further supported by the increase in the number of *tfdA* genes, which occurred in advance of the exponential phase of the mineralization. Detection of MCP and other unidentified metabolites during the degradation of MCPA have been reported in recent studies as well (10, 29).

In general, the amounts of MCPA mineralized in topsoils did not exceed a maximum of 60 to 70% of the initial concentrations. The remaining 30 to 40% can be explained by the incorporation of ^{14}C from MCPA into biomass and into soil organic matter. Mineralization potentials of this magnitude have been reported elsewhere previously (41, 61). Additionally, there is a tendency towards a slightly higher total mineralization in the subsoil experiment than in the topsoil, which can be explained by a larger degree of adsorption in the topsoil than in the subsoil. This was previously shown by Jensen et al. (29) to result in a larger bioavailability in the subsoil and thereby higher mineralization potentials, corresponding to the findings previously reported by Mortensen and Jacobsen (41) and Willems et al. (61).

Using kinetic modeling, we found that the mineralization in $Top_{2.3}$ and Top_{20} was best described by the exponential form of the 3/2-order model, in agreement with results reported previously Mortensen and Jacobsen (41), who used the exponential form for soils from three depths amended with 1 mg MCPA kg^{-1} soil. Similarly, Reffstrup et al. (47) fitted the mineralization of the phenoxypropionic herbicide mecoprop amended at 5 to 500 mg kg^{-1} to the exponential form of the 3/2-order model as well, while experiments amended with 0.0005 to 0.5 mg mecoprop kg^{-1} were fitted to the linear form of the 3/2-order model. This indicates that the initial concentration of the substrate may be important for whether growth occurs or not. However, this was not observed in the present study, which may be due to substrate concentrations that were too high. The fact that Top_{20} fitted better to the model than $Top_{2.3}$ may be a consequence of the relatively higher degree of growth in Top_{20} than in $Top_{2.3}$ compared to the substrate concentration.

In the subsoil, the result of the present study differs from what was found previously by Fomsgaard (17) and Mortensen and Jacobsen (41). They found that growth was more likely to occur in subsoil than in topsoil because the initial population of degraders in topsoils may be able to degrade the pesticide without significant growth.

Conclusion. In summary, we found that growth of microbial degraders occurs during the degradation of MCPA. The growth was more pronounced during the degradation of high concentrations (20 mg kg^{-1}) than during the degradation of low concentrations (2.3 mg kg^{-1}). This led to better fitting of mineralization data of the high-concentration scenario to a model taking exponential growth into account. In addition, we found that a shift in the degrader population occurred during the degradation period. Class I *tfdA* genes were found to be present among the naturally occurring microbial population in the topsoil, which had not been exposed to MCPA for 15 years. The concentration of these genes did not increase during the degradation period. Contrary to this, we found that degraders containing *tfdA* genes belonging to class III grew up and became dominant. We found that at least five different *tfdA*-containing genotypes grew up during the degradation period. Thus, the results of an analysis of functional genes present in soil prior to exposure with a contaminant might not necessary reflect the actual population carrying out the degradation. Last, in soils containing an initial load of *tfdA* class I genes, the metabolite MCP was detected during the degradation experiment, but no proper accumulation of metabolites from the MCPA degradation was observed.

ACKNOWLEDGMENTS

The Danish Agricultural and Veterinary Research Council supported the present study in the framework of the SOUND project.

We thank M. Nicolaisen for phylogenetic analysis of *tfdA* genes, L. F. Nielsen for initial optimization of real-time PCR, M. Andersen for the valuable technical assistance, and A. Z. Nielsen and K. L. Demant for their useful suggestions on the manuscript.

REFERENCES

1. **Acea, M. J., and M. Alexander.** 1988. Growth and survival of bacteria introduced into carbon amended soil. Soil Biol. Biochem. **20:**703–709.
2. **Acea, M. J., C. R. Moore, and M. Alexander.** 1988. Survival and growth of bacteria introduced into soil. Soil Biol. Biochem. **20:**509–515.
3. **Altschul, S. F., W. Gish, W. Miller, E. W. Myers, and D. J. Lipman.** 1990. Basic local alignment search tool. J. Mol. Biol. **215:**403–410.
4. **Amy, P. S., J. W. Schulke, L. M. Frazier, and R. J. Seidler.** 1985. Characterization of aquatic bacteria and cloning of genes specifying partial degradation of 2,4-dichlorophenoxyacetic acid. Appl. Environ. Microbiol. **49:**1237–1245.
5. **Andersen, S. M., P. B. Hertz, T. Holst, R. Bossi, and C. S. Jacobsen.** 2001. Mineralization studies of 14C-labelled metsulfuron-methyl, tribenuron-methyl, chlorsulfuron and thifensulfuron-methyl in one Danish soil and groundwater sediment profile. Chemosphere **45:**775–782.
6. **Bollag, J. M., C. S. Helling, and M. Alexander.** 1967. Metabolism of 4-chloro-2-methylphenoxyacetic acid by soil bacteria. Appl. Microbiol. **15:** 1393–1398.
7. **Brunner, W., and D. D. Focht.** 1984. Deterministic three-half-order kinetic model for microbial degradation of added carbon substrates in soil. Appl. Environ. Microbiol. **47:**167–172.
8. **Caux, P. Y., R. A. Kent, V. Bergeron, G. T. Fan, and D. D. Macdonald.** 1995. Environmental fate and effects of MCPA—a Canadian perspective. Crit. Rev. Environ. Sci. Technol. **25:**313–376.
9. **Clausen, G. B., L. Larsen, K. Johnsen, J. R. de Lipthay, and J. Aamand.** 2002. Quantification of the atrazine-degrading *Pseudomonas* sp. strain ADP in aquifer sediment by quantitative competitive polymerase chain reaction. FEMS Microbiol. Ecol. **41:**221–229.
10. **Crespin, M. A., M. Gallego, M. Valcarcel, and J. L. Gonzalez.** 2001. Study of the degradation of the herbicides 2,4-D and MCPA at different depths in contaminated agricultural soil. Environ. Sci. Technol. **35:**4265–4270.
11. **Dejonghe, W., J. Goris, S. El Fantroussi, M. Hofte, P. De Vos, W. Verstraete, and E. M. Top.** 2000. Effect of dissemination of 2,4-dichlorophenoxyacetic acid (2,4-D) degradation plasmids on 2,4-D degradation and on bacterial community structure in two different soil horizons. Appl. Environ. Microbiol. **66:**3297–3304.
12. **de Lipthay, J. R., J. Aamand, and T. Barkay.** 2002. Expression of *tfdA* genes in aquatic microbial communities during acclimation to 2,4-dichlorophenoxyacetic acid. FEMS Microbiol. Ecol. **40:**205–214.
13. **Don, R. H., and J. M. Pemberton.** 1981. Properties of 6 pesticide degradation plasmids isolated from *Alcaligenes paradoxus* and *Alcaligenes eutrophus*. J. Bacteriol. **145:**681–686.
14. **Don, R. H., and J. M. Pemberton.** 1985. Genetic and physical map of the 2,4-dichlorophenoxyacetic acid degradative plasmid pJP4. J. Bacteriol. **161:** 466–468.
15. **Don, R. H., A. J. Weightman, H. J. Knackmuss, and K. N. Timmis.** 1985. Transposon mutagenesis and cloning analysis of the pathways for degradation of 2,4-dichlorophenoxyacetic acid and 3-chlorobenzoate in *Alcaligenes eutrophus* JMP134(pJP4). J. Bacteriol. **161:**85–90.
16. **Feinberg, A. P., and B. Vogelstein.** 1983. A technique for radiolabeling DNA restriction endonuclease fragments to high specific activity. Anal. Biochem. **132:**6–13.
17. **Fomsgaard, I. S.** 1997. Modelling the mineralization kinetics for low concentrations of pesticides in surface and subsurface soil. Ecol. Model **102:** 175–208.
18. **Fukumori, F., and R. P. Hausinger.** 1993. *Alcaligenes eutrophus* JMP134 "2,4-dichlorophenoxyacetate monooxygenase" is an α-ketoglutarate-dependent dioxygenase. J. Bacteriol. **175:**2083–2086.
19. **Fukumori, F., and R. P. Hausinger.** 1993. Purification and characterization of 2,4-dichlorophenoxyacetate alpha-ketoglutarate dioxygenase. J. Biol. Chem. **268:**24311–24317.
20. **Fulthorpe, R. R., C. McGowan, O. V. Maltseva, W. E. Holben, and J. M.**

Downloaded from http://aem.asm.org/ on April 30, 2012 by guest

COR-AAD1-00002859
Bayer EX1008 (Part 6 of 9)

Tiedje. 1995. 2,4-Dichlorophenoxyacetic acid-degrading bacteria contain mosaics of catabolic genes. Appl. Environ. Microbiol. **61:**3274–3281.
21. **Gaunt, J. K., and W. C. Evans.** 1971. Metabolism of 4-chloro-2-methylphenoxyacetate by a soil pseudomonad—preliminary evidence for metabolic pathway. Biochem. J. **122:**519–526.
22. **Harker, A. R., R. H. Olsen, and R. J. Seidler.** 1989. Phenoxyacetic acid degradation by the 2,4-dichlorophenoxyacetic acid (*tfd*) pathway of plasmid pJP4: mapping and characterization of the *tfd* regulatory gene, *tfdr*. J. Bacteriol. **171:**314–320.
23. **Helweg, A.** 1987. Degradation and adsorption of C-14 MCPA in soil—influence of concentration, temperature and moisture content on degradation. Weed Res. **27:**287–296.
24. **Itoh, K., R. Kanda, Y. Sumita, H. Kim, Y. Kamagata, K. Suyama, H. Yamamoto, R. P. Hausinger, and J. M. Tiedje.** 2002. *tfdA*-like genes in 2,4-dichlorophenoxyacetic acid-degrading bacteria belonging to the *Bradyrhizobium-Agromonas-Nitrobacter-Afipia* cluster in α-*Proteobacteria*. Appl. Environ. Microbiol. **68:**3449–3454.
25. **Itoh, K., Y. Tashiro, K. Uobe, Y. Kamagata, K. Suyama, and H. Yamamoto.** 2004. Root nodule *Bradyrhizobium* spp. harbor *tfdA*α and *cadA*, homologous with genes encoding 2,4-dichlorophenoxyacetic acid-degrading proteins. Appl. Environ. Microbiol. **70:**2110–2118.
26. **Jacobsen, C. S.** 2004. Detection and quantification of microbial DNA sequences in soil by Southern- and dot/slot blot hybridization, p. 333–344. *In* G. A. Kowalchuk (ed.), Molecular microbial ecology manual. Kluwer Academic, Dordrecht, The Netherlands.
27. **Jacobsen, C. S. and J. C. Pedersen.** 1992. Mineralization of 2,4-dichlorophenoxyacetic acid (2,4-D) in soil inoculated with DBO1 (pRO101), AEO106 (pRO101) and JMP134 (pJP4): effects of inoculation level and substrate concentration. Biodegradation **2:**253–263.
28. **Jacobsen, C. S., and J. C. Pedersen.** 1992. Growth and survival of Pseudomonas cepacia DB01 (pRO101) in soil amended with 2,4-dichlorophenoxyacetic acid. Biodegradation **2:**245–252.
29. **Jensen, P. B., B. C. B. Hansen, J. Rasmussen, and O. S. Jacobsen.** 2004. Sorption-controlled degradation kinetics of MCPA in soil. Environ. Sci. Technol. **38:**6662–6668.
30. **Kamagata, Y., R. R. Fulthorpe, K. Tamura, H. Takami, L. J. Forney, and J. M. Tiedje.** 1997. Pristine environments harbor a new group of oligotrophic 2,4-dichlorophenoxyacetic acid-degrading bacteria. Appl. Environ. Microbiol. **63:**2266–2272.
31. **Kaphammer, B., J. J. Kukor, and R. H. Olsen.** 1990. Regulation of *tfdCDEF* by *tfdR* of the 2,4-dichlorophenoxyacetic acid degradation plasmid pJP4. J. Bacteriol. **172:**2280–2286.
32. **Kaphammer, B., and R. H. Olsen.** 1990. Cloning and characterization of *tfdS*, the repressor-activator gene of *tfdB*, from the 2,4-dichlorophenoxyacetic acid catabolic plasmid pJP4. J. Bacteriol. **172:**5856–5862.
33. **Kitagawa, W., S. Takami, K. Miyauchi, E. Masai, Y. Kamagata, J. M. Tiedje, and M. Fukuda.** 2002. Novel 2,4-dichlorophenoxyacetic acid degradation genes from oligotrophic *Bradyrhizobium* sp. strain HW13 isolated from a pristine environment. J. Bacteriol. **184:**509–518.
34. **Kukor, J. J., R. H. Olsen, and J. S. Siak.** 1989. Recruitment of a chromosomally encoded maleylacetate reductase for degradation of 2,4-dichlorophenoxyacetic acid by plasmid pJP4. J. Bacteriol. **171:**3385–3390.
35. **Laemmli, C. M., J. H. J. Leveau, A. J. B. Zehnder, and J. R. van der Meer.** 2000. Characterization of a second *tfd* gene cluster for chlorophenol and chlorocatechol metabolism on plasmid pJP4 in *Ralstonia eutropha* JMP134(pJP4). J. Bacteriol. **182:**4165–4172.
36. **Lee, T. H., S. Kurata, C. H. Nakatsu, and Y. Kamagata.** 2005. Molecular analysis of bacterial community based on 16S rDNA and functional genes in activated sludge enriched with 2,4-dichlorophenoxyacetic acid (2,4-D) under different cultural conditions. Microb. Ecol. **49:**151–162.
37. **Leveau, J. H. J., and J. R. van der Meer.** 1996. The *tfdR* gene product can successfully take over the role of the insertion element-inactivated TfdT protein as a transcriptional activator of the *tfdCDEF* gene cluster, which encodes chlorocatechol degradation in *Ralstonia eutropha* JMP134(pJP4). J. Bacteriol. **178:**6824–6832.
38. **Loos, M. A.** 1969. Phenoxyalkanoic acids, p. 1–128. *In* P. C. Kearney and D. D. Kaufman (ed.), Degradation of herbicides. Marcel Dekker, New York, N.Y.
39. **Matrubutham, U., and A. R. Harker.** 1994. Analysis of duplicated gene sequences associated with *tfdR* and *tfdS* in *Alcaligenes eutrophus* JMP134. J. Bacteriol. **176:**2348–2353.
40. **McGowan, C., R. Fulthorpe, A. Wright, and J. M. Tiedje.** 1998. Evidence for interspecies gene transfer in the evolution of 2,4-dichlorophenoxyacetic acid degraders. Appl. Environ. Microbiol. **64:**4089–4092.
41. **Mortensen, S. K., and C. S. Jacobsen.** 2004. Influence of frozen storage on herbicide degradation capacity in surface and subsurface sandy soils. Environ. Sci. Technol. **38:**6625–6632.
42. **Muyzer, G., E. C. Dewaal, and A. G. Uitterlinden.** 1993. Profiling of complex microbial populations by denaturing gradient gel electrophoresis analysis of polymerase chain reaction-amplified genes coding for 16S ribosomal RNA. Appl. Environ. Microbiol. **59:**695–700.
43. **Nikolausz, M., K. Sipos, S. Revesz, A. Szekely, and K. Marialigeti.** 2005. Observation of bias associated with reamplification of DNA isolated from denaturing gradient gels. FEMS Microbiol. Lett. **244:**385–390.
44. **Pemberton, J. M., B. Corney, and R. H. Don.** 1979. Evolution and spread of pesticide degrading ability among soil microorganisms, p. 287–299. *In* K. N. Timmis and A. Pühler (ed.), Plasmids of medical, environmental and commercial importance. Elsevier, Amsterdam, The Netherlands.
45. **Perkins, E. J., M. P. Gordon, O. Caceres, and P. F. Lurquin.** 1990. Organization and sequence analysis of the 2,4-dichlorophenol hydroxylase and dichlorocatechol oxidative operons of plasmid pJP4. J. Bacteriol. **172:**2351–2359.
46. **Pieper, D. H., W. Reineke, K. H. Engesser, and H. J. Knackmuss.** 1988. Metabolism of 2,4-dichlorophenoxyacetic acid, 4-chloro-2-methylphenoxyacetic acid and 2-methylphenoxyacetic acid by *Alcaligenes eutrophus* JMP134. Arch. Microbiol. **150:**95–102.
47. **Reffstrup, T. K., H. Sorensen, and A. Helweg.** 1998. Degradation of mecoprop at different concentrations in surface and subsurface soil. Pestic. Sci. **52:**126–132.
48. **Robinson, J. A.** 1985. Determining microbial kinetic-parameters using nonlinear-regression analysis—advantages and limitations in microbial ecology. Adv. Microb. Ecol. **8:**61–114.
49. **Sambrook, J., and D. W. Russell.** 2001. Molecular cloning: a laboratory manual, 3rd ed. Cold Spring Harbor Laboratory Press, Cold Spring Harbor, N.Y.
50. **Scheidleder, A.** 2000. Groundwater quality and quantity in Europe. European Environment Agency, Copenhagen, Denmark.
51. **Shaw, L. J., and R. G. Burns.** 2004. Enhanced mineralization of [U-^{14}C]2,4-dichlorophenoxyacetic acid in soil from the rhizosphere of *Trifolium pratense*. Appl. Environ. Microbiol. **70:**4766–4774.
52. **Simkins, S., and M. Alexander.** 1984. Models for mineralization kinetics with the variables of substrate concentration and population density. Appl. Environ. Microbiol. **47:**1299–1306.
53. **Smejkal, C. W., T. Vallaeys, S. K. Burton, and B. M. Lappin-Scott.** 2001. Substrate specificity of chlorophenoxyalkanoic acid-degrading bacteria is not dependent upon phylogenetically related *tfdA* gene types. Biol. Fert. Soils **33:**507–513.
54. **Streber, W. R., K. N. Timmis, and M. H. Zenk.** 1987. Analysis, cloning, and high-level expression of 2,4-dichlorophenoxyacetate monooxygenase gene *tfdA* of *Alcaligenes eutrophus* JMP134. J. Bacteriol. **169:**2950–2955.
55. **Suwa, Y., A. D. Wright, F. Fukimori, K. A. Nummy, R. P. Hausinger, W. E. Holben, and L. J. Forney.** 1996. Characterization of a chromosomally encoded 2,4-dichlorophenoxyacetic acid α-ketoglutarate dioxygenase from *Burkholderia* sp. strain RASC. Appl. Environ. Microbiol. **62:**2464–2469.
56. **Thirup, L., F. Ekelund, K. Johnsen, and C. S. Jacobsen.** 2000. Population dynamics of the fast-growing subpopulations of *Pseudomonas* and total bacteria, and their protozoan grazers, revealed by fenpropimorph treatment. Soil Biol. Biochem. **32:**1615–1623.
57. **Tonso, N. L., V. G. Matheson, and W. E. Holben.** 1995. Polyphasic characterization of a suite of bacterial isolates capable of degrading 2,4-D. Microb. Ecol. **30:**3–24.
58. **Trefault, N., P. Clement, M. Manzano, D. H. Pieper, and B. Gonzalez.** 2002. The copy number of the catabolic plasmid pJP4 affects growth of *Ralstonia eutropha* JMP134 (pJP4) on 3-chlorobenzoate. FEMS Microbiol. Lett. **212:**95–100.
59. **Vallaeys, T., R. R. Fulthorpe, A. M. Wright, and G. Soulas.** 1996. The metabolic pathway of 2,4-dichlorophenoxyacetic acid degradation involves different families of *tfdA* and *tfdB* genes according to PCR-RFLP analysis. FEMS Microbiol. Ecol. **20:**163–172.
60. **Vallaeys, T., F. Parsello-Cartieaux, N. Rouard, C. Lors, G. Laguerre, and G. Soulas.** 1997. PCR-RFLP analysis of 16S rRNA, *tfdA* and *tfdB* genes reveals a diversity of 2,4-D degraders in soil aggregates. FEMS Microbiol. Ecol. **24:**269–278.
61. **Willems, H. P. L., K. J. Lewis, J. S. Dyson, and F. J. Lewis.** 1996. Mineralization of 2,4-D and atrazine in the unsaturated zone of a sandy loam soil. Soil Biol. Biochem. **28:**989–996.

Downloaded from http://aem.asm.org/ on April 30, 2012 by guest

COR-AAD1-00002860
Bayer EX1008 (Part 6 of 9)

APPLIED AND ENVIRONMENTAL MICROBIOLOGY, May 2006, p. 3803 Vol. 72, No. 5
0099-2240/06/$08.00+0 doi:10.1128/AEM.72.5.3803.2006

ERRATUM

Degradation of 4-Chloro-2-Methylphenoxyacetic Acid in Top- and Subsoil Is Quantitatively Linked to the Class III *tfdA* Gene

Jacob Bælum, Trine Henriksen, Hans Christian Bruun Hansen, and Carsten Suhr Jacobsen

Geological Survey of Denmark and Greenland (GEUS), Department of Geochemistry, Royal Veterinary and Agricultural University (KVL), Department of Natural Sciences, and Royal Veterinary and Agricultural University (KVL), Department of Ecology, Copenhagen, Denmark

Volume 72, no. 2, p. 1476–1486, 2006. Page 1478, Table 2: The sequence for the *tfdA*** reverse primer should be GTCGCGT-GCTCGAGAAG.

Downloaded from http://aem.asm.org/ on April 30, 2012 by guest

COR-AAD1-00002861
Bayer EX1008 (Part 6 of 9)

Applied and Environmental Microbiology

TaqMan Probe-Based Real-Time PCR Assay for Detection and Discrimination of Class I, II, and III *tfdA* Genes in Soils Treated with Phenoxy Acid Herbicides

Jacob Bælum and Carsten S. Jacobsen
Appl. Environ. Microbiol. **2009, 75(9):2969. DOI: 10.1128/AEM.02051-08.**
Published Ahead of Print 27 February 2009.

Updated information and services can be found at:
http://aem.asm.org/content/75/9/2969

These include:

SUPPLEMENTAL MATERIAL
http://aem.asm.org/content/suppl/2009/04/17/75.9.2969.DC1.html

REFERENCES
This article cites 18 articles, 7 of which can be accessed free at:
http://aem.asm.org/content/75/9/2969#ref-list-1

CONTENT ALERTS
Receive: RSS Feeds, eTOCs, free email alerts (when new articles cite this article), more»

Information about commercial reprint orders: http://aem.asm.org/site/misc/reprints.xhtml
To subscribe to to another ASM Journal go to: http://journals.asm.org/site/subscriptions/

JournalsASM.org

Downloaded from http://aem.asm.org/ on April 30, 2012 by guest

APPLIED AND ENVIRONMENTAL MICROBIOLOGY, May 2009, p. 2969–2972 Vol. 75, No. 9
0099-2240/09/$08.00+0 doi:10.1128/AEM.02051-08
Copyright © 2009, American Society for Microbiology. All Rights Reserved.

TaqMan Probe-Based Real-Time PCR Assay for Detection and Discrimination of Class I, II, and III *tfdA* Genes in Soils Treated with Phenoxy Acid Herbicides▽†

Jacob Bælum[1] and Carsten S. Jacobsen[1,2]*

Geological Survey of Denmark and Greenland (GEUS), Department of Geochemistry, Øster Voldgade 10, DK-1350 Copenhagen K, Denmark,[1] and Faculty of Life Sciences, Department of Natural Sciences, University of Copenhagen, Thorvaldsensvej 40, DK-1871 Frederiksberg C, Denmark[2]

Received 4 September 2008/Accepted 19 February 2009

Separate quantification of three classes of *tfdA* genes was performed using TaqMan quantitative real-time PCR for 13 different soils subsequent to mineralization of three phenoxy acids. Class III *tfdA* genes were found to be involved in mineralization more often than class I and II *tfdA* genes.

The phenoxy acids (PA), including 2,4-dichlorophenoxyacetic acid (2,4-D), 4-chloro-2-methylphenoxyacetic acid (MCPA), and 2-(4-chloro-2-methylphenoxy)propanoic acid (MCPP), are herbicides that are intensively used for control of broadleaf weeds in cereal crops worldwide. Extensive research on these environmentally hazardous compounds has produced detailed information on pathways and gene sequences involved in their complete mineralization in several bacterial pure-culture isolates (3, 12, 15, 16).

Decomposition of the ether bond resulting in a phenolic compound and acetic or propanoic acid is accepted to be the first step in the degradation pathway (5). This step is catalyzed by an α-ketoglutarate-dependent dioxygenase encoded by the *tfdA* or *tfdA*-like genes (6). The diversity of the *tfdA* genes has been investigated in detail, and three different classes have been proposed based on sequence information (10). Recently, the *tfdA* genes have been used as biomarkers in studies of the growth of degraders during mineralization of PA in natural soil samples in situ (1, 2, 7, 8, 19), but none of these studies successfully differentiated quantities of the individual *tfdA* gene classes.

Previously, two different PCR assays were used to detect and quantify *tfdA* genes in environmental samples. Vallaeys et al. (17) developed a PCR assay suitable for targeting and proving the presence of the three classes of *tfdA* genes, while, in order to improve specificity and PCR efficiency, Bælum et al. (1) developed and used a novel PCR primer set more suitable for quantitative real-time PCR (qPCR) (1, 2, 11). Furthermore, based on endpoint analysis of PCR products, these two PCR assays have been used to study the functional diversity and dynamics of the different classes of *tfdA* genes during mineralization of phenoxyacetic acids in environmental samples. As this kind of analysis does not provide a quantitative measure of the relative composition of the different classes, the need for a tool to do this is evident. Therefore, the main objective of the present study was to develop a reliable quantitative real-time PCR-based method to separately quantify the different classes of *tfdA* genes directly in complex soil samples.

Two novel qPCR assays (*tfdA* 81-bp and TaqMan assays) and one previously described qPCR assay (*tfdA* 215-bp assay) (1) targeting the known diversity of *tfdA* genes were tested to determine their PCR efficiency and specificity for the different classes of *tfdA* genes. Due to potential problems with production of PCR artifacts, the 215-bp PCR fragment is in the longer range of the fragment size recommended for qPCR (18), explaining why we designed a novel primer set amplifying a shorter fragment. The *tfdA* 81-bp and *tfdA* 215-bp assays were based on the SYBR green dye, while the TaqMan assay was based on TaqMan probes. Also, in the TaqMan assay our novel 81-bp primer set was used to amplify the target sequences. Primers for the novel *tfdA* 81-bp assay (Table 1; see Fig. S1 in the supplemental material), as well as probes for the TaqMan assay, were designed based on *tfdA* gene sequences obtained from the GenBank database (accession numbers M16730, U25717, and AF377325 for *tfdA* classes I to III, respectively). To confirm that no unwanted targets are amplified with our primer sets, the oligonucleotides were used as queries for a BLAST search in the GenBank database (for details see the supplemental Materials and Methods in the supplemental material). In the present study we had access to instrument facilities that detect only two fluorophores simultaneously. Therefore, we were not able to test multiplex PCR, where all three *tfdA* gene classes can be quantified in a single PCR vessel, but we believe that this should be possible by using probes with three different fluorophores.

Using 10-fold standard dilution series of recombined plasmids with inserts of each of the class I, II, and III *tfdA* genes and 10^7 to 10^0 genes per reaction as a template, highly comparable PCR performances were achieved with the three different assays (see Fig. S2 and Table S2 in the supplemental material). Except for the *tfdA* 215-bp assay targeting the class II gene, consistent and reliable quantification was obtained down to a limit of 10^2 genes per reaction for all three *tfdA* classes (see Fig. S2 in the supplemental material). The com-

* Corresponding author. Mailing address: Geological Survey of Denmark and Greenland (GEUS), Department of Geochemistry, Øster Voldgade 10, DK-1350 Copenhagen K, Denmark. Phone: 45 3814 2313. Fax: 45 3814 2050. E-mail: csj@geus.dk.

† Supplemental material for this article may be found at http://aem.asm.org/.

▽ Published ahead of print on 27 February 2009.

Downloaded from http://aem.asm.org/ on April 30, 2012 by guest

COR-AAD1-00002863
Bayer EX1008 (Part 6 of 9)

TABLE 1. Primers and probes used for qPCR

Oligonucleotide	Type	Target genes	Sequence (5′–3′)[a]	Fragment size (bp)	Annealing temp (°C)
tfdA-215bp	Forward primer	*tfdA* classes I, II, and III	GAGCACTACGCRCTGAAYTCCCG	215	64
	Reverse primer		GTCGCGTGCTCGAGAAG		
tfdA-81bp	Forward primer	*tfdA* classes I, II, and III	GAGCACTACGCRCTGAAYTCCCG	81	62
	Reverse primer		SACCGGMGGCATSGCATT		
tfdA-CI	Probe	*tfdA* class I	FAM-TTGCGCTTCCGAATAGTCGGTGTC-BBQ		62
tfdA-CII	Probe	*tfdA* class II	FAM-CGTTGACTTTCAGAATACTCT GTGTCGCCA-BBQ		62
tfdA-CIII	Probe	*tfdA* class III	YAK-TTGACTTTCAGAATAGTCCGTATCGCCAAG-BBQ		62

[a] R = A or G; Y = T or C; S = G or C; M = A or C. FAM, 6-carboxyfluorescein; BBQ, blackberry quencher.

parable qPCR sensitivities for the SYBR green and TaqMan probe qPCR assays are in accordance the sensitivities reported elsewhere (4, 9, 13). Detection (i.e., the replicates were not consistent and thus unreliable quantification was obtained) could be performed with as few as 10^3 genes per reaction. Probably due to a 1-bp mismatch in the reverse primer region, reliable quantification of class II genes using the *tfdA* 215-bp assay could be obtained with only as few as 10^4 genes per reaction (see Fig. S2a in the supplemental material). Furthermore, a test with different combinations of the *tfdA* target sequences and with the three TaqMan probes together in one reaction vessel was performed in order to verify the specificity of each of the probes for its target sequence. Also, we tested the feasibility of using the probes to perform duplex real-time PCR with combinations of the class I- and III-specific probes and of the class II- and III-specific probes. These tests gave the same results for the detection level and specificity as the tests described above, indicating that duplex PCR is indeed possible with these probes (for detailed information, see the supplemental Materials and Methods in the supplemental material).

A soil microcosm experiment including 13 different soils obtained from distinct locations around the world (for further details on soils, see Table S1 in the supplemental material) was performed to test the different qPCR approaches with DNA extracted directly from a wide variety of soils. In order to allow specific degraders harboring the *tfdA* genes to proliferate, we treated the microcosms with 90 μmol of 2,4-D, MCPA, or MCPP kg^{-1} of soil. Prior to and subsequent to ≥50% mineralization (measured using evolved $^{14}CO_2$), a composite subsample consisting of 0.5 g of soil was removed, and DNA was extracted using a Power-Clean soil DNA kit (MoBio Laboratories, Carlsbad, CA) according to the manufacturer's instructions. Total DNA was quantified and the extraction efficiency was normalized by running 4-μl aliquots of extracts on a standard 1.5% agarose gel stained with ethidium bromide, and qPCR was performed using the three different approaches (for further information on the experimental setup, nucleic acid preparation, and qPCR, see the supplemental Materials and Methods in the supplemental material).

Despite the low detection limit of the qPCR approaches, we were able to detect low levels of *tfdA* genes ($<10^5$ genes g^{-1} soil) in only three soils, SjO_{reg}, Suma-Paz, and KBS_{reg} (for information on soils, see the supplemental Materials and Methods in the supplemental material) prior to PA application, while after mineralization of one of the PA (>50% mineralized) we were able to detect significant increases in the levels of *tfdA* genes in the soils. The potential to mineralize the three PA was investigated using the widely used and well-validated assay for trapping $^{14}CO_2$ in an NaOH trap during mineralization in microcosms (14). The potential to mineralize >50% of the added PA was found for all 13 soils for 2,4-D, for 9 soils for MCPA, and for 4 soils for MCPP, indicating that the potential for 2,4-D mineralization is more widespread than the potential for MCPA and MCPP mineralization. Additionally, our data suggest that 2,4-D is mineralized more rapidly than MCPA and MCPP (data not shown). In all of the soils exhibiting >50% mineralization we detected increased levels of *tfdA* genes (Fig. 1), while in the soils with very slow and insignificant mineralization no such increase was detected.

Even though there was a slight tendency for the *tfdA* 81-bp SYBR green and TaqMan assays to reveal larger quantities (Fig. 2A and 2C), the correlation between the *tfdA* quantities obtained using the three different qPCR approaches was very high (Fig. 2). Based on two-way analysis of variance statistics ($P < 0.05$), the only soil scenarios for which a difference between the quantification results could be detected were 2,4-D and MCPA in the Pradera soil and 2,4-D in the Suma-Paz soil and the KBS_{forest} soil. For the Pradera soil treated with 2,4-D the difference was especially noticeable (the outliers are shown in Fig. 2A and 2B). For this soil scenario we were able to find 6×10^8 *tfdA* genes g^{-1} soil using the *tfdA* 81-bp SYBR green assay, while with the two other assays we were able to find only $>5 \times 10^4$ *tfdA* genes g^{-1} soil. This suggests that a degrader harboring a novel class of *tfdA* genes was present, but due to difficulties in sequencing extremely short PCR amplicons we have not been able to obtain sequence information. We consider the generally high correlation between *tfdA* quantities obtained using the three qPCR assays strong evidence that these three assays are suitable for consistent and reliable quantification of the class I to III *tfdA* genes in environmental samples.

The usability of our novel TaqMan probe-based qPCR approach was demonstrated by quantifying the three different *tfdA* gene classes after mineralization of 2,4-D, MCPA, and MCPP in 13 different soils (Fig. 1; see Table S3 in the supplemental material). For most of the soils, we observed that if class III *tfdA* genes were present in a soil, they typically proliferated and became dominant among the *tfdA* genes after mineralization occurred. In the soils treated with 2,4-D this was reflected by generally higher ratios of class III *tfdA* genes to class I *tfdA* genes (Fig. 1A and 1G). This trend was even more obvious for MCPA and MCPP mineralization, where class I *tfdA* genes proliferated only in the KBS_{reg} and KBS_{forest} soils treated with MCPA (Fig. 1B), while in the remaining soils

Downloaded from http://aem.asm.org/ on April 30, 2012 by guest

COR-AAD1-00002864
Bayer EX1008 (Part 6 of 9)

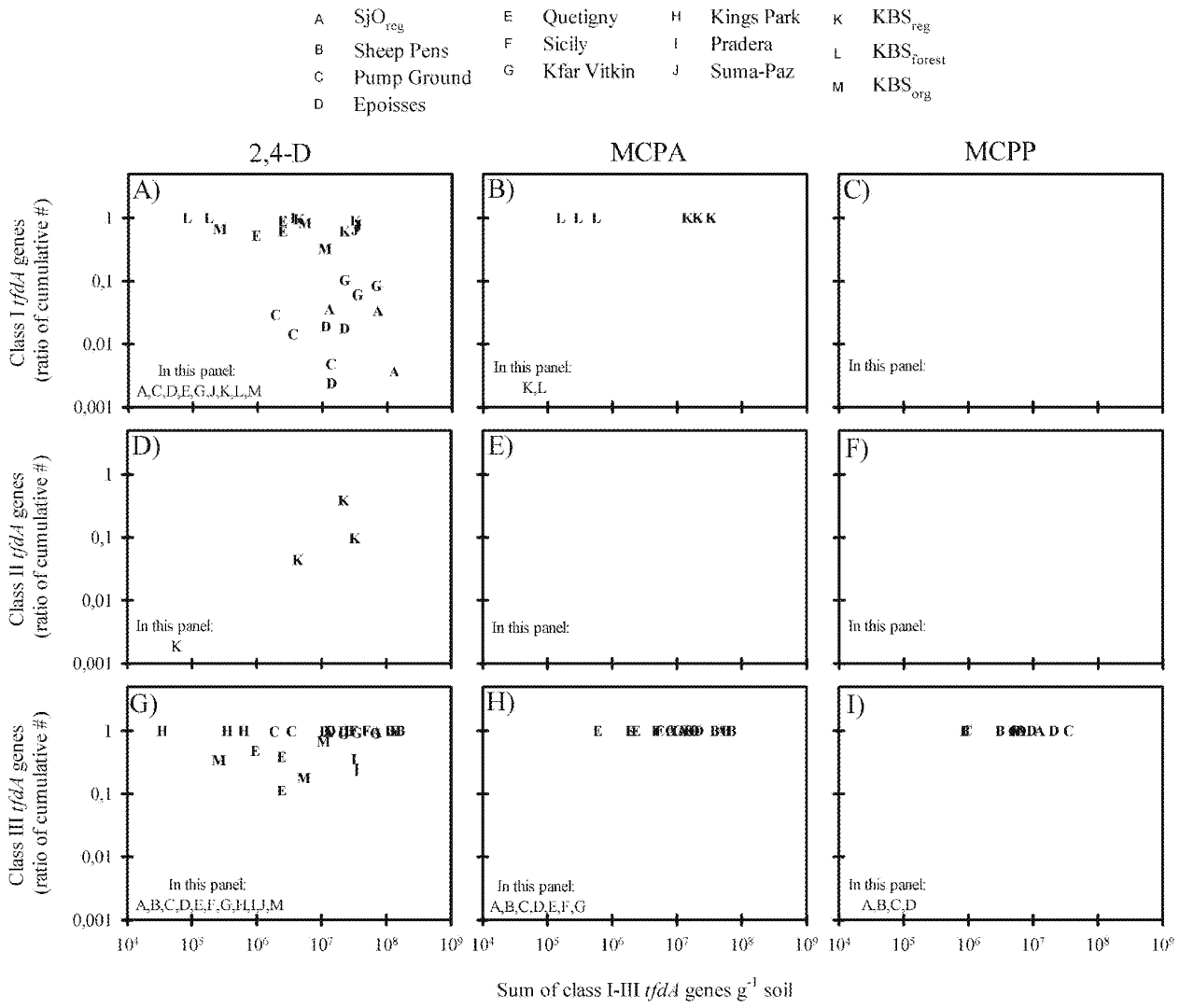


FIG. 1. Ratios of the three *tfdA* gene classes quantified using the TaqMan assay, expressed as the cumulative numbers of the three classes of *tfdA* genes in each of the 13 soils after mineralization of 2,4-D, MCPA, and MCPP. (A to C) Class I *tfdA* genes quantified in soils exposed to the three PA. (D to F) Class II *tfdA* genes quantified in soils exposed to the three PA. (G to I) Class III *tfdA* genes quantified in soils exposed to the three PA. The individual values for triplicate samples are indicated, and for clarity, the soils for which data are shown in each panel are indicated at the bottom. The exact numbers are shown in Table S3 in the supplemental material.

showing potential for MCPA and MCPP mineralization only the class III *tfdA* genes proliferated (Fig. 1B and 1I). Further proof was the fact that the KBS$_{reg}$ and KBS$_{forest}$ soils were the only soils treated with 2,4-D in which class III *tfdA* genes did not proliferate, suggesting that there was no potential for proliferation of class III *tfdA* genes, which left the PA for the organisms harboring the class I *tfdA* genes.

In previous studies we speculated that MCPA mineralization is linked to the class III *tfdA* gene (1) and 2,4-D mineralization is linked to both class I and class III *tfdA* genes (1, 2). In these studies only two different soils, originating from the same region, were studied. Furthermore, based on enrichment studies of microbial communities, Zakaria et al. (19) linked mineralization of MCPP to the class III *tfdA* gene. The present study adds significantly to our knowledge of the dynamics of *tfdA* genes during mineralization of the PA 2,4-D, MCPA, and MCPP. Here we describe a method to quantitatively measure the relative levels of the different *tfdA* gene classes in a wide variety of soils, which provides significantly better data.

In conclusion, we successfully developed a TaqMan-based qPCR method to quantify three different classes of *tfdA* genes in environmental samples. Applying the method, we were able to quantify *tfdA* genes in 13 different soils subsequent to mineralization of 2,4-D, MCPA, and MCPP. In situ in natural soils, mineralization of 2,4-D can induce growth of organisms harboring one of the three *tfdA* genes, preferentially the class I and III *tfdA* genes, and the class III *tfdA* gene is most often the dominant gene. Mineralization of MCPA induces proliferation

Downloaded from http://aem.asm.org/ on April 30, 2012 by guest

COR-AAD1-00002865
Bayer EX1008 (Part 6 of 9)

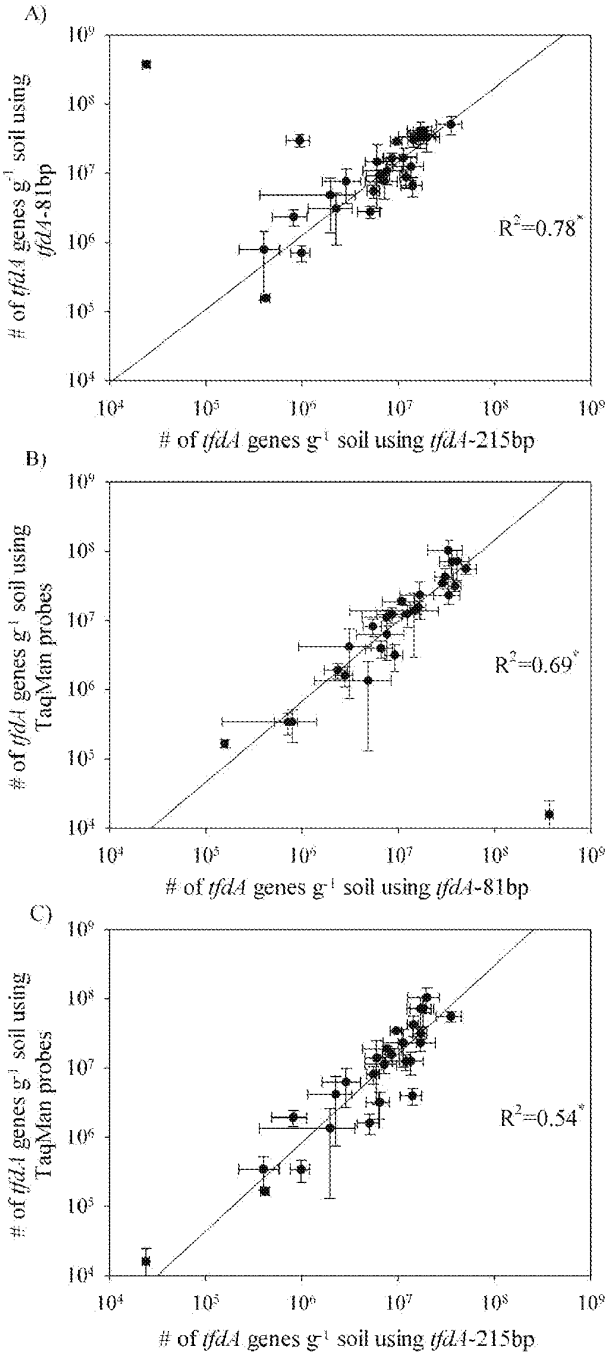


FIG. 2. Correlations between the numbers of class I to III *tfdA* genes determined using the three different approaches. (A) *tfdA* 81-bp assay compared with the *tfdA* 215-bp assay. (B) TaqMan assay compared with the *tfdA* 81-bp assay. (C) TaqMan assay compared with the *tfdA* 215-bp assay. The lines represent linear regressions, and the R^2 value is indicated in each panel. The error bars indicate standard errors of triplicate determinations.

of class III *tfdA* genes, and in cases where the potential for class III gene proliferation is absent, class I genes may proliferate as well. Mineralization of MCPP induces proliferation of only class III *tfdA* genes.

The Danish Research Council for Nature and Universe is thanked for financial support (FNU grant 274-05-0199).

Ziv Arbelli, Shai Arnon, Gary Bending, and Fabrice Martin-Laurent are thanked for kindly providing soil samples. Pia Bach Jakobsen and Szymon Kopalski are thanked for skillful technical assistance, and Kirsa Demant is thanked for proofreading the manuscript.

REFERENCES

1. **Bælum, J., T. Henriksen, H. C. B. Hansen, and C. S. Jacobsen.** 2006. Degradation of 2-methyl-4-chlorophenoxyacetic acid in top- and subsoil is quantitatively linked to the class III *tfdA* gene. Appl. Environ. Microbiol. **72:**1476–1486.
2. **Bælum, J., M. H. Nicolaisen, W. E. Holben, B. W. Strobel, J. Sørensen, and C. S. Jacobsen.** 2008. Direct analysis of *tfdA* gene expression by indigenous bacteria in phenoxy acid amended agricultural soil. ISME J. **2:**677–687.
3. **Boliag, J. M., C. S. Helling, and M. Alexander.** 1967. Metabolism of 4-chloro-2-methylphenoxyacetic acid by soil bacteria. Appl. Microbiol. **15:** 1393–1398.
4. **Demontis, M. A., S. O. Cacciola, M. Orru, V. Balmas, V. Chessa, B. E. Maserti, L. Mascia, F. Randino, G. M. B. S. Quirico, and Q. Migheli.** 2008. Development of real-time PCR systems based on SYBR Green I and TaqMan technologies for specific quantitative detection of Phoma tracheiphila in infected Citrus. Eur. J. Plant Pathol. **120:**339–351.
5. **Don, R. H., A. J. Weightman, H. J. Knackmuss, and K. N. Timmis.** 1985. Transposon mutagenesis and cloning analysis of the pathways for degradation of 2,4-dichlorophenoxyacetic acid and 3-chlorobenzoate in *Alcaligenes eutrophus* JMP134(pJP4). J. Bacteriol. **161:**85–90.
6. **Fukumori, F., and R. P. Hausinger.** 1993. *Alcaligenes eutrophus* JMP134 2,4-dichlorophenoxyacetate monooxygenase is an α-ketoglutarate-dependent dioxygenase. J. Bacteriol. **175:**2083–2086.
7. **Gonod, L. V., F. Martin-Laurent, and C. Chenu.** 2006. 2,4-D impact on bacterial communities, and the activity and genetic potential of 2,4-D degrading communities in soil. FEMS Microbiol. Ecol. **58:**529–537.
8. **Lee, T. H., S. Kurata, C. H. Nakatsu, and Y. Kamagata.** 2005. Molecular analysis of bacterial community based on 16S rDNA and functional genes in activated sludge enriched with 2,4-dichlorophenoxyacetic acid (2,4-D) under different cultural conditions. Microb. Ecol. **49:**151–162.
9. **Liu, Z. X., Y. Teng, H. Liu, Y. L. Jiang, X. Y. Xie, H. F. Li, J. Q. Lv, L. Y. Gao, J. Q. He, X. J. Shi, F. Y. Tian, J. S. Yang, and C. X. Xie.** 2008. Simultaneous detection of three fish rhabdoviruses using multiplex real-time quantitative RT-PCR assay. J. Virol. Methods **149:**103–109.
10. **McGowan, C., R. Fulthorpe, A. Wright, and J. M. Tiedje.** 1998. Evidence for interspecies gene transfer in the evolution of 2,4-dichlorophenoxyacetic acid degraders. Appl. Environ. Microbiol. **64:**4089–4092.
11. **Nicolaisen, M. H., J. Bælum, C. S. Jacobsen, and J. Sørensen.** 2008. Transcription dynamics of the functional *tfdA* gene during MCPA herbicide degradation by *Cupriavidus necator* AEO106 (pRO101) in agricultural soil. Environ. Microbiol. **10:**571–579.
12. **Pieper, D. H., W. Reineke, K. H. Engesser, and H. J. Knackmuss.** 1988. Metabolism of 2,4-dichlorophenoxyacetic acid, 4-chloro-2-methylphenoxyacetic acid and 2-methylphenoxyacetic acid by *Alcaligenes eutrophus* JMP134. Arch. Microbiol. **150:**95–102.
13. **Schonenbrucher, H., A. Abdurnawjood, K. Failing, and M. Bulte.** 2008. New triplex real-time PCR assay for detection of *Mycobacterium avium* subsp. *paratuberculosis* in bovine feces. Appl. Environ. Microbiol. **74:** 2751–2758.
14. **Sørensen, S. R., A. Schultz, O. S. Jacobsen, and J. Aamand.** 2006. Sorption, desorption and mineralisation of the herbicides glyphosate and MCPA in samples from two Danish soil and subsurface profiles. Environ. Pollut. **141:** 184–194.
15. **Streber, W. R., K. N. Timmis, and M. H. Zenk.** 1987. Analysis, cloning, and high-level expression of 2,4-dichlorophenoxyacetate monooxygenase gene *tfdA* of *Alcaligenes eutrophus* JMP134. J. Bacteriol. **169:**2950–2955.
16. **Suwa, Y., A. D. Wright, F. Fukimori, K. A. Nummy, R. P. Hausinger, W. E. Holben, and L. J. Forney.** 1996. Characterization of a chromosomally encoded 2,4-dichlorophenoxyacetic acid α-ketoglutarate dioxygenase from *Burkholderia* sp. strain RASC. Appl. Environ. Microbiol. **62:**2464–2469.
17. **Vallaeys, T., R. R. Fulthorpe, A. M. Wright, and G. Soulas.** 1996. The metabolic pathway of 2,4-dichlorophenoxyacetic acid degradation involves different families of *tfdA* and *tfdB* genes according to PCR-RFLP analysis. FEMS Microbiol. Ecol. **20:**163–172.
18. **Wang, X., and B. Seed.** 2006. High-throughput primer and probe design, p. 93–106. *In* M. T. Dorak (ed.), Real-time PCR. Taylor & Francis, New York, NY.
19. **Zakaria, B., B. Lappin-Scott, S. Burton, and C. Whitby.** 2007. Bacterial diversity in soil enrichment cultures amended with 2-(2-methyl-4-chlorophenoxy)propionic acid (mecoprop). Environ. Microbiol. **9:**2575–2587.

Downloaded from http://aem.asm.org/ on April 30, 2012 by guest

COR-AAD1-00002866
Bayer EX1008 (Part 6 of 9)

JOURNAL OF AGRICULTURAL AND FOOD CHEMISTRY

pubs.acs.org/JAFC

Characterization of Aryloxyalkanoate Dioxygenase-12, a Nonheme Fe(II)/α-Ketoglutarate-Dependent Dioxygenase, Expressed in Transgenic Soybean and *Pseudomonas fluorescens*

Samantha L. Griffin,[†] Jeffrie A. Godbey,[†] Trent J. Oman,[†] Shawna K. Embrey,[†] Anton Karnoup,[‡] Krishna Kuppannan,[‡] Brian W. Barnett,[†,§] Gaofeng Lin,[†] Nicholas V. J. Harpham,[†] Amber N. Juba,[†] Barry W. Schafer,*[,†] and Robert M. Cicchillo*[,†]

[†]Dow AgroSciences LLC, 9330 Zionsville Road, Indianapolis, Indiana 46268, United States

[‡]Analytical Sciences, BioAnalytical, The Dow Chemical Company, 1897 Building, Midland, Michigan 48667, United States

Supporting Information

ABSTRACT: Aryloxyalkanoate dioxygenase-12 (AAD-12) was discovered from the soil bacterium *Delftia acidovorans* MC1 and is a nonheme Fe(II)/α-ketoglutarate-dependent dioxygenase, which can impart herbicide tolerance to transgenic plants by catalyzing the degradation of certain phenoxyacetate, pyridyloxyacetate, and aryloxyphenoxypropionate herbicides.[1] The development of commercial herbicide-tolerant crops, in particular AAD-12-containing soybean, has prompted the need for large quantities of the enzyme for safety testing. To accomplish this, the enzyme was produced in *Pseudomonas fluorescens* (*Pf*) and purified to near homogeneity. A small amount of AAD-12 was partially purified from transgenic soybean and through various analytical, biochemical, and *in vitro* activity analyses demonstrated to be equivalent to the *Pf*-generated enzyme. Furthermore, results from *in vitro* kinetic analyses using a variety of plant endogenous compounds revealed activity with *trans*-cinnamate and indole-3-acetic acid (IAA). The catalytic efficiencies (k_{cat}/K_m) of AAD-12 using *trans*-cinnamate (51.5 M^{-1} s^{-1}) and IAA (8.2 M^{-1} s^{-1}) as substrates were very poor when compared to the efficiencies of plant endogenous enzymes. The results suggest that the presence of AAD-12 in transgenic soybean would not likely have an impact on major plant metabolic pathways.

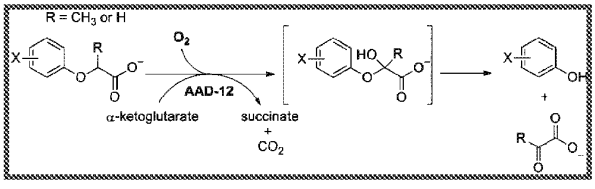
KEYWORDS: *herbicide tolerance, AAD-12, dioxygenase, nonheme Fe(II), Enlist weed control system*

INTRODUCTION

Soybean has recently been modified by insertion of the *aad-12* gene from *Delftia acidovorans* MC1.[1,2] The aryloxyalkanoate dioxygenase-12 (AAD-12) protein has been shown to confer tolerance to 2,4-dichlorophenoxyacetic acid (2,4-D) in plants. Characterization of the *aad-12* gene and the resulting translated protein is of significant importance in the safety assessment of transgenic crops.[3] For safety testing of the recombinant AAD-12 protein, large quantities are required for full characterization. Because the concentration of the AAD-12 protein in soybean is extremely low, it is technically infeasible to obtain large quantities of the active protein from transgenic plants.[4] As an alternative strategy, the protein was heterologously expressed in *Pseudomonas fluorescens* (*Pf*), which enabled the purification of a sufficient quantity of the enzyme for the current studies. However, to use the *Pf*-derived protein in safety assessment studies, biochemical and functional equivalence with the plant-derived protein needed to be established.[5]

AAD-12 is a nonheme Fe(II)/α-ketoglutarate-dependent dioxygenase, which catalyzes the degradation of various aryloxyalkanoate herbicides (Scheme 1).[1] Prior *in vitro* kinetic analyses demonstrated that AAD-12 (also known as SdpA) exhibits high catalytic efficiencies toward phenoxyalkanoate substrates.[1,6] Interestingly, AAD-12 can also utilize much larger structures such as aryloxyphenoxypropionates (AOPPs) and nitrogen-containing pyridyloxyalkanoates.[1] Studies have shown that the enzyme enantioselectively oxygenates the *S*-isomer of

Scheme 1. General Reaction Catalyzed by AAD-12



phenoxypropionate and aryloxyphenoxypropionates. The most efficiently utilized substrates reported are *S*-dichlorprop and *S*-2-(4-chloro-2-methylphenoxy)propionate (*S*-MCPP).[1,6] While monosubstituted compounds such as 2- and 4-chlorophenoxypropionates are substrates, the catalytic efficiencies are diminished significantly, suggesting the halogenation pattern on the phenoxy ring is important for substrate recognition. This notion was further substantiated by assessing the activity toward 3-phenoxypropionic acid and (*R*,*S*)-2-(2,4,5-trichlorophenoxy)propionic acid, of which neither had measurable activity under the conditions described.[6] Considerable activity was obtained using 2,4-D (a phenoxyacetate) as a substrate; however, the observed 30−50% decrease in efficiency suggests that the α-methyl group is one of the major binding

Received: January 23, 2013
Revised: May 10, 2013
Accepted: June 7, 2013
Published: June 7, 2013

ACS Publications © 2013 American Chemical Society

COR-AAD1-00002867
Bayer EX1008 (Part 6 of 9)

determinants for an efficient substrate.[1,6] Finally, extending the alkanoate chain by two carbon atoms (2,4-dichlorophenoxybutyrate) completely abolished activity. The available *in vitro* substrate specificity studies for AAD-12 and *in silico* homology modeling of SdpA from *Sphingomonas herbicidovorans* MH (~64% amino acid identity to AAD-12) suggest that the following three structural elements are important for productive substrate binding and catalysis: (1) a two- or three-carbon chain that terminates in a free carboxylate (i.e., acetates or propionates), (2) a site amenable to oxidation directly between the phenoxy oxygen and the terminal carboxylate, and (3) a phenoxy or aryloxyphenoxy group.[1,6,7]

The objective of the current study was to purify and characterize AAD-12 produced in two unique transgenic soybean lines (DAS-68416-4 and DAS-444Ø6-6) and *Pf*. A series of immunological, bioanalytical, and biochemical techniques were used to investigate biochemical and functional equivalency. Furthermore, we examined the *in vitro* substrate specificity of *Pf*-derived AAD-12 (*Pf* AAD-12) toward both xenobiotic and endogenous plant compounds.

MATERIALS AND METHODS

Chemicals. All chemicals were purchased from Sigma-Aldrich unless otherwise noted. Chlorinated *trans*-cinnamate analogues and 3-phenylglycolate (3-PGA) were prepared at Dow AgroSciences (Indianapolis, IN, USA). Indole-3-glycolic acid (IGA) was prepared according to literature procedures.[8]

Transgenic Plant Materials. The seeds used to produce the AAD-12-containing tissue (events DAS-444Ø6-6 and DAS-68416-4) were from T4 or T5 generation seed that was homozygous for the presence of the AAD-12 transgene. Leaf punches from each individual plant were harvested fresh from the greenhouse and were analyzed by a lateral flow strip assay, as described below, to confirm the presence of the AAD-12 protein. After confirmation of the presence of the AAD-12 protein, leaf and root tissues were then harvested separately, lyophilized, ground to a fine powder, and stored at −80 °C until use.

Control Plant Materials. The control plants used in this study were nontransgenic soybean plants (*Glycine max* cv. Maverick) that were the same genotype as those transformed with the *aad-12* gene. Seeds of the Maverick soybean line were planted, grown, harvested, tested, and processed under the same conditions as the transgenic plants.

Purification of AAD-12 from Soybean. The AAD-12 protein was extracted with a Tris-based buffer (50 mM Tris-HCl pH 8.0, 20 mM sodium ascorbate, 10 mM sodium metabisulfite, 250 mM NaCl, 0.5% protease inhibitor cocktail (Sigma P8849)) by macerating lyophilized leaf or root tissues in a blender (~1 g of tissue per 10 mL of buffer). The blended material was strained through four layers of cheesecloth, and the tissue was re-extracted at the same buffer-to-tissue ratio. The cheesecloth filtrates were combined and centrifuged at 10000*g* for 20 min. The resulting supernatant was filtered through diatomaceous earth. Ammonium sulfate was slowly added to the extract to a concentration of 1 M. The extract was then stirred for 1 h at 4 °C followed by centrifugation at 10000*g* for 20 min. The supernatant was collected and filtered through a 0.2 μm nylon filter, and the extract was loaded onto a 5 mL Phenyl HP Hi-Trap column (GE Healthcare) equilibrated with 1 M ammonium sulfate and 50 mM Tris-HCl pH 8.0. The column was washed with 2 column volumes (CV) of the equilibration buffer, and the bound proteins were eluted with a 20 CV elution gradient to 100% 5 mM Tris-HCl pH 8.0. Five-milliliter fractions were collected and assayed for AAD-12 content by ELISA (Acadia BioScience, LLC) and by Western blot analysis. Fractions containing the AAD-12 protein were pooled, and polyvinylpolypyrrolidone (PVPP) was added to a final concentration of 3% at 4 °C. The sample was centrifuged at 10000*g* for 10 min. The resulting supernatant was applied onto an immunoaffinity column that consisted of covalently cross-linked anti-AAD-12 monoclonal antibody (mAb 539B304, lot #609.04-2-4) to a Protein A/G resin (Thermo Scientific). The affinity resin was equilibrated with 25 mM Tris-HCl pH 8.0, 150 mM NaCl, 1 mM EDTA, 1% NP-40, and 5% glycerol, pH 7.4 (equilibration buffer), and, the PVPP-treated sample was incubated with the resin on an orbital shaker for 1 h at room temperature. The resin was pelleted by centrifugation at 1000*g* for 1 min, transferred to a gravity flow column, and washed with 15 mL of equilibration buffer followed by 2.5 mL of conditioning buffer (Thermo Scientific). The bound AAD-12 protein was eluted with 6.5 mL of elution buffer (Thermo Scientific) into tubes containing 1 M Tris-HCl pH 8.0. Fractions were collected and analyzed by SDS-PAGE, Western blot, and ELISA. The flow-through from the column contained AAD-12 protein and was reapplied to the column and purified as previously described. Fractions containing the AAD-12 protein were pooled and buffer exchanged into 5 mM ammonium bicarbonate using a PD-10 column (GE Healthcare). Aliquots were collected, lyophilized, and used for subsequent analyses.

Overexpression and Purification of AAD-12 from *P. fluorescens*. Recombinant AAD-12 protein was expressed in *Pf* strain DC57. After fermentation, samples were harvested by centrifugation at 10000*g* for 90 min, and the cell paste was frozen at −80 °C for further downstream processing. The frozen cell paste containing the AAD-12 protein was thawed and resuspended in lysis buffer (20 mM Tris-HCl pH 8.0, 1 mM EDTA, and 1 mM AEBSF) at a ratio of 1 g of wet cell paste per 4 mL of lysis buffer (i.e., 20% w/v solids). Cells were lysed by two passages through a microfluidizer (Microfluidics Corporation) at 15 000 psi. Cell debris and unbroken cells were removed by centrifugation for 30 min at 15 000 rpm at 4 °C. The extract was filtered through a 0.2 μm filter and collected in a 50 L sterile bag (Stedim Biosystems, Inc.). The clarified lysate was applied to a Q Sepharose FF column (GE Healthcare), which was equilibrated with buffer A (20 mM Tris-HCl pH 8.0, 1 mM EDTA). The column was washed with 5 CV of buffer A and then further developed by stepping to 32.5% buffer B (20 mM Tris-HC1 pH 8.0 containing 0.27 M NaCl) followed by a linear gradient from 32.5% to 60% buffer B in 7 CV, followed by a hold step at 60% buffer B. Fractions were collected and analyzed for the presence of AAD-12 by SDS-PAGE analysis. Fractions containing AAD-12 with >80% purity were pooled. Pooled fractions were diluted to 3 g L^{-1} with buffer C (20 mM Tris-HCl pH 8.0 containing 1 M NaCl), applied to a phenyl Sepharose FF column (GE Healthcare), and washed with 3 CV of buffer C. The column was then developed with an 8 CV linear gradient from 10% to 100% buffer D (20 mM Tris-HCl pH 8.0), followed by a hold at 100% D for 12 CV. Fractions were collected and analyzed for the presence of AAD-12 by SDS-PAGE. Fractions containing AAD-12 with >95% purity were pooled and buffer exchanged into 10 mM Tris-HCl pH 8.0, 0.1 M NaCl, and 2 mM dithiothreitol. After buffer exchange, trehalose was added to 1% (w/v), and the material passed through a 0.2 μm vacuum cup filter (Nalgene). The material was then frozen at −80 °C, lyophilized, and stored with desiccant packs at 4 °C.

Lateral Flow Test Strip Assay, SDS-PAGE, and Western Blot of Plant Material. To confirm the presence/absence of the AAD-12 protein in the pooled tissues, approximately 15 mg of the lyophilized tissue was weighed in a 1.5 mL microfuge tube and tested by the lateral flow test strip assay as described by the manufacturer's instructions (American Bionostica, Inc.). The soluble proteins were solubilized by adding 0.5 mL of extraction buffer, with one drop of additive, and grinding with a disposable pestle. The tubes were capped and further mixed by shaking the samples for ~10 s. The resulting supernatants were clarified by centrifuging the samples for 5 min at 20000*g*. The test strips were then incubated in the samples for 10 min. After the assay was complete, the strips were removed and allowed to air-dry, and the results were recorded.

SDS-PAGE and Western blot analysis of extracts from the transgenic events DAS-68416-4 and DAS-444Ø6-6 and nontransgenic Maverick soybean were performed using precast gels (Bio-Rad). Extracts were prepared by geno-grinding (Spex) ~75 mg of tissue with steel ball bearings in phosphate-buffered saline-Tween 20 (PBST) buffer for 3 min in a chilled Teflon microfuge tube holder. The supernatants were clarified by centrifugation for 5 min at 20000*g*, and

COR-AAD1-00002868
Bayer EX1008 (Part 6 of 9)

160 μL of each extract was mixed with 40 μL of 5× Laemmli sample buffer (LSB). The samples were then heated for 5 min at ~95 °C. After a brief centrifugation (2 min at 20000*g*), 40 μL of the supernatant was loaded directly on the gel. The microbe-derived AAD-12 and bovine serum albumin (BSA) proteins were diluted with 2× LSB to a concentration similar to that of the soybean-derived AAD-12 protein. After electrophoresis, the gel was cut in half, and one-half was stained with Thermo Scientific GelCode Blue total protein stain. The remaining half of the gel was electroblotted to a nitrocellulose membrane (Bio-Rad) and probed with an AAD-12-specific polyclonal rabbit antibody (lot #DAS F1197-167-2, 4.3 mg mL^{-1}). A conjugate of goat anti-rabbit IgG (H+L) and horseradish peroxidase (Thermo Scientific) was used as the secondary antibody. Chemiluminescent substrate (GE Healthcare, ECL Plus) was used for development and visualization of the immunoreactive protein bands. The membranes were exposed to CL-XPosure detection film (Thermo Scientific) for various time points and subsequently developed with a film developer.

Detection of Post-translational Glycosylation. The purified soybean-derived AAD-12 protein, *Pf* AAD-12, soybean trypsin inhibitor, BSA, and horseradish peroxidase were diluted with LSB, heated at ~95 °C for 5 min, and centrifuged at 20000*g* for 2 min. The resulting supernatants were applied to a Bio-Rad criterion gel and electrophoresed as described earlier. After electrophoresis, the gel was cut in half, and one-half was stained with GelCode Blue stain for total protein according to the manufacturer's protocol. The remaining half of the gel was stained with a GelCode glycoprotein staining kit (Thermo Scientific) according to the manufacturer's protocol to visualize the glycoproteins.

Peptide Mass Fingerprinting and Sequence Analysis of AAD-12. Purified soybean- and *Pf*-derived proteins were digested in-solution or in-gel. Proteins were reduced, alkylated, proteolytically digested, and subsequently analyzed by MALDI-TOF/TOF and LC-ESI-Q-TOF mass spectrometry. For in-solution digests (microbe-derived protein), AAD-12 protein samples were solubilized in 6 M guanidine hydrochloride in 400 mM ammonium bicarbonate buffer (pH 7.8) and reduced with dithiothreitol for 30 min at 65 °C. The denatured and reduced protein samples were then alkylated with iodoacetamide for 2 h in the dark at ambient temperature. The denatured, reduced, and alkylated samples were buffer exchanged into 50 mM ammonium bicarbonate buffer (pH 7.5) and digested with a combination of various endoproteases for 15 h at 37 °C. For in-gel digests (plant-derived protein), samples were analyzed using SDS-PAGE, and the band corresponding to AAD-12 protein was excised and destained. Samples were reduced, alkylated, and digested in a manner similar to that described above (see Supporting Information for endoproteases used).

For MALDI-TOF/TOF analysis, samples were desalted using ZipTip$_{C18}$ and eluted via step gradient with an increasing concentration of acetonitrile in water supplemented with 0.1% trifluoroacetic acid. Samples were mixed with an α-cyano-4-hydroxycinnamic acid matrix, deposited onto the MALDI target, and air-dried. MALDI-TOF/TOF MS and MS/MS spectra were acquired using an AB Sciex 4800 MALDI-TOF/TOF mass spectrometer.

For LC-ESI-Q-TOF analysis, a 10 μL volume of sample was injected on a Waters Acquity UPLC system equipped with an Acquity BEH C_{18} column (1.7 μm, 150 mm × 2.1 mm) heated to 50 °C and equilibrated in 5% B (solvent A = 0.1% formic acid in water; solvent B = 0.1% formic acid in acetonitrile). The sample was fractionated by employing a gradient of 5−40% B over 58 min with a 100 μL min^{-1} flow rate and was directly subjected to ESI-Q-TOF MS using a Waters Q-Tof Micro mass spectrometer. Data were acquired in ESI positive mode with leucine-enkephalin directly infused as lock mass with lock spray sampling at 7 s (MS) and 10 s (MS/MS) intervals. The acquired spectra were processed manually.

AAD-12 Colorimetric Activity Assay. A colorimetric assay was used to assess the activity of both the soybean- and *Pf*-derived enzymes. The method was adapted to 96-well plate format, and reactions were performed in a total of 150 μL as previously described.[9] Assays contained 100 mM MOPS pH 7.0, 200 μM $(NH_4)_2Fe^{II}(SO_4)_2$, 200 μM sodium ascorbate, the appropriate substrate (in DMSO), and 0.1−1 μM AAD-12. All reactions were initiated by addition of α-ketoglutarate to a final concentration of 1 mM. After the appropriate incubation time, the reaction was terminated by addition of 10 μL of 100 mM sodium EDTA. Phenol products were detected by the addition of 15 μL of pH 10 buffer (3.09 g of boric acid + 3.73 g of KCl + 44 mL of 1 N KOH), 1.5 μL of 2% 4-aminoantipyrine, and 1.5 μL of 8% potassium ferricyanide. After 3 min, the absorbance at 510 nm was recorded in a SpectraMax 190 microplate reader. Control reactions were performed excluding enzyme to account for background absorbances. Kinetic determinations were performed as described except *S*-dichlorprop was varied from 0 to 1 mM.

***P. fluorescens* AAD-12/Succinyl-CoA Synthetase-Coupled (SCS-Coupled) Activity Assay.** Enzyme assays monitoring succinate production were carried out in 96-well plates similar to those described in the literature.[10] Assays contained 100 mM MOPS pH 7.0, 1 mM PEP, 0.4 mM NADH, 0.4 mM coenzyme A, 0.4 mM ATP, 1 mM α-ketoglutarate, 0.1 mM $MgCl_2$, 0.2 mM $(NH_4)_2Fe^{II}(SO_4)_2$, and 0.2 mM sodium ascorbate. The coupling enzymes SCS (5 μM) and pyruvate kinase (6−10 units)/lactate dehydrogenase (9−14 units), along with *Pf*-derived AAD-12 (1−10 μM), were added separately in a final volume of 200 μL. The reactions were initiated by the addition of α-ketoglutarate, and activity was measured in a SpectraMax 190 plate reader monitoring the decrease in absorbance at 340 nm. The linear portion of the reaction progress curve was used to calculate the rate of NADH oxidation (ε_{340} = 6220 M^{-1} cm^{-1}). Water or dimethylsulfoxide (DMSO) replaced substrate in control reactions to account for background oxidation of NADH. Kinetic parameters for *Pf* AAD-12 were determined for nonphenoxy acids at substrate concentrations between 4 and 8000 μM, while *S*-dichlorprop was varied between 2 and 2000 μM. The data were fitted to either the Michaelis−Menten equation (eq 1) or substrate inhibition (eq 2) equation where applicable.

$$v = \frac{V_{max}[S]}{K_m + [S]} \quad (1)$$

$$v = \frac{V_{max}[S]}{K_m + \left(\frac{[S]^2}{K_i}\right) + [S]} \quad (2)$$

Fourier Transform/Mass Spectrometric (FT/MS) Analysis of *P. fluorescens*-Expressed AAD-12 Reactions. Enzymatic assays were performed as described above except that reactions were allowed to proceed for 45−60 min. Protein was removed from the sample using an Amicon Ultra centrifugal filtration device equipped with a 10 kDa molecular weight cutoff membrane. Mass spectral data were acquired for all samples on a Thermo LTQ-FT Ultra (San Jose, CA, USA). For high-resolution MS (HRMS) analyses, data were acquired in the FT cell at a nominal resolution of 12 500 in wide single-ion-monitoring with a scan range of m/z 100−450. Collisionally induced dissociation spectra were acquired in the ion trap at 35% normalized collision energy, 30 ms activation time, and an activation *Q* of 0.250. Chromatographic separation was accomplished using a Thermo Accela liquid chromatography system with 10 μL injections of sample onto a 2.1 × 50 mm, 1.9 μm Hypersil Gold (Thermo, San Jose, CA, USA) C_{18} column and eluted into the mass spectrometer using a 12 or 23 min gradient depending on the substrate analyzed. The 12 min gradient ranged from 90% buffer A (0.1% formic acid in water) to 90% buffer B (0.1% formic acid in acetonitrile), and the 23 min gradient ranged from 95% buffer A to 95% buffer B (flow rate = 0.25 mL min^{-1}). Absorption spectra from 200 to 600 nm were also acquired by using the photodiode array.

LC/TOF MS Analysis of *P. fluorescens*-Expressed AAD-12 Activity. Enzymatic assays were performed as described above, except that the SCS-coupling reagents were omitted and reactions were allowed to proceed for 120 min. The protein was removed from the sample using an Amicon Ultra centrifugal filtration device equipped with a 10 kDa molecular weight cutoff membrane. Mass spectral data were acquired in negative ion mode for all samples on an Agilent G1969A accurate-mass ESI/time-of-flight LC/MS (ESI/TOF) with a scan range of m/z 100−1000. Chromatographic separation was

COR-AAD1-00002869
Bayer EX1008 (Part 6 of 9)

accomplished using an Agilent 1200 liquid chromatography (LC) system. After removal of AAD-12, 10 μL of the flow through was injected onto an Agilent Eclipse XDB-C_{18} column (4.6 × 150 mm, 5.0 μm) and eluted into the mass spectrometer using a 21 min gradient (reaction samples were injected in triplicate). The flow rate was 1 mL min^{-1} and was split into the mass spectrometer at 0.5 mL min^{-1}. Buffer A consisted of 0.1% formic acid in water, and buffer B contained 0.1% formic acid in acetonitrile. Separation of the phenylpropanoid and flavonoid metabolites was achieved via a linear gradient from 5% buffer A to 95% buffer B. UV−visible chromatograms were obtained using a variable-wavelength detector set at 220 nm. Control assays were routinely performed using *S*-dichlorprop to verify AAD-12 activity under various conditions. Additionally, assays lacking α-ketoglutarate and AAD-12 were included to demonstrate that the presence of oxygenated products was due to the activity of AAD-12.

Quantitative Mass Spectrometric Analysis of Reactions with *trans*-2,4-Dichlorocinnamate and *trans*-Cinnamate. For *trans*-2,4-dichlorocinnamate, 47.5 μL of the reaction mixture was removed at various time points and quenched with 2.5 μL of 20% formic acid. Quenched reactions and calibration standards were diluted 10-fold in 0.1% acetic acid in water, mixed, and analyzed directly without further processing. For *trans*-cinnamate, 90 μL of the reaction mixture was removed and quenched with 10 μL of 100 mM EDTA pH 7.4. Protein was subsequently removed by filtering through an Amicon Ultra centrifugal filtration device (10 kDa MWCO membrane). Quenched reactions and calibration standards were diluted 20-fold in water, mixed, and analyzed directly without further processing. *trans*-2,4-Dichlorocinnamate and *trans*-cinnamate reactions were analyzed independently.

Matrix-matched, 12-member calibration standard curves were generated for each analyte ranging from 0.25 to 500 μM. Samples were injected on an Agilent 1290 UPLC system equipped with a BEH C_{18} column (1.7 μm, 50 mm × 2.1 mm) equilibrated in 3% buffer B (buffer A = 0.1% acetic acid in water; buffer B = 0.1% acetic acid in acetonitrile). The samples were fractionated by holding at 3% B for 30 s, then employing a gradient of 3−55% B over 3.5 min at 1.0 mL min^{-1} flow rate with a column temperature of 50 °C. UPLC eluent was directly introduced to an AB Sciex QTRAP 5500 linear ion trap quadrupole LC/MS/MS mass spectrometer without flow splitting. Data were acquired using a multiple-reaction-monitoring (MRM) scan type with previously identified and optimized transitions for the analytes monitored (Table S2 in the Supporting Information). Each sample (reactions and calibration standards) was analyzed in triplicate, and averages were reported. The calibration standards were plotted as area (counts) vs concentration (μM), and the curve was fit to linear regression with no weighting ($R^2 > 0.995$). Epoxide levels in reactions were determined from referencing the standard curve. The MRM data were integrated and analyzed using AB Sciex Analyst Software v 1.5.1 (Build 5218).

RESULTS AND DISCUSSION

During the development of AAD-12-expressing soybean, two events were selected (events DAS-68416-4 and DAS-444Ø6-6) for protein characterization, and the partially purified soybean-derived AAD-12 proteins were compared with the *Pf*-derived protein. Biophysical and biochemical data were used to investigate if the plant- and microbe-derived proteins were equivalent. Additionally, we assessed the *in vitro* substrate specificity of *Pf* AAD-12 toward a variety of xenobiotic and plant endogenous compounds.

Characterization of AAD-12 from Transgenic Soybean Events and from *P. fluorescens*. The presence of the AAD-12 protein in fresh leaf tissue (T4 or T5 generation) from events DAS-444Ø6-6 and DAS-68416-4 was confirmed using commercially available lateral flow test strips. The strips, capable of detecting between 1 and 10 ppb of AAD-12, easily discriminated between the transgenic events and nontransgenic Maverick tissue. All of the transgenic plants tested were positive for the AAD-12 protein, while none of the controls contained detectable amounts of immunoreactive protein. This result was also confirmed by the Western blot analysis using polyclonal antibodies specific to the AAD-12 protein (Figure 1).

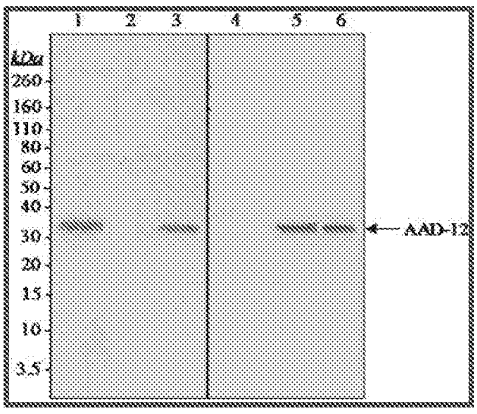


Figure 1. Western blot of AAD-12 proteins expressed in transgenic soybeans and recombinant *Pf*. Lanes 1 and 6, *Pf* AAD-12 (1 ng); lanes 2 and 4, nontransgenic leaf extract; lane 3, event DAS-444Ø6-6 leaf extract; lane 5, event DAS-68416-4 leaf extract.

To characterize the soybean-derived AAD-12 protein, the enzyme was partially purified from transgenic leaf or root tissue using hydrophobic interaction chromatography followed by immunoaffinity chromatography. The protein was examined by SDS-PAGE, which demonstrated that the final concentrated fractions contained the AAD-12 protein at an approximate molecular weight of ~32 kDa (Figure 2). Once partially purified, the biochemical and physicochemical properties of soybean-derived AAD-12 were compared with those of the *Pf*-derived protein.

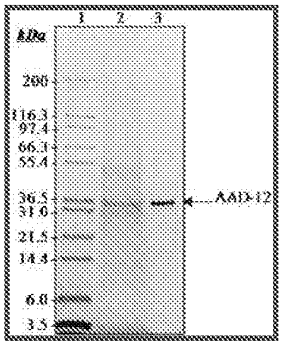


Figure 2. SDS-PAGE of AAD-12 proteins isolated from transgenic soybean and *Pf*. Lane 1, Invitrogen molecular weight markers; lane 2, event DAS-68416-4-derived AAD-12; lane 3, *Pf*-derived AAD-12 (1 μg).

The AAD-12 protein was overexpressed and purified from *P. fluorescens*. Large-scale fermentation was carried out to provide sufficient quantity of protein for toxicological and safety assessment studies. Active AAD-12 was expressed in a soluble form. Protein purification was carried out using conventional ion-exchange chromatography and hydrophobic interaction chromatography, which resulted in the recovery of purified

COR-AAD1-00002870
Bayer EX1008 (Part 6 of 9)

AAD-12 (Figure 2, lane 3). This large quantity of purified protein was used in characterization and safety studies.

Possible glycosylation of soybean- and microbe-derived AAD-12 was assessed by the GelCode glycoprotein staining kit from Thermo Scientific. The purified soybean-derived AAD-12 protein from events DAS-444Ø6-6 and DAS-68416-4 was subjected to gel electrophoresis simultaneously with a set of control and reference protein standards. Horseradish peroxidase, a glycoprotein, was loaded as a positive indicator for glycosylation. Nonglycoproteins, soybean trypsin inhibitor, and bovine serum albumin were employed as negative reference controls. SDS-PAGE gels stained for total protein demonstrated that the proteins migrated at the expected molecular weight and were readily detectable (Figure 3A; Figure S2A in

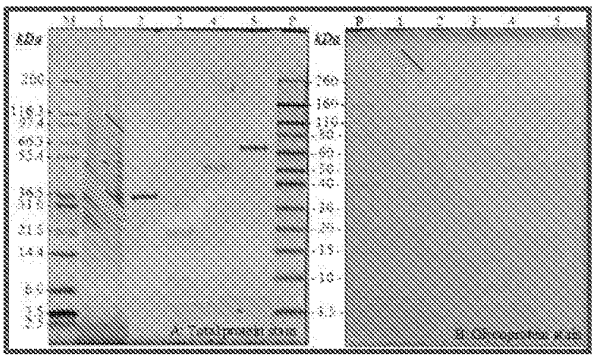


Figure 3. SDS-PAGE gels stained with (A) Coomassie blue and (B) glycoprotein stain. Lane M, Invitrogen molecular weight markers; lane 1, event DAS-68416-4-derived AAD-12; lane 2, *Pf*-derived AAD-12; lane 3, soybean trypsin inhibitor (negative control); lane 4, horseradish peroxidase (positive control); lane 5, bovine serum albumin (negative control); lane P, Novex prestained molecular weight markers.

the Supporting Information). The results of the gel stained for glycoproteins showed that neither the soybean- nor Pf-derived AAD-12 had detectable covalently linked carbohydrates, while the positive control reacted as expected (Figure 3B; Figure S2B in the Supporting Information). Additionally, the AAD-12 protein does not contain motifs that are typically required for glycosylation (Asn-Xxx-Ser/Thr).[11]

Mass spectrometry was also used to verify the amino acid sequence and any putative post-translational modifications of AAD-12 from soybean and *Pf*. Mass spectral analyses of proteolytic digests for soybean-derived AAD-12 protein from events DAS-444Ø6-6 and DAS-68416-4 resulted in peptide sequence coverage of 82.9% and 73.4%, respectively (Figures S3 and S4 in the Supporting Information). In addition, greater than 79% and 20% of the peptide sequence for DAS-444Ø6-6 and DAS-68416-4, respectively, was confirmed by MS/MS analysis, including the N- and C-terminal peptides. This analysis confirmed the microbe-derived AAD-12 protein amino acid sequence matched that of the soybean-derived protein (Figure S5 in the Supporting Information) at both the N- and C-terminus as well as a significant portion of the internal sequence. In the soybean-derived AAD-12 protein, two forms of the N-terminus were detected. The C-termini of the soybean- and microbe-derived AAD-12 proteins were indistinguishable and unmodified. A portion of the soybean-derived AAD-12 proteins was intact as predicted. In addition, a portion of the isolated proteins was missing the N-terminal methionine and the second amino acid, alanine, was acetylated. In eukaryotic (plant)-expressed proteins, this modification is observed in approximately 80−90% of the N-terminal residues.[12,13] This result implied that during or after translation in soybean and *P. fluorescens*, the N-terminal methionine was cleaved by a methionine aminopeptidase (MAP). MAPs cleave methionyl residues rapidly when the second residue on the protein is a small amino acid, such as Gly, Ala, Ser, Cys, Thr, Pro, or Val.[14] Also, it has been previously shown that proteins with serine and alanine at the N-termini are the most frequently acetylated.[15] The two co-translational processes, cleavage of an N-terminal methionine residue and N-terminal acetylation, are by far the most common modifications and occur on the vast majority of eukaryotic proteins.[15] However, examples demonstrating biological significance associated with N-terminal acetylation are rare.[16] Results of these analyses indicate that the amino acid sequence of the *Pf*-expressed protein is equivalent to that of the soybean-derived AAD-12 protein.

Comparison of Substrate Specificity and Kinetic Parameters of *P. fluorescens*-Derived and Soybean AAD-12. The substrate specificity of AAD-12 from soybean root extracts (event DAS-68416-4) and *Pf* was assessed by colorimetrically monitoring for phenol formation. The activities for the enriched soybean and purified *Pf* proteins were determined using a variety of phenoxyalkanoate substrates and AOPP graminicides (Figure 4). Both enzymes catalyzed

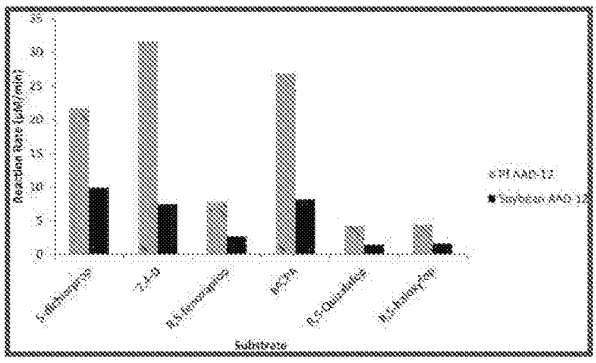


Figure 4. Substrate specificity of *Pf* AAD-12 (gray bars) and soybean AAD-12 (black bars). Reactions with contained 0.3 μM AAD-12 and 1 mM substrate (for AOPPs, 500 μM effective substrate concentration).

the degradation of the synthetic auxin herbicides 2,4-D, MCPA, and *S*-dichlorprop. The *S*-enantiospecificity was also demonstrated, as *R*-dichlorprop was not a substrate for either enzyme. The activity of the *Pf*-derived enzyme toward the AOPP herbicide had previously been established using *S*-cyhalofop.[1] Here, both enzymes demonstrated activity toward racemic mixtures of *R,S*-fenoxaprop, *R,S*-quizalofop, and *R,S*-haloxyfop (Figure 4). While the substrate specificity for both the *Pf*- and soybean-derived proteins was identical, the overall reaction rates for soybean AAD-12 were 35−50% of the purified *Pf* enzyme (>95% purity). The lowered reaction rates may be attributed to inaccuracies associated with determining the soybean AAD-12 concentration or soybean matrix interference, as AAD-12 represented only ∼1−2% of the total soluble protein.[5]

Both soybean and *Pf* enzymes displayed non-Michaelis−Menten kinetics using *S*-dichlorprop as a substrate (0−1 mM). Kinetic plots revealed that both enzymes experience substrate inhibition at *S*-dichlorprop concentrations over 200 μM;

dx.doi.org/10.1021/jf4003076 | J. Agric. Food Chem. 2013, 61, 6589−6596

COR-AAD1-00002871
Bayer EX1008 (Part 6 of 9)

Table 1. Kinetic Parameters for *Pf* AAD-12[a]

substrate	K_m (μM)	V_{max} (μM/min)	k_{cat} (s^{-1})	k_{cat}/K_m (M^{-1} s^{-1})	K_i (μM)	relative k_{cat}/K_m (M^{-1} s^{-1})
trans-cinnamate	629 ± 31.0	9.74 ± 0.14	0.032	51.5		0.019
trans-2-chlorocinnamate	322 ± 36.4	8.80 ± 0.25	0.029	90.9		0.034
trans-4-chlorocinnamate	47.4 ± 3.55	9.22 ± 0.10	0.031	647	9930 ± 467	0.242
trans-2,4-dichlorocinnamate	76.8 ± 5.11	17.2 ± 0.41	0.057	743	6610 ± 703	0.278
trans-3,4-dichlorocinnamate	12.1 ± 0.98	5.26 ± 0.11	0.018	1450	2020 ± 146	0.542
indole-3-acetic acid	3410 ± 170	16.9 ± 0.40	0.030	8.2		0.003
S-dichlorprop	21.7 ± 3.21	17.4 ± 1.00	5.80	267000	748 ± 122	100

[a]Kinetics were determined using the SCS-coupled assay.

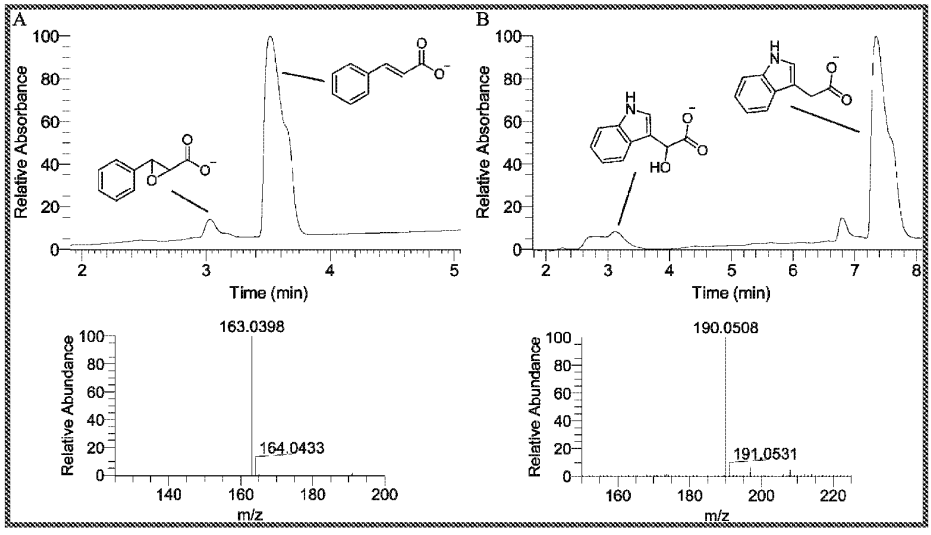


Figure 5. FTMS analysis of the *Pf* AAD-12 reactions using *trans*-cinnamate (A) and IAA (B) as substrates. Mass spectrum of 3-PGA (inset A) and IGA (inset B).

however, inhibition of *Pf* AAD-12 appears to be more pronounced than that of the enriched soybean enzyme (Figure S6 in the Supporting Information). Substrate inhibition using *S*-dichlorprop has been previously reported for SdpA.[6]

Activity of *P. fluorescens*-Derived AAD-12 toward Endogenous Plant Compounds. Activity assays were intended to determine if AAD-12 may impact important pathways when expressed in genetically modified plants. The activity of *Pf* AAD-12 was assessed using endogenous plant compounds as substrates. Relevant substrates were identified on the basis of structural similarity to herbicidal auxins, similar physiological function to known xenobiotic substrates, or presence within major primary/secondary metabolic pathways of plants. The endogenous compounds tested were separated into three groups: (1) the natural plant hormones indole-3-acetic acid (IAA), abscisic acid (ABA), and gibberellin (GA), (2) various phenylpropanoid and flavonoid secondary metabolites, (3) all 20 L-amino acids (Figures S7 and S8 in the Supporting Information). The activity toward plant endogenous compounds was initially examined by an *in vitro* enzyme-coupled system that detects succinate production (SCS-coupled assay). This system was used to guide high-resolution mass spectrometric analyses of oxidation products where applicable (either FT/MS or TOF). Together the data demonstrate that, of the endogenous compounds examined (Figure S8 in the Supporting Information), only *trans*-cinnamate and IAA were oxidized to a detectable extent and only when excessive amounts of enzyme were used. The SCS-coupled assay allowed for the determination of kinetic parameters using *trans*-cinnamic acid and IAA as substrates. The k_{cat} and K_m values for AAD-12 using *trans*-cinnamate were 0.032 s^{-1} and 629.3 μM, respectively (Table 1). The K_m was significantly elevated using IAA (~3.4 mM) and the k_{cat} was 0.03 s^{-1}. Mass spectrometry was used to identify the reaction products when *trans*-cinnamate and IAA were used as substrates. The retention times, UV−visible spectra, and MS^2 fragmentation patterns are consistent with the oxidation of *trans*-cinnamate to 3-phenylglycidate and IAA to indole-3-glycolic acid (IGA) (Figure 5).

Endogenous plant enzymes that efficiently utilize free *trans*-cinnamate have been described. Cinnamate-4-hydroxylase catalyzes the conversion of *trans*-cinnamate to *p*-coumarate during the biosynthesis of phenylpropanoids from L-phenylalanine. The enzyme from *Arabidopsis* has been characterized *in vitro* and has a K_m for *trans*-cinnamate of 0.5 μM and k_{cat}/K_m of 3.4×10^6 M^{-1} s^{-1}.[17] Additionally, the catalytic efficiency of UDP-glucose:cinnamate glucosyltransferase from strawberry has been reported.[18] The k_{cat}/K_m using *trans*-cinnamate was 0.42 μM^{-1} s^{-1}, which is ~8400-fold greater than that of *Pf* AAD-12. These kinetic parameters suggest that *trans*-cinnamate present *in planta* is efficiently directed into phenylpropanoid/flavonoid biosynthesis and that the presence of AAD-12 in transgenic crops would not likely impact the *trans*-cinnamate pool.

Indole-3-acetic acid (IAA) exists primarily as ester and amide conjugates *in planta*.[19] IAA amidosynthetase catalyzes the ATP-dependent amide bond formation between IAA and L-aspartic

COR-AAD1-00002872
Bayer EX1008 (Part 6 of 9)

acid. The enzyme from rice has a K_m of 123 μM for IAA and its k_{cat}/K_m is 2.75 × 10^3 M^{-1} s^{-1}.[20] A second enzyme, IAA glucosyltransferase, catalyzes the esterification of free IAA to glucose. The *Arabidopsis* enzyme has a K_m of 240 μM, while the enzyme from *Zea mays* has a K_m of 1.08 mM.[21,22] As with *trans*-cinnamate, the K_m and V_{max} using IAA were determined via the SCS-coupled assay (Table 1). A comparison of these kinetic parameters to endogenous plant enzymes suggests that *Pf* AAD-12 does not efficiently utilize the auxin.

Determination of Kinetic Parameters for *P. fluorescens*-derived AAD-12 Using *S*-Dichlorprop and *trans*-Cinnamates *via* the SCS-Coupled Assay. Previously, utilizing a colorimetric assay, AAD-12 kinetic measurements demonstrated that *S*-dichlorprop was utilized most efficiently followed by 2,4-D, 2-methyl-4-chlorophenoxyacetic acid (MCPA), and *S*-cyhalofop.[1] Using the SCS-coupled assay, the *Pf* AAD-12 kinetic parameters were re-evaluated with *S*-dichlorprop as a substrate (Table 1). The K_m and V_{max} were 21.7 μM and 17.42 μM min^{-1}, respectively. Additionally, a fit to eq 2 allowed for the determination of K_i, which was 748.3 μM.

Prior studies on alternative substrates for TfdA, another 2,4-D-degrading enzyme, reported the conversion of *trans*-olefins to epoxides for chloro-substituted and unsubstituted cinnamates.[23] Therefore, the substrate specificity of *Pf* AAD-12 toward *trans*-cinnamates was further expanded by determining the kinetic parameters for differentially substituted chloro-*trans*-cinnamates. The catalytic efficiencies demonstrated that the presence of chlorine atoms at positions 3,4- and 2,4- are significantly preferred over the unsubstituted phenyl (Table 1). The analyses also revealed that *Pf* AAD-12 displays substrate inhibition for all substrates except *trans*-cinnamate and *trans*-2-chlorocinnamate.

Uncoupled Succinate Production by *P. fluorescens*-Derived AAD-12. The SCS-coupled assay is limited to detection of the byproduct succinate. Under certain conditions succinate can be produced without oxidation of the primary substrate (i.e., the absence of the primary substrate or the presence of a poor substrate). This is referred to as "uncoupling" and has been demonstrated to occur among many α-ketoglutarate-dependent dioxygenases.[10,24] The drastic decrease in efficiencies using the series of *trans*-cinnamates led us to examine the extent to which uncoupled succinate production occurs. Consequently, quantitative mass spectrometry was employed to obviate detection of uncoupled succinate production by directly measuring oxygen addition to the primary substrate. To assess the extent of uncoupling catalyzed by *Pf* AAD-12, oxidized products were quantified in reactions using *trans*-2,4-dichlorocinnamate and *trans*-cinnamate as substrates. Initial rates for succinate production were simultaneously measured by the SCS-coupled assay and mass spectrometry at both 62.5 and 500 μM substrate. The rates of succinate production at 62.5 and 500 μM *trans*-2,4-dichlorocinnamate were 12.1 and 26.8 μM min^{-1}, respectively. The initial rates obtained via mass spectrometry were 3.52 and 4.91 μM min^{-1}, demonstrating that *Pf* AAD-12 catalyzes the production of succinate at approximately 0.18−0.29 the coupling efficiency when using *trans*-2,4-dichlorocinnamate as a substrate. Similar levels of uncoupling were obtained with *trans*-cinnamate (Table S2 in the Supporting Information). These results confirm that poor substrates can trigger uncoupled succinate production by *Pf* AAD-12 and suggest that the reported catalytic efficiencies determined for non-preferred substrates using the SCS-coupled assay are likely overestimated.

In conclusion, the results from this investigation support the functional and biological equivalency of soybean- and *Pf*-derived AAD-12 enzymes. This conclusion is supported by their similar immunoreactivity, physicochemical properties, and *in vitro* activity. Endogenous plant compounds were characterized as very poor substrates for *Pf* AAD-12 based on *in vitro* kinetic analyses, suggesting that the presence of the enzyme in transgenic soybean would not likely impact major plant metabolic pathways. These results are in agreement with the compositional equivalence previously reported between event DAS-68416-4 soybean and nontransgenic soybean (Maverick).[25] Collectively, these results support the use of the *Pf*-derived AAD-12 protein as a surrogate for the soybean-derived enzyme in safety studies.

ASSOCIATED CONTENT

Supporting Information

Protein sequence coverage maps for soybean- and *Pseudomonas fluorescens*-derived AAD-12 are provided. Additionally, structures of endogenous and xenobiotic compounds used in *in vitro* assays and substrate specificities are also provided. This information is available free of charge via the Internet at http://pubs.acs.org.

AUTHOR INFORMATION

Corresponding Author

*(R. M. Cicchillo) Tel: (317) 337-3846. E-mail: rmcicchillo@dow.com. (B. W. Schafer) Tel: (317) 337-3677. E-mail: bwschafer@dow.com.

Present Address

[§]BASF Plant Science, Research Triangle Park, 26 Davis Drive, North Carolina 27709, United States.

Notes

The authors declare no competing financial interest.

ACKNOWLEDGMENTS

We are grateful to Laura Tagliani, Terry Walsh, Terry Wright, Rod Herman, and Guomin Shan for their critical review of this work. The DAS-44406-6 soybean event was co-developed by Dow AgroSciences and M.S. Technologies LLC.

REFERENCES

(1) Wright, T. R.; Shan, G.; Walsh, T. A.; Lira, J. M.; Cui, C.; Song, P.; Zhuang, M.; Arnold, N. L.; Lin, G.; Yau, K.; Russell, S. M.; Cicchillo, R. M.; Peterson, M. A.; Simpson, D. M.; Zhou, N.; Ponsamuel, J.; Zhang, Z. Robust crop resistance to broadleaf and grass herbicides provided by aryloxyalkanoate dioxygenase transgenes. *Proc. Natl. Acad. Sci. U.S.A.* **2010**, *107*, 20240−20245.

(2) Wright, T. R.; Lira, J. M.; Walsh, T. A.; Merlo, D. J.; Jayakumar, P. S.; Lin, G. Novel Herbicide Resistance Genes. Patent WO 2007053482, 2007.

(3) Delaney, B.; Astwood, J. D.; Cunny, H.; Conn, R. E.; Herouet-Guicheney, C.; MacIntosh, S.; Meyer, L. S.; Privalle, L.; Gao, Y.; Mattsson, J.; Levine, M. Evaluation of protein safety in the context of agricultural biotechnology. *Food Chem. Toxicol.* **2008**, *46* (Supplement 2), S71−S97.

(4) Evans, S. L. Producing Proteins Derived from Genetically Modified Organisms for Toxicology and Environmental Fate Assessment of Biopesticides. In *The GMO Handbook: Genetically Modified Animals, Microbes, and Plants in Biotechnology*; Parekh, S. R., Ed.; Humana Press, Inc.: Totowa, NJ, 2004; pp 53−83.

COR-AAD1-00002873
Bayer EX1008 (Part 6 of 9)

(5) Raybould, A.; Kilby, P.; Graser, G. Characterising microbial protein test substances and establishing their equivalence with plant-produced proteins for use in risk assessments of transgenic crops. *Transgenic Res.* **2013**, *22*, 445−460.
(6) Westendorf, A.; Muller, R. H.; Babel, W. Purification and characterisation of the enantiospecific dioxygenases from Delftia acidovorans MC1 initiating the degradation of phenoxypropionate and phenoxyacetate herbicides. *Acta Biotechnol.* **2003**, *23*, 3−17.
(7) Muller, T. A.; Zavodszky, M. I.; Feig, M.; Kuhn, L. A.; Hausinger, R. P. Structural basis for the enantiospecificities of R- and S-specific phenoxypropionate/alpha-ketoglutarate dioxygenases. *Protein Sci.* **2006**, *15*, 1356−1368.
(8) Greenberg, J. B.; Galston, A. W.; Shaw, K. N.; Armstrong, M. D. Formation and auxin activity of indole-3-glycolic acid. *Science* **1957**, *125*, 992−993.
(9) Fukumori, F.; Hausinger, R. P. Purification and characterization of 2,4-dichlorophenoxyacetate/alpha-ketoglutarate dioxygenase. *J. Biol. Chem.* **1993**, *268*, 24311−24317.
(10) Luo, L.; Pappalardi, M. B.; Tummino, P. J.; Copeland, R. A.; Fraser, M. E.; Grzyska, P. K.; Hausinger, R. P. An assay for Fe(II)/2-oxoglutarate-dependent dioxygenases by enzyme-coupled detection of succinate formation. *Anal. Biochem.* **2006**, *353*, 69−74.
(11) Hamby, S.; Hirst, J. Prediction of glycosylation sites using random forests. *BMC Bioinf.* **2008**, *9*, 500−512.
(12) Wellner, D.; Panneerselvam, C.; Horecker, B. L. Sequencing of peptides and proteins with blocked N-terminal amino acids: N-acetylserine or N-acetylthreonine. *Proc. Natl. Acad. Sci.* **1990**, *87*, 1947−1949.
(13) Polevoda, B.; Sherman, F. N-terminal acetyltransferases and sequence requirements for N-terminal acetylation of eukaryotic proteins. *J. Mol. Biol.* **2003**, *325*, 595−622.
(14) Walsh, C. T. *Posttranslational Modification of Proteins: Expanding Nature's Inventory*; Roberts and Company Publishers: Greenwood Village, CO, 2005; Vol. *1*, p 576.
(15) Polevoda, B.; Sherman, F. The diversity of acetylated proteins. *Genome Biol.* **2002**, *3*, 1−6.
(16) Polevoda, B.; Sherman, F. N alpha-terminal acetylation of eukaryotic proteins. *J. Biol. Chem.* **2000**, *275*, 36479−36482.
(17) Chen, H.; Jiang, H.; Morgan, J. A. Non-natural cinnamic acid derivatives as substrates of cinnamate 4-hydroxylase. *Phytochemistry* **2007**, *68*, 306−311.
(18) Lunkenbein, S.; Bellido, M.; Aharoni, A.; Salentijn, E. M.; Kaldenhoff, R.; Coiner, H. A.; Munoz-Blanco, J.; Schwab, W. Cinnamate metabolism in ripening fruit. Characterization of a UDP-glucose:cinnamate glucosyltransferase from strawberry. *Plant Physiol.* **2006**, *140*, 1047−1058.
(19) Bandurski, R. S.; Schulze, A. Concentration of indole-3-acetic acid and its derivatives in plants. *Plant Physiol.* **1977**, *60*, 211−213.
(20) Chen, Q.; Zhang, B.; Hicks, L. M.; Wang, S.; Jez, J. M. A liquid chromatography-tandem mass spectrometry-based assay for indole-3-acetic acid-amido synthetase. *Anal. Biochem.* **2009**, *390*, 149−154.
(21) Jackson, R. G.; Lim, E. K.; Li, Y.; Kowalczyk, M.; Sandberg, G.; Hoggett, J.; Ashford, D. A.; Bowles, D. J. Identification and biochemical characterization of an Arabidopsis indole-3-acetic acid glucosyltransferase. *J. Biol. Chem.* **2001**, *276*, 4350−4356.
(22) Michalczuk, L.; Bandurski, R. S. Enzymic synthesis of 1-O-indol-3-ylacetyl-beta-D-glucose and indol-3-ylacetyl-myo-inositol. *Biochem. J.* **1982**, *207*, 273−281.
(23) Dunning Hotopp, J. C.; Hausinger, R. P. Alternative substrates of 2,4-dichlorophenoxyacetate/alpha-ketoglutarate dioxygenase. *J. Mol. Catal. B: Enzym.* **2001**, *15*, 155−162.
(24) Hausinger, R. P. FeII/alpha-ketoglutarate-dependent hydroxylases and related enzymes. *Crit. Rev. Biochem. Mol. Biol.* **2004**, *39*, 21−68.
(25) Herman, R. A.; Phillips, A. M.; Lepping, M. D.; Sabbatini, J. Compositional safety of DAS-68416 (AAD-12) herbicide-tolerant soybean. *J. Nutr. Food Sci.* **2011**, 1:2, doi 10.4172/215-9600.1000103.

COR-AAD1-00002874
Bayer EX1008 (Part 6 of 9)

Published on 23 April 2015 on http://pubs.rsc.org | doi:10.1039/9781782621959-00001
Downloaded on 09/07/2016 13:50:17.

CHAPTER 1

Biochemical Diversity of 2-Oxoglutarate-Dependent Oxygenases

ROBERT P. HAUSINGER*[a,b]

[a]Department of Microbiology and Molecular Genetics, [b]Department of Biochemistry and Molecular Biology, Michigan State University, East Lansing, MI 48824, USA
*E-mail: hausinge@msu.edu

1.1 Introduction

This chapter summarizes the diverse array of biochemical transformations that are catalysed by Fe(II)- and 2-oxoglutarate (2OG, also known as α-ketoglutarate)-dependent oxygenases.[1–5] As described more comprehensively in Chapter 2, most of these enzymes coordinate their active site metal at one end of a double-stranded β-helix fold (Figure 1.1A)[6–8] using a 2-His-1-carboxylate motif, bind 2OG within the core, and interact with their primary substrates using less conserved regions of the core and additional loops. Most representatives of this enzyme family catalyse hydroxylation reactions (Figure 1.1B), but desaturation, ring formation, ring expansion, halogenation and other types of chemistry are known, as described for several examples in later sections of this chapter. The mechanisms of these enzymes are detailed in Chapter 3, supported by chemical model investigations summarized in Chapter 4. A highly simplified mechanistic scheme for hydroxylases

RSC Metallobiology Series No. 3
2-Oxoglutarate-Dependent Oxygenases
Edited by Robert P. Hausinger and Christopher J. Schofield
© The Royal Society of Chemistry 2015
Published by the Royal Society of Chemistry, www.rsc.org

COR-AAD1-00002875
Bayer EX1008 (Part 6 of 9)

View Online

based on investigations of TauD (taurine hydroxylase), a well-characterized taurine-degrading enzyme (see Section 1.6.4),[9] is depicted in Figure 1.1C. As illustrated, the binding of 2OG displaces two waters from an octahedral Fe(II) site (converting state a to state b); a third water is lost as the primary substrate binds (generating state c); the newly vacant coordination site is used to react with O_2 to form an Fe(III)–superoxo species (state d); oxidative decarboxylation of 2OG yields an Fe(IV)–oxo species (state e, also known as the ferryl intermediate); this powerful oxidant abstracts a hydrogen atom from the substrate to generate a radical and Fe(III)–hydroxide (state f); and hydroxyl radical rebound (or more complex chemistry)[10] completes

Published on 23 April 2015 on http://pubs.rsc.org | doi:10.1039/9781782621959-00001
Downloaded on 09/07/2016 13:50:17.

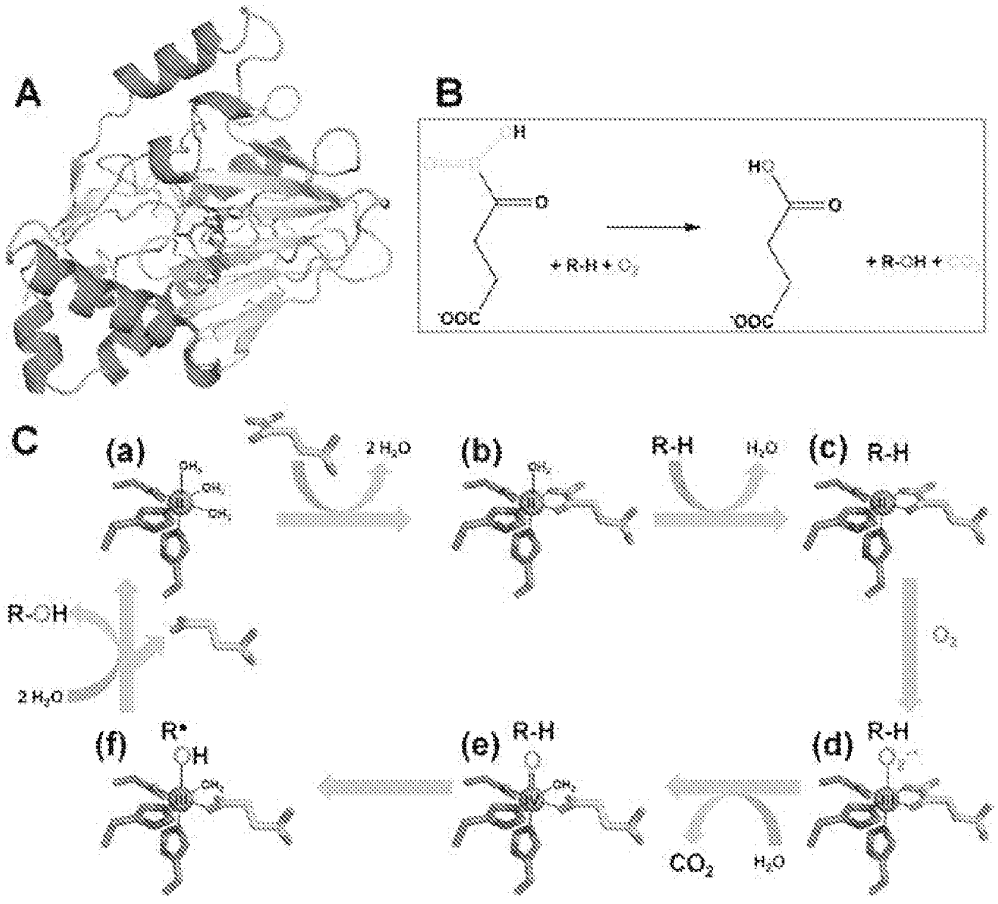


Figure 1.1 Structure and mechanism of a representative 2OG-dependent oxygenase. (A) Cartoon structure of TauD (PDB ID: 1GY9) with red α helices, yellow β strands, grey unstructured regions, Fe (orange sphere), metal ligands (sticks with blue carbons) and 2OG (sticks with cyan carbons). The major grouping of β strands forms a double-stranded β helix core. (B) Overall hydroxylation reaction in which one atom of O_2 is incorporated into substrate (R–H) in a step that is driven by the oxidative decarboxylation of 2OG; CO_2 is derived from the C-1 position of 2OG and succinate incorporates the second atom of O_2. (C) Simplified hydroxylation mechanism.

COR-AAD1-00002876
Bayer EX1008 (Part 6 of 9)

View Online

Published on 23 April 2015 on http://pubs.rsc.org | doi:10.1039/9781782621959-00001
Downloaded on 09/07/2016 13:50:17.

substrate hydroxylation and recycles the enzyme to the initial Fe(II) state. Such enzymes are dioxygenases because both atoms of oxygen are incorporated into substrates, with one atom ending up in succinate and the second in the hydroxylated product (which decomposes spontaneously in some reactions).[11] These enzymes are correctly referred to as primary substrate:2OG dioxygenases or primary substrate hydroxylases; it is incorrect to cite these enzymes as primary substrate dioxygenases or 2OG dioxygenases because these names imply both atoms of oxygen become incorporated into a single substrate. The other types of chemistries associated with this family of enzymes are also likely to utilize the Fe(IV)-oxo intermediate.

The total number of 2OG-dependent oxygenases found in biology is immense. For example, humans and other animals are thought to possess about 80 such enzymes.[7] Even more are predicted to be present in plants such as the model organism *Arabidopsis thaliana*.[12] Some 2OG-dependent oxygenases are widely distributed throughout aerobic life forms, whereas highly specialized enzymatic catalysts have evolved in various microorganisms or plants for synthesis or degradation of compounds found in their unique niches. In the following sections, the vast array of reactions catalysed by 2OG-dependent oxygenases are divided into seven categories. Section 1.2 describes the 2OG-dependent enzymes acting on proteins. These reactions may lead to structural consequences, have oxygen-sensing functions, alter histone properties, or possess other roles. Section 1.3 summarizes the metabolism of 2OG-dependent oxygenases acting on polynucleotides. The functions of these enzymes include DNA or RNA repair of alkylation damage, roles in transcriptional regulation, biosynthesis of base J in DNA or of specific tRNAs, and demethylation of 5-methylcytosine. Enzymes involved in lipid-related metabolism are discussed in Section 1.4. Examples include reactions related to carnitine biosynthesis, the degradation of phytanic acids, and the decoration of ornithine lipids or lipid A. Plant-specific representatives and close relatives are highlighted in Section 1.5. Of interest are reactions related to synthesis of flavonoids and anthocyanins, gibberellins, alkaloids, and other metabolites found predominantly in plants. Section 1.6 covers enzymes that act on a variety of small molecules including free amino acids, nucleobases or nucleosides, herbicides, sulfonates/sulfates and phosphonates. In some cases, the products resulting from these transformations are incorporated into antibiotics whereas other reactions are involved in metabolite recycling or alternative biochemical pathways. Additional 2OG-dependent oxygenases utilized for antibiotic biosynthesis are provided in Section 1.7. Examples include several halogenating enzymes and other representatives derived from bacterial and fungal sources. Finally, Section 1.8 covers enzymes that are related in structure or mechanism to the 2OG-dependent oxygenases. These include isopenicillin *N* synthase and the plant-specific ethylene-forming enzyme, which contain the 2OG oxygenase fold yet fail to utilize 2OG, and two enzymes that share a distinct fold and use the alternative oxo-acid 4-hydroxyphenylpyruvate.

COR-AAD1-00002877
Bayer EX1008 (Part 6 of 9)

View Online

1.2 2OG-Dependent Dioxygenases that Act on Proteins

This section describes 2OG-dependent dioxygenases that act directly on protein side chains or at modified sites in proteins and catalyse the reactions summarized in Figure 1.2.

Published on 23 April 2015 on http://pubs.rsc.org | doi:10.1039/9781782621959-00001
Downloaded on 09/07/2016 13:50:17.

1.2.1 Protein Substrates with Structural Roles

The earliest investigations of the 2OG-dependent dioxygenases were focused on enzymes acting on protein substrates with structural roles. For example, seminal studies from the 1960s demonstrated that prolyl 4*R*-hydroxylase (Figure 1.2A) utilizes 2OG as a cosubstrate for its function in collagen synthesis.[13,14] Similar findings were observed for two other enzymes needed to functionalize collagen, prolyl 3*S*-hydroxylase (Figure 1.2B)[15] and procollagen lysyl 5*R*-hydroxylase (PLOD, Figure 1.2C).[16] By 1982, a remarkably prescient mechanism was proposed for prolyl 4*R*-hydroxylase and contained many of the features shown in Figure 1.2C, including coordination of Fe(II) by a facial triad, bidentate coordination of 2OG, and the generation of a reactive metal–oxo intermediate.[17] Collagen, the most abundant protein in mammals, is first synthesized as procollagen, which undergoes extensive modifications including the formation of 4*R*-hydroxyproline (4Hyp, accounting for 10% of its residues), 3*S*-hydroxyproline (3Hyp, ~1% of its residues), and 5*R*-hydroxylysine (Hyl, 0.5–7% of its residues) prior to assembly into its triple helical structure and export to the extracellular matrix.[18] 4Hyp is also found in elastin and other human structural proteins, plant cell wall components, and various other proteins or peptides of algae, selected bacteria, and even a virus.[19] Similarly, 3Hyp and Hyl have been detected in non-collagen proteins. The collagen-specific prolyl 4*R*-hydroxylases form heterodimers with protein disulfide isomerase, but only the homomeric enzymes from the bacterium *Bacillus anthracis* and the alga *Chlamydomonas reinhardtii* have been crystallized.[20–22] These structures reveal the basis for stereospecificity and substrate specificity. The procollagen-specific 2OG-dependent dioxygenases are described in greater detail in Chapter 5.

1.2.2 Protein Substrates with Oxygen-Sensing Roles

An O_2-sensing role for 2OG-dependent dioxygenases was uncovered in 2001.[23,24] A key component of this signalling pathway is the hypoxia-inducible factor (HIF-1) which directs the transcription of several genes under low O_2 conditions. The two subunits of this heterodimer (HIF-α and HIF-β in humans) are constitutively synthesized, but human HIF-α is modified in cells under normoxic conditions by three HIF-α-specific prolyl 4*R*-hydroxylases (PHDs, Figure 1.2A). These enzymes act in a tissue-specific manner to oxidize Pro-402 and Pro-564 of HIF-1α, which results in enhanced affinity of the

COR-AAD1-00002878
Bayer EX1008 (Part 6 of 9)

View Online

Published on 23 April 2015 on http://pubs.rsc.org | doi:10.1039/9781782621959-00001
Downloaded on 09/07/2016 13:50:17.

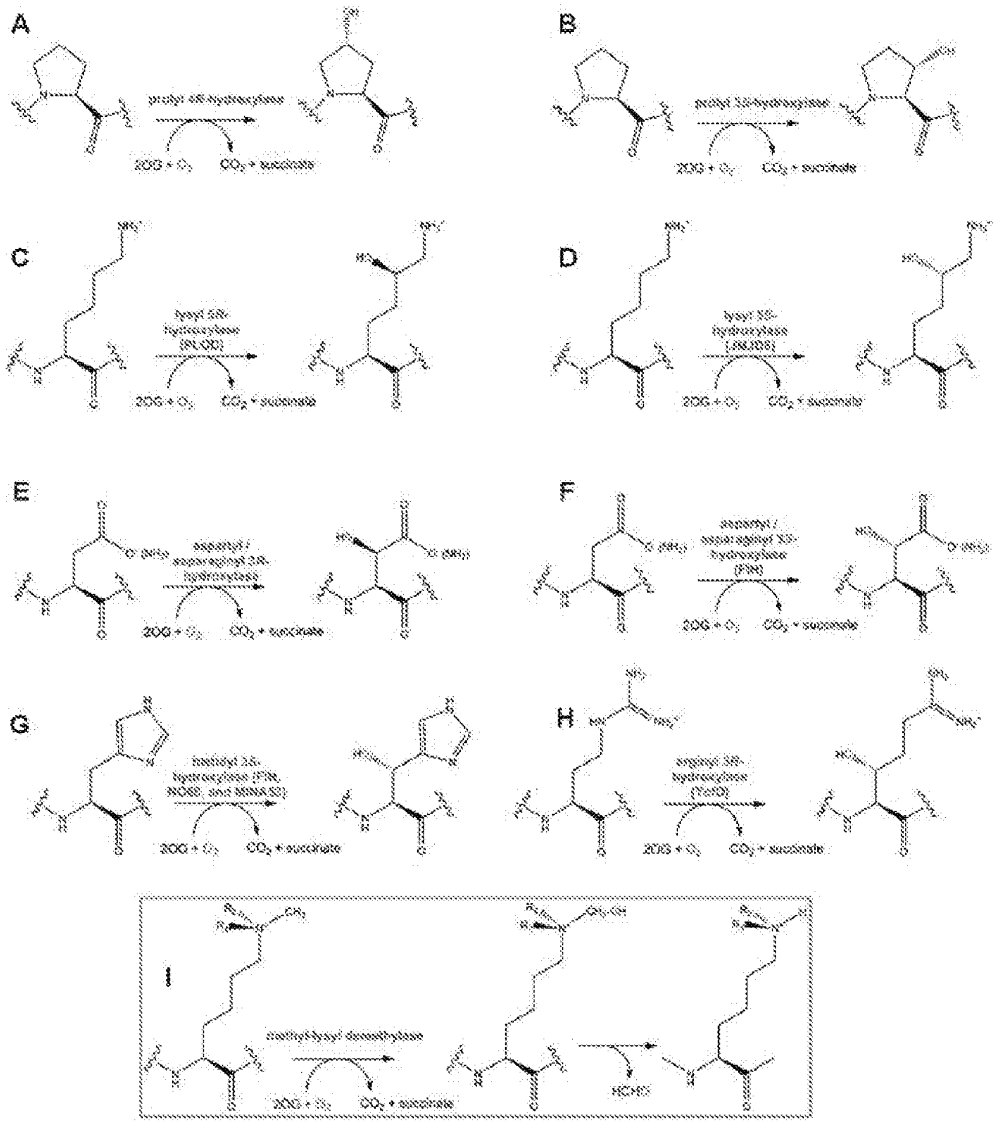


Figure 1.2 2OG-dependent dioxygenase reactions involving protein substrates. (A and B) Prolyl hydroxylases acting at the 4*R* and 3*S* positions. (C and D) Lysyl hydroxylases specific to the 5*R* and 5*S* positions. (E and F) Aspartyl or asparaginyl hydroxylases that insert oxygen at the 3*R* and 3*S* positions. (G) Histidyl 3*S*-hydroxylase. (H) Arginyl 3*R*-hydroxylase. (I) Methyl lysyl demethylases, where R_1 and R_2 are H or CH_3. A lysyl 4-hydroxylase is also known, but this reaction is not depicted because the enantiospecificity has not been reported.

protein towards the von Hipple–Lindau (VHL) tumour suppressor protein, elongin B and elongin C,[25,26] leading to polyubiquitinylation and proteosomal destruction of the transcription factor. The structure has been described for PHD2[27] and for PHD2 in complex with HIF-1α,[28] providing great insight into the geometric aspects of catalysis.

COR-AAD1-00002879
Bayer EX1008 (Part 6 of 9)

View Online

Published on 23 April 2015 on http://pubs.rsc.org | doi:10.1039/9781782621959-00001
Downloaded on 09/07/2016 13:50:17.

Independent of the PHD-specific process, a separate hydroxylation event involving Asn-803 of HIF-1α occurs in the presence of oxygen.[29] This modification is carried out by another 2OG oxygenase: factor-inhibiting HIF (FIH), an asparaginyl 3*S*-hydroxylase (Figure 1.2F).[30] The addition of a single atom of oxygen to HIF-1α results in loss of interaction with the p300/CBP transcription coactivators and abrogation of hypoxic signalling.[31,32] Several structures have been reported for FIH, including its interaction with a peptide derived from the coactivator.[33–35]

The O_2-sensing functions of the PHD and FIH 2OG-dependent dioxygenases have been summarized in several reviews,[36–38] and their structures and biological activities are described further in Chapters 2 and 6.

1.2.3 Ribosomal Protein Hydroxylases

Hydroxylation of ribosomal proteins has been demonstrated for 2OG-dependent enzymes, as first identified for cells from humans and *Escherichia coli*.[39] The human proteins NO66 and MINA53 catalyse 3*S*-hydroxylation of histidyl residues (Figure 1.2G) in Rpl8 and Prl27a, respectively, while the homologous enzyme YcfD of *E. coli* catalyses arginyl 3*R*-hydroxylation of Rpl16 (Figure 1.2H). The precise biological functions of these modifications are unclear, but when the *ycfD* strain was provided with low nutrient concentrations its growth rate was reduced compared to a wild-type strain. The crystal structure was first determined for the *E. coli* version of YcfD,[40] but additional structures quickly became available for truncated versions of NO66 and MINA53 along with the YcfD homologue of the thermophile *Rhodothermus marinus* and the same YcfD with bound substrate.[41] The structure of the yeast enzyme, known as Tpa1, had also been reported prior to identifying its role in ribosome hydroxylation.[42] A 2OG and Fe(II)-dependent oxygenase domain protein (OGFOD1) is widely found in eukaryotes, where it hydroxylates a particular prolyl residue in small ribosomal protein S23 (RPS23).[43] In mammals, loss of the enzyme leads to the formation of stress granules, stoppage of translation and growth inhibition. Whereas the human enzyme catalyses prolyl 3*S*-hydroxylation (Figure 1.2B), the corresponding enzymes from *Schizosaccharomyces pombe*, *Saccharomyces cerevisiae* (Tpa1, see above), and *Ostreococcus tauri* catalyse dihydroxylation of the cognate residues.[44] Furthermore, a *Drosophila* version of 2OGFOD1, known as Sudestada1, was studied; RNAi-mediated reduction in levels in tissue culture cells leads to smaller cell size, fewer cells and decreased translation efficiency.[45]

1.2.4 Other Protein Substrates

Some 2OG-dependent dioxygenases utilize protein substrates beyond those described above, often without a clear role being identified for the modification. Two Jumonji domain (JMJD)-containing proteins and several other examples are illustrated here.

COR-AAD1-00002880
Bayer EX1008 (Part 6 of 9)

View Online

Published on 23 April 2015 on http://pubs.rsc.org | doi:10.1039/9781782621959-00001
Downloaded on 09/07/2016 13:50:17.

The nuclear protein JMJD6 hydroxylates the C5 position of a lysyl residue in a protein associated with RNA splicing.[46] Of special interest, the stereospecificity of the enzyme is opposite to that of PLOD, yielding lysyl 5*S*-hydroxylysine (Figure 1.2D).[47] Alternatively, JMJD6 was proposed to catalyse demethylation of methylated argininyl residues,[48] and recent work extends this theme to support such a role in regulation of transcriptional pause release.[49] The crystal structure of the catalytic domain of JMJD6 is known.[50,51] Another Jumonji domain protein, JMJD4, was shown to catalyse C4 hydroxylation of a lysyl residue (not depicted in Figure 1.2 because the enantiospecificity is not reported) in the NIKS motif of eukaryotic release factor 1.[52] Hydroxylation at this site is needed for efficient translation termination.

The hydroxylation of side chains of aspartic acid and asparagine residues (Figure 1.2E) in epidermal growth factor-like domains of various vitamin K-dependent proteins, coagulation factors and complement proteins is also carried out by 2OG-dependent dioxygenases.[53,54] The resulting 3*R*-hydroxyaspartyl (Hya) and 3*R*-hydroxyasparaginyl (Hyn) groups are thought to be important because mice lacking aspartyl (asparaginyl) β-hydroxylase activity exhibit developmental defects and greater susceptibility to intestinal neoplasia.[55] In addition, overexpression of the gene encoding the enzyme is linked to cellular transformation, at least in the case of biliary epithelial cells.[56] Of related interest, a bacterial enzyme, CinX from *Streptomyces cinnamoneus*, catalyses the same type of reaction to modify an aspartyl group in a 15-residue peptide during the synthesis of cinnamycin, an antimicrobial peptide known as a lantibiotic.[57]

Aside from its O_2-sensing function related to hydroxylation of HIF-α Asn-803, FIH hydroxylates ankyrin repeat domains (ARDs) of endogenous Notch receptors.[58] The ARD modifications appear to stabilize the domains and probably affect protein–protein interactions.[59] In these roles, FIH catalyses aspartyl 3*S*-hydroxylase (Figure 1.2F)[60] and histidyl 3*S*-hydroxylase (Figure 1.2G)[61] activities using Asp and His residues in ARD domains. FIH also hydroxylates members of the apoptosis-stimulating p53-binding protein (ASPP) family, such as modification of ASPP2 at Asn-986.[62] An alternative function of type I collagen prolyl 4-hydroxylase involves oxygen addition to Pro-700 of Argonaute 2, an essential component of the RNA-induced silencing complex for RNA interference.[63] This modification is also thought to promote stabilization of the protein.

In addition to catalysing the hydroxylation of target proteins as described above, many 2OG-dependent oxygenases catalyse self-hydroxylation reactions. This process is exemplified by TfdA and TauD, described in Sections 1.6.3 and 1.6.4, which generate hydroxytryptophan and dihydroxyphenylalanine from Trp and Tyr, respectively.[64–68] It is unclear whether such modifications have any beneficial/regulatory role, but the abundance of aromatic residues near the active sites of many 2OG-dependent enzymes led to the proposal of a sacrificial function for these side chains, thus sparing the enzymes from more deleterious chemistry.[69] Other examples of

COR-AAD1-00002881
Bayer EX1008 (Part 6 of 9)

View Online

auto-catalysed oxidative modifications are found in procollagen 4*R*-hydroxylase that adds oxygen atoms to unknown sites of four of its own peptides;[70] JMJD6 that catalyses lysyl 5*S*-hydroxylation of one of its own Lys residues in the absence of its RNA splicing factor, perhaps as a regulatory mechanism;[71] FIH that catalyses the formation of hydroxytryptophan when HIF-1α is absent;[72] AlkB and ALKBH3 (both described in Section 1.3) that hydroxylate Trp and Leu residues, respectively, at their active sites.[73,74] Two reviews of autocatalysed oxidative modifications in this enzyme family have been published.[75,76]

Published on 23 April 2015 on http://pubs.rsc.org | doi:10.1039/9781782621959-00001
Downloaded on 09/07/2016 13:50:17.

1.2.5 Histone Demethylases

Another group of 2OG-dependent dioxygenases using protein substrates are those acting on N^{ε}-methylated lysine residues of histones. Eukaryotic DNA wraps around the histone core (composed of two each of histone H2A, H2B, H3 and H4) leaving the histone amino terminal regions accessible; these regions undergo several types of post-translational modification including the addition of methyl groups on specific lysyl or arginyl residues. The positions and extents of these modification have long been known to play a critical role in gene regulation.[77] In 2006, several research groups demonstrated that 2OG-dependent enzymes containing JmjC (jumonji domain C) domains catalyse demethylation reactions by hydroxylating the target methyl groups, with the hemiaminal intermediates subsequently decomposing with release of formaldehyde (Figure 1.2I).[78–82] The enzymes act on particular residues of specific histones with explicit levels of methylation. Unlike the flavin-dependent N^{ε}-methyl lysyl demethylase, the 2OG oxygenases can act on all three N^{ε}-methylation states of the modified residue. The first crystal structure for one of these enzymes was published that same year,[83] and follow-up studies have clarified the basis of the exquisite substrate specificities.[84–88] A molecular threading mechanism for the peptide substrate was proposed in the case of methylated H3K36 histone-specific KDM2A protein,[89] and the degree of methylation was suggested to influence whether the ferryl group was aligned according to the previously described 'in line' or 'off line' modes.[1] Additional discussion of this important family of enzymes is provided in Chapter 7 and selected reviews.[90–92]

1.2.6 Other Protein Demethylases

Several proteins other than histones are methylated in cells, so corresponding demethylases are likely to be identified. As one example, ALKBH4 was shown to mediate the removal of the methyl group from Lys84 in cytoplasmic actin, a reaction that regulates actin dynamics.[93] Of additional interest, ALKBH4 was also found to associate with several proteins associated with chromatin or involved in transcription, although the functions of these interactions remain unknown.[94]

COR-AAD1-00002882
Bayer EX1008 (Part 6 of 9)

View Online

1.3 2OG-Dependent Dioxygenases that Act on DNA or RNA

1.3.1 Demethylation of Alkylated DNA or RNA Substrates

Published on 23 April 2015 on http://pubs.rsc.org | doi:10.1039/9781782621959-00001
Downloaded on 09/07/2016 13:50:17.

In 2002, the *E. coli* enzyme AlkB was shown to directly repair alkylation damage to DNA by 2OG-dependent oxidation of 1-methyladenine (1meA) and 3-methylcytosine (3meC) lesions, resulting in the spontaneous loss of formaldehyde and restoration of the native base (Figure 1.3A and B).[95,96] Soon thereafter, AlkB-specific chemistry was expanded to include oxidative repair of alkylated RNA[97] and the range of lesions corrected was extended to 1-methylguanine (1meG, Figure 1.3C),[98] 3-methylthymine (3meT, Figure 1.3D),[98,99] N^6-methyladenine (N^6meA, Figure 1.3E),[100] N^2-methylguanine and N^4-methylcytosine (not shown),[101] as well as bases with slightly larger alkyl groups and exocyclic adducts (not shown). Several structures of AlkB have provided keen insights into the mechanism of substrate binding and substrate specificity.[102–105] Furthermore, the hemiaminal intermediate has been trapped in the protein by binding 3meT and exposing to oxygen.[106]

AlkB-like proteins are widely distributed in other bacteria,[107] viruses[108] and many types of eukaryotes. Of special interest, mammals have nine homologues of AlkB that are referred to as ALKBH (or ABH) followed by numbers 1–8 along with FTO (sometimes referred to as ALKBH9).[109–111] No direct evidence of polynucleotide demethylation has been identified for several of these proteins, including ALKBH4 mentioned earlier in Section 1.2.6. In contrast, ALKBH2 and ALKBH3 were shown to repair 1meA and 3meC in DNA,[112] with ALKBH3 also active with alkylated RNA.[97] Consistent with this differential specificity, knockout mouse studies demonstrated that ALKBH2 is the primary demethylase for repairing alkylated DNA.[113] The structures of ALKBH2 and ALKBH3 reveal the basis of their distinct specificities.[74,103,114–116] ALKBH1 has a more restricted specificity, acting only on 3meC in DNA and RNA,[117] but it also was proposed to be a methylated-histone demethylase[118] and is associated with lyase activity at abasic sites.[119,120] ALKBH5 exhibits N^6meA demethylase activity (Figure 1.3E) for alkylated mRNA.[121] This modification on RNA can affect its processing and has regulatory implications, such as controlling the length of the circadian clock.[122] Human and zebrafish ALKBH5 structures reveal the basis for nucleic acid recognition and catalysis.[123–125] The reaction catalysed by ALKBH8 is described in the next section. Meanwhile, the chemistries catalysed by ALKBH6 and ALKBH7 remain unknown, but the structure of ALKBH7 has been determined and shown to lack a nucleotide recognition lid consistent with a potential protein hydroxylation role.[126]

FTO is named for the fat mass and obesity-associated gene, whose inactivation protects mice from obesity.[127] Early studies reported the enzyme acts on 3meT in DNA,[128] or 3meT and 3-methyluracil (3meU, Figure 1.3F) in DNA and RNA;[129] however, more recent studies have shown that N^6meA in RNA is a major substrate.[130] The RNA-associated N^6-hydroxymethyladenine resulting

COR-AAD1-00002883
Bayer EX1008 (Part 6 of 9)

View Online

Published on 23 April 2015 on http://pubs.rsc.org | doi:10.1039/9781782621959-00001
Downloaded on 09/07/2016 13:50:17.

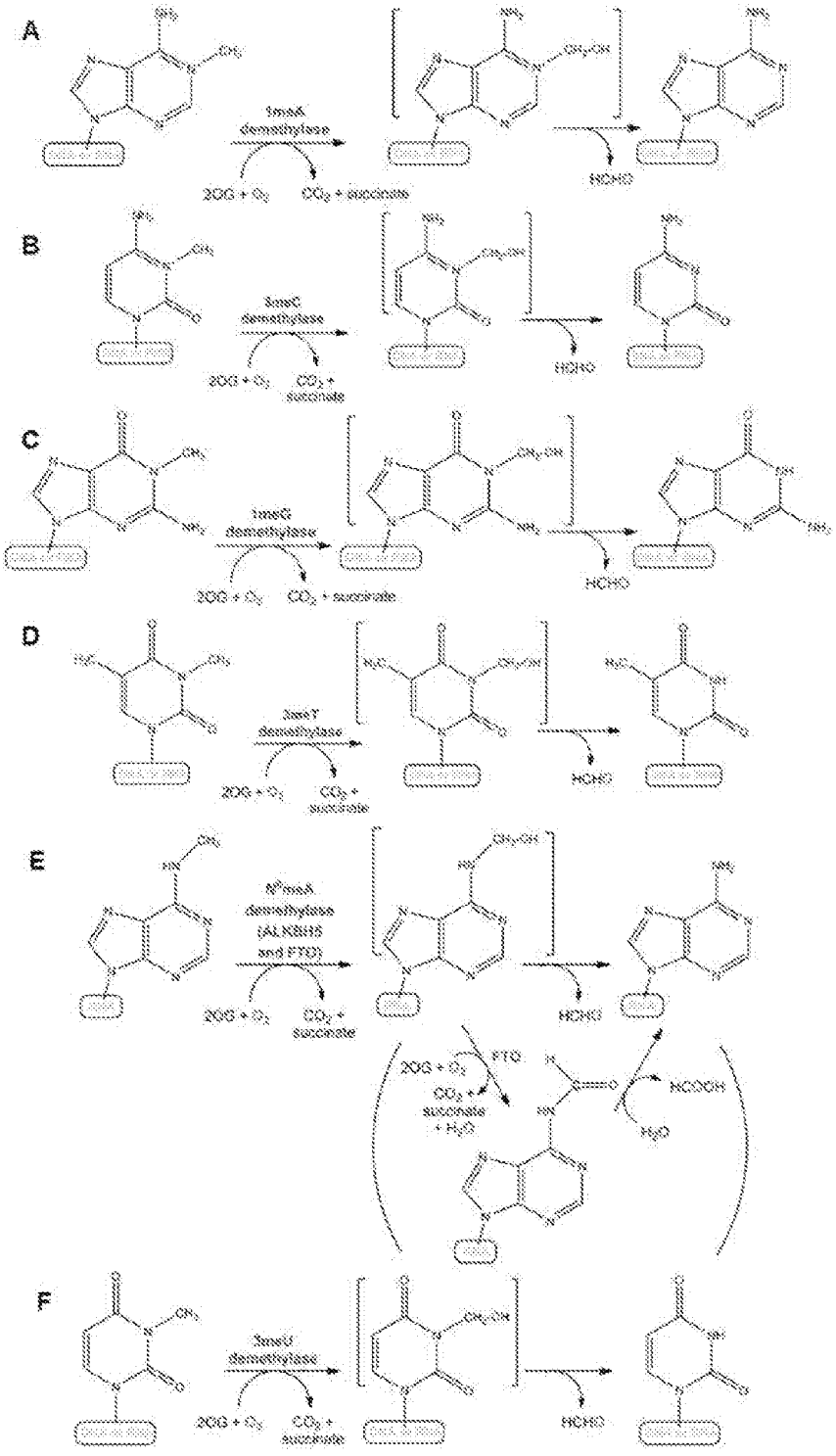


Figure 1.3 2OG-dependent dioxygenase reactions involving demethylations of alkylated DNA and RNA substrates. The reactions reverse lesions related to (A) 1meA, (B) 3meC, (C) 1meG, (D) 3meT, (E) N^6meA and (F) 3meU.

COR-AAD1-00002884
Bayer EX1008 (Part 6 of 9)

View Online

from the latter activity is sufficiently stable that it can be further hydroxylated by FTO to form N^6-formyladenine (the reaction shown in parentheses in Figure 1.3E).[131] The structure of FTO has been determined in the presence of 3meT mononucleotide and with several inhibitors.[132,133]

Further details on polynucleotide repair by AlkB and ALKBH species are found in Chapter 8, while ALKBH5 and FTO are described more fully in Chapter 9.

Published on 23 April 2015 on http://pubs.rsc.org | doi:10.1039/9781782621959-00001
Downloaded on 09/07/2016 13:50:17.

1.3.2 Other Oxidative Modifications of DNA or RNA

In addition to the oxidative demethylations of alkylated bases in DNA and RNA discussed above, 2OG-dependent dioxygenases catalyse several additional types of reaction using these substrates (Figure 1.4).

Two types of tRNA modifications have been shown to require 2OG-dependent hydroxylases. Working with an accessory protein, ALKBH8 first utilizes its RNA recognition and methyltransferase motifs to convert 5-carboxymethyluridine (cm^5U) to 5-methoxycarbonylmethyluridine (mcm^5U) at position 34 in the anticodon loop of human tRNA.[134] This modified tRNA then serves as the substrate for the hydroxylase domain of ALKBH8 which forms 5*S*-methoxycarbonylhydroxymethyluridine ($mchm^5U$) (Figure 1.4A).[135,136] The structure of the RNA recognition and hydroxylase domains of ALKBH8 has been reported.[137] Curiously, protozoan ALKBH8 catalyses both tRNA modification and DNA repair reactions.[138] Additional discussion of the biosynthesis of this unique base modification can be found in Chapter 10. A second tRNA-related hydroxylase acts on 7-(α-amino-α-carboxypropyl)wyosine known as wybutosine and abbreviated yW (Figure 1.4B), a tricyclic base that abuts the anticodon loop of $tRNA^{Phe}$ in eukaryotes and archaea.[139] Among the numerous derivatives formed from this base are hydroxylated species generated by TYW5 (tRNA-yW-synthesizing enzyme 5), a member of the JmjC domain family (see Section 1.2.4), whose structure has been reported.[140]

A family of ten-eleven translocation (TET) proteins contributes to the epigenetic regulation of a wide range of genes in many eukaryotes by controlling the methylation status of cytosine in CpG islands of DNA. For example, TET1 was shown to convert 5-methylcytosine (5meC) to 5-hydroxymethylcytosine (5hmC) in 2009 (Figure 1.4C).[141] Soon thereafter this result was confirmed and extended to TET2 and TET3.[142] More recently, TET enzymes were shown to catalyse subsequent reactions to create 5-formylcytosine (5fC)[143] and 5-carboxylcytosine (5caC),[144,145] including in a fungus.[146] In addition, the TET-catalysed oxidation of thymine to 5-hydroxymethyluracil in DNA of embryonic stem cells has been reported.[147] The various oxidized derivatives may have regulatory functions,[148] such as the hypoxic gene induction noted in neuroblastoma.[149] Moreover, the series of reactions from 5mC is suggested to play a role in active demethylation in DNA, either *via* (i) excision of 5fC or 5caC by thymine-DNA glycosylase, (ii) deamination of 5hmC followed by glycosylase removal, (iii) retro-aldol chemistry of 5hmC or 5fC with release of formaldehyde or formate, or (iv) decarboxylation of 5caC.[150] The structures of human TET2 in complex

COR-AAD1-00002885
Bayer EX1008 (Part 6 of 9)

View Online

Published on 23 April 2015 on http://pubs.rsc.org | doi:10.1039/9781782621959-00001
Downloaded on 09/07/2016 13:50:17.

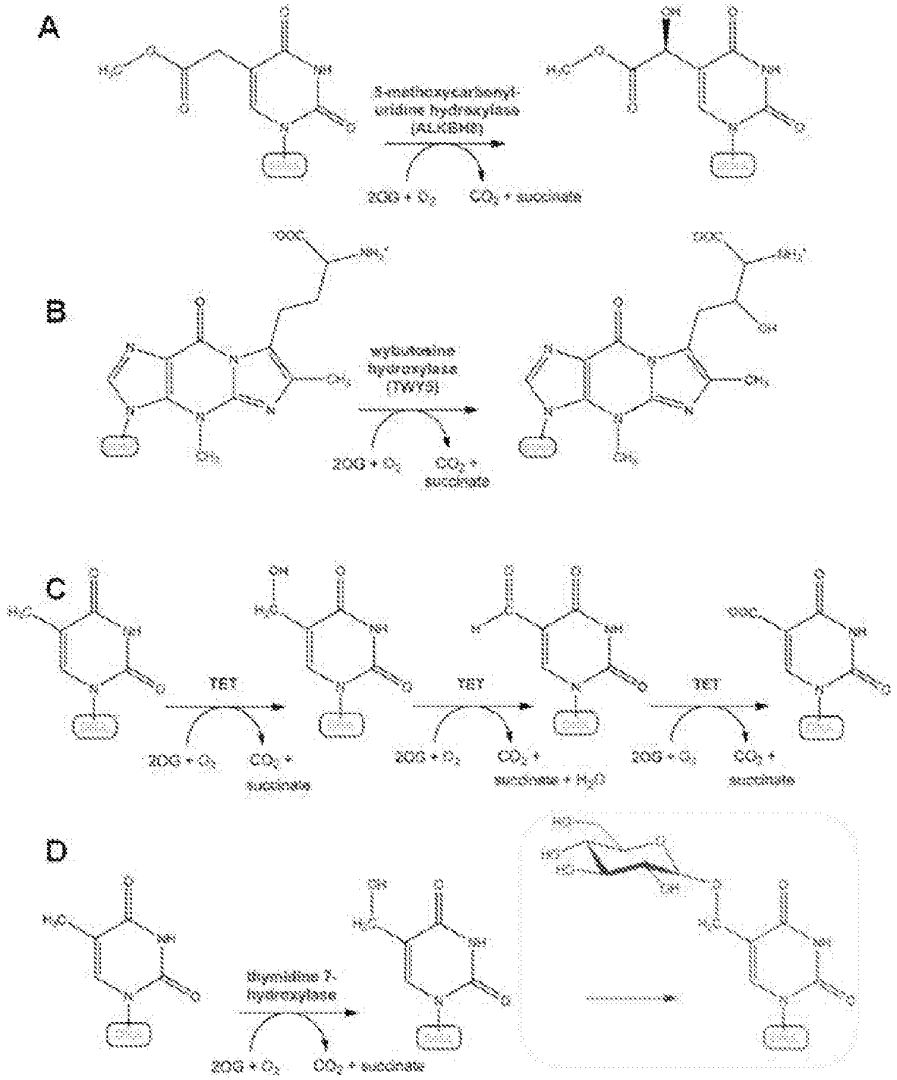


Figure 1.4 Non-demethylase 2OG-dependent dioxygenase reactions utilizing RNA or DNA substrates. (A) Action of ALKBH8 in the synthesis of a modified tRNA. (B) Wybutosine hydroxylase catalysis by TWY5. (C) The sequential reactions of TET proteins acting on 5meC to form 5hmC, 5fC and 5caC. (D) Thymidine 7-hydroxylase activity catalyses the first step in formation of base J (a subsequent glucosyl transfer reaction is highlighted in yellow).

with DNA and a TET family protein from *Naegleria gruberi* in complex with 5meC-containing DNA are reported.[151,152] Additional information on the biology of the TET proteins is provided in Chapter 11 and in reviews.[153,154]

Nuclear genomes of kinetoplastid flagellates and some unicellular flagellates contain β-D-glucopyranosyloxymethyluracil in their telomeric repeats.[155] This modified base, first identified in 1993, is also called β-D-glucosyl-hydroxymethyluracil or base J.[156] Synthesis of base J involves

COR-AAD1-00002886
Bayer EX1008 (Part 6 of 9)

View Online

Published on 23 April 2015 on http://pubs.rsc.org | doi:10.1039/9781782621959-00001
Downloaded on 09/07/2016 13:50:17.

two steps, hydroxylation of thymidine to form hydroxymethyluracil followed by glucosylation (Figure 1.4D).[157,158] JBP1, a protein that binds to and enhances the levels of base J,[159,160] was shown to belong to the 2OG-dependent dioxygenase family and is related to the TET proteins.[161,162] JBP1 along with the related JBP2, which does not bind to base J in DNA,[163] were directly demonstrated to catalyse thymidine hydroxylation.[164] Further information about the role of 2OG-dependent dioxygenases in base J biosynthesis is provided in Chapter 12.

1.4 Lipid-Related Metabolism Involving 2OG-Dependent Oxygenases

Several 2OG-dependent hydroxylase reactions are used in lipid biosynthesis (Figure 1.5).

Carnitine or γ-trimethyl-hydroxybutyrobetaine is a small molecule that becomes linked to fatty acids, allowing for their transport across the inner mitochondrial membrane and degradation in the matrix by the β-oxidation pathway.[165] The synthesis of carnitine initiates with protein-derived ε-*N*-trimethyllysine that undergoes β-hydroxylation, aldolase cleavage to glycine plus trimethylaminobutyraldehyde, dehydrogenation to γ-butyrobetaine, and another hydroxylation (Figure 1.5A). The ε-*N*-trimethyllysine hydroxylase activity was shown to require 2OG in 1978,[166] and the enzyme was purified and characterized in 2001.[167] The hydroxylation of γ-butyrobetaine was found to require 2OG in 1968,[168] and the enzyme was purified from *Pseudomonas* spp. AK1 in 1977 and from calf liver in 1981.[169,170] A detailed comparison of substrate specificities for the human and bacterial enzymes revealed surprisingly large differences in reactivity for several γ-butyrobetaine analogues.[171] The structure of human γ-butyrobetaine hydroxylase has been reported.[172,173] Further discussion of the enzymes involved in carnitine metabolism is provided in Chapter 13.

Phytanic acid (2,6,10,14-tetramethylhexadecanoic acid), a polyisoprenoid derived from the phytol moiety of chlorophyll, cannot be directly degraded *via* the β-oxidation pathway due to its 3-methyl group. To overcome this hurdle, the C-1 carbon is removed by action of a series of four enzymes: a ligase converts the molecule to phytanoyl-coenzyme A (CoA),[174] hydroxylation occurs at the C-2 position,[175] a lyase releases formyl-CoA and methylpentadecanal (pristanal),[176,177] and a dehydrogenase forms pristanic acid (2,6,10,14-tetramethylpentadecanoic acid)[178] which is a substrate for β-oxidation. Interruption of this pathway results in Refsum disease, which is associated with dysfunctions including retinitis pigmentosa, polyneuropathy and ataxia.[179] Phytanoyl-CoA hydroxylase (Figure 1.5B), shown to be a 2OG-dependent enzyme,[175] was purified from rat liver and as the recombinant human protein.[180,181] The human enzyme was structurally characterized, providing an understanding of mutations associated with Refsum disease.[182] Further description of phytanic acid metabolism is found in Chapter 14.

COR-AAD1-00002887
Bayer EX1008 (Part 6 of 9)

View Online

Published on 23 April 2015 on http://pubs.rsc.org | doi:10.1039/9781782621959-00001
Downloaded on 09/07/2016 13:50:17.

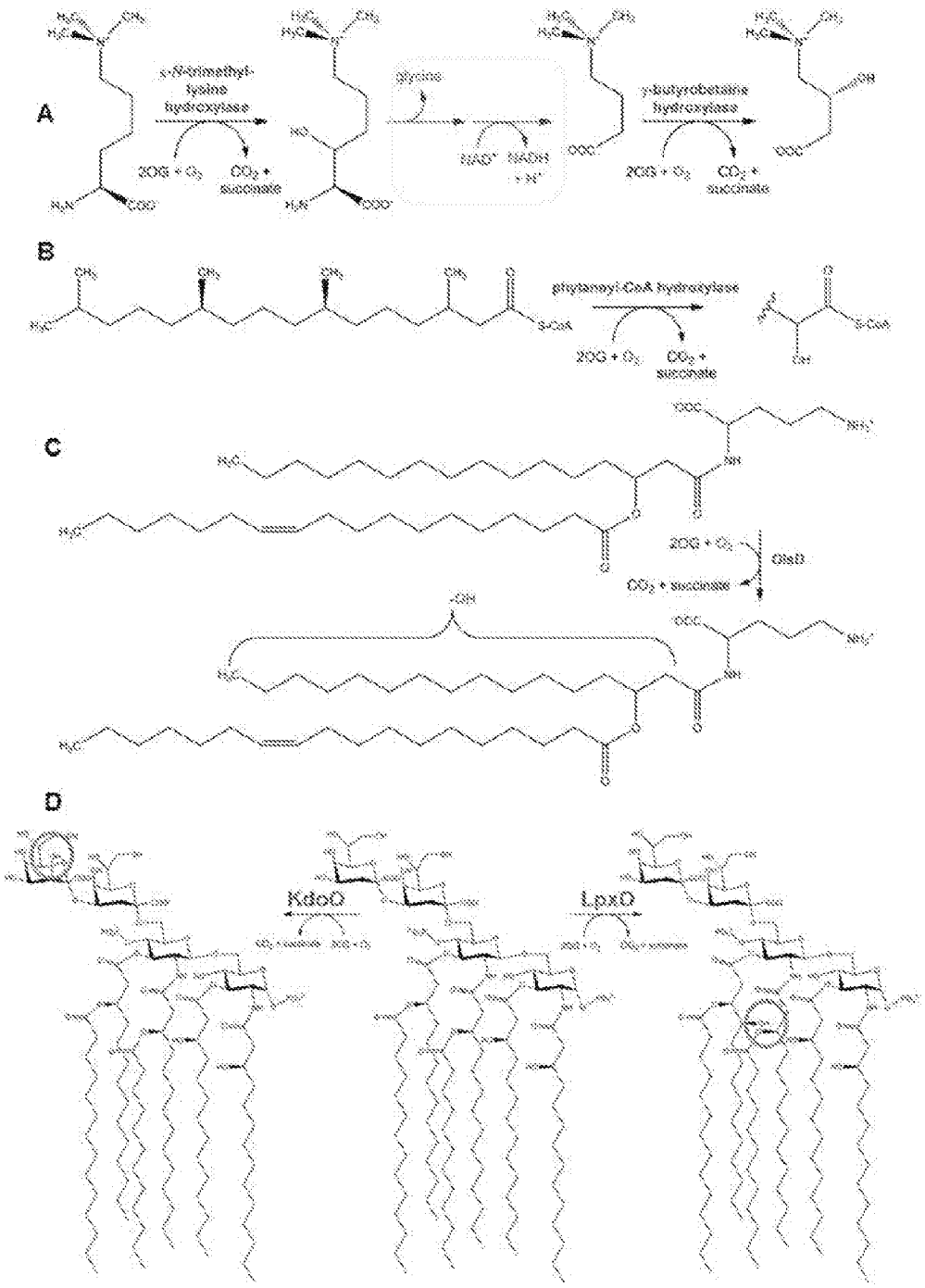


Figure 1.5 2OG-dependent dioxygenases involved in lipid metabolism. (A) Biosynthesis of the acyl group carrier molecule carnitine includes two 2OG-dependent hydroxylases that act on ε-*N*-trimethyllysine and γ-butyrobetaine (with intervening aldolase and dehydrogenase reactions highlighted in yellow). (B) Phytanic acid metabolism includes the activity of phytanoyl-CoA hydroxylase. (C) Hydroxylation of the acyl chain of ornithine lipids is catalysed by OlsD. (D) KdoO and LpxO hydroxylase reactions involving lipid A.

COR-AAD1-00002888
Bayer EX1008 (Part 6 of 9)

View Online

Published on 23 April 2015 on http://pubs.rsc.org | doi:10.1039/9781782621959-00001
Downloaded on 09/07/2016 13:50:17.

Much like phytanoyl-CoA hydroxylase, OlsD from *Burkholderia cenocepacia* (and probably from other *Burkholderia* and *Serratia* species) catalyses the hydroxylation of an acyl chain (Figure 1.5C) as part of a lipid metabolism pathway.[183] In this case, however, the pathway is biosynthetic rather than degradative. The first step of the pathway involves OlsB, an *N*-acyl transferase that transfers a 3-hydroxy fatty acyl group from the acyl carrier protein to the α-amino group of ornithine. The resulting lyso-ornithine lipid is the substrate of OlsA, an *O*-acyltransferase that transfers a fatty acyl group from the acyl carrier protein to the C-3 hydroxyl group. This ornithine-containing lipid, or its C-2 hydroxylated derivative (not shown), is the substrate of OlsD that hydroxylates somewhere on the amide-linked fatty acyl chain.

Two 2OG-dependent enzymes have been shown to modify lipid A (Figure 1.5D), with one targeting a specific acyl side chain and the other acting on the 3-deoxy-D-*manno*-oct-2-ulosonic (Kdo) moiety. *Salmonella typhimurium*, previously known to synthesize lipid A containing secondary *S*-2-hydroxyacyl chains, was demonstrated to use the O_2- and 2OG-dependent enzyme LpxO to achieve this modification.[184] LpxO was the first integral membrane protein representative of this enzyme family.[185] A Kdo 3-hydroxylase (KdoO) that adds an oxygen atom to the deoxysugar was identified in *Burkholderia ambifaria* and *Yersinia pestis*.[186] Homologues to the genes encoding these proteins are found in other Gram-negative bacteria.

1.5 Plant Metabolite Biosynthesis Using 2OG-Dependent Oxygenases

Plants possess many of the 2OG-dependent oxygenases already mentioned, but in addition they utilize members of this enzyme family for some of their unique biosynthetic needs.[187] Here we illustrate how plants (and, in a few cases, other organisms) use these enzymes for generating flavonoids, gibberellins, alkaloids and other predominantly plant-specific products.

1.5.1 2OG-Dependent Oxygenases in Flavonoid Biosynthesis

The flavonoids are polyphenolic compounds that include flavanones, flavones, isoflavones, flavonols and anthocyanins with more than 9000 such compounds known (see examples in Figure 1.6). These substances are used by plants for defence against pathogens, as signalling molecules in plant–microbe interactions, to minimize photodamage, in flower colour, and other roles.[188] When consumed by humans they function as antioxidants, antimalarials and potential anticancer agents.[189] The entrance to the main pathway shown in Figure 1.6 (indicated by the green arrow) is the flavanone naringenin, the substrate for two distinct 2OG-dependent oxygenases. Flavone synthase I (FNS) catalyses a desaturation reaction at the C-2/C-3 position forming *trans*-dihydroflavonol,[190] while flavanone 3β-hydroxylase (FHT) adds a hydroxyl group to C-3.[191] The cytochrome P450 enzyme flavanone

COR-AAD1-00002889
Bayer EX1008 (Part 6 of 9)

Published on 23 April 2015 on http://pubs.rsc.org | doi:1
Downloaded on 09/07/2016 13:50:17

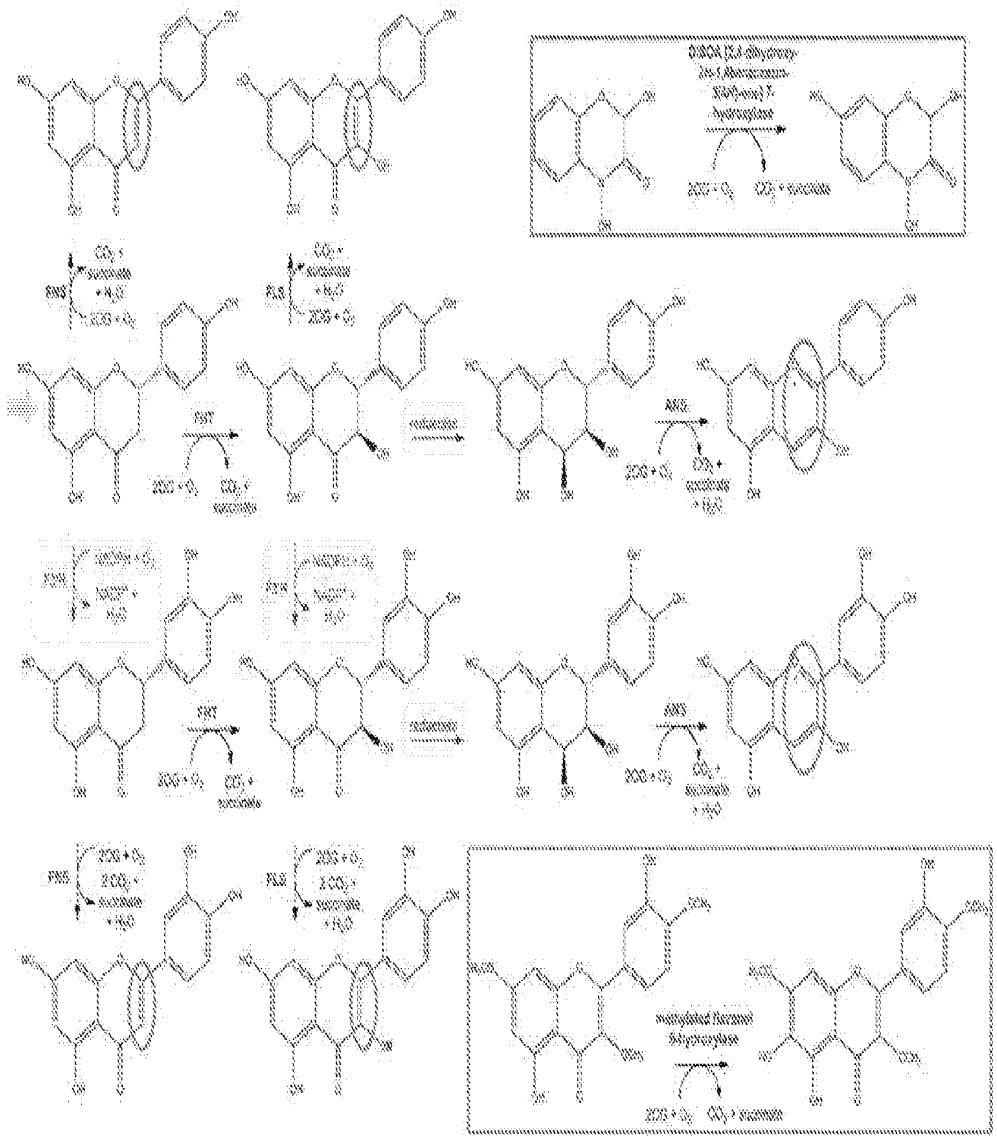


Figure 1.6 Representative 2OG-dependent oxygenases of flavonoid metabolism. Flavanone (indicated by the green arrow) can undergo desaturation by flavone synthase I (FNS), C-3 hydroxylation by flavanone 3β-hydroxylase (FHT), or C-3′ hydroxylation by flavanone 3′-hydroxylase (F3′H, not a 2OG-dependent enzyme as indicated by yellow highlighting), with the product of the latter reaction also serving as substrate for both FNS and FHT. The FHT-derived products can undergo desaturation by flavonol synthase (FLS) or can be reduced by a non-2OG enzyme (also highlighted in yellow). The reduced products are converted to anthocyanins by anthocyanidin synthase (ANS). The boxes to the upper and lower right depict the reactions of related enzymes that hydroxylate at the 7 and 6 positions of flavonoid compounds.

COR-AAD1-00002890
Bayer EX1008 (Part 6 of 9)

View Online

Published on 23 April 2015 on http://pubs.rsc.org | doi:10.1039/9781782621959-00001
Downloaded on 09/07/2016 13:50:17.

3′-hydroxylase (F3′H) uses naringenin (or its 3β-hydroxy derivative) and converts the appended phenol to a catechol, with this species also being a substrate for FNS and FHT. The FHT-derived *trans*-dihydroflavonol products are substrates for another 2OG-dependent desaturase called flavonol synthase (FLS).[192,193] Alternatively, the *trans*-dihydroflavonols can be reduced *via* non-2OG-dependent enzymes to provide leucoanthocyanidin substrates for anthocyanidin synthase (ANS).[194] The structure of ANS from *Arabidopsis thaliana* has been elucidated with the bound substrate analogue dihydroquercetin and the unnatural substrate naringenin.[192,195] Two other flavonoid-related reactions catalysed by 2OG-dependent hydroxylases are 2,4-dihydroxy-2*H*-1,4-benzoxazin-3(4*H*)-one (DIBOA) 7-hydroxylase and methylated flavonol 6-hydroxylase (see boxes in Figure 1.6).[196–200] Flavonoid biosynthesis is discussed in much greater detail in Chapter 15.[201]

1.5.2 2OG-Dependent Oxygenases of Gibberellin Biosynthesis

Tetracyclic diterpenoids known as gibberellins (GAs) are widely distributed in higher plants and are also found in some lower plants, bacteria and fungi.[202] At least 136 distinct GA structures are reported (commonly referred to as GA_1-GA_{136}; see http://www.plant-hormones.info/gibberellins.htm). A small sampling of such structures is shown in Figure 1.7, which depicts selected 2OG-dependent transformations of these molecules. Many GAs possess a carboxylate at C-7, introduced by oxidation of the GA_{12}-aldehyde to form GA_{12}, with this product undergoing partial oxidization at C-7 by a hydroxylase to form GA_{53}. Depending on their biological sources these reactions can be catalysed by either cytochrome P450 or 2OG-dependent oxygenases (Figure 1.7A).[203] The GA C20 oxidase can catalyse sequential reactions that convert the C-20 methyl group (*e.g.* GA_{12}/GA_{53}) to the alcohol (GA_{15}/GA_{44}), aldehyde (GA_{24}/GA_{19}), and in some cases the carboxylate (GA_{25}/GA_{17}) (Figure 1.7B).[204,205] Alternatively, the same enzyme can catalyse an oxidative transformation that eliminates the carboxylate as CO_2 while forming a γ-lactone (GA_9/GA_{20}).[206] GA 3β oxidase converts these products to the corresponding hydroxylated species (GA_4/GA_1).[207] GA 2β oxidase acts on the same substrates (producing GA_{51}/GA_{29}) or on the products of the prior reaction (producing GA_{34}/GA_8).[208] In addition, other 2OG-dependent enzymes can catalyse several types of desaturation reactions (not shown),[202,209] such as a recently characterized fungal GA_4 desaturase that introduces a double bond between C-1 and C-2.[210] Further information on this remarkable family of enzymes is available in Chapter 16.

1.5.3 2OG-Dependent Oxygenases in Alkaloid Synthesis

Four examples are depicted to illustrate how plants use 2OG-dependent oxygenases for alkaloid biosynthesis. Scopolamine is a hallucinogenic tropane alkaloid produced by *Hyoscyamus niger* (henbane). The last two steps in its synthesis are catalysed by hyoscyamine 6β-hydroxylase that carries out both

COR-AAD1-00002891
Bayer EX1008 (Part 6 of 9)

Downloaded on 09/07/2016 13:50:17
Published on 23 April 2015 on http://pubs.rsc.org | doi:1

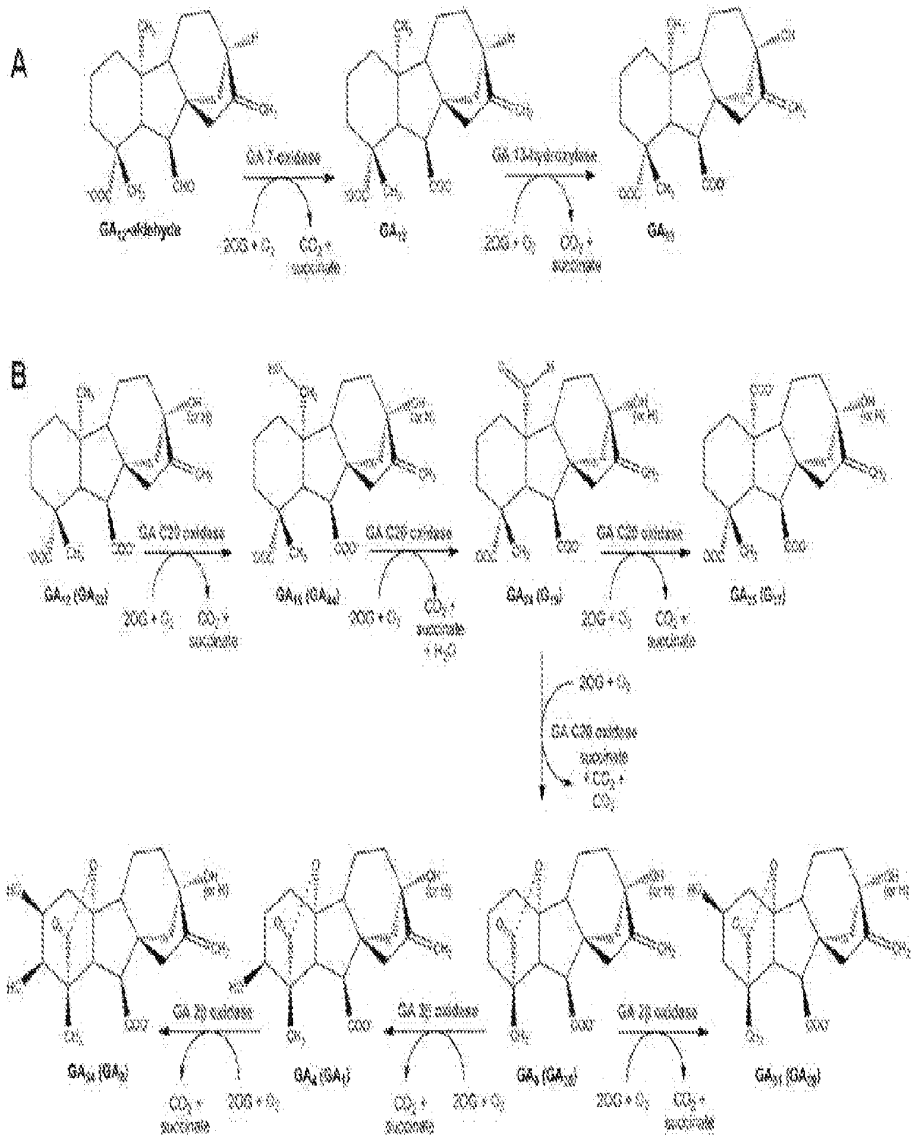


Figure 1.7 Selected 2OG-dependent oxygenases of gibberellin (GA) biosynthesis. (A) Reactions of GA 7-oxidase and GA 13-hydroxylase. (B) Three consecutive reactions of GA C20 oxidase that convert a methyl group to an alcohol, aldehyde and carboxylic acid; a distinct reaction catalysed by GA C20 oxidase to eliminate CO_2 and form a γ-lactone; GA 2β and GA 3β oxidase activities.

COR-AAD1-00002892
Bayer EX1008 (Part 6 of 9)

View Online

Published on 23 April 2015 on http://pubs.rsc.org | doi:10.1039/9781782621959-00001
Downloaded on 09/07/2016 13:50:17.

hydroxylation and epoxidation steps (Figure 1.8A).[211,212] Vinblastine and vincristine are alkaloids produced by *Caranthus roseus* (periwinkle), which have been used for treatment of Hodgkin's lymphoma and acute leukaemia. These compounds are synthesized by a complex biosynthetic pathway that utilizes a 2OG-dependent hydroxylase to generate deacetylvindoline (Figure 1.8B), which is then further modified.[213,214] Codeine and morphine are important pharmaceuticals obtained from *Papaver somniferum* (opium poppy). Their complex biosynthetic pathway includes an intermediate named thebaine, which can be demethylated at one site by thebaine 6-*O*-demethylase to produce codeinone (Figure 1.8C) or demethylated at a second site by codeine *O*-demethylase to form oripavine (Figure 1.8D).[215] These two reactions plus that catalysed by codeinone reductase yields morphine. A series of additional reactions (not shown) involving alkaloid metabolism in opium poppy are catalysed by these enzymes and the 2OG-dependent dioxygenase protopine *O*-dealkylase, PODA.[216] In the fungus *Claviceps purpurea*, a cyclization reaction (not shown) in the synthesis of D-lysergic acid alkaloid peptides is catalysed by a member of this enzyme family, and the 2OG-bound holoprotein, EasH, was structurally characterized.[217] Another fungal example is found in the synthesis of loline alkaloids by *Epichloë* species, where the 2OG-dependent oxygenase LolO introduces an ether bridge into a pyrrolizidine ring system (Figure 1.8E).[378]

1.5.4 Other Plant-Specific 2OG-Dependent Oxygenases

Additional representatives of the 2OG-dependent oxygenases that are primarily restricted to plants include enzymes involved in the biosynthesis of phytosiderophores, coumarins and glucosinolates, or the degradation of hormonal compounds.

Under iron-deficient conditions, some grasses, cereals and rice produce and secrete iron-binding compounds such as the mugineic acid-related species made by *Hordeum vulgare* (barley). This plant contains two 2OG-dependent dioxygenases, IDS2 and IDS3, that act on 2′-deoxymugineic acid to form 3-epihydroxy-2′-deoxymugineic acid and mugineic acid, respectively (Figure 1.8F).[218] 2′-Deoxymugineic acid is converted to 3-epihydroxymugineic by combined actions of the two enzymes.

Coumarins (1,2-benzopyrones) such as scopoletin and umbelliferone are synthesized by many higher plants where they are used for defence against phytopathogens. A key enzyme in the pathway used by *Arabidopsis thaliana* for generating scopoletin is a 2OG-dependent enzyme that hydroxylates the *ortho* position of feruloyl-CoA,[219] with subsequent isomerization, hydrolysis and lactonization steps providing the product (Figure 1.8G). The same activity was detected using two recombinant proteins from *Ipomoea batatas* (sweet potato), one of which also used *p*-coumaroyl-CoA to form umbelliferone (where H is present at the 3′ position in Figure 1.8G).[220] An enzyme with the latter dual activity has also been characterized from *Ruta graveolens* (the common rue).[221]

COR-AAD1-00002893
Bayer EX1008 (Part 6 of 9)

Published on 23 April 2015 on http://pubs.rsc.org | doi:1
Downloaded on 09/07/2016 13:50:17

Figure 1.8 Steps in the synthesis of selected alkaloids and other primarily plant-specific products catalysed by 2OG-dependent oxygenases. (A) Hydroxylase and epoxidase activities of hyoscyamine hydroxylase. (B) Desacetoxyvindoline 4-hydroxylase. (C) Thebaine 6-*O*-demethylase. (D) Codeine *O*-demethylase. (E) LolO-catalysed ether bridge formation in loline alkaloid biosynthesis. (F) Mugineic acid phytosiderophore synthesis. (G) Feruloyl-CoA 6′-hydroxylase and *p*-coumaroyl-CoA 2′-hydroxylase in the pathways for synthesis of scopoletin and umbelliferone (yellow highlight). (H) Action of AOP2 and AOP3 on methylsulfinylalkyl glucosinolates. (I) Indole-3-acetic acid 2-hydroxylase. (J) Salicylic acid 3-hydroxylase.

COR-AAD1-00002894
Bayer EX1008 (Part 6 of 9)

View Online

Published on 23 April 2015 on http://pubs.rsc.org | doi:10.1039/9781782621959-00001
Downloaded on 09/07/2016 13:50:17.

Glucosinolates (over 130 are known) are predominantly associated with the Brassicaceae family of plants where, following tissue disruption, they are decomposed to form compounds with diverse protective roles against herbivores and pathogens.[222] Two sequence-related 2OG-dependent enzymes in *A. thaliana*, named AOP2 and AOP3, have been shown to participate in glucosinolate biosynthesis by converting methylsulfinylalkyl glucosinolate to the alkenyl or hydroxyalkyl species (Figure 1.8H).[223] The chemistry of these reactions has not been well defined.

Indole-3-acetic acid and salicylic acid are plant hormones that play important roles in growth, development, disease resistance or other functions, but until recently their degradation pathways within plants were unclear. Using rice, a dioxygenase for auxin oxidation (DAO) has now been identified and shown to transform this substrate into 2-oxoindole-3-acetic acid (Figure 1.8I).[224] Mutants affecting the corresponding gene display male sterility and produce infertile seeds. Similarly, a salicylic acid 3-hydroxylase (Figure 1.8J) of *Arabidopsis* was identified and mutants in the corresponding *s3h* gene were found to accumulate salicylate species and exhibit early senescence.[225] When assayed *in vitro*, both 2,3- and 2,5-dihydroxybenzoate are formed; however, only the former appears to be made *in vivo*.

1.6 2OG-Dependent Oxygenases Catalysing Reactions with Free Amino Acids, Nucleobases, Herbicides and Sulfur- or Phosphorous-Containing Compounds

The reactions described in this section are diverse, but generally involve rather small-sized molecules. Several products from these reactions are precursors that become incorporated into antibiotics, whereas 2OG-dependent tailoring enzymes that act directly during antibiotic synthesis are described in Section 1.7.

1.6.1 Amino Acid Hydroxylases

2OG-Dependent hydroxylases acting on free amino acids (*i.e.* not as a side chain of a protein) are known. In the case of L-Pro, different enzymes exhibit each of four distinct specificities. Pro 4*R*-hydroxylase (Figure 1.9A, left) from *Streptomyces griseoviridus* P8648 produces the *trans*-isomer of 4-hydroxyproline that is subsequently utilized for etamycin synthesis.[226,227] This enzyme activity is also found in other bacterial strains of *Streptomyces*, *Dactylosporangium* and *Amycolatopsis*,[228] and in the pneumocandin-producing fungus *Glarea lozoyensis*.[229] L-Pro 4*S*-hydroxylase (Figure 1.9A, right), producing the *cis* isomer, has been identified in *Mesorhizobium loti* and *Sinorhizobium meliloti* where it was shown to require 2OG.[230] L-Pro 3*S*-hydroxylase (Figure 1.9B, left) has been reported in the *G. lozoyensis* fungus mentioned

COR-AAD1-00002895
Bayer EX1008 (Part 6 of 9)

View Online

Published on 23 April 2015 on http://pubs.rsc.org | doi:10.1039/9781782621959-00001
Downloaded on 09/07/2016 13:50:17.

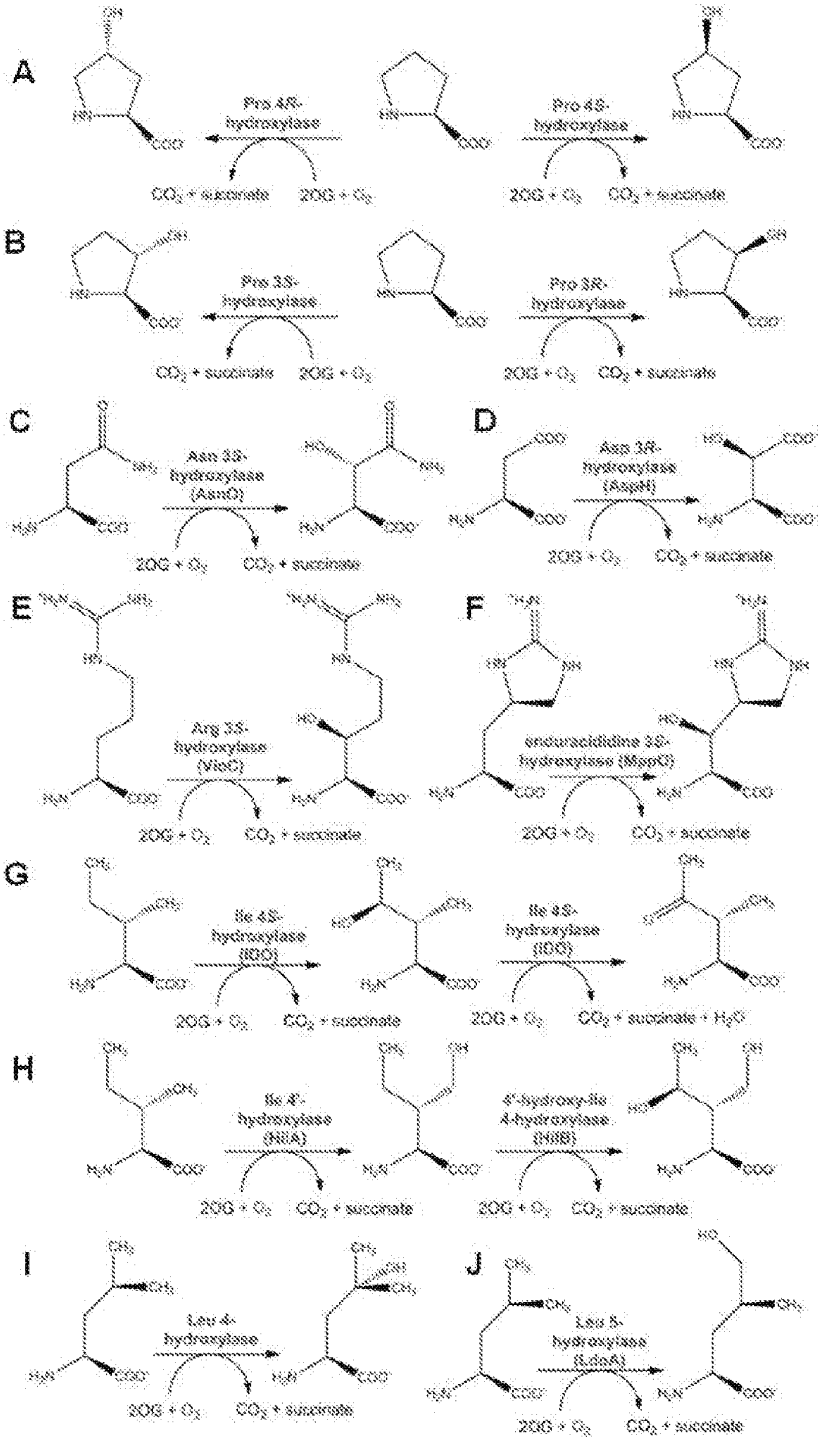


Figure 1.9 2OG-dependent hydroxylases acting on free L-amino acids. (A) Pro 4*R*- and 4*S*-hydroxylases. (B) Pro 3*S*- and 3*R*-hydroxylases. (C) Asn 3*S*-hydroxylase. (D) Asp 3*R*-hydroxylase. (E) Arg 3*S*-hydroxylase. (F) Enduracididine 3-hydroxylase. (G) Ile 4*S*-hydroxylase. (H) Ile 4′- and 4-hydroxylase. (I) Leu 4-hydroxylase. (J) Leu 5-hydroxylase.

COR-AAD1-00002896
Bayer EX1008 (Part 6 of 9)

View Online

Published on 23 April 2015 on http://pubs.rsc.org | doi:10.1039/9781782621959-00001
Downloaded on 09/07/2016 13:50:17.

above.[229] Enzymes from two actinomycetes were shown to exhibit both 3*S*- and 4*S*-hydroxylase activities using L-Pro.[231] The best studied enzyme using this substrate is L-Pro 3*R*-hydroxylase (Figure 1.9B, right), an activity identified in strains of *Streptomyces* and *Bacillus*.[232] The enzyme was purified from *Streptomyces* sp. strain TH1[233] and the structure of the apoprotein was elucidated.[234]

Several 2OG-dependent hydroxylases act on free L-amino acids with polar side chains. A 3*S*-hydroxylase of L-Asn (creating the *threo* isomer, Figure 1.9C) was characterized from recombinant cells containing *asnO* from *Streptomyces coelicolor*.[235] High-resolution crystal structures of AsnO reveal the basis of this substrate specificity. The product of the reaction is subsequently incorporated (at position nine) into a daptomycin-type lipopeptide called the calcium-dependent antibiotic. A single amino acid substitution (D241N) of AsnO led to use of L-Asp as substrate, forming the *threo* isomer of hydroxyaspartic acid (not shown).[236] By contrast, AspH from *Pseudomonas syringae* catalyses 3*R*-hydroxylation of L-Asp (and L-Asp thioesters, not shown) to form the *erythro* isomers (Figure 1.9D).[237] VioC, a 2OG-dependent Arg 3*S*-hydroxylase (Figure 1.9E), was shown to be used by *Streptomyces vinaceus* to provide a precursor for viomycin biosynthesis.[238] The VioC structure was elucidated and explains the hydroxylation specificity.[239] Enduracididine is an Arg-derived amino acid that undergoes 3*S*-hydroxylation by MppO (Figure 1.9F) to provide β-hydroxyenduracididine, which is incorporated into mannopeptimycins, glycopeptide antibiotics produced by *Streptomyces hydrogroscopicus* NRRL 30439.[240]

Hydroxylases of L-Ile and L-Leu have been widely studied since the first report of 2OG-dependent 4-hydroxyisoleucine synthesis in *Trigonella foenum-graecum* (fenugreek).[241] The recombinant enzyme (IDO) from *Bacillus thuringiensis* was shown to exhibit L-Ile 4*S*-hydroxylase activity,[242] and the enzyme was later shown to also form 2-amino-3-methyl-4-ketopentanoate, probably arising from dihydroxylation of the same carbon position to produce a gem diol that loses water (Figure 1.9G).[243] The products of two adjacent genes in *Pantoea ananatis*, HilA and HilB, catalyse sequential hydroxylation reactions at the 4′ and 4 positions, respectively, of L-Ile (Figure 1.9H).[244] Related family members were identified in a range of other bacteria, in several cases using L-Leu as the preferred substrate and yielding 4-hydroxyleucine (Figure 1.9I).[245] Alternatively, L-Leu 5-hydroxylase (LdoA, Figure 1.9J) was characterized from *Nostoc punctiforme*.[246] All of these enzymes also act on other substrates with reduced catalytic efficiencies (including Leu/Ile substitution), in various cases forming Met sulfoxide, 4-hydroxyvaline and 4-hydroxythreonine (not shown).[243–245]

Four other enzymes are mentioned in this section because they modify amino acid-like substrates or combine another reaction with amino acid hydroxylation. SadA from *Burkholderia ambifaria* acts on several *N*-substituted amino acids with hydrophobic side chains, notably catalysing 3*R* hydroxylation of *N*-succinyl-L-Leu (Figure 1.10A).[246] The structure of SadA has been reported,[247] and variants with altered specificity have been studied.[248]

COR-AAD1-00002897
Bayer EX1008 (Part 6 of 9)

View Online

Published on 23 April 2015 on http://pubs.rsc.org | doi:10.1039/9781782621959-00001
Downloaded on 09/07/2016 13:50:17.

PvcB of *Pseudomonas aeruginosa* functions in the biosynthesis of the siderophore pyoverdine by participating in the formation of 2-isocyano-6,7-dihydroxycoumarin (reminiscent of the coumarin product shown in Figure 1.8G). The *P. aeruginosa* enzyme catalyses a cyclization reaction (Figure 1.10B),[249] although the mechanistic details remain obscure, and the structure of the protein has been characterized in the absence of ligands.[249] Ectoine is an acid with a secondary amine, so the associated enzyme is described here although this tetrahydropyrimidine could alternatively be included in the next section with nucleobases and nucleosides. Bacteria synthesize ectoine and a variety of other compatible solutes to prevent excessive loss of water when grown in high salinity conditions, and some species convert ectoine

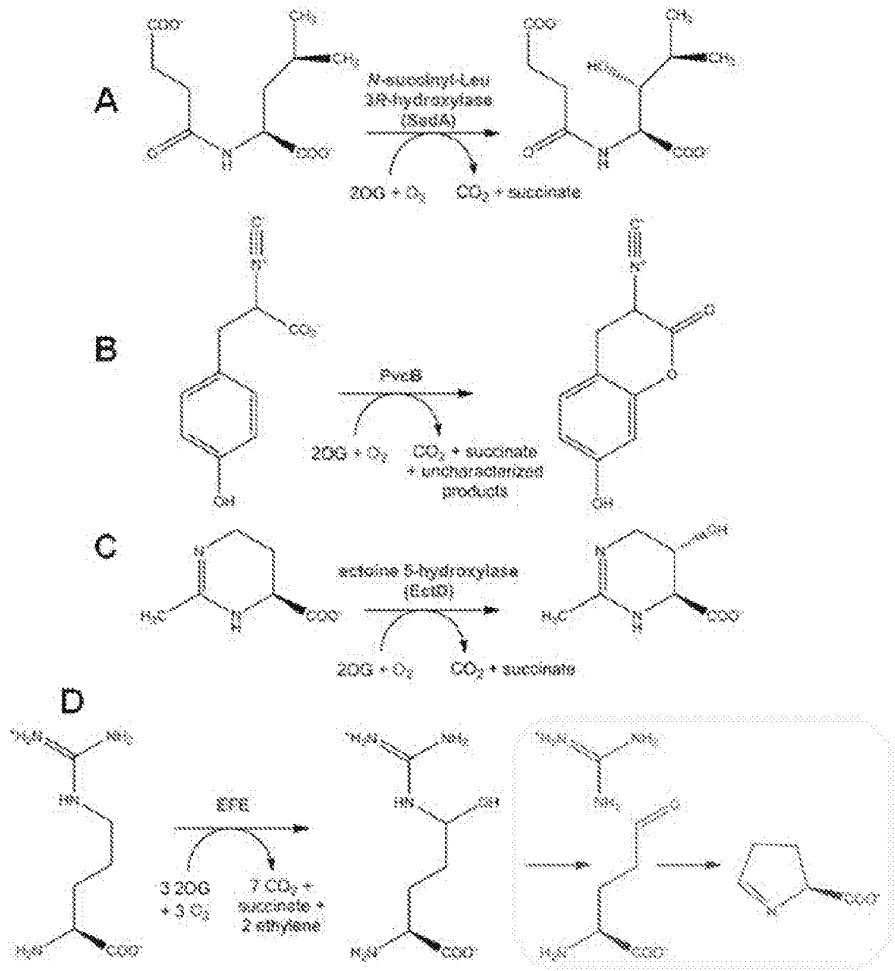


Figure 1.10 2OG oxygenases using substrates resembling amino acids. (A) *N*-succinyl-L-Leu 3*R*-hydroxylase. (B) PvcB reaction in pyoverdine biosynthesis. (C) Ectoine 5-hydroxylase. (D) A poorly characterized bacterial enzyme reported to convert 2OG to ethylene while simultaneously hydroxylating L-Arg, with subsequent spontaneous reactions shown in yellow highlight.

COR-AAD1-00002898
Bayer EX1008 (Part 6 of 9)

View Online

Published on 23 April 2015 on http://pubs.rsc.org | doi:10.1039/9781782621959-00001
Downloaded on 09/07/2016 13:50:17.

to 5-hydroxyectoine during stationary growth. EctD is a 2OG-dependent enzyme responsible for this ectoine 5-hydroxylase activity (Figure 1.10C).[250] The properties of this protein have been examined from a wide distribution of microorganisms, including extremophiles.[251] Of particular interest, the structure of EctD from *Virgibacillus* (formerly *Salibacillus*) *salexigens* in the absence of substrate has been characterized,[252] and a model of the holoprotein with ectoine and 2OG has been simulated.[253] Finally, *Pseudomonas syringae* pv. *phaseolicola* contains the ethylene-forming enzyme (EFE) which is reported to convert 2OG to ethylene and three molecules of CO_2 while simultaneously converting Arg into guanidine and Δ^1-pyrroline-5-carboxylate.[254] The presumed Arg 5-hydroxylase activity (Figure 1.10D) and formation of the resulting degradation products have not been clearly documented. 2OG-dependent ethylene formation has been observed in other microorganisms, including a mushroom,[255] and the gene encoding EFE is functional when inserted into other hosts,[256,257] including cyanobacteria,[257,258] with the latter microorganisms offering the potential for generating a biofuel from CO_2. The mechanism of 2OG conversion to ethylene by EFE is not understood.

1.6.2 Hydroxylases of Nucleobases and Nucleosides

Two distinct 2OG-dependent oxygenases are known to act on nucleobases. Thymine 7-hydroxylase from the fungus *Neurospora crassa* was among the first 2OG-dependent oxygenases to be characterized.[259,260] The enzyme catalyses sequential oxygen additions to the methyl group of the free base, forming 5-hydroxymethyluracil, 5-formyluracil and 5-carboxyuracil (Figure 1.11A).[261,262] Additional studies have focused on the purified fungal enzyme from *Rhodotorula glutinis*,[263] including analysis of its broad substrate specificity.[264,265] Xanthine hydroxylase, XanA, is a fungal enzyme that catalyses the reaction of Figure 1.11B.[266] This enzyme was discovered by studies involving a mutant strain of *Aspergillus nidulans* that was defective in xanthine dehydrogenase, a widely distributed molybdopterin-containing enzyme, yet was able to grow on xanthine as a nitrogen source. XanA was purified both from the fungal host and as a recombinant protein from *E. coli*; although differing in various types of post-translational modifications, both forms exhibited the activity shown.[267] Although no crystal structure is available for XanA, the likely active site residues were identified from mutagenesis studies and shown to support results of a homology model.[268]

Three types of 2OG-dependent oxygenases have been reported to catalyse reactions with the sugar components of nucleosides. Several fungi contain pyrimidine deoxyribonucleoside 2′-hydroxylases that form the corresponding ribonucleosides (Figure 1.11C).[269,270] Furthermore, *R. glutinis* contains a deoxyuridine or uridine 1′-hydroxylase that forms an unstable intermediate which decomposes with release of the nucleobase and formation of a lactone (Figure 1.11D).[271] Finally, a uridine-5′-monophosphate 5′-hydroxylase (Figure 1.11E) named LipL has been purified from a *Streptomyces* species where it provides a precursor for incorporation into antibiotic A-90289.[272]

COR-AAD1-00002899
Bayer EX1008 (Part 6 of 9)

View Online

Published on 23 April 2015 on http://pubs.rsc.org | doi:10.1039/9781782621959-00001
Downloaded on 09/07/2016 13:50:17.

Although the enzyme has not been characterized, it appears that a thymine 7-hydroxylase-like activity might be used for nucleoside modification during polyoxin biosynthesis in *Streptomyces avermitilis*.[273] The cells produce 14 distinct forms of polyoxins that possess a common nucleoside core containing 1-(5′-amino-5′-deoxy-β-D-allofurauronosyl)pyrimidine. The SAV_4805 open reading frame of this microorganism was shown to be associated with enhancement of structural diversity at the C-5 position of the pyrimidine ring, consistent with hydroxylation of this site by the encoded protein (Figure 1.11F).

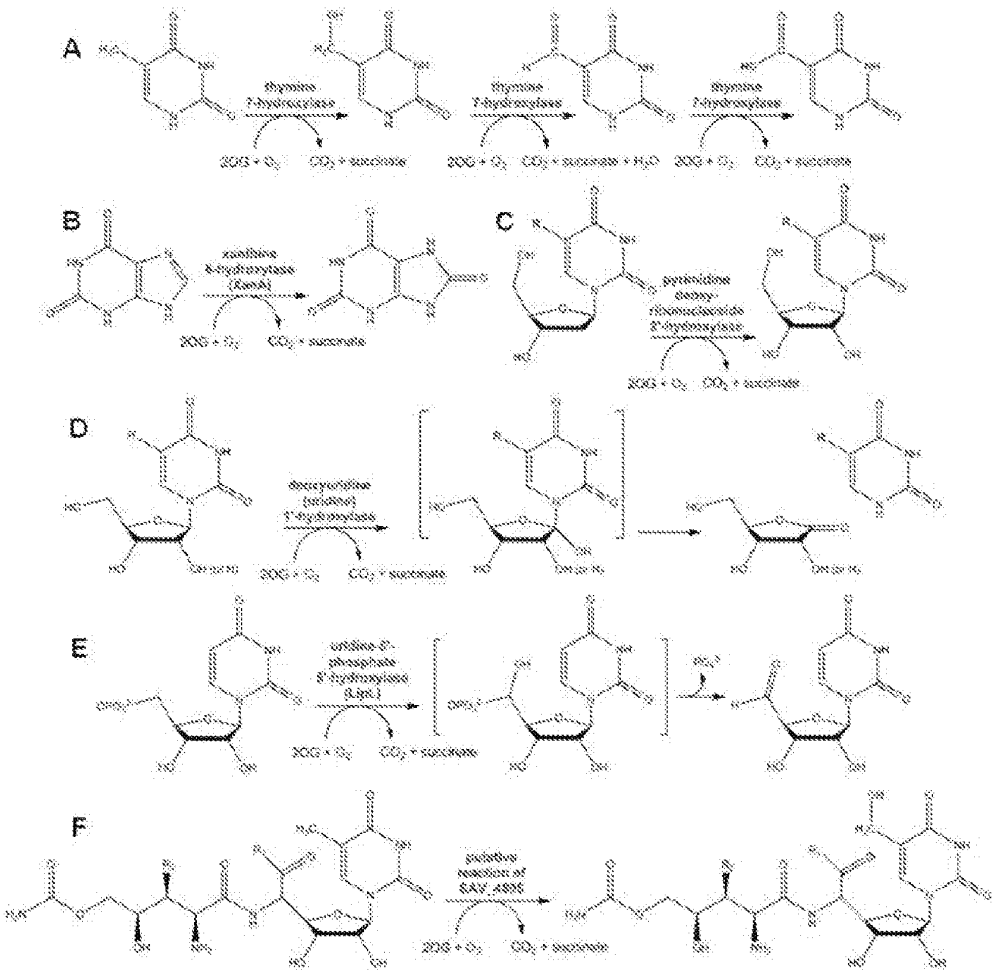


Figure 1.11 2OG-dependent oxygenase reactions involving nucleobases and nucleosides. (A) Thymine 7-hydroxylase. (B) Xanthine hydroxylase. (C) Pyrimidine deoxyribonucleoside 2′-hydroxylase. (D) Deoxyuridine (uridine) 1′-hydroxylase. (E) Uridine-5′-monophosphate 5′-hydroxylase. (F) Possible reaction catalysed by the enzyme associated with the SAV_4805 open reading frame.

COR-AAD1-00002900
Bayer EX1008 (Part 6 of 9)

View Online

Published on 23 April 2015 on http://pubs.rsc.org | doi:10.1039/9781782621959-00001
Downloaded on 09/07/2016 13:50:17.

1.6.3 Herbicide Degradation by 2OG-Dependent Oxygenases

Phenoxyalkanoic acids are widely used as herbicides for selective control of broad-leaf weeds. An important example is 2,4-dichlorophenoxyacetic acid (2,4-D), for which the biodegradative process has been extensively studied.[274] Bacteria that are capable of growth on 2,4-D as sole carbon source often possess a series of enzymes: TfdA (initially referred to incorrectly as 2,4-D monooxygenase), 2,4-chlorophenol hydroxylase (TfdB), 3,5-dichloro–catechol dioxygenase (TfdC), dichloromuconate cycloisomerase (TfdD), dienelactone hydrolase (TfdE) and maleylacetate reductase (TfdF) yielding 3-oxoadipate which enters intermediary metabolism. Using the enzyme from *Cupriavidus necator* (formerly *Ralstonia eutropha*), the reaction of TfdA was revised to be that of a 2OG-dependent hydroxylase (Figure 1.12A).[275] The properties of TfdA have been extensively characterized, including the specificity towards a diversity of phenoxyalkanoic acids, several spectroscopic features of the protein, and its ability to catalyse self-hydroxylation.[64,276,277] This was the first example of a 2OG-dependent dioxygenase being used for biodegradation of a xenobiotic compound. By incorporating *tfdA*-like genes into transgenic plants, enhanced herbicide tolerance has been obtained.[278]

2-Phenoxypropionic acids differ from phenoxyacetic acids by a single methyl group, resulting in two enantiomeric forms of these compounds. Only the (*R*) enantiomer of 2-(2,4-dichlorophenoxy)propionic acid (dichlorprop) or 2-(4-chloro-2-methyl-phenoxy)propionic acid (mecoprop) are active as herbicides. *Sphingomonas herbicidovorans* MG was shown to possess two proteins, RdpA and SdpA, specific for hydroxylating the (*R*) and (*S*) enantiomers, respectively (Figure 1.12B).[279] The structural basis of the distinct enantiospecificities for these proteins has been assessed by homology modelling, substrate docking and mutagenesis.[280]

The mechanism of herbicidal action of the above aryloxyalkanoic acids depends on the interaction of the compounds with the auxin receptor of plants. It is thus of some interest that rice possesses DAO (see Section 1.5.4), which converts indole-3-acetic acid into 2-oxoindole-3-acetic acid (Figure 1.8I).[224] The distribution of this activity in other plants remains to be defined.

1.6.4 Sulfonate and Sulfate Metabolism by 2OG-Dependent Dioxygenases

TauD is the best characterized 2OG-dependent oxygenase in terms of understanding its catalytic mechanism.[9,281] This *E. coli* enzyme hydroxylates 2-aminoethanesulfonate (taurine), with the hydroxylated sulfonate intermediate spontaneously decomposing to aminoacetaldehyde and sulfite (Figure 1.12C), which is used as a sulfur source by the cells.[282] Crystal structures are available for the *E. coli* protein as well as that from *Pseudomonas putida* KT2440.[283–285] Several of the intermediate states of catalysis

COR-AAD1-00002901
Bayer EX1008 (Part 6 of 9)

View Online

Published on 23 April 2015 on http://pubs.rsc.org | doi:10.1039/9781782621959-00001
Downloaded on 09/07/2016 13:50:17.

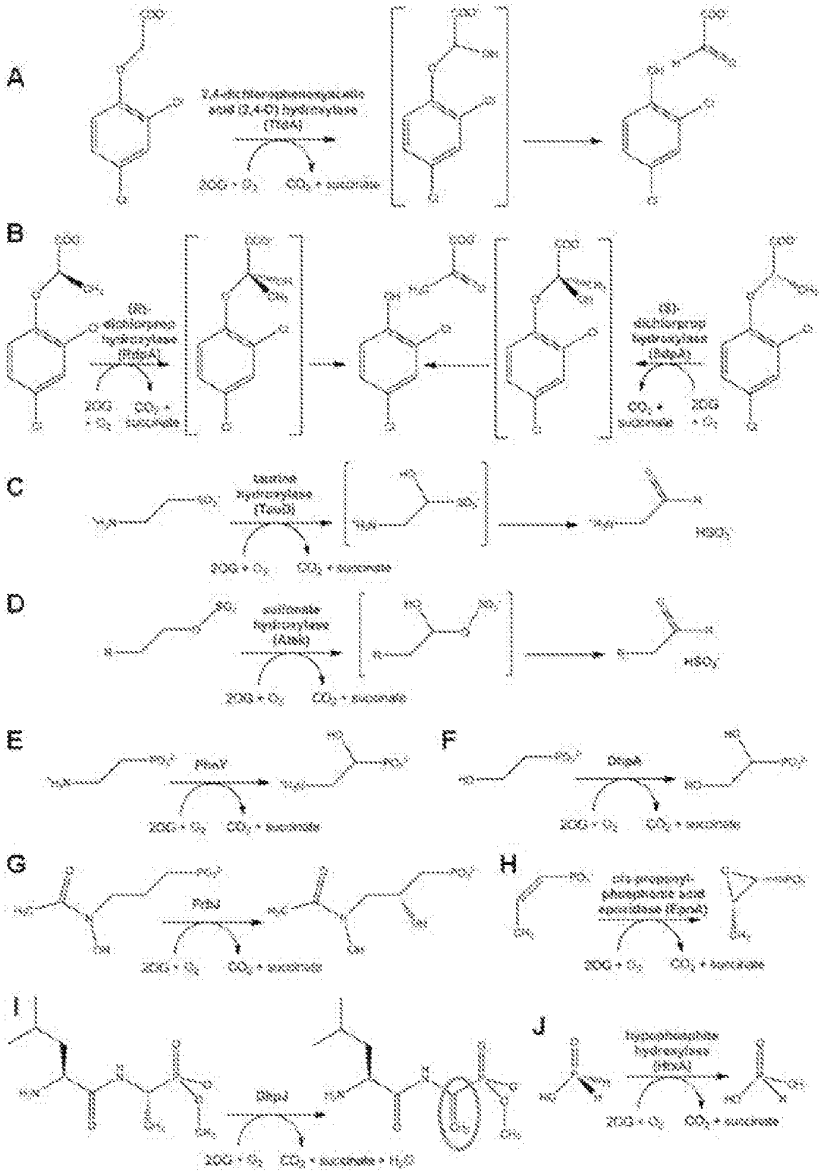


Figure 1.12 2OG-dependent oxygenases involved in metabolism of herbicides, sulfur-containing species and phosphonate compounds. (A) 2,4-D metabolism by TfdA. (B) RdpA and SdpA reactions with enantiomers of dichlorprop. (C) Taurine metabolism by TauD. (D) Sulfate metabolism by AtsK. (E) PhnY catalysed hydroxylation of 2-aminoethylphosphonate. (F) DhpA reaction with hydroxyethylphosphonate. (G) FrbJ catalysed hydroxylation. (H) Epoxidation reaction of EpoA. (I) Desaturation reaction of DhpJ. (J) HtxA conversion of hypophosphite to phosphite.

have been examined spectroscopically,[286,287] including the Fe(IV)-oxo[288–291] and later species.[10] In addition, at least two distinct types of self-hydroxylation chemistries have been studied with TauD, with one case involving a transient tyrosyl radical.[66–68] The enzyme decomposes a variety of other sulfonates (not depicted), including the widely used buffer 3-(*N*-morpholino)

COR-AAD1-00002902
Bayer EX1008 (Part 6 of 9)

View Online

propanesulfonic acid, MOPS.[282] A yeast homologue is most active with MOPS among the potential substrates tested, but physiologically it functions to degrade taurocholate – the amide formed between taurine and cholic acid.[292]

Similar to the sulfonate-degrading enzymes discussed above, 2OG-dependent hydroxylases are also used to decompose alkylsulfates (Figure 1.12D). The first such enzyme discovered was AtsK from *P. putida* S-313; this protein is 38% identical to TauD, but it exhibits no activity with taurine.[293] A related enzyme is associated with the Rv3406 locus of *Mycobacterium tuberculosis*.[294] Crystal structures have been obtained with AtsK proteins from both sources.[294–296]

Published on 23 April 2015 on http://pubs.rsc.org | doi:10.1039/9781782621959-00001
Downloaded on 09/07/2016 13:50:17.

1.6.5 2OG-Dependent Oxygenases in Phosphonate Metabolism

Several members of the 2OG oxygenase enzyme family have been shown to act on various types of phosphonate compounds. The gene encoding PhnY was identified from a screen of ocean-derived metagenomic DNA that allowed *E. coli* cells deficient in C–P lyase (*Δphn*) to grow on 2-aminoethylphosphonic acid as the sole source of phosphorus. The substrate, a close analogue of taurine, is hydroxylated by PhnY (Figure 1.12E)[297] much like the reaction of TauD; however, the hydroxylated phosphonate is stable – unlike the hydroxylated sulfonate. DhpA catalyses a very similar reaction, oxygen addition to hydroxyethylphosphonate (Figure 1.12F) or its O-phosphomonomethyl ester (not shown), in the pathway for biosynthesis of dehydrophos, a vinyl phosphonate tripeptide antibiotic of *Streptomyces luridus*.[298] A hydroxylation reaction is also catalysed by FrbJ of *Streptomyces rubellomurinus*, in this case using the antibiotic FR-900098 as substrate (Figure 1.12G).[299] Rather than hydroxylation, EpoA of *Penicillium decumbens* catalyses epoxidation using *cis*-propenylphosphonic acid (Figure 1.12H) during synthesis of the antibiotic fosfomycin.[300] Another enzyme participating in the synthesis of dehydrophos by *S. luridus* is DhpJ, which catalyses a desaturation reaction of the monomethyl diester of L-Leu-L-1-aminoethylphosphonic acid (Figure 1.12I).[301] While the substrate is not a phosphonate, it is also appropriate to mention here the phosphite-producing hypophosphite hydroxylase activity (Figure 1.12J) of HtxA from *Pseudomonas stutzeri* WM88.[302]

1.7 2OG-Dependent Oxygenases Involved in Antibiotic Biosynthesis

Several 2OG-dependent oxygenases described earlier function in the synthesis of antibiotics, but their actions typically involve provision of small precursor molecules that become incorporated into the final compounds. This section focuses on other family members that function in antibiotic biosynthesis by forming bicyclic β-lactams, tailoring terpenoids, modifying protein-bound *S*-pantetheinyl thioesters compounds, and other roles.

COR-AAD1-00002903
Bayer EX1008 (Part 6 of 9)

View Online

Published on 23 April 2015 on http://pubs.rsc.org | doi:10.1039/9781782621959-00001
Downloaded on 09/07/2016 13:50:17.

1.7.1 Bicyclic β-Lactam Antibiotic Biosynthesis

This section covers several 2OG-dependent oxygenases that participate in the formation of clinically important bicyclic β-lactam antibiotics.[303] Also of interest for this topic, Section 1.8.1 describes isopenicillin *N* synthase, a structurally-related enzyme that does not use 2OG.

Clavaminate synthase (CAS) is a remarkable trifunctional 2OG-dependent enzyme in the pathway for synthesis of clavulanic acid in *Streptomyces clavuligerus*.[304] Starting with L-Arg and glyceraldehyde-3-phosphate, the cells utilize a thiamine diphosphate-dependent enzyme to form N^2-(2-carboxyethyl)arginine, which cyclizes *via* an ATP-dependent ligase reaction to generate deoxyguanidinoproclavaminate. This compound is the substrate for CAS, which catalyses a 2OG-dependent hydroxylation reaction (Figure 1.13A, left reaction). The guanidine group is removed from the resulting guanidinoproclavaminic acid by a separate hydrolase to yield proclavaminate. This substrate is used in a 2OG-dependent cyclization reaction catalysed by CAS (Figure 1.13A, middle reaction) to form dihydroclavaminic acid, which undergoes desaturation to clavaminic acid in the third 2OG-dependent reaction of CAS (Figure 1.13A, right reaction). Subsequent amino transferase and reductase reactions provide the final clavulanic acid (with an alcohol replacing the amine in the last structure shown). Purified CAS in its various states was studied by several spectroscopic methods, which provided evidence that the binding of both substrates (2OG and the antibiotic precursors) led to the loss of all metal-bound water, thus creating an oxygen binding site on the metal.[305,306] Structures of CAS have been solved in the presence of Fe(II), 2OG and either *N*-α-acetyl-L-Arg, proclavaminic acid, or deoxyguanidinoproclavaminate (with the oxygen analogue NO bound to the metal).[307,308]

Cephalosporin biosynthesis starts with the formation of isopenicillin (see Section 1.8.1), which is epimerized to penicillin, modified by two 2OG-dependent enzymes in prokaryotes or a single dual-function enzyme in eukaryotes, and additionally tailored by other reactions, sometimes including another 2OG family member. The first two 2OG-dependent oxygenases in *S. clavuligerus* are deacetoxycephalosporin C synthase (DAOCS), which catalyses a ring expansion reaction (Figure 1.13B, left), and deacetylcephalosporin C synthase (DACS; Figure 1.13B, right), a hydroxylase.[309–311] In contrast, both reactions are catalysed by the same DAOCS/DACS enzyme from *Cephalosporium acremonium*.[312,313] Several structural studies of DAOCS included the first structure for any 2OG-dependent oxygenase[314] and reveal the modes of substrate and product binding – with the surprising finding of overlapping binding sites of 2OG and penicillin substrates.[315–319] Recent pre-steady state kinetics and binding studies have called into question the interpretations from earlier results and conclude that a ternary complex does form in the protein.[320] Modelling combined with mutagenesis studies suggest that a single residue controls whether the enzyme catalyses ring expansion or hydroxylation, and offers insight into how the *C. acremonium* DAOCS/DACS enzyme catalyses both reactions.[321] The deacetylcephalosporin C resulting

COR-AAD1-00002904
Bayer EX1008 (Part 6 of 9)

View Online

Published on 23 April 2015 on http://pubs.rsc.org | doi:10.1039/9781782621959-00001
Downloaded on 09/07/2016 13:50:17.

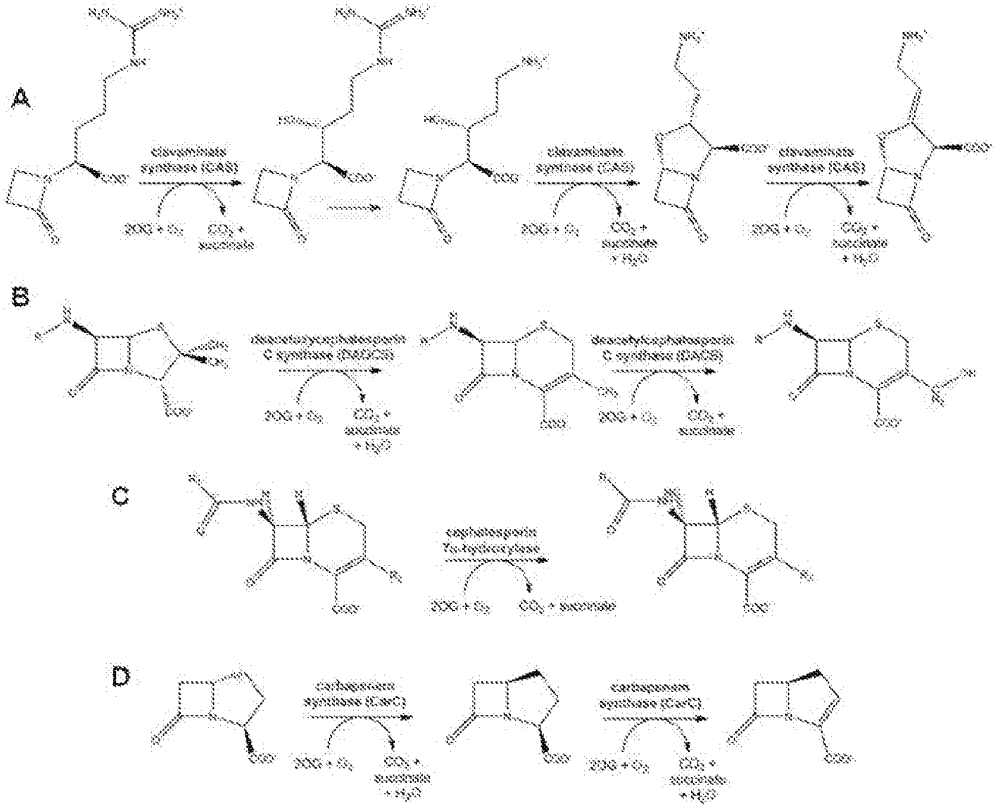


Figure 1.13 2OG-dependent oxygenases for synthesis of bicyclic β-lactam antibiotics. (A) Three reactions of clavaminic acid synthase and a separate non-CAS reaction (yellow highlight). (B) Ring expansion and hydroxylation reactions of cephalosporin biosynthesis. (C) Cephalosporin 7α-hydroxylase. (D) Carbapenem synthase epimerase (an external source of electrons is also needed for this reaction) and desaturation reactions.

from these reactions undergoes further transformations including acylation of the newly introduced hydroxyl group, 2OG-dependent hydroxylation at the 7α position (Figure 1.13C),[322] and methylation of the latter site. These enzymes are described in greater detail in Chapter 17.

Carbapenems are a third grouping of the bicyclic β-lactams that utilize a 2OG-dependent oxygenase in their synthetic pathway. *Pectobacterium carotovorum* (formerly *Erwinia carotovora*) contains the enzyme (2*S*,5*S*)-carboxymethylproline synthase (CarB) that uses glutamate semi-aldehyde and malonyl-CoA to produce the carboxymethylproline derivative. This substrate is subjected to a ligase reaction by (3*S*,5*S*)-carbapenam synthetase (CarA), forming carbapenam-3-carboxylate with its β-lactam ring. Carbapenem synthase (CarC) is a 2OG-dependent oxygenase proposed to catalyse two sequential non-hydroxylase reactions: epimerization to (3*S*,5*R*)-carbapenam-3-carboxylate and desaturation to yield (5*R*)-carbapenem-3-carboxylate (Figure 1.13D).[323] The crystal structure of CarC with bound Fe(II) and 2OG

COR-AAD1-00002905
Bayer EX1008 (Part 6 of 9)

View Online

has been elucidated.[324] The stereoinversion reaction appears to involve ferryl abstraction of a substrate hydrogen atom followed by hydrogen atom donation from a tyrosyl side chain, limiting the enzyme to a single turnover unless external electrons are provided.[325]

Published on 23 April 2015 on http://pubs.rsc.org | doi:10.1039/9781782621959-00001
Downloaded on 09/07/2016 13:50:17.

1.7.2 Synthesis of Terpenoid Antibiotics

The rich biochemistry of terpenoid metabolism includes several examples of reactions catalysed by 2OG-dependent oxygenases. The synthesis of pentalenolactone, a sesquiterpenoid produced by dozens of strains of *Streptomyces*, nicely illustrates this point. A hydroxylase reaction, the conversion of 1-deoxypentalenic acid to 11β-hydroxy-1-deoxypentalenic acid (Figure 1.14A), is catalysed by *S. avermitilis* PltH.[326] The structure of this protein in complex with Fe(II), 2OG and *ent*-1-deoxypentalenic acid (a non-reactive enantiomer), has been defined.[327] Analogous proteins appear to be present in *S. exfolatus* UC5319 and *S. arenae* TU469, where they are named PenH and PntH, respectively.[328] These three strains each possess a second 2OG-dependent oxygenase (PtlD, PenD and PntD, respectively) capable of desaturating pentalenolactone D to pentalenolactone E, with PenD and PntD subsequently forming the epoxide pentalenolactone F (Figure 1.14B). In addition, these same three enzymes can transform neopentalenolactone D to an unstable enollactone desaturation product which is hydrolysed (Figure 1.14C).[328]

Two 2OG-dependent oxygenases utilize the same substrate, fusicocca-2,10(14)-diene-8β,16-diol, to produce distinct diterpene phytohormone-like compounds in fungi.[329] An enzyme from *Alternaria brassicicola* first abstracts a hydrogen atom from the eight-membered ring, the carbon-centered radical migrates, and hydroxyl radical rebound yields the distal hydroxylated product (Figure 1.14D, left) during a step in the synthesis of cotylenin A or brassicicene C. In contrast, an enzyme from *Phomopsis amygdali* catalyses oxidation at C-16 to yield the aldehyde 8β-hydroxyfusicocca-1,10(14)-diene-16-al (Figure 1.14D, right) during fusicoccin A biosynthesis.[329]

A final example of a 2OG-dependent oxygenase involved in synthesis of a terpene glycoside antibiotic is PlaO1 from *Streptomyces* sp. Tü6071.[330] PlaO1 catalyses the critical formation of a γ-butyrolactone during synthesis of phenalinolactone (Figure 1.14E). The chemical mechanism associated with this remarkable reaction has not been detailed, but a cogent hypothesis has been proposed.[331]

1.7.3 2OG-Dependent Oxygenases Acting on Tethered Substrates in Non-Ribosomal Peptide Synthesis

Several 2OG-dependent oxygenases act on protein-tethered *S*-pantetheinyl thioesters of amino acids which undergo non-ribosomal incorporation into peptide-related antibiotics. For example, *Pseudomonas syringae* pv. *syringae* B301D produces the non-ribosomal peptide phytotoxin called syringomycin

COR-AAD1-00002906
Bayer EX1008 (Part 6 of 9)

View Online

Published on 23 April 2015 on http://pubs.rsc.org | doi:10.1039/9781782621959-00001
Downloaded on 09/07/2016 13:50:17.

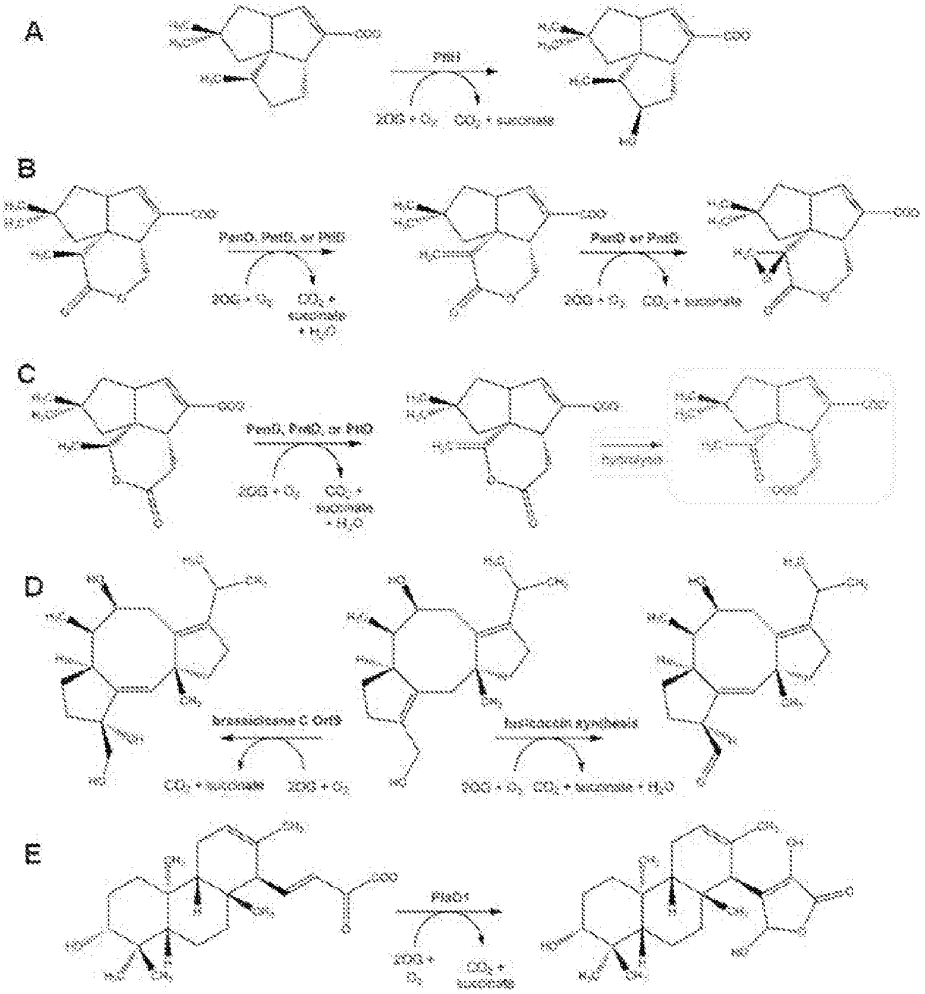


Figure 1.14 Representative 2OG-dependent oxygenases in terpenoid biosynthesis. (A) 1-deoxypentalenic acid 11β-hydroxylase, PtlH. (B) Desaturase and epoxidase reactions of PenD, PntD and PtlD using pentalenolactone D. (C) Neopentalenolactone desaturase reaction by the same enzymes, followed by spontaneous hydrolysis (yellow highlight). (D) Two reactions using fusicocca-2,10(14)-diene-8β,16-diol. (E) PlaO1-catalysed γ-butyrolactone formation in phenalinolactone synthesis.

E by assembling components on a multimodular megasynthetase, SyrE. SyrP is a 2OG-dependent hydroxylase that acts on L-Asp bound to the eighth module of SyrE to yield the *threo* isomer of 3-hydroxyaspartic acid which is inserted into the eighth position of the final phytotoxin (Figure 1.15A).[237]

Two other proteins involved in syringomycin E biosynthesis, SyrB1 and SyrB2, are required for synthesis of the 4-chloro-L-Thr located at position nine of the phytotoxin. Remarkably, SyrB2 was shown to be a 2OG-dependent oxygenase that catalyses a halogenation reaction using L-Thr tethered to SyrB1 (Figure 1.15B).[332] The enzyme also catalyses bromination, dichlorination, nitration and azidation reactions (not depicted).[333,334] The structure

COR-AAD1-00002907
Bayer EX1008 (Part 6 of 9)

View Online

Published on 23 April 2015 on http://pubs.rsc.org | doi:10.1039/9781782621959-00001
Downloaded on 09/07/2016 13:50:17.

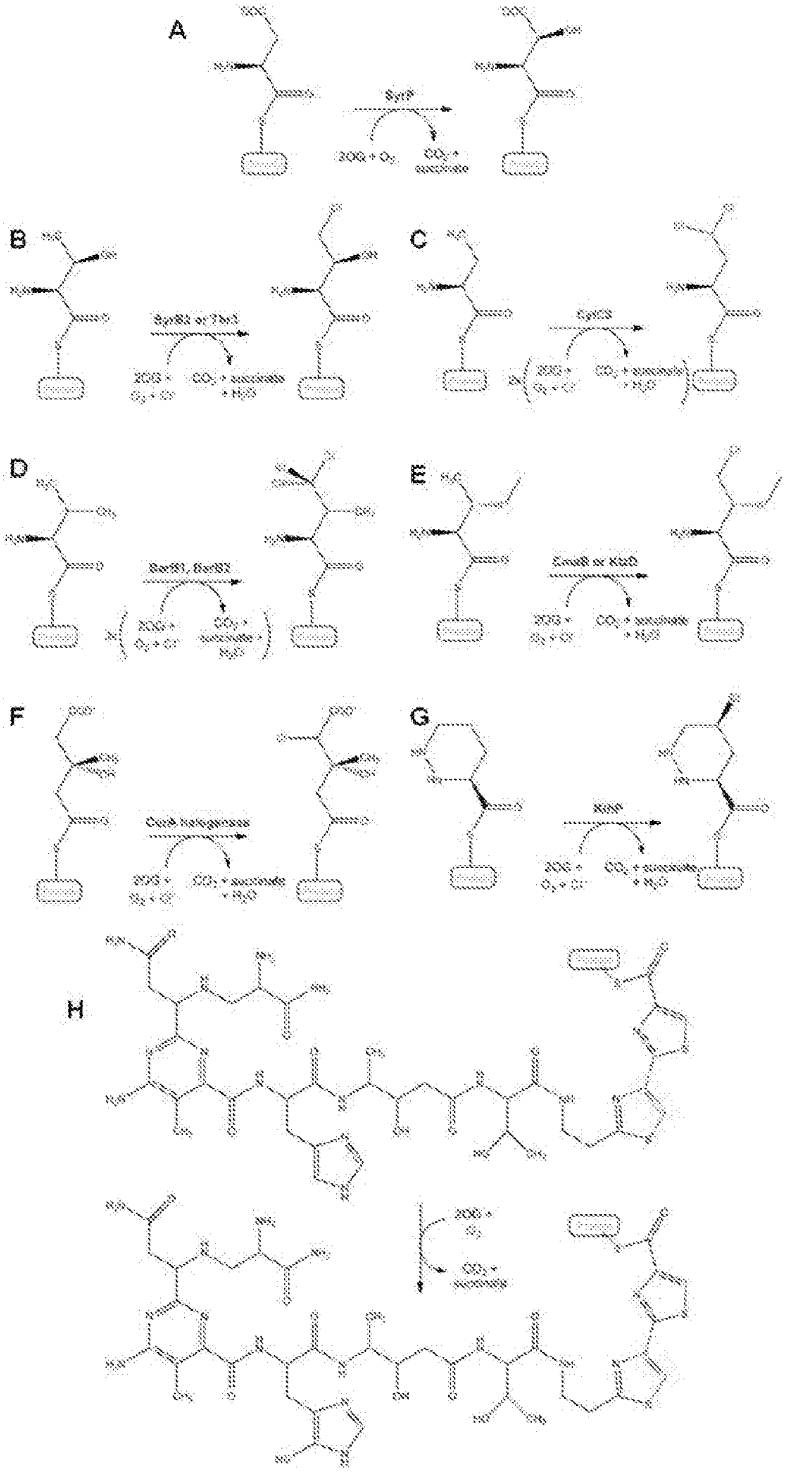


Figure 1.15 Use of protein-tethered substrates by 2OG-dependent oxygenases in antibiotic biosynthesis. (A) SyrP-catalysed formation of a 3-hydroxyaspartyl group and (B) SyrB2-dependent synthesis of a 3-chlorothreonyl group in syringomycin E synthesis. (C) CytC3 generation of the

COR-AAD1-00002908
Bayer EX1008 (Part 6 of 9)

View Online

Published on 23 April 2015 on http://pubs.rsc.org | doi:10.1039/9781782621959-00001
Downloaded on 09/07/2016 13:50:17.

of SyrB2 reveals a metallocentre in which Fe(II) is bound only by two histidyl residues (with the typical carboxylate ligand replaced by an alanyl side chain), and coordinated to 2OG and chloride ion.[335] Spectroscopic studies have revealed evidence for a chloroferryl intermediate in catalysis,[336] and studies with substrate analogues suggest that substrate positioning determines whether halogenation or hydroxylation take place.[337] *Streptomyces* sp. OH-5093 produces free 4-chlorothreonine by a similar pathway, in which Thr3 catalyses the halogenation of the tethered amino acid, followed by thioester hydrolysis.[338]

Much like the SyrB1/SyrB2 system just discussed, a cytotrienin-producing *Streptomyces* sp. uses CytC3 to catalyse halogenation of L-2-aminobutyric acid (or L-Val) tethered to CytC2 (Figure 1.15C).[339] Tandem chlorinations followed by thioesterase activity lead to the γ,γ-dichloraminobutyrate antibiotic that is released into the soil. Two interconverting Fe(IV) intermediates were detected in that study, and later work provided evidence for the formation of a bromoferryl intermediate when bromide was used to replace chloride.[340] The structure of CytC3 exhibits the same general architecture as seen for SyrB2, including an Ala residue replacing the typical aspartyl metal ligand.[341]

Five other examples illustrate additional interesting features of 2OG-dependent halogenation enzymes. The marine cyanobacterium *Lyngbya majuscula* produces barbamide, an antibiotic containing trichlorinated leucine that is active against molluscs. BarB2 converts BarA-tethered L-Leu or 4-chloro-L-Leu to the dichlorinated species and BarB1 halogenates the mono- or dichlorinated species to the trichlorinated species (Figure 1.15D).[342] *Pseudomonas syringae* pv. *tomato* DC3000 synthesizes the phytotoxin coronatine which contains 1-amino-1-carboxy-2-ethylcyclopropane (coronamic acid). Synthesis of coronamic acid derives from L-*allo*-isoleucine which is tethered to CmaD, chlorinated by CmaB (Figure 1.15E), and converted to the cyclopropane species by CmaC with elimination of chloride in this cryptic chlorination pathway.[343] An analogous system is present in the ascomycete *Kutzneria*, where KtzD chlorinates L-Ile bound to KtzC, with the product cyclized to the bound (1*S*,2*R*)-allocoronamic acid by KtzA.[344] Another example of cryptic chlorination occurs during curacin A synthesis by *L. majuscula*, the marine bacterium mentioned above. In this case, acyl carrier protein-bound (*S*)-3-hydroxy-3-methylglutarate is chlorinated by CurA (Figure 1.15F), followed by dehydration using CurC, decarboxylation *via* a CurF domain, and

mono- or dichloro L-2-aminobutyryl group in cytotrienin synthesis. (D) Trichlorination of leucine by BarB1 and BarB2 to make barbamide. (E) CmaB- or KtzD-dependent hydroxylation of isoleucyl groups for subsequent cyclization to coronamic acids. (F) CurA chlorination of a 3-hydroxy-3-methylglutaryl group as part of curacin A synthesis. (G) KthP halogenation of a piperazyl group during formation of kutznerides. (H) Hydroxylation of a histidyl group during synthesis of bleomycin, tallysomycin and zorbamycin (yellow highlight is a single bond in the case of zorbamycin).

COR-AAD1-00002909
Bayer EX1008 (Part 6 of 9)

View Online

Published on 23 April 2015 on http://pubs.rsc.org | doi:10.1039/9781782621959-00001
Downloaded on 09/07/2016 13:50:17.

reductive dechlorination by another CurF domain to yield the protein-bound (1*R*,2*S*)-2-methylcyclopropane-1-carboxylate which is incorporated into curacin A.[345] The structures of CurA in five ligand states have been elucidated.[346] *Kutzneria* sp. 744 chlorinates a protein-bound piperazate residue by using the KthP halogenase (Figure 1.15G) during biosynthesis of a family of antifungal kutznerides.[347] Finally, *Lyngbya majuscula* contains the three-domain protein HctB that catalyses dichlorination (along with hydroxylation and introduction of a vinyl chloride group) on a fatty acyl group attached to its acyl carrier domain region (not depicted).[348] Interestingly, the oxidative reactions of this enzyme are stimulated more than 200-fold by the presence of saturating concentrations of chloride, thus providing an explanation for why hydroxylation does not dominate in the absence of halide salts.[349] Further discussion of 2OG-dependent halogenases can be found in Chapter 18.

Final examples for this section relate to hydroxylation reactions during synthesis of four antitumour natural products made by non-ribosomal peptide synthesis pathways: bleomycin, tallysomycin, zorbamycin and spliceostatin made by *Streptomyces verticillus* ATCC15003, *Streptoalloteichus hindustanus* E465-94, *Streptomyces flavoviridis* ATCC21892 and *Burkholderia* spp., respectively. A 2OG-dependent hydroxylase, potentially associated with open reading frames 1, 10 and 30 of the gene clusters in the first three microbes, is thought to catalyse histidyl group hydroxylation of a large precursor of the final antibiotic species bound to carrier proteins (Figure 1.15H), rather than hydroxylating just the tethered amino acid.[350] The 3-hydroxyhistidyl group is the site of glycation and additional tailoring reactions are used to generate the final antibiotics. The *Burkholderia* enzyme catalyses the synthesis of a hemiketal group (not shown) using the 2OG-dependent mechanism.[351]

1.7.4 Other Roles for 2OG-Dependent Oxygenases in Antibiotic Synthesis

Other 2OG-dependent oxygenases serve important roles in antibiotic biosynthesis, but don't fit into the above categories. These examples are not meant to be comprehensive, but provide useful illustrations of the diversity of reactions catalysed by these enzymes. The just mentioned antibiotic tallysomycin requires TmlH for its synthesis. This enzyme catalyses two 2OG-dependent hydroxylations, at positions C-41 and C-42 (Figure 1.16A).[352] The carbanolamide produced by hydroxylation of C-41 is unstable, but appears to be immediately modified further by TlmK to produce a stable species. It remains unclear whether TlmH acts on the protein-free species as shown or if the modification takes place on the protein-tethered substrate.[350] The fumonisins are mycotoxins produced by *Fusarium verticillioides* and several other filamentous fungi *via* polyketide synthetic routes. Hydroxylation at the C-5 position (Figure 1.16B) is carried out by the 2OG-dependent enzyme Fum3p (formerly associated with the *FUM9* locus).[353,354] Another mycotoxin, verruculogen, is produced by *Aspergillus fumigatus*. The novel creation of an endoperoxide within fumitremorgin B is catalysed by the 2OG-dependent FtmOx1 protein

COR-AAD1-00002910
Bayer EX1008 (Part 6 of 9)

Published on 23 April 2015 on http://pubs.rsc.org | doi:10.1039/9781782621959-00001
Downloaded on 09/07/2016 13:50:17.

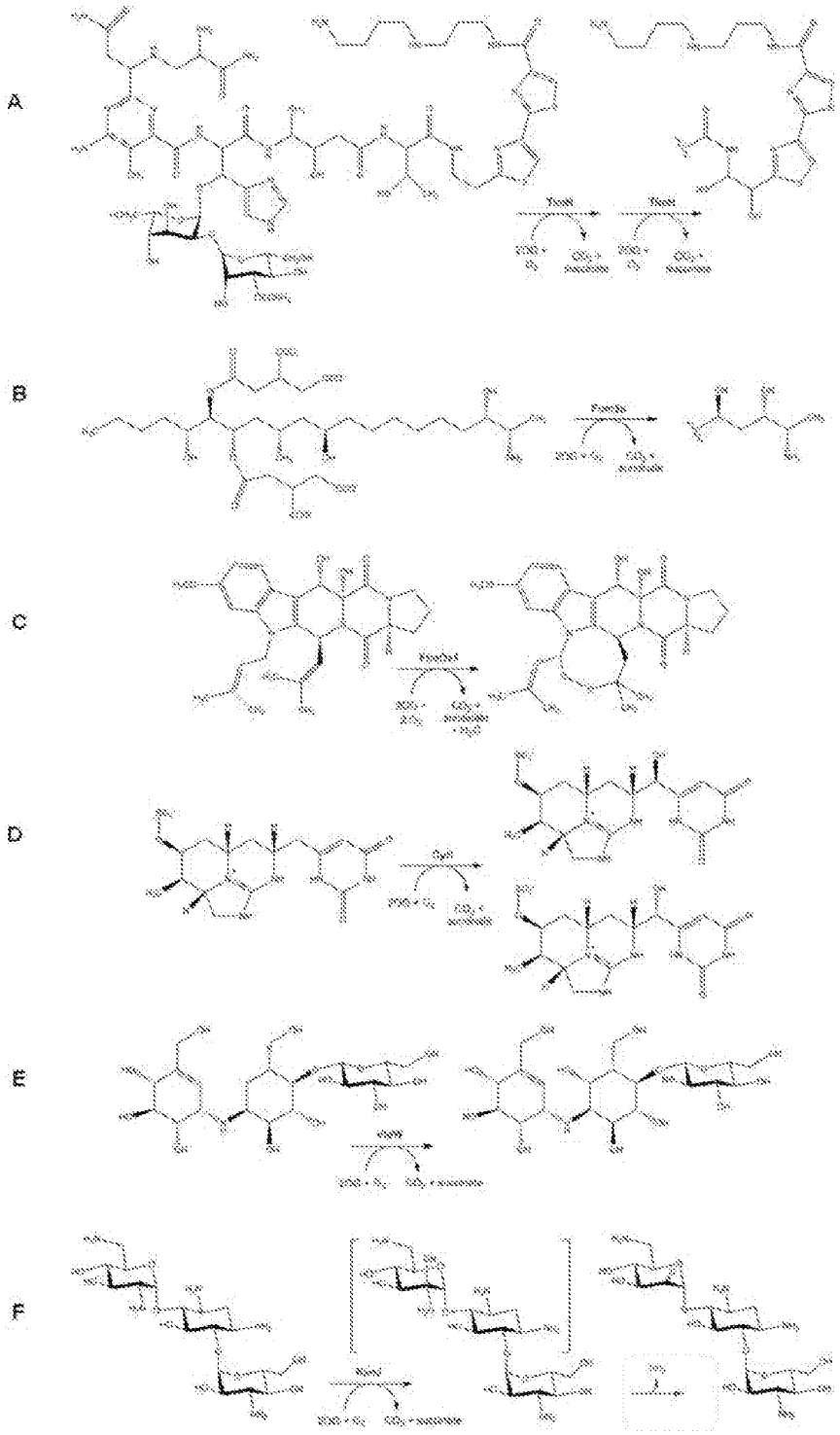


Figure 1.16 More 2OG-dependent oxygenases involved in the biosynthesis of antibiotics. (A) TlmH functioning in tallysomycin biosynthesis. (B) Fum3p modification of a fumiosin. (C) FtmOx1 creation of an endoperoxide in the verruculogen pathway. (D) CyrI production of two cylindrospermopsin products. (E) VldW role in decreasing the toxicity of a validamycin. (F) KanJ hydroxylation and a spontaneous follow-up reaction (yellow highlight) in the penultimate step of kanamycin synthesis.

COR-AAD1-00002911
Bayer EX1008 (Part 6 of 9)

View Online

(Figure 1.16C). Notably, this reaction requires two molecules of oxygen.[355] Several *Oscillatoria* and other cyanobacterial species produce the cyanotoxins cylindrospermopsin and 7-*epi*-cylindrospermopsin. The final step in the synthesis of these compounds is catalysed by the 2OG-dependent hydroxylase CyrI (Figure 1.16D).[356] *Streptomyces hydrogscopicus* subsp. *Limoneus* produces a family of validamycin compounds with antifungal activity. The main species, validamycin A, is converted to the less effective validamycin B by VldW, a 2OG-dependent hydroxylase (Figure 1.16E).[357] Finally, the penultimate step in kanamycin biosynthesis by *Streptomyces kanamyceticus* is carried out by KanJ. This protein catalyses the hydroxylation of an amino sugar (Figure 1.16F) to yield an unstable hemiaminal which decomposes with release of ammonia to yield 2′-oxokanamycin; the latter compound is the substrate for an NADPH-dependent reductase, KanK, to produce the final antibiotic.

Published on 23 April 2015 on http://pubs.rsc.org | doi:10.1039/9781782621959-00001
Downloaded on 09/07/2016 13:50:17.

1.8 Related Enzymes

1.8.1 Isopenicillin *N* Synthase

The enzyme isopenicillin *N* synthase (IPNS) catalyses the fascinating transformation of a linear tripeptide, L-δ-(α-aminoadipoyl)-L-cysteinyl-D-valine, into a bicyclic structure, as shown in Figure 1.17A. The resulting product is subsequently metabolized into penicillins and cephalosporins as described earlier in Section 1.7.1.[303] Although IPNS does not utilize 2OG as a cosubstrate, it is related in sequence and structure to the 2OG-dependent oxygenases; indeed, it was the first family member to be structurally characterized.[358] Like the 2OG-dependent enzymes, IPNS coordinates Fe(II) *via* a 2-His-1-carboxylate motif and binds substrate within a double-stranded β helix fold.[359] The thiolate sulfur atom of the substrate forms a ligand to the metallocentre. Snapshots of the reaction were structurally visualized after brief exposure of anaerobic crystals to high pressures of oxygen.[360] This remarkable enzyme is described further in Chapter 19.

1.8.2 1-Aminocyclopropane-1-Carboxylate Oxidase

Another enzyme that does not utilize 2OG, yet is related by sequence and structure to the 2OG-dependent oxygenases, is 1-aminocyclopropane-1-carboxylate oxidase (ACCO).[361,362] This plant enzyme catalyses the synthesis of ethylene (Figure 1.17B) in a reaction that is distinct from that described in Section 1.6.1. The gaseous product is a phytohormone that functions in germination, fruit ripening and senescence. The cyclopropane-containing substrate of ACCO binds to the Fe(II) site *via* its α-amino and α-carboxylate groups according to spectroscopic analyses with isotopically-labelled substrates and substrate analogues;[363,364] such coordination is reminiscent of the bidentate binding of 2OG to the metallocentre of related family members. Ascorbate is required for multiple turnovers of ACCO, but the reductant is not needed for a single turnover.[365] Surprisingly, carbon dioxide is essential

COR-AAD1-00002912
Bayer EX1008 (Part 6 of 9)

View Online

Published on 23 April 2015 on http://pubs.rsc.org | doi:10.1039/9781782621959-00001
Downloaded on 09/07/2016 13:50:17.

for catalysis in addition to being a product, and this molecule is proposed to stabilize the enzyme from undergoing inactivation reactions.[366] Oxidative inaction of ACCO occurs rapidly and can result in cleavage of the peptide backbone.[367,368] Crystal structures have been resolved for the apoprotein and holoprotein forms of ACCO,[369] and modelling studies have led to proposals for the binding sites of substrate, bicarbonate and ascorbate.[370] This enzyme is described in further detail in Chapter 20.

1.8.3 4-Hydroxyphenylpyruvate Dioxygenase and Hydroxymandelate Synthase

Hydroxymandelate synthase (HMS) and 4-hydroxyphenylpyruvate dioxygenase (HPPD) are of special interest because they transform the same substrate into distinct products (Figure 1.17C) by reactions that are mechanistically related to those carried out by the 2OG-dependent oxygenases; however, HMS and HPPD are unrelated to the latter enzymes while being closely related to each other.[371] The substrate for both enzymes is 4-hydroxyphenylpyruvate, a 2-oxo acid, and like 2OG it undergoes oxidative decarboxylation with formation of carbon dioxide and 4-hydroxyphenylacetate. The enzyme intermediate resulting from the C–C cleavage reaction is used either to hydroxylate the

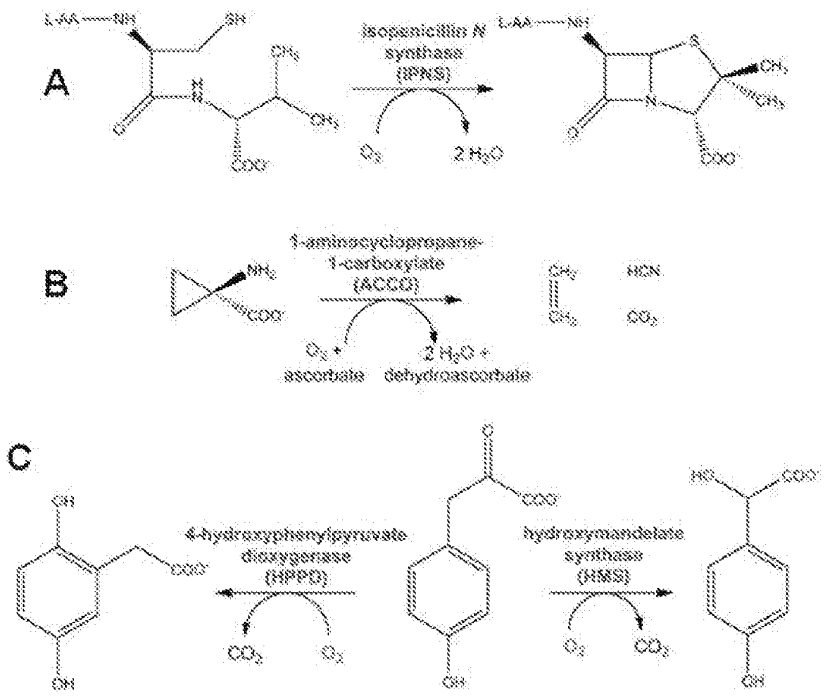


Figure 1.17 Enzymes that are structurally or functionally related to 2OG-dependent oxygenases, but do not utilize 2OG. (A) Isopenicillin *N* synthase. (B) 1-Aminocyclopropane-1-carboxylate oxidase. (C) 4-Hydroxyphenylpyruvate dioxygenase and hydroxymandelate synthase.

COR-AAD1-00002913
Bayer EX1008 (Part 6 of 9)

View Online

methylene group of 4-hydroxyphenylacetate to form hydroxymandelate (in HMS) or it catalyses the 'NIH shift' in which substituent migration and ring hydroxylation produce homogentisate (in HPPD). Isotope effect studies have provided keen insights into how the intermediate partitions to form the two products.[372] Four key residues in the active sites of these enzymes are critical for defining product specificity, and an HPPD has been engineered to exhibit HMS activity.[373] Several catalytic intermediates have been detected by using spectroscopic approaches with these enzymes.[374,375] The structure of HMS from *Amycolatopsis orientalis*[376] exhibits the same fold as found in HPPD, first reported for the enzyme from *Pseudomonas fluorescens*;[377] however, their folds are unrelated to the typical 2OG oxygenase fold. Further information on this pair of enzymes is provided in Chapter 21.

Conspectus: The 2OG-dependent oxygenases catalyze a diverse array of reactions that have profound implications in biology. The structures and mechanisms of these fascinating enzymes are discussed in Chapters 2–4 and representative topics are detailed more fully in Chapters 5–21.

Published on 23 April 2015 on http://pubs.rsc.org | doi:10.1039/9781782621959-00001
Downloaded on 09/07/2016 13:50:17.

Note added in proof

A large number of publications related to this topic have appeared since submission of this chapter, only three of which are cited here. A prolyl residue in prokaryotic elongation factor Tu is hydroxylated by a 2OG-dependent oxygenase, perhaps serving as an evolutionary precursor to prolyl hydroxylases used in oxygen sensing.[379] A review describing these enzymes in coumarin synthesis has appeared.[380] Finally, Wel05 was shown to be a 2OG-dependent halogenase acting on a free substrate (*i.e.* not tethered to a peptidyl carrier protein).[381]

Acknowledgements

2OG-dependent oxygenase work in the author's laboratory was supported by the National Institutes of Health (GM063584).

References

1. R. P. Hausinger, *Crit. Rev. Biochem. Mol. Biol.*, 2004, **39**, 21–68.
2. V. M. Purpero and G. R. Moran, *J. Biol. Inorg. Chem.*, 2007, **12**, 587–601.
3. C. Loenarz and C. J. Schofield, *Nat. Chem. Biol.*, 2008, **4**, 152–156.
4. J. M. Simmons, T. A. Müller and R. P. Hausinger, *Dalton Trans.*, 2008, **38**, 5132–5142.
5. C. Loenarz and C. J. Schofield, *TIBS*, 2010, **36**, 7–18.
6. I. J. Clifton, M. A. McDonough, D. Ehrismann, N. J. Kershaw, N. Granatino and C. J. Schofield, *J. Inorg. Biochem.*, 2006, **100**, 644–669.
7. M. A. McDonough, C. Loenarz, R. Chowdhury, I. J. Clifton and C. J. Schofield, *Curr. Opin. Struct. Biol.*, 2010, **20**, 1–14.

COR-AAD1-00002914
Bayer EX1008 (Part 6 of 9)

View Online

Published on 23 April 2015 on http://pubs.rsc.org | doi:10.1039/9781782621959-00001
Downloaded on 09/07/2016 13:50:17.

8. W. Aik, M. A. McDonough, A. Thalhammer, R. Chowdhury and C. J. Schofield, *Curr. Opin. Struct. Biol.*, 2012, **22**, 1–10.
9. D. A. Proshlyakov and R. P. Hausinger, in *Iron-containing Enzymes: Versatile Catalysts of Hydroxylation Reactions in Nature*, ed. D. Kumar and S. P. de Visser, Royal Society of Chemistry, Cambridge, U.K., 2011, pp. 67–87.
10. P. K. Grzyska, E. H. Appelman, R. P. Hausinger and D. A. Proshlyakov, *Proc. Natl. Acad. Sci. U.S.A.*, 2010, **107**, 3982–3987.
11. R. W. Welford, J. M. Kirkpatrick, L. A. McNeill, M. Puri, N. J. Oldham and C. J. Schofield, *FEBS Lett.*, 2005, **579**, 5170–5174.
12. A. G. Prescott and M. D. Lloyd, *Nat. Prod. Rep.*, 2000, **17**, 367–383.
13. J. J. Hutton, Jr., A. L. Trappel and S. Udenfriend, *Biochem. Biophys. Res. Commun.*, 1966, **24**, 179–184.
14. R. E. Rhoads and S. Udenfriend, *Proc. Natl. Acad. Sci. U.S.A.*, 1968, **60**, 1473–1478.
15. J. Risteli, K. Tryggvason and K. I. Kivirikko, *Eur. J. Biochem.*, 1977, **73**, 485–492.
16. U. Puistola, T. M. Turpeenniemi-Hujanen, R. Myllylä and K. Kivirikko, *Biochim. Biophys. Acta*, 1980, **611**, 40–50.
17. H. M. Hanauske-Abel and V. Günzler, *J. Theor. Biol.*, 1982, **94**, 421–455.
18. K. I. Kivirikko and T. Pihlajaniemi, *Adv. Enzymol. Relat. Areas Mol. Biol.*, 1998, **72**, 325–398.
19. K. L. Gorres and R. T. Raines, *Crit. Rev. Biochem. Mol. Biol.*, 2010, **45**, 106–124.
20. M. A. Culpepper, E. E. Scott and J. Limburgn, *Biochemistry*, 2010, **49**, 124–133.
21. M. K. Koski, R. Hieta, C. Böllner, K. I. Kivirikko, J. Myllyharju and R. K. Wierenga, *J. Biol. Chem.*, 2007, **282**, 37112–37123.
22. M. K. Koski, R. Hieta, M. Hirsilä, A. Rönkä, J. Myllyharju and R. K. Wierenga, *J. Biol. Chem.*, 2009, **284**, 25290–25301.
23. P. Jaakkola, D. R. Mole, Y.-M. Tian, M. I. Wilson, J. Gielbert, S. J. Gaskell, A. von Kriegsheim, H. F. Hebestreit, M. Mukherji, C. J. Schofield, P. H. Maxwell, C. W. Pugh and P. J. Ratcliffe, *Science*, 2001, **292**, 468–472.
24. M. Ivan, K. Kondo, H. Yang, W. Kim, J. Valiando, M. Ohh, A. Salic, J. M. Asara, W. S. Lane and W. G. Kaelin, Jr., *Science*, 2001, **292**, 464–467.
25. W.-C. Hon, M. I. Wilson, K. Harlos, T. D. W. Claridge, C. J. Schofield, C. W. Pugh, P. H. Maxwell, P. J. Ratcliffe, D. I. Stuart and E. Y. Jones, *Nature*, 2002, **417**, 975–978.
26. J.-H. Min, H. Yang, M. Ivan, F. Gertler, W. G. Kaelin, Jr. and N. P. Pavletich, *Science*, 2002, **296**, 1886–1889.
27. M. A. McDonough, V. Li, E. Flashman, R. Chowdhury, C. Mohr, B. M. R. Liénard, J. Zondlo, N. J. Oldham, I. J. Clifton, J. Lewis, L. A. McNeill, R. J. M. Kurzeja, K. S. Hewitson, E. Yang, S. Jordan, R. S. Syed and C. J. Schofield, *Proc. Natl. Acad. Sci. U.S.A.*, 2006, **103**, 9814–9819.
28. R. Chowdhury, M. A. McDonough, J. Mecinovíc, C. Loenarz, E. Flashman, K. S. Hewitson, C. Domene and C. J. Schofield, *Structure*, 2009, **17**, 981–989.

COR-AAD1-00002915
Bayer EX1008 (Part 6 of 9)

View Online

Published on 23 April 2015 on http://pubs.rsc.org | doi:10.1039/9781782621959-00001
Downloaded on 09/07/2016 13:50:17.

29. D. Lando, D. J. Peet, D. A. Whelan, J. J. Gorman and M. L. Whitelaw, *Science*, 2002, **295**, 858–861.
30. L. A. McNeill, K. S. Hewitson, T. D. Claridge, J. F. Seibel, L. E. Horsfall and C. J. Schofield, *Biochem. J.*, 2002, **367**, 571–575.
31. S. A. Dames, M. Martinez-Yamout, R. N. De Guzman, H. J. Dyson and P. E. Wright, *Proc. Natl. Acad. Sci. U.S.A.*, 2002, **99**, 5271–5276.
32. S. J. Freedman, Z.-Y. J. Sun, F. Poy, A. L. Kung, D. M. Livingston, G. Wagner and M. J. Eck, *Proc. Natl. Acad. Sci. U.S.A.*, 2002, **99**, 5367–5372.
33. C. E. Dann, III, R. K. Bruick and J. Deisenhofer, *Proc. Natl. Acad. Sci. U.S.A.*, 2002, **99**, 15351–15356.
34. C. Lee, S. J. Kim, D. G. Jeong, S. M. Lee and S. E. Ryu, *J. Biol. Chem.*, 2003, **278**, 7558–7563.
35. J. M. Elkins, K. S. Hewitson, L. A. McNeill, J. F. Seibel, I. Schlemminger, C. W. Pugh, P. J. Ratcliffe and C. J. Schofield, *J. Biol. Chem.*, 2003, **278**, 1802–1806.
36. C. J. Schofield and P. J. Ratcliffe, *Nat. Rev. Mol. Cell Biol.*, 2004, **5**, 343–354.
37. C. E. Dann, III and R. K. Bruick, *Biochem. Biophys. Res. Commun.*, 2005, **338**, 639–647.
38. N. S. Kenneth and S. Rocha, *Biochem. J.*, 2008, **414**, 19–29.
39. W. Ge, A. Wolf, T. Feng, C.-h. Ho, R. Sekirnik, A. Zayer, N. Granatino, M. E. Cockman, C. Loenarz, N. D. Loik, A. P. Hardy, T. D. W. Claridge, R. B. Hamed, R. Chowdhury, L. Gong, C. V. Robinson, D. C. Trudgian, M. Jiang, M. M. Mackeen, J. S. Mccullagh, Y. Gordiyenko, A. Thalhammer, A. Yamamoto, M. Yang, P. Liu-Yi, Z. Zhang, M. Schmidt-Zachmann, B. M. Kessler, P. J. Ratcliffe, G. M. Preston, M. L. Coleman and C. J. Schofield, *Nat. Chem. Biol.*, 2013, **8**, 960–962.
40. L. van Staalduinen, S. K. Novakowski and Z. Jia, *J. Mol. Biol.*, 2014, **426**, 1898–1910.
41. R. Chowdhury, R. Sekirnik, N. C. Brisset, T. Krojer, C.-h. Ho, S. S. Ng, I. J. Clifton, W. Ge, N. J. Kershaw, G. C. Fox, J. R. C. Muniz, M. Vollmar, C. Phillips, E. S. Pilka, K. L. Kavanagh, F. von Delft, U. Oppermann, M. A. McDonough, A. J. Doherty and C. J. Schofield, *Nature*, 2014, **510**, 422–426.
42. H. S. Kim, H. L. Kim, K. H. Kim, D. J. Kim, S. J. Lee, J. Y. Yoon, H. J. Yoon, H. Y. Lee, S. B. Park, S.-J. Kim, J. Y. Lee and S. W. Suh, *Nucleic Acids Res.*, 2010, **38**, 2099–2110.
43. R. S. Singleton, P. Liu-Yi, F. Formenti, W. Ge, R. Sekirnik, R. Fischer, J. Adam, P. J. Pollard, A. Wolf, A. Thalhammer, C. Loenarz, E. Flashman, A. Yamamoto, M. L. Coleman, B. M. Kessler, P. Wappner, C. J. Schofield, P. J. Ratcliffe and M. E. Cockman, *Proc. Natl. Acad. Sci. U.S.A.*, 2014, **111**, 4031–4036.
44. C. Loenarz, R. Sekirnik, A. Thalhammer, W. Ge, E. Spivakovsky, M. M. Mackeen, M. A. McDonough, M. E. Cockman, B. M. Kessler, P. J. Ratcliffe, A. Wolf and C. J. Schofield, *Proc. Natl. Acad. Sci. U.S.A.*, 2014, **111**, 4019–4024.

COR-AAD1-00002916
Bayer EX1008 (Part 6 of 9)

View Online

Published on 23 April 2015 on http://pubs.rsc.org | doi:10.1039/9781782621959-00001
Downloaded on 09/07/2016 13:50:17.

45. M. J. Katz, J. M. Acevedo, C. Loenarz, D. Galagovsky, P. Liu-Yi, M. Pérez-Pepe, A. Thalhammer, R. Sekirnik, W. Ge, M. Melani, M. G. Thomas, S. Simonetta, G. L. Boccaccio, C. J. Schofield, M. E. Cockman, P. J. Ratcliffe and P. Wappner, *Proc. Natl. Acad. Sci. U.S.A.*, 2014, **111**, 4025–4030.
46. C. J. Webby, A. Wolf, N. Gromak, M. Dreger, H. Kramer, B. Kessler, M. L. Nielsen, C. Schmitz, D. S. Butler, J. R. Yates, III, C. M. Delahunty, P. Hahn, A. Lengeling, M. Mann, N. J. Proudfoot, C. J. Schofield and A. Böttger, *Science*, 2009, **325**, 90–93.
47. M. Mantri, N. D. Loik, R. B. Hamed, T. D. W. Claridge, J. S. O. McCullagh and C. J. Schofield, *ChemBioChem*, 2011, **12**, 531–534.
48. B. Chang, Y. Chen, Y. Zhao and R. K. Bruick, *Science*, 2007, **318**, 444–447.
49. W. Liu, Q. Ma, K.-B. Wong, W. Li, K. Ohgi, J. Zhang, A. K. Aggarwal and M. G. Rosenfeld, *Cell*, 2013, **155**, 1581–1595.
50. M. Mantri, T. Krojer, E. A. Bagg, C. J. Webby, D. S. Butler, G. Kochan, K. L. Kavanagh, U. Oppermann, M. A. McDonough and C. J. Schofield, *J. Mol. Biol.*, 2010, **401**, 211–222.
51. X. Hong, J. Zang, J. White, C. Wang, C. H. Pan, R. Zhao, R. C. Murphy, S. Dai, P. Henson, J. W. Kappler, J. Hagman and G. Zhang, *Proc. Natl. Acad. Sci. U.S.A.*, 2010, **107**, 14568–14572.
52. T. Feng, A. Yamamoto, S. E. Wilkins, E. Sokolova, L. A. Yates, M. Münzel, P. Singh, R. J. Hopkinson, R. Fischer, M. E. Cockman, J. Shelley, D. C. Trudgian, J. Schödel, J. S. O. McCullagh, W. Ge, B. M. Kessler, R. J. Gilbert, L. Y. Frolova, E. Alkalaeva, P. J. Ratcliffe, C. J. Schofield and J. E. Coleman, *Mol. Cell*, 2014, **53**, 1–10.
53. J. Stenflo, E. Holme, S. Lindstedt, N. Chandramouli, L. H. T. Huang, J. P. Tam and R. B. Merrifield, *Proc. Natl. Acad. Sci. U.S.A.*, 1989, **86**, 444–447.
54. R. S. Gronke, W. J. VanDusen, V. M. Garsky, J. W. Jacobs, M. K. Sardana, A. M. Stern and P. A. Friedman, *Proc. Natl. Acad. Sci. U.S.A.*, 1989, **86**, 3609–3613.
55. J. E. Dinchuk, R. J. Focht, J. A. Kelley, N. L. Henderson, N. I. Zolotarjova, R. Wynn, N. T. Neff, J. Link, R. M. Huber, T. C. Burn, M. J. Rupar, M. R. Cunningham, B. H. Selling, J. Ma, A. A. Stern, G. F. Hollis, R. B. Stein and P. A. Friedman, *Proc. Natl. Acad. Sci. U.S.A.*, 2002, **277**, 12970–12977.
56. N. Ince, S. M. de la Monte and J. R. Wands, *Cancer Res.*, 2000, **60**, 1261–1266.
57. A. Ökesli, L. E. Cooper, E. J. Fogle and W. van der Donk, *J. Am. Chem. Soc.*, 2011, **133**, 13753–13760.
58. M. L. Coleman, M. A. McDonough, K. S. Hewitson, C. Coles, J. Mecinovic, M. Edelmann, K. M. Cook, M. E. Cockman, D. E. Lancaster, B. M. Kessler, R. J. Oldham, N. J. Ratcliffe and C. J. Schofield, *J. Biol. Chem.*, 2007, **282**, 24027–24038.
59. A. P. Hardy, I. Prokes, L. Kelly, I. D. Campbell and C. J. Schofield, *J. Mol. Biol.*, 2009, **392**, 994–1006.
60. M. Yang, W. Ge, R. Chowdhury, T. D. W. Claridge, H. B. Kramer, B. Schmierer, M. A. McDonough, L. Gong, B. M. Kessler, P. J. Ratcliffe, M. L. Coleman and C. J. Schofield, *J. Biol. Chem.*, 2011, **286**, 7648–7660.

COR-AAD1-00002917
Bayer EX1008 (Part 6 of 9)

View Online

Published on 23 April 2015 on http://pubs.rsc.org | doi:10.1039/9781782621959-00001
Downloaded on 09/07/2016 13:50:17.

61. M. Yang, R. Chowdhury, W. Ge, R. B. Hamed, M. A. McDonough, T. D. W. Claridge, B. M. Kessler, M. E. Cockman, P. J. Ratcliffe and C. J. Schofield, *FEBS J.*, 2011, **278**, 1086–1097.
62. K. Janke, U. Brockmeier, K. Kuhlmann, M. Eisenacher, J. Nolde, H. E. Meyer, H. Mairbäurl and E. Metzen, *J. Cell Sci.*, 2013, **126**, 2629–2640.
63. H. H. Qi, P. P. Ongusaha, J. Myllyharju, D. Cheng, O. Pakkanen, Y. Shi, S. W. Lee, J. Peng and Y. Shi, *Nature (London)*, 2008, **455**, 421–424.
64. A. Liu, R. Y. N. Ho, L. Que, Jr., M. J. Ryle, B. S. Phinney and R. P. Hausinger, *J. Am. Chem. Soc.*, 2001, **123**, 5126–5127.
65. R. Y. N. Ho, M. P. Mehn, E. L. Hegg, A. Liu, M. A. Ryle, R. P. Hausinger and L. Que, Jr., *J. Am. Chem. Soc.*, 2001, **123**, 5022–5029.
66. M. J. Ryle, A. Liu, R. B. Muthukumaran, R. Y. N. Ho, K. D. Koehntop, J. McCracken, L. Que, Jr. and R. P. Hausinger, *Biochemistry*, 2003, **42**, 1854–1862.
67. M. J. Ryle, K. D. Koehntop, A. Liu, L. Que, Jr. and R. P. Hausinger, *Proc. Natl. Acad. Sci. U.S.A.*, 2003, **100**, 3790–3795.
68. K. D. Koehntop, S. Marimanikkuppam, M. J. Ryle, R. P. Hausinger and L. Que, Jr., *J. Biol. Inorg. Chem.*, 2006, **11**, 63–72.
69. M. J. Ryle and R. P. Hausinger, *Curr. Opin. Chem. Biol.*, 2002, **6**, 193–201.
70. Y. Ge, B. G. Lawhorn, M. Elnaggar, S. K. Sze, T. P. Begley and F. W. McLafferty, *Protein Sci.*, 2003, **12**, 2320–2326.
71. M. Mantri, C. J. Webby, N. D. Loik, R. B. Hamed, M. L. Nielsen, M. A. McDonough, J. S. O. McCullagh, A. Böttger, C. J. Schofield and A. Wolf, *MedChemComm*, 2012, **3**, 80–85.
72. Y.-H. Chen, L. M. Comeaux, S. J. Eyles and M. J. Knapp, *Chem. Commun.*, 2008, 4768–4770.
73. T. F. Henshaw, M. Feig and R. P. Hausinger, *J. Inorg. Biochem.*, 2004, **98**, 856–861.
74. O. Sundheim, C. B. Vågbø, M. Bjørås, M. M. L. Sousa, V. Talstad, P. A. Aas, F. Drabløs, H. E. Krokan, J. A. Tainer and G. Slupphaug, *EMBO J.*, 2006, **25**, 3389–3397.
75. E. R. Farquhar, K. D. Koehntop, J. P. Emerson and L. Que, Jr., *Biochem. Biophys. Res. Commun.*, 2005, **338**, 230–239.
76. M. Mantri, Z. Zhang, M. A. McDonough and C. J. Schofield, *FEBS J.*, 2012, **279**, 1563–1575.
77. T. Jenuwein and C. D. Allis, *Science*, 2001, **293**, 1074–1080.
78. Y.-I. Tsukada, J. Fang, H. Erdjument-Bromage, M. E. Warren, C. H. Borchers, P. Tempst and Y. Zhang, *Nature*, 2006, **439**, 811–816.
79. K. Yamane, C. Toumazou, Y.-I. Tsukada, H. Erdjument-Bromage, P. Tempst, J. Wong and Y. Zhang, *Cell*, 2006, **125**, 1–13.
80. J. R. Whetstine, A. Nottke, F. Lan, M. Huart, S. Smolikov, Z. Chen, E. Spooner, E. Li, G. Zhang, M. Colaiacovo and Y. Shi, *Cell*, 2006, **125**, 467–481.
81. R. J. Klose, K. Yamane, Y. Bae, D. Zhang, H. Erdjument-Bromage, P. Tempst, J. Wong and Y. Zhang, *Nature*, 2006, **442**, 312–316.

COR-AAD1-00002918
Bayer EX1008 (Part 6 of 9)

View Online

Published on 23 April 2015 on http://pubs.rsc.org | doi:10.1039/9781782621959-00001
Downloaded on 09/07/2016 13:50:17.

82. P. A. C. Cloos, J. Christensen, K. Agger, A. Maiolica, J. Rappsilber, T. Antal, K. H. Hansen and K. Helin, *Nature*, 2006, **442**, 307–311.
83. Z. Chen, J. Zang, J. R. Whetstine, X. Hong, F. Davrazou, T. G. Kutateladze, M. Simpson, Q. Mao, C.-H. Pan, S. Dai, J. Hagman, K. Hansen, Y. Shi and G. Zhang, *Cell*, 2006, **125**, 691–702.
84. J.-F. Couture, E. Collazo, P. A. Ortiz-Tello, J. S. Brunzelle and R. C. Trievel, *Nat. Struct. Mol. Biol.*, 2007, **14**, 689–695.
85. S. S. Ng, K. L. Kavanagh, M. A. McDonough, D. Butler, E. S. Pilka, B. M. R. Lienard, J. E. Bray, P. Savitsky, O. Gileadi, F. von Delft, N. R. Rose, J. Offer, J. C. Scheinost, T. Borowski, M. Sundstrom, C. J. Schofield and U. Oppermann, *Nature*, 2007, **448**, 87–91.
86. Z. Chen, J. Zang, J. Kappler, X. Hong, F. Crawford, Q. Wang, F. Lan, C. Jiang, J. R. Whetstine, S. Dai, K. Hansen, Y. Shi and G. Zhang, *Proc. Natl. Acad. Sci. U.S.A.*, 2007, **104**, 10818–10823.
87. J. R. Horton, A. Upadhyay, H. H. Qi, Y. Shi and C. Xiaodong, *Nat. Struct. Mol. Biol.*, 2010, **17**, 38–43.
88. W. W. Yue, V. Hozjan, W. Ge, C. Loenarz, C. D. O. Cooper, C. J. Schofield, K. L. Kavanagh, U. Oppermann and M. A. McDonough, *FEBS Lett.*, 2010, **584**, 825–830.
89. Z. Cheng, P. Cheung, A. J. Kuo, E. T. Yukl, C. M. Wilmot, O. Gozani and D. J. Patel, *Genes Dev.*, 2014, **28**, 1758–1771.
90. C. Johansson, A. Tumber, K. Che, P. Cain, R. Nowak, C. Gileadi and U. Oppermann, *Epigenomics*, 2014, **6**, 89–120.
91. C. C. Thinnes, K. S. England, A. Kawamura, R. Chowdhury, C. J. Schofield and R. J. Hopkinson, *Biochim. Biophys. Acta,* 2014, **1839**, 1416–1432.
92. N. Mosammaparast and Y. Shi, *Annu. Rev. Biochem,* 2010, **79**, 155–179.
93. M.-M. Li, A. Nilsen, Y. Shi, M. Fusser, Y.-H. Ding, Y. Fu, B. Liu, Y. Niu, Y.-S. Wu, C.-M. Huang, M. Olofsson, K.-X. Jin, Y. Lv, X.-Z. Xu, C. He, M.-Q. Dong, J. M. R. Danielsen, A. Klungland and Y.-G. Yang, *Nat. Commun.*, 2013, **4**, 1832.
94. L. G. Bjørnstad, T. J. Meza, M. Otterlei, S. M. Olafsrud, L. A. Meza-Zepeda and P. Ø. Falnes, *PLoS One*, 2012, **7**, e49045.
95. S. C. Trewick, T. F. Henshaw, R. P. Hausinger, T. Lindahl and B. Sedgwick, *Nature*, 2002, **419**, 174–178.
96. P. Ø. Falnes, R. F. Johansen and E. Seeberg, *Nature*, 2002, **419**, 178–182.
97. P. A. Aas, M. Otterlei, P. Ø. Falnes, C. B. Vågbø, F. Skorpen, M. Akbari, O. Sundheim, M. Bjøras, G. Slupphaug, E. Seeberg and H. E. Krokan, *Nature*, 2003, **421**, 859–863.
98. J. C. Delaney and J. M. Essigmann, *Proc. Natl. Acad. Sci. U.S.A.*, 2004, **101**, 14051–14056.
99. P. Koivisto, P. Robins, T. Lindahl and B. Sedgwick, *J. Biol. Chem.*, 2004, **279**, 40470–40474.
100. D. Li, J. C. Delaney, C. M. Page, X. Yang, A. S. Chen, C. Wong, C. L. Drennan and J. M. Essigmann, *J. Am. Chem. Soc.*, 2012, **134**, 8896–8901.

COR-AAD1-00002919
Bayer EX1008 (Part 6 of 9)

View Online

101. D. Li, B. I. Fedeles, N. Shrivastav, J. C. Delaney, X. Yang, C. Wong, C. L. Drennan and J. M. Essigmann, *Chem. Res. Toxicol.*, 2013, **26**, 1182–1187.
102. B. Yu, W. C. Edstrom, Y. Hamuro, P. C. Weber, B. R. Gibney and J. F. Hunt, *Nature*, 2006, **439**, 879–884.
103. C.-G. Yang, C. Yi, E. M. Duguid, C. T. Sullivan, X. Jian, P. A. Rice and C. He, *Nature*, 2008, **452**, 961–965.
104. B. Yu and J. F. Hunt, *Proc. Natl. Acad. Sci. U.S.A.*, 2009, **106**, 14315–14320.
105. P. J. Holland and T. Hollis, *PLoS One*, 2010, **5**, e8680.
106. C. Yi, G. Jia, G. Hou, Q. Dai, W. Zhang, G. Zheng, X. Jian, C.-G. Yang, Q. Cui and C. He, *Nature*, 2010, **468**, 330–333.
107. E. Van den Born, A. Bekkelund, M. N. Moen, M. V. Omelchenko, A. Klungland and P. Ø. Falnes, *Nucleic Acids Res.*, 2009, **37**, 7124–7136.
108. E. van den Born, M. V. Omelchenko, A. Bekkelund, V. Leihne, E. V. Koonin, V. V. Dolja and P. Ø. Falnes, *Nucleic Acids Res.*, 2008, **36**, 5451–5456.
109. M. A. Kurowski, A. S. Bhagwat, G. Papaj and J. M. Bujnicki, *BMC Genomics*, 2003, **4**, 48.
110. L. Sanchez-Pulido and M. A. Andrade-Navarro, *BMC Biochem.*, 2007, **8**, 23.
111. D. Mielecki, D. L. Zugaj, A. Muszewska, J. Piwowarski, A. Chojnacka, M. Mielecki, J. Nieminuszczy, M. Grynberg and E. Grzesiuk, *PLoS One*, 2012, **7**, e30588.
112. T. Duncan, S. C. Trewick, P. Koivisto, P. A. Bates, T. Lindahl and B. Sedgwick, *Proc. Natl. Acad. Sci. U.S.A.*, 2002, **99**, 16660–16665.
113. J. Ringvoll, L. M. Nordstrand, C. B. Vågbø, V. Talstad, K. Reite, P. A. Aas, K. H. Lauritzen, N. B. Liabakk, A. Bjork, R. W. Doughty, P. Ø. Falnes, H. E. Krokan and A. Klungland, *EMBO J.*, 2006, **25**, 2189–2198.
114. L. Lu, C. Yi, X. Jian, G. Zheng and C. He, *Nucleic Acids Res.*, 2010, **38**, 4415–4425.
115. C. Yi, B. Chen, B. Qi, W. Zhang, G. Jia, C. J. Li, A. R. Diner, C.-G. Yang and C. He, *Nat. Struct. Mol. Biol.*, 2012, **19**, 671–676.
116. V. T. Monsen, O. Sundheim, P. A. Aas, M. P. Westbye, M. M. L. Sousa, G. Slupphaug and H. E. Krokan, *Nucleic Acids Res.*, 2010, **38**, 6447–6455.
117. M. P. Westbye, E. Feyzi, P. A. Aas, C. B. Vågbø, V. A. Talstad, B. Kavli, L. Hagen, O. Sundheim, M. Akbari, N.-B. Liabakk, G. Slupphaug, M. Otterlei and H. E. Krokan, *J. Biol. Chem.*, 2008, **283**, 25046–25056.
118. R. Ougland, D. Lando, I. Jonson, J. A. Dahl, M. N. Moen, L. M. Nordstrand, T. Rognes, J. T. Lee, A. Klungland, T. Kouzarides and E. Larsen, *Stem Cells*, 2012, **30**, 2672–2682.
119. T. A. Müller, K. Meek and R. P. Hausinger, *DNA Repair*, 2010, **9**, 58–65.
120. T. A. Müller, M. M. Andrzejak and R. P. Hausinger, *Biochem. J.*, 2013, **452**, 509–518.
121. G. Zheng, J. A. Dahl, Y. Niu, P. Fedorcsak, C.-H. Huang, C. J. Li, C. B. Vågbø, Y. Shi, W.-L. Wang, S.-H. Song, Z. Lu, R. P. G. Bosmans, Q. Dai, Y.-J. Hao, X. Yang, W.-M. Zhao, W.-M. Tong, X.-J. Wang, F. Bogdan, K. Furu, Y. Fu, G. Jia, X. Zhao, J. Liu, H. E. Krokan, A. Klungland, Y.-G. Yang and C. He, *Mol. Cell*, 2013, **49**, 18–29.

Published on 23 April 2015 on http://pubs.rsc.org | doi:10.1039/9781782621959-00001
Downloaded on 09/07/2016 13:50:17.

COR-AAD1-00002920
Bayer EX1008 (Part 6 of 9)

View Online

Published on 23 April 2015 on http://pubs.rsc.org | doi:10.1039/9781782621959-00001
Downloaded on 09/07/2016 13:50:17.

122. J.-M. Fustin, M. Doi, Y. Yamaguchi, H. Hida, S. Nishimura, M. Yoshida, T. Isagawa, M. S. Morioka, H. Kakeya, I. Manabe and H. Okamura, *Cell*, 2013, **155**, 793–806.
123. W. Aik, J. S. Scotti, H. Choi, L. Gong, M. Demetriades, C. J. Schofield and M. A. McDonough, *Nucleic Acids Res.*, 2014, **42**, 4741–4754.
124. C. Feng, Y. Liu, G. Wang, Z. Deng, Q. Zhang, W. Wu, Y. Tong, C. cheng and Z. Chen, *J. Biol. Chem.*, 2014, **289**, 11571–11583.
125. W. Chen, L. Zhang, G. Zheng, Y. Fu, Q. Ji, F. Liu, H. Chen and C. He, *FEBS Lett.*, 2014, **588**, 892–898.
126. G. Wang, Q. He, C. Feng, Y. Liu, Z. Deng, Z. Qi, W. Wu, P. Mei and Z. Chen, *J. Biol. Chem.*, **289**, 27924–27936.
127. J. Fischer, L. Koch, C. Emmerling, J. Vierkotten, T. Peters, J. C. Brüning and U. Rüther, *Nature*, 2009, **458**, 894–898.
128. T. Gerken, C. A. Girard, Y. C. Tung, C. J. Webby, V. Saudek, K. S. Hewitson, G. S. Yeo, M. A. McDonough, S. Cunliffe, L. A. McNeill, J. Galvanovskis, P. Rorsman, P. Robins, X. Prieur, A. P. Coll, M. Ma, Z. Jovanovic, I. S. Farooqi, B. Sedgwick, I. Barroso, T. Lindahl, C. P. Ponting, F. M. Ashcroft, S. O'Rahilly and C. J. Schofield, *Science*, 2007, **318**, 1469–1472.
129. G. Jia, C.-G. Yang, S. Yang, X. Jian, C. Yi, Z. Zhou and C. He, *FEBS Lett.*, 2008, **582**, 3313–3319.
130. G. Jia, Y. Fu, X. Zhao, Q. Dai, G. Zheng, Y. Yang, C. Yi, T. Lindahl, Y.-G. Yang and C. He, *Nat. Chem. Biol.*, 2011, 7, 885–887.
131. Y. Fu, G. Jia, X. Pang, R. N. Wang, X.-J. Wang, C. J. Li, S. Smemo, Q. Dai, K. A. Bailey, M. A. Nobrega, K.-L. Han, Q. Cui and C. He, *Nat. Commun.*, 2013, **4**, 1798.
132. Z. Han, T. Niu, J. Chang, X. Lei, M. Zhao, Q. Wang, W. Cheng, J. Wang, Y. Feng and J. Chai, *Nature*, 2010, **464**, 1205–1209.
133. W. Aik, M. Demetriades, M. K. K. Hamdan, E. A. L. Bagg, K. K. Yeoh, C. Lejeune, Z. Zhang, M. A. McDonough and C. J. Schofield, *J. Med. Chem.*, 2013, **56**, 3680–3688.
134. D. Fu, J. A. N. Brophy, C. T. Y. Chan, K. A. Atmore, U. Begley, R. S. Paules, P. C. Dedon, T. J. Begley and L. D. Samson, *Mol. Cell. Biol.*, 2010, **30**, 2449–2459.
135. Y. Fu, Q. Dai, W. Zhang, J. Ren, T. Pan and C. He, *Angew. Chem., Int. Ed.*, 2010, **49**, 8885–8888.
136. E. van den Born, C. B. Vågbø, L. Songe-Møller, V. Leihne, G. F. Lien, G. Leszczynska, A. Malkiewicz, H. E. Krokan, F. Kirpekar, A. Klungland and P. Ø. Falnes, *Nat. Commun.*, 2011, **2**, DOI: 10.1038/ncomms1173.
137. C. Pastore, I. Topalidou, F. Forouhar, A. C. Yan, M. Levy and J. F. Hunt, *J. Biol. Chem.*, 2012, **287**, 2130–2143.
138. D. Zdzalik, C. B. Vågbø, F. Kirpekar, E. Davydova, A. Puscian, A. M. Maciejewska, H. E. Krokan, A. Klungland, B. Tudek, E. van den Born and P. Ø. Falnes, *PLoS One*, 2014, **9**, e98729.
139. V. De Crécy-Lagard, C. Brochier-Armanet, J. Ubronavicius, B. Fernandez, G. Phillips, B. Lyons, A. Noma, S. Alvarez, L. Droogmans, J. Armengaud and H. Grosjean, *Mol. Biol. Evol.*, 2010, 27, 2062–2077.

COR-AAD1-00002921
Bayer EX1008 (Part 6 of 9)

View Online

140. M. Kato, Y. Araiso, A. Noma, A. Nagao, T. Suzuki, R. Ishitani and O. Nureki, *Nucleic Acids Res.*, 2010, **39**, 1576–1585.
141. M. Tahiliani, K. P. Koh, Y. Shen, W. A. Pastor, H. Bandukwala, Y. Brudno, S. Agarwal, L. M. Iyer, D. R. Liu, L. Aravind and A. Rao, *Science*, 2009, **324**, 930–935.
142. S. Ito, A. C. D'Alessio, O. V. Taranova, K. Hong, L. C. Sowers and Y. Zhang, *Nature*, 2010, **466**, 1129–1133.
143. T. Pfaffeneder, B. Hackner, M. Truß, M. Münzel, M. Müller, C. A. Deiml, C. Hagemeier and T. Carell, *Angew. Chem., Int. Ed.*, 2011, **50**, 7008–7012.
144. S. Ito, L. Shen, Q. Dai, S. C. Wu, L. B. Collins, J. A. Swenberg, C. He and Y. Zhang, *Science*, 2011, **333**, 1300–1303.
145. Y.-F. He, B.-Z. Li, Z. Li, P. Liu, Y. Wang, Q. Tang, J. Ding, Y. Jia, Z. Chen, L. Li, Y. Sun, X. Li, Q. Dai, C.-X. Song, K. Zhang, C. He and G.-L. Xu, *Science*, 2011, **333**, 1303–1307.
146. L. Zhang, W. Chen, L. M. Iyer, J. Hu, G. Wang, Y. Fu, M. Yu, Q. Dai, L. Aravind and C. He, *J. Am. Chem. Soc.*, 2014, **136**, 4801–4804.
147. T. Pfaffeneder, F. Spada, M. Wagner, C. Brandmayr, S. K. Laube, D. Eisen, M. Truss, J. Steinbacher, B. Hackner, O. Kotljarova, D. Schuermann, S. Michalakis, O. Kosmatchev, S. Schiesser, B. Steigenberger, N. Raddaoui, G. Kashiwazaki, U. Müller, C. G. Spruijt, M. Vermeulen, H. Leonhardt, P. Schär, M. Müller and T. Carell, *Nat. Chem. Biol.*, 2014, **10**, 574–581.
148. C.-H. Song and C. He, *TIBS*, 2013, **38**, 480–484.
149. C. J. Mariani, A. Vasanthakumar, J. Madzo, A. Yesilkanal, T. Bhagat, Y. Yu, S. Bhattacharyya, R. H. Wenger, S. L. Cohn, J. Nanduri, A. Verma, N. R. Prabhakar and L. A. Godley, *Cell Rep.*, 2014, 7, 1–10.
150. S. Schiesser, B. Hackner, T. Pfaffendeder, M. Müller, C. Hagemeier, M. Truss and T. Carell, *Angew. Chem., Int. Ed.*, 2012, **51**, 6516–6520.
151. L. Hu, Z. Li, J. Cheng, Q. Rao, W. Gong, M. Liu, Y. G. Shi, J. Zhu, P. Wang and Y. Xu, *Cell*, 2013, **155**, 1545–1555.
152. H. Hashimoto, J. E. Pais, X. Zhang, L. Saleh, Z.-Q. Fu, N. Dai, I. R. Corrèa, Jr., Y. Zheng and X. Cheng, *Nature*, 2014, **506**, 391–395.
153. Y.-C. Huang and A. Rao, *Trends Genet.*, 2014, **30**, 464–474.
154. L. Shen, C.-X. Song, C. He and Y. Zhang, *Annu. Rev. Biochem.*, 2014, **83**, 585–614.
155. P. Borst and R. Sabatini, *Annu. Rev. Microbiol.*, 2008, **62**, 235–251.
156. J. H. Gommers-Ampt, F. Van Leeuwen, A. L. de Beer, J. F. Vliegenthart, M. Dizdaroglu, J. A. Kowalak, P. F. Crain and P. Borst, *Cell*, 1993, **75**, 1129–1136.
157. J. H. Gommers-Ampt, A. J. Teixeira, G. van de Werken, W. J. van Dijk and P. Borst, *Nucleic Acids Res.*, 1993, **21**, 2039–2043.
158. F. van Leeuwen, R. Kieft, M. Cross and P. Borst, *Mol. Cell. Biol.*, 1998, **18**, 5643–5651.
159. M. Cross, R. Kieft, R. Sabatini, M. Wilm, M. de Kort, G. A. van der Marel, J. H. van Boom, F. van Leeuwen and P. Borst, *EMBO J.*, 1999, **18**, 6573–6581.

Published on 23 April 2015 on http://pubs.rsc.org | doi:10.1039/9781782621959-00001
Downloaded on 09/07/2016 13:50:17.

COR-AAD1-00002922
Bayer EX1008 (Part 6 of 9)

View Online

Published on 23 April 2015 on http://pubs.rsc.org | doi:10.1039/9781782621959-00001
Downloaded on 09/07/2016 13:50:17.

160. M. Cross, R. Kieft, R. Sabatini, A. Dirks-Mulder, I. Chaves and P. Borst, *Mol. Microbiol.*, 2002, **46**, 37–47.
161. Z. Yu, P. A. Genest, B. Ter Riet, K. Sweeney, C. DiPaolo, R. Kieft, E. Christodoulou, A. Perrakis, J. M. Simmons, R. P. Hausinger, H. G. Van Luenen, D. J. Rigden, R. Sabatini and P. Borst, *Nucleic Acids Res.*, 2007, **35**, 2107–2115.
162. L. M. Iyer, D. Zhang, R. F. de Souza, P. J. Pukkila, A. Rao and L. Aravind, *Proc. Natl. Acad. Sci. U.S.A.*, 2014, **111**, 1676–1683.
163. R. Kieft, V. Brand, D. K. Ekanayake, K. Sweeney, C. DiPaolo, W. S. Reznikoff and R. Sabatini, *Mol. Biochem. Parasitol.*, 2007, **156**, 24–31.
164. L. J. Cliffe, G. Hirsch, J. Wang, D. Ekanayake, W. Bullard, M. Hu, Y. Wang and R. Sabatini, *J. Biol. Chem.*, 2012, **287**, 19886–19895.
165. F. M. Vaz and R. J. A. Wanders, *Biochem. J.*, 2002, **361**, 417–429.
166. J. D. Hulse, S. R. Ellis and L. M. Henderson, *J. Biol. Chem.*, 1978, **253**, 1654–1659.
167. F. M. Vaz, R. Ofman, K. Westinga, J. W. Back and R. J. A. Wanders, *J. Biol. Chem.*, 2001, **276**, 33512–33517.
168. G. Lindstedt, S. Lindstedt, B. Olander and M. Tofft, *Biochim. Biophys. Acta*, 1968, **158**, 503–505.
169. G. Lindstedt, S. Lindstedt and I. Nordin, *Biochemistry*, 1977, **16**, 2181–2188.
170. A. Kondo, J. S. Blanchard and S. Englard, *Arch. Biochem. Biophys.*, 1981, **212**, 338–346.
171. A. M. Rydzik, I. K. H. Leung, G. T. Kochan, N. D. Loik, L. Henry, M. A. McDonough, T. D. W. Claridge and C. J. Schofield, *Organic and Biomolecular Chemistry*, 2014, **12**, 6354–6358.
172. K. Tars, J. Rumnieks, A. Zeltins, A. Kazaks, S. Kotelovica, A. Leonciks, J. Saripo, A. Viksna, J. Kuka, E. Liepinsh and M. Dambrova, *Biochem. Biophys. Res. Commun.*, 2010, **398**, 634–639.
173. I. K. H. Leung, T. J. Krojer, G. T. Kochan, L. Henry, F. von Delft, T. D. W. Claridge, U. Oppermann, M. A. McDonough and C. J. Schofield, *Chem. Biol.*, 2010, **17**, 1316–1324.
174. P. A. Watkins, A. E. Howard and S. J. Mihalik, *Biochim. Biophys. Acta*, 1994, **1214**, 288–294.
175. S. J. Mihalik, A. M. Rainville and P. A. Watkins, *Eur. J. Biochem.*, 1995, **232**, 545–551.
176. K. Croes, P. P. Van Veldhoven, G. P. Mannaerts and M. Casteels, *FEBS Lett.*, 1997, **407**, 197–200.
177. K. Croes, M. Casteels, S. Asselberghs, P. Herdewijn, G. P. Mannaerts and P. P. Van Veldhoven, *FEBS Lett.*, 1997, **412**, 643–645.
178. N. M. Verhoeven, D. S. M. Schor, H. J. ten Brink, R. J. A. Wanders and C. Jakobs, *Biochem. Biophys. Res. Commun.*, 1997, **237**, 33–36.
179. R. J. A. Wanders, J. Komen and S. Ferdinandusse, *Biochim. Biophys. Acta*, 2011, **1811**, 498–507.
180. G. A. Jansen, R. Ofman, S. Denis, S. Ferdinandusse, E. M. Hogenhout, C. Jakobs and R. J. A. Wanders, *J. Lipid Res.*, 1999, **40**, 2244–2254.

COR-AAD1-00002923
Bayer EX1008 (Part 6 of 9)

View Online

181. M. Mukherji, W. Chien, N. J. Kershaw, I. J. Clifton, C. J. Schofield, A. S. Wierzbicki and M. D. Lloyd, *Hum. Mol. Genet.*, 2001, **10**, 1971–1982.
182. M. A. McDonough, K. L. Kavanagh, D. Butler, T. Searls, U. Oppermann and C. J. Schofield, *J. Biol. Chem.*, 2005, **280**, 41101–41110.
183. N. González-Silva, I. López-Lara, R. Reyes-Lamothe, A. M. Taylor, D. Sumpton, J. Thomas-Oates and O. Geiger, *Biochemistry*, 2011, **50**, 6396–6408.
184. H. S. Gibbons, S. Lin, R. J. Cotter and C. R. H. Raetz, *J. Biol. Chem.*, 2000, **275**, 32940–32949.
185. H. S. Gibbons, C. M. Reynolds, Z. Guan and C. R. H. Raetz, *Biochemistry*, 2008, **47**, 2814–2825.
186. H. S. Chung and C. R. H. Raetz, *Proc. Natl. Acad. Sci. U.S.A.*, 2011, **108**, 510–515.
187. Y. Kawai, E. Ono and M. Mizutani, *Plant J.*, 2014, **78**, 328–343.
188. B. A. Bohm, *Introduction to Flavonoids*, Harwood Academic Publishers, Amsterdam, The Netherlands, 1998.
189. L. Le Marchand, *Biomed. Pharmacother.*, 2002, **56**, 296–301.
190. L. Britsch, *Arch. Biochem. Biophys.*, 1990, **282**, 152–160.
191. L. Britsch and H. Grisebach, *Eur. J. Biochem.*, 1986, **156**, 569–577.
192. R. C. Wilmouth, J. J. Turnbull, R. W. D. Welford, I. J. Clifton, A. G. Prescott and C. J. Schofield, *Structure*, 2002, **10**, 93–103.
193. F. Wellman, R. Lukacin, T. Moriguchi, L. Britsch, E. Schiltz and U. Matern, *Eur. J. Biochem.*, 2002, **269**, 4134–4142.
194. K. Saito, M. Kobayashi, Z. Gong, Y. Tanaka and M. Yamazaki, *Plant J.*, 1999, **17**, 181–189.
195. R. W. D. Welford, I. J. Clifton, J. J. Turnbull, S. C. Wilson and C. J. Schofield, *Org. Biomol. Chem.*, 2005, **3**, 3117–3126.
196. M. Frey, K. Huber, W. J. Park, D. Sicker, P. Lindberg, R. B. Meeley, C. R. Simmons, N. Yalpani and A. Gierl, *Phytochemistry*, 2003, **62**, 371–376.
197. M. Frey, K. Schullehner, R. Dick, A. Feiesselmann and A. Gierl, *Phytochemistry*, 2009, **70**, 1645–1651.
198. D. Anzellotti and R. K. Ibrahim, *Arch. Biochem. Biophys.*, 2000, **382**, 161–172.
199. D. Anzellotti and R. K. Ibrahim, *BMC Plant Biol.*, 2004, **4**, 20.
200. A. Berim and D. R. Gang, *J. Biol. Chem.*, 2013, **288**, 1795–1805.
201. A.-X. Cheng, X.-J. Han, Y.-F. Wu and H.-X. Lou, *Int. J. Mol. Sci.*, 2014, **15**, 1080–1095.
202. P. Hedden and S. G. Thomas, *Biochem. J.*, 2012, **444**, 11–25.
203. T. Lange, A. Schweimer, D. A. Ward, P. Hedden and J. E. Graebe, *Planta*, 1994, **195**, 98–107.
204. T. Lange, *Planta*, 1994, **195**, 108–115.
205. T. Lange, P. Hedden and J. E. Graebe, *Proc. Natl. Acad. Sci. U.S.A.*, 1994, **91**, 8552–8556.
206. J. L. Ward, P. Gaskin, R. G. S. Brown, G. S. Jackson, P. Hedden, A. L. Phillips, C. L. Willis and M. H. Beale, *J. Chem. Soc., Perkin Trans.*, 2002, **1**, 232–241.
207. J. Williams, A. L. Phillips, P. Gaskin and P. Hedden, *Plant Physiol.*, 1998, **117**, 559–563.

Published on 23 April 2015 on http://pubs.rsc.org | doi:10.1039/9781782621959-00001
Downloaded on 09/07/2016 13:50:17.

COR-AAD1-00002924
Bayer EX1008 (Part 6 of 9)

View Online

Published on 23 April 2015 on http://pubs.rsc.org | doi:10.1039/9781782621959-00001
Downloaded on 09/07/2016 13:50:17.

208. S. G. Thomas, A. L. Phillips and P. Hedden, *Proc. Natl. Acad. Sci. U.S.A.*, 1999, **96**, 4698–4703.
209. P. Hedden and A. L. Phillips, *Trends Plant Sci.*, 2000, **5**, 523–528.
210. A. Bhattacharya, S. Kourmpetli, D. A. Ward, S. G. Thomas, F. Gong, S. J. Powers, E. Carrera, B. Taylor, F. N. de Caceres Gonzalez, B. Tudzynski, A. L. Phillips, M. R. Davey and P. Hedden, *Plant Physiol.*, 2012, **160**, 837–845.
211. T. Hashimoto and Y. Yamada, *Eur. J. Biochem.*, 1987, **164**, 277–285.
212. T. Hashimoto, J. Matsuda and Y. Yamada, *FEBS Lett.*, 1993, **329**, 35–39.
213. E. De Carolis, F. Chan, J. Balsevich and V. De Luca, *Plant Physiol.*, 1990, **94**, 1323–1329.
214. E. De Carolis and V. De Luca, *J. Biol. Chem.*, 1993, **268**, 5504–5511.
215. J. M. Hagel and P. J. Facchini, *Nat. Chem. Biol.*, 2010, **6**, 273–275.
216. S. C. Farrow and P. J. Facchini, *J. Biol. Chem.*, 2013, **288**, 28997–29012.
217. J. Havermann, D. Vogel, B. Loll and U. Keller, *Chem. Biol.*, 2014, **21**, 146–155.
218. H. Nakanishi, H. Yamaguchi, T. Sasakuma, N. K. Nishizawa and S. Mori, *Plant Mol. Biol.*, 2000, **44**, 199–207.
219. K. Kai, M. Mizutani, N. Kawamura, R. Yamamoto, M. Tamai, H. Yamaguchi, K. Sakata and B.-I. Shimizum, *Plant J.*, 2008, **55**, 989–999.
220. S. Matsumoto, M. Mizutani, K. Sakata and B.-I. Shimizu, *Phytochemistry*, 2012, **74**, 49–57.
221. G. Vialart, A. Hehn, A. Olry, K. Ito, C. Krieger, R. Larbat, C. Paris, B. Shimizu, Y. Sugimoto, M. Mizutani and F. Bourgaud, *Plant J.*, 2012, **70**, 460–470.
222. N. Agerbirk and C. E. Olsen, *Phytochemistry*, 2012, **77**, 16–45.
223. D. J. Kliebenstein, V. M. Lambrix, M. Reichelt, J. Gershenzon and T. Mitchell-Olds, *Plant Cell*, 2001, **13**, 681–693.
224. Z. Zhao, Y. Zhang, X. Liu, X. Zhang, S. Liu, X. Yu, Y. Ren, X. Zheng, K. Zhou, L. Jiang, X. Guo, Y. Gai, C. Wu, H. Zhai, H. Wang and J. Wan, *Dev. Cell*, 2013, **27**, 113–122.
225. K. Zhang, R. Halitschke, C. Yin, C.-J. Liu and S.-S. Gan, *Proc. Natl. Acad. Sci. U.S.A.*, 2013, **110**, 14807–14812.
226. J. E. Baldwin, R. A. Field, C. C. Lawrence, K. D. Merritt and C. J. Schofield, *Tetrahedron Lett.*, 1993, **34**, 7489–7492.
227. C. C. Lawrence, W. J. Sobey, R. A. Field, J. E. Baldwin and C. J. Schofield, *Biochem. J.*, 1996, **313**, 185–191.
228. T. Shibasaki, H. Mori, S. Chiba and A. Ozaki, *Appl. Environ. Microbiol.*, 1999, **65**, 4028–4031.
229. L. Petersen, R. Olewinski, P. Salmon and N. Conners, *Appl. Microbiol. Biotechnol.*, 2003, **62**, 263–267.
230. R. Hara and K. Kino, *Biochem. Biophys. Res. Commun.*, 2009, **379**, 882–886.
231. R. Hara, N. Uchiumi and K. Kino, *J. Biotechnol.*, 2014, **172**, 55–58.
232. H. Mori, T. Shibasaki, Y. Uozaki, K. Ochiai and A. Ozaki, *Appl. Environ. Microbiol.*, 1996, **62**, 1903–1907.

COR-AAD1-00002925
Bayer EX1008 (Part 6 of 9)

View Online

233. H. Mori, T. Shibasaki, K. Yano and A. Ozaki, *J. Bacteriol.*, 1997, **179**, 5677–5683.
234. I. J. Clifton, L.-C. Hsueh, J. E. Baldwin, K. Harlos and C. J. Schofield, *Eur. J. Biochem.*, 2001, **268**, 6625–6636.
235. M. Strieker, F. Kopp, C. Mahlert, L.-O. Essen and M. A. Marahiel, *ACS Chem. Biol.*, 2007, **2**, 187–196.
236. M. Strieker, L.-O. Essen, C. T. Walsh and M. A. Marahiel, *ChemBioChem*, 2008, **9**, 374–376.
237. G. M. Singh, P. D. Fortin, A. Koglin and C. T. Walsh, *Biochemistry*, 2008, **47**, 11310–11320.
238. X. Yin and T. M. Zabriskie, *ChemBioChem*, 2004, **5**, 1274–1277.
239. V. Helmetag, S. A. Samel, M. G. Thomas, M. A. Marahiel and L.-O. Essen, *FEBS J.*, 2009, **276**, 3669–3682.
240. B. Haltli, Y. Tan, N. A. Magarvey, M. Wagenaar, X. Yin, M. Greenstein, J. A. Hucul and T. M. Zabriskie, *Chem. Biol.*, 2005, **12**, 1163–1168.
241. C. Haefelè, C. Bonfils and Y. Sauvaire, *Phytochemistry*, 1997, **44**, 563–566.
242. S. V. Smirnov, T. Kodera, N. N. Samonova, V. A. Kotlyarova, N. Y. Rushkevich, A. D. Kivero, P. M. Sokolov, M. Hibi, J. Ogawa and B. Shimizu, *Appl. Microbiol. Biotechnol.*, 2010, **88**, 719–726.
243. M. Hibi, T. Kawashima, T. Kodera, S. V. Smirnov, P. M. Sokolov, M. Sugiyama, S. Shimizu, K. Yokozeki and J. Ogawa, *Appl. Environ. Microbiol.*, 2011, **77**, 6926–6930.
244. S. V. Smirnov, P. M. Sokolov, V. A. Kotlyarova, N. N. Samsonova, T. Kodera, M. Sugiyama, T. Torii, M. Hibi, S. Shimizu, K. Yokozeki and J. Ogawa, *MicrobiologyOpen*, 2013, **2**, 471–478.
245. S. V. Smirnov, P. M. Sokolov, M. Kodera, M. Sugiyama, M. Hibi, S. Shimizu, K. Yokozeki and J. Ogawa, *FEMS Microbiol. Lett.*, 2012, **331**, 97–104.
246. M. Hibi, T. Kawashima, P. M. Sokolov, S. V. Smirnov, M. Kodera, M. Sugiyama, S. Shimizu, K. Yokozeki and J. Ogawa, *Appl. Microbiol. Biotechnol.*, 2013, **97**, 2467–2472.
247. H.-M. Qin, T. Miyakawa, M. Z. Jia, A. Nakamura, J. Ohtsuka, Y.-L. Xue, T. Kawashima, T. Kasahara, M. Hibi, J. Ogawa and M. Tanokura, *PLoS One*, 2013, **8**, e63996.
248. H.-M. Qin, T. Miyakawa, A. Nakamura, M. Hibi, J. Ogawa and M. Tanokura, *Biochem. Biophys. Res. Commun.*, 2014, **450**, 1458–1461.
249. E. J. Drake and A. M. Gulick, *J. Mol. Biol.*, 2008, **384**, 193–205.
250. J. Bursy, A. J. Pierik, N. Pica and E. Bremer, *J. Biol. Chem.*, 2007, **282**, 31147–31155.
251. N. Widderich, A. Höppner, M. Pittlekow, J. Heider, S. H. J. Smits and E. Bremer, *PLoS One*, 2014, **9**, e93809.
252. K. Reuter, M. Pittelkow, J. Bursy, A. Heine, T. Craan and E. Bremer, *PLoS One*, 2010, **5**, e10647.
253. N. Widderich, M. Pittlekow, A. Höppner, D. Mulnaes, W. Buckel, H. Gohlke, S. H. J. Smits and E. Bremer, *J. Mol. Biol.*, 2014, **426**, 586–600.

Published on 23 April 2015 on http://pubs.rsc.org | doi:10.1039/9781782621959-00001
Downloaded on 09/07/2016 13:50:17.

COR-AAD1-00002926
Bayer EX1008 (Part 6 of 9)

View Online

Published on 23 April 2015 on http://pubs.rsc.org | doi:10.1039/9781782621959-00001
Downloaded on 09/07/2016 13:50:17.

254. H. Fukuda, T. Ogawa, M. Tazaki, K. Nagahama, T. Fujii, S. Tanase and Y. Morino, *Biochem. Biophys. Res. Commun.*, 1992, **188**, 483–489.
255. D. Meng, L. Shen, R. Yang, X. Zhang and J. Sheng, *Biochim. Biophys. Acta*, 2014, **1840**, 120–128.
256. J.-P. Wang, L.-X. Wu, F. Xu, J. Lv, H.-J. Jin and S.-F. Chen, *Bioresour. Technol.*, 2010, **101**, 6404–6409.
257. F. Guerrero, V. Carbonell, M. Cossu, D. Correddu and P. R. Jones, *PLoS One*, 2012, 7, e50470.
258. J. Ungerer, L. Tao, M. Davis, M. Ghirardi, P.-C. Maness and J. Yu, *Energy Environ. Sci.*, 2012, **5**, 8998–9006.
259. M. T. Abbott, E. K. Schandl, R. F. Lee, T. S. Parker and R. J. Midgett, *Biochim. Biophys. Acta*, 1967, **132**, 525–528.
260. E. Holme, G. Lindstedt, S. Lindstedt and M. Tofft, *Biochim. Biophys. Acta*, 1970, **212**, 50–57.
261. E. Holme, G. Lindstedt, S. Lindstedt and M. Tofft, *J. Biol. Chem.*, 1971, **246**, 3314–3319.
262. C. K. Liu, C. A. Hsu and M. T. Abbott, *Arch. Biochem. Biophys.*, 1973, **159**, 180–187.
263. B. J. Warn-Cramer, L. A. Macrander and M. T. Abbott, *J. Biol. Chem.*, 1983, **258**, 10551–10557.
264. L. D. Thornburg, M.-T. Lai, J. S. Wishnok and J. Stubbe, *Biochemistry*, 1993, **32**, 14023–14033.
265. J. W. Neidigh, A. Darwanto, A. A. Williams, N. R. Wall and L. C. Sowers, *Chem. Res. Toxicol.*, 2009, 22, 885–893.
266. A. Cultrone, C. Scazzocchio, M. Rochet, G. Montero-Morán, C. Drevet and R. Fernández-Martín, *Mol. Microbiol.*, 2005, **57**, 276–290.
267. G. M. Montero-Moràn, M. Li, E. Rendóm-Huerta, F. Jourdan, D. J. Lowe, A. W. Stumpff-Kane, M. Feig, C. Scazzocchio and R. P. Hausinger, *Biochemistry*, 2007, **46**, 5293–5304.
268. M. Li, T. A. Müller, B. A. Fraser and R. P. Hausinger, *Arch. Biochem. Biophys.*, 2008, **470**, 44–53.
269. L. Bankel, G. Lindstedt and S. Lindstedt, *J. Biol. Chem.*, 1972, **247**, 6128–6134.
270. L. M. Wondrack, C. A. Hsu and M. T. Abbott, *J. Biol. Chem.*, 1978, **253**, 6511–6515.
271. J. Stubbe, *J. Biol. Chem.*, 1985, **260**, 9972–9975.
272. Z. Yang, X. Chi, M. Funabashi, S. Baba, K. Nonaka, P. Pahari, J. Unrine, J. M. Jacobsen, G. I. Elliott, J. Rohr and S. G. Van Lanen, *J. Biol. Chem.*, 2011, **286**, 7885–7892.
273. C. Zhao, T. Huang, W. Chen and Z. Deng, *Appl. Environ. Microbiol.*, 2010, **76**, 7343–7347.
274. R. P. Hausinger, F. Fukumori, D. A. Hogan, T. M. Sassanella, Y. Kamagata, H. Takami and R. E. Saari, in *Microbial Diversity and Genetics of Biodegradation*, ed. K. Horikoshi, M. Fukuda and T. Kudo, Japan Scientific Press, Tokyo, 1997, pp. 35–51.
275. F. Fukumori and R. P. Hausinger, *J. Bacteriol.*, 1993, **175**, 2083–2086.

COR-AAD1-00002927
Bayer EX1008 (Part 6 of 9)

View Online

276. F. Fukumori and R. P. Hausinger, *J. Biol. Chem.*, 1993, **268**, 24311–24317.
277. E. L. Hegg, A. K. Whiting, R. E. Saari, J. McCracken, R. P. Hausinger and L. Que, Jr., *Biochemistry*, 1999, **38**, 16714–16726.
278. S. L. Griffin, J. A. Godbey, T. J. Oman, S. K. Embrey, A. Karnoup, K. Kuppannan, B. W. Barnett, G. Lin, N. V. J. Harpham, A. N. Juba, B. W. Schafer and R. M. Cicchillo, *J. Agric. Food Chem.*, 2013, **61**, 6589–6596.
279. K. Nickel, M. J.-F. Suter and H.-P. E. Kohler, *J. Bacteriol.*, 1997, **179**, 6674–6679.
280. T. A. Müller, M. I. Zavodszky, M. Feig, L. A. Kuhn and R. P. Hausinger, *Protein Sci.*, 2006, **15**, 1356–1368.
281. J. M. Bollinger, Jr., J. C. Price, L. M. Hoffart, E. W. Barr and C. Krebs, *Eur. J. Inorg. Chem.*, 2005, 4245–4254.
282. E. Eichhorn, J. R. van der Ploeg, M. A. Kertesz and T. Leisinger, *J. Biol. Chem.*, 1997, 272, 23031–23036.
283. J. M. Elkins, M. J. Ryle, I. J. Clifton, J. C. Dunning Hotopp, J. S. Lloyd, N. I. Burzlaff, J. E. Baldwin, R. P. Hausinger and P. L. Roach, *Biochemistry*, 2002, **41**, 5185–5192.
284. J. R. O'Brien, D. J. Schuller, V. S. Yang, B. D. Dillard and W. N. Lanzilotta, *Biochemistry*, 2003, **42**, 5547–5554.
285. S. H. Knauer, O. Hartl-Spiegelhauer, S. Schwarzinger, P. Hänzelmann and H. Dobbek, *FEBS J.*, 2012, **279**, 816–831.
286. M. J. Ryle, R. Padmakumar and R. P. Hausinger, *Biochemistry*, 1999, **38**, 15278–15286.
287. R. B. Muthakumaran, P. K. Grzyska, R. P. Hausinger and J. McCracken, *Biochemistry*, 2007, **46**, 5951–5959.
288. J. C. Price, E. W. Barr, B. Tirupati, J. M. Bollinger, Jr. and C. Krebs, *Biochemistry*, 2003, **42**, 7497–7508.
289. P. J. Riggs-Gelasco, J. C. Price, R. B. Guyer, J. H. Brehm, E. W. Barr, J. M. Bollinger, Jr. and C. Krebs, *J. Am. Chem. Soc.*, 2004, **126**, 8108–8109.
290. D. A. Proshlyakov, T. F. Henshaw, G. R. Monterosso, M. J. Ryle and R. P. Hausinger, *J. Am. Chem. Soc.*, 2004, **126**, 1022–1023.
291. P. K. Grzyska, M. J. Ryle, G. R. Monterosso, J. Liu, D. P. Ballou and R. P. Hausinger, *Biochemistry*, 2005, **44**, 3845–3855.
292. D. A. Hogan, T. A. Auchtung and R. P. Hausinger, *J. Bacteriol.*, 1999, **181**, 5876–5879.
293. A. Kahnert and M. A. Kertesz, *J. Biol. Chem.*, 2000, **275**, 31661–31667.
294. K. M. Sogi, Z. J. Gartner, M. A. Breidenbach, M. J. Appel, M. W. Schelle and C. R. Bertozzi, *PLoS One*, 2013, **8**, e65080.
295. I. Müller, A. Kahnert, T. Pape, G. M. Sheldrick, W. Meyer-Klaucke, T. Dierks, M. Kertesz and I. Usòn, *Biochemistry*, 2004, **43**, 3075–3088.
296. I. Müller, C. Stückl, J. Wakeley, M. Kertesz and I. Usòn, *J. Biol. Chem.*, 2004, **280**, 5716–5723.
297. F. R. McSorley, P. B. Wyatt, A. Martinez, E. F. DeLong, B. Hove-Jensen and D. L. Zechel, *J. Am. Chem. Soc.*, 2012, **134**, 8364–8367.
298. B. T. Circello, A. C. Eliot, J.-H. Lee, W. A. van der Donk and W. W. Metcalf, *Chem. Biol.*, 2010, **17**, 402–411.

Published on 23 April 2015 on http://pubs.rsc.org | doi:10.1039/9781782621959-00001
Downloaded on 09/07/2016 13:50:17.

COR-AAD1-00002928
Bayer EX1008 (Part 6 of 9)

View Online

Published on 23 April 2015 on http://pubs.rsc.org | doi:10.1039/9781782621959-00001
Downloaded on 09/07/2016 13:50:17.

299. M. A. DeSieno, W. van der Donk and H. Zhao, *Chem. Commun.*, 2011, **47**, 10025–10027.
300. M. Watanabe, N. Sumida, S. Murakami, H. Anzai, C. J. Thompson, Y. Tateno and T. Murakami, *Appl. Environ. Microbiol.*, 1999, **65**, 1036–1044.
301. D. J. Bougioukou, S. Mukherjee and W. A. van der Donk, *Proc. Natl. Acad. Sci. U.S.A.*, 2013, **110**, 10952–10957.
302. A. K. White and W. W. Metcalf, *J. Biol. Chem.*, 2002, **277**, 38262–38271.
303. N. J. Kershaw, M. E. C. Caines, M. C. Sleeman and C. J. Schofield, *Chem. Commun.*, 2005, 4251–4263.
304. R. W. Busby, M. D.-T. Chang, R. C. Busby, J. Wimp and C. A. Townsend, *J. Biol. Chem.*, 1995, **270**, 4262–4269.
305. E. G. Pavel, J. Zhou, R. W. Busby, M. Gunsior, C. A. Townsend and E. I. Solomon, *J. Am. Chem. Soc.*, 1998, **120**, 743–753.
306. J. Zhou, W. L. Kelly, B. O. Bachmann, M. Gunsior, C. A. Townsend and E. I. Solomon, *J. Am. Chem. Soc.*, 2001, **123**, 7388–7398.
307. Z. Zhang, J. Ren, D. K. Stammers, J. E. Baldwin, K. Harlos and C. J. Schofield, *Nat. Struct. Biol.*, 2000, **7**, 127–133.
308. Z. Zhang, J.-s. Ren, K. Harlos, C. H. McKinnon, I. J. Clifton and C. J. Schofield, *FEBS Lett.*, 2002, **517**, 7–12.
309. S. Kovacevic, B. J. Weigel, M. B. Tobin, T. D. Ingolia and J. R. Miller, *J. Bacteriol.*, 1989, **171**, 754–760.
310. J. E. Dotzlaf and W.-K. Yeh, *J. Biol. Chem.*, 1989, **264**, 10219–10227.
311. B. J. Baker, J. E. Dotzlaf and W.-K. Yeh, *J. Biol. Chem.*, 1991, **266**, 5087–5093.
312. J. E. Dotzlaf and W.-K. Yeh, *J. Bacteriol.*, 1987, **169**, 1611–1618.
313. J. E. Baldwin, R. M. Adlington, J. B. Coates, M. J. C. Crabbe, N. P. Crouch, J. W. Keeping, G. C. Knight, C. J. Schofield, H.-H. Ting, C. A. Vallejo, M. Thorniley and E. P. Abraham, *Biochem. J.*, 1987, **245**, 831–841.
314. K. Valegård, A. C. Terwisscha van Scheltinga, M. D. Lloyd, T. Hara, S. Ramaswamy, A. Perrakis, A. Thompson, W.-J. Lee, J. E. Baldwin, C. J. Schofield, J. Hajdu and I. Andersson, *Nature (London)*, 1998, **394**, 805–809.
315. M. D. Lloyd, H.-J. Lee, K. Harlos, Z.-H. Zhang, J. E. Baldwin, C. J. Schofield, J. M. Charnock, C. D. Garner, T. Hara, A. C. Terwisscha Van Scheltinga, K. Valegård, J. A. C. Viklund, J. Hajdu, I. Andersson, A. Danielsson and R. Bhikhabhai, *J. Mol. Biol.*, 1999, **287**, 943–960.
316. H. J. Lee, M. D. Lloyde, I. J. Clifton, J. E. Baldwin and C. J. Schofield, *J. Mol. Biol.*, 2001, **308**, 937–948.
317. H.-J. Lee, M. D. Lloyd, I. J. Clifton, K. Harlos, A. Dubus, J. Baldwin, E., J.-M. Frere and C. J. Schofield, *J. Biol. Chem.*, 2001, **276**, 18290–18295.
318. K. Valegård, A. C. Terwisscha van Scheltinga, A. Dubus, G. Ranghino, L. M. Öster, J. Hajdu and I. Andersson, *Nat. Struct. Mol. Biol.*, 2004, **11**, 95–101.
319. L. M. Öster, A. C. Terwisscha van Scheltinga, K. Valegård, A. M. Hose, A. Dubus, J. Hajdu and I. Andersson, *J. Mol. Biol.*, 2004, **343**, 157–171.

COR-AAD1-00002929
Bayer EX1008 (Part 6 of 9)

View Online

320. H. Tarhonskaya, A. Szöllössi, I. K. H. Leung, J. T. Bush, L. Henry, R. Chowdhury, A. Iqbal, T. D. W. Claridge, C. J. Schofield and E. Flashman, *Biochemistry*, 2014, **53**, 2483–2493.
321. M. D. Lloyd, S. J. Lipscomb, K. S. Hewitson, C. M. H. Hensgens, J. E. Baldwin and C. J. Schofield, *J. Biol. Chem.*, 2004, **297**, 1540–1546.
322. X. Xiao, S. Wolfe and A. L. Demain, *Biochem. J.*, 1991, **280**, 471–474.
323. R. M. Phelan and C. A. Townsend, *J. Am. Chem. Soc.*, 2013, **135**, 7496–7502.
324. I. J. Clifton, L. X. Doan, M. C. Sleeman, M. Topf, H. Suzuki, R. C. Wilmouth and C. J. Schofield, *J. Biol. Chem.*, 2003, **278**, 20843–20850.
325. W.-c Chang, Y. Guo, C. Wang, S. E. Butch, A. C. Rosenzweig, A. K. Boal, C. Krebs and J. M. Bollinger, Jr., *Science*, 2014, **343**, 1140–1144.
326. Z. You, S. Omura, H. Ikeda and D. E. Cane, *J. Am. Chem. Soc.*, 2006, **126**, 6566–6567.
327. Z. You, S. Omura, H. Ikeda, D. E. Cane and G. Jogl, *J. Biol. Chem.*, 2007, **282**, 36552–36560.
328. M.-J. Seo, D. Zhu, S. Endo, H. Ikeda and D. E. Cane, *Biochemistry*, 2011, **50**, 1739–1754.
329. Y. Ono, A. Minami, M. Noike, Y. Higuchi, T. Toyoumasu, T. Sassa, N. Kato and T. Diari, *J. Am. Chem. Soc.*, 2011, **133**, 2548–2555.
330. M. Daum, H.-J. Schnell, S. Herrman, A. Günther, R. Murillo, R. Müller, P. Bisel, M. Müller and A. Bechthold, *ChemBioChem*, 2010, **11**, 1383–1391.
331. C. Dürr, H.-J. Schnell, A. Luzhetskyy, R. Murillo, M. Weber, K. Wetzel, A. Vente and A. Bechthold, *Chem. Biol.*, 2006, **13**, 365–377.
332. F. H. Vaillancourt, J. Yin and C. T. Walsh, *Proc. Natl. Acad. Sci. U.S.A.*, 2005, **102**, 10111–10116.
333. F. H. Vaillancourt, D. A. Vosburg and C. T. Walsh, *ChemBioChem*, 2006, 7, 748–752.
334. M. L. Matthews, W.-c. Chang, A. P. Layne, L. A. Miles, C. Krebs and J. M. Bollinger, Jr., *Nat. Chem. Biol.*, 2014, **10**, 299–315.
335. L. C. Blasiak, F. H. Vaillancourt, C. T. Walsh and C. L. Drennan, *Nature*, 2006, **440**, 368–371.
336. M. M. Matthews, C. Krest, E. W. Barr, F. Vaillancourt, C. T. Walsh, M. Green, C. Krebs and J. M. Bollinger, Jr., *Biochemistry*, 2009, **48**, 4331–4343.
337. M. L. Matthews, C. S. Neumann, L. A. Miles, T. L. Grove, S. J. Booker, C. Krebs, C. T. Walsh and J. M. Bollinger, Jr., *Proc. Natl. Acad. Sci. U.S.A.*, 2009, **106**, 17723–17728.
338. M. R. Fullone, A. Paiardini, R. Miele, S. Marsango, D. C. Gross, S. Omura, E. Ros-Herrera, M. C. Bonaccorsi di Patt, A. Laganà, S. Pacarella and I. Grgurina, *FEBS J.*, 2012, **279**, 4269–4282.
339. D. P. Galonić, E. W. Barr, C. T. Walsh, J. M. Bollinger, Jr. and C. Krebs, *Nat. Chem. Biol.*, 2007, **3**, 113–116.
340. D. G. Fujimori, E. W. Barr, M. L. Matthews, G. M. Koch, J. R. Yonce, C. T. Walsh, J. M. Bollinger, Jr., C. Krebs and P. J. Riggs-Gelasco, *J. Am. Chem. Soc.*, 2007, **129**, 13408–13409.

Published on 23 April 2015 on http://pubs.rsc.org | doi:10.1039/9781782621959-00001
Downloaded on 09/07/2016 13:50:17.

COR-AAD1-00002930
Bayer EX1008 (Part 6 of 9)

View Online

Published on 23 April 2015 on http://pubs.rsc.org | doi:10.1039/9781782621959-00001
Downloaded on 09/07/2016 13:50:17.

341. C. Wong, D. G. Fujimori, C. T. Walsh and C. L. Drennan, *J. Am. Chem. Soc.*, 2009, **131**, 4872–4879.
342. D. P. Galonić, F. H. Vaillancourt and C. T. Walsh, *J. Am. Chem. Soc.*, 2006, **128**, 3900–3901.
343. F. H. Vaillancourt, E. Yeh, D. A. Vosburg, S. E. O'Conner and C. T. Walsh, *Nature*, 2005, **436**, 1191–1194.
344. C. S. Neumann and C. T. Walsh, *J. Am. Chem. Soc.*, 2008, **130**, 14022–14023.
345. L. Gu, B. Wang, A. Kulkarni, T. W. Geders, R. V. Grindberg, L. Gerwick, K. Håkansson, P. Wipf, J. L. Smith, W. H. Gerwick and D. H. Sherman, *Nature*, 2009, **459**, 731–735.
346. D. Khare, B. Wang, L. Gu, J. Razelun, D. H. Sherman, W. H. Gerwick, K. Håkansson and J. L. Smith, *Proc. Natl. Acad. Sci. U.S.A.*, 2010, **107**, 14099–14104.
347. W. Jiang, J. R. Heemstra, Jr., R. R. Forseth, C. S. Neumann, S. Manaviazar, F. C. Schroeder, K. J. Hale and C. T. Walsh, *Biochemistry*, 2011, **50**, 6063–6072.
348. S. M. Pratter, J. Ivkovic, R. Birner-Gruenberger, R. Breinbauer, K. Zangger and G. D. Straganz, *ChemBioChem*, 2014, **15**, 567–574.
349. S. M. Pratter, K. M. Light, E. I. Solomon and G. D. Straganz, *Biochemistry*, 2014, **136**, 9385–9395.
350. U. Galm, E. Wendt-Pienkowski, L. Wang, X.-X. Huang, C. Unsin, M. Tao, J. M. Coughlin and B. Shen, *J. Nat. Prod.*, 2011, **74**, 526–536.
351. A. S. Eustáquio, J. E. Janso, A. S. Ratnayake, C. J. O'Donnell and F. E. Koehn, *Proc. Natl. Acad. Sci. U.S.A.*, 2014, **111**, E3376–E3385.
352. M. Tao, L. Wang, E. Wendt-Pienkowski, N. Zhang, D. Yang, U. Galm, J. M. Coughlin, Z. Xu and B. Shen, *Mol. Biosyst.*, 2010, **6**, 349–356.
353. J.-A. Seo, R. H. Proctor and R. D. Plattner, *Fungal Genet. Biol.*, 2001, **34**, 155–165.
354. Y. Ding, R. S. Bojja and L. Du, *Appl. Environ. Microbiol.*, 2004, **70**, 1931–1934.
355. N. Steffan, A. Grundmann, S. Afiyatullov, H. Ruan and S.-M. Li, *Org. Biomol. Chem.*, 2009, **7**, 4082–4087.
356. R. Mazmouz, F. Chapuis-Hugon, V. Pichon, A. Méjean and O. Ploux, *ChemBioChem*, 2011, **12**, 858–862.
357. K. H. Almabruk, S. Asamizu, A. Chang, S. G. Varghese and T. Mahmud, *ChemBioChem*, 2012, **13**, 2209–2211.
358. P. L. Roach, I. J. Clifton, V. Fülöp, K. Harlos, G. J. Barton, J. Hajdu, K. Andersson, C. J. Schofield and J. E. Baldwin, *Nature (London)*, 1995, **375**, 700–704.
359. P. L. Roach, I. J. Clifton, C. M. H. Hensgens, N. Shibata, C. J. Schofield, J. Hajdu and J. E. Baldwin, *Nature (London)*, 1997, **387**, 827–830.
360. N. I. Burzlaff, P. J. Rutledge, I. J. Clifton, C. M. H. Hensgens, M. Pickford, R. M. Adlington, P. L. Roach and J. E. Baldwin, *Nature*, 1999, **401**, 721–724.
361. P. John, *Physiol. Plant.*, 1997, **100**, 583–592.
362. D. R. Dilley, Z. Wang, D. K. Dadirjan-Kalbach, F. Ververidis, R. Beaudry and K. Padmanabhan, *AoB Plants*, 2013, **5**, plt031.

COR-AAD1-00002931
Bayer EX1008 (Part 6 of 9)

View Online

363. A. M. Rocklin, D. L. Tierney, V. Kofman, N. M. W. Brunhuber, B. M. Hoffman, R. E. Christoffersen, N. O. Reich, J. D. Lipscomb and L. Que, Jr., *Proc. Natl. Acad. Sci. U.S.A.*, 1999, **96**, 7905–7090.
364. D. L. Tierney, A. M. Rocklin, J. D. Lipscomb, L. Que, Jr. and B. Hoffman, *J. Am. Chem. Soc.*, 2005, **127**, 7005–7013.
365. A. M. Rocklin, K. Kato, H.-w. Liu, L. Que, Jr. and J. D. Lipscomb, *J. Biol. Inorg. Chem.*, 2004, **9**, 171–182.
366. J. Zhou, A. M. Rocklin, J. D. Lipscomb, L. Que, Jr. and E. I. Solomon, *J. Am. Chem. Soc.*, 2002, **124**, 4602–4609.
367. J. N. Barlow, Z. Zhang, P. John, J. E. Baldwin and C. J. Schofield, *Biochemistry*, 1997, **36**, 3563–3569.
368. Z. Zhang, J. N. Barlow, J. E. Baldwin and C. J. Schofield, *Biochemistry*, 1997, **36**, 15999–16007.
369. Z. Zhang, J.-S. Ren, I. J. Clifton and C. J. Schofield, *Chem. Biol.*, 2004, **11**, 1383–1394.
370. L. Brisson, N. El Bakkali-Taheri, M. Giorgi, A. Fadel, J. Kaizer, M. Réglier, T. Tron, E. H. Ajandouz and A. J. Simaan, *J. Biol. Inorg. Chem.*, 2012, **17**, 939–949.
371. P. He and G. R. Moran, *Curr. Opin. Chem. Biol.*, 2009, **13**, 443–450.
372. D. D. Shah, J. A. Conrad and G. R. Moran, *Biochemistry*, 2013, **52**, 6097–6107.
373. M. Gunsior, J. Ravel, G. L. Challis and C. A. Townsend, *Biochemistry*, 2004, **43**, 663–674.
374. K. Johnson-Winters, V. M. Purpero, M. Kavana and G. R. Moran, *Biochemistry*, 2005, **44**, 7189–7199.
375. P. He, J. A. Conrad and G. R. Moran, *Biochemistry*, 2010, **49**, 1998–2007.
376. J. Brownlee, P. He, G. R. Moran and D. H. T. Harrison, *Biochemistry*, 2008, **47**, 20002–22013.
377. L. Serre, A. Sailland, D. Sy, P. Boudec, A. Rolland, E. Pebay-Peyroula and C. Cohen-Addad, *Structure*, 1999, **7**, 977–988.
378. J. Pan, M. Bharwaj, J. R. Faulkner, P. Nagabhyru, N. D. Charlton, R. M. Higashi, A.-F. Miller, C. A. Young, R. B. Grossman and C. L. Schardl, *Phytochemistry*, 2014, **98**, 60–68.
379. J. S. Scotti, I. K. H. Leung, M. A. Bentley, J. Paps, H. B. Kramer, J. Lee, W. Aik, H. Choi, S. M. Paulsen, L. A. H. Bowman, N. D. Loik, S. Horita, C.-h. Ho, N. J. Kershaw, C. M. Tang, T. D. W. Claridge, G. M. Preston, M. A. McDonough and C. J. Schofield, *Proc. Natl. Acad. Sci. U.S.A.*, 2014, **111**, 13331–13336.
380. B.-I. Shimizu, *Front. Plant Sci.*, 2014, **5**, 549.
381. M. L. Hillig and X. Liu, *Nature Chem. Biol.*, 2014, **10**, 921–923.

Published on 23 April 2015 on http://pubs.rsc.org | doi:10.1039/9781782621959-00001
Downloaded on 09/07/2016 13:50:17.

COR-AAD1-00002932
Bayer EX1008 (Part 6 of 9)

Engineering in Life Sciences

www.els-journal.com

Sabine Leibeling[1]
Marten B. Maeß[1]
Florian Centler[1]
Sabine Kleinsteuber[1]
Martin von Bergen[2]
Martin Thullner[1]
Hauke Harms[1]
Roland H. Müller[1]

[1] Department of Environmental Microbiology, UFZ—Helmholtz Centre for Environmental Research, Leipzig, Germany

[2] Department of Proteomics and Department of Metabolomics, UFZ—Helmholtz Centre for Environmental Research, Leipzig, Germany

Research Article

Posttranslational oxidative modification of (*R*)-2-(2,4-dichlorophenoxy)propionate/ α-ketoglutarate-dependent dioxygenases (RdpA) leads to improved degradation of 2,4-dichlorophenoxyacetate (2,4-D)

Microbial activities and the versatility gained through adaptation to xenobiotic compounds are the main biological forces to counteract environmental pollution. The current results present a new adaptive mechanism that is mediated through posttranslational modifications. Strains of *Delftia acidovorans* incapable of growing autochthonously on 2,4-dichlorophenoxyacetate (2,4-D) were cultivated in a chemostat on 2,4-D in the presence of (*R*)-2-(2,4-dichlorophenoxy)propionate. Long-term cultivation led to enhanced 2,4-D degradation, as demonstrated by improved values of the Michaelis–Menten constant K_m for 2,4-D and the catalytic efficiency k_{cat}/K_m of the initial degradative key enzyme (*R*)-2-(2,4-dichlorophenoxy)propionate/ α-ketoglutarate-dependent dioxygenases (RdpA). Analyses of the *rdpA* gene did not reveal any mutations, indicating a nongenetic mechanism of adaptation. 2-DE of enzyme preparations, however, showed a series of RdpA forms varying in their p*I*. During adaptation increased numbers of RdpA variants were observed. Subsequent immunoassays of the RdpA variants showed a specific reaction with 2,4-dinitrophenylhydrazine (DNPH), characteristic of carbonylation modifications. Together these results indicate that posttranslational carbonylation modified the substrate specificity of RdpA. A model was implemented explaining the segregation of clones with improved degradative activity within the chemostat. The process described is capable of quickly responding to environmental conditions by reversibly adapting the degradative potential to various phenoxyalkanoate herbicides.

Keywords: 2,4-Dichlorophenoxyacetate (2,4-D) / (R)-2-(2,4-Dichlorophenoxy)propionate / α-ketoglutarate-dependent dioxygenases (RdpA) / Individual-based modeling / Post-translational carbonylation

Additional supporting information may be found in the online version of this article at the publisher's web-site

Received: July 3, 2012; *revised:* September 26, 2012; *accepted:* October 22, 2012

DOI: 10.1002/elsc.201100093

Correspondence: Dr. Roland H. Müller (r.mueller@ufz.de), Department of Environmental Microbiology, UFZ—Helmholtz Centre for Environmental Research, Leipzig, Germany.

Abbreviations: (*R*)-2,4-DP/(*S*)-2,4-DP, (*R*)/(*S*)-2-(2,4-dichlorophenoxy)propionate; 2,4-D, 2,4-dichlorophenoxyacetate; DNPH, 2,4-dinitrophenylhydrazine; K_m, Michaelis–Menten constant (substrate concentration at which the reaction rate is half its maximum value); k_{cat}, turnover number; MM, minimal medium; RdpA, (*R*)-2-(2,4-dichlorophenoxy)propionate/α-ketoglutarate-dependent dioxygenases; SdpA, (*S*)-2-(2,4-dichlorophenoxy)propionate/ α-ketoglutarate-dependent dioxygenases; ROS, reactive oxygen species

1 Introduction

Phenoxyalkanoates such as 2,4-dichlorophenoxyacetate (2,4-D), (4-chloro-2-methylphenoxy)acetate (MCPA), (*RS*)-2-(2,4-dichlorophenoxy)propionate (2,4-DP, dichlorprop), and (*RS*)-2-(4-chloro-2-methylphenoxy)propionate (mecoprop) have

Current address: Marten B. Maeß, Institute of Nutrition, Friedrich Schiller University Jena, Dornburger Str. 25, D-07743, Jena, Germany.

© 2013 WILEY-VCH Verlag GmbH & Co. KGaA, Weinheim

COR-AAD1-00002933
Bayer EX1008 (Part 6 of 9)

been applied as herbicides for about 80 years. Despite their xenobiotic character, they are degraded readily by microorganisms. In most cases, degradation is initiated by cleavage of the ether bond by α-ketoglutarate-dependent dioxygenases showing pronounced substrate specificity. Whereas phenoxyacetates are cleaved predominantly by 2,4-D/α-ketoglutarate dioxygenases (TfdA) [1, 2], degradation of the chiral 2-phenoxypropionates requires two enzymes with opposite enantiospecific characteristics [3–8]. (*R*)-2-(2,4-dichlorophenoxy)propionate/α-ketoglutarate-dependent dioxygenases (RdpA), which attacks the R-enantiomers of 2-phenoxypropionates, is identical in the primary amino acid sequence in *Delftia acidovorans* MC1, *Sphingobium herbicidovorans* MH, and *Rhodoferax* sp. P230, as follows from the *rdpA* gene sequences [9]. Nevertheless, significant differences in the kinetic parameters of RdpA synthesized in these three strains and upon heterologous expression in *E. coli* [10] were found, based on strain-dependent K_m (Michaelis–Menten constant) values for 4-chloro-2-methylphenoxyacetate and 2,4-D. The K_m values of RdpA synthesized in *Rhodoferax* sp. P230 were 2–5 times lower for all phenoxyalkanoates than those of RdpA derived from the other two strains. Moreover, the K_m values of strain P230 for phenoxyacetates were more similar to those for (*R*)-phenoxypropionates [10]. These differences correlated with the appearance of multiple forms of RdpA, resulting from posttranslational modification, which became visible after separation in 2D gels [10, 11].

Starting from these discoveries, the present investigation was aimed at provoking changes in RdpA that would improve the degradation of 2,4-D. Derivative strains of *D. acidovorans* MC1 (strains MC1071 and MC1073) were exposed to 2,4-D while growing chemostatically on (*R*)-2,4-DP. These mutants possess the *rdpA* gene, but are incapable of growing on 2,4-D because they lack *sdpA*, the gene encoding the relatively unspecific (*S*)-2-(2,4-dichlorophenoxy)propionate/α-ketoglutarate-dependent dioxygenases (SdpA), and *tfdA*. It was of particular interest to see whether specificity shifts of RdpA were due to genetic changes or phenotypic modification. The utilization of both substrates was followed during long-term chemostat runs. At several points in time, the kinetic characteristics of RdpA were determined, enzyme variants were visualized by 2-DE, and the *rdpA* genes of individual clones and bulk samples of the chemostat population were sequenced. The plausibility of the resulting interpretation, where long-term adaptation of a population results from the selection of cells that have acquired favorable enzyme variants, was tested by individual-based modeling.

2 Materials and methods

2.1 Organisms and cultivation

Delftia acidovorans MC1071 and MC1073 are derivatives of *D. acidovorans* MC1 [3]. They were originally identified as deviating morphotypes during growth on agar plates with (*R*)-2,4-DP as the sole growth substrate derived from a common ancestor strain deficient in SdpA activity. They grew on (*R*)-2,4-DP with rates between 0.18 h^{-1} and 0.205 h^{-1}. Both strains are incapable of growth on 2,4-D since they possess neither *sdpA* nor *tfdA*. The strains were stored and grown as described previously [11] using (*R*)-2,4-DP as the sole carbon and energy source. (*R*)-2,4-DP (Duplosan® (BASF)) had a purity of 95.6% after purification by precipitation and ether extraction in our laboratory. The cells were used to inoculate a fermenter after complete degradation of two pulses of about 1 mM (*R*)-2,4-DP. Occasionally, 2.5 g fructose L^{-1} was used as a nonherbicide growth substrate. Heterologous anaerobic expression of *rdpA* in *E. coli* Rosetta 1 (Novagen, Madison, USA) was carried out in a glove box under a 95% nitrogen/5% hydrogen atmosphere. The suspension was incubated in completely filled centrifuge tubes tightly capped and covered by parafilm to exclude atmospheric oxygen [11]. Cells were lysed by bead-beating immediately or stored under nitrogen at –20°C before further use.

2.2 Continuous cultivation and 2,4-D adaptation

Bacteria were continuously cultivated in an INFORS T4700CT laboratory fermenter (INFORS HT, Bottmingen, Switzerland) at a working volume of 1.5 l at 30°C and pH 7.5 ± 0.1; the pH was kept constant by automatic titration of 1 N HCl and 1 N NaOH. The aeration rate was set to 0.1 m^3 h^{-1}, the stirrer speed was 700 rpm, and dissolved oxygen in the suspension was ≥50% of air saturation. Cultivation was started in fed-batch mode by dosing (*R*)-2,4-DP at a rate too low to result in the accumulation of the metabolite 2,4-dichlorophenol, as verified by HPLC during the monitoring of (*R*)-2,4-DP degradation. The detection limits ranged from 0.5–1 mg L^{-1} for the analyzed compounds. When the utilization of (*R*)-2,4-DP was stable, the fermenter regime was switched to continuous cultivation by gradually increasing the dilution rate to 0.05 h^{-1}. This was achieved by feeding the medium via two separate streams of minimal medium (MM stock) and herbicide solution (herbicide stock) contributing 2/3 and 1/3 of the total volumetric flow, respectively. The MM stock contained (in mg L^{-1}): NH_4Cl, 760; KH_2PO_4, 340; K_2HPO_4, 485; $CaCl_2 \times 6\ H_2O$, 27; $MgSO_4 \times 7\ H_2O$, 71.2. The concentration of (*R*)-2,4-DP in the herbicide stock was 8.4 mM dissolved in 18 mM NaOH. In addition, a separate solution of trace elements from a stock solution of pH 2.0 was supplied at 1/1000 of the total volumetric rate. The trace elements solution contained (in mg L^{-1}): $FeSO_4 \times 7\ H_2O$, 4.98; $CuSO_4 \times 5\ H_2O$, 0.785; $MnSO_4 \times 4\ H_2O$, 0.81; $ZnSO_4 \times 7\ H_2O$, 0.44; $Na_2MoO_4 \times 2\ H_2O$, 0.25. After steady state was reached, the feed was switched to a herbicide stock solution containing 8.4 mM (*R*)-2,4-DP and 3 mM 2,4-D. Degradation and growth were followed by monitoring the stationary concentrations of the herbicides by HPLC and biomass via the OD_{700} [12]. Alternatively, chemostats were started up with 16.7 mM (*R*)-2,4-DP in the herbicide stock and when steady state was reached, they were shifted to 16.7 mM (*R*)-2,4-DP and 6 mM 2,4-D. Adaptation experiments were repeated several times. An intermittent backshift experiment was also conducted with strain MC1071. An advanced 2,4-D adaptation experiment as described above was interrupted by transient feeding of 2.5 g pyruvate L^{-1} as the sole substrate for about three generations followed by a backshift to (*R*)-2,4-DP as the only substrate for 7 days and a second prolonged period of 2,4-D adaptation.

© 2013 WILEY-VCH Verlag GmbH & Co. KGaA, Weinheim

COR-AAD1-00002934
Bayer EX1008 (Part 6 of 9)

2.3 Tracking ^{14}C uptake and incorporation into biomass

We used uniformly ring-labeled ^{14}C-2,4-D (Sigma-Aldrich) with a specific radioactivity of 5.17 mCi $mmol^{-1}$. Pulse labeling was conducted by washing in 10 mL MM solution containing 2.8 mM (*R*)-2,4-DP and 1 mM 2,4-D supplemented with ^{14}C-labeled 2,4-D to yield a specific activity of 7.64×10^5 Bq $mmol^{-1}$, without interrupting the continuous cultivation on a substrate mixture of the above-mentioned proportion. After the wash-in, the cultivation was continued by feeding nonlabeled substrate as before. Samples of 25 mL were taken from the fermenter during 1 h. Biomass was separated immediately by centrifugation, the supernatants were collected and the pellets washed two times with MM solution. The pellets were solubilized in 6 mL of Filter Count scintillation cocktail (Perkin Elmer, Boston, USA) for measuring the radiolabel in biomass; 0.5 mL of supernatant were added to 5.5 mL of the same scintillation cocktail to determine the radiolabel in the fermentation broth.

For uptake experiments biomass was obtained from the fermenter effluent, collected on ice, washed and concentrated in mineral salts medium at pH 7.5 containing 100 mM sodium carbonate/bicarbonate. A 0.99 mL suspension (containing about 0.2 mg dry mass mL^{-1}) was incubated at 30°C in an open tube with shaking for 2 min. The experiment was started by adding 10 μL of labeled 2,4-D to receive a final concentration of 250 μM. Five samples were taken in duplicate at intervals of 10 s and the cells were immediately separated from the medium by filtration through cellulose nitrate membranes (25 mm, pore width 0.2 μM; Schleicher & Schüll, Dassel, Germany), prewetted with the respective buffer containing 100 μM nonlabeled 2,4-D. The membranes were flushed three times with 1 mL quantities of the respective buffer, containing 100-μM nonlabeled 2,4-D, and transferred into scintillation vials. These contained 6 mL of Filter Count solution (Perkin Elmer).

Liquid scintillation counting was performed in a Tri-Carb 2300 RT (Packard). Calculation of the incorporation of ^{14}C-carbon was based on the mean of five individual samples.

2.4 Preparation and analysis of cell extracts

Fermenter effluent was collected in ice-cooled vials and separated by centrifugation (3500 × *g*, room temperature, 30–45 min, Varifuge 3.0). For biochemical analyses, cells were disintegrated by five passages through a precooled French pressure cell (American Instrument Company, Silver Spring, MD, USA) at 11 000 psi in 10 mM Tris/HCl-buffer, pH 7.5. Cell-free supernatant was obtained by centrifugation at 23 000 × *g* and 4°C for 10 min (Hermle Z383K). For proteomic analyses cell extracts were prepared by SDS lysis [11]. Samples for whole cell experiments were taken from the fermenter, washed and resuspended in MM solution for immediate use. *E. coli* Rosetta cells were disintegrated in a ball mill [11] after pretreatment with 1 mg lysozyme mL^{-1} for 30 min on ice. After removal of cell debris the extract was treated with 10 μL DNase mL^{-1} (5 mg mL^{-1} in 10 mM Tris/HCl buffer pH 8.0, containing 250 mM $MgCl_2$, 20 mM $CaCl_2$) and the solution was incubated for 30 min at room temperature under anoxic conditions. The protein extract obtained this way was subjected to affinity chromatography using a 10 mL Strep-Tactin Sepharose column (IBA GmbH, Göttingen, Germany). Protein was quantified according to Lowry et al. [13].

2.5 Measurement of enzyme activity in whole cells and cell-free extracts

The degradation activity of whole cells was determined by measuring the amount of herbicide degraded within a timeframe sufficient to allow maximum degradation. Cells from the fermenter were incubated at initial OD_{700} of 0.05, 0.1, or 0.2 in Erlenmeyer flasks containing MM solution. Individual phenoxyalkanoates were added at concentrations of 0.5 mM and the flasks incubated under oxic conditions on a rotary shaker at 30°C. Growth and degradation were followed by determination of OD_{700} and HPLC analysis of the remaining herbicide concentration at up to eight times during an incubation period of 24 h, with shorter intervals in the beginning. RdpA activity of cell-free extracts and purified enzyme was determined by a colorimetric assay detecting the liberation of 2,4-dichlorophenol, which is the traceable product liberated in this reaction [7, 10]]. Various herbicide concentrations were tested. GraphPad Prism software (www.graphpad.com/prism) was used to determine the catalytic parameters K_m, calculated by nonlinear regression, the catalytic efficiency (k_{cat}/K_m) and the quotient Q_{ce} of the catalytic efficiency with 2,4-D divided by the catalytic efficiency with (*R*)-2,4-DP. Since the latter represents the core activity of the enzyme, Q_{ce} is considered as a way to normalize the catalytic efficiency displaying the relative RdpA activity with both substrates at any given sample point. Q_{ce} is thus used to validate the adaptation. Since k_{cat}/K_m (min^{-1} μM^{-1}) can only be determined for purified enzymes the catalytic efficiency of cell-free extracts was specified as V_{max}/K_m. Activities were given as μM min^{-1} (mg protein)$^{-1}$ in enzyme assays and as μM min^{-1} (mg dry mass)$^{-1}$ in whole cell assays.

2.6 Purification of RdpA

RdpA from *D. acidovorans* MC1073 was partially purified by precipitation with protamine sulfate and ammonium sulfate followed by ion exchange chromatography as described elsewhere [10]. For heterologous synthesis RdpA was expressed in *E. coli* Rosetta™(DE3)pLysS (Novagene). The strain was grown on LB-medium containing 100 μg ampicillin mL^{-1}. The induction of enzyme synthesis was achieved by adding 200 μg anhydrotetracycline hydrochloride L^{-1} after the culture had reached an OD_{600} of 0.5. After 3 h the cells were harvested by centrifugation (4°C, 5000 × *g*, 15 min). Strep-tag extended RdpA obtained after expression in *E. coli* was purified by affinity chromatography on a Strep-Tactin column following the instructions of the supplier (IBA GmbH, Göttingen, Germany). Enzyme preparations were concentrated by ultrafiltration using Vivaspin 30 tubes (Vivascience, Stonehouse, UK).

© 2013 WILEY-VCH Verlag GmbH & Co. KGaA, Weinheim

COR-AAD1-00002935
Bayer EX1008 (Part 6 of 9)

2.7 Sample preparation for 2-DE and Western blot analysis

2D-PAGE followed a standard protocol [14]. Cell extracts were purified by phenol extraction [11, 15]. Isoelectric separation was performed on 7 cm Immobiline™ DryStrips™ pH 4–7 or pH 3–10NL (GE Healthcare) and replicated with individual extracts more than once. For the second dimension a 12% polyacrylamide gel was used. After separation at 25 mA, proteins were stained overnight by colloidal Coomassie Brilliant Blue G-250 [16] or transferred onto PVDF (Immobilon-P transfer membrane, pore size 0.45 μm, Millipore, Bedford, MA, USA). To detect carbonylated amino acid side chains, the protein samples were subjected to a reaction with 2,4-dinitrophenylhydrazine (DNPH) [17], leading to the formation of hydrazones that were then detected using monoclonal antibodies [11, 18]. In brief, protein preparations of 200 μg (400 μg) were resolubilized (10 min, 60°C, 1400 rpm) in 20 μL (40 μL) sample buffer containing 2% w/v SDS, derivatized with 20 μL (40 μL) DNPH (Fluka) solution (20 mM DNPH in 10% v/v TFA) for 30 min at room temperature, and processed as described earlier [11]. Appropriate controls without application of DNPH or primary antibodies revealed no positive signals in areas where RdpA is located.

2.8 Determination of p*I* of protein spots

Delta 2D software (version 3.3, Decodon, Greifswald, Germany) allowed matching spots of identical p*I* from different gels with its warping tool and thus bringing spot patterns into congruency [19]. This served to compare spot patterns obtained at different sampling times or from different experiments. p*I* values of RdpA spots were inferred from their relative positions to proteins with known p*I* on the same 2D gels (Supporting Information Table S1) [14]. p*I* values of the proteins used as reference were obtained from a database (NCBInr, National Center for Biotechnology Information, Rockville Pike, USA). To this end, 100 μg purified RdpA from strain MC1073 were admixed to 300 μg crude extract of strain MC1100. MC1100 is devoid of RdpA and provided the reference proteins for comparison of p*I* values with those of RdpA variants. As reference proteins, dominant spots were used that were distributed over the p*I* range of RdpA variants, but did not form multiple spots. They were identified by MALDI-MS after trypsin digestion as described earlier [20]. Reference proteins determined in MC1100 were also identified in crude extracts of MC1071. Based on p*I* values of reference proteins, a calibration line was established for each gel (Supporting Information Fig. S1). Spot positions were acquired using ImageJ 1.43t (Wayne Rasband, National Institute of Health, USA, http://rsb.info.nih.gov/ij).

2.9 Quantification of relative protein contents of spots

Purified RdpA of MC1073 admixed to crude extracts of strain MC1100 and crude extracts of MC1071 (backshift experiment) were subjected to protein quantification. Relative spot intensities were measured after normalization of the 2D gels using Delta 2D software. Normalization followed a common procedure and compensated for artifacts due to the sample treatment [19]. On each gel, the same section covering all RdpA spots was chosen for analysis and set to a total spot quantity of one. Within that section individual spot volumes were computed proportionally and given as relative spot intensities. Relative spot and carbonylation intensities of RdpA variants were expressed relative to the most dominant RdpA spot, which was thus set to 100%.

2.10 DNA extraction, PCR, and sequencing

The *rdpA* gene of *D. acidovorans* MC1 was cloned and transformed into *E. coli* previously [10] and used accordingly. DNA was extracted from *E. coli* and *D. acidovorans* cells using the NucleoSpin kit (Macherey Nagel, Düren, Germany) or by applying the Ultra Clean™ kit (Mo Bio Laboratories Inc., Carlsbad, CA, USA) according to the protocols of the suppliers. PCR amplification of the *rdpA* gene was performed with the Taq PCR Master Mix (Qiagen, Hilden, Germany) in reactions containing 6.25 μL master mix, 3.25 μL H_2O, 5 pmol of each primer f1 (5′-ATGCATGCTGCACTGTCCCC-3′) and r1 (5′-CTAGCGCGCCGGGCGCAC-3′), and 1 μL template DNA. The following cycling protocol was used: 94°C (45 s), 30 cycles with each 45 s at 94°C, 30 s at 64°C, 120 s at 72°C, and a final elongation step at 72°C for 6 min. Thereafter the samples were cooled to 4°C. The PCR products were checked by electrophoresis on 1.5% w/v agarose gels. The PCR products were purified using the Cycle Pure Kit (peqLab, Erlangen, Germany). Sequencing of the PCR products was performed with the BigDye RR Terminator AmpliTaq FS Kit 1.1 (Applied Biosystems) using the external primers f1 and r1 and the internal primers 2f (5′-AACGAAAGCGGGCGTGTG-3′), 2r (5′-TGCACGGTTTCACGGTCG-3′), and 3f (5′-GTGATCGGTGACGACTGG-3′), respectively. Capillary electrophoresis and data collection were carried out on an ABI PRISM 3100 Genetic Analyzer (Applied Biosystems). Data were analyzed by ABI PRISM DNA Sequencing Analysis software and the single sequences were assembled by ABI PRISM Autoassembler software (Applied Biosystems). The contig sequence was compared to the nucleotide and protein databases using BLASTX and BLASTN (www.ncbi.nlm.nih.gov/BLAST; [21]).

2.11 Modeling

The plausibility of a mechanism involving the selection of bacterial progeny enriched in favorably modified enzyme variants was tested by modeling. An individual-based model with discrete time steps was used to simulate a fixed sized population of P dividing cells. The following assumptions were made: (i) Each bacterial cell of biomass B has an enzyme content consisting of unmodified RdpA molecules (RdpA), carbonylated RdpA molecules ($RdpA_C$), and excessively carbonylated RdpA ($RdpA_{CC}$). (ii) Only $RdpA_C$ possesses enzymatic activity toward 2,4-D. (iii) The total amount of enzyme per cell remains constant. (iv) At each time step, cells acquire biomass according to their enzyme content and available substrates, and enzymes are converted from RdpA to $RdpA_C$ and further to $RdpA_{CC}$ with

© 2013 WILEY-VCH Verlag GmbH & Co. KGaA, Weinheim

COR-AAD1-00002936
Bayer EX1008 (Part 6 of 9)

a predefined probability. (v) When the proportion of $RdpA_C$ exceeds a threshold in the presence of 2,4-D, the conversion probability is increased as more reactive oxygen species (ROS; [11]) are formed during 2,4-D utilization. (vi) Cells divide when their biomass exceeds a threshold. (vii) During cell division, enzymes are distributed between both progeny cells, and unmodified RdpA molecules are added to both cells so that assumption (iii) is fulfilled. (viii) To simulate chemostatic cultivation, cell population size is kept constant by randomly removing cells from the population after cell divisions. Two scenarios were compared wherein at cell division enzyme molecules are either divided evenly among both progeny cells (symmetric division), or divided with one progeny obtaining more beneficial $RdpA_C$ and less disadvantageous $RdpA_{CC}$ molecules (asymmetric division). The model was implemented in the C++ programming language. The code keeps track of biomass and distribution of carbonylation states of RdpA for each individual cell of the simulated population. Starting with a population of P cells with each containing $RdpA^{Total}$ copies of enzyme RdpA with randomly distributed carbonylation states and random biomass, the simulation iterates over a loop consisting of four steps:

(1) Enzyme carbonylation: Each enzyme molecule RdpA ($RdpA_C$) present in the cell population is carbonylated to $RdpA_C$ ($RdpA_{CC}$) with probability p_1 (p_2). Probabilities p_1 and p_2 depend on available substrates and $RdpA_C$ concentration as follows. If only (*R*)-2,4-DP is available, or 2,4-D is additionally available but $RdpA_C$ does not exceed a threshold $RdpA_C^t$, we set $p_1 = p_1^{min}$. If both substrates are present and $RdpA_C > RdpA_C^t$, an increased carbonylation activity is modeled by setting $p_1 = p_1^{min} + m_1$ ($RdpA_C$-$RdpA_C^t$). Probability p_2 is set accordingly with parameters p_2^{min} and m_2. Note that this step only changes the carbonylation state of RdpA molecules, but does not change the total number of RdpA molecules per cell. (2) Growth: Each cell acquires biomass according to the equation $B_i = B_{i-1} + k_1\ RdpA + k_2\ RdpA_C + k_3\ RdpA_C$. Parameter k_3 describes the utilization of 2,4-D by $RdpA_C$ and is set to zero in the absence of 2,4-D. (3) Cell division: Each cell of the population with $B > B_d$ undergoes cell division. Enzymes are evenly distributed between both progeny cells. If asymmetric cell division is simulated, a normally distributed pseudo random number with mean μ and variance σ^2 determines, how many molecules of $RdpA_C$ are moved from one progeny cell to the other in exchange for $RdpA_{CC}$ molecules. After distributing all enzyme molecules of the dividing cell, RdpA molecules are added to both progeny cells so that each cell contains a total of $RdpA^{Total}$ enzyme molecules. Biomass B is set to zero for both progeny cells and the newly formed cell is added to the population. (4) Dilution: cells are randomly removed from the population until P cells remain. The parameters used for the simulation of a bacterial population are: P = 100,000, $RdpA^{Total} = 100$, $RdpA_C^t = 25$, $p_1^{min} = 5.0e\text{-}4$, $p_2^{min} = 2.5e\text{-}5$, $m_1 = 1.0e\text{-}3$, $m_2 = 5.0e\text{-}5$, $k_1 = 0.01$, $k_2 = 0.01$, $k_3 = 0.02$, $B_d = 200$, $\mu = 10$, and $\sigma^2 = 1$.

2.12 Determination of biomass

Biomass concentrations were obtained by measuring the optical density at 700 nm (OD_{700}). Corresponding dry mass was obtained in quadruple from a calibration curve of biomass samples dried to constant weight after treatment at 104°C and cooling down in a desiccator.

3 Results

3.1 Effects of long-term exposure to 2,4-D on 2,4-D degradation

D. acidovorans MC1071 and MC1073 harbor *rdpA* allowing them to grow on (*R*)-2,4-DP, but they lack *sdpA* and *tfdA*, enzymes that efficiently attack 2,4-D. Both strains were cultivated on (*R*)-2,4-DP in a chemostat at a dilution rate of D = 0.05 h^{-1} until steady state was established. Then 2,4-D was added to the feed at 36% of the molar concentration of (*R*)-2,4-DP. The concentrations of both substrates were monitored. A typical run for strain MC1071 fed with 5.6 mM (*R*)-2,4-DP and 2 mM 2,4-D is shown in Fig. 1. Wash-in of 2,4-D only reached 68% of the reservoir concentration of 2 mM. The stationary 2,4-D concentration was relatively stable until day 10. Thereafter 2,4-D steadily decreased to 0.22 mM on day 21. The (*R*)-2,4-DP concentration stayed below the detection limit during the experiment, whereas the biomass concentration increased by about 25% (approximately 0.1 g L^{-1}) indicating utilization of 2,4-D for biomass production (Fig. 1). The experiment was repeated at 50% lower substrate concentrations, while the ratio of about 3:1 of (*R*)-2,4-DP to 2,4-D was maintained. Again a decline of the stationary 2,4-D concentrations from initially 0.38 to 0.11 mM and 0.42 to 0.23 mM on day 20 was observed for strains MC1071 and MC1073, respectively (Supporting Information Fig. S2).

To test whether additional biomass was synthesized from 2,4-D, a pulse experiment with uniform ring-labeled ^{14}C-2,4-D at steady state during simultaneous substrate utilization was conducted. From the radiolabel of biomass sampled 1 h after the pulse, it was calculated that 18% of the total carbon of washed cell suspensions originated from 2,4-D. Considering that the labeling of biomass by carbon turnover might have been incomplete at that time, this is in good agreement with the 25% increase in biomass observed in the 2,4-D adaptation experiment. We did not attempt to measure incorporation of ^{14}C-2,4-D in cultures grown on (*R*)-2,4-DP alone. To be comparable with the previous experiment this would have required feeding a base concentration of non-labeled 2,4-D besides ^{14}C-2,4-D. Permitted concentrations of labeled 2,4-D alone were likely to be below the degradation threshold and might have given rise to artifacts. Simultaneous addition with unlabeled 2,4-D would have equaled the set up of the above adaptation experiment.

Degradation of 2,4-D and its utilization as a sole growth substrate were tested using fresh cells from the fermenter before exposure to 2,4-D and on days 8 and 20. The 2,4-D concentration and OD_{700} were monitored for 24 h in batches. There was an initial phase of rapid 2,4-D degradation, which then ceased. Only negligible increases of the OD_{700} accompanied the degradation of 2,4-D (data not shown). Notably, the total consumption of 2,4-D until the activity ceased was proportional to the amount of biomass for a given time of cell harvest from the fermenter (Supporting Information Fig. S3). The total turnover per

© 2013 WILEY-VCH Verlag GmbH & Co. KGaA, Weinheim

COR-AAD1-00002937
Bayer EX1008 (Part 6 of 9)

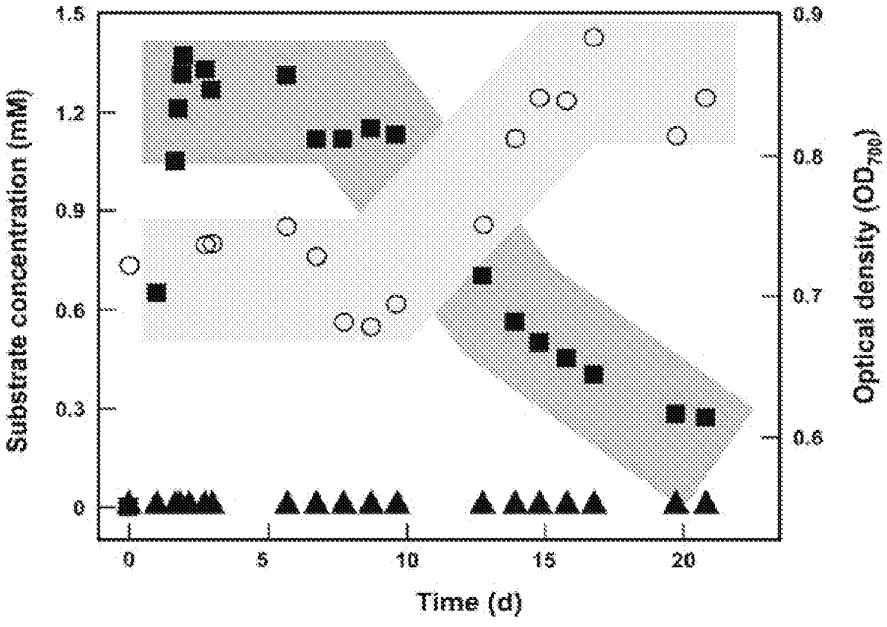


Figure 1. Development of steady-state substrate concentrations (closed symbols) and optical density (circles) during long-term chemostatic cultivation of *Delftia acidovorans* MC1071 on (*R*)-2,4-DP (triangles) and 2,4-D (squares) at 30°C and pH 7.5. The inflow concentrations of (*R*)-2,4-DP and 2,4-D were 5.6 and 2.0 mM, respectively, and the dilution rate was 0.05 h^{-1}. Shadings were included to highlight the gain of biomass at the expense of the steady-state 2,4-D concentration, while (*R*)-2,4-DP is degraded completely (detection limit) at all times.

unit biomass depended on the time of exposure to 2,4-D in the fermenter. MC1073 harvested before 2,4-D exposure degraded 139 ± 12 mg 2,4-D L^{-1} per unit OD_{700}. The same strain degraded 319 ± 64 mg L^{-1} per unit OD_{700} and 454 ± 70 mg L^{-1} per unit OD_{700} when harvested on day 8 and day 20, respectively. The same trend of adaptation leading to more efficient and lasting 2,4-D degradation was obtained with strain MC1071.

To check whether adaptation to 2,4-D led to changed uptake (due to mutation or induction), we investigated the uptake rates of ^{14}C-2,4-D in vitro with cells freshly collected from the fermenter. The rates after growth on 5.6 mM (*R*)-2,4-DP only and 5.6 mM (*R*)-2,4-DP + 2 mM 2,4-D were 8.1 ± 1.2 nmol min^{-1} (mg dry mass)$^{-1}$ and 7.7 ± 1.3 nmol min^{-1} (mg dry mass)$^{-1}$, respectively. Based on a protein content of biomass of 60% this corresponds to rates of 13.5 nmol min^{-1} (mg protein)$^{-1}$ and 12.85 nmol min^{-1} (mg protein)$^{-1}$, respectively, which is on the order found previously [22]. This indicates the presence of a functional 2,4-D uptake system that is not influenced by the adaptation process. It should be noted that the total uptake in these experiments was far below the observed 18% incorporation of C from ^{14}C-2,4-D or the 25% biomass gain in the presence of 2,4-D in adaptation experiments.

To test the stability of improved 2,4-D degradation, a culture of MC1071, which had degraded 2,4-D in the presence of (*R*)-2,4-DP for 26 days was shifted to growth on pyruvate for three generations. Thereafter continuous cultivation with 5.6 mM (*R*)-2,4-DP was resumed until steady state was reestablished. Subsequent cofeeding of 2 mM 2,4-D indicated that the culture had lost its capacity of improved 2,4-D utilization. Eight days after the shift, high concentrations (1.7 mM) of 2,4-D were found unutilized, but within 20 more days of cultivation, 2,4-D decreased to a level well below 1 mM, indicating readaptation to 2,4-D.

3.2 Kinetics of RdpA

Samples of strain MC1073 were taken from the fermenter at steady state with (*R*)-2,4-DP, and on days 8 and 19 of cofeeding with 2,4-D. RdpA was partially purified and its kinetics studied. A decrease of K_m with 2,4-D reflecting increasing affinity of RdpA for this substrate during prolonged adaptation was observed and confirmed in repeated chemostat runs (Table 1). The catalytic efficiency (k_{cat}/K_m) with (*R*)-2,4-DP changed only slightly, whereas with 2,4-D it had an upward tendency during long-term exposure. The same trend for the equivalent V_{max}/K_m was observed with strain MC1071. This strain was cultivated to study the reversibility of the observed adaptation effect in a backshift experiment (Table 2). The results indicate an even more significant decrease of K_m with 2,4-D. The quotient Q_{ce} indicating the relative activity with both substrates increased by factors of 2–5 for strains MC1071 and MC1073 (Tables 1 and 2), thus supporting our observation of truly changed kinetics of RdpA. Interestingly, K_m and V_{max}/K_m for 2,4-D returned to nearly their initial values when the strain was shifted back to continuous cultivation on (*R*)-2,4-DP for 7 days (Table 2).

For further comparison, *rdpA* was also expressed in anaerobically grown *E. coli*. RdpA was purified by affinity chromatography under anoxic conditions and included in the kinetic studies. After heterologous anaerobic synthesis, RdpA possessed a slightly lower catalytic efficiency with (*R*)-2,4-DP and did not convert 2,4-D to a measurable extent.

3.3 Sequencing of *rdpA*

To elucidate whether shifted enzyme affinities were derived from genetic changes within the *rdpA* gene, *rdpA* of MC1073 was

© 2013 WILEY-VCH Verlag GmbH & Co. KGaA, Weinheim

COR-AAD1-00002938
Bayer EX1008 (Part 6 of 9)

Table 1. Catalytic characteristics of purified RdpA derived after growth on (*R*)-2,4-DP, during long-term exposure to 2,4-D and after anaerobic expression in *E. coli*. The half-saturation constant K_m, the catalytic efficiency (k_{cat}/K_m) and quotient Q_{ce} of the catalytic efficiency with 2,4-D divided by the catalytic efficiency with (*R*)-2,4-DP were determined using GraphPad Prism software. Results are from several independent chemostat runs.

	(*R*)-2,4-DP		2,4-D		Q_{ce} ($\times 10^{-2}$)
	K_m (μM)	k_{cat}/K_m (min^{-1} μM^{-1})	K_m (μM)	k_{cat}/K_m ($\times 10^{-2}$ min^{-1} μM^{-1})	
MC1073 (2.8 mM (*R*)-2,4-DP + 1 mM 2,4-D); chemostat run 1					
Growth on (*R*)-2,4-DP, no 2,4-D	51.3 ± 3.3	1.06 ± 0.12	1104 ± 110	0.38 ± 0.08	0.36
Day 8 after exposure to 2,4-D	40.1 ± 2.4	0.94 ± 0.1	925 ± 222	0.81 ± 0.24	0.86
Day 19 after exposure to 2,4-D	41.0 ± 4.5	1.02 ± 0.22	734 ± 15	0.62 ± 0.03	0.61
MC1073 (2.8 mM (R)-2,4-DP + 1 mM 2,4-D); chemostat run 2					
Growth on (*R*)-2,4-DP, no 2,4-D	55.1 ± 3.1	1.0 ± 0.11	1305 ± 136	0.58 ± 0.1	0.58
Day 26 after exposure to 2,4-D	78.8 ± 6.8	1.26 ± 0.22	618 ± 55	1.65 ± 0.18	1.31
MC1073 (2.8 mM (R)-2,4-DP + 1 mM 2,4-D); chemostat run 3					
Day 23 after exposure to 2,4-D	53.4 ± 6.7	1.1 ± 0.14	450 ± 87	1.61 ± 0.2	1.46
Anaerobic expression in *E. coli*					
	66.0 ± 4.6	0.87 ± 0.09	No measurable activity		-

Table 2. Catalytic characteristics of RdpA from crude extracts derived after growth on (*R*)-2,4-DP, during long-term exposure to 2,4-D and after backshift. The half-saturation constant K_m, the catalytic efficiency (V_{max}/K_m) and quotient Q_{ce} of the catalytic efficiency with 2,4-D divided by the catalytic efficiency with (*R*)-2,4-DP were determined using GraphPad Prism software.

	(*R*)-2,4-DP		2,4-D		Q_{ce} ($\times 10^{-2}$)
	K_m (μM)	V_{max}/K_m ($\times 10^{-2}$ min^{-1} mg^{-1})	K_m (μM)	V_{max}/K_m ($\times 10^{-4}$ min^{-1} mg^{-1})	
MC1071 (5.6 mM (*R*)-2,4-DP + 2 mM 2,4-D)					
Growth on (*R*)-2,4-DP, no 2,4-D	33.1 ± 5.1	3.35 ± 0.6	1020 ± 117	1.34 ± 0.57	0.4
Day 5 after exposure to 2,4-D	51.4 ± 5.1	3.65 ± 0.4	987 ± 126	3.69 ± 0.5	1.01
Day 14 after exposure to 2,4-D	57.1 ± 4.7	7.35 ± 0.53	765 ± 60	9.5 ± 0.85	1.29
Day 26 after exposure to 2,4-D	49.8 ± 2.1	5.16 ± 0.23	345 ± 99	10.7 ± 0.37	2.07
Day 7 after backshift to (*R*)-2,4-DP	52.9 ± 2.2	5.29 ± 0.07	804 ± 168	5.97 ± 0.35	1.13

PCR-amplified and completely sequenced before exposure to 2,4-D and on day 19 of cofeeding (*R*)-2,4-DP and 2,4-D. In addition, PCR-products from four slightly different colony morphotypes derived from the fermenter at the end of the cultivation were completely sequenced. All *rdpA* sequences were identical to the wild-type *rdpA*.

3.4 RdpA variants

2-DE revealed that RdpA appears in distinct enzyme forms varying in their p*I* values. 2D gels were used to compare RdpA variant distributions of strains MC1071 and MC1073 obtained at steady growth with (*R*)-2,4-DP only, after various days of cofeeding with 2,4-D, after backshift to pure (*R*)-2,4-DP and after resumed cofeeding with 2,4-D, after growth with fructose and upon anaerobic expression in *E. coli*. Protein spots were identified as RdpA using MALDI-TOF-MS. Areas adjacent to the outermost RdpA spots were also subject to identification. Identification of different proteins or a lack thereof indicated that no RdpA spot was present, assuring that RdpA spot detection was not limited by the staining procedure. Table 3 summarizes a set of representative results. Anaerobically synthesized RdpA displayed only two to three enzyme variants, which were clearly less negatively charged than RdpA obtained after aerobic growth either on (*R*)-2,4-DP or on (*R*)-2,4-DP in the presence of 2,4-D. The Strep-tag extension of RdpA used for expression in *E. coli* was calculated (ExPASy Proteom Server, http://au.expasy.org; [23]) to result in a Δp*I* of 0.06 in alkaline direction and can thus not explain the extent of the observed shift, let alone the lower number of variants.

Relative changes of the distribution of RdpA spots during adaptation to 2,4-D and backshift experiments were analyzed in crude extracts of strain MC1071. Similar patterns and relative intensities of RdpA spots were found before exposure to 2,4-D and after backshift to (*R*)-2,4-DP on the one hand and during the two periods of cofeeding 2,4-D separated by the backshift on the other hand. This indicates the reversibility and phenotypic nature of the adaptation during cofeeding with 2,4-D, which is characterized by new spots appearing at more acidic and more alkaline pH. Backshifts from and to 2,4-D abolished and restored the distribution patterns, respectively (Table 3). In summary, RdpA forms spanned a broader p*I* range during adaptation to 2,4-D, while the exposure to (*R*)-2,4-DP generally caused shifts toward more acidic pH when compared to anaerobically synthesized RdpA. These shifts became more pronounced during

© 2013 WILEY-VCH Verlag GmbH & Co. KGaA, Weinheim

COR-AAD1-00002939
Bayer EX1008 (Part 6 of 9)

Table 3. Relative distributions of RdpA variants resulting from exposure of strain MC1071 to 2,4-D, after backshift experiments and anaerobic expression in *E. coli*. Normalized relative spot intensities (%) of each variant at the given p*I* in relation to the most intense spot in each lane are listed. The data show that exposure to (*R*)-2,4-DP and adaptation to 2,4-D under aerobic conditions cause shifts toward more acidic pH when compared to the anaerobically expressed RdpA. RdpA forms span a broader p*I* range while exposed to 2,4-D. Backshift experiments show the reversibility of spot distribution patterns.

	Relative spot volume (%) of RdpA variants											
p*I*	5.32 ± 0.03	5.42 ± 0.00	5.50 ± 0.00	5.59 ± 0.05	5.72 ± 0.02	5.81 ± 0.02	5.91 ± 0.02	5.97 ± 0.01	6.07 ± 0.03	6.12 ± 0.00	6.27 ± 0.02	6.41 ± 0.00
From anaerobically grown *E. coli*										22.4	71.3	100.0
Grown on (*R*)-2,4-DP, no 2,4-D				19.2	51.2	84.3	100.0					
Day 21 of exposure to 2,4-D	6.0	9.0	18.8	35.6	53.3	89.5	100.0	36.7	30.4	35.6		
Day 6 of backshift to (*R*)-2,4-DP				29.9	50.8	83.3	100.0					
Day 18 of resumed 2,4-D cofeeding	3.9	6.3	16.6	30.0	54.1	90.5	100.0	*n.i.*	22.7			

n.i., not identified.

long-term exposure to 2,4-D. The experiment was repeated with strain MC1073 showing that the RdpA variant pattern also extended after cofeeding of 2,4-D for this derivative strain (Supporting Information Table S2).

To verify that the RdpA variants resulted from oxidative modification as reported elsewhere (17), 2D gels were subjected to Western blot analyses to specifically visualize proteins containing carbonylated amino acids via their reaction with DNPH. Figure 2 places enzyme variant patterns of strain MC1073 next to the corresponding Western blots. Variations in staining intensities do not reflect differences in the expression. For normalized values refer to Supporting Information Tables S2 and S3. Figure 2 illustrates that the RdpA variants were indeed carbonylated. In contrast, a low degree of carbonylation was detected for anaerobically synthesized RdpA and cells grown on fructose, which both displayed fewer RdpA variants than cultures grown on the herbicide mixture (Fig. 2).

Comparison of the relative extent of carbonylation of RdpA variants after normalization (Supporting Information Table S3) revealed trends toward increased carbonylation of the most acidic RdpA variants and RdpA variants emerging during adaptation to 2,4-D. This and the lack of measurable degradation activity of anoxically synthesized, maximally alkaline RdpA variants indicates a correlation between more carbonylated/more acidic variants and improved degradation kinetics with 2,4-D. In addition and according to previous findings (A. Westendorf, unpublished results) no other p*I* relevant posttranslational modifications, e.g. phosphorylation or acetylation were detected using MALDI-TOF-MS. It should be noted that the dichlorocatechol dioxygenase, which was copurified by the present procedure, showed similar patterns of carbonylated variants (Fig. 2).

4 Discussion

4.1 Adaptation resulting in faster 2,4-D degradation

Experimental data show that strains of *D. acidovorans* increase the rate at which they degrade 2,4-D, when this substrate is supplied in addition to the growth substrate (*R*)-2,4-DP. The basal 2,4-D consumption (Tables 1 and 2) can be explained by some catalytic activity of RdpA with 2,4-D [5, 10] and consequently wash-in of 2,4-D into chemostat cultures growing on (*R*)-2,4-DP proceeded to stationary 2,4-D concentrations well below those in the feeding solution (Fig. 1). As 2,4-D is not a growth substrate of *D. acidovorans*, it is even more striking that during continued cultivation, further declining 2,4-D concentrations coincided with increasing biomass, while the (*R*)-2,4-DP concentration remained unchanged below the detection limit in long-term chemostat runs. This indicates that 2,4-D was increasingly used for biomass production, a finding that was further supported by the observed incorporation of ^{14}C from labeled 2,4-D by 2,4-D-adapted cells. The extent of 2,4-D incorporation matched well with the increase in biomass relative to that obtained with (*R*)-2,4-DP only. Nevertheless, the ability to grow with 2,4-D as the sole substrate was not acquired, as was seen in separate batch growth experiments where 2,4-D degradation by a given amount of biomass ceased after some time. Interestingly, the final extent of 2,4-D degradation was proportional to the

© 2013 WILEY-VCH Verlag GmbH & Co. KGaA, Weinheim

COR-AAD1-00002940
Bayer EX1008 (Part 6 of 9)

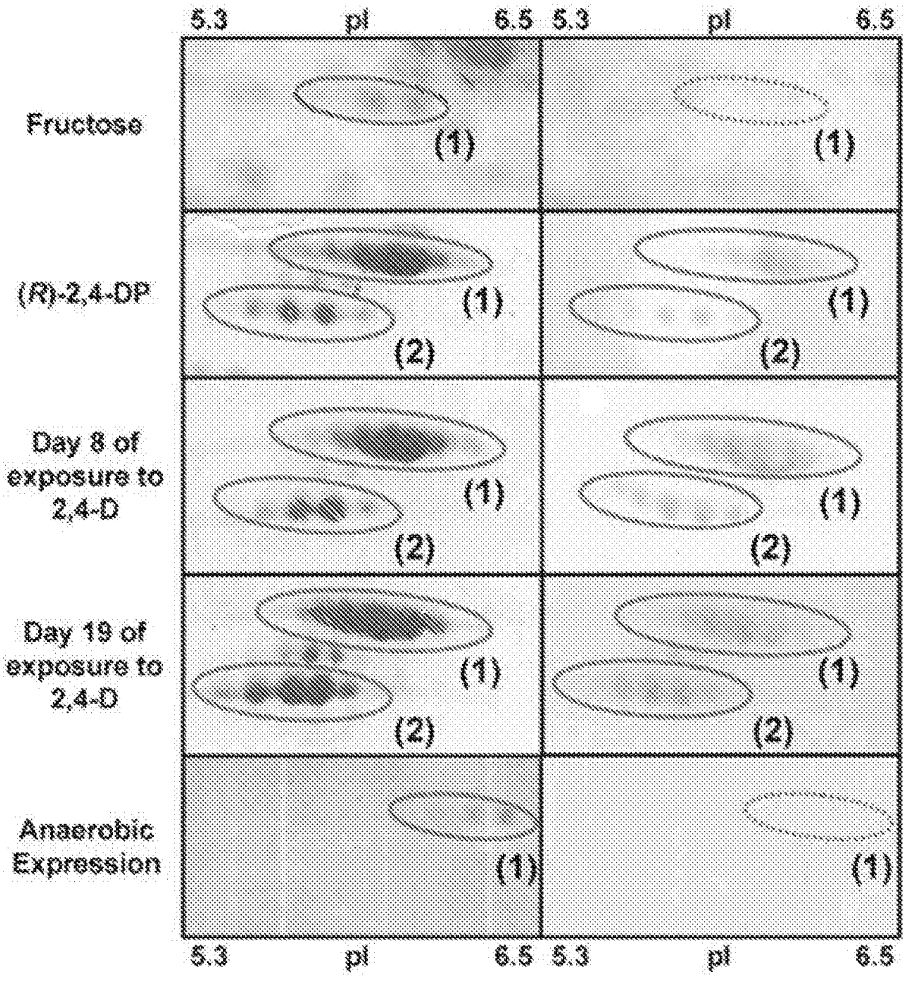


Figure 2. Sections of 2D gels and corresponding Western blots of partially purified RdpA extracts from *D. acidovorans* MC1073: Separation of variants of RdpA (1) and TfdC (2) on 2D gels (left) stained with Coomassie Brilliant Blue G-250 and detection of carbonylation on Western blots (right); sections within the molecular weight range of 25 to 40 kDa and within the pH range of 5.3 (left) to 6.5 (right) are shown. For gel electrophoresis and subsequent quantification defined amounts of partially purified RdpA from MC1073 were admixed to crude extracts of strain MC1100. Normalized spot intensities are given in Supporting Information Tables S2 and S3.

amount of biomass used in these experiments. Hence, it seemed as if the biomass or a factor in it was used up during 2,4-D degradation. It had been proposed before that the inability of $SdpA^-$ $RdpA^+$ variants of *D. acidovorans* to grow with 2,4-D is caused by difficulty in regenerating α-ketoglutarate, which is an essential co-substrate of RdpA [12, 24]. The simultaneous presence of a growth substrate that is metabolized at high rate, such as (*R*)-2,4-DP, appears to be needed to regenerate enough α-ketoglutarate to sustain the degradation of 2,4-D, while fulfilling the requirements of the strain for growth and biomass maintenance. Consequently, an adaptation leading to faster degradation of 2,4-D should partially relieve the α-ketoglutarate deficiency in the batch experiments, thus allowing prolonged 2,4-D degradation by adapted cells. Indeed, biomass obtained after 8 and 20 days of adaptation degraded up to four times more 2,4-D before the degradation ceased than the same amount of unadapted biomass (Supporting Information Fig. S3). In the light of earlier findings [12, 24], faster 2,4-D degradation thus appears to help replenish metabolites including α-ketoglutarate more efficiently by counteracting the exhaustion of metabolites for maintenance purposes. It thus seems that in adapted cells the formation of these metabolites compensated their consumption for a longer time.

4.2 Changed kinetics correlate with patterns of RdpA variants

A likely reason for the observed adaptation to faster 2,4-D degradation is a change in RdpA, since its catalytic activity is lower than the upstream and downstream reactions of uptake and further metabolism, respectively [22, 25]. Comparison of the kinetics of RdpA from three phases of the chemostat run revealed that its affinity as well as catalytic efficiency for 2,4-D indeed rose during the adaptation and declined after backshift to (*R*)-2,4-DP (Tables 1 and 2). 2-DE showed that kinetic changes coincided with the appearance of more variants of RdpA spanning a broader range of p*I* with an overall trend toward variants with more acidic p*I* values (Tables 3, Supporting Information Tables S2 and S3). The assumption that additional acidic variants were primarily responsible for improved 2,4-D degradation was supported by the observation that anoxically synthesized RdpA

 © 2013 WILEY-VCH Verlag GmbH & Co. KGaA, Weinheim

COR-AAD1-00002941
Bayer EX1008 (Part 6 of 9)

contained only highly alkaline variants, and did not exhibit measurable activity with 2,4-D. This trend is also in agreement with the earlier observation that RdpA from *Rhodoferax* sp. P230 (encoded by *rdpA* of identical sequence), which has the highest reported affinity to 2,4-D, displayed enzyme variants with highly acidic p*I* values [10]. The cooccurrence of various forms is also a likely reason for complex kinetic characteristics of RdpA preparations [10]. Unfortunately, we repeatedly failed to separate RdpA variants and to provide ultimate evidence by studying their kinetics individually.

4.3 The nature of RdpA modifications

The cooccurrence of isoenzymes varying in their kinetic properties is quite common. Isoenzymes, however, are by definition products of different genes. For instance in *Cupriavidus necator* JMP134, various isoenzymes of the modified ortho pathway for the cleavage of catechols have been found, which differ in their kinetic properties, but were encoded by separate genetic loci [26]. In contrast, the *sdpA*-deficient *D. acidovorans* strains used in the present study were derived from the *tfdA*-free strain MC1 [9] and thus contain *rdpA* as the only gene encoding a phenoxyalkanoate dioxygenase. As the appearance of mutations in the *rdpA* gene during the present experiments has been excluded by repeated sequencing, a posttranslational modification leading to the variation of RdpA is proposed. The regular series of RdpA variants on 2D gels resemble those found in *D. acidovorans* that went along with declining activity toward (*RS*)-2,4-DP [11]. In this earlier study, carbonylation and other oxidative modifications had been identified by MS, with carbonylation of lysine and arginine residues being responsible for shifts of RdpA variants to more acidic p*I* [11]. Thus oxidative modification is a likely explanation for the generation of RdpA variants also in the present study. The deletion of positive charges in alkaline amino acids due to carbonylation corresponds to distinct shifts to more acidic p*I* (Fig. 2, Table 3; Supporting Information Table S2). ROS have been proposed as the cause of oxidative modifications including carbonylation, nitration of tyrosine residues, formation of disulfide cross-links, and glycoxidation adducts [27], since the generation of ROS is a known feature of catalytic steps performed by α-ketoglutarate-dependent dioxygenases [28, 29]. In the present study, an immunoassay was used that specifically visualizes DNPH-modified carbonyl groups when combined with Western blot analysis. It showed that carbonylation was involved in the observed changes of RdpA (Fig. 2).

Whereas the exposure to phenoxyalkanoates, and particularly to the inferior substrate 2,4-D, increased the extent of carbonylation (Supporting Information Table S3), RdpA synthesized under anoxic conditions in *E. coli* was dominated by an enzyme form at p$I = 6.41$ (Table 3). Such an alkaline variant was not detected in preparations of aerobically grown cells. It might thus be that it represented the nonmodified enzyme, which for technical reasons was extended by a Strep tag that, however, can only explain a minor part of the alkalinity of this RdpA variant. When compared to the anoxically synthesized RdpA, all RdpA variants newly emerging during cofeeding with 2,4-D are still more acidic. Thus, it is likely that all forms with a p$I < 6.41$ are carbonylated to various degrees determining their positions on 2D gels. The lack of carbonylation in the anoxically synthesized RdpA is supported by the absence of a Western blot signal for the most alkaline spot. Two minor accompanying, more acidic forms can be explained by the difficulty in completely excluding oxygen throughout the preparation [11]. The formation of RdpA variants in the absence of herbicides is coincident with the observation of ROS generation in side reactions of α-ketoglutarate-dependent dioxygenases (e.g. TauD) only in the presence of α-ketoglutarate and oxygen [30]. The absence of Western blot signals of these minor spots might be due to a low degree of carbonylation and their low protein concentration. Expression of RdpA in fructose-grown cells also led to a lower degree of carbonylation, possibly reflecting the decreased activity of oxygenases [11].

Western blots indicate that TfdC might be a second target of adaptation besides RdpA. TfdC initiates the ortho-cleavage pathway by converting the dichlorocatechol intermediate into the corresponding muconic acid derivative. In consequence, improved activity of this enzyme might contribute to an enhanced overall flux and to reduced concentrations of the toxic intermediate dichlorophenol [31]. While we did not specifically address this, it is in line with experience made with *Cupriavidus necator* JMP134, which revealed that the expression of two cassettes for enzymes of the ortho-cleavage pathway resulted in a significant improvement of growth on chloroorganics [26, 32].

The obtained evidence for the carbonylation of RdpA raises the question if such changes could be responsible for the improved activity with 2,4-D. Conformational changes due to carbonylation have been reported, but typically as the cause of protein inactivation. For instance in humans, carbonylations of proteins were associated with several neurodegenerative diseases [18, 33]. In bacteria, carbonylation has been identified as symptomatic of cells that enter the non-culturable state [34]. Although positive effects of protein carbonylation have never been reported and were not found in our previous study where damaged proteins accumulated in static batch cultivations [11], in principle we do not see arguments against the possibility that carbonylation could bring about improved enzyme kinetics with an initially poor substrate. This is particularly true when assuming that enzymes with oxygenase activity should possess structures that remain active even if subjected to oxidative modification, and that cells bearing these enzymes have mechanisms to counteract inactivation. In terms of RdpA, the variants obtained from our chemostats are affected by carbonylation to a certain degree, as indicated by p*I* changes and positive signals from the carbonyl-specific immunoassay. Nevertheless RdpA is catalytically active as verified by activity measurements and though it did not exhibit a variant with a p*I* value as alkaline as the apparently nonmodified enzyme obtained after anoxic expression. Obviously, oxidatively modified variants of the enzyme represent its native state. When exposed to 2,4-D long term, increased numbers of RdpA variants associated with an increased catalytic efficiency with 2,4-D were observed. 2,4-D is structurally different from the favored substrate (*R*)-2,4-DP, being a methyl group short. Hence 2,4-D should not exactly fit into the active center, thus leaving room for oxygen involving side reactions, like carbonylation. This is likely as the catalytic efficiency is low with 2,4-D raising the feasibility that ROS generated in the catalytic cycle [35] of the

© 2013 WILEY-VCH Verlag GmbH & Co. KGaA, Weinheim

COR-AAD1-00002942
Bayer EX1008 (Part 6 of 9)

enzyme are misrouted with higher probability. A positive effect on the activity should be even more likely if selective forces act on improved enzyme variants in growing populations. Extended modification leading to enzyme inactivation by ongoing oxidative modification will finally be compensated by the common protein turnover. This is in contrast to starving cells that lack an active, regenerative metabolism and thus accumulate modifications. Altogether the essentially different settings of static batch cultivation and dynamic chemostat run may just lead to the different effects observed.

We propose a mechanism by which favorable phenotypic changes could have been selected in a reproducible way in our experimental system. Chemostat cultivation selects for organisms that grow faster at a given stationary substrate concentration or, in case of mixed substrates, use a wider range of these substrates. The observed adaptation to 2,4-D acted in both ways, as it accelerated the degradation rate and increased the extent to which 2,4-D could be coutilized for productive growth. The latter is equivalent to an apparent increase of the utilizable substrate and thus leads to a progressive increase of the stationary biomass. In ecological terms the adaptation resulted in an increase of the carrying capacity of the chemostat. Individuals hosting RdpA molecules of improved kinetics would benefit, whereas a counter selection of detrimental modifications would occur. Key to a selection on the level of individuals would then be that positive and negative modifications are separable, e.g. by uneven distribution among the progeny. The selection of positively modified enzymes in the chemostat would then occur through faster growth of the cells containing them.

4.4 Modeling the selection of favorable RdpA variants

A simple individual-based model simulating a population of dividing cells was used to test the plausibility of the hypothesis that the observed accumulation of carbonylated RdpA molecules results from enhanced carbonylation in the presence of 2,4-D.

Simulation runs show that only if cell divisions are asymmetric can cells accumulate enough $RdpA_C$ molecules to exceed the threshold at which efficient 2,4-D utilization commences, leading to an accumulation of carbonylated RdpA molecules within the population (Fig. 3). In the asymmetric case, one progeny cell inherits more molecules of $RdpA_C$ and less of $RdpA_{CC}$ than the other. When 2,4-D is added, the growth rate increases 1.2-fold for the symmetric case, and 1.9-fold for the asymmetric case (results not shown). Asymmetric distributions of molecules within cells and, moreover, asymmetric divisions of cells are actually discussed as a cause of heterogeneity in populations [36, 37], and molecular mechanisms underlying asymmetric behavior in dividing single cells have been proposed [38, 39]. Most research in this context is directed to the question of aging of bacterial cells [40–42] that takes into account the segregation of carbonylated, senescent proteins in dividing cells defining dying cell lines [43, 44]. Our present model in contrast addresses a positive effect of carbonylation. The adaptive response is finally based on the asymmetric distribution of molecular entities, in this case the various forms of the key enzymes in herbicide metabolism. Our model thus can explain a stable distribution of the subpopulations. Whether or not there actually is a directed segregation of newly synthesized (RdpA), modified ($RdpA_C$), and/or senescent ($RdpA_{CC}$) enzyme molecules cannot be answered at present. Modifications of enzyme molecules beyond the optimum would be eliminated by the same selective mechanism.

4.5 Mutational effects as alternative explanation

Though the results are consistent with posttranslational modification as an explanation for the observed adaptation of the *D. acidovorans* population and we did not find changes in *rdpA*, we cannot exclude the possibility that genetic changes in loci other than *rdpA* increased the susceptibility of *D. acidovorans* to oxidative modification or influenced 2,4-D degradation via other mechanisms. Hence, in the following we discuss the likelihood of a genetic mechanism for improved 2,4-D degradation. Assuming that a mutation caused the observed adaptation, conceivable targets are key functions of 2,4-D utilization such as the uptake of 2,4-D, the catalytic activity of RdpA via a genetically determined posttranslational modification, or the regeneration pathway of α-ketoglutarate that depends on the utilized herbicide [3].

Better specific uptake might improve the degradation of 2,4-D. Earlier experiments revealed that facilitated or active transport of phenoxyalkanoate herbicides was characterized by complex kinetics, which could suggest the presence of multiple specific transporters [22]. The latter might confer *D. acidovorans* MC1 the capability to utilize a spectrum of chlorinated and methylated phenoxyacetate- and enantiomeric phenoxypropionate derivatives. However, we can rule out an adaptation of transporters in the current work, as uptake kinetics remained unchanged during adaptation experiments, i.e. uptake rates before the application of 2,4-D and after cofeeding of this substrate were nearly identical.

A mutation changing the regulation of RdpA synthesis or a duplication of *rdpA* might explain faster 2,4-D degradation, but would not explain changed enzyme kinetics or shifted relative activities of RdpA for 2,4-D versus (*R*)-2,4-DP. Comparing the catalytic efficiency of cell extracts obtained throughout the adaptation showed rather constant figures with (*R*)-2,4-DP but increasing values with 2,4-D as the substrate (Tables 1 and 2). Hence, increased activity with 2,4-D is not caused by a dose effect of RdpA, but indicates truly improved kinetics with 2,4-D as is illustrated by a doubling of Q_{ce} values in adapted cells (Tables 1 and 2). Backshift to (*R*)-2,4-DP as sole growth substrate abolished this effect. Such an explanation would also neglect our evidence for RdpA variants. Regarding all genetically determined adaptation mechanisms, it seems highly unlikely to us that an acquired advantage in substrate utilization would be lost as reliably and quickly as observed in our experiments without bringing about advantages for the utilization of the backshift substrate (*R*)-2,4-DP. It would rather be expected that subpopulations with improved metabolic performances would keep selective advantages after genetic modifications [26, 31].

We also applied a dynamic model to test if and which conditions a mutation could become a dominant trait within the timeframe observed in our adaptation experiments (for details,

© 2013 WILEY-VCH Verlag GmbH & Co. KGaA, Weinheim

COR-AAD1-00002943
Bayer EX1008 (Part 6 of 9)

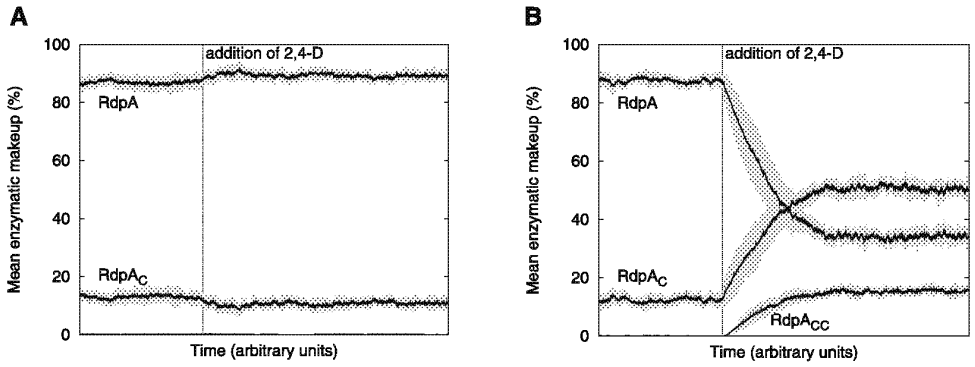


Figure 3. Simulation of a bacterial population with 100 000 cells (mean results and SDs of 20 independent simulation runs). (A) On cell division, enzymes are symmetrically, or (B) asymmetrically distributed between both progeny cells. Populations are randomly initialized; the transient phase before reaching equilibrium corresponding to the initial case with (*R*)-2,4-DP as the sole substrate is not shown.

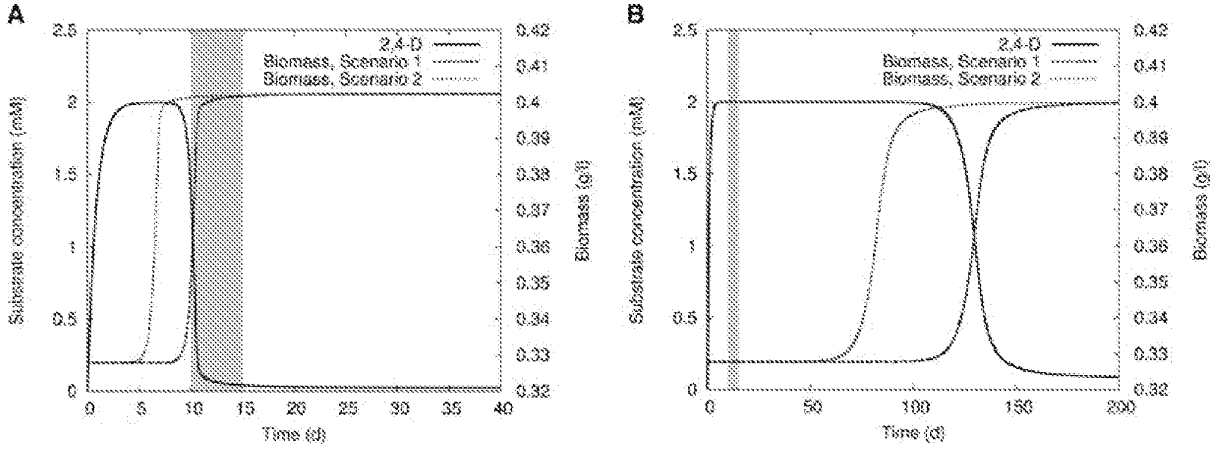


Figure 4. Chemostat simulation of the 2,4-D wash-in phase. After reaching steady state during exclusive (*R*)-2,4-DP feeding, 2,4-D is added to the chemostat feed at $t = 0$ day with a reservoir concentration of 2.0 mM. At $t = 0$ day, spontaneous mutations are assumed to yield either 1 cell (Scenario 1) or 10 000 cells (Scenario 2) being able to metabolize 2,4-D with a maximum per capita growth rate of 0.18 h^{-1} (equal to growth on (*R*)-2,4-DP, (A)) or 0.06 h^{-1} (B). In the experiment, increase of total biomass and corresponding substrate decrease occurred approximately between days 10 and 15 (shaded area).

see Supporting Information Tables S1 and S4). We took into account both a singular mutative event in one cell or in an entire subpopulation of 10^4 individuals per 5×10^{11} cells. Whereas growth on 2,4-D was not possible with the non-adapted culture, we allowed growth rates on 2,4-D with RdpA as the key enzyme up to the rate observed with (*R*)-2,4-DP as substrate, i.e. 0.18 h^{-1}. Under these conditions, the dynamics of the system allowed the single mutant to dominate the culture within 10 days (Fig. 4). The assumed growth rate is unrealistic, however, since even the adapted culture was incapable of sustained growth on 2,4-D. Assuming a maximum growth rate of 0.06 h^{-1} with 2,4-D, which results in slightly more than the observed 25% gain in biomass, up to 150 days were needed for the mutant to become dominant, and even 10^4 mutants of this kind would not dominate the culture before about 80 days.

At the present, we have strong indications, though not conclusive evidence, that random oxidative enzyme modifications in concert with selection mechanisms lead to a reversible, phenotypic adaptation to improved 2,4-D degradation by strains of *D. acidovorans*. Conclusive evidence would either require evidence for a phenotypic segregation of the population, by e.g. high-throughput single cell proteomics, or the definite exclusion of genetic mechanisms, by e.g. high-throughput single cell genomics. Both options are presently beyond our possibilities. If our favored explanation of a phenotypic adaptation should prove right, an interesting follow-up question will be whether the improved coutilization of a novel substrate via phenotypic modification can facilitate subsequent genetic adaptation by gaining dominance, lifetime and additional generations as a prerequisite for favorable mutations in the presence of the selective factor.

© 2013 WILEY-VCH Verlag GmbH & Co. KGaA, Weinheim

COR-AAD1-00002944
Bayer EX1008 (Part 6 of 9)

Practical application

Microbial metabolic activity and versatility are the main forces to counteract pollution in the environment, through degradation and mineralization of pollutants. Adaptive response to xenobiotic chemicals is commonly explained by acquisition of mutations and rearrangements of pre-existing genetic information. The present results suggest a new mechanism of adaptation, via posttranslational oxidative modifications of key enzymes in degradative pathways. In this scenario, the modifications result in increased catabolic potential of the strain and thereby enable degradation of a defined compound or compound mixtures. A sustainable process presumes a sufficient flux rate of carbon and above all energy to meet maintenance requirements. Exploitation of xenobiotic pollutants as heterotrophic substrates not only maintains the activity of a strain, but also increases its degradative potential by propagation in an autocatalytic manner. The expansion of the strain's degradative potential contributes to the elimination of pollutants in, e.g. biotopes with restricted genetic diversity. Both, any autochthonous population or strain added for bioaugmentation will take advantage of this process in general and the indicated adaptation mechanism in particular.

We thank Anja Steude for helping to establish the immonoassay for carbonylated amino acids and Peter Yau for mass spectrometric analyses. We are also grateful to Monika Neytschev for performing the chemostat runs. This study was supported by the CITE research programme of the Helmholtz Association. S. L. was supported in part by a grant from the US Department of Agriculture, award no. 2007-035107-17817 and the German Academic Exchange Service (Deutscher Akademischer Austauschdienst, DAAD).

The authors have declared no conflict of interest.

5 References

[1] Fukumori, F., Hausinger, R. P., *Alcaligenes eutrophus* JMP134 2,4-dichlorophenoxyacetate monooxygenase is an alpha-ketoglutarate-dependent dioxygenase. *J. Bacteriol.* 1993, *175*, 2083–2086.

[2] Fukumori, F., Hausinger, R. P., Purification and characterization of 2,4-dichlorophenoxyacetate alpha-ketoglutarate dioxygenase. *J. Biol. Chem.* 1993, *268*, 24311–24317.

[3] Müller, R. H., Babel, W., A theoretical study on the metabolic requirements resulting from alpha-ketoglutarate-dependent cleavage of phenoxyalkanoates. *Appl. Environ. Microbiol.* 2000, *66*, 339–344.

[4] Nickel, K., Suter, M. J., Kohler, H. P., Involvement of two alpha-ketoglutarate-dependent dioxygenases in enantioselective degradation of (*R*)- and (*S*)-mecoprop by *Sphingomonas herbicidovorans* MH. *J. Bacteriol.* 1997, *179*, 6674–6679.

[5] Saari, R. E., Hogan, D. A., Hausinger, R. P., Stereospecific degradation of the phenoxypropionate herbicide dichlorprop. *J. Mol. Catal. B-Enzym.* 1999, *6*, 421–428.

[6] Westendorf, A., Benndorf, D., Müller, R. H., Babel, W., The two enantiospecific dichlorprop/alpha-ketoglutarate-dioxygenases from *Delftia acidovorans* MC1—protein and sequence data of RdpA and SdpA. *Microbiol. Res.* 2002, *157*, 317–322.

[7] Westendorf, A., Müller, R. H., Babel, W., Purification and characterisation of the enantiospecific dioxygenases from *Delftia acidovorans* MCI initiating the degradation of phenoxypropionate and phenoxyacetate herbicides. *Acta Biotechnol.* 2003, *23*, 3–17.

[8] Zipper, C., Nickel, K., Angst, W., Kohler, H. P. E., Complete microbial degradation of both enantiomers of the chiral herbicide mecoprop [(*RS*)-2-(4-chloro-2-methylphenoxy)propionic acid] in an enantioselective manner by *Sphingomonas herbicidovorans* sp nov. *Appl. Environ. Microbiol.* 1996, *62*, 4318–4322.

[9] Schleinitz, K. M., Kleinsteuber, S., Vallaeys, T., Babel, W., Localization and characterization of two novel genes encoding stereospecific dioxygenases catalyzing 2-(2,4-dichlorophenoxy)propionate cleavage in *Delftia acidovorans* MC1. *Appl. Environ. Microbiol.* 2004, *70*, 5357–5365.

[10] Westendorf, A., Benndorf, D., Pribyl, T., Harms, H. et al., Kinetic traits and enzyme form patterns of (*R*)-2-(2,4-dichlorophenoxy)propionate/alpha-ketoglutarate dioxygenase (RdpA) after expression in different bacterial strains. *Eng. Life Sci.* 2006, *6*, 552–559.

[11] Leibeling, S., Schmidt, F., Jehmlich, N., von Bergen, M. et al., Declining capacity of starving *Delftia acidovorans* MC1 to degrade phenoxypropionate herbicides correlates with oxidative modification of the initial enzyme. *Environ. Sci. Technol.* 2010, *44*, 3793–3799.

[12] Müller, R. H., Babel, W., Pseudo-recalcitrance of chlorophenoxyalkanoate herbicides—correlation to the availability of α-ketoglutarate. *Acta Biotechnol.* 2001, *21*, 227–242.

[13] Lowry, O. H., Rosebrough, N. J., Farr, A. L., Randall, R. J., Protein measurement with the Folin Phenol Reagent. *J. Biol. Chem.* 1951, *193*, 265–275.

[14] Benndorf, D., Davidson, I., Babel, W., Regulation of catabolic enzymes during long-term exposure of *Delftia acidovorans* MC1 to chlorophenoxy herbicides. *Microbiology* 2004, *150*, 1005–1014.

[15] Benndorf, D., Vogt, C., Jehmlich, N., Schmidt, Y. et al., Improving protein extraction and separation methods for investigating the metaproteome of anaerobic benzene communities within sediments. *Biodegradation* 2009, *20*, 737–750.

[16] Neuhoff, V., Arold, N., Taube, D., Ehrhardt, W., Improved staining of proteins in polyacrylamide gels including isoelectric focusing gels with clear background at nanogram sensitivity using Coomassie Brilliant Blue G-250 and R-250. *Electrophoresis* 1988, *9*, 255–262.

[17] Mostertz, J., Hecker, M., Patterns of protein carbonylation following oxidative stress in wild-type and sigB *Bacillus subtilis* cells. *Mol. Genet. Genomics* 2003, *269*, 640–648.

[18] Levine, R. L., Carbonyl modified proteins in cellular regulation, aging, and disease. *Free Radic. Biol. Med.* 2002, *32*, 790–796.

© 2013 WILEY-VCH Verlag GmbH & Co. KGaA, Weinheim

COR-AAD1-00002945
Bayer EX1008 (Part 6 of 9)

[19] Berth, M., Moser, F. M., Kolbe, M., Bernhardt, J., The state of the art in the analysis of two-dimensional gel electrophoresis images. *Appl. Microbiol. Biotechnol.* 2007, *76*, 1223–1243.

[20] Hehemann, J. H., Redecke, L., Murugaiyan, J., von Bergen, M. et al., Autoproteolytic stability of a trypsin from the marine crab *Cancer pagurus*. *Biochem. Biophys. Res. Commun.* 2008, *370*, 566–571.

[21] Altschul, S. F., Madden, T. L., Schaffer, A. A., Zhang, J. H. et al., Gapped BLAST and PSI-BLAST: a new generation of protein database search programs. *Nucleic Acids Res.* 1997, *25*, 3389–3402.

[22] Müller, R. H., Hoffmann, D., Uptake kinetics of 2,4-dichlorophenoxyacetate by *Delftia acidovorans* MC1 and derivative strains: complex characteristics in response to pH and growth substrate. *Biosci. Biotechnol. Biochem.* 2006, *70*, 1642–1654.

[23] Gasteiger, E., Hoogland, C., Gattiker, A., Duvaud, S. E. et al., Protein identification and analysis tools on the ExPASy Server, in: Walker, J. M. (Ed.), *The Proteomics Protocols Handbook*, Springer, Totowa 2005, pp. 571–607.

[24] Müller, R. H., Activity and reaction mechanism of the initial enzymatic step specifying the microbial degradation of 2,4-dichlorophenoxyacetate. *Eng. Life Sci.* 2007, *7*, 311–321.

[25] Müller, R. H., Kleinsteuber, S., Babel, W., Physiological and genetic characteristics of two bacterial strains utilizing phenoxypropionate and phenoxyacetate herbicides. *Microbiol. Res.* 2001, *156*, 121–131.

[26] Laemmli, C. M., Leveau, J. H. J., Zehnder, A. J. B., van der Meer, J. R., Characterization of a second *tfd* gene cluster for chlorophenol and chlorocatechol metabolism on plasmid pJP4 in *Ralstonia eutropha* JMP134(pJP4). *J. Bacteriol.* 2000, *182*, 4165–4172.

[27] Nguyen, A. T., Donaldson, R. P., Metal-catalyzed oxidation induces carbonylation of peroxisomal proteins and loss of enzymatic activities. *Arch. Biochem. Biophys.* 2005, *439*, 25–31.

[28] Borowski, T., Bassan, A., Siegbahn, P. E. M., A hybrid density functional study of O-O bond cleavage and phenyl ring hydroxylation for a biomimetic non-heme iron complex. *Inorg. Chem.* 2004, *43*, 3277–3291.

[29] Zhang, Z. H., Ren, J. S., Harlos, K., McKinnon, C. H. et al., Crystal structure of a clavaminate synthase-Fe(II)-2-oxoglutarate-substrate-NO complex: evidence for metal centred rearrangements. *FEBS Lett.* 2002, *517*, 7–12.

[30] Ryle, M. J., Liu, A., Muthukumaran, R. B., Ho, R. Y. et al., O_2- and alpha-ketoglutarate-dependent tyrosyl radical formation in TauD, an alpha-keto acid-dependent non-heme iron dioxygenase. *Biochemistry* 2003, *42*, 1854–1862.

[31] Perez-Pantoja, D., Guzman, L., Manzano, M., Pieper, D. H. et al., Role of *tfdC(I)D(I)E(I)F(I)* and *tfdD(II)C(II)E(II)F(II)* gene modules in catabolism of 3-chlorobenzoate by *Ralstonia eutropha* JMP134(pJP4). *Appl. Environ. Microbiol.* 2000, *66*, 1602–1608.

[32] Leveau, J. H. J., König, F., Füchslin, H., Werlen, C. et al., Dynamics of multigene expression during catabolic adaptation of *Ralstonia eutropha* JMP134 (pJP4) to the herbicide 2,4-dichlorophenoxyacetate. *Mol. Microbiol.* 1999, *33*, 396–406.

[33] Dalle-Donne, I., Aldini, G., Carini, M., Colombo, R. et al., Protein carbonylation, cellular dysfunction, and disease progression. *J. Cell. Mol. Med.* 2006, *10*, 389–406.

[34] Desnues, B., Cuny, C., Gregori, G., Dukan, S. et al., Differential oxidative damage and expression of stress defence regulons in culturable and non-culturable *Escherichia coli* cells. *EMBO Rep.* 2003, *4*, 400–404.

[35] Kovaleva, E. G., Lipscomb, J. D., Versatility of biological non-heme Fe(II) centers in oxygen activation reactions. *Nat. Chem. Biol.* 2008, *4*, 186–193.

[36] Lawler, M. L., Brun, Y. V., A molecular beacon defines bacterial cell asymmetry. *Cell* 2006, *124*, 891–893.

[37] Müller, S., Harms, H., Bley, T., Origin and analysis of microbial population heterogeneity in bioprocesses. *Curr. Opin. Biotechnol.* 2010, *21*, 100–113.

[38] Huitema, E., Pritchard, S., Matteson, D., Radhakrishnan, S. K. et al., Bacterial birth scar proteins mark future flagellum assembly site. *Cell* 2006, *124*, 1025–1037.

[39] Lam, H., Schofield, W. B., Jacobs-Wagner, C., A landmark protein essential for establishing and perpetuating the polarity of a bacterial cell. *Cell* 2006, *124*, 1011–1023.

[40] Ackermann, M., Chao, L., Bergstrom, C. T., Doebeli, M., On the evolutionary origin of aging. *Aging Cell* 2007, *6*, 235–244.

[41] Nyström, T., A bacterial kind of aging. *PLoS Genet.* 2007, *3*, e224.

[42] Watve, M., Parab, S., Jogdand, P., Keni, S., Aging may be a conditional strategic choice and not an inevitable outcome for bacteria. *Proc. Natl. Acad. Sci. USA* 2006, *103*, 14831–14835.

[43] Aguilaniu, H., Gustafsson, L., Rigoulet, M., Nystrom, T., Asymmetric inheritance of oxidatively damaged proteins during cytokinesis. *Science* 2003, *299*, 1751–1753.

[44] Nyström, T., Role of oxidative carbonylation in protein quality control and senescence. *EMBO J.* 2005, *24*, 1311–1317.

© 2013 WILEY-VCH Verlag GmbH & Co. KGaA, Weinheim

COR-AAD1-00002946
Bayer EX1008 (Part 6 of 9)

Applied and Environmental Microbiology

Purification and Characterization of Two Enantioselective α -Ketoglutarate-Dependent Dioxygenases, RdpA and SdpA, from *Sphingomonas herbicidovorans* MH

Tina A. Müller, Thomas Fleischmann, Jan Roelof van der Meer and Hans-Peter E. Kohler
Appl. Environ. Microbiol. **2006, 72(7):4853. DOI: 10.1128/AEM.02758-05.**

Updated information and services can be found at:
http://aem.asm.org/content/72/7/4853

These include:

REFERENCES This article cites 48 articles, 15 of which can be accessed free at: http://aem.asm.org/content/72/7/4853#ref-list-1

CONTENT ALERTS Receive: RSS Feeds, eTOCs, free email alerts (when new articles cite this article), more»

Information about commercial reprint orders: http://aem.asm.org/site/misc/reprints.xhtml
To subscribe to to another ASM Journal go to: http://journals.asm.org/site/subscriptions/

Journals.ASM.org

Downloaded from http://aem.asm.org/ on April 29, 2012 by guest

COR-AAD1-00002947
Bayer EX1008 (Part 6 of 9)

APPLIED AND ENVIRONMENTAL MICROBIOLOGY, July 2006, p. 4853–4861 Vol. 72, No. 7
0099-2240/06/$08.00+0 doi:10.1128/AEM.02758-05
Copyright © 2006, American Society for Microbiology. All Rights Reserved.

Purification and Characterization of Two Enantioselective α-Ketoglutarate-Dependent Dioxygenases, RdpA and SdpA, from *Sphingomonas herbicidovorans* MH

Tina A. Müller,[1]† Thomas Fleischmann,[1] Jan Roelof van der Meer,[1,2] and Hans-Peter E. Kohler[1]*

Swiss Federal Institute of Aquatic Science and Technology (Eawag), Überlandstrasse 133, CH-8600 Dübendorf, Switzerland,[1] and Département de Microbiologie Fondamentale, Bâtiment de Biologie, University of Lausanne, 1015 Lausanne, Switzerland[2]

Received 22 November 2005/Accepted 2 May 2006

α-Ketoglutarate-dependent (*R*)-dichlorprop dioxygenase (RdpA) and α-ketoglutarate-dependent (*S*)-dichlorprop dioxygenase (SdpA), which are involved in the degradation of phenoxyalkanoic acid herbicides in *Sphingomonas herbicidovorans* MH, were expressed and purified as His_6-tagged fusion proteins from *Escherichia coli* BL21(DE3)(pLysS). RdpA and SdpA belong to subgroup II of the α-ketoglutarate-dependent dioxygenases and share the specific motif $HXDX_{24}TX_{131}HX_{10}R$. Amino acids His-111, Asp-113, and His-270 and amino acids His-102, Asp-104, and His 257 comprise the 2-His-1-carboxylate facial triads and were predicted to be involved in iron binding in RdpA and SdpA, respectively. RdpA exclusively transformed the (*R*) enantiomers of mecoprop [2-(4-chloro-2-methylphenoxy)propanoic acid] and dichlorprop [2-(2,4-dichlorophenoxy)propanoic acid], whereas SdpA was specific for the (*S*) enantiomers. The apparent K_m values were 99 μM for (*R*)-mecoprop, 164 μM for (*R*)-dichlorprop, and 3 μM for α-ketoglutarate for RdpA and 132 μM for (*S*)-mecoprop, 495 μM for (*S*)-dichlorprop, and 20 μM for α-ketoglutarate for SdpA. Both enzymes had high apparent K_m values for oxygen; these values were 159 μM for SdpA and >230 μM for RdpA, whose activity was linearly dependent on oxygen at the concentration range measured. Both enzymes had narrow cosubstrate specificity; only 2-oxoadipate was able to replace α-ketoglutarate, and the rates were substantially diminished. Ferrous iron was necessary for activity of the enzymes, and other divalent cations could not replace it. Although the results of growth experiments suggest that strain MH harbors a specific 2,4-dichlorophenoxyacetic acid-converting enzyme, *tfdA*-, *tfdA*α-, or *cadAB*-like genes were not discovered in a screening analysis in which heterologous hybridization and PCR were used.

Phenoxyalkanoic acid herbicides are widely used to control broadleaf weeds in agriculture, lawns, and industry. These compounds are systemic postemergence herbicides that act as synthetic auxins (1, 2, 28). Well-known representatives are mecoprop [2-(*R*,*S*)-2-methyl-4-chlorophenoxypropanoic acid], dichlorprop [2-(*R*,*S*)-2,4-dichlorophenoxypropanoic acid], and 2,4-D (2,4-dichlorophenoxyacetic acid). Mecoprop and dichlorprop are chiral molecules that have one stereogenic center and therefore exist as two enantiomers. In the 1950s, it was shown that only the (*R*) enantiomers had herbicidal effects (29). However, both enantiomers were and still are applied as racemic mixtures, resulting in the introduction of large amounts of unwanted chemicals into the environment (10, 50, 51). *Sphingomonas herbicidovorans* MH, an *Alphaproteobacterium*, is able to grow on both enantiomers of mecoprop and dichlorprop, as well as on 2,4-D, as sole carbon and energy sources (21, 24, 54). In batch cultures, this organism degrades the two enantiomers of mecoprop and dichlorprop sequentially, and the (*S*) enantiomers are degraded first (25, 32).

In the first reaction, both mecoprop and dichlorprop are enantioselectively converted by *S. herbicidovorans* MH to achiral phenols and pyruvate (Fig. 1). Nickel et al. (35) showed in experiments with cell extracts that two distinct enzymes are involved. These enzymes are highly specific for the corresponding enantiomers and belong to the family of α-ketoglutarate-dependent dioxygenases. The α-ketoglutarate-dependent dioxygenases are a group of enzymes which are classified on the basis of their biochemical characteristics. They are nonheme iron-dependent dioxygenases that require both oxygen and α-ketoglutarate as substrates. For many of these dioxygenases ascorbate has been used as a reducing agent. α-Ketoglutarate-dependent dioxygenases catalyze a wide range of oxidative processes, such as hydroxylations, epoxidations, desaturations, ring formations, and expansion reactions (7, 17, 27, 38, 44). Despite the diversity of their primary sequences, all of these dioxygenases have a 2-His-1-carboxylate facial triad at the catalytic center (19) and also common amino acid motifs, on the basis of which they are classified into three subgroups (20). Relevant for the work described here is subgroup II, and the representatives of this subgroup have the motif $HX(D/E)X_{23-26}(T/S)X_{114-183}HX_{10-13}R$. More prominent members of this subgroup are taurine dioxygenase (TauD) from *Escherichia coli*, which is involved in taurine utilization (11), and 2,4-D dioxygenase (TfdA) from *Cupriviadus necator* (formerly *Ralstonia eutropha*) JMP134(pJP4). TfdA is involved in 2,4-D degradation and catalyzes the oxidative cleavage of the ether bond in 2,4-D, yielding 2,4-dichlorophenol (15, 16, 18).

Recently, several genes coding for the enzymes involved in phenoxypropanoic acid herbicide degradation in *S. herbi-*

* Corresponding author. Mailing address: Swiss Federal Institute of Aquatic Science and Technology (Eawag), Überlandstrasse 133, CH-8600 Dübendorf, Switzerland. Phone: 41 1 823 5521. Fax: 41 1 823 5547. E-mail: kohler@eawag.ch.

† Present address: Microbiology and Molecular Genetics, Michigan State University, 2209 Biomedical Physical Sciences, East Lansing, MI 48824-4320.

Downloaded from http://aem.asm.org/ on April 29, 2012 by guest

COR-AAD1-00002948
Bayer EX1008 (Part 6 of 9)

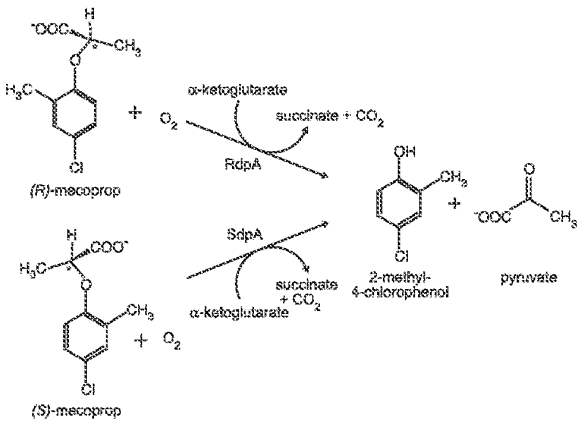


FIG. 1. Initial step in the degradation of chiral phenoxypropanoic acids in *S. herbicidovorans* MH catalyzed by the α-ketoglutarate-dependent (*R*)-dichlorprop dioxygenase (RdpA) and the α-ketoglutarate-dependent (*S*)-dichlorprop dioxygenase (SdpA).

cidovorans MH (31) and *Delftia acidovorans* MC1 (43) were identified and isolated. The genes coding for two α-ketoglutarate-dependent dioxygenases designated RdpA and SdpA were suggested to be responsible for the initial steps in the degradation of (*R*)- and (*S*)-mecoprop, respectively. The deduced amino acid sequence of RdpA from *S. herbicidovorans* MH is 30% identical to that of TfdA and 100% identical to that of RdpA from *D. acidovorans* MC1. The deduced amino acid sequence of SdpA from *S. herbicidovorans* MH exhibits only 60% identity to that of SdpA from *D. acidovorans* MC1 and about 30% identity to that of RdpA (30, 31, 43, 48).

In this study, we expressed and purified RdpA and SdpA from *S. herbicidovorans* MH as His_6-tagged fusion proteins. By measuring enzyme activities with a novel coupled enzyme assay, we verified that RdpA and SdpA are α-ketoglutarate-dependent dioxygenases belonging to subgroup II. We also characterized the kinetic behavior of the enzymes with various substrates and cosubstrates. In addition, we determined the substrate and cosubstrate specificities and obtained clear evidence that the two enzymes have opposite enantioselectivities.

MATERIALS AND METHODS

Bacterial strains and culture conditions. *E. coli* DH5α was used as a host for cloning experiments, and *E. coli* BL21(DE3)(pLysS) was used as a host for protein expression studies with pET-15b-based constructs (Novagen, Darmstadt, Germany). The *E. coli* strains were grown at 30°C or 37°C in Luria-Bertani medium (42). Ampicillin and chloramphenicol were added at final concentrations of 50 μg/ml and 25 μg/ml, respectively. Solid media were prepared by addition of 1.5% (wt/vol) agar.

Standard molecular techniques. Cloning and digestion were done by using established procedures (4, 42). Restriction enzymes and other DNA-modifying enzymes were purchased from Promega (Wallisellen, Switzerland) and Fermentas (Nunningen, Switzerland). Plasmids and cosmids were isolated by the boiling miniprep method or the alkaline lysis method described by Sambrook et al. (42) or by using an E.Z.N.A. plasmid miniprep kit II (Peqlab Biotechnologies GmbH, Baden-Dättwil, Switzerland) as suggested by the manufacturer. Purification of DNA fragments from agarose gel was carried out by using a MinElute gel extraction kit (QIAGEN AG, Basel, Switzerland) according to the protocol of the supplier.

Construction of N-terminal His_6-tagged recombinant enzyme expression plasmids. Expression plasmids pMec15 and pMec19 were constructed by reamplification by PCR of the *rdpA* and *sdpA* genes from pMec10 and pMec16, respectively, (31) with the following primers: 5′-CGC TCA TAT GCA TGC TGC ACT-3′ and 5′-AGC GGG GAT CCG CGT CGC C-3′ for *rdpA* and 5′-CAG GAG GAT TCA TAT GTC A-3′ and 5′-GCC AGC TGG ATC CGC CGA TGA-3′ for *sdpA*. In this way, an NdeI restriction site at the translational start and a BamHI restriction site after the stop codon were introduced (underlined nucleotides). The PCR-amplified fragments were first cloned into pGEM-T Easy (Promega), generating pMec14 and pMec18, which was verified by DNA sequencing. The plasmids were then digested with NdeI and BamHI, and the *rdpA* or *sdpA* inserts were recovered, purified, and ligated into the same sites of vector pET-15b. After transformation, this yielded plasmids pMec15 and pMec19.

Expression and purification of recombinant RdpA and SdpA. *E. coli* BL21-(DE3)(pLysS) harboring pMec15 or pMec19 was grown in Erlenmeyer flasks containing Luria-Bertani medium supplemented with ampicillin and chloramphenicol at 30°C with constant shaking. To express the recombinant proteins, cultures were grown until an optical density at 546 nm of 0.4 to 0.6 was reached, after which isopropyl-β-D-thiogalactopyranoside was added to a final concentration of 1 mM. The culture was incubated for another 3 h at 30°C, and the cells were harvested by centrifugation at 7,500 × *g* for 30 min at 4°C. The pellet was stored at −20°C until it was used. For preparation of cell extracts, 1 g (wet weight) of cells was resuspended in 3 ml of lysis buffer (50 mM NaH_2PO_4, 300 mM NaCl, 10 mM imidazole; pH 8.0), and the cells were broken by one passage through a French press at 1 MPa. The lysate was centrifuged for 45 min at 16,000 × *g* at 4°C, and aliquots were stored at −20°C.

His_6-tagged RdpA was purified by a one-step procedure. Up to 1 mg of protein was loaded on a 2-ml Ni-nitrilotriacetic acid (NTA) Superflow agarose column (QIAGEN) at a flow rate of 0.5 ml/min. Unbound protein was removed stepwise by washing with five bed volumes (~10 ml) of wash buffer (50 mM NaH_2PO_4, 300 mM NaCl, 20 mM imidazole; pH 8.0). After the initial washing step, wash buffers containing 50 mM imidazole and then 100 mM imidazole were applied. RdpA was then eluted with elution buffer (50 mM NaH_2PO_4, 300 mM NaCl, 250 mM imidazole; pH 8.0) at a flow rate of 0.8 ml/min and collected in 1-ml fractions. Fractions were analyzed for α-ketoglutarate-dependent dioxygenase activity; active fractions were pooled and desalted with 20 mM Tris-HCl (pH 7.5) with PD-10 columns (Amersham Biosciences, Dübendorf, Switzerland). The purified RdpA solution was stored at 4°C.

Recombinant SdpA was purified by a two-step procedure. Unless indicated otherwise, all steps were carried out at 4°C. Up to 1 mg protein was loaded on a 5-ml Superflow agarose column (QIAGEN) at a flow rate of 0.3 ml/min. Unbound protein was removed stepwise with 5 column volumes of wash buffer (50 mM NaH_2PO_4, 300 mM NaCl) containing 20 mM imidazole (pH 8) and 5 column volumes of wash buffer containing 50 mM imidazole (pH adjusted to 8). SdpA was then eluted with elution buffer (50 mM NaH_2PO_4, 300 mM NaCl, 200 mM imidazole; pH adjusted to 8) at a flow rate of 0.6 ml/min. One milliliter fractions were collected and analyzed, and active fractions were pooled and desalted with 20 mM Tris-HCl (pH 7.5) using PD-10 columns (Amersham Biosciences, Dübendorf, Switzerland) at room temperature. The SdpA solution was then loaded on a Bioscale Q2 column (Bio-Rad) equilibrated in the same buffer. The enzyme was eluted with a linear gradient from 20 mM Tris-HCl (pH 7.5) to 20 mM Tris-HCl (pH 7.5)–600 mM NaCl in 6 column volumes. SdpA was found to elute at approximately 220 mM NaCl. The fractions that exhibited activity were pooled and stored at 4°C.

Thrombin protease (Amersham Biosciences) was used to cleave the N-terminal His_6 tags of RdpA and SdpA. The N-terminal His_6 tag of approximately 10 μg enzyme was completely cleaved by 0.5 U thrombin protease within 2 h at room temperature.

Enzyme activity assays. (i) Coupled continuous assay. For purification and kinetic measurements of phenoxypropanoic acids, a coupled continuous assay with L-lactate dehydrogenase from rabbit muscle (Sigma-Aldrich, Buchs, Switzerland) as a reporter enzyme was developed. RdpA and SdpA stoichiometrically convert (substituted) phenoxypropanoic acids to the corresponding phenols and pyruvate. Pyruvate is converted by L-lactate dehydrogenase to lactate with concomitant consumption of NADH. NADH consumption was monitored spectrophotometrically by determining the decrease in absorbance at 340 nm. An extinction coefficient of 6.3 mM^{-1} cm^{-1} was used to calculate activities. The standard 0.5-ml assay mixture contained 50 mM imidazole (pH 6.75), 1 mM substrate, 1 mM α-ketoglutarate, 100 μM $(NH_4)_2Fe(SO_4)_2$, 1 mM ascorbic acid, 0.32 mM NADH, 1.2 U of L-lactate dehydrogenase, and 0.05 μg of purified RdpA or SdpA. Activity assays were done at 30°C unless indicated otherwise and were started by addition of the substrate. NADH consumption was monitored for 30 s, and the linear portion of the curve was used to calculate the activity. The substrate-specific oxidation rates were corrected for nonspecific NADH oxidation in the absence of substrate (endogenous rate). Specific activities were expressed as turnover rate (min^{-1}).

Downloaded from http://aem.asm.org/ on April 29, 2012 by guest

COR-AAD1-00002949
Bayer EX1008 (Part 6 of 9)

TABLE 1. Purification of α-ketoglutarate-dependent (*R*)-dichlorprop dioxygenase and α-ketoglutarate-dependent (*S*)-dichlorprop dioxygenase

Fraction	Vol (ml)	Total protein (mg)	Total activity (U)	Sp act (min^{-1})	Recovery (%)	Purification (*n*-fold)
α-Ketoglutarate-dependent (*R*)-dichlorprop dioxygenase						
Cell extract	10	133.1	30.9	7	100	1
Ni-NTA Superflow	7	1.8	7	133	22.7	19
α-Ketoglutarate-dependent (*S*)-dichlorprop dioxygenase						
Cell extract	3.5	42.57	18.48	14	100	1
Ni-NTA Superflow	5	1.05	7.71	247	41.70	17.1
BioScale Q2	3	0.71	6.34	299	34.32	20.7

(ii) Discontinuous assay. Experiments with alternative substrates were performed using a discontinuous assay by measuring the formation of the product by high-performance liquid chromatography. The standard assay mixture contained 50 mM imidazole (pH 6.75), 1 mM substrate, 1 mM α-ketoglutarate, 100 μM $(NH_4)_2Fe(SO_4)_2$, and 1 mM ascorbic acid. The assay mixtures were incubated at 30°C for 1 min and were inactivated in a boiling water bath for 2 min. Negative controls without enzyme were treated in the same manner. The products were analyzed on a Nucleodex α-PM column (200 by 4 mm; Macherey-Nagel, Düren, Germany) as described previously (35). Specific activity was defined as the amount of phenol derivative (μmol) that was formed per min per mg of protein. Oxidation rates were corrected for nonspecific formation of the product in the absence of the enzyme.

Oxygen electrode measurements. Kinetic measurements with oxygen were obtained with a Rank Brothers oxygen electrode at 30°C. The standard 1-ml assay mixture contained 50 mM imidazole (pH 6.75), 2 mM substrate, 2 mM α-ketoglutarate, 100 μM $(NH_4)_2Fe(SO_4)_2$, and 1 mM ascorbic acid. The assays were started by addition of the substrate, and the O_2 concentration was monitored at 2-s intervals for 15 min. An assay without substrate showed that the amount of background O_2 consumed was small and could be neglected for calculation of activities. Specific activity was defined as the amount of oxygen (μmol) reduced per min per mg of protein in the presence of a substrate and expressed as turnover rate (min^{-1}).

Kinetic measurements. The kinetic parameters K_m and k_{cat} were calculated using IgorPro software (WaveMetrics Inc., Lake Oswego, OR). The method used for calculation was based on a weighted nonlinear regression analysis of the Michaelis-Menten model. To calculate K_m and k_{cat} of RdpA with respect to oxygen, we used the first derivative (i.e., the velocity, expressed in μmol min^{-1}) of the oxygen concentration monitored with time.

Determination of the protein concentration and SDS-PAGE. Protein concentrations were determined by the Bradford method (6) with the Bio-Rad reagent dye concentrate reagent by following the instructions of the manufacturer (Bio-Rad, Reinach, Switzerland). Bovine serum albumin fraction V (Sigma-Aldrich) was used as a reference protein. Sodium dodecyl sulfate (SDS)-polyacrylamide gel electrophoresis (PAGE) was carried out with 12% acrylamide slab gels by using established procedures (26).

Molecular weight determination. Molecular weights of purified enzymes were determined by using a Superdex 200 preparation grade HiLoad 16/60 size exclusion column (Amersham Biosciences). Approximately 0.25 mg of protein was loaded on the HiLoad column and eluted at a flow rate of 0.2 ml/min with 50 mM Na_2HPO_4-KH_2PO_4 buffer (pH 7) containing 150 mM NaCl. A calibration curve was produced with the gel filtration standard from Bio-Rad containing bovine thyroglobulin (670 kDa), bovine gamma globulin (158 kDa), chicken ovalbumin (44 kDa), horse myoglobulin (17 kDa), and vitamin B_{12} (1.35 kDa). Blue dextran was used to determine the void volume.

Screening for additional α-ketoglutarate-dependent phenoxyalkanoic acid dioxygenases. To screen for *tfdA*- and *tfdA*α-like genes, we amplified DNA by PCR performed with the *tfdA*-derived primers tfdAfor (5′-TGG CAI AGC GAC AGI TCC TTT-3′), tfdArev (5′-CIG CGG TTG TCC CAI ATC IC-3′), tfdAfor2 (5′-ACG GAG TTC TG[C/T] GA[C/T] AT-3′), and tfdArev2 (5′-AAC GCA GCG [G/A]T[G/T] ATC CCA-3′) (46) in all possible combinations and with chromosomal DNA of *S. herbicidovorans* MH. The oligonucleotides used for PCR were obtained from Microsynth GmbH (Balgach, Switzerland). As a positive control, total DNA of *C. necator* JMP134(pJP4) was used.

For Southern hybridization, total DNA of *S. herbicidovorans* MH fractionated on an agarose gel was blotted on a Hybond-XL membrane (Amersham Biosciences, Dübendorf, Switzerland) with a vacuum blotter (VacuGene XL; Amersham Biosciences) by the procedure described by Ravatn et al. (40). Total DNA was hybridized with a 0.7-kb EcoRI fragment from pCBA101 (0.7-kb EcoRI fragment with *tfdA* in pGEM7; van der Meer, unpublished) and with a 1.1-kb SalI fragment of pBHS1 harboring part of *cadAB* (23). The fragments were radioactively labeled with [α-^{32}P]dATP using a Random Primed DNA labeling kit or with digoxigenin-dUTP using a DIG High Prime II DNA labeling and detection starter kit according to the protocol of the manufacturer (Roche Applied Science, Rotkreuz, Switzerland). Hybridization experiments were performed in SDS/bovine serum albumin hybridization buffer (0.5 M sodium phosphate [pH 7], 7% sodium dodecyl sulfate, 1% bovine serum albumin) at 55°C for 16 h. The membranes were washed twice with 5× SSC containing 1 mM EDTA for 2 min at room temperature and twice with 2× SSC containing 0.1% SDS for 30 min at 55°C (1× SSC is 0.15 M NaCl plus 0.015 M sodium citrate). When digoxigenin-labeled probes were used, immunological detection was carried out by using the supplier's protocol (Roche Applied Science).

Sequencing. DNA sequencing was performed with double-stranded DNA templates by using a Thermo Sequenase primer cycle sequencing kit with 7-deaza-dGTP (Amersham Biosciences) and M13 primers (5). Sequencing reaction mixtures were analyzed with an automated DNA sequencer (model 4200 IR^2; LI-COR Inc., Lincoln, NE). The primers used for sequencing were labeled at the 5′ end with IRD-700 or IRD-800 and were purchased from MWG Biotech AG (Ebersberg, Germany). Sequencing data were analyzed with DNASTAR software (DNASTAR Inc., Madison, WI) and were compared to the databases by BLAST searches (www.ncbi.nlm.nih.gov/BLAST, (45)).

Chemicals. Phenoxyalkanoic acids were purchased from Riedel-de Haën (Buchs, Switzerland) (PESTANAL; purity, 99%) or Sigma-Aldrich (purity, 97 to 99%). (*S*)-Mecoprop and (*S*)-dichlorprop were synthesized by C. Zipper (52). α-Ketoglutarate and other (di)carboxy acids were purchased from Sigma-Aldrich. All other chemicals were obtained from Fluka (Buchs, Switzerland) or from Merck AG (Dietikon, Switzerland).

RESULTS

Expression and purification of recombinant RdpA and SdpA. The *rdpA* and *sdpA* genes were expressed as N-terminal His_6-tagged fusion proteins in *E. coli* BL21(DE3)(pLysS) harboring pMec15 and pMec19, respectively. Expression resulted in high levels of recombinant RdpA and SdpA in the soluble fraction that accounted for approximately 16% and 10%, respectively, of the total protein as determined by measuring the band intensities of SDS-PAGE gels. A decrease in the incubation temperature during expression in *E. coli* did not increase the amount of the His_6-tagged enzymes in the cell extract. His_6-tagged RdpA was purified about 16-fold to apparent homogeneity by Ni-NTA affinity chromatography, whereas His_6-tagged SdpA was purified to apparent homogeneity by a two-step procedure (Table 1 and Fig. 2). The calculated molecular masses of the subunits of RdpA and SdpA were 34.9 kDa and 33.7 kDa, respectively, which was consistent with the sizes estimated by SDS-PAGE (approximately 36 kDa and 32 kDa, respectively).

Downloaded from http://aem.asm.org/ on April 29, 2012 by guest

COR-AAD1-00002950
Bayer EX1008 (Part 6 of 9)

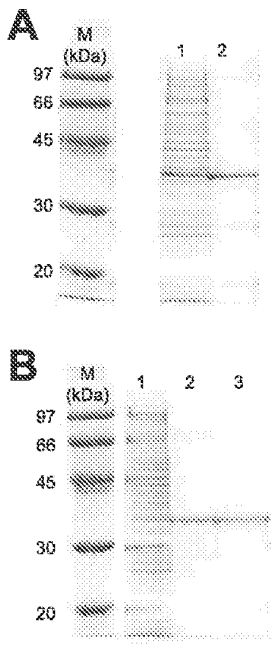


FIG. 2. Purification of RdpA (A) and SdpA (B) from *S. herbicidovorans* MH expressed as His_6-tagged fusion proteins. Protein samples were analyzed by denaturing gel electrophoresis on a 12% polyacrylamide gel and were stained with Coomassie brilliant blue. Lane M contained molecular mass markers. (A) Lane 1, extract of induced cells; lane 2, apparently pure RdpA (after Ni-NTA Superflow chromatography). (B) Lane 1, extract of induced cells; lane 2, partially purified SdpA (after Ni-NTA Superflow chromatography); lane 3, apparently pure SdpA (after ion-exchange chromatography).

The molecular weights of the native proteins were determined by size exclusion chromatography after the His_6 tag was cleaved by thrombin treatment. A molecular mass of 104 ± 7 kDa was obtained for native RdpA. This is consistent with a homotrimeric structure based on the calculated subunit molecular mass, 33.2 kDa. Native SdpA had a molecular mass of 32 kDa, a strong indication that the structure is monomeric.

The fusion proteins were treated with thrombin protease to cleave the His_6 tag, and the enzyme activities of the native and the His_6-tagged proteins were determined. In both cases, the His_6-tagged and native enzymes were equally active, showing that the His_6 tag did not affect activity. Therefore, all further experiments were carried out with the His_6-tagged recombinant proteins. Below, RdpA and SdpA refer to the to the His_6-tagged enzymes, unless indicated otherwise.

RdpA and SdpA are α-ketoglutarate-dependent dioxygenases that catalyze enantioselective reactions. RdpA and SdpA have been classified as α-ketoglutarate-dependent dioxygenases based on their amino acid sequences (31). This classification was verified by enzyme assays. RdpA and SdpA activities were completely absent in the absence of α-ketoglutarate, were strongly reduced in assays without ferrous iron, and were slightly reduced in the absence of ascorbate (Table 2).

The results of three different assays, a coupled continuous assay, a discontinuous assay, and an O_2 measurement assay, showed that there was stoichiometric product formation and substrate consumption. The specific activity of RdpA ranged from 2 to 4 U/mg protein. Determinations of the specific activity of RdpA were reproducible within single purified RdpA batches but could vary between independently induced *E. coli* cultures by a factor of two.

RdpA converted only the (*R*) enantiomers of phenoxypropanoic acids, and no activity was observed with the (*S*) enantiomers. The enantioselectivity was exactly the opposite for SdpA, which converted only the (*S*) enantiomers. In contrast to RdpA, SdpA was slightly inhibited in the presence of the nonsubstrate enantiomer (data not shown).

Physicochemical characterization. RdpA was stable at 4°C for up to 8 weeks and at room temperature for up to 7 days, but it was inactivated by several freezing and thawing cycles. Therefore, RdpA was stored at 4°C. Optimum activity was observed at pH 6.5 (Fig. 3A). Temperature dependence was also studied, but no optimum could be determined (Fig. 3B). The experiments were carried out with two independently purified RdpA batches. To avoid possible aberrant results due to inactivation of L-lactate dehydrogenase in the coupled continuous assay, specific activities were determined once by the coupled continuous assay and then by the discontinuous assay. RdpA activity was stable over a relatively wide temperature range, 20 to 55°C. Slightly higher activity was observed at 10°C and 20°C, but only in the discontinuous assay. However, the general trends for the two types of enzyme assays were similar and revealed no Arrhenius-like behavior.

SdpA was stable at room temperature for several hours and in 3 days lost less than 10% of its activity when it was stored at 4°C. Storage on ice and freeze-thaw cycles reduced the activity to about 80% of the original activity. More consistent specific activities were obtained when SdpA was prewarmed at room temperature prior to enzymatic assays. The pH optimum was pH 6.5 (Fig. 3C). In contrast to the RdpA activity, the SdpA activity had an optimum temperature between 35° and 40°C (Fig. 3D).

Substrate, cosubstrate, and cofactor specificities. Substrate specificities were determined by the coupled continuous assay for phenoxypropanoic acids and by the discontinuous assay for all other substrates. We examined the influence of the alkanoic acid group attached by an ether bond to the phenoxy ring by determining the activities with phenoxyacetic, phenoxypropanoic, and phenoxybutyric acids as substrates. The effects of different substituents, such as hydroxy, methyl, and chloride

TABLE 2. Dependence of α-ketoglutarate-dependent (*R*)- and (*S*)-dichlorprop dioxygenase activities on substrate, cosubstrate, and cofactors

Assay mixture	RdpA		SdpA	
	Activity (%)	Sp act (min^{-1})	Activity (%)	Sp act (min^{-1})
Complete	100	118.8	100	236.2
Complete without:				
(*R*)-Mecoprop	0	0	ND[a]	ND
(*S*)-Mecoprop	ND	ND	0	0
α-Ketoglutarate	0	0	0	0
Fe(II)	17.6	21.0	8.2	19.1
Ascorbate	85.3	101.4	37.8	89.2

[a] ND, not determined.

Downloaded from http://aem.asm.org/ on April 29, 2012 by guest

COR-AAD1-00002951
Bayer EX1008 (Part 6 of 9)

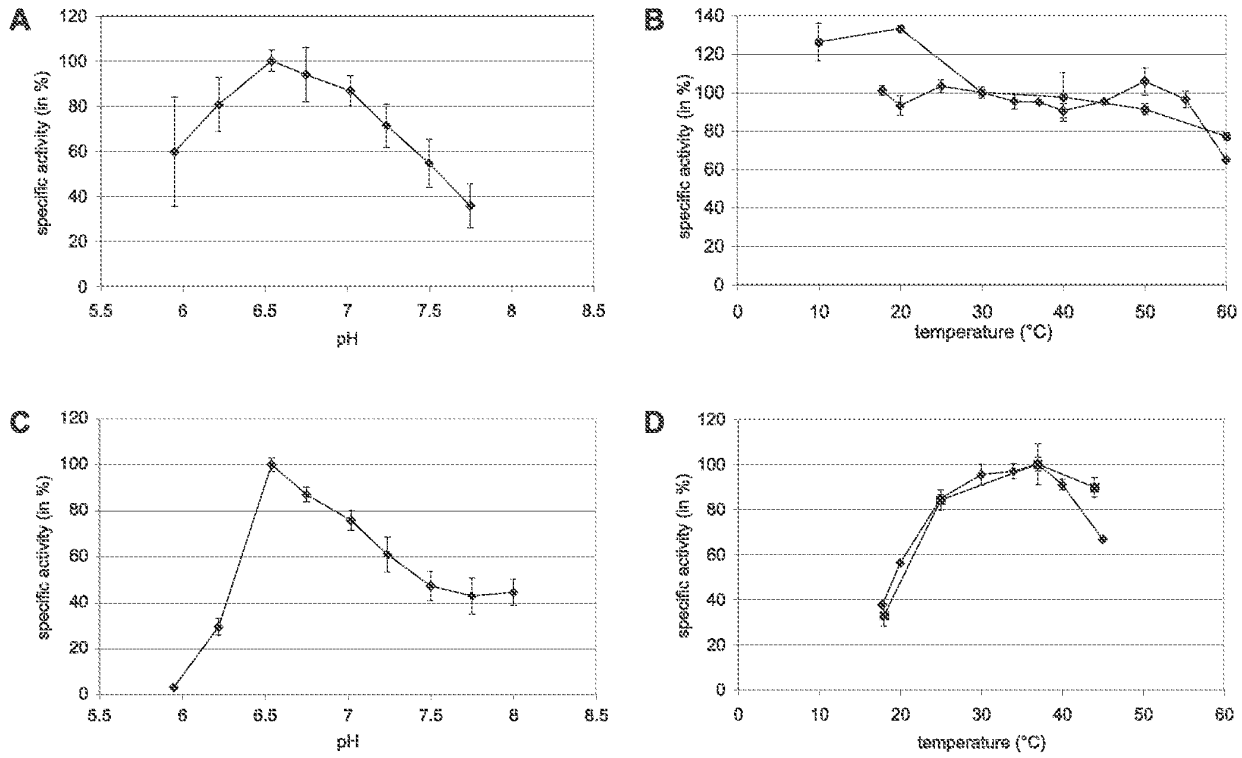


FIG. 3. Dependence of RdpA and SdpA on pH (A and C, respectively) and temperature (B and D, respectively). (A) The symbols indicate the means of six measurements. Enzyme activity was determined by the coupled continuous assay. (B) Symbols: ◆, data obtained with the discontinuous assay; ◆, data obtained with the coupled continuous assay. The experiments were performed with two independently purified RdpA samples. (C) The symbols indicate the means of six measurements for two independent experiments. Enzyme activity was determined by the coupled continuous assay. (D) Symbols: ■, data obtained with the discontinuous assay; ◆, data obtained with the coupled continuous assay. The experiments were performed with two independently purified SdpA samples.

groups on the aromatic ring, were investigated as well. RdpA converted phenoxypropanoic acids and none of the phenoxyacetic or phenoxybutyric acids except 3-methyl-5-chlorophenoxyacetic acid (MCPA). 2-(*R,S*)-4-Chlorophenoxypropanoic acid was turned over at the highest rate, followed by dichlorprop and mecoprop. Interestingly, the hydroxylated phenoxypropanoic acids and the unsubstituted phenoxypropanoic acids were converted (Table 3). SdpA exhibited the highest turnover rates with substituted phenoxypropanoic acids, and mecoprop was transformed fastest (Table 3). In contrast to RdpA, SdpA was able to convert MCPA and 2,4-D at low but measurable rates.

We also tested whether several carboxylic and dicarboxylic acids could replace α-ketoglutarate as a cofactor. Since the reporter enzyme in the coupled continuous assay, L-lactate dehydrogenase, showed activity with some cosubstrates, in this case the RdpA and SdpA activities were determined by the discontinuous assay. RdpA and SdpA were quite specific for α-ketoglutarate, with specific activities of 132.8 min^{-1} and 226.1 min^{-1}, respectively, and exhibited only low levels of activity in the presence of 2-oxoadipate (1.9% and 5%, respectively). There was no activity with any of the other carboxylic acids tested (oxaloacetate, 2-oxobutyrate, and 2-oxovalerate).

In the absence of ferrous iron, the activities of the two enzymes were substantially reduced (Table 2). The activity was independent of the iron salt, and other divalent cations could not substitute for Fe(II) (Table 4). Some of the divalent cations, including Co(II), Mg(II), Mn(II), and Ni(II), slightly inhibited enzyme activity.

Kinetic analysis. The apparent kinetic constants are shown in Table 5. For RdpA, Michaelis-Menten kinetics was observed for all substrates except oxygen; the reaction rate was linearly dependent on the oxygen concentration up to a concentration of about 1.0 mM. Therefore, apparent K_m and k_{cat} values could not be determined. However, it was possible to calculate a specificity constant (k_{cat}/K_m) for oxygen, which was 0.64 μM^{-1} min^{-1}. For the phenoxypropanoic acid substrates, RdpA exhibited the lowest K_m value and highest specificity for (*R*)-mecoprop, whereas the k_{cat} was highest for (*R,S*)-4-chlorophenoxypropanoic acid. The apparent K_m value for α-ketoglutarate was 2.8 μM; this value is below the lowest α-ketoglutarate concentration for which activity could be measured, but the data fit a Michaelis-Menten curve well, and according to the goodness of fit of the nonlinear regression analysis the value was reliable. SdpA exhibited Michaelis-Menten kinetics with all substrates and cosubstrates tested. Mecoprop was a better substrate than dichlorprop; i.e., the apparent K_m value was lower and the catalytic efficiency was higher. SdpA had an apparent K_m of 19.6 μM for α-ketoglutarate and an apparent K_m of 159 μM for oxygen.

Downloaded from http://aem.asm.org/ on April 29, 2012 by guest

COR-AAD1-00002952
Bayer EX1008 (Part 6 of 9)

TABLE 3. Substrate specificities of α-ketoglutarate-dependent (*R*)- and (*S*)-dichlorprop dioxygenases[a]

Substrate	RdpA		SdpA	
	Activity (%) (mean ± SD)	Sp act (min^{-1})	Activity (%) (mean ± SD)	Sp act (min^{-1})
(*R,S*)-Mecoprop	100	108.3/140.9[b]	100	274.8/209.7[b]
(*R,S*)-Dichlorprop	115.5 ± 3.6	125.8	65.3 ± 9.7	170.4
2-(*R,S*)-Phenoxypropanoic acid	39.7 ± 7.6	41.9	11.6 ± 2.6	31.5
2-(*R,S*)-3-Chlorophenoxypropanoic acid	14.8 ± 2.0	17.5	33.2 ± 2.5	96.6
2-(*R,S*)-4-Chlorophenoxypropanoic acid	152.1 ± 9.0	171.3	66.1 ± 3.2	198.6
2-(*R,S*)-2,4,5-Trichlorophenoxypropanoic acid	49.4 ± 4.3	55.9	71.5 ± 6.6	217.7
2-(*R,S*)-4-Hydroxyphenoxypropanoic acid	51.3 ± 7.3	55.9	19.6 ± 3.2	60.4
2,4-D[c,d]	<2	<3.5	5.6 ± 5.2	11.1
MCPA[c]	7.7 ± 4.3	10.5	20.3 ± 6.2	41.9
2,4-Dichlorophenoxybutyric acid[c,e]	<2	<3.5	<1	<3.4
4-Chloro-2-methylphenoxybutyric acid[c]	<2	<3.5	2.3 ± 1.2	4.7

[a] The substrate range was determined with RdpA and SdpA purified from two independent batches, and the enzyme activity of each batch was measured three times with all substrates.
[b] Activity determined by the coupled continuous assay/activity determined by the discontinuous assay.
[c] Enzyme activity was determined by the discontinuous assay.
[d] Only one SdpA batch showed slight activity with 2,4-D. The means might be overestimates.
[e] In one experiment, very low activity was observed. However, the 2,4-dichlorophenol concentration was below the detection limit (1 μM), and no increase in the amount of 2,4-dichlorophenol converted per unit of time was observed when the amount of RdpA in the assay was increased. Therefore, the activity was defined as <2%.

Screening for other 2,4-D-degrading genes. We screened the total DNA of *S. herbicidovorans* MH for genes encoding a TfdA-like dioxygenase and the aromatic ring-hydroxylating dioxygenase CadAB by performing hybridization and PCR experiments. Hybridization experiments with both *tfdA*- and *cadAB*-derived probes did not give positive results, and no *tfdA*-like gene could be amplified with the PCR primers derived from the conserved regions of the *tfdA* and *tfdA*α genes.

DISCUSSION

RdpA and SdpA are α-ketoglutarate-dependent dioxygenases. α-Ketoglutarate-dependent dioxygenases are grouped according to their cosubstrate and cofactor requirements. Enzyme activity measurements demonstrated that RdpA and SdpA belong to the α-ketoglutarate-dependent dioxygenase enzyme family, since their activities were strictly dependent on oxygen and α-ketoglutarate. Without ascorbate the activities were reduced to about 85% and 39%, respectively, of the highest activities. Ascorbate is not formally needed in the reaction, and it is generally thought to maintain Fe(II) in the reduced state. Two other α-ketoglutarate-dependent dioxygenases, prolyl 4-hydroxylase and lysyl hydroxylase, are almost completely inactivated within 1 min in the absence of ascorbate (9, 33, 34, 39). The inactivation is thought to involve a side reaction in which α-ketoglutarate is decarboxylated. This reaction is coupled to the oxidation of Fe(II) to Fe(III). Ascorbate reduces the ferric iron, thereby reactivating the enzyme. TfdA, on the other hand, is not as sensitive to the absence of ascorbate and is inactivated only after 30 to 40 min (16). The reductions in RdpA and SdpA activities in the absence of ascorbate indicated that α-ketoglutarate decarboxylation side reactions took place, although the inactivation was not as fast as the inactivation of the peptide hydroxylases.

Alignment of RdpA and SdpA with other α-ketoglutarate-dependent dioxygenases revealed conservation of the 2-His-1-carboxylate facial triad in RdpA and SdpA, as well as several other conserved amino acid residues (Fig. 4). RdpA and SdpA have the metal binding motif of subgroup II of the α-ketoglutarate-dependent dioxygenase family, which is $HXDX_{24}TX_{131}$

TABLE 4. Cofactor specificities of α-ketoglutarate-dependent (*R*)- and (*S*)-dichlorprop dioxygenases

Cofactor	RdpA		SdpA	
	Activity (%)	Sp act (min^{-1})	Activity (%)	Sp act (min^{-1})
$Fe(NH_4)_2(SO_4)_2$	100	97.9	100	243.2
$Fe(SO_4)$	97.5	94.4	92.8	229.1
$CaCl_2$	15.9	14.0	0	0
$CoCl_2$	0	0	0	0
$MgCl_2$	9.4	10.5	0	0
$MnCl_2$	0	0	0	0
$NiCl_2$	0	0	0	0

TABLE 5. Kinetic parameters of α-ketoglutarate-dependent (*R*)-dichlorprop dioxygenase and α-ketoglutarate-dependent (*S*)-dichlorprop dioxygenase

Substrate	K_m (μM)	k_{cat} (min^{-1})	k_{cat}/K_m (μM^{-1} min^{-1})
α-Ketoglutarate-dependent (*R*)-dichlorprop dioxygenase			
(*R*)-Mecoprop (10–2,000 μM)	98.8 ± 6.4	114.2	1.16
(*R*)-Dichlorprop (50–2,000 μM)	163.7 ± 13.5	170.1	1.04
(*R,S*)-4-Chlorophenoxypropanoic acid (120–2,000 μM)	262.4 ± 10.1	241.9	0.92
O_2 (0.02–1.0 mM)	ND[a]	ND	0.64
α-Ketoglutarate (7–1,900 μM)	2.8 ± 0.8	135.6	48.82
α-Ketoglutarate-dependent (*S*)-dichlorprop dioxygenase			
(*S*)-Mecoprop (50–2,000 μM)	132 ± 17.7	303.9	2.3
(*S*)-Dichlorprop (120–2,000 μM)	494.8 ± 43.9	284.6	0.58
O_2 (0.02–0.2 mM)	159.32	116[b]	0.75
α-Ketoglutarate (8–1,000 μM)	19.6 ± 2.5	229.7	11.72

[a] ND, not determined.
[b] The kinetic values for O_2 were determined with material from two different SdpA purification batches, both of which were less active than the purification batches used for other kinetic experiments. However, the stoichiometry of the reaction was verified with material from a third purification batch (data not shown).

Downloaded from http://aem.asm.org/ on April 29, 2012 by guest

COR-AAD1-00002953
Bayer EX1008 (Part 6 of 9)

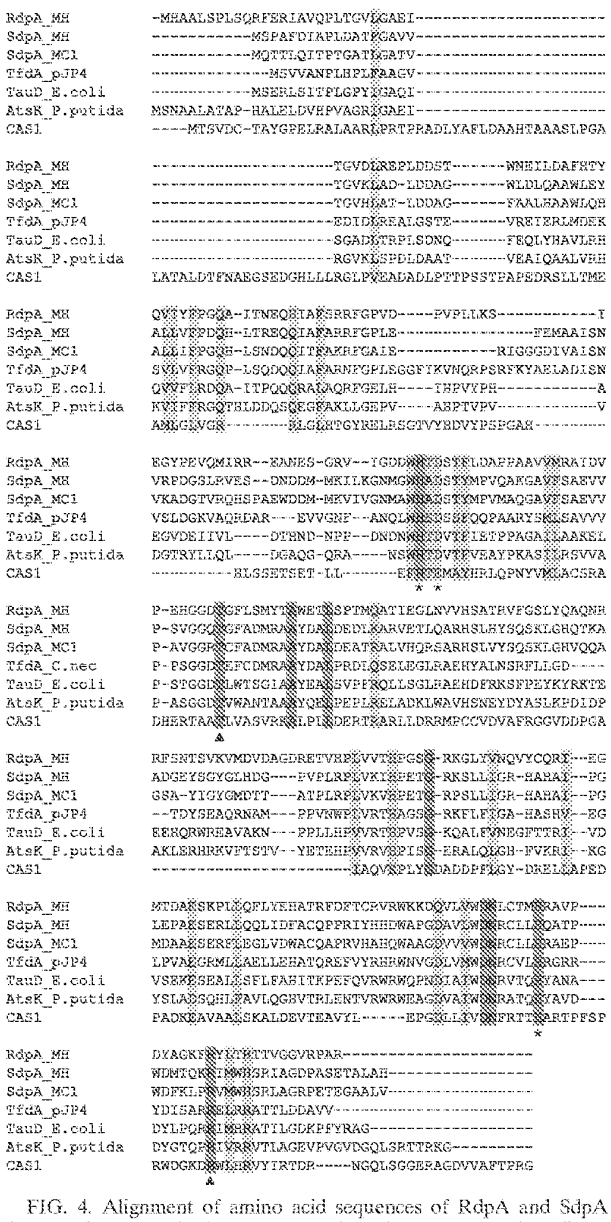


FIG. 4. Alignment of amino acid sequences of RdpA and SdpA from strain MH and other group II α-ketoglutarate-dependent dioxygenases. The alignment was performed with the T-Coffee software (http://igs-server.cnrs-mrs.fr/Tcoffee/tcoffee_cgi/index.cgi). TfdA_pJP4, 2,4-D dioxygenase from *C. necator* JMP134(pJP4) (accession no. AAA21983); RdpA_MH, (*R*)-dichlorprop dioxygenase from *S. herbicidovorans* MH (accession no. CAF32811); SdpA_MH, (*S*)-dichlorprop dioxygenase from *S. herbicidovorans* MH (accession no. CAF32813); SdpA_MC1, (*S*)-dichlorprop dioxygenase from *D. acidovorans* MC1 (accession no. AAM90963); TauD_E. coli, taurine dioxygenase from *E. coli* (accession no. AAC73471); AtsK_P. putida, alkylsulfate dioxygenase from *P. putida* (accession no. AAD31784); CAS1, clavaminate synthase from *Streptomyces clavuligeres* (accession no. A44241). Highly conserved residues (dark gray boxes) and conserved residues (light gray boxes) are highlighted. Asterisks indicate the conserved or predicted Fe(II)-binding residues, and triangles indicate the α-ketoglutarate binding residues (12, 36).

$HX_{10}R$. On the basis of the crystal structure of TauD, a structural model of TfdA, and mutagenesis studies (12, 20, 36), we concluded that His-111–Asp-113–His-270 and His-102–Asp-104–His-257 comprise the facial triads of RdpA and SdpA, respectively, which are responsible for iron binding. Residues Thr-138 and Arg-281 of RdpA and residues Thr-129 and Arg-268 of SdpA might act as α-ketoglutarate binding sites.

A comparison of kinetic data for RdpA from *S. herbicidovorans* MH with kinetic data for RdpA from *D. acidovorans* MC1 (48) revealed certain differences. Although the amino acid sequences of the enzymes are identical, the reported K_m values of the phenoxypropanoic acid derivatives for RdpA from *D. acidovorans* MC1 are less than the K_m values that we report here by a factor of about 3. The differences might be explained by the fact that different methods were used to obtain the kinetic data. In our hands, the method based on 2-aminoantipyridine (13–15) that was used for determination of the kinetic parameters of RdpA from *D. acidovorans* MC1 (48) never gave reproducible results for kinetic measurements at low substrate concentrations because of uncontrolled formation of background color. Nonspecific background activity might lead to overestimation of enzyme velocity at low substrate concentrations, which in turn might lead to underestimation of K_m values. Our problem with the aminoantipyrine method was the main reason for developing the continuous coupled enzyme assay described in Materials and Methods. With this assay, we were able to monitor the enzyme reaction continuously and to determine true initial velocities.

To our knowledge, the RdpA proteins from *S. herbicidovorans* MH and *D. acidovorans* MC1 are the only α-ketoglutarate-dependent dioxygenases with a homotrimeric structure (47). Most enzymes of this class are monomers or homodimers, such as SdpA and TfdA; tetramers, such as the alkylsulfatase from *Pseudomonas putida*, are also known (11, 16, 47).

RdpA from *S. herbicidovorans* was surprisingly insensitive to an increase in temperature (Fig. 3B). No Arrhenius-like activity profile was observed, and RdpA was found to be stable at temperatures up to 55°C. This finding correlates with the findings for an α-ketoglutarate-dependent 2,4-D dioxygenase from *Burkholderia cepacia* 2a, which also showed an unexpectedly small increase in activity with increasing temperature and at 10°C still exhibited 77% of the activity observed at 25°C (37). In contrast, TfdA from *C. necator* JMP134(pJP4) exhibits more typical temperature-dependent activity; the activity increases with higher temperatures up to 30°C, and the enzyme is completely inactivated at 40°C within 5 min (16).

RdpA and SdpA catalyze enantioselective reactions. RdpA converted only the (*R*) enantiomers of phenoxypropanoic acid herbicides, and SdpA converted only the (*S*) enantiomers. This confirmed the results of previous experiments with *S. herbicidovorans* cell extracts in which the existence of two distinct α-ketoglutarate-dependent dioxygenases in strain MH was proposed (35). We firmly concluded that *S. herbicidovorans* MH harbors two distinct enzymes with opposite enantioselectivities. Enantioselective conversion is more widespread in α-ketoglutarate-dependent dioxygenases. Also, RdpA from *D. acidovorans* MC1 did not significantly convert (*S*) enantiomers of phenoxypropanoic acids (48). Some α-ketoglutarate-dependent 2,4-D dioxygenases are also capable of enantioselective conversion of mecoprop and/or dichlorprop. For example, TfdA from *C. necator* JMP134(pJP4) and TfdA from *Burkhold-*

Downloaded from http://aem.asm.org/ on April 29, 2012 by guest

COR-AAD1-00002954
Bayer EX1008 (Part 6 of 9)

eria cepacia RASC cleave only the ether bond of (*S*)-dichlorprop, whereas TfdA from *Alcaligenes denitrificans* converts only the (*R*) enantiomer (41). This difference is surprising, given the high degree of sequence conservation among these three TfdA dioxygenases. None of the TfdA dioxygenases, however, is able to convert both enantiomers of phenoxypropanoic acids at significant catalytic rates. To oxidize both enantiomers, two distinct dioxygenases are required in strains such as *S. herbicidovorans* MH or *D. acidovorans* MC1 (31, 35, 47, 48). Kinetic investigations with site-directed variants of the enzymes demonstrated that not just one but many residues in RdpA and SdpA play a structural role in directing enantiospecificity (T. A. Müller, M. I. Zavodsky, M. Feig, L. A. Kuhn, and R. P. Hausinger, submitted for publication).

Substrate and cosubstrate specificities. RdpA exhibited narrow substrate specificity with respect to the alkyl moiety in the alkanoic acid side chain; only phenoxypropanoic acids were converted, and 2,4-D and phenoxybutyric acids were not converted. This is in contrast to SdpA, which showed measurable activity with 2,4-D. It is also in contrast to RdpA from *D. acidovorans* MC1, whose activity with 2,4-D was reported to be 14% of its activity with (*R*)-dichlorprop (48). This is yet another difference between the two enzymes for which there is not a satisfactory explanation at the moment. Neither RdpA nor TfdA from *C. necator* converted phenoxybutyric acids (16, 48). These results indicate that the active sites of RdpA and of TfdA are specific with regard to the alkanoic acid substituent and are indifferent with regard to the substituents of the aromatic ring. Additionally, RdpA was not inhibited by the (*S*) enantiomers of phenoxypropanoic acids, which indicates that there is no binding of these enantiomers at the active site.

α-Ketoglutarate-dependent dioxygenases have different cosubstrate specificities. AtsK, an alkylsulfatase from *P. putida* S-313, and TfdA, for instance, exhibit broad cosubstrate ranges, and many oxo acids substitute for α-ketoglutarate (16, 22). TauD and the inorganic α-ketoglutarate-dependent hypophosphite dioxygenase HtxA exhibited stricter specificities, and other than α-ketoglutarate, they used only 2-oxoadipate as a cosubstrate, albeit with reduced activities in the range from 4 to 23% (11, 16, 49). RdpA and SdpA showed the same cosubstrate specificities as these two enzymes, but the remaining activities with 2-oxoadipate were only 2% and 5%, respectively. The adaptation of RdpA and SdpA for α-ketoglutarate is apparent from the low apparent K_m values for α-ketoglutarate (3 to 20 μM).

A linear relationship between the O_2 concentration (0 to 1.0 mM) and the reaction rate was observed; hence, only the value for the apparent second-order rate constant k_{cat}/K_m that can be calculated from this relationship is shown in Table 5. Although the oxygen dependence of SdpA followed Michelis-Menten kinetics, the apparent K_m value (0.16 mM O_2) was also quite high. Compared to other α-ketoglutarate-dependent dioxygenases, RdpA and SdpA have unusually high apparent K_m values for oxygen. Apparent K_m values of 40 to 50 μM O_2 were observed for lysyl hydroxylase and an α-ketoglutarate-dependent 4-hydroxylase from *Catharanthus roseus* which is involved in vindoline biosynthesis (8, 39). Flavonol dioxygenase exhibits even a lower apparent K_m value, 5.26 μM (3). The activities of RdpA and SdpA are therefore highly dependent on the oxygen concentration in laboratory assays.

Existence of another dioxygenase involved in phenoxyalkanoic acid degradation in strain MH. RdpA did not convert 2,4-D, and SdpA only converted this compound at low rates. However, *S. herbicidovorans* MH does grow on 2,4-D, and it grows at a higher rate than it grows on mecoprop and dichlorprop (53). Therefore, another phenoxyalkanoic acid-converting enzyme, which is specific for 2,4-D, must be present in *S. herbicidovorans* MH. Our results of hybridization and PCR experiments suggest that *S. herbicidovorans* MH did not harbor a gene sufficiently similar to the *tfdA*, *tfdA*α, or *cadAB* genes to allow detection. Therefore, the nature of this additional enzyme in *S. herbicidovorans* MH remains unclear.

In conclusion, we describe the characteristics of two α-ketoglutarate-dependent dioxygenases, RdpA and SdpA, from *S. herbicidovorans* MH that catalyze enantioselective ether cleavage of phenoxypropanoic acids to form achiral phenols. These two dioxygenases are a good example of an enzyme pair in which each enzyme converts only one enantiomer of a chiral substrate.

ACKNOWLEDGMENT

T.A.M. was supported by Swiss National Science Foundation grant NF-3100-055468.

REFERENCES

1. **Aberg, B.** 1973. Plant growth regulators. XXXI. Some monochloro-monomethylphenoxyacetic and related optically active propionic acids. Swed. J. Agric. Res. **3**:49–62.
2. **Ahrens, W. H.** 1994. Herbicide handbook (WSSA), 7th ed. Weed Science Society of America, Champaign, Ill.
3. **Anzelotti, D., and R. K. Ibrahim.** 2000. Novel flavonol 2-oxoglutarate dependent dioxygenase: affinity purification, characterization, and kinetic properties. Arch. Biochem. Biophys. **382**:161–172.
4. **Ausubel, F. M., R. Brent, R. E. Kingston, D. D. Moore, J. G. Seidman, J. A. Smith, and K. Struhl, (ed.).** 2002. Current protocols in molecular biology. John Wiley & Sons, Inc., New York, N.Y.
5. **Benes, V., Z. Hostomosky, L. Arnold, and V. Paces.** 1993. M13 and pUC vectors with new unique restriction sites for cloning. Gene **130**:151–152.
6. **Bradford, M. M.** 1976. A rapid and sensitive method for the determination of microgram quantities of protein utilizing the principle of protein-dye binding. Anal. Biochem. **72**:248–254.
7. **Costas, M., M. P. Mehn, M. P. Jensen, and L. Que, Jr.** 2004. Dioxygen activation at mononuclear nonheme iron active sites: enzymes, models, and intermediates. Chem. Rev. **104**:939–986.
8. **de Carolis, E., and V. de Luca.** 1993. Purification, characterization, and kinetic analysis of a 2-oxoglutarate-dependent dioxygenase involved in vindoline biosynthesis from *Catharanthus roseus*. J. Biol. Chem. **268**:5504–5511.
9. **de Jong, L., S. P. J. Albracht, and A. Kemp.** 1982. Prolyl 4-hydroxylase activity in relation to the oxidation state of enzyme-bound iron. The role of ascorbate in peptidyl proline hydroxylation. Biochim. Biophys. Acta **704**:326–332.
10. **Donaldson, D., T. Kiely, and A. Grube.** 2002. Pesticides industry sales and usage. 1998 and 1999 market estimates. U.S. Environmental Protection Agency, Washington, D.C.
11. **Eichhorn, E., J. R. van der Ploeg, M. A. Kertesz, and T. Leisinger.** 1997. Characterization of α-ketoglutarate-dependent taurine dioxygenase from *Escherichia coli*. J. Biol. Chem. **272**:23031–23036.
12. **Elkins, J. M., M. J. Ryle, I. J. Clifton, J. C. Dunning Hotopp, J. S. Lloyd, N. I. Burzlaff, J. E. Baldwin, R. P. Hausinger, and P. L. Roach.** 2002. X-ray crystal structure of *Escherichia coli* taurine/α-ketoglutarate dioxygenase complexed to ferrous iron and substrates. Biochemistry **41**:5185–5192.
13. **Emerson, E.** 1943. The condensation of aminoantipyrine. II. A new color test for phenolic compounds. J. Org. Chem. **8**:532–534.
14. **Emerson, E., and K. Kelly.** 1948. The condensation of aminoantipyrine. VI. A study of the effect of excess base on the reaction of aminoantipyrine with phenolic compounds in the presence of oxidizing agents. J. Org. Chem. **13**:532–534.
15. **Fukumori, F., and R. P. Hausinger.** 1993. *Alcaligenes eutrophus* JMP134 "2,4-dichlorophenoxyacetate monooxygenase" is an α-ketoglutarate-dependent dioxygenase. J. Bacteriol. **175**:2083–2096.
16. **Fukumori, F., and R. P. Hausinger.** 1993. Purification and characterization of 2,4-dichlorophenoxyacetate/α-ketoglutarate dioxygenase. J. Biol. Chem. **268**:24311–24317.

Downloaded from http://aem.asm.org/ on April 29, 2012 by guest

COR-AAD1-00002955
Bayer EX1008 (Part 6 of 9)

17. **Hausinger, R. P.** 2004. Fe(II)/α-ketoglutarate dependent hydroxylases and related enzymes. Crit. Rev. Biochem. Mol. Biol. **39:**1–47.
18. **Hausinger, R. P., and F. Fukumori.** 1995. Characterization of the first enzyme in 2,4-dichlorophenoxyacetic acid metabolism. Environ. Health Perspect. Suppl. **103:**37–39.
19. **Hegg, E. L., and L. Que, Jr.** 1997. The 2-His-1-carboxylate facial triad—an emerging structural motif in mononuclear non-heme iron(II) enzymes. Eur. J. Biochem. **250:**625–629.
20. **Hogan, D. A., S. R. Smith, E. A. Saari, J. McCracken, and R. P. Hausinger.** 2000. Site-directed mutagenesis of 2,4-dichlorophenoxyacetic acid/α-ketoglutarate dioxygenase. J. Biol. Chem. **275:**12400–12409.
21. **Horvath, M., G. Ditzelmüller, M. Loidl, and F. Streichsbier.** 1990. Isolation and characterization of a 2-(2,4-dichlorophenoxy)propionic acid degrading soil bacterium. Appl. Microbiol. Biotechnol. **33:**213–216.
22. **Kahnert, A., and M. A. Kertesz.** 2000. Characterization of a sulfur-regulated oxygenative alkylsulfatase from *Pseudomonas putida* S-313. J. Biol. Chem. **275:**31661–31667.
23. **Kitagawa, W., S. Takami, K. Miyauchi, E. Masai, Y. Kamagata, J. M. Tiedje, and M. Fukuda.** 2002. Novel 2,4-dichlorophenoxyacetic acid degradation genes from oligotrophic *Bradyrhizobium* sp. strain HW13 isolated from a pristine environment. J. Bacteriol. **184:**509–518.
24. **Kohler, H.-P. E.** 1999. *Sphingomonas herbicidovorans* MH: a versatile phenoxyalkanoic herbicide degrader. J. Ind. Microbiol. Biotechnol. **23:**336–340.
25. **Kohler, H.-P. E., W. Angst, W. Giger, C. Kranz, S. Müller, and M. J.-F. Suter.** 1997. Environmental fate of chiral pollutants—the necessity of considering stereochemistry. Chimia **51:**947–951.
26. **Laemmli, U. K.** 1970. Cleavage of structural proteins during the assembly of the head of bacteriophage T4. Nature **227:**680–685.
27. **Lange, S. J., and L. Que.** 1998. Oxygen activating nonheme iron enzymes. Curr. Opin. Chem. Biol. **2:**159–172.
28. **Loos, M. A.** 1975. Phenoxyalkanoic acids, p. 1–128. *In* P. C. Kearney and D. D. Kaufmann (ed.), Herbicides. Chemistry, degradation and mode of action, 2nd ed., vol. 1. Marcel Dekker, Inc., New York, N.Y.
29. **Matell, M.** 1953. Stereochemical studies on plant growth regulators. VII. Optically active α-(2-methyl-4-chlorophenoxy)-propionic acid and α-(2,4-dichlorophenoxy)-*n*-butyric acid and their steric relations. Ark. Kemi **6:**365–373.
30. **Müller, R. H., S. Jorks, S. Kleinsteuber, and W. Babel.** 1999. *Comamonas acidovorans* strain MC1: a new isolate capable of degrading the chiral herbicides dichlorprop and mecoprop and the herbicides 2,4-D and MCPA. Microbiol. Res. **154:**241–246.
31. **Müller, T. A., S. M. Byrde, T. Fleischmann, J. R. van der Meer, and H.-P. E. Kohler.** 2004. Genetic analysis of phenoxyalkanoic acid degradation in *Sphingomonas herbicidovorans* MH. Appl. Environ. Microbiol. **70:**6066–6075.
32. **Müller, T. A., and H.-P. E. Kohler.** 2004. Chirality of pollutants—effects on metabolism and fate. Appl. Microbiol. Biotechnol. **64:**300–316.
33. **Myllylä, R., E.-R. Kuutti-Savolainen, and K. I. Kivirikko.** 1978. The role of ascorbate in the prolyl hydroxylase reaction. Biochem. Biophys. Res. Commun. **83:**441–448.
34. **Myllylä, R., K. Majamaa, V. Günzler, H. M. Hanauske-Abel, and K. I. Kivirikko.** 1984. Ascorbate is consumed stoichiometrically in the uncoupled reactions catalyzed by prolyl 4-hydroxylase and lysyl hydroxylase. J. Biol. Chem. **259:**5403–5405.
35. **Nickel, K., M. J.-F. Suter, and H.-P. E. Kohler.** 1997. Involvement of two α-ketoglutarate-dependent dioxygenases in enantioselective degradation of (*R*)- and (*S*)-mecoprop by *Sphingomonas herbicidovorans* MH. J. Bacteriol. **179:**6674–6679.
36. **O'Brien, J. R., D. J. Schuller, V. S. Yang, B. D. Dillard, and W. N. Lanzilotta.** 2003. Substrate-induced conformational changes in *Escherichia coli* taurine/α-ketoglutarate dioxygenase and insight into the oligomeric structure. Biochemistry **42:**5547–5554.
37. **Poh, R., X. Xia, I. J. Bruce, and A. R. Smith.** 2001. 2,4-dichlorophenoxyacetate/α-ketoglutarate dioxygenases from *Burkholderia cepacia* 2a and *Ralstonia eutropha* JMP134. Microbios **105:**43–63.
38. **Prescott, A. G., and M. D. Lloyd.** 2000. The iron(II) and 2-oxoacid-dependent dioxygenases and their role in metabolism. Nat. Prod. Rep. **17:**367–383.
39. **Puistola, U., T. M. Turpeenniemi-Hujanen, R. Myllylä, and K. I. Kivirikko.** 1980. Studies on the lysyl hydroxylase reaction. I. Initial velocity kinetics and related aspects. Biochim. Biophys. Acta **611:**40–50.
40. **Ravatn, R., S. Studer, D. Springael, A. J. B. Zehnder, and J. R. van der Meer.** 1998. Chromosomal integration, tandem amplification, and reamplification in *Pseudomonas putida* F1 of a 105-kilobase genetic element containing the chlorocatechol degradative genes from *Pseudomonas* sp. strain B13. J. Bacteriol. **180:**4360–4369.
41. **Saari, R. E., D. A. Hogan, and R. P. Hausinger.** 1999. Stereospecific degradation of the phenoxypropionate herbicide dichlorprop. J. Mol. Catal. B Enzym. **6:**421–428.
42. **Sambrook, J., E. F. Fritsch, and T. Maniatis.** 1989. Molecular cloning: a laboratory manual. Cold Spring Harbor Laboratory, Cold Spring Harbor, N.Y.
43. **Schleinitz, K. M., S. Kleinsteuber, T. Vallaeys, and W. Babel.** 2004. Localization and characterization of two novel genes encoding stereospecific dioxygenases catalyzing 2(2,4-dichlorophenoxy)propionate cleavage in *Delftia acidovorans* MC1. Appl. Environ. Microbiol. **70:**5357–5365.
44. **Schofield, C. J., and Z. Zhang.** 1999. Structural and mechanistic studies on 2-oxoglutarate-dependent oxygenases and related enzymes. Curr. Opin. Struct. Biol. **9:**722–731.
45. **Tatusova, T. A., and T. L. Madden.** 1999. BLAST 2 sequences, a new tool for comparing protein and nucleotide sequences. FEMS Microbiol. Lett. **174:**247–250.
46. **Vallaeys, T., R. R. Fulthorpe, A. M. Wright, and G. Soulas.** 1996. The metabolic pathway of 2,4-dichlorophenoxyacetic acid degradation involves different families of *tfdA* and *tfdB* genes according to PCR-RFLP analysis. FEMS Microbiol. Ecol. **20:**163–172.
47. **Westendorf, A., D. Benndorf, R. H. Müller, and W. Babel.** 2002. The two enantiospecific dichlorprop/α-ketoglutarate-dioxygenases from *Delftia acidovorans* MC1—protein and sequence data of RdpA and SdpA. Microbiol. Res. **157:**1–6.
48. **Westendorf, A., R. H. Müller, and W. Babel.** 2003. Purification and characterisation of the enantiospecific dioxygenases from *Delftia acidovorans* MC1 initiating the degradation of phenoxypropionate and phenoxyacetate herbicides. Acta Biotechnol. **23:**3–17.
49. **White, A. K., and W. W. Metcalf.** 2002. Isolation and biochemical characterization of hypophosphite/2-oxoglutarate dioxygenase. A novel phosphorus-oxidizing enzyme from *Pseudomonas stutzeri* WM88. J. Biol. Chem. **277:**38262–38271.
50. **Williams, A.** 1996. Opportunities for chiral agrochemicals. Pestic. Sci. **46:**3–9.
51. **Worthing, C. R., and R. J. Hance.** 1991. The pesticide manual—a world compendium, 9th ed. The British Crop Council, Farnham, Great Britain.
52. **Zipper, C.** 1998. Microbial degradation and environmental fate of chiral phenoxyalkanoic acid herbicides. Ph.D. thesis. ETH Zürich, Zürich, Switzerland.
53. **Zipper, C., M. Bunk, A. J. B. Zehnder, and H.-P. E. Kohler.** 1998. Enantioselective uptake and degradation of the chiral herbicide dichlorprop [(*RS*)-2-(2,4-dichlorophenoxy)propanoic acid] by *Sphingomonas herbicidovorans* MH. J. Bacteriol. **180:**3368–3374.
54. **Zipper, C., K. Nickel, W. Angst, and H.-P. E. Kohler.** 1996. Complete microbial degradation of both enantiomers of the chiral herbicide mecoprop [(*RS*)-2-(4-chloro-2-methylphenoxy)propionic acid] in an enantioselective manner by *Sphingomonas herbicidovorans* sp. nov. Appl. Environ. Microbiol. **62:**4318–4322.

Downloaded from http://aem.asm.org/ on April 29, 2012 by guest

COR-AAD1-00002956
Bayer EX1008 (Part 6 of 9)

Applied and Environmental Microbiology

Abundance and Expression of Enantioselective *rdpA* and *sdpA* Dioxygenase Genes during Degradation of the Racemic Herbicide (*R,S*)-2-(2,4-Dichlorophenoxy)Propionate in Soil

Mélanie M. Paulin, Mette H. Nicolaisen and Jan Sørensen
Appl. Environ. Microbiol. **2010, 76(9):2873. DOI: 10.1128/AEM.02270-09.**
Published Ahead of Print 19 March 2010.

Updated information and services can be found at:
http://aem.asm.org/content/76/9/2873

These include:

REFERENCES This article cites 47 articles, 12 of which can be accessed free at: http://aem.asm.org/content/76/9/2873#ref-list-1

CONTENT ALERTS Receive: RSS Feeds, eTOCs, free email alerts (when new articles cite this article), more»

Information about commercial reprint orders: http://journals.asm.org/site/misc/reprints.xhtml
To subscribe to to another ASM Journal go to: http://journals.asm.org/site/subscriptions/

Journals.ASM.org

Downloaded from http://aem.asm.org/ on June 5, 2012 by guest

COR-AAD1-00002957
Bayer EX1008 (Part 6 of 9)

APPLIED AND ENVIRONMENTAL MICROBIOLOGY, May 2010, p. 2873–2883 Vol. 76, No. 9
0099-2240/10/$12.00 doi:10.1128/AEM.02270-09
Copyright © 2010, American Society for Microbiology. All Rights Reserved.

Abundance and Expression of Enantioselective *rdpA* and *sdpA* Dioxygenase Genes during Degradation of the Racemic Herbicide (*R,S*)-2-(2,4-Dichlorophenoxy)Propionate in Soil[▽]

Mélanie M. Paulin,* Mette H. Nicolaisen, and Jan Sørensen

Section of Genetics and Microbiology, Department of Agriculture and Ecology, Faculty of Life Sciences, University of Copenhagen, Thorvaldsensvej 40, 1871 Frederiksberg C, Denmark

Received 21 September 2009/Accepted 8 March 2010

The *rdpA* and *sdpA* genes encode two enantioselective α-ketoglutarate-dependent dioxygenases catalyzing the initial step of microbial degradation of the chiral herbicide (*R,S*)-2-(2,4-dichlorophenoxy)propionate (*R,S*-dichlorprop). Primers were designed to assess abundance and transcription dynamics of *rdpA* and *sdpA* genes in a natural agricultural soil. No indigenous *rdpA* genes were detected, but *sdpA* genes were present at levels of approximately 10^3 copies g of soil^{-1}. Cloning and sequencing of partial *sdpA* genes revealed a high diversity within the natural *sdpA* gene pool that could be divided into four clusters by phylogenetic analysis. BLASTp analysis of deduced amino acids revealed that members of cluster I shared 68 to 69% identity, cluster II shared 78 to 85% identity, cluster III shared 58 to 64% identity, and cluster IV shared 55% identity to their closest SdpA relative in GenBank. Expression of *rdpA* and *sdpA* in *Delftia acidovorans* MC1 inoculated in soil was monitored by reverse transcription quantitative real-time PCR (qPCR) during *in situ* degradation of 2 and 50 mg kg^{-1} of (*R,S*)-dichlorprop. (*R,S*)-Dichlorprop amendment created a clear upregulation of both *rdpA* and *sdpA* gene expression during the active phase of ^{14}C-labeled (*R,S*)-dichlorprop mineralization, particularly following the second dose of 50 mg kg^{-1} herbicide. Expression of both genes was maintained at a low constitutive level in nonamended soil microcosms. This study is the first to report the presence of indigenous *sdpA* genes recovered directly from natural soil and also comprises the first investigation into the transcription dynamics of two enantioselective dioxygenase genes during the *in situ* degradation of the herbicide (*R,S*)-dichlorprop in soil.

It has been reported that as many as 25% of all chemical pesticides exist as chiral molecules (12), otherwise known as enantiomers. (*R,S*)-2-(2,4-Dichlorophenoxy)propionate [(*R,S*)-dichlorprop] is a chiral herbicide used mostly in agriculture, lawn care, and industry for the control of broad-leaved weeds and belongs to the family of phenoxyalkanoic herbicides, which also includes other racemates such as the structurally related phenoxypropionate (*R,S*)-2-(4-chloro-2-methylphenoxy)propionate [(*R,S*)-mecoprop]. The *R* enantiomer of both dichlorprop and mecoprop is the only form providing herbicidal activity, and several European countries have now started implementing stricter regulations on the use of chiral herbicides, e.g., banning racemic dichlorprop in favor of *R*-enantiomer-specific formulations (10). Nevertheless, it is important to evaluate the impact of the racemic mixtures as not only are they still applied in some parts of the world, but instances of enantiomerization have been reported [e.g., (*S*)-dichlorprop converting to (*R*)-dichlorprop or vice versa] (26).

Degradation of (*R,S*)-dichlorprop in the environment is mainly mediated by biological activity (22, 26, 36). As in the case of other chiral pesticides (6, 35), preferential degradation of either the *R* or the *S* enantiomer of dichlorprop during microbial degradation has been reported (13, 22, 26). (*R,S*)-Dichlorprop enantioselectivity is largely dependent upon the behavior of the microbial community at hand and can be influenced by factors such as pH (3, 23), soil type (36), and the environment (e.g., soil, water, or sludge) (4, 13, 47). The enantioselectivity observed during the microbial transformation of chiral dichlorprop implies that enzymes involved in degradation of this compound are somehow able to differentiate between enantiomers. For phenoxyalkanoic acid herbicides, the first step in the catabolic pathway usually begins with etherolytic cleavage of the side chain that is catalyzed by an α-ketoglutarate-dependent dioxygenase, thus converting the herbicides into corresponding phenols. For phenoxyacetate herbicides such as achiral 2,4-dichlorophenoxyacetate (2,4-D) and 4-chloro-2-methylphenoxyacetate (MCPA), this dioxygenase is typically encoded by the *tfdA* gene (2, 7, 11). Although a few strains are capable of degrading at least one enantiomer of dichlorprop using TfdA, increasing amounts of data have recently revealed the existence of two α-ketoglutarate-dependent dioxygenases distinct from TfdA that exhibit opposite stereoselectivities toward degradation of (*R,S*)-dichlorprop and (*R,S*)-mecoprop. These dioxygenases, designated RdpA and SdpA, target each of the two *R* and *S* enantiomers, respectively (31, 45). Unfortunately, studies focusing on enantiospecific degradative enzymes are far more scarce than studies on the involvement of TfdA during 2,4-D and MCPA degradation.

Although degradation of (*R,S*)-dichlorprop in various envi-

* Corresponding author. Mailing address: Section of Genetics and Microbiology, Department of Agriculture and Ecology, Faculty of Life Sciences, University of Copenhagen, Thorvaldsensvej 40, 1871 Frederiksberg C, Denmark. Phone: 45 3533 2627. Fax: 45 3533 2606. E-mail: mmpa@life.ku.dk.

▽ Published ahead of print on 19 March 2010.

Downloaded from http://aem.asm.org/ on June 5, 2012 by guest

COR-AAD1-00002958
Bayer EX1008 (Part 6 of 9)

ronments is well reported (for a review, see reference 32), very few bacterial strains able to oxidize both enantiomers of dichlorprop using the RdpA and SdpA enzymes have been isolated to date. The best described are *Sphingomonas herbicidovorans* MH (16, 48) and *Delftia acidovorans* MC1 (28, 29), from which *rdpA* and *sdpA* genes were first isolated and sequenced (30, 39). Enzyme activity from these strains has shown that RdpA dioxygenase is generally highly specific to the *R* enantiomer of 2-phenoxypropionates and shows very weak activity toward phenoxyacetates, whereas SdpA is enantioselective to the *S* enantiomer but can also convert certain phenoxyacetates such as 2,4-D and MCPA with various catalytic activities (27, 31, 44, 45). The genetic background has only recently become available and shows that *rdpA* sequences reported to date are nearly identical while *sdpA* sequences between *S. herbicidovorans* MH and *D. acidovorans* MC1 are far more variable (30, 39). In *D. acidovorans* MC1, plasmid-borne *rdpA* and *sdpA* genes were deduced to be constitutively expressed based on enzyme activity during induction studies with (*R*)- and (*S*)-dichlorprop in mineral salts solution (MSS) (29). Studies of *S. herbicidovorans* MH have looked specifically at mRNA and found that both genes were constitutively expressed (30), although earlier studies on enzyme activity reported constitutive activity only for SdpA (33). It is noteworthy to mention that such induction studies conducted on pure cultures grown and tested in laboratory media may not always reflect the reality observed in more complex soil environments.

Although RdpA and SdpA from a few dichlorprop-degrading strains have been biochemically characterized, there is scarcely any information available regarding the *rdpA* and *sdpA* genes when it comes to their presence, natural abundance, and activation in soil environments. In an effort to better understand the diversity of genes involved in mecoprop degradation, Zakaria et al. (46) reported the presence of *rdpA* and *sdpA* genes from soil enrichment cultures grown on either (*R*)-mecoprop or (*R,S*)-mecoprop but did not provide any quantitative data or time course analysis. This might be due to the difficulties often encountered while working with direct quantification of nucleic acids in soil. Recent advances in detection of mRNA in soil have helped overcome some of these problems and now make it possible to achieve reliable quantitative transcription analysis of functional genes in soil (34).

This work aims to provide an initial report on the natural abundance and the *in situ* transcription dynamics of *rdpA* and *sdpA* genes during degradation of (*R,S*)-dichlorprop in soil. New sets of specific primers for detection by SYBR green quantitative real-time PCR (qPCR) were designed and tested to target *rdpA* and *sdpA* genes. Soil DNA extracts were screened for the presence of these genes by qPCR followed by cloning and sequencing for phylogenetic analysis. To investigate regulation of *rdpA* and *sdpA* gene expression under *in situ* conditions, *D. acidovorans* MC1 cells were inoculated directly into soil microcosms amended with (*R,S*)-dichloprop and reverse transcription combined with qPCR was used to follow transcription dynamics over time. Herbicide degradation was followed by generating progress curves of accumulated $[^{14}C]CO_2$ evolved from (*R,S*)-[^{14}C]dichlorprop mineralization.

MATERIALS AND METHODS

Bacterial strains and culture conditions. *D. acidovorans* MC1 and *S. herbicidovorans* MH (DSMZ, Braunschweig, Germany; DSM11019), both carrying *rdpA* and *sdpA* genes, were grown and maintained under selective conditions in mineral salts solution (MSS) (29) supplemented with 400 mg liter^{-1} of (*R,S*)-dichlorprop. *Cupriavidus necator* AEO106(pRO101) carrying the *tfdA* gene was grown in LB medium supplemented with 10 mg ml^{-1} tetracycline. Incubations for growth of all strains were performed at 28°C with shaking at 200 rpm.

Soil microcosm setup and sampling. Organic agricultural topsoil classified as Typic Argiudoll (USDA soil taxonomy) with 19% clay, 18% silt, 62% sand, and 1.2% carbon and pH 7.2 was obtained from Sjællands Odde, Zeeland, Denmark, and stored at 4°C until use. Prior to setup of microcosms, soil was passed through a 4-mm sieve and water content was determined by baking a subsample at 105°C for 24 h. To prepare for inoculation into soil, *D. acidovorans* MC1 cells were grown to late stationary phase as indicated above in MSS supplemented with (*R,S*)-dichlorprop and harvested by centrifugation at 8,000 × *g* for 4 min at 4°C. Cells were washed twice and resuspended in 1× phosphate-buffered saline (PBS; 25 mM phosphate buffer, 125 mM NaCl, pH 7.4), and 1 ml was transferred to nonselective PYE medium (29) for growth overnight. Cells were once again harvested by centrifugation, washed twice, and resuspended in 1× PBS. An optical density (OD) of 1 was estimated to correspond to 5 × 10^8 CFU ml^{-1}, and cell suspensions were adjusted in order to apply 1 ml per soil microcosm to reach a cell density of 5 × 10^7 cells g of soil^{-1}. After addition of cells, soil water content was adjusted to 18% [wet weight, including subsequent addition of (*R,S*)-dichlorprop solution] with sterile Milli-Q water and soil was mixed mechanically in plastic bags and divided into glass flasks each containing 30-g soil subsamples. A stock solution of unlabeled (*R,S*)-dichlorprop was prepared in dimethyl sulfoxide (DMSO, VWR, Fontenay-sous-Bois, France) whereas (*R,S*)-[*ring*-U-^{14}C]dichlorprop (specific activity, 3.56 MBq mg^{-1}; radiochemical purity, 97.41%; Izotop, Budapest, Hungary) stock solution was prepared in methanol (LabScan, Dublin, Ireland). From these, an (*R,S*)-dichlorprop solution was prepared with 0.1 M Na_2HPO_4 (pH 8.45) and applied to each microcosm as a top amendment in a fixed volume of 1.1 ml to obtain a final concentration of 2 or 50 mg kg^{-1} unlabeled (*R,S*)-dichlorprop containing trace amounts of labeled (*R,S*)-dichlorprop (28,000 dpm g soil^{-1}). Control microcosms containing no herbicide and only 0.1 M Na_2HPO_4 were also prepared. Finally, a glass vial containing 1 ml of 1 M NaOH was placed on top of the soil in each flask to capture $[^{14}C]CO_2$ evolved during (*R,S*)-[^{14}C]dichlorprop mineralization and bottles were closed airtight and incubated in the dark at 20°C. Soil sampling and replacement of $[^{14}C]CO_2$ traps were done at appropriate time intervals during the course of herbicide degradation following the method described by Nicolaisen et al. (34). Furthermore, triplicate soil samples were taken before addition of herbicide and degrader strain to evaluate the natural diversity of *rdpA* and *sdpA* genes. All soil samples (0.5 g) were immediately frozen in liquid nitrogen and stored at −70°C until nucleic acid extraction. A second amendment with (*R,S*)-dichlorprop was made at day 13 after mineralization of the first amendment had ceased.

Mineralization curve analysis. Cumulative (*R,S*)-[^{14}C]dichlorprop mineralization data were obtained as described previously (34) and corrected for the removal of 0.5-g soil samples taken over time during herbicide degradation in (*R,S*)-[^{14}C]dichlorprop-amended soils.

Nucleic acid extraction. DNA and RNA were coextracted from soil samples as previously described (34) with the following modification: 1 μl of glycogen (Roche, Basel, Switzerland) was added during incubation with polyethylene glycol (PEG 6000) to help nucleic acid precipitation. Samples were kept on ice during the whole procedure, and final extracts were resuspended in 50 μl of DNase- and RNase-free diethyl pyrocarbonate (DEPC)-treated water (Fluka; Sigma-Aldrich, Saint Louis, MO) and stored at −70°C.

DNase treatment and reverse transcription. To eliminate contaminating DNA, 8-μl aliquots of each nucleic acid sample were treated with 2 units of RQ1 RNase-free DNase I (Promega, Madison, WI) according to the manufacturer's protocol. Immediately after, 4-μl subsamples of each DNase-treated extract were used as a template for reverse transcription with the Omniscript reverse transcription kit (Qiagen, Crawley, United Kingdom). Reaction mixtures were prepared using 400 ng of random hexamer primers (Promega), 4 U Super RNase inhibitor (Ambion, Austin, TX), and reagents provided in the kit for a final volume of 20 μl. Incubation for 90 min at 37°C was followed by inactivation of the transcriptase for 10 min at 95°C. Resulting cDNA samples were then stored at −20°C until use for quantitative real-time PCR. In parallel, DNase-treated control reaction mixtures were prepared for each RNA sample without addition of the reverse transcriptase to ensure that no DNA contamination was present.

Primer design. PCR primers for SYBR green quantitative real-time PCR (qPCR) were designed using the BioEdit v.7.0.9.0 sequence alignment software

Downloaded from http://aem.asm.org/ on June 5, 2012 by guest

COR-AAD1-00002959
Bayer EX1008 (Part 6 of 9)

TABLE 1. Oligonucleotide primers designed and used in this study for SYBR green qPCR

Target gene	Primer	Model gene(s) used for primer design	Sequence (5′→3′)	Product length (bp)[a]
rdpA	rdpA_f	16 known *rdpA* sequences in GenBank	CACTTACCAGGTCATCTA	
	rdpA_r		GTGTACATGCTCAGAAAAC	285
sdpA	sdpA_f	*D. acidovorans* MC1, *S. herbicidovorans* MH, *Rhodoferax* sp. P230	ATGCCGACAGCACCTACAT	
	sdpA_r1	*D. acidovorans* MC1	GGTCTCGGGATGCACCTT	287
	sdpA_r2	*S. herbicidovorans* MH, *Rhodoferax* sp. P230	GGTCTCGGGATGGATCTT	290

[a] PCR product lengths for different combinations of forward and reverse primers are indicated. Primer sdpA_f in combination with sdpA_r1 produces a 287-bp product while sdpA_f in combination with sdpA_r2 produces a 290-bp product.

(14) along with Primer-BLAST. Primer-BLAST is a combination of the Primer 3 primer design software (37) and BLAST (1) that searches the GenBank database (http://www.ncbi.nlm.nih.gov/GenBank/index.html) in order to avoid nontarget sequence amplification. Design of *rdpA* primers was based on the alignment of conserved regions from the 16 available *rdpA* sequences retrieved from the GenBank database, while *sdpA* primer design was based on sequences of the only three available strains known to carry *sdpA*: *D. acidovorans* MC1 (AY327575), *S. herbicidovorans* MH (AJ628860), and *Rhodoferax* sp. P230 (DQ406818). The two sdpA reverse primers differ in composition by only 2 nucleotides (Table 1) and were used separately instead of degenerate primers to enable specific detection of the gene from *D. acidovorans* MC1 (sdpA_r1). An equal mixture of sdpA_r1 and sdpA_r2 reverse primers was used only when screening for the presence of naturally occurring *sdpA* sequences. Specificity of each primer pair was further tested by qPCR (conditions indicated below) using DNA extracted as described above from pure cultures of *D. acidovorans* MC1 and *S. herbicidovorans* MH for positive controls while DNA extracted from *C. necator* AEO106(pRO101) served as a negative control. PCR amplification products were separated by 1.5% agarose gels, and fragments were purified and sequenced.

Quantitative real-time PCR. All qPCRs were performed in the Mx3000P qPCR system (Stratagene, La Jolla, CA) using the Brilliant SYBR Green QPCR Master Mix (Stratagene). Reaction mixtures were prepared with 10 μl 2× Brilliant QPCR Master Mix (including SYBR green 1 dye and PCR buffer, deoxynucleoside triphosphates [dNTPs], SureStart *Taq* DNA polymerase, and 5 mM $MgCl_2$); 0.4 μM (each) primer (DNA Technology A/S, Risskov, Denmark); 20 μg of bovine serum albumin (New England Biolabs, Ipswich, MA); 2 μl of template DNA (dilution 1/10), cDNA, or DNase-treated RNA; and DNase/RNase-free water (Sigma-Aldrich) for a final volume of 20 μl. The qPCR thermal cycling program was the same for all primer sets and consisted of an initial 15-min incubation at 95°C for enzyme activation, 40 cycles of 45 s at 95°C for denaturation, 45 s at 55°C for annealing, and 1 min at 72°C for extension with a final elongation for 2 min at 72°C. A specific dissociation curve with melting temperature (T_m) of the amplified product was generated at the end of the qPCR program by including a cycle of 95°C for 1 min and 55°C for 30 s, finally reaching 95°C by increments of 0.5°C s^{-1}, each followed by a fluorescence acquisition step. These curves were used to ensure PCR product specificity by observation of a single melting peak, and results were further confirmed by the presence of single PCR fragments of the expected size in 1.5% agarose gels.

Standard curves generated with DNA extracted from soils spiked with *D. acidovorans* MC1. To enable quantitative detection of both *rdpA* and *sdpA* genes, a standard curve was generated by adding 100 μl of *D. acidovorans* MC1 cells (following the same method as for inoculation into soil microcosms) to 7 Bio101 Lysing Matrix E tubes (MP Biomedicals, Solon, OH) each containing 500 mg of soil to reach cell densities of 10^8, 10^7, 10^6, 10^5, 10^4, 10^3, and 10^2 cells g of $soil^{-1}$. Nucleic acids were extracted as described above and used as templates for qPCR. The resulting DNA standard curve was used to quantify both DNA and mRNA from *rdpA* and *sdpA* with gene expression data being presented as ratios of mRNA normalized to DNA as first described by Nicolaisen et al. (34). Recovery rates of nucleic acids were regarded as equal for each extraction based on previously obtained extraction efficiencies from this soil where mRNA/DNA ratios remained unaffected over a wide dynamic range despite a low recovery of mRNA (34). qPCR runs always included a triplicate standard curve, and amplification efficiency (E) was calculated from the slope of the standard curve using the equation $E = 10^{(-1/\text{slope})} - 1$.

qPCR analysis of all samples collected during the soil microcosm experiments was done on the DNA, cDNA, and DNase-treated RNA fractions using the newly designed *rdpA* and *sdpA* primer sets shown in Table 1. In addition, qPCR screening for the presence of naturally occurring *rdpA* and *sdpA* genes in soil was done prior to (*R,S*)-dichlorprop exposure and degrader strain inoculation. In these cases, reaction mixtures were prepared using a mix of 0.2 μM (each) *sdpA* reverse primer in order to target all known sequences.

Cloning and sequencing. No PCR product for *rdpA* could be detected in soil samples prior to herbicide exposure. However, PCR products obtained by the sdpA primers were used to construct clone libraries. Briefly, PCR was performed using the sdpA_f and sdpA_r1/sdpA_r2 primers and reaction mixtures were prepared containing 4 μl of 5× Phusion GC buffer (Finnzymes, Helsinki, Finland), 800 μM dNTPs (Fermentas, Burlington, Canada), 0.4 μM forward sdpA primer, 0.2 μM (each) reverse sdpA primer, 20 μg of bovine serum albumin (New England Biolabs), 1.25 U of Phusion DNA polymerase (Finnzymes), and 2 μl of template DNA and DNase/RNase-free water (Sigma-Aldrich) for a final volume of 20 μl. The thermal cycling program was as follows: 98°C for 30 s followed by 35 cycles of 10 s at 98°C, 30 s at 62°C, and 30 s at 72°C and a final extension of 10 min at 72°C. PCR products were run through a SeaKem GTG 1% agarose gel, and fragments corresponding to *sdpA* were excised and purified with the Qiaquick gel extraction kit according to the manufacturer's protocol (Qiagen). Cleaned PCR products were ligated into the pCR2.1-TOPO vector and transformed into TOP10 chemically competent *Escherichia coli* cells following the manufacturer's protocol (Invitrogen, Carlsbad, CA). Forty clones were randomly selected, and both DNA strands were sequenced (Uppsala Genome Center, Uppsala, Sweden) using the M13 universal primers (Invitrogen). Resulting forward and reverse sequences were assembled into contigs and submitted to a BLASTn and BLASTp query of the GenBank database for nucleic acid and putative amino acid sequences, respectively, in order to find most homologous sequences.

Phylogenetic analysis of the *sdpA* gene sequences. The cloned gene sequences obtained with the sdpA primers were aligned with related sequences retrieved from GenBank (June 2009) using DIALIGN (25). Sites where nucleotide alignments were not resolved were excluded, and a final 190-bp alignment was used for phylogenetic analysis. The phylogenetic tree was constructed with the PAUP 4.0b10 software (40) using a neighbor-joining (NJ) analysis with 1,000 iterations to calculate bootstrap values. Tree topology was confirmed by maximum likelihood and parsimony analysis.

Nucleotide sequence accession numbers. The nucleotide sequences of *sdpA* determined in this study have been deposited in the GenBank database under the accession numbers GQ922849 to GQ922883.

RESULTS

Primer design and evaluation. Multiple alignment of the 16 *rdpA* sequences available in GenBank revealed highly conserved sequences. Aside from *rdpA* in *D. acidovorans* MC1, *S. herbicidovorans* MH, and *Rhodoferax* sp. P230 [all previously described for their involvement in (*R,S*)-dichlorprop degradation] (9, 16, 28), sequences belonged to *Burkholderia* sp. and uncultured bacterial clones. The rdpA primers designed from this alignment amplified a 285-bp region (Table 1). No product was detected when testing with *C. necator* AEO106(pRO101), which carries the *tfdA* gene instead of *rdpA*, whereas *D. acidovorans* MC1 and *S. herbicidovorans* MH, known to harbor *rdpA*, yielded amplicons of the desired length and sequence

Downloaded from http://aem.asm.org/ on June 5, 2012 by guest

COR-AAD1-00002960
Bayer EX1008 (Part 6 of 9)

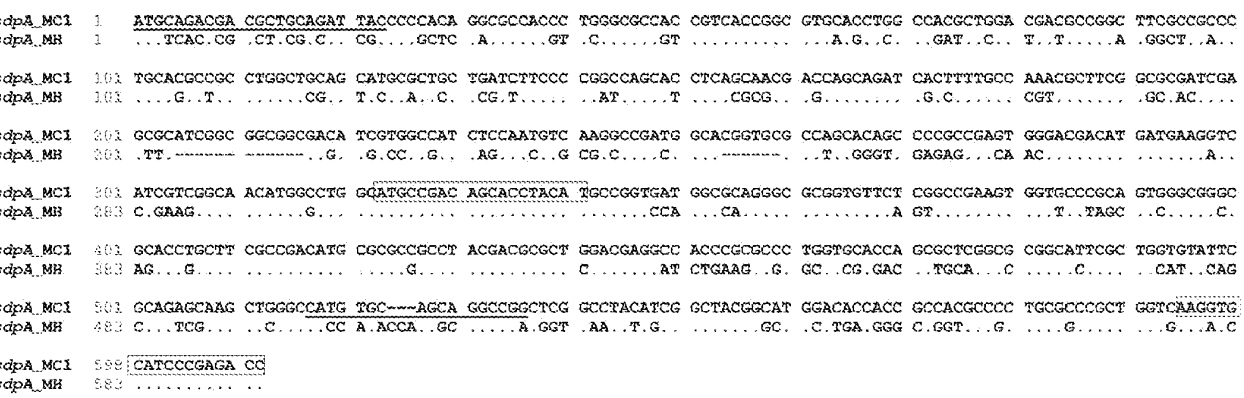


FIG. 1. Alignment of partial *sdpA* nucleic acid sequences from *D. acidovorans* MC1 (*sdpA*_MC1) and *S. herbicidovorans* MH (*sdpA*_MH) showing primer hybridization sites. Underlined sequences indicate primer sites used by Schleinitz et al. (39) based on the *D. acidovorans* MC1 SdpA peptide sequence. Primer sites designed in this study are boxed and based on all available *sdpA* nucleic acid sequences.

composition (data not shown). When tested by qPCR, dissociation curves produced a single melting peak with a T_m of approximately 89°C, thus indicating the presence of a single amplicon.

The sdpA primers were designed based on the alignment of three sequences. *S. herbicidovorans* MH and *Rhodoferax* sp. P230 have identical *sdpA* nucleic acid sequences while *D. acidovorans* MC1 shares only 75% identity to this sequence, thus restraining primer design options. A 19-mer forward primer was designed from a conserved region while two 18-mer reverse primers targeting the same area (differing only by 2 bp) had to be created for lack of a suitable consensus region (Table 1). The sdpA primers designed here were found suitable for detection of *sdpA* from all known strains, while this was not the case for previously published primers due to the presence of several mismatches at both primer hybridization sites for the *S. herbicidovorans* MH sequence (Fig. 1). The basis for using two separate reverse primers instead of one mix of degenerate primers was the intention to use sdpA_r1 to enable detection of the gene in *D. acidovorans* MC1 during transcription analysis while a combination of sdpA_r1/sdpA_r2 enabled us to better study the natural diversity of *sdpA* in soil. The strains tested for rdpA primer specificity were also used to test sdpA primer specificity and generated amplicon lengths as indicated in Table 1. Dissociation curves following qPCR produced a single melting peak at approximately 91.5°C for *D. acidovorans* MC1 and 90°C for *S. herbicidovorans* MH. For both *rdpA* and *sdpA*, primer specificity was further confirmed by the presence of a single band during agarose gel electrophoresis of qPCR products and sequencing of the amplified product (data not shown).

Standard curve performance in qPCR. Extensive testing of primer pairs is essential when generating a suitable standard curve for use in quantitative PCR since factors such as secondary structures, PCR inhibitors, or amplicon length can affect primer amplification efficiency. Both standard curves in this work were established from serial dilutions of *D. acidovorans* MC1 cells inoculated into soil anticipated to represent DNA and mRNA copy numbers, as *rdpA* and *sdpA* are presumably single-copy genes in this strain (39). The *rdpA* standard curve was linear over 6 orders of magnitude (r^2 = 1.00) from 10^8 to 10^3 copies g of soil^{-1}, while the standard curve for *sdpA* was linear over 4 orders of magnitude (r^2 = 0.999), ranging from 10^8 to 10^5 copies g of soil^{-1}. The slope of the standard curve remained consistent between different runs and indicated qPCR efficiencies of approximately 82.5% and 102% for *rdpA* and *sdpA*, respectively. The 10-fold dilutions ranging from 10^4 to 10^2 copies g of soil^{-1} for *sdpA* did not follow a linear relationship and could not be used for accurate quantification. This was caused by the presence of indigenous *sdpA* genes (see below), which in turn created two melting peaks during the dissociation curve of qPCR products with T_m values of 91.5°C and 90°C, respectively. Due to the inevitable background of *sdpA* genes in soil, linear extrapolation of the standard curve was necessary for quantification of *sdpA* genes at levels below 10^5 copies g of soil^{-1}.

Natural abundance of the *rdpA* and *sdpA* genes in agricultural soil. We first determined the natural prevalence of the *rdpA* and *sdpA* genes in the Sjællands Odde agricultural soil. No qPCR product with the rdpA primers could be detected in DNA extracts recovered from agricultural soil prior to (*R*,*S*)-dichlorprop exposure (data not shown), indicating that indigenous *rdpA* genes are present at a level below the detection limit of the qPCR or they are simply absent in this environment. In contrast, *sdpA* was consistently detected at levels below 10^5 copies g of soil^{-1}, corresponding approximately to 10^3 copies g of soil^{-1} according to the extrapolated standard curve, when soil DNA extracts were subjected to qPCR with a T_m value around 90°C.

Diversity of natural *sdpA* gene pool. To confirm that products amplified by nonquantitative PCR were indeed *sdpA*, 35 clones were recovered from soil DNA extracts and successfully sequenced and assembled into contiguous consensus sequences. Analysis revealed differences in both base composition and sequence length. None of the partial gene sequences shared more than 82% identity to other known *sdpA* sequences as verified by BLASTn analysis of GenBank. Sequence lengths varied between 269 bp and 296 bp and were shortened to an unambiguous 190-bp region obtained by multiple alignment with DIALIGN. Although phylogenetic tree construction was based on this fixed 190-bp region, NJ analysis was able to separate *sdpA* clones into four major clusters (Fig. 2). Cluster

Downloaded from http://aem.asm.org/ on June 5, 2012 by guest

COR-AAD1-00002961
Bayer EX1008 (Part 6 of 9)

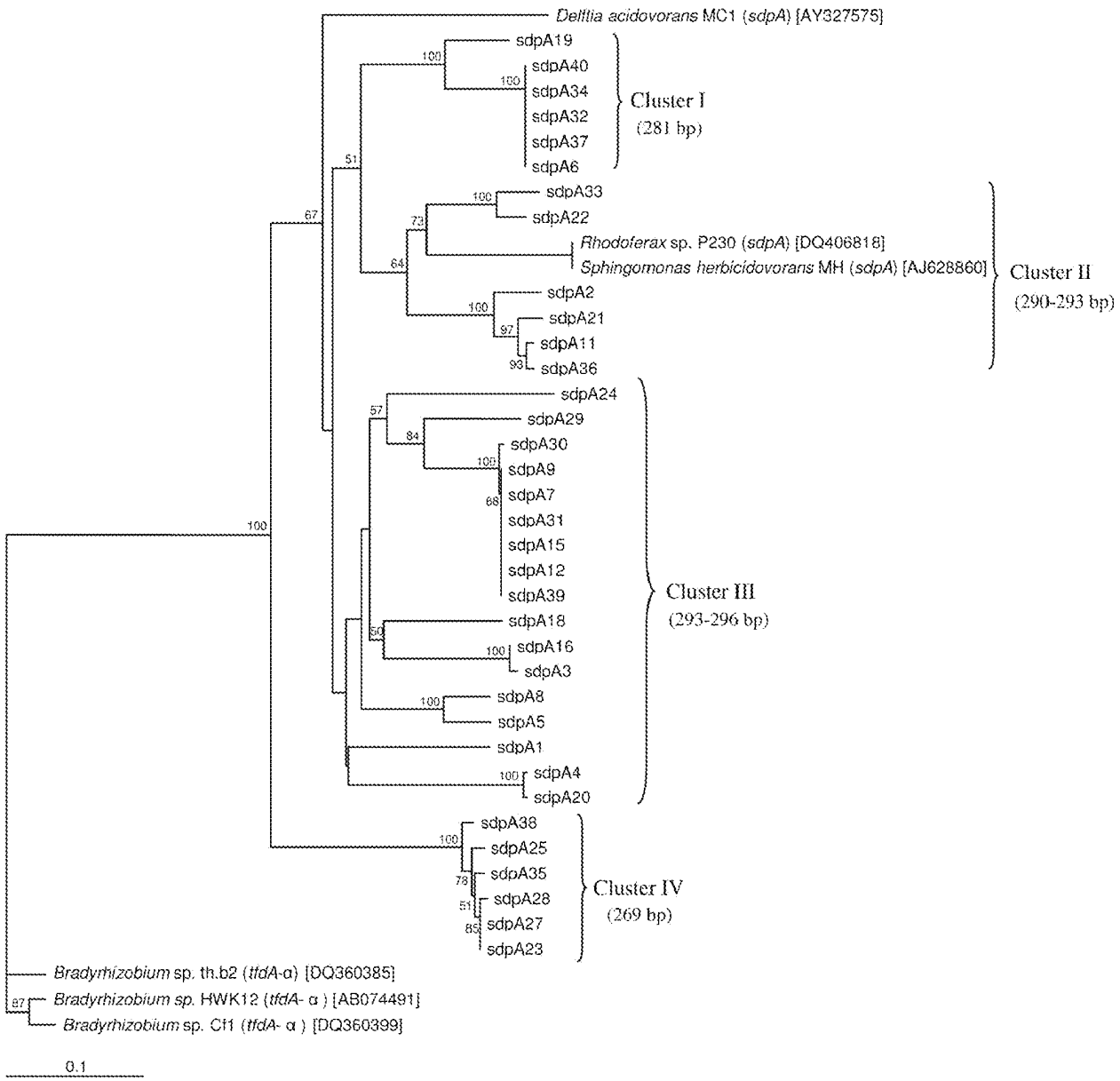


FIG. 2. Phylogenetic tree of partial *sdpA* sequences recovered from soil prior to (*R,S*)-dichlorprop exposure. Analysis was based on 190-bp unambiguously aligned *sdpA* sequences using the NJ method. Bootstrap values of >50% from 1,000 replicate samplings are displayed at the nodes. The scale bar indicates 0.1 nucleotide substitution per site. Values in parentheses below cluster numbers indicate lengths in base pairs obtained from sequencing of PCR products amplified with the sdpA primers. Strains carrying the *tfdA*-α gene were used as an outgroup. Aside from *sdpA*, *tfdA*-α genes are the most closely related to the sequences recovered in this study as determined by BLASTn analysis of the GenBank database.

I was composed exclusively of 281-bp sequences, cluster II included sequences closest to *sdpA* from *S. herbicidovorans* MH and *Rhodoferax* sp. P230 with lengths between 290 and 293 bp, and cluster III had lengths ranging from 293 to 296 bp and showed the largest diversity in base composition between sequences, while cluster IV had the shortest sequence of 269 bp. This clustering was reiterated by the tree topology obtained with maximum likelihood and parsimony analysis methods.

The phylogenetic diversity observed in the nucleic acid sequences was maintained when translated into putative amino acid sequences. BLASTp analysis indicated that all SdpA amino acid sequences shared the highest identity to both *S. herbicidovorans* and *Rhodoferax* sp. P230 (identical sequence composition) or to *D. acidovorans* MC1 (Table 2). Percent identities of partial SdpA sequences to their closest relatives in GenBank revealed a clear separation that corresponded well to each of the four clusters created by the *sdpA* phylogenetic tree (Fig. 2). The *sdpA* sequences ascribed to cluster I shared 68 to

Downloaded from http://aem.asm.org/ on June 5, 2012 by guest

COR-AAD1-00002962
Bayer EX1008 (Part 6 of 9)

TABLE 2. Identities of deduced partial amino acid sequences of SdpA recovered from agricultural soil, obtained by BLASTp analysis of the GenBank database

Uncultured bacterium clone(s)	Cluster[a]	Amino acid length[b]	% Identity[c]	Closest relative(s) in GenBank[d]
sdpA19	I	93	69 (67/97)	*S. herbicidovorans* MH, *Rhodoferax* sp. P230
sdpA40, sdpA34, sdpA32, sdpA37, sdpA6	I	93	68 (66/97)	*S. herbicidovorans* MH, *Rhodoferax* sp. P230
sdpA33, sdpA22	II	97	78 (76/97)	*S. herbicidovorans* MH, *Rhodoferax* sp. P230
sdpA2, sdpA21, sdpA11, sdpA36	II	96	85 (82/96)	*S. herbicidovorans* MH, *Rhodoferax* sp. P230
sdpA24	III	98	63 (62/98)	*S. herbicidovorans* MH, *Rhodoferax* sp. P230
sdpA29	III	98	58 (57/98)	*D. acidovorans* MC1
sdpA30, sdpA9, sdpA7, sdpA31, sdpA15, sdpA12, sdpA39	III	98	60 (59/98)	*D. acidovorans* MC1
sdpA18	III	97	64 (63/97)	*S. herbicidovorans* MH, *Rhodoferax* sp. P230
sdpA16	III	98	60 (59/98)	*S. herbicidovorans* MH, *Rhodoferax* sp. P230
sdpA3	III	98	61 (60/98)	*S. herbicidovorans* MH, *Rhodoferax* sp. P230
sdpA8, sdpA5	III	98	62 (61/98)	*S. herbicidovorans* MH, *Rhodoferax* sp. P230
sdpA1	III	97	63 (62/97)	*S. herbicidovorans* MH, *Rhodoferax* sp. P230
sdpA4, sdpA20	III	98	58 (58/99)	*D. acidovorans* MC1
sdpA38, sdpA25, sdpA35, sdpA28, sdpA27, sdpA23	IV	89	55 (53/95)	*D. acidovorans* MC1

[a] Numbers indicate clustering of the *sdpA* clones as based on the phylogenetic tree constructed from 190-bp *sdpA* gene sequences (Fig. 1).
[b] Partial amino acid sequences were translated from 269- to 296-bp nucleic acid sequences obtained by PCR-based cloning and sequencing using the sdpA primer pair sdpA_f and sdpA_r1/r2.
[c] Percent sequence identity between sequenced clone and sequence of closest relative in GenBank (number of identical amino acid hits/total number of amino acids).
[d] Strains represent the closest matches obtained by BLASTp analysis. Strain accession numbers for GenBank are the same as those indicated in Materials and Methods. More than one strain being listed indicates identical results.

69% identity, those ascribed to cluster II shared 78 to 85% identity, those ascribed to cluster III shared 58 to 64% identity, and those ascribed to cluster IV shared 55% identity to their closest match.

Expression of *rdpA* and *sdpA* is regulated by (*R,S*)-dichlorprop exposure in soil. Transcript levels of *rdpA* and *sdpA* mRNA in (*R,S*)-dichlorprop-amended soils that were not inoculated with a degrader strain were too low for quantitative detection within the time frame of this study. Therefore, *D. acidovorans* MC1 was used as a model strain to study regulation of *rdpA* and *sdpA* genes in agricultural soil. Figures 3 and 4 show the progress curves of *rdpA* and *sdpA* mRNA and DNA during *in situ* (*R,S*)-[^{14}C]dichlorprop mineralization activity at first and second amendments of the soil with 2 mg kg^{-1} and 50 mg kg^{-1} of (*R,S*)-dichlorprop, as well as progress curves for soils receiving no herbicide. Onset of mineralization was detected immediately and without lag for soils amended with 2 mg kg^{-1} and 50 mg kg^{-1} of (*R,S*)-dichlorprop. Hence, the progress curves of accumulated [^{14}C]CO_2 from mineralization of 2 mg kg^{-1} and 50 mg kg^{-1} (*R,S*)-dichlorprop could be divided into two segments: a steep segment and a plateau.

No increase of *rdpA* or *sdpA* DNA was detected in nonamended soils or soils amended with only 2 mg kg^{-1} of (*R,S*)-dichlorprop. In these cases, both *rdpA* and *sdpA* copy numbers decreased substantially following initial cell inoculation, possibly as a result of cell death or predation by protozoa, but were still maintained throughout the experiments at around 10^6 copies g of soil^{-1} (Fig. 3a and b and 4a and b). It is also noteworthy that levels of *sdpA* DNA may be slightly overestimated as a result of the low background level of indigenous *sdpA* genes in this soil. In contrast, qPCR quantification of *rdpA* and *sdpA* DNA clearly gave evidence of *D. acidovorans* MC1 cell growth during exposure to 50 mg kg^{-1} of (*R,S*)-dichlorprop. Hence, *rdpA* gene copy number, originally ~7×10^7 copies g of soil^{-1} (as verified by qPCR), reached above 10^8 copies g of soil^{-1} following 20 h of incubation (Fig. 3c). An increase in abundance of *sdpA* DNA was also observed starting at ~10^8 copies g of soil^{-1} and reaching ~2×10^8 copies g^{-1} (Fig. 4c). Approximately 1 week after initial mineralization had ceased, gene copy numbers remained stable at around 2×10^7 copies g and 4×10^7 copies g of soil^{-1} for *rdpA* and *sdpA*, respectively. A second amendment with 50 mg kg^{-1} (*R,S*)-dichlorprop at 312 h caused *rdpA* to increase to ~5×10^7 copies g^{-1} while *sdpA* underwent a higher increase compared to the first amendment, this time reaching ~3×10^8 copies g of soil^{-1} after 356 h of incubation.

Gene expression was calculated as mRNA/DNA ratios as a way of describing transcription dynamics independently of potential cell number increase (34). Detection of *rdpA* and *sdpA* transcripts from *D. acidovorans* MC1 in soil indicated similar patterns of transcription activity for the two genes. In control microcosms where *D. acidovorans* MC1 was inoculated but no (*R,S*)-dichlorprop was added, *rdpA* and *sdpA* genes were expressed at a low basal level with no apparent upregulation over the 18 days of incubation (Fig. 3d and 4d). Furthermore, no mRNA was detectable over this period for either gene in soils not amended with (*R,S*)-dichlorprop and without the degrader strain (data not shown), indicating that indigenous background expression was absent or below the detection limit. No clear increase in transcription activity could be detected in response to the first amendments with 2 mg kg^{-1} and 50 mg kg^{-1} of (*R,S*)-dichlorprop (Fig. 3e and f and 4e and f). More precisely, expression of *rdpA* and *sdpA* started off high during the first amendment with (*R,S*)-dichlorprop and slowly decreased over time to reach a minimal level of expression at around 100 h. This progressive decrease coincided well with the beginning of the plateau phase of (*R,S*)-[^{14}C]dichlorprop mineralization when most of the (*R,S*)-dichlorprop had been degraded in the soil. At that point, low transcript levels were comparable to those in control microcosms.

A second amendment with 2 mg kg^{-1} (*R,S*)-dichlorprop at 312 h caused a clear and transient increase in *rdpA* gene expression with maximal mRNA abundance being reached within 5 h to 8 h after respiking (Fig. 3e). This was in accor-

Downloaded from http://aem.asm.org/ on June 5, 2012 by guest

COR-AAD1-00002963
Bayer EX1008 (Part 6 of 9)

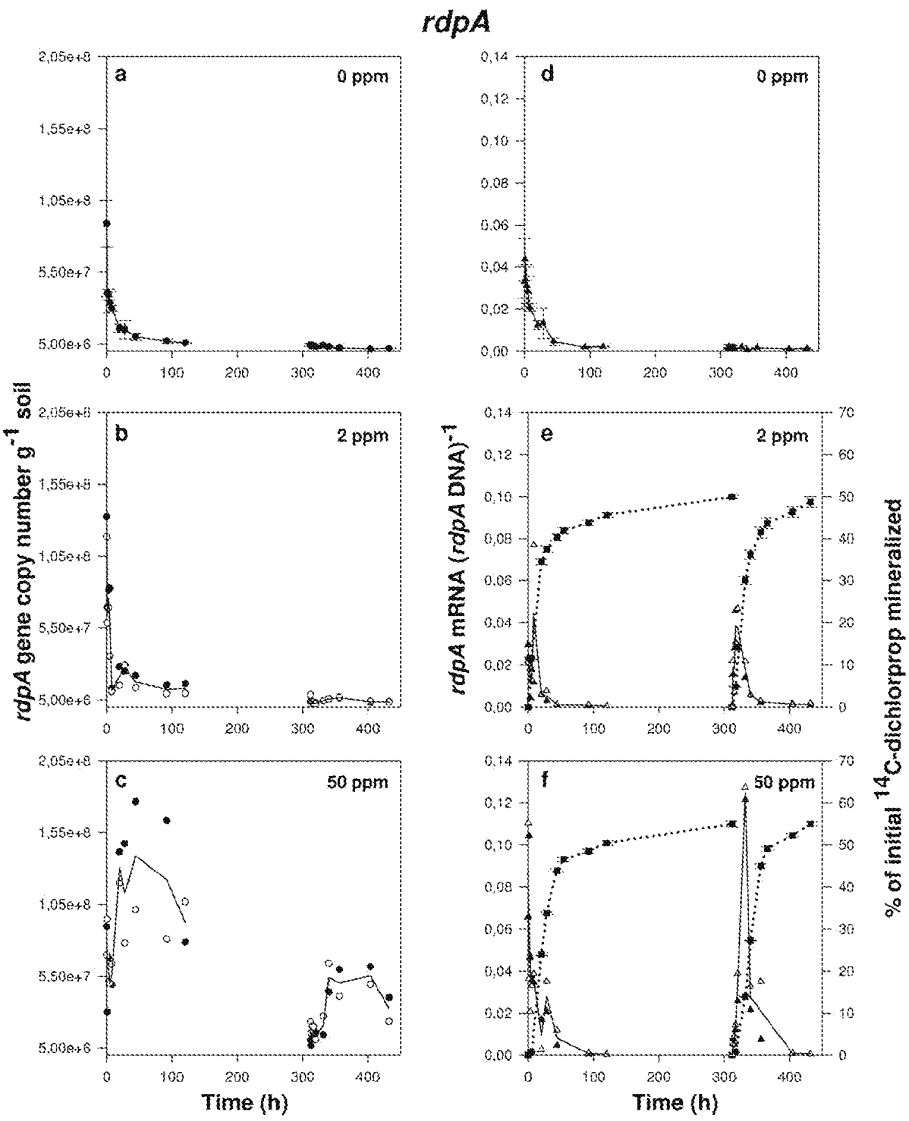


FIG. 3. Progress curves of *rdpA* gene copy numbers (a to c), *rdpA* transcription activity represented as ratios of *rdpA* mRNA to *rdpA* DNA (d to f), and (*R*,*S*)-[^{14}C]dichlorprop mineralization (e and f) during exposure of *Delftia acidovorans* MC1 to different concentrations of (*R*,*S*)-dichlorprop in soil: 0 mg kg^{-1} (a and d), 2 mg kg^{-1} (b and e), and 50 mg kg^{-1} (c and f). Amendment with (*R*,*S*)-dichlorprop was done at 0 h followed by a second amendment at 312 h. Data from microcosms not amended with (*R*,*S*)-dichlorprop (a and d) are shown from triplicate soil microcosms with error bars representing standard errors of the means. In panels b, c, e, and f, open and filled symbols each represent the data set from one individual soil microcosm while the lines running through the data points represent the means of the two replicates. Symbols: ○ and ●, *rdpA* DNA; △ and ▲, ratio of *rdpA* mRNA to *rdpA* DNA; ■, mineralization of (*R*,*S*)-dichlorprop.

dance with the high activity of the mineralization curve that quickly reached the plateau phase. However, no upregulation was observed for the *sdpA* gene in comparison to the control microcosms (Fig. 4e). In comparison, a second amendment with 50 mg kg^{-1} (*R*,*S*)-dichlorprop at 312 h caused a dramatic and transient increase in *rdpA* gene expression that reached a maximum within 20 h after respiking and decreased thereafter to levels similar to the control at 400 h of incubation (Fig. 3f). This time shift in maximal expression of *rdpA* in comparison to the 2-mg kg^{-1} (*R*,*S*)-dichlorprop amendment corresponded well to the larger amount of (*R*,*S*)-dichlorprop available for degradation in the soil. A similar progress curve was obtained for *sdpA* gene expression during the second amendment with 50 mg kg^{-1} (*R*,*S*)-dichlorprop, although abundance was clearly lower than that with *rdpA* transcripts (Fig. 4f).

DISCUSSION

The microbial degradation of (*R*,*S*)-dichlorprop and (*R*,*S*)-mecoprop is not yet fully understood and has previously been proposed to be linked to the action of microbial consortia (21, 41) with reports of some degraders carrying *tfdA* or *tfdA*-like

Downloaded from http://aem.asm.org/ on June 5, 2012 by guest

COR-AAD1-00002964
Bayer EX1008 (Part 6 of 9)

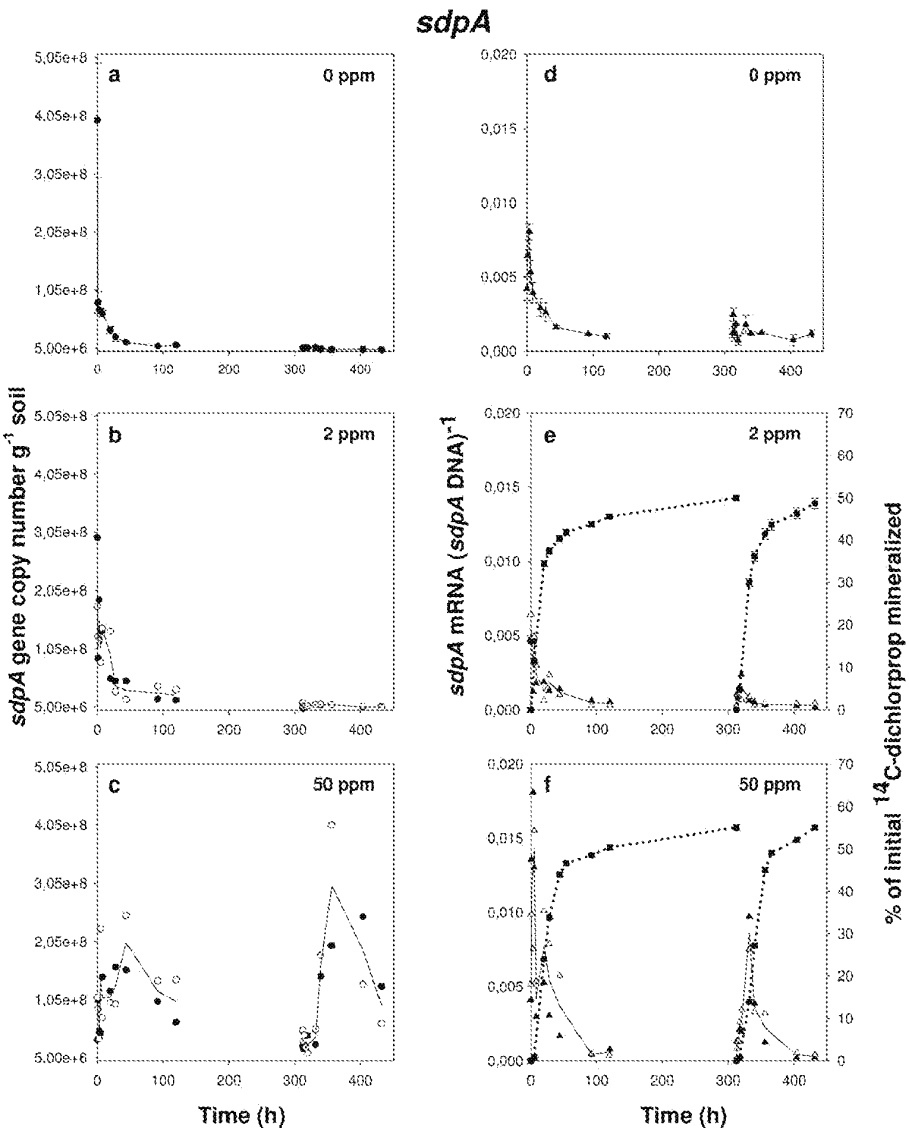


FIG. 4. Progress curves of *sdpA* gene copy numbers (a to c), *sdpA* transcription activity represented as ratios of *sdpA* mRNA to *sdpA* DNA (d to f), and (*R,S*)-[^{14}C]dichlorprop mineralization (e and f) during exposure of *Delftia acidovorans* MC1 to different concentrations of (*R,S*)-dichlorprop in soil: 0 mg kg^{-1} (a and d), 2 mg kg^{-1} (b and e), and 50 mg kg^{-1} (c and f). Amendment with (*R,S*)-dichlorprop was done at 0 h followed by a second amendment at 312 h. Data from microcosms not amended with (*R,S*)-dichlorprop (a and d) are shown from triplicate soil microcosms with error bars representing standard errors of the means. In panels b, c, e, and f, open and filled symbols each represent the data set from one individual soil microcosm while the lines running through the data points represent the means of the two replicates. Symbols: ○ and ●, *sdpA* DNA; △ and ▲, ratio of *sdpA* mRNA to *sdpA* DNA; ■, mineralization of (*R,S*)-dichlorprop.

genes and degradation pathways similar to those of 2,4-D and MCPA (38, 42). However, the recent characterization of phenoxypropionate-degrading strains that carry enantiospecific dioxygenases apart from TfdA highlights the importance of developing appropriate molecular tools for detection of these genes in the environment.

As sequence data from (*R*)- and (*S*)-dichlorprop cleaving dioxygenases have only recently become available, only one primer set for each gene has been used (39). Theoretically, the published primers for *rdpA* can amplify all sequences described to date, as they are nearly 100% identical in composition. However, rdpA primers were tested here and found unsuitable for use in SYBR green qPCR due to unsatisfactory amplification efficiency during qPCR of the standard curve (data not shown). In the case of *sdpA*, Schleinitz et al. (39) designed primers based on the peptide sequences obtained from *D. acidovorans* MC1 (43) and first reported that although *S. herbicidovorans* MH and *Rhodoferax* sp. P230 did exhibit (*S*)-dichlorprop cleaving dioxygenase activity, neither strain carried *sdpA*-like genes. Conversely, Müller et al. (30) successfully isolated and sequenced *sdpA* from *S. herbicidovorans* MH and reported that its predicted amino acid sequence shared only

Downloaded from http://aem.asm.org/ on June 5, 2012 by guest

COR-AAD1-00002965
Bayer EX1008 (Part 6 of 9)

63% identity to that of *D. acidovorans*. A closer look at this target sequence reveals that the primers designed by Schleinitz et al. (39) were unsuitable for detection of *sdpA* in strain *S. herbicidovorans* MH and that the inability to first detect *sdpA*, even under low-stringency conditions, was most likely a result of high nucleotide diversity found at the primer hybridization sites. In this work, rdpA and sdpA primers were designed based on the alignment of all available sequences and were shown to successfully amplify *rdpA* and *sdpA* from both *S. herbicidovorans* MH and *D. acidovorans* MC1.

We further report the first case of *sdpA* gene detection in natural soils even without prior (*R,S*)-dichlorprop exposure; the qPCR assay developed consistently detected levels of approximately 10^3 copies of *sdpA* DNA g of soil^{-1}. The absence of *rdpA* in the same soil was unexpected as both genes and corresponding enzymes have always been reported together in previously characterized strains (30, 39). However, given the very limited amount of information available on the distribution of these genes in the environment and the few strains isolated to date that harbor them, it is feasible that some organisms may carry only *rdpA*, *sdpA*, or a combination of both. Alternatively, *rdpA* genes could have been present but at levels below the detection limit of our method. The only other study to target *rdpA* and *sdpA* DNA in environmental samples used the primers designed by Schleinitz et al. (39) to screen mecoprop-degrading soil enrichment cultures (46). In that case, *rdpA* was detected only when cultures were enriched on (*R*)-mecoprop; although *sdpA* could not successfully be PCR amplified, dot blot hybridization was able to detect the presence of *sdpA* from the enrichment cultures grown on (*R*)- and (*R,S*)-mecoprop. The authors did not report the presence of *sdpA* or *rdpA* genes from samples not exposed to mecoprop. It can be presumed that the full extent of *sdpA* genes was not detected given the limited range of the primer set. Furthermore, no *sdpA* sequence data were provided.

The sequence diversity in *sdpA* found here corroborates well with previous, albeit limited, knowledge of *sdpA* gene sequences. As mentioned above, the DNA sequence of *sdpA* from *S. herbicidovorans* MH and *Rhodoferax* sp. P230 compared to *D. acidovorans* MC1 exhibits considerable diversity. Interestingly, the partial *sdpA* sequences that we recovered from natural soils demonstrated a high diversity not only in composition but also in length. Furthermore, phylogenetic analysis of a fixed 190-bp region for all sequences consistently divided the partial *sdpA* genes sequenced into four separate clusters. Although analysis was done on a fixed-length region, two of these clusters (cluster I and cluster IV) could easily be distinguished based on amplicon length, each being exclusively composed of 281-bp and 269-bp sequences, respectively. The diversity obtained in the nucleic acid sequences of *sdpA* was maintained when translated into partial putative amino acid sequences, indicating that it was not merely a consequence of synonymous mutations. Müller et al. (30) noted that the predicted SdpA amino acid sequence of *S. herbicidovorans* MH was 63% identical to that of *D. acidovorans* MC1 and 37% identical to the canonical TfdA sequence from *C. necator* JMP134(pJP4). In our analysis, all predicted amino acid sequences shared the closest identity to one of the previously characterized SdpA sequences and showed a fully conserved predicted α-ketoglutarate binding site as well as a Fe(II)-binding residue (31, 39). The sequences with the highest similarity to SdpA of *S. herbicidovorans* MH and *Rhodoferax* sp. P230 shared between 78 and 85% identity while the ones with the lowest similarity were the shortest sequences and shared only 55% identity to SdpA of *D. acidovorans* MC1. Comparison of the amino acid sequences to the *sdpA* gene phylogenetic tree revealed that similarly to nucleic acid sequences, sequence length could not help in distinguishing between all four clusters. However, all four clusters could be resolved by percent identities obtained through BLASTp analysis of the amino acid sequences. Hence, each of the four clusters was composed of sequences within a well-defined range of identities to their closest relative in GenBank. Nevertheless, the database of *sdpA* sequences is still too small to make any conclusions regarding the full gene diversity and the possibility of dividing sequences into different classes, as has been the case for the *tfdA* genes (20, 24).

Apart from the already described SdpA, the sequences obtained here shared some resemblance to genes belonging to the *tfdA*-α group. *Beta-* and *Gammaproteobacteria* involved in 2,4-D degradation typically carry the *tfdA* gene, which can be divided into three classes (classes I to III) (24), while *tfdA*-α is a *tfdA* homologue usually found in *Alphaproteobacteria* (18, 19). Interestingly, *tfdA* genes are widespread in the environment, even in pristine soils with no previous exposure to phenoxy acid herbicides (17, 20) and in soil organisms unable to degrade 2,4-D (15). Recently, Bælum et al. (2) detected low background levels of *tfdA* in soil prior to addition of 2,4-D and MCPA. It has been postulated that the TfdA enzyme may have undiscovered natural substrates which could help explain its widespread distribution in the environment (8, 15). Although previously characterized SdpA enzymes have a wider substrate range than RdpA and the closest relatives of SdpA are members of the TfdA enzyme family, it is unknown whether the *sdpA* gene pool detected in this soil is a result of selective pressure caused by the presence of natural substrates for SdpA. Our report on the natural abundance and diversity of *sdpA* genes in addition to the detection of *rdpA* and *sdpA* genes from soil enrichment cultures reported by Zakaria et al. (46) underscores the importance of further investigating the role of these genes during *in situ* phenoxypropionate herbicide degradation.

Patterns of *rdpA* and *sdpA* gene expression during the degradation of (*R,S*)-dichlorprop were determined from *D. acidovorans* MC1, which is able to fully degrade the herbicide following the modified *ortho*-cleavage pathway (29). This strain was chosen because of its well-characterized behavior in pure culture, while data on its activity under *in situ* soil conditions remain limited. Besides, *sdpA* and *rdpA* mRNA transcript levels were too low for detection from natural uninoculated soils during the 18 days of incubation, thus explaining the need to inoculate a degrader strain for expression studies. A time course analysis of *rdpA* and *sdpA* transcription dynamics during microbial degradation of (*R,S*)-dichlorprop was undertaken to achieve understanding of how these genes are regulated in the environment. Previously, pure culture studies with *S. herbicidovorans* MH grown on pyruvate in mineral medium showed that expression of both *rdpA* and *sdpA* genes was constitutive regardless of exposure to (*R*)-dichlorprop, (*S*)-dichlorprop, 2,4-D, or DMSO (used as a noninducing control) (30). Al-

Downloaded from http://aem.asm.org/ on June 5, 2012 by guest

COR-AAD1-00002966
Bayer EX1008 (Part 6 of 9)

though the presence of mRNA was constitutive, the study did not provide information on the actual regulation of these genes, as no quantitative expression data were presented and conclusions were based on data collected from a single time point. Constitutive gene expression was also reported for pure culture induction studies of *D. acidovorans* MC1 based on the etherolytic degradation of both enantiomers of (*R,S*)-dichlorprop but was not supported by accompanying data on mRNA transcripts (29). Nevertheless, our results also support the idea that expression of both *rdpA* and *sdpA* genes in *D. acidovorans* MC1 was constitutive and maintained at a low basal level when the strain was inoculated into soil without exposure to (*R,S*)-dichlorprop.

As observed in similar studies involving MCPA, 2,4-D, and expression of the *tfdA* genes in soil (2, 34), regulation of *rdpA* and *sdpA* gene expression may be largely dependent upon exposure to (*R,S*)-dichlorprop. Soil microcosms receiving the first amendment with 2 mg kg^{-1} or 50 mg kg^{-1} of (*R,S*)-dichlorprop did not immediately result in clear upregulation of gene expression. Hence, *rdpA* and *sdpA* mRNA (expressed as ratios of mRNA normalized to DNA) started off quite high followed by a progressive decrease until levels fell to those similar to those for unamended control soils. The preinoculation step which consisted of growth of *D. acidovorans* MC1 in (*R,S*)-dichlorprop-amended medium followed by overnight growth in nonselective PYE medium prior to soil inoculation might have been responsible for the high abundance of *rdpA* and *sdpA* transcripts detected at time zero before the first amendment. Although such pregrown cells were washed, they may have retained significant levels of mRNA as a consequence of being grown in a selective medium prior to microcosm experiments. Nonetheless, we chose this setup as a consequence of reports indicating the spontaneous loss of genes involved in etherolytic cleavage of (*R,S*)-dichlorprop when *D. acidovorans* MC1 is grown under nonselective conditions for extended periods (29, 39).

After the second amendment, however, an obvious increase in gene expression was observed in response to repeated amendments with (*R,S*)-dichlorprop, particularly in soils receiving 50 mg kg^{-1} of the herbicide. Progress curves of mRNA formation showed a sharp and transient maximum corresponding to the active phase of (*R,S*)-dichlorprop mineralization. As noted by Nicolaisen et al. (34), the subsequent decreasing levels of mRNA most likely indicate a progressive degradation of transcripts as a result of an adequate pool of degradative enzymes. Both genes were clearly upregulated in response to reexposure to high concentrations of (*R,S*)-dichlorprop, although the abundance of mRNA transcripts was higher for *rdpA* than for *sdpA*. Repeated treatment with the low concentration of herbicide (2 mg kg^{-1}) produced similar results, although expression of *sdpA* was not markedly different from that in control soils.

This study has demonstrated that *rdpA* and *sdpA* gene expression is constitutive at a basal level but is induced in response to (*R,S*)-dichlorprop degradation under *in situ* conditions. Although a basal constitutive level is not detected for the *tfdA* gene (2, 34), other degradative enzyme-encoding genes such as *atz*, involved in the initial steps of atrazine degradation, have been reported to be continuously and basally expressed with transient increases in gene expression following herbicide exposure (5). Further studies on the abundance of the *rdpA* and *sdpA* genes in various soils as well as in-depth studies of their expression in indigenous soil microbial populations exposed to (*R,S*)-dichlorprop over extended periods of time should help to gain a better understanding of how these genes are regulated in the environment.

ACKNOWLEDGMENTS

We thank R. H. Müller (Helmholtz Centre for Environmental Research, Leipzig, Germany) for kindly donating strain *Delftia acidovorans* MC1.

This study was supported by the Center for Environmental and Agricultural Microbiology (CREAM) funded by the Villum Kann Rasmussen Foundation.

REFERENCES

1. **Altschul, S. F., T. L. Madden, A. A. Schaffer, J. Zhang, Z. Zhang, W. Miller, and D. J. Lipman.** 1997. Gapped BLAST and PSI-BLAST: a new generation of protein database search programs. Nucleic Acids Res. **25**:3389–3402.
2. **Bælum, J., M. H. Nicolaisen, W. E. Holben, B. W. Strobel, J. Sørensen, and C. S. Jacobsen.** 2008. Direct analysis of *tfdA* gene expression by indigenous bacteria in phenoxy acid amended agricultural soil. ISME J. **2**:677–687.
3. **Buerge, I. J., T. Poiger, M. D. Müller, and H. R. Buser.** 2003. Enantioselective degradation of metalaxyl in soils: chiral preference changes with soil pH. Environ. Sci. Technol. **37**:2668–2674.
4. **Buser, H. R., M. D. Müller, and N. Theobald.** 1998. Occurrence of the pharmaceutical drug clofibric acid and the herbicide mecoprop in various Swiss lakes and in the North Sea. Environ. Sci. Technol. **32**:188–192.
5. **Devers, M., G. Soulas, and F. Martin-Laurent.** 2004. Real-time reverse transcription PCR analysis of expression of atrazine catabolism genes in two bacterial strains isolated from soil. J. Microbiol. Methods **56**:3–15.
6. **Diao, J. L., C. G. Lv, X. Q. Wang, Z. H. Dang, W. T. Zhu, and Z. Q. Zhou.** 2009. Influence of soil properties on the enantioselective dissipation of the herbicide lactofen in soils. J. Agric. Food Chem. **57**:5865–5871.
7. **Don, R. H., A. J. Weightman, H. J. Knackmuss, and K. N. Timmis.** 1985. Transposon mutagenesis and cloning analysis of the pathways for degradation of 2,4-dichlorophenoxyacetic acid and 3-chlorobenzoate in *Alcaligenes eutrophus* JMP134(pJP4). J. Bacteriol. **161**:85–90.
8. **Dunning Hotopp, J. C., and R. P. Hausinger.** 2001. Alternative substrates of 2,4-dichlorophenoxyacetate/alpha-ketoglutarate dioxygenase. J. Mol. Catal. B **15**:155–162.
9. **Ehrig, A., R. H. Müller, and W. Babel.** 1997. Isolation of phenoxy herbicide-degrading *Rhodoferax* species from contaminated building material. Acta Biotechnol. **17**:351–356.
10. **European Commission.** 2002. Commission regulation (EC) no. 2076/2002 of 20 November 2002 extending the time period referred to in article 8(2) of council directive 91/414/EEC and concerning the non-inclusion of certain active substances in annex I to that directive and the withdrawal of authorisations for plant protection products containing these substances. Off. J. Eur. Union **319**:3–11.
11. **Fukumori, F., and R. P. Hausinger.** 1993. Purification and characterization of 2,4-dichlorophenoxyacetate/alpha-ketoglutarate dioxygenase. J. Biol. Chem. **268**:24311–24317.
12. **Garrison, A. W.** 2006. Probing the enantioselectivity of chiral pesticides. Environ. Sci. Technol. **40**:16–23.
13. **Garrison, A. W., P. Schmitt, D. Martens, and A. Kettrup.** 1996. Enantiomeric selectivity in the environmental degradation of dichlorprop as determined by high-performance capillary electrophoresis. Environ. Sci. Technol. **30**:2449–2455.
14. **Hall, T. A.** 1999. BioEdit: a user-friendly biological sequence alignment editor and analysis program for Windows 95/98/NT. Nucleic Acids Symp. Ser. **41**:95–98.
15. **Hogan, D. A., D. H. Buckley, C. R. Nakatsu, T. M. Schmidt, and R. P. Hausinger.** 1997. Distribution of the *tfdA* gene in soil bacteria that do not degrade 2,4-dichlorophenoxyacetic acid (2,4-D). Microb. Ecol. **34**:90–96.
16. **Horvath, M., G. Ditzelmüller, M. Loidl, and F. Streichsbier.** 1990. Isolation and characterization of a 2-(2,4-dichlorophenoxy) propionic acid-degrading soil bacterium. Appl. Microbiol. Biotechnol. **33**:213–216.
17. **Itoh, K., R. Kanda, Y. Momoda, Y. Sumita, Y. Kamagata, K. Suyama, and H. Yamamoto.** 2000. Presence of 2,4-D-catabolizing bacteria in a Japanese arable soil that belong to BANA (*Bradyrhizobium-Agromonas-Nitrobacter-Afipia*) cluster in α-*Proteobacteria*. Microb. Environ. **15**:113–117.
18. **Itoh, K., R. Kanda, Y. Sumita, H. Kim, Y. Kamagata, K. Suyama, H. Yamamoto, R. P. Hausinger, and J. M. Tiedje.** 2002. *tfdA*-like genes in 2,4-dichlorophenoxyacetic acid-degrading bacteria belonging to the *Bradyrhizobium-Agromonas-Nitrobacter-Afipia* cluster in α-*Proteobacteria*. Appl. Environ. Microbiol. **68**:3449–3454.

Downloaded from http://aem.asm.org/ on June 5, 2012 by guest

COR-AAD1-00002967
Bayer EX1008 (Part 6 of 9)

19. **Itoh, K., Y. Tashiro, K. Uobe, Y. Kamagata, K. Suyama, and H. Yamamoto.** 2004. Root nodule *Bradyrhizobium* spp. harbor *tfdA*α and *cadA*, homologous with genes encoding 2,4-dichlorophenoxyacetic acid-degrading proteins. Appl. Environ. Microbiol. **70:**2110–2118.
20. **Kamagata, Y., R. R. Fulthorpe, K. Tamura, H. Takami, L. J. Forney, and J. M. Tiedje.** 1997. Pristine environments harbor a new group of oligotrophic 2,4-dichlorophenoxyacetic acid-degrading bacteria. Appl. Environ. Microbiol. **63:**2266–2272.
21. **Kelly, M. P., M. R. Heniken, and O. H. Tuovinen.** 1991. Dechlorination and spectral changes associated with bacterial degradation of 2-(2-methyl-4-chlorophenoxy) propionic acid. J. Ind. Microbiol. **7:**137–145.
22. **Lewis, D. L., A. W. Garrison, K. E. Wommack, A. Whittemore, P. Steudler, and J. Melillo.** 1999. Influence of environmental changes on degradation of chiral pollutants in soils. Nature **401:**898–901.
23. **Ma, Y., C. Xu, Y. Z. Wen, and W. P. Liu.** 2009. Enantioselective separation and degradation of the herbicide dichlorprop methyl in sediment. Chirality **21:**480–483.
24. **McGowan, C., R. Fulthorpe, A. Wright, and J. M. Tiedje.** 1998. Evidence for interspecies gene transfer in the evolution of 2,4-dichlorophenoxyacetic acid degraders. Appl. Environ. Microbiol. **64:**4089–4092.
25. **Morgenstern, B.** 2004. DIALIGN: multiple DNA and protein sequence alignment at BiBiServ. Nucleic Acids Res. **32:**W33–W36.
26. **Müller, M. D., and H. R. Buser.** 1997. Conversion reactions of various phenoxyalkanoic acid herbicides in soil. 1. Enantiomerization and enantioselective degradation of the chiral 2-phenoxypropionic acid herbicides. Environ. Sci. Technol. **31:**1953–1959.
27. **Müller, R. H.** 2007. Activity and reaction mechanism of the initial enzymatic step specifying the microbial degradation of 2,4-dichlorophenoxyacetate. Eng. Life Sci. **7:**311–321.
28. **Müller, R. H., S. Jorks, S. Kleinsteuber, and W. Babel.** 1999. *Comamonas acidovorans* strain MC1: a new isolate capable of degrading the chiral herbicides dichlorprop and mecoprop and the herbicides 2,4-D and MCPA. Microbiol. Res. **154:**241–246.
29. **Müller, R. H., S. Kleinsteuber, and W. Babel.** 2001. Physiological and genetic characteristics of two bacterial strains utilizing phenoxypropionate and phenoxyacetate herbicides. Microbiol. Res. **156:**121–131.
30. **Müller, T. A., S. A. Byrde, C. Werlen, J. R. van der Meer, and H. P. E. Kohler.** 2004. Genetic analysis of phenoxyalkanoic acid degradation in *Sphingomonas herbicidovorans* MH. Appl. Environ. Microbiol. **70:**6066–6075.
31. **Müller, T. A., T. Fleischmann, J. R. van der Meer, and H. P. E. Kohler.** 2006. Purification and characterization of two enantioselective α-ketoglutarate-dependent dioxygenases, RdpA and SdpA, from *Sphingomonas herbicidovorans* MH. Appl. Environ. Microbiol. **72:**4853–4861.
32. **Müller, T. A., and H.-P. E. Kohler.** 2004. Chirality of pollutants—effects on metabolism and fate. Appl. Microbiol. Biotechnol. **64:**300–316.
33. **Nickel, K., M. J. F. Suter, and H. P. E. Kohler.** 1997. Involvement of two α-ketoglutarate-dependent dioxygenases in enantioselective degradation of (R)- and (S)-mecoprop by *Sphingomonas herbicidovorans* MH. J. Bacteriol. **179:**6674–6679.
34. **Nicolaisen, M. H., J. Bælum, C. S. Jacobsen, and J. Sørensen.** 2008. Transcription dynamics of the functional *tfdA* gene during MCPA herbicide degradation by *Cupriavidus necator* AEO106 (pRO101) in agricultural soil. Environ. Microbiol. **10:**571–579.
35. **Qin, S. J., and J. Gan.** 2006. Enantiomeric differences in permethrin degradation pathways in soil and sediment. J. Agric. Food Chem. **54:**9145–9151.
36. **Romero, E., M. B. Matallo, A. Peña, F. Sánchez-Rasero, P. Schmitt-Kopplin, and G. Dios.** 2001. Dissipation of racemic mecoprop and dichlorprop and their pure R-enantiomers in three calcareous soils with and without peat addition. Environ. Pollut. **111:**209–215.
37. **Rozen, S., and H. Skaletsky.** 2000. Primer3 on the WWW for general users and for biologist programmers. Methods Mol. Biol. **132:**365–386.
38. **Saari, R. E., D. A. Hogan, and R. F. Hausinger.** 1999. Stereospecific degradation of the phenoxypropionate herbicide dichlorprop. J. Mol. Catal. B **6:**421–428.
39. **Schleinitz, K. M., S. Kleinsteuber, T. Vallaeys, and W. Babel.** 2004. Localization and characterization of two novel genes encoding stereospecific dioxygenases catalyzing 2(2,4-dichlorophenoxy) propionate cleavage in *Delftia acidovorans* MC1. Appl. Environ. Microbiol. **70:**5357–5365.
40. **Swofford, D. L.** 2003. PAUP*. Phylogenetic analysis using parsimony (*and other methods), v. 4. Sinauer Associates, Sunderland, MA.
41. **Tett, V. A., A. J. Willetts, and H. M. Lappinscott.** 1994. Enantioselective degradation of the herbicide mecoprop 2-(2-methyl-4-chlorophenoxy) propionic acid by mixed and pure bacterial cultures. FEMS Microbiol. Ecol. **14:**191–199.
42. **Tett, V. A., A. J. Willetts, and H. M. Lappinscott.** 1997. Biodegradation of the chlorophenoxy herbicide (R)-(+)-mecoprop by *Alcaligenes denitrificans*. Biodegradation **8:**43–52.
43. **Westendorf, A., D. Beandorf, R. H. Müller, and W. Babel.** 2002. The two enantiospecific dichlorprop/α-ketoglutarate-dioxygenases from *Delftia acidovorans* MC1—protein and sequence data of RdpA and SdpA. Microbiol. Res. **157:**317–322.
44. **Westendorf, A., D. Beandorf, T. Pribyl, H. Harms, and R. H. Müller.** 2006. Kinetic traits and enzyme form patterns of (R)-2-(2,4-dichlorophenoxy) propionate/α-ketoglutarate dioxygenase (RdpA) after expression in different bacterial strains. Eng. Life Sci. **6:**552–559.
45. **Westendorf, A., R. H. Müller, and W. Babel.** 2003. Purification and characterisation of the enantiospecific dioxygenases from *Delftia acidovorans* MC1 initiating the degradation of phenoxypropionate and phenoxyacetate herbicides. Acta Biotechnol. **23:**3–17.
46. **Zakaria, D., H. Lappin-Scott, S. Burton, and C. Whitby.** 2007. Bacterial diversity in soil enrichment cultures amended with 2 (2-methyl-4-chlorophenoxy) propionic acid (mecoprop). Environ. Microbiol. **9:**2575–2587.
47. **Zipper, C., C. Bolliger, T. Fleischmann, M. J. F. Suter, W. Angst, M. D. Müller, and H. P. E. Kohler.** 1999. Fate of the herbicides mecoprop, dichlorprop, and 2,4-D in aerobic and anaerobic sewage sludge as determined by laboratory batch studies and enantiomer-specific analysis. Biodegradation **10:**271–278.
48. **Zipper, C., K. Nickel, W. Angst, and H. P. E. Kohler.** 1996. Complete microbial degradation of both enantiomers of the chiral herbicide mecoprop [(RS)-2-(4-chloro-2-methylphenoxy)propionic acid] in an enantioselective manner by *Sphingomonas herbicidovorans* sp. Appl. Environ. Microbiol. **62:**4318–4322.

Downloaded from http://aem.asm.org/ on June 5, 2012 by guest

COR-AAD1-00002968
Bayer EX1008 (Part 6 of 9)

Applied and Environmental Microbiology

Abundance of Novel and Diverse *tfdA*-Like Genes, Encoding Putative Phenoxyalkanoic Acid Herbicide-Degrading Dioxygenases, in Soil

Adrienne Zaprasis, Ya-Jun Liu, Shuang-Jiang Liu, Harold L. Drake and Marcus A. Horn
Appl. Environ. Microbiol. **2010, 76(1):119. DOI: 10.1128/AEM.01727-09.**
Published Ahead of Print 30 October 2009.

Updated information and services can be found at:
http://aem.asm.org/content/76/1/119

These include:

SUPPLEMENTAL MATERIAL
http://aem.asm.org/content/suppl/2009/12/15/76.1.119.DC1.html

REFERENCES
This article cites 74 articles, 33 of which can be accessed free at: http://aem.asm.org/content/76/1/119#ref-list-1

CONTENT ALERTS
Receive: RSS Feeds, eTOCs, free email alerts (when new articles cite this article), more»

Information about commercial reprint orders: http://aem.asm.org/site/misc/reprints.xhtml
To subscribe to to another ASM Journal go to: http://journals.asm.org/site/subscriptions/

Journals.ASM.org

Downloaded from http://aem.asm.org/ on April 30, 2012 by guest

APPLIED AND ENVIRONMENTAL MICROBIOLOGY, Jan. 2010, p. 119–128 Vol. 76, No. 1
0099-2240/10/$12.00 doi:10.1128/AEM.01727-09
Copyright © 2010, American Society for Microbiology. All Rights Reserved.

Abundance of Novel and Diverse *tfdA*-Like Genes, Encoding Putative Phenoxyalkanoic Acid Herbicide-Degrading Dioxygenases, in Soil▽†

Adrienne Zaprasis,[1]‡ Ya-Jun Liu,[1,2]‡ Shuang-Jiang Liu,[2] Harold L. Drake,[1] and Marcus A. Horn[1]*

Department of Ecological Microbiology, University of Bayreuth, Dr.-Hans-Frisch-Straße 1-3, 95440 Bayreuth, Germany,[1] and State Key Laboratory of Microbial Resources, Institute of Microbiology, Chinese Academy of Sciences, Beijing 100101, People's Republic of China[2]

Received 21 July 2009/Accepted 20 October 2009

Phenoxyalkanoic acid (PAA) herbicides are widely used in agriculture. Biotic degradation of such herbicides occurs in soils and is initiated by α-ketoglutarate- and Fe^{2+}-dependent dioxygenases encoded by *tfdA*-like genes (i.e., *tfdA* and *tfdAα*). Novel primers and quantitative kinetic PCR (qPCR) assays were developed to analyze the diversity and abundance of *tfdA*-like genes in soil. Five primer sets targeting *tfdA*-like genes were designed and evaluated. Primer sets 3 to 5 specifically amplified *tfdA*-like genes from soil, and a total of 437 sequences were retrieved. Coverages of gene libraries were 62 to 100%, up to 122 genotypes were detected, and up to 389 genotypes were predicted to occur in the gene libraries as indicated by the richness estimator Chao1. Phylogenetic analysis of in silico-translated *tfdA*-like genes indicated that soil *tfdA*-like genes were related to those of group 2 and 3 *Bradyrhizobium* spp., *Sphingomonas* spp., and uncultured soil bacteria. Soil-derived *tfdA*-like genes were assigned to 11 clusters, 4 of which were composed of novel sequences from this study, indicating that soil harbors novel and diverse *tfdA*-like genes. Correlation analysis of 16S rRNA and *tfdA*-like gene similarity indicated that any two bacteria with $D > 20\%$ of group 2 *tfdA*-like gene-derived protein sequences belong to different species. Thus, data indicate that the soil analyzed harbors at least 48 novel bacterial species containing group 2 *tfdA*-like genes. Novel qPCR assays were established to quantify such new *tfdA*-like genes. Copy numbers of *tfdA*-like genes were 1.0×10^6 to 65×10^6 per gram (dry weight) soil in four different soils, indicating that hitherto-unknown, diverse *tfdA*-like genes are abundant in soils.

Phenoxyalkanoic acid (PAA) herbicides such as MCPA (4-chloro-2-methyl-phenoxyacetic acid) and 2,4-D (2,4-dichlorophenoxyacetic acid) are widely used to control broad-leaf weeds in agricultural as well as nonagricultural areas (19, 77). Degradation occurs primarily under oxic conditions in soil, and microorganisms play a key role in the degradation of such herbicides in soil (62, 64). Although relatively rapidly degraded in soil (32, 45), both MCPA and 2,4-D are potential groundwater contaminants (10, 56, 70), accentuating the importance of bacterial PAA herbicide-degrading bacteria in soils (e.g., references 3, 5, 6, 20, 41, 59, and 78).

Degradation can occur cometabolically or be associated with energy conservation (15, 54). The first step in the degradation of 2,4-D and MCPA is initiated by the product of *cadAB* or *tfdA*-like genes (29, 30, 35, 67), which constitutes an α-ketoglutarate (α-KG)- and Fe^{2+}-dependent dioxygenase. TfdA removes the acetate side chain of 2,4-D and MCPA to produce 2,4-dichlorophenol and 4-chloro-2-methylphenol, respectively, and glyoxylate while oxidizing α-ketoglutarate to CO_2 and succinate (16, 17).

Organisms capable of PAA herbicide degradation are phylogenetically diverse and belong to the *Alpha-*, *Beta-*, and *Gammaproteobacteria* and the *Bacteroidetes/Chlorobi* group (e.g., references 2, 14, 29–34, 39, 60, 68, and 71). These bacteria harbor *tfdA*-like genes (i.e., *tfdA* or *tfdAα*) and are categorized into three groups on an evolutionary and physiological basis (34). The first group consists of beta- and gammaproteobacteria and can be further divided into three distinct classes based on their *tfdA* genes (30, 46). Class I *tfdA* genes are closely related to those of *Cupriavidus necator* JMP134 (formerly *Ralstonia eutropha*). Class II *tfdA* genes consist of those of *Burkholderia* sp. strain RASC and a few strains that are 76% identical to class I *tfdA* genes. Class III *tfdA* genes are 77% identical to class I and 80% identical to class II *tfdA* genes and linked to MCPA degradation in soil (3). The second group consists of alphaproteobacteria, which are closely related to *Bradyrhizobium* spp. with *tfdAα* genes having 60% identity to *tfdA* of group 1 (18, 29, 34). The third group also harbors the *tfdAα* genes and consists of *Sphingomonas* spp. within the alphaproteobacteria (30).

Diverse PAA herbicide degraders of all three groups were identified in soil by cultivation-dependent studies (32, 34, 41, 78). Besides CadAB, TfdA and certain TfdAα proteins catalyze the conversion of PAA herbicides (29, 30, 35). All groups of *tfdA*-like genes are potentially linked to the degradation of PAA herbicides, although alternative primary functions of group 2 and 3 TfdAs have been proposed (30, 35). However, recent cultivation-independent studies focused on 16S rRNA genes or solely on group 1 *tfdA* sequences in soil (e.g., references 3–5, 13, and 41). Whether group 2 and 3 *tfdA*-like genes are also quantitatively linked to the degradation of PAA herbicides in soils is unknown. Thus, tools to target a broad range of *tfdA*-like genes are needed to resolve such an issue. Primers

* Corresponding author. Mailing address: Department of Ecological Microbiology, Dr.-Hans-Frisch-Str. 1-3, University of Bayreuth, 95440 Bayreuth, Germany. Phone: (49) (0)921-555620. Fax: (49) (0)921-555799. E-mail: marcus.horn@uni-bayreuth.de.

‡ Contributed equally to this study.

† Supplemental material for this article may be found at http://aem.asm.org/.

▽ Published ahead of print on 30 October 2009.

Downloaded from http://aem.asm.org/ on April 30, 2012 by guest

COR-AAD1-00002970
Bayer EX1008 (Part 6 of 9)

TABLE 1. Soil characteristics and abundances of *tfdA*-like genes

Site	pH	Clay (%)	Silt (%)	Sand (%)	C/N ratio	Reference(s)	16S rRNA gene copy no. ($\times 10^9$ g^{-1}[a])	*tfdA*-like gene copy no. ($\times 10^6$ g^{-1})			*tfdA*-like gene copy no. per 16S rRNA gene ($\times 10^{-3}$)		
								Group 2[b]	Groups 2 and 3[c]	Groups 1 to 3[d]	Group 2[b]	Groups 2 and 3[c]	Groups 1 to 3[d]
Agricultural field (Scheyern)	5.8	22	36	42	10	48	2.5 ± 0.1	12.9 ± 2.0	64.9 ± 0.7	3.0 ± 0.7	4.8 ± 0.6	26.0 ± 0.9	1.2 ± 0.3
Spruce forests													
Solling	3.3	28	58	14	33	7	1.4 ± 0.1	2.0 ± 0.7	41.5 ± 2.7	1.3 ± 0.1	1.4 ± 0.4	30.0 ± 0.2	0.9 ± 0.1
Steigerwald	3.8	18	24	58	19	8, 42	3.0 ± 0.3	4.7 ± 0.8	40.8 ± 13.6	1.3 ± 0.6	1.6 ± 0.4	13.9 ± 5.8	0.5 ± 0.2
Unterluess	3.1	3	23	74	38	7	3.5 ± 0.9	3.3 ± 1.4	9.8 ± 3.4	1.0 ± 0.6	0.9 ± 0.2	2.7 ± 0.4	0.3 ± 0.1

[a] Dry weight of soil.
[b] Gene copy numbers were determined with primer set 3 (Table 2).
[c] Gene copy numbers were determined with primer set 4 (Table 2).
[d] Gene copy numbers were determined with primer set 5 (Table 2).

used to assess the diversity of *tfdA*-like sequences used in previous studies were based on the alignment of approximately 50% or less of available sequences to date (3, 20, 29, 32, 39, 47, 58, 73). Primers specifically targeting all major groups of *tfdA*-like genes to assess and quantify a broad diversity of potential PAA degraders in soil are unavailable. Thus, the objectives of this study were (i) to develop primers specific for all three groups of *tfdA*-like genes, (ii) to establish quantitative kinetic PCR (qPCR) assays based on such primers for different soil samples, and (iii) to assess the diversity and abundance of *tfdA*-like genes in soil.

MATERIALS AND METHODS

Soil samples and bacterial strain. Samples from four different agricultural or forest soils were used (Table 1). The agricultural soil was collected at the Klostergut Scheyern experimental farm (48°30′00″N, 11°20′07″E) and was treated with MCPA in 2002. The other three soil samples were obtained from different spruce forests in Germany, which were not treated with PAA herbicides (Table 1). All soil samples were obtained from a 0- to 10-cm depth and were stored in the dark on ice during transfer. Each soil sample was homogenized, sieved (2 mm), and stored at −80°C prior to use. *Cupriavidus necator* JMP134 (DSM 4058; formerly *Ralstonia eutropha*) was cultured according to the recommendations of the DSMZ (Braunschweig, Germany) and used for testing of primer specificity (Table 2).

Nucleic acid extraction. DNA was extracted from pelleted cells of 1 ml of *C. necator* JMP134 culture (approximately 10^8 cells) or 0.5 g (wet weight) of soil according to a bead-beating protocol (22) with the following modifications: (i) 100 mM $AlNH_4(SO_4)_2$ was added in soil samples during bead beating to precipitate the humic acid in soil (9); (ii) cell lysis was performed twice for 30 s each at a speed of 5.5 m/s with intermittent cooling on ice for more than 1 min to minimize heating of the samples, and (iii) nucleic acids were precipitated on ice instead of at room temperature for more than 2 h (5). DNA was usually further purified with the MinElute PCR product purification kit (Qiagen, Hilden, Germany) according to the manufacturer's instructions. DNA extracts were stored at −20°C until further analyses.

Alignment and primer design. Fifty-four gene sequences from groups 1, 2, and 3 were obtained from publicly available databases (GenBank, http://www.ncbi.nlm.nih.gov/GenBank) and aligned with the software package ARB (http://www.arb-home.de [40]), and several degenerate primers were designed according to the conserved regions identified in alignments (Table 2). The GenBank accession numbers of the sequences from the first alignment were AY540995, AF181982, AY238495, AB025033, EF375720, BPU43196, DQ644552, DQ360372, DQ360394, DQ360397, DQ360398, DQ360399, BCU87394, AB212778, AB212779, AB212780, AB299620, AY238492, AY238493, AY238496, BSU25717, BSU43197, AFATFDA, BPU43276, AY078159, HGU22499, AY365053, AB299626, AB299627, AF182758, AY238497, AF176240, AY238494, EF600728, EF600734, EF600737, EF600748, EF600752, EF600753, DQ356907, DQ356910, DQ356912, AY554187, AY554191, AY554193, AB074490, AB074491, AB074492, AY193866, and AY554199. The GenBank accession numbers of the sequences from the second alignment containing only group 2 sequences were AB074490, AB074491, AB074492, AY193866, AY193867, AY193868, AY193869, and AY193870.

Primer evaluation and PCR conditions. Primer specificity was evaluated in silico using GenBank's BLAST tool (1), and PCR conditions were optimized by variation of Mg^{2+} and annealing temperature (Table 2). 16S rRNA genes were amplified with published primers (Table 2). Each amplification reaction was performed in a total volume of 25 μl, and the reaction mixture contained 1× PCR buffer (50 mM KCl, 10 mM Tris-HCl, 1.5 mM Mg^{2+} [5-Prime, Hamburg, Germany]) supplemented with 1.0 to 2.5 mM $MgCl_2$, 1× TaqMaster PCR enhancer (5-Prime), 60 ng/μl bovine serum albumin (BSA), 200 μM deoxynucleoside triphosphate (dNTP) mix (5-Prime), 0.2 to 1 μM of each primer (Biomers, Ulm, Germany), 1 μl of template DNA (approximating 50 ng of DNA), and 0.5 U *Taq* DNA polymerase (5-Prime). BSA was included in the reaction mixture to reduce PCR inhibition from humic substances coextracted with DNA from soil (38). The PCR was performed with a T-Gradient cycler (Biometra, Göttingen, Germany) with 10 min of initial denaturation at 95°C, followed by 45 cycles, each consisting of denaturation at 95°C for 1 min, annealing at primer-dependent temperatures (Table 2) for 1 min, and elongation at 72°C for 1 min. The final elongation was at 72°C for 5 min.

Quantification of genes in soil. qPCRs were performed with an iQ5 Real-Time qPCR cycler (Bio-Rad, Munich, Germany). All qPCRs were set up in duplicate. Negative controls with sterilized water instead of DNA template were included in every PCR setup. Standard curves were set up by serially diluting M13uni/rev PCR products of a pGEM-T vector with the appropriate insert from 10^8 to 10^1 target gene copies μl^{-1} for every primer set. qPCRs were performed in 20-μl reaction mixtures that were composed of iQ SYBR green Supermix (Bio-Rad), 60 ng/μl BSA, 0.2 to 1.6 pM of each primer (Biomers, Ulm, Germany), 5 μl of template DNA, and sterilized deionized water. Initial denaturation was at 95°C for 8 min, followed by 45 cycles of denaturation at 95°C for 40 s, annealing at temperatures appropriate for each primer set (Table 2) for 30 s, and elongation at 72°C for 15 s when fluorescence signal was recorded (i.e., a 3-step protocol was utilized). The final PCR elongation step was at 72°C for 5 min. qPCR with primer set 4 (Table 2) yielded a specific product with a melting temperature (T_m) of approximately 91°C and an unspecific product with a T_m of approximately 79°C (see Fig. S1A in the supplemental material). Agarose gel electrophoresis indicated that the latter product was primer dimers. The lower limit of quantification was 10^5 gene copy numbers μl^{-1} of DNA extract (see Fig. S1C). Thus, two more steps at 85°C (i.e., 6 s for preheating and 15 s for signal recording) were added after elongation to melt up primer dimers prior to signal recording (i.e., a 5-step protocol was utilized). After application of the 5-step protocol, primer dimers were not detected during melting curve analysis (see Fig. S1B). Melting curve analyses were performed from 70 to 95°C with increments of 0.2°C per cycle. 16S rRNA gene copy numbers were determined concomitantly for all environmental samples (Table 2) in order to quantify *tfdA*-like genes in soil relative to total bacterial 16S rRNA genes.

Inhibition of qPCR by environmental DNA extracts. Humic acids and other organic compounds coextracted from soil with nucleic acids can inhibit PCR significantly (53, 72, 75, 76). Dilution of DNA extracts and correction of threshold cycle (C_T) values are two strategies for overcoming such inhibition. For testing the inhibitory potential of environmental DNA extracts, such extracts were treated with DNase I (Fermentas, St. Leon-Rot, Germany) at 37°C for 4 h according to the manufacturer's protocol to obtain DNA-free soil extracts. Equal

Downloaded from http://aem.asm.org/ on April 30, 2012 by guest

COR-AAD1-00002971
Bayer EX1008 (Part 6 of 9)

TABLE 2. PCR primers and conditions evaluated in this study

	Primer set[a]	Sequence (5′–3′)[b]	Experimental		Target	Approx product length (bp)	PCR product of agricultural field soil[c]		Reference(s)
			Annealing temp (°C)	Mg^{2+} (mM)			Native	JMP134 spiked	
1	TfdA21F	CCTTCATCCWCTTTTCGYCG	63.0	3.0	*tfdA* (group 1)	815	−	++	This work
	TfdA836R	GCTCGGCGMAGYTCACGC							
2	TfdA334F	CTSTGGCATTSCGACAGYTC	60.0	3.0	*tfdA* (group 1)	260	−	++	This work
	TfdA608R	CSGSGTGSGTTCGVYCAG							
3	TfdAα52F	GGCGTCGATCTGCGCAAGCC	70.0 (65.0)[d]	4.0 (3.0)[d]	*tfdA*α (group 2)	360	++	++	This work
	TfdAα408R	GTTGACGACGCGCGCCGACA							
4	TfdAα421F	ACSGAGTTCGSIGAYATSC	63.6 (68.0)[d]	2.5 (3.0)[d]	*tfdA*α (groups 2 and 3)	360	++	++	Modified from references 29 and 73
	TfdAα779R	CAGCGGTTGTCCCACATCAC							
5	TfdA421dF	ACSGARTTCKSIGACATGC	53.0	3.0	*tfdA*-like (groups 1 to 3)	360	++	++	Modified from references 29 and 73
	TfdA778vkR	AGCGGTTGTCCCACATCAC							
6	TfdA421Fv	ACSGAGTTCTGYGAYATG	59.0	3.0	*tfdA*-like (group 1)	360	+−	++	Modified from reference 73
	TfdA783R	AACGCAGCGRTTRTCCCA							
7	Eub341F	CCTACGGGAGGCAGCAG	55.7	3.0	16S rRNA	190	++	++	49
	Eub534R	ATTACCGCGGCTGCTGG							

[a] Numbers in primer names indicate 5′ position of binding sites relative to the reference *tfdA* sequence of *Cupriavidus necator* JMP134 (AY365053) (primer sets 1, 2, 4, 5, and 6) and of *Alphaproteobacterium* RD5-C2 (AB074490) (primer set 3). F, forward; R, reverse.
[b] S, C/G; Y, C/T; V, A/C/G; W, A/T; M, A/C; K, G/T; R, A/G.
[c] As indicated by agarose gel electrophoresis. ++, bright band; +−, weak band; −, no band of correct size.
[d] Numbers in parentheses refer to qPCR chemicals (see Materials and Methods).

amounts of the DNase-treated soil DNA extracts (nondiluted and 10- and 50-fold diluted) were mixed with standards at 10^5 to 10^7 gene copy numbers μl^{-1} prior to qPCR with primer set 4 (Fig. 1). Standard curves obtained in the presence of nondiluted and 10-fold-diluted DNase-treated soil DNA extracts were shifted toward higher C_T values than were those obtained with pure standard DNA (controls), indicating strong PCR inhibition. The standard curve obtained in the presence of 50-fold-diluted DNase-treated soil DNA extracts was similar to that for controls, suggesting that inhibition was small. Thus, 50-fold dilutions of soil DNA were used routinely in this study for qPCR. However, inhibition still occurred at 50-fold dilution of DNA extracts, and inhibitory effects may vary with DNA extracts. Gene copy numbers in environmental samples were calculated according to the standard curve and were corrected for inhibition. Soil DNA was spiked with pure standard DNA to increase target gene copy numbers per reaction by more than 10-fold. Gene copy numbers obtained by qPCR of spiked and nonspiked DNA extracts were termed *S* and NS, respectively. *C* was the gene copy number measured for the standard DNA. The inhibition factor (IF) was calculated as IF = (*S* − NS)/*C* and theoretically ranges from 0 (complete inhibition) to 1 (no inhibition). NS was divided by IF to approximate real gene copy numbers in DNA extracts. IF varied from 0.1 to 0.91 for DNA extracts obtained from different soil samples. Representative PCR products were analyzed by agarose gel electrophoresis, and products were cloned and sequenced to check for specific amplification of target genes.

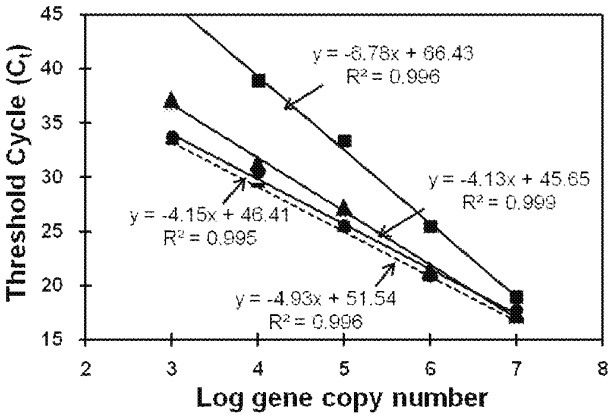


FIG. 1. Effect of inhibitors present in soil DNA extracts on standard curves generated during qPCR with primer set 4. Solid lines indicate standards spiked with various concentrations of DNA-free soil extract (■, nondiluted; ▲, 10-fold diluted; ●, 50-fold diluted); the dashed line indicates the nonspiked standard curve. Equations of linear regressions and R^2 values of every curve are given.

The recovery of target DNA from soil was estimated by spiking soil with defined amounts of a linearized, *tfdA*-like gene harboring pGEM-T. pGEM-T was linearized by digestion with SacI (New England Biolabs) overnight at 37°C, quantified by recording the A_{260} (ND1000; Peqlab), and spiked to soil prior to DNA extraction and qPCR.

Cloning, screening, and sequencing. (q)PCR products used for cloning were analyzed by gel electrophoresis on 1% agarose gels in 1× Tris-acetate-EDTA (TAE) buffer (AppliChem, Darmstadt, Germany). The gels contained ethidium bromide and were visualized under UV light. PCR products were routinely purified by cutting out the band of the expected size (Table 2) to remove primers and primer dimers with subsequent extractions using the MiniElute gel extraction kit (Qiagen, Hilden, Germany) according to the manufacturer's protocol. PCR products of all target samples were ligated into pGEM-T (Promega, Mann-

Downloaded from http://aem.asm.org/ on April 30, 2012 by guest

COR-AAD1-00002972
Bayer EX1008 (Part 6 of 9)

	Number of clones			
Primer	4		5	
(Q)PCR	A	B	A	B
Cluster				
2a	33	0	9	13
2b	0	1	1	5
2c	20	11	4	5
2d	11	19	24	30
2e	6	4	6	12
2f	1	0	2	0
3a	3	0	1	2
3b	0	0	0	2
3c	0	0	0	0
4	0	2	0	0
Class I	0	0	0	0
Class III	0	0	0	0
Class II	0	0	0	0
5	8	0	0	1

Group 2
Group 3
Group 4
Group 1
Group 5

Downloaded from http://aem.asm.org/ on April 30, 2012 by guest

COR-AAD1-00002973

Bayer EX1008 (Part 6 of 9)

heim, Germany), which was used for transformation of *Escherichia coli* JM109 competent cells (Promega, Madison, WI) according to the manufacturer's protocol. For screening of the clone libraries from (q)PCR products, the fragments were directly amplified from 1 μl of resuspended clones and electrophoresed on agarose gels (1%). The gene libraries were screened by restriction fragment length polymorphism (RFLP). PCR products of clones generated with primer set 3 (Table 2) were digested with 1 U of AluI and BsuRI (New England BioLabs, Ipswich, MA) in separate reactions, and those generated with primer sets 4 and 5 (Table 2) were likewise digested with 1 U of MspI and TaqAI (New England BioLabs) in separate reactions for 3 h at 37°C (TaqAI at 65°C). The fragments were separated on agarose gels (3%). One to 10 representative clones of each RFLP pattern per library were selected for sequencing. Representative PCR products were purified (PCR cleanup plates; Millipore, Schwalbach, Germany) according to the manufacturer's protocol and commercially sequenced (Macrogen, South Korea). Sequence comparisons and database searches were carried out by using the BLAST service at the NCBI website (http://blast.ncbi.nlm.nih.gov/).

Phylogenetic analyses. Phylogenetic analyses were performed with the ARB software package and Mega4 software (http://www.megasoftware.net/) (69). *tfdA*-like genes were retrieved from NCBI, translated in silico, and prealigned with the ClustalW algorithm, and the alignment was refined manually. The DNA was aligned according to the aligned proteins. Regions of primer binding sites were excluded from further sequence analysis. Phylogenetic trees were calculated based on amino acid sequences using the neighbor-joining algorithm (55). Tree topologies of neighbor-joining trees were verified by bootstrap analysis with 1,000 replicates.

Prealigned 16S rRNA gene sequences were retrieved from SILVA (http://www.arb-silva.de/) (52). Distance matrices for the correlation of pairwise similarities of *tfdA*-like and 16S rRNA gene sequences were generated with the ARB software package (40).

Analysis of *tfdA*-like genotype diversity. Sequences that had the same RFLP patterns as those of sequenced *tfdA*-like gene fragments were represented by the fully sequenced fragments. Distance matrices were generated from aligned amino acid sequences. DOTUR (http://schloss.micro.umass.edu/software/index.html) (57) was applied to define genotypes based on the amino acid sequence dissimilarity of proteins derived from translated *tfdA*-like sequences by the furthest-neighbor method. Sequences with maximal 3% or 20% dissimilarity (i.e., distance $D \leq 3$ or 20%) were thereby assigned to one genotype. Additional information on DOTUR is available at the publisher's website (http://schloss.micro.umass.edu/software/index.html). Coverage (C) is the number of the detected genotypes relative to their expected total number in a gene library and was calculated as $C = (1 - n \times N^{-1}) \times 100$, where n is the number of genotypes that occurred only once and N is the number of clones screened (21). The diversity of genotypes represented in gene libraries of *tfdA*-like genes was analyzed by rarefaction analysis (28), Shannon diversity index, and the genotype richness estimator Chao1 (24). All calculations were done with DOTUR (57). Rarefaction curves were produced using the Analytic Rarefaction software (version 1.2; http://www.uga.edu/strata/software/index.html).

Nucleotide sequence accession numbers. Sequences obtained in this study were deposited in the EMBL nucleotide sequences database (http://www.ebi.ac.uk) under accession numbers FN376574 to FN376845.

RESULTS

Novel primers for amplification of *tfdA*-like genes. Eight conserved regions of *tfdA*-like genes were used to design consensus primers (data not shown). Five different degenerated primer sets were designed (1 to 5, Table 2) to amplify (i) almost full-length fragments of the *tfdA* gene group 1, (ii) a partial gene fragment of *tfdA* group 1, (iii) a partial gene fragment of *tfdA*α group 2, (iv) a partial gene fragment of *tfdA*α covering group 2 genes, and (v) a partial gene fragment of *tfdA*-like genes targeting group 1 and 2 genes. Nevertheless, primer sets 4 and 5 amplified group 3 *tfdA*-like genes (Table 2; Fig. 2). In silico analyses indicated that primers of sets 1 and 2 had 1 to 4 mismatches to group 2 *tfdA*-like genes. Primer set 3 targeted a subset of group 2 *tfdA*-like genes and had more than 4 mismatches to group 1 *tfdA*. Primer set 4 covered all known group 2 *tfdA*-like genes and had one mismatch to group 1 *tfdA*. Primer set 5 had no mismatches to any known *tfdA*-like gene. In silico analyses of primer sets 4 and 5 were not performed with group 3 *tfdA*α fragments since the fragments publicly available to date were truncated. PCR products generated with primer set 6 from Scheyern soil contained only low concentrations of targets with the expected size (Table 2). However, all primer sets that were tested readily amplified fragments of the expected sizes (Table 2) from Scheyern soil that was amended with 10^4, 10^6, and 10^8 cells of *C. necator* JMP134 (harboring group 1 *tfdA*) per gram of soil, indicating that all primer sets detected target genes in soil (data not shown). The proportion of group 1 *tfdA* sequences per gene library (25 to 29 sequences per library) generated from Scheyern soil with primer set 5 approximated 15, 76, and 100% for soil amended with 10^4, 10^6, and 10^8 cells of *C. necator* JMP134 per gram of soil, respectively, indicating that the detection limit of group 1 *tfdA* in Scheyern soil with primer set 5 is below 10^4 copies per gram of soil (assuming one copy of group 1 *tfdA* per cell). Gene libraries generated from nonspiked Scheyern soil with primer sets 4 and 5 contained group 2- and 3-related *tfdA*-like genes. Primer set 3 yielded likewise specific products which were most closely related to group 2 *tfdA*-like genes (see Fig. S2 in the supplemental material). The results showed that the designed primers allowed a specific targeting of *tfdA*-like genes from soil.

Detected diversity of *tfdA*-like genes. A total number of 437 *tfdA*-positive clones (201, 119, and 117 clones for primer sets 3, 4, and 5, respectively) were screened by RFLP, and 210 representative clones were sequenced. Coverages approximated 93 and 100% at $D \leq 3\%$ and $D \leq 20\%$, respectively, for the gene library generated with primer set 3 targeting a fraction of group 2 *tfdA*-like genes (Table 3; see also Fig. S2 and S3 in the supplemental material). Coverages approximated 62 and 91% at $D \leq 3\%$ and $D \leq 20\%$, respectively, for the combined gene libraries generated with primers 4 and 5 targeting *tfdA*-like genes of groups 1 to 3 (Table 3; Fig. 2 and 3), indicating that the gene libraries were sufficiently sampled.

The gene library targeting group 2 *tfdA*-like genes (primer set 3) contained 34 and 6 genotypes at $D \leq 3\%$ and $D \leq 20\%$, respectively (Table 3). The estimated numbers of genotypes present in the gene library were 47 and 6, respectively; Shannon's diversity indices were 2.5 and 0.5, respectively (Table 3). All sequences were related to *tfdA*-like genes of cultured *Alphaproteobacteria* (*Bradyrhizobium* spp.) or *tfdA*-like genes re-

FIG. 2. Phylogenetic neighbor-joining tree of representative *tfdA*-like genes generated with primer sets 4 and 5 (approximately 110 amino acids; indicated in boldface). Accession numbers are shown in brackets, and bootstrap values above 50% are shown at nodes. The abundances of sequences in the gene library are given in parentheses. Clusters of *tfdA*-like genes containing novel sequences only are highlighted with gray boxes. The following TauD (α-ketoglutarate-dependent taurine dioxygenase) sequences were used as the outgroup: CP000699, CP000854.1, CP000124.1, AP009048, and AL590842. In the associated table, sequences generated with PCR and qPCR are indicated by A and B, respectively. The scale bar represents an estimated sequence dissimilarity of 20%.

Downloaded from http://aem.asm.org/ on April 30, 2012 by guest

COR-AAD1-00002974
Bayer EX1008 (Part 6 of 9)

TABLE 3. Summary of data from amino acid analyses of in silico-translated *tfdA*-like gene sequence fragments retrieved from Scheyern agricultural soil

Primer set(s)[a]	Target	n[b]	D[c] (%)	S[d]	C[e] (%)	Chao1[f]	H'[g]
3	*tfdA*α (group 2)	201	3	34	92.5	47	2.5
			20	6	100.0	6	0.5
4 and 5	*tfdA*-like (groups 1 to 3)	236	3	122	61.9	389	4.3
			20	48	91.1	78	3.2

[a] See Table 2.
[b] n, number of clones screened.
[c] D, maximal amino acid sequence dissimilarity used for the assignment of sequences to genotypes (see Materials and Methods).
[d] S, number of genotypes.
[e] C, coverage; see Materials and Methods for details.
[f] Richness estimator; indicative of estimated number of genotypes per gene library.
[g] H', Shannon index.

trieved from other soils (see Fig. S2 in the supplemental material). Group 2 *tfdA*-like genes retrieved from Scheyern agricultural soil were assigned to 2 phylogenetic clusters (see Fig. S2). Cluster 2 contained sequences from Scheyern soil only, indicating that phylogenetically novel *tfdA*-like genes occur in Scheyern agricultural soil. The maximal phylogenetic distance of cluster 1 sequences was 23.3%, and the cluster contained *Bradyrhizobium*-related sequences. Cluster 1 sequences generated with primer set 3 (see Fig. S2) were represented by cluster 2a in gene libraries generated with primers 4 and 5 (maximal phylogenetic distance, 23.7% [Fig. 2]).

Primer sets 4 and 5 amplified similar fragments and detected similar groups of *tfdA*-like genes (Fig. 2). Thus, the gene libraries generated with such primers were combined for further analysis and contained 122 and 48 genotypes at $D \leq 3\%$ and $D \leq 20\%$, respectively (Table 3). The estimated numbers of genotypes present in the gene library were 389 and 78, respectively; Shannon's diversity indices were 4.3 and 3.2, respectively (Table 3). All sequences of the gene library generated with primer sets 4 and 5 were related to *tfdA*-like genes from the *Alphaproteobacteria Bradyhizobium* spp. and *Sphingomonas* spp. or uncultured bacteria of other soils and were assigned to 11 clusters. Most of the clusters belonged to group 2 (90% of sequences) of *tfdA*-like genes (Fig. 2). Approximately 5% of the sequences were distantly related to any known group of *tfdA*-like genes and assigned to two novel groups, 4 and 5 (Fig. 2). Four out of the 11 clusters contained sequences from Scheyern soil only, reinforcing the conclusion that Scheyern soil harbors novel and diverse *tfdA*-like genes. The numbers of genotypes, the genotype richness estimators, and the phylogenetic diversities of *tfdA*-like genes were higher within gene libraries of primer sets 4 and 5 than within those of primer set 3 (Table 3; Fig. 2; see also Fig. S2 in the supplemental material). Thus, the detectability of *tfdA*-like gene diversity in soil was considerably higher with primer sets 4 and 5 than with primer set 3, indicating that those primers are useful tools to detect novel *tfdA*-like sequences in the environment.

Comparison of *tfdA*-like and 16S rRNA gene similarity. The comparative phylogeny of *tfdA*-like and 16S rRNA genes of bacteria harboring *tfdA*-like genes was assessed to determine if *tfdA*-like genes could be used for the identification of such organisms. Pairwise similarities of *tfdA*-like and 16S rRNA gene sequences ranged from 76.3 to 100% and 75.5 to 100% for group 1, respectively. For group 2 sequences, pairwise similarities of *tfdA*-like and 16S rRNA gene sequences ranged from 80.4 to 100% and 97.4 to 100%, respectively. Such data indicate that 16S rRNA genes are more conserved than *tfdA*-like genes (Fig. 4). Group 1 organisms that shared <77% *tfdA*-like gene similarity (or 80% protein similarity of translated *tfdA*-like genes) always shared <97% 16S rRNA gene similarity (a conservative threshold similarity for assigning two organisms to different species [65, 66]) (Fig. 4). The scattering of data points for group 1 organisms (Fig. 4) indicated horizontal gene transfer of group 1 *tfdA*, making it difficult to predict 16S rRNA gene similarities and consequently new species based on group 1 *tfdA*-like gene similarities. However, there was a correlation between 16S rRNA and group 2 *tfdA*-like gene similarity, indicating little or no horizontal gene transfer. Approximately 90% of any group 2 organisms that shared >97% 16S rRNA sequence similarity shared >82% *tfdA*-like gene similarity (equivalent to 84% protein similarity of translated *tfdA*-like genes). Thus, group 2 organisms that share ≤82% *tfdA*-like gene similarity (equivalent to ≤84% protein similarity of translated *tfdA*-like genes) have a very high probability of belonging to different species. Group 2 sequences that share ≤77% *tfdA*-like gene similarity (equivalent to ≤80% protein similarity of translated *tfdA*-like genes) have consequently an even higher probability of belonging to different species.

Quantitation and recovery of *tfdA*-like genes. Primer sets 3 to 5 were used for quantification of *tfdA*-like genes in soil by

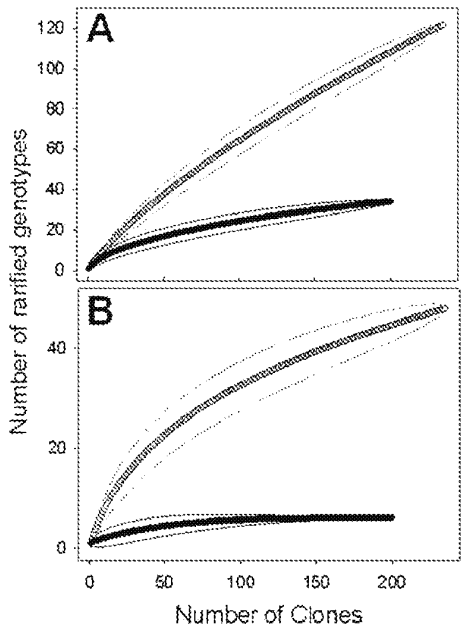


FIG. 3. Rarefaction curves of cloned *tfdA*-like gene fragments for an evolutionary distance of 3% (A) or 20% (B). *tfdA*-like sequences were retrieved from Scheyern soil with primer sets 4 and 5 (○) and primer set 3 (●). Dotted and solid lines indicate 95% confidence intervals.

Downloaded from http://aem.asm.org/ on April 30, 2012 by guest

COR-AAD1-00002975
Bayer EX1008 (Part 6 of 9)

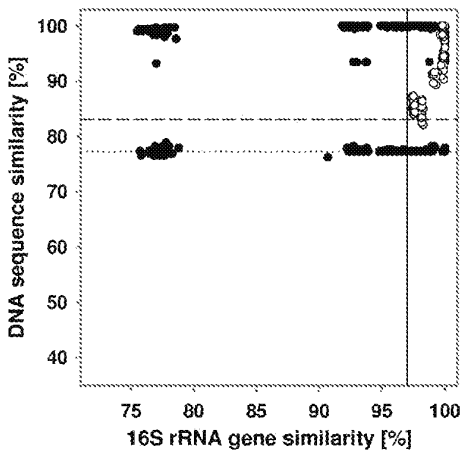


FIG. 4. Correlation of 16S rRNA gene similarity with *tfdA*-like sequence similarity of pure cultures. Group 1 (●) and 2 (○) sequences are indicated. The solid line indicates 16S rRNA gene threshold similarity values for species delineation, and the dotted line indicates threshold similarity values below which sequences are indicative of novel species with high probability. The dashed line represents the 90% quantile of pairwise sequence comparisons with a 16S rRNA similarity of >97%.

qPCR. Quantification of group 2 *tfdA*-like gene fragments with primer set 3 was reliable from 10^2 to 10^9 gene copy numbers μl of DNA extract^{-1} as indicated by the standard curve (see Fig. S3 in the supplemental material). Such qPCR products and those from environmental DNA had a T_m of approximately 90°C, and no nonspecific products were detected by agarose gel electrophoresis. Similar results were obtained with primer set 5 (see Fig. S3). Quantification of group 2 *tfdA*-like gene fragments with primer set 4 was reliable from 10^1 to 10^8 gene copy numbers μl of DNA extract^{-1} as indicated by the standard curve (see Fig. S1D).

Soils contained approximately 10^6 *tfdA*-like gene copies per gram (Table 1). Linearized pGEM-T with *tfdA*-like gene insert was added to triplicate Scheyern soil samples at final concentrations of 7.6×10^6 *tfdA*-like genes per gram of soil. *tfdA*-like gene copies per gram of soil measured by qPCR after DNA extraction were $(1.58 \pm 0.25) \times 10^6$. Thus, recovery of *tfdA*-like genes from soil approximated 20%, indicating that the DNA extraction protocol contributed to an underestimation of gene copy numbers in soil.

Quantification of *tfdA*-like genes relative to 16S rRNA genes in four different soils. To overcome the effect of various degrees of qPCR inhibition by different DNA extracts, inhibition factors were recorded per DNA extract, and the gene copy numbers obtained by qPCR were corrected accordingly (see Materials and Methods). *tfdA*-like genes were abundant in all 4 different soils. Copy numbers ranged from 1×10^6 to 65×10^6 per gram of soil, depending on the primers and the soil (Tables 1 and 2). Primer set 4 consistently detected higher *tfdA*-like gene copy numbers than did primer set 3, which is in agreement with in silico analyses (Table 2). However, primer set 5, which theoretically targeted the broadest diversity (group 1 to 3 *tfdA*-like genes), in this study yielded copy numbers that were lower than those obtained with primer set 4 (groups 2 and 3), indicating that the broader specificity of primer set 5 compromised its sensitivity toward group 2 and 3 *tfdA*-like genes. Thus, primer set 4 is recommended for the quantification of group 2 and 3 *tfdA*-like genes in soils. Nevertheless, qPCR assays utilizing any of the primer sets used were successfully used for quantification of *tfdA*-like genes in soils. 16S rRNA gene copies ranged from 1×10^9 to 3×10^9 per gram of soil (Table 1). *tfdA*-like genes were most abundant in the agricultural soil of Scheyern compared to forest soils. The proportion of *tfdA*-like genes relative to 16S rRNA genes was likewise highest in Scheyern agricultural soil, indicating that a substantial number of bacteria harbored *tfdA*-like genes.

DISCUSSION

Novel and diverse *tfdA*-like genes were detected in soil by primers developed in this study to match a broad diversity of *tfdA*-like genes (Fig. 2; Table 3; see also Fig. S2 in the supplemental material). All *tfdA*-like genes were phylogenetically distinct from *tauD* (Fig. 2; see also Fig. S2), which encodes an α-KG-dependent taurine dioxygenase with approximately 30% sequence identity to *tfdA*-like genes (74), indicating that the novel primers discriminate well against *tauD*. *tfdA*-like gene fragments recovered from an agricultural soil that was treated with MCPA in 2002 were assigned to 11 clusters and were indicative of up to 122 distinct genotypes (at $D < 3$ [Table 3]) mainly related to alphaproteobacterial *tfdA*-like genes or two hitherto-unknown groups (Fig. 2; see also Fig. S2). Other studies of *tfdA*-like gene sequence diversity in soil without prior enrichment and/or isolation are still rather scarce and detect primarily group 1 *tfdA*-like genes indicative of *Beta-* and *Gammaproteobacteria* (3–5, 20). However, enrichments and analysis of isolates from soils revealed the presence of alphaproteobacterial PAA degraders in soils (29, 34) and are consistent with the detection of alphaproteobacterial *tfdA*-like genes in this study. *Alphaproteobacteria* of the genus *Sphingomonas* numerically dominate PAA degraders in certain soils (32), and those of the genera *Sphingomonas* and *Bradyrhizobium* are often detected by isolation (11, 27, 34, 41, 51). Since highly diverse *tfdA*-like genes indicative of *Alphaproteobacteria* were detected in this study, *Alphaproteobacteria* might represent a widely distributed, more diverse group of PAA degraders in soil than previously thought.

Bradyrhizobium-related PAA degraders of the *Alphaproteobacteria* are slow-growing oligotrophs (doubling times approximate 20 h), which are sensitive to high concentrations of organic nutrients (34, 59). Such organisms were also isolated from pristine soils that never received PAA treatment (34). Group 2 *tfdA*-like gene products are capable of PAA conversion (29), indicating that those genes are potentially involved in PAA conversion in soil, despite the occurrence of alternative potential PAA-degradative genes like *cadAB* among certain *Bradyrhizobia* (30, 35). Group 2 *tfdA*-like gene products display a higher activity for nonchlorinated PAA than for chlorinated ones (29). Group 1 *tfdA*-like gene products are capable of utilizing phenoxyacetic acid and cinnamic acid derivatives which occur in soil and are produced by plants (references 26 and 61 and references therein). Cinnamic acid-related flavonoids enhanced PAA utilization by a *Bradyrhizobium* sp. strain, indicating that such naturally occurring compounds

Downloaded from http://aem.asm.org/ on April 30, 2012 by guest

COR-AAD1-00002976
Bayer EX1008 (Part 6 of 9)

might stimulate the expression of group 2 *tfdA*-like genes (58, 59). Since group 2 *tfdA*-like gene products are capable of converting PAA (29) and *tfdA*-like genes were abundant in the soil analyzed (Table 1), *tfdA*-like genes might have potential environmental relevance for (cometabolic) PAA degradation in soil. The primers developed in this study will facilitate a thorough evaluation of such a hypothesis in future studies.

The analysis of structural genes like *tfdA* might well be used for diversity studies of process-associated bacteria, but evidence for species-level diversity from such data might be obtained only if horizontal gene transfer of the structural gene in question is scarce. 16S rRNA gene similarities correlated with *tfdA*-like gene similarities for group 2 sequences but not for group 1 sequences (Fig. 4), indicating that horizontal gene transfer played a major role during evolution of group 1 rather than group 2 *tfdA*-like-gene-harboring organisms. Several lines of evidence support such a conclusion: (i) plasmid-encoded group 1 *tfdA* is common among PAA-degrading bacteria of the *Beta-* and *Gammaproteobacteria* (e.g., references 2, 14, and 18), (ii) such an encoded PAA-degrading function is transmissible (34, 46), and (iii) the degree of congruency between 16S rRNA and group 1 *tfdA*-like-gene-based phylogenetic trees is low (46). In contrast, the PAA-degrading function of group 2 and 3 *tfdA*-like gene-carrying organisms is not or only barely transmissible (34), the degree of congruency between 16S rRNA and group 2 *tfdA*-like-gene-based phylogenetic trees is high (30), and the GC contents of group 3 *tfdA*-like and housekeeping genes in *Sphingomonas* spp. are highly similar (30).

The virtual absence of horizontal gene transfer for group 2 and 3 *tfdA*-like genes allows for an estimation of species-level diversity based on group 2 and 3 *tfdA*-like gene analysis. Correlation analysis of *tfdA*-like and 16S rRNA gene similarity thus indicates that the number of *tfdA*-like genotypes that share less than 80% of translated protein sequences is a minimal estimate for species-level diversity of *tfdA*-like-gene-carrying bacteria (i.e., the true species-level diversity might be much higher). The calculated threshold similarities are well in agreement with those obtained for other structural genes (e.g., for *narG*, *nosZ*, *dsrAB*, and *amoA* gene fragments, they were 70 to 90% [25, 36, 37, 50]). The detected *tfdA*-like genes in this study consequently suggest that at least 48 distinct species of *tfdA*-like-gene-carrying bacteria occurred in agricultural soil (Table 3).

Such diverse *tfdA*-like genes were abundant in agricultural and pristine forest soils as indicated by up to 10^7 copy numbers per gram (dry weight) soil (Table 1). *tfdA*-like genes accounted for up to 3% of bacterial 16S rRNA genes. Copy numbers obtained in other studies with group 1 *tfdA*-like-gene-specific qPCR assays vary from 10^2 to 10^5 per gram (dry weight) soil prior to PAA incubation (3, 5, 20), indicating that group 2 and 3 genes outnumber group 1 genes in certain soils and highlighting a hitherto unknown PAA degradation potential in soils.

All qPCR assays in this study included a correction for inhibitory effects of environmental DNA extracts on the DNA polymerase used. Inhibition of the DNA polymerase during qPCR results in an underestimation of gene copy numbers (43). Such inhibitors include humic acids derived from plant material (53, 76). There are many approaches to overcome inhibition of qPCR, such as increase of Mg^{2+} concentration, addition of BSA, or dilution of template DNA (e.g., references 3, 23, and 38). DNA extraction and purification methods were also improved to reduce the amount of coextracted inhibitors (22, 75). However, all of these approaches failed in our study to avoid inhibition (Fig. 1 and data not shown). Thus, gene copy numbers were corrected for the inhibition caused by environmental DNA extracts. Since internal positive-control fragments are more suitable for TaqMan probe-based assays (12, 44), environmental DNA was spiked with an approximately 10-fold excess of the target gene to identify and correct for inhibition during qPCR. The quality of DNA extracts obtained with the same method from soils varies (63), necessitating the evaluation of inhibitory effects for every qPCR assay to minimize artificial variations in gene copy numbers.

Novel primers developed in this study enabled the detection of highly diverse group 2 and 3 *tfdA*-like gene sequences in soil (Fig. 2; see also Fig. S2 in the supplemental material). Such genes outnumber group 1 *tfdA*-like genes by several orders of magnitude in certain soils without prior enrichment on PAA (Table 1) (3, 4), indicating that PAA degradation is not the primary function of those genes. Inducers of gene expression of group 2 and 3 *tfdA*-like genes in soil and pure cultures need to be identified to shed light on the potential function of such genes. The present study provides a basis for such investigations.

ACKNOWLEDGMENTS

We are grateful to Stephan Schulz, Michael Schloter, Jean Charles Munch, Daniela Degelmann, and Steffen Kolb for provision of soil samples.

Support for this study was provided by the Deutsche Forschungsgemeinschaft (grant HO4020/1-1, DFG Priority Program 1315 "Biogeochemical interfaces in soil"), by the University of Bayreuth, and by a grant from the German Academic Exchange Service (DAAD) to Y.-J. Liu.

REFERENCES

1. **Altschul, S., T. Madden, A. Schaffer, J. H. Zhang, Z. Zhang, W. Miller, and D. J. Lipman.** 1997. Gapped BLAST and PSI-BLAST: a new generation of protein database search programs. Nucleic Acids Res. **25:**3389–3402.
2. **Amy, P. S., J. W. Schulke, L. M. Frazier, and R. J. Seidler.** 1985. Characterization of aquatic bacteria and cloning of genes specifying partial degradation of 2,4-dichlorophenoxyacetic acid. Appl. Environ. Microbiol. **49:**1237–1245.
3. **Bælum, J., T. Henriksen, H. C. B. Hansen, and C. S. Jacobsen.** 2006. Degradation of 4-chloro-2-methylphenoxyacetic acid in top- and subsoil is quantitatively linked to the class III *tfdA* gene. Appl. Environ. Microbiol. **72:**1476–1486.
4. **Bælum, J., and C. S. Jacobsen.** 2009. TaqMan probe-based real-time PCR assay for detection and discrimination of class I, II, and III *tfdA* genes in soils treated with phenoxy acid herbicides. Appl. Environ. Microbiol. **75:**2969–2972.
5. **Bælum, J., M. H. Nicolaisen, W. E. Holben, B. W. Strobel, J. Sørensen, and C. S. Jacobsen.** 2008. Direct analysis of *tfdA* gene expression by indigenous bacteria in phenoxy acid amended agricultural soil. ISME J. **2:**677–687.
6. **Bollag, J.-M., C. S. Helling, and M. Alexander.** 1967. Metabolism of 4-chloro-2-methylphenoxyacetic acid by soil bacteria. Appl. Environ. Microbiol. **15:**1393–1398.
7. **Borken, W., A. Muhs, and F. Beese.** 2002. Changes in microbial and soil properties following compost treatment of degraded temperate forest soils. Soil Biol. Biochem. **34:**403–412.
8. **Borken, W., Y. J. Xu, and F. Beese.** 2003. Conversion of hardwood forests to spruce and pine plantations strongly reduced soil methane sink in Germany. Global Change Biol. **9:**956–966.
9. **Braid, M. D., L. M. Daniels, and C. L. Kitts.** 2003. Removal of PCR inhibitors from soil DNA by chemical flocculation. J. Microbiol. Methods **52:**389–393.
10. **Bryant, F. O.** 1992. Biodegradation of 2,4-dichlorophenoxyacetic acid and 2,4,5-trichlorophenoxyacetic acid by dichlorophenol-adapted microorganisms from fresh-water, anaerobic sediments. Appl. Microbiol. Biotechnol. **38:**276–281.

Downloaded from http://aem.asm.org/ on April 30, 2012 by guest

COR-AAD1-00002977
Bayer EX1008 (Part 6 of 9)

11. **Chung, M. J., and J. O. Ka.** 1998. Isolation and characterization of 2,4-dichlorophenoxyacetic acid-degrading bacteria from paddy soils. J. Microbiol. **36:**256–261.
12. **Courtney, B. C., M. M. Smith, and E. A. Henchal.** 1999. Development of internal controls for probe-based nucleic acid diagnostic assays. Anal. Biochem. **270:**249–256.
13. **Cupples, A. M., and G. K. Sims.** 2007. Identification of in situ 2,4-dichlorophenoxyacetic acid-degrading soil microorganisms using DNA-stable isotope probing. Soil Biol. Biochem. **39:**232–238.
14. **Don, R. H., and J. M. Pemberton.** 1981. Properties of 6 pesticide degradation plasmids isolated from *Alcaligenes paradoxus* and *Alcaligenes eutrophus*. J. Bacteriol. **145:**681–686.
15. **Fournier, J. C.** 1980. Enumeration of the soil microorganisms able to degrade 2,4-D by metabolism or co-metabolism. Chemosphere **9:**169–174.
16. **Fukumori, F., and R. P. Hausinger.** 1993. *Alcaligenes eutrophus* JMP134 2,4-dichlorophenoxyacetate monooxygenase is an alpha-ketoglutarate-dependent dioxygenase. J. Bacteriol. **175:**2083–2086.
17. **Fukumori, F., and R. P. Hausinger.** 1993. Purification and characterization of 2,4-dichlorophenoxyacetate alpha-ketoglutarate dioxygenase. J. Biol. Chem. **268:**24311–24317.
18. **Fulthorpe, R. R., C. McGowan, O. V. Maltseva, W. E. Holben, and J. M. Tiedje.** 1995. 2,4-Dichlorophenoxyacetic acid-degrading bacteria contain mosaics of catabolic genes. Appl. Environ. Microbiol. **61:**3274–3281.
19. **Gintautas, P. A., S. R. Daniel, and D. L. Macalady.** 1992. Phenoxyalkanoic acid herbicides in municipal landfill leachates. Environ. Sci. Technol. **26:** 517–521.
20. **Gonod, L. V., F. Martin-Laurent, and C. Chenu.** 2006. 2,4-D impact on bacterial communities, and the activity and genetic potential of 2,4-D degrading communities in soil. FEMS Microbiol. Ecol. **58:**529–537.
21. **Good, I. J.** 1958. The population frequency of species and the estimation of the population parameters. Biometrics **40:**237–246.
22. **Griffiths, R. I., A. S. Whiteley, A. G. O'Donnell, and M. J. Bailey.** 2000. Rapid method for coextraction of DNA and RNA from natural environments for analysis of ribosomal DNA and rRNA-based microbial community composition. Appl. Environ. Microbiol. **66:**5488–5491.
23. **Henry, S., E. Baudoin, J. C. Lopez-Gutierrez, F. Martin-Laurent, A. Baumann, and L. Philippot.** 2004. Quantification of denitrifying bacteria in soils by *nirK* gene targeted real-time PCR. J. Microbiol. Methods **59:**327–335.
24. **Hill, T. C. J., K. A. Walsh, J. A. Harris, and B. F. Moffett.** 2003. Using ecological diversity measures with bacterial communities. FEMS Microbiol. Ecol. **43:**1–11.
25. **Horn, M. A., H. L. Drake, and A. Schramm.** 2006. Nitrous oxide reductase genes (*nosZ*) of denitrifying microbial populations in soil and the earthworm gut are phylogenetically similar. Appl. Environ. Microbiol. **72:**1019–1026.
26. **Hotopp, J. C. D., and R. P. Hausinger.** 2001. Alternative substrates of 2,4-dichlorophenoxyacetate/alpha-ketoglutarate dioxygenase. J. Mol. Catal. B Enzymatic **15:**155–162.
27. **Huong, N. L., K. Itoh, and K. Suyama.** 2007. Diversity of 2,4-dichlorophenoxyacetic acid (2,4-D) and 2,4,5-trichlorophenoxyacetic acid (2,4,5-T)-degrading bacteria in Vietnamese soils. Microbes Environ. **22:**243–256.
28. **Hurlbert, S. H.** 1971. The nonconcept of species diversity: a critique and alternative parameters. Ecology **52:**577–586.
29. **Itoh, K., R. Kanda, Y. Sumita, H. Kim, Y. Kamagata, K. Suyama, H. Yamamoto, R. P. Hausinger, and J. M. Tiedje.** 2002. *tfdA*-like genes in 2,4-dichlorophenoxyacetic acid-degrading bacteria belonging to the *Bradyrhizobium-Agromonas-Nitrobacter-Afipia* cluster in Alphaproteobacteria. Appl. Environ. Microbiol. **68:**3449–3454.
30. **Itoh, K., Y. Tashiro, K. Uobe, Y. Kamagata, K. Suyama, and H. Yamamoto.** 2004. Root nodule *Bradyrhizobium* spp. harbor *tfdA* alpha and *cadA*, homologous with genes encoding 2,4-dichlorophenoxyacetic acid-degrading proteins. Appl. Environ. Microbiol. **70:**2110–2118.
31. **Ka, J. O., W. E. Holben, and J. M. Tiedje.** 1994. Analysis of competition in soil among 2,4-dichlorophenoxyacetic acid-degrading bacteria. Appl. Environ. Microbiol. **60:**1121–1128.
32. **Ka, J. O., W. E. Holben, and J. M. Tiedje.** 1994. Genetic and phenotypic diversity of 2,4-dichlorophenoxyacetic acid (2,4-D)-degrading bacteria isolated from 2,4-D-treated field soils. Appl. Environ. Microbiol. **60:**1106–1115.
33. **Ka, J. O., W. E. Holben, and J. M. Tiedje.** 1994. Use of gene probes to aid in recovery and identification of functionally dominant 2,4-dichlorophenoxyacetic acid-degrading populations in soil. Appl. Environ. Microbiol. **60:**1116–1120.
34. **Kamagata, Y., R. R. Fulthorpe, K. Tamura, H. Takami, L. J. Forney, and J. M. Tiedje.** 1997. Pristine environments harbor a new group of oligotrophic 2,4-dichlorophenoxyacetic acid-degrading bacteria. Appl. Environ. Microbiol. **63:**2266–2272.
35. **Kitagawa, W., S. Takami, K. Miyauchi, E. Masai, Y. Kamagata, J. M. Tiedje, and M. Fukuda.** 2002. Novel 2,4-dichlorophenoxyacetic acid degradation genes from oligotrophic *Bradyrhizobium* sp. strain HW13 isolated from a pristine environment. J. Bacteriol. **184:**509–518.
36. **Kjeldsen, K. U., A. Loy, T. F. Jakobsen, T. R. Thomsen, M. Wagner, and K. Ingvorsen.** 2007. Diversity of sulfate-reducing bacteria from an extreme hypersaline sediment, Great Salt Lake (Utah). FEMS Microbiol. Ecol. **60:** 287–298.
37. **Koops, H.-P., U. Purkhold, A. Pommerening-Röser, G. Timmermann, and M. Wagner.** 2004. The lithoautotrophic ammonia-oxidizing bacteria, p. 2625–2637. *In* A. Balows, H. G. Trüper, M. Dworkin, W. Harder, and K.-H. Schleifer (ed.), The prokaryotes—an evolving electronic resource, release 3.13 ed. Springer Verlag, New York, NY.
38. **Kreader, C. A.** 1996. Relief of amplification inhibition in PCR with bovine serum albumin or T4 gene 32 protein. Appl. Environ. Microbiol. **62:**1102–1106.
39. **Lee, T. H., S. Kurata, C. H. Nakatsu, and Y. Kamagata.** 2005. Molecular analysis of bacterial community based on 16S rDNA and functional genes in activated sludge enriched with 2,4-dichlorophenoxyacetic acid (2,4-D) under different cultural conditions. Microb. Ecol. **49:**151–162.
40. **Ludwig, W., O. Strunk, R. Westram, L. Richter, H. Meier, Yadhukumar, A. Buchner, T. Lai, S. Steppi, G. Jobb, W. Forster, I. Brettske, S. Gerber, A. W. Ginhart, O. Gross, S. Grumann, S. Hermann, R. Jost, A. Konig, T. Liss, R. Lussmann, M. May, B. Nonhoff, B. Reichel, R. Strehlow, A. Stamatakis, N. Stuckmann, A. Vilbig, M. Lenke, T. Ludwig, A. Bode, and K. H. Schleifer.** 2004. ARB: a software environment for sequence data. Nucleic Acids Res. **32:**1363–1371.
41. **Macur, R. E., J. T. Wheeler, M. D. Burr, and W. P. Inskeep.** 2007. Impacts of 2,4-D application on soil microbial community structure and on populations associated with 2,4-D degradation. Microbiol. Res. **162:**37–45.
42. **Maurer, D., S. Kolb, L. Haumaier, and W. Borken.** 2008. Inhibition of atmospheric methane oxidation by monoterpenes in Norway spruce and European beech soils. Soil Biol. Biochem. **40:**3014–3020.
43. **McDevitt, J. J., P. S. J. Lees, W. G. Merz, and K. J. Schwab.** 2004. Development of a method to detect and quantify *Aspergillus fumigatus* conidia by quantitative PCR for environmental air samples. Mycopathologia **158:**325–335.
44. **McDevitt, J. J., P. S. J. Lees, W. G. Merz, and K. J. Schwab.** 2007. Inhibition of quantitative PCR analysis of fungal conidia associated with indoor air particulate matter. Aerobiologia **23:**35–45.
45. **McGhee, L., and R. G. Burns.** 1995. Biodegradation of 2,4-dichlorophenoxyacetic acid (2,4-D) and 2-methyl-4-chlorophenoxyacetic acid (MCPA) in contaminated soil. Appl. Soil Ecol. **2:**143–154.
46. **McGowan, C., R. R. Fulthorpe, A. Wright, and J. M. Tiedje.** 1998. Evidence for interspecies gene transfer in the evolution of 2,4-dichlorophenoxyacetic acid degraders. Appl. Environ. Microbiol. **64:**4089–4092.
47. **Mortensen, S. K., and C. S. Jacobsen.** 2004. Influence of frozen storage on herbicide degradation capacity in surface and subsurface sandy soils. Environ. Sci. Technol. **38:**6625–6632.
48. **Mrkonjic Fuka, M., M. Engel, A. Gattinger, U. Bausenwein, M. Sommer, J. C. Munch, and M. Schloter.** 2008. Factors influencing variability of proteolytic genes and activities in arable soils. Soil Biol. Biochem. **40:**1646–1653.
49. **Muyzer, G., E. C. De Waal, and A. G. Uitterlinden.** 1993. Profiling of complex microbial populations by denaturing gradient gel electrophoresis analysis of polymerase chain reaction-amplified genes coding for 16S rRNA. Appl. Environ. Microbiol. **59:**695–700.
50. **Palmer, K., H. L. Drake, and M. A. Horn.** 2009. Genome-derived criteria for assigning environmental *narG* and *nosZ* sequences to operational taxonomic units of nitrate reducers. Appl. Environ. Microbiol. **75:**5170–5174.
51. **Park, I. H., and J. O. Ka.** 2003. Isolation and characterization of 4-(2,4-dichlorophenoxy)butyric acid degrading bacteria from agricultural soils. J. Microbiol. Biotechnol. **13:**243–250.
52. **Pruesse, E., C. Quast, K. Knittel, B. M. Fuchs, W. G. Ludwig, J. Peplies, and F. O. Glöckner.** 2007. SILVA: a comprehensive online resource for quality checked and aligned ribosomal RNA sequence data compatible with ARB. Nucleic Acids Res. **35:**7188–7196.
53. **Radstrom, P., R. Knutsson, P. Wolffs, M. Lovenklev, and C. Lofstrom.** 2004. Pre-PCR processing—strategies to generate PCR-compatible samples. Mol. Biotechnol. **26:**133–146.
54. **Robertson, B. K., and M. Alexander.** 1994. Growth-linked and cometabolic biodegradation—possible reason for occurrence or absence of accelerated pesticide biodegradation. Pest. Sci. **41:**311–318.
55. **Saitou, N., and M. Nei.** 1987. The neighbor-joining method—a new method for reconstructing phylogenetic trees. Mol. Biol. Evol. **4:**406–425.
56. **Scheidleder, A.** 2000. Groundwater quality and quantity in Europe. European Environment Agency, Copenhagen, Denmark.
57. **Schloss, P. D., and J. Handelsman.** 2005. Introducing DOTUR, a computer program for defining operational taxonomic units and estimating species richness. Appl. Environ. Microbiol. **71:**1501–1506.
58. **Shaw, L. J., and R. G. Burns.** 2004. Enhanced mineralization of [U-^{14}C]2,4-dichlorophenoxyacetic acid in soil from the rhizosphere of *Trifolium pratense*. Appl. Environ. Microbiol. **70:**4766–4774.
59. **Shaw, L. J., and R. G. Burns.** 2005. Rhizodeposition and the enhanced mineralization of 2,4-dichlorophenoxyacetic acid in soil from the *Trifolium pratense* rhizosphere. Environ. Microbiol. **7:**191–202.
60. **Shelton, D. R., and J. S. Karns.** 1998. Pesticide bioremediation: genetic and ecological considerations, p. 181–216. *In* P. C. Kearny and T. Roberts (ed.),

Downloaded from http://aem.asm.org/ on April 30, 2012 by guest

COR-AAD1-00002978
Bayer EX1008 (Part 6 of 9)

Pesticide remediation in soils and water. John Wiley & Sons, Chichester, United Kingdom.
61. **Smejkal, C. W., T. Vallaeys, S. K. Burton, and H. M. Lappin-Scott.** 2001. Substrate specificity of chlorophenoxyalkanoic acid-degrading bacteria is not dependent upon phylogenetically related *tfdA* gene types. Biol. Fertil. Soils **33:**507–513.
62. **Smith, A. E.** 1985. Identification of 4-chloro-2-methylphenol as a soil degradation product of ring-labeled [C-14] mecoprop. Bull. Environ. Contam. Toxicol. **34:**656–660.
63. **Smith, C. J., D. B. Nedwell, L. F. Dong, and A. M. Osborn.** 2006. Evaluation of quantitative polymerase chain reaction-based approaches for determining gene copy and gene transcript numbers in environmental samples. Environ. Microbiol. **8:**804–815.
64. **Sorensen, S. R., A. Schultz, O. S. Jacobsen, and J. Aamand.** 2006. Sorption, desorption and mineralization of the herbicides glyphosate and MCPA in samples from two Danish soil and subsurface profiles. Environ. Pollut. **141:** 184–194.
65. **Stackebrandt, E., and J. Ebers.** 2006. Taxonomic parameters revisited: tarnished gold standards. Microbiol. Today **33:**152–155.
66. **Stackebrandt, E., and B. M. Goebel.** 1994. A place for DNA-DNA reassociation and 16S ribosomal-RNA sequence-analysis in the present species definition in bacteriology. Int. J. Syst. Evol. Microbiol. **44:**846–849.
67. **Streber, W. R., K. N. Timmis, and M. H. Zenk.** 1987. Analysis, cloning, and high-level expression of 2,4-dichlorophenoxyacetate monooxygenase gene *tfdA* of *Alcaligenes eutrophus* JMP134. J. Bacteriol. **169:**2950–2955.
68. **Suwa, Y., A. D. Wright, F. Fukumori, K. A. Nummy, R. P. Hausinger, W. E. Holben, and L. J. Forney.** 1996. Characterization of a chromosomally encoded 2,4-dichlorophenoxyacetic acid/alpha-ketoglutarate dioxygenase from *Burkholderia* sp. strain RASC. Appl. Environ. Microbiol. **62:**2464–2469.
69. **Tamura, K., J. Dudley, M. Nei, and S. Kumar.** 2007. MEGA4: molecular evolutionary genetics analysis (MEGA) software version 4.0. Mol. Biol. Evol. **24:**1596–1599.
70. **Thompson, D. G., G. R. Stephenson, K. R. Solomon, and A. V. Skepasts.** 1984. Persistence of (2,4-dichlorophenoxy)acetic acid and 2-(2,4-dichlorophenoxy)propionic acid in agricultural and forest soils of Northern and Southern Ontario. J. Agric. Food Chem. **32:**578–581.
71. **Tonso, N. L., V. G. Matheson, and W. E. Holben.** 1995. Polyphasic characterization of a suite of bacterial isolates capable of degrading 2,4-D. Microb. Ecol. **30:**3–24.
72. **Tsai, Y. L., and B. H. Olson.** 1992. Rapid method for separation of bacterial DNA from humic substances in sediments for polymerase chain reaction. Appl. Environ. Microbiol. **58:**2292–2295.
73. **Vallaeys, T., R. R. Fulthorpe, A. M. Wright, and G. Soulas.** 1996. The metabolic pathway of 2,4-dichlorophenoxyacetic acid degradation involves different families of *tfdA* and *tfdB* genes according to PCR-RFLP analysis. FEMS Microbiol. Ecol. **20:**163–172.
74. **van der Ploeg, J. R., E. Eichhorn, and T. Leisinger.** 2001. Sulfonate-sulfur metabolism and its regulation in *Escherichia coli*. Arch. Microbiol. **176:**1–8.
75. **Watson, R. J., and B. Blackwell.** 2000. Purification and characterization of a common soil component which inhibits the polymerase chain reaction. Can. J. Microbiol. **43:**633–642.
76. **Wilson, I. G.** 1997. Inhibition and facilitation of nucleic acid amplification. Appl. Environ. Microbiol. **63:**3741–3751.
77. **Worthing, C. R., and R. J. Hance.** 1991. The pesticide manual—a world compendium. The British Crop Protection Council, Farnham, United Kingdom.
78. **Zakaria, D., H. Lappin-Scott, S. Burton, and C. Whitby.** 2007. Bacterial diversity in soil enrichment cultures amended with 2 (2-methyl-4-chlorophenoxy) propionic acid (mecoprop). Environ. Microbiol. **9:**2575–2587.

Downloaded from http://aem.asm.org/ on April 30, 2012 by guest

COR-AAD1-00002979
Bayer EX1008 (Part 6 of 9)

JOURNAL OF AGRICULTURAL AND FOOD CHEMISTRY

pubs.acs.org/JAFC

Article

Enantioselective Catabolism of the Two Enantiomers of the Phenoxyalkanoic Acid Herbicide Dichlorprop by *Sphingopyxis* sp. DBS4

Long Zhang, Ping Hang, Xi-Yi Zhou, Wen-Jing Qiao, and Jian-Dong Jiang*

Cite This: *J. Agric. Food Chem.* 2020, 68, 6967−6976

Read Online

ACCESS | Metrics & More | Article Recommendations | Supporting Information

ABSTRACT: Dichlorprop [(*RS*)-2-(2,4-dichlorophenoxy)propanoic acid; DCPP], an important phenoxyalkanoic acid herbicide (PAAH), is extensively used in the form of racemic mixtures (*Rac*-DCPP), and the environmental fates of both DCPP enantiomers [(*R*)-DCPP and (*S*)-DCPP] mediated by microorganisms are of great concern. In this study, a bacterial strain *Sphingopyxis* sp. DBS4 was isolated from contaminated soil and was capable of utilizing both (*R*)-DCPP and (*S*)-DCPP as the sole carbon source for growth. Strain DBS4 preferentially catabolized (*S*)-DCPP as compared to (*R*)-DCPP. The optimal conditions for *Rac*-DCPP degradation by strain DBS4 were 30 °C and pH 7.0. In addition to *Rac*-DCPP, other PAAHs such as (*RS*)-2-(4-chloro-2-methylphenoxy)propanoic acid, 2,4-dichlorophenoxyacetic acid, 4-chloro-2-methylphenoxyacetic acid, and 2,4-dichlorophenoxyacetic acid butyl ester could also be catabolized by strain DBS4. Bioremediation of *Rac*-DCPP-contaminated soil by inoculation of strain DBS4 exhibited an effective removal of both (*R*)-DCPP and (*S*)-DCPP from the soil. Due to its broad substrate spectrum, strain DBS4 showed great potential in the bioremediation of PAAH-contaminated sites.

KEYWORDS: *bioremediation, degradation pathway, enantiomer-specific dioxygenase, mineralization, phenoxyalkanoic acid herbicide, Sphingopyxis sp*

Downloaded via CORTEVA AGRISCIENCE on September 9, 2020 at 14:58:04 (UTC).
See https://pubs.acs.org/sharingguidelines for options on how to legitimately share published articles.

INTRODUCTION

Phenoxyalkanoic acid herbicides (PAAHs), including 2,4-dichlorophenoxyacetic acid (2,4-D), 4-chloro-2-methylphenoxyacetic acid (MCPA), 2,4-dichlorophenoxyacetic acid butyl ester (2,4-D butyl ester), (*RS*)-2-(4-chloro-2-methylphenoxy)propanoic acid (known as MCPP or mecoprop), and (*RS*)-2-(2,4-dichlorophenoxy)propanoic acid (known as DCPP or dichlorprop) (Figure 1), are ubiquitously used to kill broad-leaved weeds, including lawn pasture industry and agriculture.[1−3] Due to their good weeding effect and low cost, PAAHs are extensively used all over the world.[4,5] Most PAAHs have high water solubility (at 25 °C, 2,4-D, 890 mg L^{-1}; MCPA, 1174 mg L^{-1}; MCPP, 895 mg L^{-1}; DCPP, 829 mg L^{-1}) and are easily leached out from the applied areas together with rain or irrigation water.[6] In Danish groundwater reservoirs, PAAHs have been frequently detected at levels above the EU limit of 0.1 mg L^{-1}.[7] Among the above-mentioned PAAHs, DCPP and MCPP are chiral compounds with one stereogenic center and therefore contain two enantiomers. Different enantiomers have been reported to have different biological activities and ecotoxicities. Notably, only (*R*)-enantiomers of PAHHs exhibited herbicidal activity as compared to their (*S*)-enantiomers.[5,8,9] In addition, (*R*)-DCPP had greater oxidative damage to maize than *Rac*-DCPP and (*S*)-DCPP[10] and could induce a higher production of reactive oxygen species (ROS) on *Scenedesmus obliquus* than that (*S*)-DCPP.[11] Currently, the pure (*R*)-enantiomer of DCPP is commercially available as dichlorprop-P. However, racemic mixtures of DCPP (*Rac*-DCPP) are still applied extensively.[6,12,13] Consequently, the inevitable release of both enantiomers of DCPP into the environment has led to a great concern regarding the environmental fates of both enantiomers.

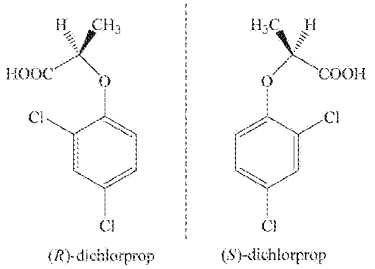


Figure 1. Structure of the chiral herbicide dichlorprop.

For the dissipation of chiral herbicides from environments, soil microorganisms have been proved to be the key driving factors. For example, over 99% of (*R*)- and (*S*)-indoxacarb was degraded in nonsterilized acidic soil after 75 days of incubation, while only 5−10% degraded in sterilized acidic

Received: February 15, 2020
Revised: May 14, 2020
Accepted: June 12, 2020
Published: June 12, 2020



ACS Publications © 2020 American Chemical Society

https://dx.doi.org/10.1021/acs.jafc.0c01066
J. Agric. Food Chem. 2020, 68, 6967−6976

COR-AAD1-00002980
Bayer EX1008 (Part 6 of 9)

soil.[34] The transformation rate of *Rac*-quizalofop-ethyl was predominantly determined by bacterial abundance and richness, and the enantioselective degradation was correlated with bacterial structures.[35] *In situ* amended *Rac*-DCPP in agricultural soil could be effectively mineralized by the indigenous microbial community and multiple α-ketoglutarate (α-KG)-dependent dioxygenase genes were found to be related to the degradation.[7] Moreover, (*R*)- and (*S*)-enantiomers could even be interconverted by soil microorganisms.[16,17] (*S*)-Indoxacarb and (*S*)-quizalofop acid had been reported to be interconverted to (*R*)-indoxacarb and (*R*)-quizalofop-acid in soils, respectively.[34,35]

A number of bacterial strains capable of degrading 2,4-D, MCPA, and 2,4-D butyl ester and utilizing them as growth substrates have been isolated.[29−35] However, few pure bacterial cultures capable of degrading the phenoxypropionate herbicides (such as DCPP and MCPP) have been reported (Table 1).[29−35] In addition, no pure strains capable of utilizing DCPP as the sole carbon and energy source for growth have been isolated since 2001.[36] The difference between the molecular structures of phenoxypropionate herbicides (e.g., DCPP) and phenoxyacetic acid herbicides (e.g., 2,4-D) is the side chain, indicating that the cleavage of the side chain from DCPP is the key step for its catabolism. The side chain of DCPP, propionic acid, is linked to the oxygen atom of the phenoxyacid moiety via the α-carbon atom adjacent to the carboxyl group, so DCPP is considered to be more recalcitrant than 2,4-D.[37]

Table 1. Reported Phenoxypropionate Herbicide Degradation by Pure Culture Strains

strain	phenoxyalkanoic acid substrates[a]	isolation source	references
Sphingomonas herbicidovorans MH	*Rac*-DCPP, *Rac*-MCPP, 2,4-D, MCPA	soil polluted with dichlorprop	31
Rhodoferax sp. P230	*Rac*-DCPP, *Rac*-MCPP, 2,4-D, MCPA	contaminated building material	32
Delftia acidovorans MC1	*Rac*-DCPP, *Rac*-MCPP, 2,4-D, MCPA	herbicide-contaminated building site	33
Stenotrophomonas maltophilia PM	*Rac*-DCPP, *Rac*-MCPP, 2,4-D, MCPA, MCPB, 4-CPA, 2,4-DB	Danish aquifer	34
Alcaligenes sp. CS1	*Rac*-DCPP, *Rac*-MCPP, 2,4-D, MCPA	agricultural soils	13
Ralstonia sp. CS2	*Rac*-DCPP, *Rac*-MCPP, 2,4-D, MCPA	agricultural soils	13
Alcaligenes denitrificans	(*R*)-MCPP	garden soil	35

[a](4-Chloro-2-methylphenoxy) butyric acid, MCPB; (4-chlorophenoxy) acetic acid, 4-CPA.

The degradation of DCPP in *Sphingobium herbicidovorans* MH and *Delftia acidovorans* MC1 has been studied on the molecular level,[31,33,38] mostly focusing on the enantiomer-specific dioxygenases (RdpA and SdpA) and their coding genes.[4,12,30] The deduced amino acid sequence of $RdpA_{MH}$ is 100% identical to that of $RdpA_{MC1}$, while the sequence of $SdpA_{MH}$ shows approximately 60% identity to that of $SdpA_{MC1}$.[5] RdpA and SdpA enantioselectively transform *Rac*-DCPP to pyruvate and the nonchiral metabolite 2,4-dichlorophenol (2,4-DCP), which is further metabolized via the classic pathway similar to that of 2,4-D.[3]

In general, compared to phenoxyacetic acid herbicides, microbial degradation of phenoxypropionate herbicides have not been extensively studied. Hence, it would be of great value and significance to discover more novel and efficient DCPP-degrading strains, which could serve as optional microbial resources to clean up DCPP-contaminated sites. In this study, we isolated and characterized a new strain of *Sphingopyxis* sp., DBS4, a versatile strain capable of utilizing various kinds of PAAHs as the sole carbon source for growth. Furthermore, the enantioselective catabolism of the two enantiomers of DCPP was systematically studied, and the bioremediation of *Rac*-DCPP-contaminated soil was also evaluated.

MATERIALS AND METHODS

Chemicals and Media. *Rac*-DCPP (CAS RN 120-36-5), (*R*)-DCPP (dichlorprop-P, CAS RN 15165-67-0), *Rac*-MCPP (CAS RN 93-65-2), (*R*)-MCPP (mecoprop-P, CAS RN 16484-77-8), 2,4-D (CAS RN 94-75-7), 2,4-DCP (CAS RN 120-83-2), MCPA (CAS RN 94-74-6), 2,4-D butyl ester (CAS RN 94-80-4), 2,4-DB [(2,4-dichlorophenoxy)butyric acid] (CAS RN 94-82-6), 2,4,5-T [(2,4,5-trichlorophenoxy)acetic acid] (CAS RN 93-76-5), and 2,4,6-trichlorophenol (CAS RN 88-06-2) were purchased from Aladdin Reagent (Shanghai, China) Co., Ltd. or Sigma-Aldrich (Shanghai, China), and their purities were all above 99%. All other chemicals and solvents were of analytical or high-performance liquid chromatography (HPLC) grade. Molecular biology reagents were purchased from TaKaRa Biotechnology (Dalian, China) Co., Ltd.

Mineral salt medium (MSM) and Luria-Bertani (LB) medium were used for the degradation experiments and culture of strains.[39] Concentrated stock solutions of the above-mentioned PAAHs (10 g L^{-1}) were prepared in methanol and filtered with 0.22 μm pore-sized nylon membranes.

Chiral Separation of *Rac*-DCPP. The two enantiomers of *Rac*-DCPP were separated at Shanghai Chiralway Biotech Co., Ltd. using autoprep HPLC (PDR-separations LLC) equipped with a Superchiral S-AD column (I.D., 2.1 cm; length, 25 cm). The mobile phase was hexane−isopropanol−formic acid (90:10:0.05, v/v/v) mixture at a flow rate of 18 mL min^{-1}. The separated (*R*)-DCPP was analyzed by HPLC (Shimadzu LC-20A, Shimadzu Corporation; Advanced Laser polarimeter @670 nm optical detector, PDR-separations LLC) equipped with a superchiral S-AS column (I.D., 0.46 cm; length, 15 cm) and checked using the purchased dichlorprop-P as the standard compound. The mobile phase was hexane−isopropanol−trifluoroacetic acid (90:10:0.05, v/v/v) mixture at a flow rate of 0.9 mL min^{-1}. The detected wavelength was the same as described below.

Isolation of the *Rac*-DCPP-Degrading Bacterial Strain. The soil sample was collected at a disused pesticide factory located in Nanjing, Jiangsu, China (31° 57′ 9.58″ N 118° 50′ 24.07″ E). Five grams of contaminated soil was added to 100 mL of sterilized MSM supplemented with 30 mg L^{-1} of *Rac*-DCPP [15 mg L^{-1} of (*R*)-DCPP plus 15 mg L^{-1} of (*S*)-DCPP]. The enrichment was incubated on a rotary shaker at 30 °C and 160 rpm for 7 days; then, 5 mL of subculture was then inoculated into 100 mL of fresh MSM containing 30 mg L^{-1} of *Rac*-DCPP and cultivated for another 7 days. After 5 rounds of cultivation, the culture was plated onto LB agar supplemented with 30 mg L^{-1} of *Rac*-DCPP. Individual colonies were checked for their capacities to degrade *Rac*-DCPP in liquid MSM by HPLC as described below. Finally, an efficient *Rac*-DCPP-degrading strain (designated DBS4) was isolated and selected for further study.

Identification and Characterization of Strain DBS4. To identify strain DBS4, morphological, physiological, and biochemical tests and 16S rRNA gene analysis were performed. The detailed procedures of the physiological and biochemical tests were similar to the previously described methods.[39,40] The 16S rRNA gene was amplified according to the method described previously.[41] The polymerase chain reaction (PCR) products were purified, ligated to a cloning vector, and sequenced at Nanjing Genscript Biotech Co., Ltd.

https://dx.doi.org/10.1021/acs.jafc.0c01066
J. Agric. Food Chem. 2020, 68, 6967−6976

COR-AAD1-00002981
Bayer EX1008 (Part 6 of 9)

(Nanjing, China). Levels of sequence similarity with closely related species were calculated through NCBI BLAST (https://blast.ncbi.nlm.nih.gov/Blast.cgi) or EzBioCloud (http://www.ezbiocloud.net/).[42] Sequence alignment and phylogenetic tree reconstruction were carried out as previously described.[39]

Biodegradation of *Rac*-DCPP, (*R*)-DCPP, and (*S*)-DCPP by Strain DBS4 in MSM. Strain DBS4 was aerobically cultured at 30 °C in 100 mL of LB to the late logarithmic period, harvested (25 °C, 6000*g*, 5 min), and washed with sterilized MSM. The washed cells were inoculated into 100 mL of MSM containing 60 mg L^{-1} of *Rac*-DCPP [30 mg L^{-1} of (*R*)-DCPP plus 30 mg L^{-1} of (*S*)-DCPP], 30 mg L^{-1} of (*R*)-DCPP, and 30 mg L^{-1} of (*S*)-DCPP, respectively, at the final OD_{600} = 0.2. The methanol in the stock solution used for the dissolution of DCPP was completely evaporated. All cultures were aerobically incubated under the same conditions, sampled at different time intervals, and then the DCPP residual and cell density were measured using HPLC and ultraviolet spectrophotometer, respectively. Inoculation with sterilized strain DBS4 cells was used as the control.

The effects of different environmental factors on the biodegradation of *Rac*-DCPP by strain DBS4 were investigated. Experiments were performed in 250 mL flasks containing 100 mL of MSM supplemented with 60 mg L^{-1} of *Rac*-DCPP [30 mg L^{-1} of (*R*)-DCPP plus 30 mg L^{-1} of (*S*)-DCPP], and the initial cell concentration (OD_{600}) was set at 0.2. The degradation efficiency was assayed at 48 h. The effects of different cultivation temperatures (16, 25, 30, 37, and 42 °C) and medium initial pH values (pH 5.0–9.0 at intervals of 1 pH unit, adjusted by 0.2 mol L^{-1} NaH_2PO_4 and Na_2HPO_4) on the biodegradation of *Rac*-DCPP were evaluated. The effects of different initial concentrations of *Rac*-DCPP (from 10 to 400 mg L^{-1}) on the biodegradation of *Rac*-DCPP were also tested. The effects of different concentrations of inoculum on biodegradation were tested by inoculating 0.2, 0.5, 1.0, 2.0, and 4.0 mL of strain DBS4 cells (initial OD_{600} = 0.5) to 100 mL of MSM.

Substrate Range of Strain DBS4. To determine the degradation capacities of strain DBS4 to other structural analogues, strain DBS4 was inoculated at a final concentration of OD_{600} = 0.2 into 20 mL of MSM containing 60 mg L^{-1} *Rac*-DCPP, *Rac*-MCPP, 2,4-D, MCPA, 2,4-D butyl ester, 2,4-DB, 2,4,5-T, 2,4-DCP, or 2,4,6-trichlorophenol. All cultures were incubated under the same conditions as described above. Samples were collected at 3 and 5 days and then the concentrations of the remaining compounds were detected. All treatments were performed in triplicate and inoculation of sterilized strain DBS4 was used as the control.

Determination of *Rac*-DCPP and Other Structural Analogues. To analyze *Rac*-DCPP and other structural analogues in a liquid medium, the pH of the solution was first adjusted to 3.0 by adding concentrated HCl, and then an equal volume of dichloromethane was added for extraction. Excessive water in the organic phase was removed with anhydrous Na_2SO_4. Spectrophotometry (UV2450, Shimadzu, Japan) was used to directly detect the residues in the organic phase at the wavelength 200–350 nm. HPLC analysis was used to accurately calculate the residue concentration of both achiral and chiral compounds. For achiral compounds, the extract was volatilized using N_2 at room temperature; the dried residue was redissolved in methanol and then filtered with a 0.22 μm nylon filter for detection by HPLC as described previously.[43] The mobile phase was 80% methanol (methanol–water, v/v) and 0.5% glacial acetic acid, the flow rate was 1.0 mL min^{-1}, and the injection volume was 20 μL. For chiral compounds, the extract was prepared similarly and detected by HPLC (Shimadzu LC-20A, Shimadzu corporation; Advanced Laser polarimeter @670 nm optical detector, PDR-separations LLC) equipped with a superchiral S-AS column (I.D., 4.6 mm; length, 150 mm). The mobile phase was hexane–isopropanol–trifluoroacetic acid (96:4:0.05, v/v/v) mixture at a flow rate of 0.8 mL min^{-1}, and the injection volume was 20 μL. All tested compounds were detected at wavelengths of 220 nm and 235 nm. The peak area ratios relative to individual standard calibration curves were used to calculate the concentrations.

Enantioselective Catabolism of *Rac*-DCPP and Identification of Metabolites. To study the enantioselective degradation of *Rac*-DCPP by strain DBS4 and identify the metabolites produced, strain DBS4 cells were inoculated into 20 mL of MSM containing 60 mg L^{-1} *Rac*-DCPP [30 mg L^{-1} (*R*)-DCPP plus 30 mg L^{-1} (*S*)-DCPP] and aerobically cultivated at 30 °C. The whole culture in each flask that had been incubated for 0, 8, 16, 24, 36, 48, 60, 72, and 96 h was frozen and dried in an FD5-4 freeze-dryer (SIM International Group Co., Ltd., Los Angeles, CA). The residual of each enantiomer of DCPP was extracted and detected using HPLC as described above. The metabolites produced from *Rac*-DCPP biodegradation were identified by an ultrahigh-pressure LC system (Dionex, Thermo) coupled with an LTQ-Orbitrap XL hybrid mass spectrometer (Thermo Fisher Scientific).

Degradation of DCPP by the Crude Enzyme Extracted from Strain DBS4. Cells of strain DBS4 were precultured (36 h) in LB medium (supplemented with 30 mg L^{-1} of *Rac*-DCPP), harvested by centrifugation (5 min, 12 000*g*) at 4 °C, and washed twice with sterilized MSM. One gram of wet cells was resuspended in 15 mL of 20 mM Tris–HCl (pH 8.0) containing 1 mM dithiothreitol. This cell suspension was disrupted by ultrasonication and then centrifuged at 12 000*g* for 20 min to remove cellular particles and membranes. Protein in the supernatant was used as the crude enzyme, and its mass concentration (varying from 10 to 15 mg mL^{-1}) was determined with the Bio-Rad Protein Assay Kit (Bio-Rad, Shanghai, China). The crude enzyme was found to retain its most enzyme activity after being stored for several weeks at −20 °C. The enzyme assays were performed in a 3 mL of imidazole buffer (50 mM, pH 6.8) at 30 °C, similarly as previously described.[6,12] If not stated otherwise, the reaction mixture contained 0.5 mL of a crude enzyme, 1 mM ascorbate, 100 mM $(NH_4)_2Fe(SO_4)_2{\cdot}6H_2O$, 1 mM α-KG, and 1 mM (*R*/*S*)-DCPP. During the incubation, the reaction mixture was gently stirred to provide sufficient oxygen. Samples were taken at appropriate time intervals and boiled for 3 min to stop the reaction. The concentrations of (*R*/*S*)-DCPP were determined by HPLC as described above. The influences of different cofactors and supplements (such as α-KG, ascorbate, Fe^{2+}, and L-cysteine) on the activities of crude enzymes were also evaluated.

Amplification of the *rdpA*, *sdpA*, and *tfd* Gene Fragments and DNA Sequence Analysis. The *rdpA* and *sdpA* genes are the only two reported genes responsible for the initial degradation of *Rac*-DCPP, which were attempted to be amplified from strain DBS4 using the primer pairs *rdpA*-f [5′-AACAGCACATCGCCTTCAG-3′]/*rdpA*-r [5′-GGTTTGCTTTCGGCATCGG-3′] and *sdpA*-f [5′-GAGATGGCCGCGATCAGCA-3′]/*sdpA*-r [5′-TGATAGATTCGCGGCGGCT-3′], targeting the 511-bp *rdpA* fragment and the 512-bp *sdpA* fragment, respectively.[5] Degenerate PCR primer pairs *tfdA*-f [5′-ACGGAGTTCTGYGAYATG-3′]/*tfdA*-r [5′-AACGCAGCGRTTRTCCCA-3′] and *tfdB*-f [5′-CGCAYATCACCAAYCARC-3′] /*tfdB*-r [5′-ATAGCGCTGRTTCATY TC-3′] were also used respectively to amplify the conserved fragments of *tfdA* (363-bp) and *tfdB* (1.1-kb) genes, which are involved in 2,4-D catabolism.[44,45]

Removal of *Rac*-DCPP from Soil by Strain DBS4. The soil used was collected from an uncontaminated site on the campus. The soil was sterilized and dried in an oven, then shredded, and mixed thoroughly; stones and debris were removed by passing the soil through a 2 mm sieve. The soil properties are listed in Table S1. Two hundred grams of soil (dry weight) was homogeneously mixed with *Rac*-DCPP (dissolved in methanol) to obtain the final concentrations of 50 mg kg^{-1} [25 mg kg^{-1} (*R*)-DCPP plus 25 mg kg^{-1} (*S*)-DCPP] and 100 mg kg^{-1} [50 mg kg^{-1} (*R*)-DCPP plus 50 mg kg^{-1} (*S*)-DCPP], respectively. Methanol was evaporated by placing the soil on a laminar flow bench for 2 h. Strain DBS4 cells were prepared as described above and then evenly inoculated to the soil at a final concentration of 8.5×10^6 CFU g^{-1} soil. Inoculation with the same volume of deionized water was used as the control. The soil water content was adjusted to 20% and incubated in the dark at 30 °C. *Rac*-DCPP residuals in the soil were analyzed at 0, 2, 4, 6, 8, 10, 12, and 14 d.

https://dx.doi.org/10.1021/acs.jafc.0c01066
J. Agric. Food Chem. 2020, 68, 6967–6976

COR-AAD1-00002982
Bayer EX1008 (Part 6 of 9)

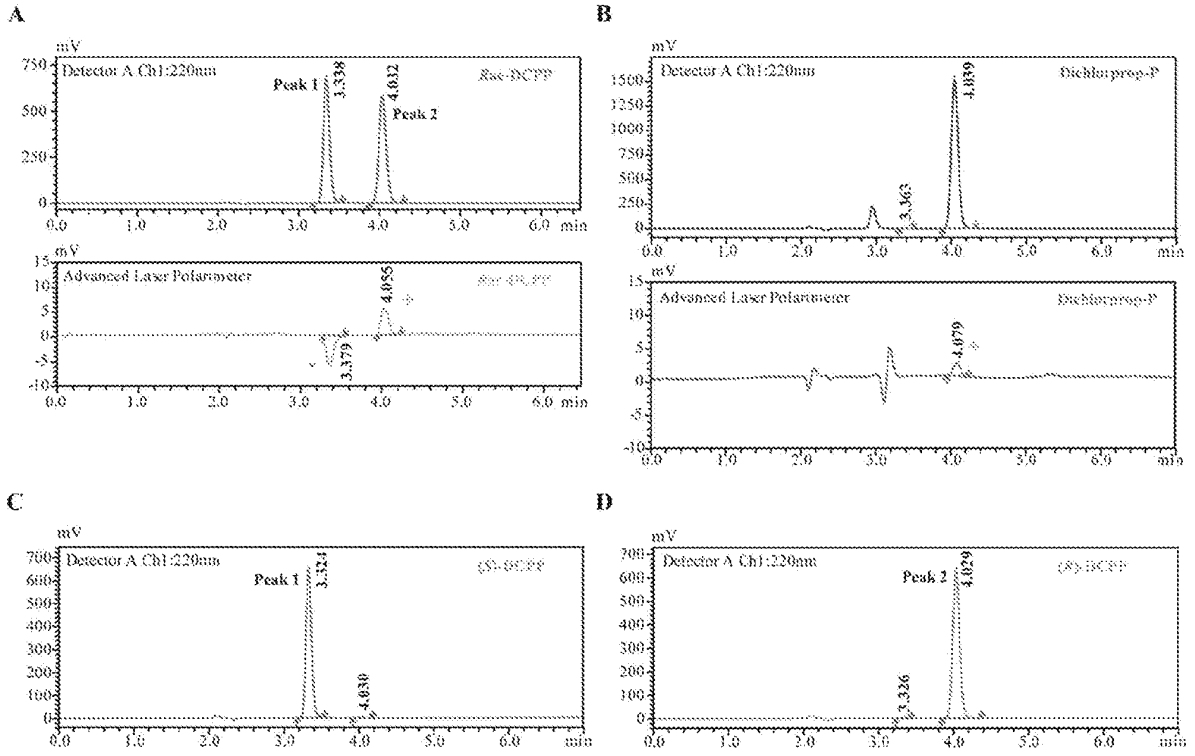


Figure 2. Chiral separation of the two enantiomers of *Rac*-DCPP.

To determine the *Rac*-DCPP in the soil, soil samples (5 g) were extracted with 30 mL of methanol−water−acetic acid (49:49:2, v/v/v) mixture and shaken for 2 h at 30 °C. Then, the extract was transferred to a 50 mL centrifugation tube, centrifuged for 10 min (6000*g*), and filtered. The above steps were repeated twice, and the filtrates were combined. To maximize extraction efficiency, the pH value was adjusted to 3.0 with concentrated HCl. The filtrate was continuously extracted three times with 30, 15, and 15 mL of dichloromethane. The combined extracts were concentrated in a rotary evaporation concentrator, dried by nitrogen, and then dissolved in 1 mL of methanol. The mean recovery efficiency of *Rac*-DCPP from the soil was about 95%. The concentration of *Rac*-DCPP was determined by HPLC as described above.

Statistical Analysis. The degradation percentages were calculated using equation $D = (C_{ck} - C_t)/C_{ck} \times 100\%$, where C_{ck} and C_t are the concentrations of the substrate in the negative control and target sample and D is degradation percentage. The degradation process of *Rac*-DCPP follows the pseudo-first-order kinetics $C_t = C_0 \times e^{-kt}$, where C_0 and C_t are the concentrations of *Rac*-DCPP at the initial time and appropriate culture time, respectively, k is the pseudo-first-order reaction rate constant, and t is the culture time. The degradation half-life ($DT_{1/2}$) was obtained by function $DT_{1/2} = \ln 2/k$, where $\ln 2$ is the natural logarithm of 2 and k is the degradation rate constant.

RESULTS

Chiral Separation of the Two Enantiomers of *Rac*-DCPP. *Rac*-DCPP was successfully separated by a Superchiral S-AD column (Chiralway Biotech Co., Ltd.) with a Shimadzu LC-20A HPLC system (Shimadzu Corporation). As shown in Figure 2A, two peaks were detected in the chromatogram, and the retention times were 3.338 min (peak 1) and 4.032 min (peak 2), respectively. The compounds corresponding to peaks 1 and 2 were then collected, and each pure enantiomer (enantiomeric excess > 98%) was obtained by removing the solvent using rotary evaporation. Compared with the retention time of the standard compound dichlorprop-P (Figure 2B) and with the advanced laser polarimeter results, the two compounds corresponding to peaks 1 and 2 were identified as (*S*)-DCPP (Figure 2C) and (*R*)-DCPP (Figure 2D), respectively.

Isolation and Identification of the *Rac*-DCPP-Degrading Strain DBS4. A bacterial strain (defined DBS4 and deposited in CCTCC under the number CCTCC M 20191082) capable of utilizing *Rac*-DCPP as the sole source of carbon for growth was isolated via the enrichment and purification procedures. Strain DBS4 was a rod-shaped, aerobic, Gram-stain-negative, and oxidase- and catalase-positive bacterium, with a size of 0.6−0.7 μm × 1.8−2.0 μm (Figure S1A). Colonies of strain DBS4 were circular, low convex with entire margins, opaque, and yellow-pigmented on LB agar (Figure S1B). The cells were urease and indole production-negative, and the optimal conditions for growth were 30 °C and pH 7.0. The 16S rRNA gene sequence of strain DBS4 (1,450 bp, GenBank no. MH553106) was obtained and sequenced. The sequence alignment showed that the 16S rRNA gene of strain DBS4 had the highest similarity to that of *Sphingopyxis taejonensis* JSS54^T (98.79%), followed by *Sphingopyxis granuli* NBRC 100800^T (98.65%). According to the results of physiological and biochemical tests and the phylogenetic analysis (Figure S2), strain DBS4 was identified as a *Sphingopyxis* species.

Degradation of DCPP versus Cell Growth of Strain DBS4 in MSM. The time course for cell growth and degradation of *Rac*-DCPP, (*R*)-DCPP, and (*S*)-DCPP by strain DBS4 in MSM are shown in Figure 3. (*S*)-DCPP (30 mg

https://dx.doi.org/10.1021/acs.jafc.0c01066
J. Agric. Food Chem. 2020, 68, 6967−6976

COR-AAD1-00002983
Bayer EX1008 (Part 6 of 9)

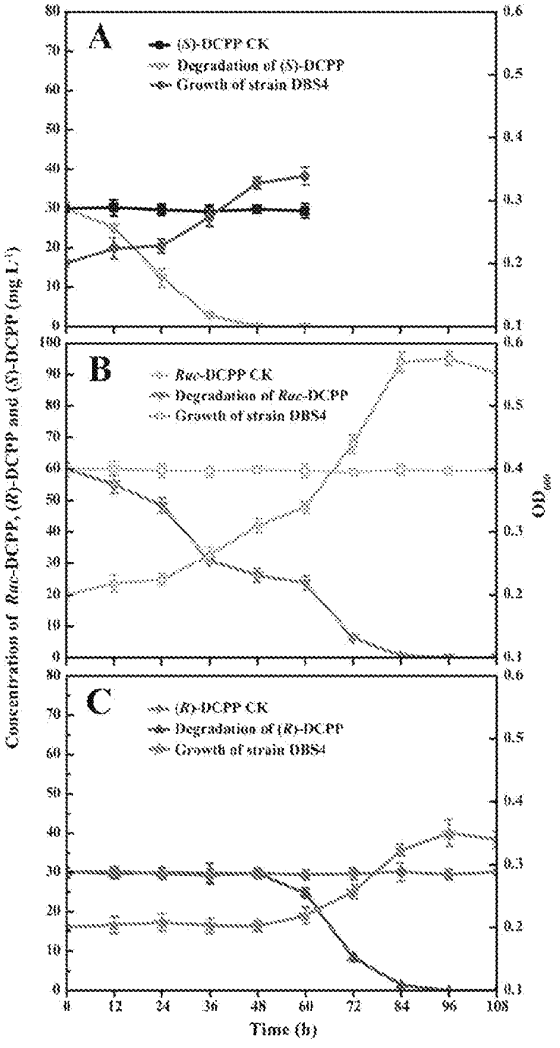


Figure 3. Cell growth and (*S*)-DCPP (A), *Rac*-DCPP (B), and (*R*)-DCPP (C) degradation by *Sphingopyxis* sp. DBS4.

L^{-1}) was degraded to none detectable level by strain DBS4 in 48 h, and the OD_{600} increased from 0.2 to 0.34 (Figure 3A). Over 50% of *Rac*-DCPP was degraded by strain DBS4 at 48 h, and *Rac*-DCPP was degraded to nondetectable level in 96 h. The cell density increased along with the degradation of *Rac*-DCPP in the first 96 h and then decreased slightly at 108 h (Figure 3B). For (*R*)-DCPP, no obvious degradation occurred in the first 48 h (Figure 3C). About 95% of (*R*)-DCPP was degraded at 84 h, and the cell density increased noticeably at this stage. No significant change in DCPP concentration was observed in the negative control. Based on these results, strain DBS4 could utilize *Rac*-DCPP, (*R*)-DCPP, and (*S*)-DCPP as the sole carbon and energy sources for growth, respectively.

Degradation Characteristics of Strain DBS4. As shown in Figure S3A, the optimal temperature for *Rac*-DCPP degradation by strain DBS4 was 30 °C. The degradation efficiency of *Rac*-DCPP was sharply decreased at 16 and 42 °C. The remarkable effect of temperature on *Rac*-DCPP biodegradation is mainly due to the significant influence of temperature on cell growth. The degradation efficiency of *Rac*-DCPP remained high at pH 6.0−8.0, with optimal at pH 7.0 (Figure S3B), indicating that strain DBS4 preferred to degrade *Rac*-DCPP under neutral pH conditions. The initial *Rac*-DCPP concentration significantly affected its degradation. Strain DBS4 could rapidly degrade *Rac*-DCPP at concentrations of 10−50 mg L^{-1} (Figure S3C). However, when the concentration of *Rac*-DCPP exceeded 200 mg L^{-1}, an obvious decrease in the degradation efficiency was observed. As expected, the degradation efficiency increased with the increasing inoculum (Figure S3D). The degradation efficiency of various structural analogues by strain DBS4 is shown in Table 2. Interestingly, besides *Rac*-DCPP, strain DBS4 could also rapidly degrade 2,4-D, MCPA, and 2,4-DCP as well as *Rac*-MCPP and 2,4-D butyl ester. However, no degradation of 2,4-DB, 2,4,5-T, or 2,4,6-trichlorophenol was observed.

Enantioselective Catabolism of the Two Enantiomers of *Rac*-DCPP and Identification of the Metabolites. Both enantiomers of the chiral herbicide DCPP were degraded by strain DBS4, and (*S*)-DCPP was preferentially degraded as compared to (*R*)-DCPP (Figure 4A), which is in agreement with the enantioselective degradation of *Rac*-MCPP/*Rac*-DCPP by *Sphingomonas herbicidovorans* MH.[46] The metabolite produced from *Rac*-DCPP degradation by strain DBS4 was extracted and identified. Based on the Liquid chromatography−mass spectrometry (LC−MS) results, only one metabolite (retention time = 6.699 min) was detected (Figure 4A,B), and was finally identified as 2,4-DCP with a *m*/*z* of 160.9556 (Figure 4B).

***Rac*-DCPP Transformation by Cell Extracts.** Cell extracts of strain DBS4 transformed both (*S*)-DCPP and (*R*)-DCPP to 2,4-DCP (Figure S4). Such kind of biotransformation was previously reported to be catalyzed by an α-KG-dependent dioxygenase, which is dependent on the cofactor Fe^{2+}.[8,12] We found that our transformation reactions strictly required α-KG, and the transformation rates were dependent on Fe^{2+} and L-ascorbic acid (Figure S). No transformant of *Rac*-DCPP was observed when a boiled crude enzyme was used. From these results, we speculated that the enzyme catalyzing *Rac*-DCPP to 2,4-DCP in strain DBS4 was also a α-KG- and Fe^{2+}-dependent dioxygenase.

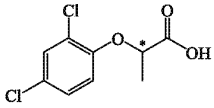
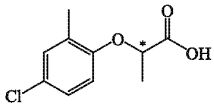
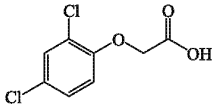
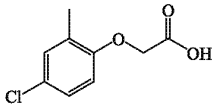
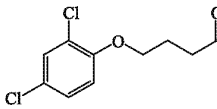
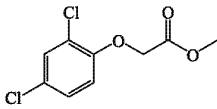
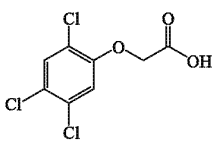
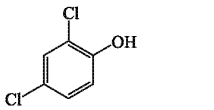
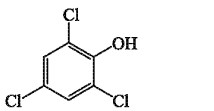
Potential Genes Involved in *Rac*-DCPP Degradation and the Metabolic Pathway in Strain DBS4. PCR amplification of the previously reported genes *rdpA* and *sdpA*, which are involved in the initial degradation of (*R*)-DCPP and (*S*)-DCPP, respectively, failed in strain DBS4. In addition, the *tfdA* gene, which is involved in the initial degradation of 2,4-D, was not amplified in strain DBS4 either. All these results indicated that there are different dioxygenases responsible for the initial degradation of PAAHs (including *Rac*-DCPP, 2,4-D, MCPA, *Rac*-MCPP, and 2,4-D butyl ester) in strain DBS4. A fragment, whose encoding protein shows 97% amino acid identity to *TfdB* (the phenol hydroxylase transforming 2,4-DCP to 3,5-dichlorocatechol during the catabolism of 2,4-D), was amplified from strain DBS4 with the degenerate primers (Figure S5). Based on the results of metabolite identification and functional gene amplification, the metabolic pathway of *Rac*-DCPP in strain DBS4 was proposed (Figure 6).[4,12]

Removal of *Rac*-DCPP from Soil by Strain DBS4. The inoculation of strain DBS4 cells at 8.5×10^6 CFU g^{-1} soil removed over 50 and 35% of *Rac*-DCPP in 4 days from soils, which had been treated with 50 and 100 mg kg^{-1} of *Rac*-DCPP, respectively (Figure S6). In 10 days, approximately 97

https://dx.doi.org/10.1021/acs.jafc.0c01066
J. Agric. Food Chem. 2020, 68, 6967−6976

COR-AAD1-00002984
Bayer EX1008 (Part 6 of 9)

Table 2. Substrate Range of Strain DBS4

Substrate	Structure	Degradation efficiency (%) [a]	
		3 days	5 days
Rac-DCPP		91.2 ± 0.3	100 ± 0.0
Rac-MCPP		85.7 ± 1.3	98.5 ± 0.4
2,4-D		98.4 ± 0.5	100 ± 0.0
MCPA		90.7 ± 1.1	98.1 ± 0.0
2,4-DB		-0.9 ± 0.6	-1.3 ± 0.8
2,4-D butyl ester		63.7 ± 0.7	89.5 ± 0.4
2,4,5-T		−0.8 ± 0.6	-2.3 ± 0.9
2,4-DCP		100 ± 0.0	100 ± 0.0
2,4,6-trichlorophenol		-0.3 ± 1.1	-1.5 ± 0.8

[a]Values indicate means of triplicate samples and standard deviation (SD).

and 62% of the 50 and 100 mg kg^{-1} of *Rac*-DCPP were removed, respectively. However, nearly no dissipation of *Rac*-DCPP was observed in the control (without inoculation of strain DBS4 cells). The degradation half-lives ($DT_{1/2}$) of *Rac*-DCPP by strain DBS4 were 7.9 days and 3.5 days in soils containing 100 and 50 mg $kg^{-1}$of *Rac*-DCPP, respectively.

DISCUSSION

PAAHs are ubiquitously applied to eliminate a broad spectrum of broad-leaved weeds in cereal crops, lawns, and grass pastures; therefore, PAAHs are frequently detected in leachates of landfills and groundwater.[1−3,5,47] The removal of PAAHs from contaminated sites by microorganisms is considered as the most potential method as compared to physical and chemical methods.[20] Although many 2,4-D- and MCPA-degrading strains have been isolated, few bacterial strains were reported to be capable of degrading racemic mixtures of chiral PAAHs, such as *Rac*-DCPP and *Rac*-MCPP. Here, a new bacterial strain DBS4, capable of utilizing most PAAHs as the growth substrates, was isolated and identified as a *Sphingopyxis* species. This study will help us to know more about the functions of *Sphingopyxis* species.

https://dx.doi.org/10.1021/acs.jafc.0c01066
J. Agric. Food Chem. 2020, 68, 6967−6976

COR-AAD1-00002985
Bayer EX1008 (Part 6 of 9)

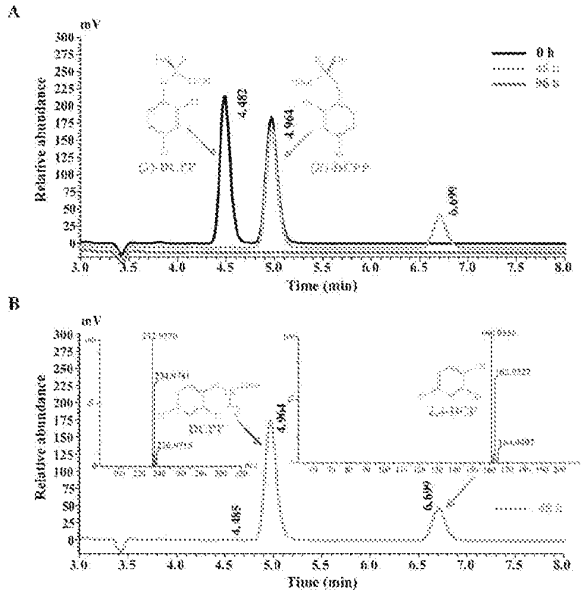


Figure 4. Detection of the enantioselective degradation of *Rac*-DCPP by HPLC (A). Identification of the metabolite from *Rac*-DCPP degradation by LC−MS (B).

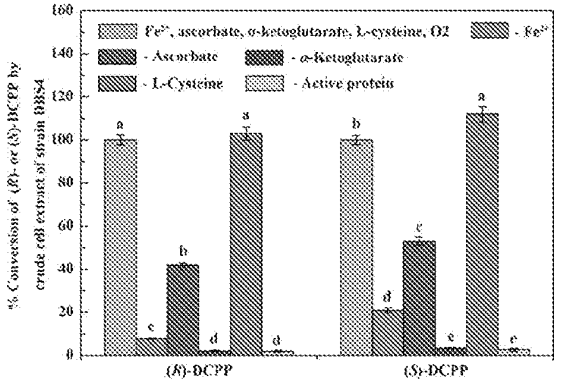


Figure 5. Effect of cofactors and supplements on the initial conversion reactions of (*R*)- and (*S*)-DCPP by the cell extracts from strain DBS4.

Sphingopyxis sp. DBS4 had a broad degrading spectrum. Besides *Rac*-DCPP, *Rac*-MCPP, 2,4-D, MCPA, and 2,4-D butyl ester could also be degraded efficiently and 2,4-D seemed to be the most favorable substrate. These data indicate that strain DBS4 has great potentials in the removal of PAAHs from contaminated sites. The effectiveness of bioaugmentation of microorganisms to clean up pesticide-polluted sites has been well confirmed.[48−54] For example, *Pseudomonas aeruginosa* strain NCIM 2074 has been applied to completely remove 10−50 mg L^{-1} chlorpyrifos in a shake flask bioreactor under controlled environmental conditions.[55] In addition, the cold-adapted strain *Oceanisphaera psychrotolerans* LAM-WHM−ZC was found to degrade 78.6 and 67.4% of 50 mg kg^{-1} of nicosulfuron in soils at 18.1 and 5 °C, respectively, within 15 days.[56] Furthermore, *Cupriavidus gilardii* T-1 has been found to efficiently degrade 2,4-D and its analogues in soils.[2] Under aerobic conditions, the phenoxypropionate herbicides are subject to rapid biodegradation, and half-lives in the top soils are usually measured in days or weeks.[7,57] However, in the subsoil or in groundwater aquifers with low or no oxygen availability, natural attenuation is generally very slow or absent.[3,58] In this study, the soil used was collected from an uncontaminated site on the campus and sterilized, nearly no dissipation of *Rac*-DCPP was observed in the control (without inoculation of strain DBS4 cells). However, the inoculation of strain DBS4 showed an encouraging result in the bioremediation of *Rac*-DCPP-contaminated soil. Approximately 97 and 62% of the 50 and 100 mg kg^{-1} *Rac*-DCPP were successfully removed from soil by inoculating strain DBS4 cells at the concentration of 8.5×10^6 CFU g^{-1} soil. This study showed that strain DBS4 is an excellent microbial resource for the bioremediation of PAAH-contaminated sites.

Strains capable of mineralizing chiral PAAHs (*Rac*-DCPP and *Rac*-MCPP) have been isolated previously. *Stenotrophomonas maltophilia* PM, *Alcaligenes* sp. CS1, and *Ralstonia* sp. CS2 were reported to efficiently degrade 60−120 mg L^{-1} of *Rac*-MCPP.[35,38] For *Rac*-DCPP, the versatile strain of *S. herbicidovorans* MH could consume 94 mg L^{-1} *Rac*-DCPP in less than 80 h. It was found that 94 mg L^{-1} (*S*)-DCPP was degraded to an undetectable level in 43 h, while no degradation of (*R*)-DCPP was observed during the first 60 h, and the complete degradation (*R*)-DCPP needed 82 h.[46] In addition, *Rhodoferax* sp. P230 and *D. acidovorans* MC1 were also reported to utilize *Rac*-DCPP as a growth substrate.[45] In our study, strain DBS4 degraded 60 mg L^{-1} of *Rac*-DCPP and *Rac*-MCPP to an undetectable level in approximately 96 h and 120 h, respectively, showing relatively high degrading efficiencies for chiral PAAHs.

Enantiomer interconversion has been reported for chiral compounds and such kind of phenomenon is frequently observed in some complex environments such as soil, lake, and river water environments. Enantiomerization was found to be biologically mediated and was not observed in sterilized soil.[17] Incubation of pure enantiomers of MCPP or DCPP in natural soils showed significant enantiomerization, (*R*)-enantiomers being transformed to (*S*)-enantiomers and vice versa.[17] In the lake and river water, MCPP and DCPP have also confirmed enantiomerization, and (*S*)-enantiomers were finally enriched.[59] However, no interconversion phenomenon of DCPP was observed in our experiments.

Sphingopyxis sp. DBS4 could use both enantiomers of DCPP as the sole source of carbon and energy for growth. However, the two enantiomers were enantioselectively degraded, with (*S*)-enantiomer preferentially degraded as compared to (*R*)-enantiomer. Such kind of phenomenon was similar to that described by Nickel et al.[32] The enantioselective catabolism of the two enantiomers of DCPP might be due to the presence of enantioselective enzymes. Two enantiomer-specific enzymes (RdpA and SdpA) have been identified in both *S. herbicidovorans* MH and *D. acidovorans* MC1.[38] The RdpA from *S. herbicidovorans* MH is 30% identical to *TfdA* and 100% identical to RdpA from *D. acidovorans* MC1, according to the deduced amino acid sequences. In regard to SdpA from *S. herbicidovorans* MH, the deduced amino acid sequence exhibits only 60% identity to SdpA from *D. acidovorans* MC1 and approximately 30% identity to RdpA.[8] The high sequence identity suggests that these two enantiomer-specific enzymes are relatively conserved in α-proteobacteria and β-proteobacteria strains. In this study, amplification of the fragments of *rdpA* and *sdpA* genes in strain DBS4 was failed, and no *tfdA*

https://dx.doi.org/10.1021/acs.jafc.0c01066
J. Agric. Food Chem. 2020, 68, 6967−6976

COR-AAD1-00002986
Bayer EX1008 (Part 6 of 9)

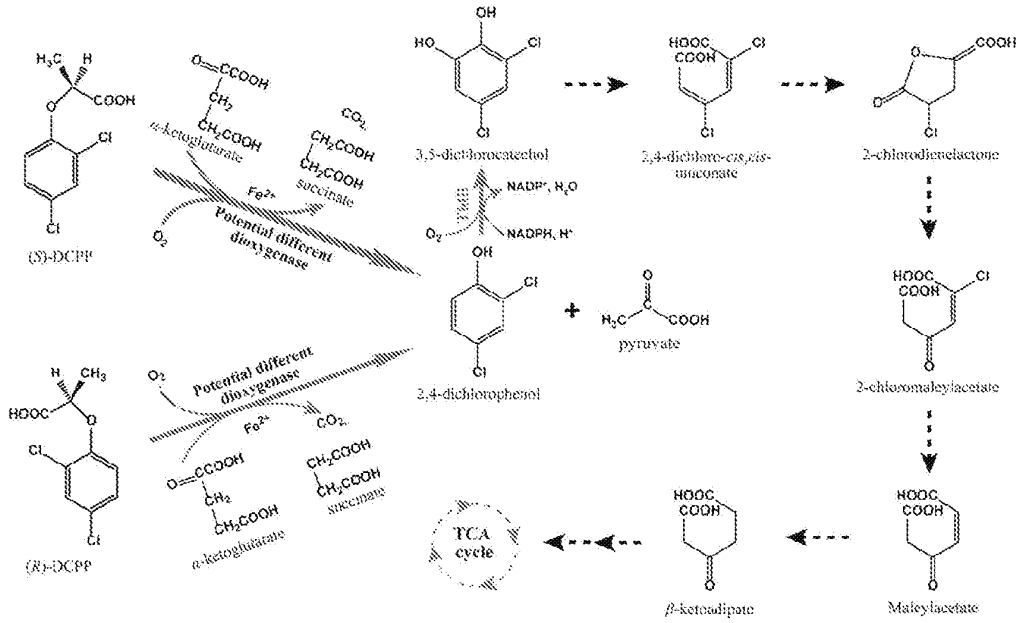


Figure 6. Proposed metabolic pathway of *Rac*-DCPP in strain DBS4.

gene was detected. Hence, we speculated that strain DBS4 might harbor different enantioselective dioxygenases, catalyzing the initial degradation of phenoxypropionate herbicides. In addition, many aromatic compounds are taken in by microorganisms through energy-dependent transport systems.[60−63] Active transport of DCPP, MCPP, and 2,4-D by three inducible and proton gradient-driven uptake systems has been confirmed to be the first step in their degradation in *S. herbicidovorans*.[46] In our study, (*S*)-enantiomer of DCPP was found to disappear much faster from culture medium than (*R*)-enantiomer. However, crude enzymes extracted from strain DBS4 showed nearly equal activities toward (*S*)-DCPP and (*R*)-DCPP (Figure S4), indicating that distinct and specific uptake systems for each DCPP enantiomer are present in strain DBS4. Further works are needed to investigate the enantiomer-specific enzymes and the enantioselective uptake systems in strain DBS4.

ASSOCIATED CONTENT

Supporting Information

The Supporting Information is available free of charge at https://pubs.acs.org/doi/10.1021/acs.jafc.0c01066.

Basic properties of the soil used (Table S1); electron transmission micrographs and morphology of strain DBS4 on LB agar (Figure S1); neighbor-joining tree of strain DBS4 (Figure S2); effects of different factors on the biodegradation of *Rac*-DCPP by strain DBS4 (Figure S3); enantioselective degradation of *Rac*-DCPP by a crude enzyme of strain DBS4 (Figure S4); PCR amplification of fragments similar to the α-ketoglutarate-dependent dioxygenase gene (*tfdA*) and the phenol hydroxylase gene (*tfdB*) (Figure S5); and removal of *Rac*-DCPP from the soil by inoculation with cells of strain DBS4 (Figure S6) (PDF)

AUTHOR INFORMATION

Corresponding Author

Jian-Dong Jiang − *Department of Microbiology, Key Lab of Microbiology for Agricultural Environment, Ministry of Agriculture, College of Life Sciences and Jiangsu Provincial Key Lab for Organic Solid Waste Utilization, Nanjing Agricultural University, 210095 Nanjing, China;* orcid.org/0000-0003-4877-5756; Phone: +86-25-84399726; Email: jiang_jjd@njau.edu.cn; Fax: +86-84396314

Authors

Long Zhang − *Department of Microbiology, Key Lab of Microbiology for Agricultural Environment, Ministry of Agriculture, College of Life Sciences, Nanjing Agricultural University, 210095 Nanjing, China; College of Life Sciences, Huaibei Normal University, 235000 Huaibei, China;* orcid.org/0000-0002-7673-7848

Ping Hang − *Department of Microbiology, Key Lab of Microbiology for Agricultural Environment, Ministry of Agriculture, College of Life Sciences, Nanjing Agricultural University, 210095 Nanjing, China*

Xi-Yi Zhou − *Department of Microbiology, Key Lab of Microbiology for Agricultural Environment, Ministry of Agriculture, College of Life Sciences, Nanjing Agricultural University, 210095 Nanjing, China*

Wen-Jing Qiao − *Department of Microbiology, Key Lab of Microbiology for Agricultural Environment, Ministry of Agriculture, College of Life Sciences, Nanjing Agricultural University, 210095 Nanjing, China*

Complete contact information is available at: https://pubs.acs.org/10.1021/acs.jafc.0c01066

Funding

This work was financially supported by the National Natural Science Foundation of China (Nos. 31670111 and 31900077), the Key Program of Natural Science Research in Colleges and

COR-AAD1-00002987
Bayer EX1008 (Part 6 of 9)

Universities in Anhui Province (KJ2020A0038), and the China Postdoctoral Science Foundation (2018M630566).

Notes

The authors declare no competing financial interest.

REFERENCES

(1) Directive G. Directive 2006/118/EC of the European Parliament and of the Council on the Protection of Groundwater against Pollution and Deterioration. In *Official Journal of the European Union, L*; Council of the European Union: Brussels, Belgium, 2006; Vol. *372*, pp 19−31.

(2) Wu, X. W.; Wang, W. B.; Liu, J. W.; Pan, D. D.; Tu, X. H.; Lv, P.; Wang, Y.; Cao, H. Q.; Wang, Y. W.; Hua, R. M. Rapid biodegradation of the herbicide 2,4-dichlorophenoxyacetic acid by *Cupriavidus gilardii* T-1. *J. Agric. Food Chem.* **2017**, *65*, 3711−3720.

(3) Feld, L.; Nielsen, T. K.; Hansen, L. H.; Aamand, J.; Albers, C. N. Establishment of bacterial herbicide degraders in a rapid sand filter for bioremediation of phenoxypropionate-polluted groundwater. *Appl. Environ. Microbiol.* **2015**, *82*, 878−887.

(4) Müller, T. A.; Byrde, S. M.; Werlen, C.; van der Meer, J. R.; Kohler, H. P. Genetic analysis of phenoxyalkanoic acid degradation in *Sphingomonas herbicidovorans* MH. *Appl. Environ. Microbiol.* **2004**, *70*, 6066−6075.

(5) Kohler, H. P. *Sphingomonas herbicidovorans* MH: a versatile phenoxyalkanoic acid herbicide degrader. *J. Ind. Microbiol. Biotechnol.* **1999**, *23*, 336−340.

(6) Rügge, K.; Juhler, R. K.; Broholm, M. M.; Bjerg, P. L. Degradation of the (*R*)- and (*S*)-enantiomers of the herbicides MCPP and dichlorprop in a continuous field-injection experiment. *Water Res.* **2002**, *36*, 4160−4164.

(7) Paulin, M. M.; Nicolaisen, M. H.; Sørensen, J. (*R,S*)-dichlorprop herbicide in agricultural soil induces proliferation and expression of multiple dioxygenase-encoding genes in the indigenous microbial community. *Environ. Microbiol.* **2011**, *13*, 1513−1523.

(8) Müller, T. A.; Fleischmann, T.; van der Meer, J. R.; Kohler, H. P. Purification and characterization of two enantioselective alpha-ketoglutarate-dependent dioxygenases, RdpA and SdpA, from *Sphingomonas herbicidovorans* MH. *Appl. Environ. Microbiol.* **2006**, *72*, 4853−4861.

(9) Zipper, C.; Nickel, K.; Angst, W.; Kohler, H. P. Complete microbial degradation of both enantiomers of the chiral herbicide mecoprop [(*RS*)-2-(4-chloro-2-methylphenoxy) propionic acid] in an enantioselective manner by *Sphingomonas herbicidovorans* sp. nov. *Appl. Environ. Microbiol.* **1996**, *62*, 4318−4322.

(10) Wu, T.; Li, X.; Huang, H.; Zhang, S. Enantioselective oxidative damage of chiral pesticide dichlorprop to maize. *J. Agric. Food Chem.* **2011**, *59*, 4315−4320.

(11) Wen, Y.; Chen, H.; Shen, C.; Zhao, M.; Liu, W. Enantioselectivity tuning of chiral herbicide dichlorprop by copper: roles of reactive oxygen species. *Environ. Sci. Technol.* **2011**, *45*, 4778−4784.

(12) Nickel, K.; Suter, M. J.; Kohler, H. P. Involvement of two alpha-ketoglutarate-dependent dioxygenases in enantioselective degradation of (*R*)- and (*S*)-mecoprop by *Sphingomonas herbicidovorans* MH. *J. Bacteriol.* **1997**, *179*, 6674−6679.

(13) Smejkal, C. W.; Vallaeys, T.; Seymour, F. A.; Burton, S. K.; Lappin-Scott, H. M. Characterization of (*R/S*)-mecoprop [2-(2-methyl-4-chlorophenoxy) propionic acid]-degrading *Alcaligenes* sp.CS1 and *Ralstonia* sp. CS2 isolated from agricultural soils. *Environ. Microbiol.* **2001**, *3*, 288−293.

(14) Sun, D.; Pang, J.; Qiu, J.; Li, L.; Liu, C.; Jiao, B. Enantioselective degradation and enantiomerization of indoxacarb in soil. *J. Agric. Food Chem.* **2013**, *61*, 11273−11277.

(15) Zhou, Q.; Zhang, X.; Huang, J. Relationship between enantioselective transformation of racemic quizalofop-ethyl and soil bacterial diversity: A destructive approach. *Chirality* **2019**, *31*, 700−710.

(16) Buser, H. R.; Müller, M. D.; Poiger, T.; Balmer, M. E. Environmental behavior of the chiral acetamide pesticide metalaxyl: Enantioselective degradation and chiral stability in soil. *Environ. Sci. Technol.* **2002**, *36*, 221−226.

(17) Müller, M. D.; Buser, H. R. Conversion reactions of various phenoxyalkanoic acid herbicides in soil. 1. Enantiomerization and enantioselective degradation of the chiral 2-phenoxypropionic acid herbicides. *Environ. Sci. Technol.* **1997**, *31*, 1953−1959.

(18) Li, Z.; Li, Q.; Cheng, F.; Zhang, W.; Wang, W.; Li, J. Enantioselectivity in degradation and transformation of quizalofop-ethyl in soils. *Chirality* **2012**, *24*, 552−557.

(19) Smith, A. E. Degradation, fate and persistence of phenoxyalkanoic acid herbicides in soil. *Rev. Weed Sci.* **1989**, *4*, 1−24.

(20) Huang, X.; He, J.; Yan, X.; Hong, Q.; Chen, K.; He, Q.; Zhang, L.; Liu, X. W.; Chuang, S. C.; Li, S. P.; Jiang, J. D. Microbial catabolism of chemical herbicides: Microbial resources, metabolic pathways and catabolic genes. *Pestic. Biochem. Physiol.* **2017**, *143*, 272−297.

(21) Smith, A. E.; Mortensen, K.; Aubin, A. J.; Molloy, M. M. Degradation of MCPA, 2,4-D, and other phenoxyalkanoic acid herbicides using an isolated soil bacterium. *J. Agric. Food Chem.* **1994**, *42*, 401−405.

(22) Kitagawa, W.; Takami, S.; Miyauchi, K.; Masai, E.; Kamagata, Y.; Tiedje, J. M.; Fukuda, M. Novel 2,4-dichlorophenoxyacetic acid degradation genes from oligotrophic *Bradyrhizobium* sp. strain HW13 isolated from a pristine environment. *J. Bacteriol.* **2002**, *184*, 509−518.

(23) Tan, L.; Hu, Q. L.; Xiong, X. Y.; Su, X. J.; Huang, Y. N.; Jiang, Z. W.; Zhou, Q. M.; Zhao, S. Y.; Zeng, W. A. Isolation and characterization of a novel 2-methyl-4-chlorophenoxyacetic acid-degrading *Enterobacter* sp. strain SE08. *Ecotoxicol. Environ. Saf.* **2013**, *96*, 198−204.

(24) Han, L. Z.; Zhao, D. G.; Li, C. C. Isolation and 2,4-D-degrading characteristics of *Cupriavidus campinensis* BJ71. *Brazilian J. Microbiol* **2015**, *46*, 433−441.

(25) Dai, Y.; Li, N. N.; Zhao, Q.; Xie, S. G. Bioremediation using *Novosphingobium* strain DY4 for 2,4-dichlorophenoxyacetic acid contaminated soil and impact on microbial community structure. *Biodegradation* **2015**, *26*, 161−170.

(26) Kumar, A.; Trefault, N.; Olaniran, A. O. Microbial degradation of 2,4-dichlorophenoxyacetic acid: insight into the enzymes and catabolic genes involved, their regulation and biotechnological implications. *Crit. Rev. Microbiol.* **2016**, *42*, 194−208.

(27) Xia, Z. Y.; Zhang, L.; Zhao, Y.; Yan, X.; Li, S. P.; Gu, T.; Jiang, J. D. Biodegradation of the herbicide 2,4-dichlorophenoxyacetic acid by a new isolated strain of *Achromobacter* sp. LZ35. *Curr. Microbiol.* **2017**, *74*, 193−202.

(28) Xiao, L.; Jia, H. F.; Jeong, I. H.; Ahn, Y. J.; Zhu, Y. Z. Isolation and characterization of 2,4-D butyl ester degrading *Acinetobacter* sp. ZX02 from a Chinese ginger cultivated soil. *J. Agric. Food Chem.* **2017**, *65*, 7345−7351.

(29) Müller, T. A.; Kohler, H. P. E. Chirality of pollutants-Effects on metabolism and fate. *Appl. Microbiol. Biotechnol.* **2004**, *64*, 300−316.

(30) Schleinitz, K. M.; Kleinsteuber, S.; Vallaeys, T.; Babel, W. Localization and characterization of two novel genes encoding stereospecific dioxygenases catalyzing 2(2,4-dichlorophenoxy) propionate cleavage in *Delftia acidovorans* MC1. *Appl. Environ. Microbiol.* **2004**, *70*, 5357−5365.

(31) Horvath, M.; Ditzelmüller, G.; Loidl, M.; Streichsbier, F. Isolation and characterization of a 2-(2,4-dichlorophenoxy) propionic acid degrading soil bacterium. *Appl. Microbiol. Biotechnol.* **1990**, *33*, 213−216.

(32) Ehrig, A.; Müller, R. H.; Babel, W. Isolation of phenoxy herbicide-degrading *Rhodoferax* species from contaminated building material. *Acta. Biotechnol.* **1997**, *17*, 351−356.

(33) Müller, R. H.; Jorks, S.; Kleinsteuber, S.; Babel, W. *Comamonas acidovorans* strain MC1: a new isolate capable of degrading the chiral herbicides dichlorprop and mecoprop and the herbicides 2,4-D and MCPA. *Microbiol. Res.* **1999**, *154*, 241−246.

https://dx.doi.org/10.1021/acs.jafc.0c01066
J. Agric. Food Chem. 2020, 68, 6967−6976

COR-AAD1-00002988
Bayer EX1008 (Part 6 of 9)

(34) Mai, P.; Jacobsen, O. S.; Aamand, J. Mineralization and co-metabolic degradation of phenoxyalkanoic acid herbicides by a pure bacterial culture isolated from an aquifer. *Appl. Microbiol. Biotechnol.* **2001**, *56*, 486−490.
(35) Tett, V. A.; Willetts, A. J.; Lappin-Scott, H. M. Biodegradation of the chlorophenoxy herbicide (*R*)-(+)-mecoprop by *Alcaligenes denitrificans*. *Biodegradation* **1997**, *8*, 43−52.
(36) Tett, V. A.; Willets, A. J.; Lappin-Scott, H. M. Enantioselective degradation of the herbicide mecoprop [2-(2-methyl-4-chlorophenoxy) propionic acid] by mixed and pure bacterial cultures. *FEMS Microbiol. Ecol.* **1994**, *14*, 191−200.
(37) Kilpi, S. Degradation of some phenoxy acid herbicides by mixed cultures of bacteria from soil treated with 2-(2-methyl-4-chloro) phenoxypropionic acid. *Microbial. Ecol.* **1980**, *6*, 261−270.
(38) Nielsen, T. K.; Rasmussen, M.; Demanèche, S.; Cecillon, S.; Vogel, T. M.; Hansen, L. H. Evolution of Sphingomonad gene clusters related to pesticide catabolism revealed by genome sequence and mobilomics of *Sphingobium herbicidovorans* MH. *Genome Biol. Evol.* **2017**, *9*, 2477−2490.
(39) Zhang, L.; Song, M.; Cao, Q.; Wu, S.; Zhao, Y.; Huang, J. W.; Chen, K.; Li, S. P.; Xia, Z. Y.; Jiang, J. D. *Camelimonas fluminis* sp. nov., a cyhalothrin-degrading bacterium isolated from river water. *Int. J. Syst. Evol. Microbiol.* **2015**, *65*, 3109−3114.
(40) Holt, J. G.; Krieg, N. R.; Sneath, P. H. A.; Staley, J. T.; Williams, S. T. *Bergey's Manual of Determinative Bacteriology*, 9th ed.; Lippincott Williams and Wilkins: Baltimore, MD, USA, 1994; pp 626−640.
(41) Zhang, L.; Chen, X. L.; Hu, Q.; Chen, K.; Yan, X.; Li, S. P.; Freilich, S.; Jiang, J. D. *Haoranjiania flava* gen. nov., sp. nov., a new member of the family *Chitinophagaceae*, isolated from activated sludge. *Int. J. Syst. Evol. Microbiol.* **2016**, *66*, 4686−4691.
(42) Yoon, S. H.; Ha, S. M.; Kwon, S.; Lim, J.; Kim, Y.; Seo, H.; Chun, J. Introducing EzBioCloud: a taxonomically united database of 16S rRNA gene sequences and whole-genome assemblies. *Int. J. Syst. Evol. Microbiol.* **2017**, *67*, 1613−1617.
(43) Zhang, L.; Hang, P.; Hu, Q.; Chen, X. L.; Zhou, X. Y.; Chen, K.; Jiang, J. D. Degradation of phenylurea herbicides by a novel bacterial consortium containing synergistically catabolic species and functionally complementary hydrolases. *J. Agric. Food Chem.* **2018**, *66*, 12479−12489.
(44) Vallaeys, T.; Fulthorpe, R. R.; Wright, A. M.; Soulas, G. The metabolic pathway of 2,4-dichlorophenoxyacetic acid degradation involves different families of *tfdA* and *tfdB* genes according to PCR-RFLP analysis. *FEMS Microbiol. Ecol.* **1996**, *20*, 163−172.
(45) Müller, R. H.; Kleinsteuber, S.; Babel, W. Physiological and genetic characteristics of two bacterial strains utilizing phenoxypropionate and phenoxyacetate herbicides. *Microbiol. Res.* **2001**, *156*, 121−131.
(46) Zipper, C.; Bunk, M.; Zehnder, A. J.; Kohler, H. P. Enantioselective uptake and degradation of the chiral herbicide dichlorprop [(*RS*)-2-(2,4-dichlorophenoxy) propanoic acid] by *Sphingomonas herbicidovorans* MH. *J. Bacteriol.* **1998**, *180*, 3368−3374.
(47) Directive G. Directive 98/83/EC of 3 November 1998 on the Quality of Water Intended for Human Consumption. In *Official Journal of the European Union, L*; Council of the European Union: Brussels, Belgium, 1998; Vol. *330*, pp 32−54.
(48) Abdelbagi, A.; Elmahi, M.; Osman, D. Organochlorine insecticides residues in Sudanese soils of intensive pesticide use and in the surface soil of a Qurashi pesticide store, University of Khartoum. *J. Agric. Sci.* **2003**, *11*, 59−68.
(49) Abdelbagi, A.; Elmahi, M.; Osman, D. Chlorinated hydrocarbon insecticide residues in the Sudanese Soils of limited or no pesticide use. *Arab. J. Plant Prot.* **2000**, *18*, 35−39.
(50) Elmahi, A. Distribution of Chlorinated Hydrocarbon Pesticides Residues in Sudan Soil. M.Sc. Thesis, University of Khartoum: Sudan, 1996.
(51) Ali, M. Naturally Occurring Soil Microorganism in Qurashi Pesticides Store and the surrounding Gezira Soil and their Potential in Degrading Endosulfan α, β and Lindane. *M.Sc. Thesis*, University of Khartoum: Sudan, 2005.
(52) Ishag, A. E. S. A.; Abdelbagi, A. O.; Hammad, A. M. A.; Elsheikh, E. E. A.; Elsaid, O. E.; Hur, J. H.; Laing, M. D. Biodegradation of chlorpyrifos, malathion, and dimethoate by three strains of bacteria isolated from pesticide-polluted soils in Sudan. *J. Agric. Food Chem.* **2016**, *64*, 8491−8498.
(53) Ishag, A. E. S. A.; Abdelbagi, A. O.; Hammad, A. M. A.; Elsheikh, E. A. E.; Elsaid, O. E.; Hur, J. H. Biodegradation of endosulfan and pendimethalin by three strains of bacteria isolated from pesticides-polluted soils in the Sudan. *Appl. Biol. Chem.* **2017**, *60*, 287−297.
(54) Abdelbagi, O. A.; Wady, A. I. A.; Ishag, A. E. S. A.; Hammad, A. M. A.; Abdalla, M. A. O.; Hur, J. H. Biodegradation of fenthion and temphos in liquid media by *Bacillus safensis* isolated from pesticides polluted soil in the Sudan. *Afr. J. Biotechnol.* **2018**, *17*, 396−340.
(55) Fulekar, M. H.; Geetha, M. Bioremediation of chlorpyrifos by *Pseudomonas aeruginosa* using scale up technique. *J. Appl. Biosci.* **2008**, *12*, 657−660.
(56) Zhou, S.; Song, J.; Dong, W.; Mu, Y.; Zhang, Q.; Fan, Z.; Wang, Y.; Kong, D.; Zhou, Y.; Jiang, X.; Zhao, B.; Han, G.; Ruan, Z. Nicosulfuron biodegradation by a novel cold-adapted strain *Oceanisphaera psychrotolerans* LAM-WHM-ZC. *J. Agric. Food Chem.* **2017**, *65*, 10243−10249.
(57) Helweg, A. Degradation and adsorption of ^{14}C mecoprop (MCPP) in surface soils and in subsoil. Influence of temperature, moisture content, sterilisation and concentration on degradation. *Sci. Total Environ.* **1993**, *132*, 229−241.
(58) Buss, S. R.; Thrasher, J.; Morgan, P.; Smith, J. W. N. A review of mecoprop attenuation in the subsurface. *Q. J. Eng. Geol. Hydrogeol.* **2006**, *39*, 283−292.
(59) Buser, H. R.; Müller, M. D. Occurrence and transformation reactions of chiral and achiral phenoxyalkanoic acid herbicides in lakes and rivers in Switzerland. *Environ. Sci. Technol.* **1998**, *32*, 626−633.
(60) Groenewegen, P. E.; Driessen, A. J.; Konings, W. N.; de Bont, J. A. Energy-dependent uptake of 4-chlorobenzoate in the coryneform bacterium NTB-1. *J. Bacteriol.* **1990**, *172*, 419−423.
(61) Locher, H. H.; Poolman, B.; Cook, A. M.; Konings, W. N. Uptake of 4-toluene sulfonate by *Comamonas testosteroni* T-2. *J. Bacteriol.* **1993**, *175*, 1075−1080.
(62) Harwood, C. S.; Nichols, N. N.; Kim, M. K.; Ditty, J. L.; Parales, R. E. Identification of the *pcaRKF* gene cluster from *Pseudomonas putida*: involvement in chemotaxis, biodegradation, and transport of 4-hydroxybenzoate. *J. Bacteriol.* **1994**, *176*, 6479−6488.
(63) Leveau, J. H.; Zehnder, A. J.; van der Meer, J. R. The *tfdK* gene product facilitates the uptake of 2,4-dichlorophenoxyacetate by *Ralstonia eutropha* JMP134 (pJP4). *J. Bacteriol.* **1998**, *180*, 2237−2243.

https://dx.doi.org/10.1021/acs.jafc.0c01066
J. Agric. Food Chem. 2020, 68, 6967−6976

COR-AAD1-00002989
Bayer EX1008 (Part 6 of 9)

BIO CITY LEIPZIG
Biotechnologisch-Biomedizinisches Zentrum

UNIVERSITÄT LEIPZIG

Center for Biotechnology and Biomedicine

4th BIOTECHNOLOGY SYMPOSIUM 2005

ABSTRACTS

Editors:
Andrea A. Robitzki
Annette G. Beck-Sickinger
Susanne Brakmann
Svenne Eichler

COR-AAD1-00002990
Bayer EX1008 (Part 6 of 9)

2005

4th Biotechnology Symposium of the University of Leipzig

June 3, 2005

ABSTRACTS

Editors:
Andrea A. Robitzki
Annette G. Beck-Sickinger
Susanne Brakmann
Svenne Eichler

UNIVERSITÄT LEIPZIG

COR-AAD1-00002992
Bayer EX1008 (Part 6 of 9)

Editors

Prof. Dr. Andrea A. Robitzki
Chair of the Center for Biotechnology and Biomedicine, Universität Leipzig

Prof. Dr. Annette G. Beck-Sickinger
Director of Institute of Biochemistry,
Faculty of Biosciences, Pharmacy and Psychology, Universität Leipzig

PD Dr. Susanne Brakmann
Head of Junior Research Group "Applied Molecular Evolution Research",
Center for Biotechnology and Biomedicine, Universität Leipzig

Dr. Svenne Eichler
Chief Executive Officer of the Center for Biotechnology and Biomedicine,
Universität Leipzig

Compilation Matthias Frölich
Center for Biotechnology and Biomedicine, Universität Leipzig

Layout wpunktw kommunikation + werbung gmbh

Print Decker Offset Druck GmbH

Editorial Deadline 31.03.2005

CONTENT

FOREWORD 23

PRESENTATIONS 25

1 PROTEIN ENGINEERING AND BIOANALYTICS 25

1.1 Creating novel proteins for therapeutic applications
Rainer Rudolph, Hauke Lilie, Ulrike Fiedler 26

1.2 Dark matter of the genome – The human genome contains thousands of non-coding RNAs
Peter F. Stadler 27

1.3 Functional annotation of high-throughput screening data with structural protein interactions and textmining
Michael Schröder 28

1.4 TRANSIL® technology – Immobilized proteins for innovative assays and for ADME prediction in drug discovery
Joachim Nöller 29

2 MOLECULAR MEDICINE AND THERAPEUTICS 31

2.1 Tumor targeting
Dario Neri 32

2.2 NAD^+-dependent regulatory processes on human monocytes/ macrophages
Sunna Hauschildt 33

2.3 Diabesity - Molecules and mechanisms
Michael Stumvoll 34

COR-AAD1-00002994

Bayer EX1008 (Part 6 of 9)

3 BIOMEDICAL AND CELL ENGINEERING 37

3.1 Modeling cardiac electric signals – From ion channels to the ECG
Olaf Dössel 38

3.2 Generation of reliable diagnostics and effective vaccines by recombinant DNA technologies
Hermann Müller 39

3.3 Microstructuring of surfaces for life science
Klaus Zimmer, Thomas Rudolph, David Ruthe, Rico Böhme, Joachim Zajadacz, Bernd Rauschenbach 40

3.4 Dopaminergic neurons from midbrain-derived neural stem cells
Sigrid C. Schwarz 41

POSTERS 43

4 PROTEIN ENGINEERING AND BIOANALYTICS 43

4.1 Characterization of *B. burgdorferi* cyst formation
Samiya Al-Robaiy, Hassan Dihazi, Johannes Kacza, Johannes Seeger, Jürgen Schiller, Daniel Huster, Reinhard K. Straubinger 44

4.2 A different approach for cloning and purification of the 5S subunit of transcarboxylase multienzyme complex
Rakesh Kumar Bhat, Stefan Berger 45

4.3 Residue specific studies of NH exchange rates performed on ubiquitin
Torsten Brand, Garreth A. Morris, Eurico J. Cabrita, Hans-Jörg Hofmann, Stefan Berger 46

4.4 Developmental pattern of tau isoforms in rat brain
Torsten Bullmann, Max Holzer, Wolfgang Härtig, Nicolas Sergeant, Andre Delacourte, Rohan de Silva, Hiroshi Mori, Thomas Arendt 47

4.5 New structural and functional aspects of phosphofructo-1-kinase from *Pichia pastoris*
Anke Edelmann, Katrin Tanneberger, Jürgen Kirchberger, Jörg Bär, Torsten Schöneberg 48

4.6 Recombinant expression and structure determination of phosphodiesterases
Roy Eylenstein, Nancy Kühn, Petra Schäfer, E. Bartholomeus Küttner, Susanne Moschütz, Norbert Sträter 49

4.7 Site-directed mutagenesis in the substrate binding region of R-3-hydroxybutyrate dehydrogenase (3-HBDH)
Claudia Feller, Marlis Grunow 50

4.8 Site-specific synthesis of Amadori-modified peptides on solid-phase
Andrej Frolov, David Singer, Ralf Hoffmann 51

4.9 Enantioselective high performance liquid chromatography of astaxanthin from microbial sources
Carola Griehl, Claudia Grewe, Sieglinde Menge 52

4.10 IZKF Leipzig Core Unit "Fluorescence Technology" – Confocal laser scanning microscopy
Jens Grosche, Andreas Reichenbach 53

4.11 Depletion of high-abundant proteins from human serum
Katja Hanisch, Tobias Langrock, Ralf Hoffmann 54

4.12 Study of antibacterial and antitumoral peptides
Jörg Hanrieder, David Singer, Laszlo Otvös Jr., Peter F. Zipfel, Vladimir N. Kokryakov, Ralf Hoffmann 55

4.13 Lipophilicity and protein binding as key descriptors for adme behavior – Innovative high-throughput screening tools
Thorsten Hartmann, Daniel Nimptsch, Cornelia Röhring, Johannes Schmitt, Joachim Nöller 56

4.14 Selection of an aptamer against the tissue inhibitor of matrix metalloproteinases
Julia Hoßbach, Rolf Gebhardt 57

4.15 Probing laminin self-interaction by chemical cross-linking and ESI-FTICR mass spectrometry
Stefan Kalkhof, Sebastian Haehn, Christian Ihling, Neil Smyth, Andrea Sinz 58

4.16 Recombinant expression and characterization of the ecto-nucleotidase CD39
Matthias Krause, Norbert Sträter 59

COR-AAD1-00002996
Bayer EX1008 (Part 6 of 9)

4.17 Crystal structure of the 2-oxoglutarate dependent dioxygenase RdpA
Jörn Krauße, Anne Westendorf, E. Bartholomeus Küttner, Roland H. Müller, Norbert Sträter 60

4.18 Application of photoactivatable GFP to investigate dynamics of human mitochondria
Christian Kukat, Katrin Pospischil, Alexandra Kneissl, Ingo Schäfer, Peter Seibel 61

4.19 Crystal structures of two thermophilic DNA nucleases as templates for protein engineering
E. Bartholomeus Küttner, Sven Pfeifer, Thomas Greiner-Stöffele, Norbert Sträter 62

4.20 Strategies for the identification of hydroxyproline-isomers and hydroxylysine in collagen
Tobias Langrock, Natividad García-Villar, Ralf Hoffmann 63

4.21 The regulatory environment for the development and approval of biopharmaceuticals
Rüdiger Laub, Ullrich Pigla 64

4.22 Discrimination of vaccinated and infected pigs by *Salmonella*-specific IgA antibodies
Jörg Lehmann, Uwe Rösler, Thomas Lindner, Thomas Kramer, Jörg Gabert, Andreas Hensel 65

4.23 Selective inhibition of protein kinases by emodin-related compounds
Katja Lerche, Lars Teich, Kurt Eger, Robert Günther, Hans-Jörg Hofmann, Rolf Gebhardt 66

4.24 Chip calorimeter as a control device for the monitoring of bioprocesses
Johannes Lerchner, Thomas Maskow, Mirko Peitsch, Hauke Harms, Gert Wolf 67

4.25 Myeloperoxidase-induced effects on spermatozoa
Jacqueline Leßig, Hans-Jürgen Glander, Uwe Paasch, Jürgen Arnhold 68

4.26 IZKF Leipzig Core Unit "Fluorescence Technology" – Flow cytometry and cell sorting
Andreas Lösche, Viola Döbel 69

COR-AAD1-00002997
Bayer EX1008 (Part 6 of 9)

4.27 IZKF Leipzig Core Unit "Fluorescence Technology" – Laser scanning cytometry
Andreas Lösche, Anja Mittag, Attila Tarnok 70

4.28 Binding proteins for advanced glycation endproducts isolated from different rat tissues
Ina Meiners, Gerald Münch, Karen Nieber 71

4.29 Characterization of recombinant antibody fragments to human CD4 expressed in transgenic tobacco
Dirk Mischke, Sunna Hauschildt, Jörg Böhme, René Brecht, Frank Emmrich, Ullrich Pigla, Rüdiger Laub 72

4.30 Separation of phosphopeptide isomers using capillary-zone-electrophoresis
Marika V. Mützelburg, Peter Hoffmann, David Singer, Ralf Hoffmann 73

4.31 Mass spectrometric methods and the investigation of the kinetic properties of cellular phospholipases
Marijana Petkovic, Jürgen Schiller, Jacqueline Leßig, Beate Fuchs, Jürgen Arnhold 74

4.32 Phenotyping of mutans streptococci by intact cell MALDI-TOF-MS after caries excavation
Stefan Rupf, Knut Merte, Knut Breitung, Susanne Kneist, Klaus Eschrich 75

4.33 Interaction of myeloperoxidase with human serum albumin
Pavel Salavei, Uta Reibetanz, Jürgen Arnhold 76

4.34 Comparing the biophysical properties of sterols in lipid membranes – What is special about cholesterol?
Holger A. Scheidt, Peter Müller, Andreas Herrmann, Klaus Arnold, Klaus Gawrisch, Daniel Huster 77

4.35 Studying calmodulin-adenylyl cyclase 8 interaction by chemical cross-linking and FTICR mass spectrometry
Andreas Schmidt, Daniela M. Schulz, Stefan Kalkhof, Christian Ihling, Annette G. Beck-Sickinger, Dermot M.F. Cooper, Andrea Sinz 78

4.36 *In vitro* evolution of a thermostabilized Exonuclease III
Ramona Schmiedel, Thomas Greiner-Stöffele 79

COR-AAD1-00002998
Bayer EX1008 (Part 6 of 9)

4.37 Purification and structural characterization of the annexin II / p11 tetramer from porcine small intestine
Daniela M. Schulz, Andreas Schmidt, Olaf Zschörnig, Stefan Kalkhof, Christian Ihling, Andrea Sinz 80

4.38 Protein-ligand interaction of S-adenosyl-L-methionine and the methyltransferase SU(VAR)3-9
Karsten Seeger, Sandro Lein, Gunter Reuter, Stefan Berger 81

4.39 Characterisation of antibodies recognizing phosphorylation dependent epitopes in the tau protein
David Singer, Daniela Volke, Ralf Hoffmann 82

4.40 Proteome analysis of *Escherichia coli* using high-performance liquid chromatography and fourier transform ion cyclotron resonance mass spectrometry
Andrea Sinz, Christian Ihling 83

4.41 Mapping protein interfaces by affinity cross-linking combined with MALDI-TOF and ESI-FTICR mass spectrometry
Andrea Sinz, Stefan Kalkhof, Christian Ihling 84

4.42 Localisation of the PHB-biosynthesis in recombinant yeasts
Claudia Stolz, Uta Breuer, Hauke Harms 85

4.43 *In vitro* selection of DNA aptamers binding ethanolamine
Beate Strehlitz, Dörthe Mann, Christine Reinemann, Regina Stoltenburg 86

4.44 The calcium-dependent regulation of TRPV4 involves the interaction with the carboxy-terminus of Calmodulin
Rainer Strotmann, Torsten Schöneberg 87

4.45 The reverse transcriptase of HIV – Generation of a polymerase with reduced replication fidelity
Sascha Stumpp, Susanne Brakmann 88

4.46 A phosphopeptide capturing Fe kit designed for selective isolation of phosphopeptides on the surface of superparamagnetic micro particles
Corinna Sykora, Peter Hoffmann, Thomas Elßner, Markus Kostrzewa, Ralf Hoffmann 89

COR-AAD1-00002999
Bayer EX1008 (Part 6 of 9)

4.47 FLOCKTYPE®recIBDV/recIBV/recNDV – The new generation of poultry virological ELISAs
Daniela Trepnau, Claudia Engemann, Katja Höschler, Roland Hackl, Michael Hess, Thorsten Arnold, Johannes-Joachim Arnold, Vikram N. Vakharia, Jörg Gabert, Jörg Lehmann 90

4.48 Novel protein microarrays for detection of posttranslational modification activities
Larissa Vasilets, Jörg Nerkamp, Carsten Voigt, Michael Braun 91

4.49 Lipid modifications of a Ras peptide lead to alteration of bilayer packing and softness as detected by 2H solid-state NMR
Alexander Vogel, Guido Reuther, Catherine Katzka, Herbert Waldmann, Klaus Arnold, Michael F. Brown, Daniel Huster 92

4.50 Characterization of the molecular distribution of bovine Tau protein with respect to its posttranslational modifications
Daniela Volke, Peter Hoffmann, Ralf Hoffmann 93

4.51 Monitoring of biotechnological processes by sodium dodecyl sulfate-polyacrylamide gel electrophoresis (SDS-PAGE)
Patrick Wunderlich, Ina Schulze, Melanie Nickel, Katrin Emmerling, Dirk Mischke, Ullrich Pigla, Rüdiger Laub 94

5 MOLECULAR MEDICINE AND THERAPEUTICS 97

5.1 A candidate gene association study in rheumatoid arthritis, strategies for gene and polymorphism selection and an application of the GENOLINK™ genotyping system
Peter Ahnert 98

5.2 Gabapentin-lactam failed to prevent rotenone-induced cell death in human neuroblastoma cells
Clemens Allgaier, Julia Kochen, Susana Garcia de Arriba, Ester Verdaguer 99

5.3 The role of β-catenin mutations and expression of glutamine synthetase in the development of hepatocellular carcinomas
Madeleine Austinat, Frank Gaunitz, Andrea Tannapfel, Rolf Gebhardt 100

COR-AAD1-00003000
Bayer EX1008 (Part 6 of 9)

5.4 *In situ* cytokine profiling of UVB-exposed human skin by combination of dermal microdialysis and protein microarrays
Marco Averbeck, Simone Beilharz, Matthias Bauer, Carl Gebhardt, Friederike Kauer, Ursula Voith, Jonathan Sleeman, Jan C. Simon, Christian Termeer 101

5.5 Large scale production of Taxol® from biosynthetical precursors by enzymatic semisynthesis
Martin Becker, Klaus Häupke, Jürgen Hensel, Daria Rybakova, Till Hornbogen, Rainer Zocher, Christian Pflieger, Doreen Liesicki, Dieter Frense, Gerald Lauckner 102

5.6 Depot-specific differences in adipocyte biology and adipose tissue gene expression-parallel regulation in humans and mice
Janin Berndt, Susan Kralisch, Mathias Fasshauer, Ralf Paschke, Michael Stumvoll, Ronald Kahn, Matthias Blüher 103

5.7 A novel approach to identify cellular target proteins of quercetin in human cells
Markus Böhl, Herwig O. Gutzeit 104

5.8 DNAzymes designed to inhibit prothrombin gene expression are outperformed by an antisense oligodeoxynucleotide
Markus Böhl, Bernd Schwenzer 105

5.9 Bioreactor "FiberReact" – The complete solution
Klaus Breese, Tanja Bloß 106

5.10 Synthesis of novel 4-phenylhydrazinopyrazolo[3,4-*d*]pyrimidines as ligands for the human A_{2A} adenosine receptor
Detlef Briel, Richard Aurich, Klaus Unverferth, Ute Egerland 107

5.11 Production and characterization of monoclonal antibodies against the nucleocapsid protein of Severe Acute Respiratory Syndrome-associated Coronavirus (SARS-CoV)
Bianca Bußmann, Sven Reiche, Lotta H. Jakob, Jan M. Braun, Christian Jassoy 108

5.12 Gene silencing in acute and persistent measles virus infection
Claire Fabian, Ute G. Brinckmann, Uwe G. Liebert 109

5.13 Reduction of VEGF gene expression by antisense oligonucleotides in bladder and breast cancer cells
Yvonne Förster, Axel Meye, Sabine Krause, Bernd Schwenzer 110

5.14 Antisense-mediated inhibition of tissue factor expression in different tumor cell lines
Yvonne Förster, Bernd Schwenzer 111

5.15 Highway for light – Müller cells as living optical fibers
Kristian Franze, Jens Grosche, Serguei N. Skatchkov, Stefan Schinkinger, Ortrud Uckermann, Kort Travis, Andreas Reichenbach, Jochen Guck 112

5.16 Phospholipid metabolism detected by ^{31}P NMR spectroscopy and MALDI-TOF mass spectrometry
Beate Fuchs, Jürgen Schiller, Klaus Arnold 113

5.17 Mechanisms of CD44 shedding in human melanoma cells – Relevance for tumor progression and target for therapeutic intervention
Carl Gebhardt, Friederike Kauer, Marco Averbeck, Verena Voelcker, Anja Saalbach, Ulf Anderegg, Jan C. Simon 114

5.18 Tauopathies' relation to axonal transport
Jens Gerdelmann, Josef A. Käs, Thomas Arendt 115

5.19 Glial cells from human retinas produce CXCL8 and express CXCR1 and CXCR2 receptors
Iwona Malgorzata Goczalik, Maik Raap, Michael Weick, Andreas Reichenbach, Mike Francke 116

5.20 Morphometrical investigations on different regions of the newborn skin
Sabine Göllnitz, Carolin Kunz, Bekele Assegedech, Dieter Reißig, Friedrich Keller 117

5.21 Experimentally induced rat brain cholinergic deficiency as a suitable tool to evaluate new radioligands for the vesicular acetylcholine transporter (VAChT) – Immunohistochemical evidence of VAChT loss after immunolesion
Udo Großmann, Wolfgang Härtig, Dietlind Sorger, Elena Kouznetsova, Reinhard Schliebs, Matthias Scheunemann, Jörg Steinbach, Osama Sabri 118

5.22 Extended tropism of HIV vectors expressing two different envelope glycoproteins
Ferenc Harmos, Theresa Möllmer, Doreen Milius, Katrin Bräutigam, Heike Tartler, Christian Jassoy 119

5.23 Expression of glutamatergic and muscarinic receptors in organotypic brain slice cultures of Munc13 knock-out mice
Maike Hartlage-Rübsamen, Kerstin Reim, Nils Brose, Steffen Roßner 120

5.24 Phenotype-dependent differential vulnerability to oxidative stress in cholinergic SN56 cells
Katrin Heinitz, J. Regino Perez-Polo, Reinhard Schliebs 121

5.25 Different vulnerability to oxidative stress in nondifferentiated and differentiated cholinergic SN56 cells
Katrin Heinitz, Reinhard Schliebs 122

5.26 Pathological changes caused by copper overload in the livers of the Wilson disease gene knock-out mice
Dominik Huster, Milton J. Finegold, Scott M. Vanderwerf, Karel Caca, Svetlana Lutsenko 123

5.27 Postnatal development of glial aquaporin and K^+ channel expression in the rat retina
Ianors Iandiev, Thomas Pannicke, Bernd Biedermann, Andreas Reichenbach, Andreas Bringmann, Peter Wiedemann 124

5.28 Detection of novel polyomaviruses by nested broad-spectrum PCR
Reimar Johne, Dirk Enderlein, Hermann Nieper, Hermann Müller 125

5.29 Atrial natriuretic peptide (ANP) inhibits osmotic Müller cell swelling in the postischemic retina of the rat
Folke Kalisch, Ortrud Uckermann, Peter Wiedemann, Andreas Reichenbach, Andreas Bringmann 126

5.30 *Borrelia burgdorferi* dissemination in the host – Comparison of the infection after intradermal and intravenous injection in mice
Jens Knauer, Reinhard K. Straubinger 127

5.31 Expression of ubiquitous phosphofructo-2-kinase/fructose-2,6-bisphosphatase in glioma cell lines
Kristin Köllner, Renate Keßler, Klaus Eschrich 128

5.32 Developmental and amyloid plaque-related changes in cerebral cortical capillaries in transgenic Tg2576 Alzheimer mice
Elena Kouznetsova, Dietlind Sorger, Osama Sabri, Jörg Steinbach, Matthias Scheunemann, Reinhard Schliebs 129

5.33 Antisense-mediated telomerase inhibition enhances the cytotoxic effects of chemotherapeutic drugs in human bladder cancer cell lines
Kai Krämer, Susanne Füssel, Uta Schmidt, Mathias Kotzsch, Manfred P. Wirth, Axel Meye 130

5.34 Proteomics reveals alterations in thyroglobulin expression and in the H_2O_2 detoxifying system in cold thyroid nodules
Kerstin Krause 131

5.35 Introducing IZKF Core facility DNA technologies
Knut Krohn, Petra Süptitz, Birgit Thiele, Kathleen Stein 132

5.36 Inhibition of C13orf19 mRNA expression by siRNA in prostate cancer cells
Doreen Kunze, Uta Schmidt, Susanne Füssel, Axel Meye, Manfred P. Wirth 133

5.37 Addition of rituximab to a CHOP-like regimen improves outcome of all patients with low risk diffuse large B-cell lymphoma (DLBCL)
Markus Löffler, Evelyn Kuhnt, Christina Rogalski, Michael Pfreundschuh 134

5.38 Keratinocyte-derived dranulocyte-macrophage colony stimulating factor accelerates wound healing in a transgenic mouse model
Amrit Mann, Kerstin Niekisch, Manfred Blessing 135

5.39 Cellular localisation of iron in the *substantia nigra* of an adult rat brain
Christoph Meinecke, Markus Morawski, Tilo Reinert, Thomas Arendt, Tilman Butz 136

COR-AAD1-00003004
Bayer EX1008 (Part 6 of 9)

5.40 Quantitative assessment of the cerebral α4β2 nicotinic acetylcholine receptors (α4β2 nAChR) in Parkinson's disease (PD) – A PET study using 2-[18F]F-A-85380 (2-FA)
Philipp Meyer, Kai Kendziorra, Henryk Barthel, Swen Hesse, Georg A. Becker, Dietlind Sorger, Andreas Schildan, Marianne Patt, Anita Seese, Thomas Lincke, Gudrun Wagenknecht, Donald Lobsien, Florian Wegner, Peter Brust, Jörg Steinbach, Claus Zimmer, Johannes Schwarz, Osama Sabri 137

5.41 Specific binding of 2-[18F]F-A-85380 (2-FA) on α4β2 nicotinic acetylcholine receptors (α4β2 nAChR) in the cerebral white matter (WM) in patients with Parkinson's disease (PD) and Alzheimer's disease (AD) – Demonstration by PET and camparison with diffusion tenso MSI (DTI)
Philipp Meyer, Kai Kendziorra, Donald Lobsien, Swen Hesse, Henryk Barthel, Georg A. Becker, Andreas Schildan, Marianne Patt, Dietlind Sorger, Anita Seese, Thomas Lincke, Annette Förschler, Florian Wegner, Peter Brust, Jörg Steinbach, Herman-Josef Gertz, Johannes Schwarz, Claus Zimmer, Osama Sabri 138

5.42 New targets for novel immunotherapeutic strategies based on natural regulatory T cells
Dirk Mischke, Sunna Hauschildt, Frank Emmrich, Ullrich Pigla, Rüdiger Laub 139

5.43 Parkinson's disease – A possible link between accumulation of iron and loss of perineuronal nets in the *substantia nigra*
Markus Morawski, Christoph Meinecke, Tilo Reinert, Anne C. Dörffel, Tilman Butz, Gert Brückner, Thomas Arendt 140

5.44 LSC as powerful tool for the analysis of DNA content in neurons
Birgit Mosch, Dominik Lenz, Attila Tarnok, Thomas Arendt 141

5.45 The role of antiinflammatory cytokines in cryptococcosis
Uwe Müller, Petra Krumbholz, Werner Stenzel, Gabriele Köhler, Melanie Kleinschek, Christoph Werner, Gesine Hansen, Manfred Blessing, Reinhard K. Straubinger, Frank Brombacher, Gottfried Alber 142

5.46 Structural alterations of the bladder wall in idiopathic urge incontinence and interstitial cystitis
Jochen Neuhaus, Thilo Schwalenberg, Lars-Christian Horn, Jens-Uwe Stolzenburg 143

5.47 Development of novel calcitonin derived carrier peptides with improved metabolic stability
Ines Neundorf, Robert Rennert, Annette G. Beck-Sickinger 144

5.48 N-methyl-D-aspartate (NMDA) receptor subunits in human and *Bennett* rat dorsal root ganglia – An immunohistochemical study
Vera Ogunlade, Ralf Schober, Stefan Grimm, Clemens Allgaier 145

5.49 Identification of P2Y receptor subtypes in human Müller glial cells
Thomas Pannicke, Julia E. Fries, Iwona Goczalik, Mike Francke, Thomas H. Wheeler-Schilling, Konrad Kohler, Sebastian Wolf, Peter Wiedemann, Andreas Bringmann, Andreas Reichenbach 146

5.50 Norchloro-fluorohomoepibatidin – PET evaluation of tracer properties in pigs
Jörg Thomas Patt, Winnie Deuther Conrad, Peter Brust, Marianne Patt, Osama Sabri, Jörg Steinbach 147

5.51 Is there an interaction of the adaptor proteins FE65 and Mint3 with MAP-tau?
Ellen Ramminger, Max Holzer, Thomas Arendt 148

5.52 Behavioural effects of the antiaggregatory therapeutic compound clopidogrel (Plavix®; Iscover®)
Ralph Regenthal, Frank Baumann, Cornelius Donat, Christian Gachet, Peter Illes, Ute Krügel 149

5.53 Brain prolyl endopeptidase expression in aging, APP transgenic mice and Alzheimer's disease
Steffen Roßner, Ingo Schulz, Ulrike Zeitschel, Reinhard Schliebs, Volker Bigl, Hans-Ulrich Demuth 150

5.54 Active cardiomyocytes on collagen gels for biohybrid systems
Markus Rüffer, Randy Kurz, Winnie Weigel, Andrée Rothermel, Jürgen Trzewik, Peter Linder, Gerhard Artmann, Andrea A. Robitzki 151

5.55 Molecular genetic diagnosis of susceptibility to malignant hyperthermia
Henrik Rüffert, Markus Wehner, Kerstin Krist, Ursula G. Froster, Derk Olthoff 152

5.56 Variability of the mitochondrial genome in cancer
Ingo Schäfer, Alexandra Kneissl, Christian Kukat, Peter Seibel 153

5.57 Interaction of interleukin-1β with muscarinic acetylcholine receptor-mediated signaling cascade in cholinergically differentiated SH-SY5Y cells
Reinhard Schliebs, Kristin Heidel, Jenny Apelt 154

5.58 Cell cycle regulatory proteins in the adult mouse neocortex
Stefanie Schmetsdorf, Ulrich Gärtner, Thomas Arendt 155

5.59 Advanced glycation endproducts activate mitogenic signal transduction pathways towards neuronal cell cycle re-entry
Angela Schmidt, Thomas Arendt, Gerald Münch 156

5.60 Neuronal activation of Ras regulates synapse formation and synaptic vesicle docking
Gudrun Seeger, Ulrich Gärtner, Thomas Arendt 157

5.61 Neuropeptide Y and the selective Y_1 receptor agonist [F7, P34] pNPY inhibit the glutamatergic synaptic transmission on cortical neurons
Kathrin Sichardt, Zacherie Vissiennon, Annette G. Beck-Sickinger, Karen Nieber 158

5.62 Flow cytometry in Alzheimer's disease diagnostics
Jens Stieler, Markus Kiefer, Thomas Arendt 159

5.63 Osmotic glial cell swelling in the rat retina is inhibited by triamcinolone acetonide
Ortrud Uckermann, Franziska Kutzera, Antje Wolf, Ianors Iandiev, Thomas Pannicke, Andreas Reichenbach, Sebastian Wolf, Peter Wiedemann, Andreas Bringmann 160

5.64 The influence of neuropeptide Y and Y_1 receptor antagonist BIBP3226 on MCF-7 tumor spheroids
Winnie Weigel, Andrée Rothermel, Markus Rüffer, Randy Kurz, Heinz-Georg Jahnke, Levin Böhlig, Annette G. Beck-Sickinger, Andrea A. Robitzki 161

5.65 Protective effects of prolyl endopeptidase inhibitors in astrocytoma cell lines and rat primary astrocytes
Ulrike Zeitschel, Susanne Rudzok, Ingo Schulz, Steffen Roßner, Hans-Ulrich Demuth 162

6 BIOMEDICAL AND CELL ENGINEERING 165

6.1 Optimisation of hepatocyte spheroid culture for application in bioartificial liver support systems
Matthias Funke, Doreen Beck, Christine Schulz, Jan-Michael Heinrich, Augustinus Bader 166

6.2 Interaction of signaling pathways during capacitation of human spermatozoa
Sonja Grunewald, Uwe Paasch, Thomas Baumann, Christian Kriegel, Hans-Jürgen Glander 167

6.3 Tissue engineered scaffolds for cartilage repair
Marcus Haberhauer, Andrea Deiwick, Augustinus Bader 168

6.4 Effects of surface coatings using bone sialoprotein, collagen, and fibronectin on cells derived from human maxillar bone
Heidegard Hilbig, Raik Rupietta, Hans-Ludwig Graf, Stefan Thalhammer, Stefan Strasser, Franz Paul Armbruster 169

6.5 Human retinal pigment epithelial cells produce and respond to placenta growth factor
Margrit Hollborn, Solveig Tenckhoff, Peter Wiedemann, Leon Kohen, Andreas Bringmann 170

6.6 Investigation of RGD-oligonucleotide conjugates with respect to their hybridization with anodically entrapped oligonucleotides (ON) on titanium alloys and their binding ability to integrines on osteoblasts
Ina Israel, Jan Michael, René Beutner, Ute Hempel, Hartmut Worch, Dieter Scharnweber, Bernd Schwenzer 171

6.7 Destruction of endogenous mtDNA – Establishing a novel method utilising a restriction endonuclease
Alexandra Kneissl, Christian Kukat, Ingo Schäfer, Peter Seibel 172

6.8 Evidence for abnormal iodination of thyroglobulin in cold thyroid nodules
Kerstin Krause, Stefan Karger, Marie-Christine Many, Sylvie Poncin, Ralf Paschke, Dagmar Führer 173

6.9 Cardiomyocytes beat for microelectrode arrays: the use of electrogenic properties for functional monitoring of autoimmune antibodies in sera of preeclamptic patients
Randy Kurz, Andrée Rothermel, Markus Rüffer, Winnie Weigel, Heinz-Georg Jahnke, Holger Stephan, Andrea A. Robitzki 174

6.10 Comparison of entrapped strategies of hepatocytes culture
Aldo Leal-Egana, Jan-Michael Heinrich, Augustinus Bader 175

6.11 Interaction of nucleic acids with titanium alloy surfaces for improved immobilization and hybridization
Jan Michael, René Beutner, Ina Israel, Hartmut Worch, Dieter Scharnweber, Bernd Schwenzer 176

6.12 Engineering of three dimensional mammalian retinal spheres by rotation cultures
Andrée Rothermel, Thomas Biedermann, Winnie Weigel, Randy Kurz, Markus Rüffer, Heinz-Georg Jahnke, Andrea A. Robitzki 177

6.13 Bioreactor technologies for culturing of skin substitutes
Thomas Rupf, Katrin Lorenz, Jürgen Salvetter, Augustinus Bader 178

6.14 Peptide mediated DNA import into mitochondria
Ingo Schäfer, Alexandra Kneissl, Christian Kukat, Martina Seibel 179

6.15 *In vitro* regeneration of liver cells
Christine Schulz, Jan-Michael Heinrich, Augustinus Bader 180

6.16 Solid-state NMR spectroscopy on bone implants
Jessica Schulz, Ina Khalaf, Mathias Pretzsch, Göran Zernia, Andrea Deiwick, Alexander Wild, Augustinus Bader, Daniel Huster 181

COR-AAD1-00003009
Bayer EX1008 (Part 6 of 9)

6.17 Novel bioreactor for simultaneous stimulation and cultivation of 3-dimensional cell constructs
Ronny Schulz, Andrea Deiwick, Nico Wüstneck, Christian Müller, Augustinus Bader 182

6.18 Automation of the 3D *in vitro* pannus-model for rheumatoid arthritis with the CyBi-Disk workstation
Anja Skodda, Simone Fuchs, Jochen Ringe, Mehdi Yahyawi, Ingrid Schmid, Peter Götz, Michael Sittinger 183

6.19 Aquaporin expression in the retina of the rat
Solveig Tenckhoff, Ianors Iandiev, Andreas Reichenbach, Peter Wiedemann, Andreas Bringmann 184

6.20 Effect of oxygen stress on the hepatocytes metabolic functions *in vitro*
Susanne Trettner, Jan-Michael Heinrich, Augustinus Bader 185

6.21 Behaviour of cells cultured on microstructured titanium surfaces
Hartwig Wolburg, Claus Burkhardt, Dieter Kern, Jochen Seebach, Friederike Pfeiffer 186

6.22 Investigation of the dynamics of the macromolecules in articular and tissue engineered cartilage by NMR spectroscopy
Göran Zernia, Stephanie Höhle, Ronny Schulz, Matthias Zscharnack, Augustinus Bader, Jürgen Schiller, Klaus Arnold, Daniel Huster 187

7 NANOBIOTECHNOLOGY AND NANOELECTRONICS 189

7.1 Protrusion forces driving rapidly translocating cells
Claudia Brunner, Michael Gögler, Allen Ehrlicher, Bernd Kohlstrunk, Detlef Knebel, Josef A. Käs 190

7.2 Lipophilic nucleic acids as building blocks for highly functional membrane surfaces
Andreas Bunge, Holger A. Scheidt, Wolfgang Flasche, Oliver Kaczmarek, Andreas Herrmann, Jürgen Liebscher, Daniel Huster 191

COR-AAD1-00003010
Bayer EX1008 (Part 6 of 9)

7.3 Binding specificity of peptides on semiconductor surfaces
Karsten Goede, Michael Bachmann, Wolfhard Janke, Marius Grundmann 192

7.4 Nano- and microstructured surfaces for selective and directed positioning of cells on electronic chips for laser-based microdissection and manipulation
Heinz-Georg Jahnke, Andrée Rothermel, Randy Kurz, Markus Rüffer, Winnie Weigel, Maik Schmidt, Andrea A. Robitzki 193

7.5 Chemosensitization of bladder cancer cells by VEGF antisense pre-treatment
Sabine Krause, Yvonne Förster, Kai Krämer, Susanne Füssel, Matthias Kotzsch, Uta Schmidt, Manfred P. Wirth, Axel Meye, Bernd Schwenzer 194

7.6 Proton microscopy – Quantitative trace element analysis with sub-micron spatial resolution
Tilo Reinert, Daniel Spemann, Markus Morawski, Thomas Arendt, Tilman Butz 195

7.7 Investigation of DNA binding proteins from the hyperthermophile *Sulfolobus acidocaldarius*
Mathias Salomo, Kati Kegler, Marc Struhalla, Jörg Reinmuth, Wiktor Skokov, Friedrich Kremer 196

7.8 Investigation of the elastic properties of single DNA molecules
Mathias Salomo, Kati Kegler, Marc Struhalla, Jörg Reinmuth, Wiktor Skokov, Friedrich Kremer 197

7.9 Release of thioflavins from nanoparticles targeting fibrillar β-amyloid in transgenic mice
Thomas Siegemund, Bernd-R. Paulke, Herbert Schmiedel, Jens Grosche, Anke Hoffmann, Tibor Harkany, Heikki Tanila, Johannes Kacza, Wolfgang Härtig 198

8 BIOINFORMATICS 201

8.1 Multiple Genome Rearrangement with conserved intervals
Matthias Bernt, Daniel Merkle, Martin Middendorf 202

COR-AAD1-00003011
Bayer EX1008 (Part 6 of 9)

8.2 Bio-Imaging platform LabImaging – A tool to develop software for biological, pharmaceutical and medical research and clinical diagnostics
Olaf Brenn 203

8.3 Identifying targets of flavonoids by virtual docking studies
Robert Günther, Rolf Gebhardt, Hans-Jörg Hofmann 204

8.4 On the potential role of biomechanics in the growth of tumors *in vitro*
Stefan Höhme, Dirk Drasdo 205

8.5 Progressive multiple sequence alignments from triplets
Matthias Kruspe, Peter F. Stadler 206

8.6 Non-coding RNAs in Ciona intestinalis
Kristin Missal, Dominic Rose, Peter F. Stadler 207

8.7 From phylogenetic footprinting to the evolution of regulatory elements
Sonja J. Prohaska, Claudia Fried, Burkhard Morgenstern, Gunter P. Wagner, Peter F. Stadler 208

8.8 Functional adaptations of dendrites of pyramidal neurons in p21H-rasVal12 transgenic mice
Andreas Schierwagen, Alexander Schubert, Alán Alpár, Ulrich Gärtner, Thomas Arendt 209

8.9 Fuzzy dynamic labeling in learning vector quantization for automatic classification of mass spectrometric data in clinical research
Frank-Michael Schleif, Barbara Hammer, Jens Decker, Ute Clauss, Thomas Villmann 210

8.10 Multiple alignments of partially coding sequences
Roman R. Stocsits, Ivo L. Hofacker, Claudia Fried, Peter F. Stadler 211

8.11 Coarse-grained polymer models – On-Lattice vs. Off-Lattice
Thomas Vogel, Michael Bachmann, Wolfhard Janke 212

CENTER FOR BIOTECHNOLOGY AND BIOMEDICINE **215**

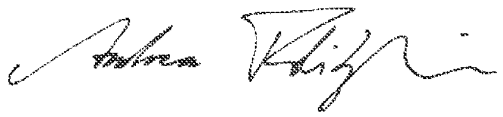
Center for Biotechnology and Biomedicine (BBZ) – An overview 216

INDEX **221**

COR-AAD1-00003012
Bayer EX1008 (Part 6 of 9)

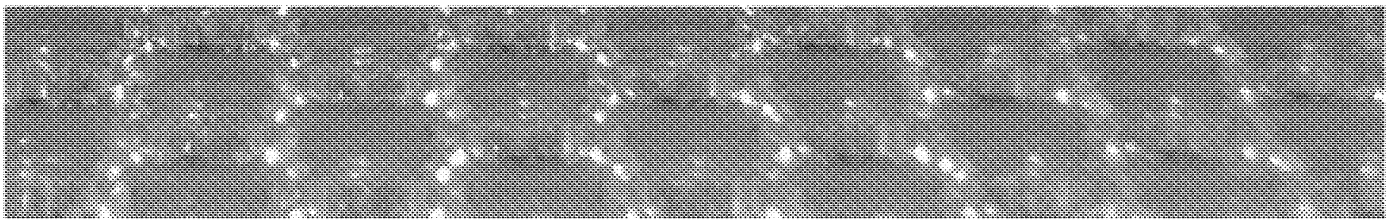
FOREWORD

The Center for Biotechnology and Biomedicine (BBZ) of the University of Leipzig is located in the BIO CITY LEIPZIG complex. Over the past few years it has established itself as partner for R&D in the fields of Protein Engineering & Bioanalytics, Molecular Medicine & Therapeutics, Biomedical & Cell Engineering as well as Nanobiotechnology & Nanoelectronics. The research center is structured in an inter- and transdisciplinal way and brings together molecular and cell biologists, pharmacologists, health professionals, (bio)chemists, (bio)physicists and engineers. At the crossways of, for example, biomedicine and biotechnology as well as micro- and nanotechnology, new modules for automation, parallelization and synchronization of analytical processes in Life Sciences are being developed. The focus is set on applied and industry-oriented bio-molecular research and development and on creating biomedical and biotechnological networks that can supply innovative approaches. The center cooperates with the most renowned national and international scientific and industrial research institutions in France and Great Britain (such as the Institute of Nanotechnology Cambridge, Nexus – European Company Network). Synergies, complementary R&D areas and expertise aiming at strengthening the European position can thus be identified and exploited: in fact, the BBZ offers services in areas such as bioanalytics, protein structure analysis as well as functional proteomics or metabolics for Pharmaceutics & Life Sciences, and it is also involved in R&D projects related to (Ultra)-High-Throughput-Screening.
The 4th Biotechnology Symposium demonstrates to which degree the alliance BBZ Leipzig, its industrial partners and research institutes are taking an active part in advancing international competition for innovative technologies.



Prof. Dr. Andrea A. Robitzki
Chair of the Center for Biotechnology and Biomedicine

1. PROTEIN ENGINEERING AND BIOANALYTICS



PRESENTATIONS

1.1 Creating novel proteins for therapeutic applications

Rainer Rudolph, Hauke Lilie, Ulrike Fiedler

Recombinant proteins are by now widely used for the treatment of various diseases. For some therapeutic applications (e.g. cancer treatment) natural proteins offer only limited strategies for therapeutic intervention. For these applications, we designed novel modular proteins. We used polyionic adaptor peptides containing cysteine residues as highly specific heterodimerization motifs. Fusion of these polyionic peptides to both a protein module recognizing specific cell surface epitopes, and another module inducing cell death resulted in disulfide-bonded immunotoxins, which possess a very high and specific cytotoxicity.

The polyionic adaptor motif was also used to specifically modify virus like particles. As modular delivery systems, composed of a specific recognition domain, *in vitro* assembled capsids, and the therapeutic cargo (e. g. DNA) specific cell transformation could be achieved.

Finally, novel binding molecules were created. For this purpose, two very stable human proteins, γ-crystallin from the eye lens, and ubiquitin were randomized in a solvent-exposed beta-sheet area. Applying suitable display and screening techniques specifically binding molecules can be isolated for both low molecular weight substances (e.g. estradiol) and globular proteins.

Prof. Dr. Rainer Rudolph

Martin-Luther-University Halle-Wittenberg

Faculty of Mathematics, Natural Sciences and Technology
Institute of Biotechnology
Protein Technology

E-Mail: rudolph@biochemtech.uni-halle.de
www.biochemtech.uni-halle.de/proteintech/

COR-AAD1-00003017
Bayer EX1008 (Part 6 of 9)

1.2 Dark matter of the genome – The human genome contains thousands of non-coding RNAs

Peter F. Stadler

In contrast to the fairly reliable and complete annotation of the protein coding genes in the human genome, comparable information is lacking for non-coding RNAs. A computational screen of vertebrate genomes evaluating sequence conservation, secondary structure conservation, and thermodynamic stability of the putative RNA structures predicts more than 30,000 structured RNAs in the human genome, almost 1,000 of which are conserved across all vertebrates. Roughly a third is found in introns of known genes, a sixth are potential regulatory elements in untranslated regions, about half are located far away of any known gene. Only a small fraction of these sequences has been described previously. EST data demonstrate, however, that the majority of them is at least transcribed. We estimate, therefore, that the human genome contains at least as many RNA genes as protein coding genes.

Prof. Dr. Peter F. Stadler

Universität Leipzig

Faculty of Mathematics and Computer Science
Institute of Computer Science
Bioinformatics

E-Mail: studla@bioinf.uni-leipzig.de
www.bioinf.uni-leipzig.de

COR-AAD1-00003018
Bayer EX1008 (Part 6 of 9)

1.3 Functional annotation of high-throughput screening data with structural protein interactions and textmining

Michael Schröder

Currently high-throughput screening with gene expression and RNAi generate large amounts of data, which need to be annotated for interpretation. I will discuss two tools to support this task by identifying potential interaction partners based on structural domain-domain interactions and by textmining using hierarchical vocabularies such as the GeneOntology. The approaches will be illustrated with example screens identifying overexpressed genes during osteoclast differentiation.

Prof. Dr. Michael Schröder

Technische Universität Dresden

Biotechnological Centre (Biotec)
Professorship for Bioinformatics

E-Mail: ms@biotec.tu-dresden.de
www.biotec.tu-dresden.de

COR-AAD1-00003019
Bayer EX1008 (Part 6 of 9)

1.4 TRANSIL® technology – Immobilized proteins for innovative assays and for ADME prediction in drug discovery

Joachim Nöller

NIMBUS' TRANSIL® platform is a proprietary bead based assay technology allowing for the biofunctionalization of solid supports. Based on this platform, we are providing bead based assays for important stages in drug discovery.

About 40 % of late-stage failures are associated with poor pharmacokinetic properties leading to a huge loss in time and money. Early profiling of drug like properties provides important information to screen out insoluble, poor absorbing and toxic compounds.

As one contribution of NIMBUS to this bottleneck in drug discovery the TRANSIL® technology allows the functional immobilization of serum proteins (e.g. Human Serum Albumin) on solid supports. After surface passivation, protein molecules are covalently attached on the bead surface taking care that important pharmacologically binding sites are freely accessible and therefore suitable for the determination of the unspecific binding to serum proteins, as an important ADME related parameter. This parameter for a compound is used in combination with the membrane affinity and the molecular weight for the prediction ADME parameters like volume of distribution or plasma organ partitioning coefficients.

Furthermore technology enables also binding assays for transmembrane proteins which will be described for the measuring the binding of AGEs (Advanced Glycation Endproducts) to the plasma membrane of Caco-2 cells.

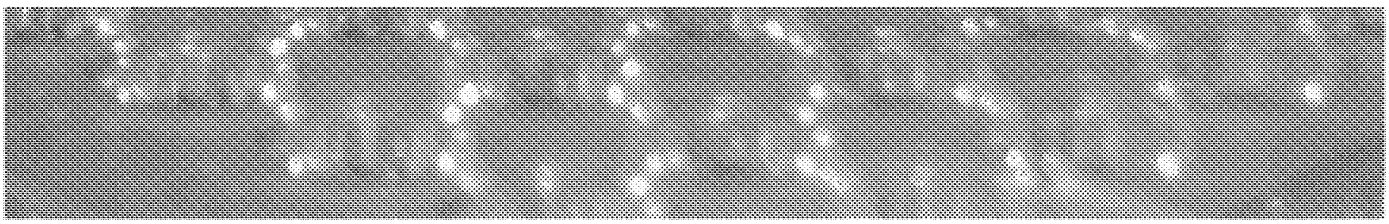
Dr. Joachim Nöller

Nimbus Biotechnologie GmbH

E-Mail: jnoeller@nimbus-biotech.com
www.nimbus-biotech.com

COR-AAD1-00003020
Bayer EX1008 (Part 6 of 9)

2. MOLECULAR MEDICINE AND THERAPEUTICS



PRESENTATIONS

Bayer EX1008 (Part 6 of 9)

2.1 Tumor targeting

Dario Neri

One avenue towards the development of more selective, better anti-cancer drugs consists in the targeted delivery of bioactive molecules (drugs, cytokines, procoagulant factors, photosensitizers, radionuclides, etc.) to the tumor environment by means of binding molecules (e.g. human antibodies) specific for tumor-associated markers.

Angiogenesis, i.e. the proliferation of new blood vessels from pre-existing ones, is an underlying process in many human diseases, including cancer, blinding ocular disorders and rheumatoid arthritis. The ability to selectively target and occlude neovasculature will be potentially useful in diagnosis and treatment of angiogenesis-related diseases.

A good-quality marker for both tumoural and non-tumoural neovasculature is the extra-domain B (ED-B) of fibronectin, a sequence of 91 aminoacids that can be inserted into the fibronectin molecule by a mechanism of alternative splicing. Anti-EDB antibodies stain vascular structures in tumour sections and selectively target tumour neovasculature, as shown in tumour-bearing mice using infrared fluorescence and radioactive techniques. The ability of the radiolabeled anti-EDB antibody L19 to target tumors in patients with cancer has recently been demonstrated using scintigraphic detection methods. A number of derivatives of the L19 antibody (fusions to cytokines, pro-coagulant factors, photosensitizers, drugs, radionuclides, etc.) have been studied in animal models. The results obtained are of therapeutic relevance, since the ED-B domain of fibronectin, a naturally-occurring marker of angiogenesis identical in mouse and man, is expressed in the majority of aggressive solid tumours, but is undetectable in normal vessels and tissues.

In the last part of my presentation, I will show how we are using the *in vivo* biotinylation of tumor bearing mice by terminal perfusion, followed by proteomic analysis of tumor specimens and normal organs, for the discovery of novel tumor-associated vascular targets.

Prof. Dr. Dario Neri

Swiss Federal Institute of Technology Zurich

Department of Chemistry and Applied Biosciences
Institute of Pharmaceutical Sciences

E-Mail: neri@pharma.ethz.ch
www.pharma.ethz.ch

COR-AAD1-00003023
Bayer EX1008 (Part 6 of 9)

2.2 NAD$^+$-dependent regulatory processes on human monocytes/macrophages

Sunna Hauschildt

Human monocytes are capable of degrading extracellular NAD^+ to biologically active compounds and to use NAD^+ as a substrate for covalent protein modification. The reactions are catalyzed by CD38 and mono-ADP-ribosyltransferases (ARTs) resp. Furthermore NAD^+ causes a rapid elevation of $[Ca^{2+}]_i$ mediated by the influx of extracellular calcium. During differentiation of monocytes to macrophages by down-regulating CD38 expression the availability of NAD^+ to serve as a substrate for ARTs increases which in turn may account for macrophage specific functions. As membrane proteins oriented towards the extracellular compartment CD38 and ecto-ARTs represent good candidates for development of drugs which will be useful tools in understanding the action and biological functions of these proteins.

Prof. Dr. Sunna Hauschildt

Universität Leipzig

Faculty of Biosciences, Pharmacy and Psychology
Institute of Biology II
Immunbiology

E-Mail: shaus@rz.uni-leipzig.de
www.uni-leipzig.de/~biowiss/zoologie/

COR-AAD1-00003024
Bayer EX1008 (Part 6 of 9)

2.3 Diabesity – Molecules and mechanisms

Michael Stumvoll

Regulation of glycaemia and body weight represents a fundamental biological principle, and failure of the regulation underlies type 2 diabetes and obesity. A myriad of molecules is likely involved in the complex aetiology of "diabesity" and dissecting the relevance of a single represents a challenge. Translation of burgeoning new basic science findings into a physiological and clinical context calls for novel and imaginative clinical experimental tools. For the purpose of this review four molecules (adiponectin [APM1], stearoyl desaturase 1 [SCD1], insulin receptor substrate-1 [IRS1], peroxisome proliferator-activated receptor γ [PPARG]) or visfatin (PBEF1), each with a plausible role in the disease process, have been selected to illustrate the use of such techniques in humans. These include procedures as diverse as isotope dilution for turnover studies (e.g. glycerol turnover as a proxy for lipolysis), conventional and modified clamp procedures, association studies of functionally relevant SNPs in candidate genes (e.g. IRS-1 and PPARγ), multivariate correlational analyses (as with plasma adiponectin), magnetic resonance spectroscopy to quantify intra-tissue lipid deposition and regional fat distribution, gas chromatography to determine fatty acid patterns in selected lipid fractions as proxy for intrahepatic enzyme activity and mRNA expression studies in selected tissues. A concerted effort by scientists from many disciplines (genetics and cell biology, physiology and epidemiology) will be required to bridge the growing gap between basic scientific concepts of biological modifiers of glycaemia and what is truly relevant for human obesity and type 2 diabetes.

Prof. Dr. Michael Stumvoll

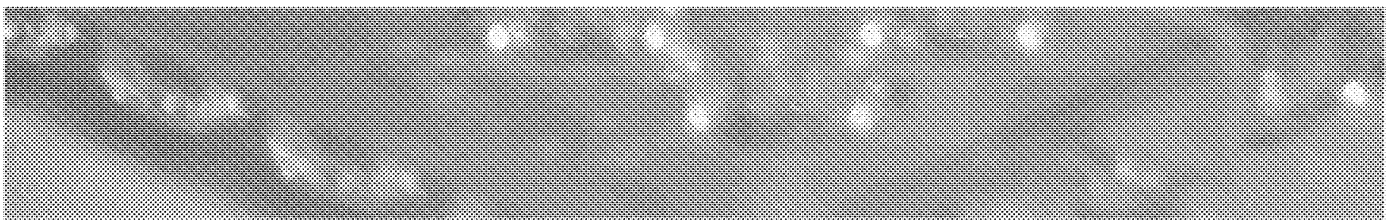
Universität Leipzig

University Hospital
Department of Internal Medicine III

E-Mail: michael.stumvoll@medizin.uni-leipzig.de
www.uni-leipzig.de/~innere/

COR-AAD1-00003025
Bayer EX1008 (Part 6 of 9)

3. BIOMEDICAL AND CELL ENGINEERING



PRESENTATIONS

COR-AAD1-00003028
Bayer EX1008 (Part 6 of 9)

3.1 Modeling cardiac electric signals – From ion channels to the ECG

Olaf Dössel

The electrocardiogramm ECG is a well-known diagnostic tool. The electrical signals that can be measured on the surface of the body originate from electrophysiological processes in the heart. The "sources" of these electric signals are the ion channels embedded into the membrane of the myocytes that open and close according to basic rules. These rules have been described mathematically first by Hodgkin and Huxley. Today the complete chain from the ion channels (nanometer scale) over the myocytes (micrometer scale) to a description of the tissue (millimeter scale) and ending with the ECG on the body surface (meter scale) can be described explicitly with mathematical models.

A large set of membrane proteins is taken into account today in order to describe the electrophysiology of isolated myocytes. A very detailed description of the electrophysiology of the heart is necessary for realistic modeling of excitation propagation. Knowing the bioelectric source distribution in the heart the time course of the body surface potential map BSPM can be calculated.

In future better therapeutic measures can be designed using computer models of the human heart. It will be possible to predict the effect of new drugs on the rhythm of the whole heart by knowing the effect on the ion channels. Optimized strategies for RF ablation can be found. Maybe also new electrode configurations and pulses for electric stimulation like they are used in a heart pacemaker or a defibrillator can be investigated.

Prof. Dr. Olaf Dössel

Universität Karlsruhe (TH)

Department of Electrical Engineering
and Information Technology
Institute of Biomedical Engineering

E-Mail: olaf.doessel@ibt.uni-karlsruhe.de
www.ibt.uni-karlsruhe.de

COR-AAD1-00003029
Bayer EX1008 (Part 6 of 9)

3.2 Generation of reliable diagnostics and effective vaccines by recombinant DNA technologies

Hermann Müller

The focus of research at the Institute for Virology is on basic science, applied science and diagnostics in the field of animal viruses and viral infections of animals. Viruses of various avian species are in the centre of these investigations. Among these are infectious bursal disease virus (IBDV) affecting developping lymphoid B cells in chickens, avian polyomaviruses such as budgerigar fledgling disease virus (BFDV)and goose hemorrhagic polyomavirus (GHPV) as well as avian circoviruses, e. g., psittacine beak and feather disease virus (BFDV) and pigeon circovirus (PiCV). To fight against these virus infections, some of which are of considerable economic importance, diagnostic tools and virus vaccines are developed by the application of the techniques of molecular biology. Some examples will be presented.

References

Zierenberg K., Raue R., Nieper H., Islam M. R., Eterradossi N., Toquin D., Müller H., Generation of serotype 1/serotype 2 viruses of the infectious bursal disease virus and their investigation in vitro and in vivo. Virus Res., 2004. 105: 23-34.

Oberländer Y., Generation and characterization of serotyp 1-/serotyp 2-recombinants of infectious bursal disease virus. PhD thesis, 2004. Universität Leipzig.

Johne R., Enderlein D., Nieper H., Müller H., Novel polyomavirus detected in the feces of a chimpanzee by nested broad-spectrum PCR, J. Virol., 2005. 79: 3883-87.

Johne R., Raue R., Grund C., Kaleta E. F., Müller H., Recombinant expression of a truncated capsid protein of beak and feather disease virus and its application in serologic tests. Avian Pathol., 2004. 33: 328.

Prof. Dr. Hermann Müller

Universität Leipzig

Faculty of Veterinary Medicine
Institute of Virology

E-Mail: virology@vetmed.uni-leipzig.de
www.vmf.uni-leipzig.de/ik/wvirologie/

COR-AAD1-00003030
Bayer EX1008 (Part 6 of 9)

3.3 Microstructuring of surfaces for life science

Klaus Zimmer, Thomas Rudolph, David Ruthe, Rico Böhme, Joachim Zajadacz, Bernd Rauschenbach

High throughput analysis sensing on cell level and one-way life science products call for microstructures, functional surfaces and eventually for microsystems. Microsystems technologies are able to meet these requirements after some adaptations and allow the fabrication of surface microstructures with defined properties. For instance the handling of minute quantities of liquid samples for analysis and agent development requires microfluidic solutions. Combining nano- and microstructures and chemical modification provide highly functionalised microstructures. Standard techniques of microsystems technologies for microstructuring and physical/chemical surface modification as well as modern processing techniques such as laser and e-beam writing, plasma and UV-engineering and replication techniques have been exploited to achieve appropriate surfaces and microstructures for life science applications.

After touching the principles of microstructuring some examples of laser micromachining of surfaces are presented. Especially the direct laser processing for etching of glass and polymers to achieve micotopographies or for chemical modified surface areas for functionalisation are considered. Different examples of microstructured surfaces for morphological investigations of cells, for modification of low cost sensors, for microfluidic systems, and for application of microspotting techniques are presented and first results of practical applications are discussed.

Dr. Klaus Zimmer

Leibniz Institute for Surface Modification

E-Mail: klaus.zimmer@iom-leipzig.de
www.iom-leipzig.de

COR-AAD1-00003031
Bayer EX1008 (Part 6 of 9)

3.4 Dopaminergic neurons from midbrain-derived neural stem cells

Sigrid C. Schwarz

Parkinson's disease (PD) is a chronic, progressive neurodegenerative movement disorder characterized by a continuous and rather selective loss of dopaminergic neurons in the *substantia nigra pars compacta* with subsequent striatal dopamine depletion. Since dopaminergic neurons are a rather small and well defined population of neurons in the brain, restorative strategies may be especially effective in PD. The use of embryonic midbrain tissue is difficult secondary to ethical and logistical problems as well variable efficacy.

We transplanted neural precursor cells (NPCs) and neuron-restricted precursor cells (nrPCs). When long-term expanded human midbrain derived NPCs or nrPCs were differentiated *in vitro,* they expressed specific markers of dopaminergic neurons and displayed neuronal characteristics including sodium currents and action potentials. Following transplantation, there was improvement of amphetamine induced rotational behaviour and survival of tyrosine-hydroxylase immunoreactive (TH-IR) cells within the graft four months after transplantation. Animals with more than 2,000 TH-IR cells in the graft showed reversal of rotational asymmetry. Four of five animals grafted with nrPCs showed functional recovery as well as minimal immune responses. Only animals that received NPCs without immunosuppression showed mild activation of astrocytes, microglia and macrophages. Histological analyses did not reveal any sign of tumor formation.

Human midbrain derived NPCs (preferably nrPCs) represent a tissue source for transplantation of homogenous and non-immunogenic cells potentially capable of reconstituting dopaminergic neurons *in vivo.*

Dr. Sigrid C. Schwarz

NeuroProgen GmbH

E-Mail: scschwarz@neuroprogen.de
www.neuroprogen.de

COR-AAD1-00003032
Bayer EX1008 (Part 6 of 9)

4. PROTEIN ENGINEERING AND BIOANALYTICS

POSTERS

4.1 Characterization of *B. burgdorferi* cyst formation

Samiya Al-Robaiy, Hassan Dihazi, Johannes Kacza, Johannes Seeger, Jürgen Schiller, Daniel Huster, Reinhard K. Straubinger

B. burgdorferi, the agent of Lyme borreliosis, has the ability to undergo morphological transformation from motile spirochetes to non-motile cystic forms in the presence of unfavourable conditions. However, little is known about cyst formation procedure.

We compared spirochetes and cysts induced under controlled conditions such as nutrient depletion or osmotic changes.

From the transmission electron microscopy it seems that cyst formation begins with membrane budding followed by spirochetal structures folding inside the pronounced budding membrane. The role of the periplasmic flagella involved in the motility and cell shape of *B. burgdorferi* was studied using a mutant lacking the major flagellar protein FlaB. Scanning electron microscopy showed that the induction of cyst formation was not affected in this mutant. Lipid analysis with MALDI demonstrated that the spirochetes and cysts contain the same lipid contents. Neither phosphatidylcholine (PC) nor phosphatidylglycerol (PG), the major phospholipids in *B. burgdorferi* which form the bilayer membrane of these cells were changed with structural transformation.

Protein profiling on western blots showed identical antigenic patterns for spirochetes and cysts with decreased expression intensities for cysts. However, an up-regulation of different low molecular proteins in the cysts was determined with SELDI.

Our results demonstrate that cyst formation is a process in which proteins as well as a physical rearrangement of the outer surface membrane are involved. Further analysis to identify the involved proteins is in progress.

Dr. Samiya Al-Robaiy

Universität Leipzig

Center for Biotechnology and Biomedicine (BBZ)
Junior Research Group "Molecular Medicine of Contagious Diseases"
and
Faculty of Veterinary Medicine
Institute of Immunology

E-Mail: robaiy@vetmed.uni-leipzig.de
www.uni-leipzig.de/~straub/

COR-AAD1-00003035
Bayer EX1008 (Part 6 of 9)

4.2 A different approach for cloning and purification of the 5S subunit of transcarboxylase multienzyme complex

Rakesh Kumar Bhat, Stefan Berger

Transcarboxylase (EC2.1.3.1) (TC) from *Propionibacterium shermanii* is a complex biotin-containing enzyme composed of 30 polypeptides of three different types. It is composed of six dimeric outer subunits associated with a central cylindrical hexameric subunit through 12 biotinyl subunits with three outer subunits on each face of the central hexamer. Each outer dimer is termed a 5S subunit, which is associated with two biotinyl subunits. The enzyme catalyzes a two-step reaction in which methylmalonyl-CoA and pyruvate form propionyl-CoA and oxalacetate, the 5S subunit specifically catalyzing one of these reactions. We report here our attempts for cloning, sequencing and expression of the monomer of the 5S subunit. The gene was identified by matching nucleotide sequences from the database available, isolated from authentic 5S peptides with the deduced sequence of an open reading frame present on a cloned *P. shermanii* genomic fragment. The cloned 5S gene encodes a protein of 519 amino acids, M, 57,793.

Initially we successfully cloned the gene into the pET 28a(+) vector. But there were problems while purification of the protein. After cleaving the His–Tag, the protein gets precipated and the cleavage was also not 100 %, which may give problems during NMR studies. Currently we tried to clone and purify the gene by a different strategy based on IMPACT-I system.

Rakesh Kumar Bhat

Universität Leipzig

Faculty of Chemistry and Mineralogy
Institute of Analytical Chemistry

E-Mail: bhat@chemie.uni-leipzig.de
www.uni-leipzig.de/~nmr/ANALYTIK/

COR-AAD1-00003036
Bayer EX1008 (Part 6 of 9)

4.3 Residue specific studies of NH exchange rates performed on ubiquitin

Torsten Brand, Garreth A. Morris, Eurico J. Cabrita, Hans-Jörg Hofmann, Stefan Berger

The aim of the present study was to establish a new method to invesigate NH exchange rates in proteins. These measurements are based on residue specific diffusion experiments and were demonstrated on human ubiquitin since it is a small protein (9 kDa, 76 residues) for which resonance assignment as well as NMR structures are available.

For NMR studies a 1.8 mM solution of uniformly ^{13}C,^{15}N-labelled ubiquitin in 90 % H_2O, 10 % D_2O was used. Experiments were carried out at 300 K on a Bruker Avance 700 spectrometer equipped with a cryo probe. In order to resolve most signals of the protein ^{1}H,^{15}N-DOSY-HSQC spectra were recorded. Diffusion Ordered Spectroscopy was used to obtain an apparent diffusion coefficient D for each separated signal.

Analysis of the apparent diffusion coefficients showed several "fast moving" NH protons. Subsequently, the exchange rates were derived directly from the decay data of the diffusion experiment by applying a model deduced from the assumption of two-site exchange with water and the "pure" diffusion coefficients of water and protein.

Molecular modelling and MD studies have been performed in an attempt to predict exchange rates from structural or dynamical features of ubiquitin. Several parameters have been checked with respect to their utility for such a prediction, including static parameters like NH bond order, partial charge at the nitrogen and accessibility of the NH protons as well as the dynamics of hydrogen bond breaking. Whereas none of the parameters examined so far yielded a strong correlation, attempts to use a weighted combination of these parameters are topic of current research.

Torsten Brand

Universität Leipzig

Faculty of Chemistry and Mineralogy
Institute of Analytical Chemistry

E-Mail: tbrand@rz.uni-leipzig.de
www.uni-leipzig.de/~nmr/ANALYTIK/

COR-AAD1-00003037
Bayer EX1008 (Part 6 of 9)

4.4 Developmental pattern of tau isoforms in rat brain

Torsten Bullmann, Max Holzer, Wolfgang Härtig, Nicolas Sergeant, Andre Delacourte, Rohan de Silva, Hiroshi Mori, Thomas Arendt

Aggregates of hyperphosphorylated microtubule associated protein tau are found in Alzheimer's disease and other neurodegenerative diseases called tauopathies. These aggregates differ in their tau isoform composition, phosphorylation of specific isoforms and filament confirmation as well as in the affected cell types and regional distribution of lesions in brain. Some studies demonstrated a link between regional variation in tau isoform expression and susceptibility to neurodegeneration. Therefore distribution of tau protein isoforms in adult rat brain and during development was studied using recently avaiable specific antibodies, western blotting and RT-PCR. Single cell RT-PCR in combination with Laser microdissection may be a useful tool to study tau mRNA splicing in human brain to clearify whether a subset of neurons posses a specific tau protein isoform pattern that renders them highly vulnerable to degeneration.

Torsten Bullmann

Universität Leipzig

Faculty of Medicine
Paul Flechsig Institute of Brain Research
Neuroanatomy

E-Mail: bullmann@rz.uni-leipzig.de
www.uni-leipzig.de/~pfi/

COR-AAD1-00003038
Bayer EX1008 (Part 6 of 9)

4.5 New structural and functional aspects of phosphofructo-1-kinase from *Pichia pastoris*

Anke Edelmann, Katrin Tanneberger, Jürgen Kirchberger, Jörg Bär, Torsten Schöneberg

The methylotrophic yeast *Pichia pastoris* is a highly efficient system for heterologous gene expression and of great interest in many biotechnological applications. Yeast growth and expression properties essentially depend on energy-providing pathways such as glycolysis. The phosphofructo-1-kinase (Pfk-1) is one of the key enzymes of glycolysis. By cloning the genes encoding the α- and β-subunits (about 100 kDa each), we could demonstrate that *P. pastoris* Pfk-1 (*Pp*Pfk-1) is a hetero-oligomer $\alpha_4\beta_4$). Surprisingly, a molecular weight of 975 kDa was determined for the native *Pp*Pfk-1. The unexpected higher molecular weight was due to a third protein component which was co-purified and partially sequenced by MALDI analyses. Based on these initial sequence data, the respective open reading frame (1,056 bp) and 2,070 bp of the 5' non-coding region were isolated. The polypeptide chain contains 351 amino acid residues and has a predicted molecular mass of 40.8 kDa. To investigate the relevance of this protein as *Pp*Pfk-1 subunit, we examined the formation of *Pp*Pfk-1 in *pfk*-deficient yeast strains. These findings provide further evidence that *Pp*Pfk-1 contains a third type of subunits, which is probably necessary for enzyme assembly and catalytic activity.

Dr. Anke Edelmann

Universität Leipzig

Faculty of Medicine
Institute of Biochemistry
Molecular Biochemistry

E-Mail: scha@medizin.uni-leipzig.de
www.uni-leipzig.de/~biochem/MolBiochem/MolBiochem.html

COR-AAD1-00003039
Bayer EX1008 (Part 6 of 9)

4.6 Recombinant expression and structure determination of phosphodiesterases

Roy Eylenstein, Nancy Kühn, Petra Schäfer, E. Bartholomeus Küttner, Susanne Moschütz, Norbert Sträter

PDEs catalyzing the hydrolysis of the 3'-5' phosphodiester bond of cyclic nucleotides (cAMP, cGMP) comprise a family of enzymes that modulate the immune response, inflammation, cell growth and many other functions. 11 families of PDEs have been described including multiple isoforms with varying selectivities for cAMP and/or cGMP. The isoforms are differentially expressed and regulated in different cell types, and they appear to modulate the location, substrate selectivity, kinetics, and response to activators or inhibitors of the enzyme. As essential regulators of cyclic nucleotide signalling, PDEs are recognized as important drug targets for the treatment of diseases such as heart failure, asthma and erectile dysfunction.

The aim of the current project is to develop expression constructs for the production of sufficient material for crystallization of full length PDEs and catalytic domains. The X-ray structures of these PDEs will allow for the rational design of specific inhibitors as therapeutics. 3D structures of the catalytic domains of PDE1, -3, -4, -5 and -9 are currently available.

For the expression of the catalytic domains we designed different truncations of PDEs to find good constructs for subsequent protein purification and crystallization. Expression in *E. coli* as well as in *P. pastoris* often yields insoluble products. To avoid the refolding processes of the proteins we also try to express the catalytic domains in an *E. coli* based cell-free *in vitro* system. This system allows for the simple modification of many expression parameters and hence it is maybe possible to directly produce soluble and active protein.

Roy Eylenstein

Universität Leipzig

Center for Biotechnology and Biomedicine (BBZ)
Professorship for Structural Analysis of Biopolymers
and
Faculty of Chemistry and Mineralogy

E-Mail: roy.eylenstein@bbz.uni-leipzig.de
www.uni-leipzig.de/~strater/

COR-AAD1-00003040
Bayer EX1008 (Part 6 of 9)

4.7 Site-directed mutagenesis in the substrate binding region of R-3-hydroxybutyrate dehydrogenase (3-HBDH)

Claudia Feller, Marlis Grunow

3-HBDH belongs to the family of short-chain dehydrogenases/reductases (SDR). At present, about 4,000 primary structures and 40 3D structures of the SDR family are annotated in sequence databases. The enzymes included in the SDR family span several EC classes, from oxidoreductases and lyases to isomerases, with NAD- or NADP-dependend oxidoreductases forming the majority. In this class, many enzymes of different substrate specificities are found acting on steroids, prostaglandins, aliphatic alcohols and xenobiotics.

The aim of our work was to gain an insight into the substrate binding mechanism of 3-HBDH. How does 3-HBDH interact with its small and hydrophilic substrate, knowing that substrates as well as coenzymes are bound in a hydrophobic substrate binding cleft, as seen by SDR structures? Because a crystal structure is not currently available, a three-dimensional model of 3-HBDH was build using known structures of five oxidoreductases as templates. Aspects of the model concerned with 3-hydroxybutyrate binding have been tested by site-directed mutagenesis of residues Gln91, His141, Lys192 and Gln193 to Ala and Lys149 to Ala and Arg. Because of their position in the substrate binding cleft of the model and their positive charge, these residues were the main candidates concidered to play a crucial role in the binding of 3-hydroxybutyrate. Enzyme variants have been characterized in terms of kinetic constants. The results obtained with enzymes mutated at positions 91, 141, 193 and in particular at Lys149 confirm the assumed interactions of these residues with the carboxylate group of the substrate.

Claudia Feller

Universität Leipzig

Faculty of Biosciences, Pharmacy and Psychology
Institute of Biochemistry
Biochemistry and Molecular Biology

E-Mail: cfeller@rz.uni-leipzig.de
www.biochemie.uni-leipzig.de/agmoerl/

COR-AAD1-00003041
Bayer EX1008 (Part 6 of 9)

4.8 Site-specific synthesis of Amadori-modified peptides on solid-phase

Andrej Frolov, David Singer, Ralf Hoffmann

Glycation of peptides and proteins is a slow chemical reaction of reducing sugars and amino groups resulting in formation of Amadori products undergoing further oxidation and degradation, leading to advanced glycation end-products - markers of ageing, diabetes mellitus and Alzheimer's disease. Here, we describe a solid-phase strategy for glycation of specific amino groups on partially protected resin bound peptides using a global post synthetic approach. The peptides were synthesized by standard Fmoc/tBu-chemistry using carbodiimide activation. The lysine to be modified was protected during the synthesis on the epsilon-amino group with the very acid labile methyltrityl group, which was cleaved after completion of the peptide synthesis selectively with 1 % TFA in dichloromethane. The partially deprotected peptide was glycated using 0.25 mol/L D-glucose in DMF at either 70 °C for 45 h or 110 °C for 25 min. The overall yields were about 35 % for the tested hexapeptides. Neighbored residues and their bulky protecting groups slightly reduced the yields to 30 %. Whereas the peptide eluted before the glycated peptide all other byproducts eluted much later on RP-HPLC allowing a simple purification even for medium-sized peptides. Thus, the general strategy presented here allows routine syntheses of Amadori peptides at reasonable yields and purities after purification by RP-HPLC using standard protocols established in most laboratories synthesizing peptides.

Andrej Frolov

Universität Leipzig

Center for Biotechnology and Biomedicine (BBZ)
Professorship for Bioanalytics
and
Faculty of Chemistry and Mineralogy

E-Mail: andrew.frolov@bbz.uni-leipzig.de
www.uni-leipzig.de/~bioanaly/

COR-AAD1-00003042
Bayer EX1008 (Part 6 of 9)

4.9 Enantioselective high performance liquid chromatography of astaxanthin from microbial sources

Carola Griehl, Claudia Grewe, Sieglinde Menge

A method for determining the enantiomers of all-E-astaxanthin (3,3'-dihydroxy-β,β-carotene-4,4'-dion), an important colorant in the feed industry, was developed. Synthetically produced the carotenoid consists of a mixture of three optical isomers in the ratio 3S,3S' : 3R,3S' : 3R,3R' 1:2:1[1]. For the separation different stationary phases were tested on their ability to resolve the optical isomers of astaxanthin: β-cyclodextrin derivatives (Chiradex, Merck), dinitrobenzoylleucin derivatives (Pirkle L-leucine, R,R-Ulmo, Regis Technology) and a cellulose-tris-3,5-dimethyl-phenylcarbamate (Chiracel OD-RH, Daicel). A sufficient separation of astaxanthin stereoisomers was only achieved employing the Daicel OD-RH as stationary and a mixture of acetonitrile and phosphate buffer as mobile phase. Direct resolution of all occurring optical isomers was achieved. Separation conditions are described allowing the determination of the isomeric forms produced in microalgae (*Scenedesmus sp.*) and yeasts (*Xanthophyllomyces dendrorhous*) as well as the identification of synthetically derived astaxanthin for example in fish feed.

Notes

1 Bjerkeng B., Coral-Hinostroza G.N., Comparative Biochemistry and Physiology Part B. 133: 437-444 (2002).

Prof. Dr. Carola Griehl

Hochschule Anhalt (FH)

Department of Biotechnology, Food Technology, Process Engineering and Environmental Engineering Biochemistry

E-Mail: carola.griehl@lbv.hs-anhalt.de
http://bio006.lbv.hs-anhalt.de/FB7/

COR-AAD1-00003043
Bayer EX1008 (Part 6 of 9)

4.10 IZKF Leipzig Core Unit "Fluorescence Technology" – Confocal laser scanning microscopy

Jens Grosche, Andreas Reichenbach

The confocal laser scanning microscopy (cLSM) has become the accepted technology for obtaining high resolution images in light microscopic morphology. The technology is based on two essential features: the application of high-energy laser light to excite the fluorophores and the placing of a pinhole in the beam path which is conjugated to the focal plane of the microscopic lens. Thus it is guaranteed that only light from the focus level contributes to the final image, while out-of-focus information is greatly reduced. In this way it is possible to generate a 3-D reconstruction of a specimen by stacking optical sections collected in series, or to reread the distribution of labeled organelles within single cells.

The cLSM is particularly advantageous when using multiple markers, because the filter settings can be adapted and optimized for each fluorophore. Even strong overlapping emission spectra can be precisely seperated from each other or from autofluorescence of the tissue.

In addition to morphological investigations, it is also possible to analyse functional parameters by cLSM. Vital dyes which react sensitively to physiological parameters can be used to measure the change of the fluorescence intensity dependent on time. Furthermore recent improvements of the emission filter setups enable the study of molecular interactions between two protein partners in living tissue by fluorescence resonance energy transfer (FRET), as long as they are located within a close proximity of 1-10 nm.

The cLSM is becoming an increasingly valuable imaging tool for a variety of applications in biological and medical basic research.

Dr. Jens Grosche

Universität Leipzig

Faculty of Medicine
Paul Flechsig Institute of Brain Research
Neurophysiology

E-Mail: groj@medizin.uni-leipzig.de
www.uni-leipzig.de/~pfi/

COR-AAD1-00003044
Bayer EX1008 (Part 6 of 9)

4.11 Depletion of high-abundant proteins from human serum

Katja Hanisch, Tobias Langrock, Ralf Hoffmann

Alzheimer's disease (AD) is considered as being the most important neuronal degenerative disease and accounts for approximately 60 % of all senile dementias. Despite all progress in recent years a valid biomarker is still missing, as neither Aβ nor tau are specific for AD and most presumably disease-specific alterations were also found in age-matched controls.

Our work aims to identify novel biomarkers in serum or cerebrospinal fluid (CSF). Difficulties in this field arise from a few dominant proteins present in these body fluids, such as serum albumin and immunoglobulins, which prevent detection of low-abundant proteins. The concentration range of proteins in human biological fluids spans over nine to twelve orders of magnitude, with 85-90 % of the total protein content being represented only by six proteins, that is, serum albumin (HSA), IgG, IgA, haptoglobin, antitrypsin and transferrin. Thus, we have tested several chromatographic techniques to deplete abundant proteins in human serum. Removing HSA with a blue column was not very effective. More effective were two commercially available columns that used specific antibodies. Whereas the POROS® Affinity Depletion Cartridges (Applied Biosystems, Langen, Germany) quantitatively removed only HSA and IgG the multiple affinity removal system (MARS, Agilent Technologies GmbH, Germany) removed HSA, IgG, IgA, haptoglobin, antitrypsin and transferrin from human serum. The depleted samples were analyzed by two-dimensional gel electrophoresis using either a colloidal coomassie or a SyproRuby stain.

Katja Hanisch

Universität Leipzig

Center for Biotechnology and Biomedicine (BBZ)
Professorship for Bioanalytics
and
Faculty of Chemistry and Mineralogy

E-Mail: katja.hanisch@bbz.uni-leipzig.de
www.uni-leipzig.de/~bioanaly/

COR-AAD1-00003045
Bayer EX1008 (Part 6 of 9)

4.12 Study of antibacterial and antitumoral peptides

Jörg Hanrieder, David Singer, Laszlo Otvös Jr.,
Peter F. Zipfel, Vladimir N. Kokryakov, Ralf Hoffmann

The increasing resistance of more and more bacteria strains against common antibiotics threatens the western societies, thus the development of new classes of antibiotics is a major focus of current pharmaceutical research. A promising approach relies on antibacterial peptides, since it appears likely that bacteria do not develop any resistance against these peptides.

Peptides with antibacterial activity prevent many organisms, especially insects but also mammals, from infections. For example, short proline rich peptides isolated from insect hemolymph show a broad spectrum of efficiency against many bacteria strains. The typical approach to identify such drug leads is to challenge insects with a bacterial infection, isolate the produced peptides and determine their structure. Based on the native sequence, more potent compounds are developed using solid-phase peptide synthesis by incorporating unnatural amino acid derivatives to enhance the antibacterial activity and to increase their protease resistance to circulate longer in the blood.

The aim of this study was to synthesize and modify native antibacterial peptides and to determine their antimicrobial activity as well as their serum stability. Furthermore, the antitumoral activity against glioblastoma and neuroblastoma cell lines was tested, for example for prophenin, which is a proline and phenylalanine rich 79mer peptide isolated from porcine lung. The bactericidal properties of the C-terminal 18 residues ("PR 18") are comparable to the full-length peptide. We will also present data on the antitumoral activity of "PR 18" and other prophenin derivatives.

Jörg Hanrieder

Universität Leipzig

Center for Biotechnology and Biomedicine (BBZ)
Professorship for Bioanalytics
and
Faculty of Chemistry and Mineralogy

E-Mail: joerg.hanrieder@gmx.de
www.uni-leipzig.de/~bioanaly/

COR-AAD1-00003046
Bayer EX1008 (Part 6 of 9)

4.13 Lipophilicity and protein binding as key descriptors for adme behavior – Innovative high-throughput screening tools

Thorsten Hartmann, Daniel Nimptsch, Cornelia Röhring, Johannes Schmitt, Joachim Nöller

Recent developments in combinatorial chemistry and robotics provide increasing numbers of lead compounds. Picking out candidates with appropriate physicochemical properties in an early drug discovery phase calls for fast and fully automated procedures.

The binding of pharmaceutically relevant molecules to neutral or ionic lipid membranes (expressed as the lipid/water partition coefficient log $D_{Lipid/Water}$) is directly related to permeation and intestinal absorption, while the binding of compounds to serum proteins like human serum albumin (HSA) determines the bound fraction (f_b) in the blood, thus affecting compound distribution. The proprietary TRANSIL® technology, based on lipids and proteins on solid supports, allows a fully automated assessment of both parameters in conventional microtiter plates (96 or 384 well) enabling high-throughput measurements of drug candidates.

TRANSIL® beads are functionalized with either a well defined single lipid-bilayer, which is no covalently attached, or with HSA, immobilized on a passivated surface. Utilizing these beads, the assay is performed in a simple set-up without using specific laboratory equipment which is presented along with their use for ADME prediction.

Dr. Joachim Nöller

Nimbus Biotechnologie GmbH

E-Mail: jnoeller@nimbus-biotech.com
www.nimbus-biotech.com

COR-AAD1-00003047
Bayer EX1008 (Part 6 of 9)

4.14 Selection of an aptamer against the tissue inhibitor of matrix metalloproteinases

Julia Hoßbach, Rolf Gebhardt

Matrix metalloproteinases (MMPs) are a group of enzymes that regulate the degradation of a variety of tissues. They play an important role in growth, development and tissue repair.

These Enzymes are regulated by their inhibitors, the TIMPs. This regulation is very sensitiv, if it fails, a diverstity of diseases may result. For example, an overproduction of TIMP may lead to fibrosis.

To interfere with the regulation of MMPs and TIMPs, we took a closer look at the possibilities to neutralize the effects of the TIMPs. One way was to select RNA species (aptamers) that may bind to the TIMPs and therefore decrease the efficiancy of the inhibiting effect of the TIMPs.

Several properties of aptamers make them attractiv agents. They act by folding a three dimensional structure, based on their nucleic acid sequence to bind their targets. The binding of aptamers is usually a very specific interaction, with the ability to discriminate between related proteins.

Systematic evolution of ligands by exponential enrichment (SELEX) was used to obtain binding species for TIMP1 out of a pool of RNA oligomers. During the selection process different methods of immobilisation of the target were tested, to avoid the problem of an enrichment of unspecific binding sequences. Using this technique three different sequences were enriched. Crosslinking studies reveal that two of the three sequences bind TIMP specifically. Further binding tests revealed a dependence of bound amounts of these sequences from the amount of TIMP present.

Julia Hoßbach

Universität Leipzig

Faculty of Medicine
Institute of Biochemistry

E-Mail: julia.hossbach@medizin.uni-leipzig.de
www.uni-leipzig.de/~biochem/

COR-AAD1-00003048
Bayer EX1008 (Part 6 of 9)

4.15 Probing laminin self-interaction by chemical crosslinking and ESI-FTICR mass spectrometry

Stefan Kalkhof, Sebastian Haehn, Christian Ihling, Neil Smyth, Andrea Sinz

We employ chemical cross-linking in combination with high-resolution fourier transform ion cyclotron resonance (FTICR) mass spectrometry to obtain structural information about self-interacting regions between N-terminal domains of laminin (LN domains). The heterotrimeric glycoprotein laminin is the main non-collagenious component of basement membranes and controls cellular activities such as adhesion or migration, differentiation and polarity, proliferation or apotosis. Laminin is essential for formation of basement membranes through interactions with itself and other components. LN domains were cross-linked with a number of homobifunctional, isotope-labeled, amine-reactive cross-linkers, such as sulfo-DSG, DSA and BS^3, bridging distances between 7 and 12 Å. The extent of cross-linking was monitored by one-dimensional SDS-PAGE of the cross-linking reaction mixtures. The bands of the created cross-linking products were cut out and digested *in gel*. For enzymatic digestion we applied a variety of proteases, such as trypsin, AspN, or LysC as well as combinations of these enzymes in order to obtain fragments of appropriate mass (m/z 500-4,000 Da) to facilitate detection of cross-linking products. The resulting mixtures of enzymatic peptides were separated by nano-HPLC which is directly coupled to the FTICR mass spectrometer equipped with nano-ESI source. The excellent resolution and mass accuracy of FTICR MS enhances confidence in the identification of cross-linking products in addition to using isotope-labeled cross-linkers. The obtained cross-linking products give information on interacting regions between LN domains.

Stefan Kalkhof

Universität Leipzig

Center for Biotechnology and Biomedicine (BBZ)
Junior Research Group "Protein-Ligand Interaction by Ion Cyclotron Resonance Mass Spectrometry"
and
Faculty of Chemistry and Mineralogy

E-Mail: stkalkhof@web.de
www.uni-leipzig.de/~sinz/

COR-AAD1-00003049
Bayer EX1008 (Part 6 of 9)

4.16 Recombinant expression and characterization of the ecto-nucleotidase CD39

Matthias Krause, Norbert Sträter

In contrast to their intracellular function as a chemical driving force, extracellular ATP and other nucleotides play an important role in autocrine and paracrine cell signalling. They are known to act as molecular cues in many physiological processes, such as thrombosis, inflammation and synaptic signalling. Cellular responses are induced by binding on specific G protein coupled receptors or ligand-gated ion channels.

Signalling effects of extracellular nucleotides are mainly controlled through the hydrolytic breakdown by extracellular nucleotidases. CD39 family members or eNTPDases (ecto-NTP-diphosphohydrolase) catalyze the sequential hydrolysis of β and γ phosphate of triphosphonucleosides. The eNTPDases are bound to the cell membrane by N- and C-terminal transmembrane helices, with their large catalytic domain facing the extracellular space.

These enzymes are now considered as potential new drug targets or drugs themselves. Soluble forms from mammalian cell culture are shown to inhibit platelet aggregation *in vivo*. This might be of high therapeutic use in treatment of coronary thrombosis and stroke. On the contrary, inhibition of eNTPDases may prolong the effect of nucleotides at their respective receptor.

We have established an *E. coli* expression system for insoluble production of the catalytic domain of CD39 and optimized the *in vitro* refolding. This allows for large scale production of active protein for further biochemical characterization and clinical application. X-ray structure determination of the refolded protein will provide valuable insights in the rational design of medically relevant inhibitors.

Matthias Krause

Universität Leipzig

Center for Biotechnology and Biomedicine (BBZ)
Professorship for Structural Analysis of Biopolymers
and
Faculty of Chemistry and Mineralogy

E-Mail: matthias.krause@bbz.uni-leipzig.de
www.uni-leipzig.de/~strater/

COR-AAD1-00003050
Bayer EX1008 (Part 6 of 9)

4.17 Crystal structure of the 2-oxoglutarate dependent dioxygenase RdpA

Jörn Krauße, Anne Westendorf, E. Bartholomeus Küttner, Roland H. Müller, Norbert Sträter

The most widespread group of mononuclear non-heme iron enzymes is the family of 2-oxoglutarate (2-OG) dependent oxygenases. Its members are found in bacteria as well as eukaryotes and catalyze a large variety of reactions. The catalysis is always coupled with the decarboxylation of 2-OG and the consumption of molecular oxygen. A 2-OG dependent oxygenase was isolated from *Delftia acidovorans* MC1. It carries enantiospecific activity for the etherolytic cleavage of R-(2,4-dichlorophenoxy)propionate (Rdp) and is thus referred to as RdpA. Its substrate belongs to the group of chlorinated phenoxyalkanoates which were widely used herbicides in agriculture and remain as severe soil pollutants. The crystal structure of RdpA is of special interest to analyze its stereospecific substrate recognition in comparison to a homologous enzyme (SdpA) which catalyzes the decomposition of S-(2,4-dichlorophenoxy)propionate (Sdp) exclusively. Such knowledge would possibly allow the design of new specific catalysts.

Initial crystallization conditions for purified RdpA were found using the sparse matrix method. Further refinement of the conditions was carried out to obtain crystals suitable for X-ray diffraction experiments. Data collection was performed at BESSY, Berlin. Orthorhombic crystals of RdpA show anisotropic diffraction up to 2.5 Å resolution. Data scaling was limited to 2.9 Å. The structure was determined by molecular replacement using the homologous protein tauD from *E. coli* as phasing model. First crystallographic data show that RdpA is a tetramer.

Jörn Krauße

Universität Leipzig

Center for Biotechnology and Biomedicine (BBZ)
Professorship for Structural Analysis of Biopolymers
and
Faculty of Chemistry and Mineralogy

E-Mail: krausze@bbz.uni-leipzig.de
www.uni-leipzig.de/~strater/

COR-AAD1-00003051
Bayer EX1008 (Part 6 of 9)

4.18 Application of photoactivatable GFP to investigate dynamics of human mitochondria

Christian Kukat, Katrin Pospischil, Alexandra Kneissl, Ingo Schäfer, Peter Seibel

Only 5 % of all mitochondrial proteins are encoded by the genome of these organelles (16,569 bp in *Homo sapiens*). The other 95 % are encoded by the nuclear genome and have to be transported to the mitochondria.

Fluorescent microscopy is a current method for studying cells and fusion proteins.

For tracing the route of the proteins through the cell and to investigate intracellular protein dynamics it would be very helpful to have the possibility to colour only a small region of the cell or only some mitochondria with fluorescent dyes.

An excellent tool for this approach is a photoactivatable GFP (PA-GFP). This is an engineered variant of the *Aequorea victoria* green fluorescent protein which was first published by Patterson and Lippincott-Schwartz[1]. After activation with 413-nm laser light it increases its natural fluorescence approximately by 100 fold when excited by 488-nm light.

By using PA-GFP as a tool for tracking photoactivated fusion proteins it is possible to reveal molecular movement in the cell by fluorescent microscopy with the focus on human mitochondrial proteins.

We engineered PA-GFP using the coding sequence of enhanced green fluorescent protein (EGFP) with the technique of site-directed mutagenesis. Using this approach we were able to convert GFP to the photoactivatable form which undergoes photoconversion upon illumination with ~400-nm light.

Our aim is to use the PA-GFP to generate different fusion proteins composed of PA-GFP and proteins that might play essential roles in mitochondrial biogenesis.

Notes

1 Patterson G.H., Lippincott-Schwartz J., Science 297(5588):1873-1877 (2002).

Christian Kukat

Universität Leipzig

Center for Biotechnology and Biomedicine (BBZ)
Professorship for Molecular Cell Therapy
and
Faculty of Medicine

E-Mail: christian.kukat@bbz.uni-leipzig.de
www.uni-leipzig.de/~mct/

COR-AAD1-00003052
Bayer EX1008 (Part 6 of 9)

4.19 Crystal structures of two thermophilic DNA nucleases as templates for protein engineering

E. Bartholomeus Küttner, Sven Pfeifer,
Thomas Greiner-Stöffele, Norbert Sträter

DNA-cleaving enzymes are a common tool in the molecular biology lab. The use of DNA applications at elevated temperatures, such as PCR, prompts the development of temperature-stable enzymes by protein engineering. Exonuclease III (ExoIII) from the mesophile bacterium *Escherichia coli* (*E. coli*) has the desired catalytical properties but lacks sufficient thermostability. In order to facilitate the design of more thermostable variants of ExoIII we determined the structures of two homologous enzymes from thermophilic archaeons. These enzymes are thermostable but lack the desired catalytical properties. The genes of exonucleases from *Methanothermobacter thermoautotrophicus* (ExoMt, 257 amino acids) and *Archeoglobus fulgidus* (ExoAf, 258 amino acids) which exhibit highest activity at 60-70 °C (ExoMt) and 70-80 °C (ExoAf) were cloned and expressed in *E. coli*. After purification both enzymes could be crystallised in space group $P2_1$ using a 10mer DNA oligonucleotide as an additive. Complete X-ray diffraction datasets were collected from cryo-cooled crystals (100 K) to a maximum resolution limit of 1.7 Å (ExoAf) or 1.8 Å (ExoMt). The three-dimensional structures were solved by the molecular replacement method using the structures of *E. coli* ExoIII (PDB id: 1AKO) [→ ExoAf] or human APE1 (PDB id: 1DEW) [ExoMt] as search models. The structural refinement of ExoAf and ExoMt with bound DNA oligonucleotides is in progress. It is hoped that the crystal structures will provide valuable insight into structural aspects of increased thermal stabilitiy in order to engineer thermostable *E. coli* ExoIII variants for applications in DNA technology.

E. Bartholomeus Küttner

Universität Leipzig
Center for Biotechnology and Biomedicine (BBZ)
Professorship for Structural Analysis of Biopolymers
and
Faculty of Chemistry and Mineralogy
E-Mail: kuettner@bbz.uni-leipzig.de
www.uni-leipzig.de/~strater/

COR-AAD1-00003053
Bayer EX1008 (Part 6 of 9)

4.20 Strategies for the identification of hydroxyproline-isomers and hydroxylysine in collagen

Tobias Langrock, Natividad García-Villar, Ralf Hoffmann

In addition to the common twenty proteinogenic amino acids several hundred co- and posttranslational modifications, mostly a result of sequence-specific enzymatic activity, are present in proteins. This study targets hydroxylation of proline and lysine in collagens. Typical for all collagen-types is their triple-helical structure formed by three collagen chains containing a high degree of glycine and proline, which is further stabilized by sequence-specific enzymatic hydroxylation. Even though collagen has been widely studied, the distribution of hydroxyproline (Hyp) and hydroxylysine (Hyl) within the sequence as well as the stereochemistry of the Hyp-residues are still not well understood.

The aim of this study was to analyze the Hyl and Hyp content of various collagens. Especially the distribution of the four Hyp isomers, i.e. cis-3-, cis-4-, trans-3- and trans-4-hydroxyproline exhibits an analytical challenge, as these four compounds have very similar physical and chemical properties and are isobaric with leucine and isoleucine. Therefore at least these six amino acids (aa) must be separated to identify them via MS-detection.

We describe two chromatographic approaches for the separation of most proteinogenic and hydroxylated AAs. A direct separation of unmodified aa relies on hydrophilic interaction chromatography (HILIC), while separation by RPC requires pre-column derivatization, in our case performed with an analogue of marfey's reagent, i.e., N^2-(5-fluoro-2,4-dinitrophenyl)-L-valine amide (L-FDVA).

In both cases, on-line coupling to an MS was essential for identification of coeluting compounds.

Tobias Langrock

Universität Leipzig
Center for Biotechnology and Biomedicine (BBZ)
Professorship for Bioanalytics
and
Faculty of Chemistry and Mineralogy
E-Mail: tobias.langrock@bbz.uni-leipzig.de
www.uni-leipzig.de/~bioanaly/

COR-AAD1-00003054
Bayer EX1008 (Part 6 of 9)

4.21 The regulatory environment for the development and approval of biopharmaceuticals

Rüdiger Laub, Ullrich Pigla

The regulatory environment for the pre-clinical development of biopharmaceuticals, the setup of clinical trials, and the application for marketing authorization is a continuously growing jungle made up of regional, national, and international guidelines and legislation.

Yet academic research on a potential investigative new drug (IND) should consider regulations laid down in the guidelines for good laboratory practice (GLP). Only pre-clinical data established under GLP are acceptable for their later inclusion in study protocols, or application trials. The manufacture of the active pharmaceutical ingredient, and its galenic formulation must comply with the guidelines for good manufacture practice (GMP) and its current 19 annexes. Guidelines for good clinical practice (GCP) have to be followed in clinical study plans and in the execution of clinical trials. Although these guidelines provide basic requirements for single steps in the development of an IND, most details are hidden inside legislations which are not harmonized among local areas. Their underestimation may block the next stage of development, and jeopardizes young biotech companies with small finance ceilings.

We here present paradigmatically important regulations which have to considered in the development of a monoclonal antibody-derived biopharmaceutical.

Dr. Rüdiger Laub

Biotectid GmbH

E-Mail: laur@medizin.uni-leipzig.de
www.biotectid.de

COR-AAD1-00003055
Bayer EX1008 (Part 6 of 9)

4.22 Discrimination of vaccinated and infected pigs by *Salmonella*-specific IgA antibodies

Jörg Lehmann, Uwe Rösler, Thomas Lindner, Thomas Kramer, Jörg Gabert, Andreas Hensel

Due to intensified stockbreeding the risk of Salmonella transmitted to man by consumption of animal food products increased. Vaccination with live attenuated vaccines is a tool for reduction of *Salmonella* burden of pig herds. Unfortunately, there exists no reliable assay to discriminate vaccinated from infected pigs so far. Ig isotype switching leads to generation of high affinity antibodies (Ab) during the immune response. This can be applied for differentiation of early and late infection stages. The aim of this study was to evaluate the applicability of a novel Ig-isotype specific *Salmonella Typhimurium* (STm) Ab ELISA for discrimination between vaccinated and infected pigs.

Serum IgM, IgG, and IgA Ab were captured by a whole cellular extract antigen of STm and detected by isotype-specific HRP-conjugated secondary Ab. Sera from vaccination/challenge experiments were used for evaluation of the test.

Using this ELISA, different patterns of specific IgM, IgG and IgA Ab were detected following immunisation with a STm live vaccine or experimental infection with a wild-type strain of STm. Interestingly, STm-specific IgA Ab represented an excellent tool for the recognition of acute infection in vaccinated pigs. Under SPF conditions, we were able to differentiate between naive, vaccinated, experimentally infected non-vaccinated and vaccinated animals. However, the highest specific IgA levels were detected in challenged vaccinated pigs. Results from field trials confirmed these findings.

This novel test offers a hopeful tool to promote the acceptance of immunisation of pig herds using live vaccines under diagnostic control.

Dr. Jörg Lehmann

Labor Diagnostik GmbH Leipzig

Research & Development
Immunology

E-Mail: jl@lab-leipzig.de
www.lab-leipzig.de

COR-AAD1-00003056
Bayer EX1008 (Part 6 of 9)

4.23 Selective inhibition of protein kinases by emodin-related compounds

Katja Lerche, Lars Teich, Kurt Eger, Robert Günther, Hans-Jörg Hofmann, Rolf Gebhardt

The enzymes CK-I, CK-II and GSK-III are ubiquitous serine/threonine protein kinases and essential for viability and multiple mechanisms of regulation in eukaryotic cells. The hydroxyanthraquinone emodin, extracted from the rhizome of *Rheum palmatum L.*, was recently described as potent, ATP-competitive inhibitor of cell cycle regulating proteins. In fact, derivatives of emodin seem to be attractive compounds for antiviral and anti-tumor chemotherapeutics.

Emodin and the derivatives rhein, emodinic acid and the emodinic acid ethyl ester are very effective (IC_{50}-values between 0.5 and 5 µM) and fairly specific (within 1:20 to 1:120 of IC_{50}-values against CK-I and GSK-III) inhibitors of protein kinase CK-II. This kinase is abnormally elevated in a wide variety of tumors. The results show, that the activity of CK-II can be highly selective inhibited.

Some of these compounds show a higher cytotoxic activity for the tumor cell line HepG2 in comparison to normal hepatocytes. By further modification, undiserable side-effects can be minimized and new therapeutically possibilities may arise.

With the help of computer-assisted analysis and molecular modelling we want to verify our results and give an outlook on new promising derivatives.

Katja Lerche

Universität Leipzig

Faculty of Medicine
Institute of Biochemistry

E-Mail: katja.lerche@medizin.uni-leipzig.de
www.uni-leipzig.de/~biochem/

COR-AAD1-00003057
Bayer EX1008 (Part 6 of 9)

4.24 Chip calorimeter as a control device for the monitoring of bioprocesses

Johannes Lerchner, Thomas Maskow, Mirko Peitsch, Hauke Harms, Gert Wolf

We demonstrated the suitability of a miniaturized calorimeter for incorporation into technical relevant bioprocesses as a monitoring device. The calorimeter is sensitive enough to detect metabolic heat production rates in microbial suspensions of few micro-litres. Due to the small time constants a fast on-line operation in connection with bioreactors is possible even for aerobic processes.

As example for the monitoring of aerobic and anaerobic processes the growth of *Escherichia coli* DH5α and *Halomonas halodentrificans* CCM 286T cultures, respectively, was calorimetrically determined. Periodically, small portions of bacterial suspension were taken out of a bioreactor and transferred into the calorimetric chip transducer of the system. The actual heat production rate of the bacterial culture was indicated with a time delay of less than five minutes. The time dependence of the heat production rate was sufficiently described by thermokinetic models.

In a second example the high flexibility of the chip calorimeter system was demonstrated by measuring the metabolic activity of a biofilm which was established inside the calorimetric chip transducer. For example, biofilms cause damages of technical tubing systems by clogging. Therefore, a great interest exists in methods for the non-destructive inspection of tubings with respect to the actual state of the contamination. As proof of principle the internal surface of several calorimetric transducers was externally loaded with *Escherichia coli* DH5α. Then, the metabolic activity of the bio-film was tested by injecting of carbon-substrate solution into the calorimetric chip transducer.

PD Dr. Johannes Lerchner

Technische Universität Bergakademie Freiberg

Faculty of Chemistry and Physics
Institute of Physical Chemistry

E-Mail: johannes.lerchner@chemie.tu-freiberg.de
www.chemie.tu-freiberg.de/phy/

COR-AAD1-00003058
Bayer EX1008 (Part 6 of 9)

4.25 Myeloperoxidase-induced effects on spermatozoa

Jacqueline Leßig, Hans-Jürgen Glander, Uwe Paasch, Jürgen Arnhold

Inflammations in the male genital tract play a steadily increasing role in the reduced male fertility. Different leukocyte subpopulations including neutrophiles, monocytes/ macrophages and lymphocytes are invading into inflammatory loci. The heme-enzyme myeloperoxidase (MPO) is released from stimulated neutrophils and becomes attached to negatively charged cell membranes. Due to its extraordinary reactivity it contributes to the production of reactive oxygen species and causes halogenation of biological material. The binding of myeloperoxidase to the spermatozoa surface could be demonstrated in connection with myeloperoxidase antibodies by confocal fluorescence microscopy. The presence of albumin in the incubation mixture decreases the binding of myeloperoxidase to spermatozoa epitopes. MPO impairs the vitality of spermatozoa in dependence on the enzyme activation with hydrogen peroxide from 52 to 31 %. MPO-derived hypochlorous acid induces the externalisation of phosphatidylserine as detected flowcytometrically with annexin V, impairs the cell vitality and induces an enhanced formation of lysophospholipids. A significant increase of annexin V binding to 43 % can be noticed at 10^{-5} mol/l hypochlorous acid, while an increasing of lysophospholipids first occurs with 10^{-4} mol/l hypochlorous acid. Vitality lost can already be seen at 10^{-6} mol/l hypochlorous acid. These results indicate drastical changes in membrane structure caused by myeloperoxide-derived hypochlorous acid whereas phosphatidylserine-exposition precedes the lysophospholipid formation.

Jacqueline Leßig

Universität Leipzig

Faculty of Medicine
Institute of Medical Physics and Biophysics

E-Mail: lesj@medizin.uni-leipzig.de
www.uni-leipzig.de/~biophys/

COR-AAD1-00003059
Bayer EX1008 (Part 6 of 9)

4.26 IZKF Leipzig Core Unit "Fluorescence Technology" – Flow cytometry and cell sorting

Andreas Lösche, Viola Döbel

Flow cytometry is a local measuring technique to analyze and/or sort suspended individual cells (or particles). Optical signals (scatter, fluorescence) are sequentially generated by each single cell and detected and displayed for cell distribution analysis.

There are three analysers in our lab (FACScan, LSR and FACSCalibur from Becton Dickinson) and a high-speed-sorter FACSVantage SE (Becton Dickinson). Up to three independent laser beam spots (UV, 488 nm, and 633 nm) are used as light sources and up to six fluorescence signals can be collected for each cell.

By correlating the forward scatter signal (FSC) and the side scatter signal (SSC), subpopulations corresponding to lymphocytes, monocytes and granulocytes can be detected in peripheral blood samples, and unwanted signals such as cell debris ar cell aggregates can be excluded from analysis.

Staining cells with fluorochrome-conjugated antibodies or fluorochromes which interact directly with specific targets such as DNA, cell subpopulations can be characterised according to phenotype and/or cell cycle phase.

The sorter has the ability to selectively deposit cells from particular populations into tubes, or other collection vessels such as wells of microtiter plates in a sterile environment.These selected cells can be used afterwards for further experiments, culture, or staining with another dye/antibody and reanalysis.

Flow cytometric applications include:

- cell cycle analysis
- apoptosis analysis
- multicolor (phenotypic) analysis
- functional analysis
- stem cell analysis
- sterile cell sorting.

Dr. Andreas Lösche

Universität Leipzig

Interdisciplinary Centre for Clinical Research (IZKF)
Core Unit "Fluorescence Technology"

E-Mail: andreas.loesche@medizin.uni-leipzig.de
www.izkf-leipzig.de

COR-AAD1-00003060
Bayer EX1008 (Part 6 of 9)

4.27 IZKF Leipzig Core Unit "Fluorescence Technology" – Laser scanning cytometry

Andreas Lösche, Anja Mittag, Attila Tarnok

The laser scanning cytometer (LSC) combines the advantages of flow cytometry, image analysis, and automated fluorescence microscopy. It allows measurements of light scatter and fluorescence but also records the position of each measured object. Cells of interest can be re-located, visualised, re-stained, re-measured and photographed. In common with flow cytometers, the LSC measures multicolour fluorescence and light scatter on a single cell basis. This technology is of particular interest if cell numbers are low, small subpopulations are being examined or morphological information is required in addition to phenotypic information.

The LSC in our lab (CompuCyte) is equipped with two lasers (Argon ion 488 nm and HeNe 633 nm) and is designed around a standard Olympus BX50 fluorescence microscope. The motorised stage has a stepper motor moving in 0.5 µm increments. In this way a pixellated bit map on the slide is built up in 0.5 µm squares. For each pixel, the fluorescence value for each measured parameter is recorded. So a number of parameters can be measured, e.g. area (the number of pixels occupied by the cell), the integral value (the sum of the fluorescence values for each pixel in the contour) and the maximum pixel (the position and value of the brightest pixel within the contour). Additional factors can also be measured, e.g. cell perimeter and "texture".

Examples of applications:

- cell cycle analysis
- cell proliferation
- apoptosis
- immunophenotyping
- enzyme kinetics
- cytogenetics
- cell-cell interaction.

Dr. Andreas Lösche

Universität Leipzig

Interdisciplinary Centre for Clinical Research (IZKF)
Core Unit "Fluorescence Technology"

E-Mail: andreas.loesche@medizin.uni-leipzig.de
www.izkf-leipzig.de

COR-AAD1-00003061
Bayer EX1008 (Part 6 of 9)

4.28 Binding proteins for advanced glycation endproducts isolated from different rat tissues

Ina Meiners, Gerald Münch, Karen Nieber

Non-enzymatic glycation of proteins by reducing sugars and subsequent metal-catalyzed oxidation leads to a formation of advanced glycation end products (AGEs). AGEs are involved in several diseases, such as Alzheimer's disease, diabetic retinopathy and nephropathy, atherosclerotic deletions of blood vessels, and inflammation reactions. The accumulation of AGEs in the body is suspected to lead to an inhibition of cellular functions and transport processes, and finally to cell dysfunction and death. AGEs are known to bind specifically to different cell surface receptors and other AGE-binding proteins. A number of AGE-binding proteins have been identified, including the receptor for advanced glycation end products (RAGE), oligosaccharyl transferase-48 (OST-48 or AGE-R1), 80K-H phosphoprotein (AGE-R2), and galectin-3 (AGE-R3). These proteins have been shown to be present in many different cell types, for example in monocytes, macrophages, endothelial cells and microglia. In the present study a method for purification of AGE-binding proteins is described. Organs from liver, lung and kidney of male Wistar rats were used. Membrane proteins were isolated by differential centrifugation and subsequent purification by an AGE-affinity chromatography. AGE-binding proteins were analyzed by 1D-SDS-PAGE and Western blot. The membrane fractions contained at least 10 proteins in all tissues interacting with AGEs. Our results indicate the existence of different binding proteins in rat tissues. This work suggests a suitable method to identify new binding proteins for AGEs

Ina Meiners

Universität Leipzig

Faculty of Biosciences, Pharmacy and Psychology
Institute of Pharmacy
Pharmacology for Natural Scientists

E-Mail: inameiners@gmx.de
www.uni-leipzig.de/~pharm/phfn/

COR-AAD1-00003062
Bayer EX1008 (Part 6 of 9)

4.29 Characterization of recombinant antibody fragments to human CD4 expressed in transgenic tobacco

Dirk Mischke, Sunna Hauschildt, Jörg Böhme, René Brecht, Frank Emmrich, Ullrich Pigla, Rüdiger Laub

The minimization of biopharmaceutical molecules is an important step to improve its performance and safety in therapeutic or *in vivo* diagnostic applications. Large proteins such as monoclonal antibodies may possess several disadvantages. They may have limited distribution, retarded clearance, and may exert other side effects simply due to their molecular size. Further, they may elicit severe immunological responses to repeated applications.

We have engineered single chain variable-fragment (scFv) and minibodies (mb) from the variable region of the heavy (VH) and light (VL) chain domains of a monoclonal antibody to human CD4, a typical surface molecule on helper T cells and monocytes. The coding sequences for the scFv and mb were cloned into a plasmid of Agrobacterium spec. which was used to transform tobacco plants.

We have established a panel of quality control analyses to test the purity of the transgenic fragments extracted and purified from plant tissues. The binding and specifity of the transgenic fragments were demonstrated by flow cytometric assays using peripheral mononuclear cells (PBMC) as indicator cells. Investigation of functional parameters revealed, that the mb but not the scFv is able to modulate the CD4 molecule on helper T cells like the parental anti-CD4 mAb does.

While important functional properties are retained, we expect from minimization better pharmacokinetic characteristics, and significantly reduced immunogenicity.

Dirk Mischke

Universität Leipzig

Faculty of Biosciences, Pharmacy and Psychology
Institute of Biology II
Immunbiology

E-Mail: dirk_immunbio@yahoo.de
www.uni-leipzig.de/~biowiss/zoologie/

COR-AAD1-00003063
Bayer EX1008 (Part 6 of 9)

4.30 Separation of phosphopeptide isomers using capillary-zone-electrophoresis

Marika V. Mützelburg, Peter Hoffmann, David Singer, Ralf Hoffmann

One of the most common posttranslational modifications of proteins is O-phosphorylation of seryl-, threonyl- and tyrosyl residues. Many proteins are phosphorylated at different sites. At the molecular level the phosphorylation pattern is often very complex and inhomogeneous. The separation of phosphopeptide isomers, which often exist in mixtures, by RP-HPLC or other techniques is very difficult or impossible due to the very similar properties. As phosphopeptide isomers have equal masses, high-resolution mass spectrometry fails too.

The tau protein, which plays an important role in the Alzheimer's disease, is a well investigated phosphoprotein. At least 26 different phosphorylation sites have been determined by immunological techniques and sequence analysis. The phosphorylation sites are mostly located in four regions of the tau protein, each region spanning about 20 amino acid residues. Singly to quadruply phosphorylated peptides are present in tryptic digests. The distribution of the phosphate groups on the molecular level, that is, the phosphopeptides isomer pattern, is still unknown.

The aim of this work was to separate singly, doubly and triply phosphorylated tau peptide isomers with capillary electrophoresis. Fused silica capillaries have been used to separate acidic and basic peptides. The impact of different buffer systems, with and without organic solvent, on the migration times and the resolution of the peptides was studied. By optimizing the separation conditions it was possible to establish a method to separate phosphopeptide isomers for both acidic and basic sequences.

Marika V. Mützelburg

Universität Leipzig
Center for Biotechnology and Biomedicine (BBZ)
Professorship for Bioanalytics
and
Faculty of Chemistry and Mineralogy
E-Mail: marika-victoria@web.de
www.uni-leipzig.de/~bioanaly/

COR-AAD1-00003064
Bayer EX1008 (Part 6 of 9)

4.31 Mass spectrometric methods and the investigation of the kinetic properties of cellular phospholipases

Marijana Petkovic, Jürgen Schiller, Jacqueline Leßig, Beate Fuchs, Jürgen Arnhold

Phospholipases are important heterogeneous group of cellular enzymes. Their activation is an important step in the intra- and inter-cellular signalling processes. Phospholipases produce various second messengers that further influence the activity of other cellular enzymes - e.g. protein kinase C.

Various methods are nowadays established for the investigation of the activity either of isolated or the cellular enzymes. A serious drawback of these methods is that most of them use modified substrate. The use of natural substrate is preferred, since in this case the phospholipase activity might not be altered. With that respect, mass spectrometric (MS) methods are advantageous over other, well established methods for the investigation of the activity of phospholipases. In the assays employing MS in most cases lipids - a substrate or one of the products - are measured. Along with kinetic parameters important structural information are easily obtained by MS.

In spite all advantages offered by MS methods in this field, there are only a few examples on their application and they concern the activity of phospholipase A_2. These applications are presented in this poster, together with experiments to use matrix-assisted laser desorption and ionisation time-of-flight MS for the investigation of the kinetics of cellular phospholipase D and phospholipase C.

Dr. Marijana Petkovic

Universität Leipzig

Faculty of Medicine
Institute of Medical Physics and Biophysics

E-Mail: petm@medizin.uni-leipzig.de
www.uni-leipzig.de/~biophys/

COR-AAD1-00003065
Bayer EX1008 (Part 6 of 9)

4.32 Phenotyping of mutans streptococci by intact cell MALDI-TOF-MS after caries excavation

Stefan Rupf, Knut Merte, Knut Breitung, Susanne Kneist, Klaus Eschrich

The study aimed to analyze the heterogeneity of *Streptococcus mutans* strains from the cavity floor of deciduous molars by intact cell matrix-assisted-laser-desorption/ionization-time-of-flight mass spectrometry (ICM).

Hard dentin samples from 32 teeth of 20 children were taken after chemo-mechanical caries excavation (T_1) and after eight weeks of temporary filling (T_2). 261 strains of mutans streptococci (MS) were isolated. Strains were identified and classified by ICM and hierarchical clustering based on known MS reference strains. Results were confirmed by species specific PCRs and 16S rDNA sequencing.

258 of the 261 MS strains were identified as *S. mutans*, two as *Streptococcus downei* and one as *Streptococcus sobrinus*. *S. mutans* was found in 19 of the 32 investigated teeth at T_1 and in 13 of 21 teeth at T_2. Identical S. mutans strains were found in the same teeth at T_1 and T_2, as well as in different teeth of individual patients. Between one to seven different phenotypes of S. mutans were found per cavity. Overall 59 phenotypes occurred in the population of 258 *S. mutans* strains. The complexity of the isolated *S. mutans* population was similar at T_1 and T_2. The overall statistical comparison of the phenotypes revealed solutions on different similarity levels.

At a low infection level clonal heterogeneity of *S. mutans* remained in carious lesions after chemomechanical caries removal which persisted after a period of temporary filling. ICM was found to be appropriate to detect rare species in a uniform MS population. The species *S. downei* was identified in a human carious lesion for the first time.

Dr. Stefan Rupf

Universität Leipzig

University Hospital
Department of Conservative Dentistry and Periodontology

E-Mail: stefan.rupf@medizin.uni-leipzig.de
www.uni-leipzig.de/~kons/

COR-AAD1-00003066
Bayer EX1008 (Part 6 of 9)

4.33 Interaction of myeloperoxidase with human serum albumin

Pavel Salavei, Uta Reibetanz, Jürgen Arnhold

Myeloperoxidase (MPO) - is a glycosylated heme-enzyme with molecular weight 140 kDa. It is present in neutrophils and in monocytes and released by activated phagocytes into the phagolysosome or into the extracellular space in responce to a variety of agonists. We investigated interaction of MPO with the plasma protein albumin. Albumin - is an important plasma protein with a molecular weight of 66 kDa. It is responsible for maintaining the transendothelial oncotic pressure gradient and regulating the transport of fatty acids, steroids, thyroxine and amino acids. Albumin also exists in the extavascular space.

The association of MPO and albumin was confirmed by ELISA technique and native gel electrophoresis. MPO (pI~10) exhibited a time-dependent binding to albumin (pI~4.7) coated microtiter plates in PBS solution by pH value 7.4 but not by pH value 5.0. This binding could also be blocked in the presence of 0.5 % Tween20 or 40 mg/ml albumin in PBS solution (pH 7.4). By FACS analysis, it was demonstrated that interaction of RITC-labelled MPO with albumin-coated silica particles can be reversed by incubation with albumin solution. We also used MALDI-TOF mass spectrometry to map the sites of MPO-mediated albumin modification. Especially modifications of methionine as well as halogenations of tyrosine residues of albumin were observed.

Pavel Salavei

Universität Leipzig

Faculty of Medicine
Institute of Medical Physics and Biophysics

E-Mail: pavel.salavei@medizin.uni-leipzig.de
www.uni-leipzig.de/~biophys/

COR-AAD1-00003067
Bayer EX1008 (Part 6 of 9)

4.34 Comparing the biophysical properties of sterols in lipid membranes – What is special about cholesterol?

Holger A. Scheidt, Peter Müller, Andreas Herrmann, Klaus Arnold, Klaus Gawrisch, Daniel Huster

Cholesterol is a major constituent of mammalian cell membranes. Its biophysical properties are essential for several membrane functions. However, a recently described generation of knock out mice, entirely lacking cholesterol[1], showed surprisingly mild phenotype. Since the cell membranes of these mice contained desmosterol, the direct precursor of cholesterol, we compared the biophysical properties of membranes containing cholesterol, desmosterol and lanosterol (a more distant precursor).

Membrane packing properties were studied by ^{2}H NMR, fluorescence, and EPR spectroscopy. It was found that cholesterol and desmosterol showed a very similar behavior, while lanosterol produced significantly weaker effects.

We also investigated the effect of the sterols on the lateral diffusion of the lipids and of the sterols, respectively, by ^{1}H PFG MAS NMR spectroscopy. In the liquid-crystalline phase, the phospholipid diffusion coefficients are decreased in the presence of all three sterols. In the lo phase this decrease strongly depends on the cholesterol concentration. Cholesterol mirrors the lipid behavior, but exhibits a slightly faster diffusion. In the lanosterol and desmosterol containing membranes, the lipid diffusion rates are somewhat higher than those for cholesterol. While desmosterol diffusion rates are also only slightly higher than for the lipids, lanosterol diffusion rates significantly exceed lipid diffusion rates. This indicates weaker interactions between the lipids and lanosterol, which explains the weaker condensation effect of lanosterol.

Notes

1 Wechsler et al., Science 302:2087 (2003).

Holger A. Scheidt

Universität Leipzig

Center for Biotechnology and Biomedicine (BBZ)
Junior Research Group "Solid-state NMR Studies of the Structure of Membrane-Associated Proteins"
and
Faculty of Medicine
Institute of Medical Physics and Biophysics

E-Mail: scheh@medizin.uni-leipzig.de
www.uni-leipzig.de/~huster/

COR-AAD1-00003068
Bayer EX1008 (Part 6 of 9)

4.35 Studying calmodulin-adenylyl cyclase 8 interaction by chemical cross-linking and FTICR mass spectrometry

Andreas Schmidt, Daniela M. Schulz, Stefan Kalkhof, Christian Ihling, Annette G. Beck-Sickinger, Dermot M.F. Cooper, Andrea Sinz

Chemical cross-linking combined with mass spectrometry has emerged as an alternative strategy to obtain low-resolution structural data of protein interfaces from low quantities of proteins within a relatively short time[1].

In our present work, we study the interaction between the C-terminal region of adenylyl cyclase 8 (AC 8) and its binding partner calmodulin (CaM). Adenylyl cyclases are a critically important family of multiply regulated signaling molecules[2]. AC 8 is regulated by Ca^{2+}/CaM and possesses an N-terminal Ca^{2+}-dependent CaM-binding motif (amino acids 35-54), as well as a Ca2+-independent IQ-motif[3] located at the C-terminus (amino acids 1197-1210).

A 25-amino acid peptide comprising the IQ-motif was synthesized. The cross-linking reaction was performed by using different amine-reactive, isotope-labeled (d_0 and d_4) cross-linkers (BS^3 and BS^2G) with varying spacer length and a zero-length cross-linker (EDC). The cross-linked 1:1 complexes were investigated by MALDI-TOFMS to check the extent of chemical cross-linking. Separation of intramolecular and intermolecular cross-linking products was carried out by one-dimensional SDS-PAGE. After excision of the bands of the cross-linked complexes, *in gel* digestion was performed using trypsin. The resulting mixtures were analyzed by nano-HPLC/ nano-ESI-FTICRMS. We expect to gain further insight into the CaM/AC 8 interaction based on the identified intermolecular cross-linking products.

Notes

1 Sinz A., J. Mass Spectrom. 38:1225-1237 (2003).

2 Gu C., Cooper D.M.F., J. Biol. Chem. 274:8012-8021 (1998).

3 Bähler M., Rhoads A., FEBS Letters 513:107-113 (2001).

Andreas Schmidt

Universität Leipzig

Center for Biotechnology and Biomedicine (BBZ)
Junior Research Group "Protein-Ligand Interaction by Ion Cyclotron Resonance Mass Spectrometry"
and
Faculty of Chemistry and Mineralogy

E-Mail: andreasschmidt.le@web.de
www.uni-leipzig.de/~sinz/

COR-AAD1-00003069
Bayer EX1008 (Part 6 of 9)

4.36 *In vitro* evolution of a thermostabilized Exonuclease III

Ramona Schmiedel, Thomas Greiner-Stöffele

Exonuclease III (ExoIII) of *Escherichia coli*, a DNA-modifying enzyme with four activities, is very frequently used in molecular biology[1]. To expand its applicability a thermostabilized variant of ExoIII could be useful for a method of recombining of homologous DNA sequences[2]. *In vitro* recombination methods have been successfully used to enhance enzyme thermostabilities[3]. Especially DNA family shuffling is a powerful tool for directed evolution combining sequences from individual genes by recombination[4]. In order to generate a library of chimaeric genes we successfully isolated, cloned and sequenced genes encoding the ExoIII gene products from four microbial species closely related to *E. coli*. DNA family shuffling was used to generate a library containing recombined sequences of these homologous genes[5]. Directed evolution experiments require selective screening of great libraries, hence we needed to be able to determine the ExoIII activity against any background activity of *E. coli* in a high throughput compatible way. We therefore established a reliable protein expression and purification protocol as well as an ExoIII activity assay using microtiter plate technology. The assay is based on contact mediated fluorescence quenching in a linear duplex DNA probe and could be shown to be qualified for sensitive screening of ExoIII activity.

Notes

1 Hoheisel J.D., Biochem. 209:238-246 (1993).

2 Koltermann A. et al., [DE 19953854] (2002).

3 Giver L. et al., Proc. Natl. Acad. Sci. USA 95:12809-12813 (1998).

4 Crameri A. et al., Nature 391:288-291 (1998).

5 Kikuchi M. et al., Gene 236:159-167 (1999).

Ramona Schmiedel

Universität Leipzig

Center for Biotechnology and Biomedicine (BBZ)
Junior Research Group "Protein Engineering"
and
Faculty of Biosciences, Pharmacy and Psychology
Institute of Biochemistry

E-Mail: rschmied@uni-leipzig.de
www.uni-leipzig.de/~tgs/

COR-AAD1-00003070
Bayer EX1008 (Part 6 of 9)

4.37 Purification and structural characterization of the annexin II / p11 tetramer from porcine small intestine

Daniela M. Schulz, Andreas Schmidt, Olaf Zschörnig, Stefan Kalkhof, Christian Ihling, Andrea Sinz

The annexin II / p11 heterotetramer (A2t) is a multifunctional protein composed of two annexin II and two p11 (S100A10) subunits. Ca^{2+}-binding mediates its interaction with phospholipids in membranes. A2t plays an important role in membrane interactions, membrane trafficking, and signaling.The purified tetrameric complex was used for structural studies of the A2t interface.

A2t was purified from pig (*Sus scrofa domestica*) small intestine[1]. Briefly, mechanically disrupted mucosal scrapings were washed repeatedly with buffer and centrifuged, retaining the pellet with membrane-bound A2t in the presence of calcium. Addition of EGTA released the tetrameric complex into the supernatant. Further purification was achieved by ion exchange chromatography. The proteins were *in gel* digested and analyzed by nano-HPLC/nano-ESI-FTICRMS and MALDI-TOFMS. The cross-linking reactions were performed using the amine-reactive, isotope-labeled cross-linkers BS^3, BS^2G (d_0 and d_4 each) and DSA (d_0 and d_8).

Sequence coverages from peptide mass fingerprinting of annexin II and p11 were 100 % and 72 %, respectively. Our data on the sequence of porcine annexin II confirm the recently published amino acid sequence[2]. The distance constraints from chemical cross-linking are in good agreement with the X-ray structure published for monomeric annexin II.

The A2t complex will be further characterized with respect to its three-dimensional structure employing chemical cross-linking and FTICRMS.

Notes

1 Gerke V., Weber K., EMBO J. 3:227-233 (1984).

2 Danielsen E.M., van Deurs B., Hansen G.H., Biochemistry 42:14670-14676, (2003).

Daniela M. Schulz

Universität Leipzig

Center for Biotechnology and Biomedicine (BBZ)
Junior Research Group "Protein-Ligand Interaction by Ion Cyclotron Resonance Mass Spectrometry"
and
Faculty of Chemistry and Mineralogy

E-Mail: dschulz@chemie.uni-leipzig.de
www.uni-leipzig.de/~sinz/

COR-AAD1-00003071
Bayer EX1008 (Part 6 of 9)

4.38 Protein-ligand interaction of S-adenosyl-L-methionine and the methyltransferase SU(VAR)3-9

Karsten Seeger, Sandro Lein, Gunter Reuter, Stefan Berger

The recently developed Saturation transfer difference (STD) NMR technique[1] was used to investigate the interaction of S-adenosyl-L-methionine (AdoMet) with SU(VAR)3-9 from *Drosophila melanogaster*. SU(VAR)3-9 has a SET domain and plays an important role in methylation of lysine-9 of histone H3 which results in formation of heterochromatin and gives rise to gene silencing.

We were able to detect a binding interaction of SU(VAR)3-9 and AdoMet in solution and determined the binding epitope of AdoMet. Comparision of the data with a crystal structure of SET7/9 ([2], another SET protein) shows a good agreement for most of the protons.

We therefore conlude, that beside differences for certain ligand protons of AdoMet, the overall binding interaction is similar for the crystal state and SU(VAR)3-9 in solution.

The binding epitope will lead to further investigation of SU(VAR)3-9 mutants with different activity. We plan to combine STD measurements with the transfer NOE technique to test possible conformational changes of the ligand.

Notes

1 Mayer M., Meyer B., J. Am. Chem. Soc. 123:6108-6117 (2002).

2 Kwon T., Chang J.H., Kwak E., Lee C.W., Joachimiak A., Kim Y.C., Lee J.W., Cho Y., EMBO J. 22:292-303 (2003).

Karsten Seeger

Universität Leipzig

Faculty of Chemistry and Mineralogy
Institute of Analytical Chemistry

E-Mail: kseeger@web.de
www.uni-leipzig.de/~nmr/ANALYTIK/

COR-AAD1-00003072
Bayer EX1008 (Part 6 of 9)

4.39 Characterisation of antibodies recognizing phosphorylation dependent epitopes in the tau protein

David Singer, Daniela Volke, Ralf Hoffmann

The microtubule-associated protein tau promotes the assembly and stabilisation of neuronal microtubules. In Alzheimer's disease, tau becomes hyperphosphorylated and self-associated to form paired helical filaments (PHF). Monoclonal antibodies (mAbs) are very useful tools to analyse the phosphorylation status of tau proteins and might be of diagnostic value, if a disease specific phosphorylation pattern is recognised. For that commercially-available polyclonal and monoclonal antibodies directed against several known phosphorylation sites, including Ser212 and Ser231, were tested for their specificity in both ELISA and Western blots. Thus, sequences corresponding to human tau-regions containing several phosphorylation sites, especially 207-219, 224-240 and 390-410 with phosphorylation sites at Ser212, Thr214, Ser217, Ser218, Ser231, Thr235, Ser396, Thr400, Ser403 and Ser404, were synthesised on solid-phase using the Fmoc/tBu-strategy. The peptides were phosphorylated on the solid-phase before deprotection by the global phosphorylation approach using phosphoamidite. After cleavage with trifluoroacetic acid, purification by RP-HPLC and characterisation by mass spectrometry, the phosphopeptides containing up to four phosphate groups were used to map the antibodies for their phosphate-specificity. Furthermore, the antibodies were tested against bovine tau by immunoblots after two-dimensional gel electrophoresis.

David Singer

Universität Leipzig

Center for Biotechnology and Biomedicine (BBZ)
Professorship for Bioanalytics
and
Faculty of Chemistry and Mineralogy

E-Mail: david.singer@bbz.uni-leipzig.de
www.uni-leipzig.de/~bioanaly/

COR-AAD1-00003073
Bayer EX1008 (Part 6 of 9)

4.40 Proteome analysis of *Escherichia coli* using high-performance liquid chromatography and fourier transform ion cyclotron resonance mass spectrometry

Andrea Sinz, Christian Ihling

The basic problem of complexity poses a significant challenge for proteomics studies. To date, 2-DE (two-dimensional gel electrophoresis) followed by enzymatic *in gel* digestion of the peptides, and subsequent identification by mass spectrometry is the most commonly used method to analyze complex protein mixtures. However, 2-DE is a slow and labor-intensive technique, which is not able to resolve all proteins of a proteome. To overcome these limitations gel-free approaches are developed based on high-performance liquid chromatography (HPLC) and Fourier transform ion cyclotron resonance mass spectrometry (FTICRMS). The high resolution and excellent mass accuracy of FTICRMS provides a basis for simultaneous analysis of numerous compounds[1]. In the present study, a small-protein subfraction of an *E. coli* cell lysate was prepared by size-exclusion chromatography and proteins were analyzed using C4 reversed phase HPLC for pre-separation followed by C18 reversed phase nano-HPLC/nano-ESI-FTICRMS for analysis of the peptide mixtures after tryptic digestion of the protein fractions[2]. We identified 231 proteins and thus demonstrated that a combination of two reversed phase separation steps - one on the protein and one on the peptide level - in combination with high-resolution FTICR mass spectrometry has the potential to become a powerful method for global proteomics studies.

Notes

1 Comisarov M.B., Marshall A.G., Chem. Phys. Lett. 25:282-283 (1974).

2 Ihling C., Sinz A., Proteomics, in press.

Dr. Andrea Sinz

Universität Leipzig

Center for Biotechnology and Biomedicine (BBZ)
Junior Research Group "Protein-Ligand Interaction by Ion Cyclotron Resonance Mass Spectrometry"
and
Faculty of Chemistry and Mineralogy

E-Mail: sinz@chemie.uni-leipzig.de
www.uni-leipzig.de/~sinz/

COR-AAD1-00003074
Bayer EX1008 (Part 6 of 9)

4.41 Mapping protein interfaces by affinity cross-linking combined with MALDI-TOF and ESI-FTICR mass spectrometry

Andrea Sinz, Stefan Kalkhof, Christian Ihling

Chemical cross-linking of proteins in combination with mass spectrometric analysis of the reaction products allows a rapid mapping of protein interfaces, which is crucial for understanding protein/protein interactions. The identification of cross-linking products from the complex mixtures created after the cross-linking reaction however remains a daunting task.

In order to facilitate the identification of cross-linking products, we are exploring the use of the trifunctional cross-linker sulfo-SBED (sulfosuccinimidyl-2-[6-(biotinamido)-2-(p-azidobenzamido)-hexanoamido]ethyl-1,3'-dithiopropionate), which possesses one amine-reactive and one photo-reactive site and additionally allows an affinity-based enrichment of cross-linker containing species via its biotin moiety. As model system, we chose the complex between calmodulin and its target peptide M13. The peptide M13 comprises 26 amino acids and represents a part of the C-terminal sequence of the skeletal muscle myosin light chain kinase.

After the cross-linking reaction, the reaction mixtures were subjected to tryptic *in solution* digestion. Biotinylated peptides were enriched on monomeric avidin beads after a number of washing steps had been performed. Peptide mixtures were analyzed by MALDI-TOF and nano-HPLC/nano-ESI-FTICR (electrospray ionization Fourier transform ion cyclotron resonance) mass spectrometry. We demonstrate that an enrichment of cross-linker containing species allows a more efficient identification of interacting amino acid sequences in protein complexes. This strategy is expected to be especially beneficial for investigating large protein assemblies.

Dr. Andrea Sinz

Universität Leipzig

Center for Biotechnology and Biomedicine (BBZ)
Junior Research Group "Protein-Ligand Interaction by Ion Cyclotron Resonance Mass Spectrometry"
and
Faculty of Chemistry and Mineralogy

E-Mail: sinz@chemie.uni-leipzig.de
www.uni-leipzig.de/~sinz/

COR-AAD1-00003075
Bayer EX1008 (Part 6 of 9)

4.42 Localisation of the PHB-biosynthesis in recombinant yeasts

Claudia Stolz, Uta Breuer, Hauke Harms

The polyester polyhydroxybutyrate (PHB), a member of the family of the polyhydroxyalkanoates (PHA), possesses similar properties as polypropylene and polyethylene, which, however, are problematical wastes. PHAs are synthesized by many bacteria as an intracellular carbon and energy storage material with yields of up to 90 % of the biomass. The most interesting properties of these materials are the biodegradability and the biocompatibility. Recently, these materials became interesting for medical applications, e.g. in implants, scaffold in tissue engineering, or as drug carriers. For the production of recombinant PHB in yeasts, the three biosynthesis enzymes (Reductase, 3-Ketothiolase and PHB-Synthase) have been transformed in *Saccharomyces cerevisiae* INVSc1. Up to now the maximally obtained PHB-yield is 6.7 % per gram biomass. To optimize and increase the PHB-synthesis in yeasts the localisation of the terminal enzyme of the biosynthesis, the PHB-Synthase (PhbC) and the polymeric product is very important. The protein phasin (PhaP) is also important in this respect; it stabilizes the developing PHB granules thus leading to an increase of the PHB-synthesis. Probably, the recombinant PHB is accumulated in yeasts within the lipid bodies because of its lipophilic properties. Up to now no microscopic analyses involving staining could differentiate between lipids and PHB. To localize the recombinant PHB in yeasts, translational fusions of the PHB-Synthase and the phasin with the fluorescent reporter yEGFP (yeast enhanced green fluorescent protein) were constructed. First results are reported.

Claudia Stolz

Centre for Environmental Research (UFZ)
Department Environmental Microbiology
E-Mail: claudia.stolz@ufz.de
www.ufz.de

COR-AAD1-00003076
Bayer EX1008 (Part 6 of 9)

4.43 *In vitro* selection of DNA aptamers binding ethanolamine

Beate Strehlitz, Dörthe Mann, Christine Reinemann, Regina Stoltenburg

Aptamers are ssDNA or RNA oligonucleotides with very high affinity to their target, developed by the SELEX-process. They bind to the target with high selectivity and specificity due to their secondary structure. Aptamers will present an attractive alternative for both *in vitro* and *in vivo* applications in the fields of clinical diagnostics and therapy.

We have identified novel aptamers binding to ethanolamine with high affinity. These specific aptamers were selected from an initial 96mer DNA-library in a FluMag-SELEX process. This process is characterized by the use of fluorescein-labeled ssDNA for quantification and magnetic beads as matrix for the immobilisation of the very small target molecule ethanolamine (M_r= 61,08). After this process the enriched aptamer pool was cloned to get individual aptamers, which were sequenced and characterized. The affinity constants (K_D) determined by binding curves range between 6-18 nM.

The aim of the development of ethanolamine specific aptamers is their use for the detection of this substance in clinical and environmental analysis. Ethanolamine is involved in the biosynthesis of glycerophospholipids and in the biosynthesis of acetylcholine as an important neurotransmitter. Disorders of this biosynthesis are connected with diseases like Schizophrenia or Alzheimer's disease as well as the storage disease Ethanolaminosis. The easy and fast determination of ethanolamine in blood or in plasma membranes should be helpful for the early diagnosis of these diseases. A biosensor based on ethanolamine aptamer receptor molecules could be a time and cost effective tool.

Dr. Beate Strehlitz

Centre for Environmental Research (UFZ)

Department Environmental Biotechnology

E-Mail: beate.strehlitz@ufz.de

www.ufz.de

COR-AAD1-00003077

Bayer EX1008 (Part 6 of 9)

4.44 The calcium-dependent regulation of TRPV4 involves the interaction with the carboxy-terminus of Calmodulin

Rainer Strotmann, Torsten Schöneberg

The calcium-permeable cation channel TRPV4 is activated by a number of stimuli, including hypotonic cell swelling, certain derivatives of arachidonic acid and phorbol esters.

A unique property of the TRPV4-mediated current is its calcium-dependent potentiation. In previous studies, we could demonstrate that the underlying molecular mechanism involves the binding of the cytosolic calcium sensor protein Calmodulin (CaM) to a C-terminal binding domain in TRPV4.

In the present study, we have used an *in vitro* proximity assay based on the AlphaScreen™ technology (Perkin Elmer) to map the TRPV4 binding site within the CaM molecule. CaM is a highly symmetrical molecule with two calcium-binding EF hand (EFH) motifs in the N- and C-terminus, respectively. Using truncated and partially calcium-binding deficient mutants, we could show that the interaction with TRPV4 occurs specifically with the C-terminus of CaM and involves the central helical and parts of the EFH3 domains. It could be shown that the AlphaScreen™ assay system can be customized to characterize protein-protein interactions on a nanomolar scale and in a high throughput fashion.

Dr. Rainer Strotmann

Universität Leipzig

Faculty of Medicine
Institute of Biochemistry
Molecular Biochemistry

E-Mail: rainer.strotmann@medizin.uni-leipzig.de
www.uni-leipzig.de/~biochem/MolBiochem/MolBiochem.html

COR-AAD1-00003078
Bayer EX1008 (Part 6 of 9)

4.45 The reverse transcriptase of HIV – Generation of a polymerase with reduced replication fidelity

Sascha Stumpp, Susanne Brakmann

Polymerases are vital for the processes of life. They maintain genetic information in every life-form in a characteristic manner. Isolated polymerases, for example, differ strongly in fidelity, processivity and substrate specificity. Our work focuses on the reverse transcriptase of HIV, which exhibits an average mutation rate of ~$5x10^{-5}$ per nucleotide per replication cycle[1]. As a result, viral offspring differs remarkably in its genotype. Genetic diversity of the virus makes medication very difficult. One possible approach is the further reduction of viral replication fidelity, driving viral progeny to complete loss of infectivity[2]. Using nucleoside analogs, extinction of HIV has been verified *in vitro*[3]. Our plan is to generate a novel reverse transcriptase with an increased error-rate. Currently we apply techniques like shuffling and error-prone PCR to generate mutant libraries and select for active variants with a genetic complementation system. In further studies, we will use a fluorescence-based assay for the identification of mutant reverse transcriptases with increased error-rates[4].

These newly generated polymerases could provide a basis for further studies of structure-function relationships and a future antiviral strategy.

Notes

1 Gao F. et al., J. Virol. 78:2426-2433 (2004).

2 Eigen M. et al., WO 94/01545, (2002).

3 Loeb L.A. et al., Proc. Natl. Acad. Sci. USA 96:1492-1497 (1999).

4 Marx A. et al., Ang. Chem. Int. Ed. 41:3620-3622 (2002).

Sascha Stumpp

Universität Leipzig

Center for Biotechnology and Biomedicine (BBZ)
Junior Research Group "Applied Molecular Evolution Research"
and
Faculty of Biosciences, Pharmacy and Psychology
Institute of Biology II

E-Mail: stumpp@rz.uni-leipzig.de
www.uni-leipzig.de/~sbrakma/

COR-AAD1-00003079
Bayer EX1008 (Part 6 of 9)

4.46 A phosphopeptide capturing Fe kit designed for selective isolation of phosphopeptides on the surface of superparamagnetic micro particles

Corinna Sykora, Peter Hoffmann, Thomas Elßner, Markus Kostrzewa, Ralf Hoffmann

Protein phosphorylation is one of the most important regulatory mechanisms in the cell. It regulates for example the activity, localisation or interaction with other proteins. Identification of phosphorylation sites is complicated due to low phosphorylation degrees, endogenous phosphatase activity, unspecific binding to metal surfaces and discrimination during the ionization process of mass spectrometrical analyses. The aim of the work presented here was to establish a general, robust method to enrich phosphopeptides from complex peptide mixtures based on immobilized metal affinity chromatography (IMAC).

The "Phosphopeptide Capturing Kit" (Bruker Daltonics, Bremen, Germany) is designed for selective enrichment of phosphopeptides, for example from protein digests. Here, purified synthetic phosphopeptides with different but well defined phosphorylation states (none, singly, doubly and triply phosphorylated) and digests of phosphoproteins as well as protein mixtures were enriched with IMAC. Thus, the enriched peptides were spotted on regular MALDI targets or Prespotted AnchorChip targets (Bruker Daltonics) and analysed using MALDI-TOF/TOF mass spectrometry.

This method worked for singly, doubly and triply phosphorylated peptides. The detection limit for singly phosphorylated peptides was approximately 500 fmol using a tryptic β-casein digest and 5 pmol for the quadruply phosphorylated peptide using a conventional AnchorChip. The "Prespotted AnchorChips" increased the sensitivity about 10 fold allowing identification of the singly phosphorylated at the 50 fmol and for the quadruply phosphorylated peptide at the 1 pmol level.

Corinna Sykora

Universität Leipzig

Center for Biotechnology and Biomedicine (BBZ)
Professorship for Bioanalytics
and
Faculty of Chemistry and Mineralogy

E-Mail: corinna.sykora@bbz.uni-leipzig.de
www.uni-leipzig.de/~bioanaly/

COR-AAD1-00003080
Bayer EX1008 (Part 6 of 9)

4.47 FLOCKTYPE®recIBDV/recIBV/recNDV – The new generation of poultry virological ELISAs

Daniela Trepnau, Claudia Engemann, Katja Höschler, Roland Hackl, Michael Hess, Thorsten Arnold, Johannes-Joachim Arnold, Vikram N. Vakharia, Jörg Gabert, Jörg Lehmann

Several ELISAs, based on inactivated viral antigens, has been developed for serological diagnosis of poultry viral infections. The standardisation of those tests runs into some problems due to the non-homogenous distribution of single antigenic components within different lots of the native antigen.

Alternatively, recombinant proteins can be used as antigens. We have cloned and expressed three recombinant proteins derived from the infectious bursal disease virus (IBDV), the infectious bronchitis virus (IBV), or the Newcastle disease virus (NDV) and developed independent ELISAs by using the respective antigen. These novel tests were proved to be useful for the detection of virus-specific IgY antibodies induced by immunisation.

To prove that the new tests lead to comparable results obtained with conventional commercial test kits, we investigated reference sera obtained from vaccinated chickens with both kinds of tests. The diagnostic specificity and sensitivity were determined to be 100 %. Additionally, a field study with vaccinated chickens revealed that the antibody titre is variable for every flock. Some of them had high antibody levels, indicating that those flocks are well protected. However, other ones had a low antibody level, indicating the need of a booster vaccination. Taken together, all three recombinant protein-based tests are very sensitive, specific and reliable tools for quantification of the vaccination state of poultry flocks. The main advantage is the standardisation in antigen production, which yields high reproducibility and reliability of the new generation of poultry virological ELISAs.

Daniela Trepnau

Labor Diagnostik GmbH Leipzig

Research & Development
Immunology

E-Mail: dt@lab-leipzig.de
www.lab-leipzig.de

COR-AAD1-00003081
Bayer EX1008 (Part 6 of 9)

4.48 Novel protein microarrays for detection of posttranslational modification activities

Larissa Vasilets, Jörg Nerkamp, Carsten Voigt, Michael Braun

One of the most extensive groups of cellular protein activities is those which produce posttranslational modification. They are characteristic of all living cells and highly significant for proteome studies as well as for the development of pharmaceuticals. These activities trigger changes in the functional properties of modified proteins. BIOSCORA is a young biotechnology company, which uses proprietary lab-on-chip technologies to perform detection of posttranslational modification activities free of radioactive or dye labelling. Our technologies enable fast and effective real time detection of protein kinase, phosphatase and protease activities in multiplex. Biosensors for the detection of protein kinase activities are designed *in silico*, cloned in expression vectors, expressed in *E. coli* and purified as heterologous proteins. Assays can be performed in wellplate as well as in microchip scale, and will find applications in proteome studies, molecular medical diagnostics, studies of disease mechanisms, high-throughput screening and toxicological studies. Examples of the new generation of activity microarrays based on the label-free electrical detection and those based on optical detection methods will be presented and discussed.

Dr. Dr. Larissa Vasilets

BIOSCORA GmbH

E-Mail: info@bioscora.de

www.bioscora.de

COR-AAD1-00003082

Bayer EX1008 (Part 6 of 9)

4.49 Lipid modifications of a Ras peptide lead to alteration of bilayer packing and softness as detected by 2H solid-state NMR

Alexander Vogel, Guido Reuther, Catherine Katzka, Herbert Waldmann, Klaus Arnold, Michael F. Brown, Daniel Huster

Many proteins involved in signal transduction are anchored to membranes by covalently attached lipid modifications. In this study, we investigated the insertion of the acyl chains of a doubly lipid-modified heptapeptide from the C-terminus of the human N-Ras protein into DMPC membranes using ^{2}H NMR. Information about the chain dynamics and membrane packing properties was obtained from powder-type samples of both deuterated DMPC with protiated ras peptide and protiated DMPC with deuterated ras peptide, at a peptide to lipid ratio of 1:15. De-Pakeing of the spectra yields a number of resolved quadrupolar splittings, which can be assigned to different CD_2 groups in the hydrocarbon chains of the peptide or the lipid, respectively. The order parameters determined for the ras chains are significantly lower than those of DMPC, meaning that the length of the alkyl groups of the peptide is adjusted to match the length of the phospholipid chains. Accordingly, the mean area per hydrocarbon chain is larger for the ras peptide than for the lipid, in good agreement with the assumption that the peptide backbone requires more space at the membrane interface than the lipid headgroups. Additionally, R_{1Z} relaxation rate measurements have been performed. While the square law plot for DMPC in the presence of ras peptide shows a straight line, the plot for ras peptide in a DMPC membrane is bent and is comparable to that of DMPC in the presence of a detergent like $C_{12}E_8$. Therefore, the hydrocarbon chains of the ras peptide are more flexible and softer than those of the surrounding lipid matrix.

Alexander Vogel

Universität Leipzig

Center for Biotechnology and Biomedicine (BBZ)
Junior Research Group "Solid-state NMR Studies of the Structure of Membrane-associated Proteins"
and
Faculty of Medicine
Institute of Medical Physics and Biophysics

E-Mail: voga@medizin.uni-leipzig.de
www.uni-leipzig.de/~huster/

COR-AAD1-00003083
Bayer EX1008 (Part 6 of 9)

4.50 Characterization of the molecular distribution of bovine tau protein with respect to its posttranslational modifications

Daniela Volke, Peter Hoffmann, Ralf Hoffmann

The brain of Alzheimer's disease (AD) patients is characterized by senile plaques (SP) and neurofibrillary tangles (NFT). The major proteinaceous component of SP is the amyloid β-peptide, Aβ. The tangles represent dense accumulations of paired helical filaments (PHF), comprising excessively phosphorylated forms of the low molecular weight microtubule associated protein, tau. Functionally, tau binds to tubulin and PHF-tau practically does not caused by its hyperphosphorylation. In recent years, this hypothesis was extended to other posttranslational modifications, such as glycosylation and isomerization. However, this hypothesis is based mostly on separation of the tau-isoforms by SDS-PAGE and probing the western blots with different sets of antibodies, without separating the modified versions of each isoform.

Our work aims to separate all tau-isoforms including their posttranslationally modified versions using 2D gel electrophoresis followed either by mass spectrometrical identification of the spots or probing them with monoclonal antibodies (mAbs) of different specificity. Thus, we could show that more than 50 tau-versions are present in bovine brain. The image of these tau-versions after 2D gel electrophoresis was independent of the preparation protocols starting from fresh calf brain samples. This indicates that the obtained pattern resembles closely the molecular distribution *in vivo*. Furthermore, we could show that all tau-versions can be enriched by affinity-chromatography using mAb BT-2. The complex pattern of posttranslational modifications as well as a novel concept to explain the data will be presented.

Daniela Volke

Universität Leipzig

Center for Biotechnology and Biomedicine (BBZ)
Professorship for Bioanalytics
and
Faculty of Chemistry and Mineralogy

E-Mail: daniela.volke@bbz.uni-leipzig.de
www.uni-leipzig.de/~bioanaly/

COR-AAD1-00003084
Bayer EX1008 (Part 6 of 9)

4.51 Monitoring of biotechnological processes by sodium dodecyl sulfate-polyacrylamide gel electrophoresis (SDS-PAGE)

Patrick Wunderlich, Ina Schulze, Melanie Nickel, Katrin Emmerling, Dirk Mischke, Ullrich Pigla, Rüdiger Laub

The manufacture of biopharmaceuticals is a complex process of biotechnological methods such as fermentation and subsequent alteration and purification of active pharmaceutical ingredients (API) based on proteins. The analysis of discrete protein species is of pivotal significance to manage single production steps, as well as for the quality control of the final processed bulk itself.

We have established a GMP-conform process to produce a monoclonal antibody (mAb) in hollow-fiber bioreactors (upstream process, USP), which is subsequently proteolytically cleaved into Fab-fragments and chemically conditioned for radiolabeling (downstream process, DSP).

SDS-PAGE was validated according to the guidelines of the International Conference on Harmonization (ICH) and was used to demonstrate the presence and the identity of the target protein in the fermentation broth (USP). In DSP, the analytical method served as inprocess control to monitor (i) the capture of the target protein by affinity chromatography, (ii) the efficiency of papain-mediated cleavage, and (iii) the results of discrete purification steps.

Moreover, gels were prepared from probes of the final processed bulk to confirm the identity of the API according to the guideline ICH Q6B.

Taken together, SDS PAGE, in conjunction with other analytical methods, has been proven as a valuable tool to facilitate supervising and controlling of complex biomanufacturing processes.

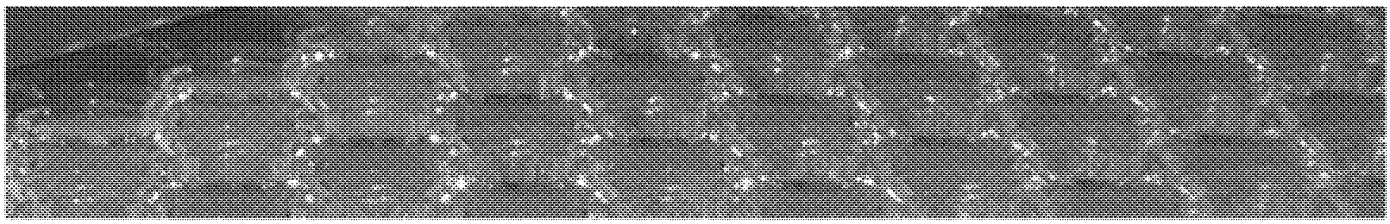
Patrick Wunderlich

Biotectid GmbH

E-Mail: wunderlich@biotectid.de
www.biotectid.de

COR-AAD1-00003085
Bayer EX1008 (Part 6 of 9)

5. MOLECULAR MEDICINE AND THERAPEUTICS



POSTERS

COR-AAD1-00003088
Bayer EX1008 (Part 6 of 9)

5.1 A candidate gene association study in rheumatoid arthritis, strategies for gene and polymorphism selection and an application of the GENOLINK™ genotyping system

Peter Ahnert

Rheumatoid Arthritis (RA) is a common complex autoimmune disease of rather unclear etiology.

There is evidence that certain patterns of specific variants of specific genes distributed throughout the whole genome are implicated in the genetic risk of RA.

Our approach is to identify such genes in a candidate gene association study.

To select genes and polymorphisms, we aim to integrate current knowledge. So we develop network analysis strategies and apply public mining tools and mainly publicly available data sources. We select SNPs for their position, frequency, ethnicity, state of validation and reported or predicted function (e.g. interference with potential transcription factor binding sites, splice sites and exonic splice site enhancers, and peptide domain architecture). Our genotyping technology is the GENOLINK™; genotyping system (Bruker Daltonics). This comprises PCR, primer extension, and MALDI-TOF analysis. We develop mostly Java™ based software tools to speed up and improve snp selection, assay design and assay optimisation.

We also apply and try to improve current data analysis methods (e.g. decision trees, max. likelihood aproaches, parametric/nonparametric methods, pattern analyses, support vector machines...). In our current undergoing study we investigate 78 different genetic variations, most of them single nucleotide polymorphisms (SNPs) in 31 candidate genes in 450 individuals. Preliminary results based on TDT tests show the association of seven genes to rheumatoid arthritis with p values ranging between 0.01 and 0.001.

Dr. Peter Ahnert

Universität Leipzig

Center for Biotechnology and Biomedicine (BBZ)
Junior Research Group "Molecular Diagnostics - Microarray Techniques"
and
University Hospital
Institute of Clinical Immunology and Transfusion Medicine

E-Mail: ahnert@uni-leipzig.de
www.uni-leipzig.de/~ahnert/

COR-AAD1-00003089
Bayer EX1008 (Part 6 of 9)

5.2 Gabapentin-lactam failed to prevent rotenone-induced cell death in human neuroblastoma cells

Clemens Allgaier, Julia Kochen, Susana Garcia de Arriba, Ester Verdaguer

Mitochondrial complex-I inhibition by rotenone is used as a model for studying neurochemical alterations associated with Parkinson's disease[1]. As recently demonstrated, the neurotoxic effect of rotenone is counteracted by activation of ATP-sensitive potassium (K-ATP) channels. Gabapentin-lactam (GBP-L) has recently been showed to be neuroprotective and this effect has been related to its K-ATP mitochondrial channel opening properties. Therefore, we investigated in human neuroblastoma (SH-SY5Y) cells the possible neuroprotective effect against rotenone-induced cell damage. Rotenone (1-100 µM for 16 h) induced necrotic cell death in SH-SY5Y cells in a dose-dependent manner. The loss of plasma membrane integrity was assessed by flow cytometry using propidium iodide. In addition, it was demonstrated by staining of cell nuclei with the fluorescent dye Hoechst 33258, DNA laddering and cytochrome c release that apoptotic pathways contribute to rotenone-induced cell death. GBP-L (10-100 µM), pre- and co-applied with rotenone was not able to reduce cell death, to prevent DNA fragmentation or cytochrome c release related to rotenone application. Instead, GBP-L showed a certain level of toxicity that became evident at 100 µM by propidium iodide staining. In conclusion, in SH-SY5Y cells GBP-L did not prevent the rotenone-induced cell damage, but induced at higher concentrations some toxic effects by its own. Accordingly, the present data do not support the idea that K-ATP channel openers such as GBP-L may be useful in the treatment of neurodegenerative diseases related to mitochondrial dysfunction.

Notes

1 Betarbet R. et al., Nat.Neurosci. 3:1301-1306 (2000).

Prof. Dr. Clemens Allgaier
Universität Leipzig
Faculty of Medicine
Rudolf Boehm Institute of Pharmacology and Toxicology
E-Mail: allgc@medizin.uni-leipzig.de
www.uni-leipzig.de/~pharma/

COR-AAD1-00003090
Bayer EX1008 (Part 6 of 9)

5.3 The role of β-catenin mutations and expression of glutamine synthetase in the development of hepatocellular carcinomas

Madeleine Austinat, Frank Gaunitz, Andrea Tannapfel, Rolf Gebhardt

Hepatocellular carcinoma (HCC) is the most frequent cancer of the liver. Although activation of the Wnt signalling pathway as indicated by nuclear localization of β-catenin is frequently observed, the prognostic value is still a matter of debate. Recently, glutamine synthetase (GS) was shown to be a putative transcriptional target of β-catenin. Mouse tumors haboring activating β-catenin mutations are stained GS positive. To verify whether this is conferrable we analysed 43 patients suffer from HCC by immunohistochemistry and mutations in the β-catenin gene.

Immunohistochemistry detected intracellular b-catenin in 22 samples. Twelve of these samples were also positively stained for GS. So far, sequence analysis of the ß-catenin gene was performed in 13 samples. In six out of seven samples showing co-localization mutations were identified within the TrCP recognition sequence, whereas in three out of six samples presenting only the β-catenin positive phenotype mutations were detected downstream of this site. Presumably, only specific activating β-catenin mutations are leading to the co-localized phenotype. Mutations in Axin1 or Axin2 may lead to positive nuclear staining of β-catenin due to deranged β-catenin degradation. This may be the case for the remaining samples where no mutations were found. Whether mutations in the Axin genes result only in an activation of β-catenin or may also lead to aberrant GS expression is currently investigated.

Only a subset of β-catenin mutations seems to lead to enhanced GS expression. This is of pathological importance, since it was shown that GS expression in HCCs is a negative prognostic marker.

Madeleine Austinat

Universität Leipzig

Faculty of Medicine
Institute of Biochemistry
Biochemistry

E-Mail: madeleine.austinat@medizin.uni-leipzig.de
www.uni-leipzig.de/~biochem/

COR-AAD1-00003091
Bayer EX1008 (Part 6 of 9)

5.4 *In situ* cytokine profiling of UVB-exposed human skin by combination of dermal microdialysis and protein microarrays

Marco Averbeck, Simone Beilharz, Matthias Bauer, Carl Gebhardt, Friederike Kauer, Ursula Voith, Jonathan Sleeman, Jan C. Simon, Christian Termeer

Investigation of real time extracellular cytokine secretion *in situ* has been limited by low-cut off filtering membranes and sample volume size. Importantly, the evolving immune response is triggered by early release of a cytokine cascade into the extracellular space. Further, it becomes more and more obvious, that the simplification of the TH-1/TH-2 model cannot copes the *in vivo* situation. Therefore, we combined the methods of intradermal microdialysis and antibody protein arraying to profile the early cascade of multiple cytokines in a complex immune response exemplified by UVB-induced inflammation. Quantitative cytokine analysis of the microdialysis fluid revealed that UVB-irradiation results in a TH2 biased immune response (IL-4, IL10) after 24 h which evolved from a strong and rapid inflammatory response, mainly depending on the secretion of TNF-α, IL-6 and IL-8 in the first 8-16 h; but also included both, TH1 and TH2 associated cytokines by secretion of IL-2, IL-12, IL-4, IL-10, and TGF-β1. The combination of the intradermal microdialysis and protein microarray analysis enable us to get a more realistic picture of the complex and rapidly changing interstitial cytokine milieu in the acute response of human skin to UVB-irradiation.

Dr. Marco Averbeck

Universität Leipzig

University Hospital
Department of Dermatology

E-Mail: marco.averbeck@medizin.uni-leipzig.de
www.uni-leipzig.de/~derma/

COR-AAD1-00003092
Bayer EX1008 (Part 6 of 9)

5.5 Large scale production of Taxol® from biosynthetical precursors by enzymatic semisynthesis

Martin Becker, Klaus Häupke, Jürgen Hensel, Daria Rybakova, Till Hornbogen, Rainer Zocher, Christian Pflieger, Doreen Liesicki, Dieter Frense, Gerald Lauckner

Taxol® or paclitaxel is a taxoid drug found in the bark and roots of several taxus species. Its unique way of action made paclitaxel one of the most successful therapeutics for treatment of different types of cancer discovered during the past decades.

From the discovery of its antitumor activities to the approval for wide spread clinical applications the supply of paclitaxel has been a constant problem. Highest concentrations of paclitaxel were found in the bark and roots of Pacific or European yews but destructing the endangered yew populations is no way to meet the growing pharmaceutical demand of the substance. Very soon the idea was born to transform biosynthetic precusors of paclitaxel from renewable parts of the yew into paclitaxel. Concentrations of paclitaxels precursor, baccatin, are small but its deacetylated precursor, 10-deacetylbaccatin, is found in the needles of the yew in concentrations up to hundred times higher than the concentration of baccatin or paclitaxel.

Since chemical acetylation of 10-DAB to baccatin is not economically feasible the aim of the presented work was to isolate an acetyltransferase from the roots of the European yew and develop a large scale semisynthetical process for the production of baccatin. Based on this enzyme a new approach for bac-catin production using an enzyme membrane reactor is presented as well as refined processes for the isolation of 10-DAB and baccatin. Semisynthetic production as large as 5 g baccatin per week was acchieved.

Dr. Martin Becker

Institute of Bioanalytics Halle GmbH

E-Mail: ifbhallegmbh@t-online.de
www.ifb-halle.de

COR-AAD1-00003093
Bayer EX1008 (Part 6 of 9)

5.6 Depot-specific differences in adipocyte biology and adipose tissue gene expression-parallel regulation in humans and mice

Janin Berndt, Susan Kralisch, Mathias Fasshauer, Ralf Paschke, Michael Stumvoll, Ronald Kahn, Matthias Blüher

Visceral and subcutaneous adipose tissue display important metabolic differences that underlie the association of visceral fat with insulin resistance, type 2 diabetes and the risk of cardiovascular disease. The functional and molecular differences contributing to this association are not completely understood. Murine and human visceral adipose tissue evidences a higher lipolytic activity and decreased insulin sensitivity in comparison to subcutaneous adipose tissue. Moreover, there is evidence for intrinsic differences in gene expression between visceral and subcutaneous adipose tissue in normal mice. Our aim was therefore to investigate whether gene expression differences detected by microarray analysis in adipose tissue of C57Bl6 mice could be confirmed in healthy humans using the same genomic approach. Gene expression analysis was performed using 10 µg of cRNA isolated from subcutaneous and visceral adipose tissue from C57Bl6 mice and hybridizd to Affymetrix oligonucleotide microarrays (MG U74A-v2 chips). In addition, RT-RCR was performed to confirm the most significant gene expression differences in mice and parallel in human. Of the 12,488 genes represented on the chip, 72 genes were identified as fat-depot-specific changed, including fatty acid synthase, lamin A, IL-6, β-adrenergic receptors, leptin, carnitine palmitoyl transferase 2,TGFβ, angiotensinogen, PKC β und δ. Our data suggest that instrinsic differences in gene expression between subcutaneous and visceral adipose tissue are evolutionary conserved and might therefore contibute to the link between visceral fat and insulin resistance.

Susan Kralisch

Universität Leipzig

University Hospital
Department of Internal Medicine III

E-Mail: susan.kralisch@medizin.uni-leipzig.de
www.uni-leipzig.de/~innere/

COR-AAD1-00003094
Bayer EX1008 (Part 6 of 9)

5.7 A novel approach to identify cellular target proteins of quercetin in human cells

Markus Böhl, Herwig O. Gutzeit

Despite the wealth of information concerning biological effects of flavonoids a systematic approach to analyse the molecular targets is still lacking and, for this reason, a rational evaluation of the risks or benefits of flavonoid- containing food or of possible pharmaceutical applications has not been possible. When the flavonoid quercetin binds to a target protein like BSA, the respective spectral properties of the protein and the ligand change. Upon excitation in UV the autofluorescence of the target protein is effectively quenched. When excited at longer wavelength a fluorescence signal is elicited in some protein/ligand combinations. This effect can be exploited to visualise quercetin target proteins in the fluorescence microscope that appear to be mainly present in the cell nucleus. For this reason we isolated nuclei of HL-60 cells and monitored the quercetin-dependent decrease of protein autofluorescence in protein fractions of nuclear extracts which were obtained by column chromatography. Those fractions containing quercetin target proteins were separated by SDS-PAGE and further analysed by MALDI-MS (collaboration with Prof. B. Hoflack, Biotec, TU Dresden). Amongst other proteins we identified actin as one of the target proteins. To verify the flavonoid/actin interaction we showed that actin autofluorescence decreases strongly after addition of quercetin. Using this approach, other target proteins of quercetin or other ligands can be identified systematically. This type of information will help to interpret the observed complex biological effects of flavonoids.

Prof. Dr. Herwig O. Gutzeit

Technische Universität Dresden

Department of Mathematics and Natural Sciences
(with Psychology)
Institute of Zoology
Zoology and Developmental Biology

E-Mail: herwig.gutzeit@mailbox.tu-dresden.de
www.biologie.tu-dresden.de/zoologie/dev-home.html

COR-AAD1-00003095
Bayer EX1008 (Part 6 of 9)

5.8 DNAzymes designed to inhibit prothrombin gene expression are outperformed by an antisense oligodeoxynucleotide

Markus Böhl, Bernd Schwenzer

DNA with nucleolytic activity towards RNA like the extensively studied 10-23 DNAzymes, has been considered to be a potential agent useful in the treatment of various diseases because of the specific mode of action. Even tho many DNAzyme based agents are reported to cleave their substrate mRNA successfully in cell free activity test systems, the number of reported DNAzymes to be effective in cell culture is much smaller. The reasons for this are well known. DNAzymes have to overcome the same hurdles like any other nucleotide based agent when they should be active in living cells and there is the additional fact, that cell free test systems utilise optimal conditions for the cleavage reaction which can not be found in cells cytoplasm. Therefore DNAzymes for the use in living cells should not be selected by a cell free activity test.

We wanted to know if the inhibition of prothrombin gene expression which was observed by us for an antisense oligodeoxynucleotide in cell culture can be outperformed by DNAzymes directed against the same target region. This approach has the benefit over other reports dealing with this topic that we were able to direct the DNAzymes against a proven accessible site within the prothrombin mRNA. The substrate binding arms of the respective DNAzymes were designed in a way, that they do always cover the exact target sequence of the original antisense oligodeoxynucleotide. We found that the DNAzymes used in this study were outperformed in their inhibition efficiency by the antisense oligodeoxynucleotide directed against the same target region.

Dr. Markus Böhl

Technische Universität Dresden

Department of Mathematics and Natural Sciences
(with Psychology)
Institute of Zoology
Zoology and Developmental Biology

E-Mail: markus.boehl@mailbox.tu-dresden.de
www.biologie.tu-dresden.de/zoologie/dev-home.html

COR-AAD1-00003096
Bayer EX1008 (Part 6 of 9)

5.9 Bioreactor "FiberReact" – The complete solution

Klaus Breese, Tanja Bloß

The FiberReact bioreactor is a complete cell cultivation system adaptable to the needs of all possible applications like production of cell mass or production of cell products like antibodies. Heart of the system are hollow fiber bundles embedded in plastic-cartridges. They are used as cultivation matrix for the cells (hydrophilic fibers) and for the oxygenation of the medium (hydrophobic fibers).

Developed for long term cell cultivation, the FiberReact system shows innovative features to make cell cultivation easier to handle, better reproducible and more cost-effective:

- online measurement and documentation of pH, pO_2 and temperature
- non-invasive, optical measurement of pH and pO_2
- use of disposables means less hands on time and less contamination risk
- modular construction system enables user specific solutions.

Additional benefit for the user can be reached by coating of the hollow fiber surface with cell specific molecules leading to better cell adhesion and higher quality of cells (e.g. specific differentiation). Appropriate technologies for the coating with bioactive molecules were developed, leading to new applications like cell specific therapies.

Dr. Klaus Breese

BECIT GmbH

E-Mail: info@becit-fibers.com
www.becit-fibers.com

COR-AAD1-00003097
Bayer EX1008 (Part 6 of 9)

5.10 Synthesis of novel 4-phenylhydrazinopyrazolo [3,4-*d*]pyrimidines as ligands for the human A_{2A} adenosine receptor

Detlef Briel, Richard Aurich, Klaus Unverferth, Ute Egerland

A prevention of dopamine receptor degeneration should lead to a synergistic action to the simultaneous administration of A_{2A}-antagonists and dopamine agonists or L-DOPA. These interactions could be the basis of new therapy conceptions of Morbus Parkinson[1-3].

Some pyrazolopyrimidines with specific substitution pattern are characterised by high receptor affinity and A_{2A}-selectivity[2].

For this reason our target was the synthesis of new 4-phenylhydrazino-pyrazolo[3,4-*d*]pyrimidine derivatives bearing a residue with low polarity at the pyrazole ring to obtain substances with A_{2A}-affinity.

Both imino-1,3-thiazines and pyrimidine carbaldehydes served as edducts. To synthesize pyrazolopyrimidines, different substituted hydrazines were used. Starting from imino-1,3-thiazines, 2-phenylsubstituted pyrazolopyrimidines were obtained. However, an alternative reaction path was favoured when pyrimidine carbaldehydes were used. Thereby the products were phenylsubstituted in the 1-position.

The affinity of the products towards the human A_{2A} adenosine receptor was determined in competitive radioligand-receptor binding experiments. Thereby the synthesized pyrazolopyrimidines proved out significant effects. A phenyl residue in the 1-position caused a higher affinity.

Notes

1 Fredholm B.B., Jzerman A.P., Jacobson K.A., Klotz K.N., Linden J., J. Pharmacol. Rev. 53:527 (2001).

2 Müller C., Drugs of the future 25, 43 (2000).

3 Warstat C., Nieber K., Deutsche Apotheker Zeitung 31:3494 (2004).

PD Dr. Detlef Briel

Universität Leipzig

Faculty of Biosciences, Pharmacy and Psychology
Institute of Pharmacy
Pharmaceutical Chemistry

E-Mail: briel@rz.uni-leipzig.de
www.uni-leipzig.de/~pharm/phache/

COR-AAD1-00003098
Bayer EX1008 (Part 6 of 9)

5.11 Production and characterization of monoclonal antibodies against the nucleocapsid protein of Severe Acute Respiratory Syndrome-associated Coronavirus (SARS-CoV)

Bianca Bußmann, Sven Reiche, Lotta H. Jakob, Jan M. Braun, Christian Jassoy

In 2002, a new virus known as the Severe Acute Respiratory Syndrome-associated Coronavirus (SARS-CoV), caused an epidemic with atypical pneumonia in China, followed by fast worldwide spreading in 2003. One of its structural proteins, the nucleocapsid (N) protein, was found in serum and different body fluids of patients early after the onset of symptoms. The detection of this protein could be used for fast diagnosis and further studies of SARS-CoV infection.

The RNA of the N protein of SARS-CoV was reverse transcribed and cloned in a bacterial expression vector. A recombinant N protein (N-MBP) was expressed consisting of the fusion protein of SARS-CoV N protein and *E. coli* maltose-binding protein (MBP). Balb/c mice were immunized and monoclonal hybridoma cultures were generated from its spleen cells. Cell culture supernatants of the hybridoma cultures were screened for production of antibodies against the N protein by ELISA, Western blot and immunofluorescence. The obtained antibodies were characterized concerning isotype and bound epitope. In immunofluorescence assay the N protein was localized mainly perinuclear but also in core.

Ten independent monoclonal cultures could be established, all were of IgG type. Until now three linear and three conformational epitopes are identified.

Altogether the immunization of mice with N-MBP led to a strong immune reaction and B-lymphocytes that could be used to generate antibody-producing hybridomas. Antibodies obtained from these cell cultures may be useful in viral diagnostic tests and research on SARS virus pathogenesis.

Bianca Bußmann

Universität Leipzig

Faculty of Medicine
Institute of Virology

E-Mail: bianca.bussmann@medizin.uni-leipzig.de
www.uni-leipzig.de/~virology/

COR-AAD1-00003099
Bayer EX1008 (Part 6 of 9)

5.12 Gene silencing in acute and persistent measles virus infection

Claire Fabian, Ute G. Brinckmann, Uwe G. Liebert

RNA interference (RNAi) is induced by short interfering RNA (siRNA) which leads to specific mRNA degradation and therefore abrogates the specific protein expression. This mechanism is highly sequence specific. Even one mismatch can inhibit the RNAi effect. The aim of the experiment presented here was to analyse the antiviral usage of siRNA in cells lytically and persistenly infected with measles virus (MV), a nonsegmented negative-stranded RNA virus. Three siRNA Expression Cassettes (SEC) were constructed. The SECs are composed of the human H1 promotor, the coding regions for sense and antisense separated by a loop region and the terminator. According to the experimental protocol described by Castanotto et al (2002) two PCRs were established and optimised to produce the SECs. SECs were designed to hybridise with the mRNA of the Nucleocapsidgene (N) at the strongly conserved 5'-region. Two viral model systems were transfected with the SEC using lipofection: Lytically infected HeLa cells and persistently infected neuroblastoma cells (SH-SY5Y). The amount of N-specific RNA was measured. It was decreased up to 43 % for the lytical and 65 % for the persistent infection. The number of cells expressing N-protein was quantified by FACS analysis using monoclonal antibodies. A decrease for N-protein was seen in both, lytical and persistent infection. The results indicate that RNAi can be induced in lytically and persistently MV infected cells.

References

Castanotto et al., RNA. 2002 Nov;8(11):1454-60.

Claire Fabian

Universität Leipzig

Faculty of Medicine
Institute of Virology

E-Mail: claire.fabian@medizin.uni-leipzig.de
www.uni-leipzig.de/~virology/

COR-AAD1-00003100
Bayer EX1008 (Part 6 of 9)

5.13 Reduction of VEGF gene expression by antisense oligonucleotides in bladder and breast cancer cells

Yvonne Förster, Axel Meye, Sabine Krause, Bernd Schwenzer

Angiogenesis plays a key role in tumor growth and metastasis. Vascular endothelial growth factor (VEGF) is one of the major angiogenic factors. In the study we have evaluated the efficiency of antisense oligodeoxynucleotides (AS-ODN) against VEGF selected from computational prediction of VEGF mRNA structure. Twenty-five different AS-ODN in two different tumor cell lines were investigated. Treatment of cell line EJ28 by VEGF723 resulted in a 83.5 % suppression of VEGF protein when compared with control-ODN. Three further AS-ODN reduced VEGF protein more than 45 % in comparison to control-ODN. This was caused by an antisense-specific downregulation of the VEGF transcript determined by real-time PCR. Furthermore, antisense-mediated inhibition of VEGF was associated by a reduced cell viability. In MCF-7 cells VEGF protein was inhibited more than 45 % by two AS-ODNs. In conclusion, we found that computational prediction of potential single strand mRNA motifs is a well suitable method to elect effective AS-ODN.

Yvonne Förster

Technische Universität Dresden

Department of Mathematics and Natural Sciences
(with Psychology)
Institute of Biochemistry

E-Mail: yvonne.foerster@chemie.tu-dresden.de
www.chm.tu-dresden.de/bc/

COR-AAD1-00003101
Bayer EX1008 (Part 6 of 9)

5.14 Antisense-mediated inhibition of tissue factor expression in different tumor cell lines

Yvonne Förster, Bernd Schwenzer

Human tissue factor (TF) is the initiator of blood coagulation. Beside this function it is involved in tumor angiogenesis and metastasis. In the study we have evaluated the efficiency of antisense oligonucleotides (AS-ODNs) against TF selected from computational prediction of TF mRNA structure. Fourteen different AS-ODNs were tested in three cell lines of different origin with a high TF content. In cell line MCF-7 TF gene expression was inhibited up to 50 % by AS-7 in comparison to reference. To investigate the dependence of inhibition efficiency on the AS-ODN position inside a potential target motive we designed further AS-ODNs shifted 2-3 nt among AS-7. One AS-ODN was found that was more effective than AS-7. In cell line T508 we found moderate effects in inhibition of TF gene expression of 30 % by AS-4. In J82 cell TF protein was inhibited up to 68.6 % by two AS-ODNs. In conclusion, we compared inhibition of TF gene expression in different cancer cell lines and found that all effective AS-ODNs were located in the translated region of TF mRNA. Suitability of a target region of an AS-ODN is relativ independent on cell line. In contrast, optimal transfection conditions are dependent on cell line.

Yvonne Förster

Technische Universität Dresden

Department of Mathematics and Natural Sciences
(with Psychology)
Institute of Biochemistry

E-Mail: yvonne.foerster@chemie.tu-dresden.de
www.chm.tu-dresden.de/bc/

COR-AAD1-00003102
Bayer EX1008 (Part 6 of 9)

5.15 Highway for light – Müller cells as living optical fibers

Kristian Franze, Jens Grosche, Serguei N. Skatchkov, Stefan Schinkinger, Ortrud Uckermann, Kort Travis, Andreas Reichenbach, Jochen Guck

Vision is one of our most important senses. The cells responsible for converting light into electrical impulses are the photoreceptor cells (PRs). However, due to the constraints of evolution, the vertebrate retina is the "wrong way round": in order for light to reach the PRs, it must first pass through several retinal layers of different types of cells. Particularly under low-light conditions additional structures are required which guarantee optimal utilization of the light. These structures ideally span the entire thickness of the retina and guide the light through all of the light-scattering layers to the PRs. Only the so-called Müller cells, the principal retinal glial cells, have these properties. Furthermore, these cells contact every single PR.

In the present work, the light guiding properties of individual Müller cells were studied. Cells were trapped between two counter-propagating, divergent infrared laser beams and additional visible light was sent through the cells. The light guiding efficiency of the cells for visible light was thereby measured.

These measurements unambiguously demonstrate the light guidance function of Müller cells. The observed intensity-dependent transmittance might serve as a protective mechanism of the inverted retina against photo damage of the PRs.

Kristian Franze

Universität Leipzig

Faculty of Medicine
Paul Flechsig Institute of Brain Research
Neurophysiology

E-Mail: franze@medizin.uni-leipzig.de
www.uni-leipzig.de/~pfi/

COR-AAD1-00003103
Bayer EX1008 (Part 6 of 9)

5.16 Phospholipid metabolism detected by ^{31}P NMR spectroscopy and MALDI-TOF mass spectrometry

Beate Fuchs, Jürgen Schiller, Klaus Arnold

Phospholipids (PL) and phospholipases A_2, C, and D play important roles in signal transduction. Alterations in PL and enzyme activities might affect membrane properties, which may have a direct impact on dysfunctions, certain pathologies or cell proliferation, differentiation and apoptosis. For successful regenerative therapy the knowledge about the details of the functional and dysfunctional PL metabolic changes are necessary.

Unfortunately, suitable methods of PL analysis are often time-consuming and tedious, since most of them include a variety of separation and derivatisation steps. Methods allowing lipid analysis in a single step would be highly useful. ^{31}P nuclear magnetic resonance (NMR) spectroscopy provides the quantitative detection of all relevant PL classes in a single step. The combination with matrix-assisted laser desorption and ionisation time-of-flight (MALDI-TOF) mass spectrometry (MS) is very useful to obtain further information about the acyl chain composition of the individual PL classes. Because of its very high sensitivity MALDI-TOF MS offers also the potential to perform measurements at low PL concentrations.

Thus, we are performing PL analyses by the combined application of ^{31}P NMR spectroscopy and MALDI-TOF MS to characterize the PL composition and metabolic changes in biological samples (tissues, cells, and body fluids). It will be shown that especially the content of lyso-phosphatidylcholine (lysoPC) represents a reliable measure of inflammation. The PC/lysoPC ratio may indicate the severity of inflammation, the success of therapy and regeneration, and may serve as an early diagnostic marker.

Dr. Beate Fuchs

Universität Leipzig

Faculty of Medicine
Institute of Medical Physics and Biophysics

E-Mail: fucb@medizin.uni-leipzig.de
www.uni-leipzig.de/~biophys/

COR-AAD1-00003104
Bayer EX1008 (Part 6 of 9)

5.17 Mechanisms of CD44 shedding in human melanoma cells – Relevance for tumor progression and target for therapeutic intervention

Carl Gebhardt, Friederike Kauer, Marco Averbeck, Verena Voelcker, Anja Saalbach, Ulf Anderegg, Jan C. Simon

Previous studies have shown that human melanoma cells (MM) can bind hyaluronic acid (HA), an extracellular matrix component, via the CD44 receptor. This interaction of HA with membrane-bound CD44 (mCD44) results in the release of autocrine growth factors from MM cells leading to proliferation and progressive tumor growth *in vivo*. On the other hand, certain MM are capable of shedding soluble CD44 (solCD44) from their surface. Interaction of solCD44 with HA abolishes proliferation of MM *in vitro* and *in vivo* by inducing apoptosis. Autocrine or drug induced secretion of solCD44 may thus exert potent anti-tumoral effects.

To elucidate the mechanism of CD44 shedding, a panel of well characterized MM cell lines differing in their capacity to shed solCD44 was analyzed. RNA analysis revealed that solCD44 is not the result of alternative splicing of CD44 mRNAs and the shedding activities are not linked with CD44 mRNA turnover. The different observed shedding activities are accompanied by similar expression of mCD44 on the cell surfaces suggesting an increased turnover of the protein. Moreover, CD44 shedding was reduced by serine protease or metalloprotease inhibitors. Further, mRNA levels of several MMPs were analyzed by realtime-RT-PCR. We found the low shedding cell line P2 lacking MMP1 and MMP3 mRNA while the high shedding cell line Bro expressed these MMPs. Addition of HA induced MMP1 and MMP3 expression in the low shedding cell line P2, indicating the regulatory role of the CD44 ligand HA. Since other authors suggested MMP14 as the main responsible protease we analysed MMP14 espression by FACS and ELISA.

Dr. Carl Gebhardt

Universität Leipzig

University Hospital
Department of Dermatology

E-Mail: carl.gebhardt@medizin.uni-leipzig.de
www.uni-leipzig.de/~derma/

COR-AAD1-00003105
Bayer EX1008 (Part 6 of 9)

5.18 Tauopathies' relation to axonal transport

Jens Gerdelmann, Josef A. Käs, Thomas Arendt

A vital function in neurons is axonal transport (AT) along microtubules. A loss of synapses and later on a loss of neurons will be the result of disturbance or even disruption of the transport. Neurodegeneration in syndromes like Alzheimer's disease (AD) or Boxer's dementia (*dementia pugilistica*; DP) are very likely related to dysfunction of axonal transport. Additional evidence are the two main deposits found in AD and DP: A-β protein in amyloid plaques and tau protein in neurofibrillary tangles. The precursor protein of A-β is thought to be an adaptor protein between vesicles and molecular motors. And tau is a microtubule-binding and stabilizing protein, which may influence the functionality of the microtubule track. Tau's microtubule-binding is mainly controlled by its phosphorylation state.

Studying the axonal transport in primary neurons and neuroblastoma cells we focus on the interaction of transport, tau phosphorylation and mechanical stress.

Jens Gerdelmann

Universität Leipzig

Faculty of Medicine
Paul Flechsig Institute of Brain Research
Neuroanatomy

E-Mail: gerdelmann@uni-leipzig.de
www.uni-leipzig.de/~pfi/

COR-AAD1-00003106
Bayer EX1008 (Part 6 of 9)

5.19 Glial cells from human retinas produce CXCL8 and express CXCR1 and CXCR2 receptors

Iwona Malgorzata Goczalik, Maik Raap, Michael Weick, Andreas Reichenbach, Mike Francke

Interleukin-8 (CXCL8) is a pro-inflammatory chemokine. Several diseases of the eye (e.g. PVR, uveitis) are associated with increased levels of CXCL8 in the vitreous. Various cell types are potential sources for the secreted CXCL8. The aim of our study was to evaluate whether retinal glial cells are able to produce and secrete CXCL8 and/or to express CXCL8 receptors. We established primary cultures of isolated glial cells from human donor retinas and used an immortalized human Müller cell line. The cultures were prepared for immunohistochemistry (IHC), Western blotting and RT-PCR. Ca^{2+} imaging was performed to test the activation of CXCL8 receptors. Additionally, we examined surgically removed PVR membranes and retinal cryosections from organ donors.

CXCL8 immunoreactivity was accompanied by GFAP immunoreactivity and was co-localized with other glial specific markers. CXCL8 mRNA could be detected in human Müller cell cultures. Immunoreactivity for CXCR1 and CXCR2 was observed in human primary cultures and in the Müller glial cell line. Western blot analysis revealed proteins with about 40 kDa. The RT-PCR method confirmed the expression of CXCR1 and CXCR2 in the human Müller cell line. Application of recombinant CXCL8 protein caused an increase in intracellular Ca^{2+} levels in subpopulations of Müller cells. We determined CXCR1 and CXCR2 expression in GFAP-positive cells in PVR membranes. It is concluded that Müller cells may participate in the inflammatory response of pathologically altered or injured eyes. Surprisingly, we also detected the expression of CXCR1 and CXCR2 in healthy retinas from organ donors by means of IHC.

Iwona Malgorzata Goczalik

Universität Leipzig

Faculty of Medicine
Paul Flechsig Institute of Brain Research
Neurophysiology

E-Mail: g-iwona@lycos.com
www.uni-leipzig.de/~pfi/

COR-AAD1-00003107
Bayer EX1008 (Part 6 of 9)

5.20 Morphometrical investigations on different regions of the newborn skin

Sabine Göllnitz, Carolin Kunz, Bekele Assegedech, Dieter Reißig, Friedrich Keller

The aim of the investigations was the elucidation of differences in the morphology of different regions in the skin of newborns. Features were the thickness of the skin and epidermis, resp. Moreover the relative amounts of collagenous fibers of type I and III in the extracellulare matrix were determined. Further features involved the depth and the distance of papillae of dermis. The investigations were carried out on conventionally stained (HE,CROSSMON) and silvered (GOMORI) histological sections of the skin of deceased newborns (six female, five male). The relevant regions were forehead, neck, upper arm, forearm, palm of the hand, thoracic and abdominal wall, back side, femoral, lower leg, sole of the foot. The data of the features of the different regions were compared to each other. A relatively uniform skin thickness was observed in the different regions by using morphometrical methods of the light microscopy. In contrast to skin thickness the thickness of the epidermis showed significant differences between some regions. Highest thickness, depths and distance of papillae of dermis were detected for the sole of the foot and the palm of the hand, the lowest for the forehead. No correlation was found between the thickness of the skin and the epidermis, resp.

The areal arrangement and orientation of the bundles of collagenous fibers and the pattern of the collagen type I and III distributions suggest a proceeded mature process at the time of birth compared to adult skin. The results of the statistical tests give hints for possible transplantations of skin regions, which resembles each other corresponding to considered feature.

Sabine Göllnitz

Universität Leipzig

Faculty of Medicine
Institute of Anatomy

E-Mail: biene-9.9@gmx.de
www.uni-leipzig.de/~anatomie/

COR-AAD1-00003108
Bayer EX1008 (Part 6 of 9)

5.21 Experimentally induced rat brain cholinergic deficiency as a suitable tool to evaluate new radioligands for the vesicular acetylcholine transporter (VAChT) – Immunohistochemical evidence of VAChT loss after immunolesion

Udo Großmann, Wolfgang Härtig, Dietlind Sorger, Elena Kouznetsova, Reinhard Schliebs, Matthias Scheunemann, Jörg Steinbach, Osama Sabri

The basal forebrain cholinergic system is known to be involved in normal brain cognitive function and cortical cholinergic deficits seem to be implicated in Alzheimer's disease and other demential disorders. The VAChT localized in the membrane of vesicles of acetylcholine storage and transport is a possible target molecule for novel vesamicol derived fluorine-18 labelled radioligands to *in vivo* image these deficits by Nuclearmedicine methods like SPET and PET.

It is the aim of this study to validate immunhistochemically (IHC) that a quantitative reduction of VAChT occurs following a single dose of intracerebroventricular applicated immunotoxin to degenerate cholinergic terminals in cholinoceptive target regions.

The IHC labelling of VAChT was performed with free-floating, coronal frozen sections from perfused paraformaldehyde-fixed rat brains 6 weeks after a unilateral ventricular stereotaxic injection of 2 µg 192 IgG-saporin. Controls received a saline injection. VAChT immunoreactivity was visualized both by immunoperoxidase and carbocyanine immunofluorescence staining, respectively, using commercially available antisera. Following immunolesion a drastic loss of VAChT-immunoreactivity in the magnocellular basal forebrain nuclei and in the vast majority of VAChT immunopositive fibres projecting to neocortex and hippocampus was observed. It was shown that the VAChT represents a potential target molecule to reflect cholinergic deficits in brain. The used animal model of cholinergic immunolesion is an appropriate tool to test novel radiolabelled analogues of vesamicol for their sensitivity to detect cholinergic reductions.

Udo Großmann

Universität Leipzig

University Hospital
Department of Nuclear Medicine

E-Mail: udo.grossmann@medizin.uni-leipzig.de
www.uni-leipzig.de/~nuklmed/

COR-AAD1-00003109
Bayer EX1008 (Part 6 of 9)

5.22 Extended tropism of HIV vectors expressing two different envelope glycoproteins

Ferenc Harmos, Theresa Möllmer, Doreen Milius, Katrin Bräutigam, Heike Tartler, Christian Jassoy

Background: Env protein of HIV-1 is assembled into stable trimer, and oligomerization is required for maintaince of viral infectivity. HIV isolates differ in use of CXCR4 and CCR5 as coreceptors for infection of target cells. Coreceptor usage depends on the particular viral glycoprotein. Simultaneous expression of genetically different glycoproteins on single virus may lead to different biological and immunological properties.

Methods: Two expression cassettes, each containing a different HIV-1 or HIV-2 glycoprotein gene were cloned into an eukaryotic expression plasmid and used for the generation of infectious replication-incompetent HIV vectors. Vector constructs were added CD4+, CXCR4 or CCR5-expressing cells in culture. Infection was monitored by determination of marker gene expression.

Results: Virus vectors with different glycoprotein have different degrees of viral infectivity. Expression of a second glycoprotein (of identical tropism) interfers with vector infectivity. HIV vectors produced with plasmids containing a CCR5-tropic HIV-1 and a CXCR4-tropic HIV-2 glycoprotein gene or the genes of two HIV-1 envelope glycoproteins of different tropism exhibited dual tropism.

Conclusion: HIV vectors generated with expression plasmids containing two different HIV glycoproteins have new biologic properties probably due to expression of a mosaic of different glycoprotein trimers on the surface of the vector particles. Different glycoprotein molecules may interact in a "dominant-recessiv" fashion.

Dr. Ferenc Harmos

Universität Leipzig

Faculty of Medicine
Institute of Virology

E-Mail: ferenc.harmos@medizin.uni-leipzig.de
www.uni-leipzig.de/~virology/

COR-AAD1-00003110
Bayer EX1008 (Part 6 of 9)

5.23 Expression of glutamatergic and muscarinic receptors in organotypic brain slice cultures of Munc13 knock-out mice

Maike Hartlage-Rübsamen, Kerstin Reim, Nils Brose, Steffen Roßner

Munc13 proteins are presynaptic phorbol ester receptors, which are essential for synaptic vesicle priming and glutamate release. Approximately 90 % of synapses are solely dependent on Munc13-1 but in a small number of synapses Munc13-1 and Munc13-2 isoforms are present. Thus, glutamate release is reduced by 90 % and 100 % in neurons of Munc13-1 knock-out mice and Munc13-1/2 double knock-out mice, respectively. The regulation of Munc13 proteins is partly mediated by binding of DAG to the Munc13 C1 domain. Several biological processes - including the proteolytical processing of the amyloid precursor protein - depend at least in part on Munc13 function. Phenotypic characteristics observed in Munc13 knock-outs are either directly due to the presynaptic functions of Munc13 proteins (i.e. vesicle fusion and glutamate release) or represent secondary consequences of impaired glutamate release (i.e. lack of stimulation of glutamate receptors). To distinguish between these scenarios, we established organotypic brains slice cultures from newborn Munc13 knock-out mice. These cultures were maintained for different periods of time and characterized with regard to the temporal expression of DAG-linked Type I metabotropic glutamate receptors (mGluR-I) and M1 muscarinic receptors (M1 mAChR) by RT-PCR, radioligand binding, and immunhistochemistry. Our results indicate that both, mGluR-I and M1 mAChR are expressed by neurons in brain slices cultured for ten to 18 days. Thus, these cultures are useful experimental tools to reveal mechansims of Munc13 function in pharmacological stimulation experiments.

Supported by IZKF, Faculty of Medicine, Universität Leipzig (proj. C17) to S.R.

Dr. Maike Hartlage-Rübsamen

Universität Leipzig

Faculty of Medicine
Paul Flechsig Institute of Brain Research
Neurochemistry

E-Mail: maikerbs@rz.uni-leipzig.de
www.uni-leipzig.de/~pfi/

COR-AAD1-00003111
Bayer EX1008 (Part 6 of 9)

5.24 Phenotype-dependent differential vulnerability to oxidative stress in cholinergic SN56 cells

Katrin Heinitz, J. Regino Perez-Polo, Reinhard Schliebs

Basal forebrain cholinergic dysfunction is a consistent feature of Alzheimer's disease, which has been suggested to cause, at least partly, the cognitive deficits observed. This has raised the question of what causes the specific degeneration of basal forebrain cholinergic cells in this disease, and moreover, whether the cholinergic system is particularly sensitive to various pathophysiological conditions. The clonal hybrid cell line SN56 derived from the medial septal region of the mouse basal forebrain, expresses typical cholinergic neuronal characteristics such as choline acetyltransferase (ChAT) and acetylcholinesterase, and thus should represent an appropriate model to study the susceptibility of cholinergic cells to pathogenic insults. Differentiated and non-differentiated SN56 cells that demonstrate different levels of ChAT expression, were exposed to increasing concentrations of H_2O_2 to induce oxidative stress. Using MTT and LDH viability assays, SN56 cells differentiated with 1 mM dbcAMP/1μM retinoic acid were shown to be more susceptible to low dosis of oxidative stress as compared to nondifferentiated cells, an effect that could partly be prevented when cells were pre-exposed to 10 μM L-nicotine. The differential vulnerability suggests a distinct activation of the cellular anti-oxidant defence system. Gene expression analyses in phenotypically different cells following oxidative stress will reveal key signaling molecules that are involved in cell maintenance.

Supported by Interdisciplinary Centre for Clinical Research (IZKF) at the University of Leipzig (proj. C29).

Kathrin Heinitz

Universität Leipzig

Faculty of Medicine
Paul Flechsig Institute of Brain Research
Neurochemistry

E-Mail: katrin.heinitz@medizin.uni-leipzig.de
www.uni-leipzig.de/~pfi/

COR-AAD1-00003112
Bayer EX1008 (Part 6 of 9)

5.25 Different vulnerability to oxidative stress in nondifferentiated and differentiated cholinergic SN56 cells

Katrin Heinitz, Reinhard Schliebs

A characteristic feature of Alzheimer's disease is the preferential loss of basal forebrain cholinergic neurons, which causes the progressive impairment of cognitive function. The mechanisms underlying the higher susceptibility of basal forebrain cholinergic neurons to pathogenic insults are still largely unknown. The disease-associated increase of oxidative stress may play an important role in the early degeneration of the cholinergic cells. The clonal hybrid cell line SN56 derived from the medial septal region of the mouse basal forebrain, expresses typical cholinergic neuronal characteristics such as choline acetyltransferase (ChAT) and acetylcholinesterase (AChE), and thus should represent an appropriate model to study the susceptibility of cholinergic cells to pathogenic insults. Differentiated and nondifferentiated SN56 cells that demonstrate different levels of ChAT and AChE expression, were exposed to oxidative stress induced by H_2O_2. Using MTT and LDH viability assays, SN56 cells differentiated with 1 mM dbcAMP/1μM retinoic acid were shown to be more susceptible to low dosis oxidative stress as compared to nondifferentiated cells. This data suggest that the cellular anti-oxidant defence system is differentially expressed in the various cell types. The different responses to oxidative stress should be investigated by performing microgene arrays. A comparison of the stress mediated responses in the phenotypically different cells may explain their differential vulnerability.

Supported by Interdisciplinary Centre for Clinical Research (IZKF) at the University of Leipzig (01KS9504/1, proj. C29 to R.S).

Kathrin Heinitz

Universität Leipzig

Faculty of Medicine
Paul Flechsig Institute of Brain Research
Neurochemistry

E-Mail: katrin.heinitz@medizin.uni-leipzig.de
www.uni-leipzig.de/~pfi/

COR-AAD1-00003113
Bayer EX1008 (Part 6 of 9)

5.26 Pathological changes caused by copper overload in the livers of the Wilson disease gene knock-out mice

Dominik Huster, Milton J. Finegold, Scott M. Vanderwerf, Karel Caca, Svetlana Lutsenko

Wilson disease (WD) is a severe genetic disorder associated with copper (Cu) accumulation in tissues, particularly in the liver. The affected gene, *ATP7B*, is well known; however, molecular mechanisms and cellular events leading to liver pathology remain poorly understood. We describe morphological, histochemical, and biochemical changes in the livers of *ATP7B*(-/-) knock-out mice at different time points.

Hepatic Cu in *ATP7B*(-/-) livers rises quickly and reaches a maximum at 5-6 weeks, approximately 20-40 fold higher than in controls. Cu accumulates predominantly in the cytosol, bound to low-molecular-weight proteins. Among organelles, nuclei accumulate proportionally more Cu, resulting in a marked increase in nuclear size and nuclear damage. High Cu concentration remains constant up to 20 weeks of age, and then declines. Histological changes associated with Cu accumulation are very striking and depend on the stage of the disease. By 6 weeks 50 % of the mice show focal to diffuse but mild necro-inflammation. At 20 weeks the changes are universal and dramatic, with extreme degrees of hepatocellular injury and dysplasia, foci of nodular regeneration and bile duct proliferation. Over the next 6 months a remarkable degree of recovery of large portions of the liver is accompanied by the localized occurrence of adenocarcinoma arising from the proliferating bile ducts. Biochemical characterization of *ATP7B*(-/-) liver homogenates revealed significant up-regulation of glutathione-S-transferase isoform Pi on protein and mRNA levels. *ATP7B*(-/-) mice represent a valuable model for analysis of Cu toxicity and regeneration in the liver.

Dr. Dominik Huster

Universität Leipzig

University Hospital
Department of Internal Medicine II

E-Mail: dominik.huster@medizin.uni-leipzig.de
www.uni-leipzig.de/~medkl2/

COR-AAD1-00003114
Bayer EX1008 (Part 6 of 9)

5.27 Postnatal development of glial aquaporin and K^+ channel expression in the rat retina

Ianors Iandiev, Thomas Pannicke, Bernd Biedermann, Andreas Reichenbach, Andreas Bringmann, Peter Wiedemann

The osmotical and ion homeostasis of the inner retina is maintained by Müller glial cells. Müller cells express various subtypes of K^+ channels in their membranes that mediate fast transglial spatial buffering K^+ currents. Osmotically coupled to the transglial K^+ currents, Müller cells mediate water fluxes that are facilitated by aquaporin (AQP) water channels. The aim of the study was to compare the postnatal expression of AQPs and K^+ channels in the retina of the rat.

Retinal slices obtained from young rats at different postnatal days (P) were stained immunohistochemically against the glial K^+ channel subunit Kir4.1, AQP-1 and -4, and glutamine synthetase. Whole-cell K^+ currents were recorded in isolated Müller cells.

Glutamine synthetase as a marker of Müller cells was expressed in the rat retina at P11 and thereafter, and was not present at P5. In slices of adult retinas, immunoreactivities (IRs) for AQP-4 and Kir4.1 are co-expressed in Müller cell membrane domains that surround the vessels and abut the inner limiting membrane. Both IRs were expressed at P15 and thereafter. The IR for AQP-1 was expressed in the outer retina at P15 and thereafter. In Müller cells of adult retinas, the most prominent membrane K^+ conductance was found in the peri-somatic membrane domain. The K^+ currents of Müller cells increased during the second and third postnatal weeks.

The proteins for glial AQP and K^+ channels are simultaneously upregulated in their expression by Müller cells during the postnatal development. The expression of glutamine synthetase precedes the expression of AQP and K^+ channels in developing Müller cells.

Dr. Ianors Iandiev

Universität Leipzig

University Hospital
Department of Ophthalmology

E-Mail: ianors.iandiev@medizin.uni-leipzig.de
www.uni-leipzig.de/~auge/

COR-AAD1-00003115
Bayer EX1008 (Part 6 of 9)

5.28 Detection of novel polyomaviruses by nested broad-spectrum PCR

Reimar Johne, Dirk Enderlein, Hermann Nieper, Hermann Müller

Mammalian polyomaviruses cause persistent subclinical infections which may develop to severe diseases after immunosuppression. Inoculation into non-permissive hosts often leads to tumor growth. Polyomaviruses of birds are primary agents of acute and chronic disease. Most of the polyomaviruses were identified by accident as contaminants of tissue cultures. In order to systematically screen for so far unknown polyomaviruses, degenerated PCR primer pairs were constructed on the basis of available polyomavirus genome sequences.

By establishing a nested PCR protocol amplifying part of the major capsid protein VP1 gene, the sensitive detection of nine different polyomavirus genomes was demonstrated. Screening of 100 field samples derived from different animal species revealed the presence of new polyomaviruses in the feces of a juvenile chimpanzee (*Pan troglodytes*) and in the inner organs of a bullfinch (*Pyrrhula pyrrhula*).

Phylogenetic analysis of the entire VP1-encoding region revealed that chimpanzee polyomavirus (ChPyV) is related to the monkey polyomavirus LPyV and the human polyomavirus JCPyV with 60.5 % and 61.0 % nucleotide sequence identity, respectively. The finch polyomavirus is most closely related to avian polyomavirus, with 50.4 % genome sequence identity. As this virus was detected in young birds died from acute systemic disease, an involvement in disease should be considered.

The results of our study indicate that polyomaviruses are widely distributed among different animal species. The application of the PCR protocol to larger sample numbers should help to assess their distribution and involvement in disease.

Dr. Reimar Johne

Universität Leipzig

Faculty of Veterinary Medicine
Institute of Virology

E-Mail: johne@vetmed.uni-leipzig.de
www.vmf.uni-leipzig.de/ik/wvirologie/

COR-AAD1-00003116
Bayer EX1008 (Part 6 of 9)

5.29 Atrial natriuretic peptide (ANP) inhibits osmotic Müller cell swelling in the postischemic retina of the rat

Folke Kalisch, Ortrud Uckermann, Peter Wiedemann, Andreas Reichenbach, Andreas Bringmann

Retinal Müller glial cells are known to play an important role in the development of retinal edema, similar to the role of astrocytes in the pathomechanism of brain edema. One main cause for edema formation is glial cell swelling. Recently, we observed that Müller cell somata in slices from postischemic retinas of the rat swell upon hypotonic stress, which was not observed under control conditions. However, Müller cell swelling could be evoked by exposing slices of control retinas to Ba^{2+}. Under both experimental conditions the glial K^+-channels are downregulated or blocked, respectively. The aim of the present study was to investigate the effect of the atrial natriuretic peptide (ANP) on osmotic glial cell swelling. Acute application of ANP (100 nM) inhibited the hypotonic swelling of Müller cell somata. ANP may activate several types of natriuretic peptide receptors (NPRs), but acts particularly on the NPR-A. Agonists of the NPR-B (CNP) and NPR-C(C-ANP-[4-23]) mimicked the effect of ANP. Pharmacological experiments suggest that the ANP-effect is mediated by activation of neuronal NPRs, which stimulates phospholipase C and evokes an increase in intracellular Ca^{2+} and an activation of proteinkinase C. These signaling steps cause the synaptic release of glutamate which, subsequently, stimulates metabotropic glutamate receptors on Müller cells. This results in a release of purinergic agonists. Autocrine stimulation of A1 receptors by adenosine finally inhibits the osmotic swelling of Müller cells. Atrial natriuretic peptides are able to prevent glial cell swelling and might be beneficial to prevent and treat edema formation.

Folke Kalisch

Universität Leipzig

Faculty of Medicine
Paul Flechsig Institute of Brain Research
Neurophysiology

E-Mail: eklof@gmx.de
www.uni-leipzig.de/~pfi/

COR-AAD1-00003117
Bayer EX1008 (Part 6 of 9)

5.30 *Borrelia burgdorferi* dissemination in the host – Comparison of the infection after intradermal and intravenous injection in mice

Jens Knauer, Reinhard K. Straubinger

Lyme disease caused by *B. burgdorferi* is characterized by disseminated inflammatory responses weeks after the infection. Most authors believe that these responses are induced by the spirochetes' presence at varying sites and in this context favour a blood-borne dissemination of the bacterium. Others, however, support a centrifugal spread of the spirochetes through the host's tissues based on clinical observations.

The aim of this work was to compare the infection pathways in mice, that received *B. burgdorferi* either intradermally (id) or intravenously (iv). Tissue and serum samples from 96 mice (6 per group) were collected in weakly intervals for six weeks and again after 26 weeks. Tissues were used for re-cultivation of spirochetes and serum samples were analyzed using ELISA and Western-Blots.

Fourteen id-injected mice and 3 iv-injected mice were positive in culture. Both experimental groups developed increasing antibody responses up to day 42. Thereafter, antibodies in iv injected mice that were mainly directed against outer surface proteins normally observed after vaccination had decreased while an increase of antibodies to a broad range of antigens was noted in the id injected group.

These data suggest, that iv injected spirochetes were unable to adapt to the host's haematogenous environment and where removed quickly form the blood stream, causing decreasing antibody titers. Id injected borrelia, however, adapted quickly and initiated a persistent infection with constant antigen exposure to the immune system. Therefore these results support the hypothesis of a centrifugal, tissue-based spreading of *B. burgdorferi*.

Jens Knauer

Universität Leipzig

Faculty of Veterinary Medicine
Institute of Immunology

E-Mail: knauer@vetmed.uni-leipzig.de
www.vmf.uni-leipzig.de/ik/wimmunologie/

COR-AAD1-00003118
Bayer EX1008 (Part 6 of 9)

5.31 Expression of ubiquitous phosphofructo-2-kinase/ fructose-2,6-bisphosphatase in glioma cell lines

Kristin Köllner, Renate Keßler, Klaus Eschrich

Many tumor cells maintain a high glycolytic rate even in the presence of oxygen (the "Warburg effect") to supply ATP and anabolic precursors essential for de novo nucleotide synthesis. High glycolytic flux correlates with tumor growth rate and malignancy.

Fructose-2,6-bisphosphate is the most powerful activator of 6-phosphofructo-1-kinase, the rate limiting enzyme of glycolysis. The synthesis and hydrolysis of fructose-2,6-bisphosphate is catalysed by the bifunctional enzyme 6-phosphofructo-2-kinase/fructose-2,6-bisphosphatase (PFK2) which is expressed in four tissue-specific isoforms (*PFKFB1-4*).

The ubiquitous PFK2 is encoded by the inducible *PFKFB3* gene which is expressed constitutively in several transformed cell lines. The mRNA of ubiquitous PFK2 contains multiple copies of the AUUUA instability motif in the 3'-untranslated region. Therefore, ubiquitous PFK2 is the first enzyme of the intermediary metabolism with proto-oncogene features.

Alternative splicing generates six different isoforms of ubiquitous PFK2. Their expression pattern was determined in different astrocytoma cell lines on mRNA and protein level. The mRNAs of isoforms 5 and 6 were predominant throughout.

The *in vivo* interacting partners of ubiquitous PFK2 will be identified with the "tandem affinity purification" method (TAP), This method allows rapid purification of protein complexes under native conditions. As a first step the cDNAs of isoforms 5 und 6 cloned in the expression vector pcDNA3 were fused with the TAP-tag. The expression of the tagged PFK2 in different astocytoma cell lines was studied.

Kristin Köllner
Universität Leipzig
Faculty of Medicine
Institute of Biochemistry
E-Mail: kristin.koellner@medizin.uni-leipzig.de
www.uni-leipzig.de/~biochem/

COR-AAD1-00003119
Bayer EX1008 (Part 6 of 9)

5.32 Developmental and amyloid plaque-related changes in cerebral cortical capillaries in transgenic Tg2576 Alzheimer mice

Elena Kouznetsova, Dietlind Sorger, Osama Sabri, Jörg Steinbach, Matthias Scheunemann, Reinhard Schliebs

There is experimental evidence that cerebral perfusion is decreased during aging and in Alzheimer's disease. To characterize the temporal relationship between amyloid deposition, plaque size and cerebrovascular abnormalities, a semiquantitative immunohistochemical study was performed in transgenic Tg2576 mice that express the Swedish double mutation of human amyloid precursor protein and progressively develop Alzheimer-like beta-amyloid deposits. Cortical cryocut sections, obtained from mice at ages ranging between 10 and 18 months, were immunostained to label glucose transporter type 1 (GLUT1), a marker of vascular endothelial cells, and thioflavine-S to visualize plaques. Regardless of age and transgene, a laminar distribution of capillaries was observed being highest in cortical layers IV and lower layer V. In transgenic mice capillary density in all cortical layers decreased steadily with age and plaque load. Around large thioflavine-S-positive plaques the capillary density was low, while diffuse plaques demonstrated a close association of capillaries with no signs of any damage. The data suggest that amyloid plaque deposition differentially affects the cerebrovascular system in an age-and plaque type-related manner.

Supported by Saxon Ministry of Science and the Fine Arts (SMWK-BEF 7531.50-03-0361-01/6). The provision of Tg2576-F1 founders by Karen Hsiao, Minnesota, USA, is gratefully acknowledged.

Dr. Elena Kouznetsova

Universität Leipzig

Faculty of Medicine
Paul Flechsig Institute of Brain Research

E-Mail: elenakouz@hotmail.com
www.uni-leipzig.de/~pfi/

COR-AAD1-00003120
Bayer EX1008 (Part 6 of 9)

5.33 Antisense-mediated telomerase inhibition enhances the cytotoxic effects of chemotherapeutic drugs in human bladder cancer cell lines

Kai Krämer, Susanne Füssel, Uta Schmidt, Mathias Kotzsch, Manfred P. Wirth, Axel Meye

Purpose: Responses of bladder cancer (BCa) to commonly used chemotherapeutical agents such as mitomycin C (MMC), cisplatin (CDDP) and gemcitabine (GEM) are often disappointing. Since hTERT is tumor-specifically expressed and contributes to immortality and malignancy of the majority of tumors, it is regarded as a suitable anti-tumor target. The aim of this study was to investigate whether combinations of hTERT antisense-oligonucleotides (AS-ODNs) with common chemotherapy (CT) schedules may improve the drug-mediated anti-tumor effects.

Material and Methods: An initial screening for the enhancement of the inhibitory effects of MMC, CDDP and GEM on viability by treatment with 2 different hTERT AS-ODNs prior to CT was performed in 4 BCa cell lines. Apoptosis was assessed by annexin V staining and detection of activated caspase-3. A nonsense (NS)-ODN was used as a control in all experiments.

Results: All cell lines responded to the anticancer agents tested. Treatment with AS+CT resulted in a significantly stronger inhibition of viability than the NS+CT control in the majority of the combinations, indicating an antisense-specific enhancement effect. For example, ASt2331+MMC reduced the viability to 17 % in contrast to NS+MMC (58 %) in EJ28 cells. All ASt2331+CT combinations specifically increased the rate of apoptosis in a range from 1.3-fold to 3.0-fold in comparison to NS+CT. Apoptosis induction was associated with caspase 3-activation.

Conclusion: The chemosensitization by hTERT AS-ODNs allows a dose reduction of the chemotherapeutics and confirms the suitability of hTERT as a target in a specific therapy approach.

Kai Krämer

Technische Universität Dresden

University Hospital Carl Gustav Carus
Department of Urology

E-Mail: titabo@gmx.de
http://urologie.uniklinikum-dresden.de

COR-AAD1-00003121
Bayer EX1008 (Part 6 of 9)

5.34 Proteomics reveals alterations in thyroglobulin expression and in the H_2O_2 detoxifying system in cold thyroid nodules

Kerstin Krause

Szintigraphically cold thyroid nodules (CTN) are frequent findings in regions with iodine deficiency. While the presence of a CTN raises the possibility of thyroid cancer probably less than 3 % of CTNs acutally represent malignancy. The molecular etiology of benign CTNs is still unresolved. We applied 2 D-gel electrophoresis in combination with MS analysis to define a protein fingerprint of CTNs as a pre-requiste to get further insights into their pathogenesis. 10 benign CTNs (colloid nodules and follicular adenoma) and corresponding normal thyroid tissue (ST) of the same patient were studied. The proteomics approach resulted in a protein resolution of ~1,500 spots/gel. Differential regulation of protein expression in CTN vs. ST was observed for 250 spots, which were subsequently identified by ESI-MS or FTICR. Proteins consistenly upregulated (>2 fold) in CTNs fell into three major categories: 1. Cellular proliferation (amyloid precursor protein), 2. Tg trafficking (cathepsin B, PDI, HSP90, calreticulin, Tg fragments) and 3. H_2O_2 detoxifying system (peroxiredoxin 2 and 6, Glutathione S-transferase π DJ-1). Western blot analysis for selective proteins e.g. APP, Cathepsin B and Tg was performed and verified the 2D-gel results.

In summary we report the first characterization of the proteome of benign CTNs. Our results suggest specific alterations in Tg expression and upregulation of the peroxide detoxification system in CTNs possibly due to a failure in the processing and iodination of thyroglobulin (Tg).

Kerstin Krause

Universität Leipzig
University Hospital
Department of Internal Medicine III
www.uni-leipzig.de/~innere/

COR-AAD1-00003122
Bayer EX1008 (Part 6 of 9)

5.35 Introducing IZKF Core facility DNA technologies

Knut Krohn, Petra Süptitz, Birgit Thiele, Kathleen Stein

The Interdisciplinary Centre for Clinical Research (IZKF) in Leipzig runs a core facility for DNA technologies to support a growing number of research groups. This well established service includes microarray technology and DNA sequencing, analysis of heterozygous DNA, fragment analysis and detection of genomic markers (e.g. SNPs, microsatellites).

As technologies rapidly change the face of modern biology and medicine, instrumentation needs a regular update. In this regard our newly available array scanner allows detection of gene expression for more than 46,000 genes on a single GeneChip as well as the analysis of more than 100,000 SNPs (single nucleotide polymorphisms) on two arrays or the re-sequencing of 30,000 Bases per chip. Moreover we extended our sequencing capacity by running a new ABI 3,100 capillary sequencer.

An the moment we serve more than 50 groups within the IZKF, the university hospital, and the university itself as well as external partners with about 15000 sequences and 300 microchip readings per year. A large part of this effort is directed to study genes (e.g. TSH receptor, thyroid peroxidase, TNF-α, Wilson gene) involved in human diseases (e.g. rheumatoid arthritis, diabetes, thyroid disorders, intestinal diseases, tumors) and to elucidate their possible molecular causes.

Moreover the core facility coordinates exchange of laboratory protocols and organizes workshops and laboratory courses for molecular topics (e.g. biocomputing, microarray technology, sequence analysis).

PD Dr. Knut Krohn

Universität Leipzig

Interdisciplinary Centre for Clinical Research (IZKF)
Core Unit "DNA Technologies"

E-Mail: krok@medizin.uni-leipzig.de
www.izkf-leipzig.de

COR-AAD1-00003123
Bayer EX1008 (Part 6 of 9)

5.36 Inhibition of C13orf19 mRNA expression by siRNA in prostate cancer cells

Doreen Kunze, Uta Schmidt, Susanne Füssel, Axel Meye, Manfred P. Wirth

Background: Human C13orf19 (NM 017569) was previously identified to be down-regulated in prostate cancer (PCa). Until now its function is unknown. We therefore inhibited the C13orf19 mRNA expression by siRNA transfection.

Material and methods: We compared the downregulation of the C13orf19 mRNA expression by different siRNA duplexes by DOTAP-mediated transfection of the PCa cell line PC-3 since these cells showed higher C13orf19 mRNA expression compared to other PCa cell lines. We optimized the transfection conditions and selected the most efficient siRNA. The mRNA expression of C13orf19 and the PBGD reference gene were measured by quantitative PCR. The relative expression values were normalized to the non-silencing siRNA-control. Cellular viability was analyzed by WST-1 viability assay and apoptosis by annexin V-propidium iodide staining. Also, cell cycle distribution and clonogenic survival were examined. In addition, the effects of C13orf19 down-regulation in combination with chemotherapy on overall cell survival were examined.

Results: The application of these siRNAs showed no obvious effects on doubling time and cellular morphology. After 24 h siRNA D5 inhibits the C13orf19 mRNA expression down to 16 %. After 72 h there is still an inhibition to 31 %. Cell cycle distribution, clonogenic survival, apoptosis and cell viability showed no alterations as compared to the controls.

Discussion: The C13orf19 mRNA inhibition by D5 has no effects on cellular growth properties. We suppose that the inhibition leads to reduced apoptosis in PCa cells. Therefore, studies on the potential chemoprotective effects of siRNA D5 are underway.

Doreen Kunze

Technische Universität Dresden

University Hospital Carl Gustav Carus
Department of Urology

E-Mail: doreen.kunze@gmx.de
http://urologie.uniklinikum-dresden.de

COR-AAD1-00003124
Bayer EX1008 (Part 6 of 9)

5.37 Addition of rituximab to a CHOP-like regimen improves outcome of all patients with low risk diffuse large B-cell lymphoma (DLBCL)

Markus Löffler, Evelyn Kuhnt, Christina Rogalski, Michael Pfreundschuh

DLBCL is a chemosensitive disease usually treated with CHOP-like chemotherapy. Adding monoclonal antibodies against the CD20-epitope (Rituximab, ROCHE/GENENTECH) has been shown to improve outcome in elderly patients[1], but there is only limited data for young low-risk patients. In an intergroup study conducted in 18 countries, untreated patients (18-60 years) with low-risk $CD20^+$ DLBCL (IPI 0 or 1, stages II-IV and stage I with bulk) were randomized to receive 6 cycles of a CHOP-like regimen (CHEMO) or CHEMO plus 375 mg/m^2 of rituximab (R-CHEMO). Radiotherapy was planned for sites of initial bulk and/or extranodal involvement. The primary endpoint was time to treatment failure (TTF). Between 05/2000 and 10/2003, 824 patients were recruited. We present here the full-set analysis on 823 evaluable patients (410 CHEMO; 413 R-CHEMO) with data base status at Oct 31st, 2004.

Patient characteristics were: median age 47 years; IPI=1: 57 %; stages III/IV: 28 %; elevated LDH: 29 %; bulk: 49 %. Toxicity was not different in the two arms. After a median observation time of 22 months, R-CHEMO patients had a significantly longer TTF ($p<0.001$), with estimated 2-year TTF rates of 61 % (CHEMO) vs 80 % (R-CHEMO).Overall survival was significantly different ($p<0.001$), with 2-year survival rates of 86 % (CHEMO) and 95 % (R-CHEMO).

The combination of six cycles of a CHOP-like regimen with rituximab sets the new treatment standard for young low-risk patients with $CDD20^+$ DLBCL. The trial also demonstrates the ability of the Coordination Centre for Clinical Trials in Leipzig to organize a multicenter, multigroup registration trial.

Notes

1 Coiffier et al., NEJM (2002).

Prof. Dr. Markus Löffler

Universität Leipzig

Faculty of Medicine
Institute of Medical Informatics, Statistics and Epidemiology

E-Mail: markus.loeffler@imise.uni-leipzig.de
www.imise.uni-leipzig.de

COR-AAD1-00003125
Bayer EX1008 (Part 6 of 9)

5.38 Keratinocyte-derived dranulocyte-macrophage colony stimulating factor accelerates wound healing in a transgenic mouse model

Amrit Mann, Kerstin Niekisch, Manfred Blessing

Poorly healing and chronic wounds represent a major clinical challenge in diverse disciplines of modern medicine as these ailments greatly contribute to the morbidity and high cost of patient care. GM-CSF has been employed in clinical trials of wound healing with some success despite the complexity and scarcity of mechanistic understanding of its role in the wound healing. In skin, granulocyte-macrophage colony stimulating factor (GM-CSF) is secreted by keratinocytes shortly after injury and mediates epidermal cell proliferation in an autocrine fashion. Many cells involved in wound healing, e.g. macrophages, lymphocytes, fibroblasts, endothelial cells, and dendritic cells synthesize GM-CSF and/or are targets of this cytokine. In the present study, effects of both augmented and decreased GM-CSF activity in the skin on excisional wound healing were evaluated. Overexpression of GM-CSF lead to accelerated wound healing, whereas overexpression of a GM-CSF antagonist lead to delayed wound healing as observed by the rate of scab rejection and reepithelialization of the wounds. Also, the wounds in the GM-CSF transgenics healed with minimal scar formation as assessed at day 14 post wounding. We propose that besides the direct effects of GM-CSF on keratinocyte proliferation, granulation tissue formation and neovascularization, also the indirect processes via the induction of beneficial secondary cytokines contribute towards wound healing. We anticipate that these animal models may contribute towards a better understanding of benefits, perils and mechanisms of GM-CSF in normal and impaired wound healing.

Dr. Amrit Mann

Universität Leipzig

Center for Biotechnology and Biomedicine (BBZ)
Professorship for Molecular Pathogenesis
and
Faculty of Veterinary Medicine

E-Mail: amrit.mann@bbz.uni-leipzig.de
www.uni-leipzig.de/~blessing/

COR-AAD1-00003126
Bayer EX1008 (Part 6 of 9)

5.39 Cellular localisation of iron in the *substantia nigra* of an adult rat brain

Christoph Meinecke, Markus Morawski, Tilo Reinert, Thomas Arendt, Tilman Butz

Iron appears to be one of the main factors in the metal induced neurodegeneration. Quantitative information on cellular, sub-cellular and cell specific distributions of iron are important to assess the correlation between metal disorder and neurodegenerative diseases. Therefore, it is important to know where the iron is localised and what quantity of iron is present in the healthy brain tissue, especially in the *substantia nigra (SN)*.

For our investigations we used an adult rat brain as a model for the healthy human brain tissue. We analysed 6 µm thick embedded, unstained brain sections containing the *substantia nigra*.

We used particle induced X-ray emission (µPIXE) measurements to determine the quantitative iron content on a cellular and sub-cellular level. Moreover, the measurements carried out with the focussed proton beam (beam-diameter below 1 µm) yielded the cellular localisation of iron quantitatively.

In an integral analysis a factor of two more iron was observed in the *SN pars reticulata* then in the *SN pars compacta*.

The analysis of the regional native iron distribution in the *SN* indicates a difference in the quantitative, elemental acquisition between different cell types (neurons and astrocytes). On the cellular level we conclude that iron is more abundant in astrocytes than in neurons.

Christoph Meinecke

Universität Leipzig

Faculty of Physics and Earth Science
Institute of Experimental Physics II
Nuclear Solid State Physics

E-Mail: meinecke@physik.uni-leipzig.de
www.uni-leipzig.de/~nfp/

COR-AAD1-00003127
Bayer EX1008 (Part 6 of 9)

5.40 Quantitative assessment of the cerebral α4β2 nicotinic acetylcholine receptors (α4β2 nAChR) in Parkinson's disease (PD) – A PET study using 2-[18F]F-A-85380 (2-FA)

Philipp Meyer, Kai Kendziorra, Henryk Barthel, Swen Hesse, Georg A. Becker, Dietlind Sorger, Andreas Schildan, Marianne Patt, Anita Seese, Thomas Lincke, Gudrun Wagenknecht, Donald Lobsien, Florian Wegner, Peter Brust, Jörg Steinbach, Claus Zimmer, Johannes Schwarz, Osama Sabri

Nicotine is assumed to have neuroprotective effects in PD mediated via the most abundant α4β2 nAChRs. By using 2-FA-PET we tested the hypothesis whether nAChR are altered in PD. Non-smoking PD (n=12) of different clinical severity and normals (n=8) of comparable age underwent brain PET following short time infusion of 370 MBq 2-FA for 7 hours. We calculated parametric images of distribution volumes DV (Logan plot after correction of the arterial input function for plasma protein binding and radioactive metabolites) and binding potential BP by MRI based ROI analysis. In parallel, dopamine transporters (DAT) in basal ganglia were assessed using [123I]FP-CIT-SPECT and ROI analysis. In comparison with controls, PD showed decreased BP in the caudate heads (caud) [paralleled by decreased target/background ratio T/B(FP-CIT) in the caud], in the frontal cortex (fctx), parietal ctx (pctx), amygdala, midbrain, pons (-39.0/-48.1 %; $p<0.05$). In both caud, put in PD, T/B was positively correlated with BP ($r=0.62, 0.79$, $p=0.01, 0.04$). Correlations of T/B in caud, put were also found with BP in fctx, temp ctx, pctx ($r=0.63$-0.83, $p=0.003$-0.04). Our data indicate alterations of α4β2 in PD not only in the striatum, but also in other (sub)cortical areas. The finding of striatal DAT state being correlated with striatal and cortical α4β2 availability might indicate a close functional interrelationship of dopaminergic and cholinergic neurotransmission in PD. Since PD patients studied here only showed mild cognitive impairment (MMSE), loss or downregulation of α4β2 nAChR might predict (later) conversion to dementia.

Philipp Meyer

Universität Leipzig

University Hospital
Department of Nuclear Medicine

E-Mail: philipp.meyer@medizin.uni-leipzig.de
www.uni-leipzig.de/~nuklmed/

COR-AAD1-00003128
Bayer EX1008 (Part 6 of 9)

5.41 Specific binding of 2-[18F]F-A-85380 (2-FA) on α4β2 nicotinic acetylcholine receptors (α4β2 nAChR) in the cerebral white matter (WM) in patients with Parkinson's disease (PD) and Alzheimer's disease (AD) – Demonstration by PET and camparison with diffusion tenso MSI (DTI)

Philipp Meyer, Kai Kendziorra, Donald Lobsien, Swen Hesse, Henryk Barthel, Georg A. Becker, Andreas Schildan, Marianne Patt, Dietlind Sorger, Anita Seese, Thomas Lincke, Annette Förschler, Florian Wegner, Peter Brust, Jörg Steinbach, Herman-Josef Gertz, Johannes Schwarz, Claus Zimmer, Osama Sabri

α4β2 on subcortical projection fibers (sPF) in WM had not been quantified *in vivo* in PD/AD. Aims of this study were to test whether 1) nAChR in WM can be quantified by 2-FA-PET, which binds on alpha4beta2, 2) nAChRs are altered in WM of PD/AD, 3) axonal integritiy is altered in WM of PD/AD studied with DTI. 25 non-smoking PD, AD or normals (N) were studied by 2-FA-PET upto 8h, a subgroup after smoking a cigarette (7h). DTI: Fractional anisotropy (fA) was assessed and normalized (rel-fA). 2-FA-PET: Distribution volumes were calculated. After co-registration with DTI-fA, binding potential (BP) and rel-fA were calculated in med./lat. periventricular WM (pvWM), ventr. capsula int. (civ), corp. callosum (cc). Smoking a cigarette resulted in displacement of 2-FA from thalamus, brainstem, pvWM. BP in PD/AD: decreased in pvWM; civ[$p<0.05$]. Rel-fA in PD/AD: increased in med pvWM; decreased in lat.pvWM[$p<0.05$], cc, civ(AD). Correlations (PD/AD/N): (N)BP vs rel-f A in pvWM, civ ($r>0.68, p<0.02$). (PD) MMSE vs BP in lat.pvWM ($r=0.59, p=0,05$), (PD)MMSE vs rel-fA in cc($r=0.83, p=0.01$), (AD)in civ ($r=-0.87, p=0.03$); (PD)MMSE vs fA in lat.pvWM($r=-0.61, p=0.08$), (AD)in civ ($R=0.90, p=0.02$). Smoking a cigarette resulting in displacement of 2-FA by nicotine (upto 45%) is *in vivo* evidence for specific 2-FA binding on sPF in WM. In PD/AD, nAChR alterations and axonal damage in pvWM and civ show a differential regional pattern. The correlations between dementia severity, nAChR availability and axonal integrity in WM measured with 2-FA-PET/fA-DTI, indicate high potential of this combined imaging to assess WM integrity and cholinergic function.

Philipp Meyer

Universität Leipzig

University Hospital, Department of Nuclear Medicine

E-Mail: philipp.meyer@medizin.uni-leipzig.de
www.uni-leipzig.de/~nuklmed/

COR-AAD1-00003129
Bayer EX1008 (Part 6 of 9)

5.42 New targets for novel immunotherapeutic strategies based on natural regulatory T cells

Dirk Mischke, Sunna Hauschildt, Frank Emmrich, Ullrich Pigla, Rüdiger Laub

The induction of immunological tolerance is an elusive clinical goal to treat autoimmune disorders.

Regulatory T-helper with high expression levels for CD25 (Treg) have been shown to exert powerful suppressive activity.

By flow cytometry, we identified a characteristic pattern of adhesion molecules which is constitutively expressed on Treg in human circulation. As compared to $CD4^+$ T cells, Treg cells express significant higher levels for CD49e, CD49f, whereas CD49d and CD62L were diminished. Following activation via CD3/CD28, Treg cells upregulate CD62L. That expression pattern suggests profound differences in migratory pathways of Treg and other Th cells.

To investigate a possible regulatory role of cytokine release by Treg cells, their cytokine release was analyzed. Beside the lead-cytokine TGF-b, we found a characteristic cytokine pattern comprising some, but not all, of the Th2 cytokines IL-4, IL-5 and IL-13. Levels for IL-6 and IL-10 were below those of Th cells. Levels of characteristic Th-1 cytokines like TNF-α, INF-γ and IL-12p70 were negligible.

We demonstrate the regulatory properties of Treg cells in cocultures with responder CD4 and CD8 T cells. Treg cells suppressed the up-regulation of CD25, CD69 on responder T cells. In contrast, Treg cells stimulated CD30, CD95, CD152 on responder T cells.In the presence of Treg cells, activated responder cells failed in down-regulation of CD62L, which is a normal cellular response of stimulation.

Novel immunotherapeutic strategies could make use of cytokines identified as being important in natural immunosuppression or regulatory cells themselves after they have been expanded *ex vivo*.

Dirk Mischke

Universität Leipzig

Faculty of Biosciences, Pharmacy and Psychology
Institute of Biology II
Immunbiology

E-Mail: dirk_immunbio@yahoo.de
www.uni-leipzig.de/~biowiss/zoologie/

COR-AAD1-00003130
Bayer EX1008 (Part 6 of 9)

5.43 Parkinson's disease – A possible link between accumulation of iron and loss of perineuronal nets in the *substantia nigra*

Markus Morawski, Christoph Meinecke, Tilo Reinert, Anne C. Dörffel, Tilman Butz, Gert Brückner, Thomas Arendt

Oxidative stress generated by iron-induced processes (e.g. Fenton reaction) might be essentially involved in neuronal cell death in Parkinson's disease (PD). Perineuronal nets (PNs), a specialized form of extracellular matrix containing large aggregating chondroitin-sulfate-proteoglycans complexed with hyaluronan and tenascin, surround subpopulations of neurons in the *substantia nigra pars reticulate* (*snpr*). Due to their glycosaminoglycan components, these PNs form polyanionical charged structures in the direct microenvironment of neurons, and might, thus, have the properties to scavenge and bind redox-active iron, thereby reducing the local oxidative potential in the neuronal microenvironment. In a previous study, we showed that PN ensheathed neurons accumulate up to 4,6-fold more iron than any other ECM structure. Here, we differentially investigated the intra- and extraneuronal iron concentrations of the *substantia nigra pars compacta* (*sn pc*) versus snpr using particle induced X-ray emission. The amount of iron in the substantia nigra was found to be increased in PD compared to healthy controls. Moreover, an almost complete loss of PNs specifically labelled by anti CSPG antibody was found in PD *snpr*. It is suggested that high levels of iron in PD might affect snpr neurons, potentially through NMDA receptors, subsequentially leading to increased GABA release which in turn might result in an increased inhibition of target neurons.Taken together, degenerative process in PD might be a consequence of the *snpr* neurons loosing their PN's, associated by a reduction of iron binding capacity and elevated levels of free iron.

Markus Morawski

Universität Leipzig

Faculty of Medicine
Paul Flechsig Institute of Brain Research
Neuroanatomy

E-Mail: morm@medizin.uni-leipzig.de
www.uni-leipzig.de/~pfi/

COR-AAD1-00003131
Bayer EX1008 (Part 6 of 9)

5.44 LSC as powerful tool for the analysis of DNA content in neurons

Birgit Mosch, Dominik Lenz, Attila Tarnok, Thomas Arendt

The laser scanning cytometer (LSC) is a microscope-based cytofluorometer closing the gap between flow cytometry and fluorescence microscopy, allowing a quantitative fluorescence analysis of tissue sections. Thus, the tissue architecture and morphological details remained conserved. Furthermore it is possible to measure many cells in a relative short time, to distinguish between different cell types by immunohistochemistry, and also to analyse the DNA content of cell populations via the propidiumiodide (PI) - fluorescence.

Alzheimer's disease (AD) is a dementia, histopathologically characterised by the formation of neuritic plaques and neurofibrillary tangles and a loss of synapses and neurons. The re-expression of cell cycle proteins in brains of AD patients leads to the assumption that a malfunction of mitogenic signaltransduction and cell cycle control triggers neurons to re-enter the cell cycle, a process that subsequently leads to cell death. Until today it is not clear, up to which point neurons progress through the cell cycle. To our knowledge, there is only one report indicating that neurons in AD brain enter the S-Phase and replicate their DNA[1]. In the present study, we developed a technique to measure the DNA content of cells in brain sections to ascertain if re-entrance into the cell cycle in neurons in AD brain is associated with partial or entire duplication of the genome.

This work was supported by a grant from the Saxon Ministry of Science and the Fine Arts (SMWK) and the Interdisciplinary Centre for Clinical Research (IZKF) of the University of Leipzig (01KS9504, project C1).

Notes

1 Yang et al. (2001).

Birgit Mosch

Universitöt Leipzig

Faculty of Medicine
Paul Flechsig Institute of Brain Research
Neuroanatomy

E-Mail: mosch@medizin.uni-leipzig.de
www.uni-leipzig.de/~pfi/

COR-AAD1-00003132
Bayer EX1008 (Part 6 of 9)

5.45 The role of antiinflammatory cytokines in cryptococcosis

Uwe Müller, Petra Krumbholz, Werner Stenzel, Gabriele Köhler, Melanie Kleinschek, Christoph Werner, Gesine Hansen, Manfred Blessing, Reinhard K. Straubinger, Frank Brombacher, Gottfried Alber

Meningoencephalitis caused by the pathogenic yeast *Cryptococcus neoformans* is an important threat for AIDS patients. As experiments of our and other groups indicated Th1 cytokines, e.g. IFN-γ and IL-12, are important stimulators of the immune system to control and eliminate this yeast. On the other hand it could be shown that Th2 cytokines can exacerbate the infection.

Cryptococcosis is an airborne infection therefore we have established a murine intranasal infection model to test the involvement of Th2 cytokines, especially IL-4 and IL-13, in pathogenesis. We could show that mice that lack IL-4, IL-13 or the shared receptor, are much more resistant to a *Cryptococcus neoformans*-infection than wild-type mice which can not control the yeast and therefore have larger cryptococcomas in the lung and the brain. These cryptococcomas cause severe problems as meningitis and pulmonary disorders. In contrast to mice that lack IL-13, mice that over express this cytokine show higher organ burdens than wild-type mice. These results clearly show the adverse role of these Th2 cytokines, for the first time for IL-13, in pathogenesis.

The future aim is to examine the cells that are influenced by these cytokines with the help of cell specific IL-4/IL-13 receptor deficient mice. These findings could help to establish new therapies against this opportunistic pathogen.

Dr. Uwe Müller

Universität Leipzig

Center for Biotechnology and Biomedicine (BBZ)
Professorship for Molecular Pathogenesis
and
Faculty of Veterinary Medicine

E-Mail: uwe.mueller@bbz.uni-leipzig.de
www.uni-leipzig.de/~blessing/

COR-AAD1-00003133
Bayer EX1008 (Part 6 of 9)

5.46 Structural alterations of the bladder wall in idiopathic urge incontinence and interstitial cystitis

Jochen Neuhaus, Thilo Schwalenberg, Lars-Christian Horn, Jens-Uwe Stolzenburg

Introduction: The high prevalence (41 %) of urinary incontinence (UI) in German female population stresses its social and economical significance. The most severe form is the interstitial cystitis (IC), a chronic disease, of which the etiology is unknown to date. Up to 0.9 % of female population has been reported with IC in the past, whereas recent epidemiological studies state at least 10-20 % prevalence of IC. Early diagnosis and effective therapies suffer from lack of physiological and histopathological basis data. Therefore, we looked for alterations of the bladder wall in patients suspected for IC.

Method: incontinence group: n=7 (f); controls (tumor patients): n=5 (f), n=6 (m). Immunolabeling (IR): nerves: S100, endothelium: CD34, gap junction proteins: Cx40, Cx43, Cx45. Evaluation of the urothelium, lamina propria and the detrusor muscle.

Results: Despite of the severe clinical symptoms, none of the patients showed the histological picture of a full-blown IC. Cx43-IR was augmented in the incontinence group ($p<0.05$); Cx45-IR was unchanged and Cx40 was restricted to blood vessels. The suburothelial myofibroblasts were strongly labeled for Cx43, indicating extensive formation of functional syncytia, while Cx45-IR was slightly elevated in these cells. The innervation of the detrusor muscle was higher in 3/7 (=43 %) of the incontinent patients. Microvascularization, however, was significantly reduced ($p<0.05$).

Conclusions: We observed distinct structural changes within the bladder wall of urge incontinent patients, which might induce more effective diagnostics and new therapeutical approaches.

Supported by the DFG, NE425/4-1.

Dr. Jochen Neuhaus

Universität Leipzig

University Hospital
Department of Urology

E-Mail: neuj@medizin.uni-leipzig.de
www.urosite.de

COR-AAD1-00003134
Bayer EX1008 (Part 6 of 9)

5.47 Development of novel calcitonin derived carrier peptides with improved metabolic stability

Ines Neundorf, Robert Rennert, Annette G. Beck-Sickinger

The use of cell penetrating peptides is limited by their rapid clearance when in contact with cellular systems. Considering that a subsequent cleavage would prevent the successive translocation of the cargo one must not forget that the metabolic stability influences also the physiological degradation of CPP. This is an important factor when used for therapeutic purposes. Therefore, the metabolic fate of CPP after permeating the lipid bilayer is of great interest.

Recently, the selected C-treminal fragment hCT(9-32) was found to internalize into excised nasal epithelium while the receptor activating N-terminal part is lacking. This led to an increased interest in using hCT-derived sequences as carrier peptides.

In previous studies it was shown that an initial degradation of hCT(9-32) occurred in its N-terminal fragment through endopeptidase activity. Thus, we developed hCT(9-32) with position 12 and 16 replaced by D-Phe or N-methyl-Phe, respectively. We could demonstrate significant improvements on the metabolic stability in human blood as well as in cell culture supernatant. Furthermore, the uptake was not affected as proven by confocal laser scanning microscopy and all the new derivatives showed no toxicity. Accordingly, a novel generation of CPPs with significantly improved properties have been identified.

Dr. Ines Neundorf

Universität Leipzig

Faculty of Biosciences, Pharmacy and Psychology
Institute of Biochemistry
Biochemistry and Bioorganic Chemistry

E-Mail: neundorf@uni-leipzig.de
www.biochemie.uni-leipzig.de/agbs/

COR-AAD1-00003135
Bayer EX1008 (Part 6 of 9)

5.48 N-methyl-D-aspartate (NMDA) receptor subunits in human and *Bennett* rat dorsal root ganglia – An immunohistochemical study

Vera Ogunlade, Ralf Schober, Stefan Grimm, Clemens Allgaier

NMDA receptors (NR) play a role in the transmission of pain signals to the central nervous system via the dorsal root ganglion (DRG) and may contribute to neuropathic pain. Therefore, information about NR subunits in DRG and spinal cord may help to understand the importance of the NR in processes related to chronic pain.

We investigated the distribution of NR subunits in the human DRG by immunohistochemistry (IHC). Possible changes in NR subunit expression in DRG were studied using the Bennett rat - a model for peripheral mononeuropathy (consisting in ligatures placed around the sciatic nerve). Lumbar human DRGs were fixed with formaldehyde. Rat DRGs were fixed by perfusion. Mayer's Hemalum counterstaining was used for IHC using anti-NR subunit-specific antibodies (Santa Cruz). NR immunoreactivity (IR) in the human DRG was found for all investigated subunits in neuronal cell bodies and axons, but also in other cell types. However, the expression pattern was found largely different among individual patients regarding the number of positive neurons and IR intensity. Mainly, the small neurons, which are supposed to be involved in nociception, were more intensively stained than the large neurons transmitting other sensory inputs. In neurons located in the ipsilateral (ligated) DRG of Bennett rats, the IR for NR2A and NR2B subunits was significantly increased as compared to the contralateral side. These alterations of NR expression were found in small and large neurons.

Our study demonstrates changes of functional significance in the expression of NR subunits presumably implicated in the development of neuropathic pain.

Dr. Vera Ogunlade

Universität Leipzig

University Hospital
Institute of Pathology
Neuropathology

E-Mail: ogunlade@medizin.uni-leipzig.de
www.uni-leipzig.de/~patho/

COR-AAD1-00003136
Bayer EX1008 (Part 6 of 9)

5.49 Identification of P2Y receptor subtypes in human Müller glial cells

Thomas Pannicke, Julia E. Fries, Iwona Goczalik, Mike Francke, Thomas H. Wheeler-Schilling, Konrad Kohler, Sebastian Wolf, Peter Wiedemann, Andreas Bringmann, Andreas Reichenbach

Nucleotides act as signaling molecules via P2 receptors. Activation of metabotropic P2Y receptors results in an increase of the intracellular Ca^{2+} concentration $[Ca^{2+}]i$. The identification of P2Y receptors expressed in the retina may improve the understanding of retinal physiology. We investigated the expression of P2Y receptors in human retinal Müller glial cells. Since the access to human tissue is limited, we confined our study to the subtypes $P2Y_1$, $P2Y_2$, $P2Y_4$, and $P2Y_6$. The use of the material was approved by the ethics committee of the University of Leipzig Medical School. Retinal tissue from patients with proliferative vitreoretinopathy was obtained during vitreoretinal surgery; Müller cells were enzymatically isolated. Because these cells express Ca^{2+}-dependent K^+ (BK) channels, an increase in $[Ca^{2+}]i$ could be recorded electrophysiologically. Application of different P2Y agonists resulted in BK current increases, pointing to the existence of different receptor subtypes in Müller cells. Subsequently to the current recording, the cytoplasm of the recorded cell was harvested into the recording electrode and expelled into a PCR tube. After reverse transcription, the cDNA from a single cell was split into two samples and separately used for a PCR reaction with $P2Y_1/P2Y_2$- (n=44) and $P2Y_4/P2Y_6$-specific (n=17) primers, respectively. The mRNA for all investigated P2Y receptor types could be found in human Müller cells, the incidence of $P2Y_2$ receptors was significantly lower than that of the other subtypes. In addition, we used human retinal tissue to demonstrate the existence of P2Y receptor subtypes immunohistochemically.

Dr. Thomas Pannicke

Universität Leipzig

Faculty of Medicine
Paul Flechsig Institute of Brain Research
Neurophysiology

E-Mail: pant@medizin.uni-leipzig.de
www.uni-leipzig.de/~pfi/

COR-AAD1-00003137
Bayer EX1008 (Part 6 of 9)

5.50 Norchloro-fluorohomoepibatidin – PET evaluation of tracer properties in pigs

Jörg Thomas Patt, Winnie Deuther-Conrad, Peter Brust, Marianne Patt, Osama Sabri, Jörg Steinbach

2-[F-18]fluoro-A-85380 (2-FA) is currently used as radiopharmaceutical for positron emission tomography (PET) imaging of α4β2 neuronal nicotinic acetylcholine receptors in the brain. Comparison of the biodistribution of both enantiomers of F-18 labeled norchloro-fluorohomoepibatidine (NCFHEB) (6-β-(2-fluoro-5-pyridinyl)-8-azabicyclo[3.2.1]octane) with 2-[F-18]fluoro-A-85380 (2-FA) in mice revealed superior properties of the enantiomers of NCFHEB. We have started the comparison of these tracer compounds by PET studies in pigs.

Radiolabeling was performed by reacting a solution of Kryptofix222/potassium carbonate/[F-18]fluoride complex with 0.3 to 0.7 mg of enantiomerically pure precursor NCBrHEB (6-β-(2-bromo-5-pyridinyl)-8-azabicyclo[3.2.1]octane) in a microwave. The product was purified by HPLC (Multospher 120 RP 18 AQ, 10x125 mm, NaH2PO4 (10 mM) pH 4, 5 % ethanol). The product peak was collected and (-)-[F-18]NCFHEB injected into a pig (20 kg bodyweight).

Precursor and product were well separated by semipreparative HPLC. (-)-[F-18]NCFHEB showed a high uptake in the brain displaying the typical distribution of α4β2 nAChR subtypes in the brain with very high accumulation in the thalamus, high accumulation in the cortex and low activity concentration in the cerebellum. The time activity curve for the thalamus showed a maximum at 115 min.

Dr. Jörg Thomas Patt

Institute of Interdisciplinary Isotope Research (IIF)

E-Mail: jpatt@iif-leipzig.de
www.iif-leipzig.de

COR-AAD1-00003138
Bayer EX1008 (Part 6 of 9)

5.51 Is there an interaction of the adaptor proteins FE65 and Mint3 with MAP-tau?

Ellen Ramminger, Max Holzer, Thomas Arendt

The main characteristic of neurodegeneration in Alzheimer's disease (AD) is progredient neuronal death within brain regions of high plasticity caused by intraneuronal neurofibrillary tangles (NFTs) and extracellular β-amyloid plaques. NFTs consist of abnormally phosphorylated tau protein, which is polymerized into paired helical filaments or straight filaments.

The role of tau protein in neurodegeneration is emphasized by pathological tau fibrils occuring separately, without β-amyloid-depositions in several neurodegenerative diseases, summarized as tauopathies. The identity of factors facilitating tau aggregation remains elusive. One approach to identify such factors is to screen for proteins that interact with human microtubule associated protein tau (MAP-tau).

FE65 was identified to be a potential MAP-tau-interacting protein by co-immunoprecipitation[1]. Colocalisation of FE65 and tau-proteins within intracellular tangles has been observed[2].

Our aim was to investigate if the proteins FE65 and a related protein Mint3 interact with human MAP-tau and to define the interacting domains by means of Yeast-two-hybrid system and co-immunoprecipitation.

Surprisingly no interaction of MAP-tau with FE65 or with Mint3 was observed using Duplex-Yeast-two-hybrid system and co-immunoprecipitation. This might indicate a transiently occurring interaction not detectable by these methods, or may point to an absence of interaction.

This work was supported by the IZKF/TP C24 and the DFG (HO2368/1-1).

Notes

1 Barbato et al., Neurobiol. Dis. 18:399.

2 Delatour et al., Am. J. of Path. 158:1585.

Ellen Ramminger

Universität Leipzig

Faculty of Medicine
Paul Flechsig Institute of Brain Research
Neuroanatomy

E-Mail: ellen.ramminger@medizin.uni-leipzig.de
www.uni-leipzig.de/~pfi/

COR-AAD1-00003139
Bayer EX1008 (Part 6 of 9)

5.52 Behavioural effects of the antiaggregatory therapeutic compound clopidogrel (Plavix®; Iscover®)

Ralph Regenthal, Frank Baumann, Cornelius Donat, Christian Gachet, Peter Illes, Ute Krügel

Clopidogrel (Plavix®; Iscover®) is an inhibitor of ADP-induced platelet aggregation via $P2Y_{12}$ receptors worldwide used for long term prevention of atherothrombotic events. It was shown that $P2Y_{12}$ receptors are present in the central nervous system, modulating behavioural changes induced by extracellular ADP. Here, the influence of clopidogrel on explorative motor activity and anxiety was investigated and its distribution in liver and brain of rats. Clopidogrel dose-dependently (1 to 25 mg/kg p.o.) reduced the explorative activity in a novelty open field situation and affected the behaviour on the elevated plus maze, a standard test for anxiety, one hour after administration. The percent of entries into the open arms and of the time spent there were significantly reduced. These results indicate that clopidogrel mediates central effects on motivation-related locomotor activity at doses used for therapy in humans (loading dose 300 mg, maintenance dose 75 mg once daily).

Clopidogrel, is a prodrug, hepatic metabolised to a highly labil active intermediate. Clopidogrel was detected in liver and brain with a maximum of tissue concentration between half and one hour after administration, which confirms with the antiaggregatory response. The concentration in the brain was much lower than in the liver (0.043 ± 0.027 vs. 0.25 ± 0.19 µg/g tissue).

It is unclear, whether clopidogrel is metabolised in the brain, or whether the active metabolite acts on endothelial cells known to be endowed with $P2Y_{12}$ receptors or passes the blood-brain barrier.

However, clopidogrel induces central side effects relevant for motivation-related behavior.

Dr. Ute Krügel

Universität Leipzig

Faculty of Medicine
Rudolf Boehm Institute of Pharmacology and Toxicology

E-Mail: ute.kruegel@medizin.uni-leipzig.de
www.uni-leipzig.de/~pharma/

COR-AAD1-00003140
Bayer EX1008 (Part 6 of 9)

5.53 Brain prolyl endopeptidase expression in aging, APP transgenic mice and Alzheimer's disease

Steffen Roßner, Ingo Schulz, Ulrike Zeitschel,
Reinhard Schliebs, Volker Bigl, Hans-Ulrich Demuth

Prolyl endopeptidase (PEP) is believed to inactivate neuropeptides that are present in the extracellular space. However, the intracellular localization of PEP suggests additional, yet unidentified physiological functions for this enzyme. We have recently demonstrated that PEP is associated with the tubulin cytoskeleton and important for the proteolytical processing of the amyloid precursor protein (APP) and for β-amyloid secretion in neuronal cell lines. Here we studied the expression, enzymatic activity and subcellular localization of PEP in adult and aged mouse brain as well as in brains of age-matched APP transgenic Tg2576 mice and in brains of Alzheimer's disease patients. In mouse brain PEP was exclusively expressed by neurons and displayed region- and age-specific differences in expression levels, with the highest PEP activity being present in cerebellum and a significant increase in hippocampal but not cortical or cerebellar PEP activity in aged mouse brain. In brains of young APP transgenic Tg2576 mice, hippocampal PEP activity was increased compared to wild-type littermates in the pre-plaque phase but not in aged mice with β-amyloid plaque pathology. This "accelerated aging" with regard to hippocampal PEP expression in young APP transgenic mice might be one factor contributing to the observed cognitive deficits in these mice in the pre-plaque phase and could also explain in part the cognition-enhancing effects of PEP inhibitors in serveral experimental paradigms.

Dr. Steffen Roßner

Universität Leipzig

Faculty of Medicine
Paul Flechsig Institute of Brain Research
Neurochemistry

E-Mail: rossn@medizin.uni-leipzig.de
www.uni-leipzig.de/~pfi/

COR-AAD1-00003141
Bayer EX1008 (Part 6 of 9)

5.54 Active cardiomyocytes on collagen gels for biohybrid systems

Markus Rüffer, Randy Kurz, Winnie Weigel, Andrée Rothermel, Jürgen Trzewik, Peter Linder, Gerhard Artmann, Andrea A. Robitzki

Cardiomyocytes show inherent contractile activity. Under the influence of stimulating agents like noradrenalin or angiotensin-II the frequency of these contractions rises. Contraction frequency can be determined optically, electrophysiologically (using Multi-Electrode-Arrays) or by a force sensor. For the detection of contractility by a force sensor a monolayer of cardiomyocytes is cultivated on a collagen gel or on a coated silicone membrane that serves as bottom of the cultivation vessel. Contracting and relaxing cardiomyocytes cause changes in tension which are detected by recording the degree of sagging of the gel or the membrane. An extremely sensitive pressure sensor is able to detect even minute changes in sagging, providing an ideal technique to automate contraction frequency and contractility determination. The system can be used to examine the influence of drugs and their antagonists on cardiomyocytes. Collagen being a vital component of the extra-cellular matrix offers the advantage of resembling more natural conditions for cells if used as substrate while culturing cells directly on the membrane allows for more sensitive detection in changes of contactility.

Markus Rüffer

Universität Leipzig

Center for Biotechnology and Biomedicine (BBZ)
Professorship for Molecular Biological-Biochemical Process Technology
and
Faculty of Biosciences, Pharmacy and Psychology
Institute of Biochemistry

E-Mail: markus.rueffer@bbz.uni-leipzig.de
www.uni-leipzig.de/~dmpt/

COR-AAD1-00003142
Bayer EX1008 (Part 6 of 9)

5.55 Molecular genetic diagnosis of susceptibility to malignant hyperthermia

Henrik Rüffert, Markus Wehner, Kerstin Krist,
Ursula G. Froster, Derk Olthoff

Malignant hyperthermia is a pharmacogenetic disorder of the skeletal muscles which may be triggered by inhalational anaesthetics and depolarizing muscle relaxants. Exposure to these agents can lead in pre-disposed individuals to a potentially life-threatening MH crisis caused by an uncontrolled intracellular calcium release from the SR into the myoplasm. A mutated ryanodine receptor subtype 1(RYR1) appears to play the outstanding role in the pathogenesis of MH. The disposition to MH is autosomal-dominantly inherited and the incidence of a MH event was estimated as 1 in 60,000 balanced anaesthesias.

The pre-clinical standard investigation to determine the MH disposition is the *in vitro* contracture test (IVCT). This test was introduced by the department of anaesthesiology and intensive care medicine in 1986. In the 90th the diagnostic approach was extended by the identification of a number of MH associated mutations in the RYR1-gene. Until 2005 23 RYR1 mutations were classified as being causative for MH by the European MH Group. From 1999-2005 we have genetically investigated 715 persons out of 135 MH families. Altogether, 231 RYR1 mutation carriers out of 62 families could be idenified. They all showed a clear pathological response in the *in vitro* contracture test, representing a strong genotype-phenotype correlation. 205 individuals did not bear the familial mutation, almost all were MH negative in the IVCT.

24 different RYR1 mutations were detected in the three hot spot regions of the gene: 9 MH causative mutations, 2 known MH associated mutations (without functional evidence) and 14 new mutations (incl. one causative).

PD Dr. Henrik Rüffert

Universität Leipzig

University Hospital
Department of Anaesthesia and Intensive Care

E-Mail: henrik.rueffert@medizin.uni-leipzig.de
www.uni-leipzig.de/~kai/

COR-AAD1-00003143
Bayer EX1008 (Part 6 of 9)

5.56 Variability of the mitochondrial genome in cancer

Ingo Schäfer, Alexandra Kneissl, Christian Kukat, Peter Seibel

ATP, cell's energy currency, derives from the partial oxidation of energy-rich biomolecules. The final steps in the complex reaction process are carried out in mitochondria. The mutation rate of the mitochondrial DNA has been found to be almost ten times higher than in nuclear DNA. This is not surprising when considering the genesis of reactive oxygen species (ROS) that are generated during the reactions of the respiratory chain as side products. In the last decade, a variety of devastating neuromuscular diseases have been associated with mutations of the mitochondrial genome. These comprise single base replacements in tRNA and rRNA genes as well as protein genes. Moreover, length variations - insertions and deletions - were reported for other patients as well.

The regulatory region of the genome, the so called D-loop (displacement loop) is a noncoding stretch of DNA of approximately 1,100 bp. Very recently, reports on mtDNA variations within the D-loop were published for several cancers, but their functional significance remains still unclear. Clusters of hypervariable regions were found where mutations occurred with much higher frequencies. As replication and the repair machinery act in part independent from cell cycle, a novel DNA variation that is created during malfunctioning DNA replication and/or repair can expand very rapidly.

The goal of this project is to characterize the variations of the mitochondrial genome during tumorigenesis. Upon finding a direct linkage between tumorigenesis and defects of the mitochondrial genome, we also want to develop a test system for simplified diagnostics.

Ingo Schäfer

Universität Leipzig

Center for Biotechnology and Biomedicine (BBZ)
Professorship for Molecular Cell Therapy
and
Faculty of Medicine

E-Mail: ingo.schaefer@bbz.uni-leipzig.de
www.uni-leipzig.de/~mct/

COR-AAD1-00003144
Bayer EX1008 (Part 6 of 9)

5.57 Interaction of interleukin-1β with muscarinic acetylcholine receptor-mediated signaling cascade in cholinergically differentiated SH-SY5Y cells

Reinhard Schliebs, Kristin Heidel, Jenny Apelt

Increased expression of interleukin (IL)-1 has been found in Alzheimer brain, raising the question whether plaque-associated up-regulation of IL-1 may contribute to neuronal loss as it is able to stimulate the amyloidogenic path of amyloid precursor protein cleavage. However, less is known on participation of IL-1 in specific cholinergic cell loss. To test for this hypothesis, the cholinergically differentiated cell line SH-SY5Y was exposed to IL-1β for various periods of time followed by stimulation of muscarinic acetylcholine receptors (mAChR) and detecting key signaling molecules. The activity of acetylcholinesterase (AChE) in SY5Y cells was dose-dependently increased following stimulation with carbachol being highest at 100 µM. Pre-exposure of SY5Y cells to various concentrations of IL-1β (ranging between 1 and 50 ng/ml) for one up to 24 hours prevented the carbachol-induced mAChR-mediated effects on AChE activity, already detectable following one hour of prexposure at 10ng/ml IL-1β. Carbachol stimulation dose-dependently stimulated the activation of the transcription factors NFkB and AP-1 as revealed by EMSA. Pre-exposure of cells with 1 ng/ml IL-1β for two hours did not affect carbachol-mediated increase in DNA binding capacity of NFkB or AP-1. However, exposure of cells with 1 ng/ml IL-1β for 24 hours suppressed the capability of SY5Y cells to respond upon mAChR stimulation with increased NFkB or AP-1 activation. The data suggest interactive mechanisms between IL-1β and mAChR signaling cascades which may contribute to the cholinergic deficits in Alzheimer's disease.

Supported by DFG Schl363/6-1 to R.S.

Prof. Dr. Reinhard Schliebs

Universität Leipzig

Faculty of Medicine
Paul Flechsig Institute of Brain Research
Neurochemistry

E-Mail: schre@medizin.uni-leipzig.de
www.uni-leipzig.de/~pfi

COR-AAD1-00003145
Bayer EX1008 (Part 6 of 9)

5.58 Cell cycle regulatory proteins in the adult mouse neocortex

Stefanie Schmetsdorf, Ulrich Gärtner, Thomas Arendt

The developmental structuring of brain is the result of a strictly coordinated process that involves controlled cell division, neuronal migration and terminal differentiation. Once differentiated, neurons are incabable of further division but retain the capability of structural and functional plasticity. In general, the cell cycle progression is regulated by the sequential expression and activation of regulatory proteins like cyclins, cyclin dependent kinases (cdk) or cdk inhibitors (cdki). In terminally differentiated neurons, cell cycle activity is arrested by enrichment of cdkis. During the development as well as during the whole lifespan neuronal elements undergo a high degree of structural and functional remodeling and establish a neuronal network. This plastic process is accompanied by dynamic rearrangements of the cytoskeleton, i.g. neurofilaments, microtubules and actin. In the present study we have examind the expression of cell cycle regulatory proteins in the adult neocortex using immunohistochemical methods. Several cyclins and cdks could be predominantly localised to pyramidal neurons of layer V. Staining was prominent both in neuronal perikarya and dendrites. In parallel to immunohistochemical studies, expression of cell cycle proteins was verified by Western blotting. Quantitative real-time PCR was used to determine mRNA expression of cyclins, cdks and cdkis in single pyramidal neurons. Findings suggest that the expression of cell cycle markers in terminal differentiated pyramidal neurons of neocortex is likely associated with additional physiological functions beyond cell cycle regulation.

Stefanie Schmetsdorf

Universität Leipzig

Faculty of Medicine
Paul Flechsig Institute of Brain Research
Neuroanatomy

E-Mail: schmetsdorf@gmx.de
www.uni-leipzig.de/~pfi/

COR-AAD1-00003146
Bayer EX1008 (Part 6 of 9)

5.59 Advanced glycation endproducts activate mitogenic signal transduction pathways towards neuronal cell cycle re-entry

Angela Schmidt, Thomas Arendt, Gerald Münch

Advanced glycation endproducts (AGE), protein-bound oxidation products of sugars, have been shown to be involved in the pathophysiological processes of Alzheimer disease (AD). In addition, AGEs contribute to inflammation and oxidative stress occurring in AD. Neurodegeneration in AD is associated with activated mitogenic signaling and signs of re-entry into the cell cycle, indicated by the presence of cell cycle specific proteins, such as cyclins, cdk´s and their inhibitors. In the present study, we analysed the colocalization of AGEs and the cell cycle marker cyclin D1 in AD. Furthermore, it is supposed that RAGE, a receptor for advanced glycation endproducts, mediates its intracellular signaling via the MAPK pathway and causes the activation of the transcription factor NfkB. In order to show that the MAPK pathway is involved in RAGE signaling, we silenced this pathway by anti-RAGE antibody and by oligo-anti-sense-RAGE. Thereby we could obtain evidence for an involvement of RAGE in cell-cycle-activation. Further, we analysed the phosphorylation of CREB and Rb, known to be critical regulators of cell-cycle-activation. Our result indicated that AGEs can potentially activate mitogenic signaling which leads to cell cycle re-entry of neurons in AD, and thus drive the progression of dementia.

This work was supported by IZKF Core Unit "Neuroimmunological Cell Biology" and AFI Application 2002.

Angela Schmidt

Universität Leipzig

Faculty of Medicine
Paul Flechsig Institute of Brain Research
Neuroanatomy

E-Mail: schmidta@medizin.uni-leipzig.de
www.uni-leipzig.de/~pfi/

COR-AAD1-00003147
Bayer EX1008 (Part 6 of 9)

5.60 Neuronal activation of Ras regulates synapse formation and synaptic vesicle docking

Gudrun Seeger, Ulrich Gärtner, Thomas Arendt

The small G protein Ras, which is a molecular switch in neurotrophic signal transduction, is implicated in synaptic plasticity and synapse development during ontogeny and in the adult nervous system. To characterise the involvement of Ras-dependent signaling in synaptogenesis, the cortical synapse-to-neuron ratio was investigated in synRas mice overexpressing Val12-Ha-Ras in postmitotic neurons[1]. The number of synapses and neurons were analysed in cortical layers II/III of the somatosensory cortex at different stages of postnatal development by stereological methods. The synapse-to-neuron ratio was still identical in wild-type and synRas mice at postnatal day 4 before the onset of transgene expression. At P12, P47 and in the adult, analyses revealed a significant increase in the synapse-to-neuron ratio in synRas mice which correlated with the strength of transgene expression. We also show that neuronal expression of Val 12-Ha-Ras enhances docking of synaptic vesicles to active zones in adult mice. The data presented here provide evidence that Ras activity might be profoundly involved in synaptogenesis by reinforcing the formation or maintenance of synapses during the development and in the adult. We conclude that neuronal Ras activity contributes to the regulation of of synaptic plasticity in adult mammalian brain at the presynaptic level.

Notes

1 Heumann et al., J. Cell. Biol. 151:1537-1548 (2000).

Dr. Gudrun Seeger

Universität Leipzig

Faculty of Medicine
Paul Flechsig Institute of Brain Research
Neuroanatomy

E-Mail: seeg@medizin.uni-leipzig.de
www.uni-leipzig.de/~pfi/

COR-AAD1-00003148
Bayer EX1008 (Part 6 of 9)

5.61 Neuropeptide Y and the selective Y_1 receptor agonist [F7, P34] pNPY inhibit the glutamatergic synaptic transmission on cortical neurons

Kathrin Sichardt, Zacherie Vissiennon, Annette G. Beck-Sickinger, Karen Nieber

Neuropeptide Y (NPY) has been shown to be one of the most abundant and widely distributed peptides in the central nervous system. In rat, NPY immunoreactivity is prevalent in the cortex and in the hippocampus. These areas are also enriched with NPY receptors (Y). Several receptor subtypes of the Y receptor superfamily have been identified in the central nervous system. The peptide agonists allow differentiation between various Y receptor subtypes in these areas. In the present study glutamatergic synaptic potentials (PSPs) induced by electrical field stimulation were measured intracellularly by microelectrodes in pyramidal cells of the rat cingulate cortex in brain slices. The type of the NPY receptor responsible for affecting the PSPs was assessed by examining the effects of different NPY agonists and the selective Y_1 receptor antagonist (R)-N2-(diphenylacetyl)-N-[(4-hydroxyphenyl)-methyl argininamide (BIBP3226). NPY had an inhibitory effect on the PSPs. It decreased concentration-dependendly the amplitude of the PSPs by a biphasic effect. The inhibitory effect induced by low concentration but not by high concentration was reversible during washout. The bath application of the selective Y_1 agonist [F7, P34] pNPY showed the same effect as NPY on PSPs. The selective Y_1 receptor antagonist BIBP3226 (50 nM) completely inhibited the effect of [F7, P34] pNPY. Accordingly, the present study demonstrates that the Y_1 receptor is involved in the inhibition of glutamatergic neurotransmission in cortical neurones of the cingulate cortex.

Kathrin Sichardt

Universität Leipzig

Faculty of Biosciences, Pharmacy and Psychology
Institute of Pharmacy
Pharmacology for Natural Scientists

E-Mail: sichardt@rz.uni-leipzig.de
www.uni-leipzig.de/~pharm/phfn/

COR-AAD1-00003149
Bayer EX1008 (Part 6 of 9)

5.62 Flow cytometry in Alzheimer's disease diagnostics

Jens Stieler, Markus Kiefer, Thomas Arendt

The search for a biomarker of Alzheimer's disease (AD) is one of the challenges in the investigation of this neurodegenerative disease. At present an early diagnosis of AD is, regardless the recent findings of molecular mechanisms and novel imaging techniques, still complex and unreliable. Several biomarkers were investigated to support or replace of the present tests. Numerous reports suggest an involvement of peripheral cell types in the pathology of AD. Isolated lymphocytes of AD patients showed an impaired response after mitogenic stimulation. The proliferative response can be analyzed by detecting the CD69 expression using flow cytometry. However, the protocol involves several elaborative and time consuming steps which make it difficult to introduce this technique into the analytical laboratory routine.

In order to reduce the methodical expenditure and enhance the reproducibility we tested the lymphocyte proliferation assay on whole blood on 22 samples (13 AD, 9 controls). Stimulation, staining and measuring of the sample can be performed in only one tube. Using this assay we could statistically significant differentiate between AD and non-AD samples.

Jens Stieler

Universität Leipzig

Faculty of Medicine
Paul Flechsig Institute of Brain Research
Neuroanatomy

E-Mail: spitz@uni-leipzig.de
www.uni-leipzig.de/~pfi/

COR-AAD1-00003150
Bayer EX1008 (Part 6 of 9)

5.63 Osmotic glial cell swelling in the rat retina is inhibited by triamcinolone acetonide

Ortrud Uckermann, Franziska Kutzera, Antje Wolf, Ianors Iandiev, Thomas Pannicke, Andreas Reichenbach, Sebastian Wolf, Peter Wiedemann, Andreas Bringmann

Anti-inflammatory corticosteroids such as triamcinolone acetonide are commonly used to treat macular edema during ischemic and inflammatory eye diseases. In addition to the leakage of blood-retinal barriers which causes extracellular edema, swelling of Müller glial cells (cytotoxic edema) has been implicated in the formation of macular edema. Recently, we have shown that hypotonic stress (that resembles hypoxia-induced cytotoxic edema in the brain) induces Müller cell swelling under multiple experimental conditions: In the postischemic retina of the rat, in retinas of eyes with LPS-induced ocular inflammation, and in control retinas in the presence of Ba^{2+}, H_2O_2, arachidonic acid, or PGE_2. Acute application of triamcinolone dose-dependently inhibited the glial cell swelling in slices of postischemic retinas and from LPS-treated eyes, as well as in control retinas. The inhibiting effect of triamcinolone on Müller cell swelling was largely abrogated in the presence of inhibitors of A1 adenosine receptors, of adenylyl cyclase and of PKA, respectively. This suggests that the effect of triamcinolone involves endogenous release or formation of adenosine and subsequent A1 receptor stimulation that results in enhancement of the intracellular cAMP level and activation of PKA. Acute application of trimacinolone rapidly inhibits the osmotic glial cell swelling which is a characteristic feature of retinas of the rat during ischemia-reperfusion and inflammation. The inhibiting effect on the cytotoxic Müller cell swelling may contribute to the edema-resolving action of triamcinolone observed in human subjects.

Dr. Ortrud Uckermann

Universität Leipzig

Faculty of Medicine
Paul Flechsig Institute of Brain Research
Neurophysiology

E-Mail: ucko@medizin.uni-leipzig.de
www.uni-leipzig.de/~pfi/

COR-AAD1-00003151
Bayer EX1008 (Part 6 of 9)

5.64 The influence of neuropeptide Y and Y_1 receptor antagonist BIBP3226 on MCF-7 tumor spheroids

Winnie Weigel, Andrée Rothermel, Markus Rüffer, Randy Kurz, Heinz-Georg Jahnke, Levin Böhlig, Annette G. Beck-Sickinger, Andrea A. Robitzki

Neuropeptide Y (NPY) and its receptors have been shown to be involved in human cancer. As revealed for breast cancer, 85 % of patients have an elevated and modified expression pattern of NPY receptors in their tumors. In normal breast tissue Y_2 receptor mRNA is predominant, whereas breast carcinomas preferentially express Y1 receptor mRNA. Tumor spheroids of the human mamma carcinoma cell line MCF-7 were incubated with NPY and Y_1 receptor antagonist (BIBP3226) to examine the effects on proliferation, apoptosis and tumor growth. In the presence of BIBP3226 the size of tumor spheroids was reduced, whereas NPY caused an increase in size compared to control spheroids. Moreover, we observed that the expression of Y_1 receptor mRNA was significantly increased by the addition of NPY. Interestingly, we could also detect an elevated mRNA expression of Y_1 receptors if tumor spheroids were treated with BIBP3226. Furthermore, an antagonist-depending reduction of apoptotic cells was shown in comparison to untreated spheroids. On the basis of these findings MCF-7 tumor spheroids can serve as a new model system to analyse the role of Y receptors in breast cancer and to develop new therapeutic strategies.

Winnie Weigel

Center for Biotechnology and Biomedicine (BBZ)
Professorship for Molecular Biological-Biochemical Process Technology
and
Faculty of Biosciences, Pharmacy and Psychology
Institute of Biochemistry

E-Mail: winnie.weigel@bbz.uni-leipzig.de
www.uni-leipzig.de/~dmpt/

COR-AAD1-00003152
Bayer EX1008 (Part 6 of 9)

5.65 Protective effects of prolyl endopeptidase inhibitors in astrocytoma cell lines and rat primary astrocytes

Ulrike Zeitschel, Susanne Rudzok, Ingo Schulz, Steffen Roßner, Hans-Ulrich Demuth

The neuroprotective effects of prolyl endopeptidase (PEP) inhibitors are well characterized in a number of experimental *in vitro* and *in vivo* models. However, several clinical conditions are associated with the death of astroyctes, whose functions are important for the maintenance of neurons. In order to demonstrate the effects of PEP inhibitors on the survival of astrocytes in stress paradigms, the astrocytoma cell lines U-343 and U-138MG as well as rat primary astrocytes were subjected to toxic stimuli by means of staurosporine-, LPS- or oncostatine M-treatment. These treatments resulted in the death of 30-70 % of the astrocytes within a period of 24 hours as demonstrated by LDH release into the culture medium. Enzymatic activity assays and immuncytochemistry using an antibody against active caspase-3 revealed the contribution of caspase3/7 in astrocytic cell death under these experimental conditions. To reveal whether or not PEP inhibitors are protective in these *in vitro* paradigms, co-incubation experiments with the stressors mentioned above and three different PEP inhibitors of distinct chemical classes were performed. We observed a dose-dependent protection from the cytotoxicity for all PEP inhibitors used but with a different potency and kinetics.

These data indicate that PEP inhibitors protect astrocytes from cell death induced by different insults. Based on the known functions of astrocytes in neuroprotection/repair it is tempting to speculate that the observed neuroprotective effects of PEP inhibitors in experimental lesion studies *in vivo* are contributed by enhanced astrocytic survival.

Dr. Ulrike Zeitschel

Universität Leipzig

Faculty of Medicine
Paul Flechsig Institute of Brain Research
Neurochemistry

E-Mail: zeiu@medizin.uni-leipzig.de
www.uni-leipzig.de/~pfi/

COR-AAD1-00003153
Bayer EX1008 (Part 6 of 9)

6. BIOMEDICAL AND CELL ENGINEERING

POSTERS

COR-AAD1-00003156
Bayer EX1008 (Part 6 of 9)

6.1 Optimisation of hepatocyte spheroid culture for application in bioartificial liver support systems

Matthias Funke, Doreen Beck, Christine Schulz,
Jan-Michael Heinrich, Augustinus Bader

In case of Hepatic Failure, the therapy options are today basically restricted to the use of biochemical and/or physical absorption and filtration process that are not suitable to substitute the complex synthetic and metabolic liver functions effectively. This task can only be fulfilled by cells of a healthy liver, namely the hepatocytes.

Our goal is the characterisation and further development of such biocomponents, especially hepatocyte spheroids, for bioartificial liver support systems. The 3D spheroid culture is characterized by the aggregation of single hepatic cells to a complex community, comparable to the native liver tissue, which promotes their viability and functionality.

The cells undergo different changes in the stages of formation and maturation of aggregates, caused by changes in mass transfer (supply with oxygen and nutrients) and by the establishment of extensive cellular contacts.

Regarding to the first point, we obsere the spheroid size and related morphological changes, especially the occurrence of necrotic or apoptotic cells inside the aggregates. At second we are focused on the differences at the formation of hepatocyte spheroids w/wo different kinds of nonparenchymal liver cells, and/or changes under the treatment with different combinations of growth factors. These experiments will result in the establishment of a continuous culture system for optimised cultivation and mass preparation of hepatocyte spheroids. The innovation of this culture system should be the production of spheroids with defined size by cutting of aggregates bigger than an upper limit, to prevent mass transfer limitations.

Matthias Funke

Universität Leipzig

Center for Biotechnology and Biomedicine (BBZ)
Professorship for Cell Techniques and
Applied Stem Cell Biology
and
Faculty of Medicine

E-Mail: matthias.funke@bbz.uni-leipzig.de
www.uni-leipzig.de/~bader/

COR-AAD1-00003157
Bayer EX1008 (Part 6 of 9)

6.2 Interaction of signaling pathways during capacitation of human spermatozoa

Sonja Grunewald, Uwe Paasch, Thomas Baumann, Christian Kriegel, Hans-Jürgen Glander

Introduction: Capacitation of sperm is a prerequisite for successful fertilization, although the exact molecular mechanism is not fully clarified. The calpain(CLP)-calmodulin(CM)-system is essential for membrane fusion during this process. Activation of caspases (CP) is a main feature of apoptotic cells. The objective of our study was to examine interactions of apoptosis signaling pathways and the CLP-CM-system during capacitation.

Material and Methods: Semen samples of donors (n=14) were washed by density gradient centrifugation. Four aliquots were incubated in BWW at 37 °C 5 % CO2 for 3h with: no additive (control); 3 % BSA (capacitation); 10 µM CLP-inhibitor III or 20 µM CM-inhibitor (Ophiobolin A). Capacitation was monitored by hyperactivation (CASA), CTC-assay and tyrosine phosphorylation (Western blot). FACS analyses were performed to evaluate CP1,-9 and -3 activation and the integrity of transmembrane mitochondrial potential (iTMP).

Results: Capacitation (proved by CTC-assay, increased levels of tyrosine phosphorylation and hyperactivation) resulted in inactivation of CP1:-9.9±8.2 %, CP9:-9.8±6.3 % and CP3: -4.8±8.3 % and improved intact TMP:+17.5±7.7 %. Inhibition of CLP during capacitation had no further impact on CP and iTMP, but diminished the capability to capacitate. In contrast, inhibition of CM resulted in both: blocking of physiological changes seen during capacitation and apoptosis (CP1:+64.0±27.2 %, CP9:+76.9±25.7 %, CP3:+78.9±25.2 %, iTMP:-68.3±20.5 %).

Conclusion: Interaction of both signaling systems seems to enable the capacitation process by prevention of apoptosis.

Dr. Sonja Grunewald

Universität Leipzig

University Hospital
Department of Dermatology

E-Mail: sonja.grunewald@medizin.uni-leipzig.de
www.uni-leipzig.de/~derma/

COR-AAD1-00003158
Bayer EX1008 (Part 6 of 9)

6.3 Tissue engineered scaffolds for cartilage repair

Marcus Haberhauer, Andrea Deiwick, Augustinus Bader

Biological restoration of cartilaginous defects of the knee joint caused by trauma remains a challenging and controversial clinical problem and a major challenge for orthopaedic surgery since these defects do not heal spontaneously because of the limited regenerative capability of the articular cartilage.

Tissue engineering offers the possibility for the construction of autologous chondrogenic grafts for reconstructive surgery and represents a promising method for the treatment of large cartilage defects.

The intent of our project is the assortment of several biocompatible materials that could be considered as a three-dimensional carrier for autologous chondrocytes.

In our work, freshly isolated porcine chondrocytes were embedded in two biological degradable matrices and cultured either in static culture system for seven days and after that transferred to a roller bottle culture system for 30 days or cultured in roller bottle culture system for 37 days right after seeding.

Immunohistochemical and biochemical analysis, confocal laser scanning microscopy and histomorphological analysis were performed at defined time points to evaluate the phenotypic changes of the embedded chondrocytes, and the quality of the newly formed cartilaginous matrix.

Our experiments show that the varying treatments combined with the different matrices used in our experiments support the proliferation and the development of a stable and cartilage-like extracellular matrix with the opportunity to create a transplant for cartilage restoration.

Marcus Haberhauer

Universität Leipzig

Center for Biotechnology and Biomedicine (BBZ)
Professorship for Cell Techniques and
Applied Stem Cell Biology
and
Faculty of Medicine

E-Mail: marcus.haberhauer@bbz.uni-leipzig.de
www.uni-leipzig.de/~bader/

COR-AAD1-00003159
Bayer EX1008 (Part 6 of 9)

6.4 Effects of surface coatings using bone sialoprotein, collagen, and fibronectin on cells derived from human maxillar bone

Heidegard Hilbig, Raik Rupietta, Hans-Ludwig Graf, Stefan Thalhammer, Stefan Strasser, Franz Paul Armbruster

The interaction between the implant material and the surrounding tissues is believed to be one of the factors determining implant success. Bone sialoprotein (BSP) is both one of the major noncollagenous protein in the extracellular matrix of bone and a marker for osteoblastic differentiation. We compared BSP-, collagen-, fibronectin- and non-coated implant material in supporting the development of adult human maxillar bone at day 3, 5, 10, 15, 20 and 25 *in vitro*. The time course of the expression of BSP and fibroblasts was visualized immunohistochemically. The distribution patterns of cells were determined on the surface of TICER and glimmer. TICER consists of titanium with hydroxy-apatite ceramic with rough surface. Glimmer has a total smooth surface.

Cell countings revealed that most of survived cells are settled on the surface of the BSP-coated implants. Significantly different values were found at the 3. and the 5. Div, exclusively. The White-test using rankings of the median values gave evidence for BSP-coatings at rank 1 followed by collagen.

Prof. Dr. Heidegard Hilbig

Universität Leipzig

Faculty of Medicine
Institute of Anatomy

E-Mail: hilbigh@medizin.uni-leipzig.de
www.uni-leipzig.de/~anatomie/

COR-AAD1-00003160
Bayer EX1008 (Part 6 of 9)

6.5 Human retinal pigment epithelial cells produce and respond to placenta growth factor

Margrit Hollborn, Solveig Tenckhoff, Peter Wiedemann, Leon Kohen, Andreas Bringmann

Placental growth factor (PlGF) is a member of the vascular endothelial growth factor (VEGF) family and shares some biological functions of this molecule. PlGF seems to be implicated in the formation of fibrovascular tissue during proliferative diabetic retinopathy (PDR), since the vitreous level of PlGF is elevated during development of PDR and PlGF immunoreactivity is expressed in fibrovascular membranes. However, it is not known whether RPE cells produce PlGF. Therefore we determine whether human retinal pigment epithelial (RPE) cells express and respond to PlGF.

Human RPE cells express mRNAs for various members of the VEGF family of growth factors and for their receptors such as for VEGF-A, -B, -C, -D, PlGF, Flt-1, KDR, and neuropilins-1 and -2. The expression levels of the mRNAs for neuropilins-1 and -2 were higher when compared to the mRNAs for Flt-1 and KDR. Exogenous PlGF enhanced the expression of neuropilin-1. The Members of the transforming growth factor (TGF)-β superfamily, BMP-4, TGF-β1 and TGF-β2 are strong inducers of the PlGF gene expression, and evoke secretion of PlGF protein by RPE cells. Exogenous PlGF-2 induces chemotaxis in RPE cells and reduces slightly the cell proliferation at high concentrations.

The finding that RPE cells secrete and respond to PlGF suggests that the factor exerts an autocrine/paracrine action on these cells. Increased retinal expression of TGF-β-related growth factors during proliferative retinopathies may cause facilitation of PlGF expression by RPE cells that may contribute to the stimulation of cell migration as a critical component of the progression of epiretinal membranes.

Dr. Margrit Hollborn

Universität Leipzig

Faculty of Medicine
Department of Ophthalmology

E-Mail: hollbm@medizin.uni-leipzig.de
www.uni-leipzig.de/~auge/

COR-AAD1-00003161
Bayer EX1008 (Part 6 of 9)

6.6 Investigation of RGD-oligonucleotide conjugates with respect to their hybridization with anodically entrapped oligonucleotides (ON) on titanium alloys and their binding ability to integrines on osteoblasts

Ina Israel, Jan Michael, René Beutner, Ute Hempel, Hartmut Worch, Dieter Scharnweber, Bernd Schwenzer

Titanium and its alloys are mainly used for implants because of their excellent biocompatibility. However, in the case of systemic diseases (e.g. diabetes) or bad local bone quality further improvement is necessary. A promising approach to stimulate the natural healing process is surface coating with components of the extracellular matrix (ECM) or peptides mimicking ECM functions. For the presented modular system different ON-conjugates were hybridized with ON which had been partially entrapped in an anodically grown oxide layer on the titanium alloy surface.

In this study complementary and non-complementary ON (with respect to the entrapped ON) were conjugated to the hexapeptide GRGDSP containing RGD as an integrine recognition sequence. Covalent linkage was carried out with suberic acid bis(N-hydroxysuccinimide ester). Characterization was accomplished by HPLC and MALDI TOF MS.

Immobilization and hybridization efficiencies were determined radioanalytically, using 32P-labeled ON. Hybridization efficiencies of the RGD-ON-conjugate and the corresponding ON were in a similar range. Thus, the bound hexapeptide hardly affects hybridization.

Successful conjugate binding to integrines on osteoblasts proved the preservation of biological activity of the GRGDSP hexapeptide.

Ina Israel

Technische Universität Dresden

Department of Mathematics and Natural Sciences
(with Psychology)
Institute of Biochemistry

E-Mail: ina.israel@chemie.tu-dresden.de
www.chm.tu-dresden.de/bc/

COR-AAD1-00003162
Bayer EX1008 (Part 6 of 9)

6.7 Destruction of endogenous mtDNA – Establishing a novel method utilising a restriction endonuclease

Alexandra Kneissl, Christian Kukat, Ingo Schäfer, Peter Seibel

A variety of human disorders are based on defects of the mitochondrial genome. Among those diseases are cases of maternally transmitted epilepsy, muscle disorders, blindness, refractory anemia or diabetes. The broad spectra of symptoms already pinpoints toward the physiological problem of these disorders: the limitation of oxidative energy supply creates tissue and developmentally critical bottlenecks in different organs that are caused by genetic defects of the oxidative phosphorylation system. Very little is known about the overall molecular mechanisms underlying these diseases especially the interaction of nuclear and mitochondrial genomes.

Therefore we developed a novel system for establishing cells devoid of any endogenous mitochondrial DNA without using mutagenic substances. This system is based on a mitochondrially targeted restriction enzyme. Upon reaching the mitochondrial matrix the mtDNA is cleaved at specific sites and hence the mitochondrial genome can undergo degradation by endogenous mitochondrial nucleases.

The cell lines established so far with this method revealed a ρ^0-state by relying on supplementation of the growth media with pyruvate and uridine. The genetic loss of the mitochondrial genome was also demonstrated by PCR analysis.

Further investigations of the interactions between the mitochondrial and nuclear genome can now be envisioned. Moreover our research interest aims for the generation of an animal model that enables the study of mitochondrial biogenesis and oxidative energy supply *in vivo*, and to shed light on the molecular pathogenesis of these diseases.

Alexandra Kneissl

Universität Leipzig

Center for Biotechnology and Biomedicine (BBZ)
Professorship for Molecular Cell Therapy
and
Faculty of Medicine

E-Mail: alex.kneissl@bbz.uni-leipzig.de
www.uni-leipzig.de/~mct/

COR-AAD1-00003163
Bayer EX1008 (Part 6 of 9)

6.8 Evidence for abnormal iodination of thyroglobulin in cold thyroid nodules

Kerstin Krause, Stefan Karger, Marie-Christine Many, Sylvie Poncin, Ralf Paschke, Dagmar Führer

Using a proteomic approach we previously observed upregulation of proteins involved in the reduction of peroxide in cold thyroid nodules. These results point to either (I) a defect in the integrity of Tg which might prevent the organification and coupling of iodide (I-) to from thyroid hormones or (II) to a principal defect in the uptake and transport of I- in CTN. To investigate the functional protein expression characteristics in CTNs in more detail, immunohistochemical analysis was performed in a series of 12 CTNs and corresponding normal thyroid tissues. The following proteins were studied: (1) proteins involved in intrathyroidal iodine metabolism (Pendrin, ThOX 1/ 2 and TPO, Tg, T4-Tg); (2) proteins involved in the antioxidative system (PDRX 5, GST π) and (III) proteins involved in Tg-processing (cathepsin B). We found (I) complete absence of T4-rich iodinated Tg in CTNs while overall Tg expression was not altered, (II) higher expression of ThOXs and TPO in CTNs compared to ST, (III) upregulation of the antioxidant enzyme PDRX 5 in CTNs and (VI) expression of pendrin depending on follicular size (upregulation only in small follicles in normal thyroid tissues). Taken together, this study confirms the data obtained by proteomics and further reinforce the hypothesis of an altered Tg function with most likely compensatory yet ineffective upregulation of the thyroid hormone synthesis apparatus in CTNs. Moreover, it is tempting to speculate that increased proliferation in combination with deranged abundant peroxide generation may contribute to somatic mutations leading to clonal CTNs.

Kerstin Krause

Universität Leipzig
University Hospital
Department of Internal Medicine III
www.uni-leipzig.de/~innere/

COR-AAD1-00003164
Bayer EX1008 (Part 6 of 9)

6.9 Cardiomyocytes beat for microelectrode arrays: the use of electrogenic properties for functional monitoring of autoimmune antibodies in sera of preeclamptic patients

Randy Kurz, Andrée Rothermel, Markus Rüffer, Winnie Weigel, Heinz-Georg Jahnke, Holger Stephan, Andrea A. Robitzki

The aim of the study was the establishment of a high-sensitive screening system that enables the electronic detection of drugs and tissue-secreted factors involved in AT_1 receptor-mediated cardiovascular diseases. Spontaneously beating neonatal rat cardiomyocytes were cultured on multielectrode arrays and used as biological sensors. After evaluation of culture parameters, computer-based electronic measurement systems have been developed for counting contractions by recording the field potential of cardiomyocytes. Using the biosensor, angiotensin II, the predominant ligand of the AT_1 receptor, was detected at very low concentrations of 10^{-11} M via altered contractions of cardiomyocytes. Moreover, we demonstrated that cardiomyocyte coupled microarrays allow the detection of blood-derived low concentrated anti-AT_1 receptor autoantibodies of pregnant women suffering from preeclampsia. This study demonstrates the first well-suited electrophysiological recording of cardiomyocytes on multielectrode arrays as a benefit for functional biomonitoring for the detection of AT_1 receptor/ligand interactions and other marker proteins in sera directed to diseases.

Randy Kurz

Universität Leipzig

Center for Biotechnology and Biomedicine (BBZ)
Professorship for Molecular Biological-Biochemical Process Technology
and
Faculty of Biosciences, Pharmacy and Psychology
Institute of Biochemistry

E-Mail: randy.kurz@bbz.uni-leipzig.de
www.uni-leipzig.de/~dmpt/

COR-AAD1-00003165
Bayer EX1008 (Part 6 of 9)

6.10 Comparison of entrapped strategies of hepatocytes culture

Aldo Leal-Egana, Jan-Michael Heinrich, Augustinus Bader

One of the principal difficulties to develop an Artificial Liver Support is the survival and the maintains of the metabolic characteristics of Hepatocytes cultured *in vitro*.

In spite of the multiples culture strategies developed, obtaining the optimal bioreactor design still remains as an unsolved problem. Nevertheless, current scientific publications show that the hepatocytes cultured in a three dimensions systems (3D) presents comparative advantages respect to the traditional culture in 2 dimensions (with adherent cells), basically due to the contact between the cells themselves.

Two techniques which allow the cell culture in a 3D system, besides aggregation culture, are the cell immobilization and the cell encapsulation, which presented other advantages, such as avoiding the shear and mechanical stress, and the possibility to freezing, maintaining a stable activity after defrost. Nevertheless, there are just a few reports which compare both systems using hepatocytes.

With the purpose to analyze the differences between both culture strategies, Mouse hepatocytes were immobilized in 500 µm diameter Alginate beads (app. 70 cells per capsule). At the same time, the same cell number was encapsulated in Poly-L-Lysine beads of the same diameter. In both cases the study was carried out without, with low and with high agitation.

The results show a clear difference in the analyzed parameters (albumin, glucose and lactate production, urea degradation, days of hepatocyte surviving) between the experiences carried out without and with low agitation, against the experiment with strong agitation, indicating that improving the mass transference could provide a potential enhancement on the survive capacity of the hepatocytes cultured *in vitro*.

Aldo Leal-Egana

Universität Leipzig

Center for Biotechnology and Biomedicine (BBZ)
Professorship for Cell Techniques and
Applied Stem Cell Biology
and
Faculty of Medicine

E-Mail: aldo.leal@bbz.uni-leipzig.de
www.uni-leipzig.de/~bader/

COR-AAD1-00003166
Bayer EX1008 (Part 6 of 9)

6.11 Interaction of nucleic acids with titanium alloy surfaces for improved immobilization and hybridization

Jan Michael, René Beutner, Ina Israel, Hartmut Worch, Dieter Scharnweber, Bernd Schwenzer

A modular system for bio-surface engineering of titanium implant materials based on anodic entrapment of single-stranded oligonucleotides (ON) and their subsequent hybridization with different ON-biomolecule conjugates was subject to further optimization.

Investigated parameters influencing interaction were
- terminal ON modification,
- pH of electrolyte,
- divalent metal ions (Mg^{2+}),
- buffer system,
- ON base composition,
- sample wettability.

Terminal phosphorylation is crucial for the extent, stability and regiospecificity of adsorption and entrapment.

Strength and quantity of immobilization depend on the pH-value of the electrolyte that influences electrostatic interaction between surface and ON. Above pH=8.0 repulsion between the - both negatively charged - titanium surface and ON is distinctly diminishing adsorption. Between pH-values of 3.0 and 8.0 Mg^{2+} acts as mediator by decreasing repulsion. Adsorption at pH=7.5 was better in TRIS buffer compared to borate buffer indicating an influence of the buffer system.

The influence of diminished surface wettability on ON adsorption due to progressive hydrocarbon contamination under atmospheric conditions was investigated comparing the interaction of water-stored (hydrophilic) and octane-treated (hydrophobic) surfaces with various ON. Their adsorption behaviour could not clearly be traced back to surface treatment or hydrophobic interactions at higher purine content. Unexpectedly, the sequences of the ON seem to influence the adsorption behaviour.

Jan Michael

Technische Universität Dresden

Department of Mathematics and Natural Sciences
(with Psychology)
Institute of Biochemistry

E-Mail: jan.michael@chemie.tu-dresden.de
www.chm.tu-dresden.de/bc/

COR-AAD1-00003167
Bayer EX1008 (Part 6 of 9)

6.12 Engineering of three dimensional mammalian retinal spheres by rotation cultures

Andrée Rothermel, Thomas Biedermann, Winnie Weigel, Randy Kurz, Markus Rüffer, Heinz-Georg Jahnke, Andrea A. Robitzki

The aim of this study was the development of a reliable three-dimensional culture system of the mammalian retina that allows the analysis of retinal development and stratification as well as cellular differentiation processes *in vitro*. For the cultivation of retinal spheres, dissociated retinal cells of neonatal rats were maintained in culture dishes on a self-made orbital shaker. Based on well-defined rotation conditions, dissociated free floating cells re-aggregate in the centre of the culture dish to form multicellular cluster. Subsequently, cells begin to proliferate, whereby they form sphere-like retinal tissues with a diameter of 180-210 µm. The characterisation of mature retinal spheres by immunocytochemistry revealed the presence of ganglion cells, amacrine cells, Müller cells, bipolar cells, and rod photoreceptors which are arranged in different retina-like layers. Although a small number of cells undergo apoptosis, retinal spheres remain viable for at least 35 days in culture as shown by fluorescein diacetate and TUNEL staining. Since proliferation, differentiation, apoptosis, and survival are also detectable in retinal spheres this novel mammalian 3D culture system is well-suited to investigate aspects of retinogenesis *in vitro* under tissue-like conditions.

Dr. Andrée Rothermel

Universität Leipzig

Center for Biotechnology and Biomedicine (BBZ)
Professorship for Molecular Biological-Biochemical Process Technology
and
Faculty of Biosciences, Pharmacy and Psychology
Institute of Biochemistry

E-Mail: andree.rothermel@bbz.uni-leipzig.de
www.uni-leipzig.de/~dmpt/

COR-AAD1-00003168
Bayer EX1008 (Part 6 of 9)

6.13 Bioreactor technologies for culturing of skin substitutes

Thomas Rupf, Katrin Lorenz, Jürgen Salvetter, Augustinus Bader

Wound coverage of extensive burn injuries and other large deep skin defects represents a major problem in dermatology. The upper limit regarding surface area is set by the availability of autologous material to cover the site of injury provided by the patient. For this reason it is necessary to develop skin equivalents for transplantation consisting of dermal and epidermal components to support the regeneration of skin.

With the aim to produce skin equivalents under controlled conditions in perfusion bioreactors, the precultivation of keratinocytes on membraneous supports becomes an important technical requirement. On the other hand, to achieve bilayered skin substitutes, preformed keratinocyte sheets have to be combined in a second step with dermal equivalents.

Meaningful key parameters for quality assessment and process control are to be characterized in order to achieve standardized protocols. Special emphasis will be put on the role of the extracellular matrix (ECM) natively synthesized in the dermal equivalents for epidermal regeneration. To prove the concept of generation of functional dermal equivalents by fibroblasts in a three-dimensional configuration we made use of a fibrous biodegradable scaffold.

Fibroblasts were inoculated into the material and cultured under conditions optimized for ECM-production. When these constructs had accomplished a smooth coherent surface at the top, they were ready for the application of keratinocytes and organotypic cocultivation in perfusion bioreactors.

Thomas Rupf

Universität Leipzig

Center for Biotechnology and Biomedicine (BBZ)
Professorship for Cell Techniques and
Applied Stem Cell Biology
and
Faculty of Medicine

E-Mail: thomas.rupf@bbz.uni-leipzig.de
www.uni-leipzig.de/~bader/

COR-AAD1-00003169
Bayer EX1008 (Part 6 of 9)

6.14 Peptide mediated DNA import into mitochondria

Ingo Schäfer, Alexandra Kneissl, Christian Kukat, Martina Seibel

Energy of eukaryotic cells is generated by the oxidative phosphorylation system located in the mitochondria. The compounds of this system are encoded either in the nuclear or the mitochondrial genome. Therefore genetic defects within the mitochondrial DNA can cause disorders in the cell's energy production and ultimately lead to neuromuscular dysfunctions. Mitochondrial DNA variations can range from single point mutations to deletions of large DNA fragments encoding for several genes.

Import of DNA from the cytoplasm into the mitochondrial matrix is an obligatory step for a site directed mutagenesis or gene therapy approach on mitochondrial DNA diseases. Up to now, no endogenous system mediating this transfer is known in mammalian cells. To close this gap we developed peptide conjugated DNA vectors that are capable of delivering nucleic acids to the mitochondrial matrix. The vector is made up of the mitochondrial signal peptide of the ornithine transcarbamylase (OTC, a nuclear encoded protein finally located in mitochondria) which is chemically cross linked to a nucleic acid component harboring the desired DNA molecule to be located in the mitochondrial matrix[1]. Due to the unique physical structure of the attached DNA, induction of regulated self-replication is emphasized upon reaching the final cellular compartment.

At the moment we focus on the composition of the DNA to achieve correct expression of the gene of interest (EGFP as marker) in the mitochondrial matrix.

Notes

1 Seibel P., Trappe J., Villani G., Klopstock T., Papa S., Reichmann H., Nucleic Acids Res. 1995 Jan 11;23(1):10-7.

Ingo Schäfer

Universität Leipzig

Center for Biotechnology and Biomedicine (BBZ)
Professorship for Molecular Cell Therapy
and
Faculty of Medicine

E-Mail: ingo.schaefer@bbz.uni-leipzig.de
www.uni-leipzig.de/~mct/

COR-AAD1-00003170
Bayer EX1008 (Part 6 of 9)

6.15 *In vitro* regeneration of liver cells

Christine Schulz, Jan-Michael Heinrich, Augustinus Bader

A special interest of regenerative medicine is the self renewing of the liver. The possibility of expanding hepatocytes *in vitro* would be an advantage for hepatocyte transplantations, liver support systems, drug screenings and especially for experimental use. Functional behaviors and growth activity of hepatocytes isolated from liver and cultured *in vitro* are incredible less in comparison to *in vivo*. The process of cell regeneration has to be divided into three phase: initiation, proliferation and termination, which are considerably controlled by different growth factors and cytokines[1,2].

This survey analyses the effect of several cytokines, growth factors and combinations on the regenerative potential of hepatocytes *in vitro*. A first the metabolic activity of cells was proved with ALAMAR-BlueTM to identify effective combinations. In addition we measured special hepatocyte behaviors i.e. albumin production rate, gluconeogenesis and cytochrome P 450 activity.

Main aim is to study intracellular signaling after treating hepatocytes with selected combinations of growth factors and cytokines. To get a global overview through changes in gene expression we used complete genome chips. After that we designed a custom made array containing approximate 500 genes which have significant roles in the regeneration process.

In summarize we can show differences in gene expression pattern after treatment with cytokines and growth factors.

Notes

1 Michalopoulos G.K., DeFrances M.C., Liver Regeneration, Science 276:60-65 (1997).

2 Zimmerman A., Liver regeneration: the emergence of new pathways, Med Sci Moint 8(3): RA53-63 (2002).

Christine Schulz

Universität Leipzig

Center for Biotechnology and Biomedicine (BBZ)
Professorship for Cell Techniques and
Applied Stem Cell Biology
and
Faculty of Medicine

E-Mail: christine_schulz@web.de
www.uni-leipzig.de/~bader/

COR-AAD1-00003171
Bayer EX1008 (Part 6 of 9)

6.16 Solid-state NMR spectroscopy on bone implants

Jessica Schulz, Ina Khalaf, Mathias Pretzsch, Göran Zernia, Andrea Deiwick, Alexander Wild, Augustinus Bader, Daniel Huster

Solid-state NMR techniques are applied to quantitatively investigate the formation of organic and inorganic bone material in animals with osteoinductive bone substitutes. To this end, mesenchymal stem cells were seeded into porous β-tricalcium phosphate (β-TCP) cylinders and subsequently implanted into the femoral condyle of rabbits. The stem cells differentiate into osteoblasts and, while new bone material is produced by these cells, the β-TCP is resorbed by the animal's organism.

The formation of inorganic bone material was investigated by ^{31}P MAS NMR spectroscopy. The implants were removed from the rabbits after 2, 3, or 4 months and the formation of hydroxyapatite determined quantitatively. The ^{31}P NMR spectra are characterized by a superposition of β-TCP and calcium-hydroxyapatite, the major inorganic component of bone. From the peak integrals, the amounts of newly formed hydroxyapatite were determined.

The main organic component of bone, collagen type I, was investigated by ^{13}C solid-state NMR spectroscopy. ^{13}C CP MAS NMR spectra exhibit the characteristic signatures of collagen type I with good resolution for all major amino acids in collagen. Comparing the intensities of the collagen peaks with the peak intensity of a test substance, we have quantified the amount of collagen produced by the osteoblasts.

Information on the dynamics of collagen segments is obtained from motionally averaged ^{13}C-1H dipolar couplings. Thus, a quantitative comparison of the dynamical properties of collagen in bone and in the implants has been carried out.

Jessica Schulz

Universität Leipzig

Center for Biotechnology and Biomedicine (BBZ)
Junior Research Group "Solid-state NMR Studies of the Structure of Membrane-Associated Proteins"
and
Faculty of Medicine
Institute of Medical Physics and Biophysics

E-Mail: jessica-schulz@gmx.de
www.uni-leipzig.de/~huster/

COR-AAD1-00003172
Bayer EX1008 (Part 6 of 9)

6.17 Novel bioreactor for simultaneous stimulation and cultivation of 3-dimensional cell constructs

Ronny Schulz, Andrea Deiwick, Nico Wüstneck, Christian Müller, Augustinus Bader

The novel bioreactor combine perfusion cultivation and mechanical stimulation of GMP-adequately produced three-dimensional, vital and mechanically resistant cartilage cell constructs in one bioreactor. The cultivated transplants can be used as substitute tissue material for the treatment of e.g. defects of the connecting and supporting tissue and degenerative articular illnesses. The main feature of the bioreactor is the transplant situated in a closed reactor area and multiply provided with *in vivo* adapted stimuli. One of these stimuli is the perfusion of the spatial cell construct with medium, which on the one hand leads to a production of organotypical shear forces at the cell membranes and on the other hand admits an increased metabolic exchange. In the closed bioreactor a piston, whose function is the application of force on the cell culture, is located above the transplant. This pressure plate is led through the bioreactor area and dynamic or static pressure stimulation is applied on the tissue transplant. Due to its degree of automation the apparatus minimizes the number of processes and thereby reduces the risk of infection for the cell culture. Furthermore, the automatic cultivation and stimulation of the transplants guarantee defined and reproducible processes. The parameters for bioreactor control include biochemical signals and the biomechanical parameters like compression, force and stiffness. Due to the constructional features of the bioreactor a closed circle is guaranteed and therefore a strictly autologous cultivation and stimulation of substitute tissue material adequate to the GMP guidelines is possible.

Ronny Schulz

Universität Leipzig

Center for Biotechnology and Biomedicine (BBZ)
Professorship for Cell Techniques and
Applied Stem Cell Biology
and
Faculty of Medicine

E-Mail: ronny.schulz@bbz.uni-leipzig.de
www.uni-leipzig.de/~bader/

COR-AAD1-00003173
Bayer EX1008 (Part 6 of 9)

6.18 Automation of the 3D *in vitro* pannus-model for rheumatoid arthritis with the CyBi-Disk workstation

Anja Skodda, Simone Fuchs, Jochen Ringe, Mehdi Yahyawi, Ingrid Schmid, Peter Götz, Michael Sittinger

The pannus-model for rheumatoid arthritis (RA) consists of a chondrocyte pellet culture interacting with RA synovial fibroblasts and was developed as a standardized screening test to analyse the effects of drugs and biological substances. Porcine chondrocytes were isolated from articular cartilage and cultured in media containing FBS. 3D cultivation was done in 96-well plates with $0{,}6 \times 10^6$ chondrocytes per well. Automated media exchange was done with the liquid handling system CyBi®-Disk (CyBio AG Jena). A control software program has been generated with the aim of minimal shear forces for the pellet culture. After two weeks the chondrocyte pellets were covered with synovial fibroblasts to complete the pannus-model. The process was compared to manual handling and effects due to automation were analysed by scans, histochemistry and real-time PCR. Histochemistry comparison of both automated and manually operated pellets showed a formation of hyaline-like cartilage matrix. Components of the extracellular matrix like type II collagen were determined by immunohistochemistry, indicating a uniform distribution. Scans demonstrated a destruction of the manually operated pellet cultures, due to unsteady pipetting resulting in intense shear forces. Pellets operated by CyBi®-Disk were homogenous within the whole 96-well plate. Additionally a great advantage of the automation is the reduction in operation time per plate, 7 min 45 sec including tip washing compared to 19 min by manual process. Successful automation of the pannus-model allows for high throughput RA drug screening experiments. The transfer in human pellet cultures is in process.

Successful automation of the pannus-model allows for high throughput RA drug screening experiments. The transfer in human pellet cultures is in process.

Dr. Ingrid Schmid

CyBio AG

E-Mail: ingrid.schmid@cybio-ag.com
www.cybio-ag.com

COR-AAD1-00003174
Bayer EX1008 (Part 6 of 9)

6.19 Aquaporin expression in the retina of the rat

Solveig Tenckhoff, Ianors Iandiev, Andreas Reichenbach, Peter Wiedemann, Andreas Bringmann

The development of retinal edema is a common complication of various ischemic and inflammatory ocular diseases. Fluid movements through the retinal tissue are facilitated by aquaporin (AQP) water channels expressed in plasma membranes of glial and neuronal cells. It is known that the retina of the rat express AQP4 and AQP1 water channel proteins while a possible expression of other members of the aquaporin protein family is unknown.

Transient retinal ischemia was induced in one eye of adult rats by elevating the intraocular pressure for 60 minutes. Total RNA was isolated and analyzed by RT-PCR. Retinal slices were immunostained against various aquaporin proteins.

The retina of the rat express mRNA for a diversity of aquaporins, including AQPs0,1,3,4,5,6,7,8,9 and 11. The mRNA for AQP2 remained under the detection level of the method used. AQP1 immunoreactivity is expressed by the outer retina and by single amacrine cells. AQP2 immunoreactivity was found at low level in horizontal cells. AQP4 immunoreactivity is strongly expressed in perivascular membranes and at the inner limiting membrane as well as in the plexiform layers. AQP5 immunoreactivity was found diffusely distributed above the whole retinal tissue. AQP9 immunoreactivity is expressed by single amacrine cells.

The retina of the rat express mRNAs for a diversity of different water channel proteins suggesting that the retinal water homeostasis is mediated by the cooperation of different aquaporins. The functional significance of the various aquaporin proteins for neuronal activity and in pathophysiological conditions remains to be determined.

Solveig Tenckhoff

Universität Leipzig

University Hospital
Department of Ophthalmology

E-Mail: s_tenckhoff@web.de
www.uni-leipzig.de/~auge/

COR-AAD1-00003175
Bayer EX1008 (Part 6 of 9)

6.20 Effect of oxygen stress on the hepatocytes metabolic functions *in vitro*

Susanne Trettner, Jan-Michael Heinrich, Augustinus Bader

With the purpose recreate in a possible closer way the function of a Liver Support System (LSS), it is necessary to determinate some specific conditions of hepatocytes culture, as the adequate supply with oxygen.

According to the physiological oxygenation conditions (Liver blood flow represents a mixture of 75-80 % of oxygen depleted venous blood and which is only 20-25 % of fully oxygenated arterial blood[1], we decide to study the effect of oxygen stress, in hypo-, norm- and hyperoxygen conditions, in a system with mouse hepatocytes cultured *in vitro*, analyzing the changes in the metabolic activity of them.

For our study we cultured adult mouse hepatocytes on a flat membrane bioreactor designed and published recently by our group[2] under controlled oxygen conditions (2,5 %, 10 %, 20 %, 30 %) coated with collagen type I.

The effect of the different oxygen concentration was analyzed by measuring hepatic specific metabolic functions, for example proliferation rate, albumin synthesis rate, LDH- as well as cytochrome P450 activity.

In conclusion, we could show differences in metabolic activity, influenced by the availability of oxygen to the hepatocytes that are important in the design and control of future bioreactors.

Notes

1 Thews G., Anatomie, Physiologie, Pathophysiologie des Menschen, Stuttgart: Wiss. Verl.-Ges. (1999).

2 Langsch A., Bader A., Longterm stability of phase I and phase II enzymes of porcine liver cells in flat membrane bioreactors., Biotechnol. Bioeng. 2001 Sep;76(2):115-25.

Dr. Jan-Michael Heinrich

Universität Leipzig

Center for Biotechnology and Biomedicine (BBZ)
Professorship for Cell Techniques and
Applied Stem Cell Biology
and
Faculty of Medicine

E-Mail: michael.heinrich@bbz.uni-leipzig.de
www.uni-leipzig.de/~bader/

COR-AAD1-00003176
Bayer EX1008 (Part 6 of 9)

6.21 Behaviour of cells cultured on microstructured titanium surfaces

Hartwig Wolburg, Claus Burkhardt, Dieter Kern, Jochen Seebach, Friederike Pfeiffer

Implantology is concerned with the cell-surface interaction. Fibroblasts seeded on microstructured epoxy resin surfaces which were sputtered with a ~50nm thick titanium layer, grow oriented according to the geometrical texture. EM analysis and immunogold labelling showed protrusions extending into the grooves and positive for vinculin. We combined the focused ion beam (FIB) technology for cutting and SEM for imaging in a CrossBeam instrument allowing site specific preparation of the internal interface at nm level. We observed tiny but numerous basal extensions of the cells where they contacted the Ti surface. This prompted us to ask for the expression of ERM-proteins (proteins connected to membrane formations such as microvilli or lamellipodia). As shown by CLSM, we observed an increased immunoreactivity against radixin on Ti versus non-Ti substrates. Then we tested the affinity of the cells on Ti versus non-Ti by means of shear-stress experiments using shear forces up to 100 dyn/cm^2. We found the attachment stronger on Ti than on non-Ti and the microstructured Ti not more effective than smooth Ti suggesting that Ti itself is more important for attachment strength than its surface geometry.

Supported by the DFG (SSP 1100) and Fortüne Program.

Prof. Dr. Hartwig Wolburg

Eberhard Karls Universität Tübingen

Faculty of Medicine
Institute of Pathology

E-Mail: hartwig.wolburg@med.uni-tuebingen.de
www.medizin.uni-tuebingen.de/~webpatho/

COR-AAD1-00003177
Bayer EX1008 (Part 6 of 9)

6.22 Investigation of the dynamics of the macromolecules in articular and tissue engineered cartilage by NMR spectroscopy

Göran Zernia, Stephanie Höhle, Ronny Schulz, Matthias Zscharnack, Augustinus Bader, Jürgen Schiller, Klaus Arnold, Daniel Huster

To understand the viscoelastic properties of articular cartilage and for the development of tissue engineered cartilage, we have studied the physicochemical properties of the tissue using ^{13}C NMR methods. Cartilage is a complicated gel with extremely well adapted shock absorbing properties. The major macromolecular components of cartilage, glycosaminoglycans and collagen, can be studied individually by high resolution NMR and solid-state NMR methods, respectively. From relaxation time measurements, the motional parameters of the glycosaminoglycans are derived. These polysaccharides undergo almost isotropic motions and fast reorientations with large amplitudes. In contrast, the collagen component of cartilage tissue is rather rigid. Only small amplitude fluctuations on the nanosecond timescale are detected using solid-state NMR methods. Considering the high water content of cartilage and the almost isotropic mobility of the glycosaminoglycan molecules it is remarkable how little this affects the collagen dynamics. Therefore, the dynamics of cartilage macromolecules is broadly distributed from almost completely rigid to highly mobile, which lends cartilage its mechanical strength and shock absorbing properties. We have also applied the NMR technology to chondrocyte cell cultures and tissue engineered cartilage. In the cell culture, ^{13}C labeling of the extracellular matrix is carried out to increase the sensitivity of the experiments. Thus, NMR methods are proposed to carry out a quality control/quality assurance analysis of tissue engineered materials.

Göran Zernia

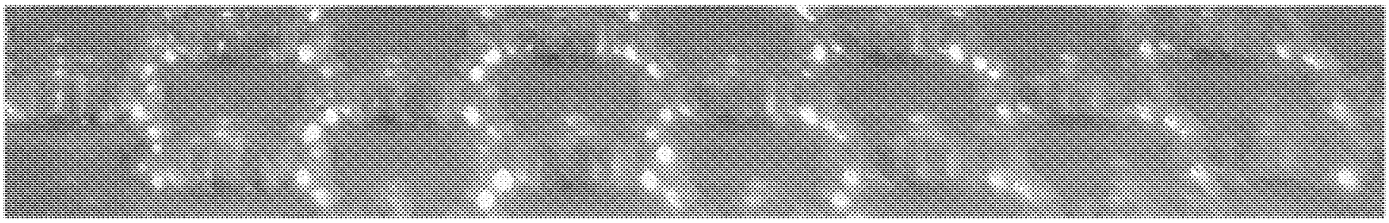
Universität Leipzig

Center for Biotechnology and Biomedicine (BBZ)
Junior Research Group "Solid-state NMR Studies of the Structure of Membrane-Associated Proteins"
and
Faculty of Medicine
Institute of Medical Physics and Biophysics

E-Mail: goeran.zernia@medizin.uni-leipzig.de
www.uni-leipzig.de/~huster/

COR-AAD1-00003178
Bayer EX1008 (Part 6 of 9)

7. NANOBIOTECHNOLOGY AND NANOELECTRONICS



POSTERS

7.1 Protrusion forces driving rapidly translocating cells

Claudia Brunner, Michael Gögler, Allen Ehrlicher, Bernd Kohlstrunk, Detlef Knebel, Josef A. Käs

Cell motility is a fundamental process of many phenomena in nature, such as immune response, wound healing, and metastasis. Mechanisms of force generation for cell migration have been described in various hypotheses1-5 requiring actin polymerization and/or molecular motors, but quantitative force measurements to date have focused on traction forces. Here we present a direct measurement of the forward force generated at the leading edge of the lamellipodium and at the cell body of a translocating fish keratocyte. To elucidate the sub-cellular force generation machinery, we additionally determined the forward force of locomoting lamellar fragments6, which lack their nuclei but remain motile. We positioned an elastic spring, the cantilever of a scanning force microscope (SFM), in front of a moving cell, which pushes this spring out of the way. The forward force was calculated using the detected vertical deflection of the cantilever in an "elastic wedge model", which considers cellular deformation. Our measurements of the propulsive forces, which are in the lower nN range and agree with expectations, will provide quantitative insight into how a polymeric network of active and passive molecular components act in concert as an active locomoting machine.

Claudia Brunner

Universität Leipzig

Faculty of Physics and Earth Science
Institute of Experimental Physics I
Soft Matter Physics

E-Mail: cbrun@uni-leipzig.de
www.softmatterphysics.com

COR-AAD1-00003181
Bayer EX1008 (Part 6 of 9)

7.2 Lipophilic nucleic acids as building blocks for highly functional membrane surfaces

Andreas Bunge, Holger A. Scheidt, Wolfgang Flasche, Oliver Kaczmarek, Andreas Herrmann, Jürgen Liebscher, Daniel Huster

The functionalization of biological surfaces has attracted much attention in the field of nanobiotechnology. We have designed lipophilic nucleosides and oligonucleotides to combine the molecular recognition mechanism of nucleic acids and the self-assembly characteristics of lipids in planar membranes. The intention of this project is to develop versatile molecular compounds that can be used to specifically bind enzymes, probes, drugs, and so on to biological surfaces. To this end, we have synthesized molecular building blocks that consist of a single adanine or uracil nucleobase attached to ribose or desoxyribose. This hydrophobic headgroup is covalently bound to various lipophilic groups such as alkynyl chains and sterodial substituents to provide membrane anchoring. Alternatively, we have synthesized lipophilic oligonucleotides that consist of a 25-mer single stranded DNA with two covalently attached hydrocarbon chains. The membrane insertion and localization of these molecules was investigated by solid-state NMR spectroscopy. All molecules can be incorporated into phospholipid membranes at high concentration without destroying the bilayer structure or the formation of non-lamellar phases as shown by ^{31}P NMR and ^{2}H NMR of deuterated phospholipids. The hydrophobic headgroup of the lipophilic nucleosides and oligonucleotides was found to be localized in the lipid water interface investigated by ^{1}H nuclear Overhauser enhancement spectroscopy under magic angle spinning. Therefore, these molecules may be useful building blocks to obtain functionalized membrane surfaces.

Andreas Bunge

Universität Leipzig

Faculty of Medicine
Institute of Medical Physics and Biophysics

E-Mail: andreas.bunge@medizin.uni-leipzig.de
www.uni-leipzig.de/~biophys/

COR-AAD1-00003182
Bayer EX1008 (Part 6 of 9)

7.3 Binding specificity of peptides on semiconductor surfaces

Karsten Goede, Michael Bachmann, Wolfhard Janke, Marius Grundmann

Hybrid systems of anorganic semiconductors and small bio-molecules constitute on the one hand an easily accessible model system for studying the fundamentally important process of molecular self-assembly. On the other hand they provide us with a multitude of possible future applications which might range from biological sensoring to nano-bio electronics. We have studied the adhesion coefficient of peptide clusters with different amino-acid sequences on various classic semiconductor materials. The adhesion crucially depends both on the electronegativity of the involved surface atoms and their spatial arrangement and on the kind and succession of side chains in the amino acids of the peptide[1]. Low adhesion comes along with the appearance of eminently large and soft clusters. Starting from these empirical findings we present first simulations of relevant peptide convolutions and phase transitions and discuss the way towards a theoretical modelling of peptide adhesion on lattice surfaces.

Notes

1 Goede K., Busch P., Grundmann, M., Nano Lett. 4(11):2115-2120 (2004).

Karsten Goede

Universität Leipzig

Faculty of Physics and Earth Science
Institute of Experimental Physics II
Semiconductor Physics

E-Mail: goede@physik.uni-leipzig.de
www.uni-leipzig.de/~hlp/goede/

COR-AAD1-00003183
Bayer EX1008 (Part 6 of 9)

7.4 Nano- and microstructured surfaces for selective and directed positioning of cells on electronic chips for laser-based microdissection and manipulation

Heinz-Georg Jahnke, Andrée Rothermel, Randy Kurz, Markus Rüffer, Winnie Weigel, Maik Schmidt, Andrea A. Robitzki

Positioning of single cells on well-defined surfaces and their directed growth is a precondition in modern biotechnology, nanotechnology and cell biology. For the reliable application of living cells on biochips and biosensors it is necessary to develop specific attracting or repelling surface topographies. Especially in neurobiology it is a great advantage if neuronal cells can be positioned in a defined neural network. Thereby, the influence of cell-cell and cell-matrix contacts or soluble factors on axon guidance or cellular growth in general can be investigated. For this purpose technical glasses or silicon-based chips were laminated with different silanes to screen their repulsive properties. Subsequently, the desired adhesive surface topography was generated easily by ablation of the silane coating via laser processing techniques. In our studies we investigated the growth of dendrites and the interactions between oligodendrocytes and nerve cells as well as the influence of chemical attractant or repellent factors like netrin. Netrin-1 is a prevalent laminin-like protein that showed both chemoattractant and repellent properties on neuronal cells. To analyse axonal growth OLN93 cells were cultured and transfected on nano- and microstructured glass chips with either sense or antisense netrin DNA constructs. Also first experiments with a lasermanipulation system were carried out because laserlight can induce and guide the growth direction of neuronal growth cones. These experiments are the basis for developing a electronic biosensor coupled with a laser-micromanipulation system.

Heinz-Georg Jahnke

Universität Leipzig

Center for Biotechnology and Biomedicine (BBZ)
Professorship for Molecular Biological-Biochemical Process Technology
and
Faculty of Biosciences, Pharmacy and Psychology
Institute of Biochemistry

E-Mail: heinz-georg.jahnke@bbz.uni-leipzig.de
www.uni-leipzig.de/~dmpt/

COR-AAD1-00003184
Bayer EX1008 (Part 6 of 9)

7.5 Chemosensitization of bladder cancer cells by VEGF antisense pre-treatment

Sabine Krause, Yvonne Förster, Kai Krämer, Susanne Füssel, Matthias Kotzsch, Uta Schmidt, Manfred P. Wirth, Axel Meye, Bernd Schwenzer

Due to the unsatisfactory success in treatment of bladder cancer and the low response rates to commonly used chemotherapeutics (CT) alternative and additive approaches have to be found. The function of vascular endothelial growth factor (VEGF) in neoangiogenesis and therefore in solid tumors makes it a promising target for a specific anti-tumor therapy. This study investigated the possibility to sensitize transitional bladder cancer cell lines (TCC) to CT by pre-treatment with VEGF antisense oligodeoxynucleotides (AS-ODNs).

The human bladder cancer cell lines EJ28 and 5637 were transiently transfected with three different anti-VEGF AS-ODNs followed by incubation with three different doses of the CT mitomycin C (MMC), gemcitabine (GEM) or cisplatin (CDDP). Both cell lines responded in a dose dependent manner to all CT. Combined treatment with VEGF-AS-ODNs and CT resulted in a reduced viability (WST-1 assay) compared to the isolated CT treatment. VEGF857 plus CT treatment could significantly reduce viability of both cell lines compared with NS-ODN plus CT treatment for all three CT ($p<0.007$). This detected chemosensitization was based on AS-mediated increase of apoptosis (annexin V staining).

One of the three AS-ODNs tested (VEGF857) significantly sensitizes human TCC cells to CT. We suggest VEGF as an additional putative target for an enhancement of therapeutical benefit for example for MMC and GEM instillation treatment schedules.

Dr. Bernd Schwenzer

Technische Universität Dresden

Department of Mathematics and Natural Sciences
(with Psychology)
Institute of Biochemistry

E-Mail: bernd.schwenzer@chemie.tu-dresden.de
www.chm.tu-dresden.de/bc/

COR-AAD1-00003185
Bayer EX1008 (Part 6 of 9)

7.6 Proton microscopy – Quantitative trace element analysis with sub-micron spatial resolution

Tilo Reinert, Daniel Spemann, Markus Morawski,
Thomas Arendt, Tilman Butz

In recent years many nuclear microprobes around the world have developed to sophisticated tools for quantitative elemental analysis with high resolutions down to one micron. The principle is similar to an electron probe microanalysis. A focussed proton beam is scanned over the sample and the characteristic X-rays are recorded (microPIXE). The main advantage is the very low background and the precise knowledge of the principles of X-ray production and detection. Therefore, nuclear microprobes are widely used in trace element analysis mainly in the field of biological and medical research. Numerous successful studies on microscopic scale structures, e.g. cells, lead to the demand for higher spatial resolution or lower detection limits. Therefore, several labs started new efforts for sub-micron resolutions.

The Leipzig microprobe laboratory LIPSION, experienced in analysing brain tissue on the cellular level, has recently improved its analytical capabilities. We are now able to perform quantitative trace element analysis with sub-micron spatial resolution and µg/g (<100 µmol/l) detection limits for most of the physiological important elements. The smallest beam diameter with analytical capabilities for elemental analysis, we achieved thus far, was about 300 nm in diameter. It enables an outstanding microPIXE resolution. This contribution shows the applicability to biological samples. We perform sub-micron trace elemental analysis on neuromelanin, an intracellular protein agglomeration with high affinity to iron.

Dr. Tilo Reinert

Universität Leipzig

Faculty of Physics and Earth Science
Institute of Experimental Physics II
Nuclear Solid State Physics

E-Mail: reinert@physik.uni-leipzig.de
www.uni-leipzig.de/~nfp/

COR-AAD1-00003186
Bayer EX1008 (Part 6 of 9)

7.7 Investigation of DNA binding proteins from the hyperthermophile *Sulfolobus acidocaldarius*

Mathias Salomo, Kati Kegler, Marc Struhalla, Jörg Reinmuth, Wiktor Skokov, Friedrich Kremer

The proteins Sac7d and Sac7e from the hyperthermophile archeon *Sulfolobus acidocaldarius* are reported to bind strongly to the minor groove of DNA and to introduce a sharp kink leading to a shortening of the DNA. Both proteins are very stable against heat, acid and chemical agents.

Our projects have the aim to investigate these proteins with optical tweezers, X-ray crystal structure analysis and evolutionary protein design.

With the help of optical tweezers we were able to establish a setup that allows to mechanically stretch and relax single DNA molecules with lengths between 1,000 bp and 6,000 bp that are immobilized between two microparticles. We can use this system to investigate changes in the elastic properties of DNA accompanying protein binding.

In the literature Sac7d is reported to bind DNA with lower affinity than Sac7e. We have crystallized Sac7e in order to solve its X-ray structure to compare it with the already known structure of Sac7d. This shall give rise to differences in the structure explaining the higher affinity of Sac7e to DNA.

Some other closely related proteins, like Sso7d isolated out of *Sulfolobus solfataricus*, own the ability to cut nucleic acids. By using evolutionary protein design we want to change the DNA binding protein Sac7d into a DNA cleaving enzyme. Therefore we randomize defined areas of Sac7d as well as the whole protein sequence generating large enzyme libraries which we will screen for the desired enzymatic activity.

Mathias Salomo

Universität Leipzig

Faculty of Biosciences, Pharmacy and Psychology
Institute of Biochemistry

E-Mail: msalomo@rz.uni-leipzig.de
www.biochemie.uni-leipzig.de

COR-AAD1-00003187
Bayer EX1008 (Part 6 of 9)

7.8 Investigation of the elastic properties of single DNA molecules

Mathias Salomo, Kati Kegler, Marc Struhalla, Jörg Reinmuth, Wiktor Skokov, Friedrich Kremer

Optical tweezers are commonly used to manipulate microscopic particles, with applications in cell manipulation, colloid research, manipulation of micromachines and studies of the properties of light beams. With their extraordinary resolution in space (~2 nm) and force (~1 pN) they became a irreplaceable tool for such purposes.

In our project we want to use them to study the elastic properties of single DNA molecules. Therefore we developed an easy and reproducible procedure for the immobilization of single double stranded DNA molecules 1,000 to 6,000 bp in length obtained by PCR between two micro particles supplying a general approach to address this problem.

A fully reversible elastic behaviour is found for the force-extension dependence of ds-DNA for relative elongations up to 50 % as described in the corresponding literature.

Mathias Salomo

Universität Leipzig

Faculty of Biosciences, Pharmacy and Psychology
Institute of Biochemistry

E-Mail: msalomo@rz.uni-leipzig.de
www.biochemie.uni-leipzig.de

COR-AAD1-00003188
Bayer EX1008 (Part 6 of 9)

7.9 Release of thioflavins from nanoparticles targeting fibrillar β-amyloid in transgenic mice

Thomas Siegemund, Bernd-R. Paulke, Herbert Schmiedel, Jens Grosche, Anke Hoffmann, Tibor Harkany, Heikki Tanila, Johannes Kacza, Wolfgang Härtig

Alzheimer's disease and age-dependent β-amyloidoses in transgenic mice are characterized by the occurrence of fibrillar amyloid (Aβ). β-sheet structures are selectively bound by fluorescent thioflavins and styrylbenzenes both in fixed tissues and after intravenous (iv.) infusion. In contrast, hydrophilic compounds such as thioflavin-T (ThT) are unable to pass the blood-brain-barrier. The modelling of brain functions with drugs only after their encapsulation with polymers suggests the targeting of Aβ using degradable, thioflavin-filled nanoparticles.

This study is based on different types of nanoparticles containing ThT or thioflavin-S. Core-shell particles were prepared by the polymerization of butyl-cyanoacrylate onto polystyrene cores containing either thioflavine or rhodamine. Purified nanoparticles had diameters between 40 and 150 nm as revealed by light scattering. The bioerosion of nanoparticles *in vivo* was mimicked by their enzymatic degradation with non-specific esterase *in vitro*. Next, aged double transgenic APP/PS1 mice displaying a high Aβ load received intrahippocampal or iv. injections of thioflavin-containing nanoparticles. Three hours or three days after injection, animals were perfused and sectioned. Thioflavin-staining of senile plaques was shown by Aβ-immunofluorescence labelling and subsequent confocal laser-scanning microscopy. For electron microscopic analyses of ThT released from nanoparticles, the fluorescent model drug was photoconverted into an electron-dense adduct and mainly found in plaques, but also in neurons and microglia. Our data suggest that drugs delivered by nanoparticles can target Aβ.

PD Dr. Wolfgang Härtig

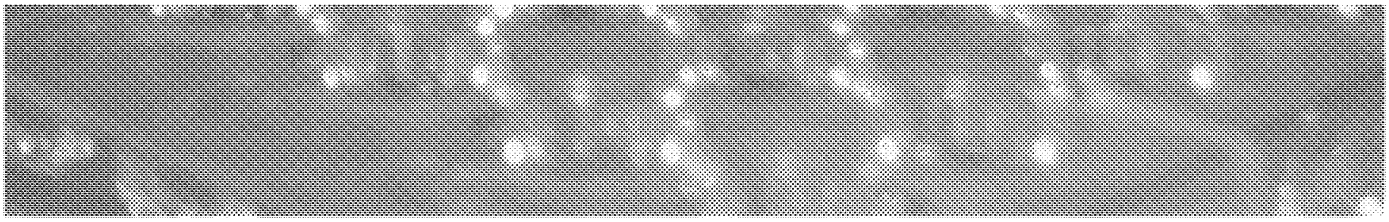
Universität Leipzig

Faculty of Medicine
Paul Flechsig Institute of Brain Research
Neurochemistry

E-Mail: hartig@medizin.uni-leipzig.de
www.uni-leipzig.de/~pfi/

COR-AAD1-00003189
Bayer EX1008 (Part 6 of 9)

8. BIOINFORMATICS



POSTERS

8.1 Multiple Genome Rearrangement with conserved intervals

Matthias Bernt, Daniel Merkle, Martin Middendorf

The Multiple Genome Rearrangement problem is to find for species that are represented by gene orders a phylogenetic tree. The phylogenetic tree should describe the most "plausible" rearrangement scenario for the gene orders with respect to some distance measure. A gene order is described by a signed permutation over a set of integers where each integer denotes a gene and the sign denotes its orientation. The rearrangement operations that are considered in our work are reversals, which reverse the order and the sign of a subsequence of neighbored genes. We have studied the special case of three given gene orders, called Median problem.

In contrast to other studies of the Median problem we consider the additional constraint that possible gene groups should not be destroyed. The concept of conserved intervals for signed permutations is employed to describe such gene groups. Our algorithm has some similarities to the well known MGR algorithm but uses a different selection process for the applied reversals. It has been shown experimentally for different types of test problems that our algorithm produces better results than MGR for the standard Median problem and has the additional property that it tries not to destroy conserved intervals. The reversal selection procedure has also been integrated into the MGR and GRAPPA algorithms. This new versions achieve a significant speedup while obtaining solutions of the same quality on the test problems.

Matthias Bernt

Universität Leipzig

Faculty of Mathematics and Computer Science
Institute of Computer Science
Parallel Computing and Complex Systems

E-Mail: bernt@informatik.uni-leipzig.de
http://pacosy.informatik.uni-leipzig.de

COR-AAD1-00003193
Bayer EX1008 (Part 6 of 9)

8.2 Bio-Imaging platform LabImaging – A tool to develop software for biological, pharmaceutical and medical research and clinical diagnostics

Olaf Brenn

Kapelan Bio-Imaging Solutions is an ambitious German company founded in the year 2000. We are developing customer specific software for biological, pharmaceutical and medical research as well as clinical diagnostics based on our own bio-imaging platform. We are mainly focused on laboratory automation and image analysis.

Supported by our own bio-imaging platform we are able to create a wide range of applications within a short development process - from prototyping up to ready-to-use applications. Our applications provide faster time to market.

The platform provides a functional library with image analysing algorithms, e.g. separation and classification of objects, which can be combined to an analysis chain. Furthermore the bio-imaging platform features a complete graphically designed interface, online and offline updates, license management and workflow orientation.

Our know-how was already implemented in a software called LabImage for analysing 1D electrophoresis gel. An earlier version of this software has been worldwide successfully distributed by Kapelan for the last four years. Also we provide OEM development.

Further applications based on the bio-imaging platform are being developed for micro blot and micro array analysis as well as the analysis of cancer cells.

The bio-imaging platform is based on Eclipse. Eclipse is a Java-based open source universal tool platform, which is pushed and influenced by IBM.

We cooperate with research and university partners.

Olaf Brenn

Kapelan GmbH

Bio-Imaging Solutions

E-Mail: olaf@kapelan.com

www.kapelan.com

COR-AAD1-00003194

Bayer EX1008 (Part 6 of 9)

8.3 Identifying targets of flavonoids by virtual docking studies

Robert Günther, Rolf Gebhardt, Hans-Jörg Hofmann

In the quest for new therapeutics, virtual screening methods have become a useful alternative to the expensive high-throughput screening (HTS) methods. Both methods have in common the testing of a great number of small compounds for interaction with one particular target to identify a lead structure. Thus, large compound libraries are needed. However, in academia and small companies often only a limited number of compounds is available, typically synthesized with special know-how. Thus, it might be of interest to identify targets interacting with these compounds.

One ansatz is the application of reverse docking methods. In contrast to common virtual screening methods, a panel of target proteins (or other macromolecules, whose 3D-structure is available) is screened for interaction with a limited number of small compounds in this approach. Beside the identification of a potential target, it is of value to know at an early stage of drug development, whether the projected therapeutic also interacts with other proteins possibly leading to undesired side effects. Furthermore, a reverse docking approach might help to shed some light on the function of hypothetical proteins.

Here, we present a preliminary reverse docking study of the screening for interaction partners of flavonoids. Flavonoids represent a vast number of compounds in higher plants. Thus, these ubiquitous plant constituents enter the food chain and might interact with various physiologically and possibly pathologically relevant proteins inside the human body.

Dr. Robert Günther

Universität Leipzig

Faculty of Biosciences, Pharmacy and Psychology
Institute of Biochemistry
Biophysical Chemistry

E-Mail: robguent@uni-leipzig.de
www.biochemie.uni-leipzig.de/aghofmann/

COR-AAD1-00003195
Bayer EX1008 (Part 6 of 9)

8.4 On the potential role of biomechanics in the growth of tumors *in vitro*

Stefan Höhme, Dirk Drasdo

Recently we have shown by computer simulations with a biophysical model that the growth kinetics of tumor spheroids and of expanding monolayers can largely be explained by a biomechanical form of contact inhibition in which growth stop can be triggered by the deformation of the cell.

Within this model each cell is represented as an individual object and parameterized by cell-biophysical and cell-kinetic parameters that can be experimentally determined.

Now we explore the consequences of this mechanism.

(1) We predict the growth kinetics in monolayers depends significantly on whether a growth stop is triggered either by a critical degree of cell deformation, or by a critical force exerted on the cell.

(2) We show, that the expansion of a tumor spheroid can largely be explained by a biomechanical form of contact inhibition while glucose (or oxygen) mainly determines the size of the necrotic core.

(3) We illustrate, that the relation between tumor diameter and tumor cell population size, and the cell size distribution in tumor spheroids is largely determined by the mechanism that controls the cell growth and propose mechanisms that are compatible with experimental observations.

(4) Based on our computations we propose a phenomenological growth law that we show covers the growth behavior of both, compact monolayers and multi-cellular spheroids.

Finally we give examples for properties of the cell environment that may significantly modify the growth kinetics of multi-cellular aggregates.

Stefan Höhme

Universität Leipzig

Interdisciplinary Centre for Bioinformatics (IZBI)

E-Mail: hoehme@izbi.uni-leipzig.de

www.izbi.de

COR-AAD1-00003196

Bayer EX1008 (Part 6 of 9)

8.5 Progressive multiple sequence alignments from triplets

Matthias Kruspe, Peter F. Stadler

The quality of progressive sequence alignments strongly depends on the performance of the pairwise alignment steps which are necessary to obtain the final alignment. The correct identification of insertions or deletions that occurred during the evolutionary history of the taxa considered is crucial. This becomes fundamental particularly for rather divergent nucleotide sequences where the information content within the sequences is scarce. The pairwise examination of the sequences only is in many cases not satisfactory.

We want to present a novel multiple alignment tool which simultaneously aligns three sequences in every step and so increases the information transfer to the alignment. This extra information is used to reliably derive the underlying phylogeny of the sequences under consideration. We use a natural gap cost model which deals with all different variations of gap openings or extensions for three sequences. Gap penalties are adjusted to global and local sequence properties. The phylogenetic history of the sequences is represented by a network which also determines the order of the three-way alignments. To speed up computation time and limit memory requirements a divide-and-conquer approach is used. We find the obtained alignments more reliable compared to alignments built with other alignment tools such as ClustalW. Because of the lesser information content compared to amino acid sequences, the benefit of our tool applies especially to RNA sequences. Furthermore we figure out that the natural gap costs model has a benefit compared to the quasi-natural gaps costs used in other algorithms.

Matthias Kruspe

Universität Leipzig

Faculty of Mathematics and Computer Science
Institute of Computer Science
Bioinformatics

E-Mail: matthias@bioinf.uni-leipzig.de
www.bioinf.uni-leipzig.de

COR-AAD1-00003197
Bayer EX1008 (Part 6 of 9)

8.6 Non-coding RNAs in Ciona intestinalis

Kristin Missal, Dominic Rose, Peter F. Stadler

Motivation: The analysis of animal genomes showed that only a minute part of their DNA codes for proteins. Recent experimental results agree, however, that a large fraction of these genomes is transcribed and hence is probably functional at the RNA level. A computational survey of vertebrate genomes has predicted thousands of previously unknown ncRNAs with evolutionary conserved secondary structures. An extension of these comparative studies beyond vertebrates is difficult, however, since most ncRNAs evolve relatively fast at the sequence level while conserving their characteristic secondary structures.

Results: Here we report on a computational screen of structured ncRNAs in the urochordate lineage based on a comparison of the genomic data from Ciona intestinalis, Ciona savignyi, and Oikopleura dioica. We predict more than 1,000 ncRNAs with an evolutionarily conserved RNA secondary structure. Of these, about a quarter is located in introns of known protein coding sequences. Only a small fraction of the RNA motifs can be identified as known RNAs, including about 300 tRNAs, some 100 snRNA genes, and a few microRNAs and snoRNAs.

Kristin Missal

Universität Leipzig

Faculty of Mathematics and Computer Science
Institute of Computer Science
Bioinformatics

E-Mail: kristin@bioinf.uni-leipzig.de
www.bioinf.uni-leipzig.de

COR-AAD1-00003198
Bayer EX1008 (Part 6 of 9)

8.7 From phylogenetic footprinting to the evolution of regulatory elements

Sonja J. Prohaska, Claudia Fried, Burkhard Morgenstern, Gunter P. Wagner, Peter F. Stadler

Regulatory elements are often conserved in non-coding DNA. A method to detect them by comparative genomics is called phylogenetic footprinting. We have developed our own method, the tracker approach (Prohaska et al.) which can handle a large set (a few tens) of genomic sequence fragments (of some hundred kb) and does not rely on a pre-supposed phylogeny among the input sequences.

Common footprinting programs based on alignments just yield high scoring alignments of conserved fragments that are in the same order and orientation. Since regulatory elements are rather insensitive to shuffling of single modules, we account for this fact in two ways. First, our method returns not only one set of consistent footprint clusters but all significant clusters, consistent and inconsistent. Second, we look for rearranged footprint clusters based on a decomposition of the detected footprint clusters into single footprints. Therefore, we dissect the clusters of conserved DNA into individual putative binding sites. Starting from this set of motifs we then look for the maximal set of footprints within a cluster of defined length that occurs in all sequences from syntenic regions independent from the order and orientation of the motifs.

The list of conserved footprint clusters or the conserved non-coding nucleotides can be passed on to statistical analyses on footprint loss and acquisition. We propose a method to test for rate differences in the modification of conserved non-coding nucleotides, as well as a method to estimate their rate of modification.

Reference

Prohaska S.J. et al., Mol. Evol. Phylog. 31:581-604 (2004).

Sonja J. Prohaska

Universität Leipzig

Faculty of Mathematics and Computer Science
Institute of Computer Science
Bioinformatics

E-Mail: sonja@bioinf.uni-leipzig.de
www.bioinf.uni-leipzig.de

COR-AAD1-00003199
Bayer EX1008 (Part 6 of 9)

8.8 Functional adaptations of dendrites of pyramidal neurons in p21H-rasVal12 transgenic mice

Andreas Schierwagen, Alexander Schubert, Alán Alpár, Ulrich Gärtner, Thomas Arendt

If compared with the wildtype, in p21H-RasVal12 transgenic mice cerebral cortex volume is increased by about 20 %, due to enlarged pyramidal cells[1]. Pyramidal neurons in layer II/III show a significant growth and establish a more complex dendritic tree[2].

In this study we used compartmental modeling to explore the design principles and functional consequences of the enlarged transgenic mice pyramids. Two sets of pyramidal neurons (28 wildtype and 26 transgenic neurons) were reconstructed and digitized using NeurolucidaTM.

Using the simulation package NEURON, we calculated the morphoelectrotonic transform (MET) of each neuron. The MET maps the neuron from anatomical space into electrotonic space, using the logarithm of voltage attenuation as the distance metric. Since attenuation depends on signal frequency and propagation direction, we calculated METs at several different frequecies and for somatopetal and somatofugal inputs, respectively.

The statistical analysis of the sample METs computed with NEURON revealed global conformity, i.e. the electrotonic architecture of the transgenic neurons scales in such a way that signal propagation in the neuron models is scarcely affected.

In conclusion, our results suggest only a minor impact of p21Ras on dendritic electroanatomy, with negligible changes of the inner part of the corresponding neuromorphic transforms.

In a next step of analysis, active membrane currents will be added to investigate further the scaling problem in these neurons.

Supported by DFG, Hirnliga, IZKF.

Notes

1 Heumann et al., J. Cell. Biol. 151:1537 (2000).

2 Alpár A. et al., J. Comp. Neurol. 467:119 (2003).

Prof. Dr. Andreas Schierwagen

Universität Leipzig

Faculty of Mathematics and Computer Science
Institute of Computer Science

E-Mail: schierwa@informatik.uni-leipzig.de
www.informatik.uni-leipzig.de/~schierwa/

COR-AAD1-00003200
Bayer EX1008 (Part 6 of 9)

8.9 Fuzzy dynamic labeling in learning vector quantization for automatic classification of mass spectrometric data in clinical research

Frank-Michael Schleif, Barbara Hammer, Jens Decker, Ute Clauss, Thomas Villmann

Proteomic profiling based on mass spectrometry is an important tool for studying cancer at the protein and peptide level.

The underlying classification algorithms are one crucial point to obtain valid and reliable results. We propose a new prototype based approach for dynamic fuzzy labeling in learning vector quantization. Thereby we allow dynamically adapted fuzzy labels to indicate the responsibility of prototypes for a class. The new learning algorithm performs a gradient descent on a cost function adapted from Soft Nearest Prototype Classification (SNPC)[1].

Thereby, to each prototype a fuzzy class information is assigned indicating the probabilities for class responsibility.

We compare this Fuzzy Dynamic Labeling SNPC with a special variant of a Genetic Algorithm (GA). It incorporates k-Nearest Neighbor- and Centroid-Clustering into an advanced GA-scheme. The different paradigms are described and their performances on data taken from a clinical prostate cancer study is demonstrated.

We show that this new method can be successfully applied to the analysis of proteomic data and used for bio marker research.

Notes

1 Seo S., Obermayer K., Soft learning vector quantization. Neural Comp. 15:1580-1604 (2003).

Frank-Michael Schleif

Bruker Daltonik GmbH

E-Mail: schleif@informatik.uni-leipzig.de
www.bdal.de

COR-AAD1-00003201
Bayer EX1008 (Part 6 of 9)

8.10 Multiple alignments of partially coding sequences

Roman R. Stocsits, Ivo L. Hofacker, Claudia Fried,
Peter F. Stadler

High quality sequence alignments of RNA and DNA sequences are an important prerequisite for the comparative analysis of genomic sequence data. Nucleic acid sequences, however, exhibit a much larger sequence heterogeneity compared to their encoded protein sequences due to the redundancy of the genetic code. It is desirable, therefore, to make use of the amino acid sequence when aligning coding nucleic acid sequences. In many cases, only a part of the sequence of interest is translated. On the other hand, overlapping reading frames may encode multiple alternative proteins, possibly with intermittent non-coding parts. Examples are, in particular, RNA virus genomes.

Therefore, the standard scoring scheme for nucleic acid alignments can be extended to incorporate simultaneously information on translation products in one or more reading frames. In our contribution, we present a multiple alignment tool, codaln, that implements a combined nucleic acid plus amino acid scoring model for pairwise and progressive multiple alignments that allows arbitrary weighting for almost all scoring parameters. Resource requirements of codaln are comparable with those of standard tools such as ClustalW.

We demonstrated the applicability of codaln to various biologically relevant types of sequences (bacteriophage Levivirus and Vertebrate Hox clusters) and showed that the combination of nucleic acid and amino acid sequence information leads to improved alignments. These, in turn, increase the performance of analysis tools that depend strictly on good input alignments such as methods for detecting conserved RNA secondary structure elements.

Dr. Roman R. Stocsits

Universität Leipzig

Interdisciplinary Centre for Bioinformatics (IZBI)

E-Mail: stocsits@izbi.uni-leipzig.de
www.izbi.de

COR-AAD1-00003202
Bayer EX1008 (Part 6 of 9)

8.11 Coarse-grained polymer models – On-Lattice vs. Off-Lattice

Thomas Vogel, Michael Bachmann, Wolfhard Janke

We investigated coarse-grained polymer models such as the HP on-lattice and the AB off-lattice formulations for heteropolymers ("proteins"). The poster will focus on the results of two problems.

Firstly, we will give results of investigations concerning designing sequences in the HP model on lattices. To this end we perform exact enumerations of the whole sequence-conformation space of HP proteins on the fcc lattice up to a certain chain length and compare with results from the simple cubic lattice.

Secondly we try to show how "far" lattice models are from "reality", or from similar off-lattice models, respectively. Therefore we simulate off-lattice AB model-like proteins with different potentials and compare putative ground states with those from on-lattice simulations.

Thomas Vogel

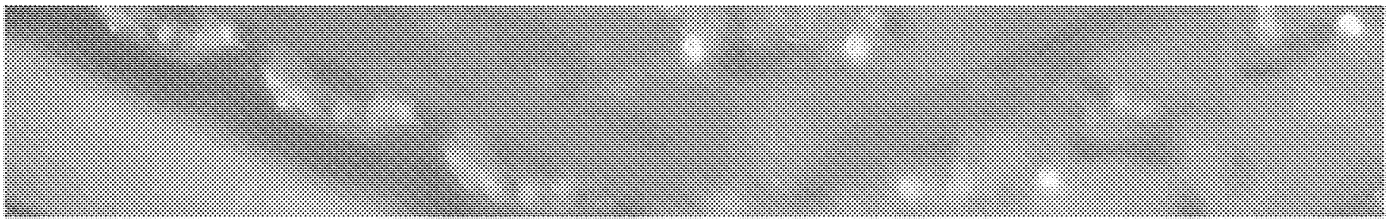
Universität Leipzig

Faculty of Physics and Earth Science
Institute of Theoretical Physics
Computer-oriented Quantum-field Theory

E-Mail: thomas.vogel@itp.uni-leipzig.de
www.physik.uni-leipzig.de/CQT/

COR-AAD1-00003203
Bayer EX1008 (Part 6 of 9)

CENTER FOR BIOTECHNOLOGY AND BIOMEDICINE



Center for Biotechnology and Biomedicine (BBZ) – An overview

In February 2003 the Center for Biotechnology and Biomedicine (BBZ) was established at the University of Leipzig. That paved the way for the BBZ to fullfill tasks set by the BBZ institutionally; which means to promote R&D in biotechnology, biomedicine and related disciplines, to initiate new degree courses and new types of in-service and further training and to facilitate the transfer of findings into economic activities.

With the framework program "The Saxon Biotechnology Offensive" in 2000 Saxony was given the pre-requisites to create such a center. The funding was granted for a period of five years (2001-2005) and was realized by the University Scientific Program and the European Regional Development Fund. The BBZ operates under the roof of BIO CITY LEIPZIG, where the city and the university combine scientific and economic activities in the fields of Biotechnology and Biomedicine and where synergies are set free for the progress of the location for science and economy in Leipzig.

The aim of the BBZ is to create an inventive atmosphere for science and development as well as for education, science and continuing education together with external research institutions, which consequently results in a transregional interest in this field by biotechnological and biomedical companies.

The concept of biotechnological biomedical focus in Leipzig is primarily being implemented by the faculty of biosciences, pharmacy and psychology, the faculty of chemistry and mineralogy, the faculty of medicine, the faculty of veterinary medicine, the faculty of mathematics and computer science as well as by the faculty of physics and earth science. These research fields all have become internationally renowned and competitive centers of research and teaching in molecular biotechnology and biomedicine in recent years.

The BBZ is an internationally competitive center which promotes research and development as well as teaching and advanced training in the areas Protein Engineering and Bioanalytics, Molecular Medicine and Therapeutics as well as Biomedical and Cell Engineering. Platform technologies and methods in biotechnology, biomedicine and nanotechnology are offered as services for academic institutions and industry. Here, the BBZ strengthens and supports collaborations between institutional and university research teams but also forms a unique interface between academia and industry in Europe. With expertise and competence, innovations are transferred to industrial utilization.

With a focus on red biotechnology and following the motive "From the molecule to the patient" the BBZ developes and offers chemical compounds, proteins and other biomolecules, cells as well as tissues as instruments and products for a wide variety of biotechnological and biomedical applications. To this end, novel analytical methods and preparative procedures are developed.

The center collaborates closely with the University Hospital and the Interdisciplinary Center for Bioinformatics (IZBI) at the University of Leipzig. A central office for management and acquisition supports the networking between science and business. In the BIO CITY LEIPZIG six academic research groups from the chemical, biological and medical sciences work under one roof with innovative biotechnological companies including many startups. In addition, 32 life science research groups in the Leipzig area are currently members of the BBZ.

COR-AAD1-00003207
Bayer EX1008 (Part 6 of 9)

The following heads of research groups are members of the Center for Biotechnology and Biomedicine:

From the Faculty of Biosciences, Pharmacy and Psychology:
- Prof. Annette Beck-Sickinger, Biochemistry / Bioorganic Chemistry
- Dr. Susanne Brakmann, Applied Molecular Evolution Research, Junior Research Group of BBZ (managing committee)
- Prof. Kurt Eger, Pharmaceutical Chemistry
- Prof. Sunna Hauschildt, Immunbiology
- Prof. Karen Nieber, Pharmacology for Natural Scientists (managing committee)
- Prof. Andrea Robitzki, Molecular Biological-Biochemical Process Technology (Chair)
- Prof. Martin Schlegel, Molecular Evolution and Animal Systematics with focus on Molecular Phylogeny (advisory)
- Dr. Thomas Greiner-Stöffele, Protein Engineering, Junior Research Group of BBZ
- Prof. Christian Wilhelm, Plant Physiology

From the Faculty of Chemistry and Mineralogy:
- Prof. Stefan Berger, Analytical Chemistry (managing committee)
- Prof. Athanassios Giannis, Organic Chemistry / Natural Products Chemistry
- Prof. Evamarie Hey-Hawkins, Inorganic Chemistry
- Prof. Ralf Hoffmann, Bioanalytics, Professorship of BBZ (managing committee)
- Prof. Helmut Papp, Technical Chemistry / Heterogeneous Catalysis
- Prof. Norbert Sträter, Structural Analysis of Biopolymers, Professorship on BBZ (managing committee)
- Dr. Andrea Sinz, Protein-Ligand Interaction by Ion Cyclotron Resonance Mass Spectrometry, Junior Research Group of BBZ

From the Faculty of Mathematics and Computer Science:
- Prof. Erhard Rahm, Informatics
- Prof. Peter Stadler, Bioinformatics (managing committee)

From the Faculty of Medicine:
- Prof. Klaus Arnold, Medical Physics and Biophysics
- Prof. Augustinus Bader, Cell Techniques and Applied Stem Cell Biology, Professorship on BBZ (advisory)
- Prof. Frank Emmrich, Clinical Immunology
- Prof. Markus Löffler, Medical Informatics, Statistics and Epidemiology
- Prof. Peter Seibel, Molecular Cell Therapy (managing committee)
- Prof. Jan C. Simon, Dermatology and Allergology
- Dr. Peter Ahnert, Molecular Diagnostics - Microarray Techniques, Junior Research Group of BBZ
- Dr. Daniel Huster, Solid-state NMR Studies of the Structure of Membrane-Associated Proteins, Junior Research Group of BBZ

COR-AAD1-00003208
Bayer EX1008 (Part 6 of 9)

From the Faculty of Veterinary Medicine:
- Prof. Gottfried Alber, Immunology
- Prof. Manfred Blessing, Molecular Pathogenesis (Vice-Chair)
- Prof. Hermann Müller, Veterinary Virology including Diagnostics
- Dr. Reimar Johne, Institute of Virology
- Dr. Reinhard Straubinger, Molecular Medicine of Contagious Diseases, Junior Research Group of BBZ

From the Faculty of Physics and Earth Science
- Prof. Josef Alfons Käs, Experimental Physics / Soft Matter Physics with focus on Cellbiophysics

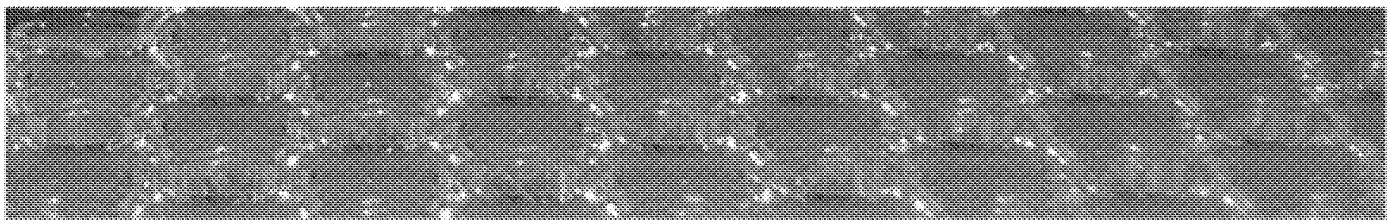
The Center for Biotechnology and Biomedicine is interested in further research divisions dealing with molecular Biotechnology and Biomedicine. Please contact the Chief Executive Officer for further information. Applications can be filed to the Chair of the Center.

Prof. Dr. Andrea Robitzki (Chair)
Dr. Svenne Eichler (Chief Executive Officer)

Universität Leipzig
Center for Biotechnology and Biomedicine (BBZ)
E-Mail: kontakt@bbz.uni-leipzig.de
www.bbz.uni-leipzig.de

COR-AAD1-00003209
Bayer EX1008 (Part 6 of 9)

INDEX



A
Ahnert, Peter 98
Alber, Gottfried 142
Allgaier, Clemens 99, 145
Alpár, Alán 209
Al-Robaiy, Samiya 44
Anderegg, Ulf 114
Apelt, Jenny 154
Arendt, Thomas 47, 115, 136, 140, 141, 148, 155, 156, 157, 159, 195, 209
Armbruster, Franz Paul 169
Arnhold, Jürgen 68, 74, 76
Arnold, Johannes-Joachim 90
Arnold, Klaus 77, 92, 113, 187
Arnold, Thorsten 90
Artmann, Gerhard 151
Assegedech, Bekele 117
Aurich, Richard 107
Austinat, Madeleine 100
Averbeck, Marco 101, 114

B
Bachmann, Michael 192, 212
Bader, Augustinus 166, 168, 175, 178, 180, 181, 182, 185, 187
Bär, Jörg 48
Barthel, Henryk 137, 138
Bauer, Matthias 101
Baumann, Frank 149
Baumann, Thomas 167
Beck, Doreen 166
Becker, Georg A. 137, 138
Becker, Martin 102
Beck-Sickinger, Annette G. 78, 144, 158, 161
Beilharz, Simone 101
Berger, Stefan 45, 46, 81
Berndt, Janin 103
Bernt, Matthias 202
Beutner, René 171, 176
Bhat, Rakesh Kumar 45
Biedermann, Bernd 124
Biedermann, Thomas
Bigl, Volker 150
Blessing, Manfred 135, 142
Bloß, Tanja 106
Blüher, Matthias 103
Böhl, Markus 104, 105
Böhlig, Levin 161
Böhme, Jörg 72
Böhme, Rico 40
Brakmann, Susanne 88
Brand, Torsten 46
Braun, Jan M. 108
Braun, Michael 91
Bräutigam, Katrin 119
Brecht, René 72
Breese, Klaus 106
Breitung, Knut 75
Brenn, Olaf 203
Breuer, Uta 85
Briel, Detlef 107
Brinckmann, Ute G. 109
Bringmann, Andreas 124, 126, 146, 160, 170, 184
Brombacher, Frank 142
Brose, Nils 120
Brown, Michael F. 92
Brückner, Gert 140
Brunner, Claudia 190
Brust, Peter 137, 138, 147
Bullmann, Torsten 47
Bunge, Andreas 191
Burkhardt, Claus 186
Bußmann, Bianca 108
Butz, Tilman 136, 140, 195

C
Cabrata, Eurico J. 46
Caca, Karel 123
Clauss, Ute 210
Cooper, Dermot M. F. 78

D
de Silva, Rohan 47
Decker, Jens 210
Deiwick, Andrea 168, 181, 182
Delacourte, Andre 47
Demuth, Hans-Ulrich 150, 162
Deuther-Conrad, Winnie 147
Dihazi, Hassan 44
Döbel, Viola 69
Donat, Cornelius 149
Dörffel, Anne C. 140

COR-AAD1-00003213
Bayer EX1008 (Part 6 of 9)

Dössel, Olaf 38
Drasdo, Dirk 205

E

Edelmann, Anke 48
Eger, Kurt 66
Egerland, Ute 107
Ehrlicher, Allen 190
Eichler, Svenne 218
Elssner, Thomas 89
Emmerling, Katrin 94
Emmrich, Frank 72, 139
Enderlein, Dirk 125
Engemann, Claudia 90
Eschrich, Klaus 75, 128
Eylenstein, Roy 49

F

Fabian, Claire 109
Fasshauer, Mathias 103
Feller, Claudia 50
Fiedler, Ulrike 26
Finegold, Milton J. 123
Flasche, Wolfgang 191
Förschler, Annette 138
Förster, Yvonne 110, 111, 194
Francke, Mike 116, 146
Franze, Kristian 112
Frense, Dieter 102
Fried, Claudia 208, 211
Fries, Julia E. 146
Frolov, Andrej 51
Froster, Ursula G. 152
Fuchs, Beate 74, 113
Fuchs, Simone 183
Führer, Dagmar 173
Funke, Matthias 166
Füssel, Susanne 130, 133, 194

G

Gabert, Jörg 65, 90
Gachet, Christian 149
Garcia de Arriba, Susana 99
García-Villar, Natividad 63
Gärtner, Ulrich 155, 157, 209
Gaunitz, Frank 100
Gawrisch, Klaus 77
Gebhardt, Carl 101, 114
Gebhardt, Rolf 57, 66, 100, 204
Gerdelmann, Jens 115
Gertz, Herman-Josef 138
Glander, Hans-Jürgen 68, 167
Goczalik, Iwona Malgorzata 116, 146
Goede, Karsten 192
Gögler, Michael 190
Göllnitz, Sabine 117
Götz, Peter 183
Graf, Hans-Ludwig 169
Greiner-Stöffele, Thomas 62, 79
Grewe, Claudia 52
Griehl, Carola 52
Grimm, Stefan 145
Grosche, Jens 53, 112, 198
Großmann, Udo 118
Grundmann, Marius 192
Grunewald, Sonja 167
Grunow, Marlis 50
Guck, Jochen 112
Günther, Robert 66, 204
Gutzeit, Herwig O. 104

H

Haberhauer, Marcus 168
Hackl, Roland 90
Haehn, Sebastian 58
Hammer, Barbara 210
Hanisch, Katja 54
Hanrieder, Jörg 55
Hansen, Gesine 142
Harkany, Tibor 198
Harmos, Ferenc 119
Harms, Hauke 67, 85
Härtig, Wolfgang 47, 118, 198
Hartlage-Rübsamen, Maike 120
Hartmann, Thorsten 56
Häupke, Klaus 102
Hauschildt, Sunna 33, 72, 139
Heidel, Kristin 154
Heinitz, Katrin 121, 122
Heinrich, Jan-Michael 166, 175, 180, 185
Hempel, Ute 171
Hensel, Andreas 65
Hensel, Jürgen 102
Herrmann, Andreas 77, 191

COR-AAD1-00003214
Bayer EX1008 (Part 6 of 9)

Hess, Michael 90
Hesse, Swen 137, 138
Hilbig, Heidegard 169
Hofacker, Ivo L. 211
Hoffmann, Anke 198
Hoffmann, Peter 73, 89, 93
Hoffmann, Ralf 51, 54, 55, 63, 73, 82, 89, 93
Hofmann, Hans-Jörg 46, 66, 204
Höhle, Stephanie 187
Höhme, Stefan 205
Hollborn, Margrit 170
Holzer, Max 47, 148
Horn, Lars-Christian 143
Hornbogen, Till 102
Höschler, Katja 90
Hoßbach, Julia 57
Huster, Daniel 44, 92, 181, 187, 191
Huster, Dominik 77, 123

I
Iandiev, Ianors 124, 160, 184
Ihling, Christian 58, 78, 80, 83, 84
Illes, Peter 149
Israel, Ina 171, 176

J
Jahnke, Heinz-Georg 161, 174, 193
Jakob, Lotta H. 108
Janke, Wolfhard 192, 212
Jassoy, Christian 108, 119
Johne, Reimar 125

K
Kacza, Johannes 44, 198
Kaczmarek, Oliver 191
Kahn, Ronald 103
Kalisch, Folke 126
Kalkhof, Stefan 58, 78, 80, 84
Karger, Stefan 173
Käs, Josef A. 115, 190
Katzka, Catherine 92
Kauer, Friederike 101, 114
Kegler, Kati 196, 197
Keller, Friedrich 117
Kendziorra, Kai 137, 138
Kern, Dieter 186
Keßler, Renate 128
Khalaf, Ina 181
Kiefer, Markus 159
Kirchberger, Jürgen 48
Kleinschek, Melanie 142
Knauer, Jens 127
Knebel, Detlef 190
Kneissl, Alexandra 61, 153, 172, 179
Kneist, Susanne 75
Kochen, Julia 99
Kohen, Leon 170
Köhler, Gabriele 142
Kohler, Konrad 146
Kohlstrunk, Bernd 190
Kokryakov, Vladimir N. 55
Köllner, Kristin 128
Kostrzewa, Markus 89
Kotzsch, Matthias 130, 194
Kouznetsova, Elena 118, 129
Kralisch, Susan 103
Krämer, Kai 130, 194
Kramer, Thomas 65
Krause, Kerstin 131, 173
Krause, Matthias 59
Krause, Sabine 110, 194
Kraße, Jörn 60
Kremer, Friedrich 196, 197
Kriegel, Christian 167
Krist, Kerstin 152
Krohn, Knut 132
Krügel, Ute 149
Krumbholz, Petra 142
Kruspe, Matthias 206
Kühn, Nancy 49
Kuhnt, Evelyn 134
Kukat, Christian 61, 153, 172, 179
Kunz, Carolin 117
Kunze, Doreen 133
Kurz, Randy 151, 161, 174, 193
Küttner, E. Bartholomeus 49, 60, 62
Kutzera, Franziska 160

L
Langrock, Tobias 54, 63
Laub, Rüdiger 64, 72, 94, 139
Lauckner, Gerald 102
Leal-Egana, Aldo 175

COR-AAD1-00003215
Bayer EX1008 (Part 6 of 9)

Lehmann, Jörg 65, 90
Lein, Sandro 81
Lenz, Dominik 141
Lerche, Katja 66
Lerchner, Johannes 67
Leßig, Jacqueline 68, 74
Liebert, Uwe G. 109
Liebscher, Jürgen 191
Liesicki, Doreen 102
Lilie, Hauke 26
Lincke, Thomas 137, 138
Linder, Peter 151
Lindner, Thomas 65
Lobsien, Donald 137, 138
Löffler, Markus 134
Lorenz, Katrin 178
Lösche, Andreas 69, 70
Lutsenko, Svetlana 123

M
Mann, Amrit 135
Mann, Dörthe 86
Many, Marie-Christine 173
Maskow, Thomas 67
Meinecke, Christoph 136, 140
Meiners, Ina 71
Menge, Sieglinde 52
Merkle, Daniel 202
Merte, Knut 75
Meye, Axel 110, 130, 133, 194
Meyer, Philipp 137, 138
Michael, Jan 171, 176
Middendorf, Martin 202
Milius, Doreen 119
Mischke, Dirk 72, 94, 139
Missal, Kristin 207
Mittag, Anja 70
Möllmer, Theresa 119
Morawski, Markus 136, 140, 195
Morgenstern, Burkhard 208
Mori, Hiroshi 47
Morris, Garreth A. 46
Mosch, Birgit 141
Moschütz, Susanne 49
Müller, Christian 182
Müller, Hermann 39, 125
Müller, Peter 77
Müller, Roland H. 60
Müller, Uwe 142
Münch, Gerald 71, 156
Mützelburg, Marika V. 73

N
Neri, Dario 32
Nerkamp, Jörg 91
Neuhaus, Jochen 143
Neundorf, Ines 144
Nickel, Melanie 94
Nieber, Karen 71, 158
Niekisch, Kerstin 135
Nieper, Hermann 125
Nimptsch, Daniel 56
Nöller, Joachim 29, 56

O
Ogunlade, Vera 145
Olthof, Derk 152
Otvös, Laszlo Jr. 55

P
Paasch, Uwe 68, 167
Pannicke, Thomas 124, 146, 160
Paschke, Ralf 103, 173
Patt, Jörg Thomas 147
Patt, Marianne 137, 138, 147
Paulke, Bernd-R. 198
Peitsch, Mirko 67
Perez-Polo, J. Regino 121
Petkovic, Marijana 74
Pfeifer, Sven 62
Pfeiffer, Friederike 186
Pflieger, Christian 102
Pfreundschuh, Michael 134
Pigla, Ullrich 64, 72, 94, 139
Poncin, Sylvie 173
Pospischil, Katrin 61
Pretzsch, Mathias 181
Prohaska, Sonja J. 208

R
Raap, Mike 116
Ramminger, Ellen 148
Rauschenbach, Bernd 40
Regenthal, Ralf 149

COR-AAD1-00003216
Bayer EX1008 (Part 6 of 9)

Reibetanz, Uta 76
Reiche, Sven 108
Reichenbach, Andreas 53, 112, 116, 124, 126, 146, 160, 184
Reim, Kerstin 120
Reinemann, Christine 86
Reinert, Tilo 136, 140, 194
Reinmuth, Jörg 196, 197
Reißig, Dieter 117
Rennert, Robert 144
Reuther, Guido 92
Reuter, Gunter 81
Ringe, Jochen 183
Robitzki, Andrea A. 151, 161, 174, 193, 218
Rogalski, Christina 134
Röhring, Cornelia 56
Rose, Dominic 207
Rösler, Uwe 65
Roßner, Steffen 120, 150, 162
Rothermel, Andrée 151, 161, 174, 193
Rudolph, Rainer 26
Rudolph, Thomas 40
Rudzok, Susanne 162
Rüffer, Markus 151, 161, 174, 193
Rüffert, Henrik 152
Rupf, Stefan 75
Rupf, Thomas 178
Rupietta, Raik 169
Ruthe, David 40
Rybakova, Daria 102

S

Saalbach, Anja 114
Sabri, Osama 118, 129, 137, 138, 147
Salavei, Pavel 76
Salomo, Mathias 196, 197
Salvetter, Jürgen 178
Schäfer, Ingo 61, 153, 172, 179
Schäfer, Petra 49
Scharnweber, Dieter 171, 176
Scheidt, Holger A. 77, 191
Scheunemann, Matthias 118, 129
Schierwagen, Andreas 209
Schildan, Andreas 137, 138
Schiller, Jürgen 44, 74, 113, 187
Schinkinger, Stefan 112
Schleif, Frank-Michael 210
Schliebs, Reinhard 118, 121, 122, 129, 150, 154
Schmetsdorf, Stefanie 155
Schmid, Ingrid 183
Schmidt, Andreas 78, 80
Schmidt, Angela 156
Schmidt, Maik 193
Schmidt, Uta 130, 133, 194
Schmiedel, Herbert 198
Schmiedel, Ramona 79
Schmitt, Johannes 56
Schober, Ralf 145
Schöneberg, Torsten 48, 87
Schröder, Michael 28
Schubert, Andreas 209
Schulz, Christine 166, 180
Schulz, Daniela M. 78, 80
Schulz, Ingo 150, 162
Schulz, Jessica 181
Schulz, Ronny 182, 187
Schulze, Ina 94
Schwalenberg, Thilo 143
Schwarz, Johannes 137, 138
Schwarz, Sigrid C. 41
Schwenzer, Bernd 105, 110, 111, 171, 176, 194
Seebach, Jochen 186
Seeger, Gudrun 157
Seeger, Johannes 44
Seeger, Karsten 81
Seese, Anita 137, 138
Seibel, Peter 61, 153, 172
Seibel, Martina 179
Sergeant, Nicolas 47
Sichardt, Kathrin 158
Siegemund, Thomas 198
Simon, Jan C. 101, 114
Singer, David 51, 55, 73, 82
Sinz, Andrea 58, 78, 80, 83, 84
Sittinger, Michael 183
Skatchkov, Serguei N. 112
Skodda, Anja 183
Skokov, Wiktor 196, 197
Sleeman, Jonathan 101
Smyth, Neil 58
Sorger, Dietlind 118, 129, 137, 138

COR-AAD1-00003217
Bayer EX1008 (Part 6 of 9)

Spemann, Daniel 195
Stadler, Peter F. 27, 206, 207, 208, 211
Stein, Kathleen 132
Steinbach, Jörg 118, 129, 137, 138, 147
Stenzel, Werner 142
Stephan, Holger 174
Stieler, Jens 159
Stocsits, Roman R. 211
Stoltenburg, Regina 86
Stolz, Claudia 85
Stolzenburg, Jens-Uwe 143
Strasser, Stefan 169
Sträter, Norbert 49, 59, 60, 62
Straubinger, Reinhard K. 44, 127, 142
Strehlitz, Beate 86
Strotmann, Rainer 87
Struhalla, Marc 196, 197
Stumpp, Sascha 88
Stumvoll, Michael 34, 103
Süptitz, Petra 132
Sykora, Corinna 89

T
Tanila, Heikki 198
Tannapfel, Andrea 100
Tanneberger, Katrin 48
Tarnok, Attila 70, 141
Tartler, Heike 119
Teich, Lars 66
Tenckhoff, Solveig 170, 184
Termeer, Christian 101
Thalhammer, Stefan 169
Thiele, Birgit 132
Travis, Kort 112
Trepnau, Daniela 90
Trettner, Susanne 185
Trzewik, Jürgen 151

U
Uckermann, Ortrud 112, 126, 160
Unverferth, Klaus 107

V
Vakharia, Vikram N. 90
Vanderwerf, Scott M. 123
Vasilets, Larissa 91
Verdaguer, Ester 99
Villmann, Thomas 210
Vissiennon, Zacharie 158
Voelcker, Verena 114
Vogel, Alexander 92
Vogel, Thomas 212
Voigt, Carsten 91
Voith, Ursula 101
Volke, Daniela 82, 93

W
Wagenknecht, Gudrun 137
Wagner, Gunter P. 208
Waldmann, Herbert 92
Wegner, Florian 137, 138
Wehner, Markus 152
Weick, Michael 116
Weigel, Winnie 151, 161, 174, 193
Werner, Christoph 142
Westendorf, Anne 60
Wheeler-Schilling, Thomas H. 146
Wiedemann, Peter 124, 126, 146, 160, 170, 184
Wild, Alexander 181
Wirth, Manfred P. 130, 133, 194
Wolburg, Hartwig 186
Wolf, Antje 160
Wolf, Gert 67
Wolf, Sebastian 146, 160
Worch, Hartmut 171, 176
Wunderlich, Patrick 94
Wüstneck, Nico 182

Y
Yahyawi, Mehdi 183

Z
Zajadacz, Joachim 40
Zeitschel, Ulrike 150, 162
Zernia, Göran 181, 187
Zimmer, Claus 40, 137, 138
Zipfel, Peter F. 55
Zocher, Rainer 102
Zscharnack, Matthias 187
Zschörnig, Olaf 80,

COR-AAD1-00003218
Bayer EX1008 (Part 6 of 9)

COR-AAD1-00003219
Bayer EX1008 (Part 6 of 9)

COR-AAD1-00003220
Bayer EX1008 (Part 6 of 9)

COR-AAD1-00003221
Bayer EX1008 (Part 6 of 9)

COR-AAD1-00003222
Bayer EX1008 (Part 6 of 9)

COR-AAD1-00003223
Bayer EX1008 (Part 6 of 9)

Insights into the enantiospecificities of (*R*)- and (*S*)-dichlorprop/α-ketoglutarate dioxygenases

Tina A. Mueller[1], Maria I. Zavodszky[2], Michael Feig[2,3], Leslie A. Kuhn[2], Robert P. Hausinger[1,2]

Departments of [1]Microbiology & Molecular Genetics, [2]Biochemistry & Molecular Biology and [3]Chemistry, Michigan State University, East Lansing.

(*R*)- and (*S*)-dichlorprop dioxygenases (RdpA and SdpA) from *Sphingomonas herbicidovorans* MH are mononuclear Fe(II)-containing α-ketoglutarate (αKG)-dependent dioxygenases that hydroxylate the side chains of their chiral substrates mecoprop [(R,S)-2-methyl-4-chlorophenoxypropanoic acid] and dichlorprop [(R,S)-2,4-dichlorophenoxypropanoic acid] to form the achiral 2-methyl-4-chlorophenol and 2,4-dichlorophenol, respectively. The substrate hydroxylation is coupled to the oxidative decarboxylation of αKG to form succinate. RdpA and SdpA share 30% amino acid identity with each other and both enzymes are strictly enantiospecific. In order to study the basis of enantiospecificity, the enzyme structures were modeled using the crystal structure of taurine/αKG dioxygenase as a template. According to the models and sequence alignments with other αKG dependent dioxygenases, the Fe(II)-binding and possible αKG-binding residues were predicted. Furthermore, several residues possibly involved in substrate binding were identified: V80, Q93, I106, G107, Y221, and R285 in RdpA, and E69, G97, N98, H208, H272, and R274 in SdpA. Site-directed mutagenesis was carried out and the kinetic parameters of the mutants were determined to assess the roles of these residues in substrate binding and enantiospecificity. Activity was abolished in the Y221A and I106G/G107N mutants of RdpA, whereas all other RdpA and SdpA mutants showed activity in the range of 0.1-65% with the corresponding mecoprop enantiomer compared to the wild type enzymes. For the V80A, Q93A, and R285A mutants of RdpA and the E69A, H272A, and G97N/N98G mutants of SdpA, the apparent K_m-values were at least ten times higher than the value of the wild type enzyme. Two SdpA mutants, E69A and G97I/N98G, showed slight activity with the (*R*)-mecoprop. These results indicate that enantiospecificity of RdpA and SdpA is due to several amino acid residues which are located at different positions of the active site cavity.

Albert-Ludwigs-Universität Freiburg

14. Jahrestagung

Deutsche Gesellschaft für Kristallographie

3. bis 6. April 2006

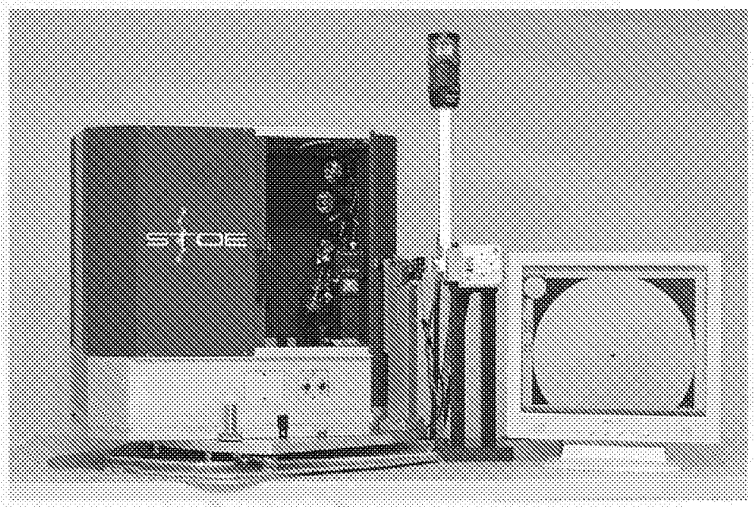
Programm

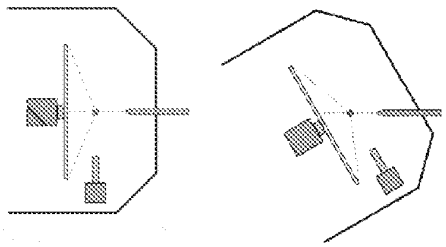
FREIBURG 2006

D G K

COR-AAD1-00003225

Bayer EX1008 (Part 6 of 9)



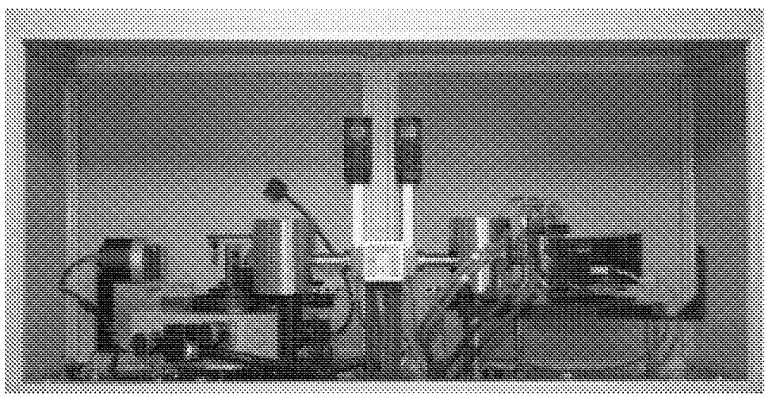


IPDS 2T

- Imaging Plate mit 2-Kreisgoniometer und maximal 77° 2θ
- Imaging Plate mit 2-Kreisgoniometer und maximal 137° 2θ
- Hoch- und Tieftemperaturzusätze

STADI P

- Hochdurchsatz- / kombinatorische Analyse
- Multi Purpose Diffraktometer
- Theta/theta- / Bragg-Brentano-Geometrie
- Transmissions- / Debye-Scherrer-Goniometer
- Verschiedene Detektorsysteme
- Hoch- und Tieftemperaturzusätze



STOE & Cie GmbH Postfach 101302 D-64213 Darmstadt
Tel.: (+49) 6151 / 98870 Fax: (+49) 6151 / 988788
E-mail: stoe@stoe.com Homepage: http://www.stoe.com

Herzlich willkommen in Freiburg

Zur 14. Jahrestagung der *Deutschen Gesellschaft für Kristallographie* begrüßen wir Sie als Tagungsteilnehmer(in) ganz herzlich.

Das wissenschaftliche Programm der Tagung basiert auf mehr als 300 Beiträgen aus allen Gebieten der Kristallographie. Dabei wurde das Konzept der letztjährigen DGK-Tagung in Köln mit Mikrosymposien (MS) zu sogenannten Themenschwerpunkten (TS) beibehalten; letztere wurden zuvor wieder von den Sprechern der Arbeitskreise (AK) fachübergreifend definiert. Auch ein weiteres Kölner Organisationsprinzip haben wir übernommen: Sämtliche Poster werden während des gesamten Tagungszeitraums präsentiert.

Wir möchten uns an dieser Stelle – auch im Namen der Deutschen Gesellschaft für Kristallographie – bei den Firmen und Institutionen bedanken, die die Tagung finanziell und materiell unterstützen. Ein Liste aller Aussteller sowie Details zur Firmenausstellung finden Sie auf S. 37.

Wir wünschen Ihnen einen angenehmen und – auch im kulturellen Sinne – erlebnisreichen Aufenthalt in der "Toskana Deutschlands" (worum es sich bei der hiesigen Region zumindest aus Sicht glühender Freiburger Lokalpatrioten handelt) und uns allen eine wissenschaftlich fruchtbare und anregende Tagung.

Das Organisationskomitee

Inhalt dieses Programmhefts

S. 5: Organisation

S. 7: Wissenschaftliches Programm

S. 10: Vortragsprogramm (Plenarvorträge und Mikrosymposien)

S. 23: Poster

S. 35: Weitere Veranstaltungen (Mitgliederversammlung, AK-Treffen, Gesellschaftsabend)

S. 36: Sehenswertes in Freiburg und Umgebung

S. 37: Liste der Sponsoren und Aussteller

S. 38: Allgemeine Hinweise (Anreise, Verpflegung, technische Hinweise)

S. 41: Lagepläne, Tagungsbüro

S. 44: Tabellarisches Gesamtprogramm

FREIBURG 2006

COR-AAD1-00003227
Bayer EX1008 (Part 6 of 9)

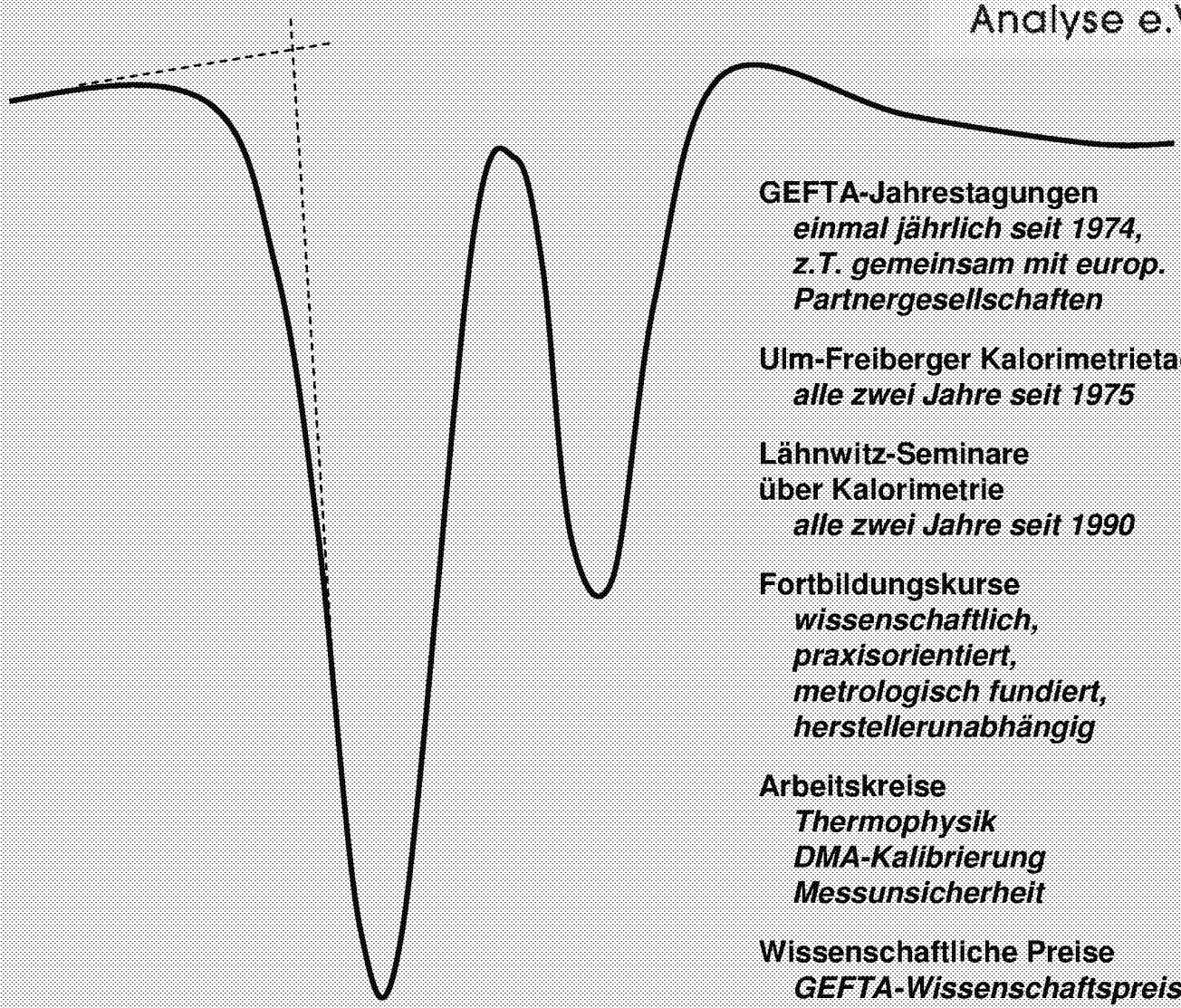
Thermische Analyse -

von den Anfängen:
Phasenanalyse und Kristallstrukturen
von Tonmineralen und anderen Silikaten
mit DTA, TG, DIL

bis heute:
Charakterisierung moderner
Werk- und Wirkstoffe
mit DTA, DSC, TG, DMA, TA-MS, TA-FTIR, ...

GEFTA

Gesellschaft
für
Thermische
Analyse e.V.



GEFTA-Jahrestagungen
einmal jährlich seit 1974, z.T. gemeinsam mit europ. Partnergesellschaften

Ulm-Freiberger Kalorimetrietage
alle zwei Jahre seit 1975

Lähnwitz-Seminare über Kalorimetrie
alle zwei Jahre seit 1990

Fortbildungskurse
wissenschaftlich, praxisorientiert, metrologisch fundiert, herstellerunabhängig

Arbeitskreise
Thermophysik
DMA-Kalibrierung
Messunsicherheit

Wissenschaftliche Preise
GEFTA-Wissenschaftspreis
NETZSCH-GEFTA-Preis
NETZSCH-GEFTA-Förderpreis
TA Instruments-Industriepreis

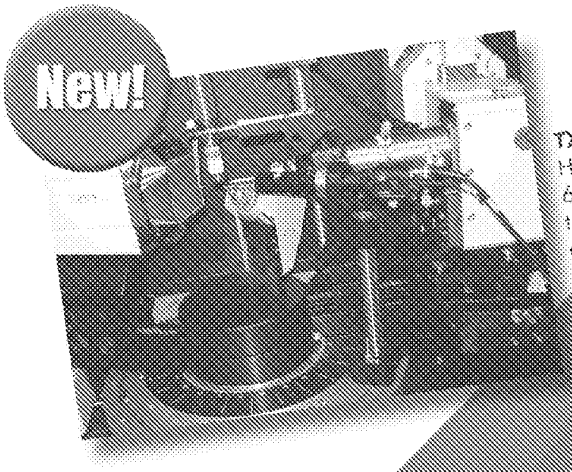
http://www.gefta.org

Organisation

- Veranstalter:
  - Albert-Ludwigs-Universität Freiburg
    - Kristallographisches Institut
    - Institut für Anorganische und Analytische Chemie
    - Institut für Organische Chemie und Biochemie
  - zusammen mit *kongress & kommunikation gGmbH*
  - unter der Schirmherrschaft der *Deutschen Gesellschaft für Kristallographie e.V.* (Vorsitzender: Wulf Depmeier, Kiel)
- Tagungsleitung und wissenschaftliches Komitee
  - Arne Cröll
  - Volker Krämer
  - Joachim Bibus
  - Andreas Danilewsky
  - Egbert Keller
  - Georg E. Schulz
  - Harald Hillebrecht
  - Caroline Röhr
- Programmgestaltung (Mikrosymposien und Postersessions) nach AKs:
  1: Dirk W. Heinz, Manfred S. Weiss, Klaus Scheffzek, Wolf-Dieter Schubert, Clemens Vonrhein, Roman Hillig (Biologische Strukturen)
  2: Ulrich Schwarz (Hochdruckkristallographie)
  3: Matthias Rodewald (Elektronenmikroskopie)
  4: Bernd Müller (Nichtkristalline und Partiellkristalline Strukturen)
  5: Jürgen Schreuer, Wolfgang W. Schmahl (Kristallphysik)
  6: Christian W. Lehmann (Molekülverbindungen)
  7: Markus Braden (Neutronenstreuung)
  9: Helmuth Zimmermann (Theoretische Kristallographie)
  10: Jörg Trempler (Mikroskopie)
  11: Ullrich Pietsch (Hochauflösende Röntgenstreuung und Synchrotron-Strahlung)
  12: Michael Fechtelkord, Georg Amthauer (NMR-Spektroskopie)
  13: Robert E. Dinnebier (Pulverdiffraktometrie)
  14: Gerhard Raabe (Computational Crystallography)
  15: Herbert Pöllmann, Horst J. Pentinghaus (Mineralogische und Technische Kristallographie)
  16: Sander van Smaalen (Aperiodische Kristalle)
  17: Reinhard Neder (Kristallographie in der Lehre)
  18: Guntram Jordan (Oberflächen und Grenzflächen)
  19: Rainer Pöttgen (Kristallchemie)
- Technische Leitung: kongress & kommunikation gGmbH, Freiburg
  - Walter Koch
  - Andrea Riegger
  - Jürgen Bächle
- Web-Seite: www.dgk-2006.de
- Tagungsort: Albert-Ludwigs-Universität Freiburg, Kollegiengebäude I (KG I)
  s. Lagepläne auf S. 38 (Stadtplan), 41 (Gebäude) und 43 (Raumpläne).

COR-AAD1-00003229
Bayer EX1008 (Part 6 of 9)

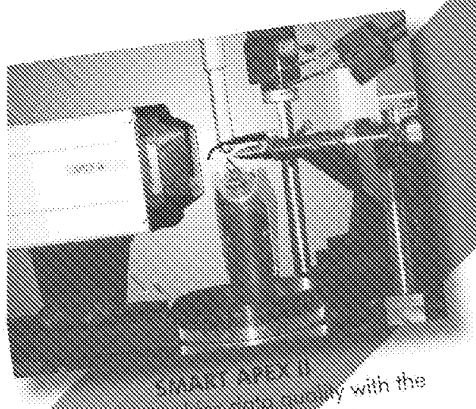
CRYSTALLOGRAPHY HAS NEVER BEEN MORE POWERFUL...



TXS with APEX II
Hottest Mo-sou
60 times the
tube. Th
cuttin



Kappa APEX II
Highest versatility with the best 4-circle goniometer available.



SMART APEX II
y with the
detector.

...AND BRUKER AXS HAS THE PERFECT INSTRUMENT TO MEET YOUR NEEDS



SMART BREEZE
easiest ever
structure
determination in a
low-maintenance
package.

BRUKER ADVANCED X-RAY SOLUTIONS

BRUKER AXS

North America: BRUKER AXS INC ■ Tel. (+1) (608) 276-3000 ■ Fax (+1) (608) 276-3006 ■ www.bruker-axs.com ■ info@bruker-axs.com
Netherlands: BRUKER AXS BV ■ Tel. (+31) (15) 215-2400 ■ Fax (+31) (15) 215-2600 ■ www.bruker-axs.nl ■ info@bruker-axs.nl
Germany: BRUKER AXS GMBH ■ Tel. (+49) (721) 595-2888 ■ Fax (+49) (721) 595-4587 ■ www.bruker-axs.de ■ info@bruker-axs.de

Wissenschaftliches Programm

Nachfolgend finden Sie als Gliederung für die Themen der Mikrosymposien und der Postersessions die AK-übergreifenden Themenschwerpunkte (TS) und die Arbeitskreise der DGK (AK):

TS 1/AK 1: Biologische Strukturen
TS 2: Kristallchemie und Hochdruck
TS 3: Kristallographie und Spektroskopie
TS 4: Instrumentierung von Großgeräten
TS 6: Strukturelle Phasenumwandlungen
TS 7: Kristallchemie und modulierte Strukturen
TS 8: Molekül- und Koordinationsverbindungen mit funktionellen Eigenschaften
TS 9: Crystal Engineering und Strukturvorhersage
TS 10: Quasi- und teilkristalline Strukturen
AK 1: Biologische Strukturen
AK 2: Hochdruckkristallographie
AK 3: Elektronenmikroskopie
AK 4: Nichtkristalline und Partiellkristalline Strukturen
AK 5: Kristallphysik
AK 6: Molekülverbindungen
AK 7: Neutronenstreuung
AK 9: Theoretische Kristallographie
AK 10: Mikroskopie
AK 11: Hochauflösende Röntgenstreuung und Synchrotron-Strahlung
AK 12: NMR-Spektroskopie
AK 13: Pulverdiffraktometrie
AK 14: Computational Crystallography
AK 15: Mineralogische und Technische Kristallographie
AK 16: Aperiodische Kristalle
AK 17: Kristallographie in der Lehre
AK 18: Oberflächen und Grenzflächen
AK 19: Kristallchemie

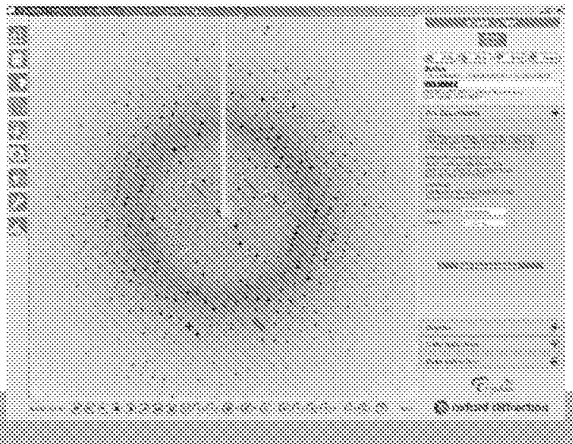
COR-AAD1-00003231
Bayer EX1008 (Part 6 of 9)

oxford diffraction

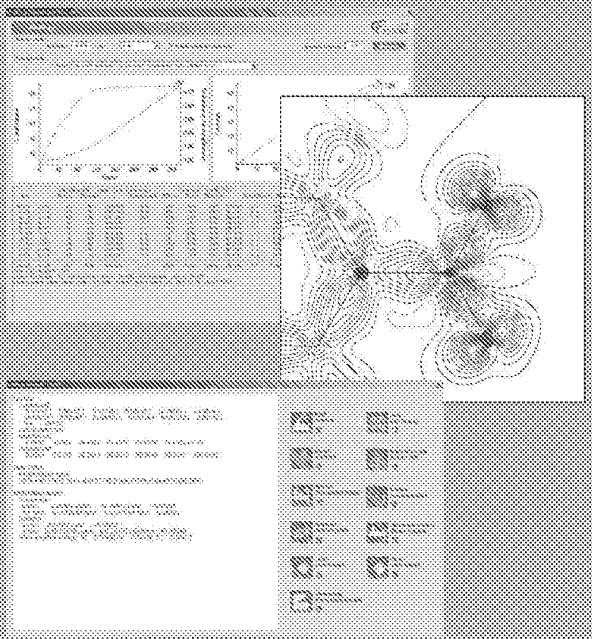
Making crystallography easier

NEW

CrysAlis Pro



- Easy to use Graphical User Interface
- Superb quality data using profile fitting
- Fully automatic data collection, parallel reduction and finalisation
- Intelligent strategy software
- Specialist 'Power Tools' for problematic data sets
- Command line access to 100's of specialist commands
- Choice of full manual control
- Remote control of cryo-devices and X-ray generators
- Real time data summary reports
- Free to ALL our existing users



Supplied with Xcalibur and Gemini diffractometers

sales@oxford-diffraction.com www.oxford-diffraction.com

Oxford Diffraction Ltd 66 Milton Park, Abingdon, Oxfordshire OX14 4RX. Tel: +44 (0)1235 443500. Fax: +44 (0)1235 443501
Oxford Diffraction Inc 300 Baker Ave, Suite 150, Concord, MA 01742, USA. Tel: +1 866 967 3606 (toll free tel: +1 978 371 2500. Fax: +1 978 369 4287
Oxford Diffraction Poland Sp. z o.o. Rogowska, 11/B, 54-440 Wrocław, Poland. Tel: +48 71 7835380. Fax: +48 71 7835381

COR-AAD1-00003232

Bayer EX1008 (Part 6 of 9)

Fritz Henning Laves (1906-1978)



Fritz Laves, dessen 100. Geburtstags wir dieses Jahr gedenken, war einer der einflussreichsten Kristallographen des 20. Jahrhunderts. Kristallographie umfasste für ihn alle geometrischen, physikalischen und chemischen Aspekte der kristallinen Materie, inklusive, aber nicht schwergewichtig, die Kristallstrukturbestimmung.

Geboren (27.2.1906) und aufgewachsen in Hannover, studierte er Mineralogie in Innsbruck (1924), Göttingen (1924-26) und Zürich (1926-29), wo er bei Paul Niggli auf dem Gebiet der Kristallchemie promovierte. Er folgte dann einer Einladung von V. M. Goldschmidt nach Göttingen (1930-43), wo er sich 1932 habilitierte. Die nächsten Stationen waren Professuren in Halle (1943-45), Marburg (1945-48) und am Geology Department der University of Chicago (1948-54). 1954 übernahm er als Nachfolger von Niggli die Leitung des Instituts für Mineralogie und Petrographie der ETH und der Universität Zürich, das entsprechend seiner neuen Orientierung in Institut für Kristallographie und Petrographie umbenannt wurde. Dieses Institut entwickelte er zu einer breit gefächerten Forschungsanstalt, deren Interdisziplinarität auch moderne Vorgaben überträfe, und die in hohem Masse die mineralogisch-kristallographische Forschung im deutschsprachigen Raum prägte. Laves ist bekannt für seine Arbeiten über geometrische Prinzipien der Kristallchemie (Bauzusammenhänge), Legierungssysteme (Lavesphasen), Ordnung-Unordnung in atomaren Strukturen vom Kristall bis zum Glas, sowie Strukturen und Phasenbeziehungen von Feldspäten. Seine wissenschaftlichen Ziele verfolgte er in Zusammenarbeit mit Mathematikern, Physikern und Chemikern mittels verschiedener Methoden wie Röntgen- und Neutronendiffraktion, Infrarot- und Kernresonanzspektroskopie sowie Elektronenmikroskopie. Seine Publikationsliste enthält 232 Titel. Für seine wissenschaftlichen Leistungen erhielt Laves zahlreiche Auszeichnungen. Er war Präsident der Deutschen Mineralogischen Gesellschaft (1956-58) und Vizepräsident der Internationalen Union für Kristallographie (1969-72). Er emeritierte 1976 und verstarb in Zürich (12. 8. 1978).

Seine Mitarbeiter bewunderten seine breite humanistische Bildung und sind ihm für seinen humanen und diskreten Führungsstil dankbar.

D. Schwarzenbach, Lausanne

COR-AAD1-00003233
Bayer EX1008 (Part 6 of 9)

Montag, 3. April 2006 (nachmittags)

Plenarvortrag

Ort: Aula

Vorsitz: W. Depmeier (Kiel)

13:30 Uhr *D. Schwarzenbach (Lausanne) und W. Hoffmann (Münster)*
Zum 100. Geburtstag von Fritz Laves (s. auch S. 9)

Mikrosymposien

Elektronenmikroskopie (AK 3)

Ort: HS 1199

Vorsitz: M. Rodewald

Abstr.: S. 9 ff

14:45 Uhr *F. Krumeich, R. Nesper*
Strukturuntersuchungen an Niob-Wolfram-Oxiden mittels Z-Kontrast

15:15 Uhr *H. Kirmse, I. Häusler, I. Hähnert, W. Neumann, F. M. Kiesling, P. Rudolph*
TEM-Untersuchungen der Struktur und Bildung von As-Ausscheidungen in GaAs

15:45 Uhr *L. A. Schmitt, R. Theissmann, K. A. Schoenau, M. Knapp, H. Kungl, H. Fuess*
TEM Untersuchungen zur Domänenstruktur und -orientierung in PZT Keramik

16:05 Uhr *H. Hofmeister, K.-D. Schicke, M. Dubiel*
Konfiguration von Kontaktzwillingen in Ag Nanopartikeln im Glas

16:25 Uhr *I. Häusler, H. Schwabe, H. Kirmse, W. Neumann*
Bestimmung der Ge-Konzentration von (Si,Ge)-Inseln mittels TEM

Kristallchemie und Hochdruck (TS 2)

Ort: HS 1010

Vorsitz: U. Schwarz (Dresden, AK 2), R. Pöttgen (Münster, AK 19)

Abstr.: S. 12 ff

14:45 Uhr *J. S. Knyrim, H. Huppertz*
Hochdrucksynthese und Kristallstruktur des silicat-ähnlichen Hafniumborates β-HfB_2O_5

15:00 Uhr *S. Lowitzer, B. Winkler, M. Tucker*
Thermoelastic behaviour of graphite from in situ high-(P,T) neutron diffraction

15:15 Uhr *C. Hejny, S. Falconi, L. F. Lundegaard, M. I. McMahon*
Phasenumwandlungen bei Tellur bei hohen Drucken und Temperaturen

COR-AAD1-00003234
Bayer EX1008 (Part 6 of 9)

15:30 Uhr *F. Liebau, X. Wang*
Stoichiometric valence and structural valence: distinct properties of atoms

15:45 Uhr *R. Demchyna, Y. Prots, U. Schwarz*
Crystal Structure of HfPdGe solved from multi-twinned Specimen

16:00 Uhr *S. Lange, T. Nilges*
Silber(I)-Tellur(id)-bromide: partiell reduzierte Materialien mit hohen Ionenmobilitäten

16:15 Uhr *N. Vojteer, H. Hillebrecht*
Das erste Lithiumboridsilicid: $Li_2B_{12}Si_2$

Mineralogische und technische Kristallographie (AK 15)

Ort: HS 1015

Vorsitz: H. Pöllmann (Halle) Abstr.: S. 16 ff

14:45 Uhr *H. Küppers, F. Liebau*
Die Durchlässigkeit von Fenstern in Zeolithen

15:15 Uhr *C. Weidenthaler, M. Mamatha, F. Schüth*
In-situ X-ray Diffraction Studies on the Dehydrogenation of Potential Hydrogen Storage Materials

15:45 Uhr *T. Wroblewski, A. Buffet*
Recrystallization of metals investigated by X-ray diffraction imaging

16:15 Uhr *U. Precht, H. J. Pentinghaus*
Röntgenografische Untersuchungen der strukturellen Relaxation in Alkalisilikatgläsern

Preisträger-Vortrag

Ort: Aula

Vorsitz: W. Depmeier (Kiel)

18:15 Uhr *Günter Schwarz (Köln):*
Die Biosynthese des Molybdäncofaktors: Von der Funktion zur Struktur und zurück

COR-AAD1-00003235
Bayer EX1008 (Part 6 of 9)

Dienstag, 4. April 2006 (vormittags)

Plenarvortrag

Ort: Aula

Vorsitz: W. Neumann (Berlin)

Abstr.: S. 3

9:00 Uhr *L. Bohatý*
Non-centrosymmetric crystals and their properties

Mikrosymposien

Instrumentierung von Großgeräten (TS 4)

Ort: HS 1199

Vorsitz: U. Pietsch (AK 11) und M. Braden (AK 7)

Abstr.: S. 18 ff

10:15 Uhr *W. Leitenberger, U. Pietsch, T. Panzner, A. Pucher, Y. Bodenthin, T. Sant*
Experiments with synchrotron radiation at the BESSY EDR-beamline

10:35 Uhr *A. Senyshyn, H. Boysen, M. Hölzel, F. Elf, H. Fuess, R. Gilles*
Powder diffractometers with positional sensitive multidetector: data treatment, correction and analysis - example of instrument SPODI

10:55 Uhr *R. U. Barz, T. B. Bekker*
Synchrotron topography of hydrothermally grown emerald single crystals

11:15 Uhr *A. Hofmann, S. van Smaalen, E. Rödel, P. Luger*
Accurate charge density of Tri-alanine. A comparison of multipole refinement and MEM

11:55 Uhr *C. Paulmann, R. Peters, K. Petermann, U. Bismayer*
Studies of disorder-induced diffuse scattering in $NaGd(WO_4)_2$:Yb^{3+} crystals

Pulverdiffraktometrie (AK 13)

Ort: HS 1010

Vorsitz: R. Dinnebier (Stuttgart, AK 7)

Abstr.: S. 21 ff

10:15 Uhr *A. Leineweber*
Kartesische Parametrisierung von Mikrodehnungsverbreiterung

10:35 Uhr *K. Sugimoto, R. E. Dinnebier*
Chlorartinite, a volcanic exhalation product also found inindustrial magnesia floors

10:55 Uhr *A. Zuev*
Die Berechnung der totalen Instrumentenfunktion in der Röntgenpulverdiffraktometrie

COR-AAD1-00003236
Bayer EX1008 (Part 6 of 9)

11:15 Uhr *S. Brühne, T. Proffen, E. Uhrig, M. Feuerbacher, C. Hu, W. Assmus, M. U. Schmidt*
Real atomic structure from analysis of synchrotron, neutron and in-house X-ray pair distribution functions (PDFs)

11:35 Uhr *J. Birkenstock, T. Messner, R. X. Fischer*
Determination of sample effects and background in XRD data using BRASS

11:55 Uhr *R. Haberkorn, H. P. Beck*
Spielarten der Verzerrungen - Bestimmung aus der Form von Beugungsprofilen und deren Interpretation

Kristallographie und Spektroskopie (TS 3)

Ort: HS 1015

Vorsitz: G. Amthauer (Salzburg) und M. Fechtelkord (Bochum)

Abstr.: S. 24 ff

10:15 Uhr *F. Haarmann, M. Armbrüster, Y. Grin*
Local ordering in $Cu_{1-x}Al_2$

10:35 Uhr *M. Fechtelkord*
Ordering of F/OH anions as a function of the Al/Mg cation distribution in the octahedral sheets of phlogopite studied by solid state NMR spectroscopy

10:55 Uhr *K. Garbev, G. Beuchle, L. Black, B. Gasharova*
Structural Features of Poorly Crystalline Calcium Silicate Hydrates of Type C-S-H (I). A Spectroscopic Study

11:15 Uhr *B. Gasharova, K. Garbev, G. Beuchle*
α-C_2SH – Dellaite Phase Transition: Single Crystal SR-IR, powder XRD and ^{29}Si NMR study

11:35 Uhr *S.-U. Weber, M. Grodzicki, C. A. Geiger, W. Lottermoser, G. Tippelt, G. Amthauer*
^{57}Fe-Mössbauer spectroscopic measurements and theoretical calculations of natural lawsonite

11:55 Uhr *M. Merz, S. Schuppler, Y. U. Idzerda, S. V. Shiryaev, S. N. Ustinovich, S. N. Barilo*
X-ray diffraction and x-ray absorption of bismuthates: Competition between bipolaronic and charge-density wave states

COR-AAD1-00003237
Bayer EX1008 (Part 6 of 9)

Dienstag, 4. April 2006 (nachmittags)

Plenarvortrag

Ort: Aula

Vorsitz: K.-W. Benz (Freiburg)

Abstr.: S. 3

13:30 Uhr *J. H. Bilgram*
Controlling of Complex Structures

Mikrosymposien

Biologische Strukturen I: New Structures (TS 1)

Ort: HS 1199

Vorsitz: Klaus Scheffzek (Heidelberg)

Abstr.: S. 27 ff

14:45 Uhr *W. Blankenfeldt, N. H. Thomae, J. S. Wray, M. Gautel, I. Schlichting*
Solving the structure of a beanpole: the story of ΔS2 from cardiac myosin II

15:00 Uhr *C. Schleberger, H. Barth, K. Aktories, G. E. Schulz*
Structure of the ADP-ribosylating component of the binary toxin C2 from *Clostridium botulinum*

15:15 Uhr *G. S. Kachalova, M. D. Hartmann, M. Bruning, G. P. Bourenkov, A. Oberschall, N. Strizhov, H. D. Bartunik:*
Structures and mechanisms of the shikimate pathway enzymes AroK, AroA, and AroF from *M. tuberculosis*

15:30 Uhr *M. Hothorn, A. Wachter, R. Gromes, T. Stuwe, T. Rausch, K. Scheffzek*
A two-component regulatory mechanism controls the key enzyme in plant glutathione biosynthesis

15:45 Uhr *G. Wille, D. Meyer, A. Steinmetz, E. Hinze, R. Golbik, K. Tittmann*
Structures of reaction intermediates in the catalytic cycle of pyruvate oxidase

16:00 Uhr *G. Hagelueken, T. M. Adams, L. Wiehlmann, U. Widow, H. Kolmar, B. Tümmler, D. W. Heinz, W.-D. Schubert*
The crystal structure of SdsA1, an alkylsulfatase from *Pseudomonas aeruginosa*, defines an independent, third mechanistic class of sulfatases

Strukturelle Phasenumwandlungen (TS 6)

Ort: HS 1010

Vorsitz: J. Schreuer (Frankfurt) und W. Schmahl (München)

Abstr.: S. 30 ff

14:45 Uhr *S. Haussühl, E. Haussühl, J. Liebertz*
Anomalous elastic behaviour of åkermanite and hardystonite near the NC-N transition

15:00 Uhr *G. Schuck, J. Karpinski, K. Rogacki, N. D. Zhigadlo, S. M. Kazakov*
Structural studies of β-pyrochlore single crystals

COR-AAD1-00003238
Bayer EX1008 (Part 6 of 9)

15:15 Uhr *D. Walter, A. Neumann*
Crystal structure and thermal stability of lanthanum hydroxide oxide

15:30 Uhr *H. Sowa*
Orientierungsbeziehungen zwischen vier AgJ-Modifikationen

15:45 Uhr *J. Davaasambuu, G. Busse, J. Hallmann, S. Techert*
Lichtinduzierte Phasenumwandlung in organischen Einkristallen

16:00 Uhr *S. Gorfman, V. Tsirelson, N. Hansen, W. Morgenroth, U. Pietsch*
Site selective response of α-$GaPO_4$ crystal to a permanent external electric field

Neutronenuntersuchungen an komplexen Überstrukturen (TS 5)

Ort: HS 1015

Vorsitz: M. Braden

Abstr.: S. 33 ff

14:45 Uhr *N. Qureshi, H. Fuess, H. Ehrenberg*
Magnetische Phasenübergänge und Strukturen des $Co_3V_2O_8$

15:05 Uhr *A. Schneidewind, M. Frontzek, A. Kreyssig, J.-U. Hoffmann, G. Behr, M. Loewenhaupt*
Magnetic structures of Tb_2PdSi_3 in fields up to 6.5 T

15:25 Uhr *D. Senff, M. Cwik, O. Schumann, A. Schneidewind, P. Link, Y. Sidis, A. Revcolevschi, M. Braden*
Magnetic structure of charge ordered systems

15:45 Uhr *B. Winkler, S. C. Vogel, D. J. Wilson, V. Milman, D. W. Brown, T. A. Sisneros*
In situ observation of the formation of TiC from the elements by neutron diffraction

Postersession I

Zwischen 16:30 und 18:00 Uhr Präsentation aller Poster; die Autorinnen und Autoren der Poster, die in den linken Spalten des Abstracts-Bandes (Nr. xx-L) abgedruckt sind, stehen für Diskussionen an den Postern zur Verfügung (Verzeichnis aller Poster siehe S. 23).

Mitgliederversammlung

Um 18:30 Uhr findet die jährliche Mitgliederversammlung der DGK in der Aula statt. Um zahlreiches Erscheinen aller Mitglieder wird hiermit herzlich gebeten!

COR-AAD1-00003239
Bayer EX1008 (Part 6 of 9)

Mittwoch, 5. April 2006 (vormittags)

Plenarvortrag

Ort: Aula

Vorsitz: C. W. Lehmann (Mülheim)

Abstr.: S. 4

9:00 Uhr *Peter Luger (Berlin)*
Schnelle Elektronendichtebestimmung - eine Routinemethode der Zukunft?

Mikrosymposien

Biologische Strukturen II: Structure Based Drug Design (AK 1/TS1)

Ort: HS 1199

Vorsitz: Roman Hillig (Berlin)

Abstr.: S. 35 ff

10:15 Uhr *M. Hennig (Roche)*
Structure based drug discovery in pharmaceutical industry

10:35 Uhr *P. Erbel, A. D'Arcy, S. Lim, M. Chaillet, N. Schiering, S. Vasudevan, U. Hommel (Novartis)*
Towards a structure of catalytic active Dengue NS3 protease in complex with a truncated NS2B cofactor

10:55 Uhr *S. G. Kauschke, N. Heine, G. Dahmann, A. Heckel, N. Stadler, T. Maurer, A. Pausch (Boehringer Ingelheim)*
PPARγ antagonists for the treatment of diabetes

11:15 Uhr *M. Schade, M. Joshi, C. Vargas, K. Moelling, P. Boisguirn, A. Diehl, G. Krause, P. Schmider, V. Hagen, H. Oschkinat (Combinature Biopharm AG)*
Fragment-based Lead Discovery by NMR: Novel modulators of PDZ domains

11:35 Uhr *T. Lundqvist (AstraZeneca)*
The important role of biophysical methods in modern drug discovery

Crystal Engineering und Strukturvorhersage (TS 9)

Ort: HS 1010

Vorsitz: C. W. Lehmann (AK 6) und G. Raabe (AK 14)

Abstr.: S. 38 ff

10:15 Uhr *T. Bredow, G. Geudtner, M. Lerch*
Defektbildung im Kationen- und Anionengitter von Zirkondioxid: quantenchemische Rechnungen

10:45 Uhr *M. U. Schmidt*
Kristall-Engineering an industriellen organischen Farbpigmenten

COR-AAD1-00003240
Bayer EX1008 (Part 6 of 9)

11:15 Uhr *M. T. Kirchner, S. A. Cirkel, R. Boese*
Zwischen Cokristallisation und chemischen Reaktionen: Manche tun es, andere nicht!

11:45 Uhr *U. Englert, C. Hu, R. Wang*
Planbare und überraschende Koordinationspolymere

Oberflächen und Grenzflächen, Biologische Materialien (AK 18)

Ort: HS 1015

Vorsitz: U. Magdans (Bochum) und G. Jordan (München) Abstr.: S. 40 ff

10:15 Uhr *K. Aldushin, G. Jordan, W. W. Schmahl*
Nanoscale alterations of phlogopite in aqueous solutions

10:30 Uhr *G. Jordan, K. Aldushin, W. W. Schmahl*
Nano-scale kinematics of surface and interlayer reactions

10:45 Uhr *U. Magdans, H. Gies, X. Torrelles, J. Rius, K. Angermund*
Interaction of glycine with the calcite-{104}-surface in aqueous solution

11:00 Uhr *K. Etzel, J. Toporski, W. Depmeier, H. Huber, R. Rachel, M. Thomm, G. Schmalz*
Effect of crystallographic orientation on microbial pyrite surface alterations

11:15 Uhr *H. Klein, O. Kaltschmidt, L. Raue, A. Preusser*
Kristallographische Texturen und anisotrope Eigenschaften von Biomaterialien

11:30 Uhr *S. Castorph, R. Hock, M. Baier*
News from the crystallographic structure of sea urchine spines of Heterocentrotus mammilatus

11:45 Uhr *C. Merkel, E. Griesshaber, R. Neuser, K. Kelm, W. Mader, W. W. Schmahl*
Microstructure and microhardness in inarticulate brachiopods

12:00 Uhr *S. Zhang, A. Klocke, B. Mihailova, B. Gasharova, B. Güttler, R. Stosch, T. Geisler, U. Bismayer*
Laser-Induced Structural changes in Dental Enamel

COR-AAD1-00003241
Bayer EX1008 (Part 6 of 9)

Mittwoch, 5. April 2006 (nachmittags)

Plenarvortrag

Ort: Aula

Vorsitz: D. W. Heinz (Braunschweig)

Abstr.: S. 4

13:30 Uhr *T. O. Yeates (Los Angeles)*
Structure of the Shell Subunits of the Carboxysome: A primitive bacterial organelle

Mikrosymposien

Biologische Strukturen III: New Methods (TS 1/AK 1)

Ort: HS 1199

Vorsitz: Clemens Vonrhein (Cambridge)

Abstr.: S. 44 ff

14:45 Uhr *C. Mueller-Dieckmann, M. S. Weiss*
On the use of longer X-rays in macromolecular crystallography

15:05 Uhr *G. M. Sheldrick*
Experimental Phasing of Macromolecules with SHELXC/D/E

15:25 Uhr *M. Ruf, C. B. Bauer*
Processing Twinned Protein Data Using the Proteum Software Package

15:45 Uhr *M. T. Stiebritz, S. Wengrzik, C. M. Jäger, Y. A. Muller*
MUMBO: Protein design algorithms to construct new interfaces, to automate ligand docking and even to fit electron densities

16:05 Uhr *M. E. Than, S. Henrich, G. P. Bourenkov, H.D. Bartunik, W. Bode*
Unequivocal determination of two Ca^{2+}-ions within the proprotein convertase furin

16:25 Uhr *S. Fielder, A. Geerlof, M. Groves, C. Hermes, W. Meyer-Klaucke, V. S. Lamzin, J. Müller-Dieckmann, S. Panjikar, A. Popov, M. Rössle , A. Schmidt, Y.-H. Song, D. Svergun, P. A. Tucker, M. S. Weiss, M. Wilmanns*
New facilities for structural biology at PETRA III

Kristallchemie und komplexe Überstrukturen (TS 7)

Ort: HS 1010

Vorsitz: A. Schönleber (AK 16) und R. Pöttgen (AK 19)

Abstr.: S. 47 ff

14:45 Uhr *C. Graf, T. Doert*
Lage- und Besetzungsmodulation in $LnSe_{2-d}$ (Ln = Pr, Gd; d ≈ 0.15)

15:15 Uhr *S.-H. Park, J. P. Parise, H. Boysen, C. Paulmann*
Dynamic and static disorder of lithium in the microporous lithosilicate RUB-29 ($Cs_{14}Li_{24}[Li_{18}Si_{72}O_{172}] \cdot 14H_2O$)

COR-AAD1-00003242
Bayer EX1008 (Part 6 of 9)

15:35 Uhr *K. Friese, H. Krüger, V. Kahlenberg, T. Balić-Žunić, H. Emerich, J.-Y. Gesland, A. Grzechnik*
Temperature dependent study of KY_3F_{10}

15:55 Uhr *M. Trömel, K. Taxer*
Bor-Wasserstoff-Bor-Brücken in $LiBH_4$

Hochauflösende Röntgenstreuung und Synchrotron-Strahlung (AK 11)

Ort: HS 1015

Vorsitz: U. Pietsch (Siegen)

Abstr.: S. 49 ff

14:45 Uhr *E. Weidner, F. Frey, B. Pedersen, M. Burghammer*
Strukturuntersuchungen an Pyroxen-Einkristallen vom Mars

15:00 Uhr *A. Danilewsky, S. Doyle, J. Göttlicher, R. Steininger, P. McNally*
Qualitätsprüfung von YB_{66}-Monochromator-Kristallen mit Röntgen-Topographie und -Diffraktometrie

15:15 Uhr *D. C. Meyer, A. A. Levin, T. Leisegang, E. Gutmann, P. Paufler, M. Reibold, W. Pompe*
Reversible Formierung von Ruddlesden-Popper Phasen in einem (001)-$SrTiO_3$-Einkristall unter Einfluss eines externen elektrischen Feldes

15:30 Uhr *H. Schlenz, A. Kirfel, M. Jansen, J. Nuss, U. Wedig, C. Lin, W. Morgenroth*
Comparison of the electron density distributions in Zn and Mg

15:45 Uhr *J. Härtwig, P. VanWaerenbergh, I. Gierz, J. Hoszowska, A. Rommeveaux, A. Chumakov, G. Carbone, S. H. Connell, M. Rebak, R. Setshedi, D. Dube, L. Mkhonza, R. Burns, J. O. Hansen*
Diamonds for X-ray optical applications at 3rd and 4th generation X-ray sources

Postersession II

Zwischen 16:30 und 18:00 Uhr Präsentation aller Poster; die Autorinnen und Autoren der Poster, die in den rechten Spalten des Abstracts-Bandes (Nr. xx-R) abgedruckt sind, stehen für Diskussionen an den Postern zur Verfügung (Verzeichnis aller Poster siehe S. 23).

Gesellschaftsabend

Ab 19:30 Uhr findet der Gesellschaftsabend im *Le Buffet* statt, s. die Hinweise auf S. 35.

COR-AAD1-00003243
Bayer EX1008 (Part 6 of 9)

Donnerstag, 6. April 2006 (vormittags)

Plenarvortrag

Ort: Aula

Vorsitz: A. Cröll (Freiburg)

Abstr.: S. 5

9:00 Uhr *T. Baumbach (Karlsruhe)*
Microdiffraction Imaging of Semiconductor Materials

Mikrosymposien

Biologische Strukturen IV: Protein-Protein Interactions (TS 1)

Ort: HS 1199

Vorsitz: W.-D. Schubert (Braunschweig)

Abstr.: S. 52 ff

10:15 Uhr *R. Jauch, M. K. Cho, S. Jäkel, K. Schreiter, C. Netter, B. Aicher, M. Zweckstetter, H. Jäckle, M. C. Wahl*
Autoinhibition via a Reprogrammed Activation Segment in MAP Kinase Interacting Kinases

10:35 Uhr *K. Büttner, K. Wenig, K.-P. Hopfner*
Structural framework for the mechanism of exosomes in RNA processing

10:55 Uhr *D. Kümmel, Y. Roske, J. J. Müller, U. Heinemann*
Structure of the Bet3-TPC6 Core of the TRAPP Tethering Complex

11:15 Uhr *T. Wollert, D. W. Heinz, W.-D. Schubert*
Structure-based re-engineering of Internalin - the intestinal invasin of *Listeria monocytogenes*

11:35 Uhr *B. Loll, J. Kern, W. Saenger, A. Zouni and J. Biesiadka*
Towards complete cofactor arrangement in the 3.0 Å resolution structure of photosystem II

Molekül- und Koordinationsverbindungen mit funktionellen Eigenschaften (TS 8)

Ort: HS 1010

Vorsitz: C. W. Lehmann (AK 6) und R. Pöttgen (AK 19)

Abstr.: S. 55 ff

10:15 Uhr *C. Näther, I. Jess, V. Suitchmezian*
Untersuchungen zur Polymorphie pharmazeutischer Wirkstoffe

10:40 Uhr *W. Frank, G. Korrell, F.-G. Wittmer, G. J. Reiß*
Kristallographische Charakterisierung von Komponenten der roten Öle der Friedel-Crafts-Reaktion

COR-AAD1-00003244
Bayer EX1008 (Part 6 of 9)

10:55 Uhr *J. Monteagudo, P. Held, M. Fleck, P. Becker, L. Bohatý*
Zur Kristallographie der Glycin-Metallhalogenide

11:10 Uhr *C. Hu, J. W. Bats, M. Bolte, V. Pashchenko, M. Lang, M. U. Schmidt*
Polymeric structures of Cu(II)-triazole complexes and their magnetic features

11:25 Uhr *K. Müller-Buschbaum, Y. Mokaddem*
Tb-Imidazolate und Tb-Benzotriazolate: Lumineszenz von Koordinationspolymeren ohne Konzentrationsquenching

11:40 Uhr *D. M. Többens, H. Schottenberger, R. Kaindl, V. Kahlenberg, M. Hummel*
Tetrakis(triacetylmethanido)zirconium(IV), a homoleptic square-antiprismatic chelate complex

Quasikristalle, inkommensurable Verbindungen und teilkristalline Strukturen (TS 10)

Ort: HS 1015

Vorsitz: B. Müller (Jena)

Abstr.: S. 58 ff

10:15 Uhr *A. Schönleber, L. Palatinus, S. van Smaalen*
The Low Temperature Structures of the Metal(III)-Oxyhalides TiOCl and TiOBr

10:35 Uhr *H. Krüger, K. Friese, V. Kahlenberg*
The modulated structure of $Na_2Si_3O_7$

10:50 Uhr *R. Kaden, G. Wagner, K. Bente*
Cylindrite $Fe_{1\pm m}Sn_{4\pm x}Pb_{3\pm y}Sb_{2\pm z}S_{14}$ - Architecture and physical properties

11:05 Uhr *H. Schlenz*
Reverse Monte Carlo Simulations of four Ni-doped sodium metaphosphate glasses

11:20 Uhr *G. Krauss, Q. Gu, S. Katrych, W. Steurer*
Zur Stabilität von d-Al-Co-Ni und i-Zn-Mg-Dy bei hohen Drücken und Temperaturen

11:40 Uhr *K. H. Hassdenteufel, W. Steurer, A. R. Oganov*
Ab initio-Simulationen an einem Approximanten von dekagonalem Al-Co-Ni

Plenarvortrag

Ort: Aula

Vorsitz: M. S. Weiss (Hamburg)

Abstr.: S. 5

12:30 Uhr *G. E. Schulz (Freiburg)*
Protein Associations

COR-AAD1-00003245
Bayer EX1008 (Part 6 of 9)

HÜTTINGER: Leistung für Kristallzucht



Kristallzucht ist ein komplexer Prozess, bei dem jede Komponente zählt. Als ein führender Hersteller von Induktionsgeneratoren für die Kristallzucht wissen wir genau worauf es ankommt. Deshalb fertigen wir unsere Generatoren mit höchster Sorgfalt. So erfüllen sie stets die hohen Anforderungen, die an sie gestellt werden. Tag für Tag. Jahr für Jahr.

Höchst zuverlässig erzeugen HÜTTINGER Induktionsgeneratoren die zur Kristallzucht benötigte Leistung. Ihre Langzeitstabilität erlaubt es unseren Kunden beste Ergebnisse zu erzielen. Eine breite Palette an Datenschnittstellen macht HÜTTINGER Induktionsgeneratoren äußerst bedienerfreundlich. Das sagen unsere Kunden: Immer wieder. Weltweit.



HÜTTINGER: Leistung für Kristallzucht

www.huettinger.com

HÜTTINGER

Poster

Die Poster sind nach Arbeitskreisen bzw. Themenschwerpunkten geordnet. Poster auf linken Seiten des Abstract-Bandes (Nr. xx-L) werden am Dienstag, die auf rechten Seiten (Nr. xx-R) am Mittwoch präsentiert. Alle Poster bleiben während der gesamten Tagung hängen.

Biologische Strukturen I: New Structures (AK 1)

63-L *C. Chan, R. Paul, U. Jenal, T. Schirmer:* Structural basis of activity and allosteric control of diguanylate cyclase

63-R *N. Sträter, K. Paithankar, R. Schultz-Heienbrok:* Structure-Function Relationships of the Domain Mobility of 5'-Nucleotidase

64-L *R. Ganesan, P. R. E. Mittl, S. Jelakovic, M. G. Grütter:* Crystal structure of caspase-3/DEVD-chloromethyl ketone complex: implications for substrate recognition and catalysis

64-R *S. Kutter, M. Spinka, S. Relle, G. Wille, M. S. Weiss, G. Hübner, S. König:* The crystal structure of pyruvate decarboxylase from *Kluyveromyces lactis*. Further arguments for the substrate activation mechanism

65-L *G. Kachalova, M. D. Hartmann, M. Bruning, G. P. Bourenkov, A. Oberschall, N. Strizhov, H. D. Bartunik*: Crystal structure of the site-specific nickase N.BspD6I

65-R *C. R. Büttner, D. W. Heinz, H. H. Niemann:* Crystal structure of the type III secretion chaperone SycT from *Yersinia enterocolitica*

66-L *K. Niefind, M. Kuzu, W. Hummel, D. Schomburg:* First structure of a water-producing NADH oxidase

66-R *L. Shkolnaya, G. P. Bourenkov, N. Strizhov, H. D. Bartunik:* Crystal structures of glutamyl- and tyrosyl-tRNA synthetases from *Mycobacterium tuberculosis*

67-L *A. Oberschall, G. P. Bourenkov, N. Strizhov, H. D. Bartunik:* Crystal structure of a universal stress protein (USP) from *Mycobacterium tuberculosis*

67-R *Y. Carius, G.-W. Kohring, F. Giffhorn, A. J. Scheidig:* Crystal Structure of Galactitol-Dehydrogenase

68-L *M. A. Klieber, O. Scholz, P. Gmeiner, W. Hillen, Y. A. Muller:* Structural insight into the discrimination of tetracycline derivatives by a new variant of the repressor protein *TetR*

68-R *M. Bublitz, D. W. Heinz, W.-D. Schubert:* Peptidoglycan and Pathogenesis: Characterization of a Listerial Autolysin

69-L *K. Fischer, A. Llamas, M. Tejada Jimenez, R. R. Mendel, E. Fernandez, G. Schwarz:* Function and Structure of the Molybdenum Cofactor Carrier Protein MCP from *Chlamydomonas rheinhardtii*

69-R *C. Bieniossek, T. Schalch, M. Bumann, M. Meister, R. Meier, U. Baumann:* The molecular architecture of the metalloprotease FtsH

70-L *S. Weyand, G. Kefala, M. S. Weiss:* The High Resolution Structure of DapC (Rv0858c) from *M. tuberculosis*

70-R *J. W. A. Koetter, G. E. Schulz:* Crystal structure of 6-hydroxy-D-nicotine oxidase from *Arthrobacter nicotinovorans*

71-L *D. P. Kloer, C. Hagel, J. Heider, G. E. Schulz:* Structure of ethylbenzene dehydrogenase: insights into anaerobic hydrocarbon degradation

71-R *T. Schulte, P. M. Wrench, S. P. Sharples, R. G. Hiller, E. Hofmann:* The structure of high-salt peridinin-chlorophyll-protein from *A.carterae* shows a modified pigment arrangement as compared to the major allele of peridin-chlorophyll-proteins

72-L *J. Kraußе, A. Westendorf, R. H. Müller, N. Sträter:* Determination of the Oligomeric Structure of the 2-Oxoglutarate Dependent Dioxygenase RdpA by X-ray Crystallography and Small Angle X-ray Scattering

72-R *S. Kutter, G. Wille, S. Relle, M. S. Weiss, G. Hübner, S. König:* Crystal structure of pyruvate decarboxylase from *Kluyveromyces lactis*. Implications for the substrate activation mechanism

COR-AAD1-00003247
Bayer EX1008 (Part 6 of 9)

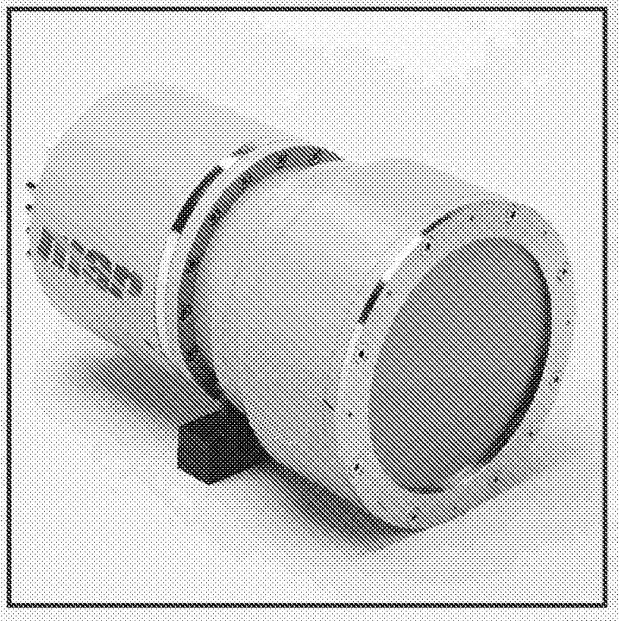
marresearch



marmosaic



mar345



marccd

World Leaders in X-ray Detectors

www.marresearch.com

Biologische Strukturen III: New Methods (AK 1)

73-L *A. Coetzee, B. Schierbeek, F. van Meurs, G. Witte, U. Curth, D. J. Manstein, R. Fedorov:* Improving data quality – the role of data collection strategy

73-R *C. Brinkmann, M. S. Weiss, E. Weckert:* Comparison of hen egg-white lysozyme in 6 different packings

74-L *U. Mueller, M. Fieber-Erdmann, M. Fuchs, R. Förster, W. Eberhardt:* The BESSY PX Beamlines: Current operational status and development plans

74-R *A. Meents, A. Wagner, R. Schneider, C. Pradervand, E. Pohl, C. Schulze-Briese:* Reduction of radiation damage with X-ray data collection at 15K: A systematic study

75-L *M. Zehnder, I. Vartaniants, E. Weckert:* Computational studies of radiation damage in protein crystals

75-R *B. Kauffmann, M. S. Weiss, V. S. Lamzin, A. Schmidt:* How to avoid premature decay of your macromolecular crystal - a chemist's approach to combat physical reality

76-L *J. Müller-Dieckmann:* High-Throughput Crystallization at the EMBL Hamburg

76-R *I. Dix, G. M. Sheldrick:* The EU BioXhit test crystal project

77-L *R. Herbst-Irmer:* Non-merohedral Twinning in Protein Crystallography

77-R *S. Panjikar, V. Parthasarathy, V. S. Lamzin, M. S. Weiss, P. A. Tucker: Auto-Rickshaw*: An automated crystal structure determination as an efficient tool to validate an X-ray diffraction experiment

Biologische Strukturen IV: Protein-Protein Interactions (AK 1)

78-L *A. Lammens, A. Schele, K.-P. Hopfner:* Structural and Biochemical Studies on the *Pfu* SMC ATPase

78-R *K. Fütterer, L. J. Alderwick, G. S. Besra, V. Molle, L. Kremer:* Molecular Structure of EmbR, a Response Element of Ser/Thr Kinase Signalling in *M. tuberculosis*

79-L *S. Panneerselvam, A. Marx, E.-M. Mandelkow, E. Mandelkow:* Catalytic and ubiquitin-associated (UBA) domains of MARK2/Par-1

79-R *S. Honnappa, W. Jahnke, J. Seelig, M. O. Steinmetz:* Control of intrinsically disordered stathmin by multisite phosphorylation

80-L *L. Hemsath, R. Dvorsky, D. Fiegen, M.-F. Carlier, M. R. Ahmadian:* A Novel Electrostatic Steering Mechanism of Cdc42 Recognition by Wiskott-Aldrich Syndrome Proteins

80-R *S. Russo, U. Baumann:* Crystal Structure of a Dodecameric Tetrahedral-shaped Aminopeptidase

81-L *A. Itzen, O. Pylypenko, R. S. Goody, A. Rak:* Nucleotide exchange via local protein unfolding – structure of Rab8 in complex with Mss4

81-R *S. Bhattacharya, J. J. Müller, Y. Roske, A. Turnbull, C. Scheich, V. Sievert, C. Quedenau, F. Götz, H. Delbrück, K. Büssow, U. Heinemann:* Crystallographic studies on the human growth arrest and DNA damage induced protein GADD45γ

Hochdruckkristallographie (AK 2)

82-L *S. C. Vogel, D. W. Brown, H. M. Volz, Y. Wang, J. Zhang:* High Pressure Deformation Study of Zirconium

82-R *E. Füglein, D. Walter:* Pressure dependency of the thermal transformation from MOOH to M_2O_3 (M=Fe, La)

83-L *E. A. Juarez-Arellano, A. Friedrich, K. Knorr, A. Lieb, B. Winkler, M. Amboage, M. Hanfland, W. Schnick:* High-pressure study on isotypic $SrYb[Si_4N_7]$ nitridosilicate and $MYb[Si_{4-x}Al_xO_xN_{7-x}]$ (M = Sr, Ba, x = 2) sialons

83-R *J. M. Engel, H. Ahsbahs, H. Ehrenberg:* Die Hochdruckphase von $K_2Co_2(MoO_4)_3$

84-L *B. Lazic, V. Kahlenberg, J. Konzett:* On a high pressure modification of $CaAl_2O_4$ isostructural with m-$CaGa_2O_4$

84-R *A. Ullrich, R. Miletich:* Static compression and strain evaluation in $NaTi^{3+}Si_2O_6$ clinopyroxene

COR-AAD1-00003249
Bayer EX1008 (Part 6 of 9)

85-L *A. Grzechnik, W. A. Crichton, W. G. Marshall, K. Friese:* High-pressure behaviours of $PbWO_4$ and $BaWO_4$ scheelites
85-R *A. Grzechnik:* Li_2ZrF_6 at high pressures and high temperatures
86-L *A. Grzechnik, T. Balić-Žunić, E. Makovicky, J.-Y. Gesland, K. Friese:* Compressibility mechanism in garnet $Li_3Na_3In_2F_{12}$
86-R *A. Friedrich, L. Wiehl, E. Haussühl, J. Schreuer, B. Winkler:* Pressure-induced phase transition of $((CH_3)_3NCH_2COO)_3MnZnCl_4$
87-L *M. Trömel, K. Taxer:* Die Wertigkeit von Eisen und Osmium unter hohen Drücken
87-R *D. Cinato, S. Johänntgen, R. Miletich:* Development of an internally heated gasket applicable to XRD at HP-HT conditions in diamond-anvil cells
88-L *C. Lathe, F. Schilling, H. J. Müller, H. J. Reichmann, J. Lauterjung:* MAX200x HASYLAB HARWI-II High pressure experiments

Nichtkristalline und Partiellkristalline Strukturen (AK 4)

89-L *B. Müller:* Integrale Strukturinvarianten

Kristallphysik und Strukturelle Phasenumwandlungen (AK 5 und TS 6)

90-L *B. Mihailova, B. Güttler, T. Malcherek, C. Paulmann, R. Stosch, M. Gospodinov, U. Bismayer:* Effect of B"-site cation on the local structure of perovskite-type relaxor ferroelectrics
90-R *D. Klimm, S. Ganschow, R. Bertram:* Segregation in $NaLn(WO_4)_2$
91-L *T. Leisegang, D. C. Meyer, P. Paufler, D. Souptel, G. Behr, B. Bergk, O. Ignatchik, J. Wosnitza, A. Ormeci, H. Rosner:* Röntgenographische Elektronendichtebestimmung von unterschiedlich synthetisierten YNi_2B_2C-Einkristallen
91-R *O. Schmidt, S. Gorfman, W. Morgenroth, A. Pucher, U. Pietsch:* X-ray diffraction study of piezoelectric tensor in BiB_3O_6
92-L *H. Grimmer:* The effect of crystal symmetry on the spectral decomposition of the linear elastic tensor
92-R *P. Becker:* Crystal growth and properties of $LaBO_2MoO_4$
93-L *L. Bohatý, S. Haussühl, J. Liebertz, P. Becker, W.-D. Stein, M. Braden:* Physical properties of PbB_4O_7 and SrB_4O_7
93-R *L. Bohatý, S. Haussühl, L. Bayarjargal, P. Becker:* Mechanical, thermomechanical and optical properties of $RE(HCOO)_3 \cdot 2\ H_2O$ (RE=Y,Er)
94-L *R. Kurtz, C. Paulmann, U. Bismayer:* Thermal Stability of Pb doped Neodymium Molybdate
94-R *L. Wiehl, J. Schreuer, E. Haussühl, K. Removic-Langer, V. Pashchenko, B. Wolf, M. Lang:* Structure and Properties of a New Compound of Copper Oxalate with Hydroxypyridine
95-L *B. Schwarz, H. Weitzel, H. Ehrenberg, H. Fuess:* Correlation between structure and magnetic properties in $Cu(Mo_xW_{1-x})O_4$
95-R *T. Malcherek, U. Bismayer, R. Miletich, C. Paulmann:* Anisotrop-diffuse Streuung in Cadmiumpyroniobat
96-L *K. Sparta, M. Merz, G. Roth, R. Stern, R. Cerny, T. Kimura:* $BaCuSi_2O_6$: structural phase transition at low temperatures
96-R *M. Mühlberg, M. Burianek, P. Görler, B. O. Hildmann, B. Joschko, D. Klimm:* Untersuchungen zum Existenzfeld von $Ca_xBa_{1-x}Nb_2O_6$ (CBN)
97-L *A. Neumann, D. Walter:* Thermoanalytische- und HT-Röntgen-pulverbeugungs-Untersuchungen an Neodymhydroxid $Nd(OH)_3$
97-R *G. Beneke, H. Schmidt, R. Müller, M. Merz, G. Heger:* The mechanism of the structural phase transition in $RbHCO_3$
98-L *K. Konias, F. Hergert, S. Jost, R. Hock, R. Enderle, M. Purwins:* Al-Cu-In intermetallic mixed crystals
98-R *S. C. Vogel, D. Bhattacharyya, G. B. Viswanathan, D. J. Williams, H. L. Fraser:* Phase Transformation Textures in Ti-6Al-4V Alloy

COR-AAD1-00003250
Bayer EX1008 (Part 6 of 9)

Molekülverbindungen (AK 6)

99-L *M. F. Bräu, A. Pfitzner:* Quecksilberhalogenidaddukte

99-R *D. Hoppe, A. Pfitzner:* $Nb_2Cl_{10}(P_4S_{10})_2$

100-L *J. Brüning, C. Buchsbaum, E. Alig, L. Fink, M. U. Schmidt:* Kristallstrukturbestimmung aus Röntgenpulverdaten: Das gelbe Fluoreszenzpigment $C_{36}H_{26}N_4O_4$

100-R *C. Buchsbaum, J. M. Schnorr, M. U. Schmidt:* Bestimmung der Kristallstruktur von $6,6'$-$(CF_3)_2$-Thiazin-Indigo aus Labor-Pulverdaten

101-L *F. Emmerling, R. Köppen, R. Becker:* Kristallstruktur von enantiomerenreinem HBCD

101-R *I. Svoboda, R. Ivaniková, B. Papánková, A. Mašlejová, H. Fuess:* Synthesis, Crystal Structure and Magnetic properties of Complexes of the Type $[M(R_1COO)_2(R_2Im)_2(H_2O)_2]$ (M = Ni,Co; R_1 = H, CH_3; Im = Imidazole, R_2 = CH_3)

102-L *Y. Wang, U. Englert:* Chiral Coordination Polymers

102-R *J. M. Rubin-Preminger, U. Englert:* Hydrogen bond motifs in substituted pyridine dimethylglyoxime cobalt (III) complexes

103-L *C. Q. Ton, O. Söntgen, G. Wagner, E. Egert:* Auf dem Weg zum Design wasserstoffbrücken-gebundener Dimere

103-R *V. W. Kuyitila, H. G. Thomas, G. Raabe:* The Structure of Dicarboxylicaciddimethylestertetramethoxytriphenylene: The Molecular Structure in the Solid State and Quantum-Chemical *ab initio* Calculations

104-L *C. B. Hübschle, B. Dittrich, P. Luger:* Visualisierung von experimentell bestimmten Ladungsdichte-Eigenschaften mit MOLISO

104-R *T. Wagner, E. Görlach:* Zooming in on Friedel Pairs - Single Reflection Intensities from a CCD detector

105-L *W. Kraus, S. Juran, F. Emmerling, H. Stephan:* Strukturelle Charakterisierung neuer Bispidinderivate und ihrer Kupfer(II)-Komplexe

105-R *S. Wallus, W. Frank:* Kaliumethansulfonat-Wasser (5/4): Kristallographische Charakterisierung eines "Scheinmonohydrates"

Theoretische Kristallographie (AK 9)

106-L *D. Orobengoa, C. Capillas, M. I. Aroyo, J. M. Perez-Mato:* SITESYM – A computer program for calculating site-symmetry induced representations of space groups

106-R *K. A. Gernoth:* Symmetries in crystalline one- and two-body densities and generalized Patterson functions: Monte Carlo studies of He quantum crystals

107-L *A. Kirfel, K. F. Fischer, H. Zimmermann:* High Resolution Structure Determination without Fourier Inversion: the Role of Inequalities

107-R *H. Zimmermann, A. Kirfel, K. F. Fischer:* High Resolution Structure Determination without Fourier Inversion: two- and three-dimensional Structures

108-L *B. Müller:* Duale Wirkungsbereichspolyeder und Dirichlet-Konstruktionen

Neutronenstreuung (AK 7)

109-L *M. Meven, V. Hutanu, G. Heger:* HEiDi und seine Anwendungen

109-R *J. Repper, M. Hofmann, U. Garbe, C. Krempaszky:* Bestimmung von Eigenspannungen und Texturen mittels Neutronen in IN718-Flachstauchproben

110-L *U. Garbe, M. Hofmann, H.-G. Brokmeier:* Textur- und Spannungsanalyse am neuen Materialwissenschaftlichen Diffraktometer STRESS-SPEC des FRM-2

110-R *W. Kockelmann, A. Kirfel, M. J. Gutmann, L. C. Chapon, P. G. Radaelli:* Neutron TOF Diffraction Tomography in Archaeometry: First Test Experiments

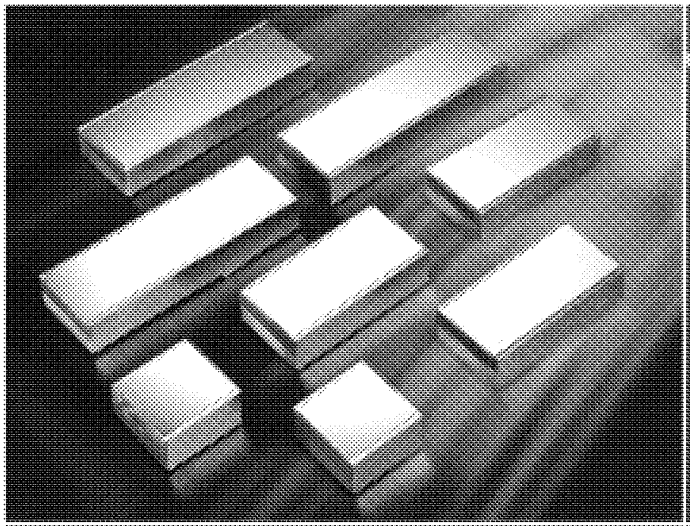
111-L *R. Gilles, D. Mukherji, M. Hoelzel, P. Strunz, D. M. Többens, B. Barbier:* Neutron and X-ray measurements on embedded and extracted precipitates of superalloys

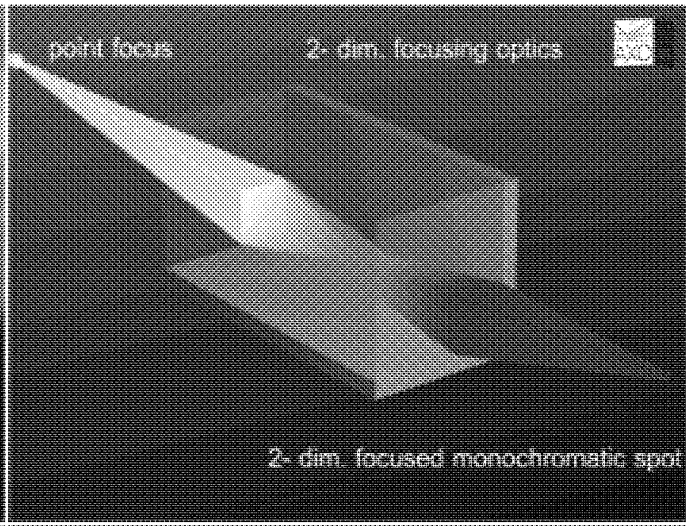
111-R *D. Schaniel, T. Woike, J. Schefer, K. W. Krämer, H. U. Güdel:* Lichtinduzierte Isonitrosyl-Konfiguration in $Na_2[Fe(CN)_5NO]\cdot 2\ H_2O$

COR-AAD1-00003251
Bayer EX1008 (Part 6 of 9)

APPLIED X-RAY OPTICS

Multilayer X-ray Optics
High Precision Deposition





collimating and focusing high precision multilayer X-ray optics for X-ray analysis

Generation of high intense X-ray beams by means of 1- and 2-dimensional X-ray optics

Application in the range of 0.1 keV up to 100 keV

- X-ray analysis
- Spectroscopy
- Tomography
- Lithography
- Astronomy
- Medicine

Services / Offers

- X-ray optical design
- Single X-ray optics
- Complex X-ray optical systems
- Up-grade of all common XRD systems
- Multilayer monochromators for XRF
- Application in XRD, XRR, XRF
- High precision large area deposition by means of PLD and sputtering

AXO

AXO Dresden GmbH
Applied X-ray Optics
Röntgenoptik und Präzisionsbeschichtung

Siegfried-Rädel-Str. 31
01809 Heidenau · Germany
phone: +49-351-2583-249
fax: -49-351-2583-314
contact@axo-dresden.de
www.axo-dresden.de

MORE THAN 10 YEARS EXPERIENCES IN X-RAY OPTICS AND HIGH PRECISION DEPOSITION

112-L *O. Kovalev, H. Gies:* Structure and dynamic of acetone intercalated RUB-18, a layered silicic acid
112-R *O. Schumann, P. Steffens, M. Braden, Y. Sidis, A. Gukasov, J. Kulda, S. Nakatsuji, Y. Maeno:* Magnetismus in 214-Ruthenaten
113-L *E. Mashkina, M. Göbbels, F. Seifert, A. Magerl:* Oxygen mobility in $Sr(Ti_{0.2}Fe_{0.8})O_{3-\delta}$
113-R *H. Kohlmann, F. Werner, K. Yvon:* Die Kristallstrukturen von SmD_3 und $SmMg_2D_7$ mit Neutronenbeugung
114-L *H. Kohlmann:* Neutronenpulverbeugung mit hoch absorbierendem ^{nat}Sm und ^{nat}Eu
114-R *W.-D. Stein, P. Becker, L. Bohatý, A. Cousson, Y. Sidis, K. Hradil, M. Braden:* Structure and lattice dynamics in bismuth triborate

Hochauflösende Röntgenstreuung und Synchrotron-Strahlung (AK 11)

115-L *J. Angelkort, S. van Smaalen, M. Niemeyer, S. O. Hauber:* Charge Density Study on $Eu(SC_{36}H_{49})_2$
115-R *J. Netzel, S. van Smaalen:* Accurate Charge Density of α-Glycine by the Maximum Entropy Method
116-L *A. Preusser, H. Klein:* Darstellung des Orientierungs- und Ortsraumes mittels Hochenergie-Synchrotronstrahlung
116-R *R. Flaig, G. Evans, A. Grant, K. McAuley, T. Sorensen, E. Duke:* Phase 1 Beamlines for Macromolecular Crystallography on Diamond
117-L *M. Hagelstein, T. Baumbach:* Das Ausbauprogramm der Synchrotronstrahlungsquelle ANKA
117-R *S. K. J. Johnas, E. Weckert:* Intensity calibration of a CCD-detector for accurate crystal structure determination
118-L *C. Paulmann, W. Morgenroth, T. Malcherek:* CCD data collection software at crystallographic beamlines D3 and F1

Kristallographie und Spektroskopie (AK 12 und TS 3)

119-L *K. Schwendtner, U. Kolitsch, E. Tillmanns:* $K(H_3O)M^{3+}(HAsO_4)_2(H_2AsO_4)$ (M^{3+} = In, Ga, Fe) – three members of a novel structure type
119-R *S. Schnabel, C. Röhr:* Alkalimetallthiooxovanadate $A_3VS_xO_{4-x}$ (A=Na,K und x=1-4) – Darstellung und Charakterisierung
120-L *J. Göttlicher, S. Mangold, A. N. Sapozhnikov, V. Tauson:* Sulfur Speciation in Lazurites with XANES Spectroscopy and XPS
120-R *W. Lottermoser, W. Treutmann, A. K. Schaper, G. Redhammer, A. Lichtenberger, G. Amthauer:* ^{57}Fe Mössbauer spectroscopy on multi-walled carbon nanotubes with metal filling
121-L *S.-U. Weber, W. Lottermoser, J. Ponahlo, G. Amthauer, A. Bieniok:* ^{57}Fe-Mössbauer spectroscopic and X-ray single-crystal investigation of natural alexandrite
121-R *M. M. Murshed, T. M. Gesing:* Synthesis and structural studies on a series of alumogallosilicate hydro-hydroxy sodalites
122-L *A. Wozniak, B. Marler, H. Gies:* Investigation of water and lithium sites during partial hydration of zeolite Li-LSX

Pulverdiffraktometrie (AK 13)

123-L *S. Schorr, M. Tovar, D. Sheptyakov:* Electronic similar elements on different structural sites: a solution by neutron powder diffraction
123-R *M. Baier, A. Magerl, R. Hock:* A laboratory high-energy diffractometer for the investigation of polycrystalline materials
124-L *J. Aufrecht, A. Leineweber, E. J. Mittemeijer:* Kugelmahlen von Fe-N-Legierungen: die Natur des erweiterten α-Fe[N]-Mischkristalls
124-R *S. Jost, F. Hergert, R. Hock, M. Purwins, R. Enderle:* Background suppression with a triple beam-stop setup

COR-AAD1-00003253
Bayer EX1008 (Part 6 of 9)

125-L *D. Trots, M. Knapp, A. Skomorokhov, H. Fuess:* Structural behaviour of superionic copper selenide, $Cu_{2-\delta}Se$ (δ = 0-0.25), in dependence on temperature
125-R *M. Martinez, E. Schweda:* In Situ Untersuchung der Nitridierung von Zirconium-Scandium-Oxiden (II)
126-L *S. Meyer, E. Schweda:* Die Reaktion von ZrO_2/CeO_2 mit NH_3
126-R *S.-H. Park, H. Boysen, M. Hölzel:* Rietveld analysis with VT neutron powder diffraction data of sogdianite
127-L *S. Lenser, H.-G. Brokmeier, V. Ventzke, M. Kocak:* Materialcharakterisierung und Texturanalyse von lasergeschweißten Al-Legierungen (AA5083H111 und AA6013T6)
127-R *K. A. Schoenau, M. Knapp, L. A. Schmitt, N. Balke, R. Theissmann, H. Fuess, H. Kungl, M. Leoni, P. Scardi:* Reaktion der Domänenstruktur von morphotropen PZT Keramiken auf elektrisches Feld – in-situ Synchrotron Pulverdiffraktion
128-L *B. Hasse, W. Reimers:* Bestimmung von Spannungsfeldern mit hoher Ortsauflösung

Computational Crystallography (AK 14)

129-L *D. J. Wilson, B. Winkler, V. Milman, P. Murray-Rust, M. Dove:* MaterialsGrid: A Dynamic Database of Calculated Crystal Properties
129-R *M. Kroeker, L. W. Finger, B. H. Toby:* DRAWxtl 5.3
130-L *T. Bredow, M.-W. Lumey, R. Dronskowski, H. Schilling, J. Pickardt, M. Lerch:* Structure and stability of TaON polymorphs
130-R *V. L. Vinograd, E. A. Juarez-Arellano, J. D. Gale, B. Winkler:* Monte Carlo simulation of crystallographic site occupancies in $SrYbSi_2Al_2O_2N_5$
131-L *R. Wang, U. Englert:* Computersimulation von Molekülverbindungen: Parametrisierung für H-Brückenbindungen und exotische Atomtypen
131-R *E. Keller, V. Krämer:* Isotype "Ionen"größendifferenzen I+II
132-L *B. Hinrichsen, F. Hergert, R. E. Dinnebier, M. Jansen, R. Hock:* Two-dimensional intensity corrections for in situ X-ray powder diffraction
132-R *R. Paneerselvam, B. Hinrichsen, M. Joswig, R. E. Dinnebier, M. Jansen:* Detection of ellipses in powder diffraction patterns using Hough transformation
133-L *V. Thome, M. Heppenstall-Butler, P. Murray-Rust:* Workflows for High-throughput Computational Crystallography

Mineralogische und Technische Kristallographie (AK 15)

134-L *A. Hösch, C. Kotré, H. McSheep:* XRD and microscopic studies on powder components of dental zinc phosphate cements
134-R *H. Pöllmann, S. Stöber:* Synthese und Charakterisierung von Metall-Phenolsulfonathydraten
135-L *P. B. Kempa, M. Herrmann:* Quantitative Analyse von Kaolin
135-R *I. P. Shakhverdova, N. Pätzke, S. K. Filatov, R. S. Bubnova, A. A. Levin, D. C. Meyer, M. I. Georgievskaya, P. Paufler:* Comparison of mechanical properties and structure of glass-like with crystalline phases of some alkali borosilicates and borates
136-L *M. Zötzl, H. Pöllmann:* Einbau von Mg + Si in einen Al-reichen Mn-Brownmillerit durch Rekristallisation aus der Schmelze
136-R *S. Stöber, M. Zötzl, H. Pöllmann:* Kristallchemie im System $Ca_2Mn_{2-2x}Al_{2x}O_{5\pm d}$ mit $0.50 < x < 0.66$
137-L *C. Weidenthaler, W. Schmidt:* Kristallographische Untersuchungen an quaternären Spinellen
137-R *U. Kolitsch, M. Wierzbicka, E. Tillmanns:* An unusually narrow Si-O-Si angle in the new disilicate $BaKYSi_2O_7$
138-L *M. Stockmeier, A. A. Rempel, M. Gomm, A. Magerl:* High-accuracy lattice constant measurements on boron and nitrogen doped 6H-SiC single crystals
138-R *U. Kolitsch, G. Giester:* Rankachite, an unusual oxidic Ca-Fe-V-W-mineral from the Clara mine, Central Black Forest: crystal structure and revision of symmetry, unit cell and chemical formula
139-L *A. Hösch, C. Kotre, H. McSheep:* Phasenanalytische Untersuchungen von Sulfatschädigungen an Betonwänden eines Stauwerks

COR-AAD1-00003254
Bayer EX1008 (Part 6 of 9)

Kristallchemie und modulierte Strukturen (AK 16 und TS 7)

140-L *I. Kaiser-Bischoff, H. Boysen, M. Lerch, C. Rödel, C. Paulmann:* Superstructures in Sc/Mg- and N-doped Zirconia

140-R *I. Kaiser-Bischoff, G. Geudtner, H. Boysen, T. Bredow:* Diffuse Streuung an Zirkonia: Experiment und ab-initio Rechnungen

141-L *J. M. Simons, M. Merz, G. Heger, A. G. Soldatov, S. V. Shiryaev, S. N. Barilo:* $DyBaCo_2O_{5+x}$: Temperaturabhängige Diffraktionsuntersuchungen an Einkristallen und Pulverproben

141-R *C. Hoch, A. Simon:* Tetramethylammoniumamalgam

142-L *W. Hornfeck, F. R. Wagner, Y. Grin, B. Harbrecht:* IrZn - Struktur und Bindung

142-R *C. Allio, D. Eppers, B. Harbrecht:* Zur Kenntnis von $RuZn_3$ und $Ru_{13-\delta}Zn_{128+\delta}$

143-L *B. Wahl, V. Dubenskyy, M. Ruck:* Mehrlingsbildung in dem Subbromid Bi_9AuBr_9

143-R *S.-H. Park, H. Boysen, C. Paulmann:* Structural defects in the zeolite-like lithosilicate RUB-30

144-L *P. Schaub, T. Weber, W. Steurer:* Bestimmung der Realstruktur fehlgeordneter Kristalle mit Hilfe der dreidimensionalen Paarverteilungsfunktion

Kristallographie in der Lehre

145-L *A. Danilewsky, J. Wittge:* Übungen zur Grundvorlesung "Kristalle" im Internet

Oberflächen und Grenzflächen (AK 18)

146-L *J. Schneider, G. Brunauer, I. Kaiser-Bischoff, W. W. Schmahl:* X-ray studies of the Cuttlefish Bone of Sepia Officinalis

146-R *X. Wang, A. Klocke, B. Mihailova, R. Stosch, B. Güttler, U. Bismayer:* Effect of bleaching on chemical and structural changes of dental hard tissues

147-L *A. Pareek, U. Magdans, H. Gies, X. Torrelles, J. Rius:* Investigation of Fluorapatite (100) surface by GIXRD techniques under different stages of hydration

147-R *L. Kirste, S. Müller, R. Kiefer, R. Quay, K. Köhler, N. Herres:* Recognition and imaging of defects by spatially resolved X-ray diffraction measurements on (Al,Ga)N/GaN/4H-SiC(0001) heterostructures for electronic devices

148-L *J. Kräußlich, C. Dubs, A. Lorenz, H. Tünnermann:* Gitterparameterbestimmung von auf kongruenten $LiNbO_3$-Substraten gewachsenen homoepitaktischen Zn:$LiNbO_3$-Schichten

Kristallchemie (AK 19)

149-L *N.-D. Van, T. Schleid:* Structure of Dicesium Undecahydromonohydroxo-*closo*-Dodecaborate-Monohydrate, $Cs_2[B_{12}H_{11}(OH)] \cdot H_2O$

149-R *N. Vojteer, H. Hillebrecht:* Einkristalle von LiB_{10}

150-L *T. Ludwig, N. Vojteer, H. Hillebrecht:* $Mg_{1.3}Si_{0.1}B_{12}$ und $Mg_{0.6}Li_{0.67}B_{12}$ – Ternäre Varianten der binären borreichen Boride α-AlB_{12} und MgB_{12}

150-R *D. Kotzott, M. Ade, M. Robertson, H. Hillebrecht:* Zwei Modifikationen von Cr_2IrB_2 mit tetrameren B_4-Einheiten

151-L *M. Ade, D. Kotzott, M. Robertson, H. Hillebrecht:* Einkristalluntersuchungen der τ-Boride $ÜM_{23-x}Ir_xB_{6+y}$ mit ÜM = Cr, Fe, Co, Ni

151-R *R.-D. Hoffmann, R. Pöttgen, B. Rohrmoser, W. Scherer:* Sc_3FeC_4 – Eine Studie zur experimentellen Elektronendichte

152-L *C. Schmolke, O. Oeckler, W. Schnick:* Die Kristallstruktur von $Sm_2[Si_4N_6C]$ und ihre Verwandtschaft mit $BaYb[Si_4N_7]$ und $Ho_2[Si_4N_6C]$

152-R *H. Schilling, H. Wolff, R. Dronskowski, M. Lerch:* Fluorite-Type Solid Solutions in the System Y-Ta-O-N: A Nitrogen-Rich Analogue to Yttria-Stabilized Zirconia (YSZ)

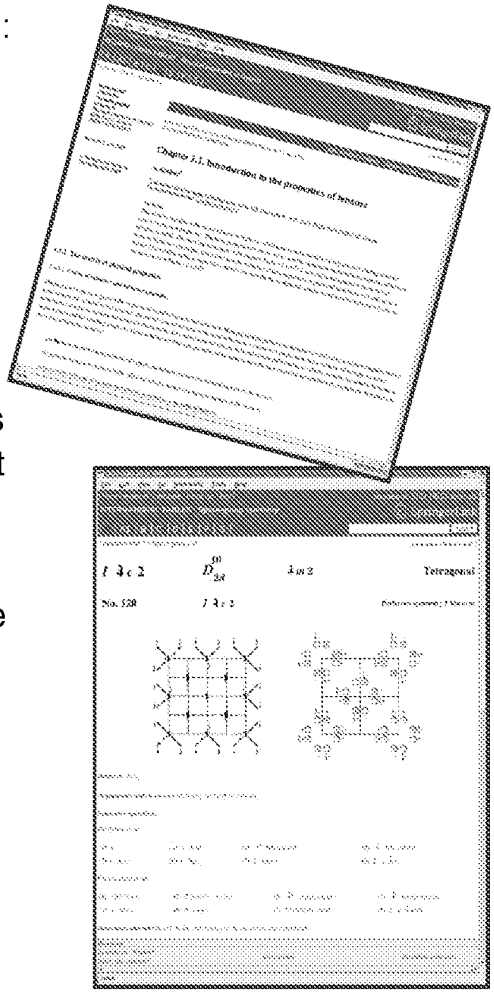
153-L *F. Lissner, T. Schleid:* $La_4N_2S_3$: Lanthanum Nitride Sulfide with an Unprecedented Crystal Structure

153-R *M. Neukirch, S. Tragl, H.-J. Meyer:* $Sm_2(CN_2)_3$ and $Dy_2(CN_2)_3$: The first rare earth carbodiimides with trivalent cations

COR-AAD1-00003255
Bayer EX1008 (Part 6 of 9)

International Tables Online

- Full text of all eight volumes (6000 pages) in pdf and html formats
- Ability to navigate rapidly through the volumes: choose to view a full chapter, a section or a subsection, a single table or just a figure
- Specific hyperlinking from each chapter to related chapters in the series
- Searching by author and by subject, and of titles, abstracts and full text. Full-text searches will link directly to the highlighted search result within the relevant section
- Comprehensive indexes with links direct to the relevant content
- Citation links to IUCr journals; CrossRef, ChemPort and PubMed linking
- Space-group tables with extensive linking between sub- and supergroups
- Updated content immediately available



Available in 2006 from the IUCr and SpringerLink

it.iucr.org

COR-AAD1-00003256
Bayer EX1008 (Part 6 of 9)

154-L *F. Gerlach, O. Büchner, M. S. Wickleder:* Tetranitratoaurate M[Au(NO_3)$_4$], (M = K, Ag, NO_2, Rb, NH_4, Cs)

154-R *T. Bongardt, A. Adam:* Synthese und Kristallstrukturen zweikerniger Chrom(II)-Komplexe des Typs $M_4[Cr_2[CO_3]_4(H_2O)_2] \cdot n\ H_2O$ mit M = K, Rb

155-L *A. Jonušaite, A. Adam:* Stabilisierung des Monomethylcarbonat-Ions in [Cs(18-Krone-6)(CH_3CO_3)]

155-R *S. Gomez Torres, G. Meyer:* Zwei Hydroacetate der Seltenerdmetalle

156-L *V. Kahlenberg, W. Wertl, A. Kremenovic, A. Schwärzler, H. Schottenberger:* Structural investigations and thermal behaviour of $(H_3O^+)[Cr(C_2O_4)_2]^- \cdot 2\ H_2O$

156-R *N. Cesur, G. Meyer:* $[Mn(II) - (C_6NO_2H_4)_{4/2}]_\infty$ – Eine Verbindung mit dimeren Mn(II)-Mn(II) Einheiten

157-L *E. Irran:* Kristallstruktur der Amidosulfate $M(NH_2SO_3)_2 \cdot 2\ H_2O$ ($M=Cd^{2+}$, Cu^{2+}) und $Cd(NH_2SO_3)_2$

157-R *A. Mietrach, I. Parchmann, M. S. Wickleder:* Synthese, Kristallstruktur und thermischer Abbau von $[Cu(H_2O)_2((NH_2)C_6H_4(SO_3))_2] \cdot 2\ H_2O$

158-L *K. Müller-Buschbaum, C. C. Quitmann:* Oligomere Bausteine beim Aufbau von Koordinationspolymeren der Lanthanoide mit Pyrazol

158-R *K. Müller-Buschbaum, Y. Mokaddem:* $^3_\infty[Eu_2(Tz)_5(TzH)_2]$, ein kristallographisch anspruchsvolles, gemischtvalentes Amid mit Raumnetzstruktur

159-L *S. Rayaprol, R. Pöttgen:* New Heavy-Fermion System Ce_2Au_2Cd

159-R *S. Lange, T. Nilges, R.-D. Hoffmann, F. M. Schappacher, R. Pöttgen:* Die Stannide $AuNiSn_2$, $AuCuSn_2$ und $AuPdSn_2$ – Synthese, Überstruktur und ^{119}Sn Mössbauer-Spektroskopie

160-L *G. Heymann, J. F. Riecken, R.-D. Hoffmann, U. C. Rodewald, S. Rayaprol, H. Huppertz, R. Pöttgen:* Die Hochdruck-Phasen der Stannide CeNiSn, CePdSn und REPtSn (RE = Ce, Pr, Nd)

160-R *W. Harms, C. Röhr:* Der binäre Schnitt $Ca(Ga_{1-x}Cd_x)_2$: Experimentelle und theoretische Untersuchungen

161-L *R. Zaremba, U. C. Rodewald, R. Pöttgen:* Synthese und Struktur der metallreichen kubischen Verbindungen RE_4RhIn (RE = Gd-Tm, Lu) und Gd_4IrIn

161-R *M. Wendorff, C. Röhr:* Ca_4AlSn_3 und Ca_2AlSn_3: Neue ternäre Phasen im System Ca-Al-Sn

162-L *M. Rhode, C. Röhr:* $Sr_{10}[Al_4Ge_6][O]$: Ein neuer Vertreter einer ungewöhnlichen Verbindungsklasse

162-R *K. Guttsche, M. Wendorff, C. Röhr:* Ba_5M_5Sn (M=Al, Ga) – Chemische Zwillinge aus Zintl- und Laves- Phase

163-L *D. Petri, C. Röhr:* Die klassische Zintl-Phase $RbSb_2$: Darstellung, Struktur und Bindung

163-R *S. T. Kong, C. Reiner, H.-J. Deiseroth:* Synthesis and structure of Lithium tin sulphide, Li_4SnS_4

164-L *T. Komm, T. Schleid:* $K_3Ho_3[PS_4]_4$: Ein Kalium-Holmium-Thiophosphat mit dreidimensionalem Aufbau

164-R *M. Gjikaj:* Ein neues Alkalimetall-Hexathiometadiphosphat, $Rb_2P_2S_6$

165-L *M. Gjikaj, A. Adam:* Stabilisierung hochreaktiver "nackter" Anionen: Darstellung, Kristallstruktur und Schwingungsspektrum von $[Na(12\text{-Krone-}4)_2]_2[P_2S_6] \cdot CH_3CN$

165-R *F. A. Weber, A. Elbe, T. Schleid:* Synthese und Kristallstruktur von Caesium-Neodym(III)-Diselenid $CsNdSe_2$ im α-$NaFeO_2$-Typ

166-L *H. Ajaz, M. Wagener, C. Reiner, H.-J. Deiseroth:* Synthesis and Crystal Structure of $PdBr_2Se_6$

166-R *C. Löhnert, D. Bichler, D. Johrendt:* $Ni_7Pd_4Te_8$ - Ein metallreiches Tellurid

167-L *M. C. Schäfer, T. Nikelski, T. Schleid:* $LaBr(BO_2)_2$: Das erste Selten-Erd-Metall(III)-Bromid-Oxoborat

167-R *G. Heymann, T. Soltner, A. Haberer, H. Huppertz:* δ-$RE(BO_2)_3$ ($\equiv$ δ-REB_3O6): Eine neue Hochdruckmodifikation der Selten-Erd *meta*-Oxoborate des Lanthans und Cers

168-L *T. M. Gesing, S. Germerott, C. H. Rüscher:* Sr Substitution in $Bi_2Al_4O_9$

168-R *M. Dogan, H.-D. Wiemhöfer, M. M. Guenter, M. Lerch, H. Boysen, D. Toebbens, E. Suard, C. Baehtz:* Sr/Mg-dotiertes Lanthangallat: Zur Korrelation zwischen elektrischer Leitfähigkeit und Kristallstruktur

COR-AAD1-00003257
Bayer EX1008 (Part 6 of 9)

169-L *T. Höfs, T. M. Gesing, C. H. Rüscher, J.-C. Buhl:* Synthesis and characterization of alumino-germanate borontetrahydride enclathrated sodalite $Na_8[AlGeO_4]_6(BH_4)_2$

169-R *I. Hartenbach, T. Schleid:* Die *Fluorapatit*-Struktur als Bauprinzip für das Europium(III)-Oxid-Oxosilicat $Eu_{4,667}O[SiO_4]_3$

170-L *D. H. Kang, T. Schleid:* $Sm_5[AsO_4][SiO_4][Si_3O_{10}]$: Ein recht ungewöhnlich aufgebautes Samarium(III)-Oxoarsenat(V)-Oxosilicat(IV)

170-R *M. Weil:* Crystal Structure of a Novel $Ca(PO_3)_2$ Polymorph

171-L *H. A. Höppe, S. Sedlmaier:* Die Kristallstruktur der späten Lanthanoid-Polyphosphate LnP_3O_9 (*Ln* = Dy, Ho, Er, Yb)

171-R *C. Lipp, T. Schleid:* $RbErCl_2[SeO_3]$: The First RbCl Derivative of $ErCl[SeO_3]$

172-L *A. Arndt, M. S. Wickleder:* $PdSeO_3$: Das erste Selenit der Platinmetalle

172-R *M. Ben Hamida, M. S. Wickleder:* Übergangsmetallarme Chlorid-Oxo-Selenate (IV) der Selten-Erd-Elemente

173-L *P. Höss, T. Schleid:* $Y_{11}ClTe_{16}O_{48}$: Ein sehr chloridarmes Yttrium-Chlorid-Oxotellurat(IV)

173-R *B. Veličkov, F. Emmerling, R. Bertram, M. Bernhagen:* Kristallchemie von $SEScO_3$ Einkristallen (SE = Dy, Gd, Sm)

174-L *S. Prinz, G. Roth:* Strukturelle Entwicklung des CaV_3O_7 zu tiefen Temperaturen

174-R *S. Prinz, G. Roth:* Struktur des $Cs_2Cl_2CuV_2O_6$

175-L *T. Debnath, C. H. Rüscher, T. M. Gesing, A. Hussain:* Phase separation into two cubic perovskites in the system $Na_{0.8}W_{1-y}Nb_yO_3$

175-R *G. Frisch, C. Röhr:* Neue Dimetallate der Alkalimetalle: $Cs_6[Cr_2O_7]$ und $Cs_6[Ge_2O_7]$

176-L *M. Wierzbicka, U. Kolitsch, E. Tillmanns:* $Rb_5Fe(MoO_4)_4$ – a novel stucture type with isolated $Fe_2Mo_8O_{32}$ clusters

176-R *T. M. Gesing, C. H. Rüscher:* Spektroskopische und Röntgen-Einkristalluntersuchungen an $Bi_2Fe_4O_9$

177-L *L. Kienle, P. Adler, J. Strempfer, B. Keimer, V. Duppel, F. Phillip:* Zur Realstruktur der Perowskitphasen $SrFeO_{3-\delta}$ ($\delta \leq 0.05$)

177-R *D. Mikhailova, H. Ehrenberg, H. Fuess:* Synthesis and structure determination of copper perrhenate, $CuReO_4$

178-L *M. Weisser, S. Tragl, H.-J. Meyer:* Aufklärung der Kristallstruktur von $Na_3[W_3Cl_{13}]$

178-R *J. Beekhuizen, G. Meyer:* Ternäre Halogenide des dreiwertigen Titans: Verbindungen vom Typ A_3TiX_6 (A = Cs-Na; X = Br-Cl)

179-L *E. Keller, V. Krämer:* Anmerkungen zum Wang-Liebau'schen Asphärizitätsvektor Φ

179-R *E. Keller, V. Krämer:* Starke Abweichungen von der Vegard'schen Regel

COR-AAD1-00003258
Bayer EX1008 (Part 6 of 9)

Weitere Veranstaltungen

Mitgliederversammlung

Die jährliche Sitzung aller Mitglieder der DGK findet am Dienstag, 18:30 Uhr, in der Aula statt.

Treffen der Arbeitskreise

Die Termine für die Treffen der Arbeitskreise (nach AK-Nummern) sind:

1: (Biologische Strukturen): Mittwoch, 18:00 Uhr (nach der Postersession II, HS 1199)

3: (Elektronenmikroskopie): Montag, 16:45 Uhr (im Anschluss an das Mikrosymposium des AK3, HS 1199)

5: (Kristallphysik): Dienstag, 16:15 Uhr (im Anschluss an das Mikrosymposium des TS6, HS 1010)

6: (Molekülverbindungen): Montag, 16:45 Uhr (HS 1010)

7: (Neutronenstreuung): Dienstag, 16:05 Uhr (im Anschluss an das Mikrosymposium zu TS 5, HS 1015)

12: (NMR-Spektroskopie): Dienstag, 12:15 Uhr (im Anschluss an das AK-Mikrosymposium, HS 1015)

13: (Pulverdiffraktometrie): Dienstag, 12:15-13:00 Uhr (im Anschluss an das AK-Mikrosymposium, HS 1010)

18: (Oberflächen und Grenzflächen): Mittwoch, 12:15 Uhr (im Anschluss an das AK-Mikrosymposium, HS 1015)

19: (Kristallchemie): Mittwoch, 16:15 Uhr (im Anschluss an das Mikrosymposium zu TS 7, HS 1010)

Termine für weitere Arbeitskreis-Treffen werden vor Ort bekanntgegeben.

Gesellschaftsabend

Am Mittwoch abend (Einlass ab 19:30 Uhr, Ende: 24:00 Uhr) findet im Restaurant *Le Buffet* (Kaufhaus Karstadt, Kaiser-Joseph-Straße 165) der Gesellschaftsabend statt. Die Kosten für die Speisen sind im Tagungsbeitrag enthalten, Getränke sind selbst zu bezahlen. Sie erhalten mit Ihren Tagungsunterlagen eine Eintrittskarte mit Wegbeschreibung. Bitte vergessen Sie nicht, diese Karte zur Abendveranstaltung mitzubringen. Im Rahmen des Gesellschaftsabends werden die Posterpreise verliehen.

COR-AAD1-00003259
Bayer EX1008 (Part 6 of 9)

Sehenswertes ...

- ... in Freiburg
  - Münster (Hochaltar von Hans Baldung Grien, 1516; Glasfenster aus dem 14. Jh.), täglich Wochenmarkt auf dem Münsterplatz; Münster-Turm leider derzeit eingerüstet und Plattform geschlossen
  - Historisches Kaufhaus von 1532 und Kornhaus von 1497 (Münsterplatz)
  - Schlossberg (mit Aussichtsturm und Biergarten)
  - Stadttore (Martinstor, Schwabentor)
  - Hotel zum Roten Bären von 1311 (am Schwabentor)
  - Mineralogisches Institut der Universität (*Geohaus*; Mineraliensammlung, Institutsviertel, Albertstr. 23b)
  - Planetarium (am Bahnhof, Bismarckallee 7g)
  - Botanischer Garten (Schänzlestr. 1)
  - Adelhauser-Museum für Natur- und Völkerkunde, Gerberau 32
  - Augustiner-Museum, Augustinerplatz 1-3 (Kunst und Kunsthandwerk vom Mittelalter bis ins 20. Jahrundert)
  - Museum für Stadtgeschichte, Münsterplatz 30
  - Museum für Ur- und Frühgeschichte, im Colombi-Schlössle, Rotteckring 5
  - Museum für Neue Kunst, Marienstr. 10a
  - Uniseum, Alte Universität, Bertoldstr. 17
  - Freiburg Kultour, Stadtführungen, Rotteckring 14
    (Tel.: 0049-761-2907447, www.freiburg-kultour.com)
  - Historix-Tour, Treffpunkt am Predigertor (nächtliche Stadtführungen)
  - Bahnhofsturm (Club Kagan, schöne Aussicht)
  - Theater und Konzerte (Großes und Kleines Haus mit Kammerbühne, Bertholdstr. 46; Konzerthaus, Konrad-Adenauer-Platz 1; E-Werk, Eschholzstr. 77; Alemannische Bühne, Gerberau 15; Theater am Martinstor, Kaiser-Joseph.Str. 237; Galli-Theater, Haslacher Str. 15; ...)
    (Karten zu Theater- und Konzert-Veranstaltungen: BZ-Kartenservice, Tel.: 01805-556656, www.freiburg-ticket.de)
  - Clubs (Jazzhaus, Schnewlinstr. 1; KGB-Sowjet-Bar, Friedrichring 23; Kagan, Bismarckallee 9; Agar, Löwenstr. 8; Waldsee, Waldseestr. 84; Jos-Fritz-Cafe, Wilhelmstr. 15; Drifters Club, Schnewelinstr. 7; ...)
- ... und Umgebung
  - Schauinsland mit Besucherbergwerk (Seilbahn derzeit leider gerade in Reparatur)
  - Süd-Schwarzwald (z.B. Titisee, Schluchsee usw. in 30 min. per Höllental-Bahn erreichbar)
  - Kaiserstuhl, Breisach (in 20 min. per Breisgau-S-Bahn erreichbar), Festung Neuf-Brisach (Frankreich)
  - Markgräflerland, Staufen mit Burg, Sulzburg (Landesbergbaumuseum und Kirche St. Cyriak, 10. Jh.)
  - Elsass, Strassbourg, Colmar, Frankreich
  - Basel (versch. Museen, Tierpark Zolli, Botanischer Garten), Schweiz (in 30 min. per ICE erreichbar)

COR-AAD1-00003260
Bayer EX1008 (Part 6 of 9)

Sponsoren und Aussteller

Die Tagungsleitung möchte sich im Namen der Deutschen Gesellschaft für Kristallographie bei den nachstehend aufgeführten Firmen und Institutionen für die finanzielle und materielle Unterstützung der Tagung bedanken.

- AXO-DRESDEN GmbH, Heidenau
- Bruker AXS GmbH, Karlsruhe
- Crystal Impact GbR, Bonn
- CrystalMaker Software Ltd., Oxfordshire
- Gesellschaft für Thermische Analyse e.V.
- Greiner Bio-One GmbH, Frickenhausen
- GE Inspection Technologies GmbH, Ahrensburg
- HÜTTINGER Elektronik GmbH + Co. KG, Freiburg
- Incoatec GmbH, Geesthacht
- International Union of Crystallography (IUCr), Chester
- JCM, Frankfurt/M.
- Linn High Therm GmbH, Eschenfelden
- Marresearch GmbH, Norderstedt
- MaTeck GmbH, Jülich
- MICOS GmbH, Eschbach
- NETZSCH-Gerätebau GmbH, Selb
- Oldenbourg Wissenschaftsverlag GmbH, München
- Oxford Diffraction Ltd., Oxfordshire
- PANalytical GmbH, Kassel
- Rigaku America Inc., The Woodlands, Texas
- Röntgenlabor Dr. Ermrich, Reinheim
- SCIMED GmbH, Isselburg
- Sintec Keramik GmbH & Co. KG, Halblech
- STOE & CIE GmbH, Darmstadt
- WILEY-VCH Verlag GmbH & Co. KGaA, Weinheim
- Well Diamantdrahtsägen GmbH, Mannheim
- XENOCS, Sassenage
- Carl Zeiss MicroImaging GmbH, Göttingen

Die Firmenausstellung findet während des gesamten Tagungszeitraums in der Eingangshalle und der Prometheus-Halle des Kollegiengebäudes I der Universität (s. Lagepläne S. 43) statt. Die Eröffnung der Ausstellung erfolgt am 3. April 2006 um 13 Uhr in der Aula der Universität Freiburg.

Wir laden Sie herzlich ein, die Firmenstände zu besuchen und sich über die neusten Methoden, Geräte und Produkte zu informieren.

Wir bedanken uns bei der Firma HÜTTINGER Elektronik GmbH + Co. KG für die Bereitstellung der Tagungstaschen und der Umhängebänder.

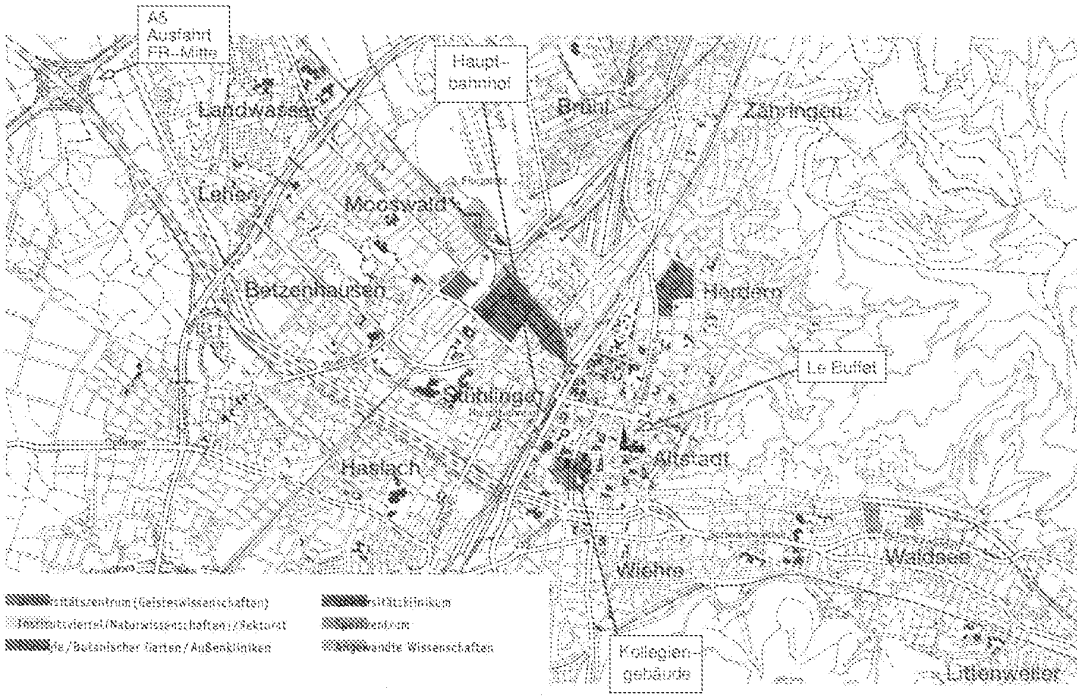




COR-AAD1-00003261
Bayer EX1008 (Part 6 of 9)

Allgemeine Hinweise

Anreise



- Mit der Bahn: Der Freiburger Hauptbahnhof ist ein EC/ICE-Haltepunkt mit stündlicher Anbindung nach Norden und Süden. Von der Stadtbahnbrücke oberhalb des Hauptbahnhofs können Sie jede Straßenbahn nehmen, die in östlicher Richtung fährt (Richtung Stadtmitte, Schwarzwald). Steigen Sie bei der ersten Haltestelle *Stadttheater* aus. Von dort sind es drei Gehminuten zum Veranstaltungsort. Sie erreichen den Veranstaltungsort ab Freiburg Hauptbahnhof auch zu Fuß in nur 10 Gehminuten.
- Mit dem Auto: Freiburg ist von Norden und Süden über die A5 erreichbar. Von der Ausfahrt Freiburg Mitte aus erreichen Sie den Tagungsort über den Autobahnzubringer-Mitte. Allerdings empfehlen wir Ihnen, den Tagungsort möglichst nicht mit dem Auto anzufahren, Parkplätze sind äußerst begrenzt und gebührenpflichtig. Bitte fahren Sie die P+R-Parkplätze bzw. Hotelparkplätze an und nehmen Sie das gute Angebot der öffentlichen Verkehrsmittel in Anspruch.
- Mit dem Flugzeug: Euro-Airport Basel-Mulhouse; von dort besteht eine Air-Bus-Verbindung (Telefon 0761/500 500) zum Zentralen Omnibusbahnhof/Hauptbahnhof Freiburg. Ab Freiburg Hauptbahnhof laufen Sie oder fahren Sie mit der Straßenbahn wie oben beschrieben zum Veranstaltungsort.

Öffentlicher Nahverkehr

Der Tagungsort kann sowohl vom Hauptbahnhof Freiburg (s.o.) als auch vom zentralen Haltepunkt der meisten Linien der VAG (Busse und Straßenbahnen), der Station *Bertholdsbrunnen*, in wenigen Minuten zu Fuß erreicht werden.

COR-AAD1-00003262
Bayer EX1008 (Part 6 of 9)

Unterkunft, Hotel-Reservierung

Hotel- und Zimmerreservierungen sind über *FIT - Freiburg Incoming & Touristik* (Am Bischofskreuz 1, 79114 Freiburg, Uni-Hotline 0761/88581-169; FAX: 0761-88581-149; E-Mail: info@freiburg-tourist.de; WEB: www.freiburg-tourist.de) möglich.

Tagungsgebühr

Die Teilnahmegebühren betragen ...

bei Bezahlung	bis zum 31.12.2005	ab dem 1.1.2006
Mitglieder	85 Euro	110 Euro
Nichtmitglieder	110 Euro	135 Euro
Studierende/Doktoranden	50 Euro	50 Euro

... und beinhalten:

- Teilnahme am wissenschaftlichen Programm
- Tagungsunterlagen
- Pausenverpflegung (exkl. Mittagessen)
- Teilnahme am Gesellschaftsabend am Mittwoch 05.04.2006 (exkl. Getränke) Hinweis: Nicht als Tagungsteilnehmer registrierte Begleitpersonen bezahlen einen Kostenbeitrag von 25 Euro.

Namensschilder

Die Namensschilder erhalten Sie im Tagungsbüro bei der Anmeldung. Sie gelten als Eintrittsausweis und sollten während der Veranstaltung getragen werden.

Verpflegung

Der Tagungsort liegt in der Innenstadt von Freiburg mit zahlreichen Restaurants, Gaststätten und Imbissmöglichkeiten. Eine Liste empfehlenswerter Lokale liegt im Tagungsbüro aus. In unmittelbarer Nähe liegt auch die Mensa Hochallee. Gäste können dort im Foyer am Service-Point gegen Pfand eine Geldkarte erhalten. Es gibt dort die verschiedensten Angebote, vom kleinen Imbiss bis zum Menü können Sie aus einem reichhaltigen Sortiment auswählen.

Internet-Zugang für Teilnehmer/innen

Im Tagungbereich ist ein offenes WLAN eingerichtet. Ferner finden Sie im Raum 1140/1141 mehrere Terminals des Rechenzentrums.

Technische Hinweise zu den Postern

Die Posterausstellung findet in der Eingangshalle sowie in der darüber liegenden Prometheushalle im Kollegiengebäude I statt (s. Lagepläne S. 43). Die maximale Postergrösse beträgt 150 x 120 cm (Höhe x Breite), Befestigungsmaterial wird gestellt und befindet sich an den Stellwänden. Alle Poster können während der gesamten Tagung präsentiert werden. In den beiden Postersessions am Dienstag und Mittwoch (jeweils 16:30 bis

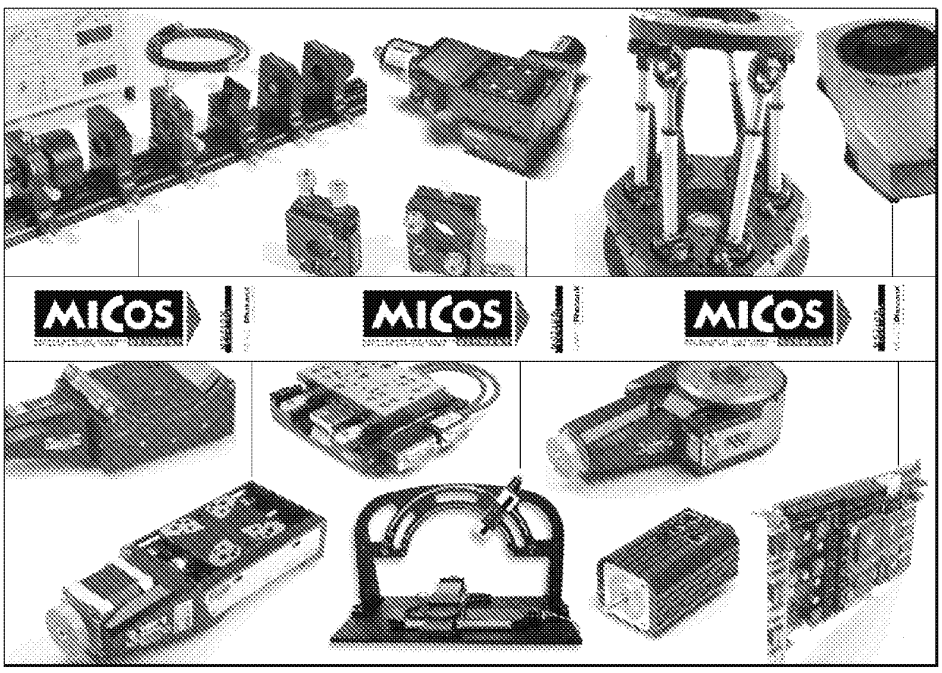
COR-AAD1-00003263
Bayer EX1008 (Part 6 of 9)

18:00 Uhr) werden die Autorinnen und Autoren der Poster, deren Abstracts in der linken (Dienstag, Nr. xx-L) bzw. rechten (Mittwoch, Nr. xx-R) Spalte des Tagungsbands abgedruckt sind, gebeten, am Poster für Fragen und Diskussionen zur Verfügung zu stehen. Entfernen Sie bitte Ihr Poster bis spätestens 6. April, 14 Uhr, danach werden nicht abgehängte Poster entsorgt.

Technische Hinweise zu den Vorträgen

In den Hörsälen Aula, 1010, 1199 und 1015 stehen Beamer und Laptops mit Internet-Zugang für ihre Präsentation zur Verfügung. Wir bitten alle Vortragende, sich spätestens eine Stunde vor Beginn des Mikrosymposiums oder des Plenarvortrags in der Medien-Annahme (R 1142) zu melden und Ihre Präsentation zu prüfen, um einen reibungslosen Ablauf der Veranstaltung zu sichern. Die Präsentation sollte auf einer Daten-CD oder einem USB-Memory-Stick zum Kopieren bereitstehen. Sie wird auf den Tagungslaptop kopiert und zusammen mit den Autoren auf Korrektheit geprüft, ggf. angepasst. Die Tagungslaptops haben als Betriebssystem Microsoft Windows XP Professional (Vers 2002; Service Pack 2). Als Präsentationsprogramme dienen MS Powerpoint (Vers. 2002) für *ppt*-Dateien, Adobe Acrobat Reader Version 7.0.7 für *pdf*-Dateien und Mozilla Firefox für *html*-Dateien. Für spezielle Anforderungen (Simulations- und Videodarstellungen o.ä.) bitten wir Sie, die Medien-Annahme rechtzeitig zu kontaktieren.

MICOS – Motion Control and Optomechanics

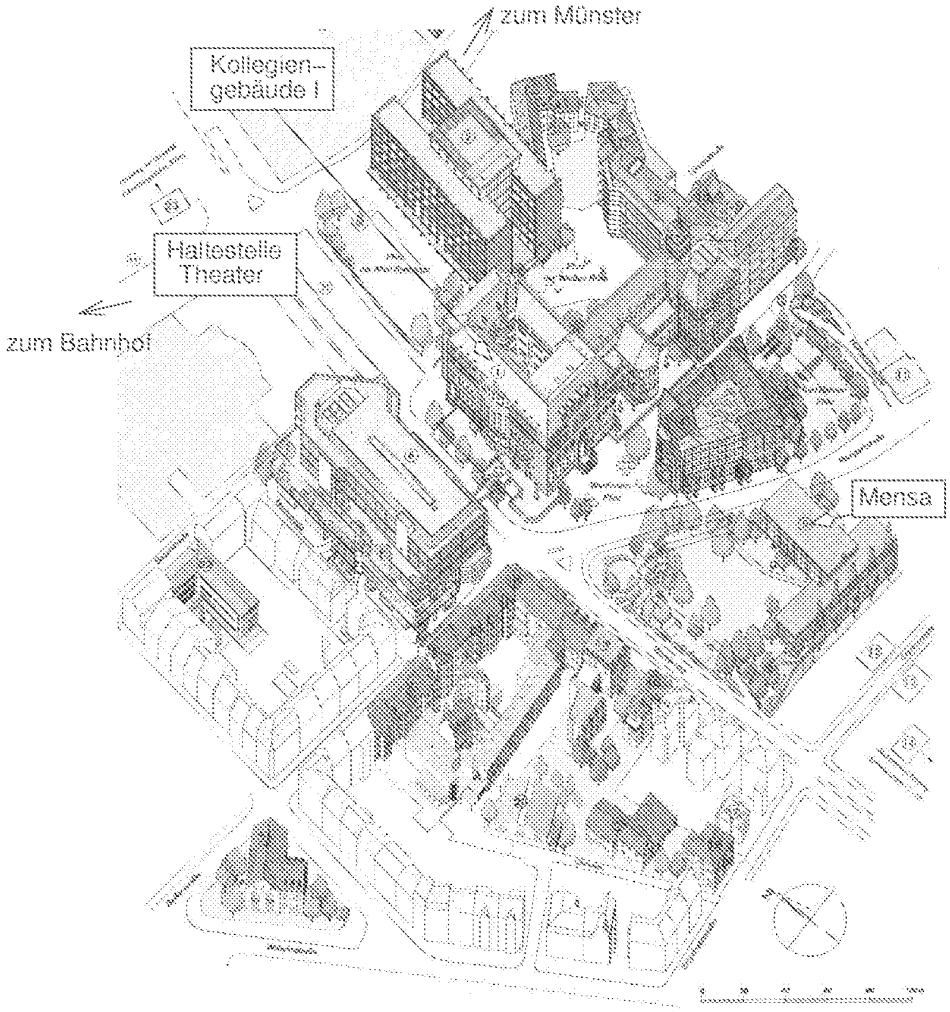


Optical benches, educational laser kits, multiaxial positioning devices
www.micos-online.com

COR-AAD1-00003264
Bayer EX1008 (Part 6 of 9)

Lagepläne, Tagungsbüro

Die Jahrestagung findet im Kollegiengebäude I (KG I; Aula, Prometheushalle, Eingangshalle und Hörsäle 1010, 1015 und 1199) der Albert-Ludwigs-Universität inmitten der Innenstadt von Freiburg statt.
Bitte beachten Sie, daß der Zugang zu den Tagungsräumen wegen Bauarbeiten am Haupteingang *Werthmann-Platz* nur über den Nordeingang am *Platz der alten Synagoge* möglich ist (s. auch die Lagepläne auf S. 43).



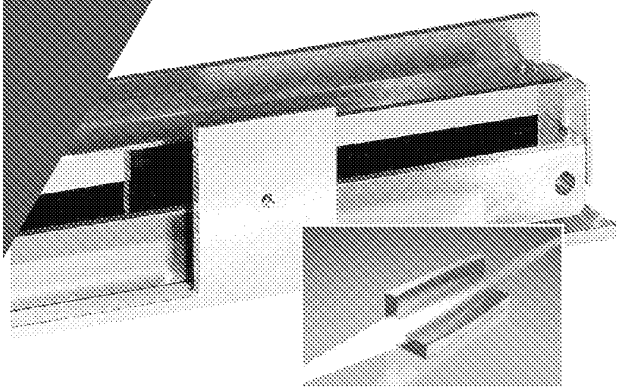
Tagungsbüro:

- Kollegiengebäude I (KG I), Eingangshalle
- Telefon 0761/270-7320
- Öffnungszeiten
  - Montag, 03.04.2006: 10:00 - 19:00 Uhr
  - Dienstag, 04.04. und Mittwoch, 05.04.2006: 8:00 - 18:30 Uhr
  - Donnerstag, 06.04.2006: 8:00 - 13:00 Uhr

COR-AAD1-00003265
Bayer EX1008 (Part 6 of 9)

Optics for Crystallography

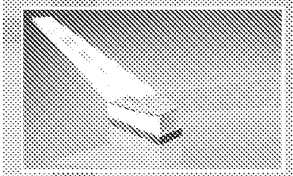
INCOATEC
innovative coating technologies gmbh



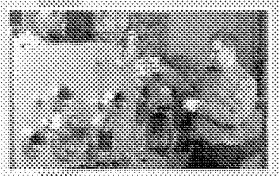
Incoatec produces ultra precise thin films according to client-specific requirements using modern deposition technology. Our main products include the latest generation of multilayer optics for

- X-ray diffraction
- X-ray spectrometry and
- synchrotron applications.

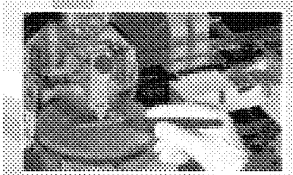
Computerized optics simulation, production of various types of substrates as well as characterization of films round off our service profile.



Simulation



Coating



Characterization

"Montel Optics"

- 2D collimation and focusing
- More than 10^9 photons/sec with sealed tubes
- More than 10^{12} photons/sec with rotating anodes
- Flux density above 10^{10} photons/sec/mm^2
- Cr, Fe, Cu and Mo radiation
- Optics with various lengths, focal distances and divergences
- Client-specific optics

Incoatec GmbH
Max-Planck-Str. 2
21502 Geesthacht · Germany
Tel.: +49 (0) 41 52 – 88 93 81
Fax: +49 (0) 41 52 – 88 93 83
email: info@incoatec.de

www.incoatec.de

INNOVATION IN CERAMICS
INNOVATION IN HIP TECHNOLOGY

HIGH
PURITY
PBN



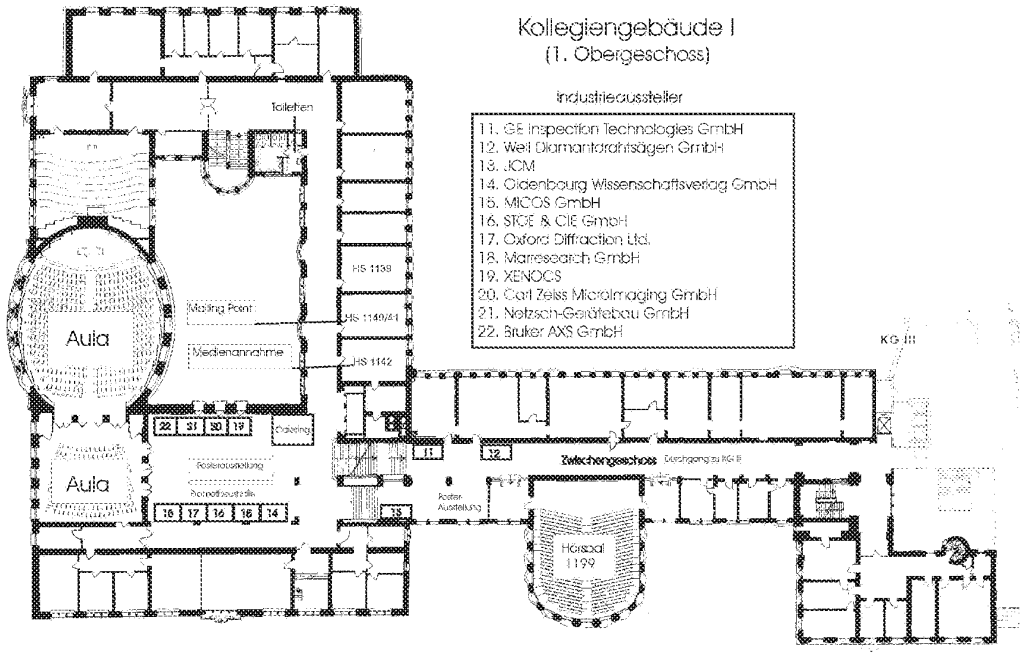
SINTEC

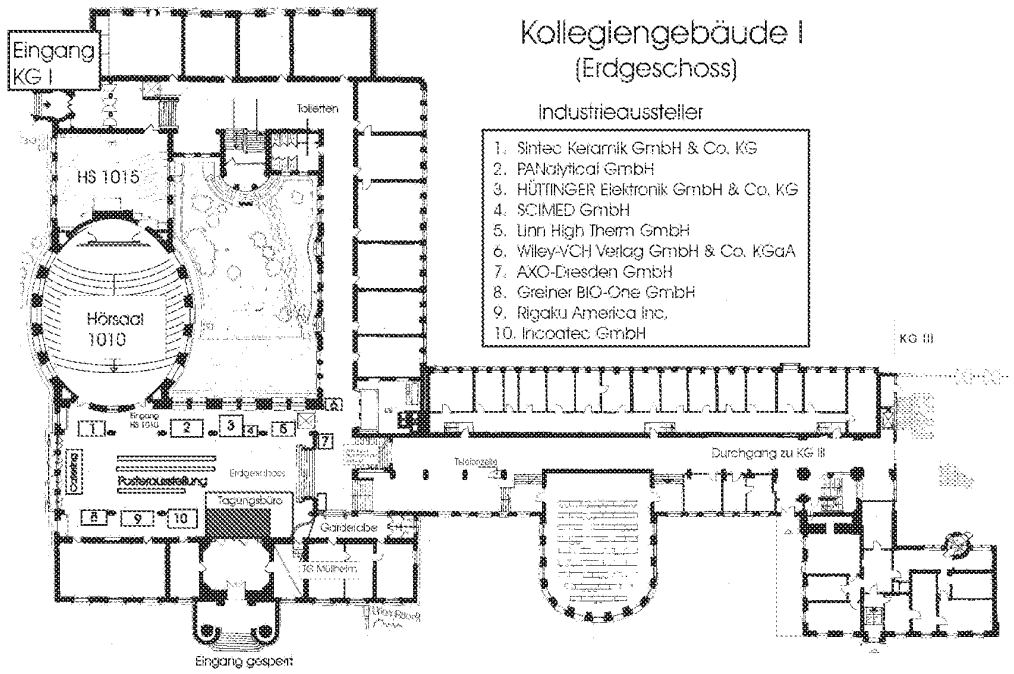
Sintec Keramik GmbH & Co. KG
info.bu.de@sintec-keramik.com

Romantische Straße 18
87642 Halblech, GERMANY

Tel.: +49-(0)8368-9101-0
Fax: +49-(0)8368-9101-30

www.sintec-keramik.com





FREIBURG 2006

COR-AAD1-00003267
Bayer EX1008 (Part 6 of 9)

Datum	Zeit	Veranstaltung (Hörsaal)		
Mo., 3.4.	13:00-13:30	Eröffnung der Tagung und der Firmenausstellung, Grußworte (Aula)		
	13:30-14:30	**PV:** D. Schwarzenbach (Lausanne), W. Hoffmann (Münster): Vortrag zum 100. Geburtstag von F. Laves (Aula)		
	14:30-14:45	– Kaffeepause –		
	14:45-17:00	**MS:** Elektronenmikroskopie, AK3 (HS 1199)	**MS:** Kristallchemie und Hochdruck, TS2 (HS 1010)	**MS:** Mineralogische und technische Kristallographie, AK15 (HS 1015)
	17:30	Empfang (Prometheus-Halle)		
	18:15	Vortrag des Max-von-Laue Preisträgers 2005, G. Schwarz (Köln): Die Biosynthese des Molybdäncofaktors (Aula)		
		Preisverleihung (Aula)		
Di., 4.4.	9:00-10:00	**PV:** L. Bohatý (Köln): Azentrische Kristalle und ihre Eigenschaften (Aula)		
	10:00-10:15	– Kaffeepause –		
	10:15-12:15	**MS:** Instrumentierung von Großgeräten, TS4 (HS 1199)	**MS:** Pulverdiffraktometrie, AK13 (HS 1010)	**MS:** Kristallographie und Spektroskopie, TS3 (HS 1015)
	12:15-13:30	– Mittagspause –		
	13:30-14:30	**PV:** J. Bilgram (Zürich): Controlling of Complex Structures (Aula)		
	14:45-16:15	**MS:** Strukturbiologie I, New Structures, AK1 (HS 1199)	**MS:** Strukturelle Phasenumwandlungen, TS6 (HS 1010)	**MS:** Neutronenuntersuchungen an komplexen Überstrukturen, TS5 (HS 1015)
	16:15-16:30	– Kaffeepause –		
	16:30-18:00	Posterpräsentation I (linke Spalten im Abstract-Band)		
	18:30	Mitgliederversammlung (Aula)		
Mi., 5.4.	9:00-10:00	**PV:** P. Luger (Berlin): Schnelle Elektronendichtebestimmung - eine Routinemethode der Zukunft? (Aula)		
	10:00-10:15	– Kaffeepause –		
	10:15-12:15	**MS:** Strukturbiologie II, Structure Based Drug Design, AK1 (HS 1199)	**MS:** Crystal Engineering und Strukturvorhersage, TS9 (HS 1010)	**MS:** Oberflächen und Grenzflächen, Biologische Materialien, AK18 (HS 1015)
	12:15-13:30	– Mittagspause –		
	13:30-14:30	**PV:** T. O. Yeates (LA): Structures of the Shell Subunits of the Carboxysome: A primitive bacterial organelle (Aula)		
	14:45-16:15	**MS:** Strukturbiologie III, New Methods, AK1 (HS 1199)	**MS:** Kristallchemie und komplexe Überstrukturen, TS7 (HS 1010)	**MS:** Hochauflösende Röntgenstreuung und Synchrotron-Strahlung, AK11 (HS 1015)
	16:15-16:30	– Kaffeepause –		
	16:30-18:00	Posterpräsentation II (rechte Spalten im Abstract-Band)		
	ab 19:30	Gesellschaftsabend (Le Buffet, Kaufhaus Karstadt, Kaiser-Joseph-Str. 165)		
Do., 6.4.	9:00-10:00	**PV:** T. Baumbach (Karlsruhe): Microdiffraction Imaging of Semiconductor Materials (Aula)		
	10:00-10:15	– Kaffeepause –		
	10:15-12:00	**MS:** Strukturbiologie IV, Protein-Protein Interactions, AK1 (HS 1199)	**MS:** Molekül- und Koordinationsverbindungen mit funktionellen Eigenschaften, TS8 (HS 1010)	**MS:** Quasikristalle, inkommensurable Verbindungen und teilkristalline Strukturen, TS10 (HS 1015)
	12:00-13:00	**PV:** G. E. Schulz (Freiburg): Protein Associations (Aula)		
	13:00	Schlußworte (Aula)		

COR-AAD1-00003268
Bayer EX1008 (Part 6 of 9)

environmental microbiology

Environmental Microbiology (2010) 12(9), 2411–2425 doi:10.1111/j.1462-2920.2010.02215.x

Novel α-ketoglutarate dioxygenase *tfdA*-related genes are found in soil DNA after exposure to phenoxyalkanoic herbicides

M. C. Gazitúa,[1,2] A. W. Slater,[1] F. Melo[1] and B. González[1,2]*

[1]*Departamento de Genética Molecular y Microbiología, Facultad de Ciencias Biológicas, Millennium Nucleus on Plant Functional Genomics, Center for Advanced Studies in Ecology and Biodiversity, Pontificia Universidad Católica de Chile, Santiago, Chile.*

[2]*Facultad de Ingeniería y Ciencias, Universidad Adolfo Ibáñez, Santiago, Chile.*

Summary

Phenoxyalkanoic herbicides such as 2,4-dichlorophenoxyacetate (2,4-D), 2,4-dichlorophenoxybutyrate (2,4-DB) or mecoprop are widely used to control broad-leaf weeds. Several bacteria have been reported to degrade these herbicides using the α-ketoglutarate-dependent, 2,4-dichlorophenoxyacetate dioxygenase encoded by the *tfdA* gene, as the enzyme catalysing the first step in the catabolic pathway. The effects of exposure to different phenoxyalkanoic herbicides in the soil bacterial community and in the *tfdA* genes diversity were assessed using an agricultural soil exposed to these anthropogenic compounds. Total community bacterial DNA was analysed by terminal restriction fragment length polymorphism of the 16S rRNA and the *tfdA* gene markers, and detection and cloning of *tfdA* gene related sequences, using PCR primer pairs. After up to 4 months of herbicide exposure, significant changes in the bacterial community structure were detected in soil microcosms treated with mecoprop, 2,4-DB and a mixture of both plus 2,4-D. An impressive variety of novel *tfdA* gene related sequences were found in these soil microcosms, which cluster in new *tfdA* gene related sequence groups, unequally abundant depending on the specific herbicide used in soil treatment. Structural analysis of the putative protein products showed small but significant amino acid differences. These *tfdA* gene sequence variants are, probably, required for degradation of natural substrate(s) structurally related to these herbicides and their presence explains self-remediation of soils exposed to phenoxyalkanoic herbicides.

Introduction

Phenoxyalkanoic (PA) herbicides are synthetic plant growth regulators that have been widely used to control broad leaf weeds since their introduction in the 40 s and 50 s (Ahrens, 1994). They usually are phenoxyacetic-, propionic- or butyric acids, with chloro and/or methyl residues in the aromatic ring (Fig. S1). Despite their foliar application, a significant amount of these herbicides reaches the ground and interacts with the soil microbiota where they can be degraded by bacteria (Fulthorpe *et al.*, 1996; Kamagata *et al.*, 1997; Kohler, 1999; Müller *et al.*, 1999) and fungi (Vroumsia *et al.*, 2005). Degradation of 2,4-dichlorophenoxyacetic acid (2,4-D) has been widely studied as a model for microbial decomposition of PA herbicides. The first step in the degradation of 2,4-D is performed by an α-ketoglutarate-dependent 2,4-D dioxygenase, encoded by the *tfdA* gene in β- and γ-*Proteobacteria* (Fukumori and Hausinger, 1993a; Suwa *et al.*, 1996; Vedler *et al.*, 2000), and by the *tfdA*α gene in α-*Proteobacteria* (Itoh *et al.*, 2002). It has been also described that some α-*Proteobacteria* use a 2,4-D monooxygenase, encoded by the *cadAB* genes, to degrade PA herbicides (Kitagawa *et al.*, 2002; Itoh *et al.*, 2004).

The archetypal TfdA enzyme, initially described in *Cupriavidus necator* JMP134 (previously named as *Ralstonia eutropha* JMP134), uses iron and catalyses the introduction of one oxygen atom into the ether bond of the PA substrate, and the other oxygen atom in the α-ketoacid co-substrate (Fukumori and Hausinger, 1993a; Fukumori and Hausinger, 1993b). This enzyme belongs to the group II of the α-ketoglutarate dependent dioxygenases (Eichhorn *et al.*, 1997), showing a clear homology to the *Escherichia coli* taurine/α-ketoglutarate dioxygenase (TauD). Based on this homology and site-directed mutagenesis studies, the conserved amino acid residues of TfdA protein that participate in binding to Fe^{2+}, α-ketoglutarate and 2,4-D have been defined (Hegg *et al.*,

Received 18 November, 2009; accepted 18 February, 2010. *For correspondence. E-mail bernardo.gonzalez@uai.cl; Tel. (+56) 2331 1619; Fax (+56) 2331 1906.

© 2010 Society for Applied Microbiology and Blackwell Publishing Ltd

COR-AAD1-00003269
Bayer EX1008 (Part 6 of 9)

1999; Hogan *et al.*, 2000; Dunning Hotopp and Hausinger, 2002; Elkins *et al.*, 2002).

It has been reported that TfdA enzymes are also involved in the first-step cleavage of other PA herbicides (Fig. S1), such as phenoxyacetic acid (PAA), 2-methyl-4-chlorophenoxyacetic acid (MCPA), 2,4,5-trichlorophenoxyacetic acid (2,4,5-T) and 2-(2,4-dichlorophenoxy) propionic acid (dichlorprop) (Fukumori and Hausinger, 1993a; Itoh *et al.*, 2002). Bacterial strains that carry *tfdA*- or *tfdA*-related genes degrade other PA compounds such as 2-methylphenoxyacetic acid (2MPA), 2 (2-methyl-4-chlorophenoxy)-propionic acid (mecoprop), 2,4-dichlorophenoxybutyric acid (2,4-DB) and 2 (2-methyl-4-chlorophenoxy)-butyric acid (Pieper *et al.*, 1988; Nickel *et al.*, 1997; Smejkal *et al.*, 2001). SdpA and RdpA are dioxygenases related to the TfdA enzyme, involved in the degradation of chiral PA compounds such as dichlorprop and mecoprop (Zipper *et al.*, 1996; Müller *et al.*, 1999; Müller *et al.*, 2006). These enzymes use the (*S*)-, or the (*R*)-isomer as substrate, respectively, with much more affinity than TfdA protein (Nickel *et al.*, 1997). These two enzymes show only 25% of amino acid identity between them, and less than 35% of amino acid identity with TfdA protein. However, SdpA and RdpA share the consensus sequence $HX(D/E)X_{136-207}HX_{10}R/K$, showing clear homology to the group II α-ketoglutarate dependent dioxygenases, as TfdA and TauD proteins (Schleinitz *et al.*, 2004).

Complete *tfdA* gene sequences have been obtained from isolated bacterial strains able to degrade PA herbicides (see as examples, Streber *et al.* 1987; Suwa *et al.*, 1996; Vedler *et al.*, 2000; Itoh *et al.*, 2002; Poh *et al.*, 2002; Hoffmann *et al.*, 2003), while numerous partial *tfdA* gene sequences have been found in total genomic DNAs by PCR amplification using degenerated primers (Shaw and Burns, 2004; Bælum *et al.*, 2006; Gonod *et al.*, 2006; Zakaria *et al.*, 2007; Bælum *et al.*, 2008). The analyses of the sequences have defined the existence of four groups of *tfdA* gene related sequences in *Proteobacteria*: *tfdA* gene classes I, II and III (Mcgowan *et al.*, 1998), and *tfdAα* genes (Itoh *et al.*, 2000). The reasons for this emerging picture of gene sequence variants are presently unknown.

In contrast with the number of studies dealing with PA degradation in bacterial isolates, very few studies have focused on the effects of PA compounds on microbial communities and, more specifically, on bacteria encoding these PA metabolizing dioxygenases (Gonod *et al.*, 2006; Macur *et al.*, 2007; Zakaria *et al.*, 2007; Bælum *et al.*, 2008). Using a culture-independent approach, it has been demonstrated that continuous exposure to *R*- or racemic mecoprop affects the soil bacterial community composition (Zakaria *et al.*, 2007). Another study has shown that exposure to different amounts of 2,4-D also modified the bacterial community structure with the highest concentration treatment resulting in a significant decrease in bacterial diversity and an enrichment of bacterial populations related to the *Burkholderia* genus (Macur *et al.*, 2007).

Using culture-independent, total genomic DNA and bioinformatic approaches, this work reports the isolation of an impressive number of novel *tfdA* gene related sequences from a single soil exposed to different PA herbicides. A new group of TfdA-related dioxygenases was defined, based on structural features of these novel sequences and the changes in the structure of the soil bacterial community and the *tfdA* gene related sequences pool upon exposure to different PA compounds. Thus, this study increases our knowledge on diversity of TfdA-related dioxygenases in microbial metabolism of PA herbicides and would help design of bioremediation strategies to clean environments polluted with these anthropogenic compounds.

Results

Total genomic DNA detection of tfdA gene related sequences in a soil exposed to different PA herbicides

To look for the presence of *tfdA* gene related sequences, a PCR detection procedure using a *tfdA* gene sequence primer pair (the so-called short PCR product) was used to scan total genomic DNA obtained from soil microcosms exposed for 4 months to different PA herbicide treatments. PCR products of the expected length (360 bp) were obtained for all treatments (data not shown), including the non-incubated soil and soil exposed to benzoic acid, or water, used as controls to track the specific effect of PA herbicides. *tfdA* gene sequence PCR products from the non-incubated soil and those from the treatment with 2,4-D and the mixture of three herbicides were cloned and subjected to RFLP analysis with the MspI endonuclease, in order to have a preliminary idea of the number of different sequences from each soil treatment. One hundred and eighty five clones were analysed (50, 75 and 60 clones from the non-incubated soil, and the soils treated with 2,4-D or the mixture of herbicides respectively) and 37 distinct MspI RFLP patterns were detected. Fifty-three clones, representing 37 unique patterns, were sequenced and their sequences were compared with the non-redundant protein sequence database at the NCBI, with the blastp software (Altschul *et al.*, 1997), revealing the presence of 46 sequences with significant identity to reported α-ketoglutarate dioxygenases. These sequences have 33–58% amino acid sequence identity with the canonical TfdA enzyme from *C. necator* JMP134, and possess characteristic residues from the active site of this enzyme (data not shown). None of these sequences matched previously reported *tfdA* gene sequences. The

COR-AAD1-00003270
Bayer EX1008 (Part 6 of 9)

new TfdA protein related sequences were optimally aligned against TauD protein from *E. coli* (data not shown). The predicted three-dimensional mapping of these TfdA protein related sequences revealed that the short PCR product targets part of the active zone, but does not cover the part of the protein that may be responsive to changes in the structure of the PA substrate.

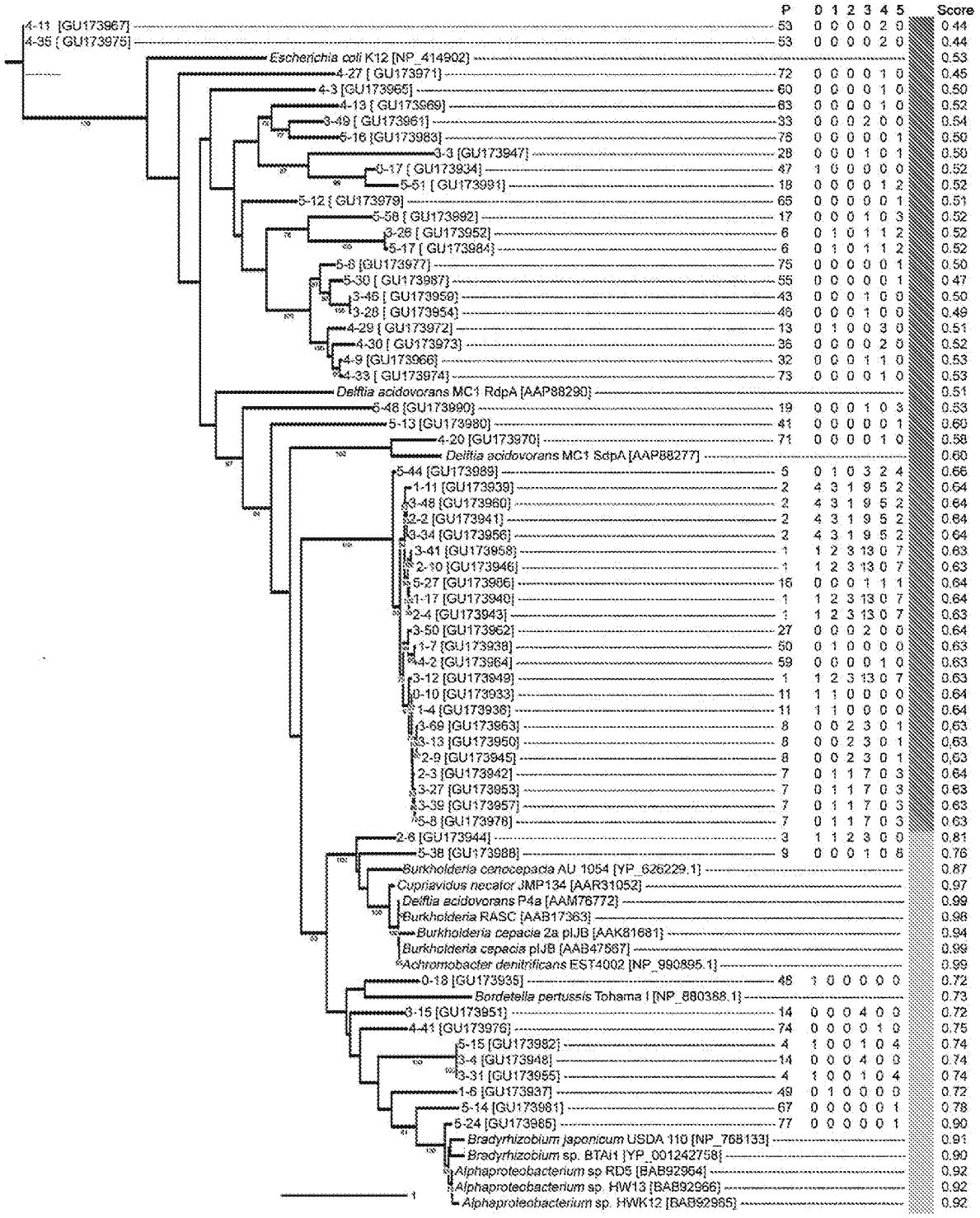
To obtain longer TfdA protein related sequences, a new set of degenerated forward primers was specifically designed to extend the amplified sequence towards the amino terminus and thus include residues involved in substrate binding. Longer PCR products for *tfdA* gene related sequences were again found in the non-incubated soil, and in soil microcosms treated with PAA, 2MPA, 2,4-D, mecoprop or 2,4-DB. PCR products of the expected length (~630 bp) were cloned and analysed by RFLP. Two hundred and twenty-two clones were analysed and 77 distinct HaeIII RFLP patterns were detected. The most frequent RFLP patterns and some found only in specific treatments (59 clones, in total) were sequenced and their sequences were aligned against the non-redundant nucleotide database using blastn program (Altschul *et al.*, 1990). These sequences were translated and aligned against the TfdA/other dioxygenases MSA, as described in *Experimental procedures*. Phylogenetic trees were built based on this final MSA using maximum likelihood optimization criteria. The phylogram is shown in Fig. 1. Eleven of the new *tfdA* gene related sequences grouped with previously reported proteobacterial TfdA protein sequences and 23 clustered close to the RdpA, SdpA or TauD oxygenases. A second group of 23 sequences appeared as the sister group of the previously reported proteobacterial TfdA protein sequences, indicating that they are part of a new family of *tfdA* gene related sequences. All sequences within this group have a very short branch length because they are closely related (above 95% sequence identity). Finally, two highly divergent sequences clustered apart of TauD and TfdA related dioxygenases (clones 4–11 and 4–35).

Based on the known TfdA sequences, a new score scheme (the T score) was designed and used to assist the classification of the new sequences (see *Experimental procedures*). The T score ranges from 0 to 1, where a value of 1 would correspond to a hypothetical TfdA protein that has at each position the most frequently observed amino acid in all known TfdAs. It should be noted that this score is based only on the known TfdA proteins and the observed frequency of occurrence of their amino acids at each position. Therefore, this score is different than the sequence alignment score used to build the dendrogram and then it should be more robust for classifying new TfdA protein related sequences. Based on the T score, three groups of TfdA protein related sequences were clearly distinguished (Fig. 1), which were named as follows: (i) TfdA protein related dioxygenases: those proteins with *T* values higher than 0.7, which include all the known α-, and β-proteobacterial TfdA proteins; (ii) TauD protein related sequences: those proteins that have *T* values lower than 0.6, which are closer to RdpA, SdpA and TauD dioxygenases; and finally (iii) PA dioxygenases, a proposed name for those protein sequences with *T* values between 0.6 and 0.7, which although appears as the sister group of the TfdA protein related dioxygenases in the phylogram (Fig. 1), their branch has not a strong statistical support (i.e. bootstraping value smaller than 50), and it is also close to the TauD protein related dioxygenase branch.

Presence of functionally important residues in the new TfdA protein related sequences

To assess the presence of functionally important residues in these new *tfdA* protein related sequences found in soil, six functional categories were defined (Table 1), based on previously described information for TauD enzyme (O'Brien *et al.*, 2003). These categories were: Fe^{2+} binding; α-ketoglutarate binding; substrate binding; substrate locking; substrate burial or accessibility; and dimer formation (see *Experimental procedures*). The relative positions of the residues in each category within the alignment were identified and selected, generating sub-alignments that were used for the generation of sequence logos (Fig. 2). Two residues involved in Fe^{2+} binding (H99, and D101 in *E. coli* TauD protein), and one involved in α-ketoglutarate binding (T126 in *E. coli* TauD protein) were found in all sequences analysed here: the previously reported TfdA protein related sequences, the TfdA protein related sequences reported here, the PA dioxygenases and the TauD protein related sequences. It should be mentioned that two important functional residues (H255, involved in iron binding and R266, participating in α-ketoglutarate binding) are not shown because they are out of the region amplified by the longer PCR primer pair. The sequence logos exhibit several conserved residues among the known TfdA protein related dioxygenases, most of which are not observed in the TauD protein related dioxygenases (Fig. 2). For example, for the substrate binding region there are three serine residues (at positions 3, 7 and 9 in the sequence logo), one asparagine (at position 6), one phenylalanine (at position 8) and one histidine (at position 11). This pattern of conservation is clearly not present in the TauD protein related dioxygenases, although part of the sequences within this group has some of these residues in common (i.e. the serine residue at fourth position in the sequence logo of the TauD protein related sequences group). Interestingly, the group of PA dioxygenases shows a somehow similar pattern to that observed in the known TfdA protein related sequences,

COR-AAD1-00003271
Bayer EX1008 (Part 6 of 9)



COR-AAD1-00003272
Bayer EX1008 (Part 6 of 9)

Fig. 1. Phylogram of *TfdA* protein sequences. The phylogenetic tree was built using maximum likelihood optimization criteria with the JTT amino acid substitution model. Only bootstrapping values higher than 50 are shown. Known TfdA proteins from α-proteobacteria, β-proteobacteria and other a-ketoglutarate dioxygenases are indicated. The new TfdA protein sequences are described by two numbers separated by a dash, with the first one corresponding to the treatment, as follows: non-incubated soil (0); PAA (1); 2MPA (2); 2,4-D (3), mecoprop (4) and 2,4-DB (5). The vertical rectangle indicates the classification of the sequences according to their T score: TfdA protein related sequences (light grey), TauD protein related sequences (dark grey) and PA dioxygenases (grey). T score values are shown at the right of the vertical rectangle while the RFLP pattern (P) and the clonal abundance found in each treatment is shown at its left side.

but with some differences. For example, the serine at third position described above is now replaced by a threonine in the PA dioxygenase group, which is an amino acid with similar physicochemical properties. Similarly, the observed NSFS pattern at positions sixth to ninth in the logo is now replaced by SKFS pattern in the PA dioxygenase group. The TauD protein related group of sequences exhibits a more diverse repertoire of amino acids, but with the phenylalanine residue typically replaced by residues with aromatic groups (tyrosine or tryptophan), which suggests a critical role of an aromatic functional group at this position in all these dioxygenases. The location of the substrate binding residues is illustrated in the three-dimensional structure model of TfdA protein from *C. necator*, along with their position in the TfdA protein primary sequence (Fig. 3). These residues belong to five independent regions in the protein, which are non-local at the sequence level, but converge in the three-dimensional space surrounding the substrate. The regions related to substrate accessibility show little conservation between the different groups. Only a glutamic acid at the first position of the sequence logo appears to be conserved in the four groups, because the serine and histidine around positions tenth and fifteenth in the sequence logo (positions 207 and 271 in the alignment), are involved in substrate binding (i.e. some residues considered in the region of substrate accessibility are included in the substrate binding region). As it was described above, the serine and histidine residues are conserved in the TfdA protein related sequences. Therefore, this glutamic acid at position 84 in the alignment may also be important for the function of these enzymes, as it was pointed out above for the aromatic group at position 144. The unique group that exhibits high conservation of the amino acids involved in substrate accessibility is the PA dioxygenase group (Fig. 2). This is because this group is highly homogeneous and by far the less diverse overall, as it can be seen from the phylogram (Fig. 1), since the 23 sequences belonging to this group share more than 95% sequence identity between them. Therefore, conservation of amino acids in this specific group of sequences should be carefully interpreted. The three-dimensional mapping of the residues belonging to the substrate accessibility region showed that these residues correspond to non-local regions at the sequence level that form three independent loops that surround the entrance of the substrate to the active site of the enzyme (Fig. 3).

The analysis of the conservation of residues involved in dimer formation (not shown) suggests that some leucine residues are critical, because they are strongly conserved in all three groups. The residues involved in dimer formation belong to two alpha helices that are located behind the active site in the structure (Fig. 3), and thus should not be interacting directly with the substrate, cofactor or products. This suggests that dimer formation may be important for the function or the regulation of the activity of these enzymes.

Distribution and abundance of TfdA protein related, PA dioxygenase and TauD protein related sequences in soils treated with different PA herbicides

The number of retrieved clones/sequences was low and could not be used to explain the *tfdA* genes diversity

Table 1. Functionally important residues in taurine dioxygenase (TauD) from *E. coli*.

Feature	TauD amino acid[a]
Fe^{2+} binding	H99, D101, H255
α-Ketoglutarate binding	T126, R266
Substrate binding[b]	H70, Y73, I83, D94, N95, N97, T100, V102, F104, S158, F159, F206, R270
Substrate locking	Y73, D94, F159, F206
Substrate burial or accessibility	68-HIHPVY-73
	155-FRKSF-159
	203-NEGF-206
Dimer formation 1	139-SVPFRQLLS-147
Dimer formation 2	214-SEKESEALLSFLFAHI-229

a. Residue numbering corresponds to that observed in the crystal structure of TauD protein (PDB code 1OS7) from *E. coli* (O'Brien *et al.*, 2003).
b. These residues were selected because they have at least one atom closer than 5.0 Å to any other atom of the substrate taurine. Although residues H99 and D101 fulfil the distance restraints mentioned above, they were not considered in the substrate-binding category because they participate directly in the binding to iron.

COR-AAD1-00003273
Bayer EX1008 (Part 6 of 9)

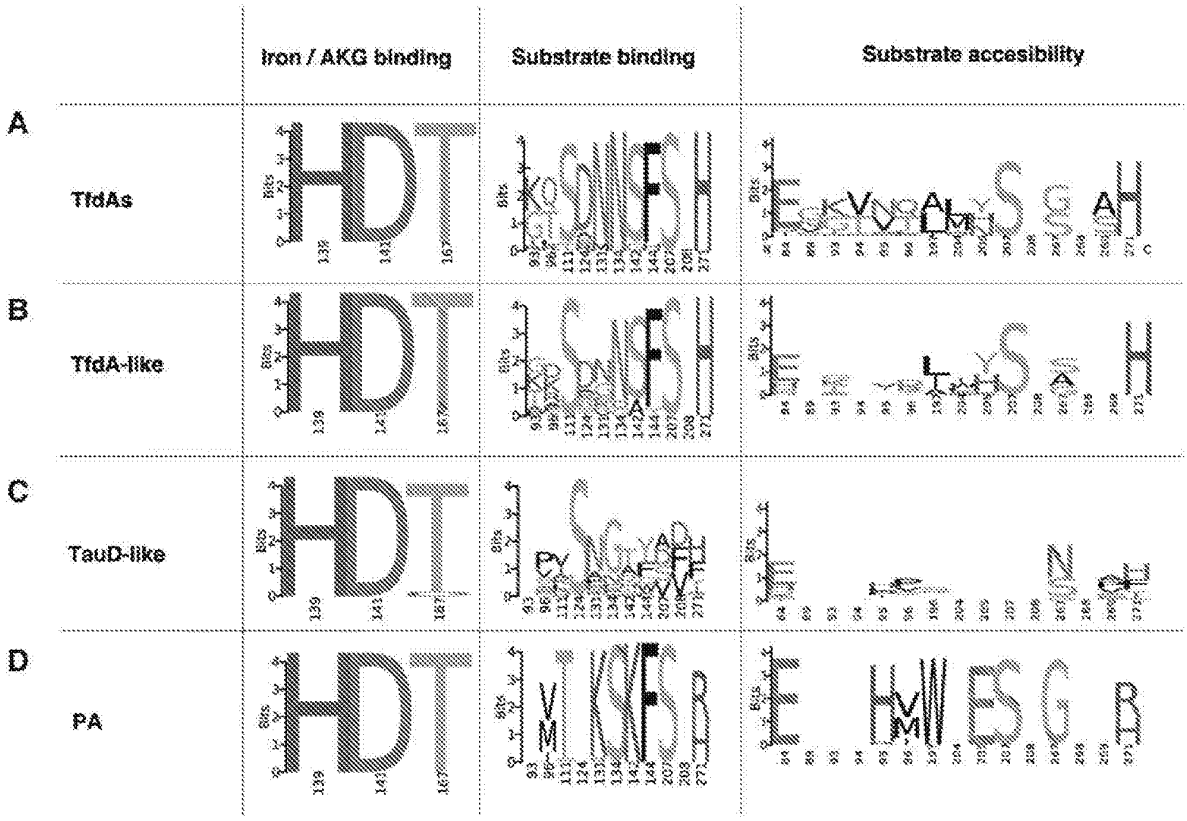


Fig. 2. Conservation of functionally important residues. Sequence logos for known (A) TfdA proteins, (B) TfdA protein related sequences, (C) TauD protein related sequences and (D) PA dioxygenases were calculated from some selected positions in the multiple sequence alignment that correspond to different functional categories, as deduced from what is known in TauD protein from *E. coli*. Numbers in the *x*-axis of the logos correspond to the sequential position number in the multiple sequence alignment. AKG, α-ketoglutarate.

found in this soil. However, the effect of specific PA treatments in the distribution and abundance of the three groups of new sequences retrieved from soil can still be analysed, with caution. Three treatments (0, 1 and 2; non-incubated soil, and exposed to PA and 2-MPA respectively) did not include chlorinated compounds as the other three (3, 4 and 5; exposed to 2,4-D, mecoprop and 2,4-DB respectively). The PA dioxygenase group and the TfdA protein related sequences group contained at least one clone from each treatment, whereas the TauD protein related sequences group was clearly biased to clones coming from treatments with each of the three chlorinated derivatives (Fig. 1). Since the low number of clones/sequences analysed, it should be kept in mind that the absence of any particular group of sequences does not necessarily means that this group is not present. The analyses carried out with short PCR products provided essentially the same trends (data not shown). The *tfdA* related sequences found in shorter fragments clustered in the three groups of dioxygenase sequences defined with longer amplicons (Fig. 1). In addition, no perfect matches or amino acid sequence identities higher than 99% were found after comparison of short with long *tfdA* sequences, further supporting the high level of diversity of these soil sequences.

RFLP analysis of 222 clones was carried out to determine the relative abundance of sequences belonging to the three groups of dioxygenases in the different soil treatments (Table 2). RFLP patterns belonging to the PA

Table 2. Relative abundance (%) of clones belonging to the three groups of TfdA-related dioxygenases.

Treatment	TfdA	PA	TauD
Non-incubated soil	3 (30.0%)	6 (60.0%)	1 (10.0%)
PAA	2 (15.4%)	9 (69.2%)	2 (15.4%)
2MPA	2 (22.2%)	7 (77.8%)	0 (0%)
2,4-D	10 (17.5%)	38 (66.7%)	9 (15.8%)
Mecoprop	1 (4.0%)	9 (36.0%)	15 (60.0%)
2,4-DB	14 (29.2%)	18 (37.5%)	16 (33.3%)

One hundred fifty two of the 222 clones were classified according to their restriction fragment length polymorphism pattern using the HaeIII endonuclease.

COR-AAD1-00003274
Bayer EX1008 (Part 6 of 9)

© 2010 Society for Applied Microbiology and Blackwell Publishing Ltd, *Environmental Microbiology*, **12**, 2411–2425

Fig. 3. Three-dimensional protein structure model of TfdA protein. Upper panel: The 3D model from *C. necator* TfdA protein (A) is shown along with the coordinates of taurine (green), α-ketoglutarate (yellow) and iron (red), modelled as block residues from the template structure of TauD protein from *E. coli* (PDB code 1OS7). The substrate taurine was modelled only to illustrate its location in the structure. Residues involved in Fe^{2+} binding are shown in blue and those involved in α-ketoglutarate binding are shown in pink. The horizontal bar at the bottom represents the primary protein sequence with the location of key residues for iron and α-ketoglutarate binding shown as vertical bars. The sequence region corresponding to the long-PCR product is shown in light brown. The region that was not amplified by PCR is shown in grey. Two key residues for Fe^{2+} and α-ketoglutarate binding that were not present in the region amplified by PCR are also shown as grey vertical bars. Bottom panel: Only the region of the TfdA protein model corresponding to the long-PCR product is shown. Key residues involved in Fe^{2+} and α-ketoglutarate binding are shown in blue colour, taurine is shown in green, α-ketoglutarate in yellow and iron as a red ball. Key residues involved in substrate binding (B), substrate accessibility (C) and dimer formation (D) are shown in red colour along with their location in the primary protein sequence.

COR-AAD1-00003275
Bayer EX1008 (Part 6 of 9)

dioxygenase group sequences were more abundant in the non-incubated soil and those soil microcosms exposed to the non-chlorinated herbicides. Although the same trend was also observed with the soil treated with 2,4-D, the relative abundance of PA dioxygenase group sequences in soil treated with 2,4-DB and mecoprop was lower. RFLP patterns belonging to TauD protein related sequences were especially abundant in soil exposed to mecoprop (Table 2), and in 2,4-DB. About 1/5-1/3 of the sequences in each treatment belonged to the TfdA protein related sequences group with the exception, again, of the soil exposed to mecoprop.

Changes in the soil bacterial community structure upon exposure to PA herbicides

To address the effect of the different soil treatments in the bacterial community structure, a terminal restriction fragment length polymorphism (T-RFLP) analysis of the total genomic DNA was carried out using PCR primer pairs targeting *tfdA* gene related sequences (the short sequences), to track functional changes, and 16S rRNA gene sequences, to follow changes in the taxonomic groups of the bacterial community structure. Gross changes in the conventional ecological indexes for richness (S), and diversity (H) were only detected in the 16S rRNA T-RFLP profiles from soils exposed to mecoprop, and the mixture containing mecoprop, 2,4-DB and 2,4-D (Table S2), but no important changes were found for the *tfdA* gene sequence T-RFLP profiles. T-RFLP profiles obtained with primer pairs tracking long *tfdA* gene sequences, carried out with selected soil microcosms showed essentially the same trends that of T-RFLP profiles with short sequences (not shown). This indicates that more subtle effects would occur upon PA exposure. The comparison among the T-RFLP profiles, based on Bray-Curtis similarity coefficients, was visualized through NMDS and cluster analyses. One-way analysis of similarity (ANOSIM) was carried out to examine the statistical significance of grouping. The NMDS visualization is shown in Fig. 4. After 4 months of incubation, the 16S rRNA T-RFLP profiles show that the structure of the bacterial communities from soil microcosms exposed to mecoprop, the herbicide mixture, and benzoate, substantially differs from all the other treatments (Fig. 4A). The same trend was observed after 2 months of incubation (data not shown). The corresponding cluster analysis (Fig. S2) demonstrated that, at the 50% similarity level, the 16S rRNA T-RFLP profiles formed four distinct clusters: the first group, with high similarity (> 70%), includes T-RFLP profiles from the non-incubated soil, the water control, and the treatments with PAA, 2,4-D or 2MPA. The second cluster corresponds to T-RFLP profiles from soils treated with 2,4-DB; the third to those treated with mecoprop and the mixture of 2,4-D + mecoprop + 2,4-DB; and the fourth to the soils treated with benzoate. The similarities within the last three clusters ranged between 65% and 85%.

The NMDS analyses of the *tfdA* gene sequences T-RFLP profiles showed significant differences for the bacterial community composition in soils treated with mecoprop, 2,4-DB, and the PA mixture (Fig. 4B). The cluster analysis of the *tfdA* gene sequences T-RFLP profiles (Fig. S2) showed that the profiles from soils treated with the mixture cluster apart from those treated with mecoprop, and that both are different from all the other soil treatment profiles. Within this last group, the T-RFLP profiles from soils treated with 2,4-DB were separated from the rest, at the 62% similarity level.

Discussion

This work reports the detection in soil total genomic DNA of sequences related to the *tfdA* gene that encodes the α-ketoglutarate dependent dioxygenase involved in the first step of the degradation of PA herbicides. An impressive variety of new *tfdA* gene related sequence variants was found. The sequence analyses of these new gene sequence variants showed small but distinguishable amino acid changes, allowing the definition of a new group of these dioxygenase sequences. The continuous exposure of soil microcosms to different PA herbicides produced significant changes in the taxonomic (16S rRNA gene marker) and functional (*tfdA* gene marker) structure of the soil bacterial community.

The finding of new *tfdA* gene related sequences in environmental DNA is not absolutely unexpected since such sequences have been reported in bacteria isolated from soils (Fulthorpe *et al.*, 1996; Vallaeys *et al.*, 1996; Kamagata *et al.*, 1997; Itoh *et al.*, 2002, 2004), aquatic ecosystems (de Lipthay *et al.*, 2002), as well as total genomic DNA samples (Ka *et al.*, 1994). The striking aspect of the findings reported here is that these novel *tfdA* genes related sequences are detected in only one soil. This soil has been subjected to standard farming practices with annual weed control based on the use of *s*-triazine herbicides such as simazine and, quite occasionally, with MCPA herbicide to control simazine resistant weeds (Manzano *et al.*, 2007). The presence of these numerous *tfdA* gene related sequences may explain the rapid turnover of 2,4-D in this soil (Manzano *et al.*, 2007). Their detection in non-incubated soil and in soil microcosms exposed to benzoic acid or water indicates that these *tfdA* genes related sequences are abundant enough to be detected in the soil total genomic DNA without a need for enrichment of the bacteria harbouring gene sequences putatively involved in degradation of specific PA herbicides.

COR-AAD1-00003276
Bayer EX1008 (Part 6 of 9)

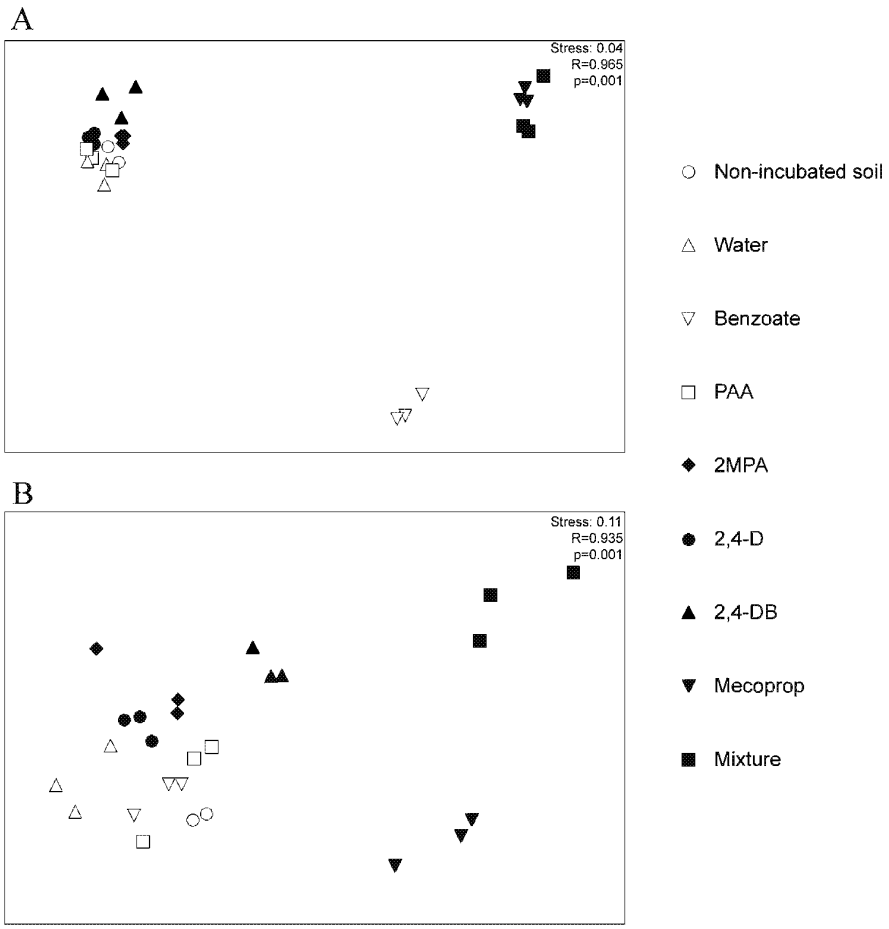


Fig. 4. Non-metric multidimensional scaling (NMDS) analysis of the 16S rRNA (A) and *tfdA* gene related sequences (B) T-RFLP profiles for total genomic DNA from soil microcosms continuously exposed for 4 months to PAA (□), 2MPA (◆), 2,4-D (●), 2,4-DB (▲), Mecoprop (▼), 2,4-D + Mecoprop + 2,4-DB (▩), water (△) or benzoate (▽). The non-incubated soil is represented by (○). Each symbol corresponds to a single T-RFLP profile. Stress values for NMDS analysis, global *R* values and significance for ANOSIM among treatments are indicated. T-RFLP data obtained with the endonuclease MspI and HaeIII for 16S rRNA and *tfdA* gene related sequences were used for this analysis respectively. Use of the endonuclease HhaI gave essentially the same results, in both cases.

The abundance and diversity of *tfdA* gene related sequences in soils may be explained by the role of α-ketoglutarate dioxygenases in catabolism of natural, more common, compounds. The enzyme from *C. necator* JMP134 is able to use cinnamic acid derivatives as substrates (Dunning Hotopp and Hausinger, 2001), which are components of plant exudates. Indoleacetic acid derivatives (Marriott *et al.*, 2000) and aryl-ether compounds released during degradation of lignin have been also proposed as natural substrates of TfdA enzyme (Hogan *et al.*, 1997). The analysis of these new sequences showed several interesting features. The general trends were observed with both the shorter and the larger PCR products. The latter includes most of the functionally relevant sequences of the TfdA protein (Fig. 3). The more relevant result of this analysis is the definition of a new group of α-ketoglutarate dioxygenases (Fig. 1). In addition to the group of proteobacterial α-ketoglutarate dioxygenases and the heterogeneous group of sequences more closely related to RdpA, SdpA and TauD dioxygenases, a third group was found. This group, comprising only novel sequences, is characterized by intermediates *T* values that indicate similarity levels equally distant from the other two groups. We have named this novel group as PA dioxygenases since their sequences were found in soils exposed to both chlorinated and non-chlorinated PA herbicides. However, biochemical and genetics studies are clearly required to define if these putative dioxygenases are involved in metabolism of PA compounds.

The *tfdA* gene related sequences that appear only distantly related to the TfdA and TauD proteins in this soil, i.e. those from clones 4–11 and 4–35 (Fig. 1), may corre-

COR-AAD1-00003277
Bayer EX1008 (Part 6 of 9)

spond to α-ketoglutarate dioxygenase performing other oxygenative reactions. Xanthine dioxygenase, involved in hydroxylation of xanthine (Cultrone *et al.*, 2005), the oxidative alkylsulfatase from *Pseudomonas putida* (Kahnert and Kertesz, 2000), or the sulfonate dioxygenase from *Saccharomyces cerevisiae* (Hogan *et al.*, 1999), are examples of these dioxygenases. However, these proteins only share some structural/functional features of α-ketoglutarate dioxygenases and have very low identity at the amino acid level with the sequences reported here.

The sequences of the three groups of dioxygenases (Figs 2 and 3), possess the three key residues (H99, D101, T126 in *E. coli* TauD protein), two for iron binding and one for α-ketoglutarate binding, strongly suggesting that most of these sequences encode functional α-ketoglutarate dioxygenases that perform dioxygenolytic cleavage of PA derivatives. Based on the conservation of substrate binding residues, it seems that the PA dioxygenases group is more similar to TfdA protein related sequences than to TauD protein related dioxygenases, thus suggesting that these enzymes could use similar substrates.

The functionality of these *tfdA* gene related sequences is also suggested by other kind of evidence. The functional structure of the soil bacterial community, i.e. the number of *tfdA* gene related sequences (functional richness), and their relative abundance, is significantly affected by the specific herbicide compound used during enrichment (Fig. 4). The shifts in the taxonomic structure of the soil bacterial community, based on tracking of the 16S rRNA gene sequences, parallel those of the functional structure, indicating that the bacterial groups that possess the *tfdA* gene related sequences are also those that react to the presence of the herbicide. Indeed, more direct approaches tracking the expression of particular *tfdA* gene related sequences are required to evaluate the functionality of these sequences, as it has been demonstrated for *tfdA* gene from *C. necator* during degradation of MCPA in an agricultural soil (Nicolaisen *et al.*, 2008). Changes in the relative abundance of variants of the *tfdA* gene sequences have been reported in soils exposed to MCPA herbicide using PCR primer pairs targeting the class III proteobacterial *tfdA* genes (Bælum *et al.*, 2006). More recently, the use of primer pairs that distinguish among subgroups of proteobacterial TfdA protein sequences allowed establishment of some differences in the contribution of specific *tfdA* gene sequences to degradation of MCPA or 2,4-D in soils (Bælum *et al.*, 2008; Bælum and Jacobsen, 2009).

Some soil treatments caused more pronounced effects than others, in both the taxonomic and functional structure of the soil bacterial community. The larger effects were observed when mecoprop, the only chiral herbicide tested, was present either alone or in the mixture. Mecoprop is metabolized by the distinct α-ketoglutarate dioxygenases, RdpA and SdpA, which are more closely related to TauD protein from *E. coli* than to the TfdA protein of 2,4-D degrading bacteria such as *C. necator* JMP134 (Fig. 1). Using SdpA, RdpA and TfdA probes in pure cultures, it has been suggested that the *rdpA* gene is involved in R-mecoprop degradation while *tfdA* and *sdpA* genes are involved in the degradation of both R- and S-mecoprop (Zakaria *et al.*, 2007). Consistently, a significant increase of sequences of the TauD protein related group was found in soil microcosms exposed to mecoprop. In contrast, PA dioxygenase sequences were more abundant in the treatments with non-chlorinated compounds.

It cannot be ruled out that the exposure to specific PA herbicides may enrich the soil community DNA in catabolic gene sequences other than *tfdA* related genes. As it is mentioned above a gene cluster encoding a 2,4-monooxygenase able to cleave PA derivatives has been reported (Kitagawa *et al.*, 2002; Itoh *et al.*, 2004). The primer pairs used in this work are unable to track *cad* genes and other, not yet described gene sequences, putatively involved in PA herbicides degradation.

On the other hand, the significant change in the soil bacterial community in soil exposed to benzoate can be explained by the toxicity of this compound and their catabolic intermediates (Lambert *et al.*, 1997; Cao and Loh, 2008). As expected, this effect is rather general than specifically related to *tfdA* gene bearing bacteria and, consistently, gross changes in bacterial community structure were also seen with the 16S rRNA marker (Fig. 4, Fig. S2).

The results reported here provide further support for the amazing catabolic abilities of microorganisms toward PA herbicides. In addition, give clues to explain the relatively fast turnover of these herbicides in soils and the natural bioremediation potential that can be observed in pristine and polluted environments (see as example, Fulthorpe *et al.*, 1996; Gonod *et al.*, 2006; Manzano *et al.*, 2007).

Experimental procedures

Soil experiments

Soil microcosms were prepared with a 28-year-old avocado (*Persea americana*) plantation soil located in central Chile (32°50′S, 71°13′W), which had been periodically treated with simazine, an herbicide not related to PA compounds, to control annual weeds, and occasionally with MCPA to control simazine resistant weeds. Rhizospheric (but not the rizhoplane) soil (3 kg) was taken from the first 20 cm of depth, at a distance of 0.5 m from the trunk of three trees, then sieved and air-dried. The original soil (also referred as non-incubated soil in experimental conditions) was stored in a dark, 4°C room. Microcosms were prepared in 20 ml glass flasks containing 10 g of soil, incubated for up to 4 months at

COR-AAD1-00003278
Bayer EX1008 (Part 6 of 9)

22 ± 5°C. Each microcosm (three replicates for each condition) was amended every two weeks with 6 μmol (approximately 120 p.p.m.) of PA herbicides (PAA, 2-MPA, 2,4-D, mecoprop, 2,4-DB, or a mixture of the last three compounds), which is close to the levels used for weed control (usually 30–50 p.p.m.); benzoic acid to test for effects of a non-PA aromatic compound, or distilled water, as a control for incubation effects.

Soil DNA isolation

Soil total genomic DNA was isolated from 1 g soil samples at the beginning of the experiment and after 4 months using the 'Ultra Clean Soil DNA Kit' (MoBio Laboratories), following the instructions of the manufacturers, and modifications reported elsewhere (Manzano *et al.*, 2007).

Terminal restriction fragment length polymorphism analysis

The T-RFLP technique was used to analyse the bacterial community structure and the diversity of the *tfdA* gene related sequences in each soil treatment. For the first case, oligonucleotide primer pairs designed for detection of bacterial 16S rRNA genes 8F (5′-AGA GTT TGA TCC TGG CTC AG-3′) (Lane, 1991) and 1392R (5′-ACG GGC GGT GTG TAC-3′) (Lane *et al.*, 1985) were used. Primer 8F was labelled at the 5′ end with the NED fluorochrome. PCR reactions were carried out in a Perkin-Elmer 2400 thermal cycler using the reaction conditions described elsewhere (Morán *et al.*, 2008). PCR product sizes (1.4 kb) were visualized after electrophoresis on 1% agarose gels prepared in TAE 1× buffer (40 mM Tris Acetate, 2 mM EDTA, pH 8) at 100 mV for 45 min and subsequent staining in ethidium bromide for 10 min. For the *tfdA* gene sequences analysis, *tfdA* gene sequence fragments of approximately 360 bp (and also those of longer sizes, see below) were amplified using degenerated primer pairs derived from conserved regions of the *tfdA* genes (Vallaeys *et al.*, 1996; Itoh *et al.*, 2002): forward primer 5′-AC(C/G) GAG TTC TG(C/T) GA(C/T) ATG-3′ and reverse primer 5′-(A/G)AC GCA GCG (G/A)TT (G/A)TC CCA-3′, the latter labelled with 6-FAM fluorochrome at the 5′ end. Each PCR reaction was performed in a total volume of 20 μL, containing 2 μL of 10× PCR buffer (200 mM Tris-HCl pH 8, 500 mM KCl), 1.2 mM $MgCl_2$, 0.2 mM of each primer, 0.2 mM of each deoxynucleotide triphosphate, 4% of dimethylsulfoxide, 50 ng μl^{-1} bovine seroalbumin, ~10–50 ng of soil DNA template and 1 U of *Taq* polymerase (Invitrogen, Brazil). PCR conditions were 94°C for 5 min, 35 cycles of 94°C for 1 min, 56°C of annealing temperature for 1 min and 72°C for 1 min, and a final extension step of 72°C for 7 min. PCR products were visualized as described for the 16S rRNA gene. PCR products were digested with endonucleases MspI or HhaI for 16S rRNA, and HaeIII or HhaI for *tfdA* gene sequences. Reactions were performed with 20 U of enzyme in a total volume of 20 μl at 37°C for 3 h, and the digested bacterial PCR products were purified by ethanol precipitation (Morán *et al.*, 2008). The DNA fragments were separated by capillary electrophoresis using a Perkin-Elmer ABI Prism 310 sequencer. The fragment sizes were determined using the internal standard ROX 500 as reference. T-RFLP data handling was carried out as described elsewhere (Morán *et al.*, 2008). Raw data sets consisted of peaks reflecting the size in bp of T-RFs and the area of each peak, measured in fluorescence units. T-RFs representing less than 0.5% of the total area and those with length sizes < 50 and > 500 bp were not included in the analyses. Technical duplicates gave essentially the same patterns and these data were averaged. Patterns from biological triplicates were treated separately. Data were standardized by calculating the area of each peak as a percentage of the total area. Profiles were plotted as peak area (relative abundance) against fragment size. Literature recommendations to minimize the drift between true and observed T-RFs were followed (Kaplan and Kitts, 2003). Richness (R) was calculated as the total T-RFs in each sample. Diversity (H') was calculated by the Shannon–Weaver index with the formula $H' = \Sigma p_i \cdot \mathrm{Ln}\ (p_i)$ (Margalef, 1958), where p is the proportion of an individual T-RF area relative to the sum of all T-RFs areas for each sample. Evenness (E) values were calculated with the formula $E = H'/\mathrm{Ln}\ (R)$ (Margalef, 1958). The T-RFs areas were analysed with the multivariate statistical software Primer 5 (Primer-E Ltd; Plymouth, UK) as described before (Morán *et al.*, 2008; Pavissich *et al.*, 2010). The statistical analysis, including non-metric multidimensional scaling (NMDS) analyses to group data according to their similarity, and one-way ANOSIM to examine the statistical significance of grouping, was performed as described elsewhere (Pavissich *et al.*, 2010). The output statistic for NMDS, R, which indicates the magnitude of difference among group samples, takes a value of 0 if there is no separation of the bacterial community structure due to the factor analysed, and 1 if total separation takes place. Values of $R \geq 0.5$ account for high differences, whereas between 0.25 and 0.5 differences are considered as moderate (Morán *et al.*, 2008; Pavissich *et al.*, 2010).

Detection and cloning of tfdA gene related sequences

Partial *tfdA* gene related sequences of approximately 360 bp were amplified using the primer pairs described above. In order to obtain longer *tfdA* gene related sequences (~630 bp), a new set of modified forward primers was specifically designed to extend the sequence towards the amino terminus, based on conserved regions of the complete *tfdA* gene sequences from β-*Proteobacteria* (Table S1). The new set of forward primers was: 5′-CAG CA(G/A) ATC GCC TT(T/C) GCG-3′. These oligonucleotides have the following predicted features that would make them suitable for PCR: melting temperature in the range 60–65°C (Panjkovich *et al.*, 2005), energy of intra-molecular interactions lower than −4 kcal mol^{-1} (Markham and Zuker, 2005), total number of contiguous inter-molecular interactions smaller than 6, total number of contiguous inter-molecular interactions at the 3′ end smaller than 5, and total number of non-contiguous inter-molecular interactions smaller than 9 bp. The reverse primer and the PCR conditions were the same indicated above.

The amplified short *tfdA* PCR products from the non-incubated soil, and from soils treated with 2,4-D and the mixture of herbicides, and the long *tfdA* PCR products from the non-incubated soil and from the treatments with PAA, 2MPA, 2,4-D, mecoprop or 2,4-DB treatments, were directly

COR-AAD1-00003279
Bayer EX1008 (Part 6 of 9)

ligated into pGEM-T Easy Vector and transformed into *E. coli* DH5α competent cells. The short *tfdA* gene related sequences clone library was analysed by RFLP with the enzyme MspI, while HaeIII was used for RFLP analysis of the long *tfdA* gene related sequences. Unique clones were sequenced and deposited in GenBank under the accession number GU173880-GU173932 (short sequences) and GU173933-GU173992 (long sequences).

Phylogenetic analysis

Thirteen *tfdA* gene related sequences, mostly of them with biochemically and or genetically supported function (Table S1), the RdpA and SdpA dioxygenase gene sequences from *D. acidovorans*, and taurine dioxygenase (TauD) from *E. coli*, were selected from the GenBank database (Benson *et al.*, 2008). A progressive block alignment procedure was carried out with ClustalW (Li, 2003). TfdA protein related sequences were divided in two groups based on taxonomic criteria: α-and β-proteobacterial sequences. Each group was independently aligned using the BLOSUM62 matrix, gap opening and extension penalties of 1.0 and 0.1 respectively. The resulting multiple sequence alignments (MSAs), were aligned as blocks based on the matrix and gap penalties indicated above, to produce a TfdA MSA. With such procedure, an alignment of two alignments is generated and the original MSAs are not internally modified. This has the advantage of preserving common and specific features that would be relevant within each group. Then, the SdpA, RdpA and TauD protein sequences were individually aligned, using ClustalW with default gap penalties, against the TfdA MSA to produce a TfdA/other dioxygenases MSA. Then, each one of the 59 clone sequences reported here was individually aligned against the TfdA/other oxygenases MSA, using default ClustalW parameters, producing the TfdA/other oxygenases/clones MSA. This MSA was manually inspected with Jalview alignment editor (Waterhouse *et al.*, 2009), and the first 47 and last 51 positions in the alignment were deleted. This editing procedure was carried out to exclude those protein regions at the N- and C-terminus that were not present in the clones. This edited MSA, containing a total of 75 sequences, was used to perform the phylogenetic and sequence analysis reported here.

A phylogenetic tree was built using maximum likelihood optimization criteria, with the PhyML package (Guindon *et al.*, 2005). The JTT amino acid substitution model was used as previously described (Jones *et al.*, 1992). Bootstrap values were calculated using one hundred replicates. Phylogenetic trees images were produced with the iTOL web server tool (Letunic and Bork, 2007) available at: http://itol.embl.de/.

Classification of new TfdA protein related sequences

To evaluate the degree of relationship between each new *tfdA* gene related sequence and those from known TfdA proteins, we created a global scoring scheme (the T score) that weights the contribution of each amino acid in the new sequence depending on its observed abundance in the same alignment position in the known TfdA proteins. Therefore, the maximum score value would be achieved by a new hypothetical TfdA protein sequence having at each position in the alignment the most frequently observed amino acid in the known TfdA proteins. Briefly, from the previously reported TfdA protein related sequences included in the alignment, the frequency of occurrence of each amino acid at each relative position in the alignment (positions 1–261 in the final MSA) was calculated. Each absolute frequency value was then divided by the total number of sequences contributing at that position (i.e. excluding gaps), thus obtaining a relative frequency value for the amino acid X at position Y in the alignment. After applying this procedure, a matrix of 261 columns (i.e. alignment positions) and 21 rows (i.e. 20 standard amino acids and a gap) was produced. This matrix was finally used to calculate the score (*T*) of each new sequence, using the following equation:

$$T = \frac{\sum_{i=1}^{261} M_{i,j}}{\sum_{i=1}^{261} \max M_{i,k}} \quad \forall k \in [1..21]$$

where *M* is the 261 × 21 matrix containing the relative frequencies, *i* is the alignment position and *j* is the amino acid of the sequence being scored found at the *i* position in the alignment.

Comparative structure modelling of C. necator TfdA protein

A comparative model of the TfdA protein sequence from *C. necator* (YP_025400) was built with MODELLER software (Sali and Blundell, 1993), using as a template the reported X-ray structure of TauD protein (PDB code 1OS7) from *E. coli* (O'Brien *et al.*, 2003). This template structure shares 29% sequence identity with the TfdA protein sequence from *C. necator*. A pairwise alignment of the sequences was generated using ClustalW software with default gap opening and extension penalty values and BLOSUM62 matrix. Taurine, α-ketoglutarate and iron heteroatom groups present in the template structure were also included and modelled as block residues. The three-dimensional modelling was carried out with MODELLER software.

Definition of relevant residues in TfdA protein

Six categories of functionally relevant amino acids were defined in the TfdA protein three-dimensional model, based on their correspondence to those amino acids already described as important in TauD protein from *E. coli* (O'Brien *et al.*, 2003) (Table 1). These functional categories included: Fe^{2+} binding, α-ketoglutarate binding, substrate binding, substrate locking, substrate burial or accessibility, and dimer formation. The relative positions of all these residues in the final MSA were determined and the corresponding subalignments of each functional category extracted. Then, sequence logos for each category were calculated using the WebLogo tool (http://weblogo.berkeley.edu/) (Crooks *et al.*, 2004).

Supplementary data

Several files, in a variety of formats, containing the high-resolution phylogram, the multiple sequence alignment, DNA

COR-AAD1-00003280
Bayer EX1008 (Part 6 of 9)

sequences, protein sequences and the *C. necator* TfdA protein three-dimensional structure model are available from the following website: http://protein.bio.puc.cl/sup-mat.html.

Acknowledgements

This work has been funded by the 'Millennium Nucleus in Microbial Ecology and Environmental Microbiology and Biotechnology' Grant P/04-007-F, the 'Plant Functional Genomics' Grant P06-009F and the FONDECYT Grant 1080158. This study is also part of the research program FONDAP 1501-0001 funded by CONICYT to the Center for Advanced Studies in Ecology and Biodiversity Program 7. Additional support from grant PBCT RED-12, and grant ICA4-CT-2002-10011 (ACCESS) contract of the European Union is acknowledged.

References

Ahrens, W.H. (1994) *Herbicide Handbook (WSSA)*, 7th edn. Champaign, IL, USA: Weed Science Society of America.

Altschul, S.F., Gish, W., Miller, W., Myers, E.W., and Lipman, D.J. (1990) Basic local alignment search tool. *J Mol Biol* **215:** 403–410.

Altschul, S.F., Madden, T.L., Schaffer, A.A., Zhang, J., Zhang, Z., Miller, W., and Lipman, D.J. (1997) Gapped BLAST and PSI-BLAST: a new generation of protein database search programs. *Nucleic Acids Res* **25:** 3389–3402.

Bælum, J., and Jacobsen, C.S. (2009) TaqMan probe-based Real-Time PCR assay for detection and discrimination of class I, II, and III *tfdA* genes in soils treated with phenoxy acid herbicides. *Appl Environ Microbiol* **75:** 2969–2972.

Bælum, J., Henriksen, T., Hansen, H.C.B., and Jacobsen, C.S. (2006) Degradation of 4-chloro-2-methylphenoxyacetic acid in top- and subsoil is quantitatively linked to the class III *tfdA* gene. *Appl Environ Microbiol* **72:** 1476–1486.

Bælum, J., Nicolaisen, M.H., Holben, W.E., Strobel, B.W., Sørensen, J., and Jacobsen, C.S. (2008) Direct analysis of *tfdA* gene expression by indigenous bacteria in phenoxy acid amended agricultural soil. *ISME J* **2:** 677–687.

Benson, D.A., Karsch-Mizrachi, I., Lipman, D.J., Ostell, J., and Wheeler, D.L. (2008) GenBank. *Nucleic Acids Res* **36:** D25–D30.

Cao, B., and Loh, K.-C. (2008) Catabolic pathways and cellular responses of *Pseudomonas putida* P8 during growth on benzoate with a proteomics approach. *Biotechnol Bioeng* **101:** 1297–1312.

Crooks, G.E., Hon, G., Chandonia, J.M., and Brenner, S.E. (2004) WebLogo: a sequence logo generator. *Genome Res* **14:** 1188–1190.

Cultrone, A., Scazzocchio, C., Rochet, M., Montero-Morán, G., Drevet, C., and Fernández-Martín, R. (2005) Convergent evolution of hydroxylation mechanisms in the fungal kingdom: molybdenum cofactor-independent hydroxylation of xanthine via alpha-ketoglutarate-dependent dioxygenases. *Mol Microbiol* **57:** 276–290.

Dunning Hotopp, J.C., and Hausinger, R.P. (2001) Alternative substrates of 2,4-dichlorophenoxyacetate/a-ketoglutarate dioxygenase. *J Mol Catal B Enzym* **15:** 155–162.

Dunning Hotopp, J.C., and Hausinger, R.P. (2002) Probing the 2,4-dichlorophenoxyacetate/alpha-ketoglutarate dioxygenase substrate-binding site by site-directed mutagenesis and mechanism-based inactivation. *Biochemistry* **41:** 9787–9794.

Eichhorn, E., van der Ploeg, J.R., Kertesz, M.A., and Leisinger, T. (1997) Characterization of alpha-ketoglutarate-dependent taurine dioxygenase from *Escherichia coli*. *J Biol Chem* **272:** 23031–23036.

Elkins, J.M., Ryle, M.J., Clifton, I.J., Dunning Hotopp, J.C., Lloyd, J.S., Burzlaff, N.I., *et al.* (2002) X-ray crystal structure of *Escherichia coli* taurine/alpha-ketoglutarate dioxygenase complexed to ferrous iron and substrates. *Biochemistry* **41:** 5185–5192.

Fukumori, F., and Hausinger, R.P. (1993a) Purification and characterization of 2,4-dichlorophenoxyacetate/α-ketoglutarate dioxygenases. *J Biol Chem* **268:** 24311–24317.

Fukumori, F., and Hausinger, R.P. (1993b) *Alcaligenes eutrophus* JMP134 '2,4-dichlorophenoxyacetate monooxygenase' is an α-ketoglutarate-dependent dioxygenase. *J Bacteriol* **175:** 2083–2086.

Fulthorpe, R.R., Rhodes, A.N., and Tiedje, J.M. (1996) Pristine soils mineralize 3-chlorobenzoate and 2,4-dichlorophenoxyacetate via different microbial populations. *Appl Environ Microbiol* **62:** 1159–1166.

Gonod, L.V., Martin-Laurent, F., and Chenu, C. (2006) 2,4-D impact on bacterial communities, and the activity and genetic potential of 2,4-D degrading communities in soil. *FEMS Microbiol Ecol* **58:** 529–537.

Guindon, S., Lethiec, F., Duroux, P., and Gascuel, O. (2005) PHYML Online - a web server for fast maximum likelihood-based phylogenetic inference. *Nucleic Acids Res* **33:** W557–W559.

Hegg, E.L., Whiting, A.K., Saari, R.E., McCracken, J., Hausinger, R.P., and Que, L. (1999) Herbicide-degrading alpha-keto acid-dependent enzyme TfdA: Metal coordination environment and mechanistic insights. *Biochemistry* **38:** 16714–16726.

Hoffmann, D., Kleinsteuber, S., Müller, R.H., and Babel, W. (2003) A transposon encoding the complete 2,4-dichlorophenoxyacetic acid degradation pathway in the alkalitolerant strain *Delftia acidovorans* P4a. *Microbiology* **149:** 2545–2556.

Hogan, D.A., Auchtung, T.A., and Hausinger, R.P. (1999) Cloning and characterization of a sulfonate/alpha-ketoglutarate dioxygenase from *Saccharomyces cerevisiae*. *J Bacteriol* **181:** 5876–5879.

Hogan, D.A., Buckley, D.H., Nakatsu, C.H., Schmidt, T.M., and Hausinger, R.P. (1997) Distribution of the *tfdA* gene in soil bacteria that do not degrade 2,4 dichlorophenoxyacetic acid, 2,4-D. *Microb Ecol* **34:** 90–96.

Hogan, D.A., Smith, S.R., Saari, E.A., McCracken, J., and Hausinger, R.P. (2000) Site-directed mutagenesis of 2,4-dichlorophenoxyacetic acid/alpha-ketoglutarate dioxygenase - Identification of residues involved in metallocenter formation and substrate binding. *J Biol Chem* **275:** 12400–12409.

Itoh, K., Kanda, R., Momoda, Y., Sumita, Y., Kamagata, Y., Suyama, K., *et al.* (2000) Presence of 2,4-D-catabolizing bacteria in a Japanese arable soil that belong to BANA

COR-AAD1-00003281
Bayer EX1008 (Part 6 of 9)

(*Bradyrhizobium-Agromonas-Nitrobacter-Afipia*) cluster in α-*Proteobacteria*. *Microbes Environ* **15:** 113–117.

Itoh, K., Kanda, R., Sumita, Y., Kim, H., Kamagata, Y., Suyama, K., *et al.* (2002) *tfdA*-like genes in 2,4-dichlorophenoxyacetic acid-degrading bacteria belonging to the *Bradyrhizobium-Agromonas-Nitrobacter-Afipia* cluster in α-*Proteobacteria*. *Appl Environ Microbiol* **68:** 3449–3454.

Itoh, K., Tashiro, Y., Uobe, K., Kamagata, Y., Suyama, K., and Yamamoto, H. (2004) Root nodule *Bradyrhizobium* spp. harbour *tfdAα* and *cadA*, homologous with genes encoding 2,4-dichlorophenoxyacetic acid-degrading proteins. *Appl Environ Microbiol* **70:** 2110–2118.

Jones, D.T., Taylor, W.R., and Thornton, J.M. (1992) The rapid generation of mutation data matrices from protein sequences. *Comput Appl Biosci* **8:** 275–282.

Ka, J.O., Holben, W.E., and Tiedje, J.M. (1994) Use of gene probes to aid in recovery and identification of functionally dominant 2,4-dichlorophenoxyacetic acid-degrading populations in soil. *Appl Environ Microbiol* **60:** 1116–1120.

Kahnert, A., and Kertesz, M.A. (2000) Characterisation of a sulfur-regulated oxygenative alkylsulfatase from *Pseudomonas putida*. *J Biol Chem* **257:** 31661–31667.

Kamagata, Y., Fulthorpe, R., Tamura, K., Takami, H., Forney, L.J., and Tiedje, J.M. (1997) Pristine environments harbour a new group of oligotrophic 2,4-dichlorophenoxyacetic acid-degrading bacteria. *Appl Environ Microbiol* **63:** 2266–2272.

Kaplan, C.W., and Kitts, C.L. (2003) Variation between observed and true terminal restriction fragment length is dependent on true TRF length and purine content. *J Microbiol Methods* **54:** 121–125.

Kitagawa, W., Takami, S., Miyauchi, K., Masai, E., Kamagata, Y., Tiedje, J.M., *et al.* (2002) Novel 2,4-dichlorophenoxyacetic acid degradation genes from oligotrophic *Bradyrhizobium* sp. strain HW13 isolated from a pristine environment. *J Bacteriol* **184:** 509–518.

Kohler, H.P.E. (1999) *Sphingomonas herbicidovorans* MH: a versatile phenoxyalkanoic acid herbicide degrader. *J Ind Microbiol Biotechnol* **23:** 336–340.

Lambert, L.A., Abshire, K., Blankenhorn, D., and Slonczewski, J.L. (1997) Proteins induced in *Escherichia coli* by benzoic acid. *J Bacteriol* **179:** 7595–7599.

Lane, D.J. (1991) *16S/23S rRNA Sequencing. Nucleic Acid Techniques in Bacterial Systematics*. New York, USA: John Wiley and Sons.

Lane, D.J., Pace, B., Olsen, G.J., Stahl, D.A., Sogin, M.L., and Pace, N.R. (1985) Rapid determination of 16S ribosomal RNA sequences for phylogenetic analyses. *Proc Natl Acad Sci USA* **82:** 6955–6959.

Letunic, I., and Bork, P. (2007) Interactive Tree Of Life (iTOL): an online tool for phylogenetic tree display and annotation. *Bioinformatics* **23:** 27–28.

Li, K.B. (2003) ClustalW-MPI: ClustalW analysis using distributed and parallel computing. *Bioinformatics* **19:** 1585–1586.

de Lipthay, J.R., Aamand, J., and Barkay, T. (2002) Expression of *tfdA* genes in aquatic microbial communities during acclimation to 2,4-dichlorophenoxyacetic acid. *FEMS Microbiol Ecol* **40:** 205–214.

Macur, R.E., Wheeler, J.T., Burr, M.D., and Inskeep, W.P. (2007) Impacts of 2,4-D application on soil microbial community structure and on populations associated with 2,4-D degradation. *Microbiol Res* **162:** 37–45.

Manzano, M., Morán, A.C., Tesser, B., and González, B. (2007) Role of eukaryotic microbiota in soil survival and catabolic performance of the 2,4-D herbicide degrading bacteria *Cupriavidus necator* JMP134. *Anton Leeuwen Int J Gen Mol Microbiol* **91:** 115–126.

Margalef, R. (1958) Information theory in ecology. *Gen Syst* **3:** 36–71.

Markham, N.R., and Zuker, M. (2005) DINAMelt web server for nucleic acid melting prediction. *Nucleic Acids Res* **33** (Web Server issue): W577–W581.

Marriott, M.W., Smejkal, C.W., and Lappin-Scott, H.M. (2000) Biodegradation of mixtures of chlorophenoxyalkanoic acid herbicides by *Alcaligenes denitrificans*. *J Ind Microbiol Biotechnol* **25:** 1–5.

McGowan, C., Fulthorpe, R., Wright, A., and Tiedje, J.M. (1998) Evidence for interspecies gene transfer in the evolution of 2,4-dichlorophenxyacetic acid degraders. *Appl Environ Microbiol* **64:** 4089–4092.

Morán, A.C., Hengst, M.B., De la Iglesia, R., Andrade, S., Correa, J.A., and González, B. (2008) Changes in bacterial community structure associated with coastal copper enrichment. *Environ Toxicol Chem* **27:** 2239–2245.

Müller, T.A., Fleischmann, T., van der Meer, J.R., and Kohler, H.P.E. (2006) Purification and characterization of two enantioselective α-ketoglutarate-dependent dioxygenases, RdpA and SdpA, from *Sphingomonas herbicidovorans* MH. *Appl Environ Microbiol* **72:** 4853–4861.

Müller, R.H., Jorks, S., Kleinsteuber, S., and Babel, W. (1999) *Comamonas acidovorans* strain MC1: a new isolate capable of degrading the chiral herbicides dichlorprop and mecoprop and the herbicides 2,4-D and MCPA. *Microbiol Res* **154:** 241–246.

Nickel, K., Suter, M.J.F., and Kohler, H.P.E. (1997) Involvement of two α-ketoglutarate-dependent dioxygenases in enantioselective degradation of (*R*)- and (*S*)-mecoprop by *Sphingomonas herbicidovorans* MH. *J Bacteriol* **179:** 6674–6679.

Nicolaisen, M.H., Baelum, J., Jacobsen, C.S., and Sorensen, J. (2008) Transcription dynamics of the functional *tfdA* gene during MCPA herbicide degradation by *Cupriavidus necator* AEO106 (pRO101) in agricultural soil. *Environ Microbiol* **10:** 571–579.

O'Brien, J.R., Schuller, D.J., Yang, V.S., Dillard, B.D., and Lanzilotta, W.N. (2003) Substrate-induced conformational changes in *Escherichia coli* taurine/alpha-ketoglutarate dioxygenase and insight into the oligomeric structure. *Biochemistry* **42:** 5547–5554.

Panjkovich, A., Norambuena, T., and Melo, F. (2005) dnaMATE: a consensus melting temperature prediction server for short DNA sequences. *Nucleic Acids Res* **33:** 570–572.

Pavissich, J.P., Silva, M., and González, B. (2010) Sulfate reduction, molecular diversity, and copper amendment effects in bacterial communities enriched from sediments exposed to copper mining residues. *Environ Toxicol Chem* **29:** 256–264.

COR-AAD1-00003282
Bayer EX1008 (Part 6 of 9)

Pieper, D.H., Reineke, W., Engesser, K.H., and Knackmuss, H.J. (1988) Metabolism of 2,4-dichlorophenoxyacetic acid, 4-chloro-2-methylphenoxyacetic acid and 2-methylphenoxyacetic acid by *Alcaligenes eutrophus* JMP134. *Arch Microbiol* **150:** 95–102.

Poh, R.P.-C., Smith, A.R.W., and Bruce, I.J. (2002) Complete characterization of *Tn5530* from *Burkholderia cepacia* strain 2a (pIJB1) and studies of 2,4-dichlorophenoxyacetate uptake by the organism. *Plasmid* **48:** 1–12.

Sali, A., and Blundell, T.L. (1993) Comparative protein modelling by satisfaction of spatial restraints. *J Mol Biol* **234:** 779–815.

Schleinitz, K.M., Kleinsteuber, S., Vallaeys, T., and Babel, W. (2004) Localization and characterization of two novel genes encoding stereospecific dioxygenases catalyzing 2(2,4-dichlorophenoxy)propionate cleavage in *Delftia acidovorans* MC1. *Appl Environ Microbiol* **70:** 5357–5365.

Shaw, L., and Burns, R.G. (2004) Enhanced mineralization of [U-14C]2,4-dichlorophenoxyacetic acid in soil from the rhizosphere of *Trifolium pretense*. *Appl Environ Microbiol* **70:** 4766–4774.

Smejkal, C.W., Vallaeys, T., Burton, S.K., and Lappin-Scott, H.M. (2001) Substrate specificity of chlorophenoxyalkanoic acid-degrading bacteria is not dependent upon phylogenetically related *tfdA* gene types. *Biol Fertil Soils* **33:** 507–513.

Streber, W.R., Timmis, KN., and Zenk, M.H. (1987) Analysis, cloning, and high-level expression of 2,4-dichlorophenoxyacetate monooxygenase gene *tfdA* of *Alcaligenes eutrophus* JMP134. *J Bacteriol* **169:** 2950–2955.

Suwa, Y., Wright, A.D., Fukumori, F., Nummy, K.A., Hausinger, R.P., Holben, W.E., and Forney, L.J. (1996) Characterization of a chromosomally encoded 2,4-dichlorophenoxyacetate/ a-ketoglutarate dioxygenase from *Burkholderia* sp. strain RASC. *Appl Environ Microbiol* **62:** 2464–2469.

Vallaeys, T., Fulthorpe, R., Wright, A.M., and Soulas, G. (1996) The metabolic pathway of 2,4-dichlorophenoxyacetic acid degradation involves different families of *tfdA* and *tfdB* genes according to PCR-RFLP analysis. *FEMS Microbiol Ecol* **20:** 163–172.

Vedler, E., Kõiv, V., and Heinaru, A. (2000) Analysis of the 2,4-dichlorophenoxyacetic acid-degradative plasmid pEST4011 of *Achromobacter xylosoxidans* subsp. *denitrificans* strain EST4002. *Gene* **255:** 281–288.

Vroumsia, T., Steiman, R., Seigle-Murandi, F., and Benoit-Guyod, J.L. (2005) Fungal bioconversion of 2,4-dichlorophenoxyacetic acid (2,4-D) and 2,4-dichlorophenol (2,4-DCP). *Chemosphere* **60:** 1471–1480.

Waterhouse, A.M., Procter, J.B., Martin, D.M.A., Clamp, M., and Barton, G.J. (2009) Jalview Version 2 - a multiple sequence alignment editor and analysis workbench. *Bioinformatics* **25:** 1189–1191.

Zakaria, D., Lappin-Scott, H., Burton, S., and Whitby, C. (2007) Bacterial diversity in soil enrichment cultures amended with 2-(2-methyl-4-chlorophenoxy)propionic acid (mecoprop). *Environ Microbiol* **9:** 2575–2587.

Zipper, C., Nickel, K., Angst W., and Kohler, H.P.E. (1996) Complete microbial degradation of both enantiomers of the chiral herbicide mecoprop [(RS)-2-(4-chloro-2-methylphenoxy)propionic acid] in an enantioselective manner by *Sphingomonas herbicidovorans* sp. *Appl Environ Microbiol* **62:** 4318–4322.

Supporting information

Additional Supporting Information may be found in the online version of this article:

Fig. S1. Chemical structure of phenoxyalkanoic herbicides. Compounds used in this study are indicated with asterisk.
Fig. S2. Cluster analysis of 16S rRNA (A) and *tfdA* gene sequences (B) T-RFLP profiles.
Table S1. TfdA protein sequences used in this study.
Table S2. Total richness (S), diversity (H) and evenness (E) values obtained from the T-RFLP profiles of the 16S rRNA and the *tfdA* gene related sequences.

Please note: Wiley-Blackwell are not responsible for the content or functionality of any supporting materials supplied by the authors. Any queries (other than missing material) should be directed to the corresponding author for the article.

© 2010 Society for Applied Microbiology and Blackwell Publishing Ltd,

COR-AAD1-00003283
Bayer EX1008 (Part 6 of 9)

Supplementary Information

Molecular Basis for Enantioselective Herbicide Degradation Imparted by Aryloxyalkanoate Dioxygenases (AADs) in Transgenic Plants

Jonathan R. Chekan[1,2,#], Chayanid Ongpipattanakul[1,#], Terry R. Wright[3], Bo Zhang[4], J. Martin Bollinger, Jr.[4,5], Lauren J. Rajakovich[4], Carsten Krebs[4,5], Robert M. Cicchillo[3],and Satish K. Nair[1,2,6,*]

[1]Department of Biochemistry, [2]Carl R. Woese Institute for Genomic Biology, and [6]Center for Biophysics and Quantitative Biology; University of Illinois, 600 S Mathews Ave, Urbana, IL, 61801, USA
and
[3]Corteva Agriscience™, Agriculture Division of DowDuPont, 9330 Zionsville Road, Indianapolis, IN, 46268, USA
and
[4]Department of Chemistry and [5]Department of Biochemistry and Molecular Biology, The Pennsylvania State University, University Park, Pennsylvania 16802

These authors contributed equally to this work
Authors to whom correspondence should be addressed: snair@illinois.edu

COR-AAD1-00003284
Bayer EX1008 (Part 6 of 9)

TABLE OF CONTENTS

Supplementary Materials and Methods.....3

Supplementary Figure 1 – Genomic Context of TfdA from *Cupriavidua necator* JMP134..... .7

Supplementary Figure 2 – Phylogenetic tree of putative AAD sequences..... 8

Supplementary Figure 3 – Genomic Context of AAD-1 and AAD-12.....9

Supplementary Figure 4 – Analytical Gel Filtration and SDS-PAGE analysis of AADs.....10

Supplementary Figure 5 – Normalized activity of AAD-2 against a panel of substrates 11

Supplementary Figure 6 - Kinetic curves for the AAD-2 reaction using various substrates.....12

Supplementary Figure 7 – Activity of AAD-2 against MCPA 13

Supplementary Figure 8 – Kinetic-difference spectra from the stopped-flow absorption experiment....14

Supplementary Figure 9 – Mössbauer spectra of a sample of the AAD-1 reaction.....15

Supplementary Figure 10 – Sequence alignment of select AADs.....16

Supplementary Table 1 – List of putative AADs identified by EFI-EST.....17

Supplementary Table 2 – Kinetic parameters of AAD-1 and AAD-2 across a panel of substrates.....19

Supplementary Table 3 – List of primers used in this study.....20

Supplementary Table 4 – Data collection and refinement statistics..... 21

Supplementary References.....22

COR-AAD1-00003285
Bayer EX1008 (Part 6 of 9)

Supplementary Materials and Methods

General Procedures, Chemicals, and Reagents

All chemical reagents were purchased from Sigma-Aldrich unless otherwise noted. All of the material used for protein production and purification were purchased from GE Healthcare. *Escherichia coli* DH5α and BL21(DE3)Rosetta (Invitrogen) strains were used for plasmid maintenance and protein overexpression respectively unless otherwise noted.

Preparation of AAD-1 for Crystallographic Studies

Lyophilized AAD-1 supplied by Corteva Agriscience was resuspended in a buffer composed of 100 mM KCl and 20 mM HEPES free acid (pH 7.5) and further purified by size exclusion chromatography using a Superdex S75-16/60 column (GE Healthcare Life Sciences) equilibrated with the same buffer. Pure fractions were collected and concentrated to 50-60 mg/mL before storage in liquid nitrogen.

Cloning, Expression and Purification of AAD-2

The *aad2* gene from *Bradyrhizobium diazoefficiens* USDA 110 cloned into a pET28-a vector using the primer listed in **Supplementary Table S2**, and the resultant plasmid was transformed into *E. coli* containing the Rosetta plasmid for subsequent expression. AAD-2 was produced by growing the cells in shaking flask of LB media at a temperature of 37 °C. When the cells reached an $O.D._{600}$ of 0.6, the cells were cooled on ice for 15 minutes. Following the addition of 0.5 mM IPTG, the cells were placed in an 18 °C shaking incubator for 18 hours. The cells were then harvested by centrifugation and resuspended in a buffer composed of 500 mM NaCl, 20 mM Tris base (pH 8.0), and 10% glycerol. Resuspended cells were lysed by sonication and the lysate was centrifuged at 14,000 rpm to remove cell debris. The cleared cell lysate was loaded onto a HisTrap column, which was subsequently washed with 1 M NaCl, 30 mM imidazole, and 20 mM Tris base (pH 8.0). Polyhistidine tagged AAD-2 was eluted using a linear gradient beginning with 1 M NaCl, 20 mM Tris base (pH 8.0), and 30 mM imidazole and ending with 250 mM imidazole. Pure fractions, as judged by SDS-PAGE, were combined and treated with thrombin (final ratio of 1:100 (w/w)) for 18 hours at 4 °C to cleave the N-terminal tag. Tag-free AAD-2 was concentrated and loaded onto a size exclusion column (Superdex S75 16/60) pre-equilibrated with containing 100 mM KCl and 20 mM HEPES free acid (pH 7.5). Pure fractions were collected and concentrated to 25 mg/mL before storage in liquid nitrogen.

AAD-1 Activity under Conditions of Stopped-Flow and Freeze-Quench Experiments.

The stopped-flow absorption and freeze-quenched Mössbauer experiments were carried out essentially as previously described (1). The stopped-flow experiments were carried out at 5 °C on an Applied

COR-AAD1-00003286
Bayer EX1008 (Part 6 of 9)

Photophysics (Leatherhead, U.K.) SX20 instrument housed in a Labmaster MBraun glovebox. The instrument was configured for single mixing with an optical path length of 1 cm and detection with a photodiode-array (PDA). In the experiments shown in Figure 3A, an air-saturated buffer solution (50 mM sodium MOPS, pH 7.5, 10% glycerol) was mixed with an equal volume of an anoxic solution containing 1.1 mM AAD-1, 1.0 mM Fe(II), 10 mM αKG and either no primary substrate, 9 mM 2,4,-D, or 9 mM d_2-2,4-D. Owing to the complexity of the kinetic traces, no attempt was made to fit the data globally according to a necessarily elaborate kinetic model. Rather, traces were fit as the sum of exponentials to provide estimates for the observed rate constants characterizing the multiple phases of the reactions with and without the 2,4-D primary substrate (or its deuterium-containing isotopologue). In the freeze-quench Mössbauer experiment shown in Figure 3B, the reactant complex contained 2.2 mM AAD-1, 2.0 mM $^{57}Fe^{2+}$, 10 mM αKG, and 9.0 mM d_2-2,4D. It was mixed at 5 °C with an equal volume of O_2-saturated buffer (the same buffer used in the stopped-flow experiments), and the reaction was quenched by rapid freezing after 0.09 s. A second sample was quenched at a reaction time of 0.28 s to verify the transient nature of the new species detected in the 0.09-s sample. Mössbauer spectra were recorded on a constant acceleration Mössbauer spectrometer from Seeco (Edina, MN) equipped with a Janis SVT-400 variable temperature cryostat. Isomer shifts are reported with respect to the centroid of the spectrum of α-iron metal at room temperature. Simulations of Mössbauer spectra were carried out with the program WMOSS (Seeco, Edina, MN).

Determination of Substrate Scope and Kinetic Parameters

To determine the substrate scope for AAD-2, we used a coupled continuous assay monitoring the decrease in absorbance of NADH at 340nm using reactions in a 96-well microplate format. Reactions contained a total volume of 150 µL, with the following composition: 20 mM MOPS (pH 7.0), 200 µM $FeSO_4 \bullet 7H_20$, 200 µM L-ascorbic acid, 10µM AAD-2, 3 mM of each respective substrate, 14 units of lactate dehydrogenase (Roche), and 400 µM NADH. Assays were initiated by the addition of α-ketoglutarate to a final concentration of 1 mM. Plates were read using an Epoch Microplate Spectrophotometer (BioTek®) and monitored using the Gen5 software (BioTek®). Reactions were carried out in triplicate. Relative V_{max} over a linear range was determined for each substrate, and then the data was normalized against the highest relative V_{max}. Prism5 (GraphPad) was used to visualize the data.

To obtain kinetic parameters for AAD-2, an end point assay monitoring the emergence of a red quinone dye at 510 nm was utilized. Reactions contained 10 µM AAD-2, the appropriate volume of each serially diluted substrate, in the following buffer: 20 mM MOPS (pH 7.0), 200 µM $FeSO_4 \bullet 7H_20$, 200 µM L-ascorbic acid. Reactions were initiated in the same manner as aforementioned. All reactions were carried

COR-AAD1-00003287
Bayer EX1008 (Part 6 of 9)

out under ambient conditions: the system may have not necessarily been saturated in O_2. After the fifteen minutes, reactions were quenched with the addition of 10 μL of 100 mM EDTA (pH 8.0). To develop each reaction for absorbance readings at 510 nm, 15 μL of pH 10 buffer (3.09 g boric acid, 3.73 g KCl, 44 mL of 1N KOH), 0.2% 4-aminoantipyrine, and 0.8% potassium ferricyanide was added to each well. The resultant color was allowed to develop for three minutes before absorbance readings were performed. Additional kinetic parameters for AAD-1 were obtained using the same experimental procedures as for AAD-2, except that only 2 μM of enzyme was used. Reactions were carried out in triplicate; Prism5 (GraphPad) was used to analyze and visualize the data.

Crystallization of AAD-1 and AAD-2

Preliminary crystals of AAD-1 in complex with Mn^{2+}, αKG, and (*R*)-dichlorprop were obtained using a sparse matrix screen. Diffraction quality crystals were grown using hanging drop vapor diffusion with 8 mg/mL AAD-1 pre-incubated with 5 mM (*R*)-dichlorprop, 5 mM αKG, and 5 mM $MnCl_2$. The protein mixture was added to mother liquor containing 25% PEG 3350, 0.3 M Li_2SO_4, and 0.1 M bicine (pH 9.0) in a 1:1 ratio at 4 °C. Crystals of AAD-1 in complex with (*R*)-cyhalofop or (*R*)-diclofop were obtained in a similar manner. Diffraction quality crystals of AAD-1 (10-15 mg/mL) in complex with (*R*)-dichlorprop (5 mM), and vanadyl sulfate (1 mM) were obtained by seeding using the same conditions described above. Addition of succinate in the drop impeded crystallization, and complexes were obtained by soaking crystals of AAD-1/vanadyl/(*R*)-dichlorprop in crystallization media supplemented with 5 mM succinate. Crystals of AAD-2 in complex with Mn^{2+} and NOG were first observed using a sparse matrix screen and refined using the hanging drop method. Briefly, AAD-2 (8-12 mg/mL), was incubated with (*S*)-dichlorprop, Mn^{2+}, and NOG (each at 2 mM) for 20 minutes and then mixed with a solution containing 22-28% PEG 4000, 0.07 M $LiSO_4$, and 0.1 M MES (pH 6.0) and equilibrated against the same solution. Crystals of all samples were briefly soaked in mother liquor supplemented with either 15% glycerol (AAD-1) or 15% ethylene glycol (AAD-2) immediately prior to vitrification by direct immersion into liquid nitrogen.

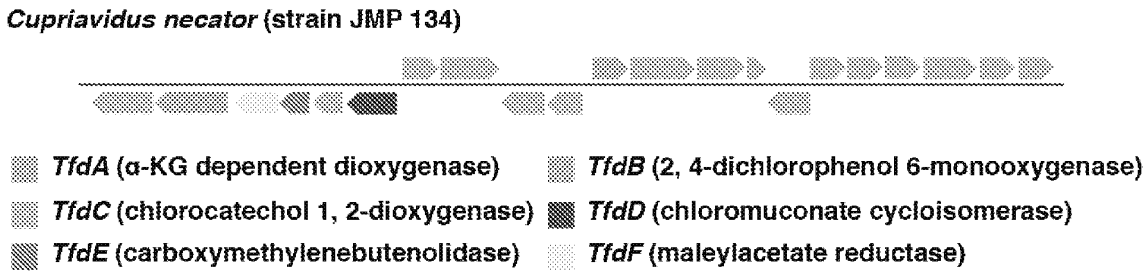
Bioinformatics

The sequence divergence of known AAD members limited identification of other AADs based solely on sequence similarities with select members of PF20668 (TauD) superfamily. Thus, the sequences of TfdA, AAD-1, and AAD-12 were each used to generate Sequence Similarity Networks (SSNs) (2) based on individual BLAST search (1000 sequences each). Gene Neighborhood Networks (GNNs) (3), using a gene window of 15 genes upstream and downstream of each sequence node, were then constructed for each SSN output. Each graphical GNN was then examined for presence for the following PFAMs:

COR-AAD1-00003288
Bayer EX1008 (Part 6 of 9)

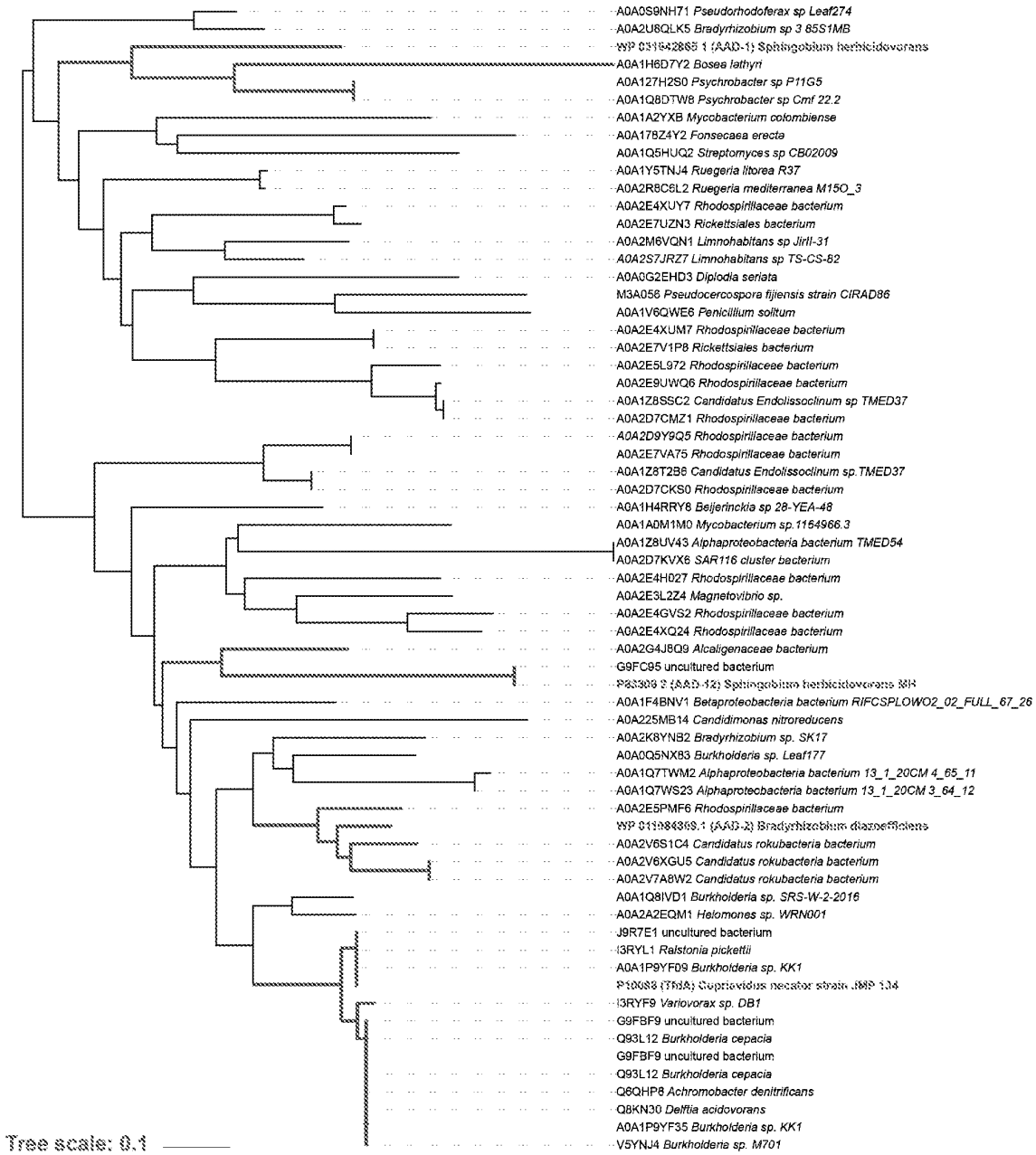
PF01494 (TfdB-like monooxygenases), or PF00775 fused to PF04444 (TfdC-like 1, 2 catechol dioxygenases). Clusters that contain mis-annotated PF01494, and PF00775 and PF04444 were included. Clusters that contained PF00775 fused to PF12391 (protocatechuate 3, 4-dioxygenases) were also included. The final SSN was generated using these sequences, along with sequences of TfdA, AAD-1, AAD-12, and 238 randomly selected members of the TauD superfamily (1/170 of all annotated TauD family members in the Uniref90 database). A representative node network at sequence similarity of 100% was used in order to filter through duplicate entries that were obtained during the initial query. Singletons (i.e. nodes with no other similar sequences) were omitted from Fig. 2 to concisely visualize the data.

COR-AAD1-00003289
Bayer EX1008 (Part 6 of 9)



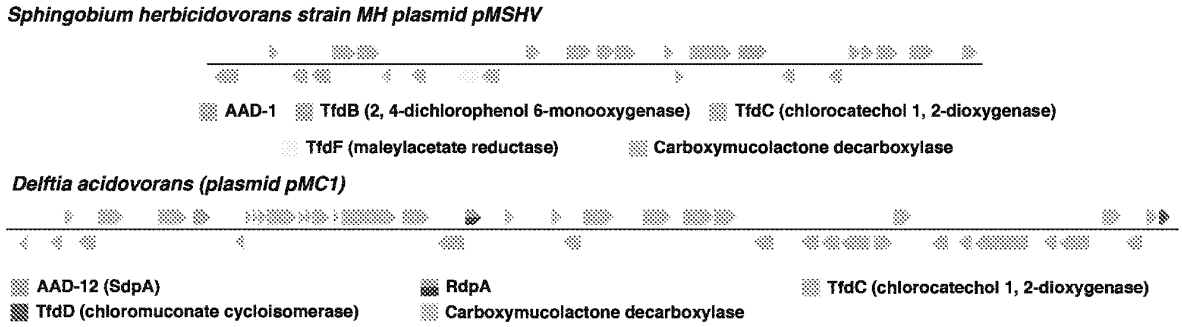
Supplementary Figure 1. Genomic context of *Tfd*A-F from the conjugative plasmid pJP4. Plasmid pJP4 was initially detected in the host bacterium *Cupriavidus necator* JMP134 (4). Genes of importance to degradation pathways are highlighted and annotated according to the legend below. Proteins that are non-essential to the pathway have been colored grey.

COR-AAD1-00003290
Bayer EX1008 (Part 6 of 9)



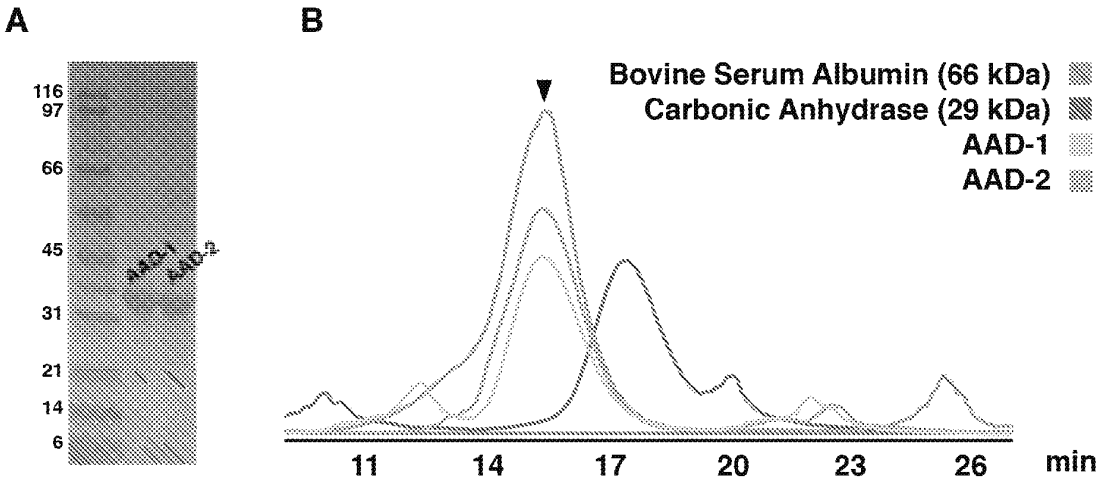
Supplementary Figure 2. Phylogenetic tree of putative AAD sequences. Sequences manually culled and used for the SNN/GNN analysis are shown in black, while sequences in blue are AADs of interest that have been biochemically characterized. Clades that contain the AADs of interest are also noted in blue.

COR-AAD1-00003291
Bayer EX1008 (Part 6 of 9)



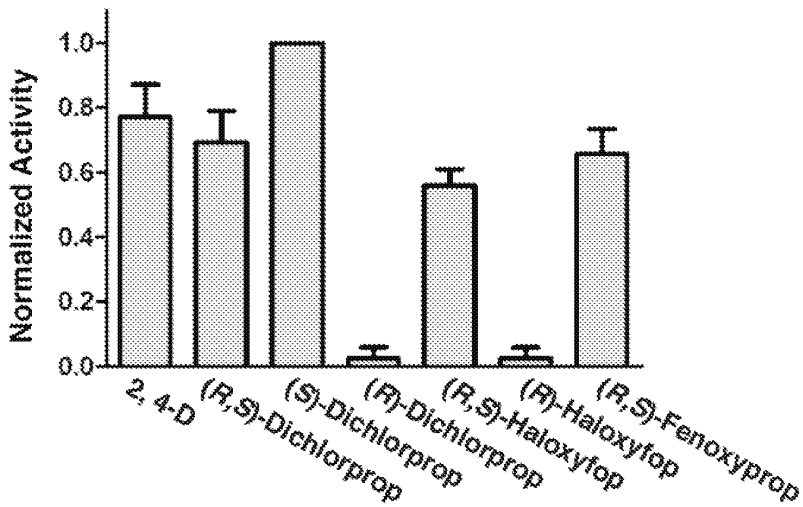
Supplementary Figure 3. Genomic context of AAD-1 and AAD-12. The genomic context highlights the distal nature of potential biosynthetic genes. We note that the genomic context of AAD-1 is that of a homolog (98% amino acid sequence similarity to the AAD-1 that was crystalized), as there is no annotated genomic data for corresponding organism and conjugative plasmid in public databases. Annotated genomic context of AAD-2 was also not available in public databases. Genes of importance to degradation pathways are highlighted and annotated according to the legend below. Proteins that are non-essential to the pathway have been colored grey.

COR-AAD1-00003292
Bayer EX1008 (Part 6 of 9)



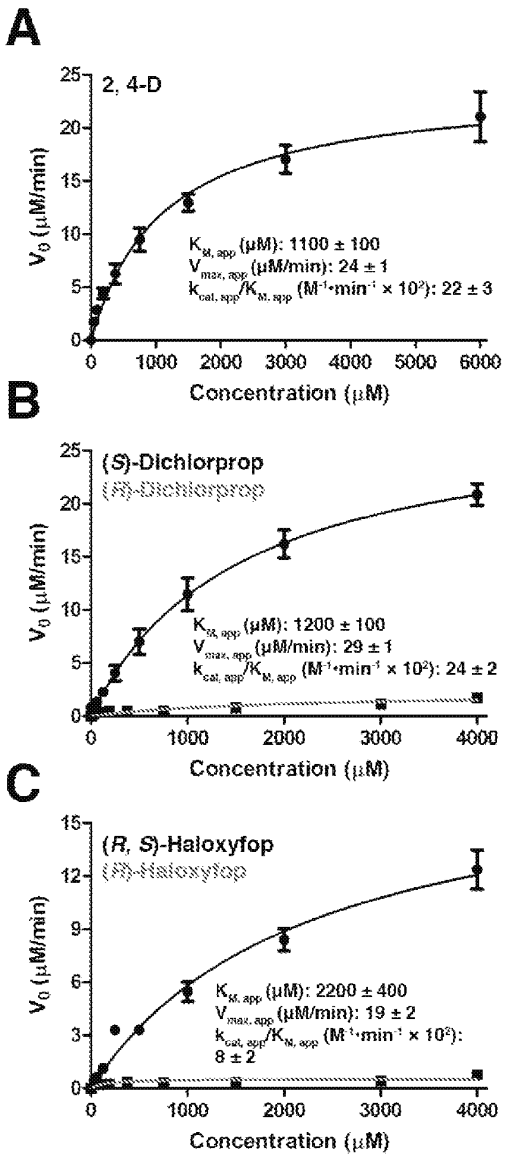
Supplementary Figure 4. Analytical Gel Filtration and SDS-PAGE analysis of AADs. (A) SDS-PAGE gel of AAD-1 and AAD-2 used for crystallographic and biochemical studies. (B) Analytical gel filtration of AAD-1 (33.2 kDa) and AAD-2 (33.6 kDa) against known standards. Elution profile suggests that AAD-1 and AAD-2 assemble as dimers in solution, denoted by the black arrow at ~15 min elution.

COR-AAD1-00003293
Bayer EX1008 (Part 6 of 9)



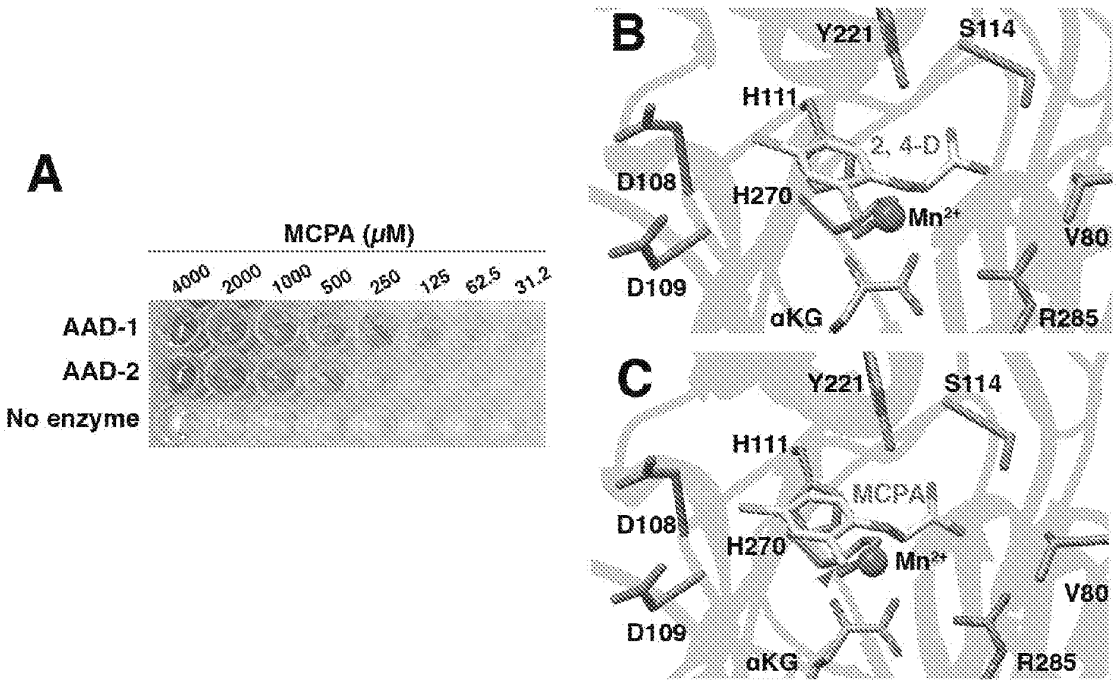
Supplementary Figure 5. Normalized activity of AAD-2 against a panel of substrates. The activity reported has been normalized to the activity of AAD-2 against (*S)*-dichlorprop, which was the substrate it most preferred amongst those tested.

COR-AAD1-00003294
Bayer EX1008 (Part 6 of 9)



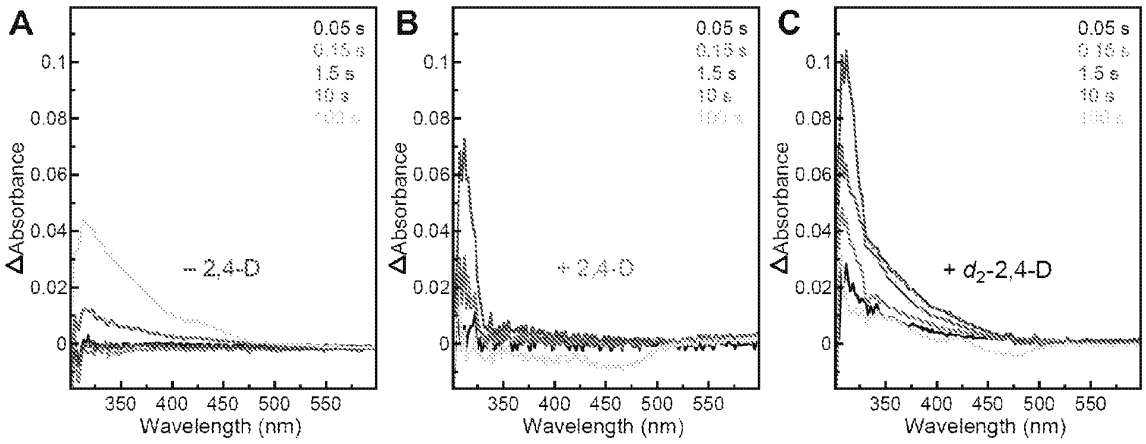
Supplementary Figure 6. Kinetic curves for the AAD-2 reaction using various substrates. (A) Kinetic curve of AAD-2 with 2,4-D at various concentrations. (B) Kinetic curves of AAD-2 with (*S*)-dichlorprop (black curve) or (*R*)-dichlorprop (red curve). (C) Kinetic curves of AAD-2 with (*R*,*S*)-haloxyfop (black curve) or (*R*)-haloxyfop (red curve). For racemic substrates, the concentration noted is the effective concentration of the (*S*) enantiomer in the sample. Kinetic parameters noted in each pane l correspond to values calculated using the black curve in each panel.

COR-AAD1-00003295
Bayer EX1008 (Part 6 of 9)



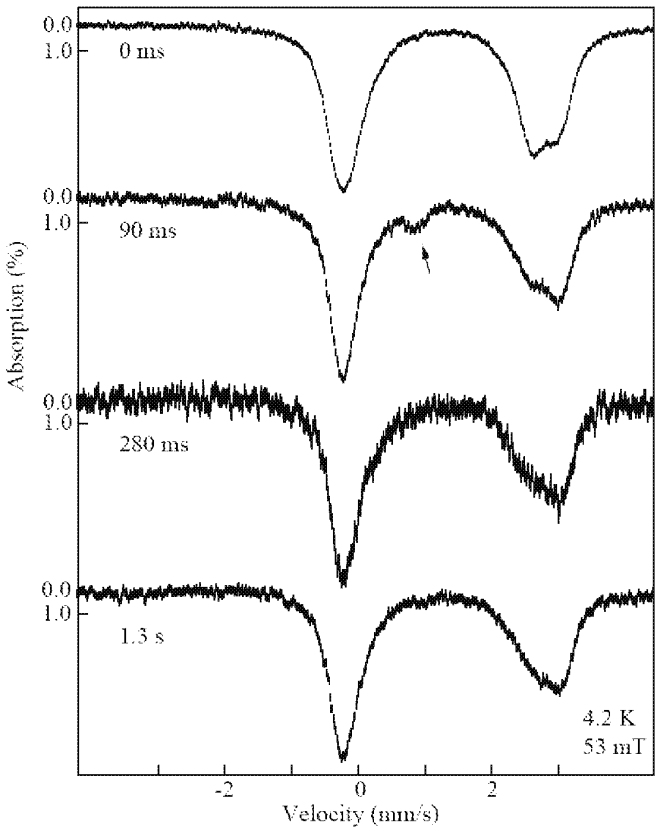
Supplementary Figure 7. AAD-1 and AAD-2 can accept MCPA as a substrate. (A) Select wells in a 96-well plate depicting the characteristic red color indicative of the presence of a phenol product (developed under basic conditions using 4-aminoantipyrine and potassium ferricyanate) as AAD-1 and AAD-2 react with MCPA at varying concentrations. The no enzyme control lane has been included to show that a null reaction will produce a pale yellow color. (B) Docking model depicting 2,4-D in the active site of AAD-1. (C) Docking model depicting MCPA in the active site of AAD-1. MCPA differs from 2,4-D only by the presence of a methyl group (brown arrow). AAD-1 was chosen to model in the achiral substrates as the structure of AAD-2 does not contain electron density for a herbicide substrate.

COR-AAD1-00003296
Bayer EX1008 (Part 6 of 9)



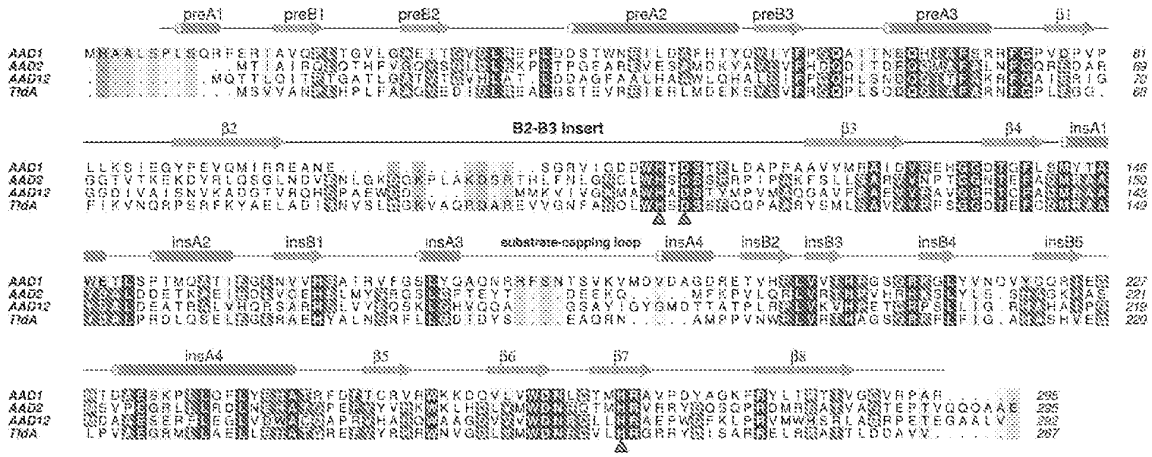
Supplementary Figure 8. Kinetic-difference spectra from the stopped-flow absorption experiment. The spectra shown here are the results of subtracting the experimental spectrum of an early reaction time (0.005 s) from the spectra taken at the reaction times indicated in the legend in the experiments with (A) no primary substrate, (B) unlabeled 2,4-D, and (C) d_2-2,4-D. The reaction conditions are given in Supplemental Materials and Methods.

COR-AAD1-00003297
Bayer EX1008 (Part 6 of 9)



Supplementary Figure 9. Mössbauer spectra of samples of the AAD-1 reaction. 4.2-K/53-mT Mössbauer spectra of a sample of the AAD-1•Fe(II) •αKG•d_2-2,4-D reactant complex (top) and samples, wherein the reactant complex was reacted for 90 ms, 280 ms, or 1.3 s. The position of the high-energy line of the ferryl intermediate is indicated with an arrow in the spectrum of the 90-ms sample. The reaction conditions are given in Supplemental Materials and Methods.

COR-AAD1-00003298
Bayer EX1008 (Part 6 of 9)



Supplementary Figure 10. Sequence alignment of select AADs. Sequence alignment of select AADs, noting secondary structure elements, and the β2β3 insert found in AAD-12 and AAD-2.

COR-AAD1-00003299
Bayer EX1008 (Part 6 of 9)

	Organism	Uniprot ID
Co-localizes with TfdB-like protein	Pseudocercospora fijiensis (strain CIRAD86)	M3A056
	Penicillium solitum	A0A1V6QWE6
	Fonsecaea erecta	A0A178Z4Y2
	Mycobacterium colombiense	A0A1A2YXB1
	Streptomyces sp. CB02009	A0A1Q5HUQ2
	Mycobacterium sp. 1164966.3	A0A1A0M1M0
	Alphaproteobacteria bacterium TMED54	A0A1Z8UV43
	SAR116 cluster bacterium	A0A2D7KVX6
	Rhodospirillaceae bacterium	A0A2D9Y9Q5
	Rhodospirillaceae bacterium	A0A2E7VA75
	Candidatus Endolissoclinum sp. TMED37	A0A1Z8T2B6
	Rhodospirillaceae bacterium	A0A2D7CKS0
	Rhodospirillaceae bacterium	A0A2E4GVS2
	Rhodospirillaceae bacterium	A0A2E4XQ24
	Magnetovibrio sp.	A0A2E3L2Z4
	Rhodospirillaceae bacterium	A0A2E4H027
	Alphaproteobacteria bacterium 13_1_20CM_4_65_11	A0A1Q7TWM2
	Alphaproteobacteria bacterium 13_1_20CM_3_64_12	A0A1Q7WS23
	Betaproteobacteria bacterium RIFCSPLOWO2_02_FULL_67_26	A0A1F4BNV1
	Alcaligenaceae bacterium	A0A2G4J8Q9
	Rhodospirillaceae bacterium	A0A2E5PMF6
	Candidatus Rokubacteria bacterium	A0A2V6XGU5
	Candidatus Rokubacteria bacterium	A0A2V7A8W2
	Burkholderia sp. SRS-W-2-2016	A0A1Q8IVD1
Co-localizes with TfdC-like protein	Diplodia seriata	A0A0G2EHD3
	Candidatus rokubacteria bacterium	A0A2V6S1C4
	Burkholderia sp. Leaf177	A0A0Q5NX83
	Bradyrhizobium sp. SK17	A0A2K8YNB2
	Halomonas sp. WRN001	A0A2A2EQM1
	Burkholderia sp. KK1	A0A1P9YF09
	Rhodospirillaceae bacterium	A0A2E4XUY7
	Rickettsiales bacterium	A0A2E7UZN3
	Rhodospirillaceae bacterium	A0A2E4XUM7
	Rickettsiales bacterium	A0A2E7V1P8

COR-AAD1-00003300
Bayer EX1008 (Part 6 of 9)

	Organism	UniprotID
Co-localizes with TfdC-like protein	Candidatus endolissoclinum sp. TMED37	A0A1Z8SSC2
	Rhodospirillaceae bacterium	A0A2D7CMZ1
	Rhodospirillaceae bacterium	A0A2E9UWQ6
	Rhodospirillaceae bacterium	A0A2E5L972
	Pseudorhodoferax sp. Leaf274	A0A0S9NH71
	Bradyrhizobium sp. 3 85S1MB	A0A2U8QLK5
	Bosea lathyri	A0A1H6D7Y2
	Beijerinckia sp. 28-YEA-48	A0A1H4RRY8
	Uncultured bacterium	G9FC95
Co-localizes with TfdB and TfdC-like proteins	uncultured bacterium	G9FBF9
	Burkholderia cepacia	Q93L12
	Achromobacter denitrificans	Q6QHP8
	Uncultured bacterium	G9FBF9
	Burkholderia cepacia	Q93L12
	Achromobacter denitrificans	Q6QHP8
	Delftia acidovorans	Q8KN30
	Burkholderia sp. KK1	A0A1P9YF35
	Burkholderia sp. M701	V5YNJ4
	Ralstonia pickettii	I3RYL1
	Uncultured bacterium	J9R7E1
	Variovorax sp. DB1	I3RYF9
	andidimonas nitroreducens	A0A225MB14
	Psychrobacter sp. P11G5	A0A127H2S0
	Psychrobacter sp. Cmf 22.2	A0A1Q8DTW8
	Ruegeria litorea R37	A0A1Y5TNJ4
	Ruegeria mediterranea M15O_3	A0A2R8C6L2
	Limnohabitans sp. JirII-31	A0A2M6VQN1
	Limnohabitans sp. TS-CS-82	A0A2S7JRZ7

Supplementary Table 1. List of Uniprot IDs of Putative AADs Identified by EFI-EST (2). The table above lists the UniprotIDs of putative AADs found using the EFI-FEST Sequence Similarity Network (SSN) and Genome Neighborhood Network (GNN) tools (3). Sequences are group to whether they co-occur (within a 15 gene window) with a TfdB homolog, TfdC homolog, or both.

COR-AAD1-00003301
Bayer EX1008 (Part 6 of 9)

Substrate	AAD-1		AAD-2	
	$K_{M,\ app}$ (μM)	$k_{cat,\ app}/K_{M,\ app}$ (M^{-1}·min^{-1} × 10^3)	$K_{M,\ app}$ (μM)	$k_{cat,\ app}/K_{M,\ app}$ (M^{-1}·min^{-1} × 10^2)
2, 4-D	683 ± 76*	27*	1100 ± 100	22 ± 3
(*R*)-dichlorprop	527 ± 38*	3380*	N. D.	N. D.
(*S*)-dichlorprop	N. D.	N. D.	1200 ± 100	24 ± 2
(*R*)-cyhalofop	96 ± 7*	1950*	N. D.	N.D.
(*R,S*)-diclofop	160 ± 40	97 ± 5	N. S.	N.A.
(*R,S*)-haloxyfop	330 ± 100	50 ± 2	2200 ± 300	8 ± 2
(*R,S*)-quizalofop	120 ±30	32 ± 3	N.S.	N.A

Supplementary Table 2. Kinetic parameters of AAD-1 and AAD-2 across a panel of substrates. Values denoted with an * were previously reported (5). The aforementioned values have been converted from $M^{-1}s^{-1} \times 10^3$ as reported, to $M^{-1}min^{-1} \times 10^3$ to provide a more direct means of comparison. Values noted with N. D. (not detected) indicate that the no activity was detected. Values noted with N. S. (not saturated) suggests that the enzyme does not prefer that compound as a substrate, i.e. only a subtle colorimetric change at 510nm was observed when 10 μM of enzyme was incubated with 4mM (effective concentration) of the accepted enantiomer of over a 15 minute incubation period. The lack in change of absorbance hindered our kinetic assays due to issues in detection. Unless otherwise noted, all other values were obtained during this study.

COR-AAD1-00003302
Bayer EX1008 (Part 6 of 9)

Primer	Sequence
AAD-2_NLIC_FP	TACTTCCAATCCAATGCAATGACGATCGCCATCCGGCAGCTT
AAD-2_NLIC_RP	TTATCCACTTCCAATGTTATTATCACTCCGCCGCCTGCTGCTG

Supplementary Table 3. List of primers used in this study.

COR-AAD1-00003303
Bayer EX1008 (Part 6 of 9)

Supplementary Table 3. Data collection, phasing and refinement statistics

	AAD-1 Mn^{2+}•αKG• (*R*)-dichlorprop	**AAD-1** Mn^{2+}•αKG• (*R*)-dicyhalofop	**AAD-1** Mn^{2+}•αKG• (*R*)-diclofop	**AAD-1** $(VO)^{2+}$•succ• (*R*)-dichlorprop	**AAD-2** Mn^{2+}•αKG
Data collection					
Space group	$P2_12_12$	$P2_12_12$	$P2_12_12$	$P2_12_12$	C2
Unit cell	85.9, 97.8, 69.9	85.5, 97.4, 69.8	85.8, 97.78, 69.9	85.9, 97.9, 69.9	266.5, 55.5, 183.7, 118.9°
Resolution	86-1.58 (1.59-1.58)	86-1.9 (1.91-1.9)	86-1.8 (1.81-1.8)	57-1.5 (1.54-1.5)	50-2.15 (2.19-2.15)
Total reflections	656,362	380,331	508,030	1,275,386	579,196
Unique	80,901	46,644	55,192	92,316	127,502
R_{sym} (%)[1]	0.093 (0.956)	0.119 (755)	0.111 (0.929)	0.072 (0.792)	0.088 (0.720)
$I/\sigma(I)$ [1]	17.5 (2.1)	17.0 (2.9)	18.7 (2.6)	20.5 (2.2)	16.1 (1.6)
Completeness	100 (95.8)	100 (97.7)	100 (97.3)	99.2 (99.4)	99.0 (92.6)
Redundancy	8.1 (7.9)	8.2 (8.3)	9.2 (9.3)	13.8 (8.2)	4.6 (3.8)
Refinement					
Resolution (Å)	54.2-1.58	56.7-1.9	48.9-1.8	25.0-1.51	25.0-2.15
# reflections	80,828	46,591	55,138	87,655	107,559
R_{work} / R_{free}[2]	16.2/19.7	17.5/21.8	16.3/20.1	19.5/21.7	18.8/23.3
# of atoms					
Protein	4,497	4,500	4,482	4,498	15,111
αKG/succinate	20	20	20	8	70
Herbicide	14	44	21	14	-
Water	734	576	668	650	1,633
B-factors					
Protein	19.4	21.5	19.6	22.0	34.7
αKG/succinate	14.6	17.5	15.5	22.8	34.1
Herbicide	22.1	32.9	32.6	38.2	-
Water	30.3	28.7	29.6	32.4	38.1
RMS deviations					
Bond lengths (Å)	0.011	0.004	0.007	0.007	0.009
Bond angles (°)	1.249	0.865	1.066	1.16	1.29

1. Highest resolution shell is shown in parenthesis.

2. R-factor = $\Sigma(|F_{obs}|-k|F_{calc}|)/\Sigma|F_{obs}|$and R-free is the R value for a test set of reflections consisting of a random 5% of the diffraction data not used in refinement.

COR-AAD1-00003304
Bayer EX1008 (Part 6 of 9)

SUPPLEMENTAL REFERENCES

1. Price JC, Barr EW, Hoffart LM, Krebs C, & Bollinger JM, Jr. (2005) Kinetic dissection of the catalytic mechanism of taurine:alpha-ketoglutarate dioxygenase (TauD) from *Escherichia coli*. *Biochemistry* 44:8138-8147.

2. Gerlt JA, *et al.* (2015) Enzyme Function Initiative-Enzyme Similarity Tool (EFI-EST): A web tool for generating protein sequence similarity networks. *Biochim Biophys Acta* 1854:1019-1037.

3. Gerlt JA (2017) Genomic Enzymology: Web tools for leveraging protein family sequence-function space and genome context to discover novel functions. *Biochemistry* 56:4293-4308.

4. Don RH & Pemberton JM (1981) Properties of six pesticide degradation plasmids isolated from Alcaligenes paradoxus and Alcaligenes eutrophus. *J Bacteriol* 145:681-686.

5. Wright TR, *et al.* (2010) Robust crop resistance to broadleaf and grass herbicides provided by aryloxyalkanoate dioxygenase transgenes. *Proc Natl Acad Sci U S A* 107:20240-20245.

COR-AAD1-00003305
Bayer EX1008 (Part 6 of 9)

Research Article

Received: 10 January 2019 Revised: 26 February 2019 Accepted article published: 3 March 2019 Published online in Wiley Online Library:

(wileyonlinelibrary.com) DOI 10.1002/ps.5393

Development of enzymes for robust aryloxyphenoxypropionate and synthetic auxin herbicide tolerance traits in maize and soybean crops

Clayton T Larue,[a*] Michael Goley,[a] Lei Shi,[a,†] Artem G Evdokimov,[a,‡] Oscar C Sparks,[a] Christine Ellis,[a] Andrew M Wollacott,[b,§] Timothy J Rydel,[a] Coralie E Halls,[a] Brook Van Scoyoc,[a] Xiaoran Fu,[b] Jeffrey R Nageotte,[b] Adewale M Adio,[a] Meiying Zheng,[a] Eric J Sturman,[a] Graeme S Garvey[a] and Marguerite J Varagona[a]

Abstract

BACKGROUND: Effective management of weedy species in agricultural fields is essential for maintaining favorable growing conditions and crop yields. The introduction of genetically modified crops containing herbicide tolerance traits has been a successful additional tool available to farmers to better control weeds. However, weed resistance challenges present a need for additional herbicide tolerance trait options.

RESULTS: To help meet this challenge, a new trait that provides tolerance to an aryloxyphenoxypropionate (FOP) herbicide and members of the synthetic auxin herbicide family, such as 2,4-dichlorophenoxyacetic acid (2,4-D), was developed. Development of this herbicide tolerance trait employed an enzyme engineered with robust and specific enzymatic activity for these two herbicide families. This engineering effort utilized a microbial-sourced dioxygenase scaffold to generate variants with improved enzymatic parameters. Additional optimization to enhance in-plant stability of the enzyme enabled an efficacious trait that can withstand the higher temperature conditions often found in field environments.

CONCLUSION: Optimized herbicide tolerance enzyme variants with enhanced enzymatic and temperature stability parameters enabled robust herbicide tolerance for two herbicide families in transgenic maize and soybeans. This herbicide tolerance trait for FOP and synthetic auxin herbicides such as 2,4-D could be useful in weed management systems, providing additional tools for farmers to control weeds.
© 2019 Society of Chemical Industry

Supporting information may be found in the online version of this article.

Keywords: agriculture biotechnology; herbicide tolerance trait; FOP herbicide tolerance; 2,4-D herbicide tolerance; applied enzyme engineering

1 INTRODUCTION

In agricultural systems, the management of weedy species in crop fields is one of many essential components to ensure favorable crop yields. Many weedy species are well adapted to compete with crops for sunlight, water, soil nutrients, and physical space. Farmers control weeds by utilizing a variety of weed management strategies, including herbicides and genetically modified herbicide-tolerant crops. However, weeds have evolved resistance to herbicides and this continues to present a challenge in agriculture today.[1] One of many strategies to manage resistant weeds is to employ multiple herbicide modes of action.

Two herbicide families of interest are the aryloxyphenoxypropionate (FOP) herbicides and members of the synthetic auxin herbicide family. FOP herbicides inhibit an enzyme variant of acetyl CoA carboxylase (ACCase) found in grasses.[2] Due to this selective nature, FOP herbicides are commonly used to control

* Correspondence to: CT Larue, Bayer Crop Science, 700 Chesterfield Parkway West, Chesterfield, Missouri 63017, USA. E-mail: clayton.larue@bayer.com

† Present address: Encodia Inc, 11125 Flintkote Avenue, San Diego, 92121 CA, USA.

‡ Present address: EnkoChem, 19 Presidential Dr, Woburn, 01801 MA, USA.

§ Present address: Visterra Inc, 275 Second Avenue, Waltham, 02451 MA, USA.

a Bayer Crop Science, Plant Biotechnology, Chesterfield, MO, USA

b Bayer Crop Science, Plant Biotechnology, Cambridge, MA, USA

COR-AAD1-00003306
Bayer EX1008 (Part 6 of 9)

grass weeds in dicot crops. The addition of a FOP herbicide tolerance trait in maize would enable the use of FOP herbicides to control grass weeds in maize fields. The synthetic auxin family of herbicides includes 2,4-dichlorophenoxyacetic acid (2,4-D), which is often used to control dicot weeds.[3] Synthetic auxin herbicides disrupt plant hormone regulatory pathways, resulting in plant death.

Two approaches have been useful in building herbicide-tolerant crops.[4] The first is to utilize a transgene expressing an insensitive variant of an enzyme that is the herbicide's target in a sensitive crop. The second approach is to utilize a transgene expressing an enzyme that deactivates the herbicide chemistry. The oxygenase enzyme α-ketoglutarate-dependent (*R*)-dichlorprop dioxygenase (RdpA), which was isolated from the common soil microbe *Sphingobium herbicidovorans*, could be utilized for the second approach.[5,6] RdpA is part of a large superfamily of dioxygenases found in microbes, plants, and animals.[7,8] RdpA catalyzes the oxidative metabolism of chemistries in the FOP (selective for the *R* enantiomers, the active form of these herbicide chemistries) and synthetic auxin herbicide groups, and has been shown to provide tolerance to these herbicides when expressed as a transgene in sensitive plants.[5,6,9]

A FOP and 2,4-D herbicide tolerance trait, when paired with other herbicide tolerance traits and selective herbicides, can aid in managing and preventing herbicide-resistant dicot and grass weeds, and provides an additional tool for effective weed management. Crops display differences in sensitivity to herbicides in the FOP and 2,4-D families. For example, maize is sensitive to FOP herbicides but displays incomplete tolerance to 2,4-D. Dicots, such as soybeans, are fully tolerant to FOP herbicides, but sensitive to 2,4-D. Therefore, we were interested in engineering an enzyme that could robustly inactivate both FOP and 2,4-D herbicides.

Here, we characterize novel optimized dioxygenase enzyme variants in maize and soybean. These new variants, named FT enzymes (FOP and 2,4-D tolerance enzymes), were engineered to improve enzymatic parameters, including enhanced enzymatic activity on selected herbicides and improved temperature stability of the enzymes. These enhanced variants could be useful in building a new generation of transgenic maize and soybeans with improved herbicide tolerance and agronomic performance when FOP and 2,4-D herbicides are used in a weed control system.

2 MATERIALS AND METHODS

2.1 Purification, enzyme assays and characterization

FT variants were synthesized and cloned into a modified pET28a vector which included a TVMV cleavable N-terminal His tag or a C-terminal His tag (Novagen, Burlington, MA). These variants were transformed into Rosetta 2 cells (Novagen) or BL21 DE3 cells (New England Biolabs, Ipswich, MA) for protein expression overnight at 20 °C. Cell pellets were lysed and FT proteins extracted using B-PER™ and Y-PER™ (ThermoFisher, Waltham, MA) plus lysozyme and benzonase (Sigma Aldrich, St. Louis, MO). Clarified extracts were Immobilized metal affinity chromatography (IMAC) purified using nickel resin (Sigma Aldrich) and eluted using 30 mM Tris pH 8, 200 mM imidazole buffer. Further purification, if needed, included dialysis or size exclusion using 30 mM Tris pH 8 and 200 mM NaCl buffer (ThermoFisher).

Enzyme assays were completed with FT proteins using a modified phenolic-based colorimetric detection assay.[10] Purified proteins (or in the case of the high-throughput screening assays, clarified *E. coli* extracts) were tested with selected substrates. Chemicals were obtained from Sigma Aldrich. For quizalofop (QFOP) and synthetic auxins, *in vitro* assays used the acid form (the active QFOP molecule in plant cells) in the racemic form (if applicable). The reaction buffer contained 20 mM MOPS pH 6.75, 50 μM $(NH_4)_2$ $Fe(SO_4)_2$, 50 μM ascorbic acid (Na salt), and 1 mM α-ketoglutarate ((α-KG)). Reactions were performed in 150 μL final reaction volumes in 96-well assay plates. All reactions for kinetic characterization were completed with four replications while high-throughput screening reactions for enzyme optimization utilized fewer replications. Reactions were stopped with 15 μL of stop solution (50 mM boric acid, 50 mM KCl, pH 10.0 (KOH) with 2% 4-aminoantipyrine w/v (in water) freshly diluted 1:10 into stop buffer). Color development agent was added (15 μL of an 8% potassium ferricyanide w/v (in water), freshly diluted 1:10). Following color development, assays were recorded with a SpectraMax spectrometer at absorbance of 510 nm. Back calculations were completed with product standards (Sigma Aldrich or custom synthesis) in simulated reactions. Control reactions without α-KG were inactive, and reactions with purified enzyme without $(NH_4)_2$ $Fe(SO_4)_2$ and ascorbic acid were significantly inhibited. Unless indicated, all reactions were completed at 22–23 °C. For the temperature stability assays shown in Fig. 2(b), the enzymes were equilibrated at the indicated temperature for 5 min before substrate (also equilibrated at the same temperature) was added and the reaction allowed to proceed at the same temperature. During the high-throughput screens focused on enhanced temperature stability, screens were run at 25 °C and 40 °C to select variants with strong activity at both temperatures. Kinetic parameters were calculated with nonlinear regression analysis using GraphPad software with default settings.

Protein melting temperatures were determined by fluorescence tracking of the hydrophobic protein binding dye SYPRO Orange (Invitrogen, Waltham, MA) with progressive increases in temperature. The assays were run in a 20 mM Tris, pH 7.75 and 150 mM NaCl buffer. Assays were also run with the addition of $(NH_4)_2$ $Fe(SO_4)_2$ and α-KG since some substrate stabilization was observed. The FT protein and a 1:100 dilution of SYPRO Orange was combined in buffer in a Bio-Rad CFX96 PCR thermocycler with a fluorescence detector. The temperature was progressively increased from room temperature to full protein denaturation. The temperature at which the protein was 50% denatured was calculated from the first derivative of the change in fluorescence in Bio-Rad CFX Manager 2.1 software.

2.2 In-plant controlled environment herbicide tolerance and temperature stability assays in maize

Several different expression vectors containing FT variants were used to transform maize immature embryos using *Agrobacterium*-mediated transformation.[11] Plants containing a single copy of the transgenic insert were identified through molecular and segregation analysis and advanced to seed production for further experimentation.[12] The FT enzymes were expressed either without a targeting peptide or targeted to the chloroplast using the malate dehydrogenase (MDH) chloroplast targeting peptide (CTP).[13] A growth chamber experiment at two different temperatures was conducted to evaluate the tolerance of F1 hybrid transgenic maize expressing MDH/FT_5, MDH/FT_T, MDH/FT_R, FT_T, or FT_R and control plants to postemergence applications of 2,4-D. For QFOP (Assure II®, formulated as an ester in the *R* enantiomer) postemergence tolerance, plants expressing MDH/FT_5, MDH/FT_C, MDH/FT_T, MDH/FT_R, FT_T, or FT_R, and control plants were assayed. The first growth chamber was set to 20 °C

 © 2019 Society of Chemical Industry

COR-AAD1-00003307
Bayer EX1008 (Part 6 of 9)

day and 20 °C night and the second growth chamber was set to 38 °C day and 30 °C night, both with 50% relative humidity and 16-h photoperiod. For each variant/targeting peptide combination tested, three different transformation events were evaluated with eight replications for each temperature regime. The herbicide treatment consisted of 2,4-D amine at 4500 g ha^{-1} (4X) applied to V3/V4 maize and QFOP at 360 g ha^{-1} (4X) plus 0.25% v/v Chemsurf™ nonionic surfactant (NIS) containing a 90% mixture of alkylarylpolyoxykane ether, isopropanol and free fatty acids applied to V2 maize in a track sprayer. Plants were visually rated 11 days after treatment (2,4-D) and 9 days after treatment (QFOP) on a scale of 0% to 100% with 0% being no injury and 100% being plant death. This scoring system is based on classical herbicide injury rating systems and includes injury to plant tissue such as chlorosis, necrosis, malformation, stunting and plant death. Injury data were averaged with standard error bars calculated in Excel.

2.3 Field-based herbicide tolerance assays in maize

Field experiments were conducted at two independent locations in Illinois, USA, to evaluate herbicide tolerance of maize expressing MDH/FT_S, MDH/FT_C, MDH/FT_T, MDH/FT_R, FT_T, or FT_R, and control maize to postemergence applications of QFOP and 2,4-D. Experimental design was a randomized complete block design with two replications. For QFOP, herbicide treatments consisted of (i) QFOP at 360 g ha^{-1} plus 0.25% v/v NIS applied to maize multiple times within the same plot, VE-V2 followed by (fb) V4 fb V8, (ii) QFOP at 720 g ha^{-1} plus 0.25% v/v NIS applied to VE-V2 fb V4 fb V8 maize, and (iii) QFOP at 1440 g ha^{-1} plus 0.25% v/v NIS applied to VE-V2 fb V4 fb V8 maize. For 2,4-D, herbicide treatments consisted of (i) 2,4-D amine at 2250 g ha^{-1} plus 0.25% v/v NIS applied to VE-V2 followed by (fb) V4 fb V8 maize, (ii) 2,4-D amine at 4500 g ha^{-1} plus 0.25% v/v NIS applied to VE-V2 fb V4 fb V8 maize, (iii) 2,4-D amine at 9000 g ha^{-1} plus 0.25% v/v NIS applied to VE-V2 fb V4 fb V8 maize, and (iv) 2,4-D amine at 18 000 g ha^{-1} plus 0.25% v/v NIS applied to VE-V2 fb V4 fb V8 maize. Herbicide treatments were applied with a CO_2 backpack or tractor-mounted sprayer calibrated to deliver 140 L ha^{-1} using air-inducted Teejet® TTI nozzles with water as the herbicide carrier. Plots were visually rated 10–14 days after V4 and V8 applications for crop injury. All data were subjected to analysis of variance and means separated at LSD or P value < 0.05.

2.4 In-plant herbicide tolerance in soybeans

Several different vectors containing FT variants were transformed into soybean using *Agrobacterium*-mediated transformation. Individuals (a transformation event) containing a single copy of the transgenes were identified and plants were advanced to seed production for further experimentation. Homozygous FT expressing plants were grown to the V3 growth stage and treated with 1680 g ha^{-1} of 2,4-D amine in controlled environment studies. Plants were assessed for visual injury approximately 7 days after treatment. Non-traited control is an average injury of four plants and the experimental treatments are the average injury of 19–39 plants. In field treatments, homozygous FT expressing plants were treated with 2240 g ha^{-1} of 2,4-D at V3 and R1 growth stages.

2.5 Data availability

Sequence information is available in GenBank:

FT_5: MH043108; FT_C: MH043109; FT_R: MH043110 and MH043111; FT_T: MH043112 and MH043113; FT_Tv3: MH043114; FT_Tv7: MH043115. Records for RdpA (AAM90965) and MDH (BT000621) have been previously submitted by other groups.[5,13]

The crystallography data referred to in this study are available in the Protein Data Bank (PDB, https://www.rcsb.org/):

6D0O, RdpA dioxygenase holoenzyme; 6D1O, FT_5 dioxygenase apoenzyme; 6D3H, FT_T dioxygenase with bound dichlorprop; 6D3I, FT_Tv7 dioxygenase with 2,4-D bound; 6D3J, FT_T dioxygenase holoenzyme; and 6D3M, FT_T dioxygenase with bound QFOP.

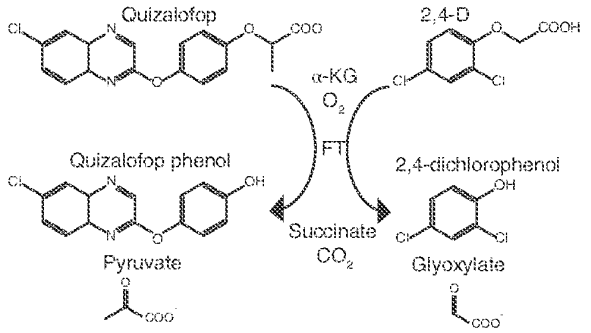


Figure 1. FT enzymes catalyze herbicide deactivation. The dioxygenase, FT, catalyzes the initial metabolism of chemistries in two herbicide chemistry families: FOP, represented by quizalofop (QFOP), and members of the synthetic auxins, represented by 2,4-D.

3 RESULTS

3.1 Introduction

The dioxygenase RdpA has been characterized as an α-ketoglutarate-dependent non-heme iron-dependent dioxygenase.[6] This enzyme utilizes α-KG, molecular oxygen and a variety of herbicide compounds to catalyze a classical dioxygenase reaction (Fig. 1). This reaction results in the release of CO_2, succinate and two breakdown products from the herbicide chemistry. However, the natural enzymatic activity of RdpA could be improved through enzyme engineering to provide tolerance to both herbicide chemistries in both monocot and dicot crops in typical field conditions. An enzyme engineering effort was thus undertaken to design optimized enzymes with enhanced activity on selected herbicide chemistries. RdpA was used as a base dioxygenase scaffold for engineering design and the optimized FT enzyme variants were screened for robust enzymatic activity on the herbicides QFOP, a FOP herbicide, and 2,4-D, a synthetic auxin. In-plant analysis of maize and soybean plants expressing selected FT variants in both controlled environment and field-based testing was essential for informing additional optimization parameters. This included a need to stabilize the enzyme for field temperature extremes and optimizing the activity of the enzyme towards the substrate 2,4-D.

3.2 Engineered FT variants demonstrated FOP tolerance in maize, but low enzyme temperature stability

At the outset of this engineering effort a series of now well-established engineering approaches were applied to RdpA to optimize activity for QFOP and 2,4-D separately and in combination (see the supporting inofrmation). Engineering approaches included homology modeling and homologous amino acid changes, scanning mutagenesis, computational protein design, rational protein design and data-driven design. At the onset of the engineering, no crystal structure of RdpA or a close

 © 2019 Society of Chemical Industry

COR-AAD1-00003308
Bayer EX1008 (Part 6 of 9)

homolog was available and therefore a homology model was generated with ICM-pro using a distant dioxygenase homolog, TauD (30% sequence identity), as a template.[14] This homology model was used for substrate docking and identification of putative active site residues for rational design to modulate protein–substrate interactions. As discussed below, we later used structural characterization of enzyme variants as crystal structures were determined to help inform additional engineering. This coupled with the enzymatic characterization of early variants described below helped further drive the computational, rational and data-driven design efforts of additional optimized variants.

The enzyme variants were assayed in a bacterial expression system and tested in a high-throughput, plate-based enzymatic assay using clarified bacterial lysates. This assay enabled screening of approximately 4000 enzyme variants in a semi-quantitative manner. Those variants identified with improved activity relative to bacterial lysate expressing RdpA were further combined in multiple rounds of optimization. The highest performing variants in the bacterial lysate screen (depending on the optimization objectives described below) were confirmed with purified protein assays. A small subset (<1% in total) of these confirmed variants were selected for *in planta* efficacy analysis.

The enzyme variant FT_5 was the first variant selected for in-plant analysis based on first round *in vitro* kinetic characterization. The FT_5 variant showed good activity with QFOP (0.44 μmol mg^{-1} min^{-1} at V_{max}) and weaker activity with 2,4-D (0.03 μmol mg^{-1} min^{-1} at V_{max}) in enzyme assays. Although this activity was lower than that observed for RdpA, FT_5 was selected early in the optimization process to benchmark in-plant tolerance assays and to direct the optimization efforts. A transformation vector with the FT_5 transgene linked to a plant CTP at the N-terminal end of the enzyme was used to transform maize. A CTP was included because FOP herbicides inhibit the enzyme ACCase. In grasses such as maize, the herbicide sensitive ACCase enzyme isoform is localized to the chloroplast.[15] Therefore, we hypothesized that localizing the FT_5 enzyme to the chloroplast would provide improved FOP tolerance.

Maize immature embryos from the germplasm LH244 were transformed with FT_5 transformation vectors using *Agrobacterium tumefaciens*. The regenerated transformed plants were spray challenged with a commercial formulation of QFOP. Following spray applications, the transformed plants were rated for tolerance using a percentage injury rating. FT_5 plants showed tolerance to the herbicide application while the control plants showed extensive tissue damage and eventual plant death (Fig. 2(a)). Treated plants with low injury ratings were grown to set seed and advanced for additional testing in the following generations.

Greenhouse testing for FT_5 was encouraging; however, a robust herbicide tolerance trait requires good performance in field-relevant environmental conditions. Therefore, the FT_5 maize plants were screened for herbicide tolerance in Midwestern USA field research plots that mimicked typical maize cropping conditions. In these trials, FT_5 expressing plants were tolerant to both QFOP and 2,4-D, showing that the FT proteins can provide tolerance to these herbicides in field conditions (Fig. 3(a) and (c)). However, tolerance in field conditions using the FT_5 variant was not as robust as desired, with injury rates exceeding 20% in some treatments. Therefore, additional characterization of the FT_5 enzyme variant and FT_5 maize plants was undertaken.

Further FT_5 enzyme characterization showed that FT_5 was unstable at elevated temperatures *in vitro* and in plants,

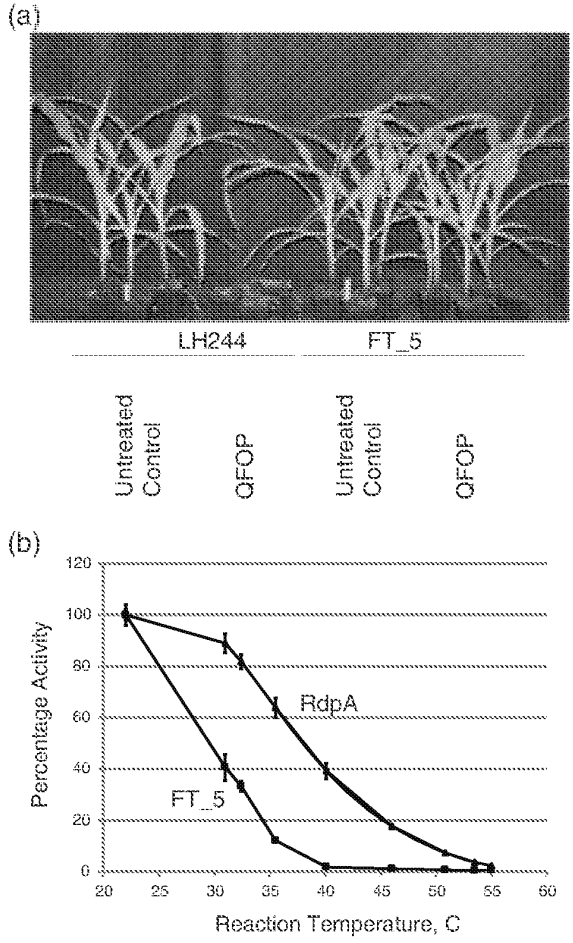


Figure 2. Characterization of FT_5. (a) Plants expressing FT_5 showed tolerance to QFOP applications in controlled environment experiments. Plants were treated with QFOP at 90 g ha^{-1}. The transformation background, LH244, served as a sensitive control while LH244 plants expressing the FT_5 enzyme (FT_5) were the test plants. Image taken 18 days after treatment. (b) Enzyme activity of FT_5 relative to RdpA with QFOP. Both FT_5 and RdpA show a progressive loss of activity with increasing reaction temperature (relative to room temperature control, which was set at 100% for both enzymes). Error bars indicate the standard error (SEM) of three replications.

suggesting that temperature stability is essential for improved in-crop performance. In the field environment, plants are exposed to large temperature swings from night to day and throughout the season. In addition, daytime temperatures in Midwestern fields commonly exceed 30 °C and can exceed 37.5 °C, the leaf surface temperature at which net photosynthesis begins to decline in well-watered maize plants.[16] A robust herbicide tolerance trait is dependent on a tolerance enzyme that can function throughout a real-world temperature range. FT_5 enzyme characterization revealed a progressive loss of enzyme function at temperatures above 30 °C with nearly complete enzyme inactivity at 40 °C with *in vitro* testing (Fig. 2(b)). While the original RdpA enzyme variant displayed somewhat more temperature stability *in vitro* than FT_5, RdpA was also temperature sensitive, with nearly 40% loss of activity at 35 °C (Fig. 2(b)). We also pre-exposed the FT_5 enzyme to an elevated temperature of 35.5 °C (a temperature which results in nearly 90% loss of activity) for various time lengths of 0 to 35 min before returning the enzyme to 22 °C for

© 2019 Society of Chemical Industry

COR-AAD1-00003309
Bayer EX1008 (Part 6 of 9)

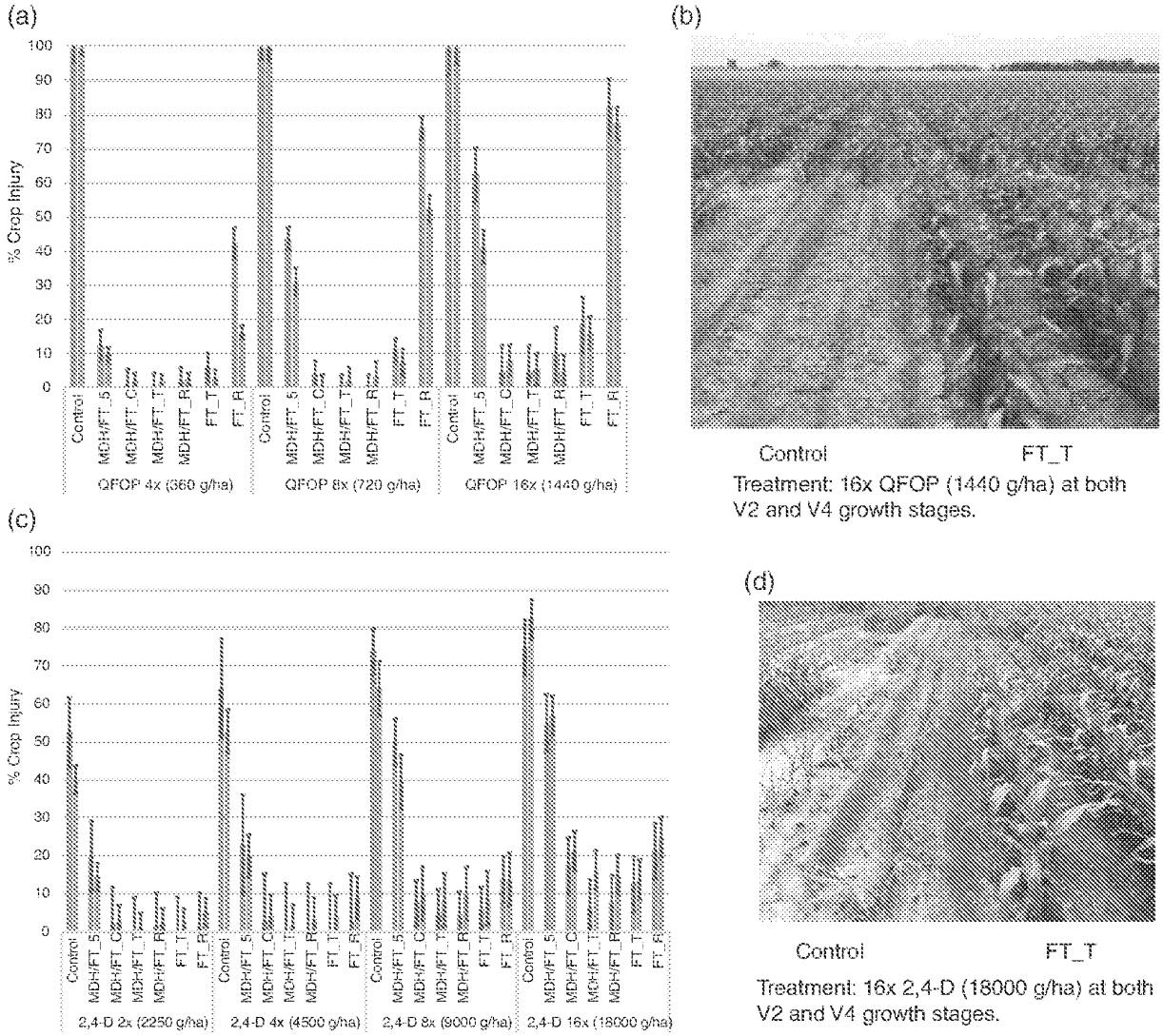


Figure 3. Field testing of FT variants. (a) Field testing confirms robust QFOP tolerance in maize. F1 plants expressing the indicated FT variants were treated at V2 and V4 (early vegetative) and V8 (late vegetative) with the indicated QFOP treatments. Injury scores were taken approximately 1 week post-treatment. The temperature-stable variants performed well when paired with a CTP. Injury ratings increased when the enzymes were expressed without a CTP. The blue bars indicate crop injury following the V4 treatments while the orange bars are following the V8 treatment, error bars indicate LSD at $P < 0.05$ with four replications. (b) Field view of MDH/FT_T (chloroplast targeted FT_T) expressing plants following the V4 application of QFOP. (c) Field testing confirmed robust 2,4-D tolerance. F1 plants expressing the indicated FT variants were treated at V2, V4 and V8 with the indicated 2,4-D treatments. Injury scores were taken approximately 1 week post-treatment. The temperature stabilized variants performed well in this assay either with or without a CTP. The blue bars indicate crop injury following the V4 treatments while the orange bars are following the V8 treatment, error bars indicate LSD at $P < 0.05$ with four replications. (d) Field view of MDH/FT_T expressing plants following V4 2,4-D application.

a traditional activity assay with QFOP. In this assay, the 10-min heat pre-treatment reduced enzyme activity by 50%, suggesting that the loss of activity at elevated temperatures is at least partly irreversible (data not shown).

To confirm that the temperature sensitivity observed in the FT_5 *in vitro* assays correlated with incomplete tolerance in plants, a series of growth chamber treatments was undertaken. Maize seedlings were moved to two temperature regimes before application of QFOP or 2,4-D herbicides. The first was a 20 °C day and night regime (non-stressed) and the second was a 38 °C day and 30 °C night regime (heat stress). FT_5 transgenic plants displayed tolerance to both herbicide applications at the non-stressed temperature regime, but in the heat stress regime these plants demonstrated increased plant injury for both herbicides (Fig. 4). Together, the *in vitro* and in-plant results confirmed that temperature sensitivity of the FT_5 enzyme contributed to incomplete FOP and 2,4-D herbicide tolerance that was observed in maize field experiments. Therefore, enzyme optimization was conducted with a focus on improving temperature stability.

3.3 Crystal structure analysis informed subsequent designs

To enhance our ability to engineer additional FT enzyme variants, crystal structures of several FT enzymes (discussed below) were analyzed. The engineered FT enzyme variants and RdpA were

 © 2019 Society of Chemical Industry

COR-AAD1-00003310
Bayer EX1008 (Part 6 of 9)

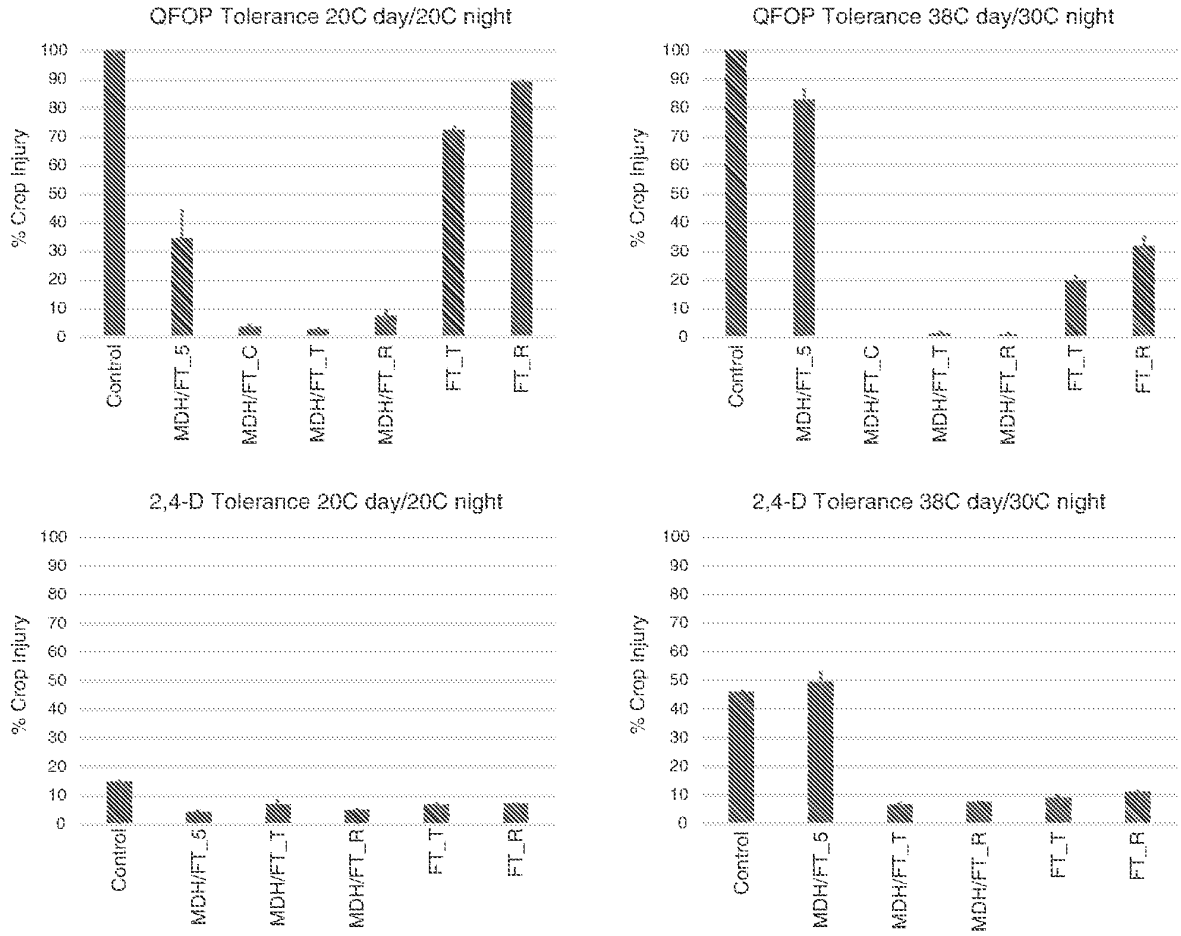


Figure 4. In-plant testing of FT enzymes in controlled environments. Controlled environment assays demonstrated differences in temperature stability of FT enzymes in maize plants. Plants were screened in non-stressed and heat-stressed conditions. Plants were grown to approximately V2 growth stage (early vegetative) and then moved to one of the two temperature regimes. After 2 days of acclimation, the plants were treated with either QFOP (4X, 360 g ha^{-1}) or 2,4-D (4X, 4500 g ha^{-1}) applications and rated for percentage injury 1 week after spray. Mean injury scores for eight replications shown with SEM indicated.

crystalized in a homotetramer asymmetric unit that contained a classical dioxygenase active pocket including a cobalt atom (replacing an iron atom found in the biologically active enzyme) coordinated by two histidine residues and one aspartic acid residue (Fig. 5 and see the supporting information, Fig. S1(a–d)). The substrates QFOP and α-KG were found to dock in the active pocket in an expected orientation for dioxygenase enzymes. A flexible loop caps the active pocket and was only observed to be well-ordered in crystal structure analysis when the enzyme contained a cobalt atom and both α-KG and a herbicide substrate.

Crystal structure analysis of the FT_5 enzyme was attempted to get a better understanding of the temperature instability. However, FT_5 was found to crystalize poorly, likely due to the instability of the enzyme (Fig. S1(e)). The enzyme could not be co-crystalized with the metal atom or substrates, and the flexible loop that was observed to become well-ordered in the crystal structures of other more stable FT variants upon substrate binding remained disordered in the FT_5 crystals. This disordered nature of the FT_5 enzyme is consistent with the inherent instability observed at higher temperatures in the enzyme assays and supports our hypothesis that the instability of FT_5 is a primary cause of reduced tolerance at higher temperatures in plants. Comparison of crystal structures of the engineered variants and RdpA helped enable additional engineering.

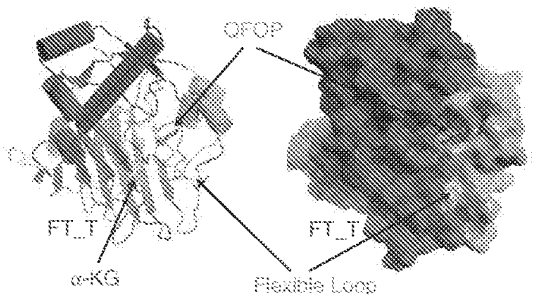


Figure 5. FT enzyme crystal structure. X-ray crystallography was used to solve the structure of FT enzymes (FT_T shown in both ribbons and space fill views). The binding of the co-substrates α-KG and QFOP (shown in light and dark green) resulted in an ordering of loops surrounding the active pocket (highlighted in purple) that also contained a metal ion. Cobalt is used to replace the iron atom during crystallization. The view as a monomer is shown for clarity.

© 2019 Society of Chemical Industry

COR-AAD1-00003311
Bayer EX1008 (Part 6 of 9)

Table 1. Characterization of selected FT enzyme variants

			RdpA	FT_R	FT_T	FT_Tv3	FT_Tv7
		Buffer	43	55	58	57	57
	Protein melting	Buffer (Fe and α-KG)	53	58	62	62	61
FOP	Quizalofop	V_{max}	2.76 (0.11)	1.60 (0.05)	1.62 (0.05)	1.51 (0.05)	1.53 (0.05)
		K_m	0.09 (0.01)	0.09 (0.01)	0.12 (0.01)	0.12 (0.01)	0.14 (0.01)
		k_{cat}/K_m	1.04	0.61	0.46	0.43	0.37
Synthetic auxins	Dichlorprop	V_{max}	5.32 (0.09)	3.03 (0.06)	2.09 (0.03)	1.29 (0.02)	1.04 (0.01)
		K_m	0.06 (0.004)	0.06 (0.01)	0.03 (0.002)	0.04 (0.003)	0.03 (0.002)
	2,4-D	V_{max}	0.25 (0.01)	0.63 (0.02)	1.17 (0.01)	3.38 (0.05)	2.91 (0.04)
		K_m	0.13 (0.02)	0.05 (0.01)	0.03 (0.002)	0.08 (0.004)	0.07 (0.004)
		k_{cat}/K_m	0.06	0.43	1.33	1.44	1.42
	MCPA	V_{max}	0.20 (0.01)	ND	1.23 (0.02)	3.64 (0.07)	2.93 (0.06)
	Mecoprop	V_{max}	4.11 (0.15)	ND	3.04 (0.07)	1.78 (0.03)	1.28 (0.02)

Lead FT variants and RdpA as a control are characterized for enzyme temperature stability and enzyme kinetics with FOP and synthetic auxin herbicides. Protein melting is recorded as the temperature (°C) in which the protein is 50% denatured in buffer alone or with supplemental Fe(II) and α-KG. Enzyme kinetic parameters are recorded for representative FOP and synthetic auxin herbicides with V_{max} (μmol mg^{-1} min^{-1}), K_m (mM) and k_{cat}/K_m (M^{-1} min^{-1}) shown. The standard error is shown in parenthesis. ND, not determined.

3.4 Temperature stable FT variants are identified

To engineer variants with improved temperature stability, structure-based design was applied in addition to the engineering approaches described above. Structure-based design leveraged a focus on the loops identified above and computational design. High-throughput screens were modified to include elevated temperatures and data-driven design enabled combinations of positive variants.

The temperature stable FT_C variant was identified with enhanced temperature stability *in vitro*. FT_C had an approximately 20 °C increase in protein melting temperature over FT_5 and maintained enzymatic activity towards QFOP (data not shown). Therefore, the FT_C variant was used as a base variant for enzyme engineering with the goal of maintaining good temperature stability while improving enzyme activity, particularly for 2,4-D as a substrate. We hypothesized that optimizing 2,4-D activity would be essential for building a 2,4-D tolerance trait in soybeans, a crop that is more sensitive to this herbicide relative to maize.

The new engineered FT variants, FT_T and FT_R, showed enhanced temperature stability with improved enzymatic activity (Table 1). Activity assays with QFOP and 2,4-D as substrates were completed with variants FT_T and FT_R (with RdpA as a control) in a range of reaction temperatures. In these assays, RdpA lost >50% activity towards QFOP at 40 °C while both FT_T and FT_R maintained >50% activity at 40 °C relative to control reactions at 25 °C (data not shown). Activity assays were also completed in which the FT_T and FT_R variants were preheated at selected temperatures (25–95 °C) before returning to 25 °C for an activity assay with QFOP. In these assays, both variants maintained approximately 50% activity with a 45 °C preheat (relative to the 25 °C preheat), further demonstrating robust temperature stability over a broad temperature range (Fig. S2). The enzymes were irreversibility inhibited at temperatures above 75 °C in this assay, consistent with the observed protein melting temperatures of approximately 60 °C (Table 1). In addition, enzymatic analysis using HPLC and mass spectrometry to confirm the reaction products demonstrated that FT_T metabolized QFOP and 2,4-D in the same manner as RdpA (Fig. S3).

3.5 FT variants with optimized 2,4-D activity are identified

FT_T showed a distinct improvement in activity towards 2,4-D relative to RdpA in the *in vitro* assays (Table 1). However, we were interested in additional engineering to determine if 2,4-D activity could be further optimized to enhance activity and crop tolerance, especially for soybean. Additional enzyme engineering, using FT_T as a base scaffold with computational protein design focused on substrate binding, resulted in the creation of variants, including FT_Tv3 and FT_Tv7. These variants had enhanced enzymatic activity when tested with 2,4-D as a substrate (Table 1), activity levels similar to SdpA, a dioxygenase characterized as having stronger activity on 2,4-D relative to RdpA (data not shown;[6,9]).

The FT variants were further characterized with FOP and auxin family herbicide chemistries (Table 1). The FT variants displayed lower activity with QFOP relative to RdpA. However, as discussed below, FT variants' FOP activity was suitable for robust in-plant tolerance, but 2,4-D activity needed to be optimized. The optimized FT variants showed enhanced 2,4-D activity with FT_Tv3 and FT_Tv7 showing a greater than 10-fold V_{max} improvement over RdpA. The 2,4-D and MCPA chemistries have two-carbon side chains that are cleaved by FT, while dichlorprop and mecoprop have three-carbon side chains identical to the FOP chemistries. The FT_Tv3 and FT_Tv7 variants have been optimized with a modified substrate preference based on the cleaved side chain, relative to RdpA. During structural analysis, several unsuccessful attempts were made to co-crystalize RdpA or FT_T with 2,4-D. FT_Tv7 was successfully co-crystalized with 2,4-D, suggesting that this variant binds 2,4-D in its active pocket better than RdpA or FT_T (Fig. S1(f)).

3.6 In-plant controlled environment and field testing demonstrates robust performance of FT variants

In-plant testing was used to further characterize selected variants. In maize, the temperature-stable variants displayed improved heat tolerance in controlled growth chamber experiments with low

 © 2019 Society of Chemical Industry

COR-AAD1-00003312
Bayer EX1008 (Part 6 of 9)

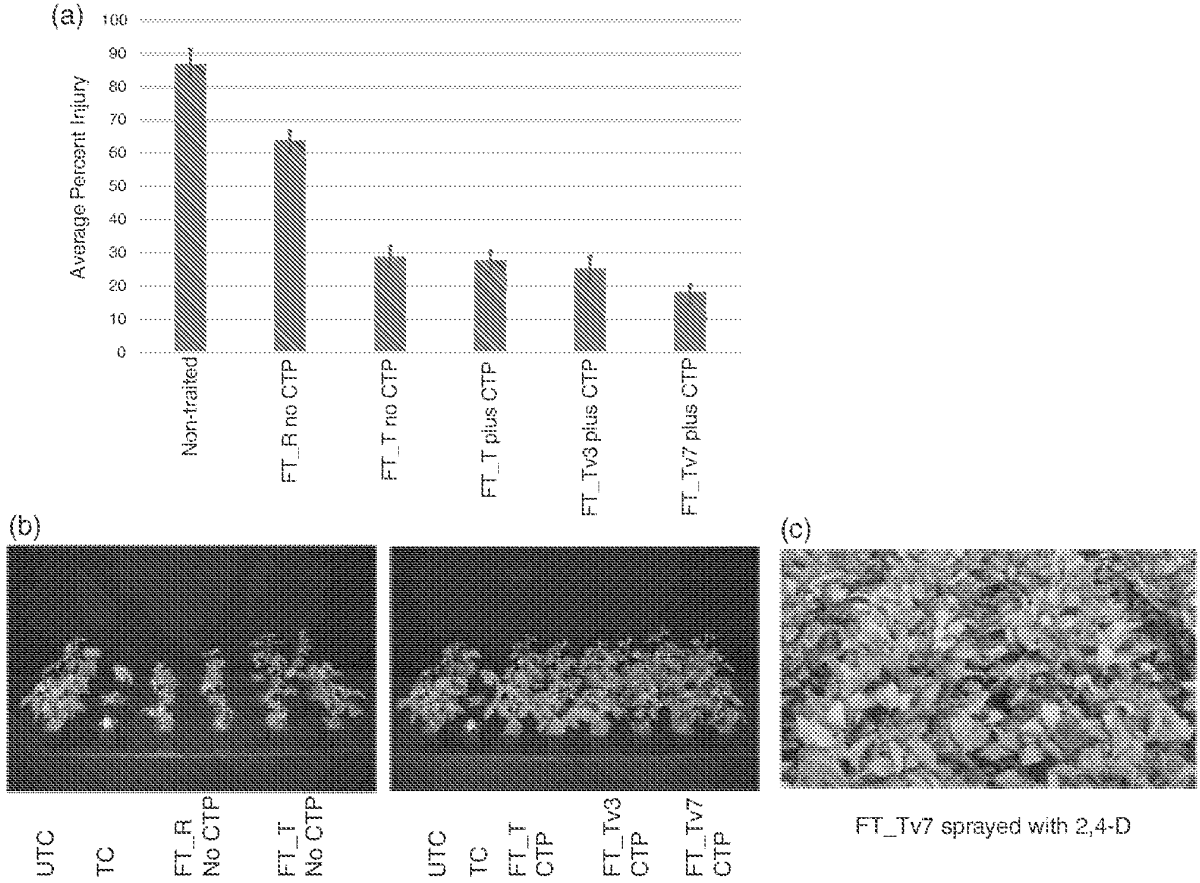


Figure 6. FT enzymes enable robust 2,4-D tolerance in soybeans. (a) Greenhouse 2,4-D spray assays in soybean demonstrated tolerance to 2,4-D in soybeans expressing FT_T, FT_Tv3 or FT_Tv7, with or without a CTP relative to control plants. Soybean lines expressing the indicated FT variant, or control plants, were treated with 2,4-D (1680 g ha^{-1}). Error bars indicate SEM. (b) Images of representative plants from (a). UTC, untreated control plants; TC, treated control plants. Control plants are in single rows of three plants; experimental plants are in double rows of three plants each. Treated control plants show extreme stunting, tissue necrosis and chlorosis. FT_R plants show some stunting and chlorosis. FT_T, FT_Tv3 and FT_Tv7 plants only show limited epinasty/malformation of upper stems and leaves. (c) Field view of FT_Tv7 expressing soybean plants following two applications (V3 and R1 growth stages) of 2,4-D (2240 g ha^{-1}) demonstrating 2,4-D tolerance.

injury ratings for both the non-stressed and heat-stressed treatments (Fig. 4). This observation confirms that the *in vitro* temperature stability of these enzyme variants directly translated to tolerance stability in plants.

Field plots with maize expressing the indicated variants were sprayed with QFOP and 2,4-D herbicides. Both QFOP and 2,4-D were tested at rates up to 16-fold over recommended agricultural field rates with repeated applications at several growth stages. In the treatments with QFOP, the control plants were completely killed while the temperature-stable variants (FT_C, FT_T and FT_R) showed little injury (Fig. 3(a) and (b)). FT_5 showed injury that increased at higher herbicide rates, demonstrating incomplete tolerance. In treatments with 2,4-D, a similar trend as with QFOP was observed (Fig. 3(c) and (d)). Maize is naturally partially tolerant to 2,4-D so complete plant death was not observed, but typical 2,4-D injury, including malformation, lodging and stunting in the control plants, was observed. Plants expressing the temperature-stable variants displayed excellent tolerance to 2,4-D, while plants expressing the FT_5 variant demonstrated incomplete tolerance at high 2,4-D rates. This demonstrated that the temperature-stable variants provided excellent tolerance to both QFOP and 2,4-D herbicide applications under field conditions in maize. Maize plants were also sprayed with clethodim, a herbicide with the same mode of action as QFOP, but a different chemical family (cyclohexanedione, DIM). As expected, no tolerance was observed for clethodim-treated FT_T expressing maize plants (data not shown). Therefore, DIM herbicides can control volunteer maize plants expressing FT in a maize-soybean crop rotation.

Maize plants were transformed to express FT variants coupled with the MDH CTP or without a CTP. As discussed above, the in-plant assays focused on using FT enzymes coupled with a CTP based on the chloroplast localization of the herbicide target. The mode of action for 2,4-D is not known to target the chloroplasts, suggesting a CTP was unlikely to improve 2,4-D tolerance.[17,18] To test these hypotheses on sub-cellular targeting, maize plants were also generated expressing FT enzymes without a CTP. The CTP-targeted FT demonstrated robust tolerance to both QFOP and 2,4-D, while the non-targeted versions of the FT enzymes (no targeting peptide) showed robust 2,4-D tolerance with reduced QFOP tolerance (Fig. 4). In the high-temperature regime, rapid growth rates appeared to somewhat, but not fully, compensate for QFOP injury observed in the non-targeted FT expressing plants. In the field-based testing, greater injury was also observed at higher QFOP rates in plants expressing FT without a CTP than FT

© 2019 Society of Chemical Industry

COR-AAD1-00003313
Bayer EX1008 (Part 6 of 9)

with a CTP (Fig. 3(a)), further suggesting that proper sub-cellular targeting of the FT enzyme improves tolerance to FOP herbicides. In addition, we also noted some increase in FT enzyme expression when FT is coupled with a CTP, suggesting this may, in part, contribute to enhanced tolerance. However, in the treatments with 2,4-D, FT enzymes with or without a CTP showed comparable performance, suggesting that the 2,4-D chemistry can be effectively deactivated both within and outside the chloroplast to provide 2,4-D herbicide tolerance (Fig. 3(c)).

In maize, the FT variants provided robust tolerance to 2,4-D herbicide applications. However, we were also interested in determining if the improved 2,4-D activity characterized for some of the temperature-stable FT variants could provide tolerance in soybeans to 2,4-D (a more sensitive crop). Therefore, we transformed a commercially relevant soybean line, A3555, using *Agrobacterium*-mediated transformation into excised embryos with several different FT enzyme variants, both with and without a CTP. Soybean plants expressing these variants were treated with 2,4-D applications. Similar to what was observed in maize, the presence or absence of the CTP did not significantly change plant 2,4-D tolerance. FT_R, a variant with improved 2,4-D activity relative to RdpA (but less activity than FT_T, FT_Tv3 and FT_Tv7; Table 1), was unable to provide good 2,4-D tolerance in soybean, with injury rates above 50%. However, FT_T, FT_Tv3 and FT_Tv7 demonstrated 2,4-D tolerance in soybean with injury rates below 30% (Fig. 6(a) and (b)). FT_Tv7 also showed commercially relevant 2,4-D tolerance in field applications of 2,4-D (Fig. 6(c)). These data support the hypothesis that engineering FT variants with optimized 2,4-D activity was essential to providing full tolerance in crops, especially sensitive crops such as soybean.

4 DISCUSSION AND CONCLUSIONS

Successful weed management is essential for ensuring robust crop yields. Here we report the successful development of engineered FT enzymes that can provide herbicide tolerance in crops to two distinct families of herbicides. Weed resistance for many herbicide families (including FOP and synthetic auxins) is already present in agricultural production areas. Therefore, successful utilization of this trait, and any herbicide tolerance trait, requires a systems-based approach to weed management. This approach includes careful consideration of the weeds present, the biology and herbicide resistance of the weed populations, the agronomic and cultural practices available and the use of combinations of herbicides encompassing multiple modes of action. The FT herbicide tolerance trait can be paired with other herbicide tolerance traits and other selective herbicides to enable additional options for farmers in their holistic weed management systems.

Ever-expanding genomics and proteomics knowledge from a variety of sources, including microbes, provides a rich source of enzyme scaffolds that can be utilized in biotechnology to design optimized enzymes. These resources can be leveraged in the optimization of enzymes for agronomically relevant properties, such as temperature stability of the FT enzymes, which may be essential for robust performance in a field setting where plants are exposed to wide temperature ranges. Another optimization target is modulating enzymatic activity with substrates of interest. For example, the FT enzymes provide tolerance to members of two herbicide families, FOP (QFOP) and synthetic auxin (2,4-D) herbicides. In conclusion, a microbial enzyme scaffold served as a starting point for the engineering of FT enzyme variants that were optimized for both enzyme activity on preferred herbicide chemistries and for enzyme temperature stability. In-plant analysis demonstrated that both elements were essential to provide robust herbicide tolerance to two herbicide families in maize and soybean crops.

SUPPORTING INFORMATION

Supporting information may be found in the online version of this article.

REFERENCES

1 Heap I, *The International Survey of Herbicide Resistant Weeds*. Available: www.weedscience.org [accessed January 2018].
2 Burton JD, Gronwald JW, Somers DA, Gengenbach BG and Wyse DL, Inhibition of corn acetyl-CoA carboxylase by cyclohexanedione and aryloxyphenoxypropionate herbicides. *Pestic Biochem Physiol* **34**:76–85 (1989).
3 Peterson MA, McMaster SA, Riechers DE, Skelton J and Stahlman PW, 2,4-D past, present, and future: a review. *Weed Technol* **30**:303–345 (2016).
4 Huang J, Ellis C, Hauge B, Qi Y and Varagona MJ, Maize protein expression: herbicide tolerance, in *Recent Advancements in Gene Expression and Enabling Technologies in Crop Plants*, ed. by Azhakanandam K, Silverstone A, Daniell H and Davey MR. Springer-Verlag, New York, pp. 213–237 (2015).
5 Schleinitz KM, Kleinsteuber S, Vallaeys T and Babel W, Localization and characterization of two novel genes encoding sterospecific dioxygenases catalyzing 2(2,4-dichlorophenoxy)propionate cleavage in *Delftia acidovorans* MC1. *Appl Environ Microbiol* **70**:5357–5365 (2004).
6 Muller TA, Fleischmann T, van der Meer JR and Kohler H-PE, Purification and characterization of two enantioselective α-ketoglutarate-dependent dioxygenases, RdpA and SdpA, from *Sphingomonas herbicidovorans* MH. *Appl Environ Microbiol* **72**:4853–4861 (2006).
7 Bugg TDH, Dioxygenase enzymes: catalytic mechanisms and chemical models. *Tetrahedron* **59**:7075–7101 (2003).
8 Hausinger RP, Fe(II)/α-ketoglutarate-dependent hydroxylases and related enzymes. *Crit Rev Biochem Mol Biol* **39**:21–68 (2004).
9 Wright TR, Shan G, Walsh TA, Lira JM, Cui C, Song P *et al.*, Robust crop resistance to broadleaf and grass herbicides provided by aryloxyalkanoate dioxygenase transgenes. *Proc Natl Acad Sci USA* **107**:20240–20245 (2010).
10 Fukomori F and Hausinger RP, Purification and characterization of 2,4-dichlorophenoxyacetate/α-ketoglutarate dioxygenase. *J Biol Chem* **268**:24311–24317 (1993).
11 Sidorov V and Duncan D, *Agrobacterium*-mediated maize transformation: immature embryos *versus* callus, in *Methods in Molecular Biology: Transgenic Maize*, Vol. **526**, ed. by Scott MP. Humana Press, New York, pp. 47–58 (2009).
12 Glenn KC, Alsop B, Bell E, Goley M, Jenkinson J, Liu B *et al.*, Bringing new plant varieties to market: plant breeding and selection practices advance beneficial characteristics while minimizing unintended changes. *Crop Sci* **57**:2906–2921 (2017).
13 Yoshida K and Hisabori T, Adenine nucleotide-dependent and redox-independent control of mitochondrial malate dehydrogenase activity in *Arabidopsis thaliana*. *Biochim Biophys Acta* **1857**:810–818 (2016).
14 O'Brien JR, Schuller DJ, Yang VS, Dillard BD and Lanzilotta WN, Substrate-induced conformational changes in *Escherichia coli* taurine/alpha-ketoglutarate dioxygenase and insight into the oligomeric structure. *Biochemistry* **42**:5547–5554 (2003).
15 Herbert D, Price LJ, Alban C, Dehaye L, Job D, Cole DJ *et al.*, Kinetic studies on two isoforms of acetyl-CoA carboxylase from maize leaves. *Biochem J* **318**:997–1006 (1996).
16 Crafts-Brandner SJ and Salvucci ME, Sensitivity of photosynthesis in a C4 plant, maize, to heat stress. *Plant Physiol* **129**:1773–1780 (2002).
17 Dharmasiri N, Dharmasiri S and Estelle M, The F-box protein TIR1 is an auxin receptor. *Nature* **435**:441–445 (2005).
18 Kepinski S and Leyser O, The Arabidopsis F-box protein TIR1 is an auxin receptor. *Nature* **435**:446–451 (2005).

 © 2019 Society of Chemical Industry

COR-AAD1-00003314
Bayer EX1008 (Part 6 of 9)

FEMS MICROBIOLOGY ECOLOGY

RESEARCH ARTICLE

Consumers of 4-chloro-2-methylphenoxyacetic acid from agricultural soil and drilosphere harbor *cadA*, *r/sdpA*, and *tfdA*-like gene encoding oxygenases

Ya-Jun Liu[1,2], Shuang-Jiang Liu[2], Harold L. Drake[1] & Marcus A. Horn[1]

[1]Department of Ecological Microbiology, University of Bayreuth, Bayreuth, Germany; and [2]State Key Laboratory of Microbial Resources, Institute of Microbiology, Chinese Academy of Sciences, Beijing, China

Correspondence: Marcus A. Horn, Department of Ecological Microbiology, Dr-Hans-Frisch-Str. 1-3, University of Bayreuth, 95440 Bayreuth, Germany. Tel.: +49 (0)921 555620; fax: +49 (0) 921 555799; e-mail: marcus.horn@uni-bayreuth.de

Present address: Ya-Jun Liu, Shandong Provincial Key Laboratory of Energy Genetics, Qingdao Institute of Bioenergy and Bioprocess Technology, Chinese Academy of Sciences, Qingdao, Shandong, China

Received 28 December 2012; revised 15 March 2013; accepted 1 May 2013.
Final version published online 23 May 2013.

DOI: 10.1111/1574-6941.12144

Editor: Kai-Uwe Totsche

Keywords
herbicide; *tfdA*-like; *cadA*; *r/sdpA*; DNA-stable isotope probing; drilosphere.

Abstract

Microbial degradation of 2-methyl-4-chlorophenoxyacetic acid (MCPA) in soil is enhanced by earthworms and initiated by *tfdA*-like, *cadA* and *r/sdpA* gene encoding oxygenases. Copy numbers of such genes increased during MCPA degradation in soil, and MCPA stimulated transcription of *tfdA*-like and *r/sdpA* genes up to 4×. Transcription of *cadA* was detected in the presence of MCPA only. DNA stable isotope probing after consumption of 0.6–0.8 mg ^{13}C-MCPA g_{dw}^{-1} in oxic microcosms indicated diverse labeled oxygenase genes in bulk soil, burrow walls, and cast. 9, 6, and 3 operational taxonomic units of *tfdA*-like, *cadA*, and *r/sdpA* genes, respectively, were labeled and affiliated with group 2 *Alphaproteobacteria* including *Bradyrhizobia* and group 1 class III *Betaproteobacteria*. New genes encoding putative MCPA degrading oxygenases were identified. Diversity of labeled OTUs tended to be lower for cast than for bulk soil. The collective data indicate (1) hitherto unknown active MCPA degraders and/or oxygenase genes in soil; (2) that multiple oxygenases are associated with MCPA degradation in soil at the same time; (3) that earthworms impact the capability of MCPA degraders in soil to respond to MCPA; and (4) the collective data enable a more in-depth analysis of MCPA degrader communities in soil by future structural gene-based experimental strategies.

Introduction

The phenoxyalkanoic acid (PAA) herbicides 4-chloro-2-methylphenoxyacetic acid (MCPA) and 2,4-dichlorophenoxyacetic acid (2,4-D) are extensively used in agricultural and nonagricultural soil for weed control (Bollag *et al.*, 1967; Loos *et al.*, 1979; Smith & Hayden, 1981; Worthing & Hance, 1991; Müller *et al.*, 2001). MCPA and 2,4-D are highly mobile in soils, potential groundwater, and soil contaminant and are classified as group 2B compounds 'possibly carcinogenic to humans' by International Agency for Research on Cancer (WHO; Thompson *et al.*, 1984; Scheidleder, 2000). MCPA is usually more persistent than 2,4-D, and thus, efficient degradation of MCPA is of concern (Audus, 1952; Smith & Hayden, 1981). PAAs are photochemically degraded when light is available and metabolized by microorganisms in soil (WHO, 2008). MCPA disappearance in the presence of fungi like *Phanerochaete chrysosporium* coincided with peroxidase activities, and 2,4-D carbon was recovered in fungal phospholipid fatty acids, thus suggesting that fungi might contribute to MCPA degradation (Castillo *et al.*, 2001; Lerch *et al.*, 2009). PAA-degrading bacteria (phyla *Actinobacteria*, *Bacteroidetes*, and *Proteobacteria*) were isolated from both pristine (i.e. noncontaminated) and herbicide pre-exposed soil (Amy *et al.*, 1985; Chaudhry & Huang, 1988; Balajee & Mahadevan, 1993; Ka *et al.*, 1994; Oh *et al.*, 1995; Huong *et al.*, 2007; Macur *et al.*, 2007; Silva *et al.*, 2007). Bacteria were classified into three main groups on the basis of their phylogeny and the sequences of genes encoding oxygenases that initiate the first step of PAA degradation (Kamagata *et al.*, 1997).

© 2013 Federation of European Microbiological Societies
Published by John Wiley & Sons Ltd. All rights reserved

Downloaded from http://femsec.oxfordjournals.org/ by guest on July 9, 2016

COR-AAD1-00003315
Bayer EX1008 (Part 6 of 9)

Group 1 microorganisms include various copiotrophic and fast-growing bacteria belonging to *Beta-* and *Gammaproteobacteria* (Fulthorpe *et al.*, 1995). α-ketoglutarate-dependent dioxygenase encoded by *tfdA* drives the first step of MCPA degradation in group 1 degraders by cleaving the ether bond of MCPA to form 2-methyl-4-chlorophenol (MCP). MCP is thereafter degraded through the pathway encoded by *tfdBCDEF* (Gaunt & Evans, 1971; Pieper *et al.*, 1988; Leveau & van der Meer, 1997; Leveau *et al.*, 1999; Shimojo *et al.*, 2009). Microorganisms of group 1 were further categorized to three classes according to *tfdA* sequences, in which *Cupriavidus necator* JMP134, *Burkholderia* sp. strain RASC, and *Rhodoferax* sp. strain P230 are model organisms of classes I, II, and III, respectively (McGowan *et al.*, 1998; Baelum *et al.*, 2006). Class III *tfdA* was primarily associated with PAA degradation to date (Baelum & Jacobsen, 2009; Rodriguez-Cruz *et al.*, 2010). Group 2 microorganisms are mainly slow-growing, oligotrophic *Bradyrhizobium* sp. of *Alphaproteobacteria* (Jordan, 1982; Kamagata *et al.*, 1997; Kitagawa *et al.*, 2002; Itoh *et al.*, 2004). *tfdA*-like genes were also detected in microorganisms of group 2, with 60% identity to group 1 *tfdA* (Fulthorpe *et al.*, 1995; Itoh *et al.*, 2002; Zaprasis *et al.*, 2010). MCPA degraders of group 3 are *Sphingomonas*-related microorganisms likewise belonging to *Alphaproteobacteria* (Ka *et al.*, 1994). Group 3 microorganisms were determined as dominant MCPA utilizers in soil by 16S rRNA gene–based stable isotope probing, and MCPA degradation was associated with the expression of *tfdA*-like genes affiliating with alphaproteobacterial sequences (Liu *et al.*, 2011a, b). Nevertheless, *cadAB* was predicted to encode an alternative 2,4-D oxygenase in groups 2 and 3 microorganisms with 46% amino acid identity to a 2,4,5-trichlorophenoxyacetic acid (2,4,5-T) oxygenase of *Burkholderia cepacia* AC1100 encoded by *tftAB* (Danganan *et al.*, 1994; Kitagawa *et al.*, 2002). *cadA* is essential for 2,4-D conversion in pure cultures of *Alphaproteobacteria* (Kitagawa *et al.*, 2002; Itoh *et al.*, 2004; Shimojo *et al.*, 2009), and gene abundance of *cadA* in soil is stimulated during MCPA degradation (Liu *et al.*, 2011b). However, the role of *cadAB* in groups 2 and 3 microorganisms for ether bond cleavage of MCPA is still unclear. Preliminary data also showed that *cadA*-like genes may occur in isolates of the *Firmicutes* and *Actinobacteria* like *Paenibacillus* sp. Ao3 (EU372719) and *Terrabacter* sp. DMA (EU372720), respectively. New groups of putative MCPA degraders were detected in soil based on phylogenetic analysis of *tfdA*-like genes (Gazitua *et al.*, 2010; Zaprasis *et al.*, 2010).

In addition to 'classic' PAA degraders who follow the degradation pathway initialized by *tfdA*-like or *cadA* gene encoding oxygenases, other potential MCPA degraders may be present in soil. Enantiomer-specific Fe (II) and α-ketoglutarate-dependent dioxygenases encoded by *rdpA* and *sdpA* genes were detected in *Delftia acidovorans* MC1 (formerly *Comamonas acidovorans* MC1), *Rhodoferax* sp. P230 of the *Betaproteobacteria*, and *Sphingobium herbicidovorans* MH [formerly *Sphingomonas herbicidovorans* MH (Takeuchi *et al.*, 2001)] of the *Alphaproteobacteria*, who are all capable of degrading the chiral phenoxypropionate herbicides 2-(2,4-dichlorophenoxy)propionate [(*RS*)-2,4-DP] and 2-(2-methyl-4-chlorophenoxy)propionate [(*RS*)-MCPP], as well as 2,4-D and MCPA (Zipper *et al.*, 1996; Ehrig *et al.*, 1997; Kohler, 1999; Müller *et al.*, 1999, 2001). *Burkholderia* strains (*Betaproteobacteria*) isolated from agricultural soil also contain *rdpA* based on GenBank database (EF373543–EF373549), but not *sdpA*. A highly conserved amino acid sequence motif of TfdA-like protein (group 2 PAA degraders) is present in both RdpA and SdpA of *D. acidovorans* MC1, but such proteins only showed 35% and 37% identity with TauD of *Pseudomonas aeruginosa* and TfdA of *C. necator* JMP134, respectively (Schleinitz *et al.*, 2004). *cadAB*-like genes are unknown to occur in *rfsdpA* gene-hosting microorganisms (Itoh *et al.*, 2004; Müller *et al.*, 2006). Information on the diversity of oxygenase genes in soil hosted by MCPA degraders is still very scarce.

MCPA degraders are subjected to various physicochemical conditions in soils impacting MCPA degradation, including those associated with the soil macrofauna. Earthworms represent the dominant macrofauna in terms of biomass and are abundant in many soils worldwide, severely impact the soil environment, and are thus often referred to as 'soil engineers' (Edwards, 2004). The drilosphere includes the burrow system, gut content, and earthworm casts and is defined as soil influenced by earthworm activities (Lavelle, 1988; Edwards, 2004). The drilosphere is considered as a zone of high microbial activity in soil due to its high nutrient availability (Scheu, 1991; Brown, 1995; Schmidt *et al.*, 1999; Tiunov & Scheu, 1999; Brown *et al.*, 2000; Drake & Horn, 2007). Earthworm movement and burrowing activity increase moisture and oxygen availability in soil and also affect the transfer of nutrients (Edwards & Bohlen, 1996; Edwards, 2004). Casts are nutritionally richer than surrounding soil because earthworms excrete mucus, which is rich in saccharides and amino acids (Bolan & Baskaran, 1996; Edwards & Bohlen, 1996; Edwards, 2004; Drake & Horn, 2007). Thus, earthworms were widely used in assisting soil bioremediation (Hickman & Reid, 2008). MCPA is degraded aerobically by microorganisms in soil (Kuhlmann *et al.*, 1995; Vink & vanderZee, 1997); thus, higher level of aeration and moisture content introduced by earthworms may benefit MCPA-degrading microorganisms and therefore accelerate MCPA degradation in soil. Our previous study suggested that the endogeic (soil-feeding) earthworm

Downloaded from http://femsec.oxfordjournals.org/ by guest on July 9, 2016

© 2013 Federation of European Microbiological Societies
Published by John Wiley & Sons Ltd. All rights reserved

COR-AAD1-00003316
Bayer EX1008 (Part 6 of 9)

Aporrectodea caliginosa (Oligochaeta, *Lumbricidae*) indeed enhances MCPA degradation in soil by stimulating both growth and activity of MCPA-degrading bacteria (Liu *et al.*, 2011b). Groups 2 and 3 microorganisms and hitherto unknown bacteria were dominant MCPA degraders in soil, and MCPA-degrading community in burrow wall and cast differed from that in bulk soil, suggesting a severe effect of earthworms in shaping soil MCPA degrader communities (Liu *et al.*, 2011a). However, data on which oxygenase genes are hosted by MCPA degraders from the drilosphere are lacking.

Thus, it was hypothesized that soil and drilosphere are a reservoir of hitherto unknown oxygenase-encoding gene diversity hosted by MCPA degraders. The objectives of the study were to (1) develop primers for the detection of *rfsdpA*; (2) determine which oxygenase genes (*tfdA*-like, *cadA*, and *rfsdpA*) are associated with MCPA degradation in agricultural soil; and (3) identify MCPA degraders and associated oxygenase genes by structural gene stable isotope probing.

Materials and methods

Chemicals

^{12}C-MCPA (chemical purity ≥ 97%, Fluka Riedel-de Haën) and ^{13}C-labeled MCPA (Phenyl-$^{13}C_6$, carbonyl-^{13}C, chemical purity ≥ 98.6%) were purchased from Sigma-Aldrich (St. Louis, MO) and IsoSciences (Country King of Prussia, PA,), respectively. Sterile 3 mM ^{12}C/^{13}C-MCPA stock solutions were prepared as described (Liu *et al.*, 2011b) prior to use.

Sampling sites

Agricultural soil samples from the top 0 to 10 cm depth were obtained in May 2009 from the experimental farm 'Klostergut Scheyern' in Germany (48°30′00″N, 11°20′07″E) where MCPA was applied in 2002. The properties of the soil are described elsewhere (Schellenberger *et al.*, 2010; Liu *et al.*, 2011a, b). Adult earthworms of the species *A. caliginosa* were collected from 0 to 15 cm depth of soil in meadow Trafo Wiese in Bayreuth (Germany) and were identified by standard protocols (Brohmer, 1984). Soil samples and earthworms were transported, stored, and prepared as described prior to use (Liu *et al.*, 2011a).

Microcosms for gene transcription analyses

Microcosms with field fresh soil were performed as described (Liu *et al.*, 2011b). In brief, 10 g_{fw} of field fresh soil was incubated in 40 mL MMS (Müller *et al.*, 2001) with 30 μg g^{-1} MCPA (*c.* 0.03 mM) under oxic condition at 15 °C in the dark. Three replicates were prepared and agitated at 150 r.p.m. for 22 days. Two millilitre of the mixed soil slurries was sampled and phase-separated by centrifugation every 2 or 3 days as described (Liu *et al.*, 2011b). Liquid and solid phases of samples were immediately used for MCPA measurements and stored at −80 °C for nucleic acids extraction, respectively.

Microcosms for ^{13}C-labeling

Soil and drilosphere material for structural gene DNA stable isotope probing (SIP) in microcosms were obtained from a previous soil column experiment (Liu *et al.*, 2011a). Microcosms analyzed in the preceding study by RNA-SIP for MCPA degraders (Liu *et al.*, 2011a) were continued, and MCPA was pulsed to stimulate growth of MCPA degraders, which is a prerequisite for structural gene DNA-SIP.

In brief, pre-incubation of MCPA-supplemented soil in the presence of earthworms was performed in soil columns. Four soil columns were set up with *c.* 1 kg_{dw} bulk soil per column. Duplicate columns were supplemented with 0.02 mg g_{dw}^{-1} ^{13}C- or ^{12}C-MCPA (nonlabeled MCPA). Ten to twelve earthworms with the biomass of 8–9 g were added per soil column. Soil columns were incubated in the dark at 15 °C for 27 days. MCPA was not detectable after (i.e. was consumed during) soil column incubation (Liu *et al.*, 2011a). Samples of bulk soil and drilosphere materials after the incubation were used for further incubation in microcosms with ^{13}C- and ^{12}C-MCPA as well as MCPA determination. Microcosms were set up for SIP in duplicates with 1–1.5 g_{fw} bulk soil or drilosphere samples (i.e. with 0–2 and 8–10 cm depth of soil, gut, burrow wall, and cast) in 4–6 mL MMS and supplemented with ^{13}C- or ^{12}C-MCPA. Soil microcosms were incubated under oxic condition as described (Liu *et al.*, 2011a) and pulsed with 0.1 mg g_{dw}^{-1} either ^{13}C- or ^{12}C-MCPA when no MCPA was detectable. One hundred microlitre supernatant was sampled from each microcosm every 2 or 3 days and analyzed for MCPA. Because DNA-SIP requires growth (replication of genomes) of organisms, one late time point was utilized for nucleic acid extraction to maximize the likelihood of incorporation of MCPA-^{13}C into DNA. The structural rather than 16S rRNA gene approach minimizes the effect of cross-feeding. Microcosms were incubated until 0.6–0.8 mg MCPA g_{dw}^{-1} was consumed in total after 55 days. Solid material was then prepared by centrifugation and stored at −80 °C for nucleic acid extraction.

Quantification of MCPA

MCPA was determined after NaOH extraction of soil (recovery of 99%) or directly in the liquid phase of

© 2013 Federation of European Microbiological Societies
Published by John Wiley & Sons Ltd. All rights reserved

Downloaded from http://femsec.oxfordjournals.org/ by guest on July 9, 2016

COR-AAD1-00003317
Bayer EX1008 (Part 6 of 9)

samples from microcosms as described (Liu *et al.*, 2011a). The concentrations of MCPA were determined by a high-performance liquid chromatography equipped with a diode array detector (Agilent 1200 series; Agilent Technologies, CA) as described previously (Liu *et al.*, 2011b). An external standard curve (10–250 μM) was prepared for every measurement. MCPA concentrations were calculated on the basis of dry weight of soil, which was determined by extracting weight loss of soil samples before and after drying at 65 °C for > 12 h.

Nucleic acid extraction

Samples collected from microcosms as well as field fresh bulk soil were used for nucleic acid extraction. DNA and RNA were co-extracted from 0.5 g_{fw} material utilizing a bead-beating protocol with humic acid precipitation as described (Persoh *et al.*, 2008; Zaprasis *et al.*, 2010; Liu *et al.*, 2011a). For quantitative PCR, DNA and RNA were separated and further purified with a RNA/DNA Mini Kit (Qiagen, Hilden, Germany). For DNA stable isotope probing, nucleic acid extracts were treated with RNase A (Fermentas GmbH, St. Leon-Rot, Germany) at room temperature for 1 h to remove RNA. All DNA and RNA samples were stored at −20 and −80 °C for further analyses, respectively.

Separation of ^{13}C- and ^{12}C-DNA

^{13}C- and ^{12}C-labeled DNAs were separated according to a modified protocol (Neufeld *et al.*, 2007b). Purified DNA extracts from duplicate soil microcosms were pooled and quantified with a Quant-iT PicoGreen DNA Assay Kit (Invitrogen, Karlsruhe, Germany) right before ultracentrifugation. Of 200–500 ng DNA was loaded per CsCl gradient. A blank control gradient was loaded with DNA-free gradient buffer (GB, Neufeld *et al.*, 2007b) to determine the buoyant density (BD) of the gradient solution per fraction after ultracentrifugation. The gradient solution was prepared by mixing 4.1 mL CsCl solution (7.16 M, BD = 1.868 g mL^{-1}) with 0.9 mL GB buffer, to obtain a desired BD of *c.* 1.725 g mL^{-1} (Neufeld *et al.*, 2007b). All solutions prepared in this study were autoclaved (121 °C, 15 P, 30 min) or filter-sterilized (0.22-μm cellulose acetate sterile filter, Minisart® NML; Sartorius Stedim Biotech S.A., Aubagne, France). Isopycnic ultracentrifugation was performed using a VTi 65.2 vertical rotor (Beckman, Fullerton, CA) at 177 200 *g*, 20 °C for 40 h. Ten fractions (450 μL each) were collected from every sample. Buoyant densities were determined by weighing 100 μL solutions from every fraction of the blank control at 20 °C. The expected density range was suggested to be *c.* 1.690–1.760 g mL^{-1} with a median density (fraction 6 or 7) of *c.* 1.725 g mL^{-1} (Neufeld *et al.*, 2007b). Buoyant densities per gradient ranged in this study from 1.704 to 1.758 g mL^{-1}, and fraction 7 had the median density of 1.726 g mL^{-1}, which was in accordance with the published protocol. Besides, a linear relationship between BD and fractions was detected. These results suggested the successful formation of gradient density. Two hundred microlitre of fractions 2–9 of every sample was precipitated at room temperature for 2 h with two volumes of 30% PEG6000, 0.1 M HEPEs, and 1.6 M NaCl (Neufeld *et al.*, 2007b). Sixty microgram of glycogen was added during precipitation to ensure the efficient precipitation of low DNA concentrations. DNA samples were collected by centrifugation in a SIGMA 1–15PK centrifuge (Rotor 12132; Sigma Laborzentrifugen GmbH, Osterode am Harz, Germany) at 13 000 *g* for 30 min at 20 °C and then washed and resuspended in 30 μL DNase-/RNase-free water. DNA concentration of every fraction was quantified with PicoGreen (Invitrogen). Fractions 3–6 and fractions 8–9 of every gradient were regarded as 'heavy' and 'light' fractions, respectively.

Amplification of *tfdA*-like, *cadA*, *r/sdpA*, and 16S rRNA genes

Polymerase chain reactions were performed with available and new primers (Table 1). Published primers were utilized for amplification of *tfdA*-like and *cadA* genes (Kitagawa *et al.*, 2002; Itoh *et al.*, 2004; Zaprasis *et al.*, 2010). *Sphingomonas* sp. TFD26 was grown as described, and colony material was used as a positive control for PCR amplification (Tonso *et al.*, 1995; Itoh *et al.*, 2004). For *r/sdpA* genes, degenerate primers (RSdpA419F/RSdpA886R) were designed in this study targeting the conserved regions identified in alignments based on 13 known *rdpA* or *sdpA* genes sequences (10 *rdpA* gene sequences and 3 *sdpA* gene sequences) obtained from NCBI database (http://www.ncbi.nlm.nih.gov). The alignment was performed with MEGA 4 (http://www.megasoftware.net/mega.html; Kumar *et al.*, 2008). The GenBank accession numbers of references for *rdpA* were as follows: EF373548, EF373549, EF373545, EF373547, EF373546, EF373543, EF373544, AF516752, AF516751, AY327575; those for *sdpA* were as follows: AJ628860, AY327575, and DQ406818. DNA from heavy fractions (i.e. fractions 3–6) of every microcosm was pooled and used as template for PCR amplification of *tfdA*-like, *cadA*, and *r/sdpA* genes. Each amplification reaction was performed in a total volume of 25 μL, and the reaction mixture contained 1X MasterMix (5-Prime, Hamburg, Germany) supplemented with 1.5 mM $MgCl_2$ (3 mM final concentration), 0.1 μg μL^{-1} bovine serum albumin (BSA), 0.2 μM of each primer (for primer TfdA421dF, 0.8 μM was added;

© 2013 Federation of European Microbiological Societies
Published by John Wiley & Sons Ltd. All rights reserved

Downloaded from http://femsec.oxfordjournals.org/ by guest on July 9, 2016

COR-AAD1-00003318
Bayer EX1008 (Part 6 of 9)

Table 1. PCR primers and conditions utilized in this study

Primer set*	Sequence (5′-3′)†	Target	Annealing temp. (°C)‡	App. product length (bp)	References
TfdA421dF	ACSGARTTCKSiGACATGC	*tfdA*-like	54.0 (53.0)	c. 360	Zaprasis *et al.* (2010)
TfdA778vkR	AGCGGTTGTCCCACATCAC				
CadA610F	AAGCTGCARTITGARAAYGG	*cadA*	50.0	c. 460	Itoh *et al.* (2004)
CadA1054R	MGGATTGAAGAAATCCTGRTA				
RSdpA419F	TGGCATRCCGACAGCACCTWC	*r/sdpA*	60.0	c. 470	This study
RSdpA886R	CAKCRKGCASMGRTTGTCCC				
Eub341F	CCTACGGGAGGCAGCAG	16S rRNA gene	55.7	c. 190	Muyzer *et al.* (1993)
Eub534R	ATTACCGCGGCTGCTGG				

*Numbers in primer names indicate position of binding sites relative to the reference sequence of *Cupriavidus necator* JMP134 (AY365053; TfdA421dF/TfdA778vkR), *Bradyrhizobium* sp. HW13 (AB062679; CadA610F/CadA1054R) and *Rhodoferax* sp. P230 (DQ406818; RSdpA419F/RSdpA886R); F forward; R reverse.

†S, C/G; Y, C/T; W, A/T; M, A/C; K, G/T; R, A/G; I, Inosine.

‡Numbers in parentheses refer to qPCR chemicals.

Biomers, Ulm, Germany), and DNA c. 2 ng (or 2 μL cDNA or RNA) as templates. PCRs were performed on a PeqStar 96 model thermal cycler (PeqLab, Erlangen, Germany) with 10 min of initial denaturation at 95 °C, followed by 45 cycles, each consisting of denaturation at 95 °C for 1 min, annealing at primer-dependent temperatures (Table 1) for 1 min, and elongation at 72 °C for 1 min. The final elongation was at 72 °C for 15 min. PCR products were investigated by 1% agarose gel electrophoresis and stored at −20 °C.

Reverse transcription of RNA

Reverse transcriptions were performed with SuperScript VILO cDNA Synthesis Kit (Invitrogen) as described (Liu *et al.*, 2011a, b). RNA was quantified with a Quant-iT RiboGreen RNA Assay Kit (Invitrogen) prior to reverse transcription. Structural gene PCRs with cDNA and RNA as template verified that (1) the reverse transcription was successful; and (2) RNA preparations were free of DNA.

Cloning, screening, and sequencing

PCR products were purified with MiniElute PCR product purification kit (Qiagen) and dissolved in 20 μL sterile water. Purified PCR products for the generation of gene libraries were ligated into pGEM-T Easy Vectors (Promega, Mannheim, Germany) according to the manufacturer's protocol, which were used to transform *Escherichia coli* JM109 competent cells. Clones hosting a vector with the correct insert were selected via blue/white and PCR-based screening with vector-specific primers M13uni/M13rev (Messing, 1983). M13-PCR products with the expected size (Table 1) were sequenced with primer M13uni (Macrogen, Seoul, South Korea). Nine gene libraries were established per structural gene, that is, one from field fresh bulk soil, four from ^{13}C-MCPA-treated microcosms (0–2 and 8–10 cm depth of bulk soil, burrow wall, and cast), and four from corresponding ^{12}C-MCPA-treated microcosms.

Phylogenetic analysis and clustering

Sequences obtained from all gene libraries were pre-aligned with MEGA 4 (http://www.megasoftware.net; Kumar *et al.*, 2008), and regions of primer binding sites and vector sequences were removed. *tfdA*-like, *cadA*, and *r/sdpA* gene sequences were then analyzed with ARB (http://www.arb-home.de/; Ludwig *et al.*, 2004). Reference sequences were retrieved from GenBank (http://www.ncbi.nlm.nih.gov). Sequences were translated *in silico* and aligned with the CLUSTALW algorithm. The alignment was refined manually. DNA was realigned according to the aligned proteins. Phylogenetic trees were calculated based on amino acid sequences using the neighbor-joining algorithm (Saitou & Nei, 1987). Tree topologies of neighbor-joining trees were verified by bootstrap analysis with 1000 replicates. Pre-aligned 16S rRNA gene sequences were retrieved from SILVA (http://www.arb-silva.de; Pruesse *et al.*, 2007). Distance matrices were generated with ARB (Ludwig *et al.*, 2004) to generate correlation plots of pairwise similarities of 16S rRNA genes with *cadA* or CadA and that of 16S rRNA gene with *r/sdpA* or R/SdpA. Such analyses were intended to yield distance cutoffs for such structural genes that could be used to identify species-level genotypes.

rdpA gene-containing microorganisms that shared 80–100% 16S rRNA gene similarity always shared > 97% *rdpA* gene similarity (Supporting Information, Fig. S1A), which indicated horizontal gene transfer of *rdpA* genes across bacteria taxa. For *sdpA* genes, only three references were found in GenBank database, which resulted in only

© 2013 Federation of European Microbiological Societies
Published by John Wiley & Sons Ltd. All rights reserved

Downloaded from http://femsec.oxfordjournals.org/ by guest on July 9, 2016

COR-AAD1-00003319
Bayer EX1008 (Part 6 of 9)

three data points of pairwise comparison (Fig. S1B). Correlation between 16S rRNA gene similarity and *cadA* gene similarity was moderate (Fig. S1C). Pairwise similarities of *cadA* and 16S rRNA gene sequences ranged from 55.6% to 100% and 77.1% to 100%, respectively. The scatting of data points was also an indicative of *cadA* gene dispersal. 84% similarity of translated *tfdA*-like genes was suggested to cover 90% of group 2 microorganisms, which shared > 97% 16S rRNA gene similarity (Zaprasis *et al.*, 2010). Thus, 16% distance of protein sequences was used as cutoff for OTU determination for *tfdA*-like, *cadA*, and *r/sdpA* genes in this study. With this distance, coverages for gene libraries of *tfdA*-like, *cadA*, and *r/sdpA* genes were 87–100%, 98–100%, and 98–100% (coverage of *r/sdpA* gene library from T_0 bulk soil was 40% because only 15 sequences were obtained), respectively. The data indicated that most of the gene libraries were sufficiently sampled.

Identification of labeled taxa

^{12}C- might comigrate with ^{13}C-containing nucleic acids toward heavy fractions during isopycnic centrifugation (Lueders *et al.*, 2004). Thus, labeled taxa were identified by comparative analyses of ^{13}C- and ^{12}C-treatments. For structural gene DNA-SIP, OTUs whose relative abundances in heavy DNA fractions from ^{13}C-treatments exceeded 5%, were higher than that in corresponding heavy fractions from ^{12}C-treatments, or only occurred in heavy fractions of ^{13}C-treatments were considered as ^{13}C-labeled OTUs, and labeling intensities were calculated (Liu *et al.*, 2011a).

Analysis of structural gene diversity

Distance matrices generated from aligned amino acid sequences were analyzed with DOTUR (http://schloss.micro.umass.edu/software/index.html; Schloss & Handelsman, 2005) to define genotypes based on the protein dissimilarity derived from translated structural gene sequences by the furthest-neighbor method. Amino acid sequences with maximal 16% dissimilarity (distance) were thereby assigned to one genotype or OTU. Coverage (*C*) was calculated to investigate the diversity of genotypes represented in gene libraries as described (Zaprasis *et al.*, 2010).

Quantification of 16S rRNA genes, structural genes, and transcripts

Quantitative PCRs (qPCRs) were performed with cDNA and DNA as templates. Samples were diluted to 1/50 first to reduce the influence of humic acids (Zaprasis *et al.*, 2010). All qPCRs were set up in duplicates. Negative controls and standards were prepared as described (Zaprasis *et al.*, 2010). Detection limits of the assays *c.* 10^{-1} copies per μL. The reaction mixture (20 μL) was composed of 1X SensiMix Reaction Mix (Bioline GmbH, Luckenwalde, Germany), 0.1 μg μL^{-1} BSA, 0.2 μM of each primer (0.8 μM for primer TfdA421dF; Biomers; Table 1), 5 μL of diluted template, and sterilized deionized water. qPCRs were performed on an iQ™5 Real-Time qPCR cycler (Bio-Rad, Munich, Germany). The initial step was at 95 °C for 8 min, followed by 45 cycles of denaturation at 95 °C for 40 s, annealing at primer-dependent temperatures (Table 1) for 30 s, and elongation at 72 °C for 15 s when fluorescence signal was recorded. The final PCR elongation step was at 72 °C for 5 min. Melting curve analyses were performed from 70 to 95 °C with increments of 0.5 °C per cycle. Inhibition factors were determined per published protocol (Zaprasis *et al.*, 2010; Liu *et al.*, 2011b), to correct copy numbers from both RNA and DNA extracts for inhibition during qPCR on a per nucleic acid extract basis. Representative qPCR products were checked by agarose gel (1%) electrophoresis. Structural gene copy numbers were normalized with 16S rRNA gene copy numbers, and the effect of MCPA treatment was expressed as relative gene frequency ratio (RGFR, i.e. the ratio of copy numbers from MCPA treatment to those from treatments without MCPA) to minimize the effect of differential cell lysis efficiencies during nucleic acid extraction (Liu *et al.*, 2011b). The RGFR of a given gene was calculated as follows:

$$RGFR_{Gene} = \frac{CN_{+MCPA}\left(ng_{DNA}^{-1}\right)}{CN_{-MCPA}\left(ng_{DNA}^{-1}\right)},$$

with CN, copy numbers. RGFRs for transcripts were calculated accordingly with the exception that transcript copy numbers were given per ng RNA.

Statistical methods

Normal distribution of the data was checked by the Jarque Bera test. One-way analyses of variance (ANOVAs) and localization of significances with Tukey's Honestly Significant Difference (HSD) as *post hoc* test were utilized. Significance was assumed at $P < 0.05$. All analyses were performed with the PAST software package (Hammer *et al.*, 2001).

Nucleotide sequence accession numbers

All gene sequences obtained in this study were deposited in the European Molecular Biology Laboratory database (http://www.ebi.ac.uk) under the accession numbers of FN659983–FN660477 (*tfdA*-like), FN660478–FN660996 (*cadA*), and FN660997–FN661491 (*r/sdpA*).

© 2013 Federation of European Microbiological Societies
Published by John Wiley & Sons Ltd. All rights reserved

Downloaded from http://femsec.oxfordjournals.org/ by guest on July 9, 2016

COR-AAD1-00003320
Bayer EX1008 (Part 6 of 9)

Results

Abundance and diversity of *tfdA*-like, *cadA*, and *r/sdpA* genes in soil

Copy numbers of *tfdA*-like, *cadA*, and *r/sdpA* per ng DNA were $(5.8 \pm 0.5) \times 10^3$, $(8.6 \pm 3.9) \times 10^0$, and $(1.0 \pm 0.3) \times 10^3$, respectively. Per gram of soil, *tfdA*-like, *cadA*, and *r/sdpA* gene copy numbers were $(5.2 \pm 3.4) \times 10^6$, $(1.1 \pm 1.1) \times 10^4$, and $(6.3 \pm 4.9) \times 10^5$, respectively. 18, 4, and 2 OTUs represented by more than one sequence were detected for *tfdA*-like, *cadA*, and *r/sdpA* genes, respectively (Fig. 1). Coverages of *tfdA*-like and *cadA* gene libraries from field fresh soil (i.e. T_0 bulk soil) were 87–100%. Coverage of *r/sdpA* gene library was 40%, suggesting that the *r/sdpA* diversity *in situ* exceeds the detected diversity. Major OTUs of *tfdA*-like genes in gene libraries of field fresh soil affiliated with *Bradyrhizobium* sp., those of *cadA* affiliated with Bradyrhizobium sp. and *Sphingomonas* sp., and those of *r/sdpA* affiliated with *Sphingobium* sp., suggesting the presence of putative Alphaproteobacterial MCPA degraders. Two likewise major OTUs of *cadA* and *r/sdpA* were distant to known sequences, indicating hitherto undetected oxygenase genes in soil (Fig. 1b and c). Such findings indicated that *tfdA*-like genes were more abundant in soil than *r/sdpA* and *cadA* and demonstrated the genetic potential of the soil microbial community to degrade MCPA.

Effect of MCPA on *tfdA*-like, *cadA*, and *r/sdpA* gene and transcript copy numbers

Approximately 0.03 mM MCPA was consumed completely within 20 days in oxic microcosms with field fresh soil (Fig. 2a). Transcript copy numbers of *tfdA*-like and *r/sdpA* genes were substantially higher in MCPA-supplemented than unsupplemented microcosms, demonstrating that transcription of such genes was concomitant to MCPA degradation (Fig. 2b). RGFRs and transcript to gene ratios of *tfdA*-like and *r/sdpA* genes peaked when more than 50% of the initial MCPA had been consumed after 16–18 days of incubation (Figs 2b and S2). Transcription of *cadA* was detected in one of the three replicate microcosms when MCPA was present (Fig. S2). Transcript to gene ratios of *cadA* peaked after 6 and 18 days of incubation (Fig. S2). Transcripts of *cadA* were below the detection limit of the assay in all microcosms without MCPA. Copy numbers of *tfdA*-like, *cadA*, and *r/sdpA* were higher in microcosms with MCPA than in those without MCPA (Fig. 2c). An increase in *tfdA*-like, *cadA*, and *r/sdpA* gene copy numbers relative to 16S rRNA genes was concomitant to MCPA degradation (Fig. 2d). Copy numbers of *tfdA*-like relative to 16S rRNA genes were 2.5×10^{-3} in bulk soil without any treatment and increased to 4×10^{-3} after incubation, which was *c.* 2 and 100 times higher than that of *r/sdpA* and *cadA* genes, respectively. Copy numbers of *r/sdpA* relative to 16S rRNA genes were four times higher after incubation than its initial abundance (3.8×10^{-4}). The abundance of *cadA* per 16S rRNA genes was orders of magnitude lower than that of *tfdA*-like and *r/sdpA* genes. The qPCR data indicated that MCPA induced the expression of *tfdA*-like, *cadA*, and *r/sdpA* genes and that soil microorganisms hosting such genes proliferated in response to MCPA. The data are indicative of simultaneous action of multiple oxygenases rather than a succession of different types of microorganisms.

Effect of MCPA treatment on detected structural gene diversity

Earthworm-pretreated soil from 0–2 and 8–10 cm depth, burrow walls, gut content, and cast material from soil columns were incubated with ^{13}C- and ^{12}C-MCPA for structural gene DNA–based stable isotope probing. Spot checks of MCPA indicated that (1) MCPA was degraded in all microcosms with the exception of those with gut content; and (2) degradation patterns of ^{13}C- and ^{12}C-MCPA were similar (data not shown), which was likewise observed in a preceding RNA-SIP study and consistent with mineralization assays applying ^{14}C-MCPA (Liu *et al.*, 2011a, b). MCPA was stable in microcosms with gut content as indicated preciously (Liu *et al.*, 2011a). Thus, such microcosms were excluded from further analyses. When 0.6–0.8 mg g_{dw}^{-1} MCPA was consumed, gene libraries were established for *tfdA*-like, *cadA*, and *r/sdpA* genes from 'heavy' DNA fractions (fraction 3–6) obtained from ^{13}C- and ^{12}C-MCPA treatments. 56 ± 14 sequences were obtained per gene library (Fig. 1). Coverages of *tfdA*-like, *cadA*, and *r/sdpA* gene libraries were 87–100%, 98–100%, and 98–100%, respectively. In total, 34, 6, and 5 OTUs represented by more than one sequence were detected for *tfdA*-like, *cadA*, and *r/sdpA* gene, respectively (Fig. 1). The numbers of detected OTUs were generally similar in field fresh soil and 0–2 cm depth of bulk soil in microcosms. However, low numbers of OTUs tended to occur in microcosms with burrow wall or cast material after incubation with MCPA when compared to field fresh soil, suggesting a selective effect of earthworms and MCPA incubations (Fig. 1).

Active MCPA-degrading bacteria hosting *tfdA*-like genes

OTUs were assigned to three clusters representing groups 1–3 of *tfdA*-like genes in soil (Fig. 1a). The majority of

Downloaded from http://femsec.oxfordjournals.org/ by guest on July 9, 2016

© 2013 Federation of European Microbiological Societies
Published by John Wiley & Sons Ltd. All rights reserved

COR-AAD1-00003321
Bayer EX1008 (Part 6 of 9)

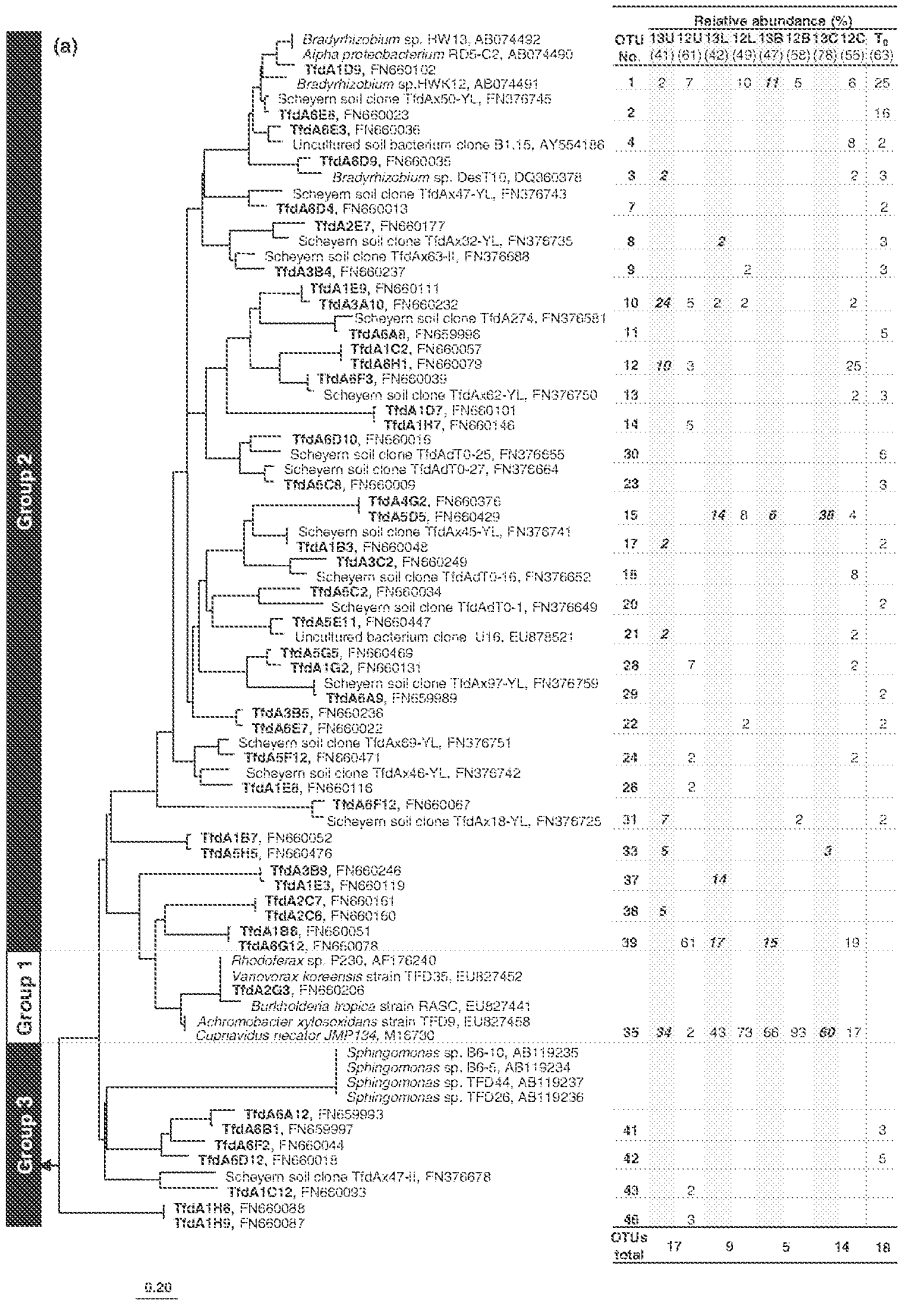


Fig. 1. Phylogenetic neighbor-joining tree of OTU representative *tfdA*-like (a), *cadA* (b), and *rlsdpA* (c) gene sequences (bold) and reference sequences. Accession numbers are provided after sequence identifiers. The trees of *tfdA*-like, *cadA*, and *rlsdpA* were calculated with 71 [position 169–239 of *Cupriavidus necator JMP134* (M16730) *tfdA*], 91 [position 271–387 of *Bradyrhizobium sp.* HW13 (AB062679) *cadA*], and 142 [positions 1–142 of *Sphingobium herbicidovorans* (AJ628860) *sdpA*] valid amino acid positions, respectively. Outgroups were TauD of *Escherichia coli* str. K-12 substr. MG1655 [(NC_000913), a] and TftAB of *Burkholderia cepacia* [(PCU11420), b and c]. The tabulated information provides OTU identifiers, origin of sequences, total numbers of OTUs per sample type, and relative sequence abundances in gene libraries per OTU. Relative abundances of OTUs that were more abundant in gene libraries from heavy fractions of 13C- than 12C-treatments are printed in bold and italics. OTUs with only one sequence are not shown. Numbers in parentheses indicate number of sequences per gene library. Abbreviations: 13 and 12, microcosms supplemented with ^{13}C- and ^{12}C-MCPA, respectively; U (upper), L (lower), b, and c, microcosm incubations with 0–2 cm depth of soil, 8–10 cm depth of soil, burrow walls, and cast materials, respectively; T_0, field fresh soil prior to incubation.

© 2013 Federation of European Microbiological Societies
Published by John Wiley & Sons Ltd. All rights reserved

Downloaded from http://femsec.oxfordjournals.org/ by guest on July 9, 2016

COR-AAD1-00003322
Bayer EX1008 (Part 6 of 9)

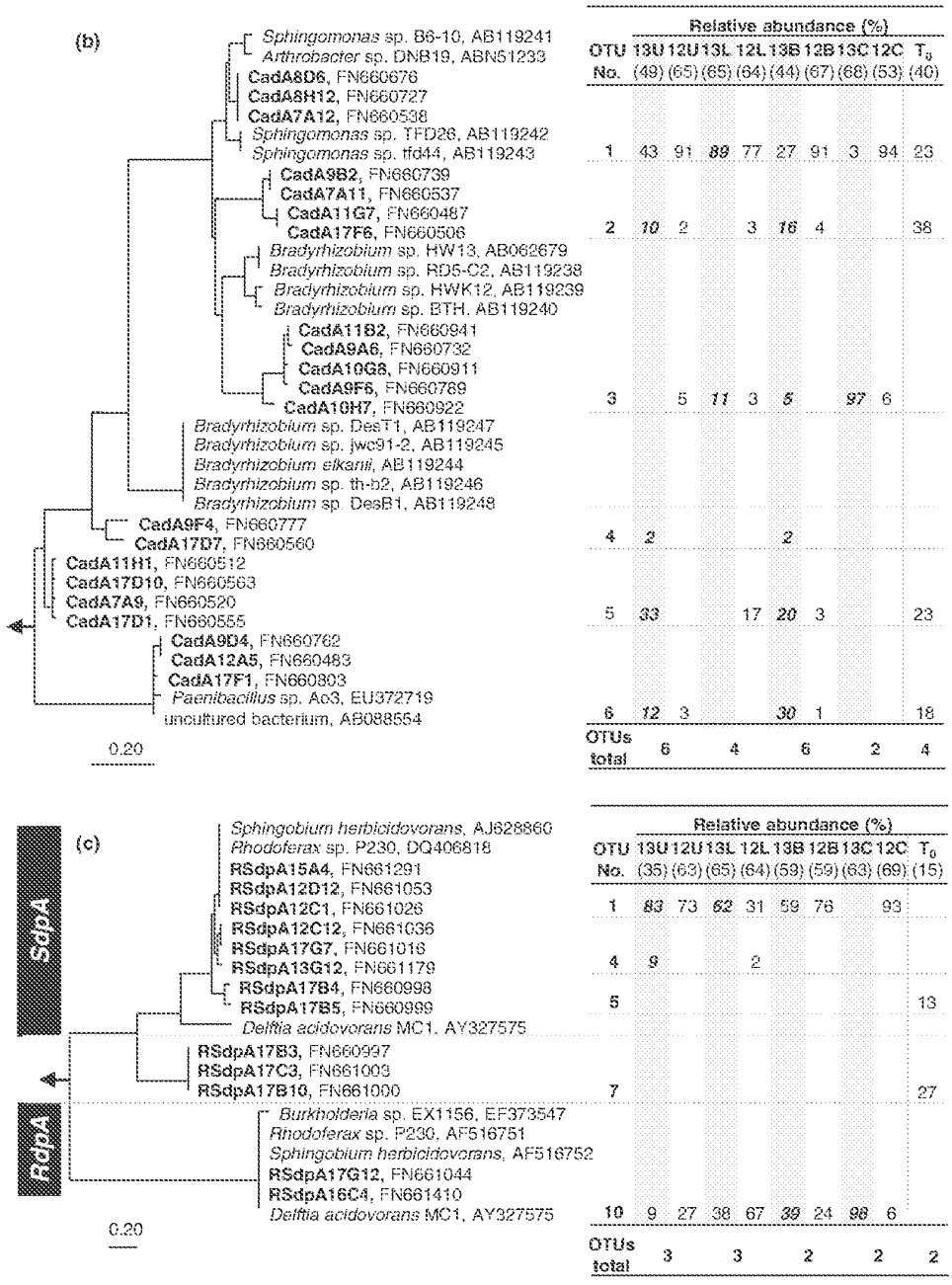


Fig. 1. Continued

OTUs were assigned to group 2. Sequences of OTU 1 were closely related to *tfdA*-like genes from known group 2 MCPA-degrading bacteria, that is, *Bradyrhizobium*-related microorganisms. Most OTUs of group 2 were related to *tfdA*-like genes from Scheyern soil or other soil samples. Some OTUs of group 2 were only distantly related to *tfdA*-like genes from known cultured or uncultured reference sequences, indicating new putative TfdA-like oxygenases. OTU 35 was closely related to *tfdA* of known group 1 MCPA-degrading bacteria. Ninety-eight percent of sequences within OTU 35 were highly similar (> 97%) to class III *tfdA*-like genes from known MCPA- or

© 2013 Federation of European Microbiological Societies
Published by John Wiley & Sons Ltd. All rights reserved

Downloaded from http://femsec.oxfordjournals.org/ by guest on July 9, 2016

COR-AAD1-00003323
Bayer EX1008 (Part 6 of 9)

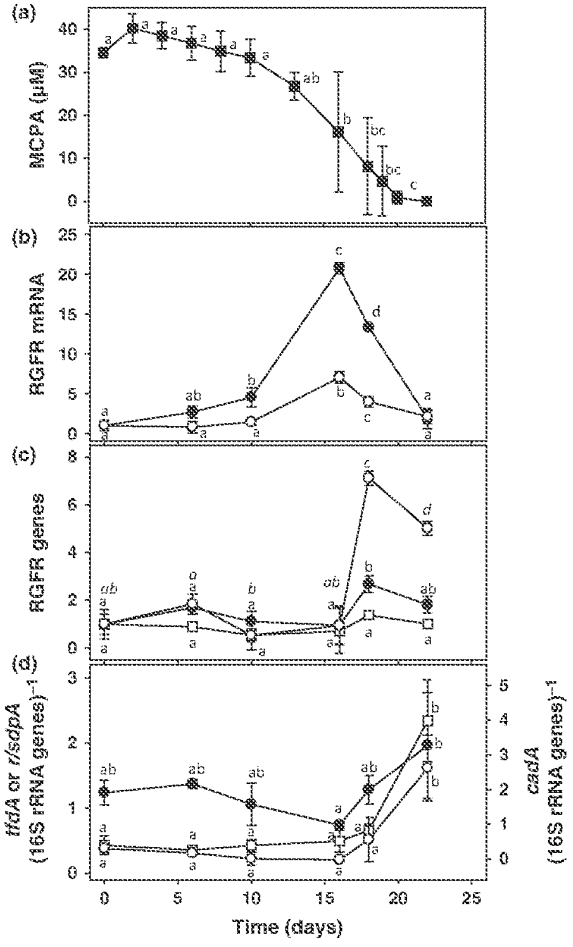


Fig. 2. Effect of MCPA (a) on transcription (b), abundance (c), and relative abundance per 16S rRNA genes (d) of *tfdA*-like ($\times 5 \times 10^{-2}$), *cadA* ($\times 10^{-5}$), and *risdpA* genes ($\times 10^{-3}$) in oxic microcosms with field fresh soil. MCPA was not detectable in unsupplemented controls. Closed squares, MCPA; open squares, *cadA*; closed circles, *tfdA*; open circles, *risdpA*. RGFR indicates transcription induced by MCPA supplementation (see Material and methods). Transcript copy numbers of *cadA* were below the detection limit of the qPCR assay for unsupplemented controls and were thus not shown. Error bars represent standard deviations based on three replicate microcosms. Different letters indicate significant differences between time points at $P < 0.05$ based on ANOVA and Tukey's HSD *post hoc* test. Letters in italics (c) apply to open circles, that is, *risdpA*.

2,4-D-degrading bacteria, for example, *Rhodoferax* sp. P230 (Müller *et al.*, 2001). Only 7 of 495 *tfdA*-like gene sequences were assigned to group 3. Six of the seven sequences were obtained from field fresh soil sample without any treatment. All group 3 sequences shared only 28–44% similarity to known sequences. Eight OTUs of groups 1 and 2 were labeled, but none of group 3 (Fig. 3a). Seven of the eight labeled OTUs affiliated with group 2 sequences. Labeled OTUs 1 and 35 affiliated with *tfdA*-like sequences from *Bradyrhizobium* and *Variovorax*, respectively, while all other labeled OTUs were new. OTU 35 that was related to class III *tfdA*-like genes of group 1 MCPA-degrading bacteria was dominantly labeled in 0–2 cm depth of bulk soil and cast (Figs 1a and 3a). OTUs 37 and 39 represented hitherto unknown *tfdA*-like genes affiliating with group 2 and were dominantly labeled in 8–10 cm depth of bulk soil and burrow wall (Figs 1a and 3a). The labeling of OTU 1 was only detected in burrow wall, indicating active *Bradyrhizobium*-related group 2 MCPA-degrading bacteria in burrow wall microcosms. OTU 15 was labeled in 8–10 cm depth of bulk soil, burrow walls, and cast materials but not in 0–2 cm depth of bulk soil, where OTUs 10, 12, and 31 were strongly labeled. This indicated that 0–2 cm depth of bulk soil microcosms harbored more diverse *tfdA*-like gene-containing MCPA degraders than the other samples and that *Alphaproteobacterial* MCPA degraders together with class III degraders of the *Betaproteobacteria* were enriched.

Active MCPA-degrading bacteria hosting *cadA* genes

Six OTUs were detected in 515 sequences (Fig. 1). OTU 1 was closely related to *cadA* of *Sphingomonas* spp. (Itoh *et al.*, 2004) and *Arthrobacter* sp. DNB19 (EF375719) of the *Alphaproteobacteria* and *Actinobacteria*, respectively. Sequences assigned to OTU 6 were closely related to a gene encoding a putative aromatic-ring-hydroxylating dioxygenase subunit-like protein of *Rhodopseudomonas palustris* DX-1 (ADFI01000001) and a putative 2,4-D monooxygenase gene of *Paenibacillus* sp. Ao3 (EU372719) of the *Alphaproteobacteria* and *Firmicutes*, respectively. Such reference sequences sharing > 95% similarity were assigned to the same *cadA* OTUs, but belonged to different phyla according to 16S rRNA gene similarity. Sequences of OTU 3 were related to *cadA* genes of some *Bradyrhizobium* spp., for example, *Bradyrhizobium* sp. HW13 (Kitagawa *et al.*, 2002) with a similarity of > 86%, and distantly related (with similarity of < 70%) to *cadA* genes of other *Bradyrhizobium* strains such as *Bradyrhizobium* sp. DesT1 (Itoh, *et al.*, 2004). These *Bradyrhizobium*-related reference microorganisms shared > 99% 16S rRNA gene similarity. This indicated the horizontal gene transfer of *cadA* or other mechanisms of gene divergence among closely related taxa. OTUs 2, 4, and 5 were not related to any known *cadA* from cultured or uncultured bacteria and indicative of hitherto unknown microorganisms carrying new *cadA* genes in soil. The composition of *cadA* gene-containing microorganisms in 0–2 cm depth of bulk soil was similar to that in burrow

© 2013 Federation of European Microbiological Societies
Published by John Wiley & Sons Ltd. All rights reserved

Downloaded from http://femsec.oxfordjournals.org/ by guest on July 9, 2016

COR-AAD1-00003324
Bayer EX1008 (Part 6 of 9)

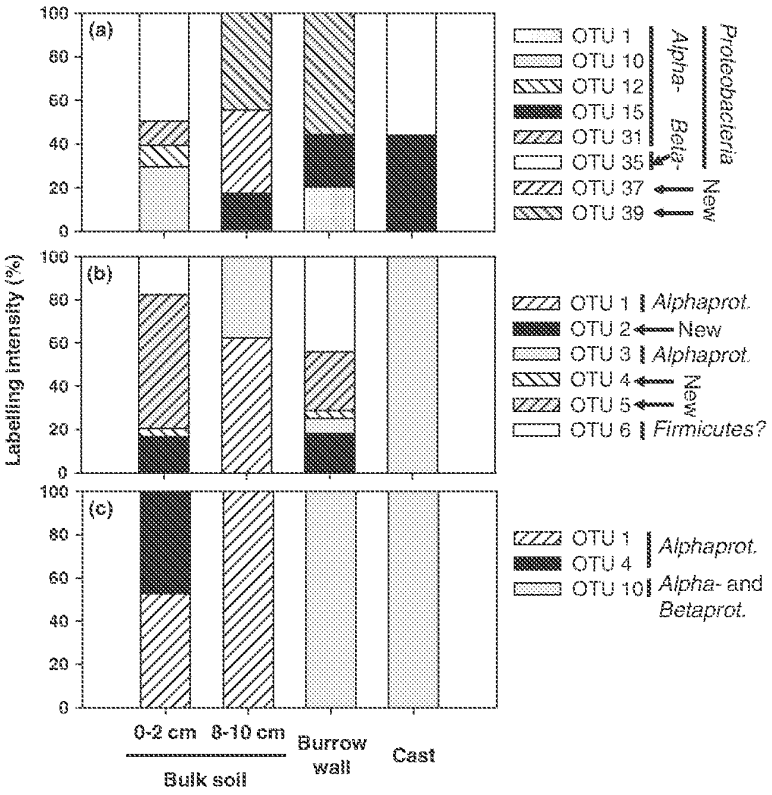


Fig. 3. Relative labeling intensity of OTUs obtained from comparative analysis of *tfdA*-like (a), *cadA* (b), and *r/sdpA* (c) libraries of 'heavy' fractions from microcosms with ^{13}C- and ^{12}C-MCPA after 55 days of incubation. OTUs were defined based on 16% dissimilarity. Labeling intensity was calculated by subtracting relative abundances of OTUs (Fig. 2) in ^{12}C-MCPA-supplemented samples from that in corresponding ^{13}C-MCPA-supplemented samples and normalized to 100%. An OTU was scored 'labeled' when its relative abundance in ^{13}C-libraries was > 5%, and its labeling intensity was > 0. Taxa OTUs were affiliating with are given in the legend. Arrows indicate new OTUs.

wall microcosms, while the composition of *cadA* gene-containing microorganisms in 8–10 cm depth of bulk soil was similar to that in cast microcosms. This indicated a change in *cadA* gene-hosting microorganisms in different samples during MCPA degradation. The relative abundances of OTU 1 in control libraries (^{12}C-MCPA-treated samples) were high in all samples (Fig. 1), and the labeling was only detected in 8–10 cm depth of bulk soil (Fig. 3b). Ninety-seven percent of sequences obtained from ^{13}C-MCPA-treated cast material were assigned to OTU 3, and only 3% of sequences from control library (^{12}C-MCPA-treated cast) were related to this OTU (Fig. 1b), which resulted in a strong labeling of OTU 3 in cast (Fig. 3b). This indicated that a group of *Bradyrhizobium*-related microorganisms harboring *cadA* was selectively stimulated during MCPA degradation in cast microcosms. OTU 3 was also strongly labeled in 8–10 cm depth of bulk soil and slightly labeled in burrow wall (Fig. 3b). OTUs 2–6 were all labeled in both 0–2 cm depth of bulk soil and burrow wall, in which OTUs 2, 4, and 5 represented novel *cadA* genes (Figs 1b and 3b). This indicated more diverse and higher abundance of novel *cadA*-containing microorganisms utilizing MCPA-derived carbon in 0–2 cm depth of bulk soil and burrow wall than in the other microcosms.

Active MCPA-degrading bacteria hosting *r/sdpA* genes

For *r/sdpA* genes, 5 OTUs that represented more than one sequence each were detected in 492 sequences. Primers targeting *r/sdpA* gene in this study were designed on the basis of both known *rdpA* and *sdpA* genes; thus, both *rdpA*- and *sdpA*-related sequences were obtained (Fig. 1c). Most of the OTUs clustered with sequences from *Alpha-* and *Betaproteobacteria*. Sequences assigned to OTUs 1 and 4 displayed a high similarity to known *sdpA* genes (Fig. 1c). In contrast, OTU 5 that clustered with *sdpA* genes was only distantly related to known *r/sdpA* genes, indicating hitherto unknown *rdpA* or *sdpA* gene-containing microorganisms in soil. Sequences in OTU 10 were closely related to known *rdpA* genes (> 96% similarity). OTU 7 clustered neither with *sdpA* nor with *rdpA* genes. Both OTUs 5 and 7 were only detected in field fresh soil (Fig. 1c). OTUs 1, 4, and 10 were detected in MCPA-treated samples rather than in field fresh soil, indicating a change in *r/sdpA* gene-hosting microorganisms during MCPA degradation. Indeed, *sdpA* (OTUs 1 and 4) and *rdpA* (OTU 10) genes were strongly labeled in bulk soil (0–2 and 8–10 cm depth) and drilosphere materials (burrow wall and cast), respectively. Such results implied that earthworm activity

© 2013 Federation of European Microbiological Societies
Published by John Wiley & Sons Ltd. All rights reserved

Downloaded from http://femsec.oxfordjournals.org/ by guest on July 9, 2016

COR-AAD1-00003325
Bayer EX1008 (Part 6 of 9)

strongly impacted the distribution of MCPA-degrading, *r/sdpA* gene-containing microorganisms, and their capability to react to MCPA in soil.

Discussion

The transcription of *tfdA*-like, *cadA*, and *r/sdpA* genes was concomitant to MCPA degradation in soil, suggesting that multiple oxygenases are involved in MCPA degradation simultaneously (Figs 1 and S2), thus extending and consolidating current knowledge that *tfdA*-like gene expression in soil is associated with MCPA degradation (Baelum *et al.*, 2006; Baelum & Jacobsen, 2009; Liu *et al.*, 2011b). Transcription of *cadA* in response to MCPA in soils and thus conversion of MCPA by *cadA* encoded oxygenases might be hypothesized based on induction of *cadA* transcription by 2,4-D in pure cultures of *Bradyrhizobium* sp. (Kitagawa *et al.*, 2002). Indeed, transcription of *cadA* in the presence of MCPA as well as an increase in *cadA* gene copy numbers supports the view that *cadA* encoded oxygenases utilize MCPA as substrate (Figs 1 and S2). Transcription of *r/sdpA* genes occurs in soil in response to (*RS*)-DP (Paulin *et al.*, 2011). SdpA accepts a broad range of phenoxyacetate derivatives besides *S*-DP as substrate, and 2,4-D as well as MCPA is readily degraded (Westendorf *et al.*, 2003; Müller, 2007). The substrate range of RdpA is very limited, and conversion of 2,4-D occurs at very slow rates (Müller & Babel, 1999; Westendorf *et al.*, 2003). *Sphingobium herbicidovorans* MH (group 3) and *D. acidovorans* MC1 (group 1) host *sdpA* genes and grow on 2,4-D and/or MCPA (Kohler, 1999; Müller *et al.*, 2001, 2004, 2006). Thus, growth on MCPA or 2,4-D in pure culture can be attributed to SdpA. Such results are in line with the observed induction of *r/sdpA* gene transcription in soil by MCPA and an increase in *r/sdpA* gene copy numbers (Figs 2 and S1). Thus, activities of *sdpA* encoded oxygenases support growth of MCPA degraders in soil.

Diverse *tfdA*-like genes were labeled with MCPA-^{13}C in soil and drilosphere material (Figs 1 and 3). Labeling of DNA during SIP requires replication of the organisms concomitant to assimilation of the ^{13}C-substrate and long incubation times and is thus prone to false positives due to cross-feeding (Manefield *et al.*, 2002; Neufeld *et al.*, 2007a). The probability of detecting labeled organisms due to cross-feeding is greatly reduced when structural genes associated with the process and physiological group of interest rather than 16S rRNA genes are analyzed. Thus, labeling patterns indicated growth of diverse *tfdA*-like, *cadA*, and *r/sdpA* gene-hosting MCPA degraders on MCPA. Most of labeled OTUs affiliated with oxygenase-encoding genes of the *Alphaproteobacteria* and to a lesser extent to those of *Betaproteobacteria* (Fig. 3), which is in line with 16S rRNA gene SIP suggesting that *Alphaproteobacteria* were dominant MCPA degraders in microcosms with bulk soil and burrow walls that received approximately half of the MCPA pulsed in this study (Liu *et al.*, 2011a). However, 16S rRNA gene SIP was indicative of *Sphingomonadaceae* rather than taxa affiliating with *Bradyrhizobium* sp. as indicated by *tfdA*-like gene SIP (Figs 1 and 3). Such a fact might indicate horizontal gene transfer of *tfdA*-like genes. Although horizontal transfer of plasmid-located group 1 *tfdA*-like and *r/sdpa* genes is likely (Fig. S1, McGowan *et al.*, 1998; Zaprasis *et al.*, 2010), such events of gene dispersal were less evident for *cadA* and chromosome-located groups 2–3 *tfdA*-like genes that occur in *Alphaproteobacteria* but cannot be excluded (Fig. S1, Zaprasis *et al.*, 2010). Publicly available *tfdA*-like genes amplified from 2,4-DCP-degrading *Sphingomonas* strains are truncated (Itoh *et al.*, 2004). Amplification of *tfdA*-like genes from *Sphingomonas* sp. TFD26 with our recently developed primers targeting group 2 *tfdA*-like genes (Zaprasis *et al.*, 2010) yielded a product of the expected size that shared (1) 99% nucleic acid similarity with *tfdA*-like gene sequences previously detected in the same soil (e.g. FN376724); and (2) 85% nucleic acid similarity with a *tfdA*-like gene of *Bradyrhizobium* sp. ApT12 isolated from the legume *Apios americana* (data not shown; Parker & Kennedy, 2006). Thus, *tfdA*-like genes of some *Sphingomonas* sp. might be subject to horizontal gene transfer and not easily differentiated from those of *Bradyrhizobia*. OTU 35 was the only taxon representing group 1 microorganisms of the *Betaproteobacteria* because sequences in OTU 35 shared > 97% similarity with *tfdA*-like genes of known group 1 PAA degraders (e.g. *Rhodoferax* sp. P230; Figs 1 and 3). Group 1 (OTU 35) *tfdA*-like gene sequences represented major MCPA-^{13}C assimilators in 0–2 cm depth and cast microcosms, suggesting that *Betaproteobacteria* were competitive MCPA degraders in such material (Fig. 3). 16S rRNA gene SIP likewise suggested that group 1 *Betaproteobacteria* dominated assimilators of MCPA-C in microcosms with cast material (Liu *et al.*, 2011a). Such group 1 sequences were not detected in T_0 bulk soil, which is in line with our previous study that group 1 microorganisms were below the detection limit of a PCR-based study in the same agricultural soil prior to MCPA incubation (Zaprasis *et al.*, 2010). The affiliation of new and known MCPA-C-labeled *tfdA*-like genes in soil with *Alpha-* and *Betaproteobacteria* was thus supported. Indeed, there is a growing body of literature that soil is still a reservoir of diverse undetected *tfdA*-like genes of unconsolidated function (Gazitua *et al.*, 2010; Zaprasis *et al.*, 2010). The present study adds new genes and associates some of those hitherto undetected *tfdA*-like gene diversity with MCPA-degrading organisms (Figs 1 and 3).

© 2013 Federation of European Microbiological Societies
Published by John Wiley & Sons Ltd. All rights reserved

Downloaded from http://femsec.oxfordjournals.org/ by guest on July 9, 2016

COR-AAD1-00003326
Bayer EX1008 (Part 6 of 9)

Groups 2 and 3 microorganisms may employ other oxygenase-encoding genes instead of *tfdA*-like genes to initialize PAA degradation, such as *cadA* and *r/sdpA* (Kitagawa *et al.*, 2002; Itoh *et al.*, 2004; Müller *et al.*, 2006). Many OTUs that did not affiliate with known *cadA* genes were also labeled in 0–2 cm depth of bulk soil and burrow wall, suggesting a high diversity of hitherto unknown *cadA*-hosting MCPA degraders involved in MCPA degradation in soil (Fig. 3). Although *cadA* gene and transcript copy numbers were low (Figs 2 and S2), *cadA* gene copy numbers increased during incubation with MCPA, and *cadA* closely related to *Sphingomonas* spp. (OTU 1) and *Bradyrhizobium* spp. (OTU 3) was strongly labeled (Fig. 3b), indicating that *cadA* gene-hosting microorganisms actively participated in MCPA degradation. The distribution of *cadA* is restricted to *Alphaproteobacteria* (Itoh *et al.*, 2002; Kitagawa *et al.*, 2002) with an exception from a *Paenibacillus* sp. (H.B. Nguyen and H.T.C. Dang, unpublished data; Fig. 1b). Group 2 *Bradyrhizobium* sp. are slow-growing oligotrophs with doubling times > 20 h that are easily outcompeted by copiotrophic groups 1 and 3 organisms like *Comamonadaceae* and *Sphingomonadaceae*, respectively (Kitagawa *et al.*, 2002; Liu *et al.*, 2011a). Copiotrophs were MCPA-C labeled as indicated by structural gene and 16S rRNA gene analysis (Fig. 3, Liu *et al.*, 2011a). Thus, *cadA*-SIP enabled a sensitive detection of putative MCPA-degrading *Bradyrhizobium* sp. in the presence of fast-growing copiotrophs, which might be overlooked by 16S rRNA gene SIP and highlight the importance of *Alphaproteobacterial* PAA degraders (Fig. 3, Kitagawa *et al.*, 2002; Huong *et al.*, 2007, 2008; Liu *et al.*, 2011a, b).

Groups 1 and 3 microorganisms hosting *r/sdpA* genes are also capable of PAA (i.e. 2,4-D and MCPA) degradation (Ehrig *et al.*, 1997; Kohler, 1999; Müller *et al.*, 1999). Transcription and abundance of *r/sdpA* were stimulated during or after MCPA degradation in soil, and *rdpA* as well as *sdpA* genes was MCPA-C labeled in one of the microcosms (Figs 2 and S2). Few isolates harbor either *rdpA* or *sdpA* but not both of such genes (Müller *et al.*, 2001, 2004; Schleinitz *et al.*, 2004). Either *sdpA* or *rdpA* gene sequences in bulk soil or drilosphere materials were labeled, respectively (Fig. 3), implying that MCPA degraders in soil hosting either *rdpA* or *sdpA* are more prevalent than previously thought. The enrichment of either *rdpA* or *sdpA* hosting organisms on *R*- or (*RS*)-MCPP lends further support to this conclusion (Zakaria *et al.*, 2007). SdpA showed lower K_m value than RdpA with phenoxyacetate derivatives (e.g. MCPA) as substrate, which is in agreement with the labeling of *sdpA* gene-hosting microorganisms (Westendorf *et al.*, 2003). Labeling of *rdpA* gene-hosting MCPA degraders might have occurred due to activities of alternative oxygenases or hitherto underappreciated activities of RdpA converting MCPA. The latter view is supported by a recent finding that the *rdpA*-hosting, non-2,4-D-degrading *D. acidovorans* acquires the capability to degrade 2,4-D via a post-translational modification of RdpA (Leibeling *et al.*, 2013).

Soil microbiota including MCPA degraders in soil is processed and impacted by earthworms (Brown, 1995; Drake & Horn, 2007; Bernard *et al.*, 2012). Earthworms stimulate MCPA degradation in soil, and group 3 *Sphingomonadaceae* are major MCPA degraders in soil and drilosphere; group 1 *Comamonadaceae* are important in burrow walls and cast (Liu *et al.*, 2011a, b). Group 1 outcompeted group 3 organisms after long-term incubation in microcosms with cast (Liu *et al.*, 2011a). Oxygenase-encoding genes labeled with MCPA-^{13}C in cast inoculated microcosms likewise affiliated with group 1 organisms (Fig. 3). Thus, gut passage that subjects ingested soil microorganisms to anoxia, high nutrient levels, a high water content, and digestive processes might enable group 1 organisms to respond quickly to MCPA and outcompete others (Drake & Horn, 2007). Indeed, the number of labeled OTUs in cast tended to be lower than in soil and burrow walls (Fig. 3), and recent studies suggest a selective effect of gut passage on ingested soil microbiota including MCPA degrader diversity (Thakuria *et al.*, 2010; Monard *et al.*, 2011; Bernard *et al.*, 2012). Such effects of earthworms on the capability of soil microorganisms to respond to MCPA, the detection of hitherto unknown structural genes that were associated with MCPA degradation, as well as evidence for the simultaneous activity of multiple oxygenases in soil during MCPA degradation broaden current knowledge and provide a basis for enhanced structural gene-based studies in the future. Thus, the assessment of microbial MCPA degradation by the analysis of multiple oxygenase genes and transcript combined with stable isotope probing allows for the analysis of hitherto overlooked PAA degraders, mining for unknown oxygenase genes associated with PAA degradation, and thus might stimulate the optimization of bioremediation strategies.

Acknowledgements

We are grateful to Kazuhito Itoh for providing *Sphingomonas* sp. TFD26 and Stephan Schulz, Michael Schloter, as well as Jean Charles Munch for provision of soil samples. Support for this study was provided by the Deutsche Forschungsgemeinschaft (DFG grant HO4020/1-1, DFG Priority Program 1315 'Biogeochemical interfaces in soil'), by the University of Bayreuth, and by a grant from the German Academic Exchange Service (DAAD) to Y.-J. Liu.

© 2013 Federation of European Microbiological Societies
Published by John Wiley & Sons Ltd. All rights reserved

Downloaded from http://femsec.oxfordjournals.org/ by guest on July 9, 2016

COR-AAD1-00003327
Bayer EX1008 (Part 6 of 9)

References

Amy PS, Schulke JW, Frazier LM & Seidler RJ (1985) Characterization of aquatic bacteria and cloning of genes specifying partial degradation of 2,4-dichlorophenoxyacetic acid. *Appl Environ Microbiol* **49**: 1237–1245.

Audus LJ (1952) The decomposition of 2,4-dichlorophenoxyacetic acid and 2-methyl-4-chlorophenoxyacetic acid in the soil. *J Sci Food Agric* **3**: 268–274.

Baelum J & Jacobsen CS (2009) TaqMan probe-based real-time PCR assay for detection and discrimination of class I, II, and III *tfdA* genes in soils treated with phenoxy acid herbicides. *Appl Environ Microbiol* **75**: 2969–2972.

Baelum J, Henriksen T, Hansen HCB & Jacobsen CS (2006) Degradation of 4-chloro-2-methylphenoxyacetic acid in top- and subsoil is quantitatively linked to the class III *tfdA* gene. *Appl Environ Microbiol* **72**: 1476–1486.

Balajee S & Mahadevan A (1993) Biodegradation of 2,4-dichlorophenoxyacetic acid in soil by *Azotobacter chroococcum*. *Toxicol Environ Chem* **39**: 169–172.

Bernard L, Chapuis-Lardy L, Razafimbelo T *et al.* (2012) Endogeic earthworms shape bacterial functional communities and affect organic matter mineralization in a tropical soil. *ISME J* **6**: 213–222.

Bolan NS & Baskaran S (1996) Characteristics of earthworm casts affecting herbicide sorption and movement. *Biol Fertil Soils* **22**: 367–372.

Bollag J-M, Helling CS & Alexander M (1967) Metabolism of 4-chloro-2-methylphenoxyacetic acid by soil bacteria. *Appl Microbiol* **15**: 1393–1398.

Brohmer P (1984) *Fauna von Deutschland*, 16th edn. Quelle und Meyer, Heidelberg.

Brown GG (1995) How do earthworms affect microfloral and faunal community diversity? *Plant Soil* **170**: 209–231.

Brown GB, Barois I & Lavelle P (2000) Regulation of soil organic matter dynamics and microbial activity in the drilosphere and the role of interactions with other edaphic functional domains. *Eur J Soil Biol* **36**: 177–198.

Castillo MD, Andersson A, Ander P, Stenstrom J & Torstensson L (2001) Establishment of the white rot fungus *Phanerochaete chrysosporium* on unsterile straw in solid substrate fermentation systems intended for degradation of pesticides. *World J Microbiol Biotechnol* **17**: 627–633.

Chaudhry GR & Huang GH (1988) Isolation and characterization of a new plasmid from a *Flavobacterium* sp which carries the genes for degradation of 2,4-dichlorophenoxyacetate. *J Bacteriol* **170**: 3897–3902.

Danganan CE, Ye RW, Daubaras DL, Xun LJ & Chakrabarty AM (1994) Nucleotide sequence and functional analysis of the genes encoding 2,4,5-trichlorophenoxyacetic acid oxygenase in *Pseudomonas cepacia* Ac1100. *Appl Environ Microbiol* **60**: 4100–4106.

Drake HL & Horn MA (2007) As the worm turns: the earthworm gut as a transient habitat for soil microbial biomes. *Ann Rev Microbiol* **61**: 169–189.

Edwards CA (2004) *Earthworm Ecology*. CRC Press, Boca Raton, FL.

Edwards CA & Bohlen PJ (1996) *Biology and Ecology of Earthworms*, 3rd edn. Chapman & Hall, London.

Ehrig A, Müller RH & Babel W (1997) Isolation of phenoxy herbicide-degrading *Rhodoferax* species from contaminated building material. *Acta Biotechnol* **17**: 351–356.

Fulthorpe RR, McGowan C, Maltseva OV, Holben WE & Tiedje JM (1995) 2,4-dichlorophenoxyacetic acid-degrading bacteria contain mosaics of catabolic genes. *Appl Environ Microbiol* **61**: 3274–3281.

Gaunt JK & Evans WC (1971) Metabolism of 4-chloro-2-methylphenoxyacetate by a soil pseudomonad – preliminary evidence for metabolic pathway. *Biochem J* **122**: 519–526.

Gazitua MC, Slater AW, Melo F & Gonzalez B (2010) Novel alpha-ketoglutarate dioxygenase *tfdA*-related genes are found in soil DNA after exposure to phenoxyalkanoic herbicides. *Environ Microbiol* **12**: 2411–2425.

Hammer Ø, Harper DAT & Ryan PD (2001) PAST: paleontological statistics software package for education and data analysis. *Palaeontol Electronica* **4**: 1–9.

Hickman ZA & Reid BJ (2008) Earthworm assisted bioremediation of organic contaminants. *Environ Int* **34**: 1072–1081.

Huong NL, Itoh K & Suyama K (2007) Diversity of 2,4-dichlorophenoxyacetic acid (2,4-D) and 2,4,5-trichlorophenoxyacetic acid (2,4,5-T)-degrading bacteria in Vietnamese soils. *Microbes Environ* **22**: 243–256.

Huong NL, Itoh K & Suyama K (2008) 2,4-dichlorophenoxyacetic acid (2,4-D)- and 2,4,5-trichlorophenoxyacetic acid (2,4,5-T)-degrading bacterial community in soil-water suspension during the enrichment process. *Microbes Environ* **23**: 142–148.

Itoh K, Kand R, Sumita Y *et al.* (2002) *tfdA*-like genes in 2,4-dichlorophenoxyacetic acid-degrading bacteria belonging to the *Bradyrhizobium–Agromonas–Nitrobacter–Afipia* cluster in α-*Proteobacteria*. *Appl Environ Microbiol* **68**: 3449–3454.

Itoh K, Tashiro Y, Uobe K, Kamagata Y, Suyama K & Yamamoto H (2004) Root nodule *Bradyrhizobium* spp. harbor *tfdA* alpha and *cadA*, homologous with genes encoding 2,4-dichlorophenoxyacetic acid-degrading proteins. *Appl Environ Microbiol* **70**: 2110–2118.

Jordan DC (1982) Transfer of *Rhizobium japonicum* Buchanan 1980 to *Bradyrhizobium* gen. nov., a genus of slow growing, root nodule bacteria from leguminous plants. *Int J Syst Bacteriol* **32**: 136–139.

Ka JO, Holben WE & Tiedje JM (1994) Genetic and phenotypic diversity of 2,4-dichlorophenoxyacetic acid (2,4-D)-degrading bacteria isolated from 2,4-D-treated field soils. *Appl Environ Microbiol* **60**: 1106–1115.

Kamagata Y, Fulthorpe RR, Tamura K, Takami H, Forney LJ & Tiedje JM (1997) Pristine environments harbor a new

© 2013 Federation of European Microbiological Societies
Published by John Wiley & Sons Ltd. All rights reserved

Downloaded from http://femsec.oxfordjournals.org/ by guest on July 9, 2016

COR-AAD1-00003328
Bayer EX1008 (Part 6 of 9)

group of oligotrophic 2,4-dichlorophenoxyacetic acid-degrading bacteria. *Appl Environ Microbiol* **63**: 2266–2272.

Kitagawa W, Takami S, Miyauchi K, Masai E, Kamagata Y, Tiedje JM & Fukuda M (2002) Novel 2,4-dichlorophenoxyacetic acid degradation genes from oligotrophic *Bradyrhizobium* sp strain HW13 isolated from a pristine environment. *J Bacteriol* **184**: 509–518.

Kohler HPE (1999) *Sphingomonas herbicidovorans* MH: a versatile phenoxyalkanoic acid herbicide degrader. *J Ind Microbiol Biotechnol* **23**: 336–340.

Kuhlmann B, Kaczmarczyk B & Schottler U (1995) Behavior of phenoxyacetic acids during underground passage with different redox zones. *Int J Environ Anal Chem* **58**: 199–205.

Kumar S, Nei m, Dudley j & Tamura K (2008) MEGA: a biologist-centric software for evolutionary analysis of DNA and protein sequences. *Brief Bioinform* **9**: 299–306.

Lavelle P (1988) Earthworm activities and the soil system. *Biol Fertil Soils* **6**: 237–251.

Leibeling S, Maeß MB, Centler F *et al.* (2013) Posttranslational oxidative modification of (R)-2-(2,4-dichlorophenoxy) propionate/α-ketoglutarate-dependent dioxygenases (RdpA) leads to improved degradation of 2,4-dichlorophenoxyacetate (2,4-D). *Eng Life Sci.* **13**: 278–291.

Lerch TZ, Dignac MF, Nunan N, Bardoux G, Barriuso E & Mariotti A (2009) Dynamics of soil microbial populations involved in 2,4-D biodegradation revealed by FAME-based stable isotope probing. *Soil Biol Biochem* **41**: 77–85.

Leveau JHJ & van der Meer JR (1997) Genetic characterization of insertion sequence ISJP4 on plasmid pJP4 from *Ralstonia eutropha* JMP134. *Gene* **202**: 103–114.

Leveau JHJ, Konig F, Fuchslin H, Werlen C & van der Meer JR (1999) Dynamics of multigene expression during catabolic adaptation of *Ralstonia eutropha* JMP134 (pJP4) to the herbicide 2,4-dichlorophenoxyacetate. *Mol Microbiol* **33**: 396–406.

Liu YJ, Liu SJ, Drake HL & Horn MA (2011a) *Alphaproteobacteria* dominate active 2-methyl-4-chlorophenoxyacetic acid herbicide degraders in agricultural soil and drilosphere. *Environ Microbiol* **13**: 991–1009.

Liu YJ, Zaprasis A, Liu SJ, Drake HL & Horn MA (2011b) The earthworm *Aporrectodea caliginosa* stimulates abundance and activity of phenoxyalkanoic acid herbicide degraders. *ISME J* **5**: 473–485.

Loos MA, Schlosser IF & Mapham WR (1979) Phenoxy herbicide degradation in soils – quantitative studies of 2,4-D-degrading and MCPA-degrading microbial populations. *Soil Biol Biochem* **11**: 377–385.

Ludwig W, Strunk O, Westram R *et al.* (2004) ARB: a software environment for sequence data. *Nucleic Acids Res* **32**: 1363–1371.

Lueders T, Manefield M & Friedrich MW (2004) Enhanced sensitivity of DNA- and rRNA-based stable isotope probing by fractionation and quantitative analysis of isopycnic centrifugation gradients. *Environ Microbiol* **6**: 73–78.

Macur RE, Wheeler JT, Burr MD & Inskeep WP (2007) Impacts of 2,4-D application on soil microbial community structure and on populations associated with 2,4-D degradation. *Microbiol Res* **162**: 37–45.

Manefield M, Whiteley AS, Griffiths RI & Bailey MJ (2002) RNA stable isotope probing, a novel means of linking microbial community function to phylogeny. *Appl Environ Microbiol* **68**: 5367–5373.

McGowan C, Fulthorpe RR, Wright A & Tiedje JM (1998) Evidence for interspecies gene transfer in the evolution of 2,4-dichlorophenoxyacetic acid degraders. *Appl Environ Microbiol* **64**: 4089–4092.

Messing J (1983) New M13 vectors for cloning. *Methods Enzymol* **101**: 20–78.

Monard C, Vandenkoornhuyse P, Le Bot B & Binet F (2011) Relationship between bacterial diversity and function under biotic control: the soil pesticide degraders as a case study. *ISME J* **5**: 1048–1056.

Müller RH (2007) Activity and reaction mechanism of the initial enzymatic step specifying the microbial degradation of 2,4-dichlorophenoxyacetate. *Eng Life Sci* **7**: 311–321.

Müller RH & Babel W (1999) Separation of two dichlorprop/alpha-ketoglutarate dioxygenases with enantiospecific properties from *Comamonas acidovorans* MC1. *Acta Biotechnol* **19**: 349–355.

Müller RH, Jorks S, Kleinsteuber S & Babel W (1999) *Comamonas acidovorans* strain MC1: a new isolate capable of degrading the chiral herbicides dichlorprop and mecoprop and the herbicides 2,4-D and MCPA. *Microbiol Res* **154**: 241–246.

Müller RH, Kleinsteuber S & Babel W (2001) Physiological and genetic characteristics of two bacterial strains utilizing phenoxypropionate and phenoxyacetate herbicides. *Microbiol Res* **156**: 121–131.

Müller TA, Byrde SA, Werlen C, van der Meer JR & Kohler HPE (2004) Genetic analysis of phenoxyalkanoic acid degradation in *Sphingomonas herbicidovorans* MH. *Appl Environ Microbiol* **70**: 6066–6075.

Müller TA, Fleischmann T, van der Meer JR & Kohler HPE (2006) Purification and characterization of two enantioselective alpha-ketoglutarate-dependent dioxygenases, RdpA and SdpA, from *Sphingomonas herbicidovorans* MH. *Appl Environ Microbiol* **72**: 4853–4861.

Muyzer G, De Waal EC & Uitterlinden AG (1993) Profiling of complex microbial populations by denaturing gradient gel electrophoresis analysis of polymerase chain reaction-amplified genes coding for 16S rRNA. *Appl Environ Microbiol* **59**: 695–700.

Neufeld JD, Dumont MG, Vohra J & Murrell JC (2007a) Methodological considerations for the use of stable isotope probing in microbial ecology. *Microbial Ecol* **53**: 435–442.

Neufeld JD, Vohra J, Dumont MG, Lueders T, Manefield M, Friedrich MW & Murrell JC (2007b) DNA stable-isotope probing. *Nat Protoc* **2**: 860–866.

Oh KH, Ahn SK, Yoon KH & Kim YS (1995) Biodegradation of the phenoxy herbicide MCPA by microbial consortia isolated from a rice field. *Bull Environ Contam Toxicol* **55**: 539–545.

Parker MA & Kennedy DA (2006) Diversity and relationships of bradyrhizobia from legumes native to eastern North America. *Can J Microbiol* **52**: 1148–1157.

© 2013 Federation of European Microbiological Societies
Published by John Wiley & Sons Ltd. All rights reserved

Downloaded from http://femsec.oxfordjournals.org/ by guest on July 9, 2016

COR-AAD1-00003329
Bayer EX1008 (Part 6 of 9)

Paulin MM, Nicolaisen MH & Sorensen J (2011) (*R, S*)-dichlorprop herbicide in agricultural soil induces proliferation and expression of multiple dioxygenase-encoding genes in the indigenous microbial community. *Environ Microbiol* **13**: 1513–1523.

Persoh D, Theuerl S, Buscot F & Rambold G (2008) Towards a universally adaptable method for quantitative extraction of high-purity nucleic acids from soil. *J Microbiol Methods* **75**: 19–24.

Pieper DH, Reineke W, Engesser KH & Knackmuss HJ (1988) Metabolism of 2,4-dichlorophenoxyacetic acid, 4-chloro-2-methylphenoxyacetic acid and 2-methylphenoxyacetic acid by *Alcaligenes eutrophus* Jmp134. *Arch Microbiol* **150**: 95–102.

Pruesse E, Quast C, Knittel K, Fuchs BM, Ludwig WG, Peplies J & Glockner FO (2007) SILVA: a comprehensive online resource for quality checked and aligned ribosomal RNA sequence data compatible with ARB. *Nucleic Acids Res* **35**: 7188–7196.

Rodriguez-Cruz MS, Baelum J, Shaw LJ *et al.* (2010) Biodegradation of the herbicide mecoprop-p with soil depth and its relationship with class III tfdA genes. *Soil Biol Biochem* **42**: 32–39.

Saitou N & Nei M (1987) The neighbor-joining method: a new method for reconstructing phylogenetic trees. *Mol Biol Evol* **4**: 406–425.

Scheidleder A (2000) *Groundwater Quality and Quantity in Europe*. European Environment Agency, Copenhagen, Denmark.

Schellenberger S, Kolb S & Drake HL (2010) Metabolic responses of novel cellulolytic and saccharolytic agricultural soil Bacteria to oxygen. *Environ Microbiol* **12**: 845–861.

Scheu S (1991) Mucus excretion and carbon turnover of endogenic earthworms. *Biol Fertil Soils* **12**: 217–220.

Schleinitz KM, Kleinsteuber S, Vallaeys T & Babel W (2004) Localization and characterization of two novel genes encoding stereospecific dioxygenases catalyzing 2(2,4-dichlorophenoxy)propionate cleavage in *Delftia acidovorans* MC1. *Appl Environ Microbiol* **70**: 5357–5365.

Schloss PD & Handelsman J (2005) Introducing DOTUR, a computer program for defining operational taxonomic units and estimating species richness. *Appl Environ Microbiol* **71**: 1501–1506.

Schmidt O, Scrimgeour CM & Curry JP (1999) Carbon and nitrogen stable isotope ratios in body tissue and mucus of feeding and fasting earthworms (*Lumbricus festivus*). *Oecologia* **118**: 9–15.

Shimojo M, Kawakami M & Amada K (2009) Analysis of genes encoding the 2,4-dichlorophenoxyacetic acid-degrading enzyme from Sphingomonas agrestis 58-1. *J Biosci Bioeng* **108**: 56–59.

Silva TM, Stets MI, Mazzetto AM *et al.* (2007) Degradation of 2,4-D herbicide by microorganisms isolated from Brazilian contaminated soil. *Braz J Microbiol* **38**: 522–525.

Smith AE & Hayden BJ (1981) Relative persistence of MCPA, MCPB, and Mecoprop in Saskatchewan soils, and the identification of MCPA in MCPB-treated soils. *Weed Res* **21**: 179–183.

Takeuchi M, Hamana K & Hiraishi A (2001) Proposal of the genus *Sphingomonas sensu stricto* and three new genera, *Sphingobium*, *Novosphingobium* and *Sphingopyxis*, on the basis of phylogenetic and chemotaxonomic analyses. *Int J Syst Evol Microbiol* **51**: 1405–1417.

Thakuria D, Schmidt O, Finan D, Egan D & Doohan FM (2010) Gut wall bacteria of earthworms: a natural selection process. *ISME J* **4**: 357–366.

Thompson DG, Stephenson GR & Sears MK (1984) Persistence, distribution and dislodgeable residues of 2,4-D following its application to turfgrass. *Pestic Sci* **15**: 353–360.

Tiunov AV & Scheu S (1999) Microbial respiration, biomass, biovolume and nutrient status in burrow walls of *Lumbricus terrestris* L. (Lumbricidae). *Soil Biol Biochem* **31**: 2039–2048.

Tonso NL, Matheson VG & Holben WE (1995) Polyphasic characterization of a suite of bacterial isolates capable of degrading 2,4-D. *Microb Ecol* **30**: 3–24.

Vink JPM & vanderZee S (1997) Effect of oxygen status on pesticide transformation and sorption in undisturbed soil and lake sediment. *Environ Toxicol Chem* **16**: 608–616.

Westendorf A, Müller RH & Babel W (2003) Purification and characterisation of the enantiospecific dioxygenases from *Delftia acidovorans* MC1 initiating the degradation of phenoxypropionate and phenoxyacetate herbicides. *Acta Biotechnol* **23**: 3–17.

WHO (2008) *Guidelines for Drinking-Water Quality*, 3rd edn. World Health Organization, Geneva.

Worthing CR & Hance RJ (1991) *The Pesticide Manual – A World Compendium*. The British Crop Protection Council, Farnham, UK.

Zakaria D, Lappin-Scott H, Burton S & Whitby C (2007) Bacterial diversity in soil enrichment cultures amended with 2 (2-methyl-4-chlorophenoxy) propionic acid (Mecoprop). *Environ Microbiol* **9**: 2575–2587.

Zaprasis A, Liu YJ, Liu SJ, Drake HL & Horn MA (2010) Abundance of novel and diverse *tfdA*-like genes, encoding putative phenoxyalkanoic acid herbicide-degrading dioxygenases, in soil. *Appl Environ Microbiol* **76**: 119–128.

Zipper C, Nickel K, Angst W & Kohler HPE (1996) Complete microbial degradation of both enantiomers of the chiral herbicide mecoprop [(RS)-2-(4-chloro-2-methylphenoxy) propionic acid] in an enantioselective manner by *Sphingomonas herbicidovorans* sp nov. *Appl Environ Microbiol* **62**: 4318–4322.

Supporting Information

Additional Supporting Information may be found in the online version of this article:

Fig. S1. Correlation plot of 16S rRNA gene with *rdpA* (A), *sdpA* (B), and *cadA* (C) gene similarity.

Fig. S2. MCPA degradation (A) and *tfdA*-like ($\times 10^{-2}$, B), *cadA* ($\times 10^{-1}$, C), and *r/sdpA* ($\times 10^{-1}$, D) transcript to gene ratios indicative of MCPA-degradation associated gene expression in MCPA supplemented oxic microcosms.

© 2013 Federation of European Microbiological Societies
Published by John Wiley & Sons Ltd. All rights reserved

Downloaded from http://femsec.oxfordjournals.org/ by guest on July 9, 2016

COR-AAD1-00003330
Bayer EX1008 (Part 6 of 9)

Structural basis for the enantiospecificities of *R*- and *S*-specific phenoxypropionate/α-ketoglutarate dioxygenases

TINA A. MÜLLER,[1] MARIA I. ZAVODSZKY,[2] MICHAEL FEIG,[2,3] LESLIE A. KUHN,[2] AND ROBERT P. HAUSINGER[1,2]

Departments of [1]Microbiology & Molecular Genetics, [2]Biochemistry & Molecular Biology, and [3]Chemistry, Michigan State University, East Lansing, Michigan 48824-4320, USA

(RECEIVED December 21, 2005; FINAL REVISION March 15, 2006; ACCEPTED March 19, 2006)

Abstract

(*R*)- and (*S*)-dichlorprop/α-ketoglutarate dioxygenases (RdpA and SdpA) catalyze the oxidative cleavage of 2-(2,4-dichlorophenoxy)propanoic acid (dichlorprop) and 2-(4-chloro-2-methyl-phenoxy)propanoic acid (mecoprop) to form pyruvate plus the corresponding phenol concurrent with the conversion of α-ketoglutarate (αKG) to succinate plus CO_2. RdpA and SdpA are strictly enantiospecific, converting only the (*R*) or the (*S*) enantiomer, respectively. Homology models were generated for both enzymes on the basis of the structure of the related enzyme TauD (PDB code 1OS7). Docking was used to predict the orientation of the appropriate mecoprop enantiomer in each protein, and the predictions were tested by characterizing the activities of site-directed variants of the enzymes. Mutant proteins that changed at residues predicted to interact with (*R*)- or (*S*)-mecoprop exhibited significantly reduced activity, often accompanied by increased K_m values, consistent with roles for these residues in substrate binding. Four of the designed SdpA variants were (slightly) active with (*R*)-mecoprop. The results of the kinetic investigations are consistent with the identification of key interactions in the structural models and demonstrate that enantiospecificity is coordinated by the interactions of a number of residues in RdpA and SdpA. Most significantly, residues Phe171 in RdpA and Glu69 in SdpA apparently act by hindering the binding of the wrong enantiomer more than the correct one, as judged by the observed decreases in K_m when these side chains are replaced by Ala.

Keywords: dioxygenase; enantiospecificity; mecoprop; site-directed mutagenesis; structural modeling; docking

Supplemental material: see www.proteinscience.org

Reprint requests to: Robert P. Hausinger, Department of Microbiology and Molecular Genetics, 6193 Biomedical Physical Sciences, Michigan State University, East Lansing, MI 48824-4320, USA; e-mail: hausinge@msu.edu; fax: (517) 353-8957.

Abbreviations: 2,4-D, 2,4-dichlorophenoxyacetic acid; AlkB, alkylation-damaged DNA repair enzyme; AtsK, alkyl sulfatase; ANS, anthocyanidin synthase; CarC, carbapenam synthase; CAS, clavaminate synthase; CSD, Cambridge Structural Database; DAOCS, deacetoxycephalosporin C synthase; dichlorprop, 2-(2,4-dichlorophenoxy)propanoic acid; FIH, factor inhibiting hypoxia-inducible factor; αKG, α-ketoglutarate; mecoprop, 2-(4-chloro-2-methyl-phenoxy)propanoic acid; NTA, nitrilotriacetic acid; PAHX, phytanoyl-coenzyme A 2-hydroxylase; PDB, Protein Data Bank; RdpA, (*R*)-specific dichlorprop/αKG dioxygenase; SdpA, (*S*)-specific dichlorprop/αKG dioxygenase; TfdA, 2,4-D/αKG dioxygenase; TauD, taurine/αKG dioxygenase; TR, tropinone reductase; SDS-PAGE, sodium dodecyl sulfate-polyacrylamide gel electrophoresis.

Article and publication are at http://www.proteinscience.org/cgi/doi/10.1110/ps.052059406.

Phenoxyalkanoic acids are systemic and post-emergence inhibitors of broadleaf weeds and are among the most widely applied herbicides in the world (Worthing and Hance 1991; Ahrens 1994; Donaldson et al. 2002). These synthetic auxins (Åberg 1973; Loos 1975; Ahrens 1994) include 2,4-dichlorophenoxyacetic acid (2,4-D) along with the chiral representatives 2-(2,4-dichlorophenoxy)-propanoic acid (dichlorprop) and 2-(4-chloro-2-methyl-phenoxy)propanoic acid (mecoprop), of which only the (*R*)-enantiomers are herbicidally active (Matell 1953). Microorganisms able to degrade these phenoxyalkanoic acid herbicides have been isolated from different environments, and their degradative pathways have been elucidated (Zipper et al. 1996; Hausinger et al. 1997; Tett et al. 1997;

 Copyright © 2006 The Protein Society

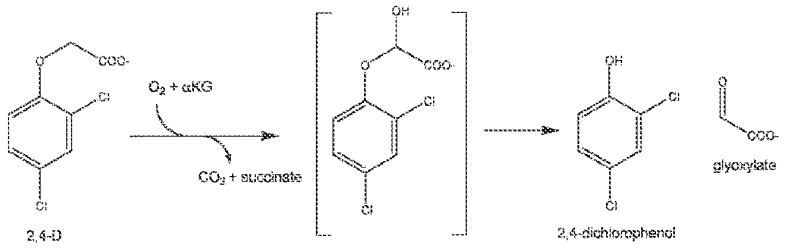
COR-AAD1-00003331
Bayer EX1008 (Part 6 of 9)

Müller et al. 1999, 2001). For example, the first step in 2,4-D metabolism is side-chain hydroxylation to form an unstable intermediate that decomposes by elimination of the phenol derivative (Scheme 1).

The 2,4-D hydroxylase (TfdA) from *Cupriavidus necator* (formerly *Ralstonia eutropha*) JMP134(pJP4) has been intensively studied and shown to require Fe^{II} as a cofactor and α-ketoglutarate (αKG) as a cosubstrate (Fukumori and Hausinger 1993a,b; Saari and Hausinger 1998; Hegg et al. 1999; Hogan et al. 2000; Dunning Hotopp and Hausinger 2002). For mecoprop or dichlorprop metabolism, best studied in the soil bacterium *Sphingomonas herbicidovorans* MH, the enantiomers are separately transported into the cell by distinct uptake systems (Nickel et al. 1997), and enantiomer-specific (*R*)- and (*S*)-dichlorprop/αKG dioxygenases (RdpA and SdpA) catalyze the initial degradation steps as illustrated in Scheme 2 (Nickel et al. 1997; Müller 2004; Müller et al. 2004b). RdpA and SdpA share 30% amino acid sequence identity to each other and 30% and 37% identity, respectively, to TfdA, with no significant gaps in alignment quality, indicating that they are all close structural homologs (Sander and Schneider 1991). The substituted phenol products released from these Fe^{II}/αKG-dependent dioxygenases are subsequently converted to the corresponding catechols and further metabolized by the modified *ortho*-cleavage pathway.

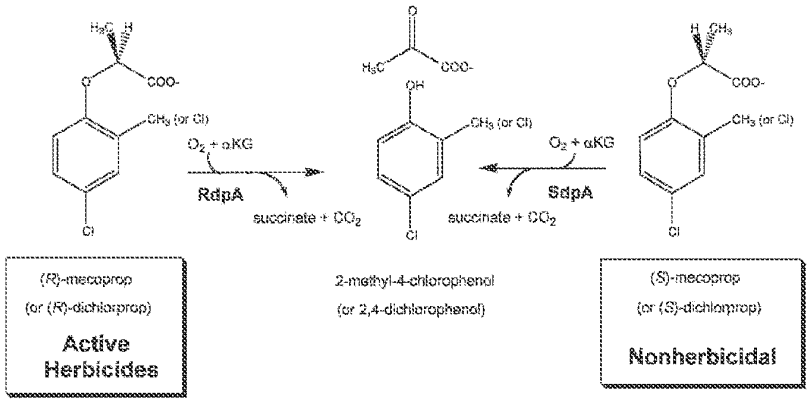
The herbicide-degrading dioxygenases belong to a large family of mononuclear, nonheme Fe^{II} enzymes that catalyze a broad array of reactions (for review, see Hausinger 2004; Clifton et al. 2006) including hydroxylations, epoxidations, desaturations, ring formation, ring expansion, and as only recently discovered, chlorinations (Vaillancourt et al. 2005a,b). Crystal structures have been elucidated for several family members including taurine/αKG dioxygenase (TauD) (Elkins et al. 2002; O'Brien et al. 2003), alkyl sulfatase (AtsK) (Müller et al. 2004a, 2005), clavaminate synthase (CAS) (Zhang et al. 2000), deacetoxycephalosporin C synthase (DAOCS) (Valegård et al. 1998), anthocyanidin synthase (ANS) (Wilmouth et al. 2002), carbapenam synthase (CarC) (Clifton et al. 2003), proline 3-hydroxylase (Clifton et al. 2001), the factor inhibiting hypoxia-inducible factor (FIH) (Dann et al. 2002; Elkins et al. 2003), phytanoyl-coenzyme A 2-hydroxylase (PAHX) (McDonough et al. 2005), and the DNA repair enzyme AlkB (Yu et al. 2006). The structures reveal a common β-jelly roll or double-stranded β-helix fold containing a metal ion-binding motif: His^1-X-Asp/Glu-X_n-His^2 (where *n* varies from 40 to 153 residues). Three water molecules occupy the remaining metal ligand positions in the resting enzyme. Two water molecules are displaced upon binding of the cosubstrate, with the αKG C-2 keto group coordinating opposite the carboxylate side chain and the αKG C-1 carboxyl group binding opposite either His^1 (TauD, AtsK, CAS, and FIH) or opposite His^2 (DAOCS, ANS, CarC, PAHX, and AlkB), with a nearby Arg residue (located 15–22 residues beyond His^2 in the sequence) providing additional stabilization to the C-1 carboxylate in the cases of TauD, AtsK, CAS, CarC, and AlkB. Another Arg residue (located in the sequence about 10 residues beyond His^2) is positioned to form an ion pair with the C-5 carboxylate of αKG in all structures except FIH, where a Lys located elsewhere in the sequence provides stabilization. Unlike other Fe^{II} sites, the αKG-bound metallocenters exhibit a characteristic metal-to-ligand charge-transfer transition (Pavel et al. 1998; Hegg et al. 1999; Ryle et al. 1999; Trewick et al. 2002) conferring a lilac color to this state of the enzymes. The primary substrate (e.g., taurine in the case of TauD) does not bind to the metal center, but the aforementioned crystallographic studies and additional spectroscopic evidence (Ho et al. 2001; Zhou et al. 2001) indicate that substrate binding leads to the loss of the final water molecule, thus creating a site for binding of oxygen. In the case of TauD, oxidative decarboxylation of αKG has been shown to produce an Fe^{IV}-oxo intermediate species that inserts oxygen into the unactivated C–H bond (Price et al. 2003a,b, 2005; Proshlyakov et al. 2004; Riggs-Gelasco et al. 2004; Grzyska et al. 2005).

Sequence alignments highlight several potential key residues of the (*R*)- and (*S*)-dichlorprop/αKG dioxygenases from *S. herbicidovorans* MH (Müller 2004). The His^1-X-Asp/Glu-X_n-His^2 motif of RdpA is comprised of residues His111, Asp113, and His270, while that of SdpA involves His102, Asp104, and His257. Fifteen residues beyond His^2 are residues predicted to interact with the C-1 carboxylate of αKG, Arg285 and His272, respectively.



Scheme 1.

COR-AAD1-00003332
Bayer EX1008 (Part 6 of 9)



Scheme 2.

Furthermore, Arg281 and Arg268 of the two proteins are predicted to form salt bridges to the αKG C-5 carboxylate, with additional interactions involving Thr138 of RdpA and Thr129 of SdpA. In contrast to these conserved residues, essentially nothing is known about the phenoxypropanoic acid-binding sites of these proteins, especially with regard to the structural basis of enantiospecificity.

Here, we describe the construction of homology models of SdpA and RdpA from *S. herbicidovorans* MH and the use of docking to identify residues likely to be involved in herbicide binding. Previous homology models have led to successes in elucidating or designing specificity-conferring interactions in ligands. For instance, homology modeling of a cercarial (human parasite) elastase led to the development of an effective elastase inhibitor (Cohen et al. 1991) and to understanding the specificity determinants for ligands binding to a parasite tRNA synthetase versus its human homolog (Sukuru et al. 2006). Here, we test by site-directed mutagenesis and kinetic analysis the residues predicted to be involved in substrate binding, enantiospecificity, or catalysis. The activity experiments are consistent with the key residues identified by modeling being involved in substrate binding. We provide additional evidence that several amino acids are responsible for the enantiospecificity of RdpA and SdpA, demonstrate that the active site of SdpA is less specific than RdpA for its substrate, and discuss the structural implications of these results.

Results

SdpA and RdpA homology models

RdpA and SdpA were aligned with TauD (Supplemental Fig. S1), and homology models were created as described in Materials and Methods (Supplemental Fig. S2) using the TauD structure as a structural template (O'Brien et al. 2003). The two phenoxypropionate-degrading proteins are predicted to contain jelly roll or double-stranded β-helix folds comprised of eight β-strands with connecting loops, as is typical of this enzyme family (Hausinger 2004; Clifton et al. 2006). The homology models contain Fe^{II}-binding sites (His111, Asp113, and His270 in RdpA or His102, Asp104, and His257 in SdpA), as expected from former sequence alignments with other Fe^{II}/αKG-dependent dioxygenases (Müller 2004). The high degree of active-site sequence identity and strong orientation of key side chains by interactions with the Fe^{II} are supportive of the active site being the most conserved and structurally accurate part of the RdpA and SdpA models. Detailed analysis of favored αKG-binding motifs in other members of this enzyme family indicate the iron is chelated by αKG with its keto group positioned opposite Asp113 of RdpA or Asp104 of SdpA and its C-1 carboxylate located so as to interact with His111 and His102, respectively. The positively charged residues Arg285 in RdpA and His272 in SdpA are well positioned to provide additional stabilization of the αKG C-1 carboxylate, and, in each protein, the C-5 carboxylate of αKG forms a salt bridge with Arg268 and Arg281, respectively. Whereas the RdpA structure represents only one subunit of the predicted trimeric protein, SdpA is suggested to be monomeric, based on gel-filtration experiments (Müller 2004).

Docking of substrates into the RdpA and SdpA structures

The natural substrates (*R*)- and (*S*)-mecoprop were docked into the active sites of RdpA and SdpA to gain insight into the basis of enzyme enantiospecificity. First, the cosubstrate αKG was modeled into the active sites of RdpA and SdpA using two distinct conformations, as found in the crystal structures of Fe^{II}/αKG-dependent dioxygenases

COR-AAD1-00003333
Bayer EX1008 (Part 6 of 9)

(Clifton et al. 2006). The flat conformation has the five-member ring formed by the metal chelate coplanar with the C-5 carboxylate, whereas the twist conformation has the two planes forming a 90° angle. The resulting four models were energy-minimized and used as targets for substrate docking with the program SLIDE (Zavodszky et al. 2002) with the assumption that the substrate carbon undergoing hydroxylation would be located approximately at the same position relative to the iron center as the key carbon atom of taurine in TauD (Elkins et al. 2002; O'Brien et al. 2003). The mecoprop-docking interactions with RdpA and SdpA were analyzed in detail, and one model of each protein was selected based on the most favorable interactions between enzyme and substrate (see below). These models are illustrated in Figure 1, with the corresponding plots of mecoprop interactions shown in Figure 2.

Binding of (R)-mecoprop to RdpA

The substrate (*R*)-mecoprop consists of a hydrophobic phenoxy ring and a polar propanoic acid, with both components needing to be accommodated and bound by the active site. The αKG conformation leading to the most favorable interactions has αKG in the twist conformation and positions the phenoxy ring of (*R*)-mecoprop as illustrated in Figure 1A (with the corresponding interactions plotted in Fig. 2A). The mecoprop carboxylate interacts with the amide nitrogen of Ser114, the hydroxyl group of Tyr221, and a guanidino nitrogen of Arg285. The Tyr221 hydroxyl group also is predicted to lie near (3.5 Å) the substrate ether oxygen atom and could play a role in directing enantiospecificity. Residues lining the hydrophobic substrate-binding pocket include Val80, Leu83, Ile106, Gly107, and Phe171 (Figs. 1A, 2A), with Val80 and Leu83 being well positioned to interact with the propanoic acid methyl group. The terminal carbon atom (CZ) of the Phe171 side chain is 4.1 Å from the phenoxy group of (*R*)-mecoprop; since LigPlot has a 4.0 Å threshold for hydrophobic interactions, this interaction is missed in Figure 2A.

To directly test the importance of potential substrate-binding residues of RdpA identified by the homology modeling and substrate docking procedures, variant forms of the enzymes were created by site-directed mutagenesis. To eliminate the bulky and polar Tyr221 and Arg285 residues, Y221A and R285A mutants were generated. In the presumed "hydrophobic pocket," Val80, Leu83, Ile106, and Phe171 each were changed to alanine to reduce hydrophobic interactions and thereby decrease the binding

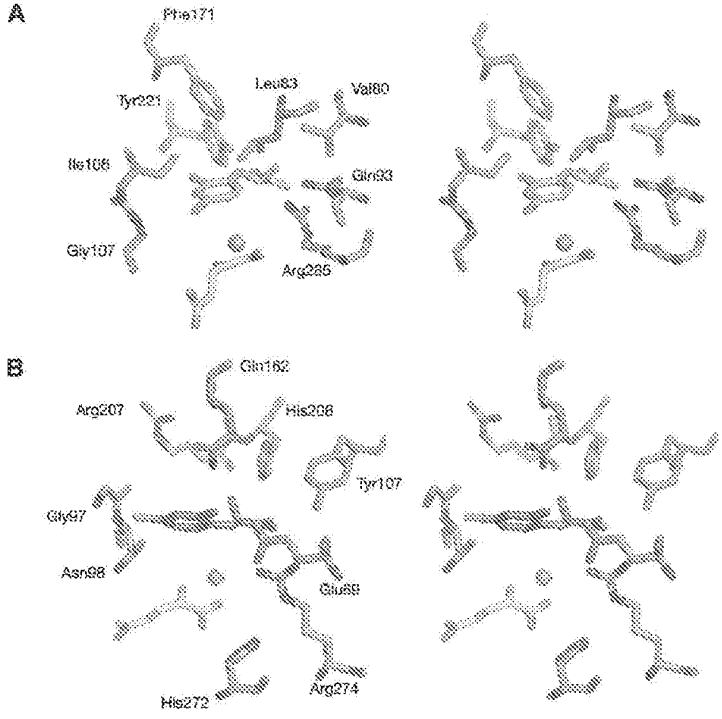


Figure 1. Stereo views of the most favorable models of the active sites of RdpA (*A*) and SdpA (*B*) with bound substrates. Shown are selected protein residues that are predicted to interact with the substrate. For clarity reasons, the Fe^{II} ligands are not depicted. (*R*)- and (*S*)-mecoprop are indicated in light blue and in turquoise, respectively, and αKG in yellow.

COR-AAD1-00003334
Bayer EX1008 (Part 6 of 9)

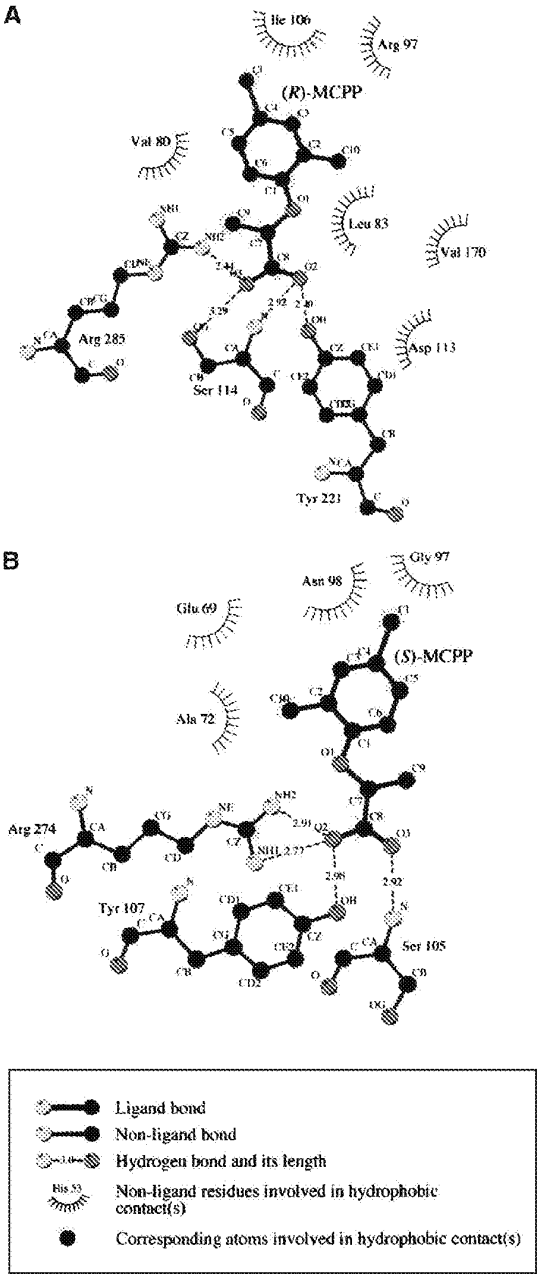


Figure 2. LIGPLOT diagrams of the active site models of RdpA (*A*) and SdpA (*B*). Shown are the most important interactions between the substrate and the active site according to the model.

affinity of (*R*)-mecoprop to the active site. Replacing Gly107—positioned near and coplanar with the phenoxy ring—with a bulkier hydrophobic residue is expected to hinder substrate binding, so this residue was mutated to Ile and Asn in the double mutants I106G/G107I and I106G/G107N, respectively.

The specific activities of the RdpA variants were tested using (*R*)-mecoprop and the racemic mixture (Table 1). The (*S*) enantiomer is not sold commercially and was available in very limited supply, so the RdpA variants were not tested with this compound. When the RdpA variants were examined using 4 mM (*R*)-mecoprop, the V80A and F171A variants exhibited ~60% of wild-type enzyme activity; I106A had ~30% of that activity and L83A, Y221A, and R285A were ~10% active. The activities of the double mutants I106G/G107I and I106G/G107N were further reduced compared with that of I106A, consistent with a bulkier side chain at position 107 presenting steric hindrance to substrate binding in a reactive conformation.

The RdpA variants retaining at least 10% of wild-type enzyme activity were subjected to more detailed kinetic characterization (Table 2). The maximal concentration of substrates that could be tested was 4 mM due to solubility limitations; therefore, K_m values higher than 800 μM are only approximations and possess large errors. The K_m values of V80A and R285A RdpA variants were at least fivefold increased over that of the wild-type enzyme, whereas that of the I106A RdpA variant was more than 20-fold greater, supporting the described docking orientation of the model. The effect on the R285A variant can be understood in terms of decreased interaction with the substrate carboxylate, while the changes observed for the V80A and I106A variants are likely to arise from loss of hydrophobic interactions. The F171A protein had a threefold lower K_m, indicating either that this residue does not interact specifically with the phenoxy ring of (*R*)-mecoprop or that F171 is actually slightly hindering (*R*)-mecoprop binding. The calculated k_{cat} of all mutant proteins was similar to the wild-type value with the exception of the R285A mutant enzyme. Arg285 is postulated to interact with both the mecoprop carboxylate and the C-1 carboxylate of αKG, so it could directly influence catalysis.

Binding of (S)-mecoprop to SdpA

The most favorable orientation of (*S*)-mecoprop was obtained with αKG in the twist conformation in SdpA and (*S*)-mecoprop bound as illustrated in Figure 1B (with the corresponding ligand interactions shown in Fig. 2B). In this model, the substrate carboxylate interacts with the amide nitrogen of Ser105, the hydroxyl group of Tyr107, and the guanidino nitrogens of Arg274. Additional active site residues near the polar carboxylate include His272 and His208. Also of interest, the substrate ether oxygen atom is predicted to lie within 3.4 Å of the two carboxyl oxygens of Glu69. If protonated or bridged by the proton of a bound water molecule, the Glu69 carboxyl group could confer specificity to the (*S*) enantiomer by making a hydrogen bond with the ether oxygen (a prediction not borne out by experimental results, vide infra). Residues predicted to be

COR-AAD1-00003335
Bayer EX1008 (Part 6 of 9)

Table 1. *Activity measurements of native and variant forms of RdpA and SdpA*

RdpA Sample	Hypothesis probed[a]	(*R*)-mecoprop (4 mM) Specific activity (U/mg protein)	(%)	(*R*)-mecoprop (2 mM) Specific activity (U/mg protein)	(%)	(*R,S*)-mecoprop (4 mM) Specific activity (U/mg protein)	(%)
Wild type	—	7.11 ± 1.34	100	5.60 ± 0.26	100	6.46 ± 0.44	100
V80A[b]	I	4.3 ± 2.1	60.5	2.06 ± 0.48	36.8	2.7 ± 0.5	41.8
L83A[c]	I, II	0.37 ± 0.09	5.2	0.24 ± 0.06	4.3	0.27 ± 0.02	4.2
Q93A[b]	II	4.3 ± 0.7	60.5	3.27 ± 0.23	58.3	2.27 ± 0.15	35.2
I106A[c]	I, II	2.14 ± 0.025	30.1	1.41 ± 0.29	25.2	1.10 ± 0.11	17.0
F171A[c]	I, II	4.83 ± 0.31	67.9	4.75 ± 0.22	84.8	4.59 ± 0.35	71.1
F171Q[c]	II	5.2 ± 0.4	73.1	4.86 ± 0.52	86.8	4.49 ± 0.31	69.5
Y221A[b]	I	0.37 ± 0.17	5.2	0.43 ± 0.02	7.7	0.31 ± 0.01	4.8
R285A[c]	I, II	1.1 ± 0.1	14.8	0.92 ± 0.06	16.4	0.80 ± 0.06	12.4
I106G/G107I[d]	I, II	0.05 ± 0.03	0.7	0.04 ± 0.03	0.7	0.05 ± 0.05	0.8
I106G/G107N[d]	I, II	0.62 ± 0.06	8.7	0.56 ± 0.05	10.0	0.53 ± 0.04	8.2

SdpA Sample	Hypothesis probed[a]	(*S*)-mecoprop (4 mM) Specific activity (U/mg protein)	(%)	(*S*)-mecoprop (2 mM) Specific activity (U/mg protein)	(%)	(*R,S*)-mecoprop (4 mM) Specific activity (U/mg protein)	(%)	(*R*)-mecoprop (4 mM) Specific activity (U/mg protein)
Wild type	—	25.5 ± 1.7	100.0	28.96 ± 3.6	100	23.5 ± 0.74	100.0	0
E69A[d]	I, II	7.85 ± 1.65	30.8	6.6 ± 1.3	22.8	5.54 ± 1.24	23.6	0.51 ± 0.22
Q162F[c]	I, II	1.22 ± 0.3	4.8	0.87 ± 0.15	3.0	0.53 ± 0.08	2.3	0
R207A[e]	I, II	4.4 ± 0.57	17.3	3.13 ± 0.52	10.8	2.08 ± 0.3	8.9	0.1 ± 0.02
R207V[c]	II	0.71 ± 0.07	2.8	0.52 ± 0.05	1.8	0.35 ± 0.04	1.5	0.01 ± 0.004
H208A[d]	I, II	0.35 ± 0.1	1.4	0.27 ± 0.07	0.9	0.14 ± 0.05	0.6	0
H272A[d]	I	0.3 ± 0.16	1.2	0.27 ± 0.16	0.9	0.25 ± 0.09	1.1	0
R274A[d]	I	0.01 ± 0.01	0.0	0.01 ± 0.01	0.0	0	0.0	0
G97N/N98G[d]	II	0.07 ± 0.03	0.3	0.06 ± 0.01	0.2	0.02 ± 0.03	0.1	0
G97I/N98G[d]	II	0.96 ± 0.27	3.8	0.93 ± 0.26	3.2	0.83 ± 0.26	3.5	0.01 ± 0.01

[a] The letters indicate whether the mutant was used to probe (I) the predicted binding mode of the substrate or (II) the enantiospecificity of the enzyme.
[b] Values were determined by measuring activities of samples isolated from three independent cell cultures.
[c] Values were determined by triplicate measurements of a single sample.
[d] Values were determined by measuring activities of samples isolated from two independent cell cultures.
[e] Values were determined by triplicate (for (*R,S*)-mecoprop) or duplicate (for (*S*)- and (*R*)-mecoprop) measurements of a single sample.

in contact with the hydrophobic ring of (*S*)-mecoprop include Ala71, Ala72, Leu82, Val84, Gly97, Asn98, Gln162, and Arg207 (with the latter four residues depicted in Fig. 1B). π-Cation interactions between positively charged side chains like Arg207 and aromatic side groups like that in mecoprop can contribute very favorably to ligand binding (Mitchell et al. 1994).

To experimentally test the importance of several of these residues for the binding of (*S*)-mecoprop in the active site of SdpA, a series of mutant proteins was constructed. Glu69, His208, His272, and Arg274 each were changed to alanine to eliminate the bulky and charged side chains proposed to interact with the substrate carboxylate. The extended side chain of Arg207 was eliminated in the R207A SdpA variant, and Gln162 was substituted with the corresponding hydrophobic residue found in RdpA to generate the Q162F variant.

The specific activities of the SdpA variants were tested using the (*S*) enantiomer, the racemic mixture, and the (*R*) enantiomer of mecoprop (Table 1). The activity of all SdpA mutants was strongly reduced. The most active SdpA variants were the E69A and R207A proteins, while all other variants exhibited <5% of the wild-type enzyme activity. No activity was detected in the R274A sample. E69A, R207A, and H208A were subjected to detailed kinetic characterization (Table 2). When analyzed with (*S*)-mecoprop, the R207A and H208A samples had 15- and 18-fold increases, respectively, in their K_m values compared with the wild-type enzyme. The H208A result is compatible with an ionic interaction between the mecoprop carboxylate group and His208. A similar interaction might be possible with the highly flexible Arg207 residue, or this side chain may participate in a π-cation interaction with the aromatic group of the substrate, in either case accounting for the large K_m change in the R207A variant. In contrast to these results, the E69A variant exhibited a lower K_m than the native SdpA, arguing against the ether oxygen having a significant role in substrate binding. With (*S*)-mecoprop, the k_{cat} was reduced four-fold for the E69A and R207A SdpA mutants compared with wild-type enzyme, and even greater reductions were noted for the H208A variant.

COR-AAD1-00003336
Bayer EX1008 (Part 6 of 9)

Table 2. *Kinetic parameters of selected variant forms of RdpA and SdpA*

RdpA Variant	(*R*)-mecoprop Range (μM)	(*R*)-mecoprop K_{to} (μM)	k_{cat} (min^{-1})	k_{cat}/K_m ($min^{-1}*\mu M^{-1}$)
Wild type	100–4000	380 ± 28	252 ± 5	0.66
V80A[a]	200–4000	2300 ± 1100	248 ± 56	0.11
Q93A[a]	200–4000	2800 ± 400	260 ± 21	0.09
I106A[b]	500–4000	8900 ± 2100	238 ± 42	0.03
F171A[b]	200–4000	108 ± 7	175 ± 2	1.62
F171Q[b]	62.5–4000	438 ± 34	203 ± 4	0.46
R285A[a]	200–4000	1550 ± 220	52 ± 4	0.03

	(*S*)-mecoprop				(*R*,*S*)-mecoprop			
SdpA Variant	Range (μM)	K_m (μM)	k_{cat} (min^{-1})	k_{cat}/K_m ($min^{-1}*\mu M^{-1}$)	Range (μM)	K_m (μM)	k_{cat} (min^{-1})	k_{cat}/K_m ($min^{-1}*\mu M^{-1}$)
Wild type	31–4000	161 ± 20	1010 ± 44	6.24	31–4000	234 ± 18	899 ± 24	3.85
E69A[c]	31–4000	91 ± 14	241 ± 8	2.65	222–4000	181 ± 38	194 ± 8.4	1.1
R207A[d]	250–4000	2500 ± 400	238 ± 20	0.1	250–4000	2780 ± 370	117 ± 8.4	0.04
H208A[c]	500–4000	2900 ± 960	21 ± 4	0.007	N.D.			
G97I/N98G[c]	250–4000	1100 ± 270	42 ± 4.4	0.04	N.D.			

N.D., not determined.
[a] Values were determined by measuring activities of samples isolated from three independent cell cultures.
[b] Values were determined by triplicate measurements of a single sample.
[c] Values were determined by measuring activities of samples isolated from two independent cell cultures.
[d] Values were determined by triplicate (for (*R*,*S*)-mecoprop) or duplicate (for (*S*)- and (*R*)-mecoprop) measurements of a single sample.

Residues determining enantiospecificity in RdpA and SdpA

A direct comparison of the active sites in the RdpA and SdpA models is shown in Figure 3. The different substrate enantiomers are predicted to bind with remarkably similar geometries in the two predicted structures, with the carboxyl groups and aromatic rings nearly overlapping but at distinct angles. RdpA residues Leu83, Gln93, Ile95 (omitted for clarity), Ile106, Phe171, and Arg285 (shown in Fig. 1A) could hinder binding of (*S*)-mecoprop; the corresponding residues in SdpA are Ala72, Leu82, Val84, Gly97, Gln162, and His272, respectively. Similarly, SdpA residues Glu69, Asn98, Ser161, His208, and Arg207 could restrict binding of (*R*)-mecoprop; Val80, Gly107, Val170, Tyr221, and Val220 occupy these positions in RdpA. Ala72, Gly97, and Gln162 are predicted to allow access by the (*S*) enantiomer. In general, side-chain interactions suggest that SdpA is less specific than RdpA for its substrate. This finding is compatible with activity measurements (Table 1), such as the activity with 2 mM (*S*)-mecoprop versus that with 4 mM of the racemate, that show inhibition of SdpA activity by (*R*)-mecoprop. However, RdpA remains completely active toward the (*R*) enantiomer in the presence of (*S*)-mecoprop (Müller 2004).

Site-directed variants of RdpA and SdpA, created and purified as described earlier, were used to test a subset of the above-mentioned residues for their importance in controlling enantioselectivity. Single substitutions included the L83A, Q93A, I106A, F171A, F171Q, and R285A variants of RdpA along with the E69A, Q162F, R207A, R207V, and H208A variants of SdpA. In addition, to test the possibility that Ile106/Gly107 (large residue/small residue) in RdpA versus Gly97/Asn98 (small residue/large residue) in SdpA confers some measure of enantiospecificity to the enzymes, the I106G/G107I and I106G/G107N double variants of RdpA along with G97N/N98G and G97I/N98G double variants of SdpA were generated. Each enzyme was tested for activity using its enantiomer, the racemate, and in the case of the SdpA mutants, with (*R*)-mecoprop, too (Tables 1, 2).

Among the RdpA variants were several that show evidence of inhibition by the (*S*) enantiomer. For example, the Q93A variant retains 60% of wild-type enzyme activity, but this dropped to 35% when the racemate was provided, suggesting that Gln93 prevents the incorrect enantiomer from binding to and inhibiting the enzyme. Significant decreases in activity also were apparent when comparing rates using the racemic mixture of mecoprop versus the (*R*)-enantiomer with the Y221A and R285A variants; these results suggest that Tyr221 and Arg285 contribute to enantiospecificity. These variant proteins exhibited ~5% to ~15% of the wild-type enzyme activity. Less dramatic differences were observed using the I106A, F171A, F171Q, and I106G/G107N variants, but in each case the activity was reduced in the presence of the incorrect enantiomer. The I106A, F171A, F171Q, and R285A proteins were subjected to detailed kinetic

COR-AAD1-00003337
Bayer EX1008 (Part 6 of 9)

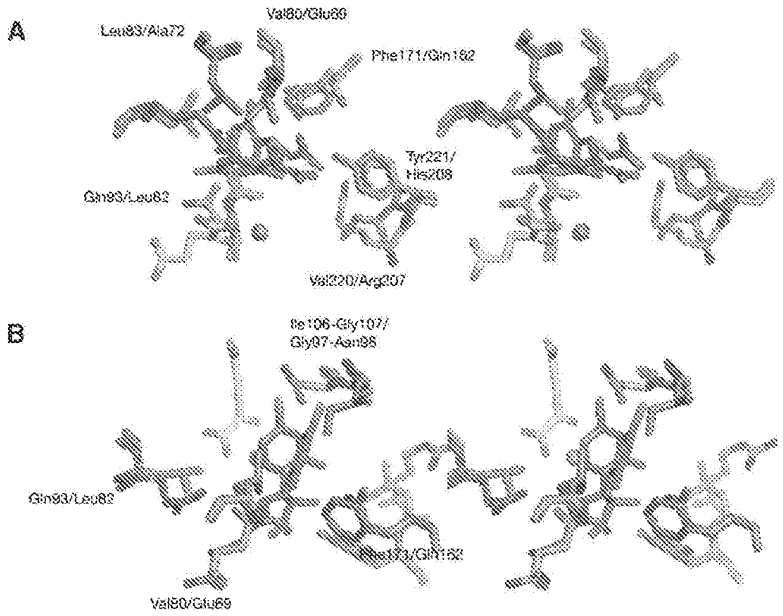


Figure 3. Stereo views of the superimposition of the substrate-bound active site models of RdpA and SdpA. Shown are selected residues predicted to be involved in dictating enantiospecificity. Amino acid residues of RdpA are depicted in pink; residues of SdpA, in green. (*R*)-mecoprop is shown in purple; (*S*)-mecoprop, in turquoise. (*A*) View with the focus on the propanoic acid moiety and its binding to the active sites. (*B*) Same as in *A* but rotated to focus on the phenoxy ring and its interaction with the amino acid residues Ile106/Gly107 in RdpA and Gly97/Asn98 in SdpA.

analysis with (*R*)-mecoprop (Table 2). With the exception of the R285A variant (which exhibited ~20% of the wild-type enzyme k_{cat}), the proteins retained >70% of the wild-type enzyme k_{cat}. The I106A and R285A variants exhibited 23- and fourfold increases in K_m; the F171Q form exhibited a K_m similar to the wild-type enzyme, and the F171A mutant had a threefold lower K_m. The latter result is consistent with Phe171 hindering binding of the correct (*R*) enantiomer while helping to exclude the (*S*) enantiomer from the RdpA active site, so that the expanded active site in the F171A variant more readily binds its substrate.

Significantly, four SdpA variants (E69A, R207A, R207V, and G97I/N98G) showed slight activity with the opposite enantiomer, (*R*)-mecoprop (Table 1). These results suggest that Glu69, Arg207, and Gly97/Asn98 contribute to determining the enantiomeric specificity, as predicted by docking. They are compatible both with the postulated interaction of Glu69 with the (*S*)-mecoprop ether oxygen and with steric constraints on (*R*)-mecoprop binding imposed by Glu69, Arg207, and Asn98. Kinetic analyses of the E69A variant (Table 2) argue against a positive, stabilizing interaction between Glu69 and the substrate ether atom, because the K_m of this variant is less than that of the wild-type enzyme. These results are most consistent with Glu69 discriminating against binding by the opposite enantiomer while slightly hindering binding of the correct enantiomer. The apparent K_m of wild-type SdpA was approximately doubled when examined using the racemic mixture, as expected from earlier work (Müller 2004). Similar results were obtained for the E69A variant, while the K_m was essentially unchanged for the R207A protein when comparing the single enantiomer versus the racemate. The R207A K_m results are consistent with both substrate enantiomers binding to the active site with similar affinities. This point was directly demonstrated by assaying the R207A enzyme with (*R*)-mecoprop, yielding a K_m of 4.0 ± 1.3 mM and a k_{cat} of ~0.16 min^{-1}. For comparison, the K_m of E69A SdpA for (*R*)-mecoprop was determined to be 5.4 ± 1.7 mM with a k_{cat} of 65 ± 15 min^{-1}. The k_{cat} was further reduced for the E69A and H208A variants when using the racemic mixture, consistent with binding and inhibition by the (*R*) enantiomer. The low activities of the H208A and G97I/N98G proteins precluded a similar analysis.

Discussion

On the basis of the modeled RdpA and SdpA structures, we identified several amino acid residues that are likely to interact with (*R*)- and (*S*)-mecoprop, including several that are likely to contribute to the enantiospecificities of

COR-AAD1-00003338
Bayer EX1008 (Part 6 of 9)

the two enzymes. The structural modeling performed here incorporated small-scale conformational changes in optimizing the protein–ligand complex through flexible docking using SLIDE and energy minimization of the structures. However, many enzymes, including selected representatives of the Fe^{II}/αKG dioxygenases (Clifton et al. 2006), are known to undergo larger-scale conformational changes upon ligand binding. The problem then becomes one of predicting protein conformational change as well as the orientation of ligand binding, a prodigious task for which no generally proven method exists. Success has been shown on subproblems for some complexes, e.g., predicting relative degrees of flexibility within a protein and how this flexibility redistributes upon complex formation (Gohlke et al. 2004), predicting large-scale conformational change between two protein states (Tama et al. 2004), evaluating conformational ensembles of the ligand and protein structures that are consistent with binding (Zavodszky et al. 2004), and predicting ligand binding by docking into a series of experimentally known enzyme conformations that approximate larger-scale protein flexibility (Lorber and Shoichet 1998). Molecular dynamics simulation of the protein–ligand complex is another option. However, it is generally difficult to access substantially different ligand orientations and protein conformations in molecular dynamics simulations. In our case, the situation is further complicated given the trimeric state of RdpA and the possible influence of subunit interfaces on active-site conformations. Therefore, the accuracy of homology modeling and prediction of (*R*)- and (*S*)-mecoprop interactions with the RdpA and SdpA enzymes may be limited by not anticipating medium- to large-scale protein conformational change. The predictive value of this modeling—identifying residues likely to be responsible for recognizing the (*R*) versus (*S*) enantiomer of mecoprop—can be assessed by consistency with the binding effects of mutations of these residues. Site-specific variants of RdpA and SdpA were created, their activities measured, and, in selected cases, detailed kinetic experiments were performed. The results confirm the residues involved in substrate or cosubstrate binding and provide useful insights into the structural basis of enantiomeric specificity.

Basis of the substrate-binding specificity of RdpA and SdpA

(*R*)- and (*S*)-mecoprop docked to the predicted structures of RdpA and SdpA, respectively, indicate that the mecoprop carboxylates and phenoxy rings are similarly positioned in the two proteins, with the substrate methyl group oriented in opposite configurations. The activity and kinetic data for R285A and Y221A variants of RdpA are compatible with the (*R*)-mecoprop carboxylate interacting with both the guanidino group of Arg285 and the hydroxyl group of Tyr221, where Tyr221 also forms a potential hydrogen bond to the ether oxygen atom. Similarly, activity and kinetic measurements of the R274A and H208A proteins are consistent with SdpA using the corresponding residues Arg274 and His208 to bind the carboxylate of (*S*)-mecoprop. Comparable Arg residues are conserved in many Fe^{II}/αKG-dependent dioxygenases, where they play a dual role of binding the primary substrate and the C1-carboxyl group of αKG (Valegård et al. 1998; Elkins et al. 2002; O'Brien et al. 2003; Hausinger 2004; Müller et al. 2004a). Such a dual role is predicted for Arg285 of RdpA, whereas Arg274 and His272 split these functions in SdpA.

Examination of the mutant forms of RdpA and SdpA also provided insights into the specificity for the distinct mecoprop enantiomers. For RdpA variants, Gln93, Ile106, and Phe171 are proposed to sterically exclude binding by the incorrect enantiomer, whereas the Q93A variant yields results consistent with inhibition by (*S*)-mecoprop. Similarly, the results with the SdpA mutants are consistent with Glu69, Asn98, and Arg207 and His208 acting to prevent binding of the (*R*) enantiomer. In particular, the E69A, R207A, and G97I/N98G variants exhibited activity with the incorrect substrate, (*R*)-mecoprop. Hydrophobic interactions are also likely to be critical for substrate discrimination. For example, Val80 and Leu83 in RdpA are predicted to be well positioned to interact with the propanoic acid methyl group, whereas Glu69 and Ala72 occupy these positions in SdpA. We conclude that several residues in each protein play a role in dictating the substrate enantiospecificity.

Comparison of the proposed RdpA- and SdpA-substrate interactions with 2,4-D binding by TfdA

RdpA and SdpA are 30% and 37% identical to TfdA, for which a homology model was previously constructed and its 2,4-D substrate docked (Elkins et al. 2002). Predicted interactions in theTfdA model previously were tested by site-directed mutagenesis and kinetic analyses (Hogan et al. 2000; Dunning Hotopp and Hausinger 2002), similar to what is described here for RdpA and SdpA. In the case of TfdA, the substrate carboxylate was suggested to interact with Arg278, His214, and Lys71. While the TfdA Arg and His residues have direct counterparts in the mecoprop-degrading enzymes (Arg285 and Tyr221 in RdpA; Arg274 and His208 in SdpA), there is no indication of a carboxylate-stabilizing Lys in RdpA or SdpA. Also of interest, Lys71 and/or Lys95 of TfdA was suggested to interact with the ether oxygen atom of 2,4-D. Again, a Lys does not appear to function in this manner in the mecoprop-degrading enzymes; however, Tyr221 of RdpA is reasonably well positioned for this role.

TfdA is slightly active with (*S*)-dichlorprop, but not with (*R*)-dichlorprop (Saari et al. 1999). Based on secondary

COR-AAD1-00003339
Bayer EX1008 (Part 6 of 9)

structure alignment, TfdA residues Ala109 and Asn110 correspond to the Gly97/Asn98 (small residue/large residue) pair in SdpA, versus Ile106/Gly107 in RdpA. Evidence described earlier is consistent with this pair of RdpA and SdpA residues contributing to the enantiospecificity of these enzymes. The presence of (*S*)-dichlorprop-degrading activity in TfdA supports this proposal. 2,4-D converting TfdAs from other strains also show slight activities with phenoxypropanoic acids. Like TfdA from *C. necator* JMP134(pJP4), TfdA from *Burkholderia cepacia* strain RASC cleaves the ether bond of (*S*)-dichlorprop (Saari et al. 1999), whereas TfdA from *Alcaligenes denitrificans* exclusively converts the (*R*) enantiomer (Tett et al. 1997). Interestingly, PCR-derived DNA fragments reveal that these enzymes share 86% amino acid sequence identity in the corresponding region of the proteins (Saari et al. 1999); if the entire proteins exhibit this level of identity, the enantiospecificity is likely to be conferred by a few key amino acid residues.

Conclusion and relationship to other enantiospecific enzymes

The stereocenter-recognition-model of Sundaresan and Abrol (2002, 2005), much like the simpler three-point interaction model (Davankov 1997), generalizes the interactions between a chiral substrate and an enzyme or a receptor by postulating that at least three points of interaction are needed to distinguish between enantiomers with one chiral center. For the enantiospecific binding of mecoprop to RdpA and SdpA, the active site could be expected to interact with the carboxylic acid, either the ether oxygen atom or the phenoxy ring, and the methyl group. The predicted substrate interactions and kinetic results for RdpA and its variants are consistent with such mecoprop interactions. That is, several protein side chains are predicted to position the carboxylate, and Tyr221 likely forms a hydrogen bond to the ether oxygen, while several residues, notably the Ile106/Gly107 pair, position the phenoxy ring, and Val80 and Leu83 interact with the methyl group. In contrast, the SdpA model displays only two clear interactions with (*S*)-mecoprop: Tyr107 and Arg274 side chains position the carboxylate, and several, including the Gly97Asn98 pair, position the phenoxy ring, but the methyl group exhibits little interaction with the active site. Therefore, the active site of SdpA appears to be inherently less enantiospecific for (*S*)-mecoprop and more easily binds the opposite (*R*) enantiomer. The observed inhibition of SdpA by the (*R*) enantiomer and the reactivity of certain SdpA variants with (*R*)-mecoprop support this hypothesis.

In general, enantioselectivity is known to arise from both stabilization of the preferred substrate and relative destabilization of binding by the other enantiomer (Sundaresan and Abrol 2002, 2005). For example, tropinone reductase (TR)-I and TR-II reduce tropinone in a stereoselective manner to produce tropine and Ψ-tropine. Tropinone is differently oriented in the active sites of the two enzymes, with both proteins providing stabilizing interactions and TR-I acting to prevent the inappropriate binding mode by a repulsion interaction involving the positively charged nitrogen of tropinone and a positively charged histidine residue (Nakajima et al. 1998). RdpA and SdpA are proposed to conform to this general pattern by using both positive and negative interactions to enhance binding by the appropriate enantiomer.

Materials and methods

Recombinant plasmids

Mutagenesis of *rdpA* and *sdpA* within pMec15 and pMec19 was carried out by using the Stratagene QuikChange System (Stratagene) and the mutagenic primers listed in Supplemental Table S1. Each mutation was confirmed by sequence analysis (Davis Sequencing). These constructs produce "wild-type" and variant enzymes as His_6-tagged fusion proteins.

Enzyme purification

Escherichia coli C41(DE3) (Miroux and Walker 1996) cells harboring pMec15, pMec151, pMec152, pMec153, pMec154, pMec155, pMec156, pMec157, pMec158, pMec160, and pMec161 were used to purify His_6-tagged wild-type RdpA and its V80A, Q93A, Y221A, R285A, I106G/G107I, I106G/G107N, L83A, I106A, F171A, and F171Q variants, respectively. Similarly, *E. coli* BL21(DE3) (Novagen) cells harboring pMec19, pMec191, pMec192, pMec193, pMec194, pMec195, pMec196, pMec197, and pMec198 were used to purify His_6-tagged wild-type SdpA and its E69A, H208A, H272A, H274A, G97N/N98G, G98I/N98G, Q162F, R207A, and R207V variants, respectively. The cells were grown with constant shaking in Erlenmeyer flasks containing terrific broth supplemented with 200 μg/mL of ampicillin. Starter cultures grown overnight at 37°C were used to inoculate (0.5% [v/v]) medium for growth at room temperature. Upon reaching an OD_{600} between 0.3 and 0.7, isopropyl-β-D-thiogalactopyranoside was added to a final concentration of 1 mM, and the cultures were grown for an additional 16–18 h. To overexpress wild-type and variant forms of His_6-tagged RdpA in *E. coli* C41(DE3) cells, it was important to fill flasks to 50% of their volume with medium and that the shaking be kept at moderate levels to minimize aeration and decrease growth rate. The cells were harvested by centrifugation at 6000*g* for 10 min at 4°C. To prepare cell extracts, each 1 g of the cell pellet was resuspended in 2.5 mL of lysis buffer (50 mM NaH_2PO_4, 300 mM NaCl, 10 mM imidazole at pH 8), and the cells were disrupted by sonication with cooling on ice between pulses. The disrupted cells were centrifuged at 130,000*g* for 60 min at 4°C, and the clarified cell extracts were stored in aliquots at –80°C. RdpA and SdpA accounted for up to 23% and 33% of the protein in the respective soluble cell extracts.

His_6-RdpA and its variants were purified by a one-step procedure carried out at room temperature. Up to 100 mg of protein was loaded onto a Ni-bound NTA-agarose column (5 × 2.5 cm; Invitrogen) in lysis buffer. Unbound proteins were removed from

COR-AAD1-00003340
Bayer EX1008 (Part 6 of 9)

the column with five column volumes of wash buffer (50 mM NaH_2PO_4, 300 mM NaCl, 50 mM imidazole at pH 8). His_6-RdpA and its variants were released from the resin with elution buffer (50 mM NaH_2PO_4, 300 mM NaCl, 200 mM imidazole at a pH adjusted to 8) containing 20% glycerol to increase stability. His_6-SdpA and its mutants were purified as described for the His_6-RdpA, except that no glycerol was included in the elution buffer (see representative purifications in Supplemental Fig. S3). Purified proteins were stored on ice for up to 4 d.

Protein concentrations were determined by using the Bio-Rad protein assay (Bio-Rad) with bovine serum albumin as the standard. Sodium dodecyl sulfate-polyacrylamide gel electrophoresis (SDS-PAGE) analysis was carried out according to established procedures (Laemmli 1970).

Assays

Typical assays contained 100 μM $(NH_4)_2Fe(SO_4)_2$, 1 mM ascorbic acid, 1 mM αKG, and the indicated amount of substrate in 100 mM imidazole buffer (pH 6.75). All assays were carried out at 30°C. To determine kinetic parameters for phenoxypropanoic acids, the coupled continuous enzyme assay was used as previously described (Müller 2004). Units of activity were defined as micromoles of product produced per min per mg protein. Values of k_{cat} were calculated using M_r 34,950 for the His_6-RdpA variants and 33,460 for the His_6-SdpA variants.

Structural modeling

Homology models of RdpA and SdpA were generated on the basis of the structure of the related taurine/αKG dioxygenase (TauD) from *E. coli* (O'Brien et al. 2003). With 33% and 29% identity to RdpA and SdpA and no significant gaps in the alignment, TauD (PDB code 1OS7, chain A) meets the criterion of at least 25% identity over at least 80 residues (Sander and Schneider 1991) to be an accurate structural template for modeling. Multiple alignments for the dichlorprop hydroxylase structures were obtained with the Bioinfo Meta Server (http://bioinfo.pl/Meta), and one was selected based on optimal agreement with predicted secondary structures. Side chains of RdpA and SdpA were reconstructed with the MMTSB Tool Set (Feig et al. 2000, 2004). Nonconserved loops and missing residues were added with Modeller (Fiser et al. 2000, 2002). The iron was placed into the active site according to the TauD structure, and the side chains in the predicted binding sites were adjusted using Insight II (Accelrys) to have similar conformations to the corresponding side chains from TauD, since conserved residues in catalytic sites tend to be highly structurally conserved. Catalytic sites are even more strongly conserved in structure when they involve a metal center, which strongly orients its ligating side chains. In particular, residues His111, Asp113, and His270 in RdpA and His102, Asp104, and His257 in SdpA were repositioned to bind the Fe^{II} metallocenter as they do in TauD, and αKG was positioned with its C-1 carboxylate plus C-2 carbonyl group chelating the metal and its C-5 carboxylate forming an ion pair with Arg268 or Arg281, respectively. The conformation of the free αKG (ID code COTPAC) was obtained from the Cambridge Structural Database (CSD).

To model αKG interactions with RdpA and SdpA as accurately as possible, multiple bound αKG conformations were retrieved from crystal structures of other αKG-dependent dioxygenases (PDB codes 1OS7, 1GY9, 1GQW, 1OII, 1OIJ, 1OIK, 1NX4, and 1NX8). This analysis revealed two distinct conformations: The flat conformation has the five-member ring formed by chelating the Fe^{II} nearly coplanar with the C-5 carboxylate, whereas the twist conformation has the two planes at a 90° angle. Both conformations could be accommodated by RdpA and SdpA, and four models (RdpA and SdpA with the flat and the twist αKG conformation) were built and energy-minimized in the context of the protein structure, with an implicit aqueous solvent (Generalized Born with solvent accessibility correction) using the MMTSB tool set and the CHARMM22 force field (Brooks et al. 1983; Feig et al. 2004).

Docking of substrates

The energy-minimized structures with each of the αKG conformations were used as targets for docking with the program SLIDE (Schnecke and Kuhn 2000; Zavodszky et al. 2002), which models the small-scale protein and ligand side-chain rotations that are ubiquitous in induced fit between proteins and their ligands (Zavodszky and Kuhn 2005). The free (*R*)-mecoprop conformation was obtained from CSD. Alternative low-energy conformations for both the (*R*) and the (*S*) enantiomer, reflecting the range of conformations likely to be energetically accessible, were generated from connectivity information using Omega v1.8.b3 (OpenEye Scientific Software). The energy window allowed for the conformers was 20 kcal/mol, ensuring a very thorough search of the ligands' conformations. Nine conformers each of (*R*)- and (*S*)-mecoprop and of the CSD structure were generated, and all 27 conformers were docked into each of the four models (RdpA with flat and twisted αKG conformations, and likewise for SdpA) with SLIDE using the default parameter set (Schnecke and Kuhn 2000; Zavodszky et al. 2002). To identify the most likely binding orientation, the dockings of mecoprop into RdpA and SdpA were filtered using the following geometric criteria for catalysis: The distance between the Fe^{II} and the C7 carbon atom of mecoprop should be ~4 Å, and the C7-H4 bond should orient toward the Fe^{II}. In addition, based on the interactions observed between enzymes of this class and their substrates, the carboxylate group of mecoprop is expected to bind in the same region and make similar interactions as the taurine sulfate group bound to TauD, anchoring the substrate for catalysis. Among the (*R*)- mecoprop dockings satisfying these criteria, the one with the most favorable interactions positioned the mecoprop phenoxy ring into the enlarged hydrophobic pocket formed by the replacement of bulky Tyr73 in TauD by Leu83 in RdpA, and the propanoic acid methyl group in the hydrophobic pocket created by replacing His70 of TauD with Val80. This comprised the favored RdpA-*(R)*-mecoprop model. The (*S*)-mecoprop dockings satisfying the above geometric criteria were very similar to each other, and the one with optimal protein-substrate hydrogen bonds was selected.

Figures 1, and 3, and Supplemental Figure S2 of RdpA and SdpA structures and active sites were produced using the program PyMOL (DeLano Scientific LLC). Ligand interactions were depicted using LIGPLOT v.4.4.2 (Wallace et al. 1995).

Electronic supplemental material

Coordinate files in PDB format containing the atomic coordinates of the modeled RdpA and SdpA structures in complex with *(R)*- and *(S)*-mecoprop and a document file containing a table, three figures, and their legends.

Acknowledgments

These studies were supported by a fellowship for prospective researchers from the Swiss National Science Foundation (to

COR-AAD1-00003341
Bayer EX1008 (Part 6 of 9)

T.A.M.), by NSF CAREER grant 0447799 (to M.F.), and by the NIH (AI53877 to L.A.K and GM063584 to R.P.H.). We thank Professor Hans-Peter Kohler for generously providing (*S*)-mecoprop and OpenEye (Santa Fe, NM) for generously providing their Omega software for our use.

References

Åberg, B. 1973. Plant growth regulators. XXXI. Some monochloro-monomethylphenoxyacetic and related optically active propionic acids. *Swed. J. Agric. Res.* **3:** 49–62.

Ahrens, W.H. 1994. *Herbicide handbook (WSSA)*. 7th ed. Weed Science Society of America, Champaign, IL.

Brooks, B.R., Bruccoleri, R.E., Olafson, B.D., States, D.J., Swaminathan, S., and Karplus, M. 1983. CHARMM: A program for macromolecular energy, minimization, and dynamics calculations. *J. Comput. Chem.* **4:** 187–217.

Clifton, I.J., Hsueh, L.-C., Baldwin, J.E., Harlos, K., and Schofield, C.J. 2001. Structure of proline 3-hydroxylase. Evolution of the family of 2-oxoglutarate dependent dioxygenases. *Eur. J. Biochem.* **268:** 6625–6636.

Clifton, I.J., Doan, L.X., Sleeman, M.C., Topf, M., Suzuki, H., Wilmouth, R.C., and Schofield, C.J. 2003. Crystal structure of carbapenem synthase (CarC). *J. Biol. Chem.* **278:** 20843–20850.

Clifton, I.J., McDonough, M.A., Ehrismann, D., Kershaw, N.J., Granatino, N., and Schofield, C.J. 2006. Structural studies on 2-oxoglutarate oxygenases and related double-stranded β-helix fold proteins. *J. Inorg. Biochem.* **100:** 644–669.

Cohen, F.E., Gregoret, L.M., Amiri, P., Aldape, K., Raily, J., and McKerrow, J.H. 1991. Arresting tissue invasion of a parasite by protease inhibitors chosen with the aid of computer modeling. *Biochemistry* **30:** 11221–11229.

Dann III, C.E., Bruick, R.K., and Deisenhofer, J. 2002. Structure of a factor-inhibiting hypoxia-inducible factor 1: An essential asparaginyl hydroxylase involved in the hypoxic response pathway. *Proc. Natl. Acad. Sci.* **99:** 15351–15356.

Davankov, V.A. 1997. The nature of chiral recognition: Is it a three-point interaction? *Chirality* **9:** 99–102.

Donaldson, D., Kiely, T., and Grube, A. 2002. *Pesticides industry sales and usage. 1998 and 1999 market estimates*, pp. 1–32. U.S. Environmental Protection Agency, Washington, D.C.

Dunning Hotopp, J.C. and Hausinger, R.P. 2002. Probing the 2,4-dichlorophenoxyacetate/α-ketoglutarate dioxygenase substrate binding site by site-directed mutagenesis and mechanism-based inactivation. *Biochemistry* **41:** 9787–9794.

Elkins, J.M., Ryle, M.J., Clifton, I.J., Dunning Hotopp, J.C., Lloyd, J.S., Burzlaff, N.I., Baldwin, J.E., Hausinger, R.P., and Roach, P.L. 2002. X-ray crystal structure of *Escherichia coli* taurine/α-ketoglutarate dioxygenase complexed to ferrous iron and substrates. *Biochemistry* **41:** 5185–5192.

Elkins, J.M., Hewitson, K.S., McNeill, L.A., Seibel, J.F., Schlemminger, I., Pugh, C.W., Ratcliffe, P.J., and Schofield, C.J. 2003. Structure of factor-inhibiting hypoxia-inducible factor (HIF) reveals mechanism of oxidative modification of HIF-1α. *J. Biol. Chem.* **278:** 1802–1806.

Feig, M., Rotkiewicz, P., Kolinski, A., Skolnick, J., and Brooks III, C.L. 2000. Accurate reconstruction of all-atom protein representations from side-chain-based low-resolution models. *Proteins* **41:** 86–97.

Feig, M., Karanicolas, J., and Brooks III, C.L. 2004. MMTSB tool set: Enhanced sampling and multiscale modeling methods for applications in structural biology. *J. Mol. Graph. Model.* **22:** 377–395.

Fiser, A., Do, R.K., and Sali, A. 2000. Modeling of loops in protein structures. *Protein Sci.* **9:** 1753–1773.

Fiser, A., Feig, M., Brooks III, C.L., and Sali, A. 2002. Evolution and physics in comparative protein structure modeling. *Acc. Chem. Res.* **35:** 413–421.

Fukumori, F. and Hausinger, R.P. 1993a. *Alcaligenes eutrophus* JMP134 "2,4-dichlorophenoxyacetate monooxygenase" is an α-ketoglutarate-dependent dioxygenase. *J. Bacteriol.* **175:** 2083–2086.

———. 1993b. Purification and characterization of 2,4-dichlorophenoxyacetate/α-ketoglutarate dioxygenase. *J. Biol. Chem.* **268:** 24311–24317.

Gohlke, H., Kuhn, L.A., and Case, D.A. 2004. Change in protein flexibility upon complex formation: Analysis of Ras-Raf using molecular dynamics and a molecular framework approach. *Proteins* **56:** 322–337.

Grzyska, P.K., Ryle, M.J., Monterosso, G.R., Liu, J., Ballou, D.P., and Hausinger, R.P. 2005. Steady-state and transient kinetic analyses of taurine/α-ketoglutarate dioxygenase: Effects of oxygen concentration, alternative sulfonates, and active site variants on the Fe(IV) intermediate. *Biochemistry* **44:** 3845–3855.

Hausinger, R.P. 2004. Fe(II)/α-ketoglutarate-dependent hydroxylases and related enzymes. *Crit. Rev. Biochem. Mol. Biol.* **39:** 21–68.

Hausinger, R.P., Fukumori, F., Hogan, D.A., Sassanella, T.M., Kamagata, Y., Takami, H., and Saari, R.E. 1997. Biochemistry of 2,4-D degradation: Evolutionary implications. In *Microbial diversity and genetics of biodegradation* (eds. K. Horikoshi et al.), pp. 35–51. Japan Scientific Press, Tokyo.

Hegg, E.L., Whiting, A.K., Saari, R.E., McCracken, J., Hausinger, R.P., and Que Jr., L. 1999. Herbicide-degrading α-keto acid-dependent enzyme TfdA: Metal coordination environment and mechanistic insights. *Biochemistry* **38:** 16714–16726.

Ho, R.Y.N., Mehn, M.P., Hegg, E.L., Liu, A., Ryle, M.A., Hausinger, R.P., and Que Jr., L. 2001. Resonance Raman studies of the iron(II)-α-keto acid chromophore in model and enzyme complexes. *J. Am. Chem. Soc.* **123:** 5022–5029.

Hogan, D.A., Smith, S.R., Saari, E.A., McCracken, J., and Hausinger, R.P. 2000. Site-directed mutagenesis of 2,4-dichlorophenoxyacetic acid/α-ketoglutarate dioxygenase. Identification of residues involved in metallocenter formation and substrate binding. *J. Biol. Chem.* **275:** 12400–12409.

Laemmli, U.K. 1970. Cleavage of structural proteins during the assembly of the head of bacteriophage T4. *Nature* **227:** 680–685.

Loos, M.A. 1975. Phenoxyalkanoic acids. In *Herbicides chemistry: Degradation and mode of action*, 2d ed. (ed. D.D. Kaufmann), pp. 1–128. Marcel Dekker, Inc, New York.

Lorber, D.M. and Shoichet, B.K. 1998. Flexible ligand docking using conformational ensembles. *Protein Sci.* **7:** 938–950.

Matell, M. 1953. Stereochemical studies on plant growth regulators. VII. Optically active α-(2-methyl-4-chlorophenoxy)-propionic acid and α-(2,4-dichlorophenoxy)-*n*-butyric acid and their steric relations. *Ark. Kemi* **6:** 365–373.

McDonough, M.A., Kavanagh, K.L., Butler, D., Searls, T., Oppermann, U., and Schofield, C.J. 2005. Structure of human phytanoyl-CoA 2-hydroxylase identifies molecular mechanisms of Refsum disease. *J. Biol. Chem.* **280:** 41101–41110.

Miroux, B. and Walker, J.E. 1996. Over-production of proteins in *Escherichia coli*: Mutant hosts that allow synthesis of some membrane protein and globular proteins at high levels. *J. Mol. Biol.* **260:** 289–298.

Mitchell, J.B.O., Nandi, L., McDonald, I.K., Thornton, J.M., and Price, S.L. 1994. Amino/aromatic interactions in proteins: Is the evidence stacked against hydrogen bonding? *J. Mol. Biol.* **239:** 315–331.

Müller, T.A. 2004. "Metabolism of phenoxyalkanoic acid herbicides in *Sphingomonas herbicidovorans* MH. Cloning and characterization of two enantiospecific α-ketoglutarate-dependent dioxygenases and degradation analysis," pp. 167. Ph.D. thesis, Swiss Federal Institute of Technology Zurich, Zurich.

Müller, R.H., Jorks, S., Kleinsteuber, S., and Babel, W. 1999. *Comamonas acidovorans* strain MC1: A new isolate capable of degrading the chiral herbicides dichlorprop and mecoprop and the herbicides 2,4-D and MCPA. *Microbiol. Res.* **154:** 241–246.

Müller, R.H., Kleinsteuber, S., and Babel, W. 2001. Physiological and genetic characteristics of two bacterial strains utilizing phenoxypropionate and phenoxyacetate herbicides. *Microbiol. Res.* **156:** 121–131.

Müller, I., Kahnert, A., Pape, T., Sheldrick, G.M., Meyer-Klaucke, W., Dierks, T., Kertesz, M., and Usón, I. 2004a. Crystal structure of the alkylsulfatase AtsK: Insights into the catalytic mechanism of the Fe(II) α-ketoglutarate-dependent dioxygenase superfamily. *Biochemistry* **43:** 3075–3088.

Müller, T.A., Byrde, S.M., Werlen, C., van der Meer, J.R., and Kohler, H.-P.E. 2004b. Genetic analysis of phenoxyalkanoic acid degradation in *Sphingomonas herbicidovorans* MH. *Appl. Environ. Microbiol.* **70:** 6066–6075.

Müller, I., Stückl, C., Wakeley, J., Kertesz, M., and Usòn, I. 2005. Succinate complex crystal structures of α-ketoglutarate-dependent dioxygenase AtsK. Steric aspects of enzyme self-hydroxylation. *J. Biol. Chem.* **280:** 5716–5723.

Nakajima, K., Yamashita, A., Akama, H., Nakatsu, T., Kato, H., Hashimoto, T., Oda, J., and Yamada, Y. 1998. Crystal structures of two tropinone reductases: Different reaction stereospecificities in the same protein fold. *Proc. Natl. Acad. Sci.* **95:** 4876–4881.

Nickel, K., Suter, M.J.-F., and Kohler, H.-P.E. 1997. Involvement of two α-ketoglutarate-dependent dioxygenases in enantioselective degradation of (*R*)- and (*S*)-mecoprop by *Sphingomonas herbicidovorans* MH. *J. Bacteriol.* **179:** 6674–6679.

O'Brien, J.R., Schuller, D.J., Yang, V.S., Dillard, B.D., and Lanzilotta, W.N. 2003. Substrate-induced conformational changes in *Escherichia coli* taurine/α-ketoglutarate dioxygenase and insight into the oligomeric structure. *Biochemistry* **42:** 5547–5554.

COR-AAD1-00003342
Bayer EX1008 (Part 6 of 9)

Pavel, E.G., Zhou, J., Busby, R.W., Gunsior, M., Townsend, C.A., and Solomon, E.I. 1998. Circular dichroism and magnetic circular dichroism spectroscopic studies of the non-heme ferrous active site in clavaminate synthase and its interaction with α-ketoglutarate cosubstrate. *J. Am. Chem. Soc.* **120:** 743–753.

Price, J.C., Barr, E.W., Glass, T.E., Krebs, C., and Bollinger Jr., J.M. 2003a. Evidence for hydrogen abstraction from C1 of taurine by the high-spin Fe(IV) intermediate detected during oxygen activation by taurine: α-ketoglutarate dioxygenase (TauD). *J. Am. Chem. Soc.* **125:** 13008–13009.

Price, J.C., Barr, E.W., Tirupati, B., Bollinger Jr., J.M., and Krebs, C. 2003b. The first direct characterization of a high-valent iron intermediate in the reaction of an α-ketoglutarate-dependent dioxygenase: A high-spin Fe(IV) complex in taurine/α-ketoglutarate dioxygenase (TauD) from *Escherichia coli*. *Biochemistry* **42:** 7497–7508.

Price, J.C., Barr, E.W., Hoffart, L.M., Krebs, C., and Bollinger Jr., J.M. 2005. Kinetic dissection of the catalytic mechanism of taurine:α-ketoglutarate dioxygenase (TauD) from *Escherichia coli*. *Biochemistry* **44:** 8138–8147.

Proshlyakov, D.A., Henshaw, T.F., Monterosso, G.R., Ryle, M.J., and Hausinger, R.P. 2004. Direct detection of oxygen intermediates in the non-heme Fe enzyme taurine/α-ketoglutarate dioxygenase. *J. Am. Chem. Soc.* **126:** 1022–1023.

Riggs-Gelasco, P.J., Price, J.C., Guyer, R.B., Brehm, J.H., Barr, E.W., Bollinger Jr., J.M., and Krebs, C. 2004. EXAFS spectroscopic evidence for an Fe=O unit in the Fe(IV) intermediate observed during oxygen activation by taurine:α-ketoglutarate dioxygenase. *J. Am. Chem. Soc.* **126:** 8108–8109.

Ryle, M.J., Padmakumar, R., and Hausinger, R.P. 1999. Stopped-flow kinetic analysis of *Escherichia coli* taurine/α-ketoglutarate dioxygenase: Interactions with α-ketoglutarate, taurine, and oxygen. *Biochemistry* **38:** 15278–15286.

Saari, R.E. and Hausinger, R.P. 1998. Ascorbic acid-dependent turnover and reactivation of 2,4-dichlorophenoxyacetic acid/α-ketoglutarate dioxygenase using thiophenoxyacetic acid. *Biochemistry* **37:** 3035–3042.

Saari, R.E., Hogan, D.A., and Hausinger, R.P. 1999. Stereospecific degradation of the phenoxypropionate herbicide dichlorprop. *J. Mol. Catal. B Enzym.* **6:** 421–428.

Sander, C. and Schneider, R. 1991. Database of homology-derived protein structures and the structural meaning of sequence alignment. *Proteins* **9:** 56–68.

Schnecke, V. and Kuhn, L.A. 2000. Virtual screening with solvation and ligand-induced complementarity. *Perspect. Drug Discov. Des.* **20:** 171–190.

Sundaresan, V. and Abrol, R. 2002. Towards a general model for protein-substrate stereoselectivity. *Protein Sci.* **11:** 1330–1339.

———. 2005. Biological chiral recognition: The substrate's perspective. *Chirality* (Suppl.) **17:** S30–S39.

Sukuru, S.C.K., Crepin, T., Milev, Y., Marsh, L.C., Hill, J.B., Anderson, R.J., Morris, J.C., Rohatgi, A., O'Mahony, G., Grøtli, M., et al. 2006. Discovering new classes of *Brugia malayi* asparaginyl tRNA synthetase inhibitors and relating specificity to conformational change. *J. Comput. Aided Mol. Des.* (in press).

Tama, F., Miyashita, O., and Brooks III, C.L. 2004. Flexible multi-scale fitting of atomic structures into low-resolution electron density maps with elastic network normal mode analysis. *J. Mol. Biol.* **337:** 985–999.

Tett, V.A., Willetts, A.J., and Lappin-Scott, H.M. 1997. Biodegradation of the chlorophenoxy herbicide (*R*)-(+)-mecoprop by *Alcaligenes denitrificans*. *Biodegradation* **8:** 43–52.

Trewick, S.C., Henshaw, T.F., Hausinger, R.P., Lindahl, T., and Sedgwick, B. 2002. Oxidative demethylation by *Escherichia coli* AlkB directly reverts DNA base damage. *Nature* **419:** 174–178.

Vaillancourt, F.H., Yeh, E., Vosburg, D.A., O'Connor, S.E., and Walsh, C.T. 2005a. Cryptic chlorination by a non-haem iron enzyme during cyclopropyl amino acid biosynthesis. *Nature* **436:** 1191–1194.

Vaillancourt, F.H., Yin, J., and Walsh, C.T. 2005b. SyrB2 in syringomycin E biosynthesis is a nonheme FeII α-ketoglutarate- and O_2-dependent halogenase. *Proc. Natl. Acad. Sci.* **102:** 10111–10116.

Valegård, K., Terwisscha van Scheltinga, A.C., Lloyd, M.D., Hara, T., Ramaswamy, S., Perrakis, A., Thompson, A., Lee, W.-J., Baldwin, J.E., Schofield, C.J., et al. 1998. Structure of a cephalosporin synthase. *Nature* **394:** 805–809.

Wallace, A.C., Laskowski, R.A., and Thornton, J.M. 1995. LIGPLOT: A program to generate schematic diagrams of protein-ligand interactions. *Protein Eng.* **8:** 127–134.

Wilmouth, R.C., Turnbull, J.J., Welford, R.W.D., Clifton, I.J., Prescott, A.G., and Schofield, C.J. 2002. Structure and mechanism of anthocyanidin synthase from *Arabidopsis thaliana*. *Structure* **10:** 93–103.

Worthing, C.R. and Hance, R.J. 1991. *The pesticide manual—A world compendium*. 9th ed. The British Crop Protection Council, Farnham, UK.

Yu, B., Edstrom, W.C., Benach, J., Hamuro, Y., Weber, P.C., Gibney, B.R., and Hunt, J.F. 2006. Crystal structures of catalytic complexes of the oxidative DNA/RNA repair enzyme AlkB. *Nature* **439:** 879–884.

Zavodszky, M.I. and Kuhn, L.A. 2005. Side-chain flexibility in protein-ligand binding: The minimal rotation hypothesis. *Protein Sci.* **14:** 1104–1114.

Zavodszky, M.I., Sanschagrin, P.C., Korde, R.S., and Kuhn, L.A. 2002. Distilling the essential features of a protein surface for improving protein-ligand docking, scoring, and virtual screening. *J. Comput. Aided Mol. Des.* **16:** 883–902.

Zavodszky, M.I., Lei, M., Day, A.R., Thorpe, M.F., and Kuhn, L.A. 2004. Modeling correlated main-chain motions in proteins for flexible molecular recognition. *Proteins* **57:** 243–261.

Zhang, Z., Ren, J., Stammers, D.K., Baldwin, J.E., Harlos, K., and Schofield, C.J. 2000. Structural origins of the selectivity of the trifunctional oxygenase clavaminic acid synthase. *Nat. Struct. Biol.* **7:** 127–133.

Zhou, J., Kelly, W.L., Bachmann, B.O., Gunsior, M., Townsend, C.A., and Solomon, E.I. 2001. Spectroscopic studies of substrate interactions with clavaminate synthase 2, a multifunctional α-KG-dependent non-heme iron enzyme: Correlation with mechanisms and reactivities. *J. Am. Chem. Soc.* **123:** 7388–7398.

Zipper, C., Nickel, K., Angst, W., and Kohler, H.-P.E. 1996. Complete microbial degradation of both enantiomers of the chiral herbicide mecoprop [(RS)-2-(4-chloro-2-methylphenoxy)propionic acid] in an enantioselective manner by *Sphingomonas herbicidovorans* sp. nov. *Appl. Environ. Microbiol.* **62:** 4318–4322.

COR-AAD1-00003343
Bayer EX1008 (Part 6 of 9)

R. H. Müller[1]

[1] UFZ, Helmholtz-Zentrum für Umweltforschung GmbH, Department Umweltmikrobiologie, Leipzig, Germany.

Research Article

Activity and Reaction Mechanism of the Initial Enzymatic Step Specifying the Microbial Degradation of 2,4-Dichlorophenoxyacetate

Dedicated to Prof. Dr. Wolfgang Babel on the occasion of his 70th birthday

The capability of *Delftia acidovorans* MC1010 ($SdpA^+$, $RdpA^-$) to degrade the herbicides 2,4-dichlorophenoxyacetate (2,4-D) and 4-chloro-2-methylphenoxyacetate (MCPA) was investigated in batch degradation experiments and interpreted in the light of the catalytic activity of the initial enzyme SdpA, an α-ketoglutarate-dependent dioxygenase, catalyzing the cleavage of the ether bond. Dense inocula of this strain degraded high initial 2,4-D concentrations quickly to below the detection limit. The specific degradation rate became slower and the degradation remained incomplete when low initial biomass concentrations and/or 2,4-D concentrations were used. With low initial 2,4-D concentrations, the degradation rate became nearly concentration-independent. This effect was less pronounced with MCPA, a substrate that is more readily degraded by SdpA than 2,4-D. (*S*)-2-(2,4-dichlorophenoxy)propionate ((*S*)-2,4-DP), the favored substrate of SdpA used as comparison, was almost completely utilized under the various conditions. The observed differences were attributed to the easier regeneration of the essential co-substrate α-ketoglutarate with MCPA and above all (*S*)-2,4-DP as a substrate compared to 2,4-D. Decreasing SdpA activity, which was observed during the starvation of MC1010, will contribute to the apparent recalcitrance of 2,4-D. Degradation of 2,4-D by *Bradyrhizobium* sp. RD5-C2, a strain initiating 2,4-D cleavage by a monooxygenase not requiring an organic intermediate as a co-substrate, proceeded to completion despite the approximately 20-fold lower degradation rates compared to those obtained with strain MC1010. However, lowering of biomass concentrations resulted in restricted degradation also with strain RD5-C2. The results were discussed in terms of the kind of co-substrate in the cleavage reaction, the availability of essential intracellular metabolites, and the cells' maintenance demands.

Keywords: Biodegradation, Enzymes, Herbicides, Xenobiotics

Received: April 3, 2007; *revised:* May 5, 2007; *accepted:* May 10, 2007

DOI: 10.1002/elsc.200720198

1 Introduction

Catabolic pathways often require the investment of co-substrates or energy equivalents in the initial metabolic steps [1]. The return is the gain of energy and metabolites from the further degradation of the substrate. A well-known example is the energy expenditure for the initial phosphorylation of glucose. The degradation of xenobiotic compounds often involves oxidative steps carried out by either monooxygenases or dioxygenases. Monooxygenase reactions rely on reduction equivalents that are obtained from the cellular pools existing under a wide range of physiological conditions. The situation is more complicated when certain kinds of dioxygenases initiate the degradation. The cleavage of the ether bond of the herbicide 2,4-dichlorophenoxyacetate (2,4-D) and related compounds is catalyzed by an α-ketoglutarate-dependent dioxygenase (see

Correspondence: R. H. Müller (r.mueller@ufz.de), UFZ, Helmholtz-Zentrum für Umweltforschung GmbH, Department Umweltmikrobiologie, Permoserstrasse 15, D-04318 Leipzig, Germany.

© 2007 WILEY-VCH Verlag GmbH & Co. KGaA, Weinheim

COR-AAD1-00003344
Bayer EX1008 (Part 6 of 9)

Scheme 1). Shortage of α-ketoglutarate as a second oxygen acceptor in the reaction was proposed to limit the degradation [2, 3]. 2,4-D was left unutilized despite the constitutive expression of the dioxygenase [2, 3]. α-Ketoglutarate-dependent dioxygenases are used by the majority of bacteria capable of degrading phenoxyalkanoates such as 2,4-D. Their substrate specificity is largely determined by the alkanoate moiety, whereas substituents of the aromatic ring are less influential. The canonical enzyme 2,4-D/α-ketoglutarate-dioxygenase (TfdA) exerts almost exclusive activity to the phenoxyacetates 2,4-D and 4-chloro-2-methyl-phenoxyacetate (MCPA) [4–6]. Bacteria degrading the racemic 2-phenoxypropionate herbicides [(*RS*)-2-(2,4-dichlorophenoxy)propionate (2,4-DP, dichlorprop) and (*R/S*)-2-(4-chloro-2-methylphenoxy)propionate (MCPP, mecoprop)] possess two enzymes with enantio- and substrate-specific properties. (*R*)-2,4-DP/α-ketoglutarate-dioxygenase (RdpA) from *Delftia acidovorans* MC1 is highly specific for the *R*-enantiomers of 2-phenoxypropionates, whereas the activity to phenoxyacetate derivatives is very weak.

In contrast, (*S*)-2,4-DP/α-ketoglutarate-dioxygenase (SdpA) of MC1 is highly specific to the corresponding *S*-enantiomers of 2-phenoxypropionates but converts phenoxyacetate derivatives also with rather high activity [7, 8]. Two enzymes with similar properties were described for *Sphingomonas herbicidovorans* MH [9, 10]. Only few bacteria use monooxygenases to attack the ether bond in phenoxyalkanoates. Gram-positive bacteria were found to employ a cytochrome P450 enzyme [11], whereas a *Burkholderia cepacia* catalyzed the cleavage of 2,4,5-trichlorophenoxyacetate with a flavoprotein type of monooxygenase [12]. *Bradyrhizobium* spp. were recently found to cleave 2,4-D using a monooxygenase (CadAB) [13, 14], although possessing also a TfdA-like enzyme, called TfdAa [15].

The requirement of α-ketoglutarate has the potential to control the metabolism of phenoxyalkanoate herbicides. Good supply of this metabolite should facilitate the cleavage reaction, whereas deficits would restrict the degradation and have consequences for the environmental fate of the phenoxy acid herbicides. The regeneration of α-ketoglutarate after its decarboxylation in the dioxygenase step (see Scheme 1) is a prerequisite for sustained degradation. Balance equations showed that α-ketoglutarate is more readily regenerated with phenoxypropionate herbicides (2,4-DP) than with phenoxyacetate derivatives [2]. The present investigation was aimed at studying the degradation of 2,4-D with cells that were completely induced. The focus was directed towards low concentrations of the herbicide, thus simulating the typical environmental situation of diffuse soil or groundwater pollution and suspecting a restriction of the regeneration of α-ketoglutarate. The main question was whether the degradation was sustainable and complete under these conditions or if the employed cleavage mechanism, i.e., a α-ketoglutarate-dependent dioxygenase or a reduction equivalent-dependent monooxygenase could explain the observation of residual concentrations in these environments. In addition, the impact of the herbicide concentration on the fate the pollutants are taken into account.

2 Materials and Methods

2.1 Strains and Cultivation

The investigations were performed with *D. acidovorans* strain MC1010 ($SdpA^+$, $RdpA^-$) and strain MC1073 ($RdpA^+$, $SdpA^-$), which are derivatives of *D. acidovorans* MC1 ($SdpA^+$, $RdpA^+$) [16], with *Ralstonia eutropha* JMP134(pJP4) (DSM 4058), and with *Bradyrhizobium* sp. strain RD5-C2 [14] which was kindly provided by Kazuhito Itoh. Strains MC1010 and MC1073 were stored on agar containing mineral salts solution (MSS) and 0.4 g/L (*RS*)-2,4-DP, pH 8.5. The MSS contained [in mg/L]: NH_4Cl, 760; KH_2PO_4, 340; K_2HPO_4, 485; $CaCl_2 \times 6\,H_2O$, 27; $MgSO_4 \times 7\,H_2O$, 71.2; $FeSO_4 \times 7\,H_2O$, 4.98; $CuSO_4 \times 5\,H_2O$, 0.785; $MnSO_4 \times 4\,H_2O$, 0.81; $ZnSO_4 \times 7\,H_2O$, 0.44; $Na_2MoO_4 \times 2\,H_2O$, 0.25. Several colonies from the agar plate were transferred to a shaking flask with PYE medium (1 g/L yeast extract, 1 g/L peptone, 0.6 g/L fructose) and cultivated overnight at 30 °C. Cells were collected under sterile conditions, washed and re-suspended in MMS at a concentration corresponding to about 1 g/L dry mass.

To assure a complete induction of the strains, 0.125 mM of (*S*)-2,4-DP for MC1010 were added, its degradation verified by HPLC analysis [17], and after its completion a further 0.125 mM of (*S*)-2,4-DP supplied. A similar procedure was used for strain MC1073 by adding (*R*)-2,4-DP for induction. Immediately after the completion of degradation, the pre-culture was diluted with MSS to 25 mg/L dry mass, unless stated otherwise. Time delay for the onset of the kinetic experiments was kept low in order to avoid any extended starvation situation which might interfere with the (onset of) herbicide degradation [3]. Phenoxyalkanoate substrates for degradation experiments at final concentrations between 0.1 and 5 mM were added to a series of 50 mL batches in 100-mL flasks. The flasks were incubated by shaking at 30 °C. Samples were taken for substrate and biomass measurements. Strain RD5-C2 was cultivated on MMS in the presence of 0.5 mM 2,4-D. Samples from this culture were diluted to the biomass concentration desired and incubated in the presence of 2,4-D, as described for the other strains.

2.2 Analytics

Phenoxyalkanoate herbicides were determined by HPLC [17]. The biomass concentration was measured by turbidity (E_{700}) and by drying pelletted aliquots to constancy at 105 °C. OD_{700} corresponds to dry mass by a factor of 0.54.

3 Results

3.1 Kinetics of Phenoxyacetate Herbicide Degradation by Strain MC1010

Growing cultures of *D. acidocorans* MC1 and a derivative strain derived from it show a constitutive expression of the respective

© 2007 WILEY-VCH Verlag GmbH & Co. KGaA, Weinheim

COR-AAD1-00003345
Bayer EX1008 (Part 6 of 9)

initial dioxygenases, i.e., RdpA and SdpA. After growth on PYE medium, e.g., the derivative strain MC1010 which harbors and expresses the *sdpA* gene, showed a cleavage activity of 3.7 mmol/h g dry mass in the presence of 0.5 mM (*S*)-2,4-DP and 1 mmol/h g dry mass in the presence of 0.5 mM 2,4-D. The cleavage activity by SdpA was not significantly increased in cell suspension washed and re-suspended in MSS by successively adding two quantities of 0.5 mM (*S*)-2,4-DP leading to an intermediate accumulation of 2,4-dichlorophenol. However, the ortho cleavage pathway was induced during this procedure enabling the complete degradation of the herbicides. Induction was completed within 3 h.

To characterize the herbicide as the variable of the cleavage reaction with whole cells, initial degradation rates were determined depending on the 2,4-D and MCPA concentration. The initial dry biomass concentration was low at 25 mg/L. The kinetic characteristics shown in Fig. 1 indicate proportionality between the rate and herbicide concentration forming a saturation-like shape. This is in general to be expected from any kinetic reaction and indicates that the rate is primarily dependent on one variable, i.e., the external substrate concentration in this case. (Deviations from pure hyperbolic patterns which became apparent in these investigations are not explicitly discussed here). The above fact has to be emphasized because the cleavage of the ether bond of phenoxyalkanoate herbicides is a two-substrate (indeed a three-substrate) reaction which is dependent on the presence of α-ketoglutarate (and oxygen). Although using cells fully induced and derived from non-starved conditions, the size of the intracellular pools of metabolites, finally α-ketoglutarate, is uncertain. Tests with cells that were immediately incubated with 2,4-D after collection from cultures growing on (*S*)-2,4-DP have shown, however, that this should not become a limiting factor for determining the initial rates under the prevailing conditions, since a comparison with cells starved for 0.5 and 2 h before adding the substrate exhibited almost identical initial rates.

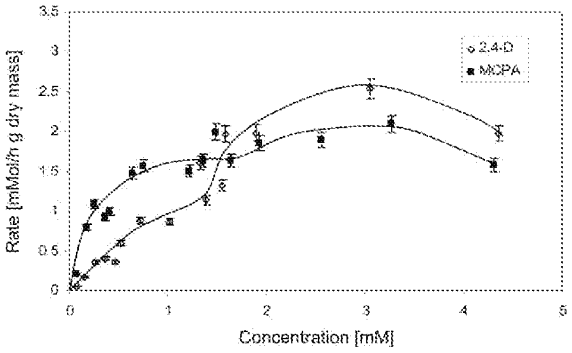


Figure 1. Degradation kinetics of 2,4-D and MCPA with *Delftia acidovorans* MC1010.
Colonies grown under selective conditions on (*RS*)-2,4-DP were used to inoculate complex (PYE) medium. The culture was grown overnight, washed and re-suspended in mineral salts medium. The cells were induced for the complete phenoxyalkanoate degradation pathway by the sequential addition of (*S*)-2,4-DP (two portions to give 0.15 mM each). After the degradation of the inductor, the cells were immediately used for the kinetic experiments. The initial rates were determined by applying strain MC1010 at a concentration of 25 mg/L biomass.

3.2 Degradation of Phenoxyacetate Herbicides at Low Rates

When the decay of substrate is followed for a longer time, the depletion curves show features that remarkably deviated from simple kinetic patterns. The approach to the zero substrate level was strongly dependent on the initial 2,4-D concentration. This is illustrated in detail in Fig. 2. Higher (initial) rates were in general observed at higher initial 2,4-D concentrations, which seems to be a trivial statement. However, the substrate utilization in the initial phases followed pseudo zero order kinetics over a wide range of 2,4-D concentrations, except some vague lag phases during the first two hours. This was succeeded by a pseudo first order pattern in the later phase (see below). Consequently, when the depletion curves that were obtained at similarly low concentrations of, e.g., ca. 0.1 mM 2,4-D were compared (see Fig. 2, inset), significant differences in the rates became evident with a culture that was started at an initial concentration of about 0.1 mM 2,4-D, for instance, and a culture that had reached this concentration after starting from, e.g., 1.5 mM 2,4-D.

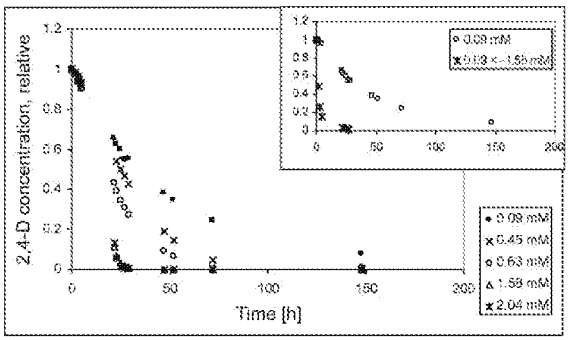


Figure 2. Decay characteristics of 2,4-D depending on the initial substrate concentration.
Pre-cultures of the strain were obtained as indicated in the legend to Fig. 1. Degradation experiments at a biomass concentration of 25 mg/L were performed in the presence of 2,4-D concentrations as indicated. The inset depicts data of 2,4-D utilization with an initial concentration of 0.09 mM as well as the degradation characteristics after attaining about 0.09 mM when starting from 1.58 mM 2,4-D.

It is quite obvious that the rate was distinctly higher with the latter culture at this concentration (0.17 mmol/g h) than with the former sample (0.0147 mmol/g h), and almost complete degradation of 2,4-D was obtained in a short time at higher initial concentrations. The change in biomass concentration which almost doubled during the experiment with the higher 2,4-D concentration that was also included in the rate calculation was not responsible for these differences. Due to

© 2007 WILEY-VCH Verlag GmbH & Co. KGaA, Weinheim

COR-AAD1-00003346
Bayer EX1008 (Part 6 of 9)

the gross differences in 2,4-D decay depending on the different initial substrate concentrations, the rate characteristics at the lower substrate concentration were investigated in more detail. Fig 3A shows graphs of the rate data which were obtained during the run of individual experiments at the low (≤ 150 μM) substrate level. The rate data at decreasing concentration followed a linear pattern which corresponds to first order kinetics. The respective rate constants which were obtained from these graphs were indicated in Fig. 3B. Apparently, the rate constant was hardly influenced at initial 2,4-D concentrations of up to 0.7 mM, whereas there was a steep, i.e. about 10-fold increase in the rate constant by increasing the initial 2,4-D concentration to 2.25 mM. This means that it is not the initial substrate concentration but rather the way of attaining the low substrate level that will influence the degradation rate under these conditions. The further increase of the first order rate constants approached almost linear dependency at the higher substrate levels which means that the rate will increasingly be determined by the initial 2,4-D concentration (see Fig. 3B). The degradation rates had consequences on biomass formation. At rates > 0.3 mmol/h g dry mass, degradation was accompanied by a significant increase of biomass. Although the individual values scattered at the lower rates, the overall picture suggests that the biomass concentration remains more or less constant at the lower range and even decreased at rates falling below 0.1 mmol/g h (see Fig. 4).

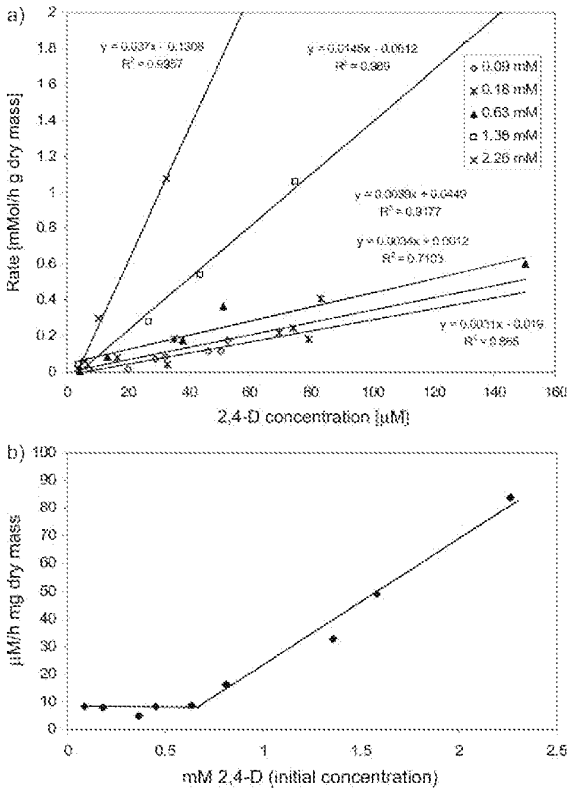


Figure 3. a) Specific rate of 2,4-D degradation at the lower substrate level.
Degradation experiments were started from different initial substrate concentrations as indicated in the legend (biomass concentration 25 mg/L). Specific rates of 2,4-D degradation at a substrate level of ≤ 0.15 mM were indicated by taking into account the changes in the biomass concentration during incubation. Linear dependency of the rate on 2,4-D at this low substrate level is verified by regression analysis.
b) Pseudo first order rate constant at low 2,4-D concentration. Rate constants derived from the 2,4-D decay at ≤ 0.15 mM were equivalent to the slopes of the specific rates over concentration as indicated in Fig. 3A.

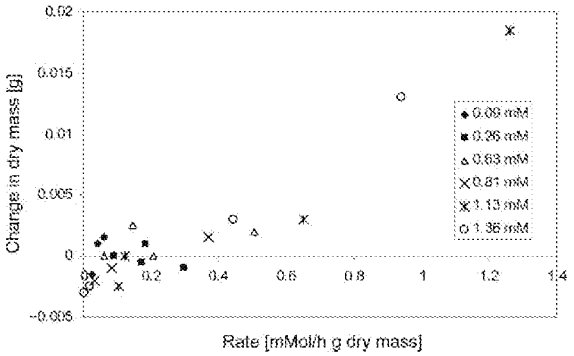


Figure 4. Change in biomass concentration as a function of the initial degradation rate.
The degradation experiments were performed as outlined in Fig. 2 by using an initial biomass concentration of 25 mg/L and substrate concentrations as indicated. The changes in biomass during the incubation intervals were determined and correlated to the degradation rates observed in these intervals.

With MCPA as the substrate of SdpA, higher initial rates were observed at the lower concentration range than were found with 2,4-D (see Fig. 1). When it is taken into account that deficits in the degradation of 2,4-D were observed above all at the lower concentrations at which the initial rates were comparatively low, the question was how MCPA behaved under these conditions. Evidently, the depletion curves deviated significantly from the pattern obtained with 2,4-D (see Fig. 5). The decay characteristics were in general steeper, and the zero substrate level was reached in quite a short time which was also true for the lowest substrate concentration supplied. The residual concentration was below 10 % of the initial one after one day of incubation, and no residual substrate was detected after 3 days with MCPA. This was in contrast to 2,4-D where residual substrate was detected after 6 days of incubation with a concentration being higher the lower the initial substrate concentration was (see Fig. 6). As the gross degradation pathways of both phenoxyacetate derivatives are similar this means that the degradation rate, i.e. finally the time required to utilize a given quantity of the substrate, decides on the fate of the various herbicides.

The addition of α-ketoglutarate (0.5 mM) to batches with low 2,4-D concentrations resulted in an increase of the initial

© 2007 WILEY-VCH Verlag GmbH & Co. KGaA, Weinheim

COR-AAD1-00003347
Bayer EX1008 (Part 6 of 9)

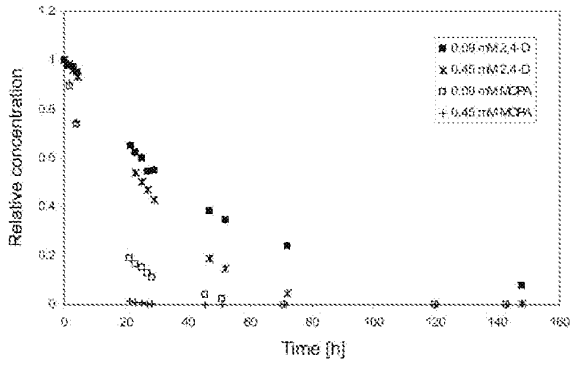


Figure 5. Degradation characteristics of 2,4-D and MCPA at different initial concentrations.
Pre-cultures of the strain were obtained as indicated in the legend to Figs. 1 and 2. Degradation experiments with strain MC1010 at a biomass concentration of 25 mg/L were performed in the presence of both 2,4-D and MCPA at the concentrations indicated.

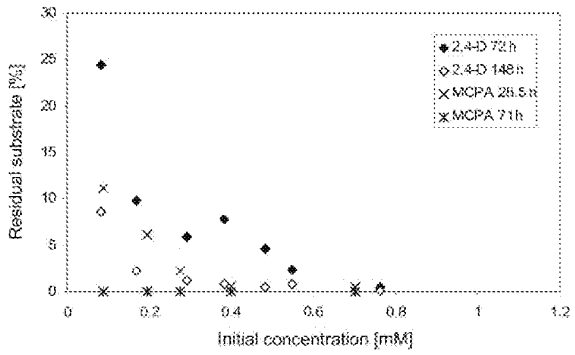


Figure 6. Residual concentration of 2,4-D and MCPA depending on the initial substrate concentration.
Strain MC1010 at a biomass concentration of 25 mg/L was incubated in the presence of the herbicides indicated. The individual data points show the residual herbicide concentrations that were found after the times of incubation as indicated in the legend after starting from different initial concentrations.

rates by a factor of 2–4 and, above all, a complete utilization of the herbicides within one day (not shown). The effect of α-ketoglutarate on the degradability of 2,4-D was verified with non-induced cells of MC1010 grown overnight on complex medium in the presence of α-ketoglutarate. Non-induced cells were used in order to "fix" the intracellular level of metabolites, i.e., to prevent replenishment of the pools through the use of the ortho cleavage pathway. Washed cells (120 mg/L dry mass), immediately derived from the growing culture or starved in substrate-free medium, respectively, were incubated in the presence of streptomycin (100 mg/L). The results showed a direct correlation between the supply of α-ketoglutarate and the extent of degradation which stagnated in the present case after 24 h of incubation. Starvation of these cultures for 4 h before adding the substrate(s) resulted in general in a decrease of the amount of 2,4-D degraded (see Fig. 7).

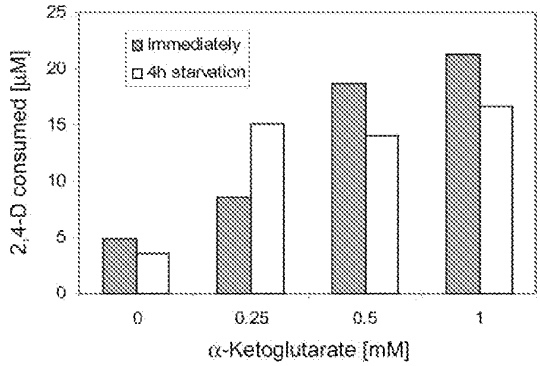


Figure 7. Effect of α-ketoglutarate on the extent of degradation of 2,4-D by strain MC1010.
The culture was grown overnight on peptone/yeast extract medium +2 mM α-ketoglutarate after inoculation with colonies of strain MC1010 grown on agar plates in the presence of (*RS*)-2,4-DP. Cells were washed and re-suspended in mineral salts medium to a concentration of 120 mg/L containing streptomycin at a concentration of 100 mg/L and 2,4-D at a concentration of 0.8 mM. α-Ketoglutarate was added to the suspension as indicated. Starved cells were treated in mineral salts medium in the presence of streptomycin for 4 h before adding α-ketoglutarate and 2,4-D.

3.3 Effect of Biomass Concentration on 2,4-D Degradation

When time is a factor that determines the degree and final result of degradation as stated above and long-lasting runs bear the potential of recalcitrance, the fate of the herbicides should likewise be controlled by the biomass concentration. The absolute quantity of biomass may be considered to be representing a pool of intracellular metabolites and the regenerative potential for α-ketoglutarate and thus, the absolute amount of this compound being present and made available over time. This quantity may be opposed to the absolute amount of the herbicide being available for degradation. Fig. 8 shows the results of degradation experiments with biomass concentrations between 0.25 mg/L and 22 mg/L while using two different 2,4-D concentrations. With a substrate level of about 0.2 mM, a slight decrease of 2,4-D at the lower biomass concentrations was observed, which leveled off later on. Accordingly, the degradation of 2,4-D was slow and incomplete under these conditions. In contrast, the degradation was effective with 22 mg/L dry mass, where the residual concentration decreased to 20.8 µM within 10 days of incubation. The latter was found in a similar manner at a 2,4-D concentration of 1.1 mM (see Fig. 8).

Comparatively high biomass concentrations have the potential, accordingly, to onset and sustain degradation, whereas there is apparently an exhaustion of the capacity at the lower biomass levels. Why a gradual decrease of 2,4-D was not observed with low biomass at the higher substrate level is not evi-

© 2007 WILEY-VCH Verlag GmbH & Co. KGaA, Weinheim

COR-AAD1-00003348
Bayer EX1008 (Part 6 of 9)

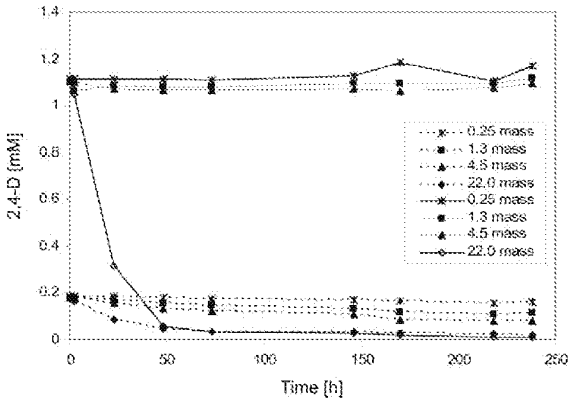


Figure 8. Degradation of 2,4-D depending on the biomass concentration.
Strain MC1010 was pre-cultivated as indicated in Figs. 1 and 2. Induced cells were incubated for a prolonged time in the presence of both 1.1 mM 2,4-D and 0.2 mM 2,4-D at different biomass concentrations ranging from 0.25 mg/L to 22 mg/L (indicated as "mass" in the legend). The degradation of 2,4-D was monitored.

dent at present. For reason of comparison, (*S*)-2,4-DP was also applied as the most favored substrate of SdpA. Degradation of 0.18 mM and 1.1 mM of (*S*)-2,4-DP, respectively, started immediately after adding substrate to the induced cells. At a biomass concentration of 1.3 mg/L and 4.5 mg/L this resulted in levels of (*S*)-2,4-DP as low as 10.85 µM and 1.06 µM, respectively, after 8 days of incubation (not shown). This means that substrates which enable high rates were consumed almost completely by SdpA as this became evident with the results regarding the substrate couple 2,4-D and MCPA (see Figs. 5 and 6). Consequently, any deficits that may result from low absolute degradative capacities, for instance with respect to regenerate α-ketoglutarate, may be compensated for by higher specific activities that enable in general higher overall substrate fluxes in the cell.

For a further reason of comparison, *C. necator* JMP134(pJP4), known to be an effective (quick) 2,4-D degrader, was used. Biomass concentrations as low as 2.5 mg/L led to a complete degradation of 0.5 mM 2,4-D within 1 day. In contrast, *D. acidovorans* MC1073 that solely expresses RdpA as the initial phenoxyalkanoate dioxygenase – an enzyme which exhibits preferred activity to the *R*-enantiomers of dichlorprop and mecoprop but only weak activity toward phenoxyacetate derivatives – did not show any significant degradation of 2,4-D after several days of incubation even with a biomass concentration as high as 250 mg/L.

3.4 Starvation Effects on SdpA Activity

As the degradation experiments lasted several days it was advisable to look for the activity of the initial key enzyme although the enzyme SdpA was constitutively expressed in MC1 and the derivative strains. Moreover, in the presence of low concentrations of 2,4-D (see Fig. 4) conditions were observed, under which growth was not obtained and almost no substrate was consumed, and the activity pattern of SdpA was recorded in starved cells. The results are shown in Fig. 9. As can be seen, within two days of starvation, the activity of MC1010 decreased to about 20 % when measured in the presence of low substrate concentrations. This was true for both 2,4-D and (*S*)-2,4-DP. In contrast, the initial rate was apparently reduced to only 50 % when measured in the presence of 1.6 mM 2,4-D. It should be mentioned, however, that the maximum rates at the respective times were obtained in the latter case only after a lag phase which amounted to 2–5 h after starvation for up to 24 h, but to about 20 h after starvation for more than 2 days. The differences in the maximum rates may potentially be referred to different pool sizes of intracellular metabolites gained after re-supplying the substrate. The fact, however, that the addition of streptomycin (100 mg/L) prevented the increase of activity but left SdpA at a level of about 25 %, when incubated in the presence of 1.6 mM 2,4-D, hints to enzyme inactivation during starvation and the involvement of de novo enzyme synthesis after substrate supply. Accordingly, different effects contribute to the recalcitrant behavior of 2,4-D under these conditions. Details on the enzymatic level remain to be clarified by further studies. It is generally known for α-ketoglutarate-dependent dioxygenases, however, that the lack of the proper substrate (e.g., 2,4-D) leads to enzyme (TfdA) inactivation [18, 19]. In the present experiments this applies for the starvation experiments but might partially apply also to conditions with low 2,4-D concentrations. The accumulation of 2,4-dichlorophenol was not observed under any conditions in degradation experiments with starved cells, which hints to the functional integrity of the ortho cleavage pathway.

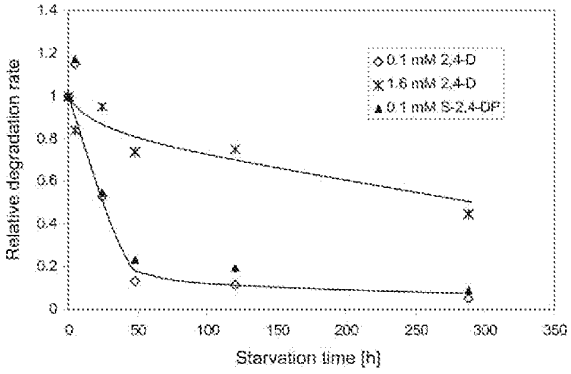


Figure 9. Degradation rate of 2,4-D and (*S*)-2,4-DP by starved cells.
Cells of strain MC1010 were pre-cultivated and induced as indicated in the legend to Fig. 1. Induced cells were re-suspended in mineral salts solution at a concentration of 25 mg/L and incubated at 30 °C without providing substrate. At the times indicated, 2,4-D was added to aliquots of the starved suspension to give concentrations of 0.1 mM and 1.6 mM and the degradation of 2,4-D was monitored. The rates were derived from that part of the progress curves where the substrate degradation was maximal. These rates were referred to the initial rates that were obtained before starting the starvation experiment.

© 2007 WILEY-VCH Verlag GmbH & Co. KGaA, Weinheim

COR-AAD1-00003349
Bayer EX1008 (Part 6 of 9)

The reduced activity in starved cells had consequences on the fate of the herbicides. The degradation was severely retarded under these conditions and about 10% of 2,4-D remained unutilized at the respective times indicated (see Fig. 10). In contrast, the degradation of 0.1 mM (*S*)-2,4-DP was complete despite the low rate.

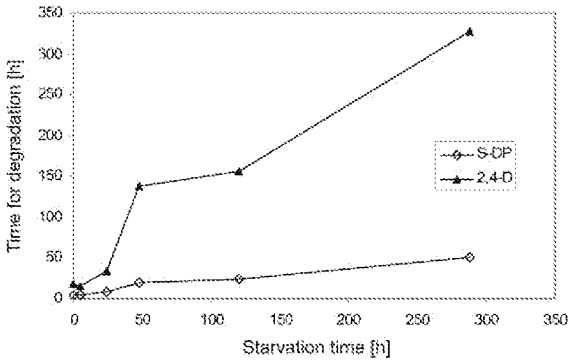


Figure 10. Time required for the degradation of 0.1 mM 2,4-D and (*S*)-2,4-DP by starved cells.
Starved cells as obtained according to the legend to Fig. 9 were incubated in the presence of various herbicides. Degradation was completed for (*S*)-2,4-DP within the time indicated. In the case of 2,4-D, about 10% of the initial substrate concentration remained unutilized at the respective times.

3.5 Monooxygenase Type Microorganisms

The use of strain *Bradyrhizobium* sp. RD5-C2, which expresses CadAB monooxygenase activity in addition to α-ketoglutarate-dependent TfdAa dioxygenase for 2,4-D cleavage, showed a different picture. The degradation rate of 2,4-D was low in general. At a 2,4-D concentration of 0.2 mM, the rate amounted to 11.8 μmol/h g dry mass. This was by a factor of 20 lower than that observed with MC1 at this concentration. The degradation with strain RD5-C2 showed that complete degradation was possible with such low specific activity at a biomass concentration of about 90 mg/L (see Fig. 11). However, by lowering the biomass concentration, the specific rate was reduced. In reducing the dry mass to e.g. 30 mg/L the specific rate decreased to 7.8 μmol/h g dry mass. At biomass concentrations of 5 mg/L, a significant degradation over a period of 15 days was not detected. Further attempts are required to elucidate this pattern in more detail.

4 Discussion

The microbial degradation of 2,4-D is known for a long time and was mainly correlated to the activity of *Ralstonia eutropha* (*Alcaligenes eutrophus*) JMP134(pJP4) [20, 21], now *Cupriavidus necator* [22]. 2,4-D appeared as an easily degradable substrate in these investigations that did not raise severe problems. However, 2,4-D may behave recalcitrant under certain conditions, although catalytic activity for attacking this compound

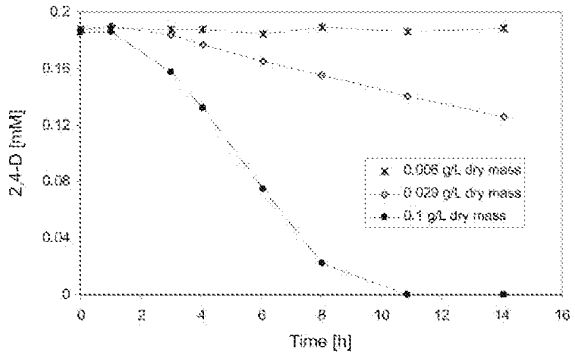


Figure 11. Degradation of 2,4-D by *Bradyrhizobium* sp. RD5-C2 depending on the biomass concentration.
The strain was pre-cultivated on 2,4-D. Biomass from a growing culture was washed and re-suspended in mineral salts solution to give the concentrations as indicated. Incubation was performed in the presence of 0.2 mM 2,4-D.

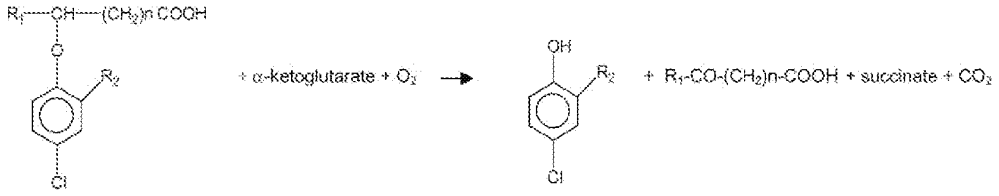
was expressed. This was experienced in earlier experiments using strains *D. acidovorans* MC1 and *Rhodoferax* sp. P230, which expressed the initial dioxygenases, involved in ether bond cleavage, but was not induced for enzymes to further degrade the phenolic intermediates. The present investigations with induced cells of *D. acidovorans* MC1010 (*sdpA*$^+$, *rdpA*$^-$), however, revealed similar deficits under certain conditions. Hence, the presence of catalytic activity is, although a prerequisite, not sufficient to enable an effective and complete degradation of 2,4-D in each case. This became evident from different observations, above all from the decay characteristics of 2,4-D in dependence of the initial conditions. For instance, lowering of the degradation rate by lowering the 2,4-D concentration or by reducing the volume activity in microcosm experiments, respectively, led to an increase of the fraction of 2,4-D that remained unutilized during the incubation with *D. acidovorans* MC1010. This means that degradation and its rates were not solely determined by 2,4-D, but to an essential extend by factors other than the external herbicide concentration. Time as a factor, that controlled several intracellular processes, seemed to play a significant role in this process. To explain the various effects in 2,4-D degradation, an answer should come from taking into account the entire metabolism of the bacterial strains involved.

The main focus was directed on the specific reaction mechanism. Cleavage of 2,4-D is carried out by an α-ketoglutarate-dependent dioxygenase in MC1010 as it holds true for phenoxyalkanoate herbicides with most of the strains. The availability of the second substrate in this reaction has the potential to control the degradation of the herbicide. α-Ketoglutarate is oxidatively decarboxylated in this step and must be regenerated in order to maintain catalysis (see Schemes 1 and 2A, B). Use and delivery of α-ketoglutarate is strongly coupled to the overall metabolism, whereas the replenishment of the metabolites, in turn, depends on the initial cleavage reaction. It is important to notice that the regeneration of α-ketoglutarate is accompanied by a substantial waste of carbon in the form of CO_2 in the case of 2,4-D, if regeneration is assumed to proceed

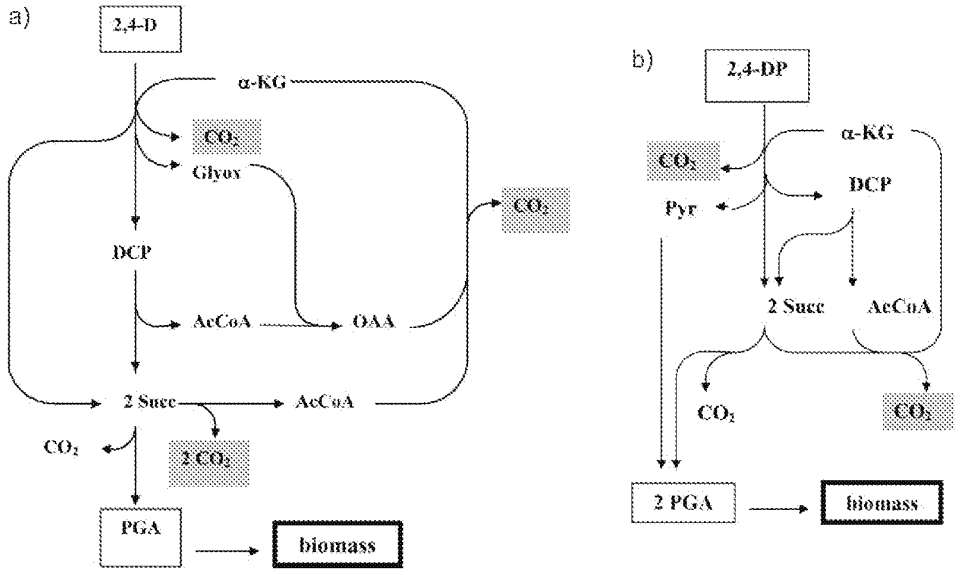
© 2007 WILEY-VCH Verlag GmbH & Co. KGaA, Weinheim

COR-AAD1-00003350
Bayer EX1008 (Part 6 of 9)

via the glyoxylate and TCA cycle (see Scheme 2A). In contrast, less than half of that amount of CO_2 is lost by regenerating α-ketoglutarate from the cleavage products of 2,4-DP (see Scheme 2B). The loss of carbon in the former case will increase the deficit in the availability of metabolites in addition to the constraints raised by kinetic terms with this substrate. The retardation and even cessation of degradation that was observed in the investigation was attributed to such processes as a likely explanation. Starvation was shown previously to result in an enforced recalcitrance of 2,4-D, which could be overcome by the addition of α-ketoglutarate [3], as was shown in the present investigation. The impact of the catalytic activity on the fate of phenoxyalkanoate herbicides was convincingly shown by applying either 2,4-D or MCPA. Both substrates use SdpA for cleavage, but the latter is favored in comparison to 2,4-D as documented by the first order rate constants (defined by k_{cat}/K_m), which were 5.9 $\mu mol^{-1}min^{-1}$ and 2 $\mu mol^{-1}min^{-1}$, respectively [7]. Consequently, MCPA was more easily degraded and almost completely utilized with strain MC1010 in comparison to 2,4-D (see Fig. 5). This was in particular true at lower substrate levels due to the higher affinity of SdpA for MCPA (see Fig. 1). Decreased activity of SdpA observed during starvation should have contributed to the overall effect of recalcitrance. The fact, however, that complete degradation was possible under these conditions with (*S*)-2,4-DP, which as the most favored substrate of this enzyme reaction enables the highest rates, supports the assumption that the level of α-ketoglutarate after the cleavage of this substrate was sufficient to satisfy the various requirements in metabolism. Similar effects with respect to enzyme activity were observed with strain MH. SdpA was shown to be constitutively expressed also in this strain [9]. However, decreased activity of SdpA was observed during starvation despite the fact that the expression of the *sdpA* gene was verified due to mRNA probing. The authors [23] explain this behavior by putative regulation effects on a transcriptional or posttranslational level.



Scheme 1. Cleavage of phenoxyalkanoate herbicides by α-ketoglutarate-dependent dioxygenase mechanism. (with R1 = H, CH_3; R2 = Cl, CH_3; n = 0, 2, in respective combinations for the usual herbicides).



Scheme 2A. Pathway proposed for the regeneration of α-ketoglutarate (a-KG) and for the synthesis of 3-phosphoglycerate (PGA) as a precursor for biomass synthesis during the conversion of 2,4-D.
(Abbreviations: AcCoA, acetyl-coenzymeA; DCP, dichlorophenol; glyox, glyoxalate; OAA. oxalacetate; Succ, succinate.
In gray: CO_2 lost during the regeneration of α-ketoglutarate).
Scheme 2B. Pathway proposed for the regeneration of α-ketoglutarate (a-KG) and for the synthesis of 3-phosphoglycerate (PGA) as a precursor for the biomass synthesis during the conversion of 2,4-DP.
Abbreviations: Pyr, pyruvate (for other details see Scheme 2A).

© 2007 WILEY-VCH Verlag GmbH & Co. KGaA, Weinheim

COR-AAD1-00003351
Bayer EX1008 (Part 6 of 9)

The main cause for exhausting metabolites should result from the demands for maintenance purposes. Cells supplied with a high initial 2,4-D concentration were expectedly fast, and the substrate was (almost) completely degraded in a comparatively short time. Cell maintenance requires a steady delivery of energy which should easily be satisfied under these conditions. Even growth occurred in such batches (see Fig. 4), which indicates that the intracellular pools seemed to be in equilibrium. Cells that started from a low initial substrate concentration did not reach a zero substrate level even after extended incubation within the framework of these experiments. Most likely, this was attributed to a deficit in metabolites, finally α-ketoglutarate. This was supported by the fact that the addition of this compound improved the degradation of 2,4-D. The specific maintenance rate is assumed to be almost constant over a wide range of growth conditions. The present investigation with *D. acidovorans* showed that consumption rates of at least 0.3 to 0.5 mmol/h g dry mass of strain MC1 were required to make 2,4-D available for biomass synthesis (see Fig. 4). Such a rate will be obtained at substrate concentrations of about 0.25–0.4 mmol 2,4-D (see Fig. 1). This is in the order of 0.4–0.6 mmol 2,4-D/g h determined in former experiments as a threshold to satisfy maintenance requirements in strain MC1 [24]. It is also similar to a value of 0.75 mmol 2,4-D/g h required for maintenance purposes of *C. necator* JMP134(pJP4) [25]. With *Bradyrhizobium* sp. RD5-C2, sustained 2,4-D consumption was apparently possible at significant lower degradation rates. At present the authors are not aware of the effects which might contribute to this behavior. In general, they assume that the reduction equivalents necessary to run the monooxygenase reaction should more easily be made available by the common metabolism. Moreover, there should be in general a reduced maintenance capability with such type of oligotrophic bacteria [26].

Substrate fluxes were apparently adequately adjusted in strains like JMP134(pJP4) for enabling fast growth on 2,4-D [21]. TfdA catalyzes 2,4-D cleavage according to a first order rate constant of 30.2 $\mu mol^{-1} min^{-1}$ [5]. But even this high level of TfdA activity was apparently not sufficient to exploit 2,4-D for effective growth. This seemed to require the presence and expression of two operons coding for the entire set of degradative enzymes [27, 28]. It was above all some gene-dose effect with the enzymes of the modified ortho cleavage pathway whose concerted action enabled adequate degradation rates [29, 30]. The degradative pathway seems to be integrated into the metabolic framework of *C. necator* JMP134 in a manner which guarantees balanced (re-)generation of α-ketoglutarate. This seems to be true also with other strains: conjugative transfer of the plasmid pJP4 that carry the degradative genes led to the establishment of strains in natural biotopes by using 2,4-D as the growth substrate [31–34]. That the metabolic background is important for using 2,4-D became evident in transconjugant strains of *Halomonas* sp. that received pJP4: these strains showed less effective utilization of 2,4-D, and growth on this substrate was more difficult to stabilize [35, 36]. In *D. acidovorans* P4a, degradative genes for 2,4-D were detected, which clustered in only one operon though some of the genes (*tfdC*, *tfdE*) were also doubled [37]. With *D. acidovorans* MC1, the genetic background of phenoxyalkanoate degradation was not completely elucidated, however, there is evidence that the initial degradative dioxygenases are singular in this strain too [38]. This means that the expression of one set of genes was in general sufficient in these strains to become productive for 2,4-D degradation, but deficits became evident when higher flux rates were required, for instance at lower substrate levels.

The present results let us speculate that the establishment of degradative microorganisms down-gradient to pollution plumes in e.g. aquifers might be limited at threshold concentrations of 2,4-D that nothing but enabled maintenance. Consequently, such low levels of pollutants will not further be productively degraded in dynamic systems and may lead to diffuse distribution of the herbicides which is frequently observed in groundwater [39–41]. It may even become a permanent problem in biotopes which (exclusively) harbor strains that express enzymes like SdpA (or RdpA). Restrictions in metabolic capability might hold for biotopes which exhibit a limited pool of genetic information and/or where the distribution of genetic information is restricted due to a low titer of microorganisms. Such a scenario might apply to environments with poor biodiversity, e.g., aquifers. Although strains, which harbor *tfdA* appear to be spread world-wide and were easily isolated from agricultural soil [18, 42–44] or contaminated sites [16, 45], undisturbed environments presented another picture. Inspection of over 700 samples from pristine soil enriched with 2,4-D and 3-chlorobenzoate (3-CB), respectively, resulted in the detection of only 5 samples which showed some sustained carbon elimination from 2,4-D, but neither of them showed stable degradative properties [46]. Most likely, this phenomenon can be explained by mechanisms as shown in the present and former investigations [2, 3], i.e., some pseudo-recalcitrance of 2,4-D due to the metabolic disposition, and finally starvation effects in potential degradative strains. This is supported by the fact that 3-CB degradation appeared more widespread due to the above study and was easily observed in the enrichment cultures [46]. This seems again to be in accordance with our initial theses according to which the kind of the oxygenase step should be of crucial impact on the degradative properties. Although this is carried out by a dioxygenase also with 3-CB but involves reduction equivalents as a co-substrate for forming the dihydro-dihydroxy-intermediate, the overall reaction becomes balanced as reduction equivalents were gained by the succeeding dehydrogenase step used for the re-aromatization of the above intermediate to catechol. The necessity of a co-substrate does, accordingly, not become a rate-determining parameter which was as effective in this intramolecular dioxygenase mechanism as found in the intermolecular mechanism with the α-ketoglutarate-dependent type of dioxygenase.

The latter should also hold for the monooxygenase-catalyzed cleavage, which in general uses reduction equivalents as a co-substrate. The experiments with strain RD5-C2 indicated that the degradation of 2,4-D down to zero was more easily enabled. Nevertheless, some impact of the biomass concentration became evident in this example too, which is in line with the above results. The final answer on the fate of 2,4-D in biotopes will be given by the joint action of degraders of different type within biocenoses. This was reflected to some extent by results in which data from laboratory models were correlated to the degradative patterns of herbicides in aquifers. Degradation was found in this study above all in biotopes from exposed sites,

© 2007 WILEY-VCH Verlag GmbH & Co. KGaA, Weinheim

COR-AAD1-00003352
Bayer EX1008 (Part 6 of 9)

whereas the herbicides resided for a long time in samples derived from untreated soil [47, 48]. Most interesting, experiments in the microgram range of 2,4-D showed that degradation did run even under these conditions and was connected to biomass synthesis down to concentration of 1 μg/L, as suggested by these authors due to the decay characteristics [49, 50]. The demonstration of complete removal of the herbicide as indicated in these experiments seems to promise the elimination of 2,4-D under in situ conditions. The fact, however, that a range of biotopes did not show degradation of this compound even after prolonged incubation [46, 49] emphasizes the relevance of asking for the degradative activity and its limits.

Acknowledgements

The author grateful acknowledges the technical assistance of Cornelia Schumann and Monika Neytschev.

Abbreviations

2,4-D	2,4-dichlorophenoxyacetate
2,4-DP	(*R*/*S*)-2-(2,4-dichlorophenoxy)propionate
MCPA	4-chloro-2-methylphenoxyacetate
MCPP	(*R*/*S*)-2-(4-chloro-2-methylphenoxy)propionate
RdpA	(*R*)-(2,4-dichlorophenoxy)propionate/α-ketoglutarate-dioxygenase
SdpA	(*S*)-(2,4-dichlorophenoxy)propionate/α-ketoglutarate-dioxygenase
TfdA	2,4-dichlorophenoxyacetate/α-ketoglutarate-dioxygenase

References

[1] W. Babel, R. H. Müller, Microorganisms as catalysts for the decontamination of ecosystems, in *Encyclopedia of Life Support Systems*, Eolss Publ., Oxford (UK) **2002**, E6-58-06-06, pp 1–24. www.eolss.net

[2] R. H. Müller, W. Babel, A theoretical study on the metabolic requirements resulting from α-ketoglutarate-dependent cleavage of phenoxyalkanoates, *Appl. Environ. Microbiol.* **2000**, *66*, 339–344.

[3] R. H. Müller, W. Babel, Pseudo-recalcitrance of phenoxyalkanoate herbicides caused by a shortage of α-ketoglutarate, *Acta Biotechnol.* **2001**, *21*, 227–242.

[4] F. Fukumori, R. P. Hausinger, *Alcaligenes eutrophus* JMP 134 "2,4-dichlorophenoxyacetate monooxygenase" is an α-ketoglutarate dependent dioxygenase, *J. Bacteriol.* **1993**, *175*, 2083–2086.

[5] F. Fukumori, R. P. Hausinger, Purification and characterization of 2,4-dichlorophenoxyacetate/α-ketoglutarate dioxygenase, *J. Biol. Chem.* **1993**, *268*, 24311–24317.

[6] E. R. Saari, D. A. Hogan, R. P. Hausinger, Stereospecific degradation of the phenoxypropionate herbicide dichlorprop, *J. Mol. Catal. B: Enzymatic* **1999**, *6*, 421–428.

[7] A. Westendorf, R. H. Müller, W. Babel, Purification and characterization of the enantiospecific dioxygenases from *Delftia acidovorans* MC1 initiating the degradation of phenoxypropionate and phenoxyacetate herbicides, *Acta Biotechnol.* **2003**, *23*, 3–17.

[8] A. Westendorf, D. Benndorf, T. Pribyl, H. Harms, R. H. Müller, Kinetic traits and enzyme form patterns of (*R*)-2,4-dichlorophenoxypropionate/α-ketoglutarate dioxygenase (RdpA) after expression in different bacterial strains. *Eng. Life Sci.* **2006**, *6*, 552–559.

[9] K. Nickel, M. J. F. Suter, H. P. E. Kohler, Involvement of two α-ketoglutarate-dependent dioxygenases in enantioselective degradation of (*R*)- and (*S*)-mecoprop by *Sphingomonas herbicidovorans* MH, *J. Bacteriol.* **1997**, *179*, 6674–6679.

[10] T. A. Muller, T. Fleischmann, J. R. van der Meer, H. P. Kohler, Purification and characterization of two enantioselective alpha-ketoglutarate-dependent dioxygenases, RdpA and SdpA, from *Sphingomonas herbicidovorans* MH, *Appl. Environ. Microbiol.* **2006**, *72*, 4853–4861.

[11] H. Sträuber, R. H. Müller, W. Babel, Evidence of cytochrome P450-catalyzed cleavage of the ether bond of phenoxybutyrate herbicides in *Rhodococcus erythropolis* K2-3, *Biodegradation* **2003**, *14*, 41–50.

[12] L. Xun, K. B. Wagnon, Purification and properties of component B of 2,4,5-trichlorophenoxyacetate oxygenase from *Pseudomonas cepacia* AC1100, *Appl. Environ. Microbiol.* **1995**, *61*, 3499–3502.

[13] W. Kitagawa, S. Takami, K. Miyauchi, E. Masai, Y. Kamagata, J. M. Tiedje et al., Novel 2,4-dichlorophenoxyacetic acid degradation genes from oligotrophic *Bradyrhizobium* sp. strain HW13 isolated from a pristine environment, *J. Bacteriol.* **2002**, *184*, 509–518.

[14] K. Itoh, Y. Tashiko, K. Uobe, Y. Kamagata, K. Suyama, H. Yamamoto, Root nodule *Bradyrhizobium* spp. harbor *tfdAa* and *cadA*, homologous with genes encoding 2,4-dichlorophenoxyacetic acid-degrading proteins, *Appl. Environ. Microbiol.* **2004**, *70*, 2110–2118.

[15] K. Itoh, R. Kanda, Y. Sumita, H. Kim, Y. Kamagata, K. Suyama, et al., *tfdA*-like genes in 2,4-dichlorophenoxyacetic acid-degrading bacteria belonging to the *Bradyrhizobium-Agromonas-Nitrobacter-Afipia* cluster in *α-Proteobacteria*, *Appl. Environ. Microbiol.* **2002**, *68*, 3449–3454.

[16] R. H. Müller, S. Kleinsteuber, W. Babel, Physiological and genetic characteristics of two bacterial strains exhibiting phenoxyacetate- and phenoxypropionate-utilizing activity, *Microbiol. Res.* **2001**, *156*, 121–131.

[17] K. H. Oh, O. H. Tuovinen, Degradation of 2,4-dichlorophenoxyacetic acid by mixed cultures of bacteria, *J. Ind. Microbiol.* **1990**, *6*, 275–278.

[18] A. Liu, Y. N. Ho, L. Que, Jr, Alternative reactivity of an α-ketoglutarate-dependent iron(II) dioxygenase: enzyme self-hydroxylation, *J. Am. Chem. Soc.* **2001**, *123*, 5126–5127.

[19] Y. M. Chiou, L. Que, Jr, Models for α-keto acid-dependent non-heme iron enzymes: structures and reactivity of $[Fe^{II}(L)(O2CCOPh)](ClO_4)$ complexes, *J. Am. Chem. Soc.* **1995**, *117*, 3999–4013.

[20] R. H. Don, J. M. Pemberton, Properties of six pesticide degradation plasmids isolated from *Alcaligenes paradoxus* and *Alcaligenes eutrophus*, *J. Bacteriol.* **1981**, *145*, 681–686.

[21] D. H. Pieper, W. Reineke, K. H. Engesser, H. J. Knackmuss, Metabolism of 2,4-dichlorophenoxyacetic acid, 4-chloro-2-

© 2007 WILEY-VCH Verlag GmbH & Co. KGaA, Weinheim

COR-AAD1-00003353
Bayer EX1008 (Part 6 of 9)

methylphenoxyacetic acid, and 2- methylphenoxyacetic acid by *Alcaligenes eutrophus* JMP 134, *Arch. Microbiol.* **1988**, *151*, 365–371.

[22] P. Vandamme, T. Coeyne, Taxonomy of the genus *Cupriavidus*: a tale of lost and found, *Int. J. System. Evol. Microbiol.* **2004**, *54*, 2285–2289.

[23] T. A. Muller, S. M. Byrde, C. Werlen, J. R. van der Meer, H. P. Kohler, Genetic analysis of phenoxyalkanoic acid degradation in *Sphingomonas herbicidovorans* MH, *Appl. Environ Microbiol.* **2004**, *70*, 6066–6075.

[24] R. H. Müller, W. Babel, *Delftia acidovorans* MC1 resists high herbicide concentrations: a study of nutristat growth on (RS)-2-(2,4-dichlorophenoxy)propionate and 2,4-dichlorophenoxyacetate, *Biosci. Biotechnol. Biochem.* **2004**, *68*, 622–630.

[25] R. H. Müller, W. Babel, Measurement of growth at very low rates ($\mu \geq 0$), an approach to study the energy requirement for the survival of *Alcaligenes eutrophus* JMP 134, *Appl. Environ. Microbiol.* **1996**, *62*, 147–151.

[26] R. Y. Morita, *Bacteria in Oligotrophic Environments*, Chapman and Hall, New York **1997.**

[27] R. Ravatn, S. Studer, D. Springael, A. J. B. Zehnder, J. R. van der Meer, Chromosomal integration, tandem amplification, and deamplification in *Pseudomonas putida* F1 of a 105-kilobase genetic element containing the chlorocatechol degradative genes from *Pseudomonas* sp. strain B13, *J. Bacteriol.* **1998**, *180*, 4360–4369.

[28] M. Klemba, B. Jacobs, R. M. Wittich, D. Pieper, Chromosomal integration of tcb chlorocatechol degradation pathway genes as a means of expanding the growth substrate range of bacteria to include haloaromatics, *Appl. Environ. Microbiol.* **2000**, *66*, 3255–3261.

[29] D. Perez-Pantoja, L. Guzman, M. Manzano, D. H. Pieper, B. Gonzales, Role of $tfdC_ID_IE_IF_I$ and $tfdC_{II}D_{II}E_{II}F_{II}$ gene modules in catabolism of 3-chlorobenzoate by *Ralstonia eutropha* JMP134 (pJP4), *Appl. Environ. Microbiol.* **2000**, *66*, 1602–1608.

[30] C. M. Laemmli, J. H. J. Leveau, A. J. B. Zehnder, J. R. van der Meer, Characterization of a second *tfd* cluster for chlorophenol and chlorocatechol metabolism on plasmid pJP4 in *Ralstonia eutropha* JMP134 (pJP4), *J. Bacteriol.* **2000**, *182*, 4165–4172.

[31] G. D. DiGiovanni, J. W. Neilson, I. L. Pepper, N. A. Sinclar, Gene transfer of *Alcaligenes eutrophus* JMP134 plasmid pJP4 to indigenous soil recipients, *Appl. Environ. Microbiol.* **1996**, *62*, 2521–2526.

[32] E. M. Top, P. van Daele, N. de Saeyer, L. J. Forney, Enhancement of 2,4-dichlorophenoxyacetic acid (2,4-D) degradation in soil by dissemination of catabolic plasmids, *Antonie van Leeuwenhoek* **1998**, *73*, 87–94.

[33] D. T. Newby, K. L. Josephson, I. L. Pepper, Detection and characterization of plasmid pJP4 transfer to indigenous soil bacteria, *Appl. Environ. Microbiol.* **2000**, *66*, 290–296.

[34] E. M. Top, D. Springael, The role of mobile genetic elements in bacterial adaptation to xenobiotic compounds, *Curr. Opin. Biotechnol.* **2003**, *14*, 262–269.

[35] S. Kleinsteuber, R. H. Müller, W. Babel, Expression of the 2,4-D degradative pathway of pJP4 in a moderately haloalkaliphilic soda lake isolate, *Halomonas* sp. EF43, *Extremophiles* **2001**, *5*, 375–384.

[36] B. Kiesel, R. H. Müller, S. Kleinsteuber, Adaptive potential of alkaliphilic bacteria towards chloroaromatic substrates assessed by a *gfp*-tagged 2,4-D degradation plasmid, *Eng. Life Sci.* **2007**, *4 (7)*, 361–372. DOI: 10.1002/elsc.200720200

[37] D. Hoffmann, S. Kleinsteuber, R. H. Müller, W. Babel, Structural organization and localization of the chlorocatechol pathway in the 2,4-D degrading alkalitolerant strain *Delftia acidovorans* P4a, *Microbiology* **2003**, *149*, 2545–2556.

[38] K. M. Schleinitz, S. Kleinsteuber, T. Vallaeys, W. Babel, The genetic background of 2,4-dichlorophenoxypropionate cleavage in *Delftia acidovorans* MC1, *Appl. Environ. Microbiol.* **2004**, *70*, 5357–5365.

[39] G. Fielding, Leaching of phenylalkanoic acid herbicides from farmland, *Sci. Total Environ.* **1995**, *168*, 11–18.

[40] R. D. Wilson, J. Geronimo, J. A. Armbruster, 2,4-D dissipation in field soils after applications of 2,4-D dimethylamine salt and 2,4-D 2-ethylhexyl ester, *Environ. Toxicol. Chem.* **1997**, *16*, 1239–1246.

[41] *Groundwater Quality and Quantity in Europe*, environmental assessment report No. 3 (Ed.: European Environment Agency), Copenhagen (Denmark) **1999**.

[42] R. R. Fulthorpe, A. H. Rhodes, O. V. Maltseva, W. E. Holben, J. M. Tiedje, 2,4-dichlorophenoxyacetic acid-degrading bacteria contain mosaics of catabolic genes, *App. Environ. Microbiol.* **1995**, *61*, 3274–3281.

[43] J. O. Ka, W. E. Holben, J. M. Tiedje, Genetic and phenotypic diversity of 2,4-dichlorophenoxyacetic acid (2,4-D)-degrading bacteria isolated from 2,4-D-treated field soils, *Appl. Environ. Microbiol.* **1994**, *60*, 1106–1115.

[44] T. Vallaeys, L. Courde, C. McGowan, A. D. Wright, R. R. Fulthorpe, Phylogenetic analyses indicate independent recruitment of diverse gene cassettes during assemblage of the 2,4-D catabolic pathway, *FEMS Microbiol. Ecol.* **1999**, *28*, 373–382.

[45] D. Hoffmann, R. H. Müller, B. Kiesel, W. Babel, Isolation and characterization of an alkaliphilic bacterium capable of growing on 2,4-dichlorophenoxyacetic acid and 4-chloro-2-methylphenoxyacetic acid, *Acta Biotechnol.* **1996**, *16*, 121–131.

[46] R. R. Fulthorpe, A. N. Rhodes, J. M. Tiedje, Pristine soils mineralize 3-chlorobenzoate and 2,4-dichlorophenoxyacetate via different microbial populations, *Appl. Environ. Microbiol.* **1996**, *62*, 1159–1166.

[47] N. Tuxen , J. R. de Lipthay, H. J. Albrechtsen, J. Aamand, P. L. Bjerg, Effect of exposure history on microbial herbicide degradation in an aerobic aquifer affected by a point source, *Environ. Sci. Technol.* **2002**, *36*, 2205–2212.

[48] J. R. de Lipthay, N. Tuxen, K. Johnsen, L. H. Hansen, H. J. Albrechtsen, P. L. Bjerg et al., In situ exposure to low herbicide concentrations affects microbial population composition and catabolic gene frequency in an aerobic shallow aquifer, *Appl. Environ. Microbiol.* **2003**, *69*, 461–467.

[49] H. J. Albrechtsen, M. S. Mills, J. Aamand, P. L. Bjerg, Degradation of herbicides in shallow Danish aquifers: an integrated laboratory and field study, *Pest Manag. Sci.* **2001**, *57*, 341–350.

[50] L. Torang, N. Nyholm, H. J. Albrechtsen, Shifts in biodegradation of the herbicides MCPP and 2,4-D at low concentrations in aerobic aquifer materials, *Environ. Sci. Technol.* **2003**, *37*, 3095–3103.

© 2007 WILEY-VCH Verlag GmbH & Co. KGaA, Weinheim

COR-AAD1-00003354
Bayer EX1008 (Part 6 of 9)

A. Westendorf[1]
D. Benndorf[1]
T. Pribyl[1]
H. Harms[1]
R. H. Müller[1]

[1]UFZ-Umweltforschungszentrum Leipzig-Halle GmbH, Leipzig, Germany.

Research Article

Kinetic Traits and Enzyme Form Patterns of (*R*)-2-(2,4-Dichlorophenoxy)propionate/ α-Ketoglutarate Dioxygenase (RdpA) after Expression in Different Bacterial Strains

The *rdpA* gene of strains *Delftia acidovorans* MC1, *Rhodoferax* sp. P230, and *Sphingobium herbicidovorans* MH proved to be identical. However, when RdpA [(*R*)-2-(2,4-dichlorophenoxy)propionate/α-ketoglutarate dioxygenase] was investigated after purification from the various strains, significant differences in the kinetics and some chemical properties of the enzymes were observed. The preference for substrates ranged in the order (*R*)-2-(2,4-dichlorophenoxy)propionate (2,4-DP) > (*R*)-2-(4-chloro-2-methylphenoxy)propionate (MCPP) >> 2,4-dichlorophenoxyacetate (2,4-D) ~ 4-chloro-2-methylphenoxyacetate (MCPA), but detailed kinetic investigations revealed significant strain-dependent differences in the k_{cat} and K_M values. While the K_M values of RdpA from the various strains were low and their range rather narrow with 2,4-DP (19–60 μM) and MCPP (35–64 μM), larger differences were observed with phenoxyacetates which were distinctly higher and spanned a wider range with 2,4-D (237–935 μM) and MCPA (164–510 μM). The lowest K_M values with 2,4-D and MCPA were found for RdpA originating from strain P230. Investigation of the enzymes from the various sources by 2D gel electrophoresis revealed up to three monomeric enzyme forms which differed in the pI value. The 2D-patterns were similar with RdpA from strains MC1 and MH, and after heterologous expression of the enzyme in *Escherichia coli*, but differed significantly from that of strain P230. The presence of enzyme forms and their different composition coincided apparently with the differences observed in the kinetic properties of RdpA in the various strains. The effects are discussed in terms of posttranslational modification of RdpA which appears to be different in extent and kind in the various strains.

Keywords: Biodegradation, Enzymes, Kinetics, Xenobiotics

Received: July 21, 2006; *revised:* September 29, 2006; *accepted:* October 1, 2006

DOI: 10.1002/elsc.200620165

1 Introduction

Phenoxyalkanoate herbicides such as 2,4-dichlorophenoxyacetate (2,4-D) have been used for about 70 years. Despite their xenobiotic character, they proved to be well degradable by microorganisms. Degradation of 2,4-D was most intensively studied with *Ralstonia eutropha* JMP134 [1–3] (now *Cupriavidus necator* [4]). The degradation of phenoxyalkanoates is initiated by cleavage of the ether bond. In most cases this step is catalyzed by α-ketoglutarate-dependent dioxygenases, e.g., 2,4-D/α-ketoglutarate dioxygenases (TfdA) [5, 6]; but monooxygenases are also known to catalyze this step [7–9]. The phenolic intermediates liberated in this step are hydroxylated and the resulting catechols broken down and connected to the general metabolism by the modified ortho cleavage pathway [10]. TfdA is highly specific for phenoxyacetate herbicides like 2,4-D or 4-chloro-2-methylphenoxyacetate (MCPA) [5, 6], it further accepts, to a lesser extend, only the (*S*)-enantiomers of 2-phenoxypropionate compounds [11].

Correspondence: R. H. Müller (r.mueller@ufz.de), UFZ-Umweltforschungszentrum Leipzig-Halle GmbH, Department Umweltmikrobiologie, Permoserstrasse 15, D-04318 Leipzig, Germany.

© 2006 WILEY-VCH Verlag GmbH & Co. KGaA, Weinheim

COR-AAD1-00003355
Bayer EX1008 (Part 6 of 9)

For the degradation of 2-phenoxypropionate herbicides, i.e., (*RS*)-2-(2,4-dichlorophenoxy)propionate (2,4-DP) or (*RS*)-2-(4-chloro-2-methylphenoxy)propionate (MCPP), which are chiral compounds, highly specialized dioxygenases with enantioselective properties were found in various strains. One of them, (*S*)-2,4-DP/α-ketoglutarate-dioxygenase (SdpA), predominantly cleaves the (*S*)-enantiomers of the racemic compounds. It does not attack the corresponding (*R*)-enantiomers, but exhibits activity to phenoxyacetate herbicides (2,4-D, MCPA) the extend of which, however, differed with SdpA from *Delftia acidovorans* MC1 [12, 13], *Rhodoferax* sp. P230 [13], and *Sphingobium herbicidovorans* MH [14]. Whereas SdpA from strains MC1 and MH shows low but distinct activity with 2,4-D and MCPA [15], SdpA from strain P230 did not use these substrates. Although the primary structure varied in SdpA of strain MC1 compared to strains MH and P230 [16, 17], these differences do not explain the entire patterns in the kinetics of these enzymes. Further effects must contribute to these differences which cannot simply be explained by differences in the primary structure of the SdpA enzymes. The elucidation of these properties is still under investigation.

Despite the knowledge about the sequence diversity of SdpA it was surprising to find that the genes encoding the (*R*)-2,4-DP/α-ketoglutarate-dioxygenase (RdpA), the other of both enantiospecific enzymes which is involved in the degradation of the corresponding (*R*)-enantiomers of 2-phenoxypropionates, were identical in all three strains [16, 17]. On a first glance, one should not expect differences in the kinetics after the expression of the *rdpA* gene in the individual strains. However, when we compared the degradative properties with respect to the various herbicides, remarkable differences became obvious in the above strains which were assumed to originate from properties of the initial key dioxygenases. For instance, whereas strain MC1 showed a high growth rate on (*R*)-2,4-DP of $> 0.2\ h^{-1}$, the rate was only 1/3 of that with strain P230 [13]. In general, 2,4-D was a bad growth substrate for both strains whereas, in contrast, strain MH preferred 2,4-D over the enantiomers of 2,4-DP [18]. Whereas 2,4-D degradation in MC1 mainly relied on SdpA [15], P230 lacking SdpA for 2,4-D cleavage nevertheless consumed this compound indicating that RdpA was apparently involved in the utilization of 2,4-D.

The present investigation was aimed at elucidating the properties of RdpA after expression in various wild type strains. RdpA was formerly studied after purification from *D. acidovorans* MC1. It showed some peculiarities with respect to the kinetics in that complex characteristics due to forming intermediary plateaus were observed [15]. This complex pattern was referred to the presence of enzyme forms of RdpA which were detected in 2D gel electrophoresis. These exhibited slight differences in the pI values, whereas the molecular weights, but above all the N-terminal sequences proved identical [19]. The presence of these enzyme forms might be of relevance for the kinetic properties, and hence, for the degradation of the various herbicides. The questions were *(i)* if the unusual pattern of RdpA observed in MC1 was a common feature of this enzyme and if so *(ii)* which consequences would arise on the kinetics after expression of RdpA in various strains. The latter was associated with the assumption that the composition of RdpA by enzyme forms might be a (strain-dependent) variable which should result from posttranslational effects.

To solve these questions we purified the enzyme and determined the kinetic characteristics of RdpA from *Rhodoferax* sp. P230 and *S. herbicidovorans* MH. In addition, the kinetics of RdpA was included after heterologous expression of the enzyme in *Escherichia coli*. The RdpA preparations were also inspected by 2D gel electrophoresis for putative multiple enzyme forms. Earlier results with *D. acidovorans* MC1 [15, 19] were re-evaluated and included for comparison.

2 Materials and Methods

2.1 Methods

Enzyme Purification

Purification was performed by the application of a GradiFrac System including pump P-1 and monitor UV-1 (Amersham Pharmacia Biotech). Unless otherwise indicated, all steps were carried out at 4 °C.

Step 1: Cells were disintegrated with a French Pressure Cell (Aminco, Silver Spring, USA) by three passages at 20,000 psi. Particle-free supernatants were obtained by centrifugation at 4 °C for 25 min at 20 000 × g.

Step 2: Ion exchange chromatography (IEX) was carried out on a poly buffer exchanger (PBE94) (Pharmacia, Sweden) column (50 × 1.5). The column was equilibrated with Tris/HCl (10 mM, pH 7.5 at room temperature) containing 0.1 M NaCl. The sample was applied at a rate of 1 mL/min and further treated with the above buffer to remove non-bound proteins. The proper elution was started at the same rate via a linearly increasing NaCl gradient (0.10–0.35 M). The total volume of the gradient solutions was 800 mL. Eluates were collected in fractions of 8 mL.

Step 3: Hydrophobic interaction chromatography (HIC) was performed on a Butyl-Sepharose (Pharmacia, Sweden) column with a bed volume of 20 mL. The column was equilibrated with Tris/HCl (10 mM, pH 7.5, at room temperature) containing different initial concentrations of ammonium sulfate ($RdpA_{P230}$: 1.07 M; $RdpA_{MH}$: 1.125 M). The protein samples derived from the IEX purification step were supplied with ammonium sulfate to reach the desired initial concentration corresponding to the column equilibrium concentration. Desorption was performed via a linearly decreasing ammonium sulfate gradient ($RdpA_{P230}$: 1.07–0.3 M; $RdpA_{MH}$: 1.125–0.45 M) at a rate of 1 mL/min. The total volume of the gradient solutions was in a range from 240 to 480 mL. Eluates were collected in fractions of 8 mL.

Enzyme Measurement

RdpA- and SdpA-activity was assayed colorimetrically after condensation of the phenolic products of the cleavage reaction with aminoantipyrine. The standard assay contained (1 mL final volume): 200 µM Fe(II)SO_4, 200 µM ascorbate, 1 mM α-ketoglutarate, 1 mM phenoxyalkanoate substrate in 10 mM

© 2006 WILEY-VCH Verlag GmbH & Co. KGaA, Weinheim

COR-AAD1-00003356
Bayer EX1008 (Part 6 of 9)

imidazol buffer pH 6 (the buffer was gassed for 30 min with air before use). Respective concentrations were varied in the case of determining kinetic constants. The reaction mixture was treated in a thermo-mixer Comfort (Eppendorf, Germany) by shaking at 950 rpm at 30 °C. Reactions were started by the addition of enzyme and stopped by the addition of 1 mM EDTA. The reaction was followed over a period of up to 2 min, and 4 samples were taken routinely at respective times. Individual sets of data were treated by linear regression analysis for deriving the respective rates.

Product formation was assayed by adding 100 μL borate buffer (3.09 g borate, 3.73 g KCl, 44 mL 1 n NaOH per liter), 10 μL 2 % 4-aminoantipyrine [w/v], and 10 μL 8 % potassium hexacyanoferrat (III) [w/v]. After 5 min shaking at 25 °C (950 rpm), the absorbance was measured at 510 nm. The extinction coefficients for 4-aminoantipyrine adducts were 14.2 $M^{-1}cm^{-1}$ for 2,4-DCP and 11.2 $M^{-1}cm^{-1}$ for 2,4-MCP as derived from calibration curves. The specific activity was defined as μmol of herbicide cleaved per minute at 1 mg of protein [U/mg].

(*R*)-2,4-DP (Dichloroprop-P) was obtained from Riedel-de-Haen (Seelze, Germany) and was 99.7 % pure. The (*R*)-enantiomer of MCPP was synthesized according to the procedure given elsewhere [18]; the preparation was free of (*S*)-DCPP as verified by HPLC analysis with an enantiospecific column (Nucleodex a-PM; Macherey Nagel, Düren, Germany). 2,4-D (98 %) was obtained from Merck (Darmstadt, Germany), and MCPA (97 %) and α-ketoglutarate from Sigma-Aldrich (Deisenhofen, Germany).

Determination of the Catalytically Active Enzyme Fraction

The catalytically active dioxygenases are able to bind α-ketoglutarate. This property was used to determine the quantity of active centers in enzyme preparations, i.e., the proportion of active enzyme. The assay contained 200 μM $(NH_4)_2Fe(SO_4)_2 \cdot 6H_2O$, 200 μM ascorbate, 50 μM α-ketoglutarate and 20 μM protein in degassed imidazol buffer (10 mM, pH 6). The mixture was incubated for 15 min at 30 °C by shaking in a thermomixer (950 rpm). Thereafter, the protein was separated by ultrafiltration (VivaSpin 2, MWCO 30000; Viva Sciences, Göttingen, Germany). α-Ketoglutarate concentration in the protein-free solution was measured by ion chromatography with suppressor technique (Dionex DX-100). As a stationary phase, an IonPacAS14 (Dionex) was used, whereas the mobile phase consisted of 5.2 mM Na_2CO_3/$NaHCO_3$ buffer (pH 10) applied with a flow rate of 2.5 mL/min. Ions were detected via their contribution to conductivity. The molar quantities of α-ketoglutarate bound were set equal to those of catalytically active monomers. The proportionality was verified by thermal inactivation studies (not shown).

Cloning of the rdpA Gene of D. acidovorans MC1

The *rdpA* gene of *D. acidovorans* MC1 was amplified by PCR using the genomic DNA of strain MC1 as a template and primers derived from the *rdpA* gene sequences [16]. The primers also contained recognition sites for the restriction endonucleases *Eco*31I (GGTCTC) and *Bpi*I (GAAGAC), respectively (as underlined). The following primers were used: *rdpA*-IBA7forward: 5′-ATG-GTA-GGT-CTC-AGC-GCA-TGC-ATG-CTG-CAC-TGT-CCC-CC-3′; *rdpA*-IBA7reverse: 5′-ATG-GTA-GGT-CTC-ATA-TCA-GCG-CGC-CGG-GCG-CAC-GCC-3′. The PCR was run for 3 min at 96 °C, followed by 11 cycles of 10 s at 94 °C, 30 s at 55 °C, and 45 s at 68 °C and by 17 identical cycles with an increment of 5 s at 68 °C using the Expand Long Template PCR system (Roche Diagnostics) and the Multicycler PTC-200 (Biozym Diagnostik). The PCR products were cloned using the pGEMT vector system (Promega). The resulting constructs were transformed into *E. coli* EZ. Transformants were screened by blue/white selection and PCR amplification of the corresponding genes using colonies as a template. Plasmids of selected clones were isolated using the Invisorb Spin Plasmid Mini Kit (Invitek) as recommended by the manufacturer.

Construction of a Plasmid for rdpA Expression in E. coli

For over-expressing the RdpA fused to an N-terminal Strep-tag, the pASK-IBA7 gene expression system (IBA, Göttingen, Germany) was used. The plasmid pGEMT::*rdpA* was digested with *Bpi*I and *Eco*31I, respectively. The resulting *rdpA* gene fragment was ligated with *Eco*31I-digested pASK7 vector DNA. The constructs were transformed in *E. coli* JM83 cells. Recombinant clones were screened by PCR amplification of the corresponding genes. For expressing the fusion proteins, the constructs were transformed in *E. coli* Rosetta™(DE3)pLysS.

DNA Sequencing

The nucleotide sequence of *rdpA* gene used for over-expression was sequenced by the automated dideoxynucleotide method using an ABI PRISM 310 Genetic Analyzer (PE Applied Biosystems). Sequence data were analyzed by the corresponding Sequence Navigator software.

Protein Expression

The protein was expressed in E. coli Rosetta™(DE3)pLysS (Novagene). The strain was grown on LB-medium containing 50 μg ampicillin per liter. The induction of enzyme synthesis was achieved by the addition of 2 ng/L anhydrotetracycline hydrochlorid after the culture had reached an OD_{550} of 0.5. After 3 hours the cells were harvested by centrifugation (4 °C, 5000 × g, 15 min). The biomass was washed (three times) and resuspended in Tris/HCl (10 mM, pH 7.5).

Purification of RdpA Fusion Protein

Cells were disrupted by using a Dyno mill (Retsch, Haan, Germany) and glass beads (150–212 microns, Sigma) for

© 2006 WILEY-VCH Verlag GmbH & Co. KGaA, Weinheim

COR-AAD1-00003357
Bayer EX1008 (Part 6 of 9)

20 min at 4 °C. Crude extracts were obtained by centrifugation at 10 000 × g for 20 min at 4 °C. Fusion proteins were purified by affinity chromatography using a StrepTactin-Superflow column (IBA, Göttingen) (bed volume 10 mL). The column was equilibrated with buffer W (0.1 M Tris/HCl, pH 8.0, 0.15 M NaCl, 0.3 mM EDTA). After loading the protein solution, the column was treated with 300 mL of buffer W, followed by 300 mL of high salt buffer (buffer W containing 0.65 M NaCl). RdpA was eluted with buffer W containing 2.5 mM D-desthiobiotin. To regenerate the chromatography material, the column was equilibrated in buffer W containing 1 mM 2-(4-hydroxyphenylazo)-benzoic acid. Enzyme preparation was performed at 4 °C, the flow rate was 1 mL/min, 10 mL fractions were collected, and protein concentration as well as enzyme activity determined.

Removal of the Strep-Tag

For cleaving off the Strep-tag, tagged proteins were incubated in Tris/HCl (50 mM, pH 8.0) containing 100 mM NaCl and 1 mM $CaCl_2$. The specific protease factor, Xa, was added to the protein solution in a proportion of 1 % [w/w] of the dioxygenase concentration. The sample was gently shaken for 18 hours at 300 rpm and 13 °C. In order to separate the remaining uncleaved protein and the tag from the product, the enzyme preparation was treated once again by Strep-tag affinity chromatography.

2D-Electrophoresis

2D-electrophoresis was performed as described previously [20, 21]. For mass spectrometric protein identification, spots of interest were excised, digested in-gel with trypsin and prepared for MS. The samples were analyzed using an AP (atmospheric pressure) MALDI/TRAP-XCT mass spectrometer (Agilent Technologies, Palo Alto, California) in automatic MS/MS mode [21]. The resulting MS/MS data were used for a database search with MASCOT (http://www.matrixscience.com) against the NCBI database.

3 Results

3.1 Enzyme Purification

The application of crude extract from *Rhodoferax* sp. P230 to IEX chromatography resulted in the separation of three protein fractions with distinct activity to the various phenoxyalkanoate herbicides. The protein fractions eluted in a broad peak at around 0.23 M ($SdpA_{P230}$-I1) and at 0.3 M ($SdpA_{P230}$-I2) sodium chloride exhibited selective activity towards the (*S*)-enantiomers of 2-phenoxypropionates. The corresponding (*R*)-enantiomers and phenoxyacetate derivatives (2,4-D) were not cleaved by the enzymes in these fractions. At a NaCl concentration of about 0.28 M a protein fraction ($RdpA_{P230}$) was eluted, which showed dominant activity to the (*R*)-enantiomers of 2-phenoxypropionates; phenoxyacetate herbicides were also cleaved by these protein fractions, although with distinctly less activity. Fractions that carried activities for (*R*)-enantiomers cleavage were pooled and applied to HIC chromatography. This resulted in a further purification of $RdpA_{P230}$. Again, the activity with respect to (*R*)-2,4-DP cleavage coincided with that for 2,4-D. Using this separation procedure, RdpA of strain P230 was enriched up to 50-fold while a loss of enzyme activity of 40 % occurred. Characterization by SDS-PAGE revealed that this purification protocol did not result in pure enzyme (see Fig. 1). Further purification steps, e.g., gel filtration, were avoided as this usually resulted in a drastic loss of activity.

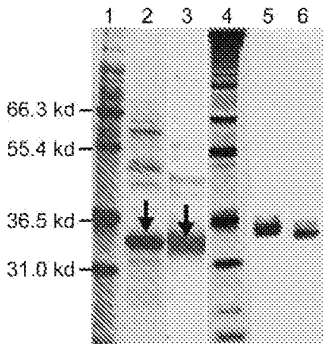


Figure 1. Analytical SDS-PAGE (12 %) of enzyme preparations of strains P230, MH and the heterologously expressed protein after purification procedures. (Lane 1+4: standard; Lane 2: $RdpA_{P230}$; Lane 3: $RdpA_{MH}$; Lane 5: $RdpA_{rec\text{-}streptag}$; Lane 6: $RdpA_{rec}$).

Treatment of crude extract from *S. herbicidovorans* MH by IEX chromatography resulted in the separation of three enzyme fractions, which also exhibited distinct activities to the various phenoxyalkanoate substrates. Analogously to the enzymes from P230, the first (0.27 M NaCl) and the third (0.3 M NaCl) protein fractions cleaved the (*S*)-enantiomers of 2-phenoxypropionates. The enzyme eluted at around 0.28 M NaCl, showed high activity for (*R*)-enantiomers ($RdpA_{MH}$). Consecutive purification of joint fractions with (*R*)-enantiomer cleaving activity by HIC chromatography resulted in a 44-fold enrichment of RdpA from strain MH, the gain in active enzyme was, however, only 14 %. The preparation still contained some impurities (see Fig. 1).

Expression of RdpA in E. coli Rosetta™(DE3)pLysS resulted in enzymatically active gene products. The specific activity of $RdpA_{rec}$ in crude extract was about half that of the value found with preparations from *D. acidovorans* MC1. The $RdpA_{rec\text{-}streptag}$ was purified to homogeneity by one-step affinity chromatography (see Fig. 1). The yield was about 50 %. Digestion of the fusion protein with protease factor Xa gave a 20 % increase in activity of $RdpA_{rec}$ showing the impact of the Strep-tag sequence on the catalytic properties.

© 2006 WILEY-VCH Verlag GmbH & Co. KGaA, Weinheim

COR-AAD1-00003358
Bayer EX1008 (Part 6 of 9)

Table 1. Kinetic parameters of RdpA enzymes from *Delftia acidovorans* MC1, *Rhodoferax* sp. P230, *Sphingobium herbicidovorans* MH, and of the heterologously expressed protein.

Enzyme	Substrate	Specific activity [U/mg]	K_M [μM]	k_{cat} [min^{-1}]	k_{cat}/K_M [$\mu M^{-1}/min$]	Hill-coefficient
$RdpA_{rec}$	(*R*)-2,4-DP	11.7 ± 2.1	49 ± 3	410 ± 73	8.4	1.7
	(*R*)-MCPP	8.6 ± 1.8	59 ± 2	301 ± 63	5.1	1.7
	2,4-D	1.3 ± 0.2	904 ± 40	46 ± 7	0.05	1.34
	MCPA	1.1 ± 0.3	510 ± 50	39 ± 10	0.08	1
$RdpA_{MC1}$	(*R*)-2,4-DP	13.9 ± 1.7	37 ± 5	487 ± 60	13.16	1.7
	(*R*)-MCPP	10 ± 1.3	64 ± 7	350 ± 46	5.47	1.6
	2,4-D	2.1 ± 0.2	900 ± 86	74 ± 7	0.08	1.2
	MCPA	1.6 ± 0.2	540 ± 63	56 ± 7	0.1	0.98
$RdpA_{P230}$	(*R*)-2,4-DP	15.9 ± 1.3	19 ± 3	557 ± 46	29.32	1.55
	(*R*)-MCPP	11.7 ± 1.0	35 ± 2	410 ± 35	11.7	1.8
	2,4-D	4.2 ± 0.5	237 ± 15	147 ± 17	0.62	1.38
	MCPA	3.7 ± 0.3	164 ± 11	130 ± 11	0.79	1.04
$RdpA_{MH}$	(*R*)-2,4-DP	13.8 ± 2.1	39 ± 3	483 ± 74	12.71	1.6
	(*R*)-MCPP	10.1 ± 1.5	58 ± 9	354 ± 53	5.8	1.3
	2,4-D	2.2 ± 0.8	634 ± 27	77 ± 28	0.12	1.2
	MCPA	1.8 ± 0.6	480 ± 25	63 ± 21	0.13	0.99

Reaction kinetics was followed by colorimetric assay [15]. Quantities of the fraction of catalytically active enzyme in the RdpA preparations were determined by the α-ketoglutarate binding capacity as described in Materials and Methods (see also legend to Fig. 2); the protein concentration in the assay was correspondingly corrected.

3.2 Kinetic Investigations

The application of (*R*)-2,4-DP in narrow concentration intervals to RdpA from strains MH and P230 resulted in complex kinetic patterns characterized by plateau regions at intermediate concentrations (see Fig. 2). Earlier results with RdpA from MC1 [15], included for comparison, were similarly complex. The enzyme from strain MH seemingly exhibited two plateaus. Statistical analysis of the data, which depended on 3 to 6 independent measurements, verified the significance of the individual rates. Consequently, the deviations from simple Michaelis-Menten kinetics are significant as well. Rates close to the final rates were obtained above 100 μM (*R*)-2,4-DP for RdpA from all strains. Similar complex shapes were observed with (*R*)-MCPP as the substrate (see Fig. 2). The specific activity with phenoxyacetates increased steadily up to 2000 μM, deviations from pure hyperbolic shape became evident also but were not as pronounced as with the 2-phenoxypropionates (data not shown). Due to the lack of an extant model for treating these complex characteristics we used a modified Michaelis equation to derive the kinetic constants. This equation includes a term for cooperative interaction (see Eq. (1)). The inhibition constant was very large in the present case and could be neglected with RdpA.

$$v = \frac{v_{max} * [S]^n}{K_M + [S]^n} \quad (1)$$

The kinetic constants were obtained by non-linear regression applying the Sigma plot software. It is evident that, due to the complex kinetics, only apparent parameters were derived by this procedure. These should nevertheless allow the individual data to be compared. The results for RdpA from the various strains are summarized in Tab. 1. These emphasize the specificity of RdpA for the (*R*)-enantiomers of 2-phenoxypropionates with (*R*)-2,4-DP being preferred over (*R*)-MCPP which was true for the enzyme from all three strains. The corresponding (*S*)-enantiomers were not cleaved (data not shown). The specific activity (k_{cat}) derived after correction for the fraction of inactive enzyme was similarly high with RdpA from different strains (references on the fraction of active enzyme are given in the legend to Fig. 2). Phenoxyacetate herbicides were substrates of RdpA too, but were converted with lower activity. Most interesting were the differences between RdpA from different strains. Whereas the relative rates with (*R*)-2,4-DP/(*R*)-MCPP/2,4-D/MCPA were about 1/0.75/0.15/0.10 with RdpA from strains MC1, MH, and after heterologous expression in *E. coli* ($RdpA_{rec}$), the relative activities with 2,4-D and MCPA were significantly higher with RdpA from strain P230 (0.26 and 0.23, respectively). Elevated activity of RdpA from strain P230 with phenoxyacetate herbicides was also reflected by 3.8- and 3.1-fold reduced K_M values for 2,4-D and MCPA compared to $RdpA_{rec}$.

The quotient of k_{cat} over K_M was used to express the enzyme specificity as the pseudo first order rate constant. This is a most suitable parameter to make evident the enzyme activity and its changes dependent on the various substrates. As a reference we used the activity of the heterologously expressed enzyme. Treatment of the data in this manner emphasized the increased activity of RdpA from strain P230 to phenoxyacetate herbicides (see Fig. 3).

3.3 Investigation of the Purified Proteins

The surprising observation of differing kinetics of RdpA expressed by the same gene motivated a further investigation of the enzymes. Fig. 4 shows the protein patterns with RdpAs prepared from different strains after separation by 2D gel electrophoresis. Obviously, the enzymes split up in various spots, indicating that the trimeric enzyme [19] was apparently com-

© 2006 WILEY-VCH Verlag GmbH & Co. KGaA, Weinheim

COR-AAD1-00003359
Bayer EX1008 (Part 6 of 9)

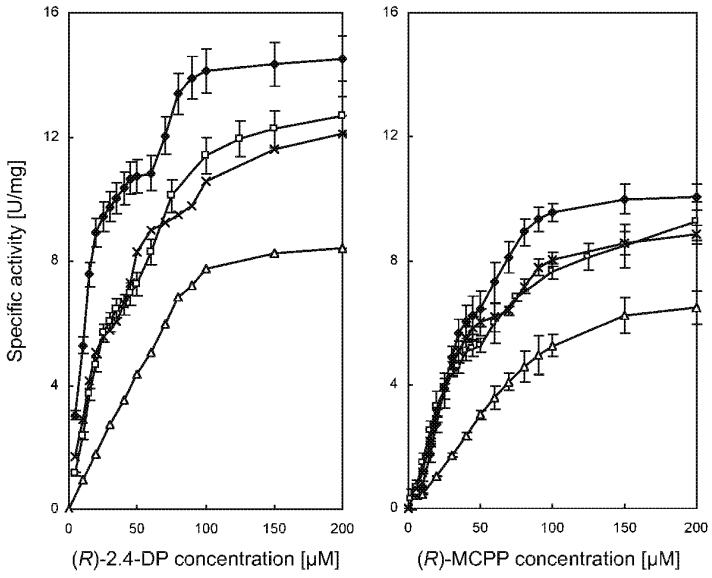


Figure 2. Michaelis plot of RdpA enzymes from *D. acidovorans* MC1 (□), *S. herbicidovorans* MH (×), *Rhodoferax* sp. P230 (◆) and heterologous protein (△) with respect to (*R*)-2-(2,4-dichlorophenoxy)propionate [(*R*)-2,4-DP] and (*R*)-2-(4-chloro-2-methylphenoxy)propionate [(*R*)-MCPP]. The specific activities were calculated by taking just the enzymatically active fraction of protein into account ($RdpA_{MC1}$ = 21 %; $RdpA_{MH}$ = 9 %; $RdpA_{P230}$ = 55 %, $RdpA_{rec}$ = 98 %). Enzyme assays contained 200 µM ascorbate, 200 µM Fe^{2+}, 1 mM a-ketoglutarate, the respective enzyme, and various amounts of herbicide in 10 mM imidazole buffer (pH 6) and were performed at 30 °C under continuous shaking.

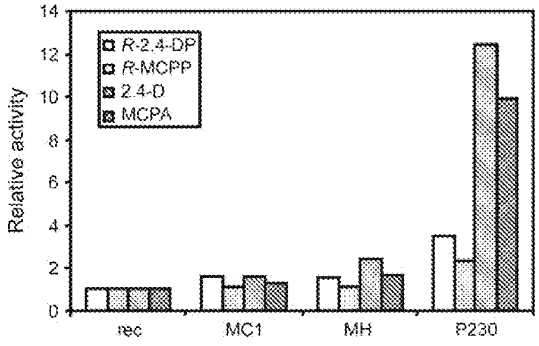


Figure 3. Comparison of relative RdpA activities after expression in different strains. The enzyme activities were referred to k_{cat}/K_M. The relative activities were derived from comparing the activities of RdpA prepared from the wild type strains (see Tab. 1) with those of the heterologously expressed enzymes in the presence of the various substrates.

posed of different monomers. These were characterized by different electrophoretic mobility (pI), whereas the molecular weight was apparently constant. Applying mass spectrometry, all RdpA monomers were identified by a significant Mowse Score higher than 50 and by at least two matching peptides per spot. The mass spectra contained no information clarifying the nature of the potential posttranslational modifications. Comparison of the electropherograms indicated that a distinct spot at pI 5.9 was present in the enzyme from all sources, and that this monomer was the main component in all RdpA preparations except for strain P230. Here the most abundant monomer had a pI of 5.8. The same spot was present also in RdpA from MC1, MH, and the recombinant enzyme, although to a less extent. Only in strain P230 was a distinct spot at pI 5.7 present. We assume that posttranslational modification was responsible for the variations in RdpA. At present we were not able to identify the nature of putative modification on the molecular level. MS-MS spectrometric investigations indicated mass differences in certain peptides but the identification of the molecular basis was without success, yet (R. Hoffmann, personal communication).

4 Discussion

The results have shown that identical *rdpA* genes in different bacteria [16, 17] brought about RdpA with different enzyme kinetics and migration behaviors in 2D gels. The most obvious deviation was found with RdpA synthesized in strain P230, which exhibited a significantly higher activity with phenoxyacetate herbicides than enzymes from the other sources. The differences were attributed to the diverging set of RdpA monomers visible in 2D

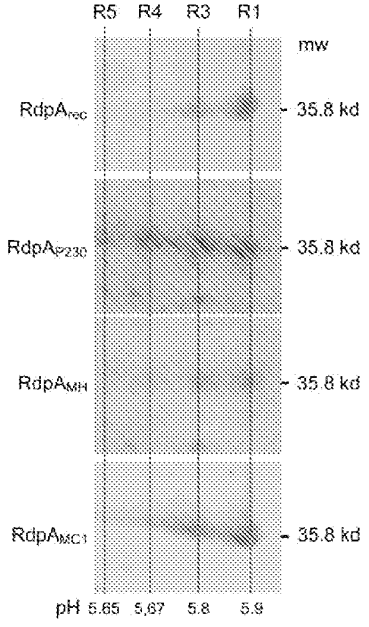


Figure 4. Patterns of the RdpA proteins in 2D gel electrophoresis after preparation from strains *D. acidovorans* MC1, *Rhodoferax* sp. P230, *S. herbicidovorans* MH, and after heterologous expression of RdpA in *E. coli*. The electropherograms show a selected part of the entire gel to close-up the enzyme form patterns.

© 2006 WILEY-VCH Verlag GmbH & Co. KGaA, Weinheim

COR-AAD1-00003360
Bayer EX1008 (Part 6 of 9)

gels. Three distinct protein spots were found differing significantly in the pI, but insignificantly in the molecular weights. The latter indicates that the enzyme forms were not caused by proteolytic attack as described for TfdA [5, 6]. In contrast, it could be shown that the primary structure was conserved in all spots due to found tryptic mass spectrometric analyses of tryptic digests. In the case of RdpA from MC1, the identity of the proteins in the various spots had also been verified by N-terminal sequencing [19].

Detailed investigation of the kinetic characteristics at a high resolution indicated significant deviations from simple Michaelis-Menten kinetics due to plateaus being formed. Such complexity would be expected from the simultaneous action of enzymes with different kinetic parameters which, in the present case, can be attributed to oligomeric native RdpA enzymes composed of various combinations of monomers. Impurities of substrate as causing artifacts in the kinetics can most likely be ruled out: (*R*)-2,4-DP, for example, which produced pronounced deviations from pure hyperbolic behavior was applied as a substrate with 99.7 % purity. Unfortunately, we were not able to separate the enzyme forms to derive their individual kinetics. This could have verified the above assumption and enable us to model the overall kinetics. Separation was prevented by very similar properties of the individual enzyme forms. In this context it should be noted that different enzyme forms were observed in a similar manner with SdpA from strain MC1 [19]. In that case we were able to separate two of the enzyme forms by preparative native electrophoresis with high resolution. Subsequent kinetic investigations revealed significant differences in the kinetic characteristics of the individual enzyme forms (A. Westendorf, unpublished results).

Unfortunately, the kind of modifications could neither be substantiated in the present investigations nor with the enzyme forms of SdpA [19]. Several attempts to apply, e.g., MALDI-TOF-MS-MS and ESI-MS-MS analysis, did not result in conclusive answers, which might be hampered also due to the lack of pure enzyme forms. Modifications of α-ketoglutarate-dependent dioxygenases are in general known. These result from the reaction that delivers reactive oxygen species (ROS). R. Hausinger and colleagues showed, that, as a side reaction in the absence of the proper substrate 2,4-D, hydroxylation of Try-112 took place in TfdA [22]. Such a mechanism might apply also in the present case but cannot be correlated to the appearance of enzyme forms of RdpA as detected by electrophoretic mobility. Hydroxylation of the arene structure is not likely accompanied by changes in charge and, hence, will not lead to the observed separation of the enzyme forms by pI. Nevertheless, hydroxylation of amino acid side chains may lead to changes in pI. It is known from several examples comprising microorganisms [23] and humans [24] that metal ion-catalyzed oxidative attack results in protein modification by carbonylation reactions [25]. Target amino acids in this irreversible reaction are especially proline, arginine, lysine, and threonine [26]. The main reaction products are glutamic semialdehyde and aminoadipic semialdehyde [25]. Although these are uncharged residues, it is the loss of the amino groups in these reactions that is accompanied by a reduction of the net-charge and will lower pI of the modified proteins. Reactions of that kind might explain the appearance of the enzyme forms in the string-of-pearl-like manner seen in Fig. 2. The fact that distinct spots became apparent indicates the regular and possibly site-specific character of these modifications.

A similar observation on multiple enzyme forms was made with superoxide dismutase (SOD1). This enzyme appeared as 4 spots in 2D gel electrophoresis. Specific assay verified carbonylated proteins which, however, were present in only one of the enzyme forms [24]. Further attempts of these authors to identify other kinds of modifications using MS techniques to explain the enzyme form pattern of SOD1 were unsuccessful as was the case in our study. To continue the investigation with α-ketoglutarate-dependent dioxygenase it will be necessary to look for putative carbonylation and to differentiate the individual enzyme forms. Then it can be evaluated to which extent such modifications would be "site-directed" due to the specific reaction mechanisms and to which extent arbitrary effects including a non-enzymatic level would contribute to modification. An answer to this would also stimulate the search for mechanisms influencing the equilibrium between the enzyme forms in the various strains.

The modification of enzymes by posttranslational effects seems to widen their substrate range. This became most evident with RdpA from P230 for which the substrate spectrum was distinctly increased. Modification in this manner might be considered as a fine-tuning of the metabolism and should become particularly effective at low substrate concentrations where slight changes in affinity strongly influence the utilization rate.

References

[1] R. H. Don, J. M. Pemberton, Properties of six pesticide degradation plasmids isolated from *Alcaligenes paradoxus* and *Alcaligenes eutrophus*, *J. Bacteriol.* **1981**, *145*, 681–686.

[2] D. H. Pieper, W. Reineke, K. H. Engesser, H. J. Knackmuss, Metabolism of 2,4-dichlorophenoxyacetic acid, 4-chloro-2-methylphenoxyacetic acid, and 2-methyl-phenoxyacetic acid by *Alcaligenes eutrophus* JMP 134, *Arch. Microbiol.* **1988**, *151*, 365–371.

[3] R. H. Don, A. J. Weightman, H. J. Knackmuss, K. N. Timmis, Transposon mutagenesis and cloning analysis of the pathways for degradation of 2,4-dichlorophenoxyacetic acid and 3-chlorobenzoate in *Alcaligenes eutrophus* JMP134(pJP4), *J. Bacteriol.* **1985**, *161*, 85–90.

[4] P. Vandamme, T. Coeyne, Taxonomy of the genus *Cupriavidus*: a tale of lost and found, *Int. J. System. Evol. Microbiol.* **2004**, *54*, 2285–2289.

[5] F. Fukumori, R. P. Hausinger, *Alcaligenes eutrophus* JMP 134 "2,4-dichlorophenoxyacetate monooxygenase" is an α-ketoglutarate-dependent dioxygenase, *J. Bacteriol.* **1993**, *175*, 2083–2086.

[6] F. Fukumori, R. P. Hausinger, Purification and characterization of 2,4-dichlorophenoxyacetate/α-ketoglutarate dioxygenase, *J. Biol. Chem.* **1993**, *268*, 24311–24317.

[7] L. Xun, K. B. Wagnon, Purification and properties of component B of 2,4,5-trichloro-phenoxyacetate oxygenase from *Pseudomonas cepacia* AC110, *Appl. Environ. Microbiol.* **1995**, *61*, 3499–3502.

© 2006 WILEY-VCH Verlag GmbH & Co. KGaA, Weinheim

COR-AAD1-00003361
Bayer EX1008 (Part 6 of 9)

[8] H. Sträuber, R. H. Müller, W. Babel, Evidence of cytochrome P450-catalyzed cleavage of the ether bond of phenoxybutyrate herbicides in *Rhodococcus erythropolis* K2-3, *Biodegradation* **2003**, *14*, 41–50.

[9] K. Itoh, Y. Tashiro, K. Uobe, Y. Kamagata, K. Suyama, H. Yamamoto, Root nodule *Bradyrhizobium* spp. harbor *tfdA*alpha and *cad*A, homologous with genes encoding 2,4-dichlorophenoxyacetic acid-degrading proteins, *Appl. Environ. Microbiol.* **2004**, 70, 2110–2118.

[10] W. Reineke, H. J. Knackmuss, Microbial degradation of haloaromatics, *Annu. Rev. Microbiol.* **1988**, *42*, 263–287.

[11] R. E. Saari, D. A. Hogan, R. P. Hausinger, Stereospecific degradation of the phenoxypropionate herbicide dichlorprop, *J. Mol. Catal. B: Enzymatic* **1999**, *6*, 421–428.

[12] R. H. Müller, W. Babel, Separation of two dichlorprop/α-ketoglutarate dioxygenases with enantiospecific properties from *Comamonas acidovorans* MC1, *Acta Biotechnol.* **1999**, *19*, 349–355.

[13] R. H. Müller, S. Kleinsteuber, W. Babel, Physiological and genetic characterization of two bacterial strains utilizing phenoxypropionate and phenoxyacetate herbicides, *Microbiol. Res.* **2001**, *156*, 121–131.

[14] K. Nickel, M. J. F. Suter, H. P. E. Kohler, Involvement of two α-ketoglutarate-dependent dioxygenase in enantioselective degradation of *(R)*- and *(S)*-mecoprop by *Sphingomonas herbicidovorans* MH, *J. Bacteriol.* **1997**, *179*, 6674–6679.

[15] A. Westendorf, R. H. Müller, W. Babel, Purification and characterization of the enantiospecific dioxygenases from *Delftia acidovorans* MC1 initiating the degradation of phenoxypropionate and phenoxyacetate herbicides, *Acta Biotechnol.* **2003**, *23*, 3–17.

[16] K. M. Schleinitz, S. Kleinsteuber, T. Vallaeys, W. Babel, The genetic backround of 2,4-dichlorophenoxypropionate cleavage in *Delftia acidovorans* MC1, *Appl. Environ. Microbiol.* **2004**, *70*, 5357–5365.

[17] T. A. Müller, H. P. E. Kohler, Chirality of pollutants-effects on metabolism and fate, *Appl. Microbiol. Biotechnol.* **2004**, *64*, 300–316.

[18] C. Zipper, K. Nickel, W. Angst, H. P. E. Kohler, Complete microbial degradation of both enantiomers of the chiral herbicide mecoprop [(*R*,*S*)-2-(4-chloro-2-methylphenoxy)propionic acid] in an enantioselective manner by *Sphingomonas herbicidovorans* sp. nov., *Appl. Environ. Microbiol.* **1996**, *62*, 4318–4322.

[19] A. Westendorf, D. Benndorf, R. H. Müller, W. Babel, The two enantiospecific dichlorprop/α-ketoglutarate-dioxygenases from *Delftia acidovorans* MC1 – protein and sequence data of RdpA and SdpA, *Microbiol. Res.* **2002**, *157*, 317–322.

[20] D. Benndorf, W. Babel, Assimilatory detoxification of herbicides by *Delftia acidovorans* MC1: Induction of two chlorocatechol 1,2-dioxygenases as response to chemostress, *Microbiology* **2002**, *148*, 2883–2888.

[21] D. Benndorf, M. Thiersch, N. Loffhagen, C. Kunath, H. Harms, *Pseudomonas putida* KT2440 responds specifically to chlorophenoxy herbicides and their initial metabolites, *Proteomics* **2006**, *6*, 3319–3329.

[22] A. Liu, R. Y. Ho, L. Que Jr., M. J. Ryle, B. S. Phinney, R. P. Hausinger, Alternative reactivity of an alpha-ketoglutarate-dependent iron(II) oxygenase: enzyme self-hydroxylation, *J. Am. Chem. Soc.* **2001**, *123*, 5126–5127.

[23] J. Mostertz, M. Hecker, Patterns of protein carbonylation following oxidative stress in wild-type and *sig*B *Bacillus subtilis* cells, *Mol. Genet. Genomics* **2003**, *269*, 640–648.

[24] J. Choi, H. D. Rees, S. T. Weintraub, A. L. Levey, L. S. Chin, L. Li, Oxidative modification and aggregation of the Cu,Zn-superoxide dismutase associated with Alzheimer and Parkinson diseases, *J. Biol. Chem.* **2005**, *280*, 11648–11655.

[25] J. R. Requena, C. C. Chao, R. L. Levine, E. R. Stadtman, Glutamic and aminoadipic semialdehydes are the main carbonyl products of metal-catalyzed oxidation of proteins, *PNAS* **2001**, *98*, 69–74.

[26] B. S. Berlett, E. R. Stadtman, Protein oxidation in aging, disease, and oxidative stress, *J. Biol. Chem.* **1997**, 272, 20313–20316.

© 2006 WILEY-VCH Verlag GmbH & Co. KGaA, Weinheim

COR-AAD1-00003362
Bayer EX1008 (Part 6 of 9)

Robust crop resistance to broadleaf and grass herbicides provided by aryloxyalkanoate dioxygenase transgenes

Terry R. Wright[a], Guomin Shan[a,1], Terence A. Walsh[a], Justin M. Lira[a], Cory Cui[a], Ping Song[a], Meibao Zhuang[a], Nicole L. Arnold[a], Gaofeng Lin[a], Kerrm Yau[a], Sean M. Russell[a], Robert M. Cicchillo[a], Mark A. Peterson[a], David M. Simpson[a], Ning Zhou[a], Jayakumar Ponsamuel[a], and Zhanyuan Zhang[b]

[a]Research and Development, Dow AgroSciences LLC, Indianapolis, IN 46268; and [b]College of Agriculture, Food, and Natural Resources, University of Missouri, Columbia, MO 65211-7140

Edited by Bruce D. Hammock, University of California, Davis, CA, and approved October 13, 2010 (received for review September 2, 2010)

Engineered glyphosate resistance is the most widely adopted genetically modified trait in agriculture, gaining widespread acceptance by providing a simple robust weed control system. However, extensive and sustained use of glyphosate as a sole weed control mechanism has led to field selection for glyphosate-resistant weeds and has induced significant population shifts to weeds with inherent tolerance to glyphosate. Additional weed control mechanisms that can complement glyphosate-resistant crops are, therefore, urgently needed. 2,4-dichlorophenoxyacetic acid (2,4-D) is an effective low-cost, broad-spectrum herbicide that controls many of the weeds developing resistance to glyphosate. We investigated the substrate preferences of bacterial aryloxyalkanoate dioxygenase enzymes (AADs) that can effectively degrade 2,4-D and have found that some members of this class can act on other widely used herbicides in addition to their activity on 2,4-D. AAD-1 cleaves the aryloxyphenoxypropionate family of grass-active herbicides, and AAD-12 acts on pyridyloxyacetate auxin herbicides such as triclopyr and fluroxypyr. Maize plants transformed with an AAD-1 gene showed robust crop resistance to aryloxyphenoxypropionate herbicides over four generations and were also not injured by 2,4-D applications at any growth stage. Arabidopsis plants expressing AAD-12 were resistant to 2,4-D as well as triclopyr and fluroxypyr, and transgenic soybean plants expressing AAD-12 maintained field resistance to 2,4-D over five generations. These results show that single AAD transgenes can provide simultaneous resistance to a broad repertoire of agronomically important classes of herbicides, including 2,4-D, with utility in both monocot and dicot crops. These transgenes can help preserve the productivity and environmental benefits of herbicide-resistant crops.

herbicide resistance | weed management | genetically modified crops | AOPP herbicides

Since their introduction in the mid-1990s, genetically modified (GM) crops have delivered many benefits to agricultural growers by providing increased productivity, reduced pesticide use, and greater flexibility and efficiency in farm management. The area devoted to GM crop plantings has steadily increased at a rate of ~20%/y globally for over a decade, with 134 million ha of GM crops planted worldwide in 2009. Continued growth is expected in the near future because of rapid adoption of this technology in developing countries (1). Over 90% of global GM crop plantings contain a trait conferring resistance to the broad-spectrum herbicide glyphosate (1). These include soybean, cotton, maize, and canola. Because glyphosate resistance provides a simple and convenient solution for control of a wide spectrum of broadleaf and grass weeds, farmers have rapidly adopted glyphosate-resistant (GR) crops. However, in many instances, traditional best agronomic practices for avoiding natural development of GR weeds in the field have been abandoned or reduced. These practices include crop rotation, herbicide mode of action rotation, tank mixing of multiple herbicide modes of action, and incorporation of mechanical weed control with chemical and cultural methods.

Glyphosate is commonly used in noncrop areas for total vegetation control. With the introduction of GR crops, glyphosate has been applied to some crop fields one to three times per year for more than 15 consecutive years. This increased application frequency, in combination with higher use rates and the increasing hectarage being treated, has placed heavy selection pressure on weed species to acquire naturally occurring resistance mechanisms to glyphosate (2–5). To date, 19 weeds, including both grass and broadleaf species, have developed natural resistance to glyphosate (6), most of which have been reported in the past 8 y, which is coincident with increasing use of GR crops (7, 8). Moreover, weeds that had previously not been an agronomic problem before the wide deployment of GR crops, such as *Ipomoea*, *Amaranthus*, *Chenopodium*, *Taraxacum*, and *Commelina* species (9–11), are now becoming more prevalent and difficult to control. With this trend, growers are rapidly losing the advantages of GR crops.

One of the most effective approaches for weed resistance management is the use of herbicides with differing modes of action, either in rotation as part of a weed management program or in combination as mixtures (12, 13). One strategy to complement and sustain the powerful weed control technology conferred by the GR trait is to deploy an additional trait that can confer resistance to herbicides with alternative modes of action. The plant hormone mimic 2,4-dichlorophenoxyacetic acid (2,4-D) was the first synthetic herbicide to be commercially developed and has been used agronomically and in noncrop applications for broad-spectrum broadleaf weed control for over 60 y (14). In addition to low cost, 2,4-D has environmentally friendly properties such as short environmental persistence and low toxicity to humans and wildlife (15, 16). Although 2,4-D remains one of the most widely used herbicides globally, its complex, plant-specific mode of action has not led to widespread natural resistance development (17), and only isolated cases of resistant weed species have been reported (6). Engineered 2,4-D resistance could offer a potentially robust, cost-effective herbicide-resistant trait that could complement glyphosate resistance.

In this work, we show that members of a class of bacterial enzymes [aryloxyalkanoate dioxygenases (AADs)], which effi-

Author contributions: T.R.W., T.A.W., C.C., and M.A.P. designed research; T.R.W., T.A.W., J.M.L., C.C., P.S., M.Z., N.L.A., G.L., K.Y., S.M.R., R.M.C., M.A.P., D.M.S., N.Z., J.P., and Z.Z. performed research; G.S., G.L., and K.Y. contributed new reagents/analytic tools; T.R.W., G.S., T.A.W., J.M.L., C.C., P.S., M.Z., R.M.C., D.M.S., and Z.Z. analyzed data; and T.R.W., G.S., and T.A.W. wrote the paper.

The authors declare no conflict of interest.

This article is a PNAS Direct Submission.

Freely available online through the PNAS open access option.

[1]To whom correspondence should be addressed. E-mail: gshan@dow.com.

This article contains supporting information online at www.pnas.org/lookup/suppl/doi:10.1073/pnas.1013154107/-/DCSupplemental.

COR-AAD1-00003363
Bayer EX1008 (Part 6 of 9)

ciently cleave 2,4-D in vitro into nonherbicidal dichlorophenol and glyoxylate, can provide robust field resistance to 2,4-D when expressed in maize and soybean crops. In addition, we have discovered that two unique members of this class of enzymes have surprisingly broad substrate ranges for xenobiotic herbicides. AAD-1 has the additional ability to inactivate potent grass-active herbicides that act through a different mode of action (inhibition of lipid biosynthesis). AAD-12 can cleave pyridyloxyacetate auxins that are structurally diverse members of the synthetic auxin herbicide family related to 2,4-D and provide extended spectra of weed control. These attributes indicate the utility of these types of enzymes for herbicide-resistant crop applications. They may offer growers options to overcome the significant developing issues of GR weeds as well as provide the ability to use herbicides that differ in both chemical structure and mode of action through a single transgene.

Results and Discussion

Identification of 2,4-D Degrading Enzymes. Previous studies have established that the enzyme TfdA is responsible for the first enzymatic step in the 2,4-D mineralization pathway of the soil bacterium *Ralstonia eutropha* (18). TfdA catalyzes the oxygenolytic cleavage of 2,4-D to nonherbicidal dichlorophenol and glyoxylate through an Fe(II)/α-keto acid-dependent dioxygenase reaction (Fig. 1*A*) (19). The enzyme was also shown to confer 2,4-D resistance when expressed in transgenic cotton plants (20). Sequences for a large number of bacterial genes that encode homologs of TfdA have now been deposited in genetic databases. However, most of these have not been biochemically characterized or more significantly, tested for attributes that could confer optimal 2,4-D resistance in transgenic crops. We identified sequences of candidate genes for potential 2,4-D–resistant crop utility by using a bioinformatic approach to identify homologs of TfdA in the National Center for Biotechnology Information (NCBI) genetic sequence database. Fe(II)/α-ketoglutarate–dependent dioxygenases typically contain a triad of conserved histidine residues comprising the Fe(II)-coordinating active site (21), and therefore, although overall similarity to TfdA may be relatively low, sequences with this histidine triad motif can be attributed to the Fe(II)/α-ketoglutarate–dependent dioxygenase family. Genes encoding candidate enzymes were synthesized and expressed in *Escherichia coli*, and the biochemical and physiological properties of the recombinant enzymes were assessed. This range-finding study enabled us to focus on two lead homologs, RdpA from *Sphingobium herbicidivorans* and SdpA from *Delftia acidovorans*, that have 28% and 31% amino acid sequence identity to TfdA, respectively.

To establish a uniform and unbiased nomenclature for the enzymes that we have characterized, we refer to these enzymes generically as AADs and further refer to RdpA and SdpA as AAD-1 and AAD-12, respectively. The chemical structures of herbicidal compounds included in the generic aryloxyalkanoate chemical family descriptor are shown in Fig. 1*B*. AAD-1 has been previously shown to cleave the herbicidally active *R*-enantiomer of dichlorprop and was also reported to have a low level of activity on 2,4-D (22). Screening an expanded set of structurally related herbicides, we unexpectedly found that AAD-1 has a unique ability to enantioselectively cleave members of the aryloxyphenoxypropionate (AOPP) class of potent grass-selective herbicides, including *R*-cyhalofop and *R*-quizalofop (Table 1). These herbicides act by an entirely different mechanism than that of the synthetic auxins and specifically inhibit the monomeric acetyl-CoA carboxylases of grasses (23). The efficiency of in vitro AOPP cleavage approaches that of the optimal substrate, *R*-dichlorprop, and is significantly higher than the activity of AAD-1 on 2,4-D (Table 1). This was surprising given the extended and bulky aryloxy substituents on the AOPPs. These data show that AAD-1 can cleave two distinct classes of herbicides covering broadleaf and grass-selective modes of action.

In contrast to AAD-1, AAD-12 has been previously reported to selectively cleave the *S*-enantiomer of dichlorprop (24). We found in our biochemical studies that AAD-12 can also cleave the *S*-enantiomers of the AOPP herbicides (Table 1). Because these are the herbicidally inactive enantiomers of these compounds, this AAD-12 activity is not of utility for providing crop resistance to these chiral herbicides. However, AAD-12 has significantly greater in vitro activity on 2,4-D (an achiral substrate) than AAD-1 (Table 1) (25). Testing a series of pyridyloxyacetate compounds as substrates, we found that AAD-12 was capable of degrading the synthetic auxin herbicides triclopyr and fluroxypyr at rates of 4% and 16%, respectively, of 2,4-D (at 1 mM substrate). AADs have not previously been shown to work on substrates containing a pyridine ring. This activity gives AAD-12 potential utility for providing resistance to a wider repertoire of synthetic auxins beyond 2,4-D and thus enables expanded broadleaf weed control.

Validation of Plant Herbicide Resistance Provided by AADs. Our initial investigations into the broad in vitro substrate specificities of the AAD-1 and AAD-12 enzymes were intriguing. Our next goal was to evaluate if expression of these enzymes in transgenic plants could provide protection against the damaging effects of 2,4-D and other herbicides. *Arabidopsis thaliana* was first used as

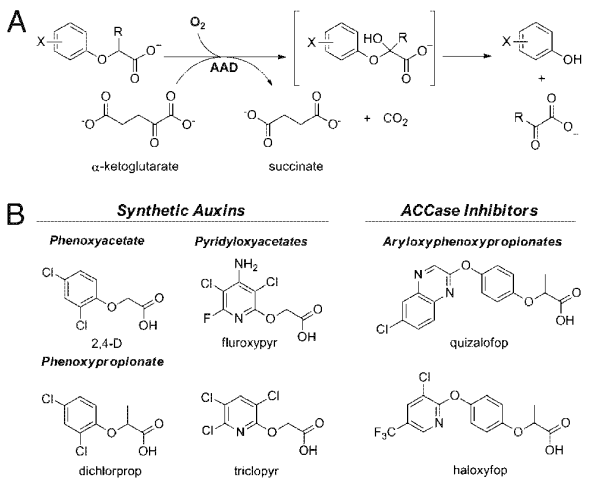


Fig. 1. (*A*) General reaction catalyzed by AAD enzyme. (*B*) Aryloxyalkanoate herbicidal compounds that are substrates for AADs.

Table 1. In vitro kinetic constants of AAD-1 and AAD-12 for various herbicide substrates

Enzyme	Substrate	K_m (μM)	k_{cat} (s^{-1})	k_{cat}/K_m ($M^{-1}\cdot s^{-1} \times 10^3$)
AAD-1				
	2,4-D	683 ± 76	0.31 ± 0.01	0.45
	MCPA	527 ± 38	0.11 ± 0.002	0.21
	R-dichlorprop	93 ± 16	5.22 ± 0.36	56.3
	R-cyhalofop	96 ± 7	3.12 ± 0.06	32.5
	R-quizalofop	144 ± 9	3.34 ± 0.09	23.3
AAD-12				
	2,4-D	185 ± 25	3.46 ± 0.14	18.6
	MCPA	283 ± 67	4.18 ± 0.60	14.7
	S-dichlorprop	118 ± 35	3.57 ± 0.46	30.2
	S-cyhalofop	279 ± 22	1.52 ± 0.08	5.43

Assays were performed using 0.1- to 1.5-μM enzyme. MCPA, 2-methyl-4-chlorophenoxyacetic acid.

COR-AAD1-00003364
Bayer EX1008 (Part 6 of 9)

a rapid and facile model system for validation of in planta activity of the AADs. An expression cassette containing either *aad*-1 or *aad*-12 genes (synthesized with plant-preferred codon usage) under control of a constitutive promoter was introduced into *Arabidopsis* plants through *Agrobacterium tumefaciens*-mediated gene delivery using phosphinothricin acetyltransferase (PAT) gene as a selectable marker (Figs. S1 and S2). T_1 generation plants were selected with glufosinate herbicide, and transformants were analyzed by Southern blot and PCR for presence of the genes and by Western blot and ELISA for expression of the appropriate proteins.

Application of 2,4-D onto untransformed *Arabidopsis* plants severely injured them, even at doses as low as 50 g acid equivalent (ae)/ha. In contrast, transgenic *Arabidopsis* plants expressing either AAD-1 and AAD-12 exhibited little or no visible signs of 2,4-D damage, even when treated with up to 3.2 kg ae/ha of the herbicide (Fig. 2 and Fig. S3). This application rate is about 5- to 10-fold higher than typical field use rates of 2,4-D and therefore, indicated that the introduced AAD enzymes could function well in plants.

In addition, plants expressing AAD-12 survived applications of triclopyr and fluroxypyr at rates of up to 2.24 kg ae/ha. Some temporary epinastic symptoms were visible on rates exceeding 0.28 g ae/ha fluroxypyr on AAD-12–expressing plants; however, the treated plants recovered, whereas control plants were severely injured or died.

Crop Transformation with AADs. For broad utility, a transgene must provide robust herbicide resistance in major crops where management of weeds is critical to maximize production. Maize, soybean, cotton, rice, and canola were chosen as crop targets for transformation with AAD-1 or AAD-12 expression cassettes similar to those used in *Arabidopsis*. Here, we describe the results obtained for maize and soybean as relevant representative monocot and dicot crops. To obtain transgenic events with adequate expression of AAD-1 and AAD-12 in these crops, various vectors with different regulatory elements were designed.

For soybean transformation, a binary vector pDAB4468 was constructed with a transfer DNA (T-DNA) insert carrying an *aad*-12 gene cassette under the control of an *A. thaliana* ubiquitin 10 promoter (AtUbi10) and a *pat* gene cassette driven by the Cassava Vein Mosaic Virus promoter (CsVMV) as the selectable marker for transformation (Fig. S4). Multiple transgenic soybean events were produced through *Agrobacterium*-mediated transformation of the public elite variety Maverick. Events with one intact copy of T-DNA insert were selected for further evaluation and characterization. T_1 seed was collected from self-pollinated T_0 putative transformants, T_1 plants were screened for resistance to glufosinate, and seeds from multiple subsequent generations of transformants (up to T_5) were collected. The heritability and stability of the gene in soybean were investigated over multiple generations. Progeny testing and molecular analysis revealed that the inheritance of the *aad*-12 gene was stable across all of the tested generations and followed typical single-locus Mendelian segregation for selected soybean events (Table 2). When sprayed with varying levels of 2,4-D, most of the transgenic soybean events showed 2,4-D resistance exceeding typical agricultural use rates, and the selected events were resistant to rates of ≥4.48 kg ae/ha under greenhouse and field conditions. The gene and herbicide resistance were heritable across multiple generations from T_0 through T_5 (Table S1 and Fig. S5). Selected events showed excellent resistance to 2,4-D at 4.48 kg ae/ha when applied at the V3 stage in field trials (eight times the recommended level of agricultural applications) (Fig. 3). Initial field studies with multiple selected soybean events at several locations in the United States showed agronomic performance equivalent to that of the nontransformed control variety, including date to flowering, lodging, phenotype, and yield. Transgenic plots were treated with 2,4-D applications comprising a seasonal total of 3.36 kg ae/ha (or 3 lb ae/acre) at both preemergence (postplant) and approximately V4 or R2 growth stages.

For maize transformation, plasmid pDAS1740 was constructed containing an *aad*-1 gene under the control of the maize ubiquitin promoter (ZmUbi1) (Fig. S6). The recipient maize line Hi-II was transformed using direct insertion of the DNA fragment from plasmid pDAS1740 through silicon carbide fiber-mediated transformation (26). Putative transgenic maize plants were screened with *R*-haloxyfop, and multiple transgenic maize events were produced. Events with one single intact copy of *aad*-1 plant transcription unit (PTU) were selected for further evaluation and characterization. Seeds from multiple generations, including self-pollinated generations (up to T_4), converted inbred generations (BC_1, BC_2, and BC_3S_1), and hybrid test crosses, were collected. Progeny testing and molecular analysis revealed that the inheritance of the *aad*-1 gene was stable across all of the generations evaluated and followed typical single-locus Mendelian segregation (Table 2).

The transgenic maize plants were resistant to applications of the grass-active AOPP herbicides (cyhalofop or quizalofop) at rates of 0.28–0.56 kg ae/ha under greenhouse and field conditions. Maize is normally highly susceptible to these herbicides. Although 2,4-D is used as a broadleaf herbicide with little or no activity on grasses, it can produce significant malformations of maize plants when applied at late seedling stages. This leads to restrictions on its use in maize to plants that are before the six-leaf stage or under 18 cm. Transgenic maize events showed resistance to 2,4-D application rates up to 4.48 kg ae/ha, with no 2,4-D–induced brace root malformations being observed. The gene and herbicide resistance was heritable over multiple generations of selfed lines (T_0 through T_4), converted inbred lines (BC_1, BC_2, and BC_3S_1), and test hybrid crosses (Table S2 and Fig. S7). Selected events showed excellent resistance to quizalofop at rates of up to 0.28 kg ae/ha when applied at the V6 stage in field trials. This is four to eight

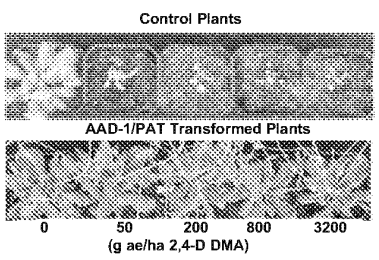


Fig. 2. *Aad*-1 transformed *Arabidopsis* response to 2,4-D in the greenhouse.

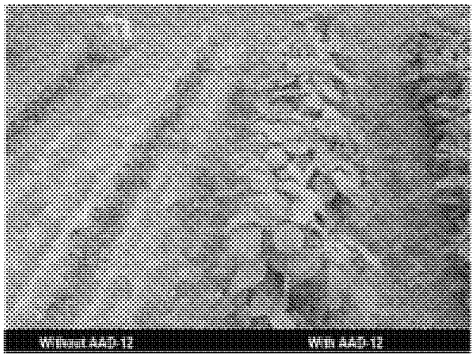


Fig. 3. Transgenic and nontransgenic soybean plants response to 2,4-D in the field.

COR-AAD1-00003365
Bayer EX1008 (Part 6 of 9)

Table 2. Inheritance of the AAD-1 maize and AAD-12 soybean

	AAD-1 maize event A T_2 seeds	AAD-1 maize event B T_2 seed	AAD-12 soybean event C F_2 seed	AAD-12 soybean event D F_2 seed	WT maize	WT soybean
Resistant	61	55	102	78	0	0
Sensitive	27	18	45	22	30	30
Totals	88	73	147	100	30	30
R (%)	69.3	75.3	69.4	78.0	0	0
S (%)	30.7	24.7	30.6	22.0	100	100
χ^2	0.2184	0.9461	2.4694	0.7866		
P value	>0.05	>0.05	>0.05	>0.05		
Ratio	3:1	3:1	3:1	3:1		

T_1 maize events were self-pollinated to produce T_2 seed; T_2 seeds were progeny-tested. Maize was sprayed with quizalofop and verified with either ELISA or Southern blot analysis. T_4 soybean events were crossed with elite soybean variety to produce F_1 seeds that were planted to produce F_2 seeds. Soybeans were sprayed with 2,4-D and verified with either ELISA or Southern blot analysis. WT, wild-type.

times the recommended field rate for control of volunteer maize, showing that the *aad*-1 gene can serve as an excellent selectable marker in field situations (Fig. 4). Initial field studies with multiple selected maize events across multiple locations in the United States showed equivalent agronomic performance to conventional controls, including date to silking, date to pollination, date to maturity, lodging, phenotype, and yield. Transgenic plots were treated with 2,4-D applications, with a seasonal total of 3.36 kg ae/ha at preemergence (postplant) and approximately V4 and V8 growth stages and/or a quizalofop application at a rate of 0.092 kg ae/ha at approximately V6 growth stage. These data show that a single *aad*-1 gene confers robust field resistance to two different herbicides with distinct modes of action. This is in contrast to other transgenic mechanisms of field-level herbicide resistance, such as glyphosate and glufosinate resistance, that confer resistance to a single herbicide chemistry.

Potential Impact of AAD-Derived Herbicide-Resistant Traits. 2,4-D is a synthetic auxin herbicide that kills the target weed by mimicking the natural plant growth hormone auxin [indole-3-acetic acid (IAA)] and binds to recently discovered IAA receptors in plants (17). It has been used effectively for over six decades to efficiently control a wide spectrum of broadleaf weeds (27). When applied to dicotyledonous plants at effective doses, 2,4-D causes uncontrolled and disorganized plant growth that leads to death (17). It can also have undesirable morphological effects on seedling grass species. Despite its widespread use, very few 2,4-D–resistant weed species have been identified (6). Of these few species, none have showed significant spread from initial sites of discovery, and none have significant economic importance (28). The lack of widespread development of 2,4-D–resistant weeds may be because of the genetic redundancy in auxin/2,4-D receptors, the essentiality of auxin perception for plant development, and/or the pleiotropic nature of the downstream auxin effects (29–31). These observations suggest that the frequency of 2,4-D–resistant weed appearance may be low.

Robust crop 2,4-D resistance can assist growers by increasing the flexibility of weed control practices at low cost. Moreover, it can help overcome or slow the development of GR weeds. A significant advantage provided by higher rates of 2,4-D is the potential for residual control of broadleaf weeds. Glyphosate is a nonresidual herbicide and does not provide control of later-germinating weeds. Resistance provided by AADs can also provide the ability to tank mix a broad-spectrum broadleaf weed control herbicide with commonly used residual weed control herbicides. These herbicides are typically applied before or at planting but often are less effective on emerged, established weeds that may exist in the field before planting. By extending the utility of aryloxyacetate auxin herbicides such as 2,4-D and fluroxypyr to include at-plant, preemergence, or preplant applications, the flexibility of residual weed control programs can be increased.

In grass crops such as maize, the AAD-1 gene confers robust resistance to grass-active AOPP herbicides, such as quizalofop and cyhalofop, that are otherwise highly injurious to these crops. AAD-1 simultaneously provides resistance to 2,4-D. The enhanced resistance of maize and other monocot crops to 2,4-D conferred by AAD-1 will enable use of these auxinic herbicides without the potential for known auxin-induced effects, such as crop leaning, inhibited leaf unfurling (rat-tailing), stalk brittleness, or deformed brace roots, that lead to the current growth-stage restrictions on 2,4-D application to grass crops.

In summary, the broad xenobiotic substrate selectivity of the AAD enzymes that we have characterized provides diverse mechanisms to incorporate additional established highly effective herbicide modes of action with the convenience of herbicide-resistant crops in an integrated weed-shift management strategy. When stacked with other herbicide resistance traits, for example, with the widely used GR traits, AAD-derived herbicide resistance will provide farmers with a practical tool to control current GR weeds, such as horseweed, as well as multiple pigweed and ragweed species and newly developing GR weeds. It also may slow weed-resistance development by diversifying herbicide selection pressures with additional modes of action and differing chemical structures. AAD-based herbicide-resistant traits will provide a tool to protect and sustain the value of current herbicides and herbicide-resistant crops.

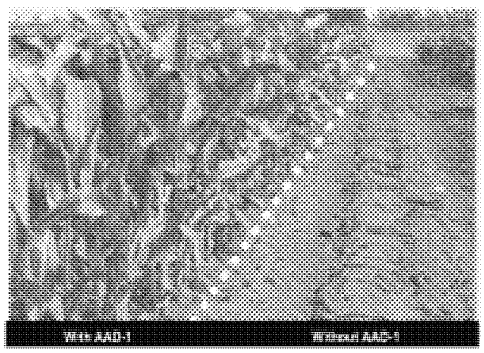


Fig. 4. Transgenic and nontransgenic maize plants response to quizalofop in the field.

Materials and Methods

Expression and Purification of AAD-1 and AAD-12 Enzymes. *Aad*-1 and *aad*-12 genes were cloned using standard PCR amplification and molecular cloning techniques. The primers were designed according to published DNA sequences to amplify the mature protein coding region (24, 25). The fragment encoding the full-length gene was then cloned in frame into a pET-based vector (pET280)

COR-AAD1-00003366
Bayer EX1008 (Part 6 of 9)

and transformed into *E. coli* BL21 (DE3) for protein expression. Typical induction conditions for the AAD-1 and AAD-12 proteins were with 75 μM isopropyl-β-D-thiogalactopyranoside (IPTG) in Luria Broth with appropriate antibodies and cells grown overnight at 25 °C for optimal soluble protein expression. Cell paste was harvested by centrifugation, and cell lysate was prepared either by using sonication or microfluidization methods. The protein was purified from the soluble fraction using standard ion exchange and hydrophobic interaction chromatography separations followed by size exclusion chromatography. Typically, after three steps of column separation, the target protein had a purity of >99%. The homogeneity and enzymatic activity of the protein were further validated by HPLC and activity assays. Protein concentration was determined by total amino acid hydrolysis.

In Vitro Enzyme Assay. AAD enzymatic activity was measured by colorimetric detection of the product phenol using a protocol modified from that of Fukumori and Hausinger (32) in a 96-well microplate format. Assays were performed in a total volume of 0.15 mL 20 mM Mops (pH 6.75) containing 200 μM NH_4FeSO_4, 200 μM sodium ascorbate, 1 mM α-ketoglutarate, and the appropriate substrate and enzyme. Assays were initiated by addition of the aryloxyalkanoate substrate, enzyme, or α-ketoglutarate at time 0. After 15 min incubation at 25 °C, the reaction was terminated by addition of 30 μL of a 1:1:1 mix of 50 mM Na EDTA, pH 10 buffer, and 0.2% 4-aminoantipyrine; then, 10 μL 0.8% potassium ferricyanide were added. After 15 min, the absorbance at 510 nm was recorded in a spectrophotometer. Blanks contained all reagents except for enzyme. Assays with pyridyloxyacetate substrates were performed in the same way, except that release of the pyridinol was directly observed by the increase of absorbance at 325 nm or by a succinyl-CoA synthetase-coupled assay (33).

Gene Redesigns for Plant Expression. Both of the *aad*-1 and *aad*-12 genes (*RdpA and SdpA*) were identified from the NCBI database (http://www.ncbi.nlm.nih.gov) with accession numbers of AF516752 and AY327575, respectively. To improve production of the recombinant protein in plants, both AAD DNA sequences were codon-optimized for plant expression. The resulting synthetic gene sequences encoded identical protein sequences, except for the addition of an alanine residue in the second position resulting from the creation of an NcoI site (CCATGG) across the ATG start codon to enable subsequent cloning operations. The plant-optimized *aad*-1 and *aad*-12 genes were synthesized at Picoscript and confirmed by sequencing.

***Constructs for testing in* Arabidopsis.** The *aad*-1 gene was cloned into plasmid pDAB726 as an NcoI–SacI fragment. The resulting construct was designated pDAB720, containing AtUbi10 /*aad*-1/Nt Osm3′UTR/AtuORF1 3′UTR. The fragment containing the described cassette in pDAB720 was then cloned into the corresponding *Not* I site of the binary vector pDAB3038. The resulting binary vector, pDAB721 (Fig. 2), containing the following cassette (AtUbi10 promoter/*aad*-1/Nt OSM 3′UTR/AtuORF1 3′UTR//CsVMV promoter/*pat*/AtuORF25/26 3′UTR) was confirmed through restriction enzyme digestion and DNA sequencing.

The *aad*-12 gene was cloned into plasmid pDAB726 as an NcoI–SacI fragment. The resulting construct was designated pDAB723, containing AtUbi10 promoter/*aad*-12/NtOsm3′UTR/AtuORF1 3′UTR. The fragment containing the described cassette in pDAB723 was then cloned into the *Not* I site of the binary vector pDAB3038. The resulting binary vector, pDAB724 (Fig. S1), containing the following cassette (AtUbi10 promoter/*aad*-12/NtOsm 3′UTR/AtuORF1 3′UTR//CsVMV promoter/*pat*/AtuORF25/26 3′UTR) was confirmed through restriction enzyme digestion and DNA sequencing.

AAD constructs for soybean and maize. *Aad*-12–containing construct pDAB4468 for soybean transformation was similar to construct pDAB724 with some modification. The T-DNA insert encompassing the *aad*-12 and *pat* expression cassettes consisted of RB7 MAR/AtUbi10 promoter/*aad*-12/AtuORF23 3′UTR//CsVMV promoter/*pat*/ AtuORF1 3′UTR (Fig. S3). The resulting binary vector, pDAB4468, was confirmed by restriction enzyme digestion and DNA sequencing.

Aad-1–containing construct pDAS1740 was derived from pDAB721 by simply eliminating the PAT expression cassette. *Aad*-1–containing construct pDAS1740 was digested by restriction enzyme FseI flanking the *aad*-1 expression cassette. The released fragment containing RB7 MAR/ZmUbi1 promoter/*aad*-1/ZmPer5 3′ UTR//RB7 MAR was purified and used for silicon carbide fiber-mediated transformation of maize (Fig. S5).

Plant Transformation. ***Agrobacterium*-mediated transformation of* Arabidopsis *and soybean.*** The genetically engineered *aad* gene cassettes in the binary vectors pDAB721 and pDAB724 were introduced into electrocompetent *A. tumefaciens* strain Z707S using a protocol from Weigel and Glazebrook (34). The presence of the gene insert in selected *Agrobacterium* colonies was verified with PCR analysis using vector-specific primers. *Arabidopsis* was transformed using the floral dip method (35).

The disarmed *A. tumefaciens* strain EHA101 carrying the binary vector pDAB4468 was used for soybean transformation. Transformation of soybean varieties was carried out by following the cotyledonary node *Agrobacterium*-mediated transformation system (36). Briefly, Maverick soybean seeds were germinated on basal media, and cotyledonary nodes were isolated and infected with *Agrobacterium.* Shoot initiation, shoot elongation, and rooting media were supplemented with cefotaxime, timentin, and vancomycin for removal of *Agrobacterium*. Glufosinate selection was used to inhibit the growth of nontransformed shoots. Selected shoots were transferred to rooting medium for root development and then, transferred to soil mix for acclimatization of plantlets. Terminal leaflets of selected plantlets were leaf-painted with glufosinate to screen for putative transformants. Surviving plantlets were deemed to be putative transformants. The screened plants were sampled and analyzed by molecular approaches to confirm the insertion of selectable marker gene and/or the gene of interest.

Silicon carbide fiber-mediated transformation of maize. DNA fragment containing the genetically engineered *aad*-1 gene cassette was released from plasmid pDAS1740 by FseI digestion and introduced into recipient maize line Hi-II through silicon carbide fiber (Whiskers)-mediated transformation (26). Immature embryos of maize were aseptically removed from the developing caryopsis, callused on semisolid media, initiated in liquid suspension cultures, cryopreserved, thawed, and reestablished as embryogenic suspensions. The reestablished suspensions were agitated with isolated pDAS1740/*Fsp* I DNA fragment and silicon carbide fibers to introduce the DNA into the cells. After 3 d of growth on nonselective, semisolid media, the cells were transferred to a medium containing the herbicide (*R*)-haloxyfop to select for cells expressing the *aad*-1 gene. The callus that survived on the herbicide-containing medium proliferated and produced embryogenic tissue that was presumably genetically transformed. Callus samples were taken for molecular analysis to verify the presence of the transgene and the absence of the ampicillin resistance gene from the vector backbone, although they were not included in the DNA fragment used for transformation. The embryogenic tissue was then manipulated to regenerate whole transgenic plants and transferred to a greenhouse. The plants were sprayed with the AOPP herbicide quizalofop to confirm herbicide resistance. Surviving plants were crossed with proprietary inbred maize lines to obtain T_1 seed from the initially transformed T_0 plants.

Characterization of Herbicide Resistance in Transformed Plants. Freshly harvested transformed *Arabidopsis* T_1 seeds were planted, and the T_1 plants at cotyledon [5 d after planting (DAP)] and two to four leaf-growth stages (10 DAP) were sprayed with glufosinate at a rate of 0.28 kg active ingredient (ai)/ha per application. Survivors (plants actively growing) were identified 5–7 d after the final spraying and transplanted individually into 3-in pots filled with potting media. Surviving T_1 plants from glufosinate spray were confirmed for expression of the PAT protein using a PAT ELISA (EnviroLogix, Inc.). Plants were then treated with various rates of 2,4-D at 0.0125 kg ae/ha and elevated rates of 0.05, 0.2, 0.8, or 3.2 kg ae/ha. Similarly, AAD-1 maize plants were selected either in the greenhouse or field with quizalofop (0.14–0.56 kg ai/ha) and subsequently challenged with 2,4-D (0.56–4.48 kg ae/ha). AAD-12 transgenic soybean plants were selected with herbicide glufosinate (0.411 kg ai/ha) and subsequently challenged with 2,4-D (0.56–4.48 kg ae/ha) in the field.

Heritability of Genes in Transgenic Plants. ***Herbicide resistance.*** T_1 and T_2 *Arabidopsis* populations (from self-pollination of T_1 plants) were screened with glufosinate. Approximately 75% of the T_2 individuals survived selective rates of glufosinate. Survivors were sprayed with varying rates of 2,4-D (0.05–3.2 kg ae/ha) as previously noted. Plant survival and level of injury were rated at 7 and 14 d after treatment (DAT). The level of injury observed among T_2 siblings was consistent with that observed in the individuals in T_1 generation. For soybean events, up to generation T_5 and the F_2 generation after crossing with elite varieties were used to study transgene heritability. For maize events, self-pollinated inbred generations (up to T_4) and back-cross generations (BC_1, BC_2, and BC_3S_1) were studied for the AAD-1 gene heritability. The data gathered indicated that the resistance is transferable across all of the tested generations (Table S1 and Fig. S6).

Southern blot analysis. For DNA analysis, total genomic DNA was isolated from individual plant tissues using the cetyltrimethylammonium bromide (CTAB) method. A total of 9 μg leaf genomic DNA or 10 μg genomic callus DNA was subjected to an overnight digestion using selected restriction enzymes. DNA was then separated by gel electrophoresis and transferred to a nylon membrane as described by Memelink et al. (37). The hybridization probes were generated using a PCR-based incorporation of a digoxigenin (DIG)-labeled nucleotide, (DIG-11)-dUTP, to DNA fragments generated by primers

COR-AAD1-00003367
Bayer EX1008 (Part 6 of 9)

specific to the gene elements and other regions from target plasmid. The PCR synthesis of the probes was performed using PCR DIG Probe Synthesis Kit (Roche Diagnostics). Labeled probes were hybridized to the target DNA on the nylon membranes using the DIG Easy Hyb Solution (Roche Diagnostics). DIG-labeled DNA molecular weight marker II was used to determine the hybridizing fragment size on the Southern blots.

DIG-labeled probes bound to the nylon membranes were visualized using CDP-Star Chemiluminescent Nucleic Acid Detection System (Roche Diagnostics). Blots were exposed to chemiluminescent film for one or more time points to detect the hybridizing fragments and visualize the molecular weight standards.

Western blot analysis. For Western blot analysis, ~50–100 mg leaf tissue were extracted with 500 μL plant extraction buffer (PBS containing 0.05% Tween 20 and 0.5% BSA) using the Geno/Grinder (Model 2000–115; Certiprep). Extracts were centrifuged, and the supernatant containing the soluble proteins was used for Western blots or ELISA. Plant extracts were incubated with Laemmli sample buffer at 95 °C for 10 min and electrophoretically separated in 8–16% Tris-Glycine Precast gel. Proteins were then electrotransferred onto nitrocellulose membrane using a standard protocol. After blocking in 4% skim milk in PBS, protein was detected by antiserum followed by goat anti-rabbit/HRP conjugates. The detected protein was visualized by chemiluminescence substrate (ECL Western Analysis Reagent; Amersham).

ELISA Analysis of Plant Tissues. ***AAD-1 ELISA.*** An AAD-1–specific monoclonal antibody (2 μg/mL) was immobilized on microtiter wells to capture AAD-1 protein in plant extracts (described above). Various concentrations of plant extracts were incubated in the wells. To prepare a standard curve, different concentrations of purified AAD-1 proteins (100, 50, 25, 12.5, 6.25, 3.13, 1.56, and 0 ng/mL) were also put into the microtiter wells on the same assay plate in duplicates. The plate was incubated for 1 h and washed four times with PBS with 0.05% Tween 20 (PBST). Biotinylated anti–AAD-1 monoclonal antibody (1 μg/mL) solution in PBST was added and incubated for 1 h to detect the bound AAD-1 protein. After another wash step, neutravidin–alkaline phosphatase (AP) conjugate (Pierce Biotech) was added to each well and incubated for another 1 h. pNPP (p-nitrophenyl phosphate) solution (AP substrate; 100 μL) was added, and after the 30- to 45-min incubation, the absorbance at 405 nm was measured using a microtiter plate reader. The concentration of proteins in plant extracts was extrapolated from a standard curve developed on the same plate.

AAD-12 ELISA. Purified rabbit antibody (1 μg/mL) was immobilized on microtiter wells to capture AAD-12 protein in plant extracts as described above for AAD-1. HRP-conjugated anti–AAD-12 monoclonal antibody (1 μg/mL) solution in PBST was added and incubated for 1 h to detect the bound AAD-12 protein. After another wash step, 3,3′,5,5′ Tetramethylbenzidine (TMB) substrate (100 μL) was added, and after the 15-min incubation, 100 μL stop solution (1 N HCl) was added to stop the reaction. The absorbance at 450 nm was measured using a microtiter plate reader.

1. James C (2009) *Global Status of Commercialized Biotech/GM Crops: 2009.* (ISAAA, Ithaca, NY), ISAAA Brief No 41.
2. Powles SB, Preston C (2006) Evolved glyphosate resistance in plants: Biochemical and genetic basis of resistance. *Weed Technol* 20:282–289.
3. Simarmata M, Kaufmann JE, Penner D (2003) Potential basis of glyphosate resistance in California rigid ryegrass (*Lolium* rigidum). *Weed Sci* 51:678–682.
4. Lorraine-Colwill DF, et al. (2003) Investigations into the mechanism of glyphosate resistance in *Lolium rigidum*. *Pestic Biochem Physiol* 74:62–73.
5. Miller SD, et al. (2003) Risks of weed spectrum shifts and herbicide resistance in glyphosate-resistant cropping systems. *Proc West Soc Weed Sci* 56:61–62.
6. Heap I (2010) The International Survey of Herbicide Resistant Weeds. Available at www.weedscience.com. Accessed August 14, 2010.
7. Cerdeira AL, Duke SO (2006) The current status and environmental impacts of glyphosate-resistant crops: A review. *J Environ Qual* 35:1633–1658.
8. Heap, I. *The International Survey of Herbicide Resistant Weeds*. Available at www.weedscience.com. Accessed August 10, 2010.
9. Coble HD, Warren LS (1997) Weed control investigations in maize, cotton, crop rotations, soybean, small grain. Annual report of the Department of Crop Science. *N C State University* 28:103–113.
10. Shaner DL (2000) The impact of glyphosate-tolerant crops on the use of other herbicides and on resistance management. *Pest Manag Sci* 56:320–326.
11. Gianessi LP (2005) Economic and herbicide use impacts of glyphosate-resistant crops. *Pest Manag Sci* 61:241–245.
12. Service RF (2007) Agbiotech. A growing threat down on the farm. *Science* 316: 1114–1117.
13. Behrens MR, et al. (2007) Dicamba resistance: Enlarging and preserving biotechnology-based weed management strategies. *Science* 316:1185–1188.
14. Industry Task Force II on 2,4-D Research Data (2005) *Issue Backgrounder*. Available at http://www.24d.org/background/24D-Backgrounder-Benefits.pdf. Accessed August 10, 2010.
15. Tu M, Hurd C, Randall JM (2001) Weed Control Methods Handbook. The Nature Conservancy, Version April 2001. Available at http://www.invasive.org/gist/handbook.html. Accessed August 10, 2010.
16. United States Environmental Protection Agency (2006) Pesticides reregistration, 2,4-D RED facts, Available at http://www.epa.gov/oppsrrd1/REDs/factsheets/24d_fs.htm. Accessed August 14, 2010.
17. Sterling TM, Hall JC (1997) Mechanism of action of natural auxins and the auxinic herbicides. *Herbicide Activity: Toxicology, Biochemistry and Molecular Biology*, eds Roe MR, Kuhr RJ, Burton JD (IOS Press, Amsterdam), pp 111–141.
18. Streber WR, Timmis KN, Zenk MH (1987) Analysis, cloning, and high-level expression of 2,4-dichlorophenixyacetic monooxygenase gene tfdA of Alcaligenes eutrophus JMP134. *J Bacteriol* 169:2950–2955.
19. Smejkal CW, et al. (2001) Substrate specificity of chlorophenoxyalkanoic acid-degrading bacteria is not dependent upon phylogenetically related tfdA gene types. *Biol Fertil Soils* 33:507–513.
20. Bayley C, et al. (1992) Engineering 2,4-D resistance into cotton. *Theor Appl Genet* 83: 645–649.
21. Hogan DA, Smith SR, Saari EA, McCracken J, Hausinger RP (2000) Site-directed mutagenesis of 2,4-dichlorophenoxyacetic acid/alpha-ketoglutarate dioxygenase. Identification of residues involved in metallocenter formation and substrate binding. *J Biol Chem* 275:12400–12409.
22. Müller TA, Byrde SM, Werlen C, van der Meer JR, Kohler HP (2004) Genetic analysis of phenoxyalkanoic acid degradation in Sphingomonas herbicidovorans MH. *Appl Environ Microbiol* 70:6066–6075.
23. Wright TR, et al. (2005) International Patent WO/2005/107437.
24. Müller TA, Fleischmann T, van der Meer JR, Kohler HP (2006) Purification and characterization of two enantioselective α-ketoglutarate-dependent dioxygenases, RdpA and SdpA, from *Sphingomonas herbicidovorans* MH. *Appl Environ Microbiol* 72: 4853–4861.
25. Westendorf A, Muller RH, Babel W (2003) Purification and characterization of the enantiospecific dioxygenases from *Delftia acidovorans* MC1 initiating the degradation of phenoxypropionates and phenoxyacetate herbicides. *Acta Biotechnol* 23:3–17.
26. Petolino JF, Arnold NL (2009) Whiskers-mediated maize transformation. *Methods in Molecular Biology: Transgenic Maize*, ed Scott MP (Humana Press, Clifton, NJ), Vol 526, pp 59–67.
27. Mockaitis K, Estelle M (2008) Auxin receptors and plant development: A new signaling paradigm. *Annu Rev Cell Dev Biol* 24:55–80.
28. Heap IM (1997) The occurrence of herbicide-resistant weeds worldwide. *Pestic Sci* 51: 235–243.
29. Devine MO, Duke SO, Fedtke C, eds (1993) *Physiology of Herbicide Action* (Prentice Hall, Englewood Cliffs, NJ).
30. Jasieniuk M, Brule-Babel AL, Morrison IN (1996) The evolution and genetics of herbicide resistance in weeds. *Weed Sci* 44:176–193.
31. Van Eerd LL, Stephenson GR, Kwiatkowski J, Grossmann K, Hall JC (2005) Physiological and biochemical characterization of quinclorac resistance in a false cleavers (Galium spurium L.) biotype. *J Agric Food Chem* 53:1144–1151.
32. Fukumori F, Hausinger RP (1993) Purification and characterization of 2,4-dichlorophenoxyacetate/α-ketoglutarate dioxygenase. *J Biol Chem* 268:24311–24317.
33. Luo L, et al. (2006) An assay for Fe(II)/2-oxoglutarate-dependent dioxygenases by enzyme-coupled detection of succinate formation. *Anal Biochem* 353:69–74.
34. Weigel D, Glazebrook J (2002) *Arabidopsis: A Laboratory Manual* (Cold Spring Harbor Laboratory Press, Plainview, NY).
35. Clough SJ, Bent AF (1998) Floral dip: A simplified method for Agrobacterium-mediated transformation of Arabidopsis thaliana. *Plant J* 16:735–743.
36. Zeng P, Vadnais DA, Zhang Z, Polacco JC (2004) Refined glufosinate selection in *Agrobacterium*-mediated transformation of soybean [Glycine max (L.) Merrill]. *Plant Cell Rep* 22:478–482.
37. Memelink J, Swords K, Harry J, Hoge C (1994) Southern, Northern, and Western Blot Analysis. *Plant Molecular Biology Manual* F1:1–23.

COR-AAD1-00003368
Bayer EX1008 (Part 6 of 9)

Protein

COVID-19 is an emerging, rapidly evolving situation.
Get the latest public health information from CDC: https://www.coronavirus.gov .
Get the latest research from NIH: https://www.nih.gov/coronavirus.
Find NCBI SARS-CoV-2 literature, sequence, and clinical content: https://www.ncbi.nlm.nih.gov/sars-cov-2/.

GenPept

2,4-dichlorophenoxyacetate monooxygenase (gtg start codon) [Cupriavidus necator]

GenBank: AAA21983.1

Identical Proteins FASTA Graphics

Go to:

```
LOCUS       AAA21983                287 aa            linear   BCT 26-APR-1993
DEFINITION  2,4-dichlorophenoxyacetate monooxygenase (gtg start codon)
            [Cupriavidus necator].
ACCESSION   AAA21983
VERSION     AAA21983.1
DBSOURCE    locus AFATFDA accession M16730.1
KEYWORDS    .
SOURCE      Cupriavidus necator (Ralstonia eutropha)
  ORGANISM  Cupriavidus necator
            Bacteria; Proteobacteria; Betaproteobacteria; Burkholderiales;
            Burkholderiaceae; Cupriavidus.
REFERENCE   1  (residues 1 to 287)
  AUTHORS   Streber,W.R., Timmis,K.N. and Zenk,M.H.
  TITLE     Analysis, cloning, and high-level expression of
            2,4-dichlorophenoxyacetate monooxygenase gene tfdA of Alcaligenes
            eutrophus JMP134
  JOURNAL   J. Bacteriol. 169 (7), 2950-2955 (1987)
   PUBMED   3036764
COMMENT     Draft entry and computer-readable sequence for [1] kindly provided
            by W.R.Streber, 30-SEP-1987.
            Method: conceptual translation.
FEATURES             Location/Qualifiers
     source          1..287
                     /organism="Cupriavidus necator"
                     /db_xref="taxon:106590"
     Protein         1..287
                     /name="2,4-dichlorophenoxyacetate monooxygenase (gtg start
                     codon)"
     Region          7..280
                     /region_name="TauD"
                     /note="Taurine catabolism dioxygenase TauD, TfdA family;
                     pfam02668"
                     /db_xref="CDD:388346"
     Site            order(114,116,141,263,274)
                     /site_type="active"
                     /db_xref="CDD:238154"
     Site            order(114,116,263)
                     /site_type="other"
                     /note="iron coordination sites [ion binding]"
                     /db_xref="CDD:238154"
     CDS             1..287
                     /coded_by="M16730.1:748..1611"
                     /transl_table=11
ORIGIN
        1 msvvanplhp lfaagvedid lrealgstev reierlmdek svlvfrgqpl sqdqqiafar
       61 nfgpleggfi kvnqrpsrfk yaeladisnv sldgkvaqrd arevvgnfan qlwhsdssfq
      121 qpaarysmls avvvppsggd tefcdmraay dalprdlqse leglraehya lnsrfllgdt
      181 dyseaqrnam ppvnwplvrt hagsgrkflf igahashveg lpvaegrmll aellehatqr
      241 efvyrhrwnv gdlvmwdnrc vlhrgrrydi sarrelrrat tlddavv
//
```


COR-AAD1-00003369
Bayer EX1008 (Part 6 of 9)

Protein

COVID-19 is an emerging, rapidly evolving situation.
Get the latest public health information from CDC: https://www.coronavirus.gov .
Get the latest research from NIH: https://www.nih.gov/coronavirus.
Find NCBI SARS-CoV-2 literature, sequence, and clinical content: https://www.ncbi.nlm.nih.gov/sars-cov-2/.

GenPept

2,4-D/alpha-ketoglutarate dioxygenase (plasmid) [Burkholderia cepacia]

GenBank: AAK81681.1

Identical Proteins FASTA Graphics

Go to:

```
LOCUS       AAK81681                287 aa            linear   BCT 23-JUL-2016
DEFINITION  2,4-D/alpha-ketoglutarate dioxygenase (plasmid) [Burkholderia
            cepacia].
ACCESSION   AAK81681
VERSION     AAK81681.1
DBSOURCE    accession AF029344.2
KEYWORDS    .
SOURCE      Burkholderia cepacia
  ORGANISM  Burkholderia cepacia
            Bacteria; Proteobacteria; Betaproteobacteria; Burkholderiales;
            Burkholderiaceae; Burkholderia; Burkholderia cepacia complex.
REFERENCE   1  (residues 1 to 287)
  AUTHORS   Poh,R., Xia,X., Bruce,I.J. and Smith,A.R.
  TITLE     2,4-dichlorophenoxyacetate/alpha-ketoglutarate dioxygenases from
            Burkholderia cepacia 2a and Ralstonia eutropha JMP134
  JOURNAL   Microbios 105 (410), 43-63 (2001)
   PUBMED   11368031
REFERENCE   2  (residues 1 to 287)
  AUTHORS   Poh,R.P., Smith,A.R. and Bruce,I.J.
  TITLE     Complete characterisation of Tn5530 from Burkholderia cepacia
            strain 2a (pIJB1) and studies of 2,4-dichlorophenoxyacetate uptake
            by the organism
  JOURNAL   Plasmid 48 (1), 1-12 (2002)
   PUBMED   12206751
REFERENCE   3  (residues 1 to 287)
  AUTHORS   Poh,R.P.C., Smith,A.R.W. and Bruce,I.J.
  TITLE     Sequence analysis and idenification of catabolic genes on plasmid
            pIJB1 from Burkholderia cepacia 2a
  JOURNAL   Unpublished
REFERENCE   4  (residues 1 to 287)
  AUTHORS   Poh,R.P.C., Bruce,I.J. and Smith,A.R.W.
  TITLE     Direct Submission
  JOURNAL   Submitted (08-OCT-1997) School of Chemical & Life Sciences,
            University of Greenwich, Wellington Street, Woolwich, London SE18
            6PF, United Kingdom
REFERENCE   5  (residues 1 to 287)
  AUTHORS   Poh,R.P.C., Bruce,I.J. and Smith,A.R.W.
  TITLE     Direct Submission
  JOURNAL   Submitted (27-JUL-2001) School of Chemical & Life Sciences,
            University of Greenwich, Wellington Street, Woolwich, London SE18
            6PF, United Kingdom
  REMARK    Sequence update by submitter
COMMENT     Method: conceptual translation supplied by author.
FEATURES             Location/Qualifiers
     source          1..287
                     /organism="Burkholderia cepacia"
                     /strain="2A"
                     /db_xref="taxon:292"
                     /plasmid="pIJB1"
     Protein         1..287
                     /product="2,4-D/alpha-ketoglutarate dioxygenase"
     Region          5..280
                     /region_name="TauD"
                     /note="Taurine catabolism dioxygenase TauD, TfdA family;
                     pfam02668"
                     /db_xref="CDD:308346"
     CDS             1..287
                     /gene="tfdA"
                     /coded_by="AF029344.2:27627..28490"
                     /experiment="experimental evidence, no additional details
```


COR-AAD1-00003370
Bayer EX1008 (Part 6 of 9)

```
                     recorded"
                     /transl_table=11
ORIGIN
        1 msitseylhp lfvgqvdkla lqgalsptev rdvehqmdqk avlvfrgqpl dqdqqiafar
       61 nfgqleggfi kvnqrpsrfk yaeladisnv svdgkvaerd arevvgnfan qlwhsdssfq
      121 qpaarysmls aivlppsggd tefcdmraay ddlpedfkke lqglraehya lnsrfilgdt
      181 dysesqrnam ppvswplvrt hagsgrkflf igahaghieg rpvaegrmll aellehatqr
      241 kfvyrhswkv gdlvmwdnrc vlhrgrrydi tarrelrrat tlddavv
//
```


COR-AAD1-00003371
Bayer EX1008 (Part 6 of 9)

Protein

COVID-19 is an emerging, rapidly evolving situation.
Get the latest public health information from CDC: https://www.coronavirus.gov .
Get the latest research from NIH: https://www.nih.gov/coronavirus.
Find NCBI SARS-CoV-2 literature, sequence, and clinical content: https://www.ncbi.nlm.nih.gov/sars-cov-2/.

GenPept

RecName: Full=Alpha-ketoglutarate-dependent 2,4-dichlorophenoxyacetate dioxygenase; Short=2,4-D dioxygenase

UniProtKB/Swiss-Prot: Q45423.1

Identical Proteins FASTA Graphics

Go to:

```
LOCUS       TFDA_BURSR               297 aa            linear   BCT 12-AUG-2020
DEFINITION  RecName: Full=Alpha-ketoglutarate-dependent
            2,4-dichlorophenoxyacetate dioxygenase; Short=2,4-D dioxygenase.
ACCESSION   Q45423
VERSION     Q45423.1
DBSOURCE    UniProtKB: locus TFDA_BURSR, accession Q45423;
            class: standard.
            created: Nov 1, 1997.
            sequence updated: Nov 1, 1996.
            annotation updated: Aug 12, 2020.
            xrefs: U25717.1, AAB17363.1
            xrefs (non-sequence databases): SMR:Q45423, KEGG:ag:AAB17363,
            KO:K06912, UniPathway:UPA00685, GO:0051213, GO:0031418, GO:0046872,
            GO:0046300, Gene3D:3.60.130.10, InterPro:IPR042098,
            InterPro:IPR003819, Pfam:PF02668
KEYWORDS    Aromatic hydrocarbons catabolism; Dioxygenase; Iron; Metal-binding;
            Oxidoreductase; Vitamin C.
SOURCE      Burkholderia sp. RASC
  ORGANISM  Burkholderia sp. RASC
            Bacteria; Proteobacteria; Betaproteobacteria; Burkholderiales;
            Burkholderiaceae; Burkholderia.
REFERENCE   1  (residues 1 to 297)
  AUTHORS   Suwa,Y., Wright,A.D., Fukimori,F., Nummy,K.A., Hausinger,R.P.,
            Holben,W.E. and Forney,L.J.
  TITLE     Characterization of a chromosomally encoded
            2,4-dichlorophenoxyacetic acid/alpha-ketoglutarate dioxygenase from
            Burkholderia sp. strain RASC
  JOURNAL   Appl. Environ. Microbiol. 62 (7), 2464-2469 (1996)
   PUBMED   8779585
  REMARK    NUCLEOTIDE SEQUENCE [GENOMIC DNA].
COMMENT     [FUNCTION] Involved in degradation of the herbicide
            2,4-dichlorophenoxyacetic acid (2,4-D). Is also able to degrade
            2-methyl-4-chlorophenoxyacetic acid and 3-chlorobenzoic acid.
            [CATALYTIC ACTIVITY] Reaction=(2,4-dichlorophenoxy)acetate +
            2-oxoglutarate + O2 = 2,4-dichlorophenol + CO2 + glyoxylate +
            succinate; Xref=Rhea:RHEA:48984, ChEBI:CHEBI:15379,
            ChEBI:CHEBI:16526, ChEBI:CHEBI:16738, ChEBI:CHEBI:16810,
            ChEBI:CHEBI:19351, ChEBI:CHEBI:30031, ChEBI:CHEBI:36655.
            [COFACTOR] Name=Fe(2+); Xref=ChEBI:CHEBI:29033;
            Evidence={ECO:0000250}; Note=Binds 1 Fe(2+) ion per subunit.
            {ECO:0000250}.
            ACTIVITY REGULATION: Activated by ascorbate. {ECO:0000305}.
            [PATHWAY] Xenobiotic degradation; (2,4-dichlorophenoxy)acetate
            degradation.
            [SIMILARITY] Belongs to the TfdA dioxygenase family. {ECO:0000305}.
FEATURES             Location/Qualifiers
     source          1..297
                     /organism="Burkholderia sp. RASC"
                     /db_xref="taxon:69003"
     gene            1..297
                     /gene="tfdA"
     Protein         1..297
                     /product="Alpha-ketoglutarate-dependent
                     2,4-dichlorophenoxyacetate dioxygenase"
                     /EC_number="1.14.11.-"
                     /note="2,4-D dioxygenase"
                     /UniProtKB_evidence="Inferred from homology"
     Region          1..297
```


COR-AAD1-00003372
Bayer EX1008 (Part 6 of 9)

```
                     /region_name="Mature chain"
                     /note="Alpha-ketoglutarate-dependent
                     2,4-dichlorophenoxyacetate dioxygenase.
                     /id=PRO_0000194018."
     Region          4..280
                     /region_name="TauD"
                     /note="Taurine catabolism dioxygenase TauD, TfdA family;
                     pfam02668"
                     /db_xref="CDD:288777"
     Region          8..283
                     /region_name="TauD"
                     /note="Taurine dioxygenase, alpha-ketoglutarate-dependent
                     [Secondary metabolites biosynthesis, transport and
                     catabolism]; COG2175"
                     /db_xref="CDD:225086"
     Site            order(114,116,141,263,274)
                     /site_type="active"
                     /db_xref="CDD:238154"
     Site            order(114,116,263)
                     /site_type="other"
                     /note="iron coordination sites [ion binding]"
                     /db_xref="CDD:238154"
     Site            114
                     /site_type="metal-binding"
                     /note="Iron; catalytic. /evidence=ECO:0000250."
     Site            116
                     /site_type="metal-binding"
                     /note="Iron; catalytic. /evidence=ECO:0000250."
     Site            141
                     /site_type="binding"
                     /note="2-oxoglutarate. /evidence=ECO:0000250."
     Site            248
                     /site_type="binding"
                     /note="2-oxoglutarate. /evidence=ECO:0000250."
     Site            263
                     /site_type="metal-binding"
                     /note="Iron; catalytic. /evidence=ECO:0000250."
     Site            274
                     /site_type="binding"
                     /note="2-oxoglutarate. /evidence=ECO:0000250."
     Site            278
                     /site_type="binding"
                     /note="2-oxoglutarate. /evidence=ECO:0000250."
ORIGIN
        1 msinseylhp lfvgqvdnla lqgalspaev rdvenemdqk avlvfrgqpl dqdqqiafar
       61 nfgqleggfi kvnqrpsrfk yaeladisnv svdgkvaead arevvgnfan qlwhsdssfq
      121 qpaarysmls aivlppsggd tefcdmraay ddlpedfkke lqglraehya lhsrfilgdt
      181 eysesqrnam ppvswplirt hagsgrkflf igahashieg rpvaegrmll aellehatqp
      241 kfvyrhswkv gdlvmwdnrc vlhrgrrydv tarrelrrat tlgrrcrlsp rgqswvq
//
```


COR-AAD1-00003373
Bayer EX1008 (Part 6 of 9)

Protein

COVID-19 is an emerging, rapidly evolving situation.
Get the latest public health information from CDC: https://www.coronavirus.gov .
Get the latest research from NIH: https://www.nih.gov/coronavirus.
Find NCBI SARS-CoV-2 literature, sequence, and clinical content: https://www.ncbi.nlm.nih.gov/sars-cov-2/.

GenPept

TfdA (plasmid) [Achromobacter denitrificans]

GenBank: AAS49436.1

Identical Proteins FASTA Graphics

Go to:

```
LOCUS       AAS49436                287 aa            linear   BCT 03-APR-2020
DEFINITION  TfdA (plasmid) [Achromobacter denitrificans].
ACCESSION   AAS49436
VERSION     AAS49436.1
DBLINK      BioSample: SAMN14224287
DBSOURCE    accession AY540995.2
KEYWORDS    .
SOURCE      Achromobacter denitrificans
  ORGANISM  Achromobacter denitrificans
            Bacteria; Proteobacteria; Betaproteobacteria; Burkholderiales;
            Alcaligenaceae; Achromobacter.
REFERENCE   1  (residues 1 to 287)
  AUTHORS   Vedler,E., Vahter,M. and Heinaru,A.
  TITLE     The completely sequenced plasmid pEST4011 contains a novel IncP1
            backbone and a catabolic transposon harboring tfd genes for
            2,4-dichlorophenoxyacetic acid degradation
  JOURNAL   J. Bacteriol. 186 (21), 7161-7174 (2004)
   PUBMED   15489427
REFERENCE   2  (residues 1 to 287)
  AUTHORS   Vedler,E.
  TITLE     Direct Submission
  JOURNAL   Submitted (04-FEB-2004) Department of Genetics, Institute of
            Molecular and Cell Biology, Tartu University, 23 Riia Street, Tartu
            51010, Estonia
REFERENCE   3  (residues 1 to 287)
  AUTHORS   Vedler,E.
  TITLE     Direct Submission
  JOURNAL   Submitted (06-FEB-2012) Department of Genetics, Institute of
            Molecular and Cell Biology, Tartu University, 23 Riia Street, Tartu
            51010, Estonia
  REMARK    Sequence update by submitter
COMMENT     Method: conceptual translation supplied by author.
FEATURES             Location/Qualifiers
     source          1..287
                     /organism="Achromobacter denitrificans"
                     /strain="EST4002"
                     /db_xref="taxon:32002"
                     /plasmid="pEST4011"
     Protein         1..287
                     /product="TfdA"
     Region          4..280
                     /region_name="TauD"
                     /note="Taurine catabolism dioxygenase TauD, TfdA family;
                     pfam02668"
                     /db_xref="CDD:280777"
     Region          8..284
                     /region_name="TauD"
                     /note="Taurine dioxygenase, alpha-ketoglutarate-dependent
                     [Secondary metabolites biosynthesis, transport and
                     catabolism]; COG2175"
                     /db_xref="CDD:225086"
     CDS             1..287
                     /gene="tfdA"
                     /coded_by="complement(AY540995.2:19666..20529)"
                     /experiment="experimental evidence, no additional details
                     recorded"
                     /note="2,4-D/alpha-ketoglutarate dioxygenase"
                     /transl_table=11
ORIGIN
        1 msitseylhp lfvgqvdkla lqgalsptev rdvehqmdqk avlvfrgqpl dqdqqiafar
```


COR-AAD1-00003374
Bayer EX1008 (Part 6 of 9)

```
       61 nfgqleggfi kvnqrpsrfk yaeladisnv svdgkvrerd arevvgnfan qlwhsdssfq
      121 qpaarysmls aivlppsggd tefcdmraay ddlpedfkke lqglraehya lnsrfilgdt
      181 dysesqrnam ppvswplvrt hagsgrkflf igahaghieg rpvaegrmll aellehatqr
      241 kfvyrhswkv gdlvmwdnrc vlhrgrrydi tarrelrrat tlddavv
//
```


COR-AAD1-00003375
Bayer EX1008 (Part 6 of 9)

Protein

COVID-19 is an emerging, rapidly evolving situation.
Get the latest public health information from CDC: https://www.coronavirus.gov .
Get the latest research from NIH: https://www.nih.gov/coronavirus.
Find NCBI SARS-CoV-2 literature, sequence, and clinical content: https://www.ncbi.nlm.nih.gov/sars-cov-2/.

GenPept

2,4-D dioxygenase (plasmid) [Burkholderia cepacia]

GenBank: AAB47567.1

Identical Proteins FASTA Graphics

Go to:

```
LOCUS       AAB47567                288 aa            linear   BCT 26-JUL-2016
DEFINITION  2,4-D dioxygenase (plasmid) [Burkholderia cepacia].
ACCESSION   AAB47567
VERSION     AAB47567.1
DBSOURCE    locus BCU87394 accession U87394.1
KEYWORDS    .
SOURCE      Burkholderia cepacia
  ORGANISM  Burkholderia cepacia
            Bacteria; Proteobacteria; Betaproteobacteria; Burkholderiales;
            Burkholderiaceae; Burkholderia; Burkholderia cepacia complex.
REFERENCE   1  (residues 1 to 288)
  AUTHORS   Maclean,K.N., Bustin,S.A., McClure,N.C., Bruce,I.J. and
            Smith,A.R.W.
  TITLE     Cloning and Sequence Analysis of the 2,4-D dioxygenase from plasmid
            pIJB
  JOURNAL   Unpublished
REFERENCE   2  (residues 1 to 288)
  AUTHORS   Maclean,K.N., Bustin,S.A., McClure,N.C., Bruce,I.J. and
            Smith,A.R.W.
  TITLE     Direct Submission
  JOURNAL   Submitted (28-JAN-1997) Surgical Unit, London Hospital Medical
            College, Whitechapel High Street, London E1 1BB, UK
FEATURES             Location/Qualifiers
     source          1..288
                     /organism="Burkholderia cepacia"
                     /strain="2a"
                     /db_xref="taxon:292"
                     /plasmid="pIJB"
     Protein         1..288
                     /product="2,4-D dioxygenase"
     Region          4..281
                     /region_name="TauD"
                     /note="Taurine catabolism dioxygenase TauD, TfdA family;
                     pfam02668"
                     /db_xref="CDD:280777"
     Region          8..286
                     /region_name="TauD"
                     /note="Taurine dioxygenase, alpha-ketoglutarate-dependent
                     [Secondary metabolites biosynthesis, transport and
                     catabolism]; COG2175"
                     /db_xref="CDD:225086"
     CDS             1..288
                     /gene="IJBA"
                     /coded_by="U87394.1:94..960"
                     /transl_table=11
ORIGIN
        1 msinseylhp lfvaeyeead lqgalsptev rdvehqmdkk avlvfrgqpl dqdqqiafar
       61 nfgqleggfi kvnqrpsrfk yaeladisnv svdgkvadre aresvgnfan nqlwhsdssf
      121 qqaaarysml sasvlpplgg dtefwdihat nlggrddlpr elqglraery lqnsrfilgd
      181 tdysesqrna mppvswplvr thagsgrkfl figahaghie grpvaegrml laellehatq
      241 rkfvyrhrwk vgdlvmwdnr cvlhrgrgyd itarrelrra ttvddgvv
//
```


COR-AAD1-00003376
Bayer EX1008 (Part 6 of 9)

Protein

COVID-19 is an emerging, rapidly evolving situation.
Get the latest public health information from CDC: https://www.coronavirus.gov .
Get the latest research from NIH: https://www.nih.gov/coronavirus.
Find NCBI SARS-CoV-2 literature, sequence, and clinical content: https://www.ncbi.nlm.nih.gov/sars-cov-2/.

GenPept

2,4-D/alpha-ketoglutarate dioxygenase [Delftia acidovorans]

GenBank: AAM76772.1

Identical Proteins FASTA Graphics

Go to:

```
LOCUS       AAM76772                287 aa            linear   BCT 26-JUL-2016
DEFINITION  2,4-D/alpha-ketoglutarate dioxygenase [Delftia acidovorans].
ACCESSION   AAM76772 AAK57006
VERSION     AAM76772.1
DBSOURCE    accession AY078159.2
KEYWORDS    .
SOURCE      Delftia acidovorans
  ORGANISM  Delftia acidovorans
            Bacteria; Proteobacteria; Betaproteobacteria; Burkholderiales;
            Comamonadaceae; Delftia.
REFERENCE   1  (residues 1 to 287)
  AUTHORS   Hoffmann,D., Kleinsteuber,S., Mueller,R.H. and Babel,W.
  TITLE     Development and application of PCR primers for the detection of the
            tfd genes in Delftia acidovorans P4a involved in the degradation of
            2,4-D
  JOURNAL   Acta Biotechnol. 21, 321-331 (2001)
REFERENCE   2  (residues 1 to 287)
  AUTHORS   Hoffmann,D., Kleinsteuber,S., Muller,R.H. and Babel,W.
  TITLE     A transposon encoding the complete 2,4-dichlorophenoxyacetic acid
            degradation pathway in the alkalitolerant strain Delftia
            acidovorans P4a
  JOURNAL   Microbiology (Reading, Engl.) 149 (PT 9), 2545-2556 (2003)
   PUBMED   12949178
REFERENCE   3  (residues 1 to 287)
  AUTHORS   Hoffmann,D., Kleinsteuber,S., Mueller,R.H. and Babel,W.
  TITLE     Structural organization and chromosomal localization of the
            chlorocatechol gene cluster in the 2,4-D degrading alkalitolerant
            strain Delftia acidovorans P4a
  JOURNAL   Unpublished
REFERENCE   4  (residues 1 to 287)
  AUTHORS   Hoffmann,D. and Kleinsteuber,S.
  TITLE     Direct Submission
  JOURNAL   Submitted (07-MAY-2001) Environmental Microbiology, UFZ Centre for
            Environmental Research, Permoserstrasse 15, Leipzig D-04318,
            Germany
REFERENCE   5  (residues 1 to 287)
  AUTHORS   Hoffmann,D. and Kleinsteuber,S.
  TITLE     Direct Submission
  JOURNAL   Submitted (07-FEB-2002) Environmental Microbiology, UFZ Centre for
            Environmental Research, Permoserstrasse 15, Leipzig D-04318,
            Germany
REFERENCE   6  (residues 1 to 287)
  AUTHORS   Hoffmann,D. and Kleinsteuber,S.
  TITLE     Direct Submission
  JOURNAL   Submitted (10-JUL-2002) Environmental Microbiology, UFZ Centre for
            Environmental Research, Permoserstrasse 15, Leipzig D-04318,
            Germany
  REMARK    Sequence update by submitter
COMMENT     On Dec 1, 2003 this sequence version replaced AAK57006.1.
FEATURES             Location/Qualifiers
     source          1..287
                     /organism="Delftia acidovorans"
                     /strain="P4a"
                     /db_xref="taxon:80866"
     Protein         1..287
                     /product="2,4-D/alpha-ketoglutarate dioxygenase"
     Region          4..280
                     /region_name="TauD"
                     /note="Taurine catabolism dioxygenase TauD, TfdA family;
                     pfam02668"
```


COR-AAD1-00003377
Bayer EX1008 (Part 6 of 9)

```
                     /db_xref="CDD:286777"
     Region          8..284
                     /region_name="TauD"
                     /note="Taurine dioxygenase, alpha-ketoglutarate-dependent
                     [Secondary metabolites biosynthesis, transport and
                     catabolism]; COG2175"
                     /db_xref="CDD:225086"
     Site            order(114,116,141,263,274)
                     /site_type="active"
                     /db_xref="CDD:238154"
     Site            order(114,116,263)
                     /site_type="other"
                     /note="iron coordination sites [ion binding]"
                     /db_xref="CDD:238154"
     CDS             1..287
                     /gene="tfdA"
                     /coded_by="complement(AY078159.2:13930..14793)"
                     /transl_table=11
ORIGIN
        1 msitseylhp lfvgqvdkla lqgalsptev rdiehqmdqk avlvfrgqpl dqdqqiafar
       61 nfgqleggfi kvnqrpsrfk yaeladisnv svdgkvaerd arevvgnyan qlwhsdssfq
      121 qpaarysmls aivlppsggd tefcdmraay ddlpedfkke lqglraehya lhsrfilgdt
      181 dysesqrnam ppvswplvrt hagsgrkflf igahashieg rpvaegrmll aellehatqr
      241 kfvyrhswkv gdlvmwdnrc vlhrgrrydi tarrelrrat tlddavv
//
```


COR-AAD1-00003378
Bayer EX1008 (Part 6 of 9)

Protein

COVID-19 is an emerging, rapidly evolving situation.
Get the latest public health information from CDC: https://www.coronavirus.gov .
Get the latest research from NIH: https://www.nih.gov/coronavirus.
Find NCBI SARS-CoV-2 literature, sequence, and clinical content: https://www.ncbi.nlm.nih.gov/sars-cov-2/.

GenPept

alpha KG dependent 2,4-D dioxygenase [alpha proteobacterium HWK12]

GenBank: BAB92965.1

Identical Proteins FASTA Graphics

Go to:

```
LOCUS       BAB92965                295 aa            linear   BCT 02-JUL-2002
DEFINITION  alpha KG dependent 2,4-D dioxygenase [alpha proteobacterium HWK12].
ACCESSION   BAB92965
VERSION     BAB92965.1
DBSOURCE    accession AB074491.1
KEYWORDS    .
SOURCE      alpha proteobacterium HWK12
  ORGANISM  alpha proteobacterium HWK12
            Bacteria; Proteobacteria; Alphaproteobacteria.
REFERENCE   1
  AUTHORS   Itoh,K., Kanda,R., Sumita,Y., Kim,H., Kamagata,Y., Suyama,K.,
            Yamamoto,H., Hausinger,R.P. and Tiedje,J.M.
  TITLE     tfdA-like genes in 2,4-dichlorophenoxyacetic acid-degrading
            bacteria belonging to the
            Bradyrhizobium-Agromonas-Nitrobacter-Afipia cluster in
            alpha-Proteobacteria
  JOURNAL   Appl. Environ. Microbiol. 68 (7), 3449-3454 (2002)
   PUBMED   12089027
REFERENCE   2  (residues 1 to 295)
  AUTHORS   Itoh,K.
  TITLE     Direct Submission
  JOURNAL   Submitted (19-NOV-2001) Kazuhito Itoh, Shimane university, Life and
            Environmental Science; Nishikawatsu 1060, Matsue, Shimane 690-8504,
            Japan (E-mail:itohkz@life.shimane-u.ac.jp, Tel:81-852-32-6521,
            Fax:81-852-32-6597)
FEATURES             Location/Qualifiers
     source          1..295
                     /organism="alpha proteobacterium HWK12"
                     /strain="HWK12"
                     /db_xref="taxon:170271"
     Protein         1..295
                     /product="alpha KG dependent 2,4-D dioxygenase"
     Region          5..288
                     /region_name="TauD"
                     /note="Taurine dioxygenase, alpha-ketoglutarate-dependent
                     [Secondary metabolites biosynthesis, transport and
                     catabolism]; COG2175"
                     /db_xref="CDD:225086"
     Region          5..281
                     /region_name="TauD"
                     /note="Taurine catabolism dioxygenase TauD, TfdA family;
                     pfam02668"
                     /db_xref="CDD:280777"
     CDS             1..295
                     /gene="tfdA-like"
                     /coded_by="AB074491.1:1..888"
                     /transl_table=11
ORIGIN
        1 mtvlirqlhk hfvgevsgvd lrkpltkqea idieagmdky avlvfhgqdi sddqqmafal
       61 nfgkrenarg gtvtkkedyr lssglndvsn lgkdgkplpk dhrthlfnlg nclwhsdssf
      121 rpipakfsll sarvvnpkgg ntefadmraa ydalddetra eiddmicehs lmysrgslgf
      181 ldytdeekqm fkpvlqrlvr thpghgrrsl ylsshagair gmsvpearvl lrdlnehats
      241 pefvyvhkwt vhdlvmwdnr qtmhrvrryd qsqprdmrra tvagtqptvv qeage
//
```


COR-AAD1-00003379
Bayer EX1008 (Part 6 of 9)

Protein

COVID-19 is an emerging, rapidly evolving situation.
Get the latest public health information from CDC: https://www.coronavirus.gov .
Get the latest research from NIH: https://www.nih.gov/coronavirus.
Find NCBI SARS-CoV-2 literature, sequence, and clinical content: https://www.ncbi.nlm.nih.gov/sars-cov-2/.

GenPept

alpha KG dependent 2,4-D dioxygenase [alpha proteobacterium HW13]

GenBank: BAB92966.1

Identical Proteins FASTA Graphics

Go to:

```
LOCUS       BAB92966                295 aa            linear   BCT 02-JUL-2002
DEFINITION  alpha KG dependent 2,4-D dioxygenase [alpha proteobacterium HW13].
ACCESSION   BAB92966
VERSION     BAB92966.1
DBSOURCE    accession AB074492.1
KEYWORDS    .
SOURCE      alpha proteobacterium HW13
  ORGANISM  alpha proteobacterium HW13
            Bacteria; Proteobacteria; Alphaproteobacteria.
REFERENCE   1
  AUTHORS   Itoh,K., Kanda,R., Sumita,Y., Kim,H., Kamagata,Y., Suyama,K.,
            Yamamoto,H., Hausinger,R.P. and Tiedje,J.M.
  TITLE     tfdA-like genes in 2,4-dichlorophenoxyacetic acid-degrading
            bacteria belonging to the
            Bradyrhizobium-Agromonas-Nitrobacter-Afipia cluster in
            alpha-Proteobacteria
  JOURNAL   Appl. Environ. Microbiol. 68 (7), 3449-3454 (2002)
   PUBMED   12089027
REFERENCE   2  (residues 1 to 295)
  AUTHORS   Itoh,K.
  TITLE     Direct Submission
  JOURNAL   Submitted (19-NOV-2001) Kazuhito Itoh, Shimane university, Life and
            Environmental Science; Nishikawatsu 1060, Matsue, Shimane 690-8504,
            Japan (E-mail:itohkz@life.shimane-u.ac.jp, Tel:81-852-32-6521,
            Fax:81-852-32-6597)
FEATURES             Location/Qualifiers
     source          1..295
                     /organism="alpha proteobacterium HW13"
                     /strain="HW13"
                     /db_xref="taxon:170272"
     Protein         1..295
                     /product="alpha KG dependent 2,4-D dioxygenase"
     Region          5..288
                     /region_name="TauD"
                     /note="Taurine dioxygenase, alpha-ketoglutarate-dependent
                     [Secondary metabolites biosynthesis, transport and
                     catabolism]; COG2175"
                     /db_xref="CDD:225086"
     Region          5..281
                     /region_name="TauD"
                     /note="Taurine catabolism dioxygenase TauD, TfdA family;
                     pfam02668"
                     /db_xref="CDD:280777"
     CDS             1..295
                     /gene="tfdA-like"
                     /coded_by="AB074492.1:1..888"
                     /transl_table=11
ORIGIN
        1 mtvlirqlhk hfvgevsgvd lrkpltkqea idieagmdky avlvfhgqdi sddqqmafal
       61 nfgkrenarg gtvtkkedyr lssglndvsn lgkdgkplpk dhrthlfnlg nclwhsdssf
      121 rpipakfsll sarvvnpkgg ntefadmraa ydalddetkt eiddmicehs lmysrgslgf
      181 ldytdeekem fkpvlqrlvr thpahgrksl ylsshagair gmsmpearll lrdltehatq
      241 pefvyvhkwt vhdlvmwdnr qtvhrvrryd qsqprdmrra tvagtqptva qeaae
//
```


COR-AAD1-00003380
Bayer EX1008 (Part 6 of 9)